IRON NUTRITION AND INTERACTIONS IN PLANTS, 2nd Edition

EDITED BY: Thomas J. Buckhout, Sebastien Thomine and Wolfgang Schmidt
PUBLISHED IN: Frontiers in Plant Science

frontiers Research Topics

ISSN 1664-8714
ISBN 978-2-88963-970-0
DOI 10.3389/978-2-88963-970-0

About Frontiers

Frontiers is more than just an open-access publisher of scholarly articles: it is a pioneering approach to the world of academia, radically improving the way scholarly research is managed. The grand vision of Frontiers is a world where all people have an equal opportunity to seek, share and generate knowledge. Frontiers provides immediate and permanent online open access to all its publications, but this alone is not enough to realize our grand goals.

Frontiers Journal Series

The Frontiers Journal Series is a multi-tier and interdisciplinary set of open-access, online journals, promising a paradigm shift from the current review, selection and dissemination processes in academic publishing. All Frontiers journals are driven by researchers for researchers; therefore, they constitute a service to the scholarly community. At the same time, the Frontiers Journal Series operates on a revolutionary invention, the tiered publishing system, initially addressing specific communities of scholars, and gradually climbing up to broader public understanding, thus serving the interests of the lay society, too.

Dedication to Quality

Each Frontiers article is a landmark of the highest quality, thanks to genuinely collaborative interactions between authors and review editors, who include some of the world's best academicians. Research must be certified by peers before entering a stream of knowledge that may eventually reach the public - and shape society; therefore, Frontiers only applies the most rigorous and unbiased reviews.
Frontiers revolutionizes research publishing by freely delivering the most outstanding research, evaluated with no bias from both the academic and social point of view. By applying the most advanced information technologies, Frontiers is catapulting scholarly publishing into a new generation.

What are Frontiers Research Topics?

Frontiers Research Topics are very popular trademarks of the Frontiers Journals Series: they are collections of at least ten articles, all centered on a particular subject. With their unique mix of varied contributions from Original Research to Review Articles, Frontiers Research Topics unify the most influential researchers, the latest key findings and historical advances in a hot research area! Find out more on how to host your own Frontiers Research Topic or contribute to one as an author by contacting the Frontiers Editorial Office: researchtopics@frontiersin.org

IRON NUTRITION AND INTERACTIONS IN PLANTS, 2nd Edition

Topic Editors:
Thomas J. Buckhout, Humboldt University of Berlin, Germany
Sebastien Thomine, UMR9198 Institut de Biologie Intégrative de la Cellule (I2BC), France
Wolfgang Schmidt, Academia Sinica, Taiwan

Publisher's note: In this 2nd edition, the following article has been updated: Eroglu S, Karaca N, Vogel-Mikus K, Kavčič A, Filiz E and Tanyolac B (2019) The Conservation of VIT1-Dependent Iron Distribution in Seeds. *Front. Plant Sci.* 10:907. doi: 10.3389/fpls.2019.00907

Citation: Buckhout, T. J., Thomine, S., Schmidt, W., eds. (2020). Iron Nutrition and Interactions in Plants, 2nd Edition. Lausanne: Frontiers Media SA.
doi: 10.3389/978-2-88963-970-0

Table of Contents

frontiers in Plant Science

EDITORIAL
published: 10 January 2020
doi: 10.3389/fpls.2019.01670

Editorial: Iron Nutrition and Interactions in Plants

Wolfgang Schmidt[1]*, *Sebastien Thomine*[2] and *Thomas J. Buckhout*[3]

[1] Institute for Plant and Microbial Biology, Taipei, Taiwan, [2] Institute de Biologie Intégrative de la Cellule (I2BC), Gif-sur-Yvette, France, [3] Institute of Biology, Humboldt University of Berlin, Berlin, Germany

Keywords: iron, iron homeostasis, iron transport, plant mineral nutrition, bio-fortification, soil biology, regulation of gene expression

Editorial on the Research Topic

Iron Nutrition and Interactions in Plants

OPEN ACCESS

Edited by:
Stefania Astolfi,
Università degli Studi della Tuscia, Italy

Reviewed by:
Gianpiero Vigani,
University of Turin, Italy

***Correspondence:**
Wolfgang Schmidt
wosh@gate.sinica.edu.tw

Specialty section:
This article was submitted to Plant Nutrition, a section of the journal Frontiers in Plant Science

Received: *11 November 2019*
Accepted: *27 November 2019*
Published: *10 January 2020*

Citation:
Schmidt W, Thomine S and Buckhout TJ (2020) Editorial: Iron Nutrition and Interactions in Plants. Front. Plant Sci. 10:1670. doi: 10.3389/fpls.2019.01670

Gold is for the mistress—silver for the maid—
Copper for the craftsman cunning at his trade!
"Good!" said the Baron, sitting in his hall,
"but iron—cold iron—is master of them all."
Rudyard Kipling

Iron is a central component of electron chains and a co-factor of many vital enzymes. Only a few bacteria are able to substitute iron with other metals, making it an essential element for virtually all life forms. In plants, iron is also required for photosynthesis and chlorophyll synthesis. The availability of iron in soils dictates the distribution of plant species in natural ecosystems and limits yield and nutritional quality of crops. Insufficient iron uptake causes retarded growth, interveinal chlorosis, and reduced fitness. Sufficient iron levels in food crops are critical to combat iron deficiency-induced anemia, one of the largest nutritional disorder worldwide. Too much iron is, however, toxic to cells. It is therefore mandatory for plants to overcome the often-restricted availability of soil iron by strategies that increase its mobility and restrict its uptake when present in excess.

Despite great leaps forward in the research into plant iron nutrition over the past decades, many facets of cellular iron homeostasis still await further clarification. Moreover, attempts to increase the iron content in edible plant parts are far from having reached sufficient improvement in dietary iron intake. The International Symposium of Iron Nutrition and Interaction in Plants (ISINIP) is a biannual meeting that covers a wide range of aspects, including but not limited to iron availability in the soil, the regulation of cellular iron homeostasis, and the exploration of novel avenues for fortifying plants with iron. The collection of mini reviews, perspectives, and original papers

presented in this Research Topic is in part associated with contributions to the 19th edition of the ISINIP held in 2018 in Taipei, Taiwan.

CHECKPOINTS, BARRIERS, AND A MINEFIELD OF INADVERTENT INTERACTIONS: THE JOURNEY OF IRON THROUGH THE CELL

While the mechanisms underlying the uptake of iron from the soil are relatively well understood, the trafficking of iron to chloroplasts and mitochondria is less well explored. Chloroplasts are loaded with transition metals and represent the iron-richest system in plant cells. Research conducted by the group of Kathrin Philipar suggested that the ATP-binding ABC-transporter subunits ABCI10 and ABCI11 are part of a novel module of a prokaryote-type ECF/ABC transporter with similarities to components of prokaryotic multi-subunit ABC transporters putatively involved in metal ion uptake (Von Voithenberg et al.). New transporters have been identified also for the transport of iron through the inner mitochondrial membrane. Jain et al. show that the Arabidopsis transporters MIT1 and MIT2 are involved in iron import into mitochondria and critical for mitochondrial function.

Iron is highly reactive and must be chelated throughout intra- and intercellular trafficking to avoid cellular damage. Nozoye et al. are reporting a collaborative approach to elucidate the function of the nicotianamine (NA) transporter EFFLUX TRANSPORTER OF NA (ENA1) in rice, which is involved in the transport of NA to the apoplast and in the import of iron into cellular compartments such as plastids. The authors conclude that in rice NA transport by ENA is critical for cellular iron homeostasis by shielding iron ions from interacting with other molecules, causing precipitation of iron and oxidative damage to the cell.

ALL FOR ONE: A MULTITUDE OF REGULATORS CONTROL CELLULAR IRON HOMEOSTASIS

The regulation of iron uptake has to meet, but not to exceed the demand of the plant to avoid undernourishment or toxicity. Therefore, cellular iron levels are controlled by a delicate signaling network that orchestrates the demand of different plant parts in the context of rapidly and constantly changing availability of iron in the soil. A key role in the regulation of iron uptake is played by bHLH proteins. Until now, 16 bHLH transcription factors of this type were shown to be involved in the control of cellular iron homeostasis; it can be expected that this number is not yet exhaustive. In their mini review, Gao et al. summarize the current knowledge regarding the complex network of bHLH proteins that cooperatively regulate iron uptake in the green lineage. The bHLH protein FIT (bHLH29) takes a central position in this regulatory network. The activity of FIT is sophisticatedly controlled by a suite of proteins, which either activate FIT or enhance its degradation. Wu and Ling review the action of proteins that have been shown to interact with FIT and post-transcriptionally fine-tune its activity.

While the mechanisms underlying the perception of the cellular iron status differs across the kingdoms of life, some actors involved in iron sensing appear to be commonly recruited by yeast, mammals, and plants. Glutaredoxins and partnering BOLAs, homologs of *Escherichia coli* BolA proteins, may represent such common actors. In their Perspective paper, Rey et al. speculate that glutaredoxins, alone or in complex with BOLAs, may function in the maintenance of iron homeostasis in plants. More evidence for a specific function in iron signaling has accumulated for a small family of hemerythrin E3 ubiquitin ligases unique to the green lineage. HRZ (Hemerythrin RING Zinc finger) proteins in rice and their homologs BTS (BRUTUS) and BTSL (BRUTUS-LIKE) in Arabidopsis modulate the activity of specific transcription factors in a negative feedback loop, and are critical in avoiding the uptake of toxic amounts of iron. In their mini review, Rodríguez Celma et al. provide an overview on what is known about the putative function in iron sensing and signaling of this enigmatic group of regulators.

Plant growth-promoting bacteria can trigger both induced systemic resistance (ISR) and a partial iron deficiency response, indicating overlap in the regulation of the two processes. Infection with growth-promoting bacteria improves plant growth, increases iron content, and boosts plant defenses, conferring resistance to pathogens and pests. Romera et al. review the available data on this "ironic liaison," and investigate the possibilities to use ISR-eliciting microbes as both pesticides and iron fertilizers in a more sustainable agriculture.

Kaisalam et al. took a different approach toward the dissection of iron signaling pathways. The authors identified two small molecules, referred to as R3 and R6, through a chemical screen and showed that both molecules efficiently compromised the iron deficiency response of Arabidopsis, likely by targeting different signaling pathways. While R6 influences the IVc clade of bHLH proteins, R3 appears to affect a so far unexplored route toward the transcription factor FIT.

Post-translational modifications of lysine residues of core histones such as acetylation or methylation are a key component of eukaryotic gene regulation. Park et al. proposed that PRC2 (Polycomb Repressive Complex 2)-mediated methylation of lysine 27 of histone 3 attenuates the induction of FIT target genes, restricting iron uptake to avoid possible overload. The authors conclude that this epigenetic feature prevents maximum induction of genes involved in iron acquisition, providing an additional mechanism to fine-tune gene activity.

MicroRNAs (miRs) are a further node in the iron-signaling network. Carrió-Seguí et al. show that miR408 targets laccase-like multicopper oxidases with putative promiscuous activities interfering with the redox homeostasis and, ultimately, with iron signaling. The study further show that modifying miR408 levels resulted in complex phenotypes characterized by increased oxidative stress, altered lignification and, as a consequence of the latter, compromised metal transport.

LIAISONS DANGEREUSES: INTERACTION OF IRON WITH OTHER MINERALS

The iron homeostasis network is sophisticatedly interwoven with the uptake and transport of other mineral nutrients, often in an antagonistic manner. Lucena et al. addressed such interactions between iron and phosphate and found that deficiencies in one nutrient resulted in transitory induction of the expression of genes encoding proteins involved in the uptake of the other. The authors speculate that this induction is possibly triggered by phloem signals originating in the shoots that interact with hormones to balance the uptake of mineral nutrients from the soil. An antagonistic crosstalk between iron and phosphate signaling was also reported with respect to the accumulation of catecholic coumarins (Chutia et al.). The authors show that phosphate availability directly influences iron deficiency-induced accumulation of coumarins, a process that appears to reflect crosstalk between the regulators controlling the responses to iron and phosphate deficiency.

Similar to what have been previously reported for strategy I plants, Nicolic et al. observed an ameliorative effect of silicon on iron deficiency stress in barley, a plant with predominant Strategy II iron acquisition. Silicon significantly modulated the expression of Strategy II genes and increased the total iron content in the youngest leaves, which was associated with a lower ROS level, elevated APX and CAT activities, and increased chlorophyll levels. Moreover, silicon improved root-to-shoot iron translocation, resulting in an increased iron content in the youngest leaves.

Studying environmental cues such as Fe deficiency in isolation covers the processes that orchestrate the hierarchy of responses to simultaneously perceived signals and stresses. Terri Long's group developed an image analysis pipeline to extract spatiotemporal metrics of GFP signals showed that subjecting the plants to both heat stress and iron deficiency affected the spatiotemporal function of the mitosis marker CYCB1;1 antagonistically, suggesting interplay between stress pathways when plants are exposed to multiple environmental factors that may modulate the response that is observed in experiments that singles out a specific stimulus (Buckner et al.).

TOO MUCH TO HANDLE: STRATEGIES TO AVOID IRON TOXICITY

If in excess, iron can react with hydrogen peroxide and trigger the formation of harmful hydroxyl radicals through Fenton chemistry. The free iron concentration drastically increases with decreasing redox potential, as it is the case for instance in flooded soils. Although genetic variation in iron tolerance suggests the evolution of adaptive strategies to cope with high external iron levels, the mechanisms underlying such adaptations have not yet been fully elucidated. Stein et al. speculated that natural variation in iron toxicity tolerance across rice cultivars is related to the composition of the root cell wall. The authors demonstrate that increased lignification in the outer layers of the cortex and in the vascular bundle may alter iron permeability, radial diffusion, and root-to-shoot translocation of iron, ultimately leading to a higher tolerance to high external iron levels. Also the interaction of iron with other nutrients appears to be important for coping with high iron levels. Wu et al. reported that the inward potassium ion (K^+) channel OsAKT1 affects the translocation of iron from roots to shoots, a process that is contributing to the tolerance to iron toxicity. Loss-of-function mutants of OsAKT1 exhibit altered K homeostasis, lower K^+ concentrations, and hyperpolarization of the plasma membrane, leading to decreased iron loading into the xylem. A further important player in the tolerance of rice to high iron levels is the vacuolar iron reductase OsFRO1, which maintains cellular iron homeostasis by tuning the iron concentrations in the cytoplasm and in the vacuole (Li et al.).

The metal chelator NA plays multifaceted roles in metal homeostasis and appears also to be important to protect the plant from iron overload. Aung et al. show that expression of the rice NA synthase *OsNAS3* strongly increased when plants were subjected to excess iron levels; *OsNAS3* knockout plants showed reduced growth and severe leaf bronzing, resulting from increased iron accumulation. The results demonstrate that NA is important for mitigating excess iron and provide a new perspective for the development of rice lines with improved tolerance to excess iron availability soils.

THE MORE, THE BETTER? FORTIFICATION OF PLANTS WITH IRON

More than 30% of the arable land are calcareous and potential iron-deficient. Low iron content of crops is the main cause of iron deficiency-induced anemia, the most common micronutrient deficiency globally. Iron-biofortification denotes the process of enhancing bioavailable iron in edible parts of staple food by agronomic approaches, biotechnology techniques, or conventional plant breeding. Biofortification is a promising approach to combat micronutrient malnutrition, which affects nearly one-third of the world's population, particularly in resource-limited settings.

Iron fertilizers are costly, not environmentally friendly, and often inefficient. Iron-humic complexes have long been known to promote iron nutrition in a multifaceted way by providing a readily available iron form in the soil and by directly impacting physiological and developmental programs. Zanin et al. review the complex issue of how humic substances affect plant performance and investigate the possibility to use iron-humic complexes as an environmentally friendly source of iron fertilizer. The supposition that increasing crop production through innovative iron fertilizers is a promising alternative to traditional iron fertilization is also supported by a study by Cieschi et al. The authors describe the action of three iron-humic nanofertilizers as a natural, low cost and environmental option to improve iron uptake of soybean grown on calcareous soils by providing iron over prolonged time periods.

Intercropping of fruit trees or crops with graminaceous plants can have beneficial effects on the iron status of iron-inefficient plants and has been proven useful for low-input/resource-limited agricultural systems. Dai et al. review the effects and mechanisms underlying the promotive effects on iron nutrition focusing on Leguminosae/Gramineae intercropping systems. Intercropping is particularly beneficial for calcifuge species adapted to acidic soils. Blueberry, a calcifuge, develops severe iron deficiency symptoms under alkaline conditions, drastically reducing plant growth and yield. Intercropping with the grasses *Festuca rubra* and *Poa pratensis* in combination with Fe-EDDHA applications was found to be effective in increasing fruit load and yield of blueberries while reducing the skin/flesh ratio and firmness of the berries (Michel et al.).

Genetic biofortification, i.e. conventional breeding and genetic engineering, is the topic of a mini review by Ludwig and Slamet-Loedin. The authors summarize the problems and advances of different biofortification strategies to enrich rice and wheat grain iron to combat "hidden hunger." Rice has employed components of both strategy I and strategy II to acquire iron from the soil. Masuda et al. reported that transgenic rice with increased phytosiderophore production and Fe(III) reduction activity conferred by introducing a gene cassette comprising a regulator of the iron deficiency responses (IRO2), a barley IDS3 genome fragment to increase PS production, and a mutationally reconstructed yeast ferric reductase exhibited enhanced tolerance to iron-deficient conditions and significantly higher yield when cultivated on calcareous soil.

The distribution of iron in seeds in a main determinant for its bioavailability, which can be severely restricted by antinutrients such as phytate that are localized in the same cellular compartments. With the goal to investigate if iron can be stored in phytate-free compartment such as plastids, Eroglu et al. investigated metal localization in seeds of more than twenty species using histochemical or X-ray based techniques. The study revealed distinct seed iron storage patterns across plant lineages. The authors further report that in Rosids iron is concentrated in the innermost cell layers, the endodermis, and in the cortex.

AUTHOR CONTRIBUTIONS

All authors wrote and approved the manuscript.

ACKNOWLEDGMENTS

We would like to express our sincere gratitude to and appreciation of all authors and reviewers that contributed to this Research Topic. We would also like to thank all the past organizers of the ISINIP for their help to keep this exciting conference series running over the past decades.

Conflict of Interest: The authors declare that the research was conducted in the absence of any commercial or financial relationships that could be construed as a potential conflict of interest.

frontiers in Plant Science

MINI REVIEW
published: 18 January 2019
doi: 10.3389/fpls.2019.00006

The Transcriptional Control of Iron Homeostasis in Plants: A Tale of bHLH Transcription Factors?

*Fei Gao†, Kevin Robe†, Frederic Gaymard, Esther Izquierdo and Christian Dubos**

BPMP, CNRS, INRA, Montpellier SupAgro, University of Montpellier, Montpellier, France

Iron is one of the most important micronutrients in plants as it is involved in many cellular functions (e.g., photosynthesis and respiration). Any defect in iron availability will affect plant growth and development as well as crop yield and plant product quality. Thus, iron homeostasis must be tightly controlled in order to ensure optimal absorption of this mineral element. Understanding mechanisms governing iron homeostasis in plants has been the focus of several studies during the past 10 years. These studies have greatly improved our understanding of the mechanisms involved, revealing a sophisticated iron-dependent transcriptional regulatory network. Strikingly, these studies have also highlighted that this regulatory web relies on the activity of numerous transcriptional regulators that belong to the same group of transcription factors (TF), the bHLH (basic helix-loop-helix) family. This is best exemplified in Arabidopsis where, to date, 16 bHLH TF have been characterized as involved in this process and acting in a complex regulatory cascade. Interestingly, among these bHLH TF some form specific clades, indicating that peculiar function dedicated to the maintenance of iron homeostasis, have emerged during the course of the evolution of the green lineage. Within this mini review, we present new insights on the control of iron homeostasis and the involvement of bHLH TF in this metabolic process.

Keywords: basic helix loop helix, bHLH, iron, homeostasis, *Arabidopsis thaliana*

OPEN ACCESS

Edited by:
Thomas J. Buckhout, Humboldt-Universität zu Berlin, Germany

Reviewed by:
Takanori Kobayashi, Ishikawa Prefectural University, Japan
Tzvetina Brumbarova, Heinrich-Heine-Universität Düsseldorf, Germany

***Correspondence:**
Christian Dubos
Christian.dubos@inra.fr

†These authors have contributed equally to this work

Specialty section:
This article was submitted to Plant Nutrition, a section of the journal Frontiers in Plant Science

Received: *16 November 2018*
Accepted: *07 January 2019*
Published: *18 January 2019*

Citation:
Gao F, Robe K, Gaymard F, Izquierdo E and Dubos C (2019) The Transcriptional Control of Iron Homeostasis in Plants: A Tale of bHLH Transcription Factors? Front. Plant Sci. 10:6. doi: 10.3389/fpls.2019.00006

INTRODUCTION

Iron (Fe) is one of the most important micronutrient elements in plants as it is involved in many cellular functions (e.g., photosynthesis and respiration). Any defect in Fe availability will impact plant growth and development as well as crop yield and plant product quality (Briat et al., 2015).

In order to cope with Fe shortage and recover Fe from soil, where it is in poorly available forms, plants have evolved two strategies. The first one, strategy I, is used by all dicots and non-graminaceous monocots. This strategy consists in rhizosphere acidification via proton extrusion in order to promote Fe solubility and involves proton-ATPase such as AHA2. The secretion by the root of Fe-mobilizing phenolic compounds facilitates this process (Fourcroy et al., 2014, 2016). Fe^{3+} is thus reduced into Fe^{2+} by ferric chelate reductases, such as FRO2 (FERRIC REDUCTION OXIDASE 2), prior to being transported across the rhizodermis cell membranes by IRT1 (IRON-REGULATED TRANSPORTER 1) (Brumbarova et al., 2015). The second strategy, strategy II, is used by graminaceous species. This strategy consists in releasing phytosiderophores into the rhizosphere to chelate Fe^{3+} (Nozoye et al., 2011). Fe^{3+}-phytosiderophores chelates are then transported into the roots by the YELLOW STRIPE 1 transporter (Curie et al., 2001). If the machinery

allowing plant Fe uptake from the soil is central for the maintenance of Fe homeostasis, this is indeed not the sole mechanism involved in this process. It also necessitates several genes encoding proteins involved in Fe transport, compartmentation and storage, at the cellular and subcellular levels, throughout the entire plant body. Such complex mechanism must thus be tightly regulated in order to avoid any physiological situation that would be deleterious to the plant.

How, at the molecular level, plants control Fe homeostasis has thus been a critical question for several years. This question has been mostly addressed by studying plant response to Fe deficiency, in particular in the model plant *Arabidopsis thaliana*. These studies have highlighted that such response involves an intricate network of basic helix-loop-helix (bHLH) transcription factors (TF) (**Figure 1**). bHLH proteins form one of the largest family of TFs found in plants that act as homo- or heterodimers to regulate the expression of their target genes. In Arabidopsis, 133 members have been identified and divided into 12 clades (Heim et al., 2003). From what is known on the role played by several members of this family of TFs in plants, it appears that their participation in the control of Fe homeostasis is unique by the number of individual TFs and different clades that are involved as well as by the intricacy of the network they form.

THE MOLECULAR REGULATION OF PLANT IRON HOMEOSTASIS

The bHLH Regulatory Network

Upstream from the regulatory network involved in Arabidopsis Fe deficiency response are four bHLH TFs belonging to the clade IVc, namely bHLH34, bHLH104, bHLH105/ILR3 (IAA-LEUCINE RESISTANT3), and bHLH115 (**Figure 1**). These four TFs, shown to interact *in vivo* in the form of homo- or heterodimers, act as transcriptional activators of the plant response to Fe deficiency and display partial redundant activities (Zhang et al., 2015; Li et al., 2016; Liang et al., 2017). Clade IVc bHLH targets consist of *bHLH47/PYE* (*POPEYE*; clade IVb) and four clade Ib bHLH genes (*bHLH38*, *bHLH39*, *bHLH100,* and *bHLH101*) (Colangelo and Guerinot, 2004; Wang et al., 2007; Yuan et al., 2008; Wang N. et al., 2013; Zhang et al., 2015). PYE acts as a transcriptional repressor. For example, PYE was shown to inhibit the expression of *NAS4* (*NICOTIANAMINE SYNTHASE 4*), a key gene involved in phloem-based transport of Fe to sink organs, and *FRO3*, a Fe reductase located in root vasculature mitochondria (Jeong and Connolly, 2009; Klatte et al., 2009; Long et al., 2010). Interestingly, PYE can interact *in vivo* with bHLH104, ILR3, and bHLH115 (Long et al., 2010; Zhang et al., 2015). Whether or not these interactions play a role in the plant response to Fe deficiency or in the control of Fe homeostasis is an important question that remains to be elucidated. In contrast, bHLH38, bHLH39, bHLH100, and bHLH101 are partially redundant proteins that function at the root epidermis as positive regulators of *FRO2* and *IRT1*. This activity relies on their interaction with FIT (Fe-deficiency induced transcription factor), a clade IIIa bHLH (Colangelo and Guerinot, 2004; Yuan et al., 2008; Wang N. et al., 2013; Maurer et al., 2014). *FIT* expression is likely controlled, at least in part, by a feed forward regulatory loop involving bHLH39 (Naranjo-Arcos et al., 2017). bHLH6/MYC2 (clade IIIe) is a master regulator of the jasmonic acid (JA) signaling pathway whose activity differentially affects the expression clade IVa bHLH (bHLH18, bHLH19, bHLH20, and bHLH25) genes to modulate FIT protein accumulation (Cui et al., 2018). This mechanism relies on the direct interaction of clade IVa bHLHs with FIT in order to promote its degradation via the 26S proteasome pathway (Cui et al., 2018). In addition, MYC2 is a JA-dependent repressor of *FIT* and clade Ib bHLH genes expression, hence inhibiting FIT-dependent Fe uptake machinery at the transcriptional and posttranslational levels (Cui et al., 2018). Interestingly, *bHLH11*, another clade IVb bHLH, was recently proposed to be a negative regulator of FIT-dependent Fe uptake mechanism effecting Fe levels in Arabidopsis plants (Tanabe et al., 2018).

Altogether, this is 16 bHLH TFs out of the 133 present in Arabidopsis that have been identified as involved in the control of the Fe deficiency response, which represent more than 12% of the members of this large family of TFs (Heim et al., 2003). Indeed, orthologous members from the above-described clades were identified in other strategy I plant species such as tomato, apple, or soybean (Ling et al., 2002; Du et al., 2015; Zhao et al., 2016b; Li et al., 2018). In soybean, it is likely that the orthologs of *FIT* (*GmbHLH57*) and clade Ib bHLH (*GmbHLH300*) genes may also play a role in nodules, a tissue where several enzymes involved in symbiotic nitrogen fixation require Fe for their activity (Tang et al., 1990; O'Hara, 2001; Li et al., 2018). With the exception of FIT, which is specific to strategy I plants, orthologs of several bHLH are present in strategy II plants, indicating that the regulatory cascade controlling plant response to Fe deficiency is mostly conserved within the plant kingdom. For instance, orthologs of clade Ib (*OsIRO2*), IVc (*OsPRI1*), *PYE* (*OsIRO3*) and *MYC2* (*OsMYC2*) genes have been characterized in rice (Ogo et al., 2007; Zheng et al., 2010; Ogawa et al., 2017; Zhang et al., 2017). However, no orthologous bHLH TF in strategy I plants has been described so far for OsbHLH133, another regulator of the Fe deficiency response in rice (Wang L. et al., 2013). Is OsbHLH133 function specific to strategy II plants as it is the case for FIT in strategy I plants? Protein sequence analysis tends to indicate that OsbHLH133 is closely related to the bHLH clade VIIIc and thus it might be that this clade plays a role in the control of Fe homeostasis in both strategy I and II plants. If this hypothesis is verified, it will certainly render more complicated our understanding of this transcriptional regulatory network. Indeed, it is not the complexity of this network that is intriguing considering that any defect in the control of Fe homeostasis might be deleterious to the plants. The main question is why so many bHLHs are involved in this process? If it is difficult to answer this question, the involvement of a large number of TFs from one family in a specific process has already been described. This is the case with the R2R3-MYB family where at least 19 members out of 122 (about 16%) are involved in the control of the phenylpropanoid pathway (Dubos et al., 2010; Zamioudis et al., 2014; Xu et al., 2015). From these observations it would be tempting to speculate that during the course of the evolution

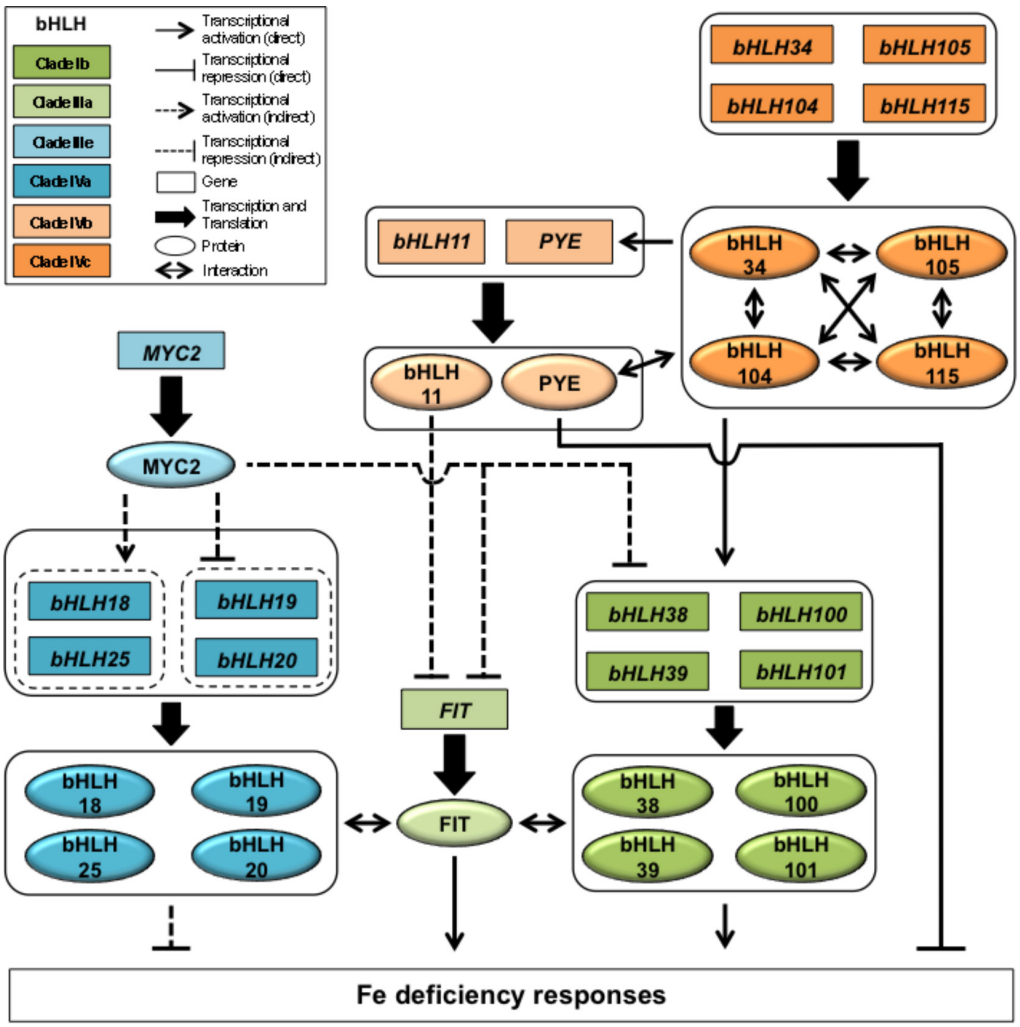

FIGURE 1 | bHLH-dependent transcriptional regulatory network controlling the iron deficiency response in *Arabidopsis thaliana*.

of the green lineage, TF families have evolved specialized roles, in which plant Fe homeostasis would be mostly regulated by TFs belonging to the bHLH gene family.

How these bHLH TFs interact with the *cis*-regulatory sequences usually present in the promoter of their target genes is an important question considering that (i) each bHLH must specifically recognized its own target and (ii) the number of bHLH involved in this complex network. Indeed, it is well known that bHLH TF bind to specific DNA motifs (*CANNTG*) named *E-box*, and in particular to the canonical *CACGTG* sequence, named *G-box* (De Masi et al., 2011). For instance, chromatin immunoprecipitation assays showed that PYE, bHLH104, bHLH115, ILR3, and FIT preferentially bound to the promoter of their target genes in region that contain *E-box* or *G-box* (Long et al., 2010; Zhang et al., 2014, 2015; Liang et al., 2017). Similar observations were made, using biochemical approaches, for MdbHLH104 and OsPRI1 (Zhao et al., 2016a; Zhang et al., 2017). Interestingly, it was demonstrated that the genomic regions flanking *E-box* binding sites influence the DNA binding specificity of TFs (Gordan et al., 2013; Ezer et al., 2017). This is for example the case for OsIRO2 that binds preferentially to *CACGTGG* motif (Ogo et al., 2007). Hence, despite the fact that several direct target genes have been identified for most of the bHLH involved in the transcriptional control of Fe homeostasis and the fact that it is possible to infer the *E-box* sequence recognized by a given bHLH dimer based on bHLH domain compositions (De Masi et al., 2011), very little is known on the actual bHLH/DNA interactions.

The Other Actors Involved in the Transcriptional Control of Plant Fe Homeostasis

Additional TFs, from several gene families, involved in the control of Fe homeostasis in both strategy I and strategy II plant species, have also been characterized.

MYB10 and MYB72, two R2R3-MYB TFs whose expression is partially dependent on FIT, are involved in Fe acquisition

and distribution by notably regulating the expression of *BGLU42* and *NAS4* (Palmer et al., 2013; Stringlis et al., 2018). A closely related apple R2R3-MYB, MdMYB58, was recently reported as potentially involved in the control of Fe transport and tissue partitioning. It is proposed that MdMYB58 activity is repressed by its heterodimerization with MdSAT1, a clade IVa bHLH (Wang et al., 2018). WRKY46 plays a critical role in Fe translocation from root to shoot by directly repressing the expression of *VITL1/VTL1* (*vacuolar iron transporter like 1*) (Yan et al., 2016). ERF4 and ERF72 (AP2/ERF TFs) play negative roles in plant response to Fe deficiency by inhibiting the expression of genes involved in Fe uptake such as *IRT1* or *AHA2* (Liu et al., 2017a,b). Two TFs (EIL family) involved in ethylene signaling (EIN3, ETHYLENE INSENSITIVE 3 and EIL1, ETHYLENE INSENSITIVE 3 LIKE 1) and ZAT12 (a C2H2-type plant-specific zinc finger TF) are also involved by modulating FIT stability (Lingam et al., 2011; Le et al., 2016). Two MYB-CC TFs (PHR1, PHOSPHATE STARVATION RESPONSE 1 and PHL1, PHR1-LIKE 1), that play a central role in the phosphate deficiency response, regulate the expression of the main Fe storage ferritin gene in Arabidopsis (*AtFER1*), indicating that they act as integrators of both the phosphate and Fe signaling pathways (Bournier et al., 2013).

IDEF1 (ABI3/VP1 family) is an early regulator of Fe deficiency response in rice that directly binds to divalent metals suggesting that IDEF1 is a cellular sensor of metal ion balance caused by changes in Fe availability (Kobayashi et al., 2009, 2012). IDEF2 (NAC family) and OsARF16 (ARF family) play also critical roles in the control of Fe homeostasis in rice by modulating the expression of Fe-related genes and by integrating auxin signals, respectively (Ogo et al., 2008; Shen et al., 2015).

THE MOLECULAR REGULATION OF THE TRANSCRIPTIONAL REGULATORY CASCADE CONTROLLING IRON HOMEOSTASIS

Post-translational Regulation of bHLH TFs

Iron deficiency results in a transcriptional response that leads to the activation of the Fe uptake machinery, which could lead to a Fe overload if it becomes suddenly available or to a toxic overaccumulation of other divalent metals (e.g., Zn, Mn, and Cd) due to the low specificity of IRT1. To cope with this, plants have developed posttranslational mechanisms such as the continuous recycling of IRT1 (Barberon et al., 2011, 2014). In addition, in Arabidopsis, IRT1 phosphorylation and ubiquitination leads to its internalization and subsequent degradation, a process that is triggered by direct binding of IRT1 to non-Fe metals (Ivanov et al., 2014; Dubeaux et al., 2018). However, maintaining Fe homeostasis requires also to tightly regulating, at the posttranslational level, the TFs involved in this process.

Fe-deficiency induced TF posttranslational regulation has been extensively investigated in Arabidopsis. For instance, it was shown that FIT heterodimerization with clade IVa bHLH promotes its degradation via the 26S proteasome pathway, whereas its interaction with clade Ib bHLH promotes its stability (Cui et al., 2018). FIT interaction with EIN3 or EIL1 also promotes its stability and contributes to Fe acquisition during the early stage of Fe deficiency (Lingam et al., 2011). In contrary, FIT interaction with ZAT12 has an inhibitory effect on its function when plants are grown under Fe sufficiency or prolonged Fe deficiency conditions (Le et al., 2016).

Several ubiquitin E3 ligases targeting bHLH TFs involved in the response to Fe deficiency have been characterized. *BRUTUS* (*BTS*), whose expression is induced upon Fe deficiency, is thought to be a Fe-sensing negative regulator in Arabidopsis (Selote et al., 2015). *In vitro* analyses suggest that BTS restricts the accumulation of ILR3 and bHLH115 through its RING E3 ligase activity and mediates their 26S proteasomal degradation (Selote et al., 2015). Whether the interaction of bHLH104 with BTS participate to its degradation remains to be demonstrated (Selote et al., 2015). The identification of two BTS ortologues in rice, namely OsHRZ1 [HEMERYTHRIN MOTIF-CONTAINING REALLY INTERESTING NEW GENE (RING) AND ZINC-FINGER PROTEIN 1] and OsHRZ2, suggests that BTS function is conserved in strategy II plants (Kobayashi et al., 2013). In addition to BTS, two closely related RING E3 ligases named BTSL1 and BTSL2 (BRUTUS LIKE 1 and 2) are proposed to negatively regulate the Fe deficiency responses by directly targeting FIT, leading to its degradation (Sivitz et al., 2011; Hindt et al., 2017; Rodriguez-Celma et al., 2018). Interestingly, it was shown in apple that a cullin-based E3 ligase mechanism, involving two BTB-TAZ proteins (MdBT1 and MdBT2) and MdCUL3, target MdbHLH104 for ubiquitin-dependent degradation via the 26S proteasome (Zhao et al., 2016a). Unlike BTS and the E3 ligase degrading FIT, *MdBT* expression and protein accumulation is induced when Fe availability is not limiting, leading to MdbHLH104 degradation (Zhao et al., 2016a). In addition, MdbHLH104 sumoylation, by the SUMO E3 ligase MdSIZ1, promotes MdbHLH104 stability, especially when Fe availability is scarce (Zhou et al., 2018). These findings suggest that the degradation of the bHLHs involved in the plant response to Fe availability may require two types of ubiquitin E3 ligases and that sumoylation may also have an important role in this process.

bHLH Promoter Activity and Protein Localization

Iron uptake and translocation to the whole plant body requires coordinating the expression of several structural genes within and between the different cell types of roots that is achieved by the involvement of several TFs, in particular bHLHs (**Figure 2**).

Clade IVc bHLHs analysis of promoter activity revealed a specific expression in the stele (pericycle) of the root in the maturation zone (Li et al., 2016; Liang et al., 2017). Root tip expression was also detected except for *bHLH115*, whereas *ILR3* was the sole bHLH from this clade to be expressed in the elongation zone of root tips and early lateral roots. These differences suggest that non-redundant biological functions may

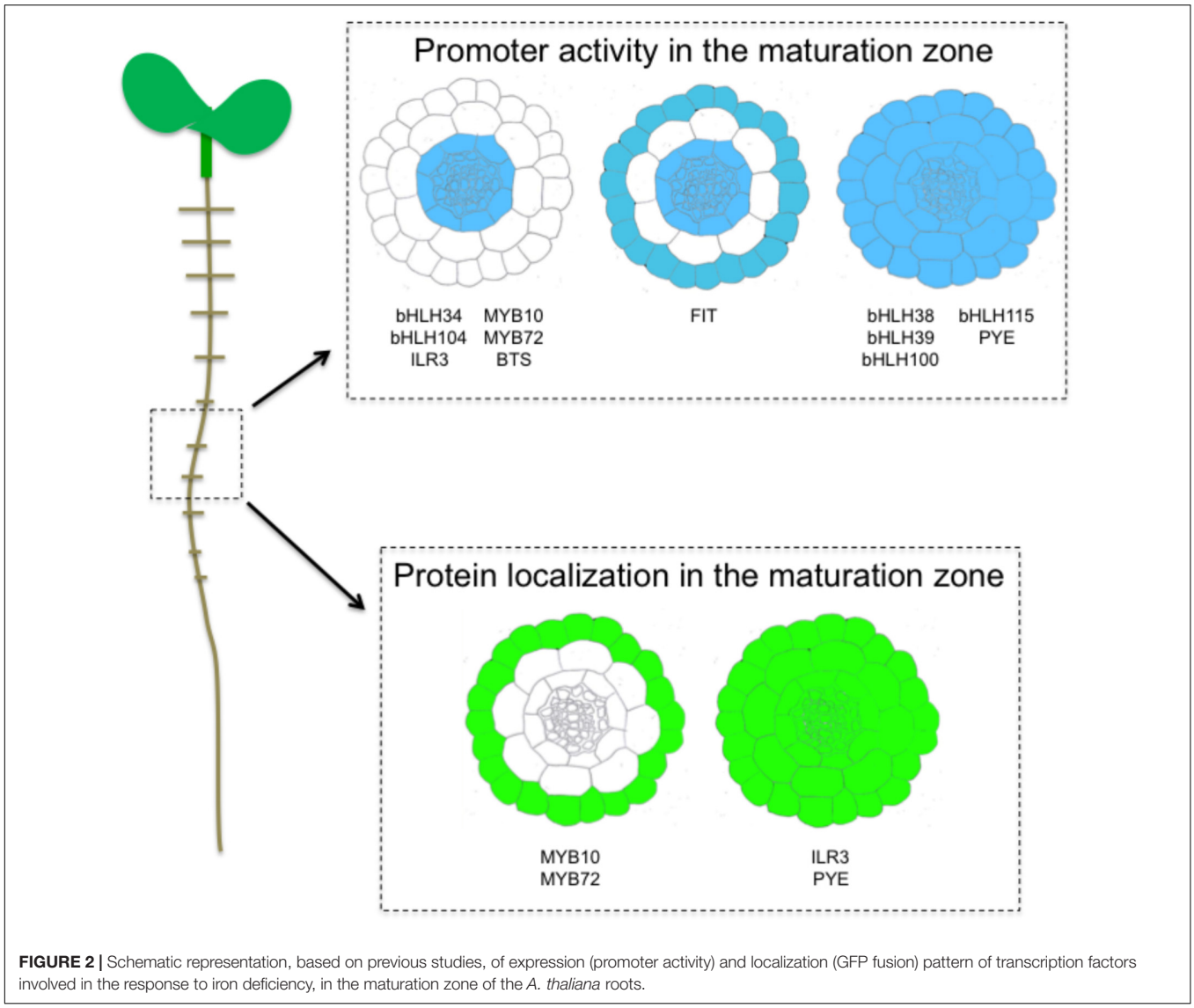

FIGURE 2 | Schematic representation, based on previous studies, of expression (promoter activity) and localization (GFP fusion) pattern of transcription factors involved in the response to iron deficiency, in the maturation zone of the *A. thaliana* roots.

exist between the members of this clade (Liang et al., 2017). For instance, ILR3 was shown to participate in the plant response to biotic and abiotic stresses (Samira et al., 2018). Perivascular expression has also been observed in the aerial part of the plants (i.e., hypocotyl and leaves) (Rampey et al., 2006; Zhang et al., 2015; Li et al., 2016; Liang et al., 2017). Promoter activity of *PYE* is similar in roots to that of *bHLH115*. In these cells PYE represses the expression of *NAS4* and *FRO3*, modulating Fe translocation to the above ground part of the plant (Long et al., 2010). Clade Ib bHLHs (except *bHLH101* whose promoter is not active in roots) were expressed throughout the root including the stele cells, which was in contrast with the expression pattern of their regulators, the clade IVc bHLH TFs (Wang et al., 2007). Clade Ib bHLHs promoter activity was essentially detected in the epidermis in the maturation zone, in the epidermis and inside the roots in the upper part zone (but not in the stele), and at the lateral root emergence site. However, a comparable pattern of expression with clade IVc bHLHs was observed in leaves. The apparent discrepancy observed in roots between the expression of clade Ib bHLHs and their transcriptional regulators suggests that clade IVc bHLH TFs may act in various cell types and thus have the ability to move from one cell type to another. In a recent study, it was shown that ILR3 protein is present in all root cell type when Fe availability is scarce (Samira et al., 2018). If this observation supports the hypothesis that ILR3 may move from the stele to other cell layers, it cannot be excluded that the promoter of *ILR3* is not sufficient for proper *ILR3* expression, and that sequences present in the coding region (e.g., introns) might be required. Interestingly, the pattern of PYE accumulation in root cells is similar to that of ILR3 (Long et al., 2010). The fact that ILR3 and PYE are present in the same cell layers and interact *in vivo* suggest that PYE function in the plant response to Fe deficiency might be tightly connected to ILR3 activity (Long et al., 2010; Selote et al., 2015). What would be the role of such heterodimers is still a matter of debate. Nevertheless, if the inter cellular trafficking of these two TFs was proven to be

true, decrypting the underlying mechanisms would be the next challenge.

Fe-deficiency induced TF expression is mostly restricted to root tissues. At the rhizodermis, *FIT* expression overlaps those of its bHLH interacting partners from clade Ib (Colangelo and Guerinot, 2004; Jakoby et al., 2004). This is in agreement with the heterodimerization of FIT with clade Ib bHLHs to regulate the expression of Fe mobilization genes such as *IRT1* and *FRO2*. Two other TFs whose expression is partly regulated by FIT in response to Fe deficiency, namely MYB10 and MYB72, are mainly localized at the rhizodermis where they control the expression of *BGLU42* (Zamioudis et al., 2014). In the maturation zone, *FIT* is expressed in the epidermis and throughout the stele (Jakoby et al., 2004). Clade IVa bHLHs promoter activity is specific to the stele, a tissues where the repressive role of the encoded proteins on FIT stability is counteracted by FIT heterodimerization with clade Ib bHLHs (Cui et al., 2018). In the aerial part of the plant, clade IVa expression follows the vasculature as it is the case for ILR3 or clade Ib bHLHs.

CONCLUSION

To date several TFs involved in the control of Fe homeostasis have been characterized and several molecular connections have been identified. However we still do not know how the expression of the most upstream TFs of this network is regulated (i.e., FIT, clade IVc bHLH), indicating that we still do not have the full set of TFs involved in this network. Whether or not the Fe deficiency and Fe excess responses are controlled by an integrated pathway involving common players is still an open question that remains to be addressed. Last, deciphering the precise localization, at the protein level, of all the TFs involved in the control of Fe homeostasis is an important task that should be achieved if one aims at fully decrypting the functioning of this intricate molecular network.

AUTHOR CONTRIBUTIONS

FeG, KR, FrG, EI, and CD wrote the manuscript. FeG, KR, and CD made the figures.

FUNDING

KR and FeG were supported by a fellowship from the Agence Nationale pour la Recherche (ANR-17-CE20-0008-01) and from the China Scholarship Council (CSC), respectively.

ACKNOWLEDGMENTS

We thank Dr. N. Berger for help in preparing this manuscript.

REFERENCES

Barberon, M., Dubeaux, G., Kolb, C., Isono, E., Zelazny, E., and Vert, G. (2014). Polarization of IRON-REGULATED TRANSPORTER 1 (IRT1) to the plant-soil interface plays crucial role in metal homeostasis. *Proc. Natl. Acad. Sci. U.S.A.* 111, 8293–8298. doi: 10.1073/pnas.1402262111

Barberon, M., Zelazny, E., Robert, S., Conejero, G., Curie, C., Friml, J., et al. (2011). Monoubiquitin-dependent endocytosis of the iron-regulated transporter 1 (IRT1) transporter controls iron uptake in plants. *Proc. Natl. Acad. Sci. U.S.A.* 108, E450–E458. doi: 10.1073/pnas.1100659108

Bournier, M., Tissot, N., Mari, S., Boucherez, J., Lacombe, E., Briat, J. F., et al. (2013). *Arabidopsis* ferritin 1 (AtFer1) gene regulation by the phosphate starvation response 1 (AtPHR1) transcription factor reveals a direct molecular link between iron and phosphate homeostasis. *J. Biol. Chem.* 288, 22670–22680. doi: 10.1074/jbc.M113.482281

Briat, J. F., Dubos, C., and Gaymard, F. (2015). Iron nutrition, biomass production, and plant product quality. *Trends Plant Sci.* 20, 33–40. doi: 10.1016/j.tplants.2014.07.005

Brumbarova, T., Bauer, P., and Ivanov, R. (2015). Molecular mechanisms governing *Arabidopsis* iron uptake. *Trends Plant Sci.* 20, 124–133. doi: 10.1016/j.tplants.2014.11.004

Colangelo, E. P., and Guerinot, M. L. (2004). The essential basic helix-loop-helix protein FIT1 is required for the iron deficiency response. *Plant Cell* 16, 3400–3412. doi: 10.1105/tpc.104.024315

Cui, Y., Chen, C. L., Cui, M., Zhou, W. J., Wu, H. L., and Ling, H. Q. (2018). Four IVa bHLH transcription factors are novel interactors of FIT and mediate JA inhibition of iron uptake in *Arabidopsis*. *Mol. Plant* 11, 1166–1183. doi: 10.1016/j.molp.2018.06.005

Curie, C., Panaviene, Z., Loulergue, C., Dellaporta, S. L., Briat, J. F., and Walker, E. L. (2001). Maize yellow stripe1 encodes a membrane protein directly involved in Fe(III) uptake. *Nature* 409, 346–349. doi: 10.1038/35053080

De Masi, F., Grove, C. A., Vedenko, A., Alibes, A., Gisselbrecht, S. S., Serrano, L., et al. (2011). Using a structural and logics systems approach to infer bHLH-DNA binding specificity determinants. *Nucleic Acids Res.* 39, 4553–4563. doi: 10.1093/nar/gkr070

Du, J., Huang, Z., Wang, B., Sun, H., Chen, C., Ling, H. Q., et al. (2015). SlbHLH068 interacts with FER to regulate the iron-deficiency response in tomato. *Ann. Bot.* 116, 23–34. doi: 10.1093/aob/mcv058

Dubeaux, G., Neveu, J., Zelazny, E., and Vert, G. (2018). Metal sensing by the IRT1 transporter-receptor orchestrates its own degradation and plant metal nutrition. *Mol. Cell* 69, 953.e5–964.e5. doi: 10.1016/j.molcel.2018.02.009

Dubos, C., Stracke, R., Grotewold, E., Weisshaar, B., Martin, C., and Lepiniec, L. (2010). MYB transcription factors in *Arabidopsis*. *Trends Plant Sci.* 15, 573–581. doi: 10.1016/j.tplants.2010.06.005

Ezer, D., Shepherd, S. J. K., Brestovitsky, A., Dickinson, P., Cortijo, S., Charoensawan, V., et al. (2017). The G-Box transcriptional regulatory code in *Arabidopsis*. *Plant Physiol.* 175, 628–640. doi: 10.1104/pp.17.01086

Fourcroy, P., Siso-Terraza, P., Sudre, D., Saviron, M., Reyt, G., Gaymard, F., et al. (2014). Involvement of the ABCG37 transporter in secretion of scopoletin and derivatives by *Arabidopsis* roots in response to iron deficiency. *New Phytol.* 201, 155–167. doi: 10.1111/nph.12471

Fourcroy, P., Tissot, N., Gaymard, F., Briat, J. F., and Dubos, C. (2016). Facilitated Fe nutrition by phenolic compounds excreted by the *Arabidopsis* ABCG37/PDR9 transporter requires the IRT1/FRO2 high-affinity root Fe(2+) transport system. *Mol. Plant* 9, 485–488. doi: 10.1016/j.molp.2015.09.010

Gordan, R., Shen, N., Dror, I., Zhou, T., Horton, J., Rohs, R., et al. (2013). Genomic regions flanking E-box binding sites influence DNA binding specificity of bHLH transcription factors through DNA shape. *Cell Rep.* 3, 1093–1104. doi: 10.1016/j.celrep.2013.03.014

Heim, M. A., Jakoby, M., Werber, M., Martin, C., Weisshaar, B., and Bailey, P. C. (2003). The basic helix-loop-helix transcription factor family in plants: a genome-wide study of protein structure and functional diversity. *Mol. Biol. Evol.* 20, 735–747. doi: 10.1093/molbev/msg088

Hindt, M. N., Akmakjian, G. Z., Pivarski, K. L., Punshon, T., Baxter, I., Salt, D. E., et al. (2017). BRUTUS and its paralogs, BTS LIKE1 and BTS LIKE2, encode important negative regulators of the iron deficiency response in *Arabidopsis thaliana*. *Metallomics* 9, 876–890. doi: 10.1039/c7mt00152e

Ivanov, R., Brumbarova, T., Blum, A., Jantke, A. M., Fink-Straube, C., and Bauer, P. (2014). SORTING NEXIN1 is required for modulating the trafficking and stability of the *Arabidopsis* IRON-REGULATED TRANSPORTER1. *Plant Cell* 26, 1294–1307. doi: 10.1105/tpc.113.116244

Jakoby, M., Wang, H. Y., Reidt, W., Weisshaar, B., and Bauer, P. (2004). FRU (BHLH029) is required for induction of iron mobilization genes in *Arabidopsis thaliana*. *FEBS Lett.* 577, 528–534. doi: 10.1016/j.febslet.2004.10.062

Jeong, J., and Connolly, E. L. (2009). Iron uptake mechanisms in plants: functions of the FRO family of ferric reductases. *Plant Sci.* 176, 709–714. doi: 10.1016/j.plantsci.2009.02.011

Klatte, M., Schuler, M., Wirtz, M., Fink-Straube, C., Hell, R., and Bauer, P. (2009). The analysis of *Arabidopsis* nicotianamine synthase mutants reveals functions for nicotianamine in seed iron loading and iron deficiency responses. *Plant Physiol.* 150, 257–271. doi: 10.1104/pp.109.136374

Kobayashi, T., Itai, R. N., Aung, M. S., Senoura, T., Nakanishi, H., and Nishizawa, N. K. (2012). The rice transcription factor IDEF1 directly binds to iron and other divalent metals for sensing cellular iron status. *Plant J.* 69, 81–91. doi: 10.1111/j.1365-313X.2011.04772.x

Kobayashi, T., Itai, R. N., Ogo, Y., Kakei, Y., Nakanishi, H., Takahashi, M., et al. (2009). The rice transcription factor IDEF1 is essential for the early response to iron deficiency, and induces vegetative expression of late embryogenesis abundant genes. *Plant J.* 60, 948–961. doi: 10.1111/j.1365-313X.2009.04015.x

Kobayashi, T., Nagasaka, S., Senoura, T., Itai, R. N., Nakanishi, H., and Nishizawa, N. K. (2013). Iron-binding haemerythrin RING ubiquitin ligases regulate plant iron responses and accumulation. *Nat. Commun.* 4:2792. doi: 10.1038/ncomms3792

Le, C. T., Brumbarova, T., Ivanov, R., Stoof, C., Weber, E., Mohrbacher, J., et al. (2016). Zinc finger of *Arabidopsis thaliana* 12 (ZAT12) interacts with FER-LIKE Iron Deficiency-Induced Transcription Factor (FIT) linking iron deficiency and oxidative stress responses. *Plant Physiol.* 170, 540–557. doi: 10.1104/pp.15.01589

Li, L., Gao, W., Peng, Q., Zhou, B., Kong, Q., Ying, Y., et al. (2018). Two soybean bHLH factors regulate response to iron deficiency. *J. Integr. Plant Biol.* 60, 608–622. doi: 10.1111/jipb.12651

Li, X., Zhang, H., Ai, Q., Liang, G., and Yu, D. (2016). Two bHLH transcription factors, bHLH34 and bHLH104, regulate iron homeostasis in *Arabidopsis thaliana*. *Plant Physiol.* 170, 2478–2493. doi: 10.1104/pp.15.01827

Liang, G., Zhang, H., Li, X., Ai, Q., and Yu, D. (2017). bHLH transcription factor bHLH115 regulates iron homeostasis in *Arabidopsis thaliana*. *J. Exp. Bot.* 68, 1743–1755. doi: 10.1093/jxb/erx043

Ling, H. Q., Bauer, P., Bereczky, Z., Keller, B., and Ganal, M. (2002). The tomato fer gene encoding a bHLH protein controls iron-uptake responses in roots. *Proc. Natl. Acad. Sci. U.S.A.* 99, 13938–13943. doi: 10.1073/pnas.212448699

Lingam, S., Mohrbacher, J., Brumbarova, T., Potuschak, T., Fink-Straube, C., Blondet, E., et al. (2011). Interaction between the bHLH transcription factor FIT and Ethylene Insensitive3/Ethylene Insensitive 3-Like1 reveals molecular linkage between the regulation of iron acquisition and ethylene signaling in *Arabidopsis*. *Plant Cell* 23, 1815–1829. doi: 10.1105/tpc.111.084715

Liu, W., Karemera, N. J. U., Wu, T., Yang, Y., Zhang, X., Xu, X., et al. (2017a). The ethylene response factor AtERF4 negatively regulates the iron deficiency response in *Arabidopsis thaliana*. *PLoS One* 12:e0186580. doi: 10.1371/journal.pone.0186580

Liu, W., Li, Q., Wang, Y., Wu, T., Yang, Y., Zhang, X., et al. (2017b). Ethylene response factor AtERF72 negatively regulates *Arabidopsis thaliana* response to iron deficiency. *Biochem. Biophys. Res. Commun.* 491, 862–868. doi: 10.1016/j.bbrc.2017.04.014

Long, T. A., Tsukagoshi, H., Busch, W., Lahner, B., Salt, D. E., and Benfey, P. N. (2010). The bHLH transcription factor POPEYE regulates response to iron deficiency in *Arabidopsis* roots. *Plant Cell* 22, 2219–2236. doi: 10.1105/tpc.110.074096

Maurer, F., Naranjo Arcos, M. A., and Bauer, P. (2014). Responses of a triple mutant defective in three iron deficiency-induced Basic Helix-Loop-Helix genes of the subgroup Ib(2) to iron deficiency and salicylic acid. *PLoS One* 9:e99234. doi: 10.1371/journal.pone.0099234

Naranjo-Arcos, M. A., Maurer, F., Meiser, J., Pateyron, S., Fink-Straube, C., and Bauer, P. (2017). Dissection of iron signaling and iron accumulation by over expression of subgroup Ib bHLH039 protein. *Sci. Rep.* 7:10911. doi: 10.1038/s41598-017-11171-7

Nozoye, T., Nagasaka, S., Kobayashi, T., Takahashi, M., Sato, Y., Uozumi, N., et al. (2011). Phytosiderophore efflux transporters are crucial for iron acquisition in graminaceous plants. *J. Biol. Chem.* 286, 5446–5454. doi: 10.1074/jbc.M110.180026

Ogawa, S., Kawahara-Miki, R., Miyamoto, K., Yamane, H., Nojiri, H., Tsujii, Y., et al. (2017). OsMYC2 mediates numerous defence-related transcriptional changes via jasmonic acid signalling in rice. *Biochem. Biophys. Res. Commun.* 486, 796–803. doi: 10.1016/j.bbrc.2017.03.125

Ogo, Y., Itai, R. N., Nakanishi, H., Kobayashi, T., Takahashi, M., Mori, S., et al. (2007). The rice bHLH protein OsIRO2 is an essential regulator of the genes involved in Fe uptake under Fe-deficient conditions. *Plant J.* 51, 366–377. doi: 10.1111/j.1365-313X.2007.03149.x

Ogo, Y., Kobayashi, T., Nakanishi Itai, R., Nakanishi, H., Kakei, Y., Takahashi, M., et al. (2008). A novel NAC transcription factor, IDEF2, that recognizes the iron deficiency-responsive element 2 regulates the genes involved in iron homeostasis in plants. *J. Biol. Chem.* 283, 13407–13417. doi: 10.1074/jbc.M708732200

O'Hara, G. (2001). Nutritional constraints on root nodule bacteria affecting symbiotic nitrogen fixation: a review. *Anim. Prod. Sci.* 41, 417–433. doi: 10.1071/EA00087

Palmer, C. M., Hindt, M. N., Schmidt, H., Clemens, S., and Guerinot, M. L. (2013). MYB10 and MYB72 are required for growth under iron-limiting conditions. *PLoS Genet.* 9:e1003953. doi: 10.1371/journal.pgen.1003953

Rampey, R. A., Woodward, A. W., Hobbs, B. N., Tierney, M. P., Lahner, B., Salt, D. E., et al. (2006). An *Arabidopsis* basic helix-loop-helix leucine zipper protein modulates metal homeostasis and auxin conjugate responsiveness. *Genetics* 174, 1841–1857. doi: 10.1534/genetics.106.061044

Rodriguez-Celma, J., Green, R. T., Connorton, J. M., Kruse, I., Cui, Y., Ling, H. Q., et al. (2018). BRUTUS-LIKE proteins moderate the transcriptional response to iron deficiency in roots. *bioRxiv* [Preprint]. doi: 10.1101/231365

Samira, R., Li, B., Kliebenstein, D., Li, C., Davis, E., Gillikin, J. W., et al. (2018). The bHLH transcription factor ILR3 modulates multiple stress responses in *Arabidopsis*. *Plant Mol. Biol.* doi: 10.1007/s11103-018-0735-8 [Epub ahead of print].

Selote, D., Samira, R., Matthiadis, A., Gillikin, J. W., and Long, T. A. (2015). Iron-binding E3 ligase mediates iron response in plants by targeting basic helix-loop-helix transcription factors. *Plant Physiol.* 167, 273–286. doi: 10.1104/pp.114.250837

Shen, C., Yue, R., Sun, T., Zhang, L., Yang, Y., and Wang, H. (2015). OsARF16, a transcription factor regulating auxin redistribution, is required for iron deficiency response in rice (*Oryza sativa* L.). *Plant Sci.* 231, 148–158. doi: 10.1016/j.plantsci.2014.12.003

Sivitz, A., Grinvalds, C., Barberon, M., Curie, C., and Vert, G. (2011). Proteasome-mediated turnover of the transcriptional activator FIT is required for plant iron-deficiency responses. *Plant J.* 66, 1044–1052. doi: 10.1111/j.1365-313X.2011.04565.x

Stringlis, I. A., Yu, K., Feussner, K., de Jonge, R., Van Bentum, S., Van Verk, M. C., et al. (2018). MYB72-dependent coumarin exudation shapes root microbiome assembly to promote plant health. *Proc. Natl. Acad. Sci. U.S.A.* 115, E5213–E5222. doi: 10.1073/pnas.1722335115

Tanabe, N., Noshi, M., Mori, D., Nozawa, K., Tamoi, M., and Shigeoka, S. (2018). The basic helix-loop-helix transcription factor, bHLH11 functions in the iron-uptake system in *Arabidopsis thaliana*. *J. Plant Res.* doi: 10.1007/s10265-018-1068-z [Epub ahead of print].

Tang, C., Robson, A., and Dilworth, M. J. (1990). The role of iron in nodulation and nitrogen fixation in *Lupinus angustifolius* L. *New Phytol.* 114, 173–182. doi: 10.1111/j.1469-8137.1990.tb00388.x

Wang, F. P., Wang, X. F., Zhang, J., Ma, F., and Hao, Y. J. (2018). MdMYB58 modulates Fe homeostasis by directly binding to the MdMATE43 promoter in plants. *Plant Cell Physiol.* 59, 2476–2489. doi: 10.1093/pcp/pcy168

Wang, H. Y., Klatte, M., Jakoby, M., Baumlein, H., Weisshaar, B., and Bauer, P. (2007). Iron deficiency-mediated stress regulation of four subgroup Ib BHLH genes in *Arabidopsis thaliana*. *Planta* 226, 897–908. doi: 10.1007/s00425-007-0535-x

Wang, L., Ying, Y., Narsai, R., Ye, L., Zheng, L., Tian, J., et al. (2013). Identification of OsbHLH133 as a regulator of iron distribution between roots and shoots in *Oryza sativa*. *Plant Cell Environ.* 36, 224–236. doi: 10.1111/j.1365-3040.2012.02569.x

Wang, N., Cui, Y., Liu, Y., Fan, H., Du, J., Huang, Z., et al. (2013). Requirement and functional redundancy of Ib subgroup bHLH proteins for iron deficiency responses and uptake in *Arabidopsis thaliana*. *Mol. Plant* 6, 503–513. doi: 10.1093/mp/sss089

Xu, W., Dubos, C., and Lepiniec, L. (2015). Transcriptional control of flavonoid biosynthesis by MYB-bHLH-WDR complexes. *Trends Plant Sci.* 20, 176–185. doi: 10.1016/j.tplants.2014.12.001

Yan, J. Y., Li, C. X., Sun, L., Ren, J. Y., Li, G. X., Ding, Z. J., et al. (2016). A WRKY transcription factor regulates fe translocation under fe deficiency. *Plant Physiol.* 171, 2017–2027. doi: 10.1104/pp.16.00252

Yuan, Y., Wu, H., Wang, N., Li, J., Zhao, W., Du, J., et al. (2008). FIT interacts with AtbHLH38 and AtbHLH39 in regulating iron uptake gene expression for iron homeostasis in *Arabidopsis*. *Cell Res.* 18, 385–397. doi: 10.1038/cr.2008.26

Zamioudis, C., Hanson, J., and Pieterse, C. M. (2014). beta-Glucosidase BGLU42 is a MYB72-dependent key regulator of rhizobacteria-induced systemic resistance and modulates iron deficiency responses in *Arabidopsis* roots. *New Phytol.* 204, 368–379. doi: 10.1111/nph.12980

Zhang, H., Li, Y., Yao, X., Liang, G., and Yu, D. (2017). Positive regulator of iron homeostasis1, OsPRI1, facilitates iron homeostasis. *Plant Physiol.* 175, 543–554. doi: 10.1104/pp.17.00794

Zhang, J., Liu, B., Li, M., Feng, D., Jin, H., Wang, P., et al. (2015). The bHLH transcription factor bHLH104 interacts with IAA-LEUCINE RESISTANT3 and modulates iron homeostasis in *Arabidopsis*. *Plant Cell* 27, 787–805. doi: 10.1105/tpc.114.132704

Zhang, Y., Wu, H., Wang, N., Fan, H., Chen, C., Cui, Y., et al. (2014). Mediator subunit 16 functions in the regulation of iron uptake gene expression in *Arabidopsis*. *New Phytol.* 203, 770–783. doi: 10.1111/nph.12860

Zhao, Q., Ren, Y. R., Wang, Q. J., Wang, X. F., You, C. X., and Hao, Y. J. (2016a). Ubiquitination-related MdBT scaffold proteins target a bHLH transcription factor for iron homeostasis. *Plant Physiol.* 172, 1973–1988. doi: 10.1104/pp.16.01323

Zhao, Q., Ren, Y. R., Wang, Q. J., Yao, Y. X., You, C. X., and Hao, Y. J. (2016b). Overexpression of MdbHLH104 gene enhances the tolerance to iron deficiency in apple. *Plant Biotechnol. J.* 14, 1633–1645. doi: 10.1111/pbi.12526

Zheng, L., Ying, Y., Wang, L., Wang, F., Whelan, J., and Shou, H. (2010). Identification of a novel iron regulated basic helix-loop-helix protein involved in Fe homeostasis in Oryza sativa. *BMC Plant Biol.* 10:166. doi: 10.1186/1471-2229-10-166

Zhou, L. J., Zhang, C. L., Zhang, R. F., Wang, G. L., Li, Y. Y., and Hao, Y. J. (2018). The SUMO E3 ligase MdSIZ1 targets MdbHLH104 to regulate plasma membrane H+-ATPase activity and iron homeostasis. *Plant Physiol.* 179, 88–106. doi: 10.1104/pp.18.00289

Conflict of Interest Statement: The authors declare that the research was conducted in the absence of any commercial or financial relationships that could be construed as a potential conflict of interest.

frontiers in Plant Science

ORIGINAL RESEARCH
published: 31 January 2019
doi: 10.3389/fpls.2019.00008

Small-Molecules Selectively Modulate Iron-Deficiency Signaling Networks in Arabidopsis

*Sakthivel Kailasam, Wei-Fu Chien and Kuo-Chen Yeh**

Agricultural Biotechnology Research Center, Academia Sinica, Taipei, Taiwan

Plant growth requires optimal levels of iron (Fe). Fe is used for energy production, numerous enzymatic processes, and is indispensable for cellular metabolism. Recent studies have established the mechanism involved in Fe uptake and transport. However, our knowledge of Fe sensing and signaling is limited. Dissecting Fe signaling may be useful for crop improvement by Fe fortification. Here, we report two small-molecules, R3 and R6 [where R denotes repressor of *IRON-REGULATED TRANSPORTER 1 (IRT1)*], identified through a chemical screening, whose use blocked activation of the Fe-deficiency response in *Arabidopsis thaliana*. Physiological analysis of plants treated with R3 and R6 showed that these small molecules drastically attenuated the plant response to Fe starvation. Small-molecule treatment caused severe chlorosis and strongly reduced chlorophyll levels in plants. Fe content in shoots was decreased considerably by small-molecule treatments especially in Fe deficiency. Small-molecule treatments attenuated the Fe-deficiency-induced expression of the Fe uptake gene *IRT1*. Analysis of FER-LIKE IRON-DEFICIENCY-INDUCED TRANSCRIPTION FACTOR (FIT) and subgroup Ib *basic helix-loop-helix* (*bHLH*) gene (*bHLH38/39/100/101*) expression showed that R3 affects the FIT-network, whereas R6 affects both the FIT and Ib bHLH networks. An assessment of the effects of the structural analogs of R3 and R6 on the induction of Fe-dependent chlorosis revealed the functional motif of the investigated chemicals. Our findings suggest that small-molecules selectively modulate the distinct signaling routes that operate in response to Fe-deficiency. R3 and R6 likely interrupt the activity of key upstream signaling regulators whose activities are required for the activation of the Fe-starvation transcriptional cascade in Arabidopsis roots.

Keywords: *Arabidopsis thaliana*, chemical biology, iron deficiency signaling, iron homeostasis, small-molecules

OPEN ACCESS

Edited by:
Thomas J. Buckhout, Humboldt-Universität zu Berlin, Germany

Reviewed by:
Ferenc Fodor, Eötvös Loránd University, Hungary
Rumen Ivanov, Heinrich-Heine-Universität Düsseldorf, Germany

***Correspondence:**
Kuo-Chen Yeh
kcyeh@gate.sinica.edu.tw

Specialty section:
This article was submitted to Plant Nutrition, a section of the journal Frontiers in Plant Science

Received: *17 November 2018*
Accepted: *07 January 2019*
Published: *31 January 2019*

Citation:
Kailasam S, Chien W-F and Yeh K-C (2019) Small-Molecules Selectively Modulate Iron-Deficiency Signaling Networks in Arabidopsis. Front. Plant Sci. 10:8. doi: 10.3389/fpls.2019.00008

INTRODUCTION

Many cellular functions occurring during plant growth and development depend on iron (Fe) availability; therefore plants regulate Fe homeostasis by tightly controlling its uptake and allocation. Fe, although abundant in soil, is not so readily available to plants in soils with high pH due to poor solubility (Colombo et al., 2014). Hence, plants employ different mechanisms for efficient acquisition of Fe from soil. To date, two mechanisms have been identified in higher plants, namely Strategy I or the reduction strategy and Strategy II or the chelation strategy (Kobayashi and Nishizawa, 2012; Connorton et al., 2017) for Fe acquisition.

Arabidopsis uses Strategy I mode to acquire Fe from soil (Kobayashi and Nishizawa, 2012). For Fe uptake, large amounts of coumarins, facilitated by PLEIOTROPIC DRUG RESISTANCE 9 (PDR9) (Fourcroy et al., 2014; Clemens and Weber, 2016) and protons, mediated by H^+-ATPASE 2 (AHA2) (Santi and Schmidt, 2009) are pumped into the rhizosphere. These processes help to solubilize and mobilize the insoluble ferric Fe (Fe^{3+}) in the rhizosphere (Chen et al., 2017; Jeong et al., 2017). Arabidopsis then reduces the soluble Fe^{3+} into ferrous Fe (Fe^{2+}) by the action of FERRIC REDUCTASE OXIDASE 2 (FRO2) (Robinson et al., 1999) at the cell surface. And the IRON-REGULATED TRANSPORTER 1 (IRT1), a plasma membrane localized divalent cation transporter, then imports ferrous Fe from the extracellular space (Connolly et al., 2002; Vert et al., 2002).

Iron uptake and transport is coordinated by the actions of transcription factors. Several basic helix-loop-helix (bHLH) transcription factors are involved in orchestrating Fe transport and utilization. A subgroup of IIIa bHLH member, FER-LIKE IRON DEFICIENCY-INDUCED TRANSCRIPTION FACTOR (FIT) is involved in controlling the Fe uptake via regulating the expression of *IRT1* and *FRO2* (Colangelo and Guerinot, 2004; Jakoby et al., 2004; Yuan et al., 2005). Members of subgroup Ib of the bHLH proteins (bHLH38/39/100/101) redundantly interact with FIT and control the Fe uptake-associated genes (Wang et al., 2007, 2013; Yuan et al., 2008). Recent studies have revealed the upstream transcriptional regulation under Fe-starvation. The subgroup IVc bHLH factors (bHLH34/104/105/115), form heterodimers among themselves, directly regulate the expression of *Ib bHLH* genes and indirectly regulate the expression of the *FIT* (Zhang et al., 2015; Li et al., 2016; Liang et al., 2017). The IVc bHLH protein levels are post-translationally controlled by BRUTUS (BTS), a hemerythrin E3 ligase, via proteosomal degradation (Selote et al., 2015). BTS has been proposed to be involved in Fe sensing (Kobayashi and Nishizawa, 2015). BTS negatively regulates the Fe-starvation responses. Hindt et al. showed that the BTS paralogs, BTS LIKE1 (BTSL1) and BTS LIKE2 (BTSL2) act redundantly as negative regulators of the Fe starvation response (Hindt et al., 2017). Therefore, both positive and negative regulators coordinately fine tune the plant responses under the Fe starvation response.

To understand the optimal balance between positive and negative regulation, it is important to shed light on the signaling that is specific to each regulator (positive or negative). By modulating selective signaling branches we might be able to dissect the Fe starvation transcriptional network and the related complicated transcriptional machinery. Many molecules/metabolites such as sucrose, putrescine, nitric oxide (NO) and *S*-nitrosoglutathione (GSNO), and the hormones auxin and ethylene participate in the signaling process and positively regulate Fe-deficiency transcription (Chen et al., 2010; Lin et al., 2015; Lucena et al., 2015; Liu et al., 2016; Zhu et al., 2016; Kailasam et al., 2018); whereas the hormones, cytokinin, abscisic acid (ABA) and jasmonic acid (JA) act negatively on the network (Liu et al., 2016; Cui et al., 2018). A recent study by Garcia et al. (2018) discussed the different signaling modes, in the form LODIS (LOng Distance Iron Signal) or LODIS-derived and also via NO/GSNO, to the transcription factors. We previously undertook a chemical screening and dissected the Fe-signaling pathway using a small-molecule named R7 (Kailasam et al., 2018). R7 blocked the transfer of the Fe-deficiency generated signal from NO to the FIT by inhibiting the cellular levels of GSNO, a carrier of NO bio-activity, whose levels are critical for the activation of *FIT* expression. By using the small-molecule R7, we clarified the signaling pathway from NO (Kailasam et al., 2018).

Despite these findings, the identity of the signal that is transferred to transcription factors from NO is still unclear. Moreover, it is not clearly known whether the Fe-dependent signal is conveyed to the transcription factors through only one route or through many routes. With this focus, we used a chemical biology approach to further dissect the signaling routes of Fe starvation response. The chemical screening undertaken yielded two small-molecules named R3 and R6 (R denotes Repressor of *IRON-REGULATED TRANSPORTER 1*), whose actions during Fe-starvation are uncovered in this report. Small-molecule treatment resulted in severe Fe-dependent chlorosis and decreased Fe levels in shoots. R6 inhibited the expression of both *FIT* and *Ib bHLH* genes whereas R3 only inhibited *FIT* expression. Our finding clearly reveals that these small-molecules modulate Fe-deficiency by targeting specific signaling branches to central transcription factors, further suggesting that multiple routes are used for transferring the Fe-deficiency born signals to the central transcription factors in roots. Our work also highlights that small-molecules can be used to decode novel signaling pathways that modulate the transcription factors responsible for Fe-deficiency.

MATERIALS AND METHODS

Plant Growth Conditions

Arabidopsis thaliana Col-0 and the reporter line Pro_{IRT1}*:LUC* (Kailasam et al., 2018) were used. Seeds were surface-sterilized for 4 min in 70% ethanol and treated for 8 min with 1.2% sodium hypochlorite containing 0.02% SDS, finally washed several times in double-distilled H_2O. Two-day-stratified seeds were grown on half-strength Murashige and Skoog (½MS) (Duchefa Biochemie) medium supplemented with 2.3 mM MES, 1% sucrose and 0.7% type A agar (Sigma-Aldrich) (pH 5.8). For Fe-sufficiency treatments [50 μM Fe(II)-EDTA], ½MS was used. For the Fe0 condition, Fe was omitted [½MS containing 0 μM Fe(II)-EDTA], whereas for the –Fe condition, 100 μM FerroZine was added to the Fe0 medium. For small molecule treatment, the indicated concentration was added in the medium, whereas in mock treatments dimethyl sulfoxide (DMSO) was added. All plants in this study were grown under a 16-h light/8-h dark photoperiod at 23°C.

Small Molecule Screening

The small molecules R3 and R6 were isolated by screening DIVERSet library (ChemBridge, United States) for inhibition of Pro_{IRT1}*:LUC* expression (Kailasam et al., 2018). Briefly, the DIVERSet library compounds were dissolved in DMSO and added a final concentration of 100 μM to 48-well plates containing –Fe medium. Two to three ½MS-grown-seedlings of

5 day old were transferred to the wells. Two days after treatment, plants were subjected to luminescence analysis. For luminescence assay, plants were submerged in 0.5 mM luciferin solution that contain 0.01% Triton X-100 and kept for 10 min in the dark. The luminescence was then captured by using the IVIS Lumina imaging system (Xenogen Corp., United States) with 1-min exposure times.

Protein Isolation and Immunoblot

Total protein isolation and western blot analysis were conducted according to (Shin et al., 2013). Ten-day-old seedlings underwent a small-molecule treatment for 3 day before analysis. Small molecules were used at a final concentration of 50 μM. Total protein from roots was extracted by using protein extraction buffer: 125 mM Tris-HCL (pH 6.8), 15% glycerol, 5.5% SDS, 0.05% 2-mercaptoethanol, and Protease Inhibitor Cocktail (Roche). SDS-PAGE followed by western-blotting was performed. Blots were probed with an anti-IRT1 antibody (Shanmugam et al., 2011).

Chlorophyll Estimation

Nine-day-old seedlings that have been grown on ½MS media were transferred onto ½MS (Fe50) or Fe0 media with 0 or 50 μM small molecules. After a 9-day treatment, the leaves were harvested and their fresh weight was measured. Total chlorophyll was extracted in 1.0 ml of 80% acetone at 4°C in the dark for 12–16 h until the leaves became white. The clear supernatant was then analyzed in a spectrophotometer (Power Wave XS; Bio-TEK) at 470, 646, and 663 nm spectra. The total chlorophyll content was calculated according to (Wellburn, 1994).

Determination of Elemental Contents

Tissue elements were estimated by inductively coupled plasma-optical emission spectrometry (ICP-OES; OPTIMA 5300; Perkin-Elmer) as described (Shanmugam et al., 2011). Ten-day-old seedlings from ½MS plates were transferred to ½MS or Fe0 media containing 0 or 50 μM small molecules and grown for 10 days. Shoots were harvested and rinsed with 10 mM $CaCl_2$ for 20 min. After washing with de-ionized water, shoots were dried at 70°C for 3 day, then digested with 1 ml 65% HNO_3 (Merck, Tracepur) and 0.5 ml H_2O_2 (Merck, Suprapur). Digested samples were analyzed in ICP-OES for quantification.

Quantitative Reverse Transcription-PCR

For gene expression analysis, 9-day-old seedlings from ½MS plates were transferred to ½MS or –Fe (½MS without Fe^{2+}-EDTA and with 100 μM FerroZine) containing 0 or 25 μM small molecules. After 3 days of treatment, the roots were harvested. RNA isolation, complementary DNA (cDNA) synthesis and quantitative reverse transcription-PCR (qPCR) analysis were conducted according to manufactures protocol. In short, the total RNA was extracted by using Total RNA isolation kit (GeneDireX). The RNA samples were treated with gDNA wipeout RNase-free DNase (Qiagen) at 42°C for 2 min for genomic DNA contamination elimination. Approximately 1 μg of total RNA was used for first-strand cDNA synthesis by using a QuantiTect Reverse Transcription kit (Qiagen). 25 ng of RNA was subjected for quantitative PCR (qPCR) using Fast SYBR Green Master Mix (Applied Biosystems) in a 7500 Fast Real-Time PCR instrument (Applied Biosystems). Three biological replicates were used for the quantification of expression of each gene. Each biological replicate was analyzed in triplicate. Relative transcript levels were calculated by normalizing to *UBC21*. Expression was calculated by using the formula $2^{-\Delta CT}$ (Schmittgen and Livak, 2008). The primers described (Zhang et al., 2015) were used for *bHLH100* and *bHLH101*. The primers described in (Shin et al., 2013) were used for *IRT1* and *UBC21*. The primers described in (Shanmugam et al., 2015) were used for *FRO2* and *FIT*. The primers described in (Kailasam et al., 2018) were used for *bHLH38* and *bHLH39*.

Statistical Analysis

All statistical significance was determined using Student's t test ($P < 0.05$) with SigmaPlot.

RESULTS

Small Molecules R3 and R6 Block Fe-Deficiency-Induced IRT1 Expression

We previously employed a chemical screen on Pro_{IRT1}:*LUC* reporter lines and isolated a small-molecule named R7 (R denotes repressor of *IRON-REGULATED TRANSPORTER 1*) that represses the Fe-deficiency response in Arabidopsis (Kailasam et al., 2018). This screen yielded two more small molecules named R3 and R6. In this report, we analyzed the physiological and molecular responses of plants to understand the role of R3 and R6 in detail. R3 or R6 treatment inhibited the Fe-deficiency-inducible Pro_{IRT1}:*LUC* expression (**Figure 1A**). Small-molecule treatment caused no luminescence in roots under Fe-deficient medium as compared to mock-treated that showed stronger luminescence. These results suggest that R3 and R6 may modulate endogenous *IRT1* expression.

First, to confirm that the small-molecule effect is not due to dysfunctional Pro_{IRT1}:*LUC* under the treatment, we analyzed the endogenous IRT1 level under both Fe sufficient and deficient conditions (**Figure 1B**). As expected, the IRT1 protein was accumulated under Fe deficiency in mock treatment, whereas R3 or R6 treatment abolished the IRT1 accumulation. This indicates that R3 and R6 (**Figure 1C**) block the accumulation of Fe-deficiency-induced IRT1 protein.

R3 and R6 Cause Severe Fe-Deficiency Chlorosis

Iron deficiency in the environment causes chlorosis and affects the chlorophyll level in plants. To investigate the effect of small-molecule treatment on plant photosynthetic capacity under Fe starvation, phenotypic analysis was conducted (**Figure 2**). Compared to mock plants whose leaves were pale-green when grown under Fe-limited conditions, small molecule-treated plants were highly chlorotic (**Figure 2A**). We further measured the chlorophyll level in both Fe sufficient and deficient

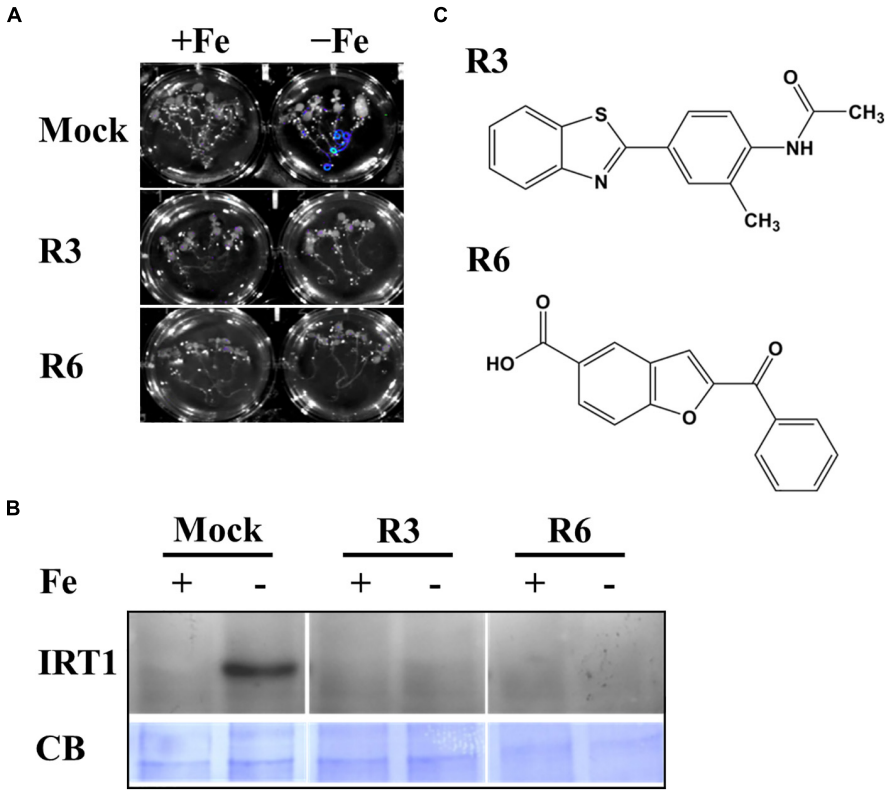

FIGURE 1 | Small-molecules block Fe-deficiency response. **(A)** Small-molecules inhibit *Pro$_{IRT1}$:LUC* expression. 6-days ½MS-grown plants were treated for 3 days under +Fe or −Fe media in the presence or absence of 50 μM indicated small-molecules. **(B)** IRT1 protein accumulation in response to small-molecules. The 10-days ½MS-grown plants were treated for 3 days under +Fe or −Fe in the presence or absence of small-molecules. IRT1 protein was detected in total protein extract of roots using an anti-IRT1 antibody. Samples were separated in the same gel. CB, coomassie blue stain. **(C)** The 2D structure of small-molecules. R3, N-[4-(1,3-benzothiazol-2-yl)-2-methylphenyl] acetamide; R6, 2-benzoyl-1-benzofuran-5-carboxylic acid.

conditions. The small molecule treatment caused a decrease in levels of chlorophyll even under Fe-sufficiency and the levels were drastically reduced under Fe-limited conditions (**Figure 2B**). These data indicate that R3 and R6 perturb the physiological responses to Fe starvation.

Small-Molecule Treatment Affects Metal Content

Perturbation in cellular levels of metals often results in chlorosis (Vert et al., 2002). R3 and R6 caused chlorosis; therefore, we next analyzed the cellular level of Fe in response to small molecule treatment (**Figure 3**). Under Fe sufficiency, R6 treatment did not alter the shoot Fe level, whereas R3 treatment led to a decrease in shoot Fe level (**Figure 3A**). In Fe-limited medium, the mock treatment showed reduced Fe levels, as expected. The small-molecule treatment caused a drastic reduction in the levels of shoot Fe under Fe-limited conditions. Since, IRT1 also transports manganese (Mn) and zinc (Zn), we then measured Mn and Zn levels. The Mn levels were significantly decreased in response to small molecule treatment under both Fe-sufficiency and -deficiency (**Figure 3B**). R3 or R6 treatment did not alter the Zn levels in shoots (**Figure 3C**). These data indicate that R3 and R6 treatment affect cellular metal contents, particularly Fe.

Fe-Acquisition Genes Are Down Regulated in Small-Molecule Treatments

The above findings suggested that small-molecule treatment might impair the transcription of genes involved in Fe uptake. To test this, we measured the expression levels of Fe-uptake-associated genes, *IRT1*, *FRO2* and *FIT*, in response to small molecule treatment in roots. Loss-of-function mutants of these genes display a decrease in cellular Fe levels and chlorosis. We found that *IRT1*, *FRO2,* and *FIT* expression was induced 51.4-, 60.7- and 5.4-fold, respectively by Fe-deficiency in mock-treated plants (**Figure 4**). The small-molecule treatment strongly inhibited the transcripts of these genes under Fe-deficiency. These results indicate that R3 and R6 inhibit the molecular response to Fe-deficiency by affecting the central transcription factor.

R3 and R6 Are Involved in Different Signaling Branches of Fe-Deficiency

FIT forms a dimeric complex with members of the Ib bHLH factors (bHLH38/39/100/101) to regulate the expression of Fe-uptake genes, *IRT1* and *FRO2*. Fe-deficiency also induces the transcripts of *Ib bHLH* genes. Hence, we wondered whether small

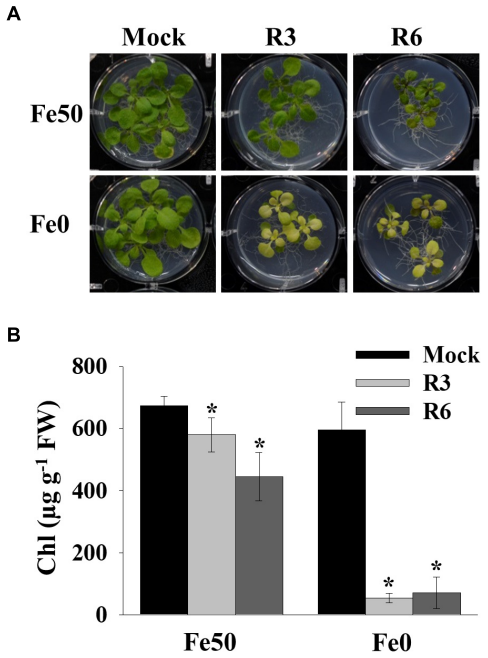

FIGURE 2 | Small-molecules cause severe Fe-deficiency chlorosis. **(A)** Phenotype of plants with small-molecule treatments. 9-days ½MS-grown plants were transferred to Fe50 or Fe0 media for 9 days in the presence or absence of 50 μM indicated small-molecules. **(B)** Total chlorophyll content of plants under small-molecules treatment. Plants were treated as in **(A)**. Data are mean ± *SD* ($n = 5$). *, significant change vs. mock at $P < 0.05$ by Student's *t* test. FW, fresh weight.

molecule treatment deregulates the expression of these genes as well or not. Expression analysis of *bHLH38/39/100/101* revealed that their transcripts are indeed induced in mock-treated plants under Fe-deficiency (**Figure 5**). Interestingly the R3 treatment did not influence the transcript levels of *Ib bHLH* genes under Fe-deficiency whereas R6 treatment inhibited the expression. The R6 inhibition level was 29.4, 17.6, 41.8, and 58.0% of the mock treatment for *bHLH38*, *bHLH39*, *bHLH100*, and *bHLH101*, respectively. These data indicate that R3 is not involved in the pathway for *Ib bHLH* gene expression whereas R6 is and further implies that small molecules R3 and R6 modulate the Fe-deficiency transcriptional networks selectively.

The reduced expression of Fe-deficiency response transcription factors under small molecule treatment could be the result of defective signaling from plant hormones/metabolites. Auxin, ethylene, NO and GSNO act as positive regulators and exogenous applications of these substances are able to improve plant molecular response and fitness under Fe-starvation. Hence, we were interested in investigating whether providing these substances could alleviate the inhibitory effects caused by R3 or R6. We monitored the Pro_{IRT1}*:LUC* expression under R3, R6, or R7, a small-molecule that blocks the signal from NO to FIT (Kailasam et al., 2018). *LUC* expression was not rescued under R3 or R6 treatment by providing any of the positive regulators [naphthaleneacetic acid (NAA) or 1-Aminocyclopropane-1-carboxylic acid (ACC) or GSNO] (**Figure 6A**). Under R7 treatment, supplying NAA or ACC did not rescue the *LUC* expression either, but supplying GSNO alleviated the R7 inhibition as demonstrated previously (Kailasam et al., 2018). Further we also measured the NO levels under these small-molecule treatments (**Figure 6B**). There was sufficient NO level, in fact higher, in roots under Fe deficiency upon treatment with any of the small-molecules. These data suggest that R3 and R6 act independently or downstream of these positive regulators.

Plant Responses to Structural Derivatives of R3 and R6

Next, to get in-depth insight into the core motif that is required for the action of R3 and R6, structural analogs of the R3 and R6 were searched online in PubChem[1] and ChemSpider[2]. We randomly selected some of the structural derivatives of R3 and R6 (**Table 1**), and assayed them. Our results showed that none of the four analogs of R3 assayed had any of the parent activity (**Figure 7**). They did not produce any observable phenotype under Fe limited conditions. In case of R6, one analog, R6SD1, mimicked the R6 activity; in fact it produced much stronger chlorosis and growth reduction than R6 under both Fe-sufficiency and deficiency (**Figure 8**). In addition, R6SD1 treatment diminished the IRT1 protein accumulation in roots under Fe-deficiency (**Figure 8C**). The structural analogs, therefore, may help to determine the active motif of the small molecule.

DISCUSSION

Crop improvement toward fortification of Fe has great significance for human health as large populations depend on plant-feeds for dietary Fe. Enhancing Fe levels in plants is therefore useful. In order to achieve this, however; an adequate knowledge of Fe homeostasis is needed. Fe homeostasis in plants is controlled through at least five cellular processes: uptake systems, internal transport and distribution, utilization, storage, and finally the regulation (Connorton et al., 2017). Of these coordinated process, uptake is the most critical, that depends on soil pH, redox environment and interactions with other minerals (Colombo et al., 2014). To overcome this kind of environment and for efficient uptake, plants have evolved sophisticated mechanisms. Until now two systems for Fe-uptake, Strategy I, and Strategy II have been identified (Kobayashi and Nishizawa, 2012). Much meticulous work has helped to establish the Fe uptake and transport and the regulation process in Arabidopsis (Brumbarova et al., 2015; Curie and Mari, 2017). However, despite this knowledge, the precise sensing, both external and internal, and the associated signaling for Fe availability is still a poorly understood process.

Small-molecule-based chemical biology is an effective approach to dissect the nutrient-starvation response, especially signaling (Bonnot et al., 2016; Kailasam et al., 2018). In the current study, we investigated the role of two small-molecules,

[1]https://pubchem.ncbi.nlm.nih.gov

[2]http://www.chemspider.com

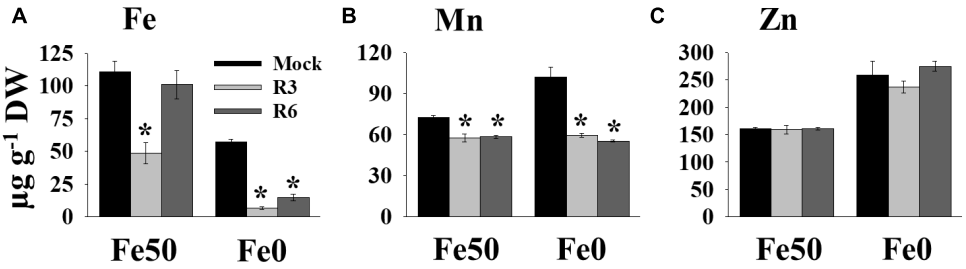

FIGURE 3 | Small-molecules affect Fe levels in plants. Effect of small molecules on Fe **(A)**, Mn **(B)**, and Zn **(C)** contents in shoots. 10-days ½MS-grown plants were treated with or without 50 μM indicated small-molecules under Fe50 or Fe0 condition for 10 days. Levels of elements were measured by ICP-OES. Data are mean ± *SD* (*n* = 3). Significant differences compared with mock by Student's *t* test: *, $P < 0.05$. DW, dry weight.

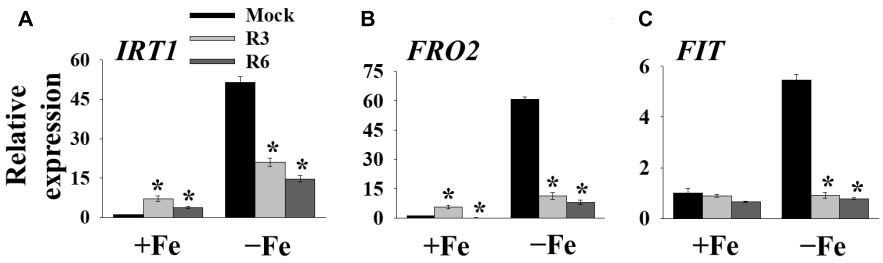

FIGURE 4 | The expression of Fe-acquisition genes is inhibited by small-molecules. qPCR analysis of expression of *IRT1* **(A)**, *FRO2* **(B)**, and *FIT* **(C)** in roots. 9-days ½MS-grown plants were transferred to +Fe or −Fe in the presence or absence of 25 μM indicated small-molecules for 3 days. The expression of *UBC21* was used to normalize mRNA levels. The gene expression levels in mock +Fe were set to 1. Data are mean ± *SE* (*n* = 3). Significant differences compared with mock by Student's *t* test: *, $P < 0.05$.

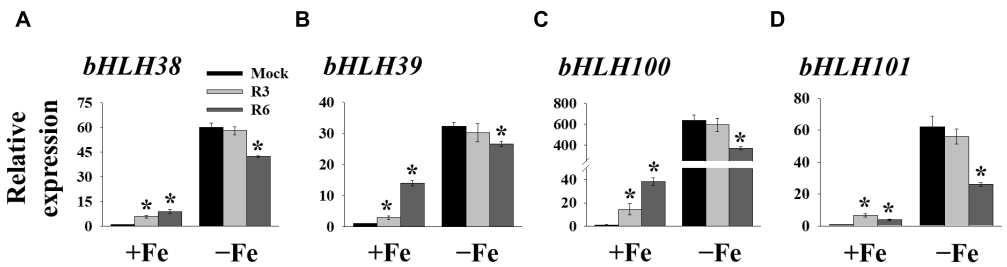

FIGURE 5 | The expression of *Ib bHLH* genes is deregulated by R6 but not by R3. qPCR analysis of expression of *bHLH38* **(A)**, *bHLH39* **(B)**, *bHLH100* **(C)**, and *bHLH101* **(D)** in roots. 9-days ½MS-grown plants were treated for 3 days under +Fe or −Fe in the presence or absence of 25 μM indicated small-molecules. The expression of *UBC21* was used to normalize mRNA levels. The gene expression levels in mock +Fe were set to 1. Data are mean ± *SE* (*n* = 3). Significant differences vs. mock by Student's *t* test: *, $P < 0.05$.

R3 and R6 in Fe deficiency response (**Table 1**). R3 and R6 blocked Fe-deficiency induced IRT1 expression (**Figure 1**). The induction of *IRT1* is important for coping with Fe-deficiency (Connolly et al., 2002; Vert et al., 2002). Physiological analysis revealed that R3 and R6 severely affected the chlorophyll levels in plants and imparted stronger chlorosis under Fe-limited conditions (**Figure 2**). This might be the result of reduced Fe levels under small molecule treatment (**Figure 3A**). Interestingly, under Fe sufficiency, R3-treated plants had a low Fe level with apparent chlorosis as well. By contrast, R6 treatment reduced the chlorophyll content, with no decrease in shoot Fe level under Fe sufficiency (**Figures 2**, **3A**). Hence, total Fe level is not the only reason for chlorosis. The missing link between Fe content and chlorosis was also observed in the triple mutant *bhlh39bhlh100bhlh101*, which showed no defective total Fe level in shoots but strong chlorosis (Maurer et al., 2014). Treatment with R3 or R6 affected the Mn level (**Figure 3B**). Surprisingly the Zn level, whose level is subjected to increase under Fe-deficiency (Korshunova et al., 1999; Vert et al., 2002), is not affected under both Fe-sufficient and -deficient conditions (**Figure 3C**). One possibility for the unchanged Zn levels in shoots is higher translocation rate for Zn. Translocation of Fe, Mn and Zn is depends on the metal-chelating nicotianamine (NA)/citrate levels in the vasculature (Durrett et al., 2007; Schuler et al., 2012). Formation of NA-Zn complexes over Fe and Mn could be favored under

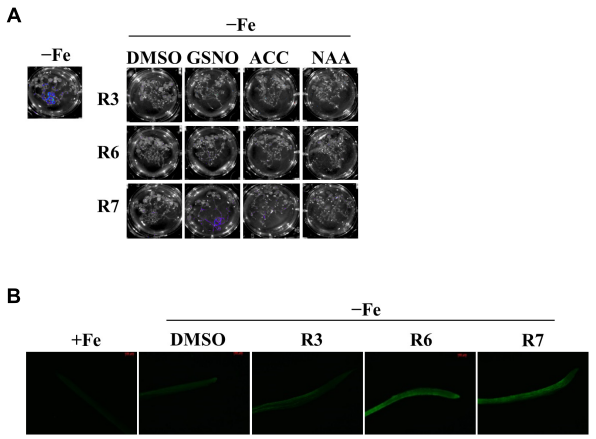

FIGURE 6 | GSNO or ACC or NAA did not rescue the inhibitory effect of R3 or R6 on Fe-deficiency response. **(A)** Reverting small-molecule effect by GSNO, ACC, and NAA. 8-days ½MS grown plants were transferred to −Fe medium with 25 μM small-molecules in the presence or absence of 100 μM GSNO or 10 μM ACC or 0.2 μM NAA for 2-days. **(B)** NO level is not affected by R3 or R6 or R7. 8-days ½MS grown plants were transferred to −Fe with or without 50 μM R3 or R6 or R7 for 4-days. The NO was imaged in root tip using 5 μM DAF-FM DA dye.

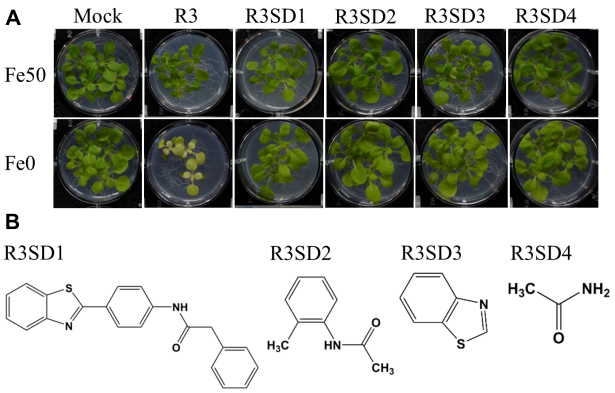

FIGURE 7 | Effect of R3 structural derivatives. **(A)** The structural derivatives do not mimic the R3 effect. 9-days ½MS-grown plants were transferred to Fe50 or Fe0 medium for 9 days in the presence or absence of 50 μM small-molecules. **(B)** The 2D structure of R3 structural derivatives.

conditions of limited Fe and the limiting levels of vasculature NA (Palmer et al., 2013). If R3 or R6 treatment brings down the levels of NA, then Zn would be the favorable substrate for the translocation. Other possibility might account for is that small-molecules may block the transport of metals in a selective manner.

Many genes are strongly induced in response to Fe-deficiency (Buckhout et al., 2009). Both R3 and R6 treatments inhibited the expression of Fe-uptake-associated genes *IRT1* and *FRO2* (**Figures 4A,B**). This inhibition is due to low transcript levels of central transcription factor *FIT* under Fe-deficiency (**Figure 4C**) upon small molecule treatment. FIT is the central modulator and is responsible for the activation of many Fe-deficiency-associated genes in root epidermal cells (Mai et al., 2016). We found that R6 downregulated the expression of *Ib bHLH* genes, FIT-partners under Fe-deficiency, whereas R3 did not (**Figure 5**). Our findings thus reveal that R3 and R6 may target the transcriptional response through distinct branches under Fe starvation.

The expression of the transcription factors responsible for Fe-deficiency is regulated by the upstream signaling molecules. Any defect in the levels or activity of these signaling-molecules causes decreased expression of transcription factors, and exogenous supply increases the transcription factor expression (Chen et al., 2010; Liu et al., 2016; Kailasam et al., 2018). Based on our data, none of the signaling-molecules (auxin/ethylene/GSNO) alleviated the inhibitory effects caused by R3 or R6 when they were supplied externally (**Figure 6**). NO levels were higher under R3 or R6 treatment than in the mock (**Figure 6C**). This supports the notion that R3 and R6 work downstream of auxin/ethylene/NO/GSNO, or alternatively that a novel pathway to the transcription factor exists independent of these hormones (**Figures 4–6**).

The observed decrease in expression of *FIT* and *Ib bHLH* transcription factors under R6 treatment (**Figures 4**, **5**) might be due to a blocked signal passage from NO. It has been demonstrated that NO acts immediately upstream to these transcription factors but downstream of auxin (Chen et al., 2010; Garcia et al., 2010; Kailasam et al., 2018). Recently it has

TABLE 1 | Characteristics of small molecules.

Small molecule	IUPAC name	MW	Molecular formula	ChemSpider ID	PubCem CID
R3	N-[4-(1,3-benzothiazol-2-yl)-2-methylphenyl]acetamide	282.36	$C_{16}H_{14}N_2OS$	349964	394824
R3SD1	N-[4-(1,3-benzothiazol-2-yl)phenyl]-2-phenylacetamide	344.43	$C_{21}H_{16}N_2OS$	1146425	1370084
R3SD2	N-(2-methylphenyl)acetamide	149.19	$C_9H_{11}NO$	10298354	–
R3SD3	1,3-benzothiazole	135.18	C_7H_5NS	6952	7222
R3SD4	Acetamide	59.06	C_2H_5NO	173	178
R6	2-benzoyl-1-benzofuran-5-carboxylic acid	266.25	$C_{16}H_{10}O_4$	6337783	8033570
R6SD1	1-benzofuran-2-yl(phenyl)methanone	222.24	$C_{15}H_{10}O_2$	21133775	–
R6SD2	(3-amino-1-benzofuran-2-yl)-phenylmethanone	237.25	$C_{15}H_{11}NO_2$	746595	854225
R6SD3	(3-amino-6-nitro-1-benzofuran-2-yl)-phenylmethanone	282.25	$C_{15}H_{10}N_2O_4$	4239080	5061996
R6SD4	1-benzofuran	118.13	C_8H_6O	8868	9223

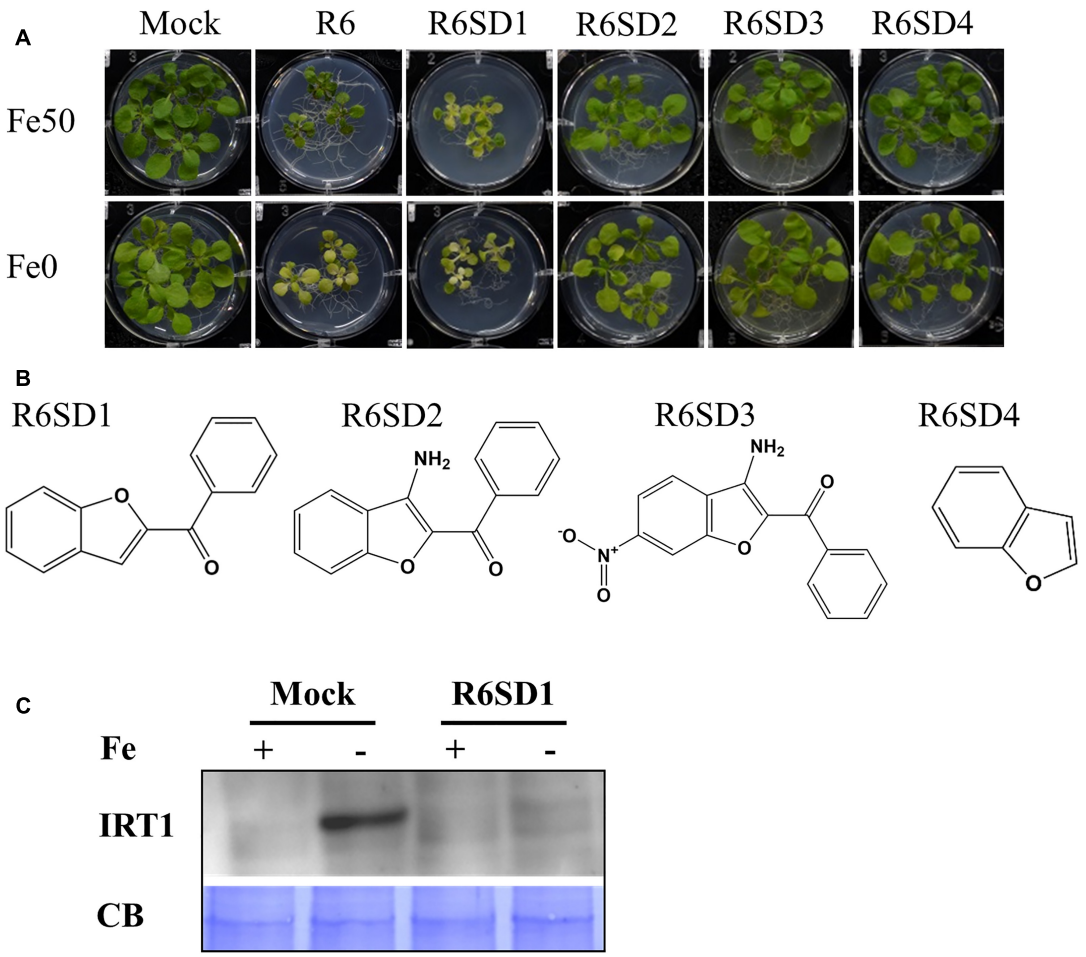

FIGURE 8 | Effect of R6 structural derivatives. **(A)** The phenotype of plants under structural derivatives treatment. 9-days ½MS-grown plants were treated in Fe50 or Fe0 for 9 days in the presence or absence of 50 μM small-molecules. **(B)** The 2D structure of R6 structural derivatives. **(C)** IRT1 protein accumulation in roots under R6SD1 treatment. 10-days ½MS-grown plants were transferred to +Fe or −Fe with or without R6SD1 for 3 days. IRT1 protein was detected using an anti-IRT1 antibody. CB, coomassie blue stain.

also been shown that IVc bHLH factors (bHLH34/104/105/115) directly control the *Ib bHLH* gene expression and indirectly control *FIT* (Zhang et al., 2015; Li et al., 2016; Liang et al., 2017). However, it is not clear whether or not IVc bHLH transcription factors work under NO. Our previous study showed that NO did not regulate the transcripts of *IVc bHLH* genes suggesting that control could be post-translational (Kailasam et al., 2018). One possibility that may account for the effect of R6 is that R6 may target these IVc bHLH proteins thereby reducing the expression of *Ib bHLH* and *FIT* genes (**Figure 9**). If this is so, it will be worth investigating how R6 regulates IVc factors.

Given that R3 treatment only affected the expression of *FIT* and not the *Ib bHLH* transcription factors (**Figures 4**, **5**) and together with the data in **Figure 6**, it is highly likely that R3 targets the signaling route that is specific to FIT alone (**Figure 9**). Similar inhibition of the expression of Fe-homeostatic genes was also found with R7 treatment (Kailasam et al., 2018); however, R7 possibly interrupts the signaling pathway from NO to FIT. GSNO has been shown to be involved in mediating the signal from NO specifically to the FIT (Kailasam et al., 2018); however, the precise mechanism and the signal identity is unknown. As the external supply of GSNO did not rescue the R3 inhibition of Pro_{IRT1}*:LUC* expression (**Figure 6**), R3 may interrupt the signal downstream of GSNO or target an independent unknown signaling pathway to FIT. We did not find any structural similarity between R3 and R7. This suggests the presence of multiple signal inputs for FIT, whose routes are selectively and independently targeted by the structurally less-related R3 and R7 compounds. Under Fe starvation, a wide range of chemical signals coordinate and trigger the transcriptional response (Liu et al., 2016). Some studies have suggested that cellular Fe, especially the levels in leaf vasculature itself act as a sensing/signaling component (Kumar et al., 2017; Garcia et al., 2018; Khan et al., 2018). Based on these findings, together with action of R3 and R7, it is clear that multilayered signaling networks exist. Importantly, there is lot of interconnection and feed-/forward-back between these signaling molecules, that

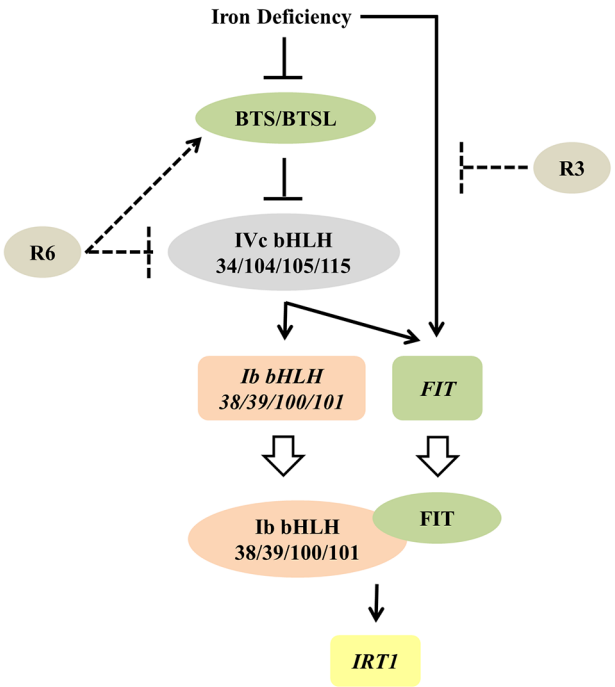

FIGURE 9 | Proposed model for the possible action of R3 and R6 in Fe-deficiency transcriptional-network of Arabidopsis. Fe-status determines the BTS/BTSL stability/function. Under Fe deficiency, BTS is likely degraded, thereby allowing the accumulation of IVc bHLH proteins, which activates the transcription of *Ib bHLH* genes (directly) and *FIT* (indirectly). R6 inhibits the Fe-deficiency-stimulated expression of these IVc bHLH targets. R6 may block the IVc bHLH function by directly affecting the stability or indirectly promoting the degradation through BTS action. In addition to these signals, an unknown Fe-deficiency born signal directly activates the *FIT* transcription. FIT forms heterodimer with each member of Ib bHLH transcription factors and regulate the Fe-uptake gene *IRT1*. R3 most likely intercepts this unknown signal, thus repressing the *FIT* expression. Solid lines indicate data-supported information from previous studies. Open arrow indicates translation. Proteins are represented by colored-ovals and the genes are indicated by colored-boxes.

influence each other, levels and activity under Fe-starvation (Garcia et al., 2011, 2018; Brumbarova et al., 2015; Liu et al., 2016). Therefore, further study of R3 may reveal the identity of a hidden unknown novel component that regulates the central transcription factor FIT.

Assaying the structural analogs of R3 did not help us to narrow down the active region of R3 and indicated that modifying the R3 parent compound will lead to loss of activity (**Figure 7**). R3 belongs to the benzothiazole class of compounds (**Figure 1C** and **Table 1**). Benzothiazole derived compounds are used in clinical studies and the benzothiazole moiety has been widely used as a template structure for the development of therapeutic agents (Ali and Siddiqui, 2013). However, the core benzothiazole (R3SD3) structure alone did not mimic the R3 effect and neither did the other R3 derivatives (**Figure 7**). Therefore, it seems that the parent structure of R3 itself is necessary for its activity. On the other hand, the structural derivatives of R6 provided some clues about the core motif required for the action of R6 (**Figure 8**). R6 is a benzofuran class compound. Benzofuran is an important pharmacophore and its derivatives are employed in medicinal chemistry for a wide range of drugs (Khanam and Shamsuzzaman, 2015). The benzofuran core (R6SD4) itself did not produce any observable phenotype under Fe-limited conditions. However, one structural derivative R6SD1 mimicked the R6 effect, in fact the phenotype caused more effect than R6 (**Figure 8**). The main difference between R6 and R6SD1 is that presence of a carboxylic moiety (-COOH) at the fifth position of the benzofuran unit. R6SD1 does not have a –COOH moiety. It should therefore be worthwhile studying the effect of the –COOH moiety in R6 on Fe-deficiency response. Further, characterizing many structural analogs of R3 and R6 might help us to better understand the core motif required for chemical activity, which will in turn benefit identification of its cellular targets, an important study.

CONCLUSION

The data presented here strongly support the view that small molecules target signaling pathways in the Fe starvation response network and specifically modulate a particular pathway. This work also shows the usefulness of small-molecules in dissecting known signal transduction pathway(s). Furthermore, the selective inhibition of signaling pathways suggests the usefulness of R3 and R6 and chemical genetics *per se* to interpret networks and to identify new components in Fe-signaling. Based on our observations, the small-molecule R3 targets a novel unknown signaling pathway to the transcription factor FIT, whereas R6 may influence the IVc bHLH transcription factors under Fe-starvation (**Figure 9**). In summary, this study unraveled a new unknown Fe-signaling route and increases our understanding of plant Fe starvation signaling.

AUTHOR CONTRIBUTIONS

K-CY conceived the research. SK designed and performed the experiments. SK and K-CY wrote the manuscript. W-FC performed the chemical library screening and western-blot. All authors read and approved the manuscript.

FUNDING

This research was supported by grants (to K-CY) from the Ministry of Science and Technology (MOST 107-2321-B-001-018) of Taiwan and Academia Sinica of Taiwan and a postdoc fellowship (to SK) from Ministry of Science and Technology (MOST 107-2811-B-001-578) of Taiwan.

ACKNOWLEDGMENTS

We thank Jing-Chi Lo and Chia-Lin Wu for their assistance.

REFERENCES

Ali, R., and Siddiqui, N. (2013). Biological aspects of emerging benzothiazoles: a short review. *J. Chem.* 2013:345198. doi: 10.1155/2013/345198

Bonnot, C., Pinson, B., Clement, M., Bernillon, S., Chiarenza, S., Kanno, S., et al. (2016). A chemical genetic strategy identify the PHOSTIN, a synthetic molecule that triggers phosphate starvation responses in *Arabidopsis thaliana*. *New Phytol.* 209, 161–176. doi: 10.1111/nph.13591

Brumbarova, T., Bauer, P., and Ivanov, R. (2015). Molecular mechanisms governing *Arabidopsis* iron uptake. *Trends Plant Sci.* 20, 124–133. doi: 10.1016/j.tplants.2014.11.004

Buckhout, T. J., Yang, T. J., and Schmidt, W. (2009). Early iron-deficiency-induced transcriptional changes in *Arabidopsis* roots as revealed by microarray analyses. *BMC Genomics* 10:147. doi: 10.1186/1471-2164-10-147

Chen, W. W., Yang, J. L., Qin, C., Jin, C. W., Mo, J. H., Ye, T., et al. (2010). Nitric oxide acts downstream of auxin to trigger root ferric-chelate reductase activity in response to iron deficiency in *Arabidopsis*. *Plant Physiol.* 154, 810–819. doi: 10.1104/pp.110.161109

Chen, Y. T., Wang, Y., and Yeh, K. C. (2017). Role of root exudates in metal acquisition and tolerance. *Curr. Opin. Plant Biol.* 39, 66–72. doi: 10.1016/j.pbi.2017.06.004

Clemens, S., and Weber, M. (2016). The essential role of coumarin secretion for Fe acquisition from alkaline soil. *Plant Signal. Behav.* 11:e1114197. doi: 10.1080/15592324.2015.1114197

Colangelo, E. P., and Guerinot, M. L. (2004). The essential basic helix-loop-helix protein FIT1 is required for the iron deficiency response. *Plant Cell* 16, 3400–3412. doi: 10.1105/tpc.104.024315

Colombo, C., Palumbo, G., He, J. Z., Pinton, R., and Cesco, S. (2014). Review on iron availability in soil: interaction of Fe minerals, plants, and microbes. *J. Soils Sediments* 14, 538–548. doi: 10.1007/s11368-013-0814-z

Connolly, E. L., Fett, J. P., and Guerinot, M. L. (2002). Expression of the IRT1 metal transporter is controlled by metals at the levels of transcript and protein accumulation. *Plant Cell* 14, 1347–1357. doi: 10.1105/tpc.001263

Connorton, J. M., Balk, J., and Rodriguez-Celma, J. (2017). Iron homeostasis in plants – a brief overview. *Metallomics* 9, 813–823. doi: 10.1039/c7mt00136c

Cui, Y., Chen, C. L., Cui, M., Zhou, W. J., Wu, H. L., and Ling, H. Q. (2018). Four IVa bHLH transcription factors are novel interactors of FIT and mediate JA inhibition of iron uptake in *Arabidopsis*. *Mol. Plant.* 11, 1166–1183. doi: 10.1016/j.molp.2018.06.005

Curie, C., and Mari, S. (2017). New routes for plant iron mining. *New Phytol.* 214, 521–525. doi: 10.1111/nph.14364

Durrett, T. P., Gassmann, W., and Rogers, E. E. (2007). The FRD3-mediated efflux of citrate into the root vasculature is necessary for efficient iron translocation. *Plant Physiol.* 144, 197–205. doi: 10.1104/pp.107.097162

Fourcroy, P., Siso-Terraza, P., Sudre, D., Saviron, M., Reyt, G., Gaymard, F., et al. (2014). Involvement of the ABCG37 transporter in secretion of scopoletin and derivatives by Arabidopsis roots in response to iron deficiency. *New Phytol.* 201, 155–167. doi: 10.1111/Nph.12471

Garcia, M. J., Corpas, F. J., Lucena, C., Alcantara, E., Perez-Vicente, R., Zamarreno, A. M., et al. (2018). A shoot Fe signaling pathway requiring the OPT3 transporter controls GSNO reductase and ethylene in *Arabidopsis thaliana* roots. *Front. Plant Sci.* 9:1325. doi: 10.3389/fpls.2018.01325

Garcia, M. J., Lucena, C., Romera, F. J., Alcantara, E., and Perez-Vicente, R. (2010). Ethylene and nitric oxide involvement in the up-regulation of key genes related to iron acquisition and homeostasis in *Arabidopsis*. *J. Exp. Bot.* 61, 3885–3899. doi: 10.1093/jxb/erq203

Garcia, M. J., Suarez, V., Romera, F. J., Alcantara, E., and Perez-Vicente, R. (2011). A new model involving ethylene, nitric oxide and Fe to explain the regulation of Fe-acquisition genes in strategy I plants. *Plant Physiol. Biochem.* 49, 537–544. doi: 10.1016/j.plaphy.2011.01.019

Hindt, M. N., Akmakjian, G. Z., Pivarski, K. L., Punshon, T., Baxter, I., Salt, D. E., et al. (2017). Brutus and its paralogs, BTS LIKE1 and BTS LIKE2, encode important negative regulators of the iron deficiency response in *Arabidopsis thaliana*. *Metallomics* 9, 876–890. doi: 10.1039/c7mt00152e

Jakoby, M., Wang, H. Y., Reidt, W., Weisshaar, B., and Bauer, P. (2004). FRU (BHLH029) is required for induction of iron mobilization genes in *Arabidopsis thaliana*. *FEBS Lett.* 577, 528–534. doi: 10.1016/j.febslet.2004.10.062

Jeong, J., Merkovich, A., Clyne, M., and Connolly, E. L. (2017). Directing iron transport in dicots: regulation of iron acquisition and translocation. *Curr. Opin. Plant Biol.* 39, 106–113. doi: 10.1016/j.pbi.2017.06.014

Kailasam, S., Wang, Y., Lo, J. C., Chang, H. F., and Yeh, K. C. (2018). S-Nitrosoglutathione works downstream of nitric oxide to mediate iron-deficiency signaling in *Arabidopsis*. *Plant J.* 94, 157–168. doi: 10.1111/tpj.13850

Khan, M. A., Castro-Guerrero, N. A., McInturf, S. A., Nguyen, N. T., Dame, A. N., Wang, J. J., et al. (2018). Changes in iron availability in *Arabidopsis* are rapidly sensed in the leaf vasculature and impaired sensing leads to opposite transcriptional programs in leaves and roots. *Plant Cell Environ.* 41, 2263–2276. doi: 10.1111/pce.13192

Khanam, H., and Shamsuzzaman. (2015). Bioactive benzofuran derivatives: a review. *Eur. J. Med. Chem.* 97, 483–504. doi: 10.1016/j.ejmech.2014.11.039

Kobayashi, T., and Nishizawa, N. K. (2012). Iron uptake, translocation, and regulation in higher plants. *Annu. Rev. Plant Biol.* 63, 131–152. doi: 10.1146/annurev-arplant-042811-105522

Kobayashi, T., and Nishizawa, N. K. (2015). Intracellular iron sensing by the direct binding of iron to regulators. *Front. Plant Sci.* 6:155. doi: 10.3389/fpls.2015.00155

Korshunova, Y. O., Eide, D., Clark, W. G., Guerinot, M. L., and Pakrasi, H. B. (1999). The IRT1 protein from *Arabidopsis thaliana* is a metal transporter with a broad substrate range. *Plant Mol. Biol.* 40, 37–44. doi: 10.1023/A:1026438615520

Kumar, R. K., Chu, H. H., Abundis, C., Vasques, K., Rodriguez, D. C., Chia, J. C., et al. (2017). Iron-Nicotianamine transporters are required for proper long distance iron signaling. *Plant Physiol.* 175, 1254–1268. doi: 10.1104/pp.17.00821

Li, X. L., Zhang, H. M., Ai, Q., Liang, G., and Yu, D. (2016). Two bHLH transcription factors, bHLH34 and bHLH104, regulate iron homeostasis in *Arabidopsis thaliana*. *Plant Physiol.* 170, 2478–2493. doi: 10.1104/pp.15.01827

Liang, G., Zhang, H., Li, X., Ai, Q., and Yu, D. (2017). bHLH transcription factor bHLH115 regulates iron homeostasis in *Arabidopsis thaliana*. *J. Exp. Bot.* 68, 1743–1755. doi: 10.1093/jxb/erx043

Lin, X. Y., Ye, Y. Q., Fan, S. K., Jin, C. W., and Zheng, S. J. (2015). Increased sucrose accumulation regulates iron-deficiency responses by promoting auxin signaling in *Arabidopsis* plants. *Plant Physiol.* 170, 907–920. doi: 10.1104/pp.15.01598

Liu, X. X., He, X. L., and Jin, C. W. (2016). Roles of chemical signals in regulation of the adaptive responses to iron deficiency. *Plant Signal. Behav.* 11:e1179418. doi: 10.1080/15592324.2016.1179418

Lucena, C., Romera, F. J., Garcia, M. J., Alcantara, E., and Perez-Vicente, R. (2015). Ethylene participates in the regulation of Fe deficiency responses in strategy I plants and in rice. *Front. Plant Sci.* 6:1056. doi: 10.3389/fpls.2015.01056

Mai, H. J., Pateyron, S., and Bauer, P. (2016). Iron homeostasis in *Arabidopsis thaliana*: transcriptomic analyses reveal novel FIT-regulated genes, iron deficiency marker genes and functional gene networks. *BMC Plant Biol.* 16:211. doi: 10.1186/S12870-016-0899-9

Maurer, F., Arcos, M. A. N., and Bauer, P. (2014). Responses of a triple mutant defective in three iron deficiency-induced *BASIC HELIX-LOOP-HELIX* genes of the subgroup Ib(2) to iron deficiency and salicylic acid. *PLoS ONE* 9:e99234. doi: 10.1371/journal.pone.0099234

Palmer, C. M., Hindt, M. N., Schmidt, H., Clemens, S., and Guerinot, M. L. (2013). MYB10 and MYB72 are required for growth under iron-limiting conditions. *PLoS Genet.* 9:e1003953. doi: 10.1371/journal.pgen.1003953

Robinson, N. J., Procter, C. M., Connolly, E. L., and Guerinot, M. L. (1999). A ferric-chelate reductase for iron uptake from soils. *Nature* 397, 694–697. doi: 10.1038/17800

Santi, S., and Schmidt, W. (2009). Dissecting iron deficiency-induced proton extrusion in *Arabidopsis* roots. *New Phytol.* 183, 1072–1084. doi: 10.1111/j.1469-8137.2009.02908.x

Schmittgen, T. D., and Livak, K. J. (2008). Analyzing real-time PCR data by the comparative C(T) method. *Nat. Protoc.* 3, 1101–1108. doi: 10.1038/nprot.2008.73

Schuler, M., Rellan-Alvarez, R., Fink-Straube, C., Abadia, J., and Bauer, P. (2012). Nicotianamine functions in the phloem-based transport of iron to sink organs, in pollen development and pollen tube growth in *Arabidopsis*. *Plant Cell* 24, 2380–2400. doi: 10.1105/tpc.112.099077

Selote, D., Samira, R., Matthiadis, A., Gillikin, J. W., and Long, T. A. (2015). Iron-binding E3 ligase mediates iron response in plants by targeting basic helix-loop-helix transcription factors. *Plant Physiol.* 167, 273–286. doi: 10.1104/pp.114.250837

Shanmugam, V., Lo, J. C., Wu, C. L., Wang, S. L., Lai, C. C., Connolly, E. L., et al. (2011). Differential expression and regulation of iron-regulated metal transporters in *Arabidopsis halleri* and *Arabidopsis thaliana* – the role in zinc tolerance. *New Phytol.* 190, 125–137. doi: 10.1111/j.1469-8137.2010.03606.x

Shanmugam, V., Wang, Y. W., Tsednee, M., Karunakaran, K., and Yeh, K. C. (2015). Glutathione plays an essential role in nitric oxide-mediated iron-deficiency signaling and iron-deficiency tolerance in *Arabidopsis*. *Plant J.* 84, 464–477. doi: 10.1111/tpj.13011

Shin, L. J., Lo, J. C., Chen, G. H., Callis, J., Fu, H., and Yeh, K. C. (2013). IRT1 degradation factor1, a ring E3 ubiquitin ligase, regulates the degradation of iron-regulated transporter1 in Arabidopsis. *Plant Cell* 25, 3039–3051. doi: 10.1105/tpc.113.115212

Vert, G., Grotz, N., Dedaldechamp, F., Gaymard, F., Guerinot, M. L., Briat, J. F., et al. (2002). IRT1, an Arabidopsis transporter essential for iron uptake from the soil and for plant growth. *Plant Cell* 14, 1223–1233. doi: 10.1105/tpc.001388

Wang, H. Y., Klatte, M., Jakoby, M., Baumlein, H., Weisshaar, B., and Bauer, P. (2007). Iron deficiency-mediated stress regulation of four subgroup Ib BHLH genes in *Arabidopsis thaliana*. *Planta* 226, 897–908. doi: 10.1007/s00425-007-0535-x

Wang, N., Cui, Y., Liu, Y., Fan, H., Du, J., Huang, Z., et al. (2013). Requirement and functional redundancy of Ib subgroup bHLH proteins for iron deficiency responses and uptake in *Arabidopsis thaliana*. *Mol. Plant* 6, 503–513. doi: 10.1093/mp/sss089

Wellburn, A. R. (1994). The spectral determination of Chlorophyll-a and Chlorophhyll-B, as well as total carotenoids, using various solvents with spectrophotometers of different resolution. *J. Plant Physiol.* 144, 307–313.

Yuan, Y. X., Wu, H. L., Wang, N., Li, J., Zhao, W. N., Du, J., et al. (2008). FIT interacts with AtbHLH38 and AtbHLH39 in regulating iron uptake gene expression for iron homeostasis in Arabidopsis. *Cell Res.* 18, 385–397. doi: 10.1038/Cr.2008.26

Yuan, Y. X., Zhang, J., Wang, D. W., and Ling, H. Q. (2005). AtbHLH29 of *Arabidopsis thaliana* is a functional ortholog of tomato FER involved in controlling iron acquisition in strategy I plants. *Cell Res.* 15, 613–621. doi: 10.1038/sj.cr.7290331

Zhang, J., Liu, B., Li, M., Feng, D., Jin, H., Wang, P., et al. (2015). The bHLH transcription factor bHLH104 interacts with IAA-LEUCINE RESISTANT3 and modulates iron homeostasis in Arabidopsis. *Plant Cell* 27, 787–805. doi: 10.1105/tpc.114.132704

Zhu, X. F., Wang, B., Song, W. F., Zheng, S. J., and Shen, R. F. (2016). Putrescine alleviates iron deficiency via NO-dependent reutilization of root cell-wall Fe in *Arabidopsis*. *Plant Physiol.* 170, 558–567. doi: 10.1104/pp.15.01617

Conflict of Interest Statement: The authors declare that the research was conducted in the absence of any commercial or financial relationships that could be construed as a potential conflict of interest.

frontiers in Plant Science

ORIGINAL RESEARCH
published: 11 February 2019
doi: 10.3389/fpls.2019.00113

Iron and Phosphate Deficiency Regulators Concertedly Control Coumarin Profiles in *Arabidopsis thaliana* Roots During Iron, Phosphate, and Combined Deficiencies

*Ranju Chutia, Steffen Abel and Jörg Ziegler**

Department of Molecular Signal Processing, Leibniz Institute of Plant Biochemistry, Halle, Germany

OPEN ACCESS

Edited by:
Thomas J. Buckhout, Humboldt-Universität zu Berlin, Germany

Reviewed by:
Brian M. Waters, University of Nebraska–Lincoln, United States
Hans-Peter Mock, Leibniz-Institut für Pflanzengenetik und Kulturpflanzenforschung (IPK), Germany

***Correspondence:**
Jörg Ziegler
joerg.ziegler@ipb-halle.de

Specialty section:
This article was submitted to Plant Nutrition, a section of the journal Frontiers in Plant Science

Received: *25 October 2018*
Accepted: *23 January 2019*
Published: *11 February 2019*

Citation:
Chutia R, Abel S and Ziegler J (2019) Iron and Phosphate Deficiency Regulators Concertedly Control Coumarin Profiles in Arabidopsis thaliana Roots During Iron, Phosphate, and Combined Deficiencies. Front. Plant Sci. 10:113. doi: 10.3389/fpls.2019.00113

Plants face varying nutrient conditions, to which they have to adapt to. Adaptive responses are nutrient-specific and strategies to ensure supply and homeostasis for one nutrient might be opposite to another one, as shown for phosphate (P_i) and iron (Fe) deficiency responses, where many genes are regulated in an opposing manner. This was also observed on the metabolite levels. Whereas root and exudate levels of catechol-type coumarins, phenylpropanoid-derived 2-benzopyranones, which facilitate Fe acquisition, are elevated after Fe deficiency, they are decreased after P_i deficiency. Exposing plants to combined P_i and Fe deficiency showed that the generation of coumarin profiles in *Arabidopsis thaliana* roots by P_i deficiency considerably depends on the availability of Fe. Similarly, the effect of Fe deficiency on coumarin profiles is different at low compared to high P_i availability. These findings suggest a fine-tuning of coumarin profiles, which depends on Fe and P_i availability. T-DNA insertion lines exhibiting aberrant expression of genes involved in the regulation of P_i starvation responses (*PHO1, PHR1, bHLH32, PHL1, SPX1*) and Fe starvation responses (*BRUTUS, PYE, bHLH104, FIT*) were used to analyze the regulation of the generation of coumarin profiles in *Arabidopsis thaliana* roots by P_i, Fe, and combined P_i and Fe deficiency. The analysis revealed a role of several Fe-deficiency response regulators in the regulation of Fe and of P_i deficiency-induced coumarin profiles as well as for P_i deficiency response regulators in the regulation of P_i and of Fe deficiency-induced coumarin profiles. Additionally, the regulation of Fe deficiency-induced coumarin profiles by Fe deficiency response regulators is influenced by P_i availability. Conversely, regulation of P_i deficiency-induced coumarin profiles by P_i deficiency response regulators is modified by Fe availability.

Keywords: *Arabidopsis thaliana*, phosphate deficiency, iron deficiency, metabolite profiling, coumarins, regulation

INTRODUCTION

Coumarins are a group of compounds derived from the phenylpropanoid pathway. They possess a 2-benzopyranone core structure and individual members of this class of compounds exhibit different substitution patterns (Shimizu, 2014). Scopoletin, the first coumarin-specific intermediate in coumarin biosynthesis, contains a methoxy group and a hydroxyl group at positions 6 and 7, respectively (**Supplementary Figure S1**). Other coumarins contain a catechol moiety, which can either be demethylated scopoletin (esculetin), or mono- and dihydroxlated scopoletin (fraxetin and sideritin) (Kai et al., 2008; Shimizu, 2014; Sisó-Terraza et al., 2016; Rajniak et al., 2018; Siwinska et al., 2018; Tsai et al., 2018). In the model plant *Arabidopsis thaliana*, these coumarins have predominantly been detected in root exudates, whereas their respective monoglucosides, such as scopolin, esculin, fraxin, and sideritin glucoside, are almost exclusively found in root extracts (Fourcroy et al., 2014, 2016; Schmid et al., 2014; Schmidt et al., 2014; Sisó-Terraza et al., 2016; Ziegler et al., 2017; Rajniak et al., 2018; Siwinska et al., 2018; Tsai et al., 2018).

In recent years, it was shown that biosynthesis and exudation of coumarins, especially of catechol type coumarins, contribute to iron acquisition under iron limiting conditions (Rodríguez-Celma et al., 2013; Fourcroy et al., 2014, 2016; Schmid et al., 2014; Schmidt et al., 2014; Sisó-Terraza et al., 2016; Rajniak et al., 2018; Siwinska et al., 2018; Tsai et al., 2018). It was shown that iron deficiency-induced accumulation of coumarins was under positive control of the major regulator of iron deficiency responses FIT (FER-like Iron deficiency-induced Transcription Factor) (Schmid et al., 2014), a basic helix loop helix type transcription factor (bHLH 29) (Colangelo and Guerinot, 2004). FIT is part of a comprehensive network of transcriptional regulators required to orchestrate responses which enable the plant to cope with iron limiting conditions. Although many responses seem to be regulated by FIT alone, its interaction with the bHLH type transcription factors 38, 39, 100, and 101 is required to mediate a subset of iron deficiency responses (Colangelo and Guerinot, 2004; Yuan et al., 2008; Wang et al., 2013). Expression of *bHLH38*, *39*, *100*, and *101* is positively regulated by the transcription factor bHLH 104 (Li et al., 2016), which was shown to interact with BRUTUS (BTS), an E3 ubiquitin ligase protein with metal ion binding and DNA binding domains (Selote et al., 2015; Zhang et al., 2015). BTS, a negative regulator, is assumed to be responsible for fine tuning of iron deficiency responses by monitoring iron status through its metal ion binding domain (Kobayashi et al., 2013; Selote et al., 2015). Opposing effects on plant growth and development also suggest an interaction of BTS with the bHLH transcription factor POPEYE (PYE), which positively regulates several iron deficiency responses (Long et al., 2010). However, with the exception of FIT, the contribution of these regulators to iron deficiency-induced coumarin accumulation has not been investigated so far.

Recently, we observed changes in the levels of coumarins in Arabidopsis root exudates as well as of coumarin glucoside in Arabidopsis roots after plants have been subjected to phosphate (P_i) deficiency (Ziegler et al., 2016). We observed an accumulation for a subset of coumarins, i.e., esculin, esculetin, scopolin, and scopoletin, whereas the levels of sideritin and its glucoside were strongly decreased, thus contrasting the iron deficiency-induced accumulation of all coumarins, especially of highly oxygenated ones, such as sideritin (Schmid et al., 2014; Rajniak et al., 2018). Several regulators of P_i deficiency responses have been described. The major regulator is PHR1, which binds to the PBS domain in the promoter of many phosphate starvation genes, thereby inducing their transcription (Rubio et al., 2001; Bustos et al., 2010; Briat et al., 2015). SPX proteins, for which three isoforms are known, negatively regulate P_i deficiency-induced gene expression. High intracellular P_i concentrations promote the interaction between PHR1 and SPX preventing PHR1 to bind to its target sites on the promoters. At low intracellular P_i concentrations, PHR1 is released from the PHR1-SPX complex, allowing it to activate gene expression (Puga et al., 2014; Wang et al., 2014). PHR1 was shown to regulate the transcription of about 60% of P_i starvation responsive genes (Bustos et al., 2010). Other genes, which are not controlled by PHR1, are mainly regulated by PHL transcription factors (PHR1-Like), for which several isoforms have been described (Bustos et al., 2010). Although conceivable, it has not yet been elucidated whether or not regulation by PHL proceeds through P_i mediated interaction with SPX protein, as is the case with PHR1. On the other hand, negative regulation of P_i starvation responses by the transcription factor bHLH32 was shown to be independent of P_i content (Chen et al., 2007). PHOSPHATE1 (PHO1) was identified as eukaryotic P_i exporter. Mutants with impaired *PHO 1* expression showed reduced shoot but increased root P_i levels indicating a disturbed shoot to root distribution of P_i (Poirier et al., 1991; Hamburger et al., 2002). Reduced transcriptional activation of P_i starvation response genes despite low P_i levels in shoots of *pho1* mutants as well as the presence of known P_i regulatory motifs in the PHO1 protein suggests a role for PHO1 in the coordination of P_i starvation responses (Rouached et al., 2011; Wege et al., 2016). Although many P_i starvation responses are controlled by these regulators, their involvement in the changes in P_i deficiency-induced coumarin profiles is unknown.

The different coumarin profiles observed after either P_i or Fe deficiency treatments alone, especially the opposing effects on sideritin levels (Ziegler et al., 2016), raises the question on the response after combined deficiency, specifically, whether withdrawal of Fe affects P_i deficiency induced changes in coumarin levels and vice versa. Furthermore, as mentioned above, FIT has been shown to play an important role in the accumulation of coumarins after Fe deficiency (Schmid et al., 2014), but no regulator of P_i deficiency induced alteration in coumarin profiles have been identified yet. Also, regulators of possible modifications of Fe deficiency-induced coumarin profiles by P_i deficiency and vice versa are not known.

In this report, we studied the effect of P_i deficiency, Fe deficiency, and combined P_i and Fe deficiency on coumarin profiles in *Arabidopsis thaliana* roots. Several mutants were included in order to elucidate the contribution of either P_i or Fe deficiency response regulators in the establishment of coumarin profiles. Since we were mainly interested in the regulation of coumarin biosynthesis rather than on coumarin exudation, we

focused our analysis on coumarin glucosides, which are almost exclusively found inside roots and which most likely represent the major storage form of newly biosynthesized coumarins before being cleaved and exuded. Additionally, we could recently show that coumarin glucoside profiles obtained from root tissue are qualitatively and quantitatively correlated to coumarin aglycone profiles in exudates (Ziegler et al., 2016, 2017).

MATERIALS AND METHODS

Plant Lines and Growth Conditions

Arabidopsis thaliana accession Columbia (Col-0) was used as WT throughout the study. All T-DNA insertion lines (Col-0 background) were provided by the Nottingham Arabidopsis Stock Center (NASC). Homozygous plants were generated by selfing heterozygous plants, and homozygosity was confirmed by PCR with the primers listed in **Supplementary Table S1**.

Seeds were surface sterilized with chlorine gas and individually placed with a toothpick on sterile agar plates containing 5 mM KNO_3, 0.5 mM KH_2PO_4, 2 mM $MgSO_4$, 2 mM $Ca(NO_3)_2$, 50 μM Fe-EDTA, 70 μM H_3BO_3, 14 μM $MnCl_2$, 0.5 μM $CuSO_4$, 1 μM $ZnSO_4$, 0.2 μM Na_2MoO_4, 10 μM $CoCl_2$, and 5 g l^{-1} of sucrose buffered with 2.5 mM Mes-KOH to pH 5.6. For $-P_i$ medium, the concentration of KH_2PO_4 was reduced to 5 μM, for −Fe medium, Fe-EDTA was omitted. Agar (Phyto Agar, Duchefa, Haarlem, Netherlands) was routinely purified as described (Ward et al., 2008) and added to a concentration of 1% (w/v). Plates were incubated for 2 days in the dark at 4°C to synchronize seed germination. Afterward, agar plates were kept in a vertical position in a growth chamber at 22°C under illumination for 16 h daily (170 μmol s^{-1} m^{-2}; Osram LumiluxDeLuxe Cool daylight L58W/965, Osram, Augsburg, Germany). After 5 days of growth, plants were transferred to fresh agar plates containing the respective conditions ($+P_i$,+Fe; $-P_i$,+Fe; $+P_i$,−Fe; $-P_i$,−Fe). After additional 6 days of growth, roots were separated from the shoots, their fresh weight recorded and frozen in liquid nitrogen until further processing. One biological replicate consisted of roots from two plants (coumarin concentration) or shoots and roots from one plant (P_i concentration). The phenotypes of WT plants and mutant plants grown under the four applied treatments were recorded at the time of harvest after and are shown in **Supplementary Figure S2**.

Metabolite Analysis

Frozen tissues (1–5 mg of fresh weight) were ground using 5 mm steel beads in a bead mill at 25 s^{-1} for 50 s, and the resulting powder was extracted by vigorous shaking for 20 min with 100 μl of 70% (v/v) methanol containing 2 nmol of 4-methyl-umbelliferon and 5 nmol [2,2,3,3-^{2}H] succinic acid as internal standards for coumarin and P_i quantification, respectively. Targeted coumarin profiling was performed as described (Ziegler et al., 2016, 2017). For the determination of P_i concentrations, 10 μl of the extracts were evaporated to dryness, methoxylated with 20 μl of 20 mg ml^{-1} of methoxyamine in pyridine (Sigma-Aldrich, St. Louis, MO, United States) for 1.5 h at room temperature, and silylated for 30 min at 37°C with 35 μl of Silyl 991 (Macherey-Nagel, Düren, Germany). Gas chromatography (GC)-MS/MS was performed as described (Ziegler et al., 2016) with some modifications. Briefly, the Agilent 7890 GC system was equipped with an OPTIMA 5 column (10 m × 0.25 mm, 0.25 μm; Macherey-Nagel, Düren, Germany) and coupled to an Agilent 7000B triple quadrupole mass spectrometer operated in the positive chemical ionization mode (reagent gas: methane, gas flow: 20%, ion source temperature; 230°C). One microliter was injected [pulsed (25 psi) splitless injection] at 220°C. The initial temperature of 60°C was held for 1 min, followed by increases at 35°C min^{-1} to 200°C and 50°C min^{-1} to 340°C. The final temperature of 340°C was held for 5 min. Helium was used as the carrier at 2.39 ml min^{-1}. The transfer line was set to a temperature of 250°C. Helium and N_2 were used as quench and collision gasses, respectively (2.25 and 1.5 ml min^{-1}). Multiple reaction monitoring parameters for the detection of P_i (3TMS) and [2,2,3,3-^{2}H] succinic acid (2TMS) are indicated in **Supplementary Table S2**. The IntelliQuant algorithm of the Analyst 1.6.2 software (AB Sciex, Darmstadt, Germany) or the Agile algorithm of the MassHunter Quantitative Analysis software (version B06.00, Agilent, Waldbronn, Germany) were used to integrate the peaks for coumarins or P_i, respectively. Coumarins and P_i concentrations were quantified using 4-methyl-umbelliferon and [2,2,3,3-^{2}H] succinic acid, respectively, and the calculated amounts were divided by the fresh weight. In order to account for variations in absolute coumarin concentrations between independent experiments, all values within individual experiments were normalized to the average values of the biological replicates of the Col0 $+P_i$+Fe treatment in the respective experiment. The raw data are available in **Supplementary Dataset S1**.

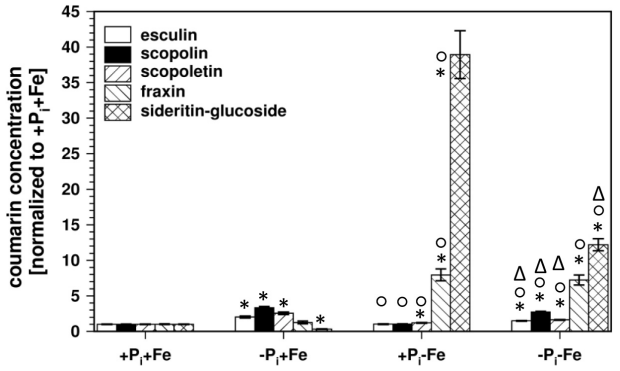

FIGURE 1 | Normalized coumarin concentrations in roots of WT plants (normalized to $+P_i$+Fe, average absolute amounts: esculin (open bars): 0.64 pmol mg^{-1} FW; scopolin (solid bars): 702 pmol mg^{-1} FW; scopoletin (hatched/bars): 16.8 pmol mg^{-1} FW; fraxin (hatched\bars): 1.9 pmol mg^{-1} FW; sideritin glucoside (cross hatched bars): 3.6 pmol mg^{-1} FW). Plants were grown for 5 days on $+P_i$+Fe agar plates, transferred to the indicated conditions and allowed to grow for additional 6 days before harvest. $+P_i$: 500 μM, $-P_i$: 5 μM, +Fe: 50 μM, –Fe: no Fe added. Error bars indicate SE ($n \geq 35$). Significance analyses between treatments were performed by Student's *t*-test (two tailed, equal variances). $^*P \leq 0.05$ compared to $+P_i$+Fe; $^\circ P \leq 0.05$ compared to $-P_i$+Fe; $^\Delta P \leq 0.05$ compared to $+P_i$–Fe.

RESULTS

Root Coumarin Profiles in Response to P_i Deficiency, Fe Deficiency, and Combined P_i and Fe Deficiency

At first we analyzed the coumarin glucoside profile in roots of Col0 wild-type plants after P_i and Fe deficiency, as well as after combined deficiency (**Figure 1**). In P_i depleted conditions (−P_i, +Fe), sideritin glucoside concentration in roots was decreased by about 70%, whereas esculin, scopolin, and scopoletin levels increased two- to three-fold. The slight increase in the concentration of fraxin (1.2-fold) was of low statistical significance ($P = 0.22$). As reported (Schmid et al., 2014; Schmidt et al., 2014; Sisó-Terraza et al., 2016; Rajniak et al., 2018; Tsai et al., 2018), fraxin and sideritin glucoside levels strongly increased almost 8- and 40-fold, respectively, after Fe deficiency (+P_i, −Fe). For esculin and scopolin, statistically significant ($P \leq 0.05$) changes could not be detected, whereas scopoletin levels slightly increased by 20%. Interestingly, Fe deficiency-induced sideritin glucoside levels were lower in case plants experienced additional P_i limitation (−P_i, −Fe). However, the amount of fraxin was not affected. After combined deficiency, esculin, scopolin, and scopoletin levels approached those observed after P_i deficiency alone (−Pi, +Fe), but were still significantly ($P \leq 0.05$) lower. Consistently, the P_i deficiency response, decrease in sideritin glucoside and accumulation of esculin, scopolin, and scopoletin, was different in the absence than in the presence of Fe (two way ANOVA: $P \leq 0.01$). Similarly, the Fe deficiency response was dependent on the applied P_i concentration. Whereas the increase in sideritin glucoside levels was lower in the absence compared to the presence of P_i (two way ANOVA: 5.8 e^{-12}), fraxin accumulation was unaffected, and esculin, scopolin, and scopoletin levels rather declined (two way ANOVAs: $P = 6.5\ e^{-4}$, 6.9 e^{-3}, 1.6 e^{-7}, respectively). These results indicate a cross-talk between Fe and P_i nutrition in the generation of coumarin profiles, especially the impact of P_i limitation on Fe deficiency-induced coumarin accumulation. In order to evaluate whether this is due to internal or external P_i concentrations, we measured the P_i content in roots and shoots.

Correlation Between Coumarin Profiles and P_i Content

Lowering the P_i concentration in the medium from 500 to 5 μM resulted in a decrease of root P_i by 70% (**Figure 2**). Simultaneous Fe deficiency (−P_i, −Fe) led to a further decrease by 30%, whereas growth in Fe-depleted conditions alone (+P_i, −Fe) did not alter P_i levels. Shoot P_i levels followed a similar pattern. From these data it seems that decreased P_i levels lead to decreased sideritin glucoside, and increased esculin, scopolin, and scopoletin concentrations irrespective of the presence of iron, suggesting that coumarin profiles in roots of plants grown in control as well as in Fe deficient conditions are modulated by the internal P_i status. To further elaborate such a correlation we analyzed the *pho1* mutant which exhibits an aberrant P_i distribution between roots and shoots (**Figure 3**) (Poirier et al., 1991; Hamburger et al., 2002; Rouached et al., 2011). In case changes in sideritin glucoside, esculin, scopolin, and scopoletin levels would be due to root P_i status, roots of *pho1* plants showing higher P_i concentrations should exhibit increased sideritin glucoside and decreased esculin, scopolin, and scopoletin levels compared to WT. However, by comparing **Figures 3**, **4**, *pho1* roots rather displayed lower sideritin glucoside and increased esculin levels compared to WT under nutrient sufficient conditions (+P_i,+Fe) despite higher P_i concentrations in roots. Also,

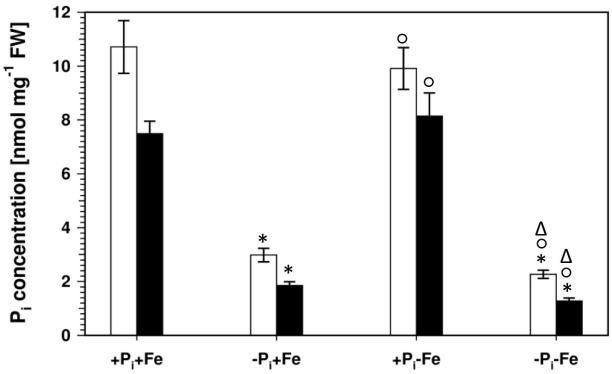

FIGURE 2 | P_i concentrations in roots (open bars) and shoots (solid bars) of WT plants. Plants were grown for 5 days on +P_i+Fe agar plates, transferred to the indicated conditions and allowed to grow for additional 6 days before harvest. +P_i : 500 μM, –P_i : 5 μM, +Fe: 50 μM, –Fe: no Fe added. Error bars indicate SE ($n \geq 35$). Significance analyses between treatments were performed by Student's *t*-test (two tailed, equal variances). $^{*}P \leq 0.05$ compared to +P_i+Fe; $^{\circ}P \leq 0.05$ compared to –P_i+Fe; $^{\Delta}P \leq 0.05$ compared to +P_i–Fe.

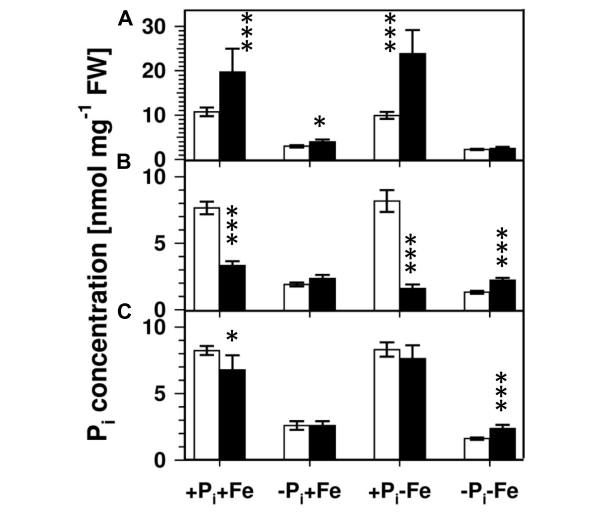

FIGURE 3 | P_i concentrations in roots **(A)**, shoots **(B)**, and seedlings **(C)** of WT (open bars) and *pho1* (solid bars). Plants were grown for 5 days on +P_i+Fe agar plates, transferred to the indicated conditions and allowed to grow for additional 6 days before harvest. +P_i : 500 μM, –P_i : 5 μM, +Fe: 50 μM, –Fe: no Fe added. Error bars indicate SE ($n \geq 8$). Significance analyses between *pho1* and Col0 were performed by Student's *t*-test (two tailed, equal variances): $^{*}P \leq 0.05$; $^{**}P \leq 0.01$; $^{***}P \leq 0.001$.

sideritin glucoside and esculin levels in *pho1* roots exposed to Fe deficiency (+P_i, −Fe) are similar or slightly increased, respectively, although root P_i levels are higher. Only the elevated P_i levels in *pho1* roots exposed to P_i limiting conditions (−P_i, +Fe) coincided with higher sideritin glucoside levels, but esculin and fraxin concentrations were strongly elevated compared to WT. Considering the P_i status of whole seedlings grown in nutrient sufficient condition (+P_i, +Fe), lower levels of P_i in *pho1* corresponded to decreased sideritin glucoside and increased esculin levels in *pho*1 roots compared to WT, suggesting that the levels of sideritin glucoside and esculin levels are negatively and positively correlated, respectively, to the P_i concentration of the whole seedling. However, although seedling P_i levels were higher in *pho1* compared to WT under conditions of combined deficiency (−P_i, −Fe), sideritin glucoside levels were indistinguishable between the mutant and Col0, and esculin levels were about threefold higher in *pho1*. These results show that the effect of P_i deficiency on coumarin profiles can only be partially attributed to cellular P_i concentration. Remarkably, P_i limitation resulted in a strong accumulation of fraxin in roots of P_i starved *pho1* roots, which was not observed in WT roots.

The observation that coumarin profiles are modified by P_i starvation raised the question whether P_i deficiency response or Fe deficiency response regulators are involved. Therefore, T-DNA lines harboring insertions in several known regulatory genes of both responses were tested for their coumarin profiles under the four conditions described above.

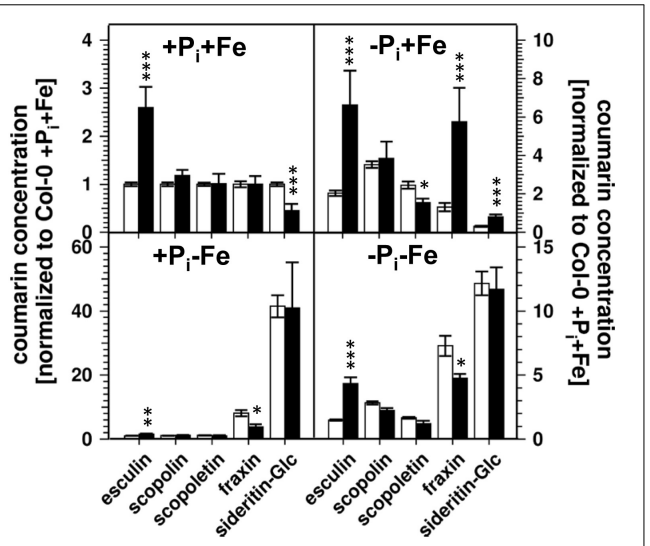

FIGURE 4 | Normalized coumarin concentrations in roots of WT (open bars) and *pho1* (solid bars) plants (normalized to Col-0 +P_i+Fe, average absolute amounts: esculin: 0.64 pmol mg^{-1} FW; scopolin: 702 pmol mg^{-1} FW; scopoletin: 16.8 pmol mg^{-1} FW; fraxin: 1.9 pmol mg^{-1} FW; sideritin glucoside: 3.6 pmol mg^{-1} FW). Plants were grown for 5 days on +P_i +Fe agar plates, transferred to the indicated conditions and allowed to grow for additional 6 days before harvest. +P_i: 500 μM, –P_i: 5 μM, +Fe: 50 μM, –Fe: no Fe added. Error bars indicate SE ($n \geq 8$). Significance analyses between *pho1* and Col0 were performed by Student's *t*-test (two tailed, equal variances): $^*P \leq 0.05$; $^{**}P \leq 0.01$; $^{***}P \leq 0.001$.

Effect of Fe Deficiency Response Regulator Mutants on Coumarin Profiles

The *fit* mutant, which is deficient in the expression of a regulator mediating many Fe deficiency responses, was previously shown to exhibit reduced root fluorescence after Fe deficiency compared to WT, indicating lower coumarin accumulation (Schmid et al., 2014). Our analysis showed that sideritin glucoside and fraxin levels were strongly reduced (50- and 20- fold, respectively) in these plants compared to WT after exposure to Fe limiting conditions (+P_i, −Fe), scopolin and scopoletin levels were diminished by 30%, whereas esculin levels were indistinguishable to WT (**Figure 5** and **Supplementary Figure S3**). Other Fe deficiency response regulators (bHLH104, BRUTUS, PYE) exerted a less pronounced influence on coumarin profiles. Changes in these mutants were most obvious for sideritin glucoside and fraxin. Compared to WT, sideritin glucoside levels were increased in roots of *pye* and *bts* after P_i (−P_i, +Fe) and combined deficiency (−P_i, −Fe), respectively, whereas decreased levels were measured for *bhlh104* after combined deficiency. The most pronounced difference to WT was observed for fraxin, showing more than twofold higher levels in *bts* roots after Fe (+P_i, −Fe) and combined deficiency (−P_i, −Fe).

In addition to compare coumarin content between mutants and WT under each condition, differences in the responsiveness to the treatments between mutants and WT were evaluated. Fe deficiency response regulator mutants exhibited several statistically significant (two way ANOVA $P \leq 0.05$) differences in the coumarin response to the treatments compared to WT plants (**Supplementary Figure S4**). In contrast to WT which responded to P_i deficiency in the presence of Fe (−P_i, +Fe) with decreased levels of sideritin glucoside, *fit* plants reacted with a slight (1.8-fold) accumulation of sideritin glucoside levels (P = 0.0009 compared to +P_i,+Fe conditions). P_i deficiency-induced esculin accumulation was absent in these plants. *Fit* plants were also impaired in the response to Fe deficiency with respect to sideritin glucoside and fraxin accumulation. This defect was more pronounced under P_i limiting conditions, where *fit* plants completely lost the ability to respond to Fe deficiency with sideritin glucoside accumulation, and even showed decreasing fraxin levels (−Fe/+Fe response at low P_i). Furthermore, the reduction of Fe deficiency-induced sideritin glucoside levels by concomitant P_i limitation observed in WT plants, was absent in *fit* plants (−P_i/+Pi response at −Fe). Under the same conditions, *fit* plants accumulated scopolin to a weaker extent than WT, and exhibited a decline in esculin levels. The P_i deficiency response in plants with impaired expression of *BRUTUS* affected the accumulation of scopoletin in the presence of Fe, whereas it was indistinguishable from WT in the absence of Fe. More differences in the response to Fe deficiency under P_i limiting condition could be observed. As such, *bts* plants exhibited a more pronounced accumulation of sideritin glucoside and fraxin, but no decline in esculin and scopoletin levels. Fe deficiency-induced fraxin accumulation was also enhanced under P_i sufficient conditions (16 *vs.* 7-fold, respectively, two way ANOVA $p = 2\ e^{-5}$). Plants

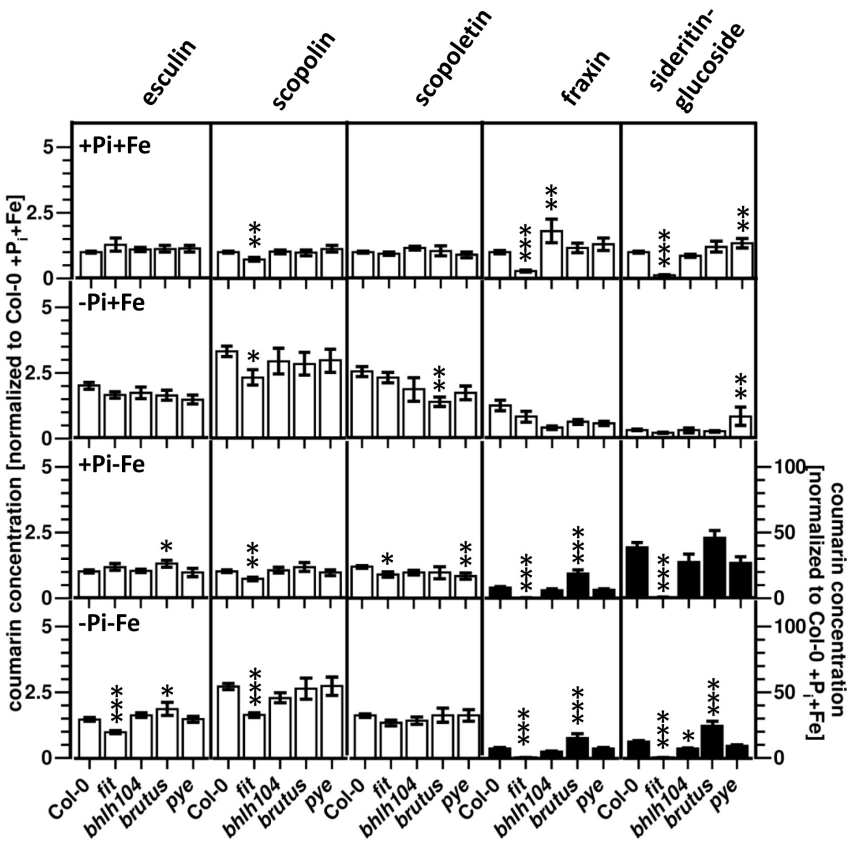

FIGURE 5 | Normalized coumarin concentrations in roots of WT, *fit*, *bhlh104*, *brutus*, and *pye* plants (normalized to Col-0 +P_i+Fe, average absolute amounts: esculin: 0.64 pmol mg^{-1} FW; scopolin: 702 pmol mg^{-1} FW; scopoletin: 16.8 pmol mg^{-1} FW; fraxin: 1.9 pmol mg^{-1} FW; sideritin glucoside: 3.6 pmol mg^{-1} FW). Plants were grown for 5 days on +P_i+Fe agar plates, transferred to the indicated conditions and allowed to grow for additional 6 days before harvest. +P_i: 500 μM, –P_i: 5 μM, +Fe: 50 μM, –Fe: no Fe added. Error bars indicate SE ($n \geq 8$). Significance analyses between mutants and Col0 were performed by Student's *t*-test (two tailed, equal variances): $^*P \leq 0.05$; $^{**}P \leq 0.01$; $^{***}P \leq 0.001$. Note that the values for fraxin and sideritin glucoside in the lower two panels (black bars) refer to the y-axis to the right.

deficient in the expression of *PYE* and *bHLH104* affected the response to Fe deficiency with respect to scopoletin accumulation at high P_i (*bhlh104*) and low P_i (*pye*) conditions. Additionally, Fe deficiency-induced sideritin accumulation was lower in *bhlh104* plants in the presence of low P_i. Both mutants strongly responded to P_i deficiency with decreasing fraxin levels, but only in the presence of Fe. *Pye* mutants also failed to accumulate esculin under these conditions. The P_i deficiency response in the absence of Fe was indistinguishable from WT for both mutants.

Effect of P_i Deficiency Response Regulator Mutants on Coumarin Profiles

Of all four mutants with impaired expression of P_i deficiency response regulators, the *phr1* mutant exhibited the most comprehensive changes in coumarin profiles compared to WT (**Figure 6** and **Supplementary Figure S3**). With respect to coumarin levels, *phr1* roots were most different to WT under P_i limiting conditions, in the presence as well as in the absence of Fe. In the presence of Fe, *phr1* plants exposed to P_i limitation (−P_i, +Fe) exhibited higher levels of sideritin glucoside and fraxin, and lower levels of scopoletin compared to WT. In the additional absence of Fe (−P_i, −Fe), sideritin glucoside levels were elevated, while scopolin and fraxin levels were lower. Fraxin as well as esculin concentrations in *phr1* roots were lower when plants were grown in P_i and Fe sufficient conditions (+P_i, +Fe), whereas scopoletin content was increased. There were no statistically significant ($P \leq 0.05$) changes in coumarin levels between *phr1* and WT roots in conditions of Fe deficiency in the presence of P_i (+P_i, −Fe). The *spx1* mutant exhibited opposite effects compared to *phr1* with respect to the levels of fraxin under nutrient sufficient conditions (+P_i, +Fe) as well as to the levels of scopoletin under P_i limiting conditions in the presence of Fe (−P_i, +Fe). Additionally, aberrant *spx1* expression led to increased levels of esculin, scopolin, and fraxin in roots exposed to Fe deficiency (+P_i, −Fe) and of scopoletin after exposure to combined deficiency (−P_i, −Fe). In *bhlh32* plants, only the concentrations of the glucosides of the catechol type coumarins were altered, showing elevated levels of sideritin glucoside after Fe deficiency at high P_i (+P_i, −Fe), and of fraxin after P_i deficiency in the presence of Fe (−P_i, +Fe). Aberrant expression of the *phr1* homologue *phl1* only mildly affected

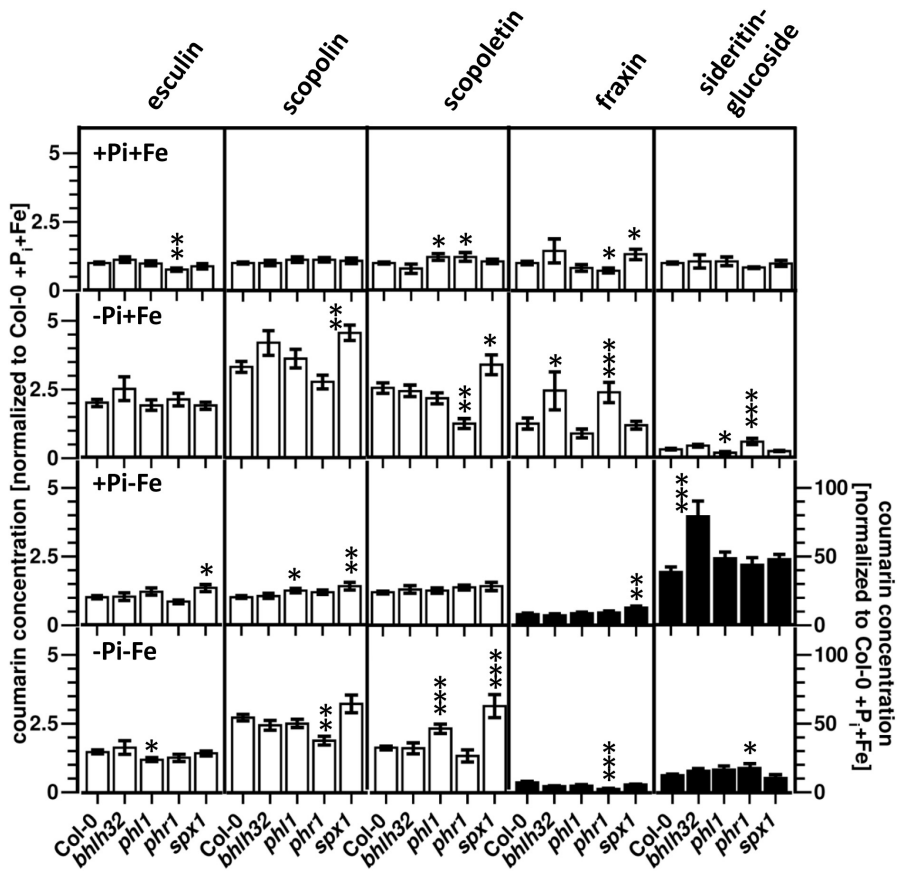

FIGURE 6 | Normalized coumarin concentrations in roots of WT, *bhlh32*, *phl1*, *phr1*, and *spx1* plants (normalized to Col-0 +P_i+Fe, average absolute amounts: esculin: 0.64 pmol mg^{-1} FW; scopolin: 702 pmol mg^{-1} FW; scopoletin: 16.8 pmol mg^{-1} FW; fraxin: 1.9 pmol mg^{-1} FW; sideritin glucoside: 3.6 pmol mg^{-1} FW). Plants were grown for 5 days on +P_i+Fe agar plates, transferred to the indicated conditions and allowed to grow for additional 6 days before harvest. +P_i: 500 μM, –P_i: 5 μM, +Fe: 50 μM, –Fe: no Fe added. Error bars indicate SE ($n \geq 8$). Significance analyses between mutants and Col0 were performed by Student's *t*-test (two tailed, equal variances): $^*P \leq 0.05$; $^{**}P \leq 0.01$; $^{***}P \leq 0.001$. Note that the values for fraxin and sideritin glucoside in the lower two panels (black bars) refer to the y-axis to the right.

coumarin profiles. These were most pronounced in roots exposed to combined Fe and P_i deficiencies (−P_i, −Fe), and, interestingly, affected coumarins which were not affected in the *phr1* mutant, such as esculin and scopoletin.

Consistent with the changes in coumarin profiles, the coumarin response of *phr1* was also most different compared to WT for −P_i treatments, in the absence as well as in the presence of Fe (**Supplementary Figure S4**). As such, the P_i deficiency-induced decrease in sideritin glucoside levels observed in WT roots was less pronounced in *phr1* plants, but only in the presence of Fe. The effect of P_i deficiency in *phr1* plants on fraxin concentration depended on Fe availability. In the presence of Fe, P_i deficiency induced fraxin accumulation, whereas a reduction in fraxin levels was observed in the absence of Fe. Scopoletin levels, which were induced by P_i limitation in WT roots, were not affected in *phr1*. The Fe deficiency response of *phr1* in the presence of high Pi was indistinguishable from WT, but in P_i depleted conditions, the Fe deficiency-induced reduction in scopoletin levels was less pronounced. Also the response with respect to the accumulation of sideritin glucoside was lower (37-fold in WT vs. 29-fold in *phr1*). Compared to WT, low P_i treatment induced stronger scopolin and scopoletin accumulation in *spx1* in the presence and in the absence of Fe, respectively. However, differences in the −P_i response with respect to esculin and fraxin were only observed in the absence of Fe. The Fe deficiency response was also affected in *spx1*, but only in the presence of high P_i. Here, induction of esculin levels was detected, which was not observed in WT, and fraxin accumulation was more pronounced. Interestingly, the majority of effects of plants with aberrant expression of the P_i deficiency response regulator *bHLH32* were detected after Fe deficiency. In the presence of high P_i, Fe deficiency-induced sideritin glucoside accumulation was twice as strong in *bhlh32* plants compared to WT, whereas in low P_i, a stronger reduction and weaker induction of scopolin and fraxin levels, respectively, was observed. Compared to WT, changes in the P_i deficiency response in *bhlh32* were only detectable in the absence of Fe, there only affecting sideritin glucoside levels. For *phl1*, different responses were observed for P_i deficiency-induced changes in the absence of Fe, exhibiting a lack of esculin accumulation and stronger

induction of scopoletin levels, and for Fe deficiency-induced changes in low P_i conditions, showing unaltered scopoletin levels.

DISCUSSION

The impact of Fe-deficiency on root coumarin profiles has been well-established in recent years (Fourcroy et al., 2014, 2016; Schmid et al., 2014; Schmidt et al., 2014; Sisó-Terraza et al., 2016; Rajniak et al., 2018; Siwinska et al., 2018; Tsai et al., 2018). In order to cope with iron limiting conditions, Arabidopsis roots strongly accumulate coumarin glucosides, especially catechol-type coumarins glucosides, which are assumed to support Fe chelation and ferric ion reduction in order to facilitate Fe uptake after coumarin aglycones have been exuded to the rhizosphere. We recently showed an opposite effect of P_i deficiency on coumarin profiles, resulting in reduced exudation and reduced accumulation especially of catechol type coumarins and their glucosides (Ziegler et al., 2016). These observations prompted us to investigate coumarin profiles in Arabidopsis roots exposed to P_i, Fe, and combined P_i and Fe deficiencies. Our results show that P_i deficiency resulted in lower sideritin glucoside and higher scopolin, scopoletin, and esculin levels. Furthermore, Fe deficiency-induced sideritin glucoside accumulation is dampened at low P_i conditions ($-P_i$, $-$Fe), while scopolin, scopoletin, and esculin levels are slightly higher compared to Fe deficiency in the presence of high P_i ($+P_i$, $-$Fe). These results indicate an antagonistic cross talk between Fe and P_i deficiency responses with respect to coumarin accumulation, which is most evident considering catechol-type coumarins. This cross-talk could be mediated by differences in the formation of Fe–P complexes, which depend on the concentrations of Fe and P_i supplied in the medium. As such, high P_i availability could lead to a relative decrease in available Fe, resulting in the accumulation of catechol-type coumarins. On the other hand, low P_i availability could lead to a relative increase in available Fe, which would result in decreased levels of catechol-type coumarins. These scenarios might apply to Fe sufficient conditions, in which relatively more iron would be available at low compared to high P_i concentrations in the medium, however, Fe availability in our Fe deficiency conditions with complete omission of any Fe sources should be independent of the external P_i concentration. Indeed, it was shown that P_i deficiency only led to increased iron concentrations in roots when plants were exposed to Fe sufficient conditions, whereas iron accumulation was not observed when plants were grown in the absence of Fe (Ward et al., 2008; Muller et al., 2015). Furthermore, if altered root Fe status because of changes in Fe–P complex formation would be the reason for P dependent changes in coumarin profiles, the levels catechol-type coumarins should be negatively correlated with P_i levels. However, compared to WT roots, sideritin glucoside and fraxin levels are lower in *pho1* roots exposed to nutrient sufficient and Fe deficient conditions, respectively, although P_i concentration is twice as high as in WT roots. Based on these results, we conclude that P dependent modifications of coumarin profiles are not solely due to altered Fe availability, and that P_i availability directly interferes with Fe deficiency-induced accumulation of catechol type coumarins.

The biosynthesis of coumarins proceeds via the generation of scopoletin/scopolin through the action of feruloyl CoA hydroxylase 1 (F6′H1), and subsequent hydroxylation reactions to fraxetin/fraxin and sideritin/sideritin glucoside (Kai et al., 2008; Rajniak et al., 2018; Siwinska et al., 2018; Tsai et al., 2018). Thus, P_i deficiency-induced accumulation of early coumarin intermediates, such as scopoletin/scopolin and esculin could be either due to increased biosynthesis, or to reduced conversion to coumarins exhibiting more elaborate hydroxylation patterns, or both. In most large scale gene expression studies, *F6′H1* mRNA levels were not altered in roots exposed to P_i deficiency (Bustos et al., 2010; Puga et al., 2014; Hoehenwarter et al., 2016; Mora-Macias et al., 2017). Instead, all studies reported strongly reduced expression of the gene At3G12900 (Bustos et al., 2010; Puga et al., 2014; Li and Lan, 2015; Hoehenwarter et al., 2016). This gene, whose expression and protein level are highly induced by Fe-deficiency, was recently characterized as scopoletin 8 hydroxylase (S8H), catalyzing the conversion of scopoletin to fraxetin (Rajniak et al., 2018; Siwinska et al., 2018; Tsai et al., 2018). We therefore assume that P_i deficiency-induced accumulation of scopolin and scopoletin is due to reduced conversion to downstream products. The increase in esculin might be a consequence of scopolin/scopoletin demethylation, although it is not clear yet, whether esculetin/esculin are actually derived from scopolin/scopoletin, or from caffeoyl CoA by a F6′H1-like reaction. Despite the reported P_i deficiency-induced reduction in *S8H* mRNA levels, our coumarin profiling did not show P_i deficiency-induced alterations in fraxin levels, neither in the presence nor in the absence of Fe. An explanation for this discrepancy could be that the subsequent hydroxylation step converting fraxetin/fraxin to sideritin/sideritin glucoside is impaired to a similar extent as the S8H reaction, which would lead to the observed constant fraxin level. Indeed, gene expression data generated in our group revealed a strong downregulation of the gene At4G31940 by P_i deficiency. At4G31940 encodes the P450 dependent monooxygenase CYP82C4 (Hoehenwarter et al., 2016). Reduced *CYP82C4* mRNA levels by P_i deficiency were also observed by other groups (Bustos et al., 2010; Li and Lan, 2015). Similar to *S8H* mRNA levels, *CYP82C4* mRNA levels strongly increase after Fe deficiency (Colangelo and Guerinot, 2004; Long et al., 2010; Lan et al., 2011; Rajniak et al., 2018). CYP82C4 protein was recently shown to catalyze the hydroxylation of fraxetin at position 5, yielding sideritin as product (Rajniak et al., 2018). Thus, the coumarin profiling data presented in this study and gene expression data from several studies suggest a P_i deficiency-induced negative regulation of the hydroxylation steps downstream of scopoletin/scopolin and fraxetin/fraxin, leading to reduced sideritin glucoside and increased scopoletin, scopolin, and esculin levels.

The analysis of mutants impaired in the expression of P_i and Fe deficiency response regulators revealed specificity of several transcription factors with respect to the nutrient conditions and to the biosynthesis of distinct coumarins, mainly of catechol type coumarins. The RING E3 ligase BRUTUS, known to negatively regulate Fe deficiency responses (Kobayashi et al.,

2013; Selote et al., 2015; Zhang et al., 2015), also negatively regulates the accumulation of fraxin and sideritin glucoside, as suggested by the increased accumulation of both compounds in Fe depleted conditions in the *bts* mutant. Interestingly, Fe deficiency-induced hyper-accumulation of sideritin glucoside was only detectable in low P_i conditions. Thus, the reduction of Fe deficiency-induced sideritin glucoside levels by simultaneous P_i deficiency is less pronounced in *bts* plants compared to WT plants, indicating that the attenuation of Fe deficiency-induced sideritin glucoside accumulation by low P_i is mediated at least partially by BRUTUS. Whereas compared to WT, sideritin glucoside levels are elevated in roots of *bts*, they are reduced in *bhlh104* roots under conditions of combined P_i and Fe deficiency. This suggests that the proposed network consisting of the negative Fe deficiency response regulator BRUTUS, which targets bHLH104 (Selote et al., 2015), a positive regulator, is involved in the generation of coumarin profiles. However, the role of bHLH104 seems to be more complex, since it also affects fraxin levels under nutrient sufficient conditions. It was shown, that bHLH104 together with bHLH34 regulates the expression of PYE, as well as of bHLH38/39/100/101 transcription factors (Li et al., 2016), which contribute to FIT action by the formation of heterodimers (Colangelo and Guerinot, 2004; Yuan et al., 2008; Wang et al., 2013). The impact of the *fit* mutant is more pronounced compared to the *pye* mutant, suggesting that the FIT network represents the downstream target for BRUTUS and bHLH104 in the generation of coumarin profiles rather than PYE. FIT positively regulates mainly the accumulation of the catechol type coumarins sideritin glucoside and fraxin, which is corroborated by the absence of Fe deficiency-induced accumulation of *S8H* transcripts in *fit* plants (Colangelo and Guerinot, 2004). Interestingly, although FIT is known to regulate F6′H1 expression (Colangelo and Guerinot, 2004; Schmid et al., 2014), *fit* mutants still produce appreciable levels of scopolin, scopoletin, and esculin, indicating that other factors are involved in the control of constitutive levels of coumarins upstream of fraxin.

Of all tested P_i deficiency response regulators, bHLH32 and SPX1 seem to play a role in the generation of Fe deficiency-induced coumarin profiles, mainly in the presence of high P_i. BHLH32 was identified as negative regulator of several P_i starvation responses (Chen et al., 2007). Our data showing increased sideritin glucoside levels in *bhlh32* mutants imply a role of this transcription factor also in the negative regulation of the biosynthesis of catechol type coumarins during Fe deficiency. SPX1, which interferes with the induction of P_i starvation responses (Puga et al., 2014; Wang et al., 2014), also regulates Fe deficiency-induced coumarin biosynthesis at high P_i, as seen by the increased fraxin, esculin, and scopolin levels in *spx1* mutants. It is interesting that *phr1* plants do not show alteration of coumarin profiles in Fe depleted roots at high P_i, since SPX1 was shown to exert its role by binding to PHR1 preventing its binding to the promoters of Pi starvation responsive genes (Puga et al., 2014; Wang et al., 2014). Possibly, SPX1 has additional targets, which are required to initialize the Fe deficiency-induced coumarin response at high P_i availability. However, the coumarin profiles suggest that P_i deficiency-induced changes in coumarin biosynthesis are mediated by PHR1, and to minor extent, by PHL1. Higher sideritin glucoside and fraxin levels in *phr1* plants grown on low P_i/high Fe media indicate that downregulation of catechol type coumarin biosynthesis by P_i deficiency is controlled by PHR1. In low P_i/Fe depleted media, *phr1* plants show increased sideritin glucoside, but decreased fraxin levels, which might be due to the loss of suppression of fraxin conversion suggesting that the conversion of fraxin to sideritin glucoside is more strongly controlled by PHR1 than the S8H reaction. It was already shown that modulation of expression of other Fe deficiency responsive genes by P_i starvation, such as *FERRIC REDUCTASE OXIDASE FRO3*, *IRON REGULATED TRANSPROTER IRT1*, IRT2, *NICOTIANAMINE SYNTHASE NAS1*, and *FRO6* was PHR1 and PHL1 dependent (Bustos et al., 2010). However, transcriptome data did not reveal PHR1 dependent downregulation of S8H and CYP82C4 by P_i deficiency (Bustos et al., 2010).

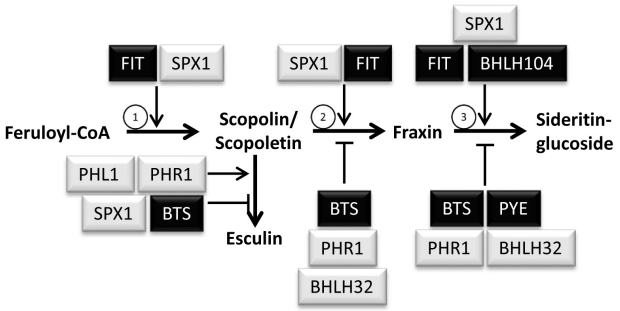

FIGURE 7 | Tentative model depicting possible mode and site of action of P_i and Fe deficiency regulators in the regulation of coumarin profiles. Note that the model was drafted according to the coumarin profiling data generated in this study and is not supposed to indicate transcriptional control of individual biosynthetic steps. Regulators of Fe and P_i deficiency responses are shown in black and gray background, respectively. Encircled numbers indicate the enzymes catalyzing the respective step: (1) F6′H1; (2) S8H; (3) CYP82C4.

Taken together, several P_i and Fe deficiency response regulators are involved in the generation of Fe and P_i dependent coumarin profiles. A model was drafted summarizing possible modes and sites of action for each regulator irrespective of the growth condition (**Figure 7**). In this model, it was taken into account that changes in the level of coumarin compounds could be either due to changes in their biosynthesis, or to changes in their turnover, or to changes in the activity of the whole pathway.

According to this model, BRUTUS, PHR1, and bHLH32 negatively regulate both hydroxylation steps downstream of scopoletin/scopolin, whereas PYE seems to negatively impact solely the last hydroxylation reaction from fraxin to sideritin glucoside. The decreased levels of fraxin in *phr1* under nutrient sufficient conditions as well as under combined P_i and Fe deficiency was interpreted to be a consequence of higher fraxin to sideritin glucoside turnover. BHLH104, which is known to regulate several Fe starvation responses in an opposing way compared to BRUTUS, was placed in the model as a positive regulator of the conversion from fraxin to sideritin glucoside, based on decreased sideritin glucoside levels under conditions

of combined P_i and Fe deficiency in *bhlh104* mutants. Increased fraxin levels observed in *bhlh104* in nutrient sufficient conditions, were interpreted as a consequence of impaired fraxin turnover to sideritin glucoside. FIT promotes both hydroxylation reactions leading to the generation of fraxin and sideritin glucoside and it also positively regulates the committed step in the pathway, the conversion of feruloyl CoA to scopoletin. Accumulation of scopoletin/scopolin in *phr1* and *phl1* also indicates positive regulation of this step by PHR1 and PHL1. However, since esculin concentrations are also reduced in both mutants, we rather assume that PHR1 and PHL1 might positively regulate the generation of esculin, which, if missing, indirectly might lead to the accumulation of scopoletin/scopolin. This is in contrast to the *bts* mutant, which exhibited increased esculin and decreased scopoletin levels, and which was therefore placed in the model as a negative regulator of esculin generation. The coumarin profiles in roots of *spx1* posed the major problem to fit this negative regulator of P_i deficiency responses into the model. Increased scopolin/scopoletin as well as esculin concentrations in *spx1* were interpreted as positive and negative regulation of scopolin/scopoletin and esculin generation, respectively, by SPX1, which would match the antagonistic interaction between PHR1 or PHL1 and SPX1. In contrast, if increased fraxin concentrations in *spx1* would be the consequence of impaired negative regulation of fraxin biosynthesis by SPX1, both SPX1 as well as PHR1 would be negative regulators of the same step. In order to preserve the antagonistic roles of both regulators, we decided to place SPX1 as a positive regulator of fraxin to sideritin glucoside conversion. However, we want to emphasize, that it is currently unknown whether the regulations shown in the model are due to transcriptional control of the respective genes. Only FIT was shown to regulate mRNAs levels for F6′H1, S8H, and CYP82C4 (Colangelo and Guerinot, 2004). As such, in the future, the elucidation of the molecular mechanism underlying the differential control of catechol-type coumarin biosynthesis will be interesting in order to see whether P_i and Fe deficiency response regulators such as PHR1 and FIT independently inactivate or activate the transcription of respective genes. The presence of the P_i deficiency responsive *PHR1 Binding site* (*P1BS*) and the Fe deficiency responsive IDRS *cis*-acting element in the AtFER1 promoter suggests that transcriptional control of this gene by Fe as well as by P_i deficiency is mediated by binding of Fe and P_i deficiency response regulators to different sites of the promoter (Bournier et al., 2013). It remains to be elucidated whether this also applies to the differential regulation of coumarin biosynthesis genes, or, alternatively, whether P_i and Fe deficiency response regulators might interact on the protein level, thus interfering with each other in the activation of the promoters.

AVAILABILITY OF DATA AND MATERIAL

Metabolite profiling data have been deposited to the EMBL-EBI MetaboLights database (doi: 10.1093/nar/gks1004. PubMed PMID: 23109552) with the identifier MTBLS831.

The complete **dataset** can be accessed here https://www.ebi.ac.uk/metabolights/MTBLS831.

AUTHOR CONTRIBUTIONS

RC designed the study, performed most of the measurements and biological experiments, and co-wrote the manuscript. JZ designed the study, supported the measurements, and wrote the manuscript. SA designed the study and co-wrote the manuscript. All authors have read and approved the final version of the manuscript.

FUNDING

This work was supported by core funding to the Leibniz Institute of Plant Biochemistry from the state of Saxony-Anhalt and the Federal Republic of Germany. RC was supported by the BRAVE scholarship program funded by the ERASMUS MUNDUS Action 2 program of the European Union.

ACKNOWLEDGMENTS

We thank Birgit Ortel and Pascal Rudewig for technical assistance.

SUPPLEMENTARY MATERIAL

The Supplementary Material for this article can be found online at: https://www.frontiersin.org/articles/10.3389/fpls.2019.00113/full#supplementary-material

FIGURE S1 | Chemical structures of coumarins measured in this study. [a]Note that the position of the glucoside (R5, R7, or R8) in sideritin glucoside has not been confirmed yet by NMR studies.

FIGURE S2 | (A) Pictures of WT and mutant seedlings 6 days after transfer from $+P_i$+Fe (5 days) to $+P_i$+Fe. The height of each panel corresponds to 7 cm. $+P_i$: 500 μM; +Fe: 50 μM. **(B)** Pictures of WT and mutant seedlings 6 days after transfer from $+P_i$+Fe (5 days) to $-P_i$+Fe. The height of each panel corresponds to 7 cm. $+P_i$: 500 μM; +Fe: 50 μM; $-P_i$: 5 μM. **(C)** Pictures of WT and mutant seedlings 6 days after transfer from $+P_i$+Fe (5 days) to $+P_i$−Fe. The height of each panel corresponds to 7 cm. $+P_i$: 500 μM; +Fe: 50 μM; −Fe: no Fe added. **(D)** Pictures of WT and mutant seedlings 6 days after transfer from $+P_i$+Fe (5 days) to $-P_i$−Fe. The height of each panel corresponds to 7 cm. $+P_i$: 500 μM; +Fe: 50 μM; $-P_i$: 5 μM; −Fe: no Fe added.

FIGURE S3 | Coumarin concentrations in roots of mutants relative to Col-0 (Col-0 set to one). The fold changes compared to Col-0 are color coded according to the scale bar. Gray squares indicate no difference to Col0-0 at $P \leq 0.05$ (Student's *t*-test, paired, two sided).

FIGURE S4 | Coumarin response **(A)** upon P_i starvation in the presence or absence of Fe, and **(B)** upon Fe deficiency in the presence of high (500 μM) or low (5 μM) P_i. The fold changes compared to the respective nutrient sufficient conditions are color coded. For Col-0, only changes at $P \leq 0.05$ (Student's *t*-test, two tailed equal variance) are color coded. For the mutants, the fold changes compared to the respective nutrient sufficient conditions are color coded, if the response was different compared to the WT response at $P \leq 0.05$ (two way ANOVA). Gray indicates no differences.

TABLE S1 | Primers used for genotyping.

TABLE S2 | MS parameters for MRM transitions.

DATASET S1 | Raw data of all the analysis presented in this study.

REFERENCES

Bournier, M., Tissot, N., Mari, S., Boucherez, J., Lacombe, E., Briat, J. F., et al. (2013). Arabidopsis ferritin 1 (AtFer1) gene regulation by the phosphate starvation response 1 (AtPHR1) transcription factor reveals a direct molecular link between iron and phosphate homeostasis. *J. Biol. Chem.* 288, 22670–22680. doi: 10.1074/jbc.M113.482281

Briat, J.-F., Rouached, H., Tissot, N., Gaymard, F., and Dubos, C. (2015). Integration of P, S, Fe and Zn nutrition signals in *Arabidopsis thaliana*: potential involvement of Phosphate Starvation Response 1 (PHR1). *Front. Plant Sci.* 6:290. doi: 10.3389/fpls.2015.00290

Bustos, R., Castrillo, G., Linhares, F., Puga, M. I., Rubio, V., Perez-Perez, J., et al. (2010). A central regulatory system largely controls transcriptional activation and repression responses to phosphate starvation in Arabidopsis. *PLoS Genet.* 6:e1001102. doi: 10.1371/journal.pgen.1001102

Chen, Z. H., Nimmo, G. A., Jenkins, G. I., and Nimmo, H. G. (2007). BHLH32 modulates several biochemical and morphological processes that respond to Pi starvation in Arabidopsis. *Biochem. J.* 405, 191–198. doi: 10.1042/BJ20070102

Colangelo, E. P., and Guerinot, M. L. (2004). The essential basic helix-loop-helix protein FIT1 is required for the iron deficiency response. *Plant Cell* 16, 3400–3412. doi: 10.1105/tpc.104.024315

Fourcroy, P., Siso-Terraza, P., Sudre, D., Saviron, M., Reyt, G., Gaymard, F., et al. (2014). Involvement of the ABCG37 transporter in secretion of scopoletin and derivatives by Arabidopsis roots in response to iron deficiency. *New Phytol.* 201, 155–167. doi: 10.1111/nph.12471

Fourcroy, P., Tissot, N., Gaymard, F., Briat, J. F., and Dubos, C. (2016). Facilitated Fe nutrition by phenolic compounds excreted by the Arabidopsis ABCG37/PDR9 transporter requires the IRT1/FRO2 high-affinity root Fe(2+) transport system. *Mol. Plant* 9, 485–488. doi: 10.1016/j.molp.2015.09.010

Hamburger, D., Rezzonico, E., Macdonald-Comber Petetot, J., Somerville, C., and Poirier, Y. (2002). Identification and characterization of the Arabidopsis PHO1 gene involved in phosphate loading to the xylem. *Plant Cell* 14, 889–902. doi: 10.1105/tpc.000745

Hoehenwarter, W., Monchgesang, S., Neumann, S., Majovsky, P., Abel, S., and Muller, J. (2016). Comparative expression profiling reveals a role of the root apoplast in local phosphate response. *BMC Plant Biol.* 16:106. doi: 10.1186/s12870-016-0790-8

Kai, K., Mizutani, M., Kawamura, N., Yamamoto, R., Tamai, M., Yamaguchi, H., et al. (2008). Scopoletin is biosynthesized via ortho-hydroxylation of feruloyl CoA by a 2-oxoglutarate-dependent dioxygenase in *Arabidopsis thaliana*. *Plant J.* 55, 989–999. doi: 10.1111/j.1365-313X.2008.03568.x

Kobayashi, T., Nagasaka, S., Senoura, T., Itai, R. N., Nakanishi, H., and Nishizawa, N. K. (2013). Iron-binding haemerythrin RING ubiquitin ligases regulate plant iron responses and accumulation. *Nat. Commun.* 4:2792. doi: 10.1038/ncomms3792

Lan, P., Li, W., Wen, T. N., Shiau, J. Y., Wu, Y. C., Lin, W., et al. (2011). iTRAQ protein profile analysis of Arabidopsis roots reveals new aspects critical for iron homeostasis. *Plant Physiol.* 155, 821–834. doi: 10.1104/pp.110.169508

Li, W., and Lan, P. (2015). Genome-wide analysis of overlapping genes regulated by iron deficiency and phosphate starvation reveals new interactions in Arabidopsis roots. *BMC Res. Notes* 8:555. doi: 10.1186/s13104-015-1524-y

Li, X., Zhang, H., Ai, Q., Liang, G., and Yu, D. (2016). Two bHLH transcription factors, bHLH34 and bHLH104, regulate iron homeostasis in *Arabidopsis thaliana*. *Plant Physiol.* 170, 2478–2493. doi: 10.1104/pp.15.01827

Long, T. A., Tsukagoshi, H., Busch, W., Lahner, B., Salt, D. E., and Benfey, P. N. (2010). The bHLH transcription factor POPEYE regulates response to iron deficiency in Arabidopsis roots. *Plant Cell* 22, 2219–2236. doi: 10.1105/tpc.110.074096

Mora-Macias, J., Ojeda-Rivera, J. O., Gutierrez-Alanis, D., Yong-Villalobos, L., Oropeza-Aburto, A., Raya-Gonzalez, J., et al. (2017). Malate-dependent Fe accumulation is a critical checkpoint in the root developmental response to low phosphate. *Proc. Natl. Acad. Sci. U.S.A.* 114, E3563–E3572. doi: 10.1073/pnas.1701952114

Muller, J., Toev, T., Heisters, M., Teller, J., Moore, K. L., Hause, G., et al. (2015). Iron-dependent callose deposition adjusts root meristem maintenance to phosphate availability. *Dev. Cell* 33, 216–230. doi: 10.1016/j.devcel.2015.02.007

Poirier, Y., Thoma, S., Somerville, C., and Schiefelbein, J. (1991). A Mutant of Arabidopsis deficient in xylem loading of phosphate. *Plant Physiol.* 97, 1087–1093. doi: 10.1104/pp.97.3.1087

Puga, M. I., Mateos, I., Charukesi, R., Wang, Z., Franco-Zorrilla, J. M., De Lorenzo, L., et al. (2014). SPX1 is a phosphate-dependent inhibitor of Phosphate Starvation Response 1 in Arabidopsis. *Proc. Natl. Acad. Sci. U.S.A.* 111, 14947–14952. doi: 10.1073/pnas.1404654111

Rajniak, J., Giehl, R. F. H., Chang, E., Murgia, I., Von Wiren, N., and Sattely, E. S. (2018). Biosynthesis of redox-active metabolites in response to iron deficiency in plants. *Nat. Chem. Biol.* 14, 442–450. doi: 10.1038/s41589-018-0019-2

Rodríguez-Celma, J., Lin, W.-D., Fu, G.-M., Abadía, J., López-Millán, A.-F., and Schmidt, W. (2013). Mutually exclusive alterations in secondary metabolism are critical for the uptake of insoluble iron compounds by Arabidopsis and *Medicago truncatula*. *Plant Physiol.* 162, 1473–1485. doi: 10.1104/pp.113.220426

Rouached, H., Stefanovic, A., Secco, D., Bulak Arpat, A., Gout, E., Bligny, R., et al. (2011). Uncoupling phosphate deficiency from its major effects on growth and transcriptome via PHO1 expression in Arabidopsis. *Plant J.* 65, 557–570. doi: 10.1111/j.1365-313X.2010.04442.x

Rubio, V., Linhares, F., Solano, R., Martin, A. C., Iglesias, J., Leyva, A., et al. (2001). A conserved MYB transcription factor involved in phosphate starvation signaling both in vascular plants and in unicellular algae. *Genes Dev.* 15, 2122–2133. doi: 10.1101/gad.204401

Schmid, N. B., Giehl, R. F. H., Döll, S., Mock, H.-P., Strehmel, N., Scheel, D., et al. (2014). Feruloyl-CoA 6′-Hydroxylase1-Dependent coumarins mediate iron acquisition from alkaline substrates in Arabidopsis. *Plant Physiol.* 164, 160–172. doi: 10.1104/pp.113.228544

Schmidt, H., Gunther, C., Weber, M., Sporlein, C., Loscher, S., Bottcher, C., et al. (2014). Metabolome analysis of *Arabidopsis thaliana* roots identifies a key metabolic pathway for iron acquisition. *PLoS One* 9:e102444. doi: 10.1371/journal.pone.0102444

Selote, D., Samira, R., Matthiadis, A., Gillikin, J. W., and Long, T. A. (2015). Iron-binding E3 ligase mediates iron response in plants by targeting basic helix-loop-helix transcription factors. *Plant Physiol.* 167, 273–286. doi: 10.1104/pp.114.250837

Shimizu, B. (2014). 2-Oxoglutarate-dependent dioxygenases in the biosynthesis of simple coumarins. *Front. Plant Sci.* 5:549. doi: 10.3389/fpls.2014.00549

Sisó-Terraza, P., Luis-Villarroya, A., Fourcroy, P., Briat, J.-F., Abadía, A., Gaymard, F., et al. (2016). Accumulation and secretion of coumarinolignans and other coumarins in *Arabidopsis thaliana* roots in response to iron deficiency at high pH. *Front. Plant Sci.* 7:1711. doi: 10.3389/fpls.2016.01711

Siwinska, J., Siatkowska, K., Olry, A., Grosjean, J., Hehn, A., Bourgaud, F., et al. (2018). Scopoletin 8-hydroxylase: a novel enzyme involved in coumarin biosynthesis and iron-deficiency responses in Arabidopsis. *J. Exp. Bot.* 69, 1735–1748. doi: 10.1093/jxb/ery005

Tsai, H. H., Rodriguez-Celma, J., Lan, P., Wu, Y. C., Velez-Bermudez, I. C., and Schmidt, W. (2018). Scopoletin 8-Hydroxylase-Mediated fraxetin production is crucial for iron mobilization. *Plant Physiol.* 177, 194–207. doi: 10.1104/pp.18.00178

Wang, N., Cui, Y., Liu, Y., Fan, H., Du, J., Huang, Z., et al. (2013). Requirement and functional redundancy of Ib subgroup bHLH proteins for iron deficiency responses and uptake in *Arabidopsis thaliana*. *Mol. Plant* 6, 503–513. doi: 10.1093/mp/sss089

Wang, Z., Ruan, W., Shi, J., Zhang, L., Xiang, D., Yang, C., et al. (2014). Rice SPX1 and SPX2 inhibit phosphate starvation responses through interacting with PHR2 in a phosphate-dependent manner. *Proc. Natl. Acad. Sci. U.S.A.* 111, 14953–14958. doi: 10.1073/pnas.1404680111

Ward, J. T., Lahner, B., Yakubova, E., Salt, D. E., and Raghothama, K. G. (2008). The effect of iron on the primary root elongation of Arabidopsis during phosphate deficiency. *Plant Physiol.* 147, 1181–1191. doi: 10.1104/pp.108.118562

Wege, S., Khan, G. A., Jung, J. Y., Vogiatzaki, E., Pradervand, S., Aller, I., et al. (2016). The EXS domain of PHO1 participates in the response of shoots to phosphate deficiency via a root-to-shoot signal. *Plant Physiol.* 170, 385–400. doi: 10.1104/pp.15.00975

Yuan, Y., Wu, H., Wang, N., Li, J., Zhao, W., Du, J., et al. (2008). FIT interacts with AtbHLH38 and AtbHLH39 in regulating iron uptake gene expression for iron homeostasis in Arabidopsis. *Cell Res.* 18, 385–397. doi: 10.1038/cr.2008.26

Zhang, J., Liu, B., Li, M., Feng, D., Jin, H., Wang, P., et al. (2015). The bHLH transcription factor bHLH104 interacts with IAA-LEUCINE RESISTANT3 and modulates iron homeostasis in Arabidopsis. *Plant Cell* 27, 787–805. doi: 10.1105/tpc.114.132704

Ziegler, J., Schmidt, S., Chutia, R., Muller, J., Bottcher, C., Strehmel, N., et al. (2016). Non-targeted profiling of semi-polar metabolites in Arabidopsis root exudates uncovers a role for coumarin secretion and lignification during the local response to phosphate limitation. *J. Exp. Bot.* 67, 1421–1432. doi: 10.1093/jxb/erv539

Ziegler, J., Schmidt, S., Strehmel, N., Scheel, D., and Abel, S. (2017). Arabidopsis transporter ABCG37/PDR9 contributes primarily highly oxygenated coumarins to root exudation. *Sci. Rep.* 7:3704. doi: 10.1038/s41598-017-03250-6

Conflict of Interest Statement: The authors declare that the research was conducted in the absence of any commercial or financial relationships that could be construed as a potential conflict of interest.

frontiers in Plant Science

MINI REVIEW
published: 13 February 2019
doi: 10.3389/fpls.2019.00098

Hemerythrin E3 Ubiquitin Ligases as Negative Regulators of Iron Homeostasis in Plants

*Jorge Rodríguez-Celma[1,2], Hsuan Chou[3], Takanori Kobayashi[4], Terri A. Long[3] and Janneke Balk[1,2]**

[1] Department of Biological Chemistry, John Innes Centre, Norwich, United Kingdom, [2] School of Biological Sciences, University of East Anglia, Norwich, United Kingdom, [3] Department of Plant and Microbial Biology, North Carolina State University, Raleigh, NC, United States, [4] Research Institute for Bioresources and Biotechnology, Ishikawa Prefectural University, Nonoichi, Japan

Iron (Fe) is an essential nutrient for plants, but at the same time its redox properties can make it a dangerous toxin inside living cells. Homeostasis between uptake, use and storage of Fe must be maintained at all times. A small family of unique hemerythrin E3 ubiquitin ligases found in green algae and plants play an important role in avoiding toxic Fe overload, acting as negative regulators of Fe homeostasis. Protein interaction data showed that they target specific transcription factors for degradation by the 26S proteasome. It is thought that the activity of the E3 ubiquitin ligases is controlled by Fe binding to the N-terminal hemerythrin motifs. Here, we discuss what we have learned so far from studies on the HRZ (Hemerythrin RING Zinc finger) proteins in rice, the homologous BTS (BRUTUS) and root-specific BTSL (BRUTUS-LIKE) in Arabidopsis. A mechanistic model is proposed to help focus future research questions towards a full understanding of the regulatory role of these proteins in Fe homeostasis in plants.

Keywords: micronutrient, iron deficiency, bHLH, FBXL5, zinc finger, sensor

OPEN ACCESS

Edited by:
Thomas J. Buckhout, Humboldt-Universität zu Berlin, Germany

Reviewed by:
Rumen Ivanov, Heinrich Heine Universität Düsseldorf, Germany
Xiaosa Xu, Cold Spring Harbor Laboratory, United States

***Correspondence:**
Janneke Balk
janneke.balk@jic.ac.uk

Specialty section:
This article was submitted to Plant Nutrition, a section of the journal Frontiers in Plant Science

Received: *21 November 2018*
Accepted: *22 January 2019*
Published: *13 February 2019*

Citation:
Rodríguez-Celma J, Chou H, Kobayashi T, Long TA and Balk J (2019) Hemerythrin E3 Ubiquitin Ligases as Negative Regulators of Iron Homeostasis in Plants. Front. Plant Sci. 10:98. doi: 10.3389/fpls.2019.00098

INTRODUCTION

Plants are stationary, therefore the ability to detect environmental stimuli, interpret them and activate proper physiological responses is crucial for survival, growth, and development. Plants rely on different sensors such as cell receptors to detect and respond to light, hormones, abiotic/biotic stimuli and nutrients. Many of the molecular mechanisms and pathways involved in sensing and responding to these environmental cues have been well studied (Galvão and Fankhauser, 2015; Larrieu and Vernoux, 2015; Ranty et al., 2016). In contrast, very little is known about how plants sense micronutrients such as iron (Fe), zinc (Zn), manganese, copper, and boron. In this review, we focus on a small family of proteins that have been proposed to function as the elusive Fe sensors in plants.

Plants are very efficient in mining the soil for Fe, even though Fe is mostly insoluble in its oxidised form. The uptake of Fe, and the expression of many genes involved in this process, is tightly regulated in line with the requirement of Fe for new growth and photosynthesis (Kobayashi and Nishizawa, 2012; Connorton et al., 2017). It is therefore important to constantly monitor the Fe status, linked to signalling pathways to balance supply and demand.

The molecular mechanisms for Fe sensing and signalling are very diverse in bacteria, fungi and animals (Kobayashi and Nishizawa, 2014; Outten, 2017). Regardless of the differences, Fe sensor

systems all require direct binding of Fe or Fe-containing prosthetic groups (Fe-S clusters and heme) which then bring about changes in transcription, translation or protein turnover.

The mammalian protein FBXL5 (F-BoX and Leucine-rich repeat 5) regulates Fe homeostasis by targeting IRP2 (Iron Regulated Protein 2) for degradation (Salahudeen et al., 2009; Vashisht et al., 2009; Thompson et al., 2012). FBXL5 consists of an N-terminal hemerythrin (Hr) motif that binds a redox-active di-iron centre, an F-box domain that forms part of a multi-subunit E3 ubiquitin ligase, and a leucine-rich repeat for protein interactions (**Figure 1A**). When Fe is bound, the Hr domain is folded and the FBXL5-E3 ligase complex interacts with IRP2, promoting its degradation. When Fe is low, the Hr domain unfolds and FBXL5 is degraded, thus leaving IRP2 intact to stabilise transcripts encoding Fe uptake proteins. At the same time, IRP2 binding blocks the translation of the Fe storage protein ferritin. FBXL5 is also stabilised by oxygen, but the mechanism is not fully understood (Ruiz and Bruick, 2014). Recently, proteins with distant homology to FBXL5 have been identified in plants (Kobayashi et al., 2013). Here, we present relevant data about this novel family of putative Fe sensors, including the HRZ, BTS, and BTSL proteins, and their involvement in controlling Fe accumulation in plants.

PHYLOGENY AND PROTEIN MOTIFS

The HRZ/BTS/BTSL proteins are found throughout the green lineage. They are characterised by 2 – 3 Hr motifs at the N-terminus and a RING-type E3 ubiquitin ligase at the C-terminal end (**Figure 1A**). This unique combination of protein domains is not found in other kingdoms of life (Matthiadis and Long, 2016). The small gene family is represented by one copy in the green alga *Chlamydomonas reinhardtii* (Urzica et al., 2012), two *HRZ* genes in rice, and three genes – *BTS*, *BTSL1,* and *BTSL2* – in Arabidopsis (Kobayashi et al., 2013). Phylogenetic analysis shows that the genes can be divided in two clades; *HRZ*/*BTS* "sensu stricto" are found in all green organisms, whereas the *BTSL* genes are only present in dicotyledon species (bioRxiv: Rodríguez-Celma et al., 2017).

The N-terminus with Hr motifs makes up two-thirds of the ∼140 kDa protein. Hr motifs typically form a bundle of four α-helices, with the di-iron cofactor in the middle bound by histidines and acidic residues. The two Fe ions are bridged by an oxygen or hydroxyl group (**Figure 1B**; Ruiz and Bruick, 2014). HRZ/BTS proteins have 3 Hr motifs, but BTSL proteins only retain the 1st and 3rd motif. Instead of the 2nd Hr motif, a predicted α-helical bundle is found but not the residues for Fe binding. HRZ2 in rice was initially annotated with one Hr motif corresponding to the 3rd motif in HRZ1 (Kobayashi et al., 2013), however, the open reading frame extends 5′ to reveal another 2 Hr motifs. Thus, 2 or 3 Fe-binding Hr motifs are found in all HRZ/BTS/BTSL proteins and are likely to be critical for their function in plants, in contrast to a single N-terminal Hr motif in the mammalian FBXL5 protein.

E3 ubiquitin ligases form a large family of proteins, with more than 1400 family members in Arabidopsis (Lee and Kim, 2011). By forming specific protein interactions, E3 ligases ubiquitinate target proteins, followed, in most cases, by proteasomal degradation. The E3 ligase domain of HRZ/BTS/BTSL has striking amino acid similarity (∼57%) with human/mouse RCHY1 (also called Pirh2), which belongs to a small subfamily of RING-type E3 ubiquitin ligases (**Figure 1A**). NMR structures of the three subdomains of RCHY1 revealed 9 Zn-binding sites in different types of Zn fingers: the CHY-type, the CTCHY-type and the RING-type that interacts with the E2 ubiquitin-conjugating enzyme (Sheng et al., 2008). Protein motif searches identified a rubredoxin motif at the very end of the protein, but the NMR structure showed Zn binding rather than Fe. The Zn-binding cysteine and histidine residues are fully conserved in plant HRZ/BTS proteins (Matthiadis and Long, 2016), but an additional Zn-finger motif is present in BTSL proteins (**Figure 1A**). Specific amino acids in the C- and N-terminal domains of RCHY1 have been identified that interact with one of its ubiquitination targets (Sheng et al., 2008), but these are not conserved in plants. Plants have an additional 3–4 homologues of RCHY1, for example MYB30-INTERACTING E3 LIGASE 1 (MIEL1) in Arabidopsis was shown to ubiquitinate the transcription factors MYELOBLASTOSIS (MYB) 30 and MYB96 (Marino et al., 2013; Lee and Seo, 2016).

In summary, bioinformatics analyses show that the domain structure of HRZ/BTS/BTSL is conserved in the green lineage. In dicotyledons, the BTS and BTSL proteins belong to separate phylogenetic clades with differences in the second Hr motif and the Zn-finger domain.

EXPRESSION PATTERNS AND MUTANT STUDIES

Expression behaviour and mutant phenotypes provide evidence that *HRZ1* and *HRZ2* in rice, *BTS* in several plant species and the two redundant *BTSL* genes in Arabidopsis play comparable roles in Fe homeostasis, acting as negative regulators.

Microarray analysis of root tissues showed that *BTS* is up-regulated as early as 12–24 h after transferring seedlings to medium lacking Fe, especially in the root stele above the differentiation zone (Dinneny et al., 2008; Long et al., 2010). Further expression analysis of shoots and roots showed that *BTS* transcripts are much more abundant in shoots than in roots (Rodríguez-Celma et al., 2013; Hindt et al., 2017). Initial promoter-GUS studies in young seedlings showed no Fe-dependent regulation of *BTS* in the leaves (Selote et al., 2015), contrasting with RNAseq data of >10-fold induction under Fe deficiency (Rodríguez-Celma et al., 2013; Hindt et al., 2017). Possibly, sequences outside the cloned promoter region may contribute to the transcriptional regulation of *BTS*, but further investigation is needed.

Rice *HRZ1* and *HRZ2* are also induced within 1 day after transfer to Fe-deficient medium, and transcript levels increase further over the next 6 days without Fe (Kobayashi et al., 2013). Both *HRZ* paralogs are expressed in roots and shoots, but about 10 times higher in shoots (Kobayashi et al., 2013).

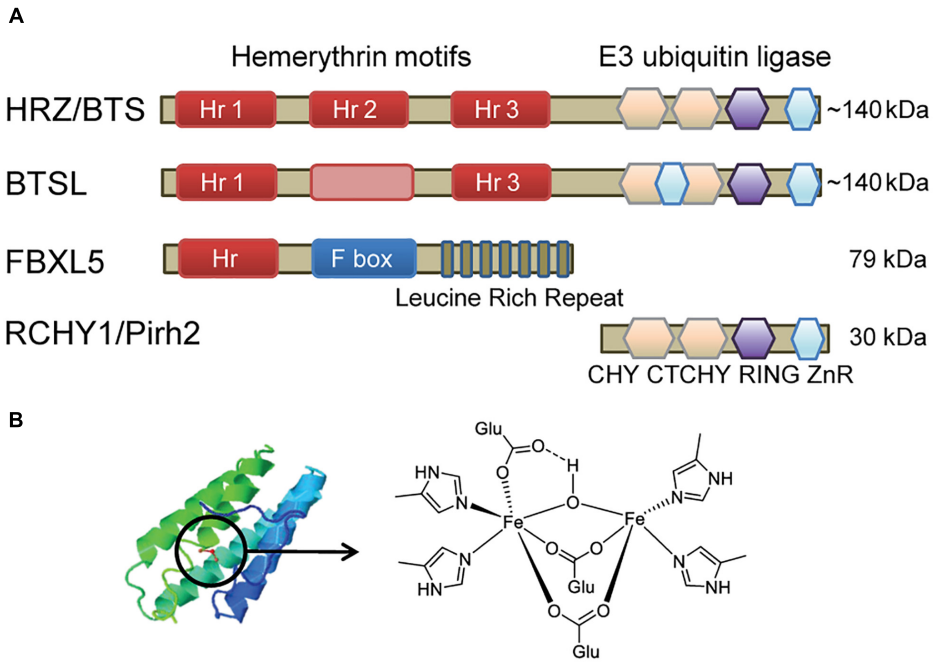

FIGURE 1 | Diagram depicting the main features of hemerythrin E3-ligases. **(A)** Domain organisation of HRZ/BTS/BTSL proteins in plants and algae, compared to homologous proteins in animals. The pink box in BTSL represents a degenerate hemerythrin (Hr) motif with a predicted alpha-helical bundle but lacking the Fe-binding histidine and glutamate residues. The E3 ubiquitin ligase domain has a sequence of different zinc fingers, including CHY-type, CTCHY-type, RING-type and a zinc ribbon (ZnR). **(B)** Typical alpha-helical structure of Hr proteins and the structure of the di-iron centre (Fe-O-Fe) in FBXL5 (Ruiz and Bruick, 2014).

The expression of *BTSL1* and *BTSL2* in Arabidopsis is restricted to the roots under Fe deficiency (Hindt et al., 2017; Rodríguez-Celma et al., 2017). Promoter-GUS studies revealed expression in the root hairs, epidermis, cortex and endodermis (Rodríguez-Celma et al., 2017). The *BTSL* genes are coregulated with the root ferrome (Schmidt and Buckhout, 2011), suggesting common upstream transcription factors.

BTSL2 was de-regulated in the *fit-1* and *fit-3* mutants lines, which are defective in FER-LIKE IRON DEFICIENCY INDUCED TRANSCRIPTION FACTOR (FIT), the main regulator of Fe uptake in dicotyledonous plants (Colangelo and Guerinot, 2004; Jakoby et al., 2004). *HRZ1* and *HRZ2* expression was transiently enhanced in lines overexpressing the *IDEF1*, the IRON-DEFICIENCY-RESPONSIVE ELEMENT (IDE) BINDING FACTOR 1, but not *IDEF2* (Kobayashi et al., 2013). Overall, Fe deficiency affects the expression levels of Arabidopsis *BTS* and *BTSL* genes more than any other stress condition (**Supplementary Table 1**[1]).

Knockout alleles of *BTS* are embryo lethal (McElver et al., 2001; Selote et al., 2015), but lines with a T-DNA insertion in the promoter are viable despite lower seed production (Long et al., 2010; Selote et al., 2015). The mutants accumulate Fe in the whole plant but especially in the seeds which is the likely cause of embryo lethality. Viable *bts* mutants also showed increased acidification of the rhizosphere and ferric-chelate reductase activity under Fe deficiency (Selote et al., 2015). Recently, a new allele of *BTS* was found in a mutant screen for altered element profiles (Hindt et al., 2017). The *bts-3* allele carries a missense mutation affecting the second Zn-finger of the RING motif (Pro1174Leu). *bts-3* plants accumulated more Fe than the promoter mutant *bts-1* (244 and 32% over wild-type, respectively) and growth of *bts-3* was severely compromised in the presence of Fe.

In contrast to *BTS*, knockout mutants of Arabidopsis *BTSL* are viable (Hindt et al., 2017; Rodríguez-Celma et al., 2017). Phenotypes are only observed in the *btsl* double mutant, which retained more chlorophyll than wild type under Fe deficiency and has increased Fe levels in both roots and shoots. A triple mutant with *bts-1* displayed an enhanced phenotype (Hindt et al., 2017).

To study the function of the rice *HRZ* genes, RNAi lines and insertion mutants have been generated. Two different *hrz1* alleles, *hrz1-1* with decreased transcript levels and *hrz1-2* with a frameshift predicted to remove the E3 ligase domain, were more tolerant to Fe deficiency than wild type, accumulated Fe in the seeds and had lower grain yield (Kobayashi et al., 2013; Zhang et al., 2017). For *HRZ2*, RNAi lines and the *hrz2-1* mutant also showed tolerance to Fe deficiency and accumulated Fe in leaves and seeds (Kobayashi et al., 2013). Interestingly, detailed phenotypic and gene expression studies of the mutants showed that the *HRZ* genes also have a function in Fe sufficiency and excess (Zhang et al., 2017; Aung et al., 2018).

The *BTS* homologue in the legume *Lotus japonicus* is strongly upregulated in developing root nodules (Shimomura et al., 2006), perhaps correlated with the high demand for Fe in the

[1]www.araport.org

plant-bacterial symbiosis (Brear et al., 2013). RNAi silencing of the gene resulted in chlorosis, retarded growth and roots which failed to nodulate. The growth phenotypes could not be rescued by exogenous nitrogen supply, which usually overcomes a lack of symbiotic nitrogen fertilisation. However, Fe-dependent regulation and phenotypes have not been investigated to date. Another report identified the BTS homologue in tobacco, *Nicotiana tabacum*, in the context of tobacco mosaic virus infection (Yamaji et al., 2010).

To sum up, *HRZ*/*BTS*(*L*) transcript levels are strongly induced under Fe deficiency, and mutant lines have an enhanced or constitutive response to Fe deficiency, resulting in Fe accumulation in all tissues.

METAL BINDING, PROTEIN STABILITY AND LOCALISATION

The HRZ/BTS/BTSL proteins are predicted to bind metals both in the Hr motifs and the Zn-fingers. Hemerythrins bind 2 Fe ions, thus HRZ and BTS are predicted to bind a total of 6 Fe in their 3 Hr motifs, and BTSLs are likely to bind 4 Fe. Conservation of the Zn-binding sites in the C-terminal domain of HRZ/BTS proteins compared to RCHY1/Pirh2 suggests 9 Zn ions are required for structural integrity (Sheng et al., 2008). Experimental data for HRZ and BTS to date falls well short of these numbers. Full-length recombinant BTS purified from *Escherichia coli* was found to bind 2 Fe and 5 Zn (Selote et al., 2015). Full length HRZ1 co-purified with 2 Fe and 1 Zn, and the truncated version of the HRZ2 protein bound 2 Fe and 2 Zn ions (Kobayashi et al., 2013). Despite the lower than expected number of Zn ions binding to the E3 ligase domain, the recombinant HRZ and BTS proteins had ubiquitin transferase activity, evident from self-ubiquitination (Kobayashi et al., 2013; Selote et al., 2015; Zhang et al., 2017). Most likely, a small proportion of HRZ/BTS protein had a full complement of Zn ions among mostly apo-protein.

The HRZ/BTS/BTSL proteins appear highly unstable. Attempts to detect the endogenous protein *in vivo* have been unsuccessful to date, and even full-length GFP fusions of HRZ or BTS are difficult to detect either by western blot analysis or fluorescence microscopy (Kobayashi et al., 2013; Selote et al., 2015). Interestingly, a truncated version of BTS lacking the Hr domain is easily detectable in roots and complements *bts-1* phenotypes (Selote et al., 2015). This suggests that the Hr domain may contribute to the instability of HRZ/BTS proteins. Furthermore, root extracts from rice (but not shoot extracts) were able to degrade recombinant HRZ1 and HRZ2 in a MG132-dependent manner, pointing at proteasomal degradation following self-ubiquitination or ubiquitination by other E3 ligases (Kobayashi et al., 2013; Zhang et al., 2017).

The HRZ/BTS proteins localised to the nucleus when full-length GFP fusions were transiently expressed in onion cells and *Nicotiana benthamiana*, respectively (Kobayashi et al., 2013; Selote et al., 2015). No data is yet available about the localisation of BTSL proteins, but they are presumably also nuclear. Interestingly, a truncated version of BTS lacking the Hr domain but preserving the first N-terminal amino acids was localised to the cytosol (Selote et al., 2015). Truncated versions of BTS containing only the Hr motifs or lacking the RING motif were localised to both the cytosol and the nucleus (Selote et al., 2015). A similar observation was made for HRZ2 in Kobayashi et al. (2013), using a truncated version of HRZ2 containing only the third hemerythrin motif and the C-terminal E3 ligase domain.

How does Fe binding to the Hr motifs relate to protein stability? This key question has been addressed using transient expression of BTS-GFP in *N. benthamiana* leaves and by using a wheat germ *in vitro* translation system (Selote et al., 2015). BTS-GFP fluorescence was only observed when deferoxamine, an Fe chelator, was co-infiltrated. Addition of micromolar amounts of Fe to the wheat germ extract prevented accumulation of BTS protein, but it was produced upon deletion of the entire Hr domain. Selective mutagenesis of putative Fe-binding ligands in the first or second Hr motif, but not the third, also stabilised the BTS protein (Selote et al., 2015). Thus, these data suggest that BTS is destabilised by Fe binding to the Hr motifs, in contrast to the mammalian FBXL5 protein, which is stabilised by Fe binding. Given there are 3 Hr domains in the plant proteins, Fe binding properties are likely to be more complex than a simple de/stabilisation effect, as discussed below.

Thus, the data obtained by different experimental approaches suggest that the abundance and subcellular localisation of HRZ/BTS/BTSL proteins are tightly controlled, regulated by Fe binding to the N-terminal Hr domain and self-ubiquitination.

INTERACTION PARTNERS

A yeast-2-hybrid screen with BTS as bait against a root-specific cDNA library identified several potential interaction partners, including the basic Helix-Loop-Helix (bHLH) transcription factors bHLH104 and bHLH115 which are involved in Fe homeostasis (Long et al., 2010). *In planta* bimolecular fluorescence complementation (BiFC) and co-immunoprecipitation confirmed that BTS interacts with bHLH104, bHLH115, and also with bHLH105 (ILR3), but not with the bHLH protein POPEYE (PYE) (Selote et al., 2015). Further investigation using an *in vitro* cell-free degradation assay with or without the inhibitor MG132 indicated that BTS mediates the degradation of ILR3 and bHLH115 (Selote et al., 2015).

A similar yeast-2-hybrid screen using rice HRZ1 identified the bHLH transcription factor POSITIVE REGULATOR OF IRON HOMEOSTASIS 1 (PRI1) as interaction partner, which is the homologue of Arabidopsis ILR3 (Zhang et al., 2017). Co-localisation of transiently produced HRZ1 and PRI1 in the nucleus and co-immunoprecipitation further supported the interaction (Zhang et al., 2017). PRI1 promotes the expression of *IRO2* and *IRO3*, which are orthologs of *bHLH38/39* and *PYE*, respectively (Kobayashi and Nishizawa, 2012). Interestingly, the homology of the interaction partners in Arabidopsis and rice suggest that this part of the Fe-regulatory circuit is conserved in dicot and monocot species.

Protein interaction screens have so far not been reported for the BTSL proteins but phenotypic studies have provided some clues. When the *btsl* double mutant was exposed to Fe-deficiency

and resupply treatments, a specific pattern of mis-regulated expression of the Fe uptake genes *FERRIC REDUCTASE OXIDASE 2* (*FRO2)* and *IRON-REGULATED TRANSPORTER 1* (*IRT1)* suggested that FIT, or a transcription factor further upstream, is a target for degradation by BTSLs (Rodríguez-Celma et al., 2017). Previous studies by Sivitz et al. (2011) found that FIT protein levels are controlled by proteasomal degradation, but the E3 ligase had not been identified. Physical interaction between BTSL1/2 and FIT has been shown *in vitro* using far-Western blot analysis (Rodríguez-Celma et al., 2017). FIT functions as a heterodimer with bHLH38/39, the expression of which is controlled by ILR3 and bHLH104 (Zhang et al., 2015; Li et al., 2016). Interestingly, mis-regulation of *bHLH38/39* expression is also found in the *btsl* double mutant (Rodríguez-Celma et al., 2017). This suggests that BTSLs may have additional targets such as ILR3 and/or bHLH104.

Very recently, it was shown that BTS interacts with another set of transcription factors, VASCULAR PLANT ONE-ZINC FINGER (VOZ) 1 and VOZ2 (Selote et al., 2018). VOZ1 and VOZ2 negatively regulate drought and cold responses, and VOZ2 has previously been shown to be degraded by the 26 proteasome. VOZ1/2 are primarily present in the cytosol, but likely translocate to the nucleus through phosphorylation to interact with BTS (Yasui et al., 2012; Koguchi et al., 2017; Selote et al., 2018). Importin (IMP) α-4. Localised in the nucleus, interacts with BTS but is not a target for degradation (Selote et al., 2018). This suggests that IMPα-4 may play a role in nuclear localisation of BTS and BTS-interacting proteins.

These findings suggest HRZ/BTS/BTSL might be involved in other stress conditions that are sensitive to Fe levels, possibly due to the role of Fe in the reactive oxygen species (ROS) response (Tripathi et al., 2018). Future studies to characterise HRZ/BTS/BTSL interacting proteins will help to shed light on how these Fe sensors may integrate multiple stress responses.

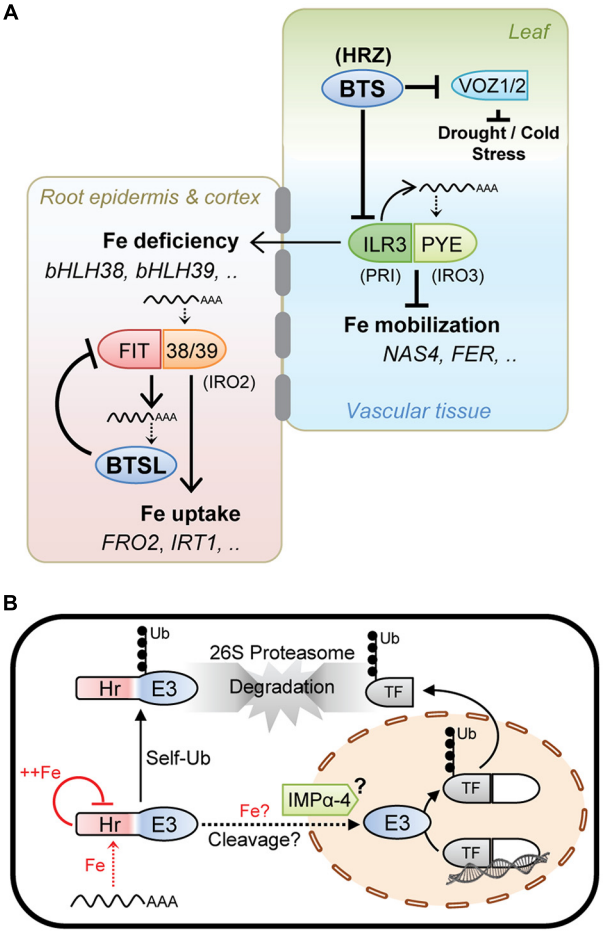

FIGURE 2 | Working model of the hemerythrin E3 ligases as negative regulators of the Fe deficiency response. **(A)** HRZ/BTS/BTSL protein function integrated with the iron homeostasis regulatory cascade. The Arabidopsis gene acronyms are used, with rice orthologs in brackets. BTSL represents two mostly redundant proteins in Arabidopsis, and HRZ represents the HRZ1 and HRZ2 proteins. **(B)** Cellular mode of action of HRZ/BTS/BTSL proteins. Fe levels are thought to affect protein translation and stability. Protein stability is further controlled via self-ubiquitination activity and proteasomal degradation. HRZ/BTS have been shown to localise in the nucleus. Protein interaction data indicate that importin (IMP) α-4 may facilitate nuclear import of BTS and that the hemerythrin (Hr) domain may be cleaved off. Once in the nucleus, HRZ/BTS/BTSL catalyse the ubiquitination of specific transcription factors followed by proteasomal degradation.

WORKING MODEL

Taken together, the experimental data on HRZ, BTS, and BTSL, although patchy in places, suggests a similar mode of action of these proteins, namely they provide a negative feedback loop to moderate the activity of specific transcription factors and hence limit Fe accumulation (**Figure 2A**).

Present in all plant species, HRZ/BTS proteins act in shoots and root vascular tissue to moderate the Fe deficiency response and Fe mobilisation (**Figure 2A**). The BTSL proteins are found in dicotyledonous plants only and inhibit Fe uptake. These two regulatory loops are connected through the expression of *bHLH38* and *bHLH39*, two transcription factors needed for Fe uptake whose expression is regulated by ILR3, a target of BTS (**Figure 2A**).

The transcript levels of *HRZ*/*BTS*/*BTSL* are strongly induced by Fe deficiency. Protein translation may depend on low amounts of Fe to allow folding of the N-terminal Hr domain (**Figure 2B**), as shown for FBXL5 in mammals, and to proceed with translation of the C-terminal E3 ligase domain. Because FIT is required for *BTSL* transcription and also for replenishing Fe in the cytosol, this creates a time delay in the feedback loop. Interestingly, Sivitz et al. (2011) observed that FIT protein starts being turned over ∼48 h after its upregulation in response to Fe deficiency.

On the other hand, Fe binding to the Hr domain was shown to negatively control the levels of BTS protein (**Figure 2B**). Possibly, once sufficient Fe is available, most of the BTS is degraded, leaving only a residual amount functioning under Fe sufficiency and excess. HRZ/BTS/BTSL protein levels would also be tightly controlled by self-ubiquitination leading to proteasomal degradation (**Figure 2B**).

Since truncated BTS-GFP lacking the Hr domains is stable and functionally complemented the *bts-1* mutant, it is tempting to speculate that the Hr domain is cleaved off, resulting in a ∼40 kDa protein which is small enough for nuclear import facilitated by the interaction with the importin IMPα-4 (**Figure 2B**). A precedent for such a relocation mechanism is provided by the Fe-regulated transcription factor Aft1 in yeast, which shuttles between the cytosol and nucleus depending on the Fe status of the cell (Outten, 2017). A possible role of Fe binding to the hemerythrin motifs in the cleavage or relocation of the protein cannot be ruled out (**Figure 2B**). Once in the nucleus, the E3 ligase domain would be able to interact with and ubiquitinate its target transcription factors for degradation.

From expression networks and promoter-GUS studies, it has become clear that BTS and BTSLs have diverged functions in dicotyledonous plants. *BTSLs* are expressed in root tissues that take up Fe from the soil, whereas *BTS* acts in the stele and shoots. The presence of 2 or 3 Hr motifs, respectively, suggests that they respond to different Fe setpoints on each side of the endodermis, a cell layer that performs a critical function in nutrient uptake (Barberon et al., 2016).

To further test the working model, the following research questions will need to be addressed:

- Determine how Fe binding to the Hr domain alters the stability and localisation of the HRZ/BTS/BTSL proteins, and whether this domain is removed for nuclear import. For this, detection of the endogenous proteins will be key.
- Identify possible phosphorylation sites that could affect nuclear import.
- Investigate if the di-iron cofactors are redox active, and whether the HRZ/BTS proteins are modulated by oxygen levels, as is the case for FBXL5.
- Test the "different Fe setpoint hypothesis" for roots and shoots by swapping the Hr domains of BTS and BTSLs and expressing them in the respective mutants.
- In dicots, investigate possible connexions between the BTS and BTSL feedback loops, for example through the expression of bHLH38/39.
- Identify the transcription factors that regulate *BTS* expression, and confirm those that are likely to regulate the *HRZ* and *BTSL* genes.

AUTHOR CONTRIBUTIONS

All authors contributed to the writing of the manuscript, including discussion, and proofreading.

FUNDING

Our work was funded by the Biotechnology and Biological Sciences Research Council (BBSRC) grant BB/N001079/1 (JR-C and JB); the National Science Foundation (NSF) awards #1247427 and #1517058 (TL and HC); and the Japan Society for the Promotion of Science (JSPS) KAKENHI grant number 15H05617 (TK).

SUPPLEMENTARY MATERIAL

The Supplementary Material for this article can be found online at: https://www.frontiersin.org/articles/10.3389/fpls.2019.00098/full#supplementary-material

REFERENCES

Aung, M. S., Kobayashi, T., Masuda, H., and Nishizawa, N. K. (2018). Rice HRZ ubiquitin ligases are crucial for the response to excess iron. *Physiol. Plant* 163, 282–296. doi: 10.1111/ppl.12698

Barberon, M., Vermeer, J. E. M., De Bellis, D., Wang, P., Naseer, S., Andersen, T. G., et al. (2016). Adaptation of root function by nutrient-induced plasticity of endodermal differentiation. *Cell* 164, 447–459. doi: 10.1016/j.cell.2015.12.021

Brear, E. M., Day, D. A., and Smith, P. M. C. (2013). Iron: an essential micronutrient for the legume-rhizobium symbiosis. *Front. Plant Sci.* 4:359. doi: 10.3389/fpls.2013.00359

Colangelo, E. P., and Guerinot, M. L. (2004). The essential Basic Helix-Loop-Helix protein FIT1 is required for the iron deficiency response. *Plant Cell* 16, 3400–3412. doi: 10.1105/tpc.104.024315

Connorton, J. M., Balk, J., and Rodríguez-Celma, J. (2017). Iron homeostasis in plants-a brief overview. *Metallomics* 9, 813–823. doi: 10.1039/c7mt00136c

Dinneny, J. R., Long, T. A., Wang, J. Y., Jung, J. W., Mace, D., Pointer, S., et al. (2008). Cell identity mediates the response of Arabidopsis roots to abiotic stress. *Science* 320, 942–946. doi: 10.1126/science.1153795

Galvão, V. C., and Fankhauser, C. (2015). Sensing the light environment in plants: photoreceptors and early signaling steps. *Curr. Opin. Neurobiol.* 34, 46–53. doi: 10.1016/j.conb.2015.01.013

Hindt, M. N., Akmakjian, G. Z., Pivarski, K. L., Punshon, T., Baxter, I., Salt, E., et al. (2017). *BRUTUS* and its paralogs, *BTS LIKE1* and *BTS LIKE2*, encode important negative regulators of the iron deficiency response in *Arabidopsis thaliana*. *Metallomics* 9, 876–890. doi: 10.1039/C7MT00152E

Jakoby, M., Wang, H. Y., Reidt, W., Weisshaar, B., and Bauer, P. (2004). FRU (BHLH029) is required for induction of iron mobilization genes in *Arabidopsis thaliana*. *FEBS Lett.* 577, 528–534. doi: 10.1016/j.febslet.2004.10.062

Kobayashi, T., Nagasaka, S., Senoura, T., Itai, R. N., Nakanishi, H., and Nishizawa, N. K. (2013). Iron-binding haemerythrin RING ubiquitin ligases regulate plant iron responses and accumulation. *Nat. Commun.* 4:2792. doi: 10.1038/ncomms3792

Kobayashi, T., and Nishizawa, N. K. (2012). Iron uptake, translocation, and regulation in higher plants. *Annu. Rev. Plant Biol.* 63, 131–152. doi: 10.1146/annurev-arplant-042811-105522

Kobayashi, T., and Nishizawa, N. K. (2014). Iron sensors and signals in response to iron deficiency. *Plant Sci.* 224, 36–43. doi: 10.1016/j.plantsci.2014.04.002

Koguchi, M., Yamasaki, K., Hirano, T., and Sato, M. H. (2017). Vascular plant one-zinc-finger protein 2 is localized both to the nucleus and stress granules under heat stress in Arabidopsis. *Plant Signal. Behav.* 12, 1–7. doi: 10.1080/15592324.2017.1295907

Larrieu, A., and Vernoux, T. (2015). Comparison of plant hormone signalling systems. *Essays Biochem.* 58, 165–181. doi: 10.1042/bse0580165

Lee, H. G., and Seo, P. J. (2016). The Arabidopsis MIEL1 E3 ligase negatively regulates ABA signalling by promoting protein turnover of MYB96. *Nat. Commun.* 7:12525. doi: 10.1038/ncomms12525

Lee, J. H., and Kim, W. T. (2011). Regulation of abiotic stress signal transduction by E3 Ubiquitin Ligases in Arabidopsis. *Mol. Cells* 31, 201–208. doi: 10.1007/s10059-011-0031-9

Li, X., Zhang, H., Ai, Q., Liang, G., and Yu, D. (2016). Two bHLH transcription factors, bHLH34 and bHLH104, regulate iron homeostasis in *Arabidopsis thaliana*. *Plant Physiol.* 170, 2478–2493. doi: 10.1104/pp.15.01827

Long, T. A., Tsukagoshi, H., Busch, W., Lahner, B., Salt, D. E., and Benfey, P. N. (2010). The bHLH transcription factor POPEYE regulates response to iron deficiency in Arabidopsis roots. *Plant Cell* 22, 2219–2236. doi: 10.1105/tpc.110.074096

Marino, D., Froidure, S., Canonne, J., Khaled, S., Ben Khafif, M., Pouzet, C., et al. (2013). Arabidopsis ubiquitin ligase MIEL1 mediates degradation of the transcription factor MYB30 weakening plant defence. *Nat. Commun.* 4, 1–9. doi: 10.1038/ncomms2479

Matthiadis, A., and Long, T. A. (2016). Further insight into BRUTUS domain composition and functionality. *Plant Signal. Behav.* 11, e1204508. doi: 10.1080/15592324.2016.1204508

McElver, J., Tzafrir, I., Aux, G., Rogers, R., Ashby, C., Smith, K., et al. (2001). Insertional mutagenesis of genes required for seed development in *Arabidopsis thaliana*. *Genetics* 159, 1751–1763.

Outten, C. E. (2017). Checks and balances for the iron bank. *J. Biol. Chem.* 292, 15990–15991. doi: 10.1074/jbc.H117.785741

Ranty, B., Aldon, D., Cotelle, V., Galaud, J.-P., Thuleau, P., and Mazars, C. (2016). Calcium sensors as key hubs in plant responses to biotic and abiotic stresses. *Front. Plant Sci.* 7:327. doi: 10.3389/fpls.2016.00327

Rodríguez-Celma, J., Green, R. T., Connorton, J. M., Kruse, I., Cui, Y., Ling, H.-Q., et al. (2017). Brutus-like proteins moderate the transcriptional response to iron deficiency in roots. *bioRxiv* [Preprint]. doi: 10.1101/231365

Rodríguez-Celma, J., Pan, I. C., Li, W., Lan, P., Buckhout, T. J., and Schmidt, W. (2013). The transcriptional response of Arabidopsis leaves to Fe deficiency. *Front. Plant Sci.* 4:276. doi: 10.3389/fpls.2013.00276

Ruiz, J. C., and Bruick, R. K. (2014). F-box and leucine-rich repeat protein 5 (FBXL5): sensing intracellular iron and oxygen. *J. Inorg. Biochem.* 133, 73–77. doi: 10.1016/j.jinorgbio.2014.01.015

Salahudeen, A. A., Thompson, J. W., Ruiz, J. C., Ma, H.-W., Kinch, L. N., Li, Q., et al. (2009). An E3 ligase possessing an iron-responsive hemerythrin domain is a regulator of iron homeostasis. *Science* 326, 722–726. doi: 10.1126/science.1176326

Schmidt, W., and Buckhout, T. J. (2011). A hitchhiker's guide to the Arabidopsis ferrome. *Plant Physiol. Biochem.* 49, 462–470. doi: 10.1016/j.plaphy.2010.12.001

Selote, D., Matthiadis, A., Gillikin, J. W., Sato, M. H., and Long, T. A. (2018). The E3 ligase BRUTUS facilitates degradation of VOZ1/2 transcription factors. *Plant Cell Environ.* 41, 2463–2474. doi: 10.1111/pce.13363

Selote, D., Samira, R., Matthiadis, A., Gillikin, J. W., and Long, T. A. (2015). Iron-binding E3 ligase mediates iron response in plants by targeting basic Helix-Loop-Helix transcription factors. *Plant Physiol.* 167, 273–286. doi: 10.1104/pp.114.250837

Sheng, Y., Laister, R., Lemak, A., Wu, B., Tai, E., Duan, S., et al. (2008). Molecular basis of Pirh2-mediated p53 ubiquitylation. *Nat. Struct. Mol. Biol.* 15, 1334–1342. doi: 10.1038/nsmb.1521.Molecular

Shimomura, K., Nomura, M., Tajima, S., and Kouchi, H. (2006). LjnsRING, a novel RING finger protein, is required for symbiotic interactions between *Mesorhizobium loti* and *Lotus japonicus*. *Plant Cell Physiol.* 47, 1572–1581. doi: 10.1093/pcp/pcl022

Sivitz, A., Grinvalds, C., Barberon, M., Curie, C., and Vert, G. (2011). Proteasome-mediated turnover of the transcriptional activator FIT is required for plant iron-deficiency responses. *Plant J.* 66, 1044–1052. doi: 10.1111/j.1365-313X.2011.04565.x

Thompson, J. W., Salahudeen, A. A., Chollangi, S., Ruiz, J. C., Brautigam, C. A., Makris, T. M., et al. (2012). Structural and molecular characterization of iron-sensing hemerythrin-like domain within F-box and leucine-rich repeat protein 5 (FBXL5). *J. Biol. Chem.* 287, 7357–7365. doi: 10.1074/jbc.M111.308684

Tripathi, D. K., Singh, S., Gaur, S., Singh, S., Yadav, V., Liu, S., et al. (2018). Acquisition and homeostasis of iron in higher plants and their probable role in abiotic stress tolerance. *Front. Environ. Sci.* 5:86. doi: 10.3389/fenvs.2017.00086

Urzica, E. I., Casero, D., Yamasaki, H., Hsieh, S. I., Adler, L. N., Karpowicz, S. J., et al. (2012). Systems and trans-system level analysis identifies conserved iron deficiency responses in the plant lineage. *Plant Cell* 24, 3921–3948. doi: 10.1105/tpc.112.102491

Vashisht, A. A., Zumbrennen, K. B., Huang, X., Powers, D. N., Durazo, A., Sun, D., et al. (2009). Control of iron homeostasis by an iron-regulated ubiquitin ligase. *Science* 326, 718–721. doi: 10.1002/9781118343371.refs

Yamaji, Y., Hamada, K., Yoshinuma, T., Sakurai, K., Yoshii, A., Shimizu, T., et al. (2010). Inhibitory effect on the tobacco mosaic virus infection by a plant RING finger protein. *Virus Res.* 153, 50–57. doi: 10.1016/j.virusres.2010.07.005

Yasui, Y., Mukougawa, K., Uemoto, M., Yokofuji, A., Suzuri, R., Nishitani, A., et al. (2012). The phytochrome-interacting vascular plant one-zinc finger1 and VOZ2 redundantly regulate flowering in Arabidopsis. *Plant Cell* 24, 3248–3263. doi: 10.1105/tpc.112.101915

Zhang, H. M., Li, Y., Yao, X. N., Liang, G., and Yu, D. (2017). Positive regulator of Iron Homeostasis1, OsPRI1, positively regulates iron homeostasis in rice. *Plant Physiol.* 175, 543–554. doi: 10.1104/pp.17.00794

Zhang, J., Liu, B., Li, M., Feng, D., Jin, H., Wang, P., et al. (2015). The bHLH transcription factor bHLH104 interacts with IAA-LEUCINE RESISTANT3 and modulates iron homeostasis in Arabidopsis. *Plant Cell* 27, 787–805. doi: 10.1105/tpc.114.132704

Conflict of Interest Statement: The authors declare that the research was conducted in the absence of any commercial or financial relationships that could be construed as a potential conflict of interest.

frontiers in Plant Science

REVIEW
published: 11 March 2019
doi: 10.3389/fpls.2019.00287

Induced Systemic Resistance (ISR) and Fe Deficiency Responses in Dicot Plants

Francisco J. Romera[1], María J. García[2], Carlos Lucena[2], Ainhoa Martínez-Medina[3], Miguel A. Aparicio[4], José Ramos[4], Esteban Alcántara[1], Macarena Angulo[1] and Rafael Pérez-Vicente[2]*

[1] Department of Agronomy, Campus de Excelencia Internacional Agroalimentario CeiA3, Universidad de Córdoba, Córdoba, Spain, [2] Department of Botany, Ecology and Plant Physiology, Campus de Excelencia Internacional Agroalimentario CeiA3, Universidad de Córdoba, Córdoba, Spain, [3] Molecular Interaction Ecology, German Centre for Integrative Biodiversity Research (iDiv) Halle-Jena-Leipzig, Leipzig, Germany, [4] Department of Microbiology, Campus de Excelencia Internacional Agroalimentario CeiA3, Universidad de Córdoba, Córdoba, Spain

Plants develop responses to abiotic stresses, like Fe deficiency. Similarly, plants also develop responses to cope with biotic stresses provoked by biological agents, like pathogens and insects. Some of these responses are limited to the infested damaged organ, but other responses systemically spread far from the infested organ and affect the whole plant. These latter responses include the Systemic Acquired Resistance (SAR) and the Induced Systemic Resistance (ISR). SAR is induced by pathogens and insects while ISR is mediated by beneficial microbes living in the rhizosphere, like bacteria and fungi. These root-associated mutualistic microbes, besides impacting on plant nutrition and growth, can further boost plant defenses, rendering the entire plant more resistant to pathogens and pests. In the last years, it has been found that ISR-eliciting microbes can induce both physiological and morphological responses to Fe deficiency in dicot plants. These results suggest that the regulation of both ISR and Fe deficiency responses overlap, at least partially. Indeed, several hormones and signaling molecules, like ethylene (ET), auxin, and nitric oxide (NO), and the transcription factor MYB72, emerged as key regulators of both processes. This convergence between ISR and Fe deficiency responses opens the way to the use of ISR-eliciting microbes as Fe biofertilizers as well as biopesticides. This review summarizes the progress in the understanding of the molecular overlap in the regulation of ISR and Fe deficiency responses in dicot plants. Root-associated mutualistic microbes, rhizobacteria and rhizofungi species, known for their ability to induce morphological and/or physiological responses to Fe deficiency in dicot plant species are also reviewed herein.

Keywords: dicotyledons, ethylene, iron, ISR, rhizobacteria, rhizofungi, rhizosphere, stress responses

OPEN ACCESS

Edited by:
Thomas J. Buckhout, Humboldt-Universität zu Berlin, Germany

Reviewed by:
Christos Zamioudis, Democritus University of Thrace, Greece
Louis Grillet, Academia Sinica, Taiwan

****Correspondence:***
Francisco J. Romera
ag1roruf@uco.es

Specialty section:
This article was submitted to Plant Nutrition, a section of the journal Frontiers in Plant Science

Received: *19 December 2018*
Accepted: *21 February 2019*
Published: *11 March 2019*

Citation:
Romera FJ, García MJ, Lucena C, Martínez-Medina A, Aparicio MA, Ramos J, Alcántara E, Angulo M and Pérez-Vicente R (2019) Induced Systemic Resistance (ISR) and Fe Deficiency Responses in Dicot Plants. Front. Plant Sci. 10:287. doi: 10.3389/fpls.2019.00287

INTRODUCTION

In the last decades, crop productivity has been mainly based on the use of high-yielding varieties and in the application of high amounts of fertilizers and pesticides. Despite crop protection measures, current losses are estimated at 20–40% for the major food crops world-wide (Savary et al., 2012). Hence, novel strategies for crop production, with less reliance on chemical products need to be developed. In relation to plant mineral nutrition, two strategies that can contribute to

this goal are the development of crop varieties more efficient in nutrient acquisition and better management of the rhizosphere (Shen et al., 2013). The rhizosphere, the soil volume influenced by the root system, is one of the most energy-rich habitats on Earth, allowing the life of a myriad of microbes (Pieterse et al., 2014; Pii et al., 2015). Many of them are pathogenic and threaten plant growth. However, there are also many others that are beneficial for plants, like rhizobacteria ("PGPB or PGPR: Plant Growth-Promoting Bacteria or Rhizobacteria") and fungi ("PGPF: Plant Growth-Promoting Fungi"), which can improve plant growth and benefit the adaptation of plants to adverse conditions (Yang et al., 2008; de Zelicourt et al., 2013; Pieterse et al., 2014; Pii et al., 2015; Verbon and Liberman, 2016). Some rhizosphere microbes can have negative effects on plant mineral nutrition, for example, by competing with plants for some nutrients. However, several genera of the rhizosphere microbiota can facilitate nutrient acquisition by plants, thus having positive effects. These beneficial microbes include, among others, mycorrhizal fungi and *Rhizobium*, which establish mutualistic symbiosis with plant roots that improve phosphorus (P) or nitrogen (N) nutrition, respectively (Guinel, 2015; Wang W. et al., 2017). Additionally, there are free-living mutualistic microbes that can improve plant nutrition through different mechanisms, such as the release of nutrient solubilizing compounds or the modification of root physiology and architecture (Jin et al., 2014; Mimmo et al., 2014; Zamioudis et al., 2014, 2015; Contreras-Cornejo et al., 2015; Li et al., 2015; Pii et al., 2015; García-López et al., 2016; Garnica-Vergara et al., 2016; Verbon et al., 2017).

Among the essential mineral nutrients required by plants, iron (Fe), along with P and N, represent the major constraints for crop productivity worldwide (Pii et al., 2015; Scagliola et al., 2016; Tsai and Schmidt, 2017b). Iron deficiency is widely distributed, mainly in calcareous soils (approximately one third of cultivated lands) which are abundant in arid and semiarid regions (Briat et al., 2015). To cope with Fe deficiency, plants develop morphological and physiological responses, mainly in their roots, aimed to facilitate its acquisition (see following Section; Kobayashi and Nishizawa, 2012; Brumbarova et al., 2015; Lucena et al., 2015). Despite these responses, in many cases it is necessary to apply Fe fertilizers to correct Fe deficiency. For Fe supply in the field, the most common practice is the application of Fe chelates to soils, which are generally expensive and therefore restricted to high added-value field-grown crops (Briat et al., 2015). An alternative is the use of more Fe efficient plant genotypes. However, different results obtained with sterile soils have shown that, even with these genotypes, the cooperation of rhizosphere microbes is necessary for an adequate Fe acquisition (Jin et al., 2014; Pii et al., 2015).

Several studies demonstrated that the application of some beneficial microbes to soils can improve the Fe nutrition of plants (de Santiago et al., 2009, 2013; Zhang et al., 2009; Freitas et al., 2015; Li et al., 2015; Ipek et al., 2017; Sonbarse et al., 2017; Aras et al., 2018; Arıkan et al., 2018). However, the main mechanisms driving such effects are complex and not fully understood. One possible mechanism is the release of Fe solubilizing compounds to soils (Jin et al., 2014; Mimmo et al., 2014; Pii et al., 2015). Moreover, the rhizosphere mutualistic microbiota can also improve plant Fe uptake by the alteration of the root physiology and architecture (Zamioudis et al., 2014, 2015; Contreras-Cornejo et al., 2015; Garnica-Vergara et al., 2016; Scagliola et al., 2016; Verbon et al., 2017). In the last years it has been found that some rhizosphere microbes can induce physiological and morphological responses in roots of dicot plants similar to the ones induced by plants under Fe deficiency (Zhang et al., 2009; Orozco-Mosqueda et al., 2013; Jin et al., 2014; Pieterse et al., 2014; Zamioudis et al., 2014, 2015; Zhao et al., 2014; Pii et al., 2016b; Zhou et al., 2016a; Martínez-Medina et al., 2017; Verbon et al., 2017). It is remarkable that these rhizosphere microbes are also capable of eliciting the Induced Systemic Resistance (ISR) against pathogens and insects. This observation suggests that both processes (ISR and Fe deficiency responses) might be closely interconnected, and opens new possibilities for optimizing the management of the rhizosphere microbiota for improving Fe nutrition and health (Pieterse et al., 2014; Zamioudis et al., 2014, 2015; Verbon et al., 2017). However, the nodes of convergence between the two processes remain unclear.

Elucidating the main nodes of interconnection between the pathways regulating microbe-elicited ISR and Fe uptake is critical for optimizing the use of plant mutualistic microbes in agriculture. This review summarizes the progress in the understanding of the molecular overlap in the regulation of ISR and Fe deficiency responses in dicot plants. We further describe and evaluate rhizobacteria and rhizofungi species, known for their ability to induce morphological and/or physiological responses to Fe deficiency in dicot plants and with potential for a future use as Fe biofertilizers.

Fe DEFICIENCY RESPONSES IN DICOT PLANTS

Iron (Fe) is abundant in most soils, mainly as Fe^{3+}, although its availability to plants is low, especially in calcareous soils (Briat et al., 2015). Based on the mechanisms used by plant roots to facilitate mobilization and uptake of Fe, plants are classified into Strategy I species (dicots and non-grass monocots) and Strategy II species (grasses; Kobayashi and Nishizawa, 2012; Ivanov et al., 2012). Dicots, such as *Arabidopsis* and tomato, are Strategy I species which have to reduce Fe^{3+} to Fe^{2+} at the root surface, by means of a ferric reductase (encoded by *FRO2* in *Arabidopsis*), prior to its subsequent uptake through a Fe^{2+} transporter (encoded by *IRT1* in Arabidopsis; Ivanov et al., 2012; Kobayashi and Nishizawa, 2012). This review is devoted to dicots, where ISR mechanisms have been more extensively studied (Balmer et al., 2013). Consequently, the mechanisms described thereafter correspond to Strategy I plant species. For details about the Strategy II plant species readers are referred to other articles in this special issue.

When grown under Fe deficiency, Strategy I species develop several physiological and morphological responses, mainly in roots, known as Fe deficiency responses. Those responses are aimed at facilitating Fe mobilization and uptake (Ivanov et al., 2012; Kobayashi and Nishizawa, 2012; Brumbarova et al., 2015; Lucena et al., 2015). Among the physiological responses are: an enhanced ferric reductase activity due to upregulation of the *FRO*

genes; an enhanced Fe^{2+} uptake capacity due to upregulation of the *IRT1* genes; the acidification of the rhizosphere due to upregulation of *AHA* or *HA* (H^+-ATPase) genes (Waters et al., 2007; Brumbarova et al., 2015; Lucena et al., 2015); an increase of the synthesis and release of organic acids, like citrate and malate, to the medium (Kabir et al., 2012; Schmidt et al., 2014); an increase of the synthesis and release of phenolic compounds to the medium due to upregulation of genes like *F6′H1*, *S8H*, *BGLU42*, and *ABCG37* (Schmid et al., 2014; Schmidt et al., 2014; Zamioudis et al., 2014; Tsai and Schmidt, 2017a; Siwinska et al., 2018; Tsai et al., 2018); and an increase of the synthesis and release of flavins to the medium (Rodríguez-Celma and Schmidt, 2013). The acidification facilitates the solubilisation of Fe and the functioning of the ferric reductase which has an optimum pH around 5.0 (Lucena et al., 2007; Waters et al., 2007). Organic acids can act as chelating agents for Fe in the soil and also inside the plant (Durrett et al., 2007; Schmidt et al., 2014). In fact, Fe is moved through the xylem chelated with citrate (Durrett et al., 2007; Schmidt et al., 2014). Phenolic compounds, like coumarins, and flavins can act as chelating and reducing agents of Fe^{3+}, thus facilitating its mobilization in the rhizosphere (Rodríguez-Celma and Schmidt, 2013; Tsai and Schmidt, 2017a; Rajniak et al., 2018). The *F6′H1* ("Feruloyl-CoA 6′-Hydroxylase1") and *S8H* ("Scopoletin 8-Hydroxylase") genes encode enzymes involved in the last steps of the synthesis of the coumarins scopoletin and fraxetin (Schmid et al., 2014; Schmidt et al., 2014; Tsai and Schmidt, 2017a; Siwinska et al., 2018; Tsai et al., 2018). The *ABCG37* gene (also named *PDR9*) encodes an ABC transporter involved in the release of coumarins to the medium (Fourcroy et al., 2014, 2016; Zamioudis et al., 2014) while the *BGLU42* gene encodes a β-glucosidase, possibly required for the processing of glycosylated phenolic compounds as an essential step for their secretion in the root vicinity (Zamioudis et al., 2014; Stringlis et al., 2018b). Among the morphological responses are: development of subapical root hairs, cluster roots, and transfer cells, all of which are aimed to increase the surface of contact with the soil (Römheld and Marschner, 1986; Lucena et al., 2015; Romera et al., 2017). Both physiological and morphological responses are mainly located in the subapical regions of the roots (Römheld and Marschner, 1986).

The regulation of the physiological and morphological responses described above is not fully understood but in the last years several transcription factors (TFs) that participate in the activation of most of their associated genes have been described (Ivanov et al., 2012; Kobayashi and Nishizawa, 2012; Brumbarova et al., 2015; Zhang et al., 2015; Li et al., 2016; Liang et al., 2017). In *Arabidopsis*, the master regulator of most of these genes is FIT (bHLH29), homolog of the tomato FER (Bauer et al., 2007 and references therein). The FIT regulatory network comprises other bHLH TFs of the Ib subgroup, such as bHLH38, bHLH39, bHLH100, and bHLH101. All of them have redundant functions and can interact with FIT to form heterodimers that activate the expression of the Fe acquisition genes *FRO2* and *IRT1* (Yuan et al., 2008; Wang N. et al., 2013; Brumbarova et al., 2015). *FIT/FER* is induced in roots in response to Fe deficiency while the other Ib bHLH genes cited above are induced in both roots and leaves in response to Fe deficiency (Brumbarova et al., 2015 and references therein). FIT also controls MYB10 and MYB72, two other TFs essential for plant growth on low Fe conditions (Palmer et al., 2013; Zamioudis et al., 2014, 2015). Besides the FIT/Ib bHLH regulatory network, there is another regulatory network related to the POPEYE (PYE; bHLH47) TF and associated with the vasculature (Brumbarova et al., 2015). In the last years, it has been found that, under Fe-deficiency conditions, IVc subgroup bHLH TFs [bHLH34, bHLH104, bHLH105(ILR3), and bHLH115] activate *FIT/bHLH38/39/100/101* and *PYE* expression (Zhang et al., 2015; Li et al., 2016; Liang et al., 2017). Upstream of the IVc subgroup bHLH TFs is the BRUTUS (BTS) protein, which possesses Fe-binding domains and that interacts with IVc bHLH TFs, targeting them for proteasomal degradation (Zhang et al., 2015; Liang et al., 2017). Since the IVc bHLH TFs act as positive regulators of Fe deficiency responses, the current data suggests that BTS is a negative regulator of Fe deficiency responses (Zhang et al., 2015; Hindt et al., 2017).

The mechanisms by which plants perceive Fe deficiency and how this perception is transmitted to the activation of the responses is not fully understood. Several studies support a role for hormones and other plant signaling molecules in the activation of FIT and other TFs and, consequently, in the upregulation of the ferric reductase, the Fe^{2+} transporter and other Fe-related genes. Within them, the plant hormone ethylene (ET) has been found to play a key role in the regulation of most of the physiological and morphological responses to Fe deficiency (**Figure 1**; reviewed in Lucena et al., 2015; Li and Lan, 2017; Romera et al., 2017). Besides ET, auxin, nitric oxide (NO), sucrose, and glutathione (GSH) have also been involved in the regulation of Fe deficiency responses; all of them increase in Fe-deficient roots although their specific roles are not fully understood (Romera et al., 1999, 2011, 2017; Lucena et al., 2006, 2015; Graziano and Lamattina, 2007; Waters et al., 2007; Bacaicoa et al., 2009, 2011; García et al., 2010, 2011; Chen et al., 2010; Lingam et al., 2011; Meiser et al., 2011; Koen et al., 2012; Yang et al., 2014; Shanmugam et al., 2015; Lin et al., 2016; Li and Lan, 2017; Kailasam et al., 2018). By contrast to these activating signals, other ones have been implicated in the suppression of Fe deficiency responses, like cytokinins (Séguéla et al., 2008), jasmonic acid (JA; Maurer et al., 2011), brassinosteroids (Wang et al., 2012), and some phloem Fe-related signals (García et al., 2013, 2018). To integrate both positive and negative signals in the regulation of Fe acquisition genes in roots, a model has been proposed where auxin/ET/NO would act as activators of their expression, while LODIS ("LOng Distance Iron Signal": a phloem Fe-related signal) would act to repress them (Lucena et al., 2006; García et al., 2011, 2018; Romera et al., 2011, 2017).

INDUCED SYSTEMIC RESISTANCE (ISR)

Besides responses to abiotic stresses, plants also respond to biotic stresses provoked by biological agents, like pathogens or insects (Pieterse et al., 2014; Martínez-Medina et al., 2017; Verbon et al., 2017). Some of these responses are localized but others are systemic, spreading far from the attacked organ and inducing defensive responses in the entire

plant (Pieterse et al., 2014; Verbon et al., 2017). Within this second possibility, induced resistance is a physiological state of enhanced defensive capacity of the plant triggered by biological or chemical inducers, which protects plant tissues not exposed to the initial attack against future attack by pathogens and herbivorous insects (Van Loon et al., 1998). Induced resistance can be triggered in plants by the infection of pathogens, in response to insect herbivory, or upon root colonization by certain rhizosphere mutualistic microbes. Two of the most studied forms of induced resistance are SAR (Systemic Acquired Resistance), triggered by plant pathogens, and ISR, triggered by root-colonizing mutualistic microbes, like *Pseudomonas simiae* (syn. *Pseudomonas fluorescens*), *Paenibacillus polymyxa*, or *Trichoderma* spp. (**Table 1**; Zhang et al., 2009; Pieterse et al., 2012, 2014; Alizadeh et al., 2013; Zamioudis et al., 2014, 2015; Zhao et al., 2014; Martínez-Medina et al., 2017; Verbon et al., 2017). SAR and ISR are mainly differentiated on the basis of the elicitor and the regulatory pathways involved, though the signaling pathways that regulate SAR and ISR share some components (Pieterse et al., 1998, 2002, 2012, 2014; Van Loon et al., 1998; Choudhary et al., 2007).

Over the last years, SAR and ISR have been extensively reviewed (Van Loon et al., 1998; Choudhary et al., 2007; Pieterse et al., 2012, 2014), so here we only discuss major principles in both responses. In systemic tissues, SAR is characterized by increased levels of the hormone salicylic acid (SA) which, through the redox-regulated protein NON-EXPRESSOR OF *PR* GENES1 (NPR1), activates the expression of a large set of *PATHOGENESIS-RELATED* (*PR*) genes, involved in defense responses (**Figure 1**; Pieterse et al., 1998, 2002, 2012, 2014; Van Loon et al., 1998; Choudhary et al., 2007). By contrast to SAR, ISR is generally mediated by an SA-independent pathway where JA and ET are the central players, and typically functions without *PR* gene activation (**Figure 1**; Pieterse et al., 1998, 2002, 2012, 2014; Van Loon et al., 1998; Choudhary et al., 2007). Despite these differences, it has been shown that NPR1 is also required for the JA/ET-dependent ISR triggered by rhizosphere microbes although its role seems to be different in both processes (**Figure 1**; Pieterse et al., 2014; Nie et al., 2017). In SA signaling, NPR1 is related to a function in the nucleus while in JA/ET signaling it is related to a cytosolic function (Pieterse et al., 2014). Despite these general differences, in some particular cases, ISR can require SA accumulation (Ryu et al., 2003; Alizadeh et al., 2013). Moreover, the signaling pathways involved in the induction of ISR can be different depending on the microbial species and the plant species (Ryu et al., 2003; Jankiewicz and Koltonowicz, 2012; Alizadeh et al., 2013).

The discovery of ISR occurred around 1991, when several researchers showed that root colonization by certain non-pathogenic bacterial races promoted the health of plants upon the stimulation of their defense responses (reviewed in Pieterse et al., 2014). After these pioneering works with bacteria, ISR was further extended to rhizosphere fungi, like *Trichoderma* spp. or *Piriformospora indica* (**Table 1**; Segarra et al., 2009; Alizadeh et al., 2013; Pieterse et al., 2014).

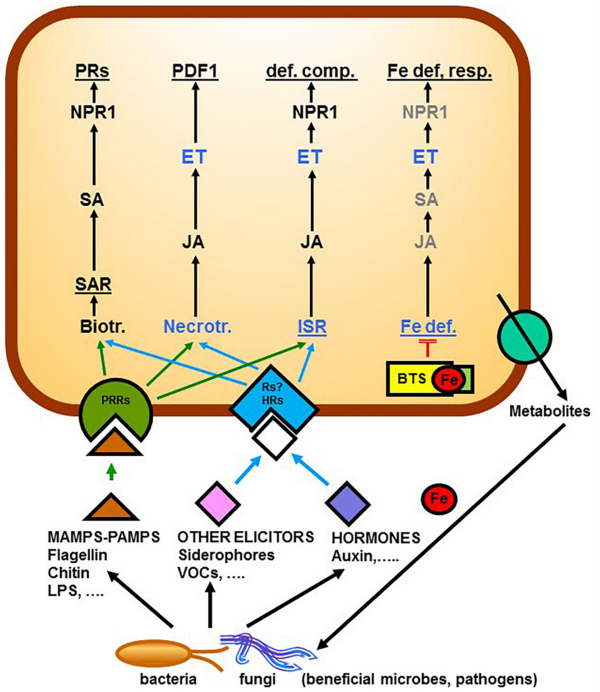

FIGURE 1 | Relationship between Fe deficiency responses in dicots and responses to pathogens (necrotrophs or biotrophs that elicit SAR) or to beneficial microbes that elicit ISR. Microbes can produce Microbe-Associated Molecular Patterns (MAMPs) or Pathogen-Associated Molecular Patterns (PAMPs), like flagellin, that are perceived by PRRs, or other elicitors, like Volatile Organic Compounds (VOCs), or siderophores, that are perceived by Rs (some of them unknown). In some cases, microbes themselves can produce hormones, like auxin, that are perceived by HRs. After the perception of the eliciting or hormonal signals by receptors, there is activation of signaling pathways including hormones that lead to the activation of the different responses. In the case of Fe, BTS binds Fe (probably a chelated form of Fe) and, in this way, blocks the signaling pathway leading to the activation of Fe deficiency responses. In several of these pathways (responses to necrotrophs, ISR and Fe deficiency) ET plays a key role. Roots can also release different metabolites, like coumarins, that can shape the rhizosphere microbiome. In gray are components whose participation in the process is not yet clear. BTS (Brutus protein), def. comp. (defensive compounds), ET (Ethylene), Fe def. resp. (Fe deficiency responses), HRs (Hormonal Receptors), ISR (Induced Systemic Resistance), JA (Jasmonic Acid), LPS (Lipopolysaccharides), MAMPs (Microbe-Associated Molecular Patterns), NPR1 (Nonexpressor of PR genes1), PAMPs (Pathogen-Associated Molecular Patterns), PDF1 (Plant Defensin), PRs (Pathogenic-Related proteins), PRRs (Pattern Recognition Receptors), SA (Salicylic Acid), Rs (Receptors), SAR (Systemic Acquired Resistance), VOCs (Volatile Organic Compounds). Based on Pieterse et al., 1998, 2012; Lucena et al., 2015; García et al., 2018; Stringlis et al., 2018b; Tyagi et al., 2018.

How Is ISR Triggered by Beneficial Rhizosphere Microbes?

The ways beneficial rhizosphere microbes elicit ISR are not totally understood but several microbial elicitors have been proposed to be responsible for its onset. These elicitors, upon perception, would trigger the ISR through the action of diverse plant hormones (**Figure 1**; Pieterse et al., 2012, 2014; Sharifi and Ryu, 2018; Tyagi et al., 2018). Among these elicitors,

there are Microbe-Associated Molecular Patterns (MAMPs) and other elicitors, like Volatile Organic Compounds (VOCs) or siderophores (**Figure 1**; Zhang et al., 2007, 2009; Jankiewicz and Koltonowicz, 2012; Orozco-Mosqueda et al., 2013; Pieterse et al., 2014; Zamioudis et al., 2015; Garnica-Vergara et al., 2016; Martínez-Medina et al., 2017; Sharifi and Ryu, 2018; Tyagi et al., 2018; Villena et al., 2018). MAMPs (when produced by pathogens are named Pathogen-Associated Molecular Patterns: PAMPs) are conserved microbial molecules released by the microbes, like flagellin, chitin, and lipopolysaccharides (LPS; Zeidler et al., 2004; Pieterse et al., 2014; Villena et al., 2018). VOCs are low molecular weight compounds derived from different biosynthetic pathways, with high vapor pressure and that can evaporate and disperse easily (Sharifi and Ryu, 2018; Tyagi et al., 2018). At present, over 1000 volatile compounds (including alkanes, alcohols, esters, ketones, sulfides, terpenoids, and sesquiterpenes) have been identified (Tyagi et al., 2018). Those derived from beneficial microbes can trigger drastic changes in plant growth patterns, generally by altering hormone signaling (Garnica-Vergara et al., 2016; Martínez-Medina et al., 2017; Sharifi and Ryu, 2018; Tyagi et al., 2018). Siderophores are Fe chelating agents released by the bacteria to further acquire Fe from the medium (Lemanceau et al., 2009; Aznar and Dellagi, 2015; Aznar et al., 2014, 2015).

Microbe-Associated Molecular Patterns are perceived by Pattern Recognition Receptors (PRRs) while other elicitors could be perceived by other Receptors (Rs), not known in all cases (**Figure 1**; Jankiewicz and Koltonowicz, 2012; Pieterse et al., 2014; Aznar and Dellagi, 2015; Aznar et al., 2015; Sharifi and Ryu, 2018; Tyagi et al., 2018; Villena et al., 2018). Upon perception, the elicitors trigger the ISR by affecting diverse plant hormones that act as central players in the plant immune signaling network leading to the activation of the defense responses (**Figure 1**; Pieterse et al., 2012, 2014; Sharifi and Ryu, 2018; Tyagi et al., 2018). In some cases, the microbes themselves can also produce different hormones, like auxin or cytokinins, that upon perception by the plant hormonal receptors (HRs) can cause changes in the root physiology and morphology (Grady et al., 2016; Scagliola et al., 2016; Asari et al., 2017; Kudoyarova et al., 2017; Patel and Saraf, 2017). Among the hormones implicated in the ISR, JA, ET, auxin, and NO play a key role (Knoester et al., 1999; Ton et al., 2001; Shoresh et al., 2005; Zhang et al., 2007; Van der Ent et al., 2008; Camehl et al., 2010; Acharya et al., 2011; Pieterse et al., 2014; Garnica-Vergara et al., 2016; Hossain et al., 2017; Martínez-Medina et al., 2017; Nie et al., 2017; Nascimento et al., 2018; Stringlis et al., 2018a).

ISR Characteristics

One general characteristic of the microbial elicitors that induce ISR is their redundancy. This redundancy implies that microbial mutants defective in one elicitor can induce ISR through other elicitors (Meziane et al., 2005; Pieterse et al., 2014; Zamioudis et al., 2015). For example, the siderophore pseudobactin was as effective in inducing ISR as live bacteria but a mutant defective in pseudobactin biosynthesis was equally effective (Meziane et al., 2005). Beneficial ISR-eliciting microbes do not directly activate defense responses but sensitize the whole plant (a phenomenon called priming) for a faster and stronger activation of defense responses upon invasion by pathogens (Choudhary et al., 2007; Berendsen et al., 2012; Jung et al., 2012; Pieterse et al., 2014; Martinez-Medina et al., 2016). A high percentage of the genes, predominantly associated with defense responses, induced by the elicitors, like flagellin, are suppressed by the ISR-eliciting microbes to allow the establishment of a mutually beneficial interaction with the host root (Stringlis et al., 2018a). There is increasing evidence that beneficial soil-borne microbes hijack plant hormone signaling pathways to suppress the host defenses (Pieterse et al., 2012). This is also the case for the symbiotic relationship between legumes and rhizobia where the defense reactions set up by the plant are quickly suppressed, allowing microbial entry and the potential successful rhizobial establishment in plant roots (Guinel, 2015).

To elicit ISR, beneficial rhizobacteria must reach a minimal concentration equal to 10^5–10^7 colony forming unit (CFU) per gram of root for several days (Jankiewicz and Koltonowicz, 2012; Bakker et al., 2013; Pieterse et al., 2014). It should be noted that in the rhizosphere, the microbial density can range from 10^8 to 10^9 bacteria per gram and that its diversity is generally less than in the bulk soil since plant exudates specifically stimulate or repress members of the microbial community shaping the root microbiome (**Figure 1**; Berendsen et al., 2012; Bakker et al., 2013; Pii et al., 2016a; Stringlis et al., 2018b). In this sense, very recently it has been found that the release of the antimicrobial coumarin scopoletin by roots of Arabidopsis plants inoculated with the rhizobacterium *P. simiae* inhibits some soil-borne pathogens but not the rhizobacterium (Stringlis et al., 2018b). Coumarins are phenolic compounds that are also released by Fe-deficient roots to favor the Fe acquisition of plants (Schmid et al., 2014; Schmidt et al., 2014; Tsai and Schmidt, 2017a; Siwinska et al., 2018; Tsai et al., 2018; see also Section "Fe deficiency responses in dicot plants"). Consequently, the ISR-eliciting microbes, by inducing the release of coumarins and other Fe deficiency responses in plants, can improve the Fe nutrition of plants but, at the same time, they can benefit from a niche where their competitors are eliminated or restricted (Stringlis et al., 2018b).

INTERRELATIONSHIP BETWEEN ISR AND Fe DEFICIENCY RESPONSES IN DICOT PLANTS

Since Fe acquisition is a limiting factor in most soils, Fe is a central player in the tripartite interaction among beneficial microbes, pathogens, and plants (López-Berges et al., 2013; Naranjo-Arcos and Bauer, 2016; Verbon et al., 2017). This close interrelation is in good agreement with the already described relationship between Fe homeostasis and defense responses against pathogens in plants (Lemanceau et al., 2009; Aznar et al., 2015; Verbon et al., 2017) and with the crosstalk between ISR and Fe deficiency responses (Pieterse et al., 2014; Verbon et al., 2017). The relationship between plant defense responses and Fe deficiency is complex and depends on several factors, like the plant genotype, the kind of pathogens and the intensity and duration of the deficiency. In some cases, plants are more tolerant to pathogens under conditions of Fe deficiency,

TABLE 1 | Microbial species that induce Fe deficiency responses when applied to dicot plants.

Microbial species	Plant species	Mode appl.	Signals	Fe def. resp.	Fe genes	Fe Gr.	Refs
Rhizobacteria							
Azospirillum brasilense	*Solanum lycopersicum*	gm(a)	ET Auxin	Root hairs	nd	∧	Ribaudo et al., 2006
Azospirillum brasilense	*Cucumis sativus*	gm(ns)	nd	FCR, pH	*FIT FRO1 IRT1 HA1*	Fe	Pii et al., 2016b
Bacillus subtilis	*Arabidopsis thaliana*	gm(a)	VOCs	FCR, pH	*FIT FRO2 IRT1*	Fe	Zhang et al., 2009
*Arthrobacter agilis**	*Medicago truncatula*	gm(a)	VOCs	FCR, pH	nd	Fe ∧	Orozco-Mosqueda et al., 2013
Pseudomonas simiae	*Arabidopsis thaliana*	gm(a)	VOCs Auxin NO	FCR phenolics	*FIT FRO2 bHLH38 bHLH39 IRT1 F6′H1 MYB72 BGLU42 ABCG37*		Zamioudis et al., 2014, 2015; Stringlis et al., 2018b
*Enterobacter** *Pseudomonas*	*Cucumis sativus*	gm(ns)	Auxin	FCR	nd	nd	Scagliola et al., 2016
Paenibacillus polymyxa	*Arabidopsis thaliana*	gm(a)	Auxin	FCR, pH, phenolics	*FIT FRO2 IRT1 MYB72 F6′H1*	Fe ∧	Zhou et al., 2016a
Bacillus amyloliquefaciens	*Arabidopsis thaliana*	gm(a)	VOCs Auxin NO	FCR	*FIT FRO2 IRT1*	Fe ∧	Wang J. et al., 2017; Zhou et al., 2017
Burkholderia cepacia	*Astragalus sinicus*	ri(s)	Auxin	FCR, pH, flavins	*FIT FRO2 IRT1 AHA2*	Fe ∧	Zhou et al., 2018
Rhizofungi							
Trichoderma asperellum	*Cucumis sativus*	gm(s)	nd	FCR	nd	Fe ∧	Zhao et al., 2014
Trichoderma asperellum, *T. harzianum*	*Arabidopsis thaliana*	gm(a)	VOCs	FCR, root hairs	*FIT FRO2 bHLH38 bHLH39 IRT1 MYB72*	nd	Martínez-Medina et al., 2017
Trichoderma asperellum, *T. harzianum*	*Solanum lycopersicum*	gm(a)	VOCs	FCR, root hairs	*FER FRO1 IRT1*	nd	Martínez-Medina et al., 2017

*Mode appl., mode of application of the microbes (gm, application to the growth medium; ri, root immersion; a, agar; ns, nutrient solution; s, soil); Signals, elicitors and hormones involved; Fe def. resp., Fe deficiency responses; FCR, ferric chelate reductase activity; pH, acidification; Fe genes, Fe acquisition genes; Fe Gr., increased shoot Fe concentration (Fe) and increased shoot growth (∧); nd, not determined; *, microbial species whose association with ISR is not yet clear.*

probably because pathogens require an adequate quantity of Fe for full virulence (Kieu et al., 2012; López-Berges et al., 2013). However, in other cases, plants are more susceptible to pathogens under Fe-deficient conditions (Verbon et al., 2017 and references therein). The competition for Fe between soil-borne pathogens and their antagonistic microorganisms has been related to disease suppression; siderophores produced in the rhizosphere by PGPR can inhibit growth of the pathogens by depriving them of Fe (Verbon et al., 2017). In contrast to the negative effect of some soil-borne pathogens on Fe acquisition, there are several recent reviews showing an important role of beneficial rhizosphere microbes on the Fe nutrition of plants (Jin et al., 2014; Mimmo et al., 2014; Pii et al., 2015; İpek and Esitken, 2017). These microbes can directly improve Fe nutrition through the release of H^+ and/or Fe- solubilizing compounds to soils, like siderophores and organic acids, or by inducing changes in root physiology and architecture, which can improve the acquisition of Fe and also of other nutrients (Orozco-Mosqueda et al., 2013; Jin et al., 2014; Mimmo et al., 2014; Zhao et al., 2014; Contreras-Cornejo et al., 2015; Pii et al., 2015, 2016b; Garnica-Vergara et al., 2016; Scagliola et al., 2016; Verbon and Liberman, 2016; Zhou et al., 2016a,b; Martínez-Medina et al., 2017; Sonbarse et al., 2017; Sharifi and Ryu, 2018; Stringlis et al., 2018a). In this way, it has been demonstrated that ISR-eliciting microbes can induce Fe deficiency responses in their host roots, such as enhanced ferric reductase activity, acidification of the rhizosphere, release of phenolics and flavins, and development of root hairs; and the expression of the genes associated with these responses, such as *FIT*, *bHLH38*, *bHLH39*, *MYB72*, *MYB10*, *FRO2*, *IRT1*, *AHA*, *F6′H1*, *BGLU42*, *ABCG37*, and others (**Figures 1**, **2** and **Table 1**; Ribaudo et al., 2006; Zhang et al., 2009; Zamioudis et al., 2014, 2015; Zhao et al., 2014; Pii et al., 2016b; Scagliola et al., 2016; Verbon and Liberman, 2016; Zhou et al., 2016a,b, 2018; Martínez-Medina et al., 2017; Verbon et al., 2017; see also Section "Fe deficiency responses in dicot plants" and Section "Rhizosphere microbial species that induce Fe deficiency responses and improve Fe acquisition").

Since bacteria that elicit ISR can release siderophores to the medium, it has been speculated that perhaps these Fe chelating agents could deprive plants of Fe and in this way cause the induction of Fe deficiency responses (Van der Ent, 2008; Aznar et al., 2014; Pieterse et al., 2014; Aznar and Dellagi, 2015; Zamioudis et al., 2015). However, mutants defective in siderophore biosynthesis also induce Fe deficiency responses, which suggests that they could induce these responses through other mechanisms (Meziane et al., 2005; Pieterse et al., 2014; Zamioudis et al., 2015). A possibility could be through alteration of hormone biosynthesis and signaling in the plants. In this sense, the plant hormone ET has been implicated in both the activation of ISR (Knoester et al., 1999; Ton et al., 2001; Shoresh et al., 2005; Camehl et al., 2010; Pieterse et al., 2012; Garnica-Vergara et al., 2016; Hossain et al., 2017; Nie et al., 2017) and the activation of Fe deficiency responses (**Figures 1**, **2**; reviewed in Lucena et al., 2015; Li and Lan, 2017; Romera et al., 2017). Besides

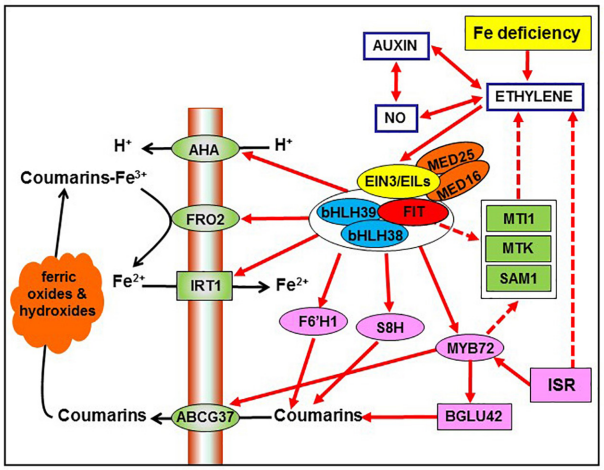

FIGURE 2 | Possible interrelationship between ISR and Fe deficiency responses through the common participation of ethylene in both processes (see **Figure 1**). Ethylene, through the activation of the transcription factors FIT, bHLH38, and bHLH39, can up-regulate the expression of several genes associated with Fe deficiency, like *AHA*, *FRO2*, *IRT1*, *F6'H1*, and *S8H*. Additionally, FIT/bHLH38/bHLH39 can up-regulate the expression of *MYB72*, which activates the β-glucosidase BGLU42 and the phenolic efflux transporter ABCG37, both being implicated in the secretion of phenolic compounds, like coumarins. Moreover, FIT and MYB72 could indirectly act by affecting ethylene synthesis, through the upregulation of *SAM1*, *MTK*, and *MTI1*. Besides ethylene, auxin, and nitric oxide (NO) can also affect these Fe-related genes since they are closely interrelated with ethylene. Based on Lucena et al. (2015). For more details, see Section "Interrelationship between ISR and Fe deficiency responses."

ET, other hormones and signaling molecules, like auxin, and NO, have also been implicated in both processes (García et al., 2010; Acharya et al., 2011; Romera et al., 2011, 2017; Zamioudis, 2012; Jin et al., 2014; Contreras-Cornejo et al., 2015; Garnica-Vergara et al., 2016; Poupin et al., 2016; Stringlis et al., 2018a). Moreover, the root-specific MYB72 TF, that plays a key role in the onset of ISR (Van der Ent et al., 2008; Segarra et al., 2009; Zamioudis et al., 2014; Verbon et al., 2017; Stringlis et al., 2018b), is also essential for plant growth on low Fe conditions (**Figure 2**; García et al., 2011; Palmer et al., 2013; Zamioudis et al., 2014, 2015; Lucena et al., 2015; Verbon et al., 2017; see also Section "Fe deficiency responses in dicot plants"). This indicates that MYB72 is a node of convergence between ISR and Fe deficiency responses (Van der Ent et al., 2008; Segarra et al., 2009; Pieterse et al., 2014; Zamioudis et al., 2014, 2015; Verbon et al., 2017). All these results suggest that the regulatory pathways of ISR and Fe deficiency responses overlap. In the following paragraphs the main common components shared by ISR and Fe deficiency responses are described and analyzed.

Ethylene and Other Hormones and Signaling Molecules

As previously stated (see Section "Induced Systemic Resistance"), ISR is generally mediated by a pathway where JA and ET are the central players (**Figure 1**; Pieterse et al., 1998, 2002, 2012, 2014; Van Loon et al., 1998; Choudhary et al., 2007). In this pathway, JA acts upstream of ET, and ET upstream of the NPR1 protein (**Figure 1**; Pieterse et al., 1998, 2002, 2012, 2014; Van Loon et al., 1998; Choudhary et al., 2007). NPR1 functions in the nucleus as a transcriptional coactivator of SA-responsive genes during the SAR pathway, but NPR1 also plays a cytosolic function in the JA/ET signaling during the ISR pathway (**Figure 1**; Pieterse et al., 2014). In relation to these components (ET, JA, SA, and NPR1), ET has been clearly implicated in the regulation of Fe deficiency responses in Strategy I plants and in rice, that presents characteristics of both Strategy I and II plant species (reviewed in Lucena et al., 2015; Li and Lan, 2017; Romera et al., 2017). However, the roles of the other components (JA, SA, and NPR1) on Fe deficiency responses are not yet clear. For instance, JA has been implicated in the regulation of Fe deficiency responses in Strategy I plants but as a suppressor of these responses (Maurer et al., 2011). In rice, JA has been shown to activate the expression of some Fe deficiency responses at the very early stages of the Fe deficiency (0.5–1 h) but strongly suppresses them later on (3–6 h; Kobayashi et al., 2016). In relation to the role of SA on the regulation of Fe deficiency responses, the results are contrasting. It was shown that Arabidopsis lines overexpressing the SA-inducible transcription factor OBF−BINDING PROTEIN 3 (OBP3) present upregulation of *bHLH038* and *bHLH039*, encoding two TFs that play a key role in the activation of Fe acquisition genes (Kang et al., 2003; see Section "Fe deficiency responses in dicot plants"). In the same way, exogenous application of SA to Arabidopsis plants upregulates the expression of *YELLOW STRIPE-LIKE1* (*YSL1*) and *YSL3*, which are involved in Fe translocation and homeostasis (Chen et al., 2014; Kumar et al., 2017). Shen et al. (2016) further found that Fe deficiency increases SA contents in shoots and roots of Arabidopsis plants, and that the SA biosynthesis defective mutant *phytoalexin deficient 4* (*pad4*) presents altered Fe deficiency responses, suggesting a link between SA and Fe deficiency. However, Maurer et al. (2014) found that SA and SA signaling through NPR1 (**Figure 1**) do not affect Fe deficiency responses. To complete this network of interactions, some Fe-related TFs, such as ILR3 (bHLH105; belonging to the IVc bHLH subgroup; Zhang et al., 2015; see also Section "Fe deficiency responses in dicot plants"), can affect JA and SA biosynthesis (Aparicio and Pallás, 2017). After analyzing all these results, it is clear that the role of JA and SA on the regulation of Fe deficiency responses in dicots deserves further research.

In relation to ET, this plant hormone is synthetized from the amino acid methionine, through a pathway requiring SAMS (S-adenosyl methionine synthetase), ACS [1-aminocyclopropane-1-carboxylic acid (ACC) synthase], and ACO (ACC oxidase; Sauter et al., 2013; Wang F. et al., 2013; Dubois et al., 2018):

$$\text{Methionine} \xrightarrow{SAMS} \text{SAM} \xrightarrow{ACS} \text{ACC} \xrightarrow{ACO} \text{Ethylene}$$

Although ET's mode of action is not fully understood, a linear signaling pathway has been proposed in Arabidopsis

(Shakeel et al., 2013; Wang F. et al., 2013; Dubois et al., 2018):

$$\text{ET} \dashv\!\| \text{ ET receptors} \rightarrow \text{CTR1} \dashv\!\| \text{ EIN2} \rightarrow \text{EIN3/EILs} \rightarrow \text{ERFs} \rightarrow \text{ET responses}$$

In this signaling pathway, all the components are proteins and, within them, EIN3/EILs and ERFs are TFs (for more details, see Shakeel et al., 2013; Wang F. et al., 2013; Lucena et al., 2015; Dubois et al., 2018).

The participation of ET in the regulation of Fe deficiency responses was first proposed by Romera and Alcántara (1994) and has been further supported by many experimental data (recently reviewed in Lucena et al., 2015; Li and Lan, 2017; Romera et al., 2017). As more recent evidence, it should be mentioned that FIT (master regulator of Fe acquisition genes in Arabidopsis; see Section "Fe deficiency responses in dicot plants") interacts with the EIN3 and EIL1 TFs, associated with ET signaling, and with MED16 and MED25, Mediators, to form a complex implicated in the transcription of Fe acquisition genes (**Figure 2**; Lingam et al., 2011; Yang et al., 2014; Brumbarova et al., 2015). In the same way, recently it has been found that the ERF4 and ERF72 TFs, that are also associated with ET signaling, are induced under Fe deficiency and participate in the regulation of Fe deficiency responses (Liu et al., 2017a,b). Fe deficiency causes the upregulation of genes involved in both ET synthesis, like *SAM*, *ACS*, *ACO*, *MTK*, *MTI1*, *MPK3*, and *MPK6*, and signaling, like *EIN2*, *EIN3*, *EIL1*, *EIL3*, *ERF4*, and *ERF72*, in roots of different dicot plants (García et al., 2010; Ye et al., 2015; Li and Lan, 2017; Romera et al., 2017). MTK (5-methylthioribose kinase) and MTI1 (5-methylthioribose-1-phosphate isomerase1) participate in the Yang cycle and are necessary for ET biosynthesis (Pommerrenig et al., 2011; Sauter et al., 2013). Both *MTK* and *MTI1*, besides their upregulation under Fe deficiency, are also regulated by ET, probably through FIT (**Figure 2**; Colangelo and Guerinot, 2004; García et al., 2010). *MTI1* (At2g05830) was previously identified as eIF-2B, a putative eukaryotic translation initiation factor (García et al., 2010; Pommerrenig et al., 2011). The mitogen-activated protein kinases 3 and 6 (MPK3/MPK6) are related to ET (Li et al., 2012; Contreras-Cornejo et al., 2015; Dubois et al., 2018) and can activate ACS2/6 in Fe deficiency-induced ET production (Ye et al., 2015).

Ethylene has been involved in the regulation of both morphological and physiological responses to Fe deficiency in Strategy I plants (Romera and Alcántara, 1994, 2004; Lucena et al., 2015; Li and Lan, 2017; Romera et al., 2017). In relation to the morphological responses, ET has been implicated in the formation of subapical root hairs, cluster roots, and transfer cells (reviewed in Lucena et al., 2015). In relation to the physiological responses, ET has been implicated in the upregulation of *FIT* (or its tomato homolog *FER*), *bHLH38*, *bHLH39*, and *MYB72*, encoding key TFs (**Figure 2**; Lucena et al., 2006; García et al., 2010; Lingam et al., 2011). bHLH38 and bHLH39 interact with FIT to form heterodimers that activate the expression of the Fe acquisition genes *FRO2* (ferric reductase) and *IRT1* (iron transporter) (**Figure 2**; Yuan et al., 2008; Wang N. et al., 2013). Similarly, the acidification capacity, depending on *AHA*-like genes (Colangelo and Guerinot, 2004), is also activated by FIT and consequently by ET (**Figure 2**; Waters et al., 2007; Lucena et al., 2015). In relation to the excretion of phenolics, it has been found that the expression of *F6′H1* and *S8H*, involved in their synthesis, is dependent on FIT (**Figure 2**; García et al., 2010; Schmid et al., 2014; Tsai and Schmidt, 2017a; Tsai et al., 2018; see also "Fe deficiency responses in dicots"). Consequently, both of them would also be dependent on ET (**Figure 2**). In supporting this view, *S8H* (At3g12900) is greatly induced in Fe deficient roots and drastically inhibited by ethylene inhibitors (García et al., 2010). Besides all the above genes related to Fe acquisition, ET also participates in the activation of *NAS1* (nicotianamine synthase1), *NAS2*, and *FRD3* (ferric reductase defective3), that are very important for internal Fe mobilization and homeostasis (García et al., 2010).

Besides its involvement in Fe deficiency responses, ET has also been implicated in the development of ISR triggered by root-colonizing microbes, acting downstream of JA (**Figure 1**; Knoester et al., 1999; Ton et al., 2001; Shoresh et al., 2005; Ribaudo et al., 2006; Van Loon et al., 2006; Van der Ent, 2008; Camehl et al., 2010; Pieterse et al., 2012; Zamioudis, 2012; Contreras-Cornejo et al., 2015; Garnica-Vergara et al., 2016; Hossain et al., 2017; Nie et al., 2017; Nascimento et al., 2018). In general, root colonization by ISR-eliciting microbes does not induce a direct enhancement of ET and JA biosynthesis (Knoester et al., 1999; Pieterse et al., 2014) except in some cases (Ribaudo et al., 2006; Contreras-Cornejo et al., 2015). However, the expression of genes involved in ET biosynthesis, like *ACSs* and *ACOs*, and signaling, like *ETR1*, *EIL3*, *CTR1*, and *ERFs*, is frequently upregulated in roots by ISR-eliciting microbes (Shoresh et al., 2005; Ribaudo et al., 2006; Van der Ent et al., 2008; Velivelli et al., 2015; Zamioudis et al., 2015; Poupin et al., 2016). For example, root colonization by *P. simiae* WCS417 induced the upregulation of *ACS2*, *ACS6*, and *EIL3* in Arabidopsis roots (Van der Ent et al., 2008; Zamioudis et al., 2015), which are also upregulated under Fe deficiency (García et al., 2010; Ye et al., 2015).

In both processes, ISR and Fe deficiency responses, ET can have a dual role. It is necessary for the activation of Fe deficiency responses (Lucena et al., 2015; Li and Lan, 2017; Romera et al., 2017) and for the onset of ISR (Knoester et al., 1999; Ton et al., 2001; Shoresh et al., 2005; Ribaudo et al., 2006; Pieterse et al., 2012, 2014; Garnica-Vergara et al., 2016; Hossain et al., 2017; Nie et al., 2017; Nascimento et al., 2018). However, when accumulated in excess, ET can have negative effects on the responses to Fe deficiency (Romera et al., 1999), on the growth of plants and on the mutualistic interactions with beneficial microbes (Pierik et al., 2007; Camehl et al., 2010; Gamalero and Glick, 2015; Nascimento et al., 2018). This dual role also occurs for the nodulation between legumes and rhizobia, where ET is crucial for the proper development of the rhizobial colonization but also acts as a negative regulator to limit the number of rhizobial infections (Zamioudis, 2012; Guinel, 2015). To avoid the detrimental effects of ET, some beneficial microbes and plant species possess the enzyme ACC deaminase, that eliminates the ET

precursor ACC (Gamalero and Glick, 2015; Singh et al., 2015; Nascimento et al., 2018).

The participation of ET on morphological and physiological responses to Fe deficiency and on ISR probably follows different ET signaling pathways. While several Arabidopsis ethylene insensitive mutants, like *etr1*, *ein2*, *ein3*, and *eir1*, are blocked in their capacity to mount the ISR (Knoester et al., 1999; Ton et al., 2001; Van Loon et al., 2006; Camehl et al., 2010; Zamioudis, 2012; Alizadeh et al., 2013; Contreras-Cornejo et al., 2015; Hossain et al., 2017; Nie et al., 2017), and to develop morphological responses to Fe deficiency (Romera and Alcántara, 2004), they can induce most of the physiological responses to Fe deficiency (Romera and Alcántara, 2004; Lucena et al., 2006; García et al., 2010). These differences are perhaps related to the existence of an alternate route for ethylene signaling, besides the conventional one that includes EIN2 (see above; Shakeel et al., 2013). At this point, it has been suggested that for several physiological responses, ET could act through a pathway where EIN2 is not strictly required (Lucena et al., 2015).

Besides ET, other hormones and signaling molecules, such as auxin, GSH and NO have also been involved in both ISR and Fe deficiency responses (Ribaudo et al., 2006; Graziano and Lamattina, 2007; Bacaicoa et al., 2009, 2011; Chen et al., 2010; García et al., 2010, 2011, 2018; Acharya et al., 2011; Romera et al., 2011, 2017; Jin et al., 2014; Contreras-Cornejo et al., 2015; Shanmugam et al., 2015; Zamioudis et al., 2015; Garnica-Vergara et al., 2016; Poupin et al., 2016; Zhou et al., 2016a, 2017, 2018; Wang J. et al., 2017; Gullner et al., 2018; Kailasam et al., 2018; Sharifi and Ryu, 2018; Stringlis et al., 2018a; Sumayo et al., 2018; Tyagi et al., 2018). All of them increase in roots under Fe deficiency and frequently upon colonization of roots by ISR-eliciting microbes (Romera et al., 1999; Ribaudo et al., 2006; Graziano and Lamattina, 2007; Bacaicoa et al., 2009, 2011; Chen et al., 2010; Contreras-Cornejo et al., 2015; Shanmugam et al., 2015; Zamioudis et al., 2015; Zhou et al., 2016a, 2017; Wang J. et al., 2017; Kailasam et al., 2018). Some microbial elicitors, like VOCs or LPS, can affect ET, auxin or NO production and/or signaling, and in this way upregulate Fe-related genes (Zeidler et al., 2004; Zhang et al., 2007, 2009; Kwon et al., 2010; Liu and Zhang, 2015; Zamioudis et al., 2015; Garnica-Vergara et al., 2016; Zhou et al., 2017; Wang J. et al., 2017; Sharifi and Ryu, 2018; Tyagi et al., 2018). As examples, VOCs from *Bacillus subtilis* GB03 upregulated the expression of several ET biosynthesis genes (Kwon et al., 2010) and VOCs from *P. simiae* WCS417 or *Bacillus amyloliquefaciens* BF06 caused NO accumulation in Arabidopsis roots and upregulated several Fe-related genes (Zamioudis et al., 2015; Wang J. et al., 2017). Moreover, some of these hormones and signaling molecules can affect the perception of microbial elicitors. For example, the PRR for flagellin (FLAGELLIN-SENSING 2-FLS2) is regulated by ET (Boutrot et al., 2010).

Ethylene, auxin, and NO are closely interrelated since each one can affect the synthesis and/or action of the others (**Figure 2**; Ribaudo et al., 2006; Chen et al., 2010; García et al., 2011, 2018; Romera et al., 2011, 2017; Contreras-Cornejo et al., 2015; Garnica-Vergara et al., 2016; Poupin et al., 2016; Zhou et al., 2017). As a probe of their close interrelationship, *FIT*, *MYB72*, and other Fe- and ISR-related genes are similarly affected by ET, auxin, or NO treatments. They are upregulated by these molecules, or their precursors, and downregulated by their inhibitors (Graziano and Lamattina, 2007; Chen et al., 2010; García et al., 2010, 2011; Zamioudis et al., 2015; Wang J. et al., 2017; Zhou et al., 2017; Stringlis et al., 2018a; Sumayo et al., 2018).

In the last years, the roles of GSH and NO in the activation of responses to Fe deficiency are becoming more complex since several experimental results have shown that *S*-nitrosoglutathione (GSNO), derived from GSH and NO, specifically works in such an activation having a different role that the one of NO (García et al., 2018; Kailasam et al., 2018). NO, GSH, and GSNO have also been implicated in plant defense responses against pathogens, and NO and GSH in ISR (Zamioudis et al., 2015; Yun et al., 2016; Gullner et al., 2017, 2018). Moreover, in plant defense responses, NO and GSNO exhibit additive functions and, by extension, may have distinct or overlapping molecular targets (Yun et al., 2016). The roles of GSH and GSNO in these processes have been related to their capacity to detoxify toxins (by their conjugation with GSH), to their interconnection with reactive oxygen species and SA, and to their capacity to modulate the redox state of NPR1 and to *S*-nitrosylate defense-related TFs and transcriptional coregulators (Yun et al., 2016; Gullner et al., 2017, 2018). However, to our knowledge, only NO has been implicated in the signaling processes leading to the activation of Fe acquisition genes by ISR-eliciting microbes (Zamioudis et al., 2015) while GSH and GSNO have not yet been studied in relation to this activation, which deserves further research.

MYB72 and Other Transcription Factors

Some years ago, it was found that the *MYB72* gene, encoding a TF, was greatly induced in Arabidopsis roots under Fe deficiency (Colangelo and Guerinot, 2004) and also upon their colonization with the ISR-eliciting rhizobacterium *P. simiae* WCS417 (Verhagen et al., 2004; Van der Ent, 2008; Van der Ent et al., 2008). Later on, *MYB72* upregulation has also been demonstrated with other ISR-eliciting microbes (Segarra et al., 2009; Alizadeh et al., 2013; Pieterse et al., 2014; Martínez-Medina et al., 2017; Verbon et al., 2017). Furthermore, Arabidopsis *myb72* knockout mutants are defective in the activation of ISR which suggests that MYB72 plays a key role in the early signaling steps of this process (**Figure 2**; Van der Ent, 2008; Van der Ent et al., 2008; Segarra et al., 2009; Alizadeh et al., 2013; Zamioudis et al., 2014, 2015; Stringlis et al., 2018b). However, overexpression of MYB72 did not result in enhanced resistance against any of the pathogens tested, demonstrating that MYB72 is not sufficient for the expression of ISR (Van der Ent et al., 2008). In both Fe deficiency and ISR, *MYB72* is upregulated along with *MYB10*, also encoding a TF (Colangelo and Guerinot, 2004; Zamioudis, 2012; Palmer et al., 2013; Zamioudis et al., 2015). MYB72 and MYB10 physically interact *in vivo* and function redundantly in regulating the expression of genes involved in the shikimate, the phenylpropanoid and the nicotianamine (NA) biosynthesis pathways (Zamioudis, 2012; Zamioudis et al., 2014, 2015; Stringlis et al., 2018b). Under

Fe deficiency, both MYB72 and MYB10 act early in the Fe deficiency regulatory cascade to drive gene expression of *NAS2* and *NAS4*, two NA synthase genes (Palmer et al., 2013). An important difference of the participation of MYB72 and MYB10 in ISR and Fe deficiency responses is that the Arabidopsis *myb72* mutants are defective in the activation of ISR (see above) while they behave apparently normal when grown on alkaline soil, a condition that favors Fe deficiency (Palmer et al., 2013). However, the *myb10myb72* double mutant displays seedling lethality when grown on alkaline soil (Palmer et al., 2013). This suggests that MYB10 and MYB72 have overlapping roles in relation to Fe deficiency (Palmer et al., 2013). In relation to ISR, MYB72, and MYB10 coordinately suppress the expression of a large group of defense-related genes upon root colonization by *P. simiae* WCS417, enabling the bacteria to establish long-term associations with host roots (Zamioudis, 2012). The bacteria can also colonize roots of the *myb72* mutant (Van der Ent et al., 2008), suggesting that MYB10 may compensate in defense suppression (Zamioudis, 2012).

MYB72 is consequently a node of convergence between ISR and Fe deficiency responses in dicots. This convergence is further supported when considering that *MYB72* expression is controlled by FIT either under Fe deficiency or upon colonization of roots by ISR-eliciting microbes (**Figure 2**; Colangelo and Guerinot, 2004; Sivitz et al., 2012; Palmer et al., 2013; Zamioudis et al., 2015). Moreover, FIT interacts with the bHLH38 TF to control *MYB72* expression upon colonization of roots by ISR-eliciting microbes (Zamioudis et al., 2015), as occurred with *FRO2* and *IRT1* expression under Fe deficiency (Yuan et al., 2008). *FIT*, *bHLH38*, and *MYB72* expression is activated by ET (García et al., 2010, 2011), which suggests a connection between the regulation of Fe deficiency responses and ISR through this plant hormone. In supporting this view, several *P. simiae* WCS417-inducible MYB72 target genes, like *BGLU42* (β-glucosidase), *CYP71B5* (cytochrome P450), *At5g55620* (unknown function), and *bHLH39* (TF), are all induced by Fe deficiency and also activated by ET (García et al., 2010; Zamioudis et al., 2014). Moreover, *MYB72* and *BGLU42* present ET-responsive elements in their promoters (García et al., 2010). Similarly, there are genes associated with the biosynthesis and release of coumarins to the rhizosphere, like *F6′H1*, *S8H*, and *ABCG37*, that are upregulated both under Fe deficiency and upon colonization of roots by ISR-eliciting microbes. These genes are dependent on FIT (*F6′H1*, *S8H*) or MYB72 (*ABCG37*) and, consequently, on ET (**Figure 2**; García et al., 2010; Schmid et al., 2014; Schmidt et al., 2014; Zamioudis et al., 2014; Tsai and Schmidt, 2017a; Siwinska et al., 2018; Tsai et al., 2018; see also Section "Fe deficiency responses in dicot plants").

The results about the relationship of MYB72 and ET are controversial. For example, Van der Ent et al. (2006) showed that *MYB72* transcript levels accumulated after treatment with the ET precursor ACC and that they did not accumulate in the Arabidopsis ethylene insensitive mutant *ein2-1* upon root colonization with the ISR-eliciting bacterium *P. simiae* WCS417. However, later on, these authors found that *MYB72* transcript levels did not accumulate after treatment with ACC while they accumulated in the *ein2-1* mutant upon treatment with *P. simiae* WCS417 (Van der Ent et al., 2008). After these latter results, they concluded that *MYB72* expression was not regulated by ET (Van der Ent et al., 2008). Similarly, it was found, by using yeast two-hybrid screening, that MYB72 physically interacted *in vitro* with EIL3, a TF associated with ET signaling (Van der Ent et al., 2008) while later on it was found, by using Bimolecular Fluorescence Complementation, that MYB72 and EIL3 did not interact *in vivo* (Zamioudis, 2012). Curiously, *EIL3* expression is upregulated both under Fe deficiency (García et al., 2010) and upon colonization of roots with *P. simiae* WCS417 (Van der Ent et al., 2008). Today, there is enough evidence to support the regulation of *FIT*, *bHLH38*, and *bHLH39* by ET and, consequently, the one of *MYB72*. For example, both *FIT* and *MYB72* are upregulated by ET treatment (García et al., 2010). In relation to FIT regulation, it has been shown that the ET-signaling TFs EIN3 and EIL1 interact with FIT to favor its stability and activity (Lingam et al., 2011; Yang et al., 2014; Brumbarova et al., 2015; see Subsection "Ethylene and other hormones and signaling molecules"). The upregulation of *MYB72* in the *ein2-1* mutant could be explained by taking into account the upregulation of *FIT*, *bHLH38*, and *bHLH39* in this mutant (García et al., 2010). This could be related to the existence of an alternate route for ethylene signaling, besides the conventional one including EIN2 (Shakeel et al., 2013; Lucena et al., 2015). The complexity of the relationship between MYB72 and ET is also manifested when considering that MYB72 can also affect ET biosynthesis: the *SAM1* gene, encoding a SAM synthetase enzyme involved in ET synthesis, is upregulated by MYB72 (**Figure 2**; Zamioudis et al., 2014) and also is upregulated under Fe deficiency in Arabidopsis roots (García et al., 2010). In accordance with the influence of MYB72 on ET, the exogenous application of ACC induced wild-type levels of resistance in the Arabidopsis *myb72-1* mutant, suggesting that MYB72 acts upstream of ET in the ISR pathway (Van der Ent et al., 2008).

Besides the participation of the MYB72, MYB10, FIT, bHLH38, and bHLH39 TFs in both ISR and Fe deficiency responses, there are other TFs that also play a key role in both processes. Among them, the EIN3/EIL1 (related to ET signaling) and MED16 (Mediator) TFs can be highlighted (see Subsection "Ethylene and other hormones and signaling molecules"). These TFs are required to activate the expression of Fe acquisition genes by interacting with FIT (**Figure 2**; Lingam et al., 2011; Yang et al., 2014; Zhang et al., 2014; Brumbarova et al., 2015; Lucena et al., 2015). In relation to ISR, the Arabidopsis *ein3-1* mutant did not express ISR in response to treatment with the bacterium *P. simiae* WCS417, which suggests that the EIN3 TF also plays a key role in this process (Knoester et al., 1999). MED16 is a key component in the JA/ET-mediated immunity against necrotrophic pathogens (Wang et al., 2015). In addition, and besides affecting the expression of Fe acquisition genes, it greatly influences the expression of *MYB72* and *MYB10* (Zhang et al., 2014), two important components in both Fe deficiency responses and ISR (see above). Probably, the physical interaction of MED16 with FIT is necessary for the activation of *MYB72* and *MYB10* expression (**Figure 2**).

TABLE 2 | Microbial species that improve Fe nutrition when applied to dicot plants grown in calcareous soils (or in artificial calcareous soils).

Microbial species	Plant species	Mode appl.	Fe def. resp.	Fe Gr.	Refs
Rhizobacteria					
Bacillus subtilis	*Manihot esculenta*	ri	nd	Fe ∧	Freitas et al., 2015
Paenibacillus polymyxa	*Arabidopsis thaliana*	ri	nd	Fe	Zhou et al., 2016a
Bacillus sp. *Agrobacterium* sp.* *Alcaligenes* sp.* *Pantoea* sp.*	*Pyrus communis*	ri	FCR organic acids	Fe	Ipek et al., 2017
Alcaligenes sp.* *Pantoea* sp.*	*Malus domestica*	i	FCR organic acids	Fe	Aras et al., 2018
Bacillus sp. *Agrobacterium* sp.* *Alcaligenes* sp.* *Staphylococcus* sp.*	*Prunus persica*	ri	FCR organic acids	Fe	Arıkan et al., 2018
Rhizofungi					
Trichoderma asperellum	*Lupinus albus*	gm and ri	nd	Fe	de Santiago et al., 2009
Trichoderma asperellum	*Cucumis sativus*	ri	nd	Fe	de Santiago et al., 2013

*Mode appl., mode of application of the microbes (gm, application to the growth medium; i, through the irrigation system; ri, root immersion). FCR, ferric chelate reductase activity; Fe Gr., increased shoot Fe concentration (Fe) and increased shoot growth (∧); nd, not determined; *, microbial species whose association with ISR is not yet clear.*

Internal Fe Content

Eethylene, auxin, and NO greatly activate the expression of Fe acquisition genes in plants grown with low levels of Fe (or without Fe), but have much less effect in plants grown with high levels of Fe (Lucena et al., 2006; Graziano and Lamattina, 2007; Chen et al., 2010; García et al., 2011). This suggests that the upregulation of Fe acquisition genes does not solely depend on hormones and signaling molecules (such as ET, auxin, or NO), that would act as activators, but also on the internal Fe content of plants, that would act as a repressor (Lucena et al., 2006; García et al., 2011, 2013, 2018; Romera et al., 2011, 2017). However, different results suggest that total Fe in roots is not the repressor of Fe acquisition genes but instead it is a Fe-related signal moving from shoots to roots through the phloem (García et al., 2013, 2018). Very recently, it has been found that this shoot Fe-related signal can affect the synthesis of ET on roots (García et al., 2018). To integrate all these regulatory components, a model has been proposed where ET/auxin/NO act as activators of Fe acquisition genes while a phloem Fe-related signal acts as repressor (García et al., 2011, 2013, 2018; Lucena et al., 2015; Romera et al., 2017).

In relation to ISR, there are also several results showing that the effects of ISR-eliciting microbes on the induction of Fe deficiency responses could also be dependent on the Fe concentration of the medium. For example, the expression of two Fe-related genes, like *MYB72*, and *FRO2*, was induced by *P. simiae* WCS417 independently of the Fe concentration in the medium but their absolute values were decreased when the Fe concentration increased (Zamioudis et al., 2015). Other examples, the expression of *FIT*, *IRT1* and *FRO2*, and the ferric reductase activity, decreased in Arabidopsis plants inoculated with *P. polymyxa* BFKC01 when the Fe concentration in the medium increased (Zhou et al., 2016a). The expression of *FIT*, *IRT1*, *FRO1*, and *HA1*, and the ferric reductase activity, in cucumber plants inoculated with *Azospirillum brasilense* Cd(DSM-1843) or other rhizobacterial species, decreased when the Fe concentration in the medium increased (Pii et al., 2016b; Scagliola et al., 2016). The acidification capacity induced by the rhizobacterium *Arthrobacter agilis* in *Medicago truncatula* roots was lower in plants grown with high levels of Fe than in those grown with low levels of Fe (Orozco-Mosqueda et al., 2013). Moreover, the expression of several Fe-related genes induced by *P. simiae* WCS417, like *MYB72*, *FRO2*, and *IRT1*, is transitory (Zamioudis et al., 2015). This suggests that, after the induction of the Fe acquisition genes by ISR-eliciting microbes, plants acquire enough Fe and turn off these genes, to avoid toxicity and to conserve energy. The same occurs when plants induce the Fe acquisition genes under Fe deficiency and, as a consequence, they get sufficient Fe (Vert et al., 2003; Lucena et al., 2015).

RHIZOSPHERE MICROBIAL SPECIES THAT INDUCE Fe DEFICIENCY RESPONSES AND IMPROVE Fe ACQUISITION

As previously stated, beneficial rhizosphere microbes can contribute to improve Fe acquisition. This is most likely due to their capacity to induce Fe deficiency responses, such as enhanced ferric reductase activity, acidification of the rhizosphere, release of phenolics and flavins, and development of root hairs (see Section "Interrelationship between ISR and Fe deficiency responses in dicot plants"). These Fe deficiency responses are induced in a similar way as they are induced under Fe deficiency conditions. For example, ISR-eliciting microbes induce the upregulation of the genes associated with the Fe deficiency responses, like *FRO2*, *IRT1*, *AHA*, *F6′H1*, *BGLU42*, *ABCG37*, and others, and these genes are activated by the

TFs that activate them under Fe deficiency, like FIT(FER), bHLH38, bHLH39, MYB72, and MYB10 (**Figure 2**; Zhang et al., 2009; Palmer et al., 2013; Zamioudis et al., 2014, 2015; Zhao et al., 2014; Pii et al., 2016b; Scagliola et al., 2016; Verbon and Liberman, 2016; Zhou et al., 2016a, 2017, 2018; Martínez-Medina et al., 2017; Verbon et al., 2017; Wang J. et al., 2017; Stringlis et al., 2018a,b). Moreover, the hormones and signaling molecules related to the activation of these TFs, like ET, auxin, and NO, are similar in both ISR and Fe deficiency responses (see Subsection "Ethylene and other hormones and signaling molecules").

Among the beneficial rhizosphere microbes that can activate the ISR are rhizobacteria, like *P. simiae* (syn. *P. fluorescens*), *B. subtilis*, *P. polymyxa* and *A. brasilense*; rhizofungi, like *Trichoderma* spp.; mycorrhizal fungi, like *Rhizophagus irregularis* (syn. *Glomus intraradices*) and *P. indica*; and non-pathogenic races of *Fusarium oxysporum* (Segarra et al., 2009; Zhang et al., 2009; Patil et al., 2011; Pieterse et al., 2012, 2014; Alizadeh et al., 2013; Zamioudis et al., 2014, 2015; Zhao et al., 2014; Pii et al., 2016b; Martínez-Medina et al., 2017; Verbon et al., 2017). In the case of mycorrhizal fungi, the enhanced defensive capacity provoked by them is also named MIR ("Mycorrhiza-Induced Resistance") and can favor P acquisition (Jung et al., 2012; Cameron et al., 2013). Furthermore, it has been suggested that MIR can involve an ISR component elicited by bacteria in the mycorrhizosphere (Cameron et al., 2013). This is supported by the synergistic effects in defense responses when both arbuscular mycorrhiza and rhizobacteria are simultaneously applied (Pérez de Luque et al., 2017). The synergy between both kind of microbes paves the way to study the consortia of mycorrhiza and rhizobacteria in relation to the acquisition of Fe and P, and perhaps of other nutrients.

In **Table 1** are summarized several rhizobacteria and rhizofungi species (most of them trigger ISR) that have been shown to induce Fe deficiency responses and to improve Fe acquisition and/or growth when applied to dicot plants. In **Table 2** are summarized the ones that have been shown to cause similar effects when applied to dicot plants grown in calcareous soils (or in artificial calcareous soils).

CONCLUDING REMARKS AND FUTURE PERSPECTIVES

The ability of ISR-eliciting microbes to trigger both defense responses and Fe deficiency responses opens the way to use them as biopesticides and also as Fe biofertilizers. This represents a very important opportunity to diminish the application of fertilizers and pesticides in a more sustainable agriculture. However, and in relation to Fe nutrition, the use of ISR-eliciting microbes is in its infancy since it is not sufficiently known the behavior of these microbes on crops grown in calcareous soils. Most research works about the realtionship of these microbes with the Fe nutrition of plants have been carried out with Arabidopsis plants grown on agar plates. For their application to crop plants in the field it would be also necessary to study the behavior of these microbes with plant species growing in calcareous soils, including their capacity to thrive in these soils and to compite with wild soil microbes. More research is also needed to know the best ways for their application, by analyzing and comparing, both biologically and economically, the different possibilities, like direct application to soil, root immersion of plantlets before transplanting them (in the case of crop trees), application to seeds, and application into the irrigation systems (probably as spores). In the same way, it is necessary to study whether it is better to apply individual microbial species or consortia of different microbial species (Alizadeh et al., 2013; Sonbarse et al., 2017). In this latter case, and since ET can play a dual role in both ISR and Fe deficiency responses, it would be interesting to analyze the interactions between plant species and microbial species possesing the ACC deaminase enzyme and those that do not. Anyway, the research about ISR-eliciting microbes and Fe nutrition is a very fascinating topic for the near future.

AUTHOR'S NOTE

We apologize to authors whose works were not cited in this review due to our ignorance and to manuscript length restrictions. We encourage authors with papers relating ISR and Fe nutrition in dicot plants to send them to us: we are preparing a website (http://www.uco.es/rhizosferrum) to keep updated all the microbial species that elicit ISR, induce Fe deficiency responses, and improve Fe acquisition.

AUTHOR CONTRIBUTIONS

FR, MG, and CL revised the information related to ISR and Fe deficiency signaling. RP-V revised the information related to volatile compounds. EA, JR, MAA, and MA revised the information related to the different microbial species and their effects on Fe nutrition. FR wrote a first draft of the manuscript. JR, RP-V, and AM-M corrected and improved the manuscript.

FUNDING

This work was supported by "Plan Propio" Universidad de Córdoba (Spain), the "Junta de Andalucía" (Research Groups AGR115, BIO159, and BIO202) and "LABORATORIOS JAER S.A." (company related to the production of micronutrient fertilizers which is starting to work on micronutrient biofertilizers). The funder played no role in the study design, the collection, analysis or interpretation of data, the writing of this paper or the decision to submit it for publication.

ACKNOWLEDGMENTS

We thank Dr. Brian M. Waters of the University of Nebraska (Lincoln, United States), for the English correction and valuable suggestions in the editing of the manuscript, and Gabriel Martí ("LABORATORIOS JAER S.A.") for funding the publication of this Review.

REFERENCES

Acharya, K., Chandra, S., Chakraborty, N., and Acharya, R. (2011). Nitric oxide functions as a signal in induced systemic resistance. *Arch. Phytopathol. Plant Protect.* 44, 1335–1342. doi: 10.1080/03235408.2010.496552

Alizadeh, H., Behboudi, K., Ahmadzadeh, M., Javan-Nikkhah, M., Zamioudis, C., Pieterse, C. M. J., et al. (2013). Induced systemic resistance in cucumber and *Arabidopsis thaliana* by the combination of *Trichoderma harzianum* Tr6 and *Pseudomonas* sp. Ps14. *Biol. Control* 65, 14–23. doi: 10.1016/j.biocontrol.2013.01.009

Aparicio, F., and Pallás, V. (2017). The coat protein of Alfalfa mosaic virus interacts and interferes with the transcriptional activity of the bHLH transcription factor ILR3 promoting salicylic acid-dependent defence signaling response. *Mol. Plant Pathol.* 18, 173–186. doi: 10.1111/mpp.12388

Aras, S., Arıkan, S., İpek, M., Esitken, A., Pırlak, L., Dönmez, M. F., et al. (2018). Plant growth promoting rhizobacteria enhanced leaf organic acids, FC-R activity and Fe nutrition of apple under lime soil conditions. *Acta Physiol. Plant.* 40:120. doi: 10.1007/s11738-018-2693-9

Arıkan, S., Esitken, A., İpek, M., Aras, S., Sahin, M., Pırlak, L., et al. (2018). Effect of plant growth promoting rhizobacteria on Fe acquisition in peach (*Prunus persica* L.) under calcareous soil conditions. *J. Plant Nutr.* 41, 2141–2150. doi: 10.1080/01904167.2018.1482910

Asari, S., Tarkowská, D., Rolčík, J., Novák, O., Velázquez-Palmero, D., Bejai, S., et al. (2017). Analysis of plant growth-promoting properties of *Bacillus amyloliquefaciens* UCMB5113 using *Arabidopsis thaliana* as host plant. *Planta* 245, 15–30. doi: 10.1007/s00425-016-2580-9

Aznar, A., Chen, N. W., Rigault, M., Riache, N., Joseph, D., Desmaële, D., et al. (2014). Scavenging iron: a novel mechanism of plant immunity activation by microbial siderophores. *Plant Physiol.* 164, 2167–2183. doi: 10.1104/pp.113.233585

Aznar, A., Chen, N. W. G., Thomine, S., and Dellagi, A. (2015). Immunity to plant pathogens and iron homeostasis. *Plant Sci.* 240, 90–97. doi: 10.1016/j.plantsci.2015.08.022

Aznar, A., and Dellagi, A. (2015). New insights into the role of siderophores as triggers of plant immunity: what can we learn from animals? *J. Exp. Bot.* 66, 3001–3010. doi: 10.1093/jxb/erv155

Bacaicoa, E., Mora, V., Zamarreño, A. M., Fuentes, M., Casanova, E., and García-Mina, J. M. (2011). Auxin: a major player in the shoot-to-root regulation of root Fe-stress physiological responses to Fe deficiency in cucumber plants. *Plant Physiol. Biochem.* 49, 545–556. doi: 10.1016/j.plaphy.2011.02.018

Bacaicoa, E., Zamarreño, A. M., Leménager, D., Baigorri, R., and García-Mina, J. M. (2009). Relationship between the hormonal balance and the regulation of iron deficiency stress responses in cucumber. *J. Am. Soc. Hortic. Sci.* 134, 589–601. doi: 10.21273/JASHS.134.6.589

Bakker, P. A. H. M., Doornbos, R. F., Zamioudis, C., Berendsen, R. L., and Pieterse, C. M. J. (2013). Induced systemic resistance and the rhizosphere microbiome. *Plant Pathol. J.* 29, 136–143. doi: 10.5423/PPJ.SI.07.2012.0111

Balmer, D., Planchamp, C., and Mauch-Mani, B. (2013). On the move: induced resistance in monocots. *J. Exp. Bot.* 64, 1249–1261. doi: 10.1093/jxb/ers248

Bauer, P., Ling, H. Q., and Guerinot, M. L. (2007). *FIT*, the *FER-LIKE IRON DEFICIENCY INDUCED TRANSCRIPTION FACTOR* in *Arabidopsis*. *Plant Physiol. Biochem.* 45, 260–261. doi: 10.1016/j.plaphy.2007.03.006

Berendsen, R. L., Pieterse, C. M., and Bakker, P. A. (2012). The rhizosphere microbiome and plant health. *Trends Plant Sci.* 17, 478–486. doi: 10.1016/j.tplants.2012.04.001

Boutrot, F., Segonzac, C., Chang, K. N., Qiao, H., Ecker, J. R., Zipfel, C., et al. (2010). Direct transcriptional control of the *Arabidopsis* immune receptor FLS2 by the ethylene-dependent transcription factors EIN3 and EIL1. *Proc. Natl. Acad. Sci. U.S.A.* 107, 14502–14507. doi: 10.1073/pnas.1003347107

Briat, J. F., Dubos, C., and Gaymard, F. (2015). Iron nutrition, biomass production, and plant product quality. *Trends Plant Sci.* 20, 33–40. doi: 10.1016/j.tplants.2014.07.005

Brumbarova, T., Bauer, P., and Ivanov, R. (2015). Molecular mechanisms governing *Arabidopsis* iron uptake. *Trends Plant Sci.* 20, 124–133. doi: 10.1016/j.tplants.2014.11.004

Camehl, I., Sherameti, I., Venus, Y., Bethke, G., Varma, A., Lee, J., et al. (2010). Ethylene signalling and ethylene-targeted transcription factors are required to balance beneficial and nonbeneficial traits in the symbiosis between the endophytic fungus *Piriformospora indica* and *Arabidopsis thaliana*. *New Phytol.* 185, 1062–1073. doi: 10.1111/j.1469-8137.2009.03149.x

Cameron, D. D., Neal, A. L., van Wees, S. C. M., and Ton, J. (2013). Mycorrhiza-induced resistance: more than the sum of its parts? *Trends Plant Sci.* 18, 539–545. doi: 10.1016/j.tplants.2013.06.004

Chen, C. C., Chien, W. F., Lin, N. C., and Yeh, K. C. (2014). Alternative functions of *Arabidopsis* YELLOW STRIPE-LIKE3: from metal translocation to pathogen defense. *PLoS One* 9:e98008. doi: 10.1371/journal.pone.0098008

Chen, W. W., Yang, J. L., Qin, C., Jin, C. W., Mo, J. H., Ye, T., et al. (2010). Nitric oxide acts downstream of auxin to trigger root ferric-chelate reductase activity in response to iron deficiency in *Arabidopsis thaliana*. *Plant Physiol.* 154, 810–819. doi: 10.1104/pp.110.161109

Choudhary, D. K., Prakash, A., and Johri, B. N. (2007). Induced systemic resistance (ISR) in plants: mechanism of action. *Indian J. Microbiol.* 47, 289–297. doi: 10.1007/s12088-007-0054-2

Colangelo, E. P., and Guerinot, M. L. (2004). The essential basic helix-loop-helix protein FIT1 is required for the iron deficiency response. *Plant Cell* 16, 3400–3412. doi: 10.1105/tpc.104.024315

Contreras-Cornejo, H. A., López-Bucio, J. S., Méndez-Bravo, A., Macías-Rodríıguez, L. I., Ramos-Vega, M., Guevara-García, Á. A., et al. (2015). Mitogen-activated protein kinase 6 and ethylene and auxin signaling pathways are involved in *Arabidopsis* root-system architecture alterations by *Trichoderma atroviride*. *Mol. Plant Microbe Interact.* 28, 701–710. doi: 10.1094/MPMI-01-15-0005-R

de Santiago, A., García-López, A. M., Quintero, J. M., Avilés, M., and Delgado, A. (2013). Effect of *Trichoderma asperellum* strain T34 and glucose addition on iron nutrition in cucumber grown on calcareous soils. *Soil Biol. Biochem.* 57, 598–605. doi: 10.1016/j.soilbio.2012.06.020

de Santiago, A., Quintero, J. M., Avilés, M., and Delgado, A. (2009). Effect of *Trichoderma asperellum* strain T34 on iron nutrition in white lupin. *Soil Biol. Biochem.* 41, 2453–2459. doi: 10.1016/j.soilbio.2009.07.033

de Zelicourt, A., Al-Yousif, M., and Hirt, H. (2013). Rhizosphere microbes as essential partners for plant stress tolerance. *Mol. Plant* 6, 242–245. doi: 10.1093/mp/sst028

Dubois, M., Van den Broeck, L., and Inzé, D. (2018). The pivotal role of ethylene in plant growth. *Trends Plant Sci.* 23, 311–323. doi: 10.1016/j.tplants.2018.01.003

Durrett, T. P., Gassmann, W., and Rogers, E. E. (2007). The FRD3-mediated efflux of citrate into the root vasculature is necessary for efficient iron translocation. *Plant Physiol.* 144, 197–205. doi: 10.1104/pp.107.097162

Fourcroy, P., Sisó-Terraza, P., Sudre, D., Saviróon, M., Reyt, G., Gaymard, F., et al. (2014). Involvement of the ABCG37 transporter in secretion of scopoletin and derivatives by *Arabidopsis* roots in response to iron deficiency. *New Phytol.* 201, 155–167. doi: 10.1111/nph.12471

Fourcroy, P., Tissot, N., Reyt, G., Gaymard, F., Briat, J. F., and Dubos, C. (2016). Facilitated Fe nutrition by phenolic compounds excreted by the *Arabidopsis* ABCG37/PDR9 transporter requires the IRT1/FRO2 high-affinity root Fe2+ transport system. *Mol. Plant* 9, 485–488. doi: 10.1016/j.molp.2015.09.010

Freitas, M. A., Medeiros, F. H. V., Carvalho, S. P., Guilherme, L. R. G., Teixeira, W. D., Zhang, H., et al. (2015). Augmenting iron accumulation in cassava by the beneficial soil bacterium *Bacillus subtilis* (GBO3). *Front. Plant Sci.* 6:596. doi: 10.3389/fpls.2015.00596

Gamalero, E., and Glick, B. R. (2015). Bacterial modulation of plant ethylene levels. *Plant Physiol.* 169, 13–22. doi: 10.1104/pp.15.00284

García, M. J., Corpas, F. J., Lucena, C., Alcántara, E., Pérez-Vicente, R., Zamarreño, Á. M., et al. (2018). A shoot Fe signaling pathway requiring the OPT3 transporter controls GSNO Reductase and ethylene in *Arabidopsis thaliana* roots. *Front. Plant Sci.* 9:1325. doi: 10.3389/fpls.2018.01325

García, M. J., Lucena, C., Romera, F. J., Alcántara, E., and Pérez-Vicente, R. (2010). Ethylene and nitric oxide involvement in the up-regulation of key genes related to iron acquisition and homeostasis in *Arabidopsis*. *J. Exp. Bot.* 61, 3885–3899. doi: 10.1093/jxb/erl189

García, M. J., Romera, F. J., Stacey, M. G., Stacey, G., Villar, E., Alcántara, E., et al. (2013). Shoot to root communication is necessary to control the expression of iron-acquisition genes in Strategy I plants. *Planta* 237, 65–75. doi: 10.1007/s00425-012-1757-0

García, M. J., Suárez, V., Romera, F. J., Alcántara, E., and Pérez-Vicente, R. (2011). A new model involving ethylene, nitric oxide and Fe to explain the regulation

of Fe-acquisition genes in Strategy I plants. *Plant Physiol. Biochem.* 49, 537–544. doi: 10.1016/j.plaphy.2011.01.019

García-López, A. M., Avilés, M., and Delgado, A. (2016). Effect of various microorganisms on phosphorus uptake from insoluble Ca-phosphates by cucumber plants. *J. Plant Nutr. Soil Sci.* 179, 454–465. doi: 10.1002/jpln.201500024

Garnica-Vergara, A., Barrera-Ortiz, S., Muñoz-Parra, E., Raya-González, J., Méndez-Bravo, A., Macías-Rodríguez, L., et al. (2016). The volatile 6-pentyl-2H-pyran-2-one from *Trichoderma atroviride* regulates *Arabidopsis thaliana* root morphogenesis via auxin signaling and ETHYLENE INSENSITIVE 2 functioning. *New Phytol.* 209, 1496–1512. doi: 10.1111/nph.13725

Grady, E. N., MacDonald, J., Liu, L., Richman, A., and Yuan, Z. C. (2016). Current knowledge and perspectives of *Paenibacillus*: a review. *Microb. Cell Fact.* 15:203. doi: 10.1186/s12934-016-0603-7

Graziano, M., and Lamattina, L. (2007). Nitric oxide accumulation is required for molecular and physiological responses to iron deficiency in tomato roots. *Plant J.* 52, 949–960. doi: 10.1111/j.1365-313X.2007.03283.x

Guinel, F. C. (2015). Ethylene, a hormone at the center-stage of nodulation. *Front. Plant Sci.* 6:1121. doi: 10.3389/fpls.2015.01121

Gullner, G., Komives, T., Király, L., and Schröder, P. (2018). Glutathione S-transferase enzymes in plant-pathogen interactions. *Front. Plant Sci.* 9:1836. doi: 10.3389/fpls.2018.01836

Gullner, G., Zechmann, B., Künstler, A., and Király, L. (2017). "The signaling roles of glutathione in plant disease resistance," in *Glutathione in Plant Growth, Development, and Stress Tolerance*, eds M. A. Hossain, M. G. Mostofa, P. D. Vivancos, D. J. Burritt, M. Fujita, and L. S. P. Tran (Cham: Springer International Publishing), 331–357. doi: 10.1007/978-3-319-66682-2_15

Hindt, M. N., Akmakjian, G. Z., Pivarski, K. L., Punshon, T., Baxter, I., Salt, D. E., et al. (2017). BRUTUS and its paralogs, BTS LIKE1 and BTS LIKE2, encode important negative regulators of the iron deficiency response in *Arabidopsis thaliana*. *Metallomics* 9, 876–890. doi: 10.1039/c7mt00152e

Hossain, M. M., Sultana, F., and Hyakumachi, M. (2017). Role of ethylene signalling in growth and systemic resistance induction by the plant growth-promoting fungus *Penicillium viridicatum* in Arabidopsis. *J. Phytopathol.* 165, 432–441. doi: 10.1111/jph.12577

Ipek, M., Aras, S., Arıkan, S., Esitken, A., Pırlak, L., Dönmez, M. F., et al. (2017). Root plant growth promoting rhizobacteria inoculations increase ferric chelate reductase (FC-R) activity and Fe nutrition in pear under calcareous soil conditions. *Sci. Hortic.* 219, 144–151. doi: 10.1016/j.scienta.2017.02.043

İpek, M., and Eşitken, A. (2017). "The actions of PGPR on micronutrient availability in soil and plant under calcareous soil conditions: an evaluation over Fe nutrition," in *Plant-Microbe Interactions in Agro-Ecological Perspectives*, Vol. 2, eds D. Singh, H. Singh, and R. Prabha (Singapore: Springer), 81–100.

Ivanov, R., Brumbarova, T., and Bauer, P. (2012). Fitting into the harsh reality: regulation of iron-deficiency responses in dicotyledonous plants. *Mol. Plant* 5, 27–42. doi: 10.1093/mp/ssr065

Jankiewicz, U., and Koltonowicz, M. (2012). The involvement of *Pseudomonas* bacteria in induced systemic resistance in plants (Review). *Appl. Biochem. Microbiol.* 48, 244–249. doi: 10.1134/S0003683812030052

Jin, C. W., Ye, Y. Q., and Zheng, S. J. (2014). An underground tale: contribution of microbial activity to plant iron acquisition via ecological processes. *Ann. Bot.* 113, 7–18. doi: 10.1093/aob/mct249

Jung, S. C., Martinez-Medina, A., Lopez-Raez, J. A., and Pozo, M. J. (2012). Mycorrhiza-Induced Resistance and priming of plant defenses. *J. Chem. Ecol.* 38, 651–664. doi: 10.1007/s10886-012-0134-6

Kabir, A. H., Paltridge, N. G., Able, A. J., Paull, J. G., and Stangoulis, J. C. R. (2012). Natural variation for Fe-efficiency is associated with up-regulation of Strategy I mechanisms and enhanced citrate and ethylene synthesis in *Pisum sativum* L. *Planta* 235, 1409–1419. doi: 10.1007/s00425-011-1583-9

Kailasam, S., Wang, Y., Lo, J. C., Chang, H. F., and Yeh, K. C. (2018). S-nitrosoglutathione works downstream of nitric oxide to mediate iron deficiency signaling in *Arabidopsis. Plant J.* 94, 157–168. doi: 10.1111/tpj.13850

Kang, H. G., Foley, R. C., Onate-Sanchez, L., Lin, C., and Singh, K. B. (2003). Target genes for OBP3, a Dof transcription factor, include novel basic helix-loop-helix domain proteins inducible by salicylic acid. *Plant J.* 35, 362–372. doi: 10.1046/j.1365-313X.2003.01812.x

Kieu, N. P., Aznar, A., Segond, D., Rigault, M., Simond-Côte, E., Kunz, C., et al. (2012). Iron deficiency affects plant defence responses and confers resistance to *Dickeya dadantii* and *Botrytis cinerea*. *Mol. Plant Pathol.* 13, 816–827. doi: 10.1111/J.1364-3703.2012.00790.X

Knoester, M., Pieterse, C. M. J., Bol, J. F., and Van Loon, L. C. (1999). Systemic resistance in *Arabidopsis* induced by rhizobacteria requires ethylene-dependent signaling at the site of application. *Mol. Plant Microbe Interact.* 12, 720–727. doi: 10.1094/MPMI.1999.12.8.720

Kobayashi, T., Itai, R. N., Senoura, T., Oikawa, T., Ishimaru, Y., Ueda, M., et al. (2016). Jasmonate signaling is activated in the very early stages of iron deficiency responses in rice roots. *Plant Mol. Biol.* 91, 533–547. doi: 10.1007/s11103-016-0486-3

Kobayashi, T., and Nishizawa, N. K. (2012). Iron uptake, translocation, and regulation in higher plants. *Annu. Rev. Plant Biol.* 63, 131–152. doi: 10.1146/annurev-arplant-042811-10552

Koen, E., Szymańska, K., Klinguer, A., Dobrowolska, G., Besson-Bard, A., and Wendehenne, D. (2012). Nitric oxide and glutathione impact the expression of iron uptake- and iron transport-related genes as well as the content of metals in *A. thaliana* plants grown under iron deficiency. *Plant Signal. Behav.* 7, 1246–1250. doi: 10.4161/psb.21548

Kudoyarova, G. R., Vysotskaya, L. B., Arkhipova, T. N., Kuzmina, L. Y., Galimsyanova, N. F., Sidorova, L. V., et al. (2017). Effect of auxin producing and phosphate solubilizing bacteria on mobility of soil phosphorus, growth rate, and P acquisition by wheat plants. *Acta Physiol. Plant.* 39:253. doi: 10.1007/s11738-017-2556-9

Kumar, R. K., Chu, H. H., Abundis, C., Vasques, K., Rodriguez, D. C., Chia, J. C., et al. (2017). Iron-nicotianamine transporters are required for proper long distance iron signaling. *Plant Physiol.* 175, 1254–1268. doi: 10.1104/pp.17.00821

Kwon, Y. S., Ryu, C.-M., Lee, S., Park, H. B., Han, K. S., Lee, J. H., et al. (2010). Proteome analysis of *Arabidopsis* seedlings exposed to bacterial volatiles. *Planta* 232, 1355–1370. doi: 10.1007/s00425-010-1259-x

Lemanceau, P., Expert, D., Gaymard, F., Bakker, P. A. H. M., and Briat, J. F. (2009). Role of iron in plant-microbe interactions. *Adv. Bot. Res.* 51, 491–549. doi: 10.1016/S0065-2296(09)51012-9

Li, G., Meng, X., Wang, R., Mao, G., Han, L., Liu, Y., et al. (2012). Dual-level regulation of ACC synthase activity by MPK3/MPK6 cascade and its downstream WRKY transcription factor during ethylene induction in *Arabidopsis*. *PLoS Genet.* 8:e1002767. doi: 10.1371/journal.pgen.1002767

Li, R.-X., Cai, F., Pang, G., Shen, Q.-R., Li, R., and Chen, W. (2015). Solubilisation of phosphate and micronutrients by *Trichoderma harzianum* and its relationship with the promotion of tomato plant growth. *PLoS One* 10:e0130081. doi: 10.1371/journal.pone.0130081

Li, W., and Lan, P. (2017). The understanding of the plant iron deficiency responses in Strategy I plants and the role of ethylene in this process by omic approaches. *Front. Plant Sci.* 8:40. doi: 10.3389/fpls.2017.00040

Li, X., Zhang, H., Ai, Q., Liang, G., and Yu, D. (2016). Two bHLH transcription factors, bHLH34 and bHLH104, regulate iron homeostasis in *Arabidopsis thaliana*. *Plant Physiol.* 170, 2478–2493. doi: 10.1104/pp.15.01827

Liang, G., Zhang, H., Li, X., Ai, Q., and Yu, D. (2017). bHLH transcription factor bHLH115 regulates iron homeostasis in *Arabidopsis* thaliana. *J. Exp. Bot.* 68, 1743–1755. doi: 10.1093/jxb/erx043

Lin, X. Y., Ye, Y. Q., Fan, S. K., Jin, C. W., and Zheng, S. J. (2016). Increased sucrose accumulation regulates iron-deficiency responses by promoting auxin signaling in *Arabidopsis* plants. *Plant Physiol.* 170, 907–920. doi: 10.1104/pp.15.01598

Lingam, S., Mohrbacher, J., Brumbarova, T., Potuschak, T., Fink-Straube, C., Blondet, E., et al. (2011). Interaction between the bHLH transcription factor FIT and the ETHILENE INSENSITIVE3/ ETHYLENE INSENSITIVE3-LIKE1 reveals molecular linkage between the regulation of iron acquisition and ethylene signaling in *Arabidopsis*. *Plant Cell* 23, 1815–1829. doi: 10.1105/tpc.111.084715

Liu, W., Karemera, N. J. U., Wu, T., Yang, Y., Zhang, X., Xu, X., et al. (2017a). The ethylene response factor AtERF4 negatively regulates the iron deficiency response in *Arabidopsis thaliana*. *PLoS One* 12:e0186580. doi: 10.1371/journal.pone.0186580

Liu, W., Li, Q., Wang, Y., Wu, T., Yang, Y., Zhang, X., et al. (2017b). Ethylene response factor AtERF72 negatively regulates *Arabidopsis thaliana* response to iron deficiency. *Biochem. Biophys. Res. Commun.* 491, 862–868. doi: 10.1016/j.bbrc.2017.04.014

Liu, X. M., and Zhang, H. (2015). The effects of bacterial volatile emissions on plant abiotic stress tolerance. *Front. Plant Sci.* 6:774. doi: 10.3389/fpls.2015.00774

López-Berges, M., Turra, D., Capilla, J., Schafferer, L., Matthijs, S., Jöchl, C., et al. (2013). Iron competition in fungus-plant interactions: the battle takes place in the rhizosphere. *Plant Signal. Behav.* 8:e23012. doi: 10.4161/psb.23012

Lucena, C., Romera, F. J., García, M. J., Alcántara, E., and Pérez-Vicente, R. (2015). Ethylene participates in the regulation of Fe deficiency responses in Strategy I plants and in rice. *Front. Plant Sci.* 6:1056. doi: 10.3389/fpls.2015.01056

Lucena, C., Romera, F. J., Rojas, C. L., García, M. J., Alcántara, E., and Pérez-Vicente, R. (2007). Bicarbonate blocks the expression of several genes involved in the physiological responses to Fe deficiency of Strategy I plants. *Funct. Plant Biol.* 34, 1002–1009. doi: 10.1071/FP07136

Lucena, C., Waters, B. M., Romera, F. J., García, M. J., Morales, M., Alcántara, E., et al. (2006). Ethylene could influence ferric reductase, iron transporter and H+-ATPase gene expression by affecting FER (or FER-like) gene activity. *J. Exp. Bot.* 57, 4145–4154. doi: 10.1093/jxb/erl189

Martinez-Medina, A., Flors, V., Heil, M., Mauch-Mani, B., Pieterse, C. M. J., Pozo, M. J., et al. (2016). Recognizing plant defense priming. *Trends Plant Sci.* 21, 818–822. doi: 10.1016/j.tplants.2016.07.009

Martínez-Medina, A., Van Wees, S. C. M., and Pieterse, C. M. J. (2017). Airborne signals from *Trichoderma* fungi stimulate iron uptake responses in roots resulting in priming of jasmonic acid dependent defences in shoots of *Arabidopsis thaliana* and *Solanum lycopersicum*. *Plant Cell Environ.* 40, 2691–2705. doi: 10.1111/pce.13016

Maurer, F., Müller, S., and Bauer, P. (2011). Suppression of Fe deficiency gene expression by jasmonate. *Plant Physiol. Biochem.* 49, 530–536. doi: 10.1016/j.plaphy.2011.01.025

Maurer, F., Naranjo Arcos, M. A., and Bauer, P. (2014). Responses of a triple mutant defective in three iron deficiency-induced Basic Helix-Loop-Helix genes of the subgroup Ib(2) to iron deficiency and salicylic acid. *PLoS One* 9:e99234. doi: 10.1371/journal.pone.0099234

Meiser, J., Lingam, S., and Bauer, P. (2011). Post-transcriptional regulation of the Fe deficiency bHLH transcription factor FIT is affected by iron and nitric oxide. *Plant Physiol.* 157, 2154–2166. doi: 10.1104/pp.111.183285

Meziane, H., Van der Sluis, I., Van Loon, L. C., Höfte, M., and Bakker, P. A. (2005). Determinants of *Pseudomonas putida* WCS358 involved in inducing systemic resistance in plants. *Mol. Plant Pathol.* 6, 177–185. doi: 10.1111/j.1364-3703.2005.00276.x

Mimmo, T., Del Buono, D., Terzano, R., Tomasi, N., Vigani, G., Crecchio, C., et al. (2014). Rhizospheric organic compounds in the soil-microorganism-plant system: their role in iron availability. *Eur. J. Soil Sci.* 65, 629–642. doi: 10.1111/ejss.12158

Naranjo-Arcos, M. A., and Bauer, P. (2016). "Iron nutrition, oxidative stress, and pathogen defense," in *Nutritional Deficiency*, eds P. Erkekoglu and B. Kocer-Gumusel (Rijeka: InTechOpen), 63–98. doi: 10.5772/63204

Nascimento, F. X., Rossi, M. J., and Glick, B. R. (2018). Ethylene and 1-aminocyclopropane-1-carboxylate (ACC) in plant–bacterial interactions. *Front. Plant Sci.* 9:114. doi: 10.3389/fpls.2018.00114

Nie, P., Li, X., Wang, S., Guo, J., Zhao, H., and Niu, D. (2017). Induced systemic resistance against *Botrytis cinerea* by *Bacillus cereus* AR156 through a JA/ET- and NPR1-dependent signaling pathway and activates PAMP-triggered immunity in *Arabidopsis*. *Front. Plant Sci.* 8:238. doi: 10.3389/fpls.2017.00238

Orozco-Mosqueda, M. C., Velázquez-Becerra, C., Macías-Rodríguez, L. I., Santoyo, G., Flores-Cortez, I., Alfaro-Cuevas, R., et al. (2013). *Arthrobacter agilis* UMCV2 induces iron acquisition in *Medicago truncatula* (Strategy I plant) in vitro via dimethylhexadecylamine emission. *Plant Soil* 362, 51–66. doi: 10.1007/s11104-012-1263-y

Palmer, C. M., Hind, M. N., Schmidt, H., Clemens, S., and Guerinot, M. L. (2013). MYB10 and MYB72 are required for growth under iron-limiting conditions. *PLoS Genet.* 9:e1003953. doi: 10.1371/journal.pgen.1003953

Patel, T., and Saraf, M. (2017). Biosynthesis of phytohormones from novel rhizobacterial isolates and their in vitro plant growth-promoting efficacy. *J. Plant Interact.* 12, 480–487. doi: 10.1080/17429145.2017.1392625

Patil, S., Sriram, S., Savitha, M. J., and Arulmani, N. (2011). Induced systemic resistance in tomato by non-pathogenic *Fusarium* species for the management of *Fusarium* wilt. *Arch. Phytopathol. Plant Protect.* 44, 1621–1634. doi: 10.1080/03235408.2010.526774

Pérez de Luque, A., Tille, S., Johnson, I., Pascual-Pardo, D., Ton, J., and Cameron, D. D. (2017). The interactive effects of arbuscular mycorrhiza and plant growth-promoting rhizobacteria synergistically enhance host plant defences against pathogens. *Sci. Rep.* 7:16409. doi: 10.1038/s41598-017-16697-4

Pierik, R., Sasidharan, R., and Voesenek, L. A. C. J. (2007). Growth control by ethylene: adjusting phenotypes to the environment. *J. Plant Growth Regul.* 26, 188–200. doi: 10.1007/s00344-006-0124-4

Pieterse, C. M. J., Van der Does, D., Zamioudis, C., Leon-Reyes, A., and Van Wees, S. C. M. (2012). Hormonal modulation of plant immunity. *Annu. Rev. Cell Dev. Biol.* 28, 489–521. doi: 10.1146/annurev-cellbio-092910-154055

Pieterse, C. M. J., Van Wees, S. C. M., Ton, J., Van Pelt, J. A., and Van Loon, L. C. (2002). Signalling in rhizobacteria-lnduced systemic resistance in *Arabidopsis thaliana*. *Plant Biol.* 4, 535–544. doi: 10.1055/s-2002-354411

Pieterse, C. M. J., Van Wees, S. C. M., van Pelt, J. A., Knoester, M., Laan, R., Gerrits, H., et al. (1998). A novel signaling pathway controlling induced systemic resistance in *Arabidopsis*. *Plant Cell* 10, 1571–1580. doi: 10.1105/tpc.10.9.1571

Pieterse, C. M. J., Zamioudis, C., Berendsen, R. L., Weller, D. M., Van Wees, S. C. M., and Bakker, P. A. H. M. (2014). Induced systemic resistance by beneficial microbes. *Annu. Rev. Phytopathol.* 52, 347–375. doi: 10.1146/annurev-phyto-082712-102340

Pii, Y., Borruso, L., Brusetti, L., Crecchio, C., Cesco, S., and Mimmo, T. (2016a). The interaction between iron nutrition, plant species and soil type shapes the rhizosphere microbiome. *Plant Physiol. Biochem.* 99, 39–48. doi: 10.1016/j.plaphy.2015.12.002

Pii, Y., Marastoni, L., Springeth, C., Fontanella, M. C., Beone, G. M., Cesco, S., et al. (2016b). Modulation of Fe acquisition process by *Azospirillum brasilense* in cucumber plants. *Environ. Exp. Bot.* 130, 216–225. doi: 10.1016/j.envexpbot.2016.06.011

Pii, Y., Mimmo, T., Tomasi, N., Terzano, R., Cesco, S., and Crecchio, C. (2015). Microbial interactions in the rhizosphere: beneficial influences of plant growth-promoting rhizobacteria on nutrient acquisition process. A review. *Biol. Fertil. Soils* 51, 403–415. doi: 10.1007/s00374-015-0996-1

Pommerrenig, B., Feussner, K., Zierer, W., Rabinovych, V., Klebl, F., Feussner, I., et al. (2011). Phloem-specific expression of Yang cycle genes and identification of novel Yang cycle enzymes in *Plantago* and *Arabidopsis*. *Plant Cell* 23, 1904–1919. doi: 10.1105/tpc.110.079657

Poupin, M. J., Greve, M., Carmona, V., and Pinedo, I. (2016). A complex molecular interplay of auxin and ethylene signaling pathways is involved in *Arabidopsis* growth promotion by *Burkholderia phytofirmans* PsJN. *Front. Plant Sci.* 7:492. doi: 10.3389/fpls.2016.00492

Rajniak, J., Giehl, R. F. H., Chang, E., Murgia, I., von Wirén, N., and Sattely, E. S. (2018). Biosynthesis of redox-active metabolites in response to iron deficiency in plants. *Nat. Chem. Biol.* 14, 442–450. doi: 10.1038/s41589-018-0019-2

Ribaudo, C. M., Krumpholz, E. M., Cassán, F. D., Bottini, R., Cantore, M. L., and Curá, J. A. (2006). *Azospirillum* sp. promotes root hair development in tomato plants through a mechanism that involves ethylene. *J. Plant Growth Regul.* 24, 175–185. doi: 10.1007/s00344-005-0128-5

Rodríguez-Celma, J., and Schmidt, W. (2013). Reduction-based iron uptake revisited. On the role of secreted iron-binding compounds. *Plant Signal. Behav.* 8:e26116. doi: 10.4161/psb.26116

Romera, F. J., and Alcántara, E. (1994). Iron-deficiency stress responses in cucumber (*Cucumis sativus* L.) roots. A possible role for ethylene? *Plant Physiol.* 105, 1133–1138.

Romera, F. J., and Alcántara, E. (2004). Ethylene involvement in the regulation of Fe-deficiency stress responses by Strategy I plants. *Funct. Plant Biol.* 31, 315–328. doi: 10.1071/FP03165

Romera, F. J., Alcántara, E., and De la Guardia, M. D. (1999). Ethylene production by Fe-deficient roots and its involvement in the regulation of Fe-deficiency stress responses by Strategy I plants. *Ann. Bot.* 83, 51–55. doi: 10.1006/anbo.1998.0793

Romera, F. J., García, M. J., Alcántara, E., and Pérez-Vicente, R. (2011). Latest findings about the interplay or auxin, ethylene and nitric oxide in the regulation of Fe deficiency responses by Strategy I plants. *Plant Signal. Behav.* 6, 167–170. doi: 10.4161/psb.6.1.14111

Romera, F. J., Lucena, C., García, M. J., Alcántara, E., and Pérez-Vicente, R. (2017). "The role of ethylene and other signals in the regulation of Fe deficiency responses by dicot plants," in *Stress Signaling in Plants: Genomics and Proteomics Perspectives*, Vol. 2, eds M. Sarwat, A. Ahmad, M. Z. Abdin, and M. Ibrahim (Cham: Springer), 277–300.

Römheld, V., and Marschner, H. (1986). Mobilization of iron in the rhizosphere of different plant species. *Adv. Plant Nutr.* 2, 155–204. doi: 10.1007/BF02220801

Ryu, C.-M., Hu, C.-H., Reddy, M. S., and Kloepper, J. W. (2003). Different signaling pathways of induced resistance by rhizobacteria in *Arabidopsis thaliana* against two pathovars of *Pseudomonas syringae*. *New Phytol.* 160, 413–420. doi: 10.1046/j.1469-8137.2003.00883.x

Sauter, M., Moffatt, B., Saechao, M. C., Hell, R., and Wirtz, M. (2013). Methionine salvage and *S*-adenosylmethionine: essential links between sulfur, ethylene and polyamine biosynthesis. *Biochem. J.* 451, 145–154. doi: 10.1042/BJ20121744

Savary, S., Ficke, A., Aubertot, J. N., and Hollier, C. (2012). Crop losses due to diseases and their implications for global food production losses and food security. *Food Secur.* 4, 519–537. doi: 10.1007/s12571-012-0200-5

Scagliola, M., Pii, Y., Mimmo, T., Cesco, S., Ricciuti, P., and Crecchio, C. (2016). Characterization of plant growth promoting traits of bacterial isolates from the rhizosphere of barley (*Hordeum vulgare* L.) and tomato (*Solanum lycopersicon* L.) grown under Fe sufficiency and deficiency. *Plant Physiol. Biochem.* 107, 187–196. doi: 10.1016/j.plaphy.2016.06.002

Schmid, N. B., Giehl, R. F. H., Döll, S., Mock, H. P., Strehmel, N., Scheel, D., et al. (2014). Feruloyl-CoA 6'-Hydroxylase1-dependent coumarins mediate iron acquisition from alkaline substrates in *Arabidopsis*. *Plant Physiol.* 164, 160–172. doi: 10.1104/pp.113.228544

Schmidt, H., Günther, C., Weber, M., Spörlein, C., Loscher, S., Böttcher, C., et al. (2014). Metabolome analysis of *Arabidopsis thaliana* roots identifies a key metabolic pathway for iron acquisition. *PLoS One* 9:e102444. doi: 10.1371/journal.pone.0102444

Segarra, G., Van der Ent, S., Trillas, I., and Pieterse, C. M. J. (2009). MYB72, a node of convergence in induced systemic resistance triggered by a fungal and a bacterial beneficial microbe. *Plant Biol.* 11, 90–96. doi: 10.1111/j.1438-8677.2008.00162.x

Séguéla, M., Briat, J. F., Vert, G., and Curie, C. (2008). Cytokinins negatively regulate the root iron uptake machinery in *Arabidopsis* through a growth-dependent pathway. *Plant J.* 55, 289–300. doi: 10.1111/j.1365-313X.2008.03502.x

Shakeel, S. N., Wang, X., Binder, B. M., and Schaller, G. E. (2013). Mechanisms of signal transduction by ethylene: overlapping and non-overlapping signalling roles in a receptor family. *AoB Plants* 5:lt010. doi: 10.1093/aobpla/plt010

Shanmugam, V., Wang, Y. W., Tsednee, M., Karunakaran, K., and Yeh, K. C. (2015). Glutathione plays an essential role in nitric oxide-mediated iron-deficiency signaling and iron-deficiency tolerance in *Arabidopsis*. *Plant J.* 84, 464–477. doi: 10.1111/tpj.13011

Sharifi, R., and Ryu, C. M. (2018). Sniffing bacterial volatile compounds for healthier plants. *Curr. Opin. Plant Biol.* 44, 88–97. doi: 10.1016/j.pbi.2018.03.004

Shen, C., Yang, Y., Liu, K., Zhang, L., Guo, H., Sun, T., et al. (2016). Involvement of endogenous salicylic acid in iron-deficiency responses in Arabidopsis. *J. Exp. Bot.* 67, 4179–4193. doi: 10.1093/jxb/erw196

Shen, J., Li, C., Mi, G., Li, L., Yuan, L., Jiang, R., et al. (2013). Maximizing root/rhizosphere efficiency to improve crop productivity and nutrient use efficiency in intensive agriculture of China. *J. Exp. Bot.* 64, 1181–1192. doi: 10.1093/jxb/ers342

Shoresh, M., Yedidia, I., and Chet, I. (2005). Involvement of jasmonic acid/ethylene signaling pathway in the systemic resistance induced in cucumber by *Trichoderma asperellum* T203. *Phytopathology* 95, 76–84. doi: 10.1094/PHYTO-95-0076

Singh, R. P., Shelke, G. M., Kumar, A., and Jha, P. N. (2015). Biochemistry and genetics of ACC deaminase: a weapon to "stress ethylene" produced in plants. *Front. Microbiol.* 6:937. doi: 10.3389/fmicb.2015.00937

Sivitz, A. B., Hermand, V., Curie, C., and Vert, G. (2012). *Arabidopsis* bHLH100 and bHLH101 control iron homeostasis via a FIT-independent pathway. *PLoS One* 7:e44843. doi: 10.1371/journal.pone.0044843

Siwinska, J., Siatkowska, K., Olry, A., Grosjean, J., Hehn, A., Bourgaud, F., et al. (2018). Scopoletin 8-hydroxylase: a novel enzyme involved in coumarin biosynthesis and iron-deficiency responses in *Arabidopsis*. *J. Exp. Bot.* 69, 1735–1748. doi: 10.1093/jxb/ery005

Sonbarse, P. P., Sharma, P., and Parvatam, G. (2017). PGPR's mix treatment to *Moringa* improved plant growth and iron content in foliage as substantiated by biochemical and molecular methods. *J. Plant Interact.* 12, 526–532. doi: 10.1080/17429145.2017.1400125

Stringlis, I. A., Proietti, S., Hickman, R., Van Verk, M. C., Zamioudis, C., and Pieterse, C. M. J. (2018a). Root transcriptional dynamics induced by beneficial rhizobacteria and microbial immune elicitors reveal signatures of adaptation to mutualists. *Plant J.* 93, 166–180. doi: 10.1111/tpj.13741

Stringlis, I. A., Yua, K., Feussnerb, K., de Jonge, R., Van Bentum, S., Van Verk, M. C., et al. (2018b). MYB72-dependent coumarin exudation shapes root microbiome assembly to promote plant health. *Proc. Natl. Acad. Sci. U.S.A.* 115, E5213–E5222. doi: 10.1073/pnas.1722335115

Sumayo, M. M., Son, J.-S., and Ghim, S.-Y. (2018). Exogenous application of phenylacetic acid promotes root hair growth and induces the systemic resistance of tobacco against bacterial soft-rot pathogen *Pectobacterium carotovorum* subsp. *carotovorum*. *Funct. Plant Biol.* 45, 1119–1127. doi: 10.1071/FP17332

Ton, J., Davison, S., Van Wees, S. C. M., Van Loon, L. C., and Pieterse, C. M. J. (2001). The *Arabidopsis ISR1* locus controlling rhizobacteria-mediated induced systemic resistance is involved in ethylene signaling. *Plant Physiol.* 125, 652–661. doi: 10.1104/pp.125.2.652

Tsai, H. H., Rodríguez-Celma, J., Lan, P., Wu, Y. C., Vélez-Bermúdez, I. C., and Schmidt, W. (2018). Scopoletin 8-Hydroxylase-mediated fraxetin production is crucial for iron mobilization. *Plant Physiol.* 177, 194–207. doi: 10.1104/pp.18.00178

Tsai, H. H., and Schmidt, W. (2017a). Mobilization of iron by plant-borne coumarins. *Trends Plant Sci.* 22, 538–548. doi: 10.1016/j.tplants.2017.03.008

Tsai, H. H., and Schmidt, W. (2017b). One way. Or another? Iron uptake in plants. *New Phytol.* 214, 500–505. doi: 10.1111/nph.14477

Tyagi, S., Mulla, S. I., Lee, K. J., Chae, J. C., and Shukla, P. (2018). VOCs-mediated hormonal signaling and crosstalk with plant growth promoting microbes. *Crit. Rev. Biotechnol.* 38, 1277–1296. doi: 10.1080/07388551.2018.1472551

Van der Ent, S. (2008). *Transcriptional Regulators of Rhizobacteria Induced Systemic Resistance*. Ph.D. Thesis, Utrecht University Repository, Utrecht.

Van der Ent, S., Pozo, M. J., Verhagen, B. W. M., Bakker, D., Van Loon, L. C., and Pieterse, C. M. J. (2006). Transcription factors in roots and shoots of *Arabidopsis* involved in rhizobacteria-induced systemic resistance. *IOBC/WPRS Bull.* 29, 157–161.

Van der Ent, S., Verhagen, B. W. M., Van Doorn, R., Bakker, D., Verlaan, M. G., Pel, M. J. C., et al. (2008). MYB72 is required in early signaling steps of rhizobacteria induced systemic resistance in *Arabidopsis*. *Plant Physiol.* 146, 1293–1304. doi: 10.1104/pp.107.113829

Van Loon, L. C., Bakker, P. A. H. M., and Pieterse, C. M. J. (1998). Systemic resistance induced by rhizosphere bacteria. *Annu. Rev. Phytopathol.* 36, 453–483. doi: 10.1146/annurev.phyto.36.1.453

Van Loon, L. C., Geraats, B. P. J., and Linthorst, H. J. M. (2006). Ethylene as a modulator of disease resistance in plants. *Trends Plant Sci.* 11, 184–191. doi: 10.1016/j.tplants.2006.02.005

Velivelli, S. L. S., Lojan, P., Cranenbrouck, S., Dupré de Boulois, H., Suarez, J. P., Declerck, S., et al. (2015). The induction of Ethylene Response Factor 3 (ERF3) in potato as a result of co-inoculation with *Pseudomonas* sp. R41805 and *Rhizophagus irregularis* MUCL 41833 - a possible role in plant defense. *Plant Signal. Behav.* 10:e988076. doi: 10.4161/15592324.2014.988076

Verbon, E. H., and Liberman, L. M. (2016). Beneficial microbes affect endogenous mechanisms controlling root development. *Trends Plant Sci.* 21, 218–229. doi: 10.1016/j.tplants.2016.01.013

Verbon, E. H., Trapet, P. L., Stringlis, I. A., Kruijs, S., Bakker, P. A. H. M., and Pieterse, C. M. J. (2017). Iron and immunity. *Annu. Rev. Phytopathol.* 55, 355–375. doi: 10.1146/annurev-phyto-080516-035537

Verhagen, B. W. M., Glazebrook, J., Zhu, T., Chang, H.-S., Van Loon, L. C., and Pieterse, C. M. J. (2004). The transcriptome of rhizobacteria-induced systemic resistance in *Arabidopsis*. *Mol. Plant Microbe Interact.* 17, 895–908. doi: 10.1094/MPMI.2004.17.8.895

Vert, G. A., Briat, J. F., and Curie, C. (2003). Dual regulation of the Arabidopsis high-affinity root iron uptake system by local and long-distance signals. *Plant Physiol.* 132, 796–804. doi: 10.1104/pp.102.016089

Villena, J., Kitazawa, H., Van Wees, S. C. M., Pieterse, C. M. J., and Takahashi, H. (2018). Receptors and signaling pathways for recognition of bacteria in livestock and crops: prospects for beneficial microbes in healthy growth strategies. *Front. Immunol.* 9:2223. doi: 10.3389/fimmu.2018.02223

Wang, B., Li, Y., and Zhang, W. H. (2012). Brassinosteroids are involved in response of cucumber (*Cucumis sativus*) to iron deficiency. *Ann. Bot.* 110, 681–688. doi: 10.1093/aob/mcs126

Wang, C., Yao, J., Du, X., Zhang, Y., Sun, Y., Rollins, J. A., et al. (2015). The *Arabidopsis* Mediator Complex Subunit16 is a key component of basal resistance against the necrotrophic fungal pathogen *Sclerotinia sclerotiorum*. *Plant Physiol.* 169, 856–872. doi: 10.1104/pp.15.00351

Wang, F., Cui, X., Sun, Y., and Dong, C. H. (2013). Ethylene signaling and regulation in plant growth and stress responses. *Plant Cell Rep.* 32, 1099–1109. doi: 10.1007/s00299-013-1421-6

Wang, N., Cui, Y., Liu, Y., Fan, H., Du, J., Huang, Z., et al. (2013). Requirement and functional redundancy of Ib subgroup bHLH proteins for iron deficiency responses and uptake in *Arabidopsis thaliana*. *Mol. Plant* 6, 503–513. doi: 10.1093/mp/sss089

Wang, J., Zhou, C., Xiao, X., Xie, Y., Zhu, L., and Ma, Z. (2017). Enhanced iron and selenium uptake in plants by volatile emissions of *Bacillus amyloliquefaciens* (BF06). *Appl. Sci.* 7:85. doi: 10.3390/app7010085

Wang, W., Shi, J., Xie, Q., Jiang, Y., Yu, N., and Wang, E. (2017). Nutrient exchange and regulation in arbuscular mycorrhizal symbiosis. *Mol. Plant* 10, 1147–1158. doi: 10.1016/j.molp.2017.07.012

Waters, B. M., Lucena, C., Romera, F. J., Jester, G. G., Wynn, A. N., Rojas, C. L., et al. (2007). Ethylene involvement in the regulation of the H+-ATPase *CsHA1* gene and of the new isolated ferric reductase *CsFRO1* and iron transporter *CsIRT1* genes in cucumber plants. *Plant Physiol. Biochem.* 45, 293–301. doi: 10.1016/j.plaphy.2007.03.011

Yang, J., Kloepper, J. W., and Ryu, C. M. (2008). Rhizosphere bacteria help plants tolerate abiotic stress. *Trends Plant Sci.* 14, 1–4. doi: 10.1016/j.tplants.2008.10.004

Yang, Y., Ou, B., Zhang, J., Si, W., Gu, H., Qin, G., et al. (2014). The *Arabidopsis* Mediator subunit MED16 regulates iron homeostasis by associating with EIN3/EIL1 through subunit MED25. *Plant J.* 77, 838–851. doi: 10.1111/tpj.12440

Ye, L., Li, L., Wang, L., Wang, S., Li, S., Du, J., et al. (2015). MPK3/MPK6 are involved in iron deficiency-induced ethylene production in Arabidopsis. *Front. Plant Sci.* 6:953. doi: 10.3389/fpls.2015.00953

Yuan, Y. X., Wu, H. L., Wang, N., Li, J., Zhao, W. N., Du, J., et al. (2008). FIT interacts with AtbHLH038 and AtbHLH039 in regulating iron uptake gene expression for iron homeostasis in *Arabidopsis*. *Cell Res.* 18, 385–397. doi: 10.1038/cr.2008.26

Yun, B. W., Skelly, M. J., Yin, M., Yu, M., Mun, B. G., Lee, S. U., et al. (2016). Nitric oxide and *S*-nitrosoglutathione function additively during plant immunity. *New Phytol.* 211, 516–526. doi: 10.1111/nph.13903

Zamioudis, C. (2012). *Signaling in Arabidopsis Roots in Response to Beneficial Rhizobacteria*. Ph.D. Thesis, Utrecht University, Utrecht.

Zamioudis, C., Hanson, J., and Pieterse, C. M. J. (2014). β-Glucosidase BGLU42 is a MYB72-dependent key regulator of rhizobacteria-induced systemic resistance and modulates iron deficiency responses in *Arabidopsis* roots. *New Phytol.* 204, 368–379. doi: 10.1111/nph.12980

Zamioudis, C., Korteland, J., Van Pelt, J. A., van Hamersveld, M., Dombrowski, N., Bai, Y., et al. (2015). Rhizobacterial volatiles and photosynthesis-related signals coordinate MYB72 expression in *Arabidopsis* roots during onset of induced systemic resistance and iron-deficiency responses. *Plant J.* 84, 309–322. doi: 10.1111/tpj.12995

Zeidler, D., Zähringer, U., Gerber, I., Dubery, I., Hartung, T., Bors, W., et al. (2004). Innate immunity in *Arabidopsis thaliana*: lipopolysaccharides activate nitric oxide synthase (NOS) and induce defense genes. *Proc. Natl. Acad. Sci. U.S.A.* 101, 15811–15816. doi: 10.1073/pnas.0404536101

Zhang, H., Kim, M. S., Krishnamachari, V., Payton, P., Sun, Y., Grimson, M., et al. (2007). Rhizobacterial volatile emissions regulate auxin homeostasis and cell expansion in *Arabidopsis*. *Planta* 226, 839–851. doi: 10.1007/s00425-007-0530-2

Zhang, H., Sun, Y., Xie, X., Kim, M. S., Dowd, S. E., and Paré, P. W. (2009). A soil bacterium regulates plant acquisition of iron via deficiency inducible mechanisms. *Plant J.* 58, 568–577. doi: 10.1111/j.1365-313X.2009.03803.x

Zhang, J., Liu, B., Li, M., Feng, D., Jin, H., Wang, P., et al. (2015). The bHLH transcription factor bHLH104 interacts with IAA-LEUCINE RESISTANT3 and modulates iron homeostasis in *Arabidopsis*. *Plant Cell* 27, 787–805. doi: 10.1105/tpc.114.132704

Zhang, Y., Wu, H., Wang, N., Fan, H., Chen, C., Cui, Y., et al. (2014). Mediator subunit 16 functions in the regulation of iron uptake gene expression in *Arabidopsis*. *New Phytol.* 203, 770–783. doi: 10.1111/nph.12860

Zhao, L., Wang, F., Zhang, Y., and Zhang, J. (2014). Involvement of *Trichoderma asperellum* strain T6 in regulating iron acquisition in plants. *J. Basic Microbiol.* 54, S115–S124. doi: 10.1002/jobm.201400148

Zhou, C., Guo, J., Zhu, L., Xiao, X., Xie, Y., Zhu, J., et al. (2016a). *Paenibacillus polymyxa* BFKC01 enhances plant iron absorption via improved root systems and activated iron acquisition mechanisms. *Plant Physiol. Biochem.* 105, 162–173. doi: 10.1016/j.plaphy.2016.04.025

Zhou, C., Ma, Z., Xiao, X., Xie, Y., Zhu, J., and Wang, J. (2016b). Potential enhancement of plant iron assimilation by microbial-induced root exudation of phenolic compounds. *Res. Rev. J. Bot. Sci.* 5, 34–37.

Zhou, C., Zhu, L., Ma, Z., and Wang, J. (2017). *Bacillus amyloliquefaciens* SAY09 increases cadmium resistance in plants by activation of auxin-mediated signaling pathways. *Genes* 8:E173. doi: 10.3390/genes8070173

Zhou, C., Zhu, L., Ma, Z., and Wang, J. (2018). Improved iron acquisition of *Astragalus sinicus* under low iron-availability conditions by soil-borne bacteria *Burkholderia cepacia*. *J. Plant Interact.* 13, 9–20. doi: 10.1080/17429145.2017.1407000

Conflict of Interest Statement: The authors declare that the research was conducted in the absence of any commercial or financial relationships that could be construed as a potential conflict of interest.

frontiers in Plant Science

ORIGINAL RESEARCH
published: 12 March 2019
doi: 10.3389/fpls.2019.00255

Sustainable Strategies to Prevent Iron Deficiency, Improve Yield and Berry Composition in Blueberry (*Vaccinium* spp.)

*Lucía Michel[1], Álvaro Peña[1], Claudio Pastenes[1], Pablo Berríos[1], Adamo Domenico Rombolà[2] and José Ignacio Covarrubias[1]**

[1] Facultad de Ciencias Agronómicas, Universidad de Chile, Santiago, Chile, [2] Department of Agricultural and Food Sciences, University of Bologna, Bologna, Italy

The aim of this investigation was to study the effect of sustainable strategies to correct iron deficiency in blueberries, based on Fe-heme applications or intercropping with graminaceous species, on yield, and berry quality variables. The experiment was conducted in a blueberry orchard established in a sub-alkaline soil. The association with grasses increased the crop load and yield (only *Festuca rubra*), and decreased the skin/flesh ratio. In addition, these treatments increased anthocyanins as well as some hydroxybenzoic acids, hydroxycinnamic acids, flavanols, and flavonol concentrations in skins with a similar effectiveness as Fe-EDDHA, whereas the Fe-heme applications did not influence such parameters. Moreover, data revealed that the association with both grasses decreased the firmness of the berries, whereas none of the treatments assessed changed the soluble solids, pH, acidity, and the soluble solids/acidity rate compared to the control. These results suggest that Fe nutrition is crucial for yield and berry quality in blueberry, and that intercropping with grasses may be an effective and sustainable alternative to counteract Fe deficiency in blueberry, with a similar effect on berries to that achieved with Fe-EDDHA.

Keywords: intercropping, Fe-heme, iron deficiency, phenolic compounds, fruit quality

OPEN ACCESS

Edited by:
Wolfgang Schmidt, Academia Sinica, Taiwan

Reviewed by:
Ajay Kumar Pandey, National Agri-Food Biotechnology Institute, India
Tomoko Nozoye, Meiji Gakuin University, Japan

***Correspondence:**
José Ignacio Covarrubias
jcovarru@uchile.cl

Specialty section:
This article was submitted to Plant Nutrition, a section of the journal Frontiers in Plant Science

Received: *06 December 2018*
Accepted: *18 February 2019*
Published: *12 March 2019*

Citation:
Michel L, Peña Á, Pastenes C, Berríos P, Rombolà AD and Covarrubias JI (2019) Sustainable Strategies to Prevent Iron Deficiency, Improve Yield and Berry Composition in Blueberry (Vaccinium spp.). Front. Plant Sci. 10:255. doi: 10.3389/fpls.2019.00255

INTRODUCTION

Recently, the daily consumption of functional foods for the prevention of some human diseases has become highly promoted by several health organizations in the world. In this context, the demand for blueberries (*Vaccinium* spp.) has progressively increased in some countries due to the high phenolic compounds concentration in their skins, which are characterized by a great antioxidant capacity (Cordes et al., 2016). Blueberry is a species evolved in rainy areas characterized by soils with an acidic pH from 4.5 to 5.5 (Retamales and Hancock, 2012), and when it is cultivated in lower rainfall zones, often characterized by alkaline or sub-alkaline soils, frequently manifest severe symptoms of iron (Fe) deficiency, drastically reducing plant growth and yield (Rombolà and Tagliavini, 2006).

Even though a few studies have assessed the effect of Fe deficiency on fruit chemical composition and quality in some fruit crops, knowledge regarding the impact of Fe chlorosis on blueberry quality, and healthiness is scarce. In peach fruits, some experiences indicate that Fe deficiency decreases fruit firmness and the red skin color, increasing organic anion concentrations (particularly succinate and quinate), vitamin C,

and total phenolic compounds (Álvarez-Fernández et al., 2003). In grapevines, Fe deficiency has been shown to increase the phenolic compounds accumulation in berries (Bavaresco et al., 2010). In contrast, in the model plant *Perilla frutescens*, anthocyanin synthesis was negatively affected by Fe deficiency, likely associated to a reduced activity of the anthocyanidin synthase (ANS), an enzyme involved in the anthocyanidin synthesis (Saito et al., 1999; Turnbull et al., 2000; Nakajima et al., 2001), and whose activity requires a ferrous Fe center. The controversy on the impact of Fe deficiency on the secondary metabolites concentration in fruits might be due to a subtle effect of the environment on the biosynthetic regulatory signals, or a species dependent sensitivity. Even though blueberries are considered as a healthy nutritional fresh produce, precisely because of their fruit chemical composition, and also as a highly sensitive crop to Fe deficiency, rather scarce knowledge is available in this regard.

In blueberry orchards located in sub-alkaline areas, soil acidification by means of elemental sulfur (S) previous to planting or with sulfuric or phosphoric acid applications during the growing season through the irrigation system, is a common field practice worldwide. In the former case, soil pH varies after long periods of time since microorganisms mediate the transformation of S into inorganic acids. Moreover, depending on the initial soil pH values and the buffer capacity of the soil, extremely high S amounts should be applied to shift the pH down to optimal levels for blueberry (Horneck et al., 2004). As for sulfuric acid applications, soil pH is more quickly reduced, especially in weakly buffered soils. However, this material is hazardous and difficult for farm workers to use (Horneck et al., 2004), and repeated soil applications of sulfuric acid may have a detrimental effect on the microbial biomass and mycorrhizal fungi populations, and on carbon dioxide emissions to the atmosphere. On the other hand, the treatment for Fe chlorosis with Fe chelates is costly and not environmental nor human friendly (Rombolà and Tagliavini, 2006) due to the high risk of metals and chelating agents leaching into the deep soil layers and into the water table (Rombolà and Tagliavini, 2006).

The above mentioned evidences of the negative impact of traditional Fe corrective measures, have led to the use of natural Fe sources to control Fe deficiency. In this context, animal blood-derived compounds, composed of a relatively high Fe content (20–30 g Fe kg^{-1}) chelated by a heme group related to hemoglobin (López-Rayo et al., 2015), have been shown to be highly stable and capable of maintaining available Fe for plants in calcareous soils (Yunta et al., 2013). In controlled experiments conducted on grapevines cultivated in a calcareous soil, Fe-heme applications have increased the leaf chlorophyll concentration, plant growth, and potassium content in leaves (López-Rayo et al., 2015). On the other hand, some investigations have reported that intercropping systems with grasses are effective at preventing Fe chlorosis in co-cultivated crops (Cañasveras et al., 2014, Covarrubias et al., 2014, Granja and Covarrubias, 2018). The mechanism involved in improving Fe nutrition in associated plants is attributed to the ability of monocotyledoneous species to extrude mugineic acid family phytosiderophores (MAs), which are chelating compounds that form a soluble complex with Fe^{3+}, increasing its availability also for the associated crops (Takagi, 1976; Ma et al., 2003; Xiong et al., 2013). For example, some authors have described that the main phytosiderophore secreted by *Festuca rubra* is 2′-deoxymugineic acid (DMA), whereas the graminaceous species *Poa pratensis* exudes DMA, avenic acid A (AVA) and 2′hydroxyavenic acid A (HAVA) (Ma et al., 2003; Ueno et al., 2007). Other studies have reported positive results from this sustainable management technique to prevent Fe chlorosis in fruit tree crops (Cañasveras et al., 2014, Covarrubias et al., 2014), however, to date there have been no reports published on a species highly susceptible to Fe deficiency like blueberry. In addition, some authors have described the possibility of the Fe^{3+}-DMA complex being directly absorbed by intercropped peanut roots, since a functional Fe^{3+}-DMA transporter, AhYSL1, was identified in this species (Xiong et al., 2013).

Even though investigations have been conducted on the effect of alternative and more sustainable management techniques for Fe correction in calcareous soils in blueberry productive and vegetative variables (Michel et al., 2019), the impact on the berry composition is lacking. Indeed, the use of animal blood-derived compounds and/or intercropping with graminaceous species implies the modification of soil nutrition properties related to nitrogen (N) availability, eventual phytoalexins, or simply modification of the competition for light, water and nutrients with eventual impacts on the fruit yield and metabolism (Michel et al., 2019). Accordingly, the present study is focused to evaluate the effect of Fe-heme applications or intercropping with graminaceous species on productive and berry quality variables in blueberry cv. Emerald, cultivated in a sub-alkaline soil.

MATERIALS AND METHODS

Plant Material, Treatments, and Design of the Experiment

The experiment was undertaken from May 2014 to April 2015 (2014–2015 season) in a blueberry orchard located in the Valparaiso Region, Chile (32°42′S and 70°54′W) in an alluvial soil composed of 4% total calcium carbonate, 2% active lime, 1.1% organic matter and pH 8.1. These properties provided chemical conditions inducing Fe chlorosis in blueberries. The trial was conducted on highbush blueberries cv. Emerald (interspecific origin based largely on *Vaccinium corymbosum* L. with some genes from *Vaccinium darrowi* Camp), planted in September 2011 at a distance of 3 m between the rows and 0.8 m between plants along the row.

In autumn 2014, five contiguous rows were selected, homogeneous in size and degree of Fe chlorosis in the plants. The treatments tested were: (1) Control: bare soil; (2) Soil-applied Fe-ethylenediamine-N,N'-bis (2-hydroxyphenyl)acetic acid (Fe-EDDHA) chelate; (3) Soil-applied bovine blood compound (Fe-heme); (4) intercropping with *F. rubra* (graminaceous species), and (5) intercropping with *P. pratensis* L. (graminaceous species). A Latin square design (5 × 5) was used to take into account the slope and drip line as possible independent sources of variance.

Each treatment was replicated five times. The experimental plot for each treatment was composed of 6 plants, and the treatments along the same row were separated by 2 plants between them.

Experimental Conditions and Sample Collection

The Fe chelate was applied to the soil from August 2014 according to the SPAD value in order to maintain an intensive green color in the leaves (SPAD index > 35). Doses of 500 mL per plant of a 5% Fe-EDDHA solution (4 g Fe-EDDHA L^{-1}) were occasionally applied to the soil, reaching 1 g of Fe applied per plant at the end of the season. The Fe-heme was applied through a dried bovine blood formulation composed of 2,675 mg Fe kg^{-1}. Bovine blood was diluted in distilled water to a concentration of 20 g L^{-1} and applied to the soil at doses of 500 mL per plant every 15 days, reaching 0.27 g of Fe applied per plant at the end of the season. The Fe-EDDHA and Fe-heme applications were carried out manually, from the onset of bud break (spring 2014) to the summer flush growth. The graminaceous species *F. rubra* L. and *P. pratensis* L were sown over the rows in autumn 2014 at a density of 20,000 seeds m^{-2}. During the season, the graminaceous species were cut manually to a height of 5 cm every time they reached 15 cm. The plants were irrigated daily through two 2 L h^{-1} in-line microdrip emitters, maintaining a constant soil moisture level, close to field capacity (40% saturation). The soil water content was measured daily using one tensiometer per experimental plot. In intercropped plants, an additional water supply was added according to the tensiometers record to maintain a similar soil moisture between treatments. The agronomic management of pruning, phytosanitary control, and fertilization with macro and micronutrients, except for Fe, were performed regularly throughout the season.

Leaf chlorophyll concentration is an accepted tool to monitor Fe status in fruit crops provided other nutrient deficiencies are excluded, given that leaf Fe concentrations cannot be used for this purpose (Römheld, 2000; Kosegarten et al., 2001). At harvest time, the leaf chlorophyll concentration (μg cm^{-2}) was measured on the first completely expanded leaf of 16 shoots per experimental plot.

All harvested fruits were manually collected, when the skin color reached the 75% Blue stage, used for commercial purposes. The harvest took place on 5 different days, according to the fruit maturation rate. At each harvest, yield, and number of fruits per plant were measured for 6 plants in each replicate. At the end of the season, the total yield and crop load recorded at each harvest were determined, and the average berry weight was calculated.

In the third harvest (December 11, 2014), which was the largest and most representative (55% of the harvested fruit), berry samples (one composed of 40 and two of 200 berries) were collected from each experimental unit. The berries were sampled at random, considering that their size was representative of the experimental unit. The samples composed of 40 berries were used for firmness determinations, whereas one of the samples composed of 200 berries was used for chemical analysis, and the others were frozen at −80°C for phenolic compound determinations.

Firmness of Berries

Firmness of the berries was measured in samples of 40 berries per experimental unit, within a few hours of the harvest. Firmness was determined in each berry using a fruit texture analyzer (FTA 65-14, GÜSS, Strand, South Africa) with a plunger 3 cm in diameter.

Physio-Chemical Analysis of Berries

These measurements were taken in samples of 200 berries per experimental unit. Blueberries were peeled, weighed, and the skin/flesh ratio was determined. Successively, a composite sample was made by mixing and grinding the mesocarp of the 200 fruits per experimental unit. The ground pulp was then filtered and divided into two aliquots for chemical analysis. Soluble solids (SS), reported as °Brix, were determined with a digital refractometer thermocompensated at 20°C (PAL-1, Atago Co, Ltd., Tokyo, Japan). Titratable acidity (expressed as a percentage of citric acid) was measured with NaOH 0.1 N up to pH 8.2, and the pH of the mesocarp was measured with a pH meter (pHep-HI98107, Hanna Instrument, Padua, Spain).

Determination of Phenolic Compounds

For the extraction, the skins of 200 berries per experimental unit, frozen at −80°C, were peeled, weighed and placed in a methanol:water solution (80:20 v/v) at a 1:5 ratio. The samples were homogenized, shaken (BioScan OS-20, LabTec, Chile) for 30 min and centrifuged (Universal 320, Hettich Lab, Germany) for 10 min at 1,500 rpm at 20°C. Successively, the liquid part was refrigerated and the supernatant was again macerated, shaken and centrifuged, following the previous procedure. Once this second extraction was complete, the liquid fraction was recovered and added to the first, and the final solution was centrifuged at 4,000 rpm at 20°C for 15 min. Thereafter, the samples were filtered under vacuum through a PVDF membrane, porosity 8 μm.

Total anthocyanin concentration was determined according to García-Barceló (1990), based on bisulfite discoloration. The extract was diluted 100 times, and 1 mL of the diluted extract was added with 1 mL of acid alcohol and 20 mL of 2% HCl. The resulting solution was separated into two test tubes, and to each one 4 mL of $NaHSO_3$ (sodium metabisulfite), and 4 mL of distilled water were added. After placing the tubes in the dark for 20 min, absorbance was measured by spectrophotometry (Lambda 25, PerkinElmer, Hartford, United States) at 520 nm with 10 mm glass cuvettes. Total phenols concentration was determined in the extract (diluted at 1:100) according to García-Barceló (1990), using gallic acid as the standard. The analysis was performed by spectrophotometry at 280 nm with 10 mm quartz cuvettes. Total tannins concentrations were assessed as described by the Bate-Smith (1972) methodology, which is based on tannins hydrolysis in acidic medium. After 1:50 dilution of the extract, 4 mL of the sample were placed in two test tubes, and 2 mL of distilled water and 6 mL of 35% HCl were added. Then, one tube was subjected to a water bath at 90°C for 30 min, and the other at room temperature. Both samples were evaluated with spectrophotometry at 550 nm with 10 mm glass cuvettes.

The anthocyanins profile were determined according to Peña-Neira et al. (2007), using high-performance liquid chromatography (Agilent Technologies 1100 series HPLC system, Santa Clara, CA, United States), consisting of a photodiode array detector (DAD), model G1315B; a quaternary pump, model QuatPump G1311A; a degasser, model G1379A; and an autosampler, model G1329A. A RP-18 reverse-phase column (Merck Hitachi, Tokyo, Japan), 5 μm pore size, 250 mm × 4 mm was used. One-hundred mL of each extract was filtered through a 0.45 mm pore size and then subjected to reverse-phase chromatographic separation at 20°C. The quantification was carried out by peak area measurements at 520 nm. Anthocyanins were quantified and expressed as mg of g^{-1} of berry skin of malvidin-3-glucoside. The calibration curves at 520 nm were obtained by injecting different volumes of standard solutions under the same conditions as for the samples analyzed.

The low molecular weight phenolic compounds were quantified as described by Peña-Neira et al. (2007), using the same Agilent model HPLC-DAD equipment as described for anthocyanin determinations. A Nova Pack C18 reverse-phase column (4 μm, 3.9 mm i.d. × 300 mm; Waters Corp.) was used. Both chromatographs were coupled to an Agilent Chem Station (version B.04.03) data processing station. Signals were detected at 280 nm, at 20°C and with an injection volume of 10 μm. The low molecular weight phenolic compounds were identified by comparing their absorption spectrum and retention time to their respective standard. The calibration curves at 280 nm were obtained by injecting different volumes of standard solutions under the same conditions as for the samples analyzed. The phenolic compounds were expressed as mg of each phenolic compound g^{-1} of berry skin.

Statistics

The analysis of variance (ANOVA) was performed under the framework of mixed linear models (MLM). In the case of significant differences between treatments, the DGC test for multiple comparisons was used ($\alpha = 0.05$). The statistical software used was InfoStat v. 2013.

RESULTS

Leaf Chlorophyll Concentration, Crop Load, Plant Production, Berry Weight, and Skin/Flesh Ratio

At harvest time, the leaf chlorophyll concentration ($\mu g\ cm^{-2}$) average measured on the first completely expanded leaf of 16 shoots per experimental plot was the following: (1) Control: 7.3 units ± 1.6; (2) Soil-applied Fe-EDDHA chelate: 13.1units ± 1.5; (3) Soil-applied Fe-heme: 8.1 units ± 1.7; (4) Intercropping with *P. pratensis* L.: 9.8 units ± 1.6; (5) Intercropping with *F. rubra*: 11.6 units ± 1.6. Such leaf chlorosis is attributed to Fe deficiency since the leaf mineral concentration analysis revealed values in the sufficiency range for the other nutrients (data not reported). In addition, plants treated with Fe-EDDHA showed the highest values, with significant differences in comparison with the control plants.

The association with *F. rubra* and *P. pratensis* as well as the Fe-EDDHA applications increased the crop load, whereas the fertilization with Fe-heme did not modify this variable compared to control plants (**Figure 1A**). As for yield, however, only the intercropping with *F. rubra* treatment increased this variable compared to control, while the Fe-heme treated plants were the less yielding plants, similar to untreated plants (**Figure 1B**). Regarding the berry weight, in general no marked differences were observed between treatments, but two opposite and significant results were clear between the Fe-EDDHA and the Fe-heme treated plants, the latter with the lowest berry weight (**Figure 1C**). Also, regarding fruit physical properties, some treatments reduced the skin to flesh weight ratio, such as the intercropping with *F. rubra* and *P. pratensis* and, particularly, fruits from plants treated with the Fe-EDDHA chelate, all of them with significant lower averages of this parameter compared to control fruits (**Figure 1D**).

Firmness and Chemical Berry Composition

From **Table 1**, it is clear that none of the Fe correction treatments induced significant changes on the ripening of fruits since the SS concentration, pH, acidity and the SS/acidity ratio were similar between treatments. In fact, the extreme values for each of these parameters between treatments accounted for an 11, 3, 20, and 13% for SS, pH, acidity and SS to acidity ratio, respectively. As for fruit firmness, however, differences were observed between treatments, in which the association with both grasses decreased the firmness compared with the control and with plants treated with Fe-heme, whereas the berries collected from plants treated with Fe-EDDHA reached intermediate values (**Table 1**).

Phenolic Compounds Concentration in Berry Skins

The Fe treatments, except for the Fe-heme, had an impact on the berry skin composition of the blueberries considering total anthocyanins and total phenols, but no effect was observed in total tannins (**Table 2**). Regarding total anthocyanins, the intercropping and the Fe-EDDHA applications were the more promising treatments. As for total phenols, the intercropping treatments and the Fe-EDDHA applications were equally effective, inducing nearly a 40% increase in the concentration, in average, compared to control (**Table 2**).

Interestingly, the treatments implemented in the present study not only affected the total anthocyanins in the blueberry skins, but also its composition. Regardless of the treatment, four anthocyanin classes were found; all of them were 3-O-glycoside conjugates: malvidin, delphinidin, cyanidin and petunidin (**Table 3**). Glycosylation with galactose, glucose and arabinose were the forms found for malvidin and delphnidin, only galactose for cyanidin and, for petunidin, galactose, and arabinose additions were detected (**Table 3**). Of all, malvidin 3-galactoside and delphinidin 3-galactoside were the most abundant forms found in the berry skins. In agreement with

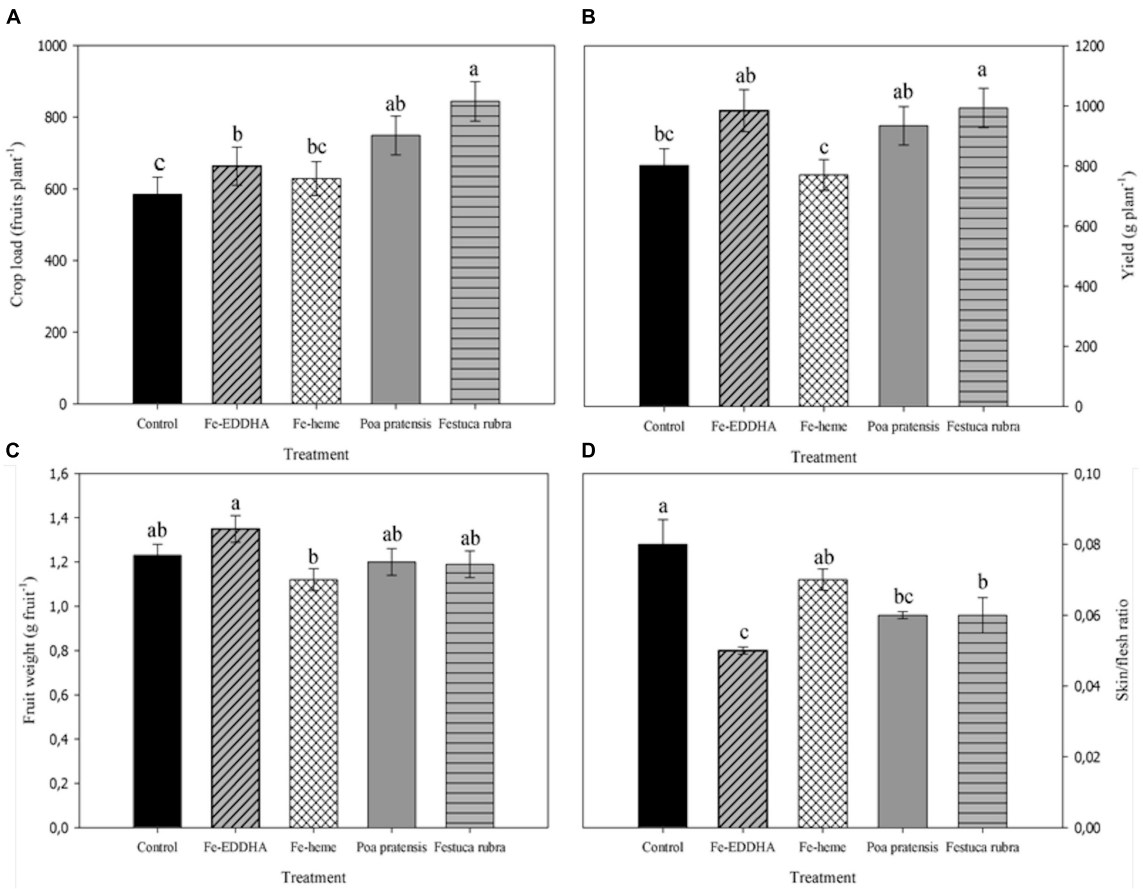

FIGURE 1 | Crop load **(A)**, yield **(B)**, berry weight **(C)**, and skin/flesh ratio **(D)** at harvest in "Emerald" blueberries under different treatments to prevent Fe deficiency. Adjusted means with different letters between treatments indicate significant differences according to DGC test ($p < 0.05$). Vertical bars indicate the standard error.

TABLE 1 | Firmness (N), soluble solids (°Brix), pH, acidity (%), and soluble solids/acidity ratio at harvest in "Emerald" blueberries under different treatments to prevent Fe deficiency.

Treatment	Firmness (N)	Soluble solids (°Brix)	pH	Acidity (% citric acid)	Soluble solids/acidity
Control	3.11 ± 0.07*a*	15.9 ± 0.19	3.63 ± 0.06	0.45 ± 0.03	33.1 ± 4.03
Fe-EDDHA	2.99 ± 0.07*ab*	16.5 ± 1.23	3.68 ± 0.06	0.58 ± 0.04	28.7 ± 1.04
Fe-heme	3.07 ± 0.07*a*	14.6 ± 0.59	3.69 ± 0.05	0.48 ± 0.03	30.5 ± 1.82
Poa pratensis	2.91 ± 0.07*bc*	15.1 ± 0.58	3.57 ± 0.07	0.50 ± 0.02	32.6 ± 3.44
Festuca rubra	2.88 ± 0.07*c*	14.9 ± 0.63	3.62 ± 0.06	0.56 ± 0.03	28.9 ± 1.11
Significance	$p = 0.0016$	NS	NS	NS	NS

In each column the adjusted mean @ standard error is presented. Adjusted means with different letters in the same column indicate significant differences between treatments according to the DGC test ($p < 0.05$). NS, not significant.

data from **Table 2**, the higher concentrations of anthocyanins corresponded to berries from plants treated with Fe-EDDHA and from those intercropped with grasses (**Table 3**). In general, the Fe-EDDHA applications and the association with *P. pratensis* increased the malvidin, delphinidin and petunidin glycosides and cyanidin-3-galactoside concentrations in comparison with the control and Fe-heme plants (**Table 3**), whereas the association with *F. rubra* increased only delphinidin and some malvidin glycosides (**Table 3**). The Fe-heme applications, on the other hand, did not influence the skin anthocyanin composition compared to the control (**Table 3**).

As for the phenolic acid compounds, the gallic and vanillic hydroxybenzoic acids and the chlorogenic and *trans*-caffeic hydroxycinnamic acids, were the most abundant on a weight basis in blueberry skins. Protocatechuic and ferulic acids were also detected but in a lower concentration and with no significant differences between treatments. Regarding hydroxybenzoic acids, the association with both grasses increased the gallic acid

TABLE 2 | Total anthocyanins (mg g skin^{-1}), total phenols (mg g skin^{-1}) and total tannins (mg g skin^{-1}) at harvest in "Emerald" blueberries under different treatments to prevent Fe deficiency.

Treatment	Total anthocyanins (mg g skin^{-1})	Total phenols (mg g skin^{-1})	Total tannins (mg g skin^{-1})
Control	13.7 ± 1.6c	54.3 ± 5.5b	0.38 ± 0.03
Fe-EDDHA	24.2 ± 1.6a	78.1 ± 5.4a	0.43 ± 0.01
Fe-heme	14.7 ± 1.8c	53.2 ± 5.5b	0.41 ± 0.02
Poa pratensis	21.8 ± 1.8b	75.0 ± 5.3a	0.40 ± 0.03
Festuca rubra	19.5 ± 2.1b	72.4 ± 4.8a	0.36 ± 0.02
Significance	$p < 0.0001$	$p = 0.0193$	NS

In each column the adjusted mean @ standard error is presented. Adjusted means with different letters in the same column indicate significant differences between treatments according to the DGC test ($p < 0.05$). NS, not significant.

concentration as compared with the control berries, but not the Fe-heme treatment (**Table 4**). Also, the Fe-EDDHA applications increased the gallic and vanillinic acid berry skin concentrations compared to control (**Table 4**).

As for hydroxycinnamic acids, the association with graminaceous species and the fertilization with Fe-EDDHA increased the chlorogenic acid concentration compared to both, control and the Fe-heme treatments (**Table 4**). Besides, the intercropping with *P. pratensis* and application of Fe-EDDHA increased the *trans*-caffeic acid in skins more than in the control and Fe-heme, whereas the association with *F. rubra* reached intermediate values (**Table 4**). The treatments did not modify the ferulic acid concentration in the berry skins (**Table 4**).

Results concerning flavanols in skins revealed that intercropping with graminaceous species and Fe-EDDHA treatments increased the catechin and epicatechin concentrations compared to the control, whereas Fe-heme did not influence such concentrations (**Table 5**). In the case of procyanidin dimmers, no differences were registered between treatments (**Table 5**). In the di-Oh flavonol, a trend similar to the catechin and epicatechin was registered for the astilbin acid concentration, whereas no differences were recorded for the flavonol quercetin. In the case of coumarins, data revealed that Fe-EDDHA increased the esculetin concentration in comparison with Fe-heme and the control, whereas intercropping treatments reached intermediate values (**Table 5**).

DISCUSSION

Data collected in our experiment indicate that those treatments resulting in higher leaf chlorophyll concentrations at harvest (see section "Materials and Methods"), such as intercropping with *F. rubra* and *P. pratensis*, together with Fe-EDDHA applications, were effective in inducing changes in some productive and berry morphological characteristics compared to the control and Fe-heme plants. Indeed, these treatments increased the fruit load and, for plants intercropped with *F. rubra*, also an increase in the yield per plant was evident. In addition, the same treatments decreased the skin/flesh ratio (**Figure 1**). The skin to flesh ratio is affected by the berry volume, as it might be the case for the Fe-EDDHA treated plants, with the highest fruit average weight as well as the lowest skin/flesh relationship (**Figures 1C,D**), but may be also due to a more thick epidermis tissue. The lower crop load recorded in plants with a lower leaf chlorophyll concentration, that is control and Fe-heme, could be related to a lower fruit set or a higher early abscission of berries in these plants, considering that Fe chlorosis promotes the expression of genes involved in the synthesis and signaling of ethylene, resulting in the abscission of young fruits (Iqbal et al., 2013). Also, blueberries are regarded as a highly sensitive species to sink/source relationship (Jorquera-Fontena et al., 2018; Petridis et al., 2018), where the non-structural carbon reserves status in shoots and storage organs are determinant in the extent of the post-fruit set fall (Buwalda and Smith, 1990; Mehouachi et al., 1995). In fact, it is well known that the Fe status of plants is closely linked to the photosynthetic capacity of leaves (Briat et al., 2007), and in citrus, Fe deficiency induced reductions in the carbon status of plants, increasing the early fruit fall (Gómez-Cadenas et al., 2000). In our study, a lower leaf net photosynthesis during the season was registered, precisely, in control and Fe-heme plants in comparison with those treated with Fe-EDDHA and intercropping with grasses (Michel et al., 2019). Likewise, the effect of Fe nutrition on the carbon availability within the plant could contribute to explain the higher pulp fraction in relation to the skin in berries collected from plants with a better Fe status, such as those treated with Fe-EDDHA and intercropped with graminaceous, as well as the higher yield in plants associated with *F. rubra* than the control plants.

The ripening process, on the other hand, regarding SS, pH, acidity and SS acidity ratio were not altered by any of the Fe-correcting strategies (**Table 1**). This result, suggests that any eventual impact of the treatments on yield was rather the result of a sink to source balance, with no impact on the primary metabolism of the berries. Similar results from Fe nutrition studies have been reported for peach, citrus and pear (Álvarez-Fernández et al., 2003, 2011; Bañuls et al., 2003). However, as for berry firmness, a relevant trait for post-harvest market considerations, differences between the treatments assessed in the present study were recorded (**Table 1**). Firmness is associated to a combination of ripening stages, water content and cell wall properties in berries. In blueberry, the berry firmness varies according the ripeness status, being maximum before berry veraison and progressively decreasing after it, and the SS to acidity ratio has been reported as a very reliable indicator of the ripening stage and fruit firmness (Moggia et al., 2017). As for our results, no significant differences in the SS/acidity ratio was observed between treatments, even though differences of up to a 13% between the minimum -Fe-EDDHA- and maximum –intercropping with *P. pratensis*- were detected, both treatments with significant differences in the berry firmness. This might suggest that the primary metabolites and their ratio, suggested as a proxy for ripening state in fruits, are highly variable as compared to firmness. Alternatively, a more subtle effect of the treatments might be indirectly affecting the water status and physical skin properties of the berries, such as plant vigor and light interception and temperature on fruits, but those were not evident from our observations.

TABLE 3 | Anthocyanin (mg g skin^{-1}) profile at harvest in 'Emerald' blueberries under different treatments to prevent Fe deficiency.

Anthocyanins (mg g skin^{-1})	Treatment					
	Control	Fe-EDDHA	Fe-heme	*Poa pratensis*	*Festuca rubra*	Significance
Malvidin 3-galactoside	0.080 ± 0.010bc	0.110 ± 0.010a	0.070 ± 0.010c	0.100 ± 0.010ab	0.100 ± 0.010ab	$p = 0.0180$
Malvidin 3-glucoside	0.039 ± 0.004c	0.062 ± 0.004a	0.037 ± 0.004bc	0.057 ± 0.004a	0.052 ± 0.004ab	$p = 0.0053$
Malvidin 3-arabinoside	0.030 ± 0.003b	0.050 ± 0.003a	0.030 ± 0.003b	0.050 ± 0.003a	0.050 ± 0.003a	$p = 0.0134$
Delphinidin 3-galactoside	0.080 ± 0.010c	0.120 ± 0.010a	0.090 ± 0.010bc	0.120 ± 0.010a	0.110 ± 0.010ab	$p = 0.0084$
Delphinidin 3-glucoside	0.026 ± 0.007b	0.039 ± 0.007a	0.026 ± 0.007b	0.037 ± 0.007a	0.034 ± 0.007a	$p = 0.0063$
Delphinidin 3-arabinoside	0.050 ± 0.010b	0.070 ± 0.004a	0.050 ± 0.004b	0.070 ± 0.010a	0.070 ± 0.010a	$p = 0.0104$
Cyanidin 3-galactoside	0.060 ± 0.010b	0.080 ± 0.004a	0.060 ± 0.004b	0.080 ± 0.010a	0.070 ± 0.010ab	$p = 0.0185$
Petunidin 3-galactoside	0.030 ± 0.002c	0.046 ± 0.002a	0.030 ± 0.002c	0.038 ± 0.002b	0.034 ± 0.002bc	$p = 0.0011$
Petunidin 3-arabinoside	0.026 ± 0.002b	0.036 ± 0.002a	0.025 ± 0.002b	0.034 ± 0.002a	0.031 ± 0.002ab	$p = 0.0195$

In each column the adjusted mean @ standard error is presented. Adjusted means with different letters in the same column indicate significant differences between treatments according to the DGC test ($p < 0.05$).

TABLE 4 | Hydroxybenzoic acid (mg g skin^{-1}) and hydroxycinnamic acid (mg g skin^{-1}) profiles at harvest in "Emerald" blueberries under different treatments to prevent Fe deficiency.

Treatment	Hydroxybenzoic acids (mg g skin^{-1})			Hydroxycinnamic acids (mg g skin^{-1})		
	Protocatechuic	Gallic	Vanillinic	Ferulic	Chlorogenic	*Trans* caffeic
Control	0.0043 ± 0.0007	0.025 ± 0.002c	0.046 ± 0.002b	0.006 ± 0.002	0.37 ± 0.08b	0.06 ± 0.01*b*
Fe-EDDHA	0.0056 ± 0.0005	0.032 ± 0.001a	0.059 ± 0.002a	0.008 ± 0.002	0.70 ± 0.07a	0.10 ± 0.02*a*
Fe-heme	0.0040 ± 0.0006	0.026 ± 0.002bc	0.043 ± 0.003b	0.006 ± 0.002	0.35 ± 0.07b	0.07 ± 0.01*b*
Poa pratensis	0.0052 ± 0.0006	0.031 ± 0.003a	0.050 ± 0.002ab	0.009 ± 0.003	0.67 ± 0.07a	0.10 ± 0.01*a*
Festuca rubra	0.0052 ± 0.0005	0.030 ± 0.002ab	0.049 ± 0.002ab	0.009 ± 0.004	0.73 ± 0.08a	0.09 ± 0.02*ab*
Significance	NS	$p = 0.0194$	$p = 0.029$	NS	$p < 0.0001$	$p = 0.0446$

In each column the adjusted mean @ standard error is presented. Adjusted means with different letters in the same column indicate significant differences between treatments, according to DGC test ($p < 0.05$). NS, not significant.

TABLE 5 | Flavanols (mg g skin^{-1}), flavonols (mg g skin^{-1}) and coumarins (mg g skin^{-1}) profiles at harvest in "Emerald" blueberries under different treatments to prevent Fe deficiency.

Treatment	Flavanols (mg g skin^{-1})			Flavonols (mg g skin^{-1})		Coumarins (mg g skin^{-1})
	Procyanidin dimmers	Catechin	Epicatechin	Quercetin	Astilbin	Esculetin
Control	0.010 ± 0.003	0.04 ± 0.01d	0.10 ± 0.01c	0.016 ± 0.003	0.05 ± 0.02b	8.2*E* − 05 ± 0.000*bc*
Fe-EDDHA	0.014 ± 0.005	0.07 ± 0.02c	0.16 ± 0.01a	0.023 ± 0.003	0.14 ± 0.03a	1.2*E* − 04 ± 0.000*a*
Fe-heme	0.011 ± 0.003	0.05 ± 0.01d	0.11 ± 0.02bc	0.020 ± 0.002	0.07 ± 0.02b	6.3*E* − 05 ± 0.000*c*
Poa pratensis	0.011 ± 0.003	0.09 ± 0.01b	0.16 ± 0.01a	0.023 ± 0.004	0.17 ± 0.04a	9.7*E* − 05 ± 0.000*ab*
Festuca rubra	0.020 ± 0.006	0.13 ± 0.02a	0.14 ± 0.01b	0.019 ± 0.003	0.19 ± 0.04a	1.0*E* − 04 ± 0.000*ab*
Significance	NS	$p < 0.0001$	$p < 0.0001$	NS	$p = 0.0007$	$p = 0.0016$

In each column the adjusted mean @ standard error is presented. Adjusted means with different letters in the same column indicate significant differences between treatments according to the DGC test ($p < 0.05$). NS, not significant.

Data concerning anthocyanin content in 'Emerald' blueberries from our study, revealed the presence of 9 different compounds in the skins (**Table 3**), while 13 were reported in Italy (Giovanelli and Buratti, 2009), 15 in France (Kader et al., 1996), 25 in Canada (Gao and Mazza, 1994), 15 in United States (Ballington et al., 1987; Mazza and Miniati, 1993), and 10 in other countries and other varieties (Sapers et al., 1984). The anthocyanin compounds identified in berry skins were galactosides, glucosides and arabinosides of delphinidin, cyanidin, petunidin and malvidin, similar to previous studies (Kader et al., 1996; Taruscio et al., 2004; Giovanelli and Buratti, 2009). However, and in contrast with other investigations, peonidin was not detected (Kader et al., 1996; Tomás-Barberán and Espín, 2001; Lohachoompol et al., 2008; Giovanelli and Buratti, 2009). In addition, the

major anthocyanins concentration corresponded to delphinidin 3-galactoside and malvidin 3-galactoside, followed by cyanidin 3-galactoside and delphinidin 3-arabinoside. Also, and consistent with determinations from different *Vaccinium corymbosum* varieties, anthocyanin compounds reached 30–35% of total phenols (Moyer et al., 2002; Sellapan et al., 2002; Lee et al., 2004; Giovanelli and Buratti, 2009).

As for low molecular weight phenols, the hydroxycinnamic acids were the largest group contained in skins. Within that group, the highly antioxidant molecule chlorogenic acid predominated, while ferulic acid was present in lower concentrations (**Table 4**), similar to previous reports (Häkkinen and Törrönen, 2000; Taruscio et al., 2004). As for the hydroxybenzoic acids group, the highest compound identified was vanillinic acid, followed by gallic and protocatechuic acids (**Table 4**). In the flavanols group, epicatechin predominated over catechin (**Table 5**), as seen in nine different *Vaccinium* species (Taruscio et al., 2004). Between di-OH flavanols and flavonols, astilbin showed a higher concentration than quercetin, and no myricetin or kaempferol was detected (**Table 5**), as reported by Taruscio et al. (2004). In this sense, Kader et al. (1996) and Sellapan et al. (2002) found kaempferol, although in a smaller amount than quercetin, a molecule regarded as the more abundant flavonol in blueberry (Kader et al., 1996, Häkkinen et al., 1998). Up to our knowledge, this is the first report on the phenolic composition in "Emerald" blueberries grown in Chile. Thus, although the phenolic composition and antioxidant capacity of blueberry is more influenced by the genotype than by the growing season, it is advisable to evaluate the same species for several producing seasons in order to precisely determine whether the genotype maintains its phenolic composition over environmental variations.

It has been widely reported that changes in berry weight usually leads to changes in phenol concentration in berries, as these compounds are affected by the berry size due to a dilution factor (Ojeda et al., 2002; Roby et al., 2004). In contrast, our results did not reveal significant differences between treatments in total phenol, total anthocyanin and total tannin concentrations, when are expressed as mg g^{-1} berry (data not reported), despite the effect of treatments on the skin/flesh ratio. This suggest, that the phenol content in berries were not necessarily the result of berry size variations but to an actual positive differential synthesis vs. degradation activities in skins. Indeed, our results are expressed as for skin weight basis (**Tables 2–5**). Data related to total phenols and total anthocyanins (**Table 2**) as well as the anthocyanins and low molecular weight phenols profiles (**Tables 3–5**) revealed a higher accumulation of these compounds in skins from plants treated with Fe-EDDHA and in intercropped plants than the control and Fe-heme. These results suggest that by better counteracting the Fe deficiency of blueberry plants, the Fe-chelate as well as the intercropping treatments favored the berry fruits chemical composition. Fe is a cofactor of the ANS enzyme, which is involved in the anthocyanin synthesis pathway (Saito et al., 1999; Turnbull et al., 2000), the activity of which requires a ferrous Fe center to catalyze the reaction that converts dihydroflavones (flavan-3,4-diol) into anthocyanidins (Turnbull et al., 2004). Similarly, for the low molecular weight phenols, Fe is also involved in its synthesis pathway as a cofactor of flavanone-3β-hydroxylase (F3H) and flavonol synthase (FLS) enzymes, which catalyze the consecutive conversion of flavanones to flavanonols, and of flavanonols to flavonols, respectively. In this sense, the oxidation reactions involving Fe-dependent enzymes play a crucial role in flavonoid biosynthesis (Saito and Yamazaki, 2002; Springob et al., 2003), and clearly, corrective and effective field practices regarding Fe nutrition have a positive impact on berry quality in field grown blueberries.

On the other hand, data related to both cinnamic and benzoic acids suggest that Fe might also be participating in the non-flavonoid compounds concentration in blueberry skins, but further studies are needed to clarify this issue. The synthesis and accumulation of phenolic compounds are strongly influenced by the photosynthetic capacity of plants (Smart and Robinson, 1991) which, in our study, was higher in plants treated with Fe-EDDHA and intercropped with the graminaceous species (data not shown). In fact, the synthesis of the shikimate pathway precursors come from hexoses derived from photosynthesis, ending in the formation of polyphenols such as flavonols, flavanols, anthocyanins, or tannins. Whether the higher benzoic and cinnamic acid concentrations results purely from a more favorable carbon supply condition in the Fe chelate and intercropping with grasses treatments, or a more subtle effect are involved, as it could be the need for antioxidant defenses and related systemic acquired resistance in Fe-deficient plants, depleting benzoic acids intermediates, is not clear and needs further investigations.

In view of the strong and positive relationship among the antioxidant capacity and the total phenol and anthocyanin content (Ehlenfeldt and Prior, 2001; Moyer et al., 2002; Sellapan et al., 2002), the study of sustainable management techniques, such as intercropping with grasses, that affect the crop and influence the phenolic accumulation of the fruits, will be useful to providing the consumer with a better product.

DATA AVAILABILITY

The datasets generated for this study are available on request to the corresponding author.

AUTHOR CONTRIBUTIONS

JC conceived the work and wrote the manuscript. LM conducted the experiment and measured the field. ÁP performed the chemical analysis in berries. CP, PB, and AR contributed to the manuscript writing.

FUNDING

This work was supported by the Comisión Nacional de Investigación Científica y Tecnológica (CONICYT) of Chile (FONDECYT project no. 11130328).

REFERENCES

Álvarez-Fernández, A., Melgar, J. C., Abadía, J., and Abadía, A. (2011). Effects of moderate and severe iron deficiency chlorosis on fruit yield, appearance and composition in pear (*Pyrus communis L.*) and peach (*Prunus persica L.* Batsch). *Environ. Exp. Bot.* 71, 280–286. doi: 10.1016/j.envexpbot.2010.12.012

Álvarez-Fernández, A., Paniagua, P., Abadía, J., and Abadía, A. (2003). Effects of Fe deficiency chlorosis on yield and fruit quality in peach (*Prunus persica L.* Batsch). *J. Agric. Food Chem.* 51, 5738–5744. doi: 10.1021/jf034402c

Ballington, J. R., Ballinger, W. E., and Maness, E. P. (1987). Interspecific differences in the percentage of anthocyanins, aglycones and aglycone-sugars in the fruit of seven species of blueberry. *J. Am. Soc. Hortic. Sci.* 112, 859–864.

Bañuls, J., Quiñones, A., Martín, B., Primo-Millo, E., and Legaz, F. (2003). Effects of the frequency of iron chelate supply by fertigation on iron chlorosis in citrus. *J. Plant Nutr.* 26, 1985–1996. doi: 10.1081/PLN-120024258

Bate-Smith, E. C. (1972). Detection and determination of ellagitannins. *Phytochemistry* 11, 1153–1156. doi: 10.1016/S0031-9422(00)88470-8

Bavaresco, L., van Zeller, M. I., Civardi, S., Gatti, M., and Ferrari, F. (2010). Effects of traditional and new methods on overcoming lime-induced chlorosis of grapevine. *Am. J. Enol. Vitic.* 61, 186–190.

Briat, J. F., Curie, C., and Gaymard, F. (2007). Iron utilization and metabolism in plants. *Curr. Opin. Plant Biol.* 10, 276–282. doi: 10.1016/j.pbi.2007.04.003

Buwalda, J. G., and Smith, G. S. (1990). Effects of partial defoliation at various stages of the growing season on fruit yields, root growth and return bloom of kiwifruit vines. *Sci. Hortic.* 42, 29–44. doi: 10.1016/0304-4238(90)90145-5

Cañasveras, J. C., Del Campillo, M. C., Barrón, V., and Torrent, J. (2014). Intercropping with grasses helps to reduce iron chlorosis in olive. *J. Soil Sci. Plant Nutr.* 14, 554–564.

Cordes, H., Iriarte, A., and Villalobos, P. (2016). Evaluating the carbon footprint of chilean organic blueberry production. *Int. J. Life Cycle Assess.* 21, 281–292. doi: 10.1016/j.scitotenv.2017.03.147

Covarrubias, J. I., Pisi, A., and Rombolà, A. D. (2014). Evaluation of sustainable management techniques for preventing iron chlorosis in the grapevine. *Aust. J. Grape Wine Res.* 20, 149–159. doi: 10.1111/ajgw.12055

Ehlenfeldt, M. K., and Prior, R. L. (2001). Oxygen radical absorbance capacity (ORAC) and phenolic and anthocyanin concentrations in fruit and leaf tissues of highbush blueberry. *J. Agric. Food Chem.* 49, 2222–2227. doi: 10.1021/jf0013656

Gao, L., and Mazza, G. (1994). Quantitation and distribution of simple and acylated anthocyanins and other phenolics in blueberries. *J. Food Sci.* 59, 1057–1059. doi: 10.1111/j.1365-2621.1994.tb08189.x

García-Barceló, J. (1990). *Técnicas Analíticas Para Vinos*. San Francisco, CA: Scribd Inc.

Giovanelli, G., and Buratti, S. (2009). Comparison of polyphenolic composition and antioxidant activity of wild Italian blueberries and some cultivated varieties. *Food Chem.* 112, 903–908. doi: 10.1016/j.foodchem.2008.06.066

Gómez-Cadenas, A., Mehouachi, J., Tadeo, F. R., Primo-Millo, E., and Talon, M. (2000). Hormonal regulation of fruitlet abscission induced by carbohydrate shortage in citrus. *Planta* 210, 636–643. doi: 10.1007/s004250050054

Granja, F., and Covarrubias, J. I. (2018). Evaluation of acidifying nitrogen fertilizers in avocado trees with iron deficiency symptoms. *J. Soil Sci. Plant Nutr.* 18, 157–172. doi: 10.4067/S0718-95162018005000702

Häkkinen, S. H., Kärenlampi, S. O., Heinonen, I. M., Mykkänen, H. M., and Törrönen, A. R. (1998). HPLC method for screening of flavonoids and phenolic acids in berries. *J. Sci. Food Agric.* 77, 543–551. doi: 10.1002/(SICI)1097-0010(199808)77:4<543::AID-JSFA78>3.0.CO;2-I

Häkkinen, S. H., and Törrönen, A. R. (2000). Content of flavonols and selected phenolic acids in strawberries and *Vaccinium* species: influence of cultivar, cultivation site and technique. *Food Res. Int.* 33, 517–524. doi: 10.1016/S0963-9969(00)00086-7

Horneck, D., Hart, J., Stevens, R., Petrie, S., and Altland, J. (2004). *Acidifying Soil for Crop Production West of the Cascade Mountains (Western Oregon and Washington)*. Oregon: Oregon State University.

Iqbal, N., Trivellini, A., Masood, A., Ferrante, A., and Khan, N. (2013). Current understanding on ethylene signaling in plants: the influence of nutrient availability. *Plant Physiol. Biochem.* 73, 128–138. doi: 10.1016/j.plaphy.2013.09.011

Jorquera-Fontena, E., Pastenes, C., Meriño-Gergichevich, C., and Franck, N. (2018). Effect of source/sink ratio on leaf and fruit traits of blueberry fruiting canes in the field. *Sci. Hortic.* 241, 51–56. doi: 10.1016/j.scienta.2018.06.041

Kader, F., Rove, B., Girardin, M., and Metche, M. (1996). Fractionation and identification of the phenolic compounds of highbush blueberries (*Vaccinium corymbosum, L.*). *Food Chem.* 55, 35–40. doi: 10.1016/0308-8146(95)00068-2

Kosegarten, H., Hoffmann, B., and Mengel, K. (2001). The paramount influence of nitrate in increasing apopastic pH of young sunflower leaves to induce Fe deficiency chlorosis, and the re-greening effect brought about by acidic foliar sprays. *J. Plant Nutr. Soil Sci.* 164, 155–163. doi: 10.1002/1522-2624(200104)164:2<155::AID-JPLN155>3.0.CO;2-F

Lee, J., Finn, C. E., and Wrolstad, R. E. (2004). Anthocyanin pigment and total phenolic content of three *Vaccinium* species native to the Pacific Northwest of North America. *Hortic. Sci.* 39, 959–964.

Lohachoompol, V., Mulholland, M., Srzednicki, G., and Craske, J. (2008). Determination of anthocyanins in various cultivars of highbush and rabbiteye blueberries. *Food Chem.* 111, 249–254. doi: 10.1016/j.foodchem.2008.03.067

López-Rayo, S., Di Foggia, M., Bombai, G., Yunta, F., Rodrigues, E., Filippini, G., et al. (2015). Blood-derived compounds can efficiently prevent iron deficiency in the grapevine. *Aust. J. Grape Wine Res.* 21, 135–142. doi: 10.1111/ajgw.12109

Ma, J. F., Ueno, H., Ueno, D., Rombolà, A. D., and Iwashita, T. (2003). Characterization of phytosiderophore secretion under Fe deficiency stress in *Festuca rubra*. *Plant Soil.* 256, 131–137. doi: 10.1023/A:1026285813248

Mazza, G., and Miniati, E. (1993). *Small Fruits. Anthocyanins in Fruits, Vegetables and Grain*. Boca Raton: CRC Press.

Mehouachi, J., Serna, D., Zaragoza, S., Agustí, M., Talon, M., and Primo-Millo, E. (1995). Defoliation increases fruit abscission and reduces carbohydrate levels in developing fruits and woody tissues of Citrus unshiu. *Plant Sci.* 107, 189–197. doi: 10.1016/0168-9452(95)04111-7

Michel, L., Beyá-Marshall, V., Rombolà, A. D., Pastenes, C., and Covarrubias, J. I. (2019). Evaluation of Fe-heme applications or intercropping for preventing iron deficiency in blueberry. *J. Soil Sci. Plant Nutr.* doi: 10.1007/s42729-019-0017-9

Moggia, C., Graell, J., Lara, I., González, G., and Lobos, G. A. (2017). Firmness at harvest impacts postharvest fruit softening and internal browning development in mechanically damaged and non-damaged highbush blueberries (*Vaccinium corymbosum L.*). *Front Plant Sci.* 8:535. doi: 10.3389/fpls.2017.00535

Moyer, R. A., Hummer, K. E., Finn, C. E., Frei, B., and Wrolstad, R. E. (2002). Anthocyanins, phenolics, and antioxidant capacity in diverse small fruits: *Vaccinium*, *Rubus*, and *Ribes*. *J. Agric. Food Chem.* 50, 519–525. doi: 10.1021/jf011062r

Nakajima, J., Tanaka, Y., Yamazaki, M., and Saito, K. (2001). Reaction mechanism from leucoanthocyanidin to anthocyanidin 3-glucoside, a key reaction for coloring in anthocyanin biosynthesis. *J. Biol. Chem.* 276, 25797–25803. doi: 10.1074/jbc.M100744200

Ojeda, H., Andary, C., Kraeva, E., Carbonneau, A., and Deloire, A. (2002). Influence of pre and postveraison water deficit on synthesis and concentration of skin phenolic compounds during berry growth of Vitis vinifera cv. Shiraz. *Am. J. Enol. Vitic.* 53, 261–267.

Peña-Neira, A., Cáceres, A., and Pastenes, C. (2007). Low molecular weight phenolic and anthocyanin composition of grape skins from cv. Syrah (Vitis vinifera L.) in the Maipo valley (Chile): effect of clusters thinning and vineyard yield. *Food Sci. Technol. Int.* 13, 153–158. doi: 10.1177/1082013207077920

Petridis, A., van der Kaay, J., Chrysanthou, E., McCallum, S., Graham, J., and Hancock, R. D. (2018). Photosynthetic limitation as a factor influencing yield in highbush blueberries (*Vaccinium corymbosum*) grown in a northern European environment. *J. Exp. Bot.* 69, 3069–3080. doi: 10.1093/jxb/ery118

Retamales, J., and Hancock, F. (2012). *Blueberries*. Wallingford: CABI.

Roby, G., Harbertson, J. F., Adams, D. A., and Matthews, M. A. (2004). Berry size and vine water deficits as factors in winegrape composition: anthocyanins and tannins. *Aust. J. Grape Wine Res.* 10, 100–107. doi: 10.1111/j.1755-0238.2004.tb00012.x

Rombolà, A., and Tagliavini, M. (2006). "Iron nutrition of fruit tree crops," in *Iron Nutrition in Plants and Rhizospheric Microorganisms*, eds L. Barton and J. Abadía (Dordrecht: Springer), 61–83. doi: 10.1007/1-4020-4743-6_3

Römheld, V. (2000). The chlorosis paradox: Fe inactivation as a secondary event in chlorotic leaves of grapevine. *J. Plant Nutr.* 23, 1629–1643. doi: 10.1080/01904160009382129

Saito, K., Kobayshi, M., Gong, Z. Z., Tanaka, Y., and Yamazaki, M. (1999). Direct evidence for anthocyanidin synthase as a 2-oxoglutarate-dependent oxygenase: molecular cloning and functional expression of cDNA from a red forma of *Perilla frutescens*. *Plant J.* 17, 181–189. doi: 10.1046/j.1365-313X.1999.00365.x

Saito, K., and Yamazaki, M. (2002). Biochemistry and molecular biology of the late-stage of biosynthesis of anthocyanin: lessons from *Perilla frutescens* as a model plant. *New Phytol.* 155, 9–23. doi: 10.1046/j.1469-8137.2002.00440.x

Sapers, G. M., Burguer, A. M., Phillips, J. G., Jones, S. B., and Stone, E. G. (1984). Color and composition of highbush blueberry cultivars. *J. Am. Soc. Hortic. Sci.* 109, 105–111.

Sellapan, S., Akoh, C. C., and Krewer, G. (2002). Phenolic composition and antioxidant capacity of Georgia grown blueberries and blackberries. *J. Agric. Food Chem.* 50, 2432–2438. doi: 10.1021/jf011097r

Smart, R. E., and Robinson, M. D. (1991). *Sunlight into Wine: a Handbook for Winegrape Canopy Management*. Adelaide: Winetitles.

Springob, K., Nakajima, J., Yamazakia, M., and Saito, K. (2003). Recent advances in the biosynthesis and accumulation of anthocyanins. *Nat. Prod. Rep.* 20, 288–303. doi: 10.1039/b109542k

Takagi, S. (1976). Naturally occurring iron-chelating compounds in oat- and rice-root washings. *Soil Sci. Plant Nutr.* 22, 423–433. doi: 10.1080/00380768.1976.10433004

Taruscio, T. G., Barney, D. L., and Exon, J. (2004). Content and profile of flavanoid and phenolic acid compounds in conjunction with the antioxidant capacity for a variety of northwest *Vaccinium* berries. *J. Agric. Food Chem.* 52, 3169–3176. doi: 10.1021/jf0307595

Tomás-Barberán, F. A., and Espín, J. C. (2001). Phenolic compounds and related enzymes as determinants of quality in fruits and vegetables. *J. Sci. Food Agric.* 81, 853–876. doi: 10.1002/jsfa.885

Turnbull, J. J., Nakajima, J., Welford, E. D., Yamazaki, M., Saito, K., and Schofield, C. J. (2004). Mechanistic studies on three 2-oxoglutarate-dependent oxygenases of flavonoid biosynthesis: anthocyanidin synthase, flavonol synthase and flavanone 3-hydroxylase. *J. Biol. Chem.* 279, 1206–1216. doi: 10.1074/jbc.M309228200

Turnbull, J. J., Sobey, W. J., Aplin, R. T., Hassan, A., Firmin, J. L., Schofield, C. J., et al. (2000). Are anthocyanidins the immediate products of anthocyanidin synthase? *Chem. Commun.* 32, 2473–2474. doi: 10.1039/b007594i

Ueno, D., Rombolà, A. D., Iwashita, T., Nomoto, K., and Ma, J. F. (2007). Identification of two novel phytosiderophores secreted by perennial grasses. *New Phytol.* 173, 304–310. doi: 10.1111/j.1469-8137.2007.02056.x

Xiong, H., Kakei, Y., Kobayashi, T., Guo, X., Nakazono, M., Takahashi, H., et al. (2013). Molecular evidence for phytosiderophore-induced improvement of iron nutrition of peanut intercropped with maize in calcareous soil. *Plant Cell Environ.* 36, 1888–1902. doi: 10.1111/pce.12097

Yunta, F., Di Foggia, F., Bellido, V., Morales, M., Tessarin, P., López-Rayo, S., et al. (2013). Blood meal-based compound. Good choice as iron fertilizer to be used in organic farming. *J. Agric. Food Chem.* 61, 3995–4003. doi: 10.1021/jf305563b

Conflict of Interest Statement: The authors declare that the research was conducted in the absence of any commercial or financial relationships that could be construed as a potential conflict of interest.

frontiers in Plant Science

ORIGINAL RESEARCH
published: 02 April 2019
doi: 10.3389/fpls.2019.00324

OPEN ACCESS

Edited by:
Wolfgang Schmidt, Academia Sinica, Taiwan

Reviewed by:
Gang Liang, Xishuangbanna Tropical Botanical Garden (CAS), China
Diqiu Yu, Xishuangbanna Tropical Botanical Garden (CAS), China
Rongrong Guo, Guangxi Academy of Agricultural Science, China

***Correspondence:**
Lola Peñarrubia
lola.penarrubia@uv.es; penarrub@uv.es

†Present address:
Àngela Carrió-Seguí, Instituto de Biología Molecular y Celular de Plantas (CSIC-Universidad Politécnica de Valencia), Valencia, Spain
Omar Ruiz-Rivero, Instituto Valenciano de Investigaciones Agrarias (IVIA), Centro de Protección Vegetal y Biotecnología, Valencia, Spain
Laura Villamayor-Belinchón, Instituto de Medicina Genómica, Universitat de València, Valencia, Spain

Specialty section:
This article was submitted to Plant Nutrition, a section of the journal Frontiers in Plant Science

Received: *18 December 2018*
Accepted: *28 February 2019*
Published: *02 April 2019*

Citation:
Carrió-Seguí À, Ruiz-Rivero O, Villamayor-Belinchón L, Puig S, Perea-García A and Peñarrubia L (2019) The Altered Expression of microRNA408 Influences the Arabidopsis Response to Iron Deficiency. Front. Plant Sci. 10:324. doi: 10.3389/fpls.2019.00324

The Altered Expression of *microRNA408* Influences the Arabidopsis Response to Iron Deficiency

Àngela Carrió-Seguí[1†], Omar Ruiz-Rivero[2†], Laura Villamayor-Belinchón[1†], Sergi Puig[2], Ana Perea-García[2] and Lola Peñarrubia[1*]

[1]Departament de Bioquímica i Biologia Molecular, Estructura de Recerca Interdisciplinar en Biotecnologiaia i Biomedicina (ERI BIOTECMED), Universitat de València, Valencia, Spain, [2]Departamento de Biotecnología, Instituto de Agroquímica y Tecnología de Alimentos (IATA), Consejo Superior de Investigaciones Científicas (CSIC), Valencia, Spain

MicroRNAs contribute to the adaptation of plants to varying environmental conditions by affecting systemic mineral nutrient homeostasis. Copper and iron deficiencies antagonistically control the expression of *Arabidopsis thaliana microRNA408* (*miR408*), which post-transcriptionally regulates laccase-like multicopper oxidase family members *LAC3*, *LAC12*, and *LAC13*. In this work, we used *miR408* T-DNA insertion mutants (408-KO1 and 408-KO2) and a previously characterized transgenic line overexpressing *miR408* (35S:408-14) to explore how *miR408* influences copper- and iron-dependent metabolism. We observed that the altered expression of *miR408* diminished plant performance and the activation of the iron-regulated genes under iron-deficient conditions. Consistently with the low expression of the *miR408*-target laccases, we showed that the vascular bundle lignification of the *35S:408-14* plants diminished. The decrease in the phenoloxidase and ferroxidase activities exhibited by wild-type plants under iron deficiency did not occur in the 408-KO1 plants, probably due to the higher expression of laccases. Finally, we observed that the hydrogen peroxide levels under iron starvation were altered in both the *408-KO1* and *35S:408-14* lines. Taken together, these results suggest that Arabidopsis plants with modified *miR408* levels undergo multiple deregulations under iron-deficient conditions.

Keywords: Arabidopsis, hydrogen peroxide, iron deficiency, lignin, microRNA408

INTRODUCTION

Systemic signaling between roots and shoots is required to maintain mineral nutrient homeostasis in plants cultivated under varying environmental conditions. The nutrient itself, but also other molecules such as microRNAs, transmits and signals nutritional status information for whole plant adaptation (Sunkar et al., 2007; Kehr, 2013; Zhang et al., 2016; Chien et al., 2017). In *Arabidopsis thaliana*, a group of conserved small RNAs, denoted as Cu-miRNAs, are upregulated under copper (Cu) deficiency to target nonessential cuproproteins (Abdel-Ghany and Pilon, 2008). Cu-miRNAs *miR397*, *miR398*, and *miR408* are highly conserved, which supports the

importance of small RNA-mediated regulation in plant Cu homeostasis (Pilon, 2017). Apart from regulating local Cu deficiency responses, Cu-miRNAs also act as phloem-mediated systemic signals during Cu allocation and adaptation to metal deficiency (Buhtz et al., 2010; Kehr, 2013).

Experimental evidence indicates the interplay between Cu and iron (Fe) homeostases during different processes, including the antagonistic control of miRNA expression (Buhtz et al., 2010; Waters et al., 2012). *miR398* regulates the mRNAs of genes *CSD1* and *CSD2*, which encode cytosolic and chloroplastic Cu/Zn superoxide dismutases (Cu/ZnSODs), respectively (Yamasaki et al., 2007). Under Cu deficiency conditions, transcription factor SQUAMOSA-PROMOTER BINDING-LIKE PROTEIN 7 (SPL7) upregulates *miR398* to replace Cu/ZnSOD with the Fe superoxide dismutase (FeSOD) counterpart, probably to economize Cu for essential cuproproteins such as plastocyanin (Yamasaki et al., 2007, 2009). Conversely under Fe deficiency conditions, the downregulation of *miR398* contributes to FeSOD replacement with Cu/ZnSOD (Waters et al., 2012). Another antagonistically regulated miRNA by Cu and Fe deficiencies in phloem sap is *miR408* (Buhtz et al., 2010), but its physiological significance remains uncovered. *miR408* expression in Arabidopsis is abundant and spatially ubiquitous (Sunkar et al., 2006; Zhang and Li, 2013). *miR408* is required for proper vegetative development and is involved in the adaptation to different abiotic stresses (Zhang and Li, 2013; Zhang et al., 2014; Ma et al., 2015). *miR408* regulation under Cu deficiency is mediated by SPL7 through the binding to the GTAC motifs within the *miR408* promoter (Yamasaki et al., 2009; Bernal et al., 2012; Zhang and Li, 2013). Besides, *miR408* is also a target of HY5 (elongated Hypocotyl 5), a transcription factor that mediates responses to light (Zhang et al., 2014). *miR408* overexpression partially compensates the effects in the *spl7* and *hy5* mutants under low Cu conditions by improving the plastocyanin function (Zhang and Li, 2013; Zhang et al., 2014). Based on its role in responses to light and Cu through the HY5-SPL7 gene network, *miR408* has been proposed to act as an integrator of environmental signals in order to properly deliver Cu to plastocyanin for photosynthesis (Zhang et al., 2014). Thus a constitutive *miR408* expression improves photosynthetic performance, increases the Cu content of chloroplasts, and improves biomass and seed yield in diverse plant species (Zhang et al., 2017; Pan et al., 2018; Song et al., 2018). Cupredoxin, plantacyanin, and uclacyanin mRNAs are *miR408* targets (Abdel-Ghany and Pilon, 2008). These are blue cuproproteins that function as electron transfer shuttles between proteins (Nersissian et al., 1998; Choi and Davidson, 2011). *miR408* targets the mRNAs of the *LAC3*, *LAC12*, and *LAC13* genes encoding laccase-like multicopper oxidases (LMCOs) (LC, EC 1.10.3.2) (Abdel-Ghany and Pilon, 2008). LMCOs are extracellular glycoproteins that catalyze the oxidation of many substrates *in vitro* with simultaneous oxygen reduction (McCaig et al., 2005; Turlapati et al., 2011). Based on the wide range of substrates, it has been proposed that higher plant LMCOs could play more varied functions than initially expected (Reiss et al., 2013). Some LMCO functions could be involved in processes that affect Fe homeostasis, such as lignification, ferroxidase activity, and oxidative stress, which might account for their regulation under Fe deficiency through *miR408*.

Some LMCOs are involved in the oxidative polymerization of lignins from monolignols in secondary cell-wall formation (Berthet et al., 2011; Choi and Davidson, 2011; Zhao et al., 2013; Wang et al., 2014), and their activities are affected by *miRNA* expression (Lu et al., 2013). Cell-wall modifications through cross-linking have been suggested to affect metal chelation and mobilization (Le Gall et al., 2015; Curie and Mari, 2017). Among the potential interactions between Cu and Fe homeostases, we find metal competition for ligands during long-distance traffic under scarcity conditions (Alvarez-Fernández et al., 2014). In addition to laccases, the peroxidases that use hydrogen peroxide (H_2O_2) as a substrate also contribute to lignin biosynthesis *in vivo,* and H_2O_2 itself plays a role in cell-wall cross-linking and loosening (O'Brien et al., 2012; Kärkönen and Kuchitsu, 2015). H_2O_2 scavenging in the culture medium significantly decreases the amount of extracellular lignin formed in Norway spruce, and the inhibition of superoxide (O_2^-) synthesis, or its dismutation to H_2O_2 by superoxide dismutases reduces lignin content (Kärkönen et al., 2002; Karlsson et al., 2005). Rice OsLAC3 has been shown to induce H_2O_2 accumulation, which affects the seed setting rate and mitochondria integrity in vascular tissues and root tips (Yu et al., 2017). Given the striking similarity between OsLAC3 and L-ascorbate oxidases, a role in oxidizing ascorbate, which drives to restrain H_2O_2 removal, has been proposed to explain the observed phenotypes. Reactive oxygen species (ROS) could also affect Cu-Fe interactions under metal deficiency conditions (Ravet and Pilon, 2013). The delicate balance between ROS, particularly H_2O_2, production and scavenging during metal stress is important for diverse signaling pathways, and there is evidence for a correlation between H_2O_2 and plant metal tolerance (Cuypers et al., 2016).

The role proposed for certain LMCOs as putative ferroxidases would be another *miR480*-controlled process that could participate in the interplay between Cu and Fe homeostases. LMCOs participate in Fe traffic in organisms other than plants (Hoopes and Dean, 2004). Some LMCO members could be involved in redox cycles, which are necessary for the mobilization and trafficking of Fe as they contain the residues expected for this purpose (Quintanar et al., 2007; Kosman, 2010a; Turlapati et al., 2011). Among other factors, the Fe redox state depends on the ratio between ferroxidase and ferrireductase activities (Kosman, 2010b, 2018). However, experimental evidence for LMCOs being involved in metal oxidation, by acting as ferroxidases, in plants is scarce (Müller et al., 2015). All plants, except grasses, acquire Fe after the reduction of Fe^{3+} chelates by a plasma membrane ferric chelate reductase which, in *Arabidopsis,* is encoded by *FERRIC REDUCTASE 2* (*FRO2*) (Robinson et al., 1999). Upon reduction, Fe^{2+} is incorporated into the cell through a transporter encoded by IRON REGULATED TRANSPORTER 1 (IRT1) (Eide et al., 1996; Vert et al., 2002). IRT1 substrate availability

depends on free external Fe (not bound to inorganic and organic complexes) and the Fe^{2+}/Fe^{3+}ratio, according to external redox status conditions and the enzymatic activity of ferrireductases. Helix-loop-helix type transcription factor FIT (bHLH29) is involved in Fe acquisition and remobilization (Colangelo and Guerinot, 2004). Other bHLH subgroup Ib factors (bHLH38, bHLH39, bHLH100, and bHLH101) could act in concert with FIT (Yuan et al., 2008; Wang et al., 2013). In the present work, we explore the effect of Fe deficiency on seedlings with altered *miR408* levels by analyzing *LMCO* mRNA levels, enzymatic activities, and Fe deficiency responses.

MATERIALS AND METHODS

Plant Growth Conditions and Treatments

Arabidopsis thaliana ecotype *Columbia* (Col-0) was used as the control wild type (WT). The three *miR408* altered expression transgenic lines used herein, the *miR408*-overexpressing line 14 driven by the cauliflower mosaic virus 35S promoter (35S:408-14) and the two T-DNA insertion lines SALK_038860 (408-KO1) and SALK_121013.28.25.n (408-KO2), have been previously described (Zhang and Li, 2013; Ma et al., 2015). Seeds were surface-sterilized by sequential washes in 70% ethanol (5 min), bleach (5 min), and water (2 × 2 min) and were resuspended in 0.1% agar (w/v) and grown on plates containing 1/2 Murashige and Skoog (MS) medium supplemented with sucrose 1% (w/v). The 1/2 MS medium containing 1 μM $CuSO_4$ and 50 μM Fe citrate was used for the metal sufficiency control conditions (50 μM Fe). Metal deficiency was obtained by home-made 1/2 MS with no added $CuSO_4$ (0 μM Cu) or 5 μM Fe citrate for slight Fe deficiency (5 μM Fe) and 0 μM Fe citrate for severe Fe deficiency (0 μM Fe). For the assays of phenoloxidase and ferroxidase activities, 100 μM ferrozine, a Fe chelator, was included to provide severe deficiency growing conditions (-Fe). For severe Cu deficiency conditions, 100 μM of Cu chelator bathocuproine disulfonate (BCS) was added to the growth medium (-Cu). Intermediate photoperiodic conditions (12 h light, 20–23°C/12 h darkness, 16°C) were applied. Root length was measured by the Image J 1.42 q software.[1]

Chlorophyll and Hydrogen Peroxide Contents and Lignin Staining

The chlorophyll-a content of the Arabidopsis seedlings was determined by the trichlorometric method (Parsons and Strickland, 1963) and estimated by the equation of Lichtenthaler (1987). Hydrogen peroxide (H_2O_2) was detected by the brown polymerization product, formed by a reaction with diaminobenzidine tetrahydrochloride (DAB) (Jambunathan, 2010).

Lignin staining was done using 0.1% phloroglucinol saturated with HCl (Wiesner stain) (Liljegren, 2010). Between 5 and 7 seedlings of each genotype and condition were placed inside an Eppendorf tube with 700 μl of the reagent mixture to be incubated for 5 min. Afterward, seedlings were washed with sterile water and photographed.

Metal Content Determination

The fresh Arabidopsis material was washed once with 20 μM EDTA and three times with MilliQ H_2O before being dried at 65°C for 2 days and digested with 65% (v/v) HNO_3 and H_2O_2 30% (v/v) at 140°C. The digested samples were then diluted with Millipore H_2O (*Purelab Ultra*). The Cu and Fe contents were determined by mass spectrometry with inductively coupled plasma (ICP-MS Agilent technologies) at the SCSIE (Universitat de València) using the manufacturer's standard solutions for the calibration curves.

Gene Expression Analysis by Real-Time Quantitative PCR

The total RNA isolation, reverse transcription, and RT-qPCR analyses were performed as described in Carrió-Seguí et al. (2016). The forward (F) and reverse (R) sequences for the specific primers are shown in **Table SI**. To transform the fluorescent intensity measurements into relative mRNA levels, a two-fold dilution series of a mixture containing an equal amount of each cDNA sample was used, and standard curves were constructed for all the studied genes. The *UBIQUITIN10* reference gene was used for data normalization. Each sample was analyzed in biological replicates, and the mean ratios ± SD were calculated.

Phenoloxidase and Ferroxidase Activities

Total proteins were extracted from the 7-day-old seedlings frozen in liquid nitrogen in the extraction buffer [400 mM NaCl, 2 mM $MgCl_2$, 0.2% (p/v) sucrose, 20 mM Tris, PMSF 1 mM, pH 8.0, with HCl] at a ratio of 1:2 (p/v). Samples were centrifuged at 12,000 rpm for 10 min (4°C), and the supernatant was used as a crude extract. Total proteins were quantified (Bradford, 1976), and 500 μg were loaded with the nondenaturing loading buffer in the 12% SDS gels.

The phenoloxidase activity in gels was detected by using 3 mM p-phenylenediamine as the substrate (Lang et al., 2012). For the ferroxidase assay, the protocol of Hoopes and Dean (2004) was slightly modified as follows: gel was incubated for 1 h in 100 mM sodium acetate buffer, pH 5, with 5% (v/v) glycerol and 10 mM $CuSO_4$, followed by a 1 h incubation period in 100 mM sodium acetate buffer, pH 5, with 0.4 mM $FeSO_4$. After washing twice with distilled water and kept in the darkness at a relative humidity of 30% overnight, gel was revealed with 15 mM ferrozine. In the phenoloxidase assay, the bands around 65 kDa were quantified three times with the Image J 1.42 q software.[1]

Statistical Analyses

The statistical differences in gene expression analyses were identified by the pair-wise fixed reallocation randomization test ($p < 0.05$) (Pfaffl et al., 2002). One-way ANOVAs were performed for the other parameters. The significant differences between means were established after the Duncan test using

[1]https://imagej.nih.gov/ij/

the Infostat Statistics software, version 2018.[2] Data are provided as the mean values ± SD of the different biological samples indicated in the figure legends. Asterisks indicate statistical differences ($p < 0.05$) in relation to the WT value.

RESULTS

Phenotypic Characterization of Plants With an Altered *miR408* Expression Under Iron Deficiency

The potential role of LMCOs in Fe homeostasis prompted us to conduct a physiological study of those plants with altered *miR408* expression grown under Fe deficiency. To this end, the wild-type (WT) plants, a T-DNA mutant line (408-KO1), and a transgenic line overexpressing *miR408* (35S:408-14) (Ma et al., 2015) were grown under Fe sufficiency (50 μM Fe) and under mild (5 μM Fe) and severe (0 μM Fe) Fe deficiency (**Figures 1** and **S1**). The root length measurements indicated that only the 408-KO1 seedlings were slightly affected under the severe Fe deficiency conditions (**Figure S1A**). Regarding the chlorosis symptoms observed when Fe was scarce (**Figure 1A**; 0 μM Fe), the chlorophyll-a content of both the plants with altered *miR408* levels was significantly lower than that of the WT under severe Fe deficiency (**Figure 1B**; 0 μM Fe). However under Fe sufficiency and mild Fe deficiency, the chlorophyll-a content of the three lines was roughly similar (**Figure 1B**). To ascertain whether the altered *miR408* expression could influence metal content, Fe and Cu levels were measured in the aerial parts of the WT, 408-KO1, and 35S:408-14 lines (**Figures 1C** and **S1B**). As previously reported (Waters et al., 2012), the Cu levels in the WT seedlings were slightly higher under Fe deficiency

[2]http://www.infostat.com.ar

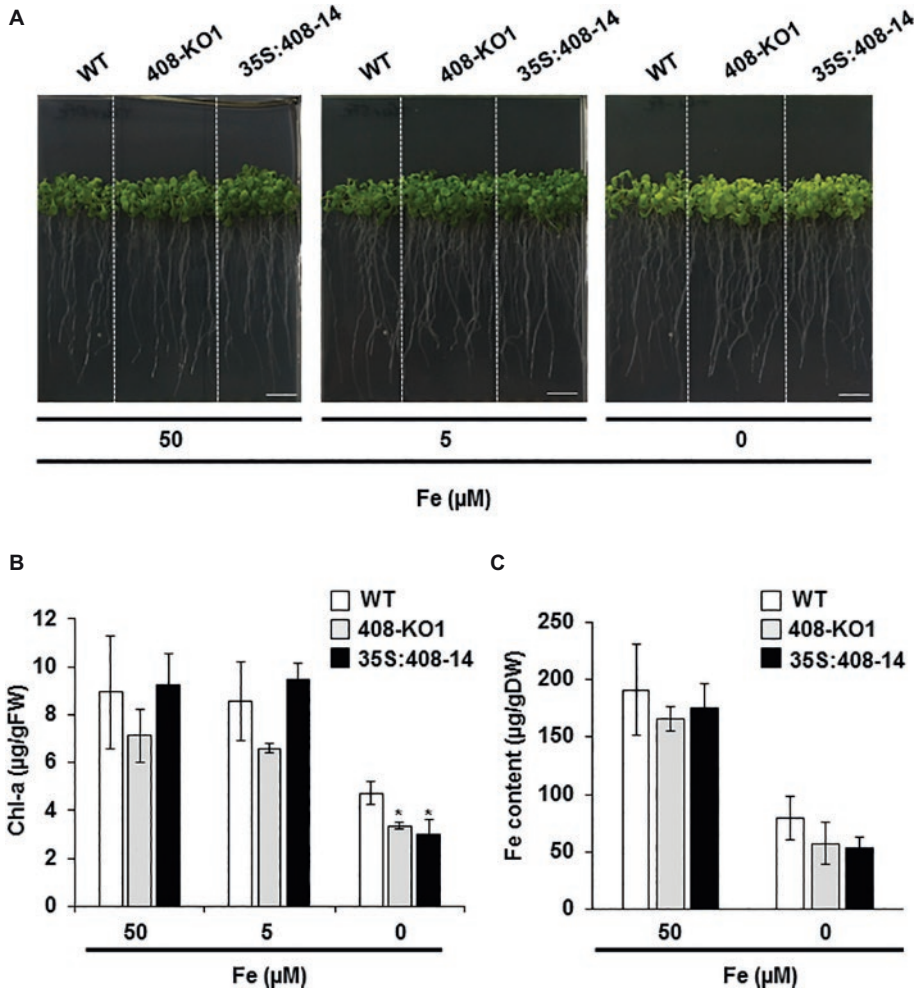

FIGURE 1 | Phenotypic characterization under iron deficiency of the seedlings with altered *miR408* expression. **(A)** Photographs of representative 15-day-old seedlings grown on 1/2 MS plates containing 50, 5, and 0 μM Fe citrate. **(B)** Chlorophyll-a content and **(C)** iron content in aerial tissues measured from the wild-type (WT), 408-KO1, and 35S:408-14 seedlings grown under the same conditions as indicated in panel A. Bars represent the means ± standard deviation of three biological replicates of $n \geq 15$ plants for each genotype. Asterisks denote statistical differences ($p < 0.05$) compared to the WT value according to the Duncan test.

compared to Fe sufficiency. Cu content did not change in the plants with altered *miR408* expression under Fe deprivation compared to the control under these experimental conditions (**Figure S1B**). The Fe content in the 408-KO1 and 35S:408-14 lines remained essentially identical to the WT plants (**Figure 1C**). These results indicate that proper *miR408* expression is necessary for Arabidopsis plants to adequately perform under iron-deficient conditions.

Lignification Under Iron Deficiency Is Affected in the Plants With Altered *miR408* Expression

As certain LMCOs have been involved in the lignification process (Liang et al., 2006; Bonawitz and Chapple, 2010), we wondered whether there was a correlation between the degree of *LMCO* gene expression (*LAC3*, *LAC12*, and *LAC13*) and lignification. To this end, the WT, 408-KO1, and 35S:408-14 seedlings were grown under the control, slight, and severe Fe deficiency conditions (**Figures 2** and **S2**). As previously reported (Rodríguez-Celma et al., 2016), we observed that the lignin staining of the WT vascular cylinder increased under the low Fe conditions (**Figures 2** and **S2**). The lignification of the vascular bundles in the WT seedlings was more evident in the aerial part (**Figure S2**). The general reduction in lignin content observed in both the seedlings with altered *miR408* expressions under the Fe deficiency conditions was noteworthy (**Figures 2** and **S2**).

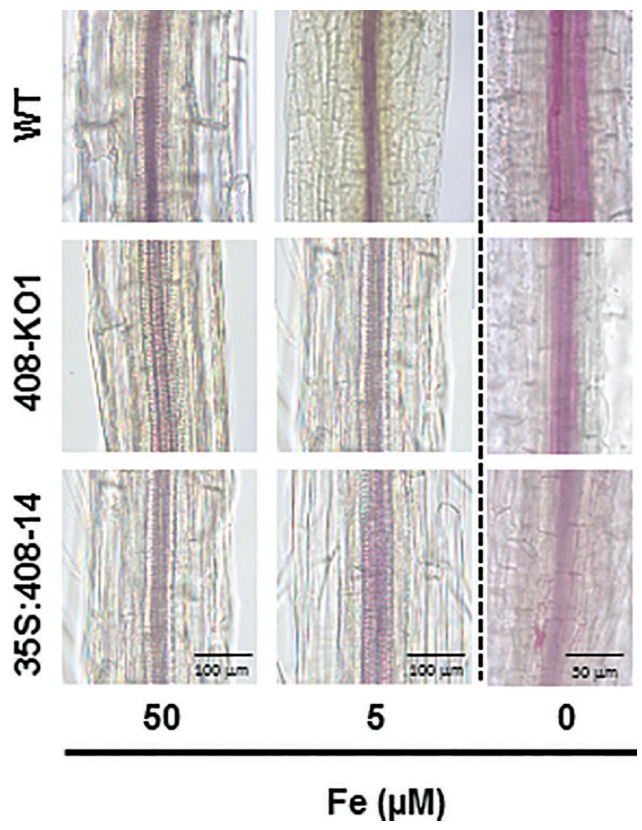

FIGURE 2 | Lignin staining under iron deficiency conditions of the altered *miR408* expression seedlings. Photographs of the representative lignin stained stems from the 20-day-old seedlings from the wild-type (WT), 408-KO1, and 35S:408-14 lines grown on 1/2 MS plates containing 50, 5, and 0 µM Fe citrate, pH 5.6. Stems ($n \geq 10$ for each genotype) were stained with phloroglucinol saturated with HCl and photographed under a microscope. The length of the bars indicates 100 µm in 50 and 5 µM Fe citrate conditions and 50 µm in 0 µM Fe citrate.

To study the *miR408* expression effects, we first corroborated that the *miR408* levels were downregulated in the 408-KO1 and were overexpressed in the 35S:408-14 lines under our experimental conditions (**Figure S3A**). Previous studies had shown that *miR408* is oppositely regulated by Fe and Cu deficiencies in phloem sap (Buhtz et al., 2010). In line with these data, *miR408* expression increased in the WT seedlings under Cu deficiency, but decreased under the Fe deficiency conditions (**Figure S3B**). The expression of *miR408* target transcript *LAC3* was checked in the WT and *miR408* mutant seedlings, with a second 408-KO line (408-KO2), under the control (1 µM Cu) and Cu-deficient conditions (0 µM Cu) (**Figure S3C**). As expected, the *LAC3* mRNA levels lowered in response to Cu limitation in the WT seedlings. Moreover, its levels lowered in the *miR408* overexpressing plants, but increased in the 408-KO mutants (**Figure S3C**), which indicates that the *LAC3* target expression responded to both the *miR408* levels and Cu deficiency in accordance with *miR408* being upregulated. To address the target responses to Fe deficiency, the WT and mutant *miR408* seedlings were grown under the control (50 µM Fe) and Fe deficiency (0 µM Fe) conditions, and the mRNA expression of *miR408* targets *LAC3*, *LAC12*, *LAC13*, and plantacyanin (*ARPN*), encoding a cyanin (Yamasaki et al., 2007), was checked by RT-qPCR (**Figure 3**). In agreement with *miR408* being downregulated, all the studied *miR408* targets were upregulated by Fe deficiency in the WT plants (**Figure 3**). Moreover, the *miR408* targets were upregulated in the 408-KO mutants and downregulated in the 35S:408-14 line under the metal sufficiency conditions, and the same results were also observed for Fe starvation (**Figure 3**). These results indicate that the *miR408* mRNA targets under study are properly regulated by Fe limitation and respond accordingly to the altered *miR408* expression under both the control and metal deficiency conditions (**Figures 3** and **S3C**).

We analyzed whether the expression of the specific molecular markers involved in the lignin biosynthetic process (*F6'H1´*, β-*GLU23*, *CCR1*, and *LAC17;* Bonawitz and Chapple, 2010) were affected in the plants with the altered *miR408* expression grown under Fe deficiency (**Figure 4**). Under the Fe-limited conditions, the expression of the studied lignification-related genes significantly reduced in the 408-KO lines compared to the WT plants (**Figure 4**). However in the 35S:408-14 line, the mRNA levels of the lignification-related genes increased under low Fe to reach the same levels observed in the WT, except for *CCR1*, which was not induced (**Figure 4**). As these genes are not direct *miR408* targets, their downregulation in the 408-KO mutants is probably due to an indirect effect. With the 35S:408-14 line, the mRNA levels of the lignification-related genes increased when Fe was low, except for *CCR1,* which encodes a cinnamoyl-CoA reductase (**Figure 4**). These

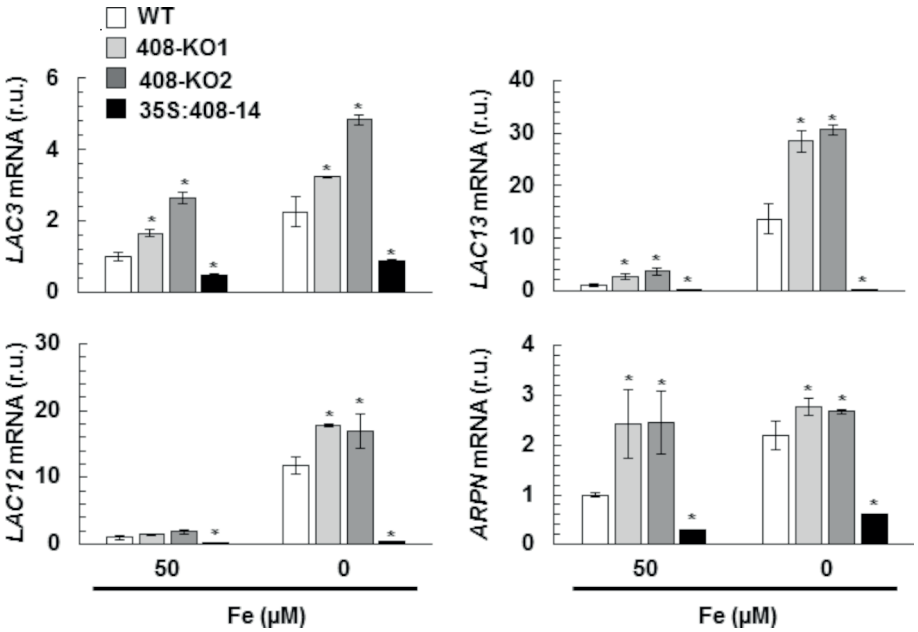

FIGURE 3 | Gene expression of the *miR408* targets under iron deficiency. *LAC3, LAC12, LAC13,* and *ARPN* relative expression. The 15-day-old wild-type (WT), 408-KO1, 408-KO2, and 35S:408-14 seedlings grown in 1/2 MS medium containing 50 and 0 μM Fe citrate. Total RNA was extracted and analyzed by RT-qPCR with specific oligonucleotides for *LAC3, LAC12, LAC13*, and *ARPN.* The *UBIQUITIN10* gene was used for data normalization, and the expression is shown in relative units (r.u.). Values correspond to the arithmetic means ($2^{-\Delta\Delta Ct}$) ± standard deviation of at least three biological replicates ($n \geq 25$ plants). Asterisks denote significant differences for the same group of samples compared to the WT line ($p < 0.05$) based on the pair-wise fixed reallocation randomization test.

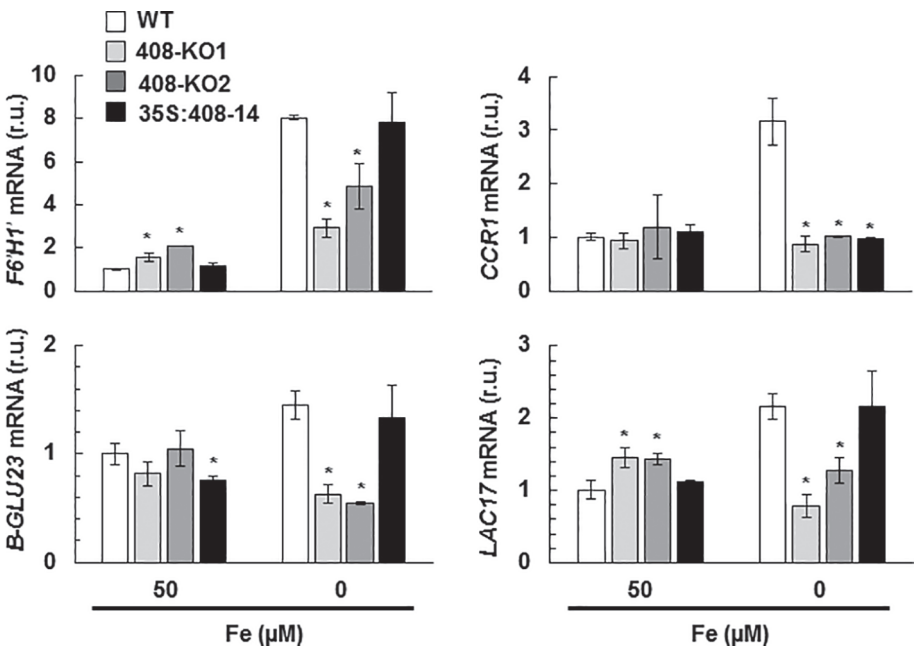

FIGURE 4 | Gene expression of the lignification-related genes under iron deficiency in the seedlings with altered *miR408* expression. *F6'H1', B-GLU23, LAC17*, and *CCR1* relative expression. The 15-day-old wild-type (WT), 408-KO1, 408-KO2, and 35S:408-14 seedlings grown in 1/2 MS medium containing 50 and 0 μM Fe citrate. Total RNA was extracted and analyzed by RT-qPCR with specific oligonucleotides for *F6'H1', B-GLU23, LAC17*, and *CCR1.* The *UBIQUITIN10* gene was used for data normalization, and the expression is shown in relative units (r.u.). Values correspond to the arithmetic means ($2^{-\Delta\Delta Ct}$) ± standard deviation of at least three biological replicates ($n \geq 3$). Asterisks depict significant differences for the same group of samples *versus* the WT line ($p < 0.05$) based on the pair-wise fixed reallocation randomization test.

results show that *miR408* influences the expression of the genes implicated in lignin biosynthesis.

Iron Deficiency Responses Are Affected in Altered *miR408* Expression Plants

To determine how the plants with the altered *miR408* expression perceived Fe status, the expression of a group of molecular Fe deficiency markers was analyzed under the Fe sufficiency and deficiency conditions. The genes involved in Fe remobilization and incorporation, such as *FRO2*, *FRO3*, and *IRT1*, and Fe-regulated Cu transporter *COPT2* (Perea-García et al., 2013) were induced under Fe limitation in the WT plants (**Figure 5**). Unexpectedly, the expression of these Fe deficiency markers lowered in the plants with the altered *miR408* expression grown under Fe scarcity (**Figure 5**). In order to check the regulation of the Fe deficiency responses, the expression of transcriptional activators *bHLH39* and *FIT* (Colangelo and Guerinot, 2004; Yuan et al., 2008; Wang et al., 2013) was also analyzed (**Figure 5**). A differential response was observed in the 408-KO and 35S-408-14 lines. Whereas *bHLH39* expression decreased by three times in the 408-KO lines, an 8-fold reduction in *FIT* expression took place in the 35S-408-14 line compared to the WT under Fe deprivation (**Figure 5**).

Characterization of Phenoloxidase and Ferroxidase Activities in Plants With Altered *miR408* Expression

The wide range of substrates that LMCOs can oxidize suggests that they could be involved in many other processes apart from lignification (Reiss et al., 2013). Therefore, we decided to determine phenoloxidase activity in gel in the WT and *miR408* mutant seedlings grown under the control and Fe deficiency conditions (Lang et al., 2012; **Figures 6A** and **S4**). Remarkably, the phenoloxidase activity of the WT plants decreased under Fe

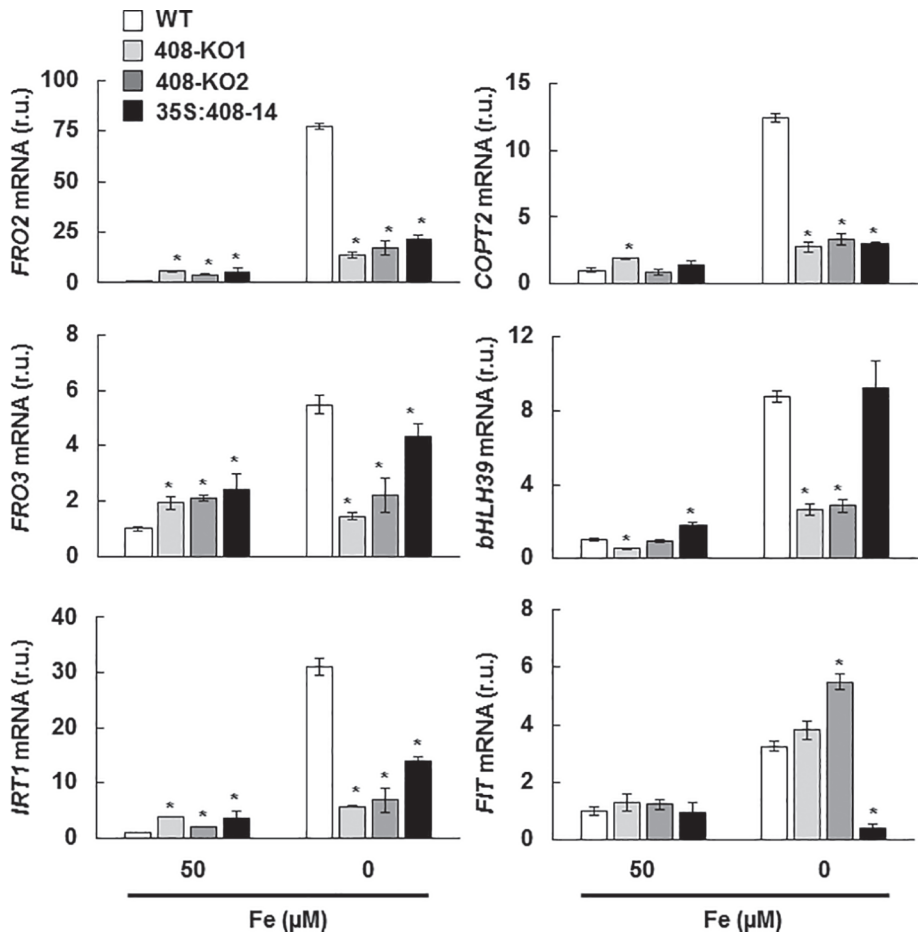

FIGURE 5 | Expression of the metal homeostasis-related genes under iron deficiency in the seedlings with altered *miR408* expression. *FRO2, FRO3, IRT1, COPT2, bHLH39*, and *FIT1* relative expression. The 15-day-old wild-type (WT), 408-KO1, 408-KO2, and 35S:408-14 seedlings grown in 1/2 MS medium containing 50 and 0 μM Fe citrate. Total RNA was extracted and analyzed by RT-qPCR with specific oligonucleotides for *FRO2, FRO3, IRT1, COPT2, bHLH39*, and *FIT1*. The *UBIQUITIN10* gene was used for data normalization and the expression is shown in relative units (r.u.). Values correspond to the arithmetic means ($2^{-\Delta\Delta Ct}$) ± standard deviation of at least three biological replicates ($n \geq 25$). Asterisks indicate significant differences for the same group of samples *versus* the WT line ($p < 0.05$) based on the pair-wise fixed reallocation randomization test.

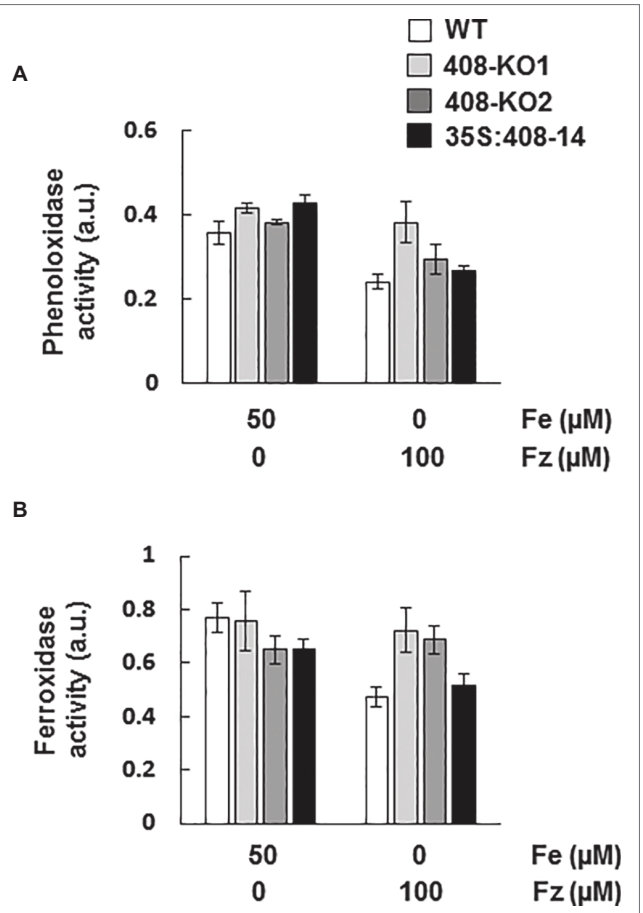

FIGURE 6 | Phenoloxidase and ferroxidase activities in the seedlings with altered *miR408* expression. **(A)** Phenoloxidase and **(B)** ferroxidase activities in the gels from the 7-day-old wild-type (WT), 408-KO1, 408-KO2, and 35S:408-14 seedlings grown on 1/2 MS plates containing 50 μM Fe citrate and 100 mM ferrozine. About 100 μg of total protein extraction were used for each sample. The relative intensities of the bands corresponding to the LMCO expected MW are shown as arbitrary units (a.u.). Values are the means ± SD of three technical replicates. A representative quantification of at least three independent experiments is shown.

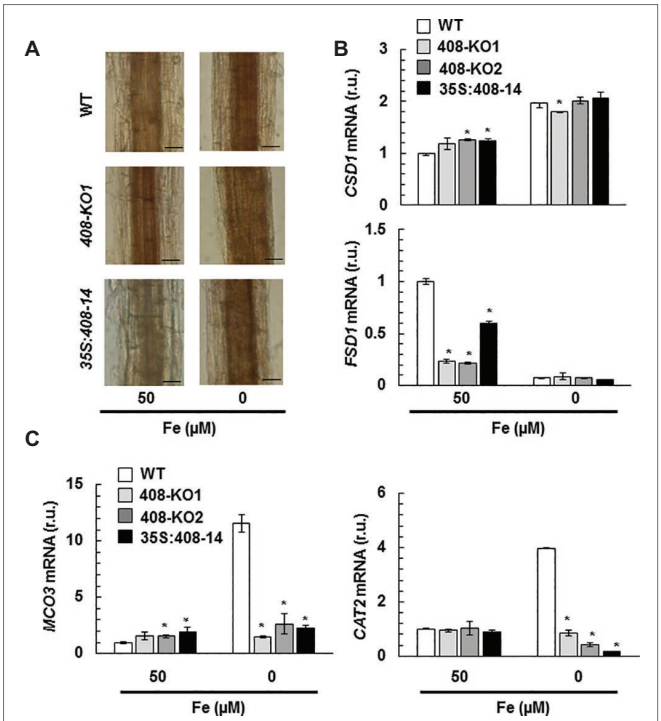

FIGURE 7 | Hydrogen peroxide detection in the plants with altered *miR408* expression. **(A)** Hydrogen peroxide detected in the roots of the 15-day-old wild-type (WT), 408-KO1, and 35S:408-14 seedlings grown in 50 and 5 μM Fe citrate media. Photographs of the representative roots, where a brown polymerization product was formed by the reaction of hydrogen peroxide with diaminobenzidine tetrahydrochloride. n = 15 plants were stained for each genotype and condition. The length of the bars indicates 100 μm in 50 and 5 μM Fe citrate. **(B)** *FSD1* and *CSD1* **(C)** *CAT2* and *MCO3* relative expression. The 7-day-old wild-type (WT), 408-KO1, 408-KO2, and 35S:408-14 seedlings grown in 1/2 MS medium containing 50 and 0 μM Fe citrate. Total RNA was extracted and analyzed by RT-qPCR with specific oligonucleotides for *FSD1*, *CSD1*, *CAT2*, and *MCO3.* The *UBIQUITIN10* gene was used for data normalization, and the expression is shown in relative units (r.u.). Values correspond to the arithmetic means ($2^{-\Delta\Delta Ct}$) ± standard deviation of at least three biological replicates ($n \geq 25$ plants). Asterisks indicate significant differences for the same group of samples *versus* the WT line ($p < 0.05$) based on the pair-wise fixed reallocation randomization test.

deficiency (**Figure 6A**), despite us having shown that the *miR408*-dependent *LMCO* expression increased under these growth conditions (**Figure 3**). Phenoloxidase activity was slightly higher in mutants 408-KO than in the WT under Fe starvation (**Figure 6A**).

All laccases exhibit the characteristic conserved Cu-binding domains of LMCOs. Apart from the different Cu-binding domains formed by histidine residues, *Saccharomyces cerevisiae* ferroxidase Fet3 (Askwith et al., 1994) possesses an essential aspartic residue (D409) within its ferroxidase domain (Quintanar et al., 2007). The alignment of the *A. thaliana* laccase sequences and yeast Fet3 showed that LAC3, LAC4, LAC5, LAC10, LAC11, LAC12, LAC13, and LAC17 were LMCOs which conserved the essential ferroxidase aspartic residue (**Figure S5**). Among the different Cu-miRNAs with *LMCO* mRNAs as targets (Abdel-Ghany and Pilon, 2008), *miR408* is the only Cu-microRNA to target LMCO mRNAs, which encode proteins containing an aspartic residue potentially involved in Fe-binding. Thus, we hypothesized that *miR408* expression could affect ferroxidase activity. To study this possibility, ferroxidase activity was checked in gels (Hoopes and Dean, 2004) in the same samples used to measure phenoloxidase activity (**Figures 6B** and **S4**). Similar to phenoloxidase, ferroxidase activity reduced under Fe deficiency in the WT plants (**Figure 6B**), despite the increase in the *miR408*-dependent *LMCO* mRNAs (**Figure 3**). It was noteworthy that ferroxidase activity did not decrease in mutants 408-KO (**Figure 6B**), probably due to the expression of laccases being higher than in the WT plants (**Figure 3**).

Hydrogen Peroxide Levels in Plants With Altered *miR408* Expression

Previous data have shown that hydrogen peroxide (H_2O_2) increases in the vascular bundles of WT plants under Fe

deficiency (Alvarez-Fernández et al., 2014). Thus, we decided to study H_2O_2 levels by diaminobenzidine tetrahydrochloride (DAB) staining in the 15-day-old seedling roots from the WT and *miR408* mutants grown under the control and slight Fe deficiency conditions (**Figure 7A**). Under the control conditions, high H_2O_2 levels were observed in the vascular bundles of mutant 408-KO1, whereas the 35S:408-14 line displayed low levels *versus* the WT plants. Moreover, when Fe was scarce, the H_2O_2 levels increased in all the genotypes and were higher in mutant 408-KO1 and lower in the 35S:408-14 line compared to the WT line (**Figure 7A**). Therefore, we checked whether the expression of a set of oxidative stress genes involved in H_2O_2 metabolism was affected under Fe deprivation in the plants with altered *miR408* expression (**Figures 7B,C**). We tested the expression of genes related either to H_2O_2 synthesis, such as *SODs* (*CSD1, FSD1*), or elimination, such as ascorbate oxidase *MCO3* and catalase *CAT2* (Cuypers et al., 2016). We observed that *FSD1* expression significantly reduced in mutants *miR408* compared to the WT plants under Fe sufficiency (**Figure 7B**). However under Fe deficiency, the most relevant result was the low expression of *MCO3* and *CAT2* compared to the WT in the plants with altered *miR408* expression (**Figure 7C**). These data reveal that *miR408* expression determines H_2O_2 levels and the expression of the genes related to oxidative stress.

DISCUSSION

Previous work has shown the antagonistic effects of Cu and Fe deficiencies on Arabidopsis *miR408* expression (Buhtz et al., 2010). In response to Cu starvation, SPL7 binds to Cu-responsive elements within the *miR408* promoter and activates its expression (Yamasaki et al., 2009). As all *miR408* targets are mRNAs that encode apoplastic cuproproteins, a role in Cu redistribution has been postulated for *miR408* under Cu depletion (Abdel-Ghany and Pilon, 2008; Zhang et al., 2014). The mRNAs from the internal cuproproteins showed enhanced expression when *miR408* was overexpressed and its targets putatively reduced (Ma et al., 2015). From this viewpoint, an apparently pernicious effect could take place under Fe deficiency because *miR408* downregulation would increase the extracellular Cu quota *versus* the internal Cu, which could harm internal metalloprotein substitutions such as the FeSOD replacement for its Cu counterpart (Abdel-Ghany and Pilon, 2008). We ruled out a putative role of *miR408* expression in metalloprotein substitution because no significant changes in *SODs* expression were observed under Fe deficiency in the plants with altered *miR408* expression (**Figure 7B**).

The signaling pathway that drives to *miR408* Fe deficiency repression and its physiological relevance remain unknown. *miR408* is both induced and repressed when faced with different abiotic stresses (Ma et al., 2015). Indeed signaling during Cu starvation would display similarities to other stresses that induce *miR408* expression, such as cold, salinity, and oxidative stress, whereas Fe deficiency signaling could converge with the stress signals that inhibit *miR408* expression, such as drought and osmotic stress (Ma et al., 2015). Based on both the physiological and molecular effects that plants with altered *miR408* expression showed under Fe limitation, the results offered herein could explain the antagonistic Fe and Cu regulation on *miR408* expression (**Figure 8**). Both the 35S:408-14 overexpressing line and mutants 408-KO exhibited reduced chlorophyll-a content under low Fe conditions (**Figure 1**). According to previous results (Ma et al., 2015), 35S:408-14 plants are resistant to the type of stresses that induce *miR408* expression and are sensitive to the stresses that inhibit its expression, among which we can now include Fe deficiency. However, whereas Fe sensitivity was observed in the 35S:408-14 seedlings, adult plants produced more seeds than the WT plants under Fe starvation (results not shown). Different possibilities were explored to understand these phenotypes. First, the role of the *miR408 LMCO* mRNA targets in the lignification process, which could affect metal translocation to the aerial part and shoot-to-root Fe deficiency signaling (Le Gall et al., 2015; Curie and Mari, 2017). Second, the potential function of LMCOs as ferroxidases and their influence on both Fe incorporation and mobilization. Finally, a putative role of LMCOs in oxidative stress and, more specifically, in H_2O_2 generation could affect metal transport.

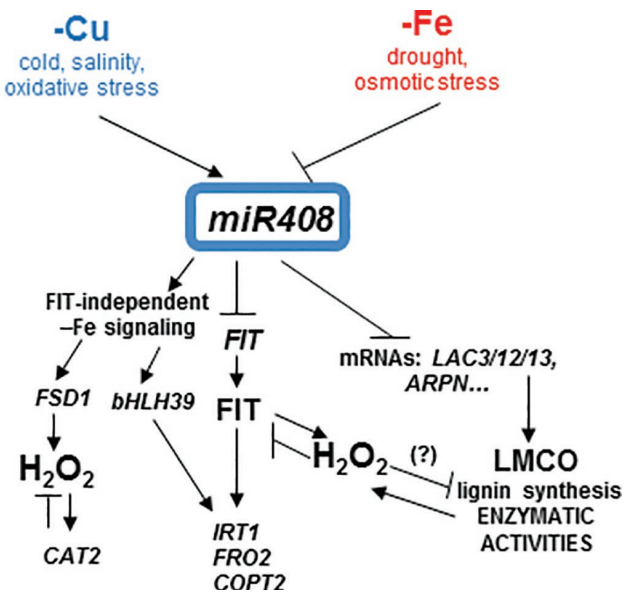

FIGURE 8 | Model for the copper and iron homeostasis interplays through *miR408* regulation. Schematic representation of the main *miR408* effects on the Fe-deficiency responses observed in the present work. *miR408* directly affects the expression of the target genes, such as the mRNA from LMCOs *LAC3*, *LAC12*, *LAC13* (*LAC3/12/13*), and cyanins (i.e., *ARPN*) and their putative promiscuous LMCO role in lignin synthesis and enzymatic activities, such as phenoloxidase, ferroxidase, and ascorbate oxidase. In addition to other abiotic stresses, Cu and Fe deficiencies had the opposite effects on *miR408* regulation and their subsequent enzymatic activities. The FIT-independent and FIT-dependent signaling pathways under Fe deficiency were induced or repressed by *miR408*, respectively. Fe deficiency induced oxidative stress and hydrogen peroxide (H_2O_2) could play a role in the observed *miR408* effects. H_2O_2 could affect LMCO enzymatic activities, and at least part of the *miR408* function could be able to counteract this effect under Fe deficiency.

Regarding the lignification process, some laccases, such as LAC4, LAC15, and LAC17, are directly involved in lignin synthesis in Arabidopsis (Liang et al., 2006; Berthet et al., 2011). Lignification is affected by *miR857* and *miR397* in both Arabidopsis and trees, such as Populus, where miRNAs act as negative regulators of laccase expression and are involved in the control of the secondary growth of vascular tissues (Lu et al., 2013; Wang et al., 2014; Zhao et al., 2015). Long-distance regulatory circuits have been identified for Fe deficiency signaling. Fe homeostasis is controlled at local and systemic levels by a wide range of signaling molecules, including ions, hormones, and metabolites (Giehl et al., 2009). Fe deficiency promotes increased lignification (Alvarez-Fernández et al., 2014). If laccases LAC3, LAC12, and LAC13 were involved in lignification, the repression of *miR408* by Fe deprivation (**Figure S3B**), and the subsequent increase in *LAC3*, *LAC12* and *LAC13* expression (**Figure 3**), if redounded in increased protein activity, would lead to enhanced lignification under Fe deficiency, as was indeed observed (**Figure 2**). By applying the same reasoning, lignification should be higher in 408-KO mutants and lower in the 35S:408-14 line as *LAC3*, *LAC12*, and *LAC13* expression was up- and downregulated, respectively (**Figure 3**). Instead, lignification under Fe deficiency was impaired in both 408-KO mutants and the 35S:408-14 line (**Figure 2**). However, we cannot rule out a direct role of the *miR408* target *LMCOs* in the lignification process, and it is possible that their upregulated expression would cause reduced Cu availability for other LMCOs, including those involved in lignin biosynthesis. The inhibited expression of the key regulatory genes in the lignin pathway in both 408-KO mutants and the 35S:408-14 line (**Figure 4**) could account for the reduction observed in lignin in these lines.

Although both the 35S:408-14 line and the 408-KO mutants showed slightly increased responses in the expression of the Fe deficiency markers under Fe sufficiency, as well as a general defect under Fe deficiency, the molecular reasons behind these effects differed in both plant types. A reduced *FIT* expression was observed in the 35S:408-14 line under low Fe conditions, which suggests that low *miR408* levels could be required for *FIT* expression and the subsequent Fe deficiency responses. Accordingly, FIT-independent Fe deficiency responses have been described for limited Cu, when *miR408* expression is induced (Waters et al., 2012). On the contrary, 408-KO mutants displayed problems in *bHLH39* expression, which could also account for their defective Fe deficiency responses. Different processes that are independent of FIT affect the expression of the Ib subgroup *bHLH* genes, including *bHLH39*. IVc subgroup members of the bHLH transcription factor family bind to the promoters of the Ib subgroup *bHLH* genes, and positively regulate Fe deficiency responses (Zhang et al., 2015). The dimethylation of histone H4R3 in the chromatin of the Ib subgroup *bHLH* genes is involved in Fe deficiency responses (Fan et al., 2014). Taken together, distinctive circumstances that depend on FIT or bHLH39 could be responsive of the defective Fe deficiency signaling in plants with high and low *miR408* expression levels, respectively.

A significant decrease in both phenoloxidase and ferroxidase activities was observed under Fe deficiency in the WT plants (**Figure 6**), but its cause remains unsolved. These activities also reduced in the *spl7* mutant, which exhibits exacerbated defects in root-to-shoot Fe translocation under low Cu conditions, but no responsive enzymes were identified (Bernal et al., 2012). In our study, Fe deficiency downregulated *miR408* and led to the increase in *miR408* target *LMCO* expression (**Figure 3**), which suggests a compensatory effect to counteract the negative effect of Fe scarcity on enzymatic activities. Thus, no decrease in phenoloxidase and ferroxidase activities was observed in mutants 408-KO at higher levels of *miR408* target *LMCOs*. This result could indicate that both activities were affected by the *miR408* expression levels, which would evidence a rather promiscuous range of activity for LMCOs, as previously suggested (Reiss et al., 2013).

LOW PHOSPHATE RESPONSE1 (LPR1), a cell wall-targeted ferroxidase, is involved in root growth inhibition when phosphate deficiency occurs by triggering Fe-stimulated apoplastic ROS generation and cell wall modifications, which impair cell-to-cell communication and meristem maintenance (Müller et al., 2015). Our results matched the concomitant increase in ferroxidase activity and ROS generation in mutant 408-KO under Fe scarcity conditions compared to the WT (**Figures 6B, 7A**). The results shown herein also agree with the proposed role of LMCOs functioning as ascorbate oxidases and, subsequently, with increasing H_2O_2 levels by competing with ascorbate peroxidases for reduced ascorbate (Yu et al., 2017). Hence according to the levels of the *miR408* target *LMCOs* (**Figures 3, 7A**), H_2O_2 levels increased in mutant 408-KO and decreased in the 35S:408-14 line compared to the WT. Moreover, the fact that H_2O_2 levels increased in all cases under low Fe conditions (**Figure 7A**), which agrees with a higher *LMCOs* expression (**Figure 3**), could explain the previous studies in which Fe deficiency produced enhanced root H_2O_2 concentrations (Alvarez-Fernández et al., 2014). However, a role for other LMCOs, such as *MCO3,* that function as ascorbate oxidases (Yamamoto et al., 2005) cannot be ruled out because *MCO3* expression was enhanced under Fe deficiency, but its expression considerably reduced in the plants with altered *miR408* levels (**Figure 7C**).

Redox signaling has been shown to mediate *microRNA* expression (Sunkar et al., 2012; Jagadeeswaran et al., 2014). The results obtained with antioxidant activities in mutants 408-KO (**Figures 7B,C**) suggest that H_2O_2 accumulation under Fe deprivation could be due to the poor capacity to detoxify it (Jelali et al., 2014). H_2O_2 content was enhanced in an FIT-dependent manner under low Fe conditions, and the FIT protein was stabilized by H_2O_2 in the presence of zinc-finger transcription factor ZAT12, which demonstrates that H_2O_2 serves as a signal for Fe deficiency responses (Le et al., 2016). If the presence of FIT is a prerequisite for H_2O_2 accumulation in Fe-deficient roots, the difficulties shown by the 35S:408-14 overexpressing line to express *FIT* (**Figure 5**) would agree with the drop in H_2O_2 (**Figure 7A**). In addition, the fact that H_2O_2 participates in lignification would make lignin biosynthesis in these plants even more difficult (**Figures 2** and **S2**).

One potential explanation to justify the reduced LMCO activities observed under Fe limitation comes from previous data, indicating that H_2O_2 inhibits the ferroxidase activity of the major human plasma multicopper oxidase ceruloplasmin

(Shukla et al., 2006; Olivieri et al., 2011; Barbariga et al., 2015). Ceruloplasmin oxidation induces the structural changes that release Cu atoms from multicopper oxidase sites, which further increases oxidative stress (Shukla et al., 2006). Subsequently, reduced extracellular ferroxidase activity redounded in intracellular Fe retention (Olivieri et al., 2011). According to these data, it is tempting to speculate that increased oxidative stress under low Fe could also inactivate ferroxidase in Arabidopsis. If this were the case, plants would face a conflict under Fe deficiency as inhibited ferroxidase activity would make Fe mobilization difficult, while a subsequent Cu increase would further compete with scarce Fe for long-distance transport. In this scenario, the downregulation of *miR408* and the subsequent increase in *LMCOs* expression could partially compensate for the negative effects of Fe depletion on ferroxidase activity. If *miR408* mediates a process whose aim is to counteract the post-translational Fe deficiency effects on LMCO activities, the opposite *miR408* regulation under Cu and Fe deficiencies could be justified.

In summary, these results suggest that Fe deficiency responses include an increase in oxidative stress, which comes in the form of H_2O_2, drives to enhanced lignification and affects shoot-to-root Fe signaling responses. In addition to their role in lignin biosynthesis, *miR408* and probably other Cu-miRNAs that target *LMCO* mRNAs with putative promiscuous activities, such as ferroxidases and ascorbate oxidases, would interfere with Fe deficiency responses in a complex manner.

DATA AVAILABILITY

All datasets generated for this study are included in the manuscript and/or the **Supplementary Files**.

AUTHOR CONTRIBUTIONS

LP and SP conceived the idea and wrote the manuscript. ÀC-S, LV-B, and OR-R performed the physiological and molecular experiments in the mutant plants. AP-G processed the data and helped to write the manuscript.

FUNDING

This work was supported by grant BIO2017-87828-C2-1-P from the Spanish Ministry of Economy, Industry and Competitiveness, and by FEDER funds from the European Union. ÀC-S and AP-G were recipients of predoctoral FPI and post-doctoral Juan de la Cierva Formación contracts, respectively, from the Spanish Ministry of Economy, Industry and Competitiveness.

ACKNOWLEDGMENTS

We acknowledge the SCSIE (Universitat de València) for the ICP-MS and greenhouse services. The T-DNA mutants lines (408-KO1 and 408-KO2) and the transgenic line overexpressing *miR408* (35S:408-14) were kindly provided by Ma et al. (2015).

SUPPLEMENTARY MATERIAL

The Supplementary Material for this article can be found online at: https://www.frontiersin.org/articles/10.3389/fpls.2019.00324/full#supplementary-material

REFERENCES

Abdel-Ghany, S. E., and Pilon, M. (2008). MicroRNA-mediated systemic down-regulation of copper protein expression in response to low copper availability in Arabidopsis. *J. Biolumin. Chemilumin.* 283, 15932–15945. doi: 10.1074/jbc.M801406200

Alvarez-Fernández, A., Díaz-Benito, P., Abadía, A., López-Millán, A.-F., and Abadía, J. (2014). Metal species involved in long distance metal transport in plants. *Front. Plant Sci.* 5:105. doi: 10.3389/fpls.2014.00105

Askwith, C., Eide, D., Van Ho, A., Bernard, P. S., Li, L., Davis-Kaplan, S., et al. (1994). The FET3 gene of *S. cerevisiae* encodes a multicopper oxidase required for ferrous iron uptake. *Cell* 76, 403–410. doi: 10.1016/0092-8674(94)90346-8

Barbariga, M., Curnis, F., Andolfo, A., Zanardi, A., Lazzaro, M., Conti, A., et al. (2015). Ceruloplasmin functional changes in Parkinson's disease-cerebrospinal fluid. *Mol. Neurodegener.* 10:59. doi: 10.1186/s13024-015-0055-2

Bernal, M., Casero, D., Singh, V., Wilson, G. T., Grande, A., Yang, H., et al. (2012). Transcriptome sequencing identifies SPL7-regulated copper acquisition genes FRO4/FRO5 and the copper dependence of iron homeostasis in *Arabidopsis*. *Plant Cell* 24, 738–761. doi: 10.1105/tpc.111.090431

Berthet, S., Demont-Caulet, N., Pollet, B., Bidzinski, P., Cézard, L., Le Bris, P., et al. (2011). Disruption of LACCASE4 and 17 results in tissue-specific alterations to lignification of *Arabidopsis thaliana* stems. *Plant Cell* 23, 1124–1137. doi: 10.1105/tpc.110.082792

Bonawitz, N. D., and Chapple, C. (2010). The genetics of lignin biosynthesis: connecting genotype to phenotype. *Annu. Rev. Genet.* 44, 337–363. doi: 10.1146/annurev-genet-102209-163508

Bradford, M. M. (1976). A rapid and sensitive method for the quantitation of microgram quantities of protein utilizing the principle of protein-dye binding. *Anal. Biochem.* 72, 248–254. doi: 10.1016/0003-2697(76)90527-3

Buhtz, A., Pieritz, J., Springer, F., and Kehr, J. (2010). Phloem small RNAs, nutrient stress responses, and systemic mobility. *BMC Plant Biol.* 10:64. doi: 10.1186/1471-2229-10-64

Carrió-Seguí, À., Romero, P., Sanz, A., and Peñarrubia, L. (2016). Interaction between ABA signaling and copper homeostasis in Arabidopsis thaliana. *Plant Cell Physiol.* 57, 1568–1582. doi: 10.1093/pcp/pcw087

Chien, P. S., Chiang, C. B., Wang, Z., and Chiou, T. J. (2017). MicroRNA-mediated signaling and regulation of nutrient transport and utilization. *Curr. Opin. Plant Biol.* 39, 73–79. doi: 10.1016/j.pbi.2017.06.007

Choi, M., and Davidson, V. L. (2011). Cupredoxins: a study of how proteins may evolve to use metals for bioenergetic processes. *Metallomics* 3, 140–151. doi: 10.1039/c0mt00061b

Colangelo, E. P., and Guerinot, M. L. (2004). The essential basic helix-loop-helix protein FIT1 is required for the iron deficiency response. *Plant Cell* 16, 3400–3412. doi: 10.1105/tpc.104.024315

Curie, C., and Mari, S. (2017). New routes for plant iron mining. *New Phytol.* 214, 521–525. doi: 10.1111/nph.14364

Cuypers, A., Hendrix, S., Amaral Dos Reis, R., De Smet, S., Deckers, J., Gielen, H., et al. (2016). Hydrogen peroxide, signaling in disguise during metal phytotoxicity. *Front. Plant Sci.* 7:470. doi: 10.3389/fpls.2016.00470

Eide, D., Broderius, M., Fett, J., and Guerinot, M. L. (1996). A novel iron-regulated metal transporter from plants identified by functional expression in yeast. *Proc. Natl. Acad. Sci. U.S.A* 93, 5624–5628.

Fan, H., Zhang, Z., Wang, N., Cui, Y., Sun, H., Liu, Y., et al. (2014). SKB1/PRMT5-mediated histone H4R3 dimethylation of Ib subgroup bHLH genes negatively regulates iron homeostasis in *Arabidopsis thaliana*. *Plant J.* 77, 209–221. doi: 10.1111/tpj.12380

Giehl, R. F., Meda, A. R., and von Wirén, N. (2009). Moving up, down, and everywhere: signaling of micronutrients in plants. *Curr. Opin. Plant Biol.* 12, 320–327. doi: 10.1016/j.pbi.2009.04.006

Hoopes, J. T., and Dean, J. F. (2004). Ferroxidase activity in a laccase-like multicopper oxidase from *Liriodendron tulipifera*. *Plant Physiol. Biochem.* 42, 27–33. doi: 10.1016/j.plaphy.2003.10.011

Jagadeeswaran, G., Li, Y. F., and Sunkar, R. (2014). Redox signaling mediates the expression of a sulfate-deprivation-inducible microRNA395 in *Arabidopsis*. *Plant J.* 77, 85–96. doi: 10.1111/tpj.12364

Jambunathan, N. (2010). Determination and detection of reactive oxygen species (ROS), lipid peroxidation, and electrolyte leakage in plants. *Methods Mol. Biol.* 639, 292–298. doi: 10.1007/978-1-60761-702-0_18

Jelali, N., Donnini, S., Dell'Orto, M., Abdelly, C., Gharsalli, M., and Zocchi, G. (2014). Root antioxidant responses of two Pisum sativum cultivars to direct and induced Fe deficiency. *Plant Biol.* 16, 607–614. doi: 10.1111/plb.12093

Kärkönen, A., Koutaniemi, S., Mustonen, M., Syrjänen, K., Brunow, G., Kilpeläinen, I., et al. (2002). Lignification related enzymes in *Picea abies* suspension cultures. *Physiol. Plant.* 114, 343–353. doi: 10.1034/j.1399-3054.2002.1140303.x

Kärkönen, A., and Kuchitsu, K. (2015). Reactive oxygen species in cell wall metabolism and development in plants. *Phytochemistry* 112, 22–32. doi: 10.1016/j.phytochem.2014.09.016

Karlsson, M., Melzer, M., Prokhorenko, I., Johansson, T., and Wingsle, G. (2005). Hydrogen peroxide and expression of hipI-superoxide dismutase are associated with the development of secondary cell walls in *Zinnia elegans*. *J. Exp. Bot.* 56, 2085–2093. doi: 10.1093/jxb/eri207

Kehr, J. (2013). Systemic regulation of mineral homeostasis by micro RNAs. *Front. Plant Sci.* 4:145. doi: 10.3389/fpls.2013.00145

Kosman, D. J. (2010a). Multicopper oxidases: a workshop on copper coordination chemistry, electron transfer, and metallophysiology. *J. Biol. Inorg. Chem.* 15, 15–28. doi: 10.1007/s00775-009-0590-9

Kosman, D. J. (2010b). Redox cycling in iron uptake, efflux, and trafficking. *J. Biolumin. Chemilumin.* 285, 26729–26735. doi: 10.1074/jbc.R110.113217

Kosman, D. J. (2018). The teleos of metallo-reduction and metallo-oxidation in eukaryotic iron and copper trafficking. *Metallomics* 10, 370–377. doi: 10.1039/c8mt00015h

Lang, M., Braun, C. L., Kanost, M. R., and Gorman, M. J. (2012). Multicopper oxidase-1 is a ferroxidase essential for iron homeostasis in *Drosophila melanogaster*. *Proc. Natl. Acad. Sci. U.S.A* 109, 13337–13342. doi: 10.1073/pnas.1208703109

Le, C. T., Brumbarova, T., Ivanov, R., Stoof, C., Weber, E., Mohrbacher, J., et al. (2016). Zinc finger of *Arabidopsis thaliana*12 (ZAT12) interacts with FER-like iron deficiency-induced transcription factor (FIT) linking iron deficiency and oxidative stress responses. *Plant Physiol.* 170, 540–557. doi: 10.1104/pp.15.01589

Le Gall, H., Philippe, F., Domon, J. M., Gillet, F., Pelloux, J., and Rayon, C. (2015). Cell wall metabolism in response to abiotic stress. *Plants* 4, 112–166. doi: 10.3390/plants4010112

Liang, M., Davis, E., Gardner, D., Cai, X., and Wu, Y. (2006). Involvement of AtLAC15 in lignin synthesis in seeds and in root elongation of Arabidopsis. *Planta* 224, 1185–1196. doi: 10.1007/s00425-006-0300-6

Lichtenthaler, H. K. (1987). Chlorophylls and carotenoids: pigments of photosynthetic biomembranes. *Methods Enzymol.* 148, 350–382.

Liljegren, S. (2010). Phloroglucinol stain for lignin. *Cold Spring Harb. Protoc.* 1:pdb.prot4954. doi: 10.1101/pdb.prot4954

Lu, S., Li, Q., Wei, H., Chang, M. J., Tunlaya-Anukit, S., Kim, H., et al. (2013). Ptr-miR397a is a negative regulator of laccase genes affecting lignin content in *Populus trichocarpa*. *Proc. Natl. Acad. Sci. U.S.A* 110, 10848–10853. doi: 10.1073/pnas.1308936110

Ma, C., Burd, S., and Lers, A. (2015). miR408 is involved in abiotic stress responses in *Arabidopsis*. *Plant J.* 84, 169–187. doi: 10.1111/tpj.12999

McCaig, B. C., Meagher, R. B., and Dean, J. F. (2005). Gene structure and molecular analysis of the laccase-like multicopper oxidase (LMCO) gene family in Arabidopsis thaliana. *Planta* 221, 619–636. doi: 10.1007/s00425-004-1472-6

Müller, J., Toev, T., Heisters, M., Teller, J., Moore, K. L., Hause, G., et al. (2015). Iron-dependent callose deposition adjusts root meristem maintenance to phosphate availability. *Dev. Cell* 33, 216–230. doi: 10.1016/j.devcel.2015.02.007

Nersissian, A. M., Immoos, C., Hill, M. G., Hart, P. J., Williams, G., Herrmann, R. G., et al. (1998). Uclacyanins, stellacyanins, and plantacyanins are distinct subfamilies of phytocyanins: plant-specific mononuclear blue copper proteins. *Protein Sci.* 7, 1915–1929. doi: 10.1002/pro.5560070907

O'Brien, J. A., Daudi, A., Butt, V. S., and Bolwell, G. P. (2012). Reactive oxygen species and their role in plant defence and cell wall metabolism. *Planta* 236, 765–779. doi: 10.1007/s00425-012-1696-9

Olivieri, S., Conti, A., Iannaccone, S., Cannistraci, C. V., Campanella, A., Barbariga, M., et al. (2011). Ceruloplasmin oxidation, a feature of Parkinson's disease CSF, inhibits ferroxidase activity and promotes cellular iron retention. *J. Neurosci.* 31, 18568–18577. doi: 10.1523/JNEUROSCI.3768-11.2011

Pan, J., Huang, D., Guo, Z., Kuang, Z., Zhang, H., Xie, X., et al. (2018). Overexpression of microRNA408 enhances photosynthesis, growth, and seed yield in diverse plants. *J. Integr. Plant Biol.* 60, 323–340. doi: 10.1111/jipb.12634

Parsons, T., and Strickland, J. (1963). Discussion of spectrophotometric determination of marine-plant pigments, with revised equations for ascertaining chlorophyll-a and carotenoids. *J. Mar. Res.* 21, 105–156.

Perea-García, A., Garcia-Molina, A., Andrés-Colás, N., Vera-Sirera, F., Pérez-Amador, M. A., Puig, S., et al. (2013). Arabidopsis copper transport protein COPT2 participates in the cross talk between iron deficiency responses and low-phosphate signaling. *Plant Physiol.* 162, 180–194. doi: 10.1104/pp.112.212407

Pfaffl, M. W., Horgan, G. W., and Dempfle, L. (2002). Relative expression software tool (REST) for group-wise comparison and statistical analysis of relative expression results in real-time PCR. *Nucleic Acids Res.* 30:e36. doi: 10.1093/nar/30.9.e36

Pilon, M. (2017). The copper microRNAs. *New Phytol.* 213, 1030–1035. doi: 10.1111/nph.14244

Quintanar, L., Stoj, C., Taylor, A. B., Hart, P. J., Kosman, D. J., and Solomon, E. I. (2007). Shall we dance? How a multicopper oxidase chooses its electron transfer partner. *Acc. Chem. Res.* 40, 445–452. doi: 10.1021/ar600051a

Ravet, K., and Pilon, M. (2013). Copper and iron homeostasis in plants: the challenges of oxidative stress. *Antioxid. Redox Signaling* 19, 919–932. doi: 10.1089/ars.2012.5084

Reiss, R., Ihssen, J., Richter, M., Eichhorn, E., Schilling, B., and Thöny-Meyer, L. (2013). Laccase versus laccase-like multi-copper oxidase: a comparative study of similar enzymes with diverse substrate spectra. *PLoS One* 8:e65633. doi: 10.1371/journal.pone.0065633

Robinson, N. J., Procter, C. M., Connolly, E. L., and Guerinot, M. L. (1999). A ferric-chelate reductase for iron uptake from soils. *Nature* 397, 694–697. doi: 10.1038/17800

Rodríguez-Celma, J., Lattanzio, G., Villarroya, D., Gutierrez-Carbonell, E., Ceballos-Laita, L., Rencoret, J., et al. (2016). Effects of Fe deficiency on the protein profiles and lignin composition of stem tissues from *Medicago truncatula* in absence or presence of calcium carbonate. *J. Proteomics* 140, 1–12. doi: 10.1016/j.jprot.2016.03.017

Shukla, N., Maher, J., Masters, J., Angelini, G. D., and Jeremy, J. Y. (2006). Does oxidative stress change ceruloplasmin from a protective to a vasculopathic factor? *Atherosclerosis* 187, 238–250. doi: 10.1016/j.atherosclerosis.2005.11.035

Song, Z., Zhang, L., Wang, Y., Li, H., Li, S., Zhao, H., et al. (2018). Constitutive expression of miR408 improves biomass and seed yield in *Arabidopsis*. *Front. Plant Sci.* 8:2114. doi: 10.3389/fpls.2017.02114

Sunkar, R., Chinnusamy, V., Zhu, J., and Zhu, J. K. (2007). Small RNAs as big players in plant abiotic stress responses and nutrient deprivation. *Trends Plant Sci.* 12, 301–309. doi: 10.1016/j.tplants.2007.05.001

Sunkar, R., Kapoor, A., and Zhu, J. K. (2006). Posttranscriptional induction of two Cu/Zn superoxide dismutase genes in Arabidopsis is mediated by downregulation of miR398 and important for oxidative stress tolerance. *Plant Cell* 18, 2051–2065. doi: 10.1105/tpc.106.041673

Sunkar, R., Li, Y. F., and Jagadeeswaran, G. (2012). Functions of microRNAs in plant stress responses. *Trends Plant Sci.* 17, 196–203. doi: 10.1016/j.tplants.2012.01.010

Turlapati, P. V., Kim, K. W., Davin, L. B., and Lewis, N. G. (2011). The laccase multigene family in *Arabidopsis thaliana*: towards addressing the mystery of their gene function(s). *Planta* 233, 439–470. doi: 10.1007/s00425-010-1298-3

Vert, G., Grotz, N., Dédaldéchamp, F., Gaymard, F., Guerinot, M. L., Briat, J. F., et al. (2002). IRT1, an Arabidopsis transporter essential for iron uptake from the soil and for plant growth. *Plant Cell* 14, 1223–1233. doi: 10.1105/tpc.001388

Wang, N., Cui, Y., Liu, Y., Fan, H., Du, J., Huang, Z., et al. (2013). Requirement and functional redundancy of Ib subgroup bHLH proteins for iron deficiency responses and uptake in Arabidopsis thaliana. *Mol. Plant.* 6, 503–513. doi: 10.1093/mp/sss089

Wang, C. Y., Zhang, S., Yu, Y., Luo, Y. C., Liu, Q., Ju, C., et al. (2014). MiR397b regulates both lignin content and seed number in Arabidopsis via modulating a laccase involved in lignin biosynthesis. *Plant Biotechnol. J.* 12, 1132–1142. doi: 10.1111/pbi.12222

Waters, B. M., McInturf, S. A., and Stein, R. J. (2012). Rossette iron deficiency transcript and microRNA profiling reveals links between copper and iron homeostasis in *Arabidopsis thaliana*. *J. Exp. Bot.* 63, 5903–5918. doi: 10.1093/jxb/ers239

Yamamoto, A., Bhuiyan, M. N., Waditee, R., Tanaka, Y., Esaka, M., Oba, K., et al. (2005). Suppressed expression of the apoplastic ascorbate oxidase gene increases salt tolerance in tobacco and *Arabidopsis* plants. *J. Exp. Bot.* 56, 1785–1796. doi: 10.1093/jxb/eri167

Yamasaki, H., Abdel-Ghany, S. E., Cohu, C. M., Kobayashi, Y., Shikanai, T., and Pilon, M. (2007). Regulation of copper homeostasis by micro-RNA in Arabidopsis. *J. Biolumin. Chemilumin.* 282, 16369–16378. doi: 10.1074/jbc.M700138200

Yamasaki, H., Hayashi, M., Fukazawa, M., Kobayashi, Y., and Shikanai, T. (2009). SQUAMOSA promoter binding protein-like7 is a central regulator for copper homeostasis in *Arabidopsis*. *Plant Cell* 21, 347–361. doi: 10.1105/tpc.108.060137

Yu, Y., Li, Q. F., Zhang, J. P., Zhang, F., Zhou, Y. F., Feng, Y. Z., et al. (2017). Laccase-13 regulates seed setting rate by affecting hydrogen peroxide dynamics and mitochondrial integrity in rice. *Front. Plant Sci.* 8:1324. doi: 10.3389/fpls.2017.01324

Yuan, Y., Wu, H., Wang, N., Li, J., Zhao, W., Du, J., et al. (2008). FIT interacts with AtbHLH38 and AtbHLH39 in regulating iron uptake gene expression for iron homeostasis in *Arabidopsis*. *Cell Res.* 18, 385–397. doi: 10.1038/cr.2008.26

Zhang, H., and Li, L. (2013). SQUAMOSA promoter binding protein-like7 regulated microRNA408 is required for vegetative development in Arabidopsis. *Plant J.* 74, 98–109. doi: 10.1111/tpj.12107

Zhang, J., Liu, B., Li, M., Feng, D., Jin, H., Wang, P., et al. (2015). The bHLH transcription factor bHLH104 interacts with IAA-LEUCINE RESISTANT3 and modulates iron homeostasis in Arabidopsis. *Plant Cell* 27, 787–805. doi: 10.1105/tpc.114.132704

Zhang, J. P., Yu, Y., Feng, Y. Z., Zhou, Y. F., Zhang, F., Yang, Y. W., et al. (2017). MiR408 regulates grain yield and photosynthesis via a phytocyanin protein. *Plant Physiol.* 175, 1175–1185. doi: 10.1104/pp.17.01169

Zhang, H., Zhao, X., Li, J., Cai, H., Deng, X. W., and Li, L. (2014). MicroRNA408 is critical for the HY5-SPL7 gene network that mediates the coordinated response to light and copper. *Plant Cell* 26, 4933–4953. doi: 10.1105/tpc.114.127340

Zhang, Z., Zheng, Y., Ham, B. K., Chen, J., Yoshida, A., Kochian, L. V., et al. (2016). Vascular-mediated signalling involved in early phosphate stress response in plants. *Nat. Plants* 2:16033. doi: 10.1038/nplants.2016.33

Zhao, Y., Lin, S., Qiu, Z., Cao, D., Wen, J., Deng, X., et al. (2015). MicroRNA857 is involved in the regulation of secondary growth of vascular tissues in Arabidopsis. *Plant Physiol.* 169, 2539–2552. doi: 10.1104/pp.15.01011

Zhao, Q., Nakashima, J., Chen, F., Yin, Y., Fu, C., Yun, J., et al. (2013). Laccase is necessary and nonredundant with peroxidase for lignin polymerization during vascular development in Arabidopsis. *Plant Cell* 25, 3976–3987. doi: 10.1105/tpc.113.117770

Conflict of Interest Statement: The authors declare that the research was conducted in the absence of any commercial or financial relationships that could be construed as a potential conflict of interest.

frontiers in Plant Science

ORIGINAL RESEARCH
published: 05 April 2019
doi: 10.3389/fpls.2019.00416

Silicon Alleviates Iron Deficiency in Barley by Enhancing Expression of Strategy II Genes and Metal Redistribution

Dragana B. Nikolic[1], Sofija Nesic[1], Dragana Bosnic[1], Ljiljana Kostic[2], Miroslav Nikolic[2] and Jelena T. Samardzic[1]*

[1] Laboratory for Plant Molecular Biology, Institute of Molecular Genetics and Genetic Engineering, University of Belgrade, Belgrade, Serbia, [2] Plant Nutrition Research Group, Institute for Multidisciplinary Research, University of Belgrade, Belgrade, Serbia

The beneficial effects of silicon (Si) have been shown on plants using reduction-based strategy for iron (Fe) acquisition. Here we investigated the influence of Si on Fe deficiency stress alleviation in barley (*Hordeum vulgare*), a crop plant which uses the chelation-based strategy for Fe acquisition. Analyses of chlorophyll content, ROS accumulation, antioxidative status, concentrations of Fe and other micronutrients, along with the expression of Strategy II genes were studied in response to Si supply. Si successfully ameliorated Fe deficiency in barley, diminishing chlorophyll and biomass loss, and improving the activity of antioxidative enzymes, resulting in lowered reactive oxidative species accumulation in the youngest leaves. Alleviation of Fe deficiency stress correlated well with the Si-induced increase of Fe content in the youngest leaves, while it was decreased in root. Moreover, Si nutrition lowered accumulation of other micronutrients in the youngest leaves of Fe deprived plants, by retaining them in the root. On the transcriptional level, Si led to an expedient increase in the expression of genes involved in Strategy II Fe acquisition in roots at the early stage of Fe deficiency stress, while decreasing their expression in a prolonged stress response. Expression of Strategy II genes was remarkably upregulated in the leaves of Si supplied plants. This study broadens the perspective of mechanisms of Si action, providing evidence for ameliorative effects of Si on Strategy II plants, including its influence on accumulation and distribution of microelements, as well as on the expression of the Strategy II genes.

Keywords: iron deficiency, silicon, Strategy II Fe acquisition, gene expression, barley (*Hordeum vulgare*), microelement accumulation

OPEN ACCESS

Edited by:
Thomas J. Buckhout, Humboldt-Universität zu Berlin, Germany

Reviewed by:
Christof Alfred Engels, Humboldt-Universität zu Berlin, Germany
Ping Lan, Institute of Soil Science (CAS), China

****Correspondence:***
Dragana B. Nikolic
dragana.nikolic@imgge.bg.ac.rs

Specialty section:
This article was submitted to Plant Nutrition, a section of the journal Frontiers in Plant Science

Received: *19 December 2018*
Accepted: *19 March 2019*
Published: *05 April 2019*

Citation:
Nikolic DB, Nesic S, Bosnic D, Kostic L, Nikolic M and Samardzic JT (2019) Silicon Alleviates Iron Deficiency in Barley by Enhancing Expression of Strategy II Genes and Metal Redistribution. Front. Plant Sci. 10:416. doi: 10.3389/fpls.2019.00416

INTRODUCTION

Iron (Fe) is an essential element for all living organisms. Due to its ability to undergo a reversible valence change between ferrous (Fe^{2+}) and ferric (Fe^{3+}), Fe is involved in vital cellular processes such as photosynthesis and nitrogen fixation. It is a component of numerous proteins and enzymes, including some antioxidative enzymes. However, the same redox properties easily make Fe toxic when present in excess. Free Fe^{2+} ions react directly with O_2 or catalyze Fenton reaction, leading

to oxidative damage; therefore, it must always be in complex with chelators (Broadley, 2012). Although Fe is one of the most abundant elements in Earth's crust, it is present mostly in the form of ferric hydroxide [$Fe(OH)_3$], which is poorly soluble and unavailable to plants (Boukhalfa and Crumbliss, 2002). This problem is emphasized in calcareous soils which make up 30% of the world's agricultural soils (Guerinot and Yi, 1994). Iron deficiency, hence, is one of the major nutritional concerns, lowering a crop's yield and nutritional quality. Plants have developed two distinct strategies for iron acquisition from soil (Marschner and Römheld, 1994; Connorton et al., 2017). Dicotyledonous and non-graminaceous monocotyledonous plant species use reduction-based Strategy I, employing ferric chelate reductases (FRO) to reduce Fe(III) to Fe(II) which is then taken up by IRT (Iron Regulated Transporter). Graminaceous monocotyledonous plant species (Poaceae) developed a chelation-based strategy for Fe acquisition (Strategy II). They synthesize metal chelators, mugineic acid (MA) phytosiderophores (PS) and release them into the rhizosphere *via* TOM1 (transporter of mugineic acid family phytosiderophores 1) (Mori, 1999; Nozoye et al., 2011). Iron-phytosiderophore complexes are then taken up by the root cells via yellow stripe1 (YS1) transporters (Curie et al., 2001; Murata et al., 2006; Inoue et al., 2009). Phytosiderophores are synthesized from methionine via S-adenosylmethionine and nicotianamine (NA), in the subsequent steps catalyzed by the enzymes S-adenosyl methionine synthetase (SAMS), nicotianamine synthase (NAS), nicotianamine aminotransferase (NAAT) and deoxymugineic acid synthase (DMAS) (Mori, 1999; Bashir et al., 2006). Genes encoding MA transporters and biosynthetic enzymes are upregulated by Fe deficiency. Phytosiderophores and their precursor non-proteinogenic amino acid NA are also required for both cellular Fe homeostasis and long-distance Fe transport within the plant. While organic acids like citrate are main Fe ligands in apoplast, NA and MAs are essential for Fe chelation and transport in symplast. Moreover, MAs have been identified in the xylem as well as in the phloem, and are considered to be important for long-distance metal transport (Kawai et al., 2001; Nishiyama et al., 2012).

Although not accepted as an essential element, silicon (Si) is well known for its beneficial effects in plants and protection against biotic and abiotic stresses (Hernandez-Apaolaza, 2014; Liang et al., 2015; Pontigo et al., 2015; Coskun et al., 2019); nonetheless the mechanisms of its action are poorly understood. Despite being the second most abundant element in Earth's crust, intensive crop production without Si fertilizing have reduced the amount of Si in soils available for plants. Therefore, Si fertilizers are being applied increasingly to improve crops' resistance and yields (Ma and Yamaji, 2006). Recently, an ameliorative effect of Si on micronutrient deficiency has been reported; Si mitigated Fe deficiency symptoms in cucumber, soybean and *Vallerianella locusta* (Gottardi et al., 2012; Gonzalo et al., 2013; Pavlovic et al., 2013). Silicon is considered to enhance metal ion pools in the root and leaf apoplast in conditions of sufficient supply and to intensify its reutilization and transport when plants encounter a lack of the metal micronutrient (Hernandez-Apaolaza, 2014; Liang et al., 2015).

In dicots, Si upregulated the expression of genes involved in the reduction-based strategy for Fe acquisition (Strategy I), as well as genes participating in biosynthesis of Fe-chelating compounds (e.g., organic acids and phenolics), thereby enhancing Fe mobilization from the rhizosphere and reutilization of root apoplastic Fe, as well as xylem translocation of Fe toward the shoot (Pavlovic et al., 2013; Stevic et al., 2016). Moreover, it has been demonstrated that Si increases re-translocation of Fe from old to young leaves associated with upregulated expression of *CsNAS1* and *CsYSL1* as well as increased leaf concentration of NA (Pavlovic et al., 2016).

Si-mediated mitigation of Fe deficiency stress has only been reported for Strategy I plants, and it has even been suggested that Si application has no effect on alleviation of such stress in Strategy II plants (Bityutskii et al., 2010). The distinction between strategy I and strategy II plants is not considered so strict anymore, however, although dicotyledonous plants synthesize phenolic chelating compounds they still require FRO2 and IRT1 to take up iron, and even though functional IRT transporter is found among the Gramineae it is mainly utilized in low oxygen conditions keeping the chelating strategy predominant for Fe entry (Ishimaru et al., 2006; Pedas et al., 2008; Fourcroy et al., 2016). Recently, Gattullo et al. (2016) reported that Fe deficient barley plants promoted mineral weathering, dissolving amorphous mineral phases in the soil and increasing the amount of smectite, by exudation of phytosiderophores. The exudates further drove dissolution of smectite and increased uptake of Si in Fe deficient plants compared to those adequately supplied with Fe.

The objective of the present work was to investigate the ability of Si to ameliorate Fe deficiency stress in a graminaceous plant which uses predominantly the chelation-based strategy for Fe acquisition. Barley (*Hordeum vulgare*) was chosen as a representative plant for this strategy. As we found stress alleviation in Si treated barely, we further analyzed accumulation of Fe and other microelements in leaves, as well as expression of genes involved in Strategy II Fe acquisition, searching for elucidation of the molecular mechanisms underlying the process.

MATERIALS AND METHODS

Plant Materials and Growth Conditions

After soaking in 1 mM $CaSO_4$ overnight, seeds of barley (*Hordeum vulgare,* cultivar Rekord; kindly provided by Institute for cereals, Kragujevac, Serbia) were germinated between two sheets of filter paper moistened with saturated $CaSO_4$. The 4 days old seedlings were then transferred to a complete nutrient solution containing (in mM): 0.7 K_2SO_4, 0.1 KCl, 2.0 $Ca(NO_3)_2$, 0.5 $MgSO_4$, 0.1 KH_2PO_4, and (in μM): 0.5 $MnSO_4$, 0.5 $ZnSO_4$, 0.2 $CuSO_4$, 0.01$(NH_4)_6Mo_7O_{24}$, 1 H_3BO_3. Fe was supplied as $NaFe^{III}EDTA$. Plants were pre-cultured for 4 days in nutrient solution supplied with 20 μM Fe and then grown in either +Fe (80 μM) or in -Fe (Fe-free) nutrient solution, without (−Si) or with (+Si) supply of Si. Si-treatments started after the 4 days preculture, simultaneously with Fe withdrawal. If applied, Si was in the form of $Si(OH)_4$ at 1.5 mM. This was freshly prepared

by passing Na_2SiO_3 (Merck, Sodium silicate solution, extra pure, Fe $\leq$ 0.005%) through a column filled with cation-exchange resin (Amberlite IR-120, H+ form; Fluka, Buchs SG, Switzerland). Amberlite IR-120 is also capable of removing ionic Fe forms (Schmid and Gerloff, 1961) from Na_2SiO_3, thus preventing any possible contamination of the nutrient solution with Fe. The pH of nutrient solutions was adjusted to 6.0 and the nutrient solutions were renewed completely every 2 days and continuously aerated. Plants (15 seedlings per pot of 3L) were grown under controlled environmental conditions with a photoperiod of 16 h:8 h and temperature regime of 25°C:21°C (light:dark), photon flux density of 250 μmol m^{-2} s^{-1} at plant height.

Chlorophyll Determination

Chlorophyll content in the youngest fully developed leaves was approximated non-destructively using a portable ChlorophyllMeter SPAD-502 device (Minolta Camera Co., Osaka, Japan).

Determination of Microelements in Plant Tissues

After harvest roots are washed in 1 mM EDTA, and twice in destiled water. Roots and leaves were oven dried at 70°C for 48 h, weighed and hand ground. Dry plant material (0.2 g) was digested in 3 ml concentrated HNO_3 + 2 ml H_2O_2 for 1 h in a microwave oven (Speedwave MWS-3+; Berghof Products + Instruments GmbH, Eningen, Germany). Samples were then transferred into 25 ml plastic flasks and flask volume was adjusted to 25 ml with deionized H_2O. Fe was determined by inductively coupled plasma optical emission spectroscopy (ICP-OES, SpectroGenesis EOP II; Spectro Analytical Instruments GmbH, Kleve, Germany).

Determination of Si concentration was performed as described in Pavlovic et al. (2013).

ROS Detection

For fluorescent ROS (reactive oxygen species) detection, the youngest leaves were vacuum infiltrated with dichloro-dihydrofluorescein (H2DCF DA; Sigma-Aldrich) essentially as described in Zhang and Qiu (2007). The leaves were visualized by Olympus BX51 fluorescent microscope with appropriate filters for detection of SpectrumGreen. All images were taken using the same settings (exposure 0.02, bright 166, black 107).

Assay of Antioxidative Enzymes and Compounds

Leaves were homogenized in 50 mM potassium phosphate buffer (pH 7.0) including 0.1 mM EDTA and 2% (v/v) PVP. The homogenates were centrifuged at 14,000 g for 15 min at 4°C and the supernatants used for enzyme activity assays. The protein content was determined according to Bradford (1976) with bovine serum albumin as a standard.

APX (ascorbate peroxidase, EC 1.11.1.11) activity was determined according to Nakano and Asada (1981) by following the rate of ascorbate oxidation at 290 nm. Reaction mixture contained 50 mM potassium phosphate buffer, pH 7.0, 0.1 mM of EDTA, 0.25 mM ascorbate, 1.27 mM H_2O_2 and leaf extract. The enzyme activity was determined using an extinction coefficient of 2.8 mM^{-1} cm^{-1}. One unit of APX activity was defined as the amount of enzyme needed for the oxidation of 1 μmol of ascorbate per minute and the specific activity was expressed as units per mg protein.

SOD (Superoxide dismutase, E.C. 1.15.1.1) activity was determined essentially as described by Giannopolitis and Ries (1977) by measuring its ability to inhibit photochemical reduction of nitroblue tetrazolium (NBT) at 560 nm. The reaction mixture contained 50 mM potassium phosphate buffer (pH 7.0), 0.1 mM of EDTA, 75 μM NBT, 13 mM methionine, 2 μM riboflavin and leaf extract. One SOD unit was taken to be the amount of enzyme causing 50% inhibition of NBT reduction and expressed in units per mg protein.

CAT (catalase, E.C.1.11.1.6) activity was determined by following the consumption of H_2O_2 at 240 nm according to the method of Aebi (1984). The reaction mixture contained 50 mM potassium phosphate buffer (pH 7.0), 0.1 mM of EDTA, 15 mM H_2O_2 and leaf extract. One unit of CAT activity was defined as the amount of enzyme that catalyzes the decomposition of 1 μmol of H_2O_2 per minute and the specific activity was expressed as units per mg protein (extinction coefficient 0.0436 mM^{-1} cm^{-1}).

Total glutathione concentration was determined essentially as described in Tommasi et al. (2001). Total ascorbate was measured following method described in Vidović et al. (2015).

RNA Extraction and cDNA Synthesis

Root and leaf tissue samples (0.5–1 g FW) were frozen in liquid N_2 and ground thoroughly in a mortar. RNA was isolated using the RNeasy® Mini Kit (Qiagen) as described in the RNeasy® Mini Handbook. Before cDNA synthesis DNA was removed from RNA samples using Ambion DNA-free DNase Treatment and Removal Reagents. First strand cDNA was synthesized from 1 μg of RNA with M-MuLV reverse transcriptase (Thermo Scientific) and random hexamer primers (Applied Biosystems, FosterCity, CA, United States) according to the manufacturer's instructions. The cDNA was diluted 1:5 (v/v) with nuclease-free H_2O (except when determining target genes expressed at low levels, *HvTOM1* and *HvNAS1* in leaves) and used as a template for Real-time PCR with primers designed for barley.

Real-Time Quantitative PCR

Real-time PCR reactions were performed in 25 μl volume containing 400 nM of each primer and 1X SYBER Green PCR master mix (Thermo Fisher Scientific), on the ABI Prism 7500 Sequence Detection System (Applied Biosystem), as described in Pavlovic et al. (2013). Actin gene was used as the endogenous control. Primers and accession numbers of housekeeping and target genes are listed in **Supplementary Table S1**. Level of expression in control plants, grown in optimal Fe supply, was used as a calibrator, i.e., all the expression levels that were normalized to the level of actin gene were subsequently normalized to the expression in the control plants, according to Pfaffl method (Pfaffl, 2001). Gene expression level of plants supplied with Fe was set to 1.0.

FIGURE 1 | Effect of Si nutrition on visual symptoms of Fe deficiency in barley (*Hordeum vulgare*). Plants were pre-cultured for 4 days in a nutrient solution supplied with 20 μM NaFeIIIEDTA and then grown for 3 weeks in Fe-free nutrient solution, with or without a supply of 1.5 mM $Si(OH)_4$ (+Si and −Si, respectively). Control plants (C) were grown in solution supplied with 80 μM NaFeIIIEDTA, without Si.

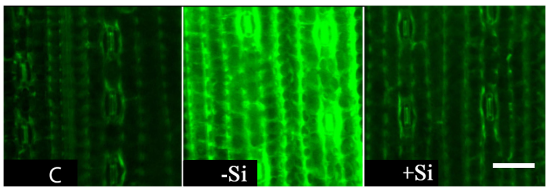

FIGURE 2 | Effect of Si nutrition on ROS accumulation in leaves of iron-deficient barley seedlings. Representative fluorescent microscopy images of the youngest fully expanded leaves showing ROS accumulation as green fluorescence with the probe H_2DCF DA. The plants were treated as described in the legend of **Figure 1** (C- control plants grown optimally supplied with Fe; −Si – plants grown in the absence of Fe and Si; +Si – plants grown in the absence of Fe and supplied with Si). Scale bar = 40 μm.

Statistical Analysis

Data were subjected to analysis of variance using the statistical software SPSS for windows and means were compared by Tukey's test at 5% significance level ($p < 0.05$).

RESULTS

Si Alleviates Fe Deficiency Symptoms and Oxidative Stress in Barley

To examine whether Si alleviates Fe deficiency in Strategy II plants, barley has been chosen as a representative of gramineous plants, which predominantly use the chelating strategy for Fe acquisition. Si successfully mitigated Fe deficiency symptoms in barley pre-cultured for 4 days with 20 μM $NaFe^{III}EDTA$ and further grown in hydroponics for 3 weeks without Fe (**Figure 1**).

Plants grown without Si were severely chlorotic, while in Si-supplied plants chlorosis was alleviated. The effect was the most prominent in the youngest fully expanded leaves. These observations were confirmed by measuring Spectral Plant Analysis Diagnostic (SPAD) index. The relative chlorophyll content was significantly higher in leaves of Si fed plants. Si also promoted the growth of Fe deprived plants. Fresh and dry biomasses of the youngest leaves were considerably higher in Si supplied plants (**Table 1**).

One of the consequences of Fe deprivation can be oxidative stress due to decreased activity of electron transport chains and reduced activity of some antioxidative enzymes. Therefore, we examined levels of reactive oxygen species (ROS) in the youngest, chlorotic leaves. Intracellular ROS accumulation was monitored using fluorescent dye DCF-DA. An intense fluorescent signal was detected in leaves of iron deprived plants, indicating highly elevated accumulation of ROS. The signal was markedly reduced in leaves of Si treated plants, reversing it to the control level (**Figure 2**).

Since ROS accumulation observed in leaves of iron-deficient plants may be, in part, a result of the reduced activity of antioxidative enzymes, we measured the activity of ascorbate peroxidase, catalase and superoxide dismutase (**Table 2**). As previously reported for different plant species (Ranieri et al., 2001; Zaharieva et al., 2004; Sun et al., 2007; Ramírez et al., 2013) iron deficiency caused a huge decrease in the activity of the heme-containing enzymes ascorbate peroxidase and catalase in barley leaves. Silicon supply remarkably improved the activities of both enzymes, restoring them to the levels found under iron-sufficient conditions. On the other hand, aside from the Fe isoform, SOD also comprises Mn and Cu-Zn isoforms and we did not detect any significant change in its activity among the treatments. The non-enzymatic antioxidants ascorbate and glutathione are also involved in keeping the cellular redox homeostasis and their levels are found to be altered during Fe deprivation (Zaharieva et al., 2004; Ramírez et al., 2013). We detected a significant increase in glutathione content in the youngest leaves under Fe deficiency, irrespective of Si supply. The level of ascorbate did not change significantly among the treatments (**Table 2**).

TABLE 1 | Effect of Si nutrition on dry weight (DW) of root, old leaf (L1), and mature leaf (L2) and FW, DW, and chlorophyll content (SPAD units) of the youngest fully expanded leaves of barley.

				Youngest leaf		
Treatments	**DW per root (mg)**	**DW per old leaf (mg)**	**DW per mature leaf (mg)**	**FW per leaf (mg)**	**DW per leaf (mg)**	**SPAD**
C	6.8 ± 1.2 ab	13.3 ± 0.5 a	13.0 ± 1.7 a	219.2 ± 1.7 a	21.3 ± 0.2 a	29.7 ± 2.7 a
−Si	6.6 ± 0.7 b	11.9 ± 0.7 b	12.3 ± 0.6 a	177.5 ± 7.3 c	17.3 ± 0.7 c	10.2 ± 1.5 b
+Si	7.9 ± 0.8 a	13.0 ± 0.3 a	13.0 ± 0.0 a	210.9 ± 4.6 b	20.6 ± 0.4 b	27.5 ± 3.3 a

*Plants were grown as described in the legend of **Figure 1** (C- control plants grown optimally supplied with Fe; −Si – plants grown in the absence of Fe and Si; +Si – plants grown in the absence of Fe and supplied with Si). Data shown are means ± s.d. (n = 3). Significant differences (P < 0.05) between treatments are indicated by different letters.*

Si Increases Total Fe Concentration and Content and Modulates Concentration and Content of Some Other Microelements in the Youngest Leaves of Fe Deficient Barley

Increased chlorophyll content as well as APX and CAT activities under Si supply, indicated increased iron concentration and content in the youngest leaves. Along with Fe we also measured the leaf content and concentration of Mn, Zn, and Cu, to obtain information for other elements that could be perturbed during iron deficiency. As we have expected, Si significantly raised Fe concentration and content in the youngest leaves of barley (**Table 3** and **Figure 3A**).

On the other hand, concentrations of Mn, Zn, and Cu were increased in Fe deficient leaves (**Table 3**), and were above critical levels of toxicity according to Pedas et al. (2014) and Ryzhenko et al. (2016). However, concentrations of all three elements, as well as leaf contents of Mn and Zn in Si-treated Fe deprived plants were significantly reduced, implying the additional protective role of Si (**Table 3** and **Figure 3**). Increased concentration of Si was also shown in the youngest leaves of Si treated plants (**Table 3**).

To determine Fe distribution in plant organs during the Fe deprivation we measured Fe content in roots and three leaf maturity stages (L1–L3) (**Figures 4**, **5**). More than half of Fe in control plant is deposited in roots; in leaves the majority of Fe is present in the youngest ones. Under Fe deficiency only one third of Fe is present in roots and distribution of Fe among leaves is also changed, the highest content is determined in the oldest leaves. In Si supplied plants, grown without Fe, Fe content in roots decreased even more; only 17% of the total Fe in plant was retained in this organ. The youngest leaves of silicon fed plants were the most abundant in Fe content.

In parallel, we also measured contents of other essential metals, such as Mn, Zn, and Cu and investigated differences in their distribution under Fe deficiency and upon Si supply (**Figure 4**). All the metals showed similar pattern of the distribution between organs in Fe deficient plants – increase of the content in the roots and leaves compared with the control, with the exception of Mn in L1 and L2 which were equal to the control plants. Si nutrition additionally increased the metal content in roots (except Cu). Significant decrease in Cu content, under influence of Si, was detected in old and mature leaves (L1 and L2), in contrast to Mn and Zn that were less present only in the youngest leaves. Mn and Zn contents were almost unchanged in L1 and L2, in respect to Si supply. Concentrations of Fe, Mn, Zn, and Cu in root, old and mature leaf are given in a **Supplementary Table S2**.

Si Accelerates Increase in Expression of Genes Related to Strategy II Fe Acquisition in Roots and Upregulates the Gene Expression in Leaves of Fe Deficient Barley

Previous studies have shown modulation of the expression of genes involved in Strategy I Fe acquisition and Fe re-translocation upon Si treatment (Pavlovic et al., 2013, 2016). In this work, we monitored changes in the expression of genes participating in Strategy II Fe acquisition: *HvDMAS1*, *HvTOM1,* and *HvYS1*, responsible for phytosiderophore DMA biosynthesis and release, and metal-DMA complex uptake, respectively. We also analyzed the expression of *HvNAS1,* the gene for nicotianamine synthase, involved in the biosynthesis pathway of phytosiderophores.

TABLE 2 | Effect of Si supply on activity of antioxidative enzymes and concentration of non-enzymatic antioxidants in the youngest fully expanded leaves.

Treatment	APX	CAT	SOD	GSH	Asc
C	0.120 ± 0.048 a	171 ± 29 a	134 ± 16 a	156 ± 10 b	2043 ± 205 a
−Si	0.051 ± 0.012 b	124 ± 27 b	133 ± 4 a	201 ± 9 a	2165 ± 185 a
+Si	0.143 ± 0.022 a	177 ± 10 a	124 ± 10 a	200 ± 12 a	2261 ± 228 a

Enzyme activities are given as u/mg protein; GSH and Asc in nmol g^{-1} FW. The plants were treated as described in the legend of ***Figure 1*** *(C- control plants grown optimally supplied with Fe; −Si – plants grown in the absence of Fe and Si; +Si – plants grown in the absence of Fe and supplied with Si). Data shown are means ± s.d. (n = 3). APX, Ascorbate peroxidase; CAT, catalase; SOD, superoxide dismutase; GSH, glutathione; Asc, ascorbate. Significant differences (P < 0.05) between treatments are indicated by different letters.*

TABLE 3 | Concentration of microelements and Si in the youngest leaves of barley, 3 weeks after Fe withdrawal.

	Microelement concentration in the youngest leaves (μg g^{-1} DW)				
Treatment	Fe	Mn	Zn	Cu	Si (% DW)
C	104.1 ± 31.7 a	54.0 ± 13.0 c	75.1 ± 27.8 b	11.3 ± 3.7 c	0.61 ± 0.09 b
−Si	37.9 ± 8.2 c	154.0 ± 16.6 a	188.2 ± 25.0 a	31.2 ± 5.6 a	0.40 ± 0.14 b
+Si	64.5 ± 11.5 b	100.1 ± 9.6 b	114.6 ± 15.2 b	22.1 ± 5.7 b	1.26 ± 0.11 a

The plants were treated as described in the legend of ***Figure 1*** *(C- control plants grown optimally supplied with Fe; −Si – plants grown in the absence of Fe and Si; +Si – plants grown in the absence of Fe and supplied with Si). Data shown are means ± s.d. (n ≥ 3). Significant differences (P < 0.05) between treatments are indicated by different letters.*

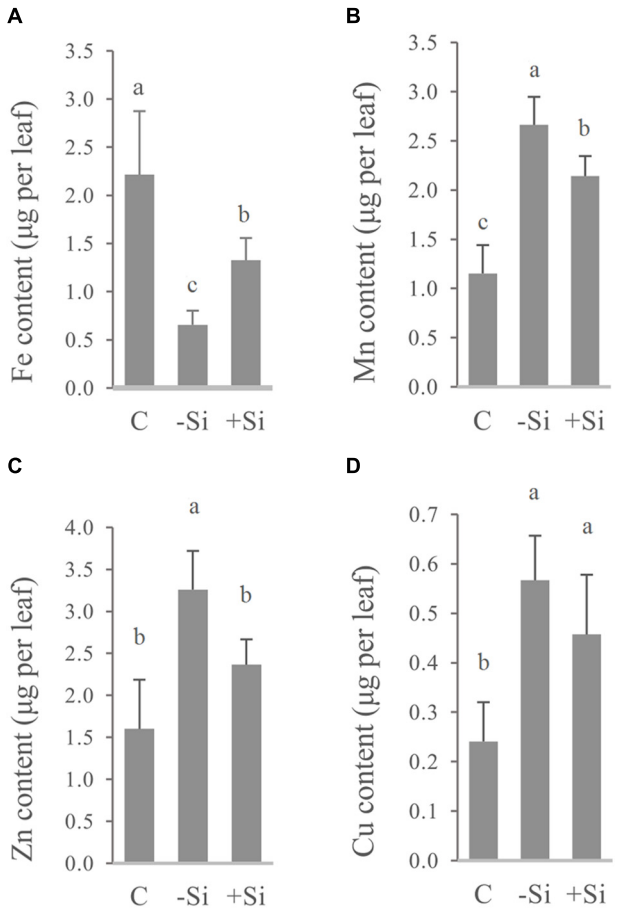

FIGURE 3 | Effect of Si nutrition on micronutrient content in the youngest fully developed barley leaves (third leaves, L3), 3 weeks after Fe withdrawal. Total leaf content of **(A)** Fe, **(B)** Mn, **(C)** Zn, and **(D)** Cu. The plants were treated as described in the legend of **Figure 1** (C- control plants grown optimally supplied with Fe; −Si – plants grown in the absence of Fe and Si; +Si – plants grown in the absence of Fe and supplied with Si). Data shown are means ± s.d. ($n \geq 3$). Significant differences ($P < 0.05$) between treatments are indicated by different letters.

When compared to the gene expression level in the control plants (which was shown set to 1, on the graph in **Figure 6**, as it was used as the calibrator), the expression of all the examined genes was unchanged or slightly increased in Fe-deficient roots, 5 h after Fe withdrawal. In Si treated roots, however, when compared to both the control and Fe-deficient plants, the expression level of all genes, except *HvTOM1,* was instantly and significantly elevated 5 h after Fe withdrawal. Si-dependent acceleration of gene expression response is most evident for *HvYS1* and *HvNAS1* genes, which were increased more than twofold in +Si roots in comparison to −Si roots. On the first and second day, the expression of all examined genes was higher from the control level in both −Si and +Si roots, however, on the second day, the expression in Si supplied roots was decreased compared to −Si roots. The biggest differences in the transcript levels between treatments were observed on the seventh day. While in the −Si roots the expression of all the genes was kept on the same high level as before (*HvYS1* and *HvNAS1*) or raised even higher (*HvDMAS1* and *HvTOM1*), in Si supplied roots the expression of all genes decreased greatly, even compared to the control (**Figure 6**).

Si also influenced gene expression in the leaves, however, it was regulated differently compared to the roots (**Figure 7**). Changes in expression were slower and the greatest influence of Si was seen on the third day. Si remarkably increased expression of *HvNAS1* and *HvTOM1* genes on the third day of Fe deprivation, 134- and 137-fold, respectively. *HvNAS1* was also upregulated on the first and seventh day. *HvTOM1* gene expression was not influenced by Si on the first day, and a small upregulation was detected on the seventh day. On the other hand, no significant change in transcript level of *HvYS1* was detected at any of the tested time points, while *HvDMAS1* expression slightly decreased or remained unaffected.

DISCUSSION

Recent publications have reported an ameliorative effect of silicon on iron deficient Strategy I plants, in particular cucumber, pumpkin and soybean (Bityutskii et al., 2010; Gonzalo et al., 2013; Pavlovic et al., 2013). Si increased the apoplastic Fe pool in cucumber roots and enhanced Fe acquisition and translocation toward apical shoot parts by the accumulation of Fe-mobilizing compounds and acceleration and enhancement of the expression response of the relevant genes (Pavlovic et al., 2013; Bityutskii et al., 2014). To date, beneficial effects of Si on Fe deficiency stress in Strategy II plants have not been reported; moreover, it has been suggested that Si cannot alleviate stress in the chelation-based strategy (Bityutskii et al., 2010). In the present study we have clearly demonstrated an ameliorative effect of Si on Fe deficiency stress in barley, a plant with predominant Strategy II Fe acquisition and shown Si-induced modulation of Strategy II genes expression.

The most obvious effect of Si was successfully prevented chlorosis and biomass reduction of the youngest leaves (**Table 1**). One of the consequences of iron deprivation can also be an imbalance of cellular redox homeostasis. We have shown a high intracellular accumulation of ROS in the youngest leaves of Fe deficient barley, as detected by DCF-DA fluorescent dye, and a decrease in ROS level in the presence of Si (**Figure 2**). ROS may serve as signaling molecules, which trigger stress responses to various abiotic and biotic stresses, but their accumulation could also lead to oxidative damage of cellular components (Mittler et al., 2004). These dual effects have also been observed, although not completely understood, in iron deficiency stress. Prolonged Fe deficiency can result in the accumulation of ROS in leaves, due to lowered activity of Fe-dependent antioxidative enzymes and perturbances in electron transport chains in mitochondria and chloroplasts (Ranieri et al., 2001; Sun et al., 2007; Ramírez et al., 2013). ROS accumulation in Fe deprived leaves, and a restoration of basal ROS level in the youngest leaves of Si-supplied barley (**Figure 2**) was associated with changes in antioxidative enzyme activities. APX and CAT activities were significantly decreased in Fe deficient plants, but recovered upon

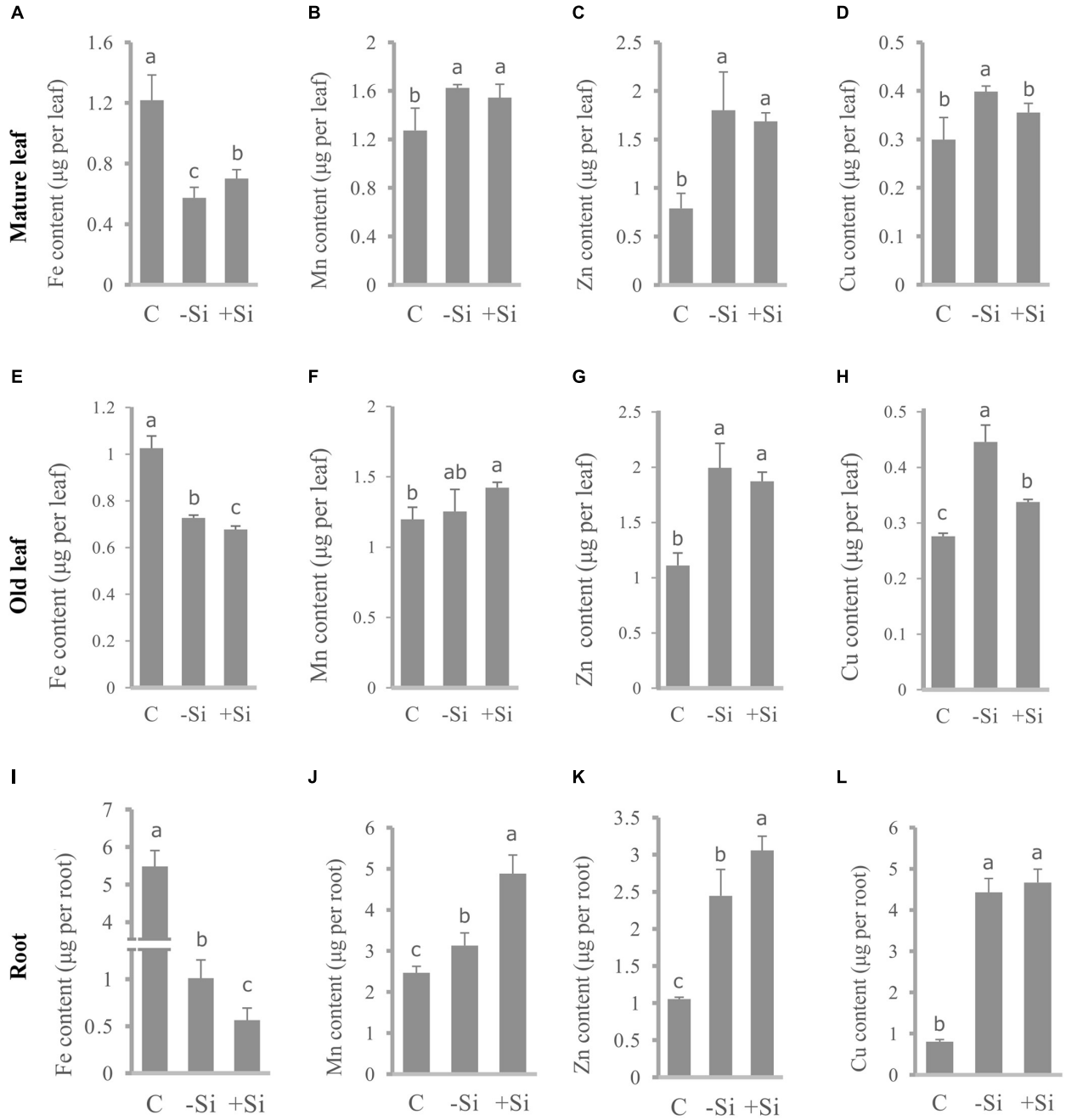

FIGURE 4 | Effect of Si nutrition on micronutrient content in different organs of barley, 3 weeks after Fe withdrawal. Mature leaf (second leaf, L2): **(A–D)**. Old leaf (first leaf, L1): **(E–H)**. Root: **(I–L)**. Content of Fe: **(A,E,I).** Content of Mn: **(B,F,J)**. Content of Zn: **(C,G,K)**. Content of Cu: **(D,H,L)**. The plants were treated as described in the legend of **Figure 1** (C- control plants grown optimally supplied with Fe; −Si – plants grown in the absence of Fe and Si; +Si – plants grown in the absence of Fe and supplied with Si). Data shown are means ± s.d. (n = 3). Significant differences ($P < 0.05$) between treatments are indicated by different letters.

Si treatment, while SOD activity was not significantly changed (**Table 2**). APX and CAT are heme-containing enzymes and their activities are strongly dependent on Fe status, while SOD exists in three isoforms containing Fe, Mn, or Cu/Zn, allowing maintenance of enzyme activity in respect to metal availability. Important players in maintaining cellular redox homeostasis are components of the ascorbate – glutathione cycle. Among other functions, ASC and GSH are found to protect *Arabidopsis* from iron deficiency, preserving redox homeostasis and improving internal iron availability (Zaharieva et al., 2004; Ramírez et al., 2013). However, even though we found an increased GSH level in barley leaves as a response to Fe deprivation, the influence of Si was not detected. ASC content was not altered among the treatments (**Table 2**).

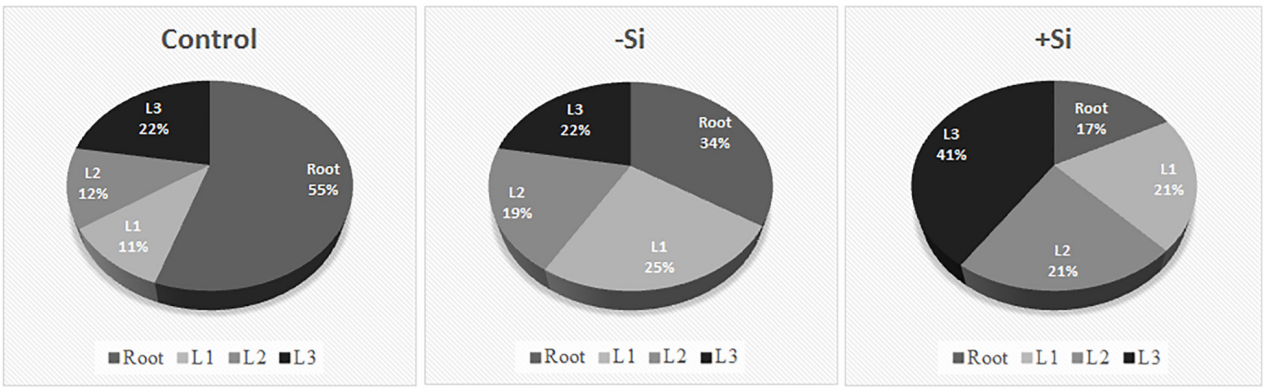

FIGURE 5 | Relative distribution of Fe content in different plant organs. Plants were treated as described in **Figure 1**. Leaf positions (from the base to the youngest leaf): L1, L2, L3.

As we assumed, silicon significantly increased the total iron content in the youngest leaves (**Figure 3A**), which was in accordance with a lower ROS level, elevated APX and CAT activities and chlorophyll level. It has already been shown that Si accelerates utilization of Fe from root apoplast in cucumber (Pavlovic et al., 2013). However, unlike the cucumber where the older leaves are the source of iron that is used for its Si-induced remobilization to younger leaves, we have found that in the barley the older leaves are of minor importance, with the main source of iron actually being the root.

The Fe pool translocated from root is much greater in Si supplied plants, compared to −Si plants, which constitutes a sufficient supply of Fe for the youngest leaves. It is also important to note that even though the root Fe content and concentration were depleted, roots of Si-fed plants appear to be superior in sustaining the stress, having higher biomass (DW) compared to roots of both −Si and control plants. It would suggest that Si does not stimulate remobilization of Fe from vital compartments, but rather from the deposits such as apoplast and root surface, which otherwise stay unused in −Si plants. In rice, the high resolution images, using SEM-EDX and LA-ICP-MS techniques, revealed that under Fe deficiency, Si supply has significantly decreased the Fe concentration in epidermal cells and root surface, but has, on the other hand, increased its concentration in the endodermal and vascular cylinder cells (Carrasco-Gil et al., 2018). The authors have suggested that the Fe plaque formed on root surface, during the Fe sufficient period, could function as an Fe source when plants need it.

The enhanced expression of the Fe acquisition genes in the early phase of the stress, as well as the greatly increased expression of the genes involved in phytosiderophores biosynthesis and transport in leaves, may have additively contributed to the efficient translocation of Fe from root to shoot.

Si led to an expedient increase in the expression of genes involved in Strategy II Fe acquisition in roots at the early stage of Fe deficiency stress. NA synthase and genes involved in phytosiderophore DMA synthesis and uptake of Fe-DMA complexes (*HvDMAS* and *HvYS1*) were induced by Si as soon as 5 h after withdrawal of Fe from the nutrient medium, while in the absence of Si a rise in their expression was delayed 1 or 2 days (**Figure 6**). Acceleration of gene expression response has previously been shown for Strategy I Fe acquisition genes *FRO2*, *IRT1,* and *HA1*, however the response was slower compared to the response of Strategy II genes examined in this study. Si-induced enhancement of their expression was greatest 1 and 3 days after Fe withdrawal (Pavlovic et al., 2013).

A dramatic increase in the expression of *HvNAS1* and *HvTOM1* genes in the leaves 3 days after Fe withdrawal (**Figure 7**) could play an important role in utilization and redistribution of iron within the shoot. *NAS1* encodes the enzyme responsible for biosynthesis of nicotianamine (NA), an important Fe ligand involved in Fe transport through phloem as well as in intracellular Fe chelation and short distance transport (Scholz et al., 1992; Hell and Stephan, 2003). Moreover, NA is also a biosynthetic precursor of deoxymugineic acid. *HvTOM1* is a phytosiderophore efflux transporter. The *TOM1* gene from rice was upregulated in both roots and leaves under Fe deficiency, and its promoter activity was detected in leaf phloem. *Xenopus laevis* oocytes expressing *TOM1* or *HvTOM1* were found to release DMA but not NA (Nozoye et al., 2011). It is possible that elevated expression of *HvNAS1* under the influence of Si, is necessary as an important step in DMA biosynthesis, and that phytosiderophores are crucial not only for Fe acquisition from the rhizosphere, but also in Fe utilization and re-translocation in the shoots of graminaceous plants. The importance of DMA in plant internal metal transport was suggested by chemical speciation of iron-binding ligands that revealed DMA as a dominant chelator in rice phloem sap (Nishiyama et al., 2012). Phytosiderophores were also detected in the xylem sap of rice and barley plants (Mori et al., 1991; Kawai et al., 2001).

Although we have not detected changes in *HvDMAS1* and *HvYS1* transcript levels in leaves, we cannot exclude the possibility of regulation of their expression on the post-transcriptional level. Besides, other members of the *YSL* gene family may also be influenced by Si.

Dynamics of the changes in gene expression suggest that processes important for Si-enhanced remobilization of Fe from root apoplast and translocation from root to shoot could occur

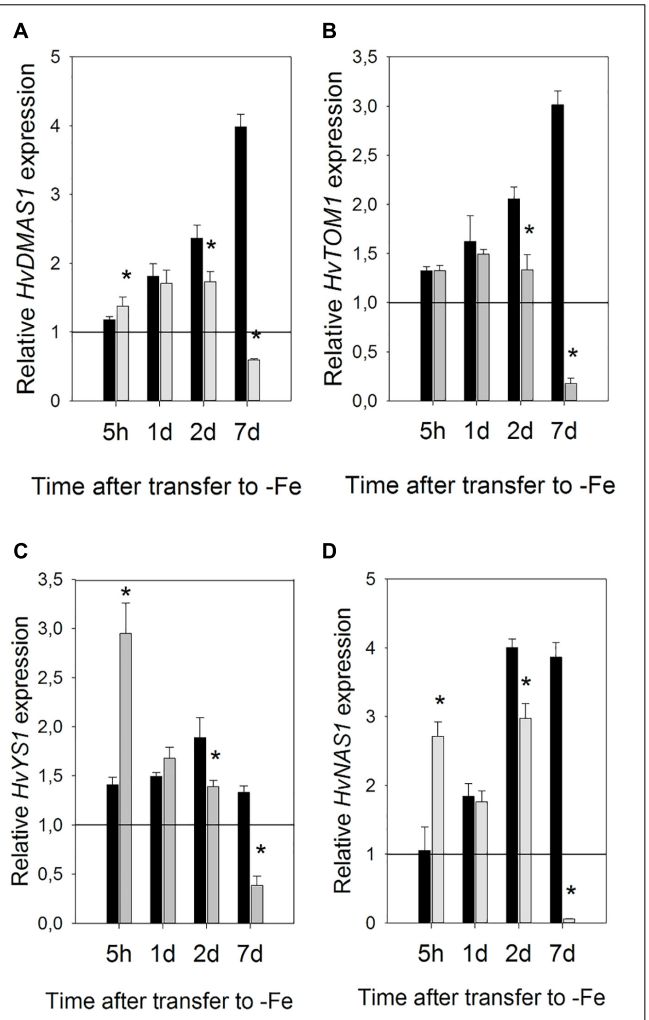

FIGURE 6 | Effect of Si supply on the relative expression level of **(A)** *HvDMAS*, **(B)** *HvTOM*, **(C)** *HvYS1* and **(D)** *HvNAS1* in barley roots 5 h and 1, 2, and 7 days after iron withdrawal from the nutrient solution. The plants were treated as described in the legend of **Figure 1** (−Si – plants grown in the absence of Fe and Si; +Si – plants grown in the absence of Fe and supplied with Si). Gene expression is normalized to the values obtained for control plants grown in optimal Fe supply, which was set to 1.0. Black bars −Si; gray bars +Si. Data shown are means ± s.d. (n = 3). Significant differences ($P < 0.05$) between −Si and +Si treatments for each time point are indicated by asterisks.

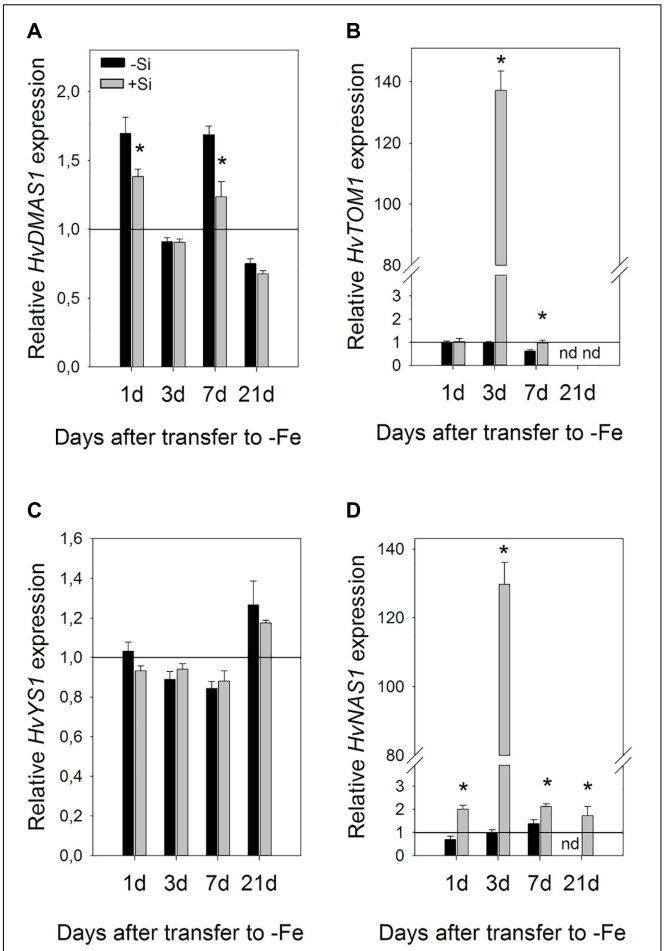

FIGURE 7 | Effect of Si supply on the relative expression level of **(A)** *HvDMAS*, **(B)** *HvTOM*, **(C)** *HvYS1,* and **(D)** *HvNAS1* in the barley leaves 1, 3, 7, and 21 days after iron withdrawal from the nutrient solution. The plants were treated as described in the legend of **Figure 1** (−Si – plants grown in the absence of Fe and Si; +Si – plants grown in the absence of Fe and supplied with Si). Gene expression is normalized to the values obtained for control plants grown in optimal Fe supply, which was set to 1.0. Black bars −Si; gray bars +Si. Data shown are means ± s.d. (n = 3). Significant differences ($P < 0.05$) between −Si and +Si treatments for each time point are indicated by asterisks.

mostly in the early phase of the stress response: in root already 5 h after Fe removal and in shoot around the third day. It is possible that the pool of Fe is firstly translocated from roots to the first leaves which are the only ones expanded by the 7th day, and that subsequently the pool is re-mobilized to the younger developing leaves.

It is also possible that Fe is translocated from root during expansion of the second and the third leaf, too, and that the pool of Fe is directly transferred from root to the leaf that is the youngest and developing in at that moment. Direct translocation of Fe from roots to young leaves via phloem, in graminaceous plants, have been indicated by the visualization of the real-time translocation of iron (Fe) in barley using a positron-emitting tracer imaging system (PETIS) (Tsukamoto et al., 2009). We have observed huge substantial changes only in HvTOM1 and HvNAS1 expression on the 3rd day, and smaller differences between treatments on the 7th and 21st, however, we have no insight into the fluctuation of the gene expression and production of phytosiderophores during the whole treatment and so that we cannot exclude the possibility that they fluctuate dynamically in order to support remobilization of Fe to developing leaves when it is needed the most.

Iron deficiency can perturb the homeostasis of some other essential elements. Increased concentrations of Mn, Co, Zn, and Cd were found in A. thaliana under iron deficiency (Baxter et al., 2008). Le et al. (2016) suggested that down-regulation of the Fe acquisition machinery in prolonged Fe deprivation is required in order to prevent damage from the accumulation of other metals.

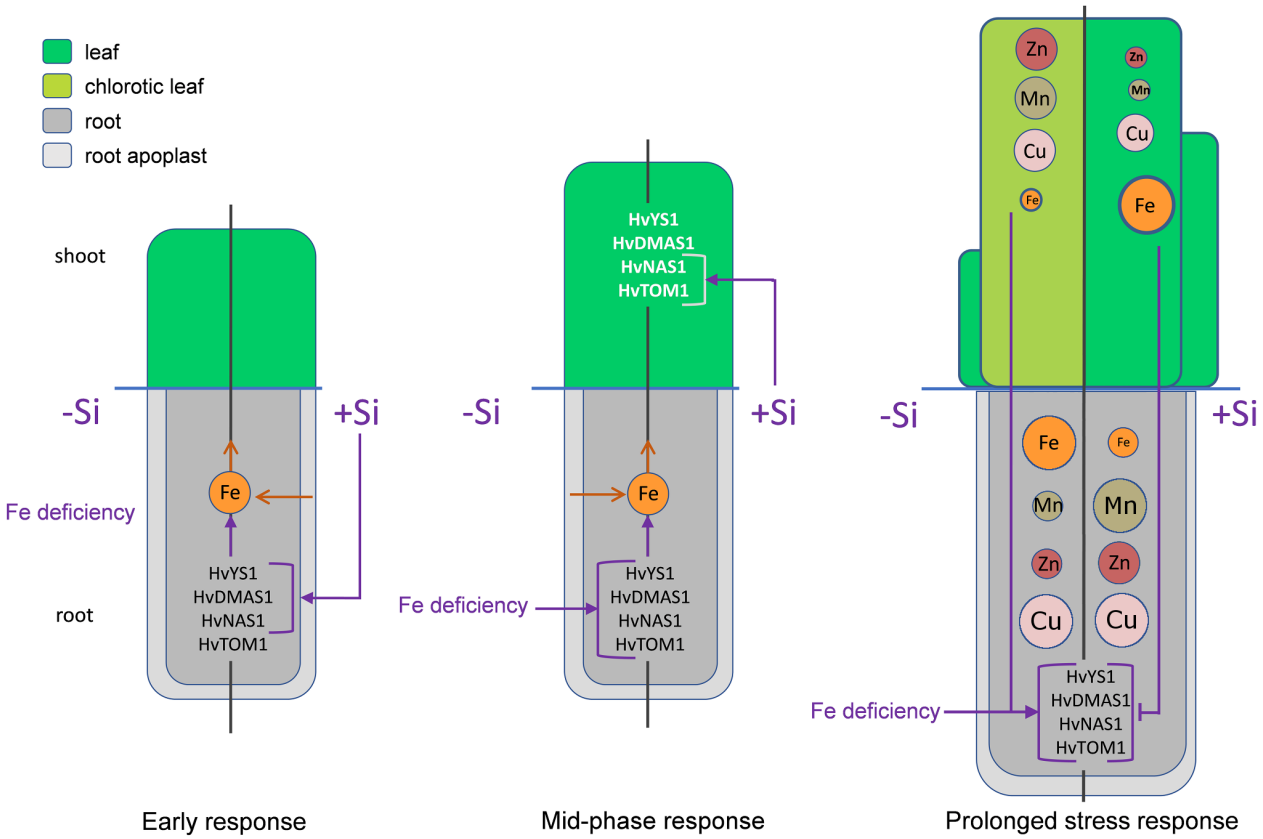

FIGURE 8 | The proposed model of Si-mediated alleviation of Fe deficiency in barley. In the early phase (5 h after Fe withdrawal) Si stimulates the expression of Strategy II genes in root, enhancing that way Fe uptake from the root apoplast and its remobilization toward shoot. In the mid-phase response (2 and 3 days after Fe withdrawal) the expression of Strategy II genes in root starts to increase under the influence of Fe deficiency. In this phase, Si enhances the expression of *HvTOM1* and *HvNAS1* in the leaf. As a consequence, after prolonged period of Fe deficiency, the status of Fe in the youngest leaf of Si treated plants is improved compared to the low Fe concentration in the plants grown without Si. Low Fe status in leaf of −Si plants is a signal for further increase in the gene expression in the root. On the contrary, improved Fe status in Si treated plants inhibits the expression of Strategy II genes. Another consequence of the reduced leaf Fe concentration is an increased uptake of other metals, which leads to elevated concentrations of Zn, Mn, and Cu in shoot. Si treatment increases concentrations and contents of Mn and Zn in root, resulting in decreased translocation toward shoot and lowered accumulation of these metals in the youngest leaves. The left halves of the schemes represent plants grown in the absence of Si, the right halves represent plants supplied with Si. Purple arrows – positive influence, purple T-end lines – inhibitory influence, brown open arrows – flow of the metal ions. Metal ions are represented by circles; the size of the circles in the youngest leaf corresponds to the concentration of the element.

As shown in **Table 3** and **Figure 3**, Si significantly decreased Mn, Zn, and Cu concentrations and Mn and Zn content in the youngest fully expanded leaves, contrary to its effect on Fe content. The reduced accumulation of Mn and Zn may have also contributed to the Si-induced lowering of ROS level. It is noteworthy that expression of all the examined genes remained elevated in roots even in prolonged iron deficiency in the absence of Si, while Si supply decreased greatly their expression on the seventh day of treatment (**Figure 6**). Fe acquisition machinery can only have positive effects on Fe uptake from root apoplast in the early stages of Fe deprivation, but in a longer period of total absence of Fe it cannot further improve Fe status. In our opinion, faster Fe mobilization in the root and its improved availability in leaves reduced Fe deficiency stress in Si treated plants, which resulted in decreased expression of Fe acquisition genes during prolonged treatment. Lowered expression of Strategy II genes in the prolonged stress may have led to the reduced uptake of some metal ions. However, the increased content of Mn and Zn in the root, while being lowered in the youngest leaves, may suggest that Si protects young, developing plant organs by retaining the potentially harmful metals in the root. Further investigation, employing imaging techniques, may give us information about localization and distribution of different metals within the root and contribute to elucidation of the mechanism of Si-induced metal deposition in root.

CONCLUSION

In conclusion, an ameliorative effect of Si on Fe deficiency in barley, a gramineous plant, was shown. Si improved Fe translocation from root to shoot, resulting in an increased Fe content in the youngest leaves. Another protective effect of Si during Fe deficiency stress was decreased accumulation

of Mn and Zn in the youngest leaves, by retaining them in root. The influence of Si on the genes involved in Strategy II Fe acquisition is presented for the first time, indicating a role of phytosiderophores in Si-induced stress alleviation. The expedient increase in the expression of Strategy II iron acquisition genes and *HvNAS1* in roots and strongly enhanced *HvTOM1* and *HvNAS1* expression in leaves, was observed in Si supplied plants. We propose a mechanism of Si protective activity in Fe deficient barley and its influence on Strategy II genes (**Figure 8**). Fe deficiency leads to low yield and plant fitness, but also to the reduced nutritional value of cereal crops widely used for human and animal consumption. In that light, formulation of new eco-friendly Si-based fertilizers might be an important approach to surmount these shortcomings.

AUTHOR CONTRIBUTIONS

DN designed and performed the experiments, analyzed data, and wrote the manuscript. SN performed the experiments and analyzed data. DB contributed to the experiments. LK performed ICP-OES measurements. MN and JS initiated the project, analyzed, and discussed the data.

FUNDING

This work was supported by the Serbian Ministry of Education, Science and Technological Development (Grant Nos. ON-173005 and ON-173028).

ACKNOWLEDGMENTS

We thank Nathaniel Aaron Sprinkle and Dr. Milorad Kojic (IMGGE) for English language editing.

SUPPLEMENTARY MATERIAL

The Supplementary Material for this article can be found online at: https://www.frontiersin.org/articles/10.3389/fpls.2019.00416/full#supplementary-material

REFERENCES

Aebi, H. (1984). [13] Catalase in vitro. *Methods Enzymol.* 105, 121–126. doi: 10.1016/S0076-6879(84)05016-3

Bashir, K., Inoue, H., Nagasaka, S., Takahashi, M., Nakanishi, H., Mori, S., et al. (2006). Cloning and characterization of deoxymugineic acid synthase genes from graminaceous plants. *J. Biol. Chem.* 281, 32395–32402. doi: 10.1074/jbc.M604133200

Baxter, I. R., Vitek, O., Lahner, B., Muthukumar, B., Borghi, M., Morrissey, J., et al. (2008). The leaf ionome as a multivariable system to detect a plant's physiological status. *Proc. Natl. Acad. Sci. U.S.A.* 105, 12081–12086. doi: 10.1073/pnas.0804175105

Bityutskii, N., Pavlovic, J., Yakkonen, K., Maksimović, V., and Nikolic, M. (2014). Contrasting effect of silicon on iron, zinc and manganese status and accumulation of metal-mobilizing compounds in micronutrient-deficient cucumber. *Plant Physiol. Biochem.* 74, 205–211. doi: 10.1016/j.plaphy.2013.11.015

Bityutskii, N., Yakkonen, K., and Zlotina, M. (2010). Vliyanie kremniya na proyavlenie khlorosa rasteniy v usloviyakh defizita zhelesa i marganza. *Agrokhimiia* 2:e51.

Boukhalfa, H., and Crumbliss, A. L. J. B. (2002). Chemical aspects of siderophore mediated iron transport. *Biometals* 15, 325–339. doi: 10.1023/A:1020218608266

Bradford, M. M. (1976). A rapid and sensitive method for the quantitation of microgram quantities of protein utilizing the principle of protein-dye binding. *Anal. Biochem.* 72, 248–254. doi: 10.1016/0003-2697(76)90527-3

Broadley, M. R. (2012). *Marschner's Mineral Nutrition of Higher Plants*. Amsterdam: Elsevier.

Carrasco-Gil, S., Rodríguez-Menéndez, S., Fernández, B., Pereiro, R., de la Fuente, V., Hernandez-Apaolaza, L. J. P. P., et al. (2018). Silicon induced Fe deficiency affects Fe, Mn, Cu and Zn distribution in rice (*Oryza sativa* L.) growth in calcareous conditions. *Plant Physiol. Biochem.* 125, 153–163. doi: 10.1016/j.plaphy.2018.01.033

Connorton, J. M., Balk, J., and Rodríguez-Celma, J. (2017). Iron homeostasis in plants–a brief overview. *Metallomics* 9, 813–823. doi: 10.1039/c7mt00136c

Coskun, D., Deshmukh, R., Sonah, H., Menzies, J. G., Reynolds, O., Ma, J. F., et al. (2019). The controversies of silicon's role in plant biology. *New Phytol.* 221, 67–85. doi: 10.1111/nph.15343

Curie, C., Panaviene, Z., Loulergue, C., Dellaporta, S. L., Briat, J.-F., and Walker, E. L. (2001). Maize yellow stripe1 encodes a membrane protein directly involved in Fe (III) uptake. *Nature* 409, 346–349. doi: 10.1038/35053080

Fourcroy, P., Tissot, N., Gaymard, F., Briat, J.-F., and Dubos, C. J. M. P. (2016). Facilitated Fe nutrition by phenolic compounds excreted by the *Arabidopsis* ABCG37/PDR9 transporter requires the IRT1/FRO2 high-affinity root Fe2+ transport system. *Mol. Plant* 9, 485–488. doi: 10.1016/j.molp.2015.09.010

Gattullo, C. E., Allegretta, I., Medici, L., Fijan, R., Pii, Y., Cesco, S., et al. (2016). Silicon dynamics in the rhizosphere: connections with iron mobilization. *J. Plant Nutr. Soil Sci.* 179, 409–417. doi: 10.1002/jpln.201500535

Giannopolitis, C., and Ries, S. (1977). Purification and quantitative relationship with water-soluble protein in seedling. *Plant Physiol.* 59, 315–318. doi: 10.1104/pp.59.2.315

Gonzalo, M. J., Lucena, J. J., and Hernández-Apaolaza, L. (2013). Effect of silicon addition on soybean (*Glycine max*) and cucumber (*Cucumis sativus*) plants grown under iron deficiency. *Plant Physiol. Biochem.* 70, 455–461. doi: 10.1016/j.plaphy.2013.06.007

Gottardi, S., Iacuzzo, F., Tomasi, N., Cortella, G., Manzocco, L., Pinton, R., et al. (2012). Beneficial effects of silicon on hydroponically grown corn salad (*Valerianella locusta* (L.) Laterr) plants. *Plant Physiol. Biochem.* 56, 14–23. doi: 10.1016/j.plaphy.2012.04.002

Guerinot, M. L., and Yi, Y. (1994). Iron: nutritious, noxious, and not readily available. *Plant Physiol.* 104, 815–820. doi: 10.1104/pp.104.3.815

Hell, R., and Stephan, U. W. (2003). Iron uptake, trafficking and homeostasis in plants. *Planta* 216, 541–551.

Hernandez-Apaolaza, L. (2014). Can silicon partially alleviate micronutrient deficiency in plants? a review. *Planta* 240, 447–458. doi: 10.1007/s00425-014-2119-x

Inoue, H., Kobayashi, T., Nozoye, T., Takahashi, M., Kakei, Y., Suzuki, K., et al. (2009). Rice OsYSL15 is an iron-regulated iron (III)-deoxymugineic acid transporter expressed in the roots and is essential for iron uptake in early growth of the seedlings. *J. Biol. Chem.* 284, 3470–3479. doi: 10.1074/jbc.M806042200

Ishimaru, Y., Suzuki, M., Tsukamoto, T., Suzuki, K., Nakazono, M., Kobayashi, T., et al. (2006). Rice plants take up iron as an Fe3+-phytosiderophore and as Fe2+. *Plant J.* 45, 335–346. doi: 10.1111/j.1365-313X.2005.02624.x

Kawai, S., Kamei, S., Matsuda, Y., Ando, R., Kondo, S., Ishizawa, A., et al. (2001). Concentrations of iron and phytosiderophores in xylem sap of iron-deficient barley plants. *Soil Sci. Plant Nutr.* 47, 265–272. doi: 10.1080/00380768.2001.10408390

Le, C. T. T., Brumbarova, T., Ivanov, R., Stoof, C., Weber, E., Mohrbacher, J., et al. (2016). Zinc finger of arabidopsis thaliana12 (zat12) interacts with fer-like iron deficiency-induced transcription factor (fit) linking iron deficiency

and oxidative stress responses. *Plant Physiol.* 170, 540–557. doi: 10.1104/pp.15.01589

Liang, Y., Nikolic, M., Bélanger, R., Gong, H., and Song, A. (2015). *Silicon in Agriculture. Silicon in Agriculture: from Theory to Practice*. Berlin: Springer, 45–68. doi: 10.1007/978-94-017-9978-2

Ma, J. F., and Yamaji, N. (2006). Silicon uptake and accumulation in higher plants. *Trends Plant Sci.* 11, 392–397. doi: 10.1016/j.tplants.2006.06.007

Marschner, H., and Römheld, V. (1994). Strategies of plants for acquisition of iron. *Plant Soil* 165, 261–274. doi: 10.1007/BF00008069

Mittler, R., Vanderauwera, S., Gollery, M., and Van Breusegem, F. (2004). Reactive oxygen gene network of plants. *Trends Plant Sci.* 9, 490–498. doi: 10.1016/j.tplants.2004.08.009

Mori, S. (1999). Iron acquisition by plants. *Curr. Opin. Plant Biol.* 2, 250–253. doi: 10.1016/S1369-5266(99)80043-0

Mori, S., Nishizawa, N., Hayashi, H., Chino, M., Yoshimura, E., and Ishihara, J. (1991). "Why are young rice plants highly susceptible to iron deficiency?," in *Iron Nutrition and Interactions in Plants*, ed. Y. Chen (Berlin: Springer), 175–188.

Murata, Y., Ma, J. F., Yamaji, N., Ueno, D., Nomoto, K., and Iwashita, T. (2006). A specific transporter for iron (III)–phytosiderophore in barley roots. *Plant J.* 46, 563–572. doi: 10.1111/j.1365-313X.2006.02714.x

Nakano, Y., and Asada, K. (1981). Hydrogen peroxide is scavenged by ascorbate-specific peroxidase in spinach chloroplasts. *Plant Cell Physiol.* 22, 867–880.

Nishiyama, R., Kato, M., Nagata, S., Yanagisawa, S., and Yoneyama, T. (2012). Identification of Zn–nicotianamine and Fe–2'-deoxymugineic acid in the phloem sap from rice plants (*Oryza sativa* L.). *Plant Cell Physiol.* 53, 381–390. doi: 10.1093/pcp/pcr188

Nozoye, T., Nagasaka, S., Kobayashi, T., Takahashi, M., Sato, Y., Sato, Y., et al. (2011). Phytosiderophore efflux transporters are crucial for iron acquisition in graminaceous plants. *J. Biol. Chem.* 286, 5446–5454. doi: 10.1074/jbc.M110.180026

Pavlovic, J., Samardzic, J., Kostic, L., Laursen, K. H., Natic, M., Timotijevic, G., et al. (2016). Silicon enhances leaf remobilization of iron in cucumber under limited iron conditions. *Ann. Bot.* 118, 271–280. doi: 10.1093/aob/mcw105

Pavlovic, J., Samardzic, J., Maksimović, V., Timotijevic, G., Stevic, N., Laursen, K. H., et al. (2013). Silicon alleviates iron deficiency in cucumber by promoting mobilization of iron in the root apoplast. *New Phytol.* 198, 1096–1107. doi: 10.1111/nph.12213

Pedas, P., Stokholm, M. S., Hegelund, J. N., Ladegård, A. H., Schjoerring, J. K., and Husted, S. (2014). Golgi localized barley MTP8 proteins facilitate Mn transport. *PLoS One* 9:e113759. doi: 10.1371/journal.pone.0113759

Pedas, P., Ytting, C. K., Fuglsang, A. T., Jahn, T. P., Schjoerring, J. K., and Husted, S. (2008). Manganese efficiency in barley: identification and characterization of the metal ion transporter HvIRT1. *Plant Physiol.* 148, 455–466. doi: 10.1104/pp.108.118851

Pfaffl, M. W. (2001). A new mathematical model for relative quantification in real-time RT–PCR. *Nucleic Acids Res.* 29:e45. doi: 10.1093/nar/29.9.e45

Pontigo, S., Ribera, A., Gianfreda, L., de la Luz Mora, M., Nikolic, M., and Cartes, P. (2015). Silicon in vascular plants: uptake, transport and its influence on mineral stress under acidic conditions. *Planta* 242, 23–37. doi: 10.1007/s00425-015-2333-1

Ramírez, L., Bartoli, C. G., and Lamattina, L. (2013). Glutathione and ascorbic acid protect *Arabidopsis* plants against detrimental effects of iron deficiency. *J. Exp. Bot.* 64, 3169–3178. doi: 10.1093/jxb/ert153

Ranieri, A., Castagna, A., Baldan, B., and Soldatini, G. F. (2001). Iron deficiency differently affects peroxidase isoforms in sunflower. *J. Exp. Bot.* 52, 25–35. doi: 10.1093/jexbot/52.354.25

Ryzhenko, N. O., Kavetsky, S., and Kavetsky, V. M. (2016). Heavy Metals (Cd, Pb, Zn, and Cu) uptake by spring barley in polluted soils. *Pol. J. Soil Sci.* 48:111.

Schmid, W. E., and Gerloff, G. C. (1961). A naturally occurring chelate of iron in xylem exudate. *Plant Physiol.* 36:226. doi: 10.1104/pp.36.2.226

Scholz, G., Becker, R., Pich, A., and Stephan, U. (1992). Nicotianamine-a common constituent of strategies I and II of iron acquisition by plants: a review. *J. Plant Nutr.* 15, 1647–1665. doi: 10.1080/01904169209364428

Stevic, N., Korac, J., Pavlovic, J., and Nikolic, M. (2016). Binding of transition metals to monosilicic acid in aqueous and xylem (*Cucumis sativus* L.) solutions: a low-T electron paramagnetic resonance study. *Biometals* 29, 945–951. doi: 10.1007/s10534-016-9966-9

Sun, B., Jing, Y., Chen, K., Song, L., Chen, F., and Zhang, L. (2007). Protective effect of nitric oxide on iron deficiency-induced oxidative stress in maize (*Zea mays*). *J. Plant Physiol.* 164, 536–543. doi: 10.1016/j.jplph.2006.02.011

Tommasi, F., Paciolla, C., de Pinto, M. C., and Gara, L. D. (2001). A comparative study of glutathione and ascorbate metabolism during germination of *Pinus pinea* L. seeds. *J. Exp. Bot.* 52, 1647–1654. doi: 10.1093/jexbot/52.361.1647

Tsukamoto, T., Nakanishi, H., Uchida, H., Watanabe, S., Matsuhashi, S., Mori, S., et al. (2009). (52)Fe translocation in barley as monitored by a positron-emitting tracer imaging system (PETIS): evidence for the direct translocation of Fe from roots to young leaves via phloem. *Plant Cell Physiol.* 50, 48–57. doi: 10.1093/pcp/pcn192

Vidović, M., Morina, F., Milić, S., Albert, A., Zechmann, B., Tosti, T., et al. (2015). Carbon allocation from source to sink leaf tissue in relation to flavonoid biosynthesis in variegated Pelargonium zonale under UV-B radiation and high PAR intensity. *Plant Physiol. Biochem.* 93, 44–55. doi: 10.1016/j.plaphy.2015.01.008

Zaharieva, T., Gogorcena, Y., and Abadì, J. (2004). Dynamics of metabolic responses to iron deficiency in sugar beet roots. *Plant Sci.* 166, 1045–1050. doi: 10.1016/j.plantsci.2003.12.017

Zhang, Z. C., and Qiu, B. S. (2007). Reactive oxygen species metabolism during the cadmium hyperaccumulation of a new hyperaccumulator *Sedum alfredii* (Crassulaceae). *J. Environ. Sci.* 19, 1311–1317. doi: 10.1016/S1001-0742(07)60214-9

Conflict of Interest Statement: The authors declare that the research was conducted in the absence of any commercial or financial relationships that could be construed as a potential conflict of interest.

frontiers in Plant Science

ORIGINAL RESEARCH
published: 05 April 2019
doi: 10.3389/fpls.2019.00413

Eco-Friendly Iron-Humic Nanofertilizers Synthesis for the Prevention of Iron Chlorosis in Soybean (*Glycine max*) Grown in Calcareous Soil

María T. Cieschi[1], Alexander Yu Polyakov[2,3], Vasily A. Lebedev[4], Dmitry S. Volkov[4,5], Denis A. Pankratov[4], Alexey A. Veligzhanin[6], Irina V. Perminova[4] and Juan J. Lucena[1]**

[1] Department of Agricultural Chemistry and Food Science, Autonomous University of Madrid, Madrid, Spain, [2] Kurnakov Institute of General and Inorganic Chemistry, Russian Academy of Sciences, Moscow, Russia, [3] Department of Materials Science, Lomonosov Moscow State University, Moscow, Russia, [4] Department of Chemistry, Lomonosov Moscow State University, Moscow, Russia, [5] Department of Chemistry and Physical Chemistry of Soils, V.V. Dokuchaev Soil Science Institute, Moscow, Russia, [6] National Research Center "Kurchatov Institute", Moscow, Russia

OPEN ACCESS

Edited by:
Thomas J. Buckhout,
Humboldt-Universität zu Berlin,
Germany

Reviewed by:
Roberto Pinton,
University of Udine, Italy
Zeno Varanini,
University of Verona, Italy

***Correspondence:**
Irina V. Perminova
iperm@org.chem.msu.ru
Juan J. Lucena
juanjose.lucena@uam.es

Specialty section:
This article was submitted to Plant Nutrition, a section of the journal Frontiers in Plant Science

Received: 14 January 2019
Accepted: 19 March 2019
Published: 05 April 2019

Citation:
Cieschi MT, Polyakov AY, Lebedev VA, Volkov DS, Pankratov DA, Veligzhanin AA, Perminova IV and Lucena JJ (2019) Eco-Friendly Iron-Humic Nanofertilizers Synthesis for the Prevention of Iron Chlorosis in Soybean (Glycine max) Grown in Calcareous Soil. Front. Plant Sci. 10:413. doi: 10.3389/fpls.2019.00413

Iron deficiency is a frequent problem for many crops, particularly in calcareous soils and iron humates are commonly applied in the Mediterranean basin in spite of their lesser efficiency than iron synthetic chelates. Development and application of new fertilizers using nanotechnology are one of the potentially effective options of enhancing the iron humates, according to the sustainable agriculture. Particle size, pH, and kinetics constrain the iron humate efficiency. Thus, it is relevant to understand the iron humate mechanism in the plant–soil system linking their particle size, characterization and iron distribution in plant and soil using ^{57}Fe as a tracer tool. Three hybrid nanomaterials (F, S, and M) were synthesized as iron-humic nanofertilizers (^{57}Fe-NFs) from leonardite potassium humate and ^{57}Fe used in the form of $^{57}Fe(NO_3)_3$ or $^{57}Fe_2(SO_4)_3$. They were characterized using Mössbauer spectroscopy, X-ray diffraction (XRD), extended X-ray absorption fine structure spectroscopy (EXAFS), transmission electron microscopy (TEM) and tested for iron availability in a calcareous soil pot experiment carried out under growth chamber conditions. Three doses (35, 75, and 150 μmol pot^{-1}) of each iron-humic material were applied to soybean iron deficient plants and their iron nutrition contributions were compared to ^{57}FeEDDHA and leonardite potassium humate as control treatments. Ferrihydrite was detected as the main structure of all three ^{57}Fe-NFs and the plants tested with iron-humic compounds exhibited continuous long-term statistically reproducible iron uptake and showed high shoot fresh weight. Moreover, the ^{57}Fe from the humic nanofertilizers remained available in soil and was detected in soybean pods. The Fe-NFs offers a natural, low cost and environmental option to the traditional iron fertilization in calcareous soils.

Keywords: iron nanoparticles, iron nutrition, humic substances, leonardite, ^{57}Fe, soybean, ferrihydrite

INTRODUCTION

Iron (Fe) is an essential micronutrient for humans and plants. Iron deficiency is very common in the human diet and affects an estimated two billion people in the world (Briat et al., 2015). Iron chlorosis is a widespread agricultural problem occurring in about 30–50% of cultivated soils (Cakmak, 2002) and one of the major limiting factor of crop production in calcareous soils. Farmers apply iron synthetic chelates to alleviate iron deficiency in cash crops. Despite the high costs of these fertilizers, they tend to lixiviate and the chelating agents may avoid the precipitation and enhance mobilization of heavy metals (Ylivainio, 2010). Many crops are sensitive to the iron chlorosis, such as citrus and fruit trees but soybean (*Glycine max* L.) is one of the most studied iron Strategy I plant (Fuentes et al., 2018). Moreover, soybean production reaches levels of about 230 million metric tons per year across the world (Vasconcelos and Grusak, 2014) and this legume is a highly nutritious crop which contains more protein (40%) and oil (20%) than any other ordinary food source (Bolon et al., 2010).

According to the United Nations [UN] (2013), the rapidly growing world population is projected to reach 9.6 billion by the year 2050 and Food and Agriculture Organization of the United Nations [FAO] (2017) has predicted that the global grain production is required to increase by 70% to meet these demands. Therefore, new approaches should be developed for alleviation of iron deficiency in plants and new ecofriendly fertilizers are needed in order to enhance crop environmental quality. Iron fertilizers based on HSs extracted from lignites, such as leonardite, are used in the Mediterranean area (as liquid concentrates) in drip irrigation (Kovács et al., 2013). This kind of iron fertilizers is more ecofriendly than synthetic iron chelates but they are less efficient in correcting iron chlorosis. Moreover, field experiments have demonstrated that the synthetic chelate has a fast effect while the iron humate fertilizers provide increasing iron availability in the root–soil interface resulting in slow uptake of Fe by the plants (Cieschi et al., 2017). Kulikova et al. (2017) have demonstrated that only iron from very small and amorphous nanoparticles of ferric polymers incorporated into humic matrix is readily taken up by plants. Therefore, the synthesis of iron humates should be optimized for developing efficient NFs.

According to Naderi and Danesh-Shahraki (2013), NFs are the most important products of nanotechnology with regard to agriculture. Nanosized active ingredients (from 1 to 100 nm in diameter) have a large specific surface area that can result in significantly enhanced reactivity, and this feature increases absorption of nutritional elements and essential compounds for plant growth and plant metabolism (Janmohammadi et al., 2016). Many attempts has been made to prepare inorganic Fe nanofertilizers. As example Sánchez-Alcalá et al. (2012) synthesized nanosiderite ($FeCO_3$) and demonstrated that it was highly effective in preventing iron chlorosis in chickpea and had a great residual effect. Ghafariyan et al. (2013) reported that low concentrations of superparamagnetic Fe-NPs significantly increased the chlorophyll contents in sub-apical leaves of soybeans in a greenhouse test under hydroponic conditions, suggesting that soybean could use this type of Fe-NPs as source of Fe and reduce chlorotic symptoms of Fe deficiency. However, the research on natural Fe nano-humate complexes is now in progress. Dholakia (2016) developed the preparation of nanoparticulate liquid organic fertilizers employing humic acids. In addition, Kulikova et al. (2017) have synthesized well-defined iron (hydr)oxide NPs of feroxyhyte stabilized by traces of HS (a model of iron-based engineered NPs) and water-soluble Fe-HS complexes of the proven high availability to plants tested their iron materials in wheat plants under hydroponic conditions. These promising results motivated us to follow the research on Fe NFs stabilized with humates.

According to Dimkpa and Bindraban (2017), up to now, the bulk of research in plant nanoscience either consists of experiments conducted in artificial media, such as nutrient solutions, agar, sand, or other non-soil media. Moreover, Liu and Lal (2015) recommend that micronutrient research should focus on enhancing the bioavailability (plant-uptake rate) of NFs to address the field leaching associated with the conventional micronutrient fertilizers and compare the beneficial effects of these micronutrient NFs with commercially available micronutrient counterparts [e.g., FeNPs vs. $FeCl_3$ or Fe(EDTA) as Fe sources] under the field condition. Therefore, it is of particular importance to test the ^{57}Fe-NFs in a soil system in a long-term experiment which would enable for completion of the full growth cycle crop in order to be closer to agronomical conditions. Since the efficacy of an iron fertilizer is related to the iron that the plants can take from the fertilizer, the use of iron isotopes is highly beneficial for monitoring iron uptake by plants (Cesco et al., 2002; Nikolic et al., 2003; Tomasi et al., 2013). The use of stable Fe isotopes instead of radioactive ones gives a high flexibility in the experimental designs and can include field studies, because special safety measurements and trained staff are not required. Moreover, long-term assays can be carried out without taking care of radioactivity decay over time. In addition, the generation of radioactive wastes is avoided (Benedicto et al., 2011). Many studies about ^{57}Fe application in soils experiments (Nadal et al., 2012; Martín-Fernández et al., 2017a,b) were reported, but this work is the first one in preparing ^{57}Fe-NFs and applying them in a calcareous soil.

Here, three ^{57}Fe-labeled humic nanomaterials (F, S, and M) were synthesized using potassium humate as a parent humic material and ^{57}Fe in the form of $^{57}Fe(NO_3)_3$ (product F) and $^{57}Fe_2(SO_4)_3$ (products S and M), characterized for iron speciation and phase composition of nanoparticles, and tested

Abbreviations: ^{57}Fe-NFs, iron-humic nanofertilizers isotopically labeled; ANOVA, analysis of variance; DAF, days after fertilizers applications; DTPA, diethylenetriaminepentaacetic acid; E.C., electrical conductivity; ED, electron diffraction; EELS, electron energy loss spectra; EXAFS, extended X-ray absorption fine structure spectroscopy; Fe-MCC, iron-maximum complexing capacity; Fe-Nps, iron nanoparticles; FeHBED, iron (III) *N*,*N*'-bis(*o*-hydroxybenzyl)-ethylenediamine-*N*,*N*'-diacetic acid complex; HEPES, *N*-(2-hydroxyethyl) piperazine *N*'-(2-ethanesulfonic acid); HS, humic substances; ICP-OES, inductively coupled plasma – optical emission spectrometry; ICP-MS, inductively coupled plasma mass spectrometry; L, leonardite potassium humate; NFs, nanofertilizers; *o*-*o*EDDHA, ethylenediamine-di (*o*-*o* hydroxyphenylacetic acid); OM, soil organic matter; SAED, selected area electron diffraction; SPAD, soil–plant analysis development; TEM, transmission electron microscopy; XANES, X-ray absorption near edge structure; XAS, X-ray absorption spectra; XRD, X-ray diffraction.

for bioavailability to soybean iron deficient plants grown in calcareous soils under growth chamber conditions. This was to establish a link between the Fe-NPs characteristics and their behavior in the soil–plant system using ^{57}Fe as a tracer tool.

MATERIALS AND METHODS

Reagents

All reagents used were of recognized analytical grade, and solutions were prepared with type-I grade water (ISO 3696:1987, 1987) free of organic contaminants (Millipore, Milford, CT, United States).

Synthesis of ^{57}Fe-NFs

Prior to the synthesis, a known weight of leonardite potassium humate (C 34.9%, H 3.89%, N 0.72%, S 0.06%, Fe 0.45%) (Powhumus, Humintech Ltd., Germany) was dissolved in distilled water and centrifuged at 10,000 min^{-1} for 10 min to separate and discard any insoluble mineral components. The obtained solution contained 70 g L^{-1} of leonardite potassium humate (L solution) and was used for the further NF synthesis.

A $^{57}Fe_2(SO_4)_3$ solution (0.20 M in ^{57}Fe) was prepared from metallic ^{57}Fe (Isoflex, 96.28% ^{57}Fe isotopic enrichment) by dissolving 0.4008 g in 34 mL 1M H_2SO_4 and heating till complete dissolution. After that, two products (S and M) were obtained by interaction of potassium humate with $^{57}Fe_2(SO_4)_3$ solution. In brief, the product S was synthesized as in Sorkina et al. (2014), 17 mL of 0.2M $^{57}Fe_2(SO_4)_3$ solution was added dropwise to 14.3 mL of the L solution and pH was maintained at a value of 10 by adding slowly 1M KOH when needed. For the synthesis of the product M, 17 mL of $^{57}Fe_2(SO_4)_3$ solution was slowly added to 40 mL of L solution, maintaining the pH at 9 with 1M KOH. The product M was prepared with the 90% of its maximum complexing capacity (Fe-MCC). Determination of Fe-MCC was conducted as described in Villén et al. (2007) and presented in the **Supplementary Figure SM1**. According to the obtained titration curve, an amount of 190 mg of Fe (III) per g org C^{-1} was necessary to obtain 200 mg of complexed Fe (III) per g org C^{-1} at the MCC.

Similarly, for the preparation of F product, a $^{57}Fe(NO_3)_3$ solution was prepared from the same metallic ^{57}Fe by dissolving 0.2004 g in 5 mL HNO_3 (70%, 1,401 g/mL density) and then diluted. The obtained solution was added dropwise to 32 mL of the L solution, maintaining the pH at 9 with 1M KOH.

In all syntheses described above, the final reaction mixtures were frozen "as is" using liquid N_2 and freeze-dried using Labconco FreeZone freeze dry system (-50°C, 0.03 mbar pressure).

It should be noted, that the high hydrolysis rate is required to obtain ultradispersed (nanosized) iron (hydr)oxide nanoparticles from iron (III) sulfate or nitrate solutions. For this, we added $^{57}Fe_2(SO_4)_3$ and $^{57}Fe(NO_3)_3$ dropwise but rapidly to the strongly alkaline medium of potassium humate solution and prevented the pH drop by simultaneous addition of KOH. The pH values between 9 and 10 were chosen to ensure formation of the disordered and chemically labile iron oxy-hydroxide phases instead of well-crystalline iron oxides like Fe_3O_4, Fe_2O_3 or rigid α-FeOOH.

The content of soluble iron in the synthesized fertilizers was determined using ICP AES. It was (in % mass) 2.9, 2.3, and 2.1 in the samples F, S, and M, respectively. The Fe:org C ratios were 0.27, 0.52, and 0.12 (g Fe g C org^{-1}) in the samples F, S, and M, respectively.

Characterization of ^{57}Fe-NFs

The freeze dried preparations of ^{57}Fe-NFs were exhaustively characterized using XRD, TEM with ED, EELS and energy filtered transmission electron microscopy (EFTEM), X-ray absorption spectroscopy (XANES and EXAFS) and Mössbauer spectroscopy. The XRD patterns were collected at CuKα on Rigaku D-MAX 2500 diffractometer in Theta/2Theta geometry. Reference samples, such as ferrihydrite and goethite were synthesized according to the procedure proposed by Schwertmann and Cornell (1992) and described by López-Rayo et al. (2015).

The TEM data were obtained with the use of Zeiss Libra 200MC microscope, equipped with monochromator and Omega-filter. For the TEM measurements, samples were dissolved in distilled water, dropped on the lacey-carbon coated copper grid for the few minutes with the following removal of the solution excess to reduce the concentration of mineral salts in the sample. Details of energy filtered TEM and SAED acquisition and processing are described in the corresponding part and in **Supplementary Materials**. Image processing was performed with the use of Gwyddion (Nečas and Klapetek, 2012), further data treatment – with the use of *scipy* and *matplotlib* (Hunter, 2007). The EELS spectra were acquired using the omega-filter, and integrated with DigitalMicrograph2 (DM2) software, Gatan. The variable slit of 3.5 eV width was placed in the Omega-filter to select the elastic part of scattered electrons. Two EFTEM images were collected with the background signal differing in intensity in the pre-edge energy area, and one image – with the combined signals of iron and background – was collected on the Fe M-line. Final iron distribution map was calculated using the DM2 software.

X-ray absorption spectra were measured at the STM beamline of Kurchatov Synchrotron Source facility, National Research Center "Kurchatov Institute", Moscow, Russia. The Si (111) channel-cut monochromator was used. Ionization chambers with length of 10 cm filled with argon were used as detectors of incidence and transmitted beams. The samples were used as dry powders mounted onto the kapton tape. Thickness of each sample was adjusted to yield the absorption value of 3. All spectra for the iron-containing NFs under study and the iron (hydr)oxide references were measured by absorption using Fe foil as a reference sample. XAS of the parent humate (L) was measured using fluorescence due to the low iron content in this sample. The Amptek X-123 SDD detector was used for this purpose. Six spectra were acquired for each sample and averaged. All spectra were handled with the use of Athena software. The further modeling and refinements were done using the Artemis software. Refinements were performed by k^2-weighted spectra in the range of 3–14 Å^{-1} in the k-space, and of 1–3.5 Å in the R-space, Hanning window

function was used. The value of S_0^2 = 1 was fixed during the refinements.

Mössbauer absorption spectra were obtained on MS1104EM Express Mössbauer spectrometer (Cordon GmbH, Rostov-on-Don). The radiation source with an activity of 6 mCi was ^{57}Co in a metal rhodium matrix (RITVERC GmbH, St. Petersburg, Russia). The spectra were obtained at room temperature (295 ± 3 K) and in a vacuumed cryostat at a liquid nitrogen temperature (77.5 ± 0.5 K). The spectra were collected until the signal to noise ratio was less than 1%. Mathematical processing was carried out for spectra with a high resolution (1,024 points) using SpectrRelax 2.4 (Lomonosov MSU, Russia) software. The isomer shift was determined relative to α Fe.

Soil Pot Experiment

Fertilizers

A stock solution (1,000 μmol Fe L^{-1}) of each ^{57}Fe-humic NF (F, S, and M) at pH 7 was prepared from the freeze dried products (^{57}Fe-NFs) previously obtained, as it was described above A stock solution of ^{57}FeEDDHA (1,000 μmol Fe L^{-1}) was prepared by chelation with Fe^{3+} from $Fe(NO_3)_3$ and *o-o*EDDHA [ethylenediamine-di (*o-o* hydroxyphenylacetic acid)] obtained from LGC Standards, Teddington, United Kingdom (93.12%), previously dissolved with three mol of NaOH per mol of chelating agent. The solution was adjusted at pH 7 with 1M KOH.

In order to test the ^{57}Fe-NFs as correctors of iron chlorosis, three doses (35, 75, and 150 μmol ^{57}Fe pot^{-1}) were applied to iron deficient soybean plants and compared to ^{57}FeEDDHA (50 μmol pot^{-1}), as a positive control, and L (providing 8.9 μmol Fe pot^{-1}). The treatments were applied over the soil surface 2 days after the soybean plants were transferred to the pots. Five replicates (five pots) per fertilizer were carried out.

Plant Material

Soybeans (*Glycine max AG1835* Asgrow Seed Co.) were germinated in the dark at room temperature on filter paper moistened with distilled water. After germination (7 days), seedlings were transferred to the growth chamber where they grew until the end of the experiment in a Dycometal-type CCK growth chamber provided with fluorescent and sodium vapor lamps with a 16 h, 25°C and 40% humidity day and 8 h, 20°C and 60% humidity night regime. Seedlings were placed on containers filled with 1/5 diluted nutrient solution of the full-strength solution with the following composition: macronutrients (mM) 1.0 $Ca(NO_3)_2$, 0.9 KNO_3, 0.3 $MgSO_4$, and 0.1 KH_2PO_4; cationic micronutrients (μM) 2.0 FeHBED, 2.5 $MnSO_4$, 1.0 $CuSO_4$, 10.0 $ZnSO_4$, 1.0 $CoSO_4$, 1.0 $NiCl_2$, and 115.5 $EDTANa_2$; anionic micronutrients (μM) 35.0 NaCl, 10.0 H_3BO_3, and 0.05 Na_2MoO_4 and 0.1 mM HEPES. The pH was adjusted to 7.5 with 1.0M KOH. After 8 days, the diluted nutrient solution was replaced by the full-strength solution without Fe. Seedlings were kept in this solution for 2 days in order to induce iron deficiency. In order to simulate calcareous conditions, $CaCO_3$ (0.1 g L^{-1}) was added to each pot. The deficient iron soybean plants (three plants per pot) were transferred into 600 g polystyrene pots filled in with the soil/sand 70/30% (w/w) mixture. The soil was obtained from the top 20 cm of a citrus farm at Picassent, Valencia, Spain (39°21′41.28″ N, 0°27′42.58″ W). Physicochemical characteristics of this soil are described in **Table 1**. Texture, pH, soil E.C., OM, C/N ratio, $CaCO_3$ were measured according to the official methods (MAPA, 1994) and micronutrients availability was determined as described by Soltanpour and Schwab (1977). Normalized calcareous sand (2–4 mm) was used. One day before transferring the seedlings, pots were irrigated till field capacity. Water and iron free nutrient solution were added every day. Two samplings were carried out, at 15 and 48 days after the fertilizers (DAF) were applied.

TABLE 1 | Physical and chemical properties of the soil used for both pot experiments.

Parameter	Picassent soil
[1]Sand (g · kg^{-1})	435
[1]Silt (g · kg^{-1})	80
[1]Clay (g · kg^{-1})	485
pH (H_2O)	7.9
$E.C._{1:5}$ (dS m^{-1})	2.0
[2]OM (g kg^{-1})	9.2
[3]N Kjeldahl (g kg^{-1})	0.3
C/N	30.7
[5]$CaCO_3$ (g · kg^{-1})	380
[6]$CaCO_3$ active (g · kg^{-1})	89
[8]DTPA Zn (mg · kg^{-1})	3.00
[8]DTPA Fe (mg · kg^{-1})	5.3
[8]DTPA Mn (mg · kg^{-1})	4.5
[8]DTPA Cu (mg · kg^{-1})	1.1

E.C., electrical conductivity; OM, organic matter. [1]Densitometry Bouyoucos's method. [2]Walkley-Black's method. [3]Kjeldahl's method. [5]Williams's calcimeter. [6]Droinean's method. [7]Exchangeable cations extracted with NH_4Ac pH = 7. [8]Soltanpour and Swab's method.

Analytical Procedures

The sampled roots, stems, and leaves were separated, weighted, and washed with 0.1% HCl and 0.01% non-ionic detergent (Tween 80) solutions, rinsed with distilled water (Álvarez-Fernández et al., 2001) and dried in a forced air oven at 65°C for 3 days. Thereafter, samples were milled and calcined in a muffle furnace (480°C). The ashes were digested using 7M HNO_3 Suprapour.

Soil soluble fraction was obtained by washing the soil with distilled water (600 mL) by stirring for 10 min on a rotary shaker at 90 min^{-1}. An aliquot of 40 mL was centrifuged at 9,000 min^{-1} for 10 min (Sorvall Legend XFR, Thermo Fisher Scientific, United States), the supernatant was first filtered with ashless filters paper (Grade 1238, Filter Lab) and then, through syringe cellulose filters (0.45 μm) (OlimPeak, Teknokroma). Nitric acid (Suprapur, Merck) was added to achieve a 1% acid matrix.

Soil available fraction was obtained from the solid residue in the centrifuge tube by extraction for 20 min with 25 mL using Soltanpour and Schwab (1977) extractant (DTPA + ammonium bicarbonate). After that, the samples were filtered. The extraction was made in triplicate, the extracts joined in a single extract, and volume made up to 100.0 mL. An aliquot of 7.165 mL of 65% HNO_3 was added to eliminate the excess of bicarbonate and to allow an acid media for the analytical determinations.

Isotope quantification in the plant organs and soil fractions (soluble and available) were determined by ICP-MS (7500c, Agilent Technologies, Santa Clara, CA, United States) using ^{57}Fe standards and correcting Ca and Ar interferences by means of a collision cell quadrupole ICP-MS instrument.

The specific contribution of each iron fertilizer to the soil and plant nutrition was calculated by isotope pattern deconvolution analysis considering the two iron sources, with a modification of the method proposed by Rodríguez-Castrillón et al. (2008) In brief, the mass balance for the Fe natural isotope can be expressed as shown by matrix notation:

$$\begin{bmatrix} {}^{54}A_{Total} \\ {}^{56}A_{Total} \\ {}^{57}A_{Total} \\ {}^{58}A_{Total} \end{bmatrix} = \begin{bmatrix} {}^{54}A_{Fer} & {}^{54}A_{Nat} \\ {}^{56}A_{Fer} & {}^{56}A_{Nat} \\ {}^{57}A_{Fer} & {}^{57}A_{Nat} \\ {}^{58}A_{Fer} & {}^{58}A_{Nat} \end{bmatrix} \times \begin{bmatrix} x_{Fer} \\ x_{Nat} \end{bmatrix} + \begin{bmatrix} {}^{54}e \\ {}^{56}e \\ {}^{57}e \\ {}^{58}e \end{bmatrix}$$

where each A_{Total} is the isotope abundance of each Fe isotope in the plant sample. A_{Fer} is the corresponding isotope abundance in the tracer, and A_{Nat} is the natural isotope abundance. Moreover, x_{Fer} and x_{Nat} denote the molar fractions of Fe in the isotopically altered sample arising from the two different sources of the element (fertilizer or natural). The best values of x_{Nat} and x_{Fer} are found by least-squares fitting of the error vector e (minimizing the square sum of errors) using the SOLVER tool in Excel®.

To evaluate the influence of Fe on leaf chlorophyll, the SPAD Index was measured every 2 or 3 days, using a Minolta Chlorophyll Meter SPAD-502 (Minolta, Osaka, Japan) after the first application of the Fe fertilizers.

Statistical Analysis

In order to verify the homogeneity of the data, the Levene test was used first, prior to testing the differences between Fe treatments for significance by one-way ANOVA. Means were compared using the Duncan multiple range test ($P < 0.05$). Results of two-way ANOVA are expressed as ns (not significant), $^{*}P < 0.05$, $^{**}P < 0.01$, and $^{***}P < 0.001$. All the calculations were performed using SPSS v.24.0 software.

RESULTS

Characterization of ^{57}Fe-NFs

The main characterization tools used in this work were ^{57}Fe Mössbauer spectroscopy, XRD, EXAFS, and TEM. They were applied to identify the iron phases in the ^{57}Fe-NFs and to estimate the particle size. According to the XRD data, the major crystalline phases in all three samples of ^{57}Fe-NFs are mineral salts of potassium and sodium: nitrates in the product F, and sulfates in the products S and M, the collected data are shown in **Supplementary Figure SM2**. No iron-containing crystalline phases were observed in the obtained XRD patterns. The XRD data on the synthesized reference samples – ferrihydrite and goethite – are shown in **Supplementary Figure SM3**.

TEM data demonstrate that all ^{57}Fe-NFs samples contain large low density particles typical for HSs. Inside of these particles the nano-sized contrast variations can be observed, which correspond to the NPs with sizes < 5 nm (**Figures 1a,b**). Some aggregates of ∼20 nm were observed in the product S (**Figure 1c**). These NPs can be clearly seen in the zero loss images of the products F and M (**Supplementary Figure SM3**). **Figure 2** shows TEM images, Fe M-line EFTEM, EELS spectra and the scheme of EFTEM measurements for the F sample, which was of particular interest for this study, because its synthesis was specifically run under conditions favoring formation of ferrihydrite phase. The Fe M- and L-lines were clearly observed in the EELS spectrum of this sample (**Figure 2**). This confirmed the presence of iron in the region of interest. The spatial distribution of iron was investigated using three-point EFTEM, which yielded the pattern of iron-containing NPs (bright inclusions) in the darker matrix (HSs). The obtained results are indicative of the iron-containing composition of the formed NPs. In order to investigate the structures of the observed NPs, the SAED patterns were measured (**Supplementary Figure SM6**) and compared to the ED of the parent HS (L) and XRD pattern of the synthesized pure two-line ferrihydrite (Ferrihydrite). ED patterns of all iron containing samples were characterized with appearance of two additional reflexes as compared to the parent L sample (**Figure 3**). The smaller peak was observed at 0.15 nm, and the larger one – at 0.25–0.30 nm. Such a combination of reflexes is similar to the two-line ferrihydrite diffraction pattern. However, for refining this assignment additional information was desirable and obtained with the use of XANES and EXAFS spectroscopy.

The acquired XANES spectra of the samples obtained in this study are shown in **Supplementary Figure SM7** and their first derivatives are presented in **Figure 4A**. The spectra obtained for all samples under study were rather similar and demonstrated the presence of ferric ions in octahedral coordination (Manceau and Gates, 1997). EXAFS spectra of the same samples (**Figure 4B** and **Supplementary Figure SM8**) were fitted to the two-shell model (Maillot et al., 2011). It assumes that the first shell contains two different oxygen positions (Fe-O), whereas the second one- three iron position (Fe–Fe) with the same value of σ^2. The obtained results for ferrihydrite and goethite reference samples (**Table 2**) are in good agreement with the reported values for Fe–O and Fe–Fe distances (Maillot et al., 2011). For the samples under study, the values of Fe–Fe distances were very close to those of ferrihydrite (**Table 2**). For example, in the F sample (HS-ferrihydrite), they were 2.98 Å, 3.14 Å, and 3.53 Å, whereas in the reference sample – 2.91 Å, 3.06 Å, and 3.46 Å. These distances belong to face-sharing, edge-sharing, and corner-sharing octahedra in ferrihydrite, respectively (Manceau and Gates, 1997). Coordination number of iron at 2.91 Å and 3.06 Å for all three samples of the NFs are similar and indicative of ferrihydrite (Maillot et al., 2011). The high value of R-factor for the "S" sample results from the poorest quality of its approximation by the above two-shell model. This might be caused by heterogeneity of the S sample which contained different phases of iron (hydr)oxides. The iron in the parent humate resembles closely goethite phase. The differences in Fe–O distances between the reference ferrihydrite (1.82 Å and 1.97 Å) and the samples obtained in the presence of HS (1.94 Å and 2.11 Å) may be connected to very small size of the particles formed (<5 nm) and to respective surface effects. In the ideal

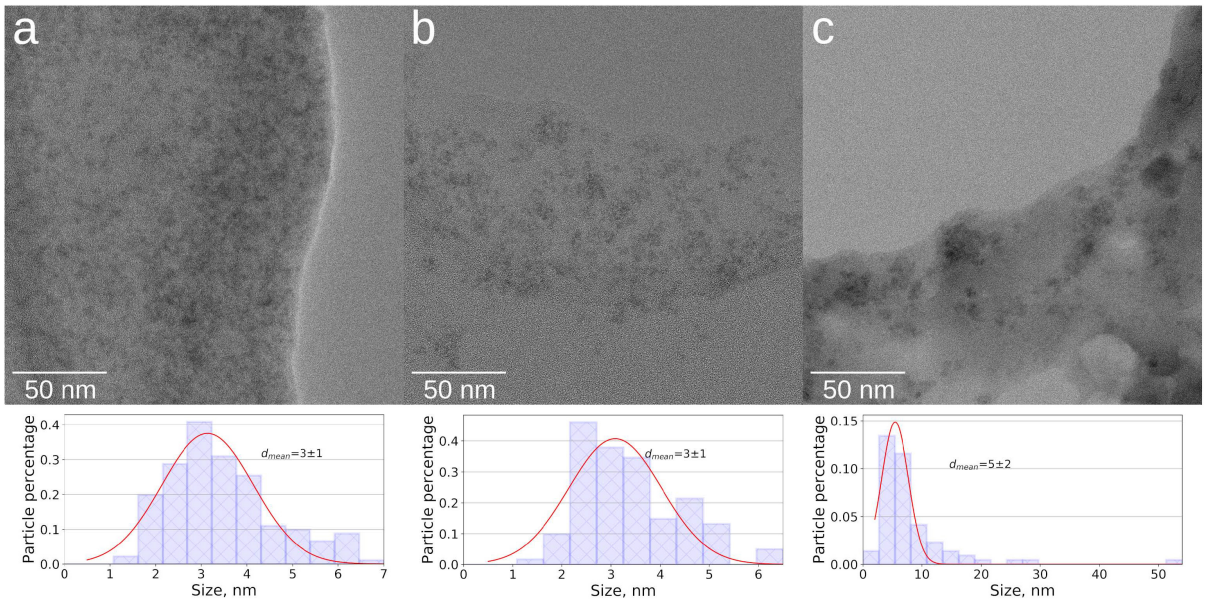

FIGURE 1 | TEM images and size statistics for the three ^{57}Fe-nanofertilizer samples under study: **(a)** F, **(b)** M, **(c)** S.

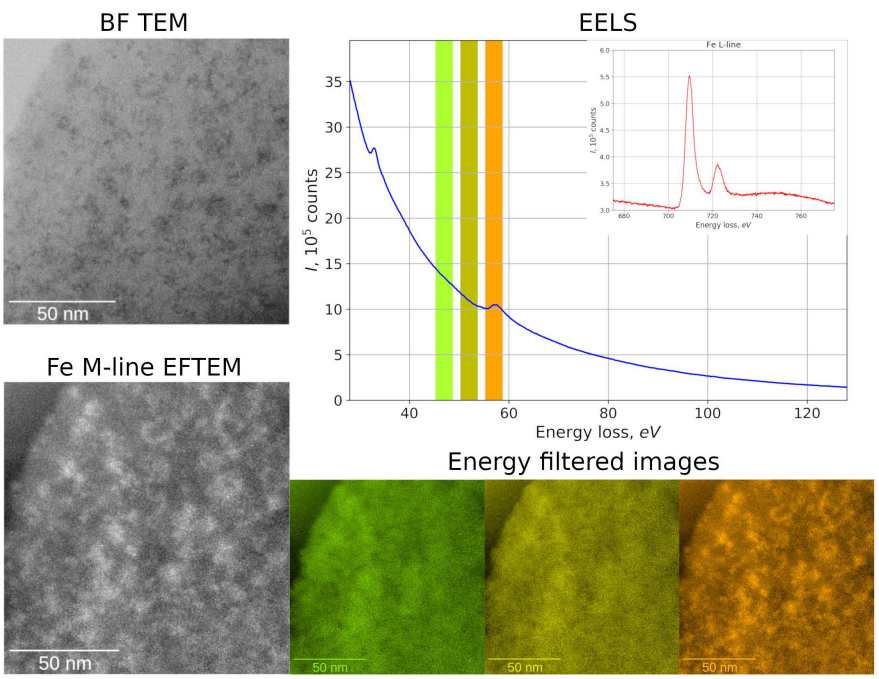

FIGURE 2 | TEM, Fe M-line EFTEM, EELS spectra and the scheme of EFTEM measurements for the product F.

ferrihydrite, the relation between tetrahedral Fe (IV Fe) and octahedral Fe (VI Fe) is 1:4. However, according to Michel et al. (2007), the size reduction of ferrihydrite particles leads to a decrease in IV Fe number. Moreover, Manceau and Gates (1997) demonstrated that 1.86Å Fe–O distance observed in the EXAFS spectra could not be directly assigned to the IV Fe due to the presence of short Fe–(O,OH) bonds on the surface. It means that the surface contamination and size reduction in the HS-stabilized ferrihydrite particles may lead to a decrease in a number of short Fe–O bonds as compared to the reference ferrihydrite. The applied EXAFS model involved only two Fe–O distances due to restriction on the amount of independent parameters, the most intense paths for each sample were chosen. The obtained data allow a conclusion that all three samples of the

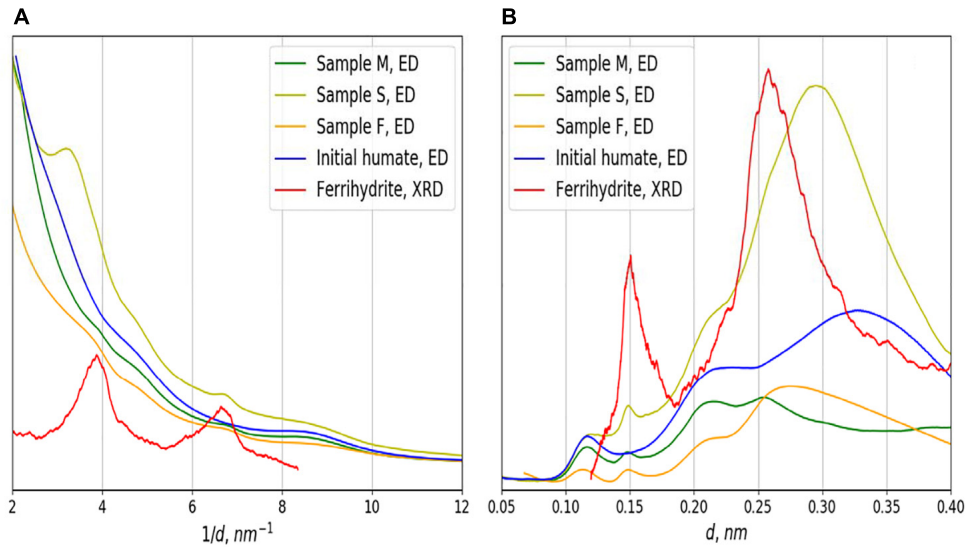

FIGURE 3 | Results of ED integration in reciprocal space **(A)** and in direct space, after background removal **(B)** for the products F, M, S. and initial humate (L) in comparison with the XRD data for ferrihydrite.

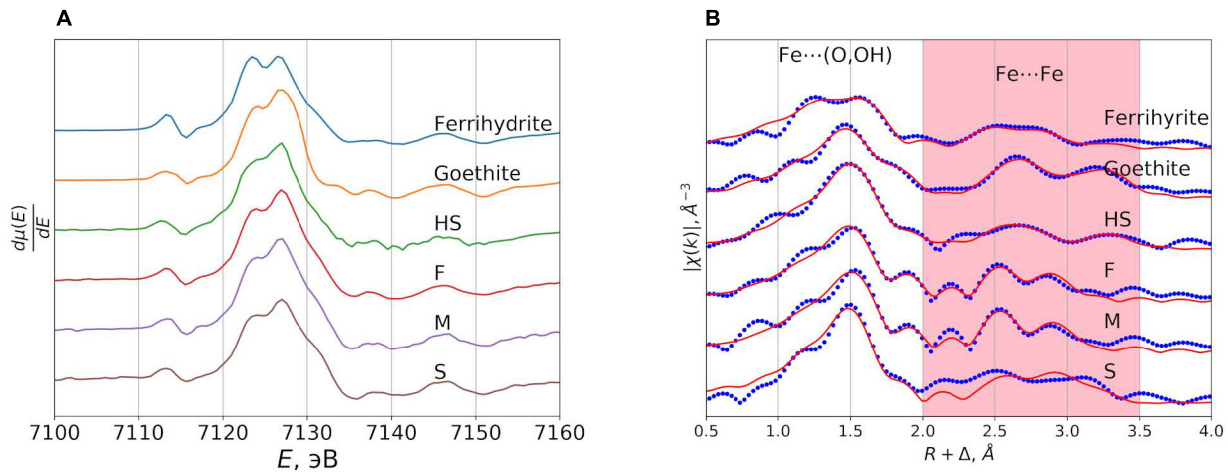

FIGURE 4 | The first derivatives of the XANES spectra shown in **Supplementary Figure SM7 (A)** and the results of model approximation of the EXAFS spectra in R-space **(B)** for the ^{57}Fe-labeled nanofertilizer samples under study.

synthesized NFs were very similar with regard to the iron phase and contained iron (hydr)oxide with the polyhedral arrangement motif of the ferrihydrite.

The results of Mössbauer spectroscopy investigation yielded additional support to this conclusion. The Mössbauer spectra of M and F samples recorded at room temperature and at liquid nitrogen showed broadened electric quadrupole doublets as it is demonstrated in **Figure 5A** on the example of M-sample. The Mössbauer spectra of F-sample is shown in **Supplementary Figure SM11**. This could be explained by the distribution of gradients of the electric field (**Supplementary Figure SM10**). For these samples, the distribution of quadrupole splittings has a bimodal character, similar to the distribution for high-temperature spectra of a reference sample of ferrihydrite (**Supplementary Figure SM10**). The small size of the particles under study and the low blocking temperature might be the reasons for a lack of substantial broadening of the resonance lines as well as the absence of a magnetically ordered fraction in the spectra at low temperature. Even for the reference sample of ferrihydrite with the larger particles as compared to the NPs stabilized by humate, the magnetic ordering (**Supplementary Figure SM10**) was not observed at the boiling point of liquid nitrogen (Schwertmann et al., 1999).

The spectra of S sample at these temperatures, in addition to very similar quadrupole doublets, contained extended absorption with low intensity, which can be conditionally described by a singlet line of a large width (**Figure 5B**). The relative area of extended absorption in the S sample did not

TABLE 2 | The model parameters calculated from the EXAFS spectra for three ^{57}Fe-NFs samples used in this study.

Sample	R_f (%)	ΔE (eV)		*N*	R (Å)	$\sigma^2 \times 10^3$
"L"	1.5%	−0.9	O	2.7 ± 0.9	1.94 ± 0.02	2 ± 2
			O	1.3 ± 0.4	2.08 ± 0.04	
			Fe	2.1 ± 0.8	3.05 ± 0.03	10*
			Fe	1.8 ± 1.2	3.24 ± 0.06	
			Fe	2.4 ± 0.9	3.48 ± 0.03	
Ferrihydrite	2.9%	-7	O	1.2 ± 0.4	1.82 ± 0.04	3 ± 3
			O	2.3 ± 0.8	1.97 ± 0.02	
			Fe	0.5 ± 0.3	2.91 ± 0.04	0 ± 6
			Fe	0.5 ± 0.4	3.06 ± 0.04	
			Fe	0.3 ± 0.2	3.46 ± 0.04	
Goethite	1.5%	−0.1	O	2.7 ± 0.6	1.94 ± 0.02	3 ± 2
			O	2.2 ± 0.4	2.09 ± 0.02	
			Fe	3.3 ± 1.4	3.07 ± 0.02	9 ± 3
			Fe	2.8 ± 1.6	3.30 ± 0.04	
			Fe	3.6 ± 1.3	3.47 ± 0.03	
"F"	3.0%	0.3	O	2.6 ± 0.8	1.94 ± 0.02	3 ± 3
			O	1.3 ± 0.4	2.11 ± 0.04	
			Fe	0.7 ± 0.4	2.98 ± 0.02	0 ± 4
			Fe	0.9 ± 0.5	3.14 ± 0.03	
			Fe	0.1 ± 10.2	3.49 ± 0.3	
"M"	2.9%	0.2	O	2.8 ± 1.1	1.94 ± 0.02	3 ± 3
			O	1.1 ± 0.5	2.10 ± 0.0C	
			Fe	0.9 ± 0.5	2.97 ± 0.02	0 ± 3
			Fe	0.9 ± 0.5	3.13 ± 0.03	
			Fe	0.2 ± 0.2	3.53 ± 0.09	
"S"	4.7%	3.2	O	1.4 ± 0.3	1.95 ± 0.02	0.5 ± 2.5
			O	2.0 ± 0.5	2.10 ± 0.03	
			Fe	0.9 ± 0.7	3.01 ± 0.03	2 ± 7
			Fe	1.1 ± 0.8	3.16 ± 0.04	
			Fe	0.4 ± 0.5	3.51 ± 0.07	

* *Fixed value.*

change with temperature indicating that it is not related to superparamagnetism. This can be connected with weak spin–spin interactions between iron (III) atoms in strongly inhomogeneous and disordered medium. These interactions could be precisely observed because of the use of ^{57}Fe (Pankratov et al., 2013). Distribution of quadrupole splitting in the S sample is unimodal and it has significantly larger dispersion as compared to those in the samples M and F. This might be indicative of the larger diversity of the local environments of iron atoms in the S sample. The further details on Mössbauer data can be found in the **Supplementary Table SM1** and Supplementary text. In general, the data of Mössbauer spectroscopy are in good agreement with the data of TEM and X-ray spectroscopy.

Soil Pot Experiment

In order to evaluate the ^{57}Fe-NFs effect in the plant growth, the SPAD index and the fresh weight of soybean shoots and roots at 48 DAF were measured and presented in **Table 3**. There was no leaf chlorosis observed and the plants presented SPAD indexes > 25, which is indicative of sufficient iron nutrition (Martín-Fernández et al., 2017b). The shoot biomass of the fertilized plants (in case of F3, S1, S2, S3, and M2) was larger as compared to FeEDDHA. There was no significant differences observed in the root biomass of the plants fertilized with the NFs under study (except for F3, which showed the largest fresh weight of roots). In our former studies, the plants fertilized with the leonardite humates accumulated slightly higher fresh weight than those fertilized with the iron chelate. According to Rose et al. (2014), the HSs generally increase the shoot and root growth by 15–25%. Canellas et al. (2015) reported that the growth response of monocotyledonous plants to exogenously applied HS is more sensitive as compared to for dicotyledonous plants, and the plant physiological responses to HS isolated from brown coal (e.g., lignite, leonardite, and subbituminous coals) are less than those observed in response to the addition of HS isolated from peat, composts or vermicomposts.

The ^{57}Fe tracer technique allowed monitoring Fe from the fertilizer (Fe_{Fer}) in the soil experiment and distinguishing it from the native Fe contained in the soil (Fe_{Nat}). The Fe_{Total} was calculated as the sum of Fe_{Fer} and Fe_{Nat}. A combination of ^{57}Fe isotope and mathematical deconvolution was a relevant tool to evaluate the efficacy between different NFs to correct iron deficiency.

The contents of Fe_{Fer}, Fe_{Nat}, and Fe_{Total} (μmol pot^{-1}) in soybean shoots were calculated as the sum of the first (15 DAF) and second samplings (48 DAF) and presented in **Figure 6**. The effect of type and doses of the ^{57}Fe-NFs on the contents of Fe_{Fer}, Fe_{Nat} and Fe_{Total} in soybean shoots was studied by ANOVA two-way statistical analysis and presented in **Table 4**. Significant differences were observed between ^{57}Fe-NFs types and doses. The product M provided the highest Fe_{Fer} content to the soybean shoots mainly when the third dose was applied (150 μmol ^{57}Fe pot^{-1}). The content of Fe_{Total} expressed as the sum of the Fe_{Fer} and Fe_{Nat} showed significant differences only between the doses, and the third dose seemed to be the most adequate. **Table 5** presents the Fe_{Total} (mg kg^{-1}) concentration in soybean leaves at 15 and 48 DAF. It ranged from 36.8 mg kg^{-1} (F1) to 53.6 mg kg^{-1} (M1) at 15 DAF and from 34.6 mg kg^{-1} (S1) to 39.9 (S3) mg kg^{-1} at 48 DAF. According to the iron concentration obtained in a previous work (Rodríguez-Lucena et al., 2010) and the SPAD index detected (**Table 4**), the soybean plants are sufficiently iron nourished and did not present symptoms of iron chlorosis. Moreover, the iron concentration in leaves decreased for the second sampling because iron was a priority for the pods production, even for plants fertilized with ^{57}FeEDDHA.

Differences in Fe_{Fer} uptake (nmol plant^{-1}) in soybean leaves between the first (15 DAF) and the second samplings (48 DAF) were calculated and plotted in **Figure 7**. The plants fertilized with the ^{57}Fe-NFs, nominally, with S2, M2 and F3, have taken up 93, 88, and 70 nmol Fe_{Fer} plant^{-1} in leaves in 33 days, whereas the plants fertilized with FeEDDHA stopped providing Fe_{Fer} to the leaves after the first sampling. The products S and M, prepared from $^{57}Fe_2(SO_4)_3$, at their second dose (75 μmol ^{57}Fe pot^{-1}) and the product F, prepared from $^{57}Fe(NO_3)_3$ at the third dose (150 μmol ^{57}Fe pot^{-1}) showed the highest Fe_{Fer} increase between sampling times. These results are consistent with our previous data (Cieschi et al., 2017) on

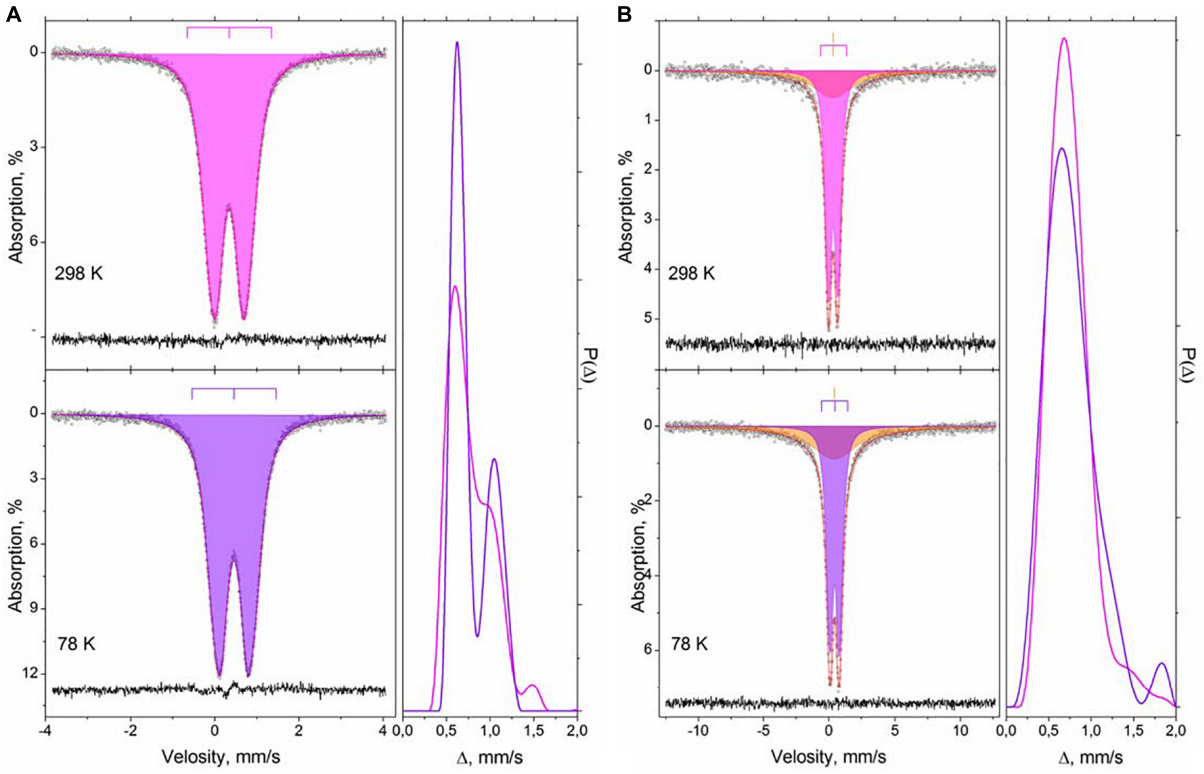

FIGURE 5 | Mössbauer spectra of the M and S samples (**A,B**, respectively) recorded at 295K and 78K and the quadrupole splitting distributions for these spectra.

fertilization with iron leonardite humate which sustained slow and increasing iron nutrition to citrus growth under conditions of calcareous soil and yielded results similar to FeEDDHA with regard to efficacy of iron deficiency correction during the first year of application.

TABLE 3 | SPAD index at the last level of trifoliate well developed soybean leaves and fresh weight (FW) of shoots and roots of soybean control (L) plants and plants fertilized with the ^{57}Fe products F, S, and M in three doses: (1) 35, (2) 75, and (3) 150 μmol ^{57}Fe pot^{-1} or 50 μmol ^{57}FeEDDHA pot^{-1} at 48 DAF.

Treatments	SPAD	Shoot FW (g pot^{-1})	Root FW (g pot^{-1})
L	41.8 ± 2.04^{abc}	13.9 ± 0.47^{a}	5.69 ± 0.62^{b}
F1	37.1 ± 1.55^{cd}	13.4 ± 0.50^{ab}	7.33 ± 0.61^{ab}
F2	39.2 ± 1.03^{bc}	13.8 ± 0.09^{a}	6.90 ± 0.22^{ab}
F3	45.9 ± 0.50^{ab}	14.6 ± 0.39^{a}	8.15 ± 0.60^{a}
S1	40.2 ± 1.75^{bc}	14.0 ± 0.73^{a}	6.80 ± 0.40^{ab}
S2	38.4 ± 1.98^{bc}	14.5 ± 0.55^{a}	7.03 ± 0.97^{ab}
S3	30.8 ± 4.75^{d}	13.9 ± 0.48^{a}	6.61 ± 0.32^{ab}
M1	39.1 ± 3.70^{bc}	13.4 ± 0.16^{ab}	6.81 ± 0.54^{ab}
M2	42.4 ± 2.84^{abc}	13.7 ± 0.45^{a}	6.34 ± 0.25^{ab}
M3	40.6 ± 2.44^{bc}	13.3 ± 1.13^{ab}	7.22 ± 0.79^{ab}
FeEDDHA	48.9 ± 1.53^{a}	11.5 ± 0.74^{b}	5.70 ± 0.45^{b}

For each series different letters denote significant differences among the treatments according to Duncan's Test ($p < 0.05$). Results are expressed as averages ± standard error, n = 5.

Of particular interest are the contents of Fe_{Fer}, Fe_{Nat} and Fe_{Total} (μmol pot^{-1}) in soybean pods at 48 DAF, which are presented in **Figure 8**. The Fe_{Fer} content in pods increased along with an increase in the dose of ^{57}Fe-NFs. The significant differences were observed between the doses and the ^{57}Fe-NF type when the obtained results were compared using ANOVA two-way statistical analysis (**Table 4**). As in case of the shoots, the product M provided the higher content of Fe_{Fer} as compared to the other two ^{57}Fe-NFs to the soybean pods and the third dose was the most efficient. Moreover, the similar Fe_{otal} contents in soybean pods were observed for the plants treated with ^{57}Fe-NFs (except for F2) or FeEDDHA, and the product M was the most efficient in providing Fe_{Total} to the soybean pods regardless of the dose applied. **Table 5** shows the Fe_{Total} concentration (mg kg^{-1}) in soybean pods at 48 DAF. It ranged from 32.6 mg kg^{-1} (F2) to 57.8 mg kg^{-1} (M2) for the plants fertilized with ^{57}Fe-NFs. According to Römheld and Nikolic (2007), the accumulation of total iron in pods for soybean plants reaches 50 mg kg^{-1} under conditions of sufficient nourishment. Nadal et al. (2012) and Martín-Fernández et al. (2017a) have observed ^{57}Fe in soybean fruit of plants fertilized with *o,o*EDDHA/$^{57}Fe^{3+}$ and HBED/$^{57}Fe^{3+}$. Still, this study is the first one when ^{57}Fe supplied by iron humates was detected in soybean pods. Shoots of plants fertilized with FeEDDHA showed the highest Fe_{Fer}, the lowest Fe_{Nat} and the highest Fe_{Total} contents. The pods showed similar results for Fe_{Fer} and Fe_{Nat} contents.

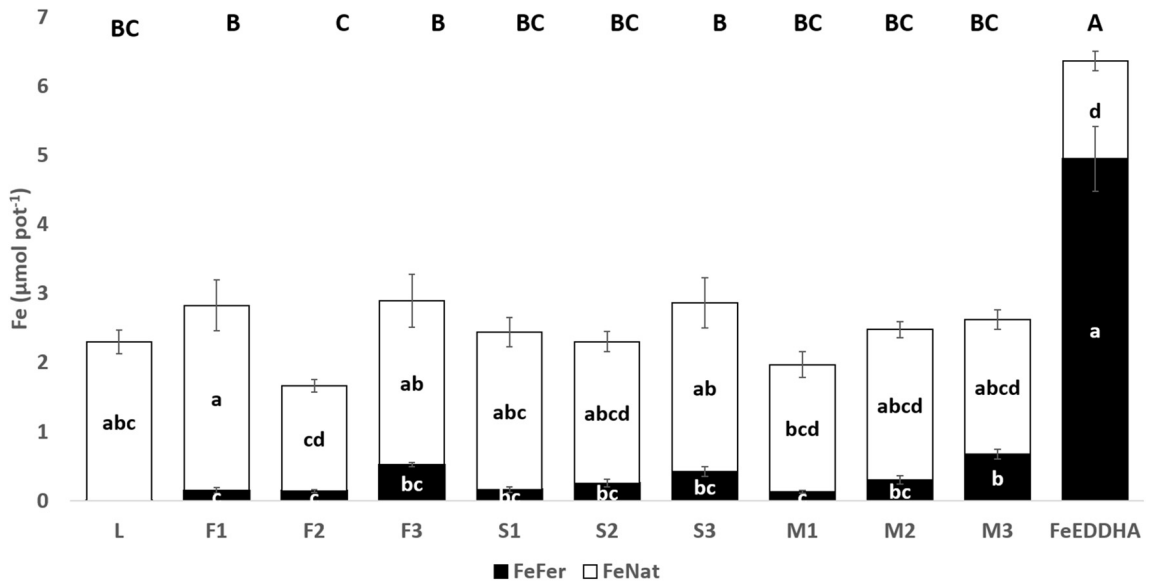

FIGURE 6 | Fe_{Fer} and Fe_{Nat} (μmol pot^{-1}) contents in soybean shoots of control plants (L) and plants fertilized with the ^{57}Fe products F, S, and M in three doses: (1) 35, (2) 75, and (3) 150 μmol ^{57}Fe pot^{-1} or 50 μmol $^{57}FeEDDHA$ pot^{-1}, calculated as the sum of the first (15 DAF) and second sampling (48 DAF). For each series different letters denote significant differences among the treatments according to Duncan's Test ($p < 0.05$). Lowercase letters correspond to Fe_{Fer} and Fe_{Nat} and capital letters correspond to Fe_{Total} statistical results. Results are expressed as averages ± standard error, $n = 5$.

TABLE 4 | Effect of doses (D) and nanofertilizers (NFs) related to the contents of Fe_{Fer}, Fe_{Nat}, and Fe_{Total} (μmol pot^{-1}) in soybean shoots, roots, pods, soluble and available soil fraction for soybean plants fertilized with the products F, S, and M with three doses (35, 75, and 150 μmol pot^{-1}) at 48 DAF.

					Nanofertilizers			Doses (μmol pot^{-1})		
		D	NFs	DxNFs	F	S	M	35	75	150
Shoots	Fe_{Fer}	***	*	*	0.27 ± 0.03^{b}	0.28 ± 0.03^{b}	0.35 ± 0.03^{a}	0.15 ± 0.03^{c}	0.23 ± 0.03^{b}	0.54 ± 0.03^{a}
	Fe_{Nat}	ns	ns	ns	2.19 ± 0.15	2.26 ± 0.15	1.99 ± 0.15^{ns}	2.27 ± 0.15	1.92 ± 0.15	2.25 ± 0.15^{ns}
	Fe_{Total}	*	ns	ns	2.44 ± 0.16	2.53 ± 0.16	2.36 ± 0.16^{ns}	2.41 ± 0.16^{ab}	2.15 ± 0.16^{b}	2.77 ± 0.16^{a}
Pods	Fe_{Fer}	***	*	ns	0.20 ± 0.04^{b}	0.19 ± 0.16^{b}	0.34 ± 0.16^{a}	0.11 ± 0.04^{c}	0.22 ± 0.04^{b}	0.40 ± 0.04^{a}
	Fe_{Nat}	ns	ns	ns	0.94 ± 0.09	0.97 ± 0.09	1.08 ± 0.09^{ns}	1.15 ± 0.09	0.94 ± 0.09	0.90 ± 0.09^{ns}
	Fe_{Total}	ns	*	*	1.14 ± 0.10^{b}	1.14 ± 0.11^{b}	1.42 ± 0.10^{a}	1.27 ± 0.10	1.22 ± 0.10	1.27 ± 0.10^{ns}
Roots	Fe_{Fer}	***	ns	ns	1.64 ± 0.29	1.21 ± 0.29	1.15 ± 0.29^{ns}	0.45 ± 0.30^{b}	0.75 ± 0.29^{b}	2.80 ± 0.27^{a}
	Fe_{Nat}	ns	ns	ns	77.7 ± 8.23	71.8 ± 8.23	77.8 ± 8.23^{ns}	67.6 ± 8.23	74.4 ± 8.23	85.2 ± 8.23^{ns}
	Fe_{Total}	ns	ns	ns	79.4 ± 8.34	73.1 ± 8.34	79.0 ± 8.34^{ns}	68.2 ± 8.34	75.2 ± 8.34	88.0 ± 8.34^{ns}
Soluble	Fe_{Fer}	**	*	*	0.16 ± 0.11^{b}	0.20 ± 0.11^{b}	0.53 ± 0.10^{a}	0.18 ± 0.10^{b}	0.06 ± 0.11^{b}	0.65 ± 0.11^{a}
	Fe_{Nat}	ns	ns	ns	5.24 ± 3.49	9.80 ± 3.49	15.6 ± 3.49^{ns}	10.6 ± 3.49	6.19 ± 3.49	13.8 ± 3.49^{ns}
	Fe_{Total}	ns	ns	ns	5.39 ± 3.43	10.0 ± 3.57	16.2 ± 3.43^{ns}	10.8 ± 3.43	6.36 ± 3.43	14.5 ± 3.57^{ns}
Available	Fe_{Fer}	***	***	***	27.3 ± 2.51^{a}	10.3 ± 2.51^{c}	17.7 ± 2.51^{b}	7.83 ± 2.51^{a}	17.3 ± 2.51^{b}	30.1 ± 2.51^{c}
	Fe_{Nat}	ns	*	ns	179 ± 55.8^{b}	169 ± 58.1^{b}	364 ± 55.8^{a}	255 ± 55.8	212 ± 55.8	245 ± 58.1^{ns}
	Fe_{Total}	ns	*	ns	207 ± 56.8^{b}	179 ± 59.2^{b}	382 ± 56.8^{a}	263 ± 56.8	230 ± 56.8	274 ± 59.2^{ns}

*Means (n = 5) in the same row followed by the same letter do not differ significantly according to the Duncan test (P < 0.05). Two-way ANOVA results. *P < 0.05, **P < 0.01, ***P < 0.001; ns, not significant.*

The content of Fe_{Fer} (μmol pot^{-1}) in soybean roots as well as the contents of soluble and available soil fractions at 48 DAF are presented in **Figure 9**. In general, an increase in the content of Fe_{Fer} in soybean roots was observed when the plants were treated with the ^{57}Fe-NFs (**Figure 9A**). The significant differences between the doses were confirmed by the ANOVA two-way statistical analysis (**Table 4**). The third dose was the most prone to store Fe_{Fer} in roots, in particular, in case of the F sample.

The Fe_{Fer} content in the soluble soil fraction was increasing along with the dose of the ^{57}Fe-NFs. The results obtained for F3, S3, M3, and FeEDDHA were similar, though the highest Fe_{Fer} content was observed in the pots treated with M3 (**Figure 9B**). The ANOVA two-way statistical analysis has confirmed these results when the effect of the ^{57}Fe-NF type and doses were compared (**Table 4**). Relating to the Fe_{Fer} content in the available soil fraction, the pots fertilized with the product F differed

TABLE 5 | Fe_{Total} (mg kg^{-1}) concentration in soybean leaves and pods of plants fertilized with the ^{57}Fe products F, S, and M in three doses: (1) 35, (2) 75, and (3) 150 μmol ^{57}Fe pot^{-1} or 50 μmol $^{57}FeEDDHA$ pot^{-1} at 15 and 48 DAF and soybean pods at 48 DAF.

Treatments	Leaves 15 DAF	Leaves 48 DAF	Pods
L	38.1 ± 2.85^{d}	48.3 ± 5.65^{b}	49.5 ± 5.40^{ab}
F1	36.8 ± 1.10^{d}	38.6 ± 3.52^{bc}	46.1 ± 9.53^{ab}
F2	41.3 ± 3.38^{cd}	37.5 ± 2.60^{bc}	32.6 ± 6.85^{b}
F3	40.2 ± 3.61^{d}	39.4 ± 2.40^{bc}	38.9 ± 4.00^{b}
S1	38.2 ± 3.11^{d}	34.6 ± 1.43^{c}	45.7 ± 5.38^{ab}
S2	38.9 ± 2.73^{d}	35.8 ± 1.97^{c}	45.7 ± 5.58^{ab}
S3	38.1 ± 2.59^{d}	39.9 ± 1.81^{bc}	45.9 ± 3.26^{ab}
M1	53.6 ± 4.29^{b}	35.4 ± 0.53^{c}	51.3 ± 2.90^{ab}
M2	46.1 ± 1.20^{bcd}	35.5 ± 2.61^{c}	57.9 ± 7.43^{a}
M3	50.7 ± 3.11^{bc}	39.5 ± 2.16^{bc}	49.8 ± 3.63^{ab}
FeEDDHA	139 ± 5.60^{a}	108 ± 6.99^{a}	46.7 ± 3.13^{ab}

For each series different letters denote significant differences among the treatments according to Duncan's Test ($p < 0.05$). Results are expressed as averages ± standard error, n = 5.

substantially from the others, in particular, in case of the third dose (**Figure 9C** and **Table 4**). In general, the Fe_{Fer} from the product F at the highest dose (150 μmol ^{57}Fe pot^{-1}) remained mostly available in soil (**Figure 9C**) or in the roots (**Figure 9A**).

Figure 10 shows the ^{57}Fe (%) distribution in soybean plants (shoots, pods and roots) of plants fertilized with the ^{57}Fe products F, S and M in three doses (35, 75 and 150 μmol ^{57}Fe pot^{-1}) and in the soil (soluble and available fraction). In general, the ^{57}Fe-NFs remained in soil and ranged from 80% (S1) to 95% (F1), mainly in the available soil fraction. With respect to the plant, the highest percentage of ^{57}Fe was detected in plants fertilized with S1 (18%), but mainly in roots. The ^{57}Fe content in shoots increased along with the dose for plants fertilized with F and M.

DISCUSSION

In our work, three ^{57}Fe-NFs (F, M, and S) were obtained and exhaustively characterized by XRD, TEM with ED, EELS and EFTEM, X-ray absorption spectroscopy (XANES and EXAFS) and Mössbauer spectroscopy. There were similarities among them with regard to the iron phase and iron (hydr)oxide content with the polyhedral arrangement motif of the ferrihydrite. Most agricultural soils contain natural ferrihydrite NPs, which may contribute to iron nutrition of plants. Many authors (Römheld and Nikolic, 2007; Colombo et al., 2012; Cieschi et al., 2017) reported ferrihydrite formation during the iron humate synthesis, they characterized and studied the relationship between the particle size, pH and stability. Angelico et al. (2014) and Colombo et al. (2015) have shown that the phase of iron (hydr)oxide formed in the presence of HS depends on pH, oxidation rate, and Fe:HS ratio.

Our pot experiments revealed that the ^{57}Fe-NFs were capable of supplying ^{57}Fe to the plants and it was transported from root to shoot and reached the pods (**Figures 6**, **8**, **9A**). In particular, we have observed that the plants fertilized with the product M presented the highest contents of ^{57}Fe in shoots, pods and the soil soluble fraction, according to the two-way ANOVA statistical analysis (**Table 4**). This iron humate was prepared taking into account its maximum complexing capacity in order to avoid the iron flocculation in calcareous conditions. Then, the Fe:HS ratio obtained after the synthesis was the lowest (0.12 g Fe g org. C^{-1})

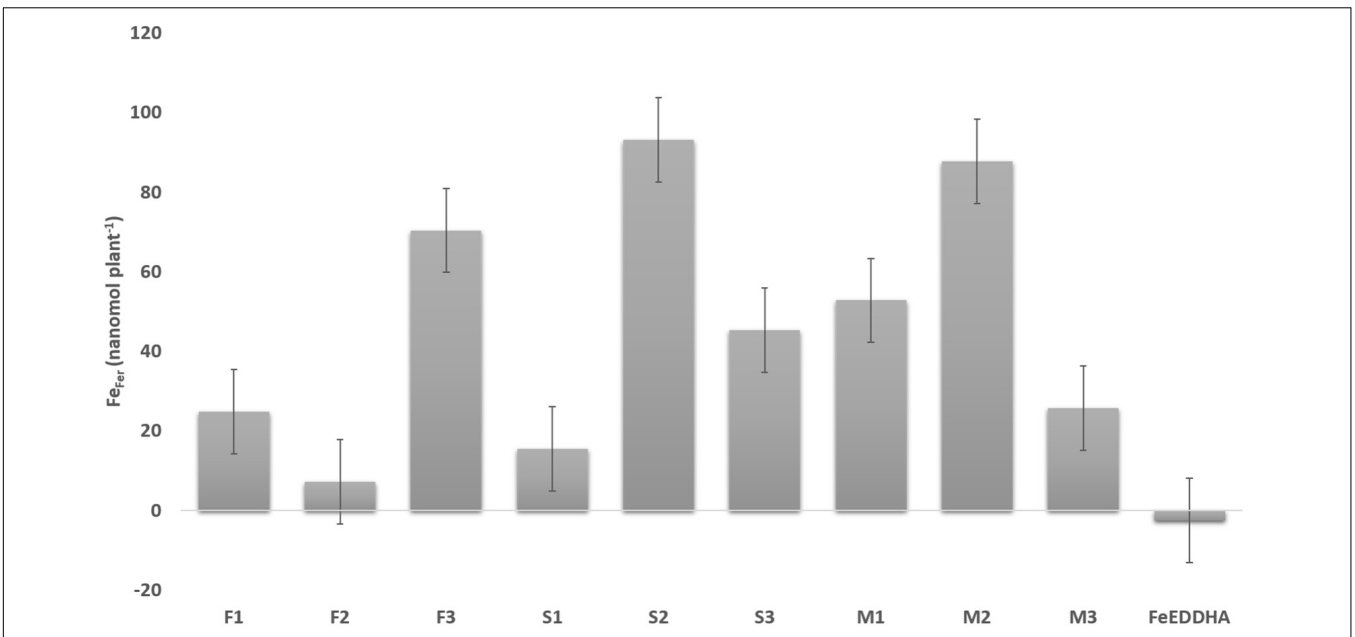

FIGURE 7 | Differences in Fe_{Fer} uptake (%) in soybean leaves of plants fertilized with the ^{57}Fe products F, S, and M in three doses: (1) 35, (2) 75, and (3) 150 μmol ^{57}Fe pot^{-1} or 50 μmol $^{57}FeEDDHA$ pot^{-1}, between the first (15 DAF) and the second sampling (48 DAF). Results are expressed as averages ± standard error, $n = 5$.

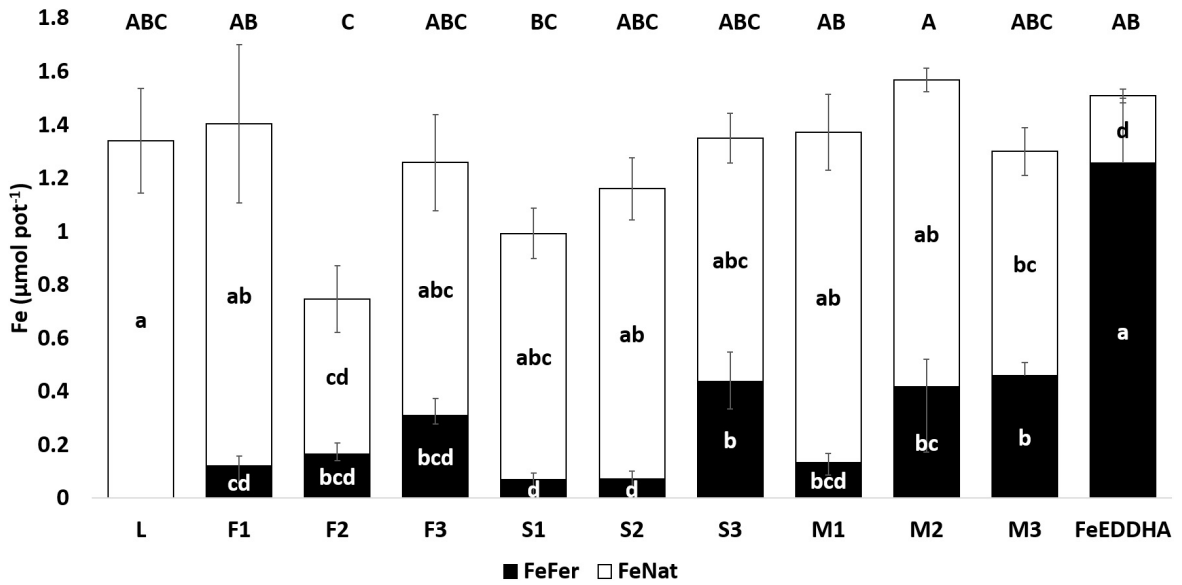

FIGURE 8 | Fe_{Fer} and Fe_{Nat} (µmol pot^{-1}) contents in soybean pods of control plants (L) and plants fertilized with the ^{57}Fe products F, S, and M in three doses: (1) 35, (2) 75, and (3) 150 µmol ^{57}Fe pot^{-1} or 50 µmol $^{57}FeEDDHA$ pot^{-1} at 48 DAF. For each series different letters denote significant differences among the treatments according to Duncan's Test ($p < 0.05$). Lowercase letters correspond to Fe_{Fer} and Fe_{Nat} and capital letters correspond to Fe_{Total} statistical results. Results are expressed as averages ± standard error, $n = 5$.

which suggested that the high content of HS has stabilized the poorly ordered ^{57}Fe structures entrapped into humic matrix and favored the iron uptake by the soybean plants. Similar results were obtained by Kulikova et al. (2017) for their product Fe-HA (4% Fe, 68% HA) which was tested with wheat plants grown under hydroponic conditions.

In soil, the ^{57}Fe-NFs presented an increasing tendency to remain available to the plant requirements for the different growth stages (**Figure 9C**). In addition, the slow and continuous iron release from these NFs has confirmed their long-term effect in providing iron in calcareous conditions in contrast to the short-term effect of the iron synthetic chelate (**Figure 7**), reported in the previous studies (Cieschi et al., 2017). Moreover, in a recent hydroponic assay (Cieschi and Lucena, 2018), plants fertilized with FeEDDHA presented the highest Fe contents in roots after 10 days but at longer term exposition (60 days) of the plants treated with iron humates yielded iron uptake similar to the plants fertilized with the iron synthetic chelate. We hypothesized that an increase in iron humate concentration in the rhizosphere might cause a decrease in the transcription level of the genes involved in the iron transport and shoot growth, and so the iron transport from root to shoot decelerated. Several authors (Aguirre et al., 2009; Tomasi et al., 2013; Olaetxea et al., 2015; Zamboni et al., 2016) suggested that the efficiency of the root transcriptional response to Fe supply depends on the nature (physicochemical characteristics) of the ligand and its capability to activate Fe uptake mechanisms and translocations. In particular, Zamboni et al. (2016) demonstrated that Fe complexed to water-extractable HSs from peat did not cause relevant changes in the root transcriptome of tomato plants with respect to Fe-deficient plants. However, Aguirre et al. (2009) observed that high doses of a purified humic acid from leonardite applied to cucumber plants promoted the upregulation of CsFRO1 and CsIRT1 gene expression for 48 and 72 h while these genes were downregulated for 96 h. The authors suggested that it may be associated to root iron accumulation and/or iron translocation. Olaetxea et al. (2018) proposed that it is very likely that the action of HS on plant mineral nutrition involves a coordinated functional crosstalk between indirect and direct HS effects on the soil–plant system. Soil and, in particular, the rhizosphere are extremely complex environments with a large degree of heterogeneity down to the nanoscale where the interactions between soil constituents, plant roots, and microorganisms take place (Mimmo et al., 2014). Thus, the long-term effect would be an expected result.

With respect to the uptake of nanoparticles by plants, Kulikova et al. (2014) have observed that particles of HA were transferred from root to shoot of wheat seedlings through the plant vascular system and Nardi et al. (2002) have previously observed the same mechanism for low molecular weight fraction of HA (<2.5 kDa). Furthermore, Pariona et al. (2016) have recently detected by 3D microscopic techniques, clusters of hematite and ferrihydrite NPs in endodermis, xylem, phloem vessels, and cell walls of the xylem vessels of maize stems of plants grown in hydroponic conditions. The extensive studies of R. Pinton and S. Cesco's group (Cesco et al., 2000, 2002; Nikolic et al., 2003; Colombo et al., 2012, 2014; Tomasi et al., 2013; Mimmo et al., 2014) modeled variety of interactions in soils of iron humate complexes according to the molecular weight of HS. They have demonstrated that low-molecular weight HS can form soluble complexes of Fe and move toward the root, acting as natural substrates for the membrane Fe (III)-chelate reductase

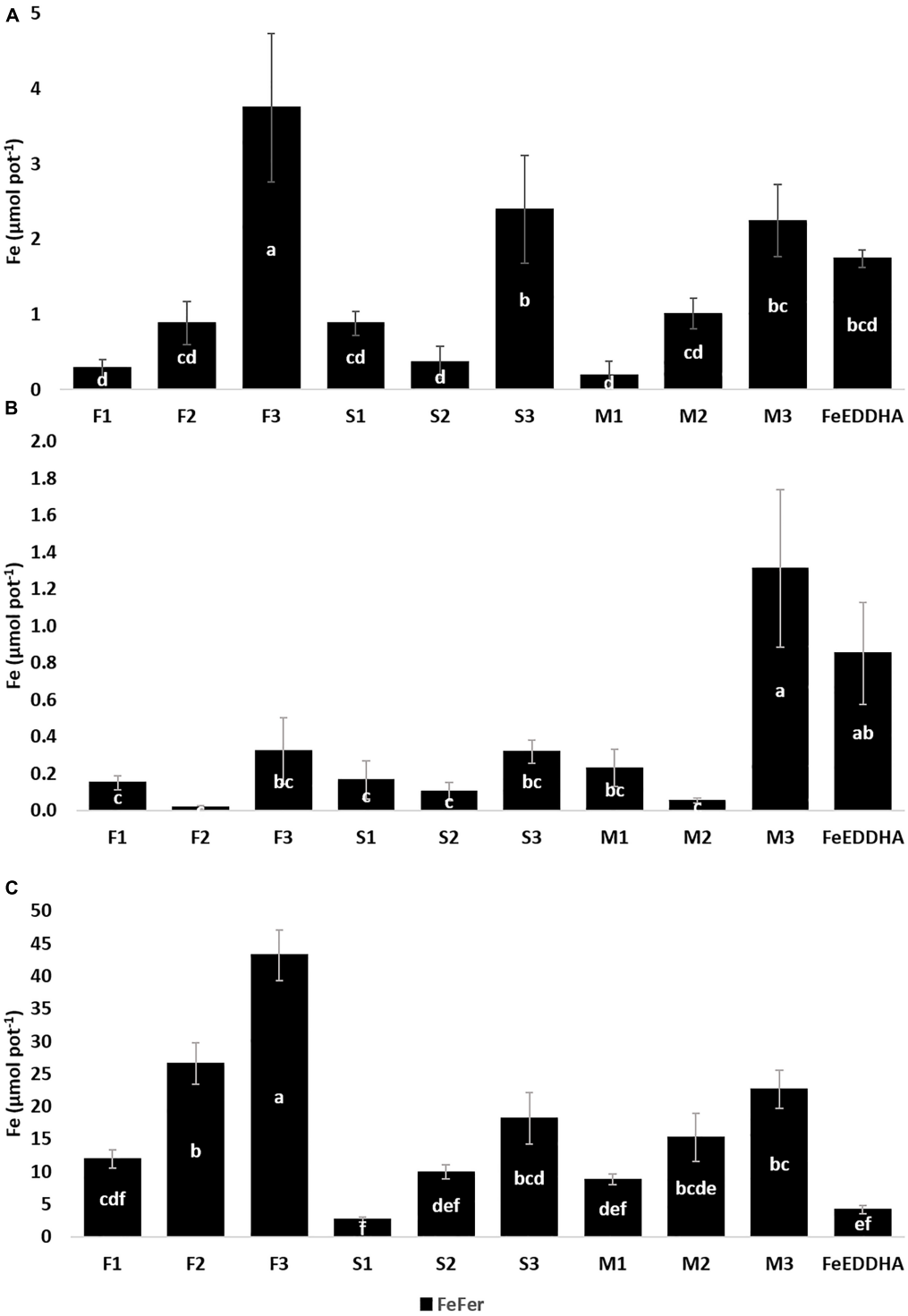

FIGURE 9 | Fe_{Fer} (µmol pot^{-1}) content in soybean roots of plants fertilized with the ^{57}Fe products F, S, and M in three doses: (1) 35, (2) 75, and (3) 150 µmol ^{57}Fe pot^{-1} or 50 µmol $^{57}FeEDDHA$ pot^{-1} **(A)**, soluble soil fraction **(B)**, and available soil fraction **(C)** at 48 DAF. For each series different letters denote significant differences among the treatments according to Duncan's Test ($p < 0.05$). Results are expressed as averages ± standard error, $n = 5$.

and stimulate the proton release promoting the Fe acquisition for Strategy I plants. Recently, Homonnay et al. (2016) have carried out a preliminary study about iron nanoparticles in plant nutrition and hypothesized that it would be possible to consider for plant nutrition supply in the soil iron-based oxide or oxy-hydroxide nanoparticles since storage of iron in cells

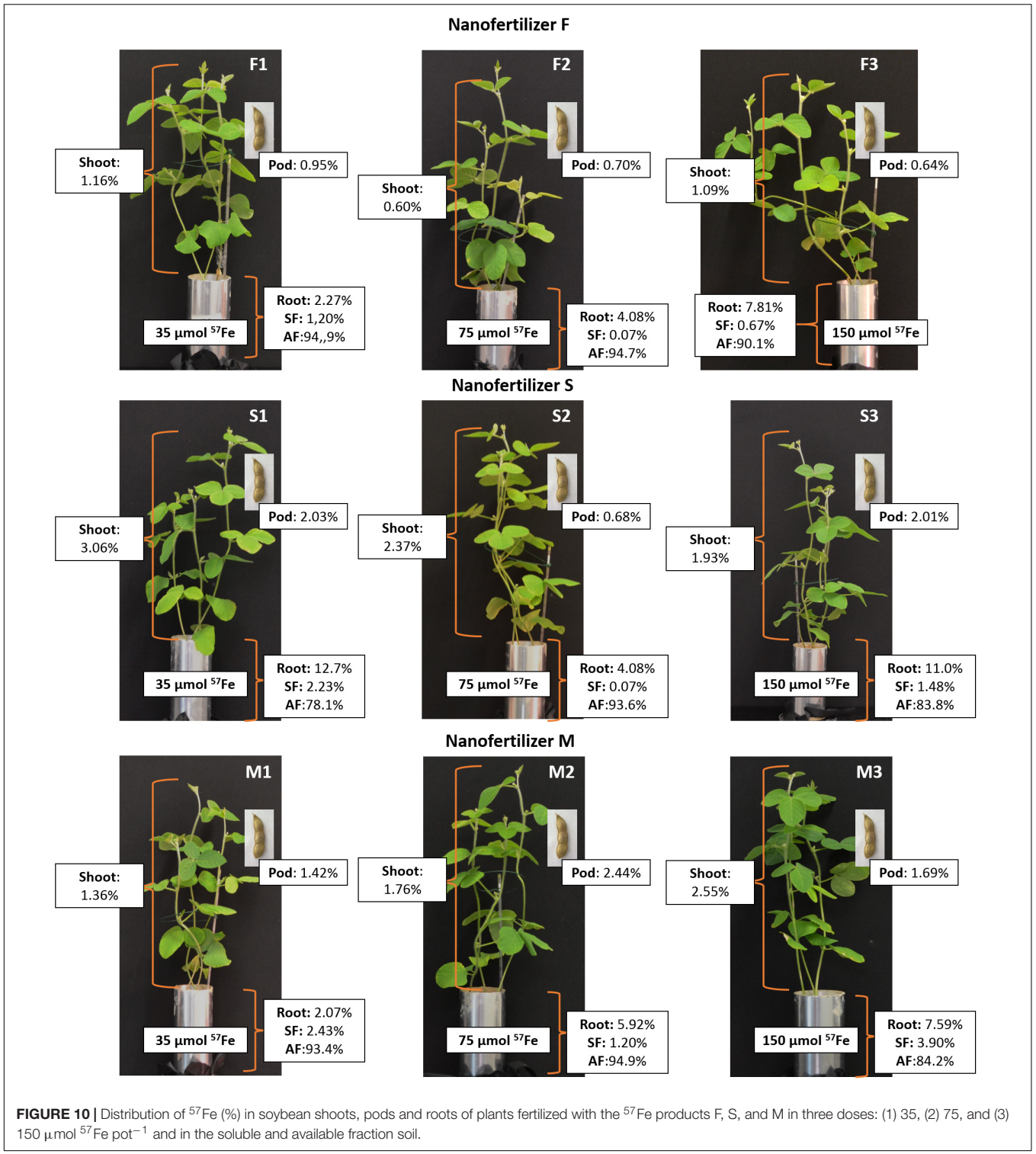

FIGURE 10 | Distribution of ^{57}Fe (%) in soybean shoots, pods and roots of plants fertilized with the ^{57}Fe products F, S, and M in three doses: (1) 35, (2) 75, and (3) 150 µmol ^{57}Fe pot^{-1} and in the soluble and available fraction soil.

usually implies formation of ferritin which has a certain similarity with ferrihydrite/ferric hydrous oxide nanoparticles with variable amounts of phosphate.

Further research is needed to redesign the classical model of the iron uptake by plant with more studies that consider uptake from the Fe-NPs.

CONCLUSION

According to Lal (2008), in the context of sustainable agriculture, applying innovative nanotechnology in agriculture is regarded as one of the promising approaches to significantly increase crop production. The Fe-NFs can be considered as a part of

a novel technology in line with the precision and sustainable agriculture. They are iron-natural complex NPs synthetized from leonardite and they contain ferrihydrite in their structures which was properly and widely characterized. Moreover, the ^{57}Fe-NFs used in this paper are capable of supplying Fe to the plants, transport it from root to shoot and reach the soybean pods. The slow and continuous iron release of these ^{57}Fe-NFs confirms their long-term effect in providing iron in calcareous conditions while in soil, they tends to remain available to the plant requirements for the different growth stages.

Although further research is needed about the contribution of iron nanoparticles in plant nutrition, the Fe-NFs offers a natural, low cost and environmental option to the traditional iron fertilization in calcareous soils.

AUTHOR CONTRIBUTIONS

MC: synthesis of ^{57}Fe-NFs, carried out of the soil experiment, data processing, and manuscript preparation. AP: synthesis of ^{57}Fe-NFs and manuscript preparation. VL: XRD, TEM, and EXAFS data processing. DV: ICP AES analysis of ^{57}Fe-NFs samples. DP: Mössbauer spectroscopy. AV: EXAFS spectroscopy. IP: design and supervision of the synthesis and characterization of the ^{57}Fe-NFs, data interpretation, and manuscript preparation. JL: design and supervision of the soil experiment, data interpretation, and manuscript preparation.

FUNDING

The Russian Science Foundation (16-14-00167), the Russian Foundation for Basic Research (18-29-25065), and the Spanish Ministry of Science and Innovation (AGL2013-44474-R) have financially supported this research.

ACKNOWLEDGMENTS

The authors would like to acknowledge generous help and professional assistance of Dr. Oleg Schlaykhtin with freeze-drying the samples of NFs. MC expresses acknowledgment to Erasmus+ International Credit Mobility Program Alliance 4 Universities (A-4U) KA-107 for an academic stay at the Lomonosov MSU devoted to synthesis of ^{57}Fe-labeled NFs. JL and MC acknowledge the financial support of the Spanish Ministry of Science and Innovation (grant AGL2013-44474-R). JL and MC also acknowledge to the Comunidad de Madrid (Spain) and Structural Funds 2014-2020 (ERDF and ESF) for the financial support (project AGRISOST-CM S2018/BAA-4330). AP, VL, DV, and IP acknowledge financial support of the Russian Science Foundation (grant # 16-14-00167) in part of the ICP-OES, XRD, TEM, and EFTEM measurements. VL and IP acknowledge support of Russian Foundation for Basic Research project 18-29-25065 for EXAFS measurements and interpretations of the obtained samples of ^{57}Fe-labeled NFs. The use of the Carl Zeiss Libra 200MC TEM is supported by Lomonosov Moscow State University Program of Development. XAS were measured at the unique scientific facility Kurchatov Synchrotron Radiation Source supported by the Ministry of Education and Science of the Russian Federation (project code RFMEFI61917X0007).

SUPPLEMENTARY MATERIAL

The Supplementary Material for this article can be found online at: https://www.frontiersin.org/articles/10.3389/fpls.2019.00413/full#supplementary-material

REFERENCES

Aguirre, E., Leménager, D., Bacaicoa, E., Fuentes, M., Baigorri, R., Zamarreño, A. M., et al. (2009). The root application of a purified leonardite humic acid modifies the transcriptional regulation of the main physiological root responses to Fe deficiency in Fe-sufficient cucumber plants. *Plant Physiol. Biochem.* 47, 215–223. doi: 10.1016/j.plaphy.2008.11.013

Álvarez-Fernández, A., Pérez-Sanz, A., and Lucena, J. J. (2001). Evaluation of effect of washing procedures on mineral analysis of orange and peach leaves sprayed with seaweed extracts enriched with iron. *Commun. Soil Sci. Plant Anal.* 32, 157–170. doi: 10.1081/CSS-100103000

Angelico, R., Ceglie, A., He, J. Z., Liu, Y. R., Palumbo, G., and Colombo, C. (2014). Particle size, charge and colloidal stability of humic acids coprecipitated with ferrihydrite. *Chemosphere* 99, 239–247. doi: 10.1016/j.chemosphere.2013.10.092

Benedicto, A., Hernandez-Apaolaza, L., Rivas, I., and Lucena, J. J. (2011). Determination of 67Zn distribution in navy bean (*Phaseolus vulgaris* L.) after foliar application of 67Zn-lignosulfonates using isotope pattern deconvolution. *J. Agric. Food. Chem.* 59, 8829–8838. doi: 10.1021/jf2002574

Bolon, Y. T., Joseph, B., Cannon, S. B., Graham, M. A., Diers, B. W., Farmer, A. D., et al. (2010). Complementary genetic and genomic approaches help characerize the linkage group I seed protein QTL. *BMC Plant Biol.* 10:41. doi: 10.1186/1471-2229-10-41

Briat, J. F., Dubos, C., and Gaymard, F. (2015). Iron nutrition, biomass production, and plant product quality. *Trends Plant Sci.* 20, 33–40. doi: 10.1016/j.tplants.2014.07.005

Cakmak, I. (2002). Plant nutrition research: priorities to meet human needs for food in sustainable ways. *Plant Soil* 247, 3–24. doi: 10.1007/978-94-017-2789-1_1

Canellas, L. P., Olivares, F. L., Aguiar, N. O., Jones, D. L., Nebbioso, A., Mazzei, P., et al. (2015). Humic and fulvic acids as biostimulants in horticulture. *Sci. Hortic.* 196, 15–27. doi: 10.1016/j.scienta.2015.09.013

Cesco, S., Nikolic, M., Römheld, V., Varanini, Z., and Pinton, R. (2002). Uptake of 59Fe from soluble 59Fe-humate complexes by cucumber and barley plants. *Plant Soil* 241, 121–128. doi: 10.1023/A:1016061003397

Cesco, S., Römheld, V., Varanini, Z., and Pinton, R. (2000). Solubilization of iron by water-extractable humic substances. *J. Plant Nutr. Soil Sci.* 163, 285–290. doi: 10.1002/1522-2624(200006)163:3<285::AID-JPLN285>3.0.CO;2-Z

Cieschi, M. T., Caballero-Molada, M., Menéndez, N., Naranjo, M. A., and Lucena, J. J. (2017). Long-term effect of a leonardite iron humate improving Fe nutrition as revealed in silico, in vivo, and in field experiments. *J. Agric. Food Chem.* 65, 6554–6563. doi: 10.1021/acs.jafc.7b01804

Cieschi, M. T., and Lucena, J. J. (2018). Iron and humic acid accumulation on soybean roots fertilized with leonardite iron humates under calcarous conditions. *J. Agric. Food Chem.* 66, 13386–13396. doi: 10.1021/acs.jafc.8b04021

Colombo, C., Palumbo, G., He, J. Z., Pinton, R., and Cesco, S. (2014). Review on iron availability in soil: interaction of Fe minerals, plants, and microbes. *J. Soils Sediments* 14, 538–548. doi: 10.1007/s11368-013-0814-z

Colombo, C., Palumbo, G., Sellitto, V. M., Cho, H. G., Amalfitano, C., and Adamo, P. (2015). Stability of coprecipitated natural humic acid and ferrous iron under oxidative conditions. *J. Geochem. Explor.* 151, 50–56. doi: 10.1016/j.gexplo.2015.01.003

Colombo, C., Palumbo, G., Sellitto, V. M., Rizzardo, C., Tomasi, N., Pinton, R., et al. (2012). Characteristics of insoluble, high molecular weight iron-humic substances used as plant iron sources. *Soil Sci. Soc. Am. J.* 76, 1246–1256. doi: 10.2136/sssaj2011.0393

Dholakia, P. V. (2016). Preparation of nanopartical liquid organic fertilizer and its effect on various crops. *Int. J. Sci. Res. Sci. Eng. Tech.* 2, 781–785.

Dimkpa, C. O., and Bindraban, P. S. (2017). Nanofertilizers: new products for the industry? *J. Agric. Food Chem.* 66, 6462–6473. doi: 10.1021/acs.jafc.7b02150

Food and Agriculture Organization of the United Nations [FAO] (2017). *The Future of Food and Agriculture. Trends and Challenges*. Rome: FAO.

Fuentes, M., Bacaicoa, E., Rivero, M., Zamarreño, ÁM., and García-Mina, J. M. (2018). Complementary evaluation of iron deficiency root responses to assess the effectiveness of different iron foliar applications for chlorosis remediation. *Front. Plant Sci.* 9:351. doi: 10.3389/fpls.2018.00351

Ghafariyan, M. H., Malakouti, M. J., Dadpour, M. R., Stroeve, P., and Mahmoudi, M. (2013). Effects of magnetite nanoparticles on soybean chlorophyll. *Environ. Sci. Technol.* 47, 10645–10652. doi: 10.1021/es402249b

Homonnay, Z., Tolnai, G., Fodor, F., Solti, Á, Kovács, K., Kuzmann, E., et al. (2016). Iron oxide nanoparticles for plant nutrition? A preliminary Mössbauer study. *Hyperfine Interact.* 237, 1–9. doi: 10.1007/s10751-016-1334-1

Hunter, J. D. (2007). Matplotlib: a 2D graphics environment. *Comput. Sci. Eng.* 9, 99–104. doi: 10.1109/MCSE.2007.55

ISO 3696:1987 (1987). *Water for Analytical Laboratory Use–Specification and Test Methods*. Available at: https://www.iso.org/standard/9169.html (accessed April, 1987).

Janmohammadi, M., Navid, A., Segherloo, A. E., and Sabaghnia, N. (2016). Impact of nano-chelated micronutrients and biological fertilizers on growth performance and grain yield of maize under deficit irrigation condition. *Biologija* 62, 134–147. doi: 10.6001/biologija.v62i2.3339

Kovács, K., Czech, V., Fodor, F., Solti, A., Lucena, J. J., Santos-Rosell, S., et al. (2013). Characterization of Fe-leonardite complexes as novel natural iron fertilizers. *J. Agric. Food Chem.* 61, 12200–12210. doi: 10.1021/jf404455y

Kulikova, N., Badun, G. A., Korobkov, V. I., Chernysheva, M. G., Tsvetkova, E. A., Abroskin, D. P., et al. (2014). Accumulation of coal humic acids by wheat seedlings: direct evidence using tritium autoradiography and occurrence in lipid fraction. *J. Plant Nutr. Soil Sci.* 177, 875–883. doi: 10.1002/jpln.201300648

Kulikova, N. A., Polyakov, A. Y., Lebedev, V. A., Abroskin, D. P., Volkov, D. S., Pankratov, D. A., et al. (2017). Key roles of size and crystallinity of nanosized iron hydr(oxides) stabilized by humic substances in iron bioavailability to plants. *J. Agric. Food Chem.* 65, 11157–11169. doi: 10.1021/acs.jafc.7b03955

Lal, R. (2008). Promise and limitations of soils to minimize climate change. *J. Soil Water Conserv.* 63, 113A–118A. doi: 10.2489/jswc.63.4.113A

Liu, R., and Lal, R. (2015). Potentials of engineered nanoparticles as fertilizers for increasing agronomic productions. *Sci. Total Environ.* 514, 131–139. doi: 10.1016/j.scitotenv.2015.01.104

López-Rayo, S., Di Foggia, M., Bombai, G., Yunta, F., Rodrigues Moreira, E., Filippini, G., et al. (2015). Blood-derived compounds can efficiently prevent iron deficiency in the grapevine. *Aust. J. Grape Wine Res.* 21, 135–142. doi: 10.1111/ajgw.12109

Maillot, F., Morin, G., Wang, Y., Bonnin, D., Ildefonse, P., Chaneac, C., et al. (2011). New insight into the structure of nanocrystalline ferrihydrite: EXAFS evidence for tetrahedrally coordinated Iron (III). *Geochim. Cosmochim. Acta* 75, 2708–2720. doi: 10.1016/j.gca.2011.03.011

Manceau, A., and Gates, W. (1997). Surface structural model for ferrihydrite. *Clays Clay Miner.* 45, 448–460. doi: 10.1346/CCMN.1997.0450314

MAPA (1994). *Métodos Oficiales De Análisis. Servicio De Publicaciones. Spanish Ministry of Agriculture, F. and F. MAPA Official Methods of Analysis*, Vol. III. Madrid: MAPA.

Martín-Fernández, C., López-Rayo, S., Hernández-Apaolaza, L., and Lucena, J. J. (2017a). Timing for a sustainable fertilisation of Glycine max by using HBED/Fe3+ and EDDHA/Fe3+ chelates. *J. Sci. Food Agric.* 97, 2773–2781. doi: 10.1002/jsfa.8105

Martín-Fernández, C., Solti, Á, Czech, V., Kovács, K., Fodor, F., Gárate, A., et al. (2017b). Response of soybean plants to the application of synthetic and biodegradable Fe chelates and Fe complexes. *Plant Physiol. Biochem.* 118, 579–588. doi: 10.1016/j.plaphy.2017.07.028

Michel, F. M., Ehm, L., Antao, S. M., Lee, P. L., Chupas, P. J., Liu, G., et al. (2007). The structure of ferrihydrite, a nanocrystalline material. *Science* 316, 1726–1729. doi: 10.1126/science.1142525

Mimmo, T., Del Buono, D., Terzano, R., Tomasi, N., Vigani, G., Crecchio, C., et al. (2014). Rhizospheric organic compounds in the soil-microorganism-plant system: their role in iron availability. *Eur. J. Soil Sci.* 65, 629–642. doi: 10.1111/ejss.12158

Nadal, P., García-Delgado, C., Hernández, D., López-Rayo, S., and Lucena, J. J. (2012). Evaluation of Fe-N,N'-Bis(2-hydroxybenzyl)ethylenediamine-N,N'-diacetate (HBED/Fe3+) as Fe carrier for soybean (*Glycine max*) plants grown in calcareous soil. *Plant Soil* 360, 349–362. doi: 10.1007/s11104-012-1246-z

Naderi, M. R., and Danesh-Shahraki, A. (2013). Nanofertilizers and their roles in sustainable agriculture. *Int. J. Agric. Crop Sci.* 5, 2229–2232.

Nardi, S., Pizzeghello, D., Muscolo, A., and Vianello, A. (2002). Physiological effects of humic substances on higher plants. *Soil Biol. Biochem.* 34, 1527–1536. doi: 10.1016/S0038-0717(02)00174-8

Nečas, D., and Klapetek, P. (2012). Gwyddion: an open-source software for SPM data analysis. *Cent. Eur. J. Phys.* 10, 181–188. doi: 10.2478/s11534-011-0096-2

Nikolic, M., Cesco, S., Römheld, V., Varanini, Z., and Pinton, R. (2003). Uptake of iron (59Fe) Complexed to water-extractable humic substances by sunflower leaves. *J. Plant Nutr.* 26, 2243–2252. doi: 10.1007/s11104-009-0091-1

Olaetxea, M., De Hitaa, D., Garcia, A., Fuentes, M., Baigorri, R., Mora, V., et al. (2018). Hypothetical framework integrating the main mechanisms involved in the promoting action of rhizospheric humic substances on plant root- and shootgrowth. *Appl. Soil Ecol.* 123, 521–537. doi: 10.1016/j.apsoil.2017.06.007

Olaetxea, M., Mora, V., Bacaicoa, E., Garnica, M., Fuentes, M., Casanova, E., et al. (2015). Abscisic acid regulation of root hydraulic conductivity and aquaporin gene expression is crucial to the plant shoot growth enhancement caused by rhizosphere humic acids. *Plant Physiol.* 169, 2587–2596. doi: 10.1104/pp.15.00596

Pankratov, D. A., Dolzhenko, V. D., Stukan, R. A., Al Ansari, Y. F., Savinkina, E. V., and Kiselev, Y. M. (2013). Investigation of Iron (III) complex with crown-porphyrin. *Hyperfine Interact.* 222, 1–11. doi: 10.1007/s10751-011-0378-5

Pariona, N., Martinez, A. I., Hdz-García, H. M., Cruz, L. A., and Hernandez-Valdes, A. (2016). Effects of hematite and ferrihydrite nanoparticles on germination and growth of maize seedlings. *Saudi J. Biol. Sci.* 24, 1547–1554. doi: 10.1016/j.sjbs.2016.06.004

Rodríguez-Castrillón, J. Á, Moldovan, M., García Alonso, J. I., Lucena, J. J., García-Tomé, M. L., and Hernández-Apaolaza, L. (2008). Isotope pattern deconvolution as a tool to study iron metabolism in plants. *Anal. Bioanal. Chem.* 390, 579–590. doi: 10.1007/s00216-007-1716-y

Rodríguez-Lucena, P., Hernández, D., Hernández-Apaolaza, L., and Lucena, J. J. (2010). Revalorization of a two-phase olive mill waste extract into a micronutrient fertilizer. *J. Agric. Food Chem.* 58, 1085–1092. doi: 10.1021/jf903185z

Römheld, V., and Nikolic, M. (2007). "Iron," in *Handbook of Plant Nutrition*, eds A. V. Barker and D. J. Pilbeam (Boca raton, FL: CRC Press).

Rose, M. T., Patti, A. F., Little, K. R., Brown, A. L., Jackson, W. R., and Cavagnaro, T. R. (2014). A meta-analysis and review of plant-growth response to humic substances: practical implications for agriculture. *Adv. Agron.* 124, 37–89. doi: 10.1016/B978-0-12-800138-7.00002-4

Sánchez-Alcalá, I., del Campillo, M. C., Barrón, V., and Torrent, J. (2012). Pot evaluation of synthetic nanosiderite for the prevention of iron chlorosis. *J. SCI. Food Agric.* 92, 1964–1973. doi: 10.1002/jsfa.5569

Schwertmann, U., and Cornell, R. (1992). *Iron Oxides in the Laboratory: Preparation and Characterization*. Hoboken, NJ: John Wiley & Sons.

Schwertmann, U., Friedl, J., and Stanjekl, H. (1999). From Fe (III) ions to ferrihydrite and then to hematite. *J. Colloid Interface Sci.* 209, 215–223. doi: 10.1006/jcis.1998.5899

Soltanpour, P. N., and Schwab, A. P. (1977). A new soil test for simultaneous extraction of macro- and micro-nutrients in alkaline soils. *Commun. Soil Sci. Plant Anal.* 8, 195–207. doi: 10.1080/00103627709366714

Sorkina, T. A., Polyakov, A. Y., Kulikova, N. A., Goldt, A. E., Philippova, O. I., Aseeva, A. A., et al. (2014). Nature-inspired soluble iron-rich humic compounds: new look at the structure and properties. *J. Soils Sediments* 14, 261–268. doi: 10.1007/s11368-013-0688-0

Tomasi, N., De Nobili, M., Gottardi, S., Zanin, L., Mimmo, T., Varanini, Z., et al. (2013). Physiological *and* molecular characterization of fe acquisition by tomato plants from natural Fe complexes. *Biol. Fertil. Soils* 49, 187–200. doi: 10.1007/s00374-012-0706-1

United Nations [UN] (2013). *World Population Prospects: The 2012 Revision*. Available at: https://population.un.org/wpp/Publications/Files/WPP2012_HIGHLIGHTS.pdf (accessed December 1, 2018).

Vasconcelos, M. W., and Grusak, M. A. (2014). Morpho-physiological parameters affecting iron deficiency chlorosis in soybean (*Glycine max* L.). *Plant Soil* 374, 161–172. doi: 10.1007/s11104-013-1842-6

Villén, M., Lucena, J. J., Cartagena, M. C., Bravo, R., García-Mina, J., and de la Hinojosa, M. I. M. (2007). Comparison of two analytical methods for the evaluation of the complexed metal in fertilizers and the complexing capacity of complexing agents. *J. Agric. Food Chem.* 55, 5746–5753. doi: 10.1021/jf070422t

Ylivainio, K. (2010). Effects of iron (III) chelates on the solubility of heavy metals in calcareous soils. *Environ. Pollut.* 158, 3194–3200. doi: 10.1016/j.envpol.2010.07.004

Zamboni, A., Zanin, L., Tomasi, N., Avesani, L., Pinton, R., Varanini, Z., et al. (2016). Early transcriptomic response to Fe supply in Fe-deficient tomato plants is strongly influenced by the nature of the chelating agent. *BMC Genomics* 17:35. doi: 10.1186/s12864-015-2331-5

Conflict of Interest Statement: The authors declare that the research was conducted in the absence of any commercial or financial relationships that could be construed as a potential conflict of interest.

frontiers in Plant Science

ORIGINAL RESEARCH
published: 30 April 2019
doi: 10.3389/fpls.2019.00502

Characterization of the Nicotianamine Exporter ENA1 in Rice

Tomoko Nozoye[1,2], Nicolaus von Wirén[3], Yoshikatsu Sato[4], Tetsuya Higashiyama[4], Hiromi Nakanishi[2] and Naoko K. Nishizawa[2,5]*

[1] Center for Liberal Arts, Meiji Gakuin University, Tokyo, Japan, [2] Graduate School of Agricultural and Life Sciences, The University of Tokyo, Tokyo, Japan, [3] Molecular Plant Nutrition, Leibniz Institute of Plant Genetics and Crop Plant Research, Gatersleben, Germany, [4] Institute of Transformative Bio-Molecules (WPI-ITbM), Nagoya University, Nagoya, Japan, [5] Research Institute for Bioresources and Biotechnology, Ishikawa Prefectural University, Nonoichi, Japan

Under iron (Fe) deficiency, graminaceous plants produce and secrete Fe-chelating phytosiderophores of the mugineic acid (MA) family into the rhizosphere to solubilize and mediate uptake of sparingly soluble Fe in the soil. MAs and their biosynthetic intermediate, nicotianamine (NA), are also important for the translocation of divalent metals such as Fe and zinc (Zn) throughout the plant body. In this study, the physiological role of the efflux transporter EFFLUX TRANSPORTER OF NA (ENA1), which exports NA out of cells, was analyzed in rice. *Promoter-GUS* analysis showed that *ENA1* was mainly expressed in roots, and strongly upregulated under Fe-deficient conditions. In epidermal onion cells and rice roots, green fluorescent protein-tagged ENA1 localized mainly to the plasma membrane, while a part of the fluorescence was observed in vesicular structures in the cytoplasm. In the younger stage after germination, *ENA1*-overexpressing rice plants exhibited truncated roots with many root hairs compared to wild-type plants, while these phenotype were not observed in high Zn-containing medium. In *Arabidopsis*, which use a different strategy for Fe uptake from rice, *ENA1* overexpression did not show any apparent phenotypes. Oligo DNA microarray analysis in rice showed that *ENA1* knockout affects the response to stress, especially in root plastids. These results suggest that ENA1 might be recycling between the plasma membrane and cellular compartments by vesicular transport, playing an important role in the transport of NA, which is important for the physiological response to Fe deficiency.

Keywords: iron chelator, mugineic acid, nicotianamine (NA) export, graminaceous plant, transporter

OPEN ACCESS

Edited by:
Thomas J. Buckhout, Humboldt University of Berlin, Germany

Reviewed by:
Stephane Mari, Institut National de la Recherche Agronomique (INRA), France
Michael Frei, University of Bonn, Germany

****Correspondence:***
Tomoko Nozoye
atom1210@mail.ecc.u-tokyo.ac.jp

Specialty section:
This article was submitted to Plant Nutrition, a section of the journal Frontiers in Plant Science

Received: *31 January 2019*
Accepted: *01 April 2019*
Published: *30 April 2019*

Citation:
Nozoye T, von Wirén N, Sato Y, Higashiyama T, Nakanishi H and Nishizawa NK (2019) Characterization of the Nicotianamine Exporter ENA1 in Rice. Front. Plant Sci. 10:502. doi: 10.3389/fpls.2019.00502

INTRODUCTION

Iron (Fe) is an essential element for all living organisms. In plants, Fe plays a key role in electron transfer in both photosynthetic and respiratory reactions in chloroplasts and mitochondria. Fe deficiency leads to leaf chlorosis and decreased plant yield. On the other hand, excess Fe is toxic, because it catalyzes the generation of free radicals. To acquire Fe from the rhizosphere, plants have evolved two strategies (Marschner et al., 1986). In strategy-I plants, Fe is mobilized via coumarin-type siderophores (Schmid et al., 2014; Rajniak et al., 2018; Tsai et al., 2018) and Fe(III) reduction prior to uptake in the form of ferrous Fe (Eide et al., 1996; Robinson et al., 1999; Vert et al., 2002). In strategy-II plants, Fe is mobilized via chelation through mugineic acid

(MA)-type phytosiderophores (Takagi, 1976) and uptake of intact Fe(III)-phytosiderophore complexes (Römheld and Marschner, 1986). It has been believed that most plants acquire Fe by strategy-I, while only graminaceous plant species acquire Fe by strategy-II (Marschner, 1995).

In graminaceous plants, MAs are synthesized through a conserved pathway, in which three sequential enzymatic reactions convert *S*-adenosyl methionine to 2′-deoxymugineic acid (DMA) (Mori and Nishizawa, 1987; Shojima et al., 1990; Ma and Nomoto, 1993; Ma et al., 1999; Mori, 1999; Arco and Satrústegui, 2005). Expression of the genes involved in MAs biosynthesis is strongly induced by Fe deficiency. MAs are also involved in metal transport in planta (Mori et al., 1991; Kawai et al., 2001; Suzuki et al., 2006; Kakei et al., 2009). Only in the phytosiderophore biosynthesis pathway of graminaceous plants, nicotianamine (NA) acts as the direct precursor for the synthesis of DMA, whereas NA is synthesized in all plants including those that employ strategy-I for Fe acquisition (Noma and Noguchi, 1976; Rudolph et al., 1985). NA is structural analog of MAs and chelates metal cations, including Fe and zinc (Zn), manganese (Mn), and copper (Cu) (Beneš et al., 1983; Von Wirén et al., 1999). In both Strategy I and II plants, NA functions as metal chelator for intracellular metal trafficking and for long-distance metal transport between different organs (Takahashi et al., 2003; Bashir et al., 2010; Kobayashi and Nishizawa, 2012), including phloem-mediated transport of Fe from source to sink organs (Hell and Stephan, 2003; Takahashi et al., 2003; Schuler et al., 2012). In graminaceous plants, it was reported that NA is a main chelator of Zn in the phloem sap (Nishiyama et al., 2012). Intracellularly, NA was suggested to be important for vacuolar sequestration in the detoxification of excess Fe (Pich et al., 2001). In *Arabidopsis halleri*, one of the intensively studied hyperaccumulator species, NA concentrations can be extremely high (Deinlein et al., 2012), suggesting that NA plays a key role in Zn hyperaccumulation.

Fe translocation and cellular Fe transport are regulated by different transporters. MAs are secreted from the roots via TRANSPORTER OF MAs (TOM1) (Nozoye et al., 2011, 2013) to solubilize Fe in the rhizosphere. The resulting Fe(III)–MAs complexes are then taken up through the action of YELLOW STRIPE 1 (YS1) transporters (Mihashi and Mori, 1989; Curie et al., 2001; Inoue et al., 2009). Transgenic rice plants with repressed expression of *TOM2*, which is a homolog of *TOM1* and can efflux DMA, showed impaired growth because of a defect in Fe mobilization (Nozoye et al., 2015). These results corroborate that DMA solubilizes and mobilizes precipitated Fe in the apoplast. ZINC-INDUCED FACILITATOR 1 (ZIF1), a homolog of TOM1 in *Arabidopsis*, is a tonoplast-localized transporter believed to transport NA from the cytoplasm to the vacuoles (Haydon and Cobbett, 2007; Haydon et al., 2012). *ZINC-INDUCED FACILITATOR 1*-overexpressing *Arabidopsis* plants showed interveinal chlorosis and had higher Fe but lower Zn concentrations in their shoots than wild-type (WT) plants, while the opposite tendency occurred in roots (Haydon et al., 2012). These results suggested that NA is involved in the subcellular distribution and inter-organ partitioning of Fe and Zn, and that perturbing NA transport may have significant impact on Fe and Zn nutrition. However, the association between Fe, Zn, and NA, and MAs remains unclear. EFFLUX TRANSPORTER OF NA (ENA1), a rice gene belonging to the major facilitator superfamily as the TOM family and ZIF1, has been described to transport NA out of cells, when expressed in *Xenopus* oocytes (Nozoye et al., 2011). The expression of *ENA1* was strongly induced in Fe-deficient roots, suggesting that ENA1 is involved in Fe homeostasis in rice. However, its physiological function *in planta* has not been identified. In this study, different approaches were taken to investigate the physiological function of ENA1 in planta.

MATERIALS AND METHODS

Construction of Plant Expression Vectors and Transgenic Plants

To construct the β-glucuronidase (GUS) reporter fusion genes, an 1.5-kb fragment of the 5′-upstream region of *ENA1* (*Os11g0151500*) was amplified from genomic DNA extracted from rice leaves (cv. Nipponbare) using the primer pairs 5′-AAGCTTTTGGTCCAACTCTAAGAGAT-3′ and 5′-ACTAGTCAGTGGCTTCAGAACCCTCA-3′ and ligated into the pCR4 Blunt-TOPO vector (Invitrogen). Gene fragments were then excised and subcloned into the pIG121Hm vector (Hiei et al., 1994) upstream of the GUS open-reading frame to generate the *ENA1* promoter-GUS construct. To assess the subcellular localization of *ENA1* in onion epidermal cells or rice plants, an attL/attR substrate recombination reaction between pENA1 and pH7FWG2 (Karimi et al., 2002) was used to generate the CaMV *35S promoter–ENA1–enhanced green fluorescent protein* (*eGFP*) cassette. To confirm subcellular localization of ENA1 in rice plants, *ENA1–GFP* or *GFP–ENA1* cassettes were cloned into the pDEST35S–sGFP binary vector (Ishimaru et al., 2005) using LR Clonase (Invitrogen) according to the manufacturer's instructions for expression under control of the 35S promoter as described previously (Nozoye et al., 2011, 2015). *Agrobacterium tumefaciens* strain C58 carrying these constructs was used to transform rice (cv. Tsukinohikari) plants (Hiei et al., 1994).

Histochemical Localization and Subcellular Localization of ENA1

β-Glucuronidase activity in the roots and shoots of *ENA1 promoter::GUS* transgenic plants was determined using a histochemical assay, as described previously (Inoue et al., 2003; Nozoye et al., 2011, 2015). Subcellular localization of ENA1 in onion epidermal cells or rice roots was observed as described previously (Nozoye et al., 2011, 2015). FM-64 (1 mM; Molecular Probes) was used for staining the plasma membranes by incubation of rice roots section on glass slides at room temperature. Confocal images of rice roots were acquired with a laser scanning microscope (LSM Pascal and LSM 780, Zeiss,

Germany) equipped with a 10×/0.45 M27 objective. Excitation/emission wavelengths of 488 nm/490–540 nm or ∼515 nm/640 nm were used for detection of GFP or FM4-64 fluorescence, respectively.

Characterization of *ena1* Mutants

Five *ena1 Tos17* mutant lines, namely, *NG1014*, *NG1060*, *ND1041*, *ND0824*, and *NC0379*, generated through retrotransposon insertion (Hirochika et al., 1996) were obtained from the former National Institute of Agricultural Sciences (NIAS) [https://tos.nias.affrc.go.jp/ in Japanese; present organization is Institute of Agrobiological Sciences (NARO)]. To confirm the insertion of *Tos17* into the *ENA1* gene, PCR was performed using the *Tos17* left-border specific primers (Tos17L) and *ENA1*-specific primers (pE1 for *NG1060*, pE2 for *NG1014*, pE3 for *ND8024*, pE4 for *ND1041*, and pE5 for *NC0379*) (**Supplementary Table S1** and **Supplementary Figure S3**). When the *Tos17* fragment was inserted into *ENA1* gene, PCR fragments were expected to be amplified. To explore whether *ENA1* disruption by *tos17* was homozygous or heterozygous, PCR on genomic DNA using primers amplifying the fragment between the *tos17* insertion regions was performed. Primer sets were as follows: pE1 and pE2 for *NG1060*; pE1 and pE5 for *NG0379*; and pE1 and pE4 for *NG1014*, *ND8024*, and *ND1041*. If the *Tos17* insertion was homozygous, fragments of 1.3, 3, or 1.6 kb were not expected to be amplified by the primer sets for NG1060, NC0379, or other lines, respectively, since insertion of *tos17* into these regions would disrupt the *ENA1* sequence. When the amplified fragment was the same sizes as in WT, although they carry a *Tos17* insertion in ENA1, these plants were handled as being heterozygous.

For DNA microarray analysis, rice plants were grown hydroponically. Rice seeds (*Oryza sativa* L. cv. Nipponbare) were surface-sterilized using 2.5% sodium hypochlorite and then germinated for 1 week on Murashige and Skoog (MS) medium. After germination, the seedlings were transferred to a 20-L plastic container containing a nutrient solution of the following composition: 0.7 mM K_2SO_4, 0.1 mM KCl, 0.1 mM KH_2PO_4, 2.0 mM $Ca(NO_3)_2$, 0.5 mM $MgSO_4$, 10 μM H_3BO_3, 0.5 μM $MnSO_4$, 0.2 μM $CuSO_4$, 0.5 μM $ZnSO_4$, 0.05 μM Na_2MoO_4, and 0.1 mM Fe(III)–EDTA. The pH of the nutrient solution was adjusted daily to 5.5 with 1 M HCl. The Fe-deficiency treatment was initiated 4 weeks after germination by transferring the plants to an Fe(III)–EDTA-free nutrient solution. Experiments were performed in triplicate.

For germination analysis under high Zn conditions, rice seeds were germinated on MS medium (control) or MS medium containing 2 mM $ZnSO_4$ (high Zn) according to Song et al. (2011), and cultured under a 14-h photoperiod at 320 μmol photons m^{-2} s^{-1} at 30°C. Plants were harvested at 12 days after germination, and the lengths of shoots and roots were measured. Nine plants for each line were used for each analysis. The concentrations of Fe, Zn, Mn, and phosphorus (P) were determined using inductively coupled plasma–mass spectroscopy, as described previously (Nozoye et al., 2014a).

Semiquantitative Reverse Transcription (RT)-PCR

Total RNA was extracted from the roots of three plants per line using the RNeasy Plant Kit (Qiagen) according to the manufacturer's instructions. Using ReverTra Ace qPCR RT Master Mix with gDNA Remover (Toyobo, Tokyo, Japan), contaminating genomic DNA was removed from total RNA and first-strand cDNA was synthesized. The forward and reverse primers used for *ENA1* were 5′-ACAAATTGGCAAGGAACTGA-3′ and 5′-CAAGATTGTG GCGTTACAAC-3′. The forward and reverse primers used for *OsActin1* were 5′-ACACCGGTGTCATGGTCGG-3′ and 5′-ACACGGAGCTCGTTGTAGAA-3′. The sizes of the amplified fragments were confirmed by agarose gel electrophoresis.

Analysis of Rice Genes Overexpressed in *Arabidopsis thaliana*

Transgenic *Arabidopsis* plants overexpressing *ENA1*, *OsIRO2* (Ogo et al., 2006), *DMAS1*, *TOM2*, and *TOM3* generated previously by Kondou et al. (2009) were obtained from the rice full-length cDNA overexpressing *Arabidopsis* mutant database[1] (Ichikawa et al., 2006). *Arabidopsis* seeds were surface-sterilized and germinated on 1/2 MS medium containing 100 μM Fe(III)-EDTA, 1/2 MS medium without Fe, 1/2 MS medium replacing Fe(III)-EDTA with 1 μM $FeCl_2$, or 1/2 MS medium replacing Fe(III)-EDTA with 1 mM Fe(III)-citrate. Shoots were harvested 1 month after germination and used for analysis of metal concentrations as described above.

Oligo DNA Microarray Analysis

Microarray expression analysis was performed as described previously (Nozoye et al., 2011). Total RNA was extracted from shoots and roots of *ena1* mutants (ND0824 #A, NG1060 #A, and NG1060 #D) and WT plants using the RNeasy Plant Kit (Qiagen), labeled with Cy-3 or Cy-5, and hybridized to Agilent rice 44K oligo DNA microarrays (Agilent Technologies). For each line, a mixture of three plants was used to extract RNA. For expression analysis, gene expression ratios were calculated by (signal value of *ena1* mutant sample)/(signal value of WT sample), and genes whose expression levels were increased or decreased by at least twofold were categorized as upregulated or downregulated, respectively. To assess reproducibility of the microarray analysis, genes whose expression levels were changed in all three independent lines (ND0824 #A, NG1060 #A, and NG1060 #D) were further analyzed.

To identify upregulated genes under Fe-deficient conditions, the ratio was calculated as (signal value of Fe-deficient [–Fe] sample)/(signal value of Fe-sufficient [+Fe] sample), and these ratios were used to identify Fe deficiency-induced genes, as described previously (Nozoye et al., 2011). Genes showing differential expression

[1]http://ricefox.psc.riken.jp/index.php?contents=top&subcontents=research&research=foxh

with a significant difference according to Student's *t*-test ($P < 0.05$) were analyzed. To evaluate the function of *ENA1 in planta*, we performed gene ontology (GO) analysis using agriGO (Du et al., 2010; Tian et al., 2017). agriGO is designed to identify enriched GO terms in a list of microarray probe sets[2]. Three categories were included in the analysis, namely biological process, molecular function, and cellular component.

RESULTS

Promoter-GUS Analysis of ENA1

In Fe-sufficient plants, *ENA1* promoter activity was low in primary and branched lateral roots (**Figures 1A,B,E**), where *ENA1* expression was localized to the epidermis and cortex (**Figures 1G,I**). Under Fe-deficient conditions, *ENA1* promoter activity was strongly enhanced in both, primary and lateral roots, except in root tips (**Figures 1C,D,F,H,J**). Root cross-sections further revealed that *ENA1* promoter activity was confined to the epidermis near the root tips, while it was detected across all tissues in basal root zones (**Figures 1H,J**). In shoots, *ENA1* expression was also induced by Fe deficiency but only observed near the root-to-shoot junction, where translocation spots exist between xylem and phloem (**Figures 1K,L**). In leaves, *ENA1* expression was not observed (data not shown).

Intracellular Localization of ENA1

To investigate the subcellular localization of ENA1, *ENA1–GFP*, or *GFP–ENA1* fusion constructs were transiently expressed in onion epidermal cells (**Supplementary Figure S1**). Both ENA1–GFP and GFP–ENA1 fusion proteins were observed in the plasma membrane and in the cytoplasm. In the cytoplasm, some of the GFP–ENA1 and ENA1–GFP fusion proteins were localized to vesicular structures. This localization was more common with the ENA1–GFP fusion protein than the GFP–ENA1 fusion protein. To confirm the cellular localization in rice plants, *ENA1–GFP* or *GFP–ENA1* fusion genes were stably expressed in rice plants, in which expression was observed in roots. There ENA1–GFP-dependent fluorescence was mainly localized to the plasma membrane (**Figure 2** and **Supplementary Figures S2A–F**). A part of ENA1–GFP fusion proteins was observed in intracellular compartments. The fluorescence intensity from the GFP–ENA1 fusion protein was much weaker than that of the ENA1–GFP fusion, while the mRNA levels of *GFP–ENA1* and *ENA1–GFP* fusion genes were similar (**Supplementary Figure S2G**). The expression pattern was not affected by the Fe concentration of the medium.

Analysis of the tos17 Insertion Line in ENA1 Loci

Five *tos17* insertion mutants with retrotransposon fragments inserted in *ENA1* (NG1014, NG1060, ND1041, ND0824, and NC0379) were identified (**Figure 3A** and **Supplementary Figure S3A**). Nested PCR was performed to confirm the insertion of *tos17* in *ENA1*, which showed that three lines

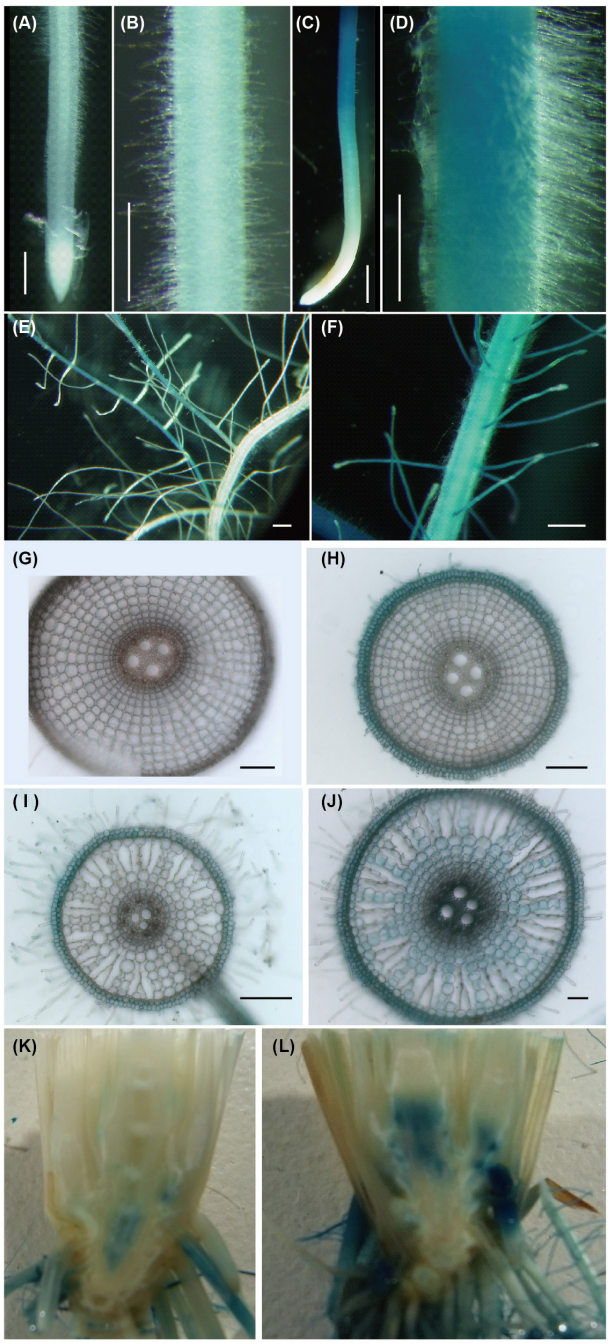

FIGURE 1 | Promoter activity of ENA1 in rice during vegetative growth as indicated by GUS staining. **(A,B,E,G,I)** Iron (Fe)-sufficient root. **(C,D,F,H,I)** Fe-deficient root. **(G,H)** Cross-sections of the elongation zone. **(I,J)** Cross-sections of the root near the basal part. **(K,L)** Tissue distribution of *ENA1* promoter activity in root–shoot junctions under Fe-sufficient **(K)** or Fe-deficient **(L)** conditions. The basal part of the shoot was cut vertically and the interior tissue is shown. Scale bars: 1 mm **(A–F)**; 200 μm **(G–J)**.

[2]http://bioinfo.cau.edu.cn/agriGO/index.php

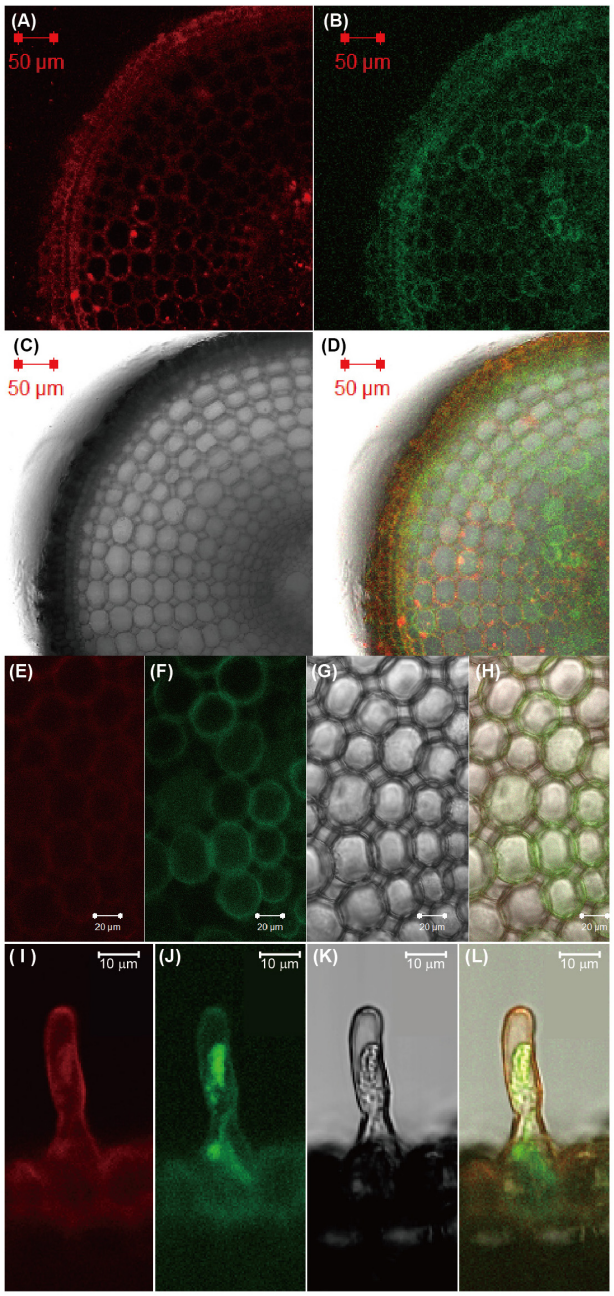

FIGURE 2 | Subcellular localization of ENA1-GFP in rice roots. **(A,E,I)** Fluorescence image of FM65-stained rice roots. **(B,F,J)** Fluorescence image of GFP. **(C,G,K)** Differential interference contrast image. **(D,H,L)** Overlay.

of NG1014 (#C, #D, #E), three of NG1060 (#A, #C, #D), two of ND1041 (#D, #E), two of ND0824 (#B, #C), and two of NC0379 (#A, #D) carried a *tos17* insertion in the *ENA1* gene (**Supplementary Figure S3B**). Next, to explore whether the transgenic plants harboring the *tos17* retrotransposon in *ENA1* were in a homozygous or heterozygous state, genomic PCR amplifying the *tos17* insertion region was performed (**Supplementary Figure S3C**). NG1014 (#D), NG1060 (#A, #C, #D), ND1041 (#D, #E), and NC0379 (#A) were heterozygous, while NG1014 (#C, #E), ND0824 (#B, #C), and NC0379 (#D) were homozygous. RT-PCR showed that *ENA1* was knocked-out in NG1014 (#C, #E), NG1060 (#A, #D), ND1041 (#E), and NC0379 (#A, #D) (**Figure 3B** and **Supplementary Figure S3B**). *ENA1* fragments in ND0824 (#B, #C) were not absent, although the *tos17* insertion in *ENA1* was homozygous, and their sizes were smaller than in the WT. In ND0824, *Tos17* was inserted at the junction of the intron and exon of *ENA1*, which could influence the size of *ENA1*.

To analyze the function of ENA1 in planta, plants were cultivated hydroponically under Fe-sufficient or Fe-deficient conditions, and plant characteristics such as plant height, root length, chlorophyll content, and metal concentrations were analyzed (**Supplementary Figure S4**). However, there were no apparent differences among *ena1* knockout mutants, *ENA1–GFP-* or *GFP–ENA1*-overexpression lines, or WT plants.

Since ENA1 has the ability to export NA (Nozoye et al., 2011), it was speculated that the function of ENA1 *in planta* might be similar to that of ZIF1, a putative NA exporter in *Arabidopsis*, and involved in Fe and Zn homeostasis (Haydon and Cobbett, 2007; Haydon et al., 2012). Interveinal chlorosis of *ZIF1*-overexpressing Arabidopsis was recovered by addition of Fe, while this phenotype became more severe under high Zn conditions (Haydon et al., 2012). Therefore, the phenotypes of *ena1* knockout mutants in rice, NG1060 #A and NC0379 #A, the *ENA1–GFP-* or *GFP–ENA1*-overexpressing lines, and WT were compared in MS medium with adequate nutrient supply or excess Zn supply (**Figure 4**). Under adequate nutrient supply, roots of *ENA1–GFP-* and *GFP–ENA1*-overexpressing rice plants were shorter than those of WT and *ena1* knockout mutants (**Figures 4A,F**). The *ENA1–GFP-* and *GFP–ENA1*-overexpressing plants had more root hairs compared to WT and *ena1* knockout mutants (**Figures 4A,C,D**). Under high Zn conditions, the short-root phenotype and enhanced root hair formation of *ENA1–GFP-* and *GFP–ENA1*-overexpressing rice plants were no longer observed (**Figure 4B**). These phenotypes were not observed when the plants were grown hydroponically (**Supplementary Figure S4E**). Under adequate nutrient supply, Fe concentrations in shoots were lower in *ENA1*-overexpressing rice plants and *ena1* knockout mutant 1060#A compared to WT (**Figure 4G**). Under adequate nutrient supply, root Fe concentrations in *ENA1–GFP*-overexpressing rice plants were slightly lower than in WT and *ena1* knockout plants. Under high Zn conditions, Fe concentrations in the shoots were not significantly different among *ENA1*-overexpressing rice plants, *ena1* knockout mutants, and WT plants. Under high Zn conditions, root Fe concentrations in *GFP–ENA1*-overexpressing rice plants and *ena1* knockout mutants 1060#A were slightly higher compared with WT plants. Zn concentrations did not significantly differ among *ENA1*-overexpressed rice plants, *ena1* knockout mutants, and WT under both adequate nutrient supply and high Zn condition (**Figure 4H**). Under adequate nutrient supply, P concentrations in shoots were slightly lower in *ENA1–GFP*-overexpressing rice plants and the *ena1* knockout line 1060#A compared to WT (**Figure 4I**). Under high Zn conditions,

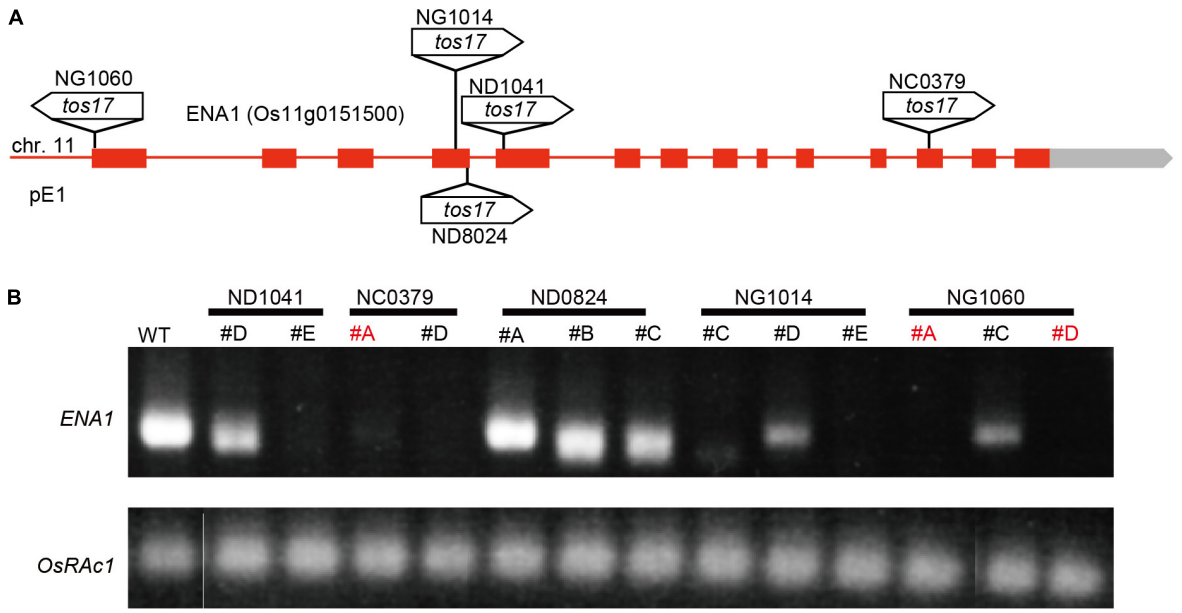

FIGURE 3 | *Tos17* insertion positions and *ENA1* expression in the mutants. **(A)** Schematic representation of *ENA1* and insertion positions of the *tos17* fragments. **(B)** RT-PCR was performed to verify the expression of *ENA1* in *ena1 tos17* insertion lines. The *ena1* knockout mutant lines NC0379#A, and NG1060#A and #D, were further analyzed.

shoot P concentrations were slightly higher in both *ENA1–GFP* and *ENA1–GFP* overexpressing rice plants compared to WT and *ena1* knockout mutants. In roots, there was no difference in P concentrations among these lines. There were no differences in Mn concentrations following modification of *ENA1* expression (**Figure 4J**).

Analysis of ENA1-Overexpressing Arabidopsis

ZINC-INDUCED FACILITATOR 1-overexpressing *Arabidopsis* exhibited a drastic phenotypes with interveinal chlorosis and higher shoot Fe (Haydon and Cobbett, 2007; Haydon et al., 2012). To examine whether this phenotype could be reproduced by overexpression of *ENA1*, transgenic *Arabidopsis* plants overexpressing *ENA1* were analyzed (**Figure 5**). Transgenic *Arabidopsis* plants overexpressing rice Fe homeostasis-related genes including *OsIRO2*, *TOM1*, *TOM2*, *TOM3*, and *OsDMAS1* were also analyzed. The plant appearance of *ENA1*-, *OsIRO2*-, and *TOM2*-overexpressing *Arabidopsis* was not different from WT, irrespective of Fe treatment (**Figure 5A**). One month after germination, plants were harvested and the metal concentrations in shoots were analyzed (**Figure 5C**). No significant differences in shoot Fe, Zn, or Mn concentrations were observed between WT plants and transgenic plants overexpressing *ENA1*, *OsIRO2*, and *TOM2*, independent of external Fe treatment. Mn concentrations in *ENA1*-overexpressing *Arabidopsis* shoots were higher than in WT plants when grown with an Fe(III) source. Fe and Zn concentrations in *OsIRO2*-overexpressing *Arabidopsis* shoots were lower than in WT plants when grown with an Fe(III) source. *Arabidopsis* plants overexpressing *DMAS1* and *TOM3* exhibited impaired germination and were unable to survive (**Figure 5C**). *TOM1*-overexpressing *Arabidopsis* seeds did not germinate, although the seed age was similar to that of WT and other transgenic *Arabidopsis* seeds (data not shown).

Oligo DNA Microarray Analysis of *ena1* Knockout Mutant Lines

To analyze the molecular function of *ENA1 in planta*, genome-wide changes in shoot and root gene expression were compared in *ena1* knockout and WT plants using oligo DNA microarray analysis. To exclude the effect of *Tos17* insertions in the genome other than in the *ENA1* locus, only those genes were analyzed, whose expression level was at least twofold upregulated or downregulated in all plants of two *ena1* knockout mutants (NC0379#A, NG1060#A, and NG1060#D). Among the 29,864 unique genes on the oligo DNA microarray, 116 and 213 genes were upregulated in shoots and roots, respectively, of the *ena1* knockout mutants under Fe-sufficient conditions (**Figure 6A**). Under Fe deficiency, 366 and 201 genes were upregulated in *ena1* shoots and roots, respectively. In contrast, 210 and 179 genes were downregulated in shoots and roots of the *ena1* knockout mutants under Fe-sufficient conditions, while 719 and 362 were downregulated in *ena1* shoots and roots, respectively, under Fe-deficient conditions. The upregulated and downregulated genes in shoots and roots under both Fe-sufficient and Fe-deficient conditions of the *ena1* knockout mutants compared to WT are listed in **Tables 1**, **2**. In the list of upregulated genes, almost all genes are unknown and have not yet been characterized (**Table 1**). On top of the

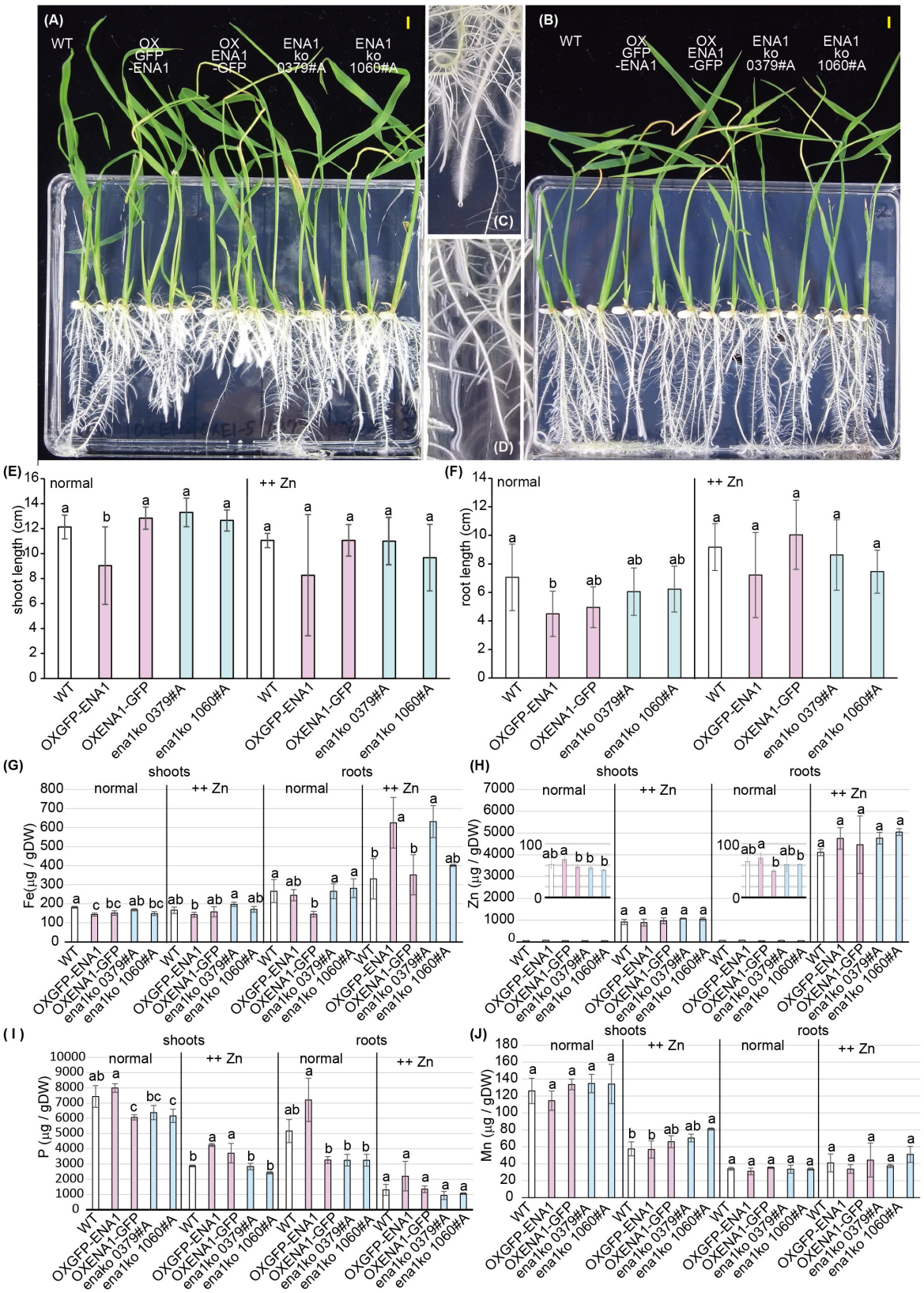

FIGURE 4 | Plant phenotype of *ena1* knockout mutants (0379#A and 1060#A), *GFP-ENA1*- or *ENA1-GFP*-overexpressing rice plants, and WT. Rice plants grown on MS medium (normal) or MS medium with high zinc (Zn) concentrations (++Zn). **(A–D)** Plant appearance at 12 days after germination under normal **(A,C,D)** or high

(*Continued*)

FIGURE 4 | Continued
Zn **(B)** conditions. Scale bars represent 0.5 cm. Roots pictures of *ENA1-GFP* overexpressing **(C)** or wild-type (WT) plants **(D)** under normal conditions are enlarged. **(E,F)** Shoot length **(E)** and root length **(F)** were measured 12 days after germination. Error bars represent the standard error (n = 9). **(G–J)** Fe, Zn, manganese (Mn), and phosphorus (P) concentrations in the shoots and roots of *ena1* knockout mutants, *GFP-ENA1-* or *ENA1-GFP*-overexpressed rice plants, and WT. Values represent means of three replicates. Error bars represent standard deviations. DW, dry weight. Different letters indicate significant differences according to the Tukey–Kramer HSD test (n = 9, $P < 0.05$).

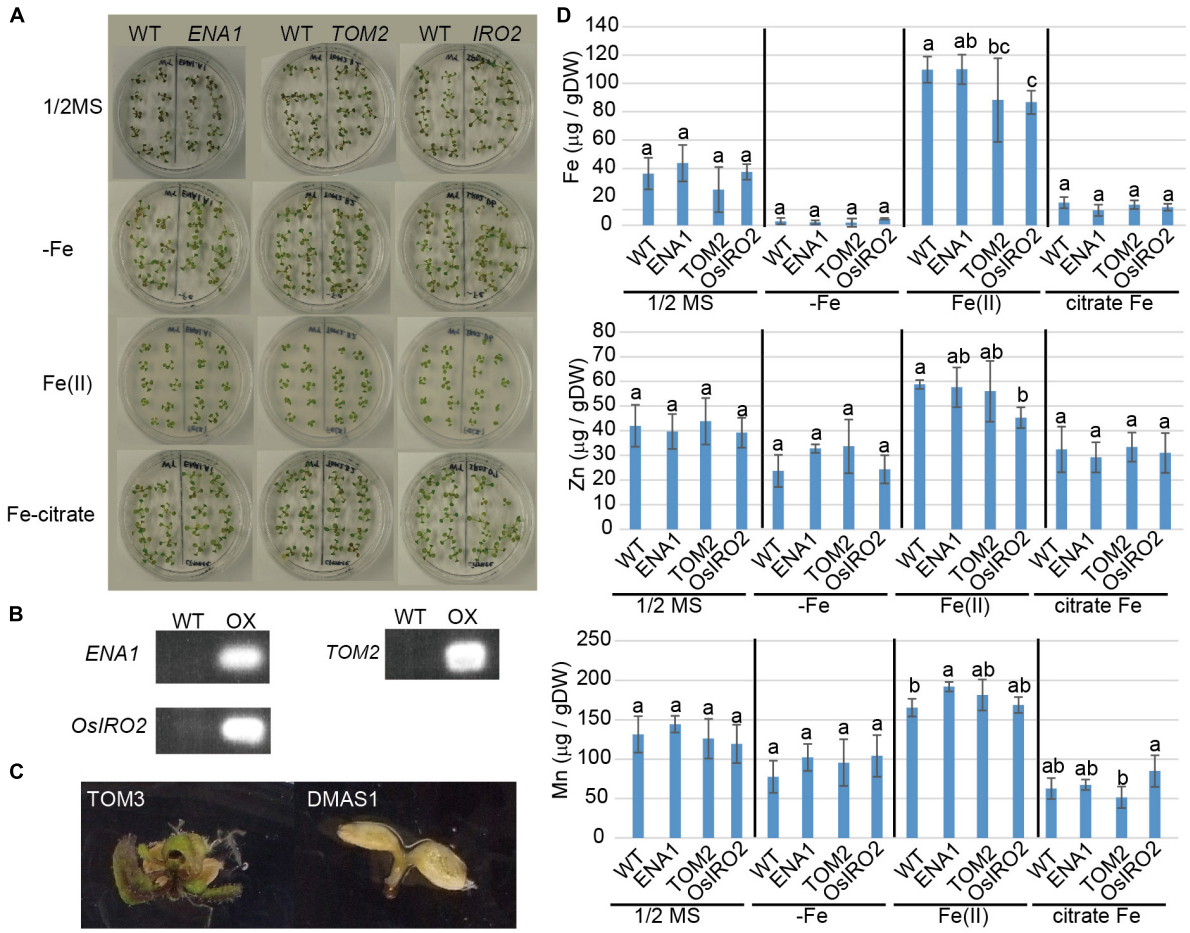

FIGURE 5 | Phenotype of transgenic *Arabidopsis* plants overexpressing *ENA1*, *TOM2*, *TOM3*, *OsIRO2*, or *OsDMAS1*. **(A)** Plant appearance at 1 month after germination. *ENA1*-, *TOM2*-, or *OsIRO2*-overexpressing *Arabidopsis* plants were grown next to WT plants in the same medium. **(B)** RT-PCR analysis of the expression of *ENA1*, *TOM2*, and *OsIRO2* in *Arabidopsis* shoots. **(C)** Plant appearance of *Arabidopsis* plants overexpressing *TOM3* or *OsDMAS1* at 1 month after germination. **(D)** Fe, Zn, and Mn concentrations in the shoots of transgenic *Arabidopsis* overexpressing *ENA1*, *TOM2*, or *OsIRO2*. Values are the means of three to six replicates. Error bars represent standard deviation. DW, dry weight. Letters indicate significant differences according to Tukey–Kramer HSD test (n = 3–6, $P < 0.05$).

downregulated genes in the *ena1* knockout mutants was a gene homologous to PV72, a seed-specific vacuolar sorting receptor (Watanabe et al., 2004), whose expression was downregulated in roots and upregulated in shoots of the WT by Fe deficiency (**Table 2**).

Under Fe deficiency, we observed significant changes in gene expression, reflecting how plants cope with the stress and maintain Fe homeostasis. Therefore, it was analyzed whether the expression of Fe deficiency-regulated genes was altered in *ena1* knockout mutants (**Figure 6B**). Among the genes whose expression was different from the WT in *ena1* knockout mutants, 13.5% and 16.8% of genes in shoots under Fe-sufficient and Fe-deficient conditions, respectively, were genes modulated by Fe deficiency (**Figure 6B**). In roots, the corresponding numbers were 24.2% and 40.9%. Among the Fe deficiency-modulated genes, whose expression was up-regulated in *ena1* knockout mutants compared with the WT under Fe-sufficient conditions, the ratio of the upregulated genes by Fe deficiency was higher than that of the down-regulated genes, especially in the roots. Under Fe-deficient condition, this trend was opposite. The ratio of downregulated genes by Fe deficiency was higher than that of upregulated genes among the upregulated genes in the

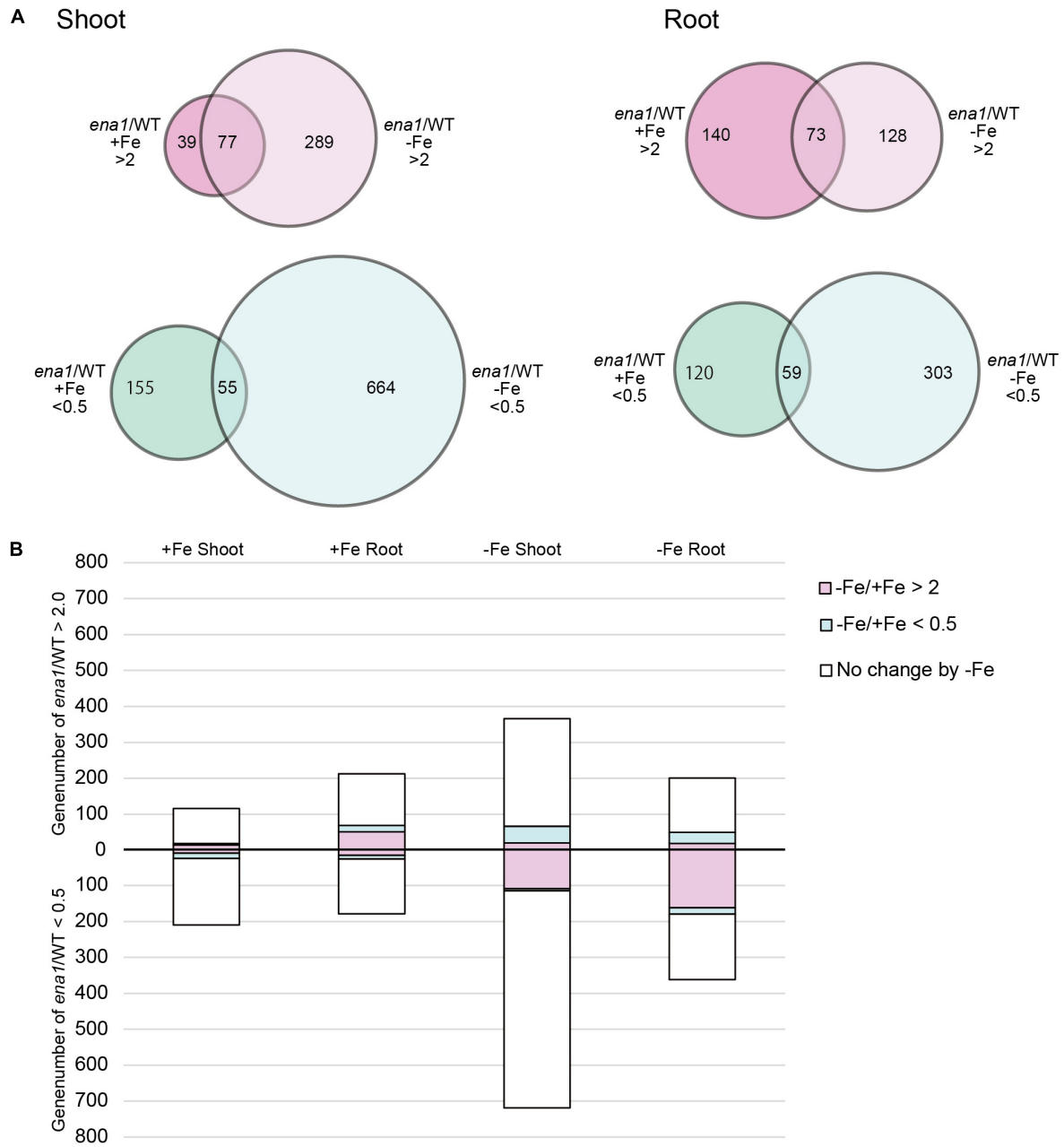

FIGURE 6 | Gene expression analysis in *ena1* knockout mutants and WT plants. **(A)** Venn diagrams represent genes differentially expressed in roots of *ena1* knockout mutants compared to WT plants under Fe-sufficient or Fe-deficient conditions. Of a total of 29,864 genes, 2,102 (746 upregulated and 1,356 downregulated) were differentially expressed by at least twofold between *ena1* knockout mutants compared to WT plants under both Fe-sufficient and Fe-deficient conditions compared with the gene list in **Supplementary Table S2**. **(B)** Graphs representing the numbers of Fe deficiency-responsive genes among the 2,102 genes, whose expression levels were upregulated or downregulated in *ena1* knockout mutants compared to WT shoots and roots under Fe-sufficient or Fe-deficient conditions. Pink or blue colors indicate the ratios of genes that showed upregulation (–Fe/+Fe > 2) or downregulation (–Fe/+Fe < 0.5), respectively, by at least twofold under Fe-deficient conditions in the WT.

ena1 knockout mutants compared with WT, while the ratio of upregulated genes by Fe deficiency was higher than that of down-regulated genes by Fe deficiency among the down-regulated genes in the *ena1* knockout mutants compared with WT. Expression changes of Fe homeostasis-related genes in the *ena1* knockout mutants compared with WT were analyzed (**Table 3**). The expression of *OsNAS1*, *OsNAS2*, *OsDMAS1*, *TOM1*, and *OsYSL15* tended to be lower in Fe-deficient shoots of *ena1* knockout mutants than of WT plants.

To gain further insights into ENA1-dependent processes, an agriGO analysis was carried out to identify enriched categories among the genes, whose expression level was altered in the

TABLE 1 | Upregulated genes in the *ena1* knockout mutants.

	Gene description	*ena1* ko/WT				−Fe/+Fe	
RAP locus		**Fe-sufficient shoot**	**Fe-deficient shoot**	**Fe-sufficient root**	**Fe-deficient root**	**Root**	**Shoot**
Os03g0115800	Conserved hypothetical protein	171.58	221.22	164.98	202.44	0.72	0.80
Os06g0265100	Hypothetical protein	89.11	238.59	80.07	98.16	1.02	0.88
Os01g0692400	Conserved hypothetical protein	72.39	57.63	16.23	15.58	0.99	0.61
Os02g0252400	Zn-finger, Dof-type domain containing protein	52.81	27.39	41.84	54.43	0.98	0.98
Os07g0511400	Hypothetical protein	24.39	54.23	2095.42	2403.44	0.72	0.90
Os12g0428300	Retrotransposon gag protein family protein	20.92	33.42	8.90	15.25	1.11	1.09
Os06g0215900	Oxo-phytodienoic acid reductase	19.11	38.59	20.56	39.15	1.16	0.97
Os06g0216000	Oxo-phytodienoic acid reductase	18.47	17.24	7.70	6.62	1.38	1.02
Os03g0629800	Conserved hypothetical protein	14.53	29.03	50.96	83.70	0.66	0.25
Os04g0390800	Short-chain dehydrogenase/reductase SDR family protein	10.56	4.89	5.76	33.58	0.47	3.91
Os06g0261300	Hypothetical protein	9.01	5.74	8.84	6.26	1.07	1.48
Os07g0457200	Non-protein coding transcript, putative npRNA	7.92	13.78	5.41	18.80	1.93	1.42
Os02g0216200	Hypothetical protein	7.30	13.45	3.00	2.26	0.82	0.97
Os07g0511100	Glycine-rich protein precursor	7.30	8.71	280.70	389.21	0.98	2.14
Os08g0441700	Hypothetical protein	6.46	9.09	9.07	11.95	0.46	1.00
Os11g0491900	(No hit)	5.59	23.16	4.86	16.77	0.54	0.77
Os04g0607800	(No hit)	5.31	23.89	5.06	15.19	0.84	0.65
Os01g0108500	(No hit)	4.13	6.22	11.49	13.75	0.97	0.35
Os07g0122000	Conserved hypothetical protein	3.93	11.01	3.80	5.67	0.86	0.42
Os01g0538200	Conserved hypothetical protein	2.09	3.98	4.40	4.36	1.25	1.07

Listed are the genes whose expression levels were upregulated at least twofold in the ena1 knockout (ko) mutants compared to wild type (WT). Shown are the averages of the expression ratios calculated by (signal value of the enal ko mutants line)/(signal value of the corresponding WT) in the three ena1 ko lines (NC0379#A, NG1060#A, and NG1060#D). The ratios calculated by (signal value in WT under Fe-deficient condition)/(signal value in WT under Fe-sufficient condition) are also represented. Upregulated or downregulated genes are shaded in pink or blue, respectively.

ena1 knockout mutants (**Supplementary Figures S5–8**). In Fe-deficient roots of *ena1* plants, the most significantly enriched GO term for biological processes was "photosynthesis, light harvesting" (GO:0009765) (**Supplementary Figure S5A**). GO enrichment analysis also revealed enrichment of genes involved in the biological processes "oxylipin metabolism," "jasmonic acid biosynthesis," and "systemic acquired resistance." The molecular function "tetrapyrrole binding" (GO:0046906) (**Supplementary Figure S5B**) and the cellular compartments "membrane-bound vesicle" (GO:0031988) and "cytoplasmic membrane-bound vesicle" (GO:0016023) (**Supplementary Figure S5C**) were also strongly enriched among the genes downregulated in Fe-deficient roots of the *ena1* knockout. In Fe-deficient shoots of *ena1* knockout mutants, "DNA replication" (GO:0006260) and "methylammonium transmembrane transporter activity" (GO:0015200) were the only significantly enriched terms in biological process and molecular function, respectively (**Supplementary Figures S6A,B**). Interestingly, "membrane-bound vesicle" (GO:0031988) and "cytoplasmic membrane-bound vesicle" (GO:0016023) were also the most significantly enriched GO terms for cellular compartments among genes downregulated in Fe-deficient shoots of the *ena1* knockout mutants (**Supplementary Figure S6C**). The molecular function "Zn ion binding" (GO:0008270) was enriched in the Fe-sufficient shoots of the *ena1* knockout mutants (**Supplementary Figure S8A**), whereas the cellular compartments "membrane-bound vesicle" (GO:0031988) and "cytoplasmic membrane-bound vesicle" (GO:0016023) were again the most significantly enriched GO terms in both Fe-sufficient roots (**Supplementary Figure S7**) and shoots (**Supplementary Figure S8B**). These GO terms were not enriched among the genes upregulated in the *ena1* knockout mutants compared to WT.

TABLE 2 | Downregulated genes in the *ena1* knockout mutants.

		ena1 ko/WT				−Fe/+Fe	
RAP locus	**Gene description**	**Fe-sufficient shoot**	**Fe-deficient shoot**	**Fe-sufficient root**	**Fe-deficient root**	**Root**	**Shoot**
Os11g0190700	PV72. A seed-specific vacuolar sorting receptor	0.09	0.05	0.11	0.07	0.16	18.11
Os03g0323700	(No hit)	0.10	0.05	0.17	0.16	1.09	0.89
Os02g0534700	Pectinesterase inhibitor domain containing protein	0.22	0.31	0.37	0.28	1.00	0.98
Os01g0129200	Zn-finger, C_2H_2-type domain containing protein	0.25	0.24	0.24	0.29	0.97	0.98
Os01 g0522400	ARM repeat fold domain containing protein	0.27	0.28	0.25	0.28	0.98	0.99
Os03g0294100	Conserved hypothetical protein	0.29	0.29	0.26	0.25	0.99	0.98
Os03g0151000	Hypothetical protein	0.29	0.28	0.27	0.25	0.99	1.63
Os12g0168500	Hypothetical protein	0.30	0.26	0.28	0.31	0.99	0.99
Os01g0213700	Conserved hypothetical protein	0.31	0.25	0.30	0.18	0.94	0.70
Os09g0254600	MtN3 and saliva-related transmembrane protein family protein	0.31	0.24	0.26	0.26	0.99	0.73
Os10g0500300	MTD2. Zinc finger, RING/FYVE/PHD-type domain containing protein	0.32	0.35	0.30	0.35	0.97	0.97
Os12g0117800	Protein of unknown function DUF1191 family protein	0.33	0.38	0.27	0.29	1.25	0.98
Os06g0545200	Glycoside hydrolase, family 28 protein	0.35	0.34	0.39	0.32	0.98	0.98
Os08g0392200	Conserved hypothetical protein	0.35	0.42	0.40	0.29	0.87	0.99
Os02g0452900	Hypothetical protein	0.39	0.26	0.27	0.29	0.74	2.12
Os01g0339500	Conserved hypothetical protein	0.40	0.41	0.17	0.26	1.28	0.95

Listed are the genes whose expression levels were downregulated by at least twofold in the ena1 knockout (ko) mutants compared to WT. Shown are the averages of the expression ratios calculated by (signal value of the enal ko mutants line)/(signal value of the corresponding WT) in the three ena1 ko lines (NC0379#A, NG1060#A, and NG1060#D). The ratios calculated by (signal value in WT under Fe-deficient condition)/(signal value in WT under Fe-sufficient condition) are also presented. Upregulated or downregulated genes are shaded in pink or blue, respectively.

DISCUSSION

Since the discovery of MAs, we have explored strategies to acquire insoluble Fe from the soil, and meanwhile the molecular machinery involved in Fe acquisition in graminaceous plants has been largely identified (Kobayashi et al., 2018). MAs and NA are involved in the translocation and intracellular transport of metals, including Fe (Kakei et al., 2009; Nishiyama et al., 2012), however, the intracellular transport of Fe by MAs and NA remains largely unexplored. It has been suggested that the transporters for MAs and NA are involved in the regulation of metal flows *in planta*. In this study, we characterized ENA1, which can export NA out of the cell (Nozoye et al., 2011).

ENA1 May Be Involved in the Transport of NA From the Intracellular Compartment Outside Cells in Roots

Promoter-GUS analysis showed that under Fe-sufficient conditions *ENA1* is mainly expressed in lateral roots (**Figure 1**). In root cross-sections, *ENA1* expression was observed in the root epidermis. Under Fe-deficient conditions, *ENA1* expression was strongly induced in roots, except near the root tip. Near the root tips, *ENA1* expression was observed only in the epidermis, while *ENA1* expression was observed in whole roots including the epidermis, cortex, and vascular bundle near the basal area of the roots. These results are consistent with previous studies, in which laser micro-dissection analysis showed that *ENA1* was mainly expressed in roots and expression in the cortex was induced by Fe deficiency (Ogo et al., 2014). The expression patterns of *ENA1* in roots were similar to those of the DMA exporters *TOM1* and *TOM2*, and of the Fe importers *OsYSL15* and *OsIRT1* (Ishimaru et al., 2006; Inoue et al., 2009; Nozoye et al., 2011, 2015). In the leaf and stem, *ENA1* expression was not observed under Fe-sufficient or Fe-deficient conditions. Interestingly, *ENA1* expression was observed in the discrimination center (DC) at the basal part of the shoots, where Fe accumulates after absorption and translocation from xylem to phloem in barley (Tsukamoto et al., 2009). *ENA1* expression in the DC was strongly induced by Fe deficiency. *TOM2*, a DMA exporter

TABLE 3 | Expression changes of Fe homeostasis-related genes in the *ena1* knockout (ko) mutants.

	Gene	*ena1* ko/WT			
RAP locus		**Fe-sufficient shoot**	**Fe-deficient shoot**	**Fe-sufficient root**	**Fe-deficient root**
Biosynthesis ofmugineic acid family phytosiderophores					
Os03g0307300	*OsNAS1*	0.74	**0.38**	0.71	1.02
Os03g0307200	*OsNAS2*	1.12	**0.38**	0.73	1.02
Os07g0689600	*OsNAS3*	0.94	1.04	0.89	1.01
Os02g0306400	*OsNAAT1*	1.05	1.20	0.83	1.03
Os03g0237100	*OsDMAS1*	0.77	***0.45***	0.82	0.85
Methionin cycle					
Os01g0323600	*OsSAMS2*	0.92	0.92	1.01	1.06
Os06g0112200	*MTN*	1.06	0.81	1.04	0.99
Os12g0589100	*OsAPT1*	0.86	0.57	0.82	0.84
Os04g0669800	*OsMTK1*	0.91	0.61	0.96	0.87
Os11g0216900	*Os/D/2*	0.94	1.12	0.64	1.24
Os04g0306400	*RPI*	1.06	0.74	0.79	0.84
Os11g0484000	*DEP*	1.10	0.75	1.05	0.93
Os06g0486900	*FDH*	***3.05***	1.66	***2.11***	***2.71***
Os06g0486800	*FDH*	0.88	0.55	0.93	0.79
Os09g0453800	*Os/D/4*	1.06	0.60	0.87	0.88
Transcriptional regulation of Fe-deficiency responses					
Os01g0952800	*OsIR02*	0.88	0.96	0.81	0.92
Os03g0379300	*OsIR03*	0.99	1.07	0.95	1.08
Os08g0101000	*IDEF1*	1.18	1.22	1.08	1.05
Os05g0426200	*IDEF2*	1.02	1.21	1.09	1.04
Os01g0689300	*OsHRZ1*	1.00	1.15	1.06	0.90
Os05g0551000	*OsHRZ2*	1.20	1.11	0.87	0.98
Fe uptake and/or translocation					
Os11g0134900	*TOM1*	0.61	***0.35***	0.56	0.90
Os11g0135000	*TOM2*	1.18	1.27	1.72	1.14
Os11g0135900	*TOM3*	1.16	1.39	0.75	0.85
Os02g0650300	*OsYSL15*	***2.11***	***0.32***	0.88	1.17
Os02g0649900	*OsYSL2*	***0.46***	1.57	***0.50***	1.09
Os03g0667500	*OsIRT1*	0.67	0.61	1.73	1.30

Listed are Fe deficiency-inducible genes involved in Fe uptake and utilization and transcriptional regulators of Fe-deficiency responses. Shown are the averages of the expression ratios calculated by (signal value of the enal ko mutants line)/(signal value of the corresponding WT) in the three ena1 ko lines (NC0379#A, NG1060#A, and NG1060#D). Upregulated or downregulated genes are shaded in pink or blue, respectively. Ratios upregulated or downregulated by at least twofold in all three lines are indicated in bold, while if at least one replicate was not upregulated or downregulated by at least twofold, values are indicated in italics

and homolog of *TOM1*, is strongly expressed in the DC under both Fe-sufficient and Fe-deficient conditions (Nozoye et al., 2015). *TOM2* repression in rice plants impaired plant growth, suggesting that *TOM2* is involved in DMA transport, which is important for Fe mobilization in the plant body. These results suggested that Fe mobilization in the DC is important for Fe homeostasis. ENA1 may be involved in Fe mobilization in the DC by NA efflux.

The subcellular localization of ENA1 was examined in onion epidermal cells (**Supplementary Figure S1**) and rice root cells (**Figure 2** and **Supplementary Figure S2**). GFP–ENA1 and ENA1–GFP fusion proteins were localized in the plasma membrane and in the cytoplasm of onion epidermal cells. There, the GFP–ENA1 and ENA1–GFP fusion protein partly localized to vesicular structures. In rice roots, the ENA1–GFP fusion protein localized mainly to the plasma membrane, and partially to intracellular vesicular structures. MA biosynthesis through NA has been proposed to occur in intracellular vesicles (Nishizawa and Mori, 1987; Negishi et al., 2002; Nozoye et al., 2004, 2014a,b). MA secretion in barley and rice follows a diurnal rhythm and occurs 2–3 h after sunrise while its production is constant (Takagi et al., 1984; Nozoye et al., 2014a). These observations suggested that MAs are stored in cells until secretion. Vesicles surrounded by ribosomes have been shown to accumulate near the plasma membrane just before sunrise in Fe-deficient barley and rice roots (Nishizawa and Mori, 1987; Negishi et al., 2002; Nozoye et al., 2014a). These vesicles are not observed in Fe-sufficient roots. Therefore, these vesicles were considered to contain MAs, and to store these until secretion. It has been proposed that all enzymes involved in MAs biosynthesis localize to these vesicles. Indeed, a fusion protein of GFP with the rice NA synthase 2 (OsNAS2), one of the MAs biosynthetic enzymes, was observed as dot-like structures in rice root cells, suggesting that at least NA is synthesized in MAs-containing vesicles (Nozoye et al.,

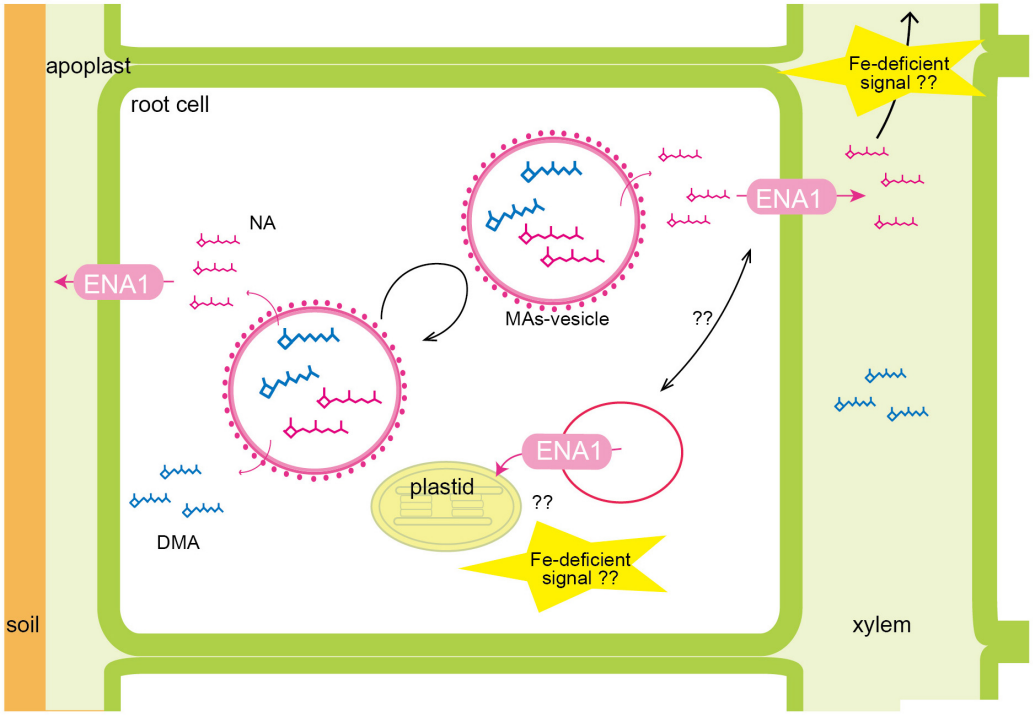

FIGURE 7 | Schematic of the putative roles of ENA1 in rice. NA and DMA are predicted to be produced in intracellular vesicles, recognized as MAs-synthesizing vesicle. Since MAs-synthesizing vesicles are surrounded by rough endoplasmic reticulum, NA and DMA are exported into the cytoplasm, and then transported out of the cell via ENA1. ENA1 is mainly localized to the plasma membrane, where it transports NA to the apoplast. Regarding an intracellular function, ENA1 might export NA from vesicles for subsequent Fe loading of plastids. ENA1 transport functions are upregulated under Fe deficiency.

2014a). In this study, ENA1–GFP mainly localized to the plasma membrane. Since MAs-synthesizing vesicles were supposed to be surrounded by rER, it was thought that MAs-synthesizing vesicles are not fused to the plasma membrane. It was speculated that NA and/or DMA produced in MAs-synthesizing vesicles were secreted to the cytoplasm and then transported out of cells. ENA1 might be involved in the efflux of NA from the cytoplasm to the apoplast (**Figure 7**).

In the cytoplasm, ENA1–GFP was observed in part also vesicular structures, which differed from the dot-like structures observed for NAS2-GFP, since the number and form of vesicles differed. ENA1 fused to GFP at the N-terminus (ENA1–GFP) also localized to the plasma membrane and cellular vesicular structures. However, in onion epidermal cells the number of vesicular structures was higher for ENA1–GFP than GFP–ENA1. The fluorescence of GFP–ENA1 in rice roots was too weak to be detected, suggesting that GFP might interfere with the intracellular localization of ENA1 in rice cells. Both *ENA1–GFP*- and *GFP–ENA1*-overexpressing plants showed truncated roots with large number of root hairs, when plants were grown in MS medium with adequate Fe supply (**Figure 4**), suggesting that ENA1–GFP and GFP–ENA1 might be functional in rice plants. However, the changes in metal concentrations differed among *ENA1–GFP* and *GFP–ENA1*-overexpressing plants. This may be a consequence of protein mistargeting due to protein overload. To evaluate the phenotypes of *ENA1–GFP* and *GFP–ENA1*-overexpressing plants, rice plants overexpressing *ENA1* without a *GFP* tag would be required. Further analyses are also necessary to confirm the intracellular localization of ENA1.

The Mechanism of NA Transport Differs Between Rice and Arabidopsis

To examine the physiological role of ENA1 *in planta*, characteristics of *ena1* knockout mutants carrying *tos17* insertions (**Supplementary Figure S3**) and *ENA1–GFP*- or *GFP–ENA1*-overexpressing rice plants was analyzed (**Figure 3**). However, in hydroponics there were no apparent differences (**Supplementary Figure S4**). In rice, NA is an intermediate of MAs biosynthesis and DMA is the final product. DMA and NA are involved in metal translocation in the plant body (Suzuki et al., 2006; Kakei et al., 2009; Nishiyama et al., 2012; Nozoye et al., 2015). On the other hand, *Arabidopsis* produces NA but not DMA. In rice, transporters of DMA, such as members of the TOM family, may compensate or even take over transport functions that are mediated by ENA1 in Arabidopsis. Such a view is supported by the fact that YS1-type transporters also transport both, DMA and NA (Schaaf et al., 2004).

Under Fe-adequate conditions, root growth of *ENA1–GFP*- or *GFP–ENA1*-overexpressing rice plants was significantly impaired, but this impairment was not observed under high Zn conditions (**Figure 4**). The roots of *ENA1–GFP*- or *GFP–ENA1*-overexpressing rice plants were shorter and had more root hairs than the WT. Fe concentrations were slightly lower in shoots of

ENA1–GFP or *GFP–ENA1* overexpressing rice plants. However, these phenotypes were rather moderate compared to those of *ZIF1*-overexpressing *Arabidopsis* or *zif1* mutants (Haydon and Cobbett, 2007; Haydon et al., 2012). Since the root phenotype is similar to the response under P starvation (Peret et al., 2014), we determined P concentrations (**Figure 4**). However, differences in root P concentrations were not correlated with changes in *ENA1* expression. In shoots, the P concentration in *ENA1–GFP*-overexpressing rice plants was slightly lower than in WT plants under adequate nutrient supply, but slightly higher than in WT plants under elevated Zn supply, although these differences were not large. NA transport by ENA1 may be affected in part by both, Fe and P nutrition *in planta*.

When *ENA1* was overexpressed in *Arabidopsis,* plants grew well and metal concentrations in the leaves were not significantly different from WT, unlike under overexpression of ZIF1. A difference was only observed in the Mn concentration of shoots. Based on amino acid homology, ZIF1 is most closely related to TOM1, which may be the main transporter responsible for DMA secretion from roots into rhizosphere (Nozoye et al., 2011). However, it has been shown that TOM1 can efflux DMA, but not NA. In rice, *TOM2* and *TOM3* are homologs of *TOM1*. It has been shown that TOM2 is also a DMA exporter that plays a role in metal translocation in the plant body (Nozoye et al., 2015). Since both NA and DMA are involved in long-distance metal translocation, TOM2 might complement ENA1 functions in rice. In this study, similar to the case with ENA1, *TOM2*-overexpressing *Arabidopsis* did not show any obvious phenotypes (as opposed to *ZIF1*-overexpressing *Arabidopsis*), while *TOM1*-, *TOM3*-, and *OsDMAS1*-overexpressing *Arabidopsis* could not germinate. *Arabidopsis* NAS (AtNAS1-4) did not localize to vesicular structures in the cytoplasm like OsNAS2-GFP did in rice (Nozoye et al., 2014b). These results suggest that the cellular compartments producing NA may differ between rice and *Arabidopsis*, and these cellular compartments may be relevant for the function of NA.

Oligo DNA Microarray Analysis Suggests That Intracellular Transport of NA Through ENA1 May Be Involved in Maintaining Fe Homeostasis, and ENA1 Knockouts Influence Plastid Function in Roots

To examine the molecular function of *ENA1*, oligo DNA microarray analysis was performed. In *ena1* knockout mutants, the number of genes whose expression level was downregulated was larger than that of upregulated genes relative to the WT. Previously, we identified genes whose expression was upregulated under Fe deficiency, including transcription factors, MAs biosynthetic enzymes, and Fe transporters (Nozoye et al., 2011, 2014a). Under Fe-sufficient conditions, genes whose expression was induced under Fe deficiency tended to be upregulated in *ena1* knockout mutants compared to WT (**Figure 6B**). By contrast, under Fe-deficient conditions, genes whose expression level was induced by Fe deficiency tended to be downregulated in *ena1* knockout mutants (**Figure 6B**). Indeed, the expression levels of the genes involved in MAs biosynthesis and transport were lower in the Fe-deficient shoots (**Table 3**). These results suggest that *ena1* mutants respond to Fe deficiency even under Fe-sufficient conditions; however, *ena1* mutants could not respond to Fe deficiency under Fe-deficient conditions. agriGO analysis showed that genes whose expression levels were downregulated in *ena1* mutant roots under Fe-deficient conditions are involved in photosynthesis, jasmonic acid biosynthetic processes, and innate immunity. Further molecular functions of these genes are related to chlorophyll binding. In addition, cellular components were involved in cytoplasmic membrane-bound vesicles. Fe is important for photosynthesis in chloroplasts since it plays a role as enzyme cofactor in chlorophyll biosynthesis. In *Arabidopsis*, it has been shown that chlorophyll biosynthesis in leaves is downregulated and metabolite changes under Fe-deficient conditions allow plants to prevent photo-oxidative damage (Rodriguez-Celma et al., 2013). In general, plastids synthesize chlorophylls, carotenoids, and fatty acids, and are involved in aromatic amino acid biosynthesis, and reduce several inorganic nutrients (Buchanan et al., 2015). As some of these Fe-dependent functions are also relevant for root plastids, Fe must be imported also into root plastids. NA transport through ENA1 may take over such a function to adjust metabolism and prevent the stress response under Fe deficiency, such as the production of reactive oxygen species (**Figure 7**). As mentioned above, OsNAS2-GFP fusion proteins localized as dot-like structures in rice root cells (Nozoye et al., 2014a). In this study, the expression levels of *OsNAS1*, *OsNAS2*, and *OsDMAS1* were lower in the Fe-deficient shoots of *ena1* knockouts than in the WT (**Table 3**), suggesting that ENA1 expression is involved in DMA and NA biosynthesis, which may take place in intracellular vesicles. Other than WT plants, *ena1* mutants could not induce Fe deficiency-inducible genes under Fe deficiency. This result may indicate that ENA1 is involved in Fe trafficking into cellular compartments such as plastids. Further studies on the intracellular trafficking of Fe by Fe transporters including ENA1 will be important to characterize the mechanisms maintaining Fe homeostasis *in planta*.

AUTHOR CONTRIBUTIONS

TN, HN, and NN designed the research. TN carried out the experiments with assistance from NvW, YS, and TH, and analyzed the data. TN wrote the manuscript with contributions and discussion from all of the co-authors.

FUNDING

This research was supported by an Advanced Low Carbon Technology Research and Development Program (Grant Number JPMJAL1107) from the Japan Science and Technology Agency (to NN), JSPS KAKENHI [Grant Numbers 15K18658 (to TN), 15KK0286 (to TN), and JP16H06280 (to TH)], and by a grant from Uragami-zaidan (to TN).

ACKNOWLEDGMENTS

We thank Dr. Y. Nagamura (NIAS) and Ms. R. Motoyama (NIAS) for their assistance with the oligo-microarray analysis; Ricardo F. H. Giehl for assistance with the confocal microscopy and valuable suggestion for the manuscript; and Dr. M. Minami (RIKEN), Dr. H. Hirochika (NIAS), and Dr. K. Oda for providing transgenic *Arabidopsis* seeds.

SUPPLEMENTARY MATERIAL

The Supplementary Material for this article can be found online at: https://www.frontiersin.org/articles/10.3389/fpls.2019.00502/full#supplementary-material

FIGURE S1 | Subcellular localization of ENA1 in onion epidermal cells. **(A)** GFP-ENA1. **(B)** ENA1-GFP.

FIGURE S2 | Subcellular localization of ENA1-GFP in rice roots. **(A,D)** Differential interference contrast image. **(B,E)** Fluorescence image. **(C,F)** Overlay. **(G)** GFP expression was examined by RT-PCR in *ENA1-GFP*- or *GFP-ENA1*-overexpressed rice plants and WT.

FIGURE S3 | Insertion positions and *ENA1* expression in the mutants. **(A)** Schematic representation of *ENA1* and insertion positions of *tos17* fragments. Primer positions used for *tos17* insertion checks are represented by arrows. Blue arrows indicate primer Tos17L and black arrows indicated primers pE1, pE2, pE3, pE4, and pE5 (**Supplementary Table S1**). **(B,C)** Confirmation of integration of *tos17* **(B)** and the homozygous status of *ena1* mutants. **(B)** Nested PCR with primers; Tos17L primer located in *tos17* and pE1–5 located in the *ENA1* gene were used. **(C)** Primers pE1–5 located in *ENA1* interposing *tos17* were used. Fragments of 1.3, 3, or 1.6 kb were predicted to be amplified in NG1060, NC0379, and other lines, respectively, when *tos17* was not inserted. **(D)** RT-PCR was performed to verify the expression of *ENA1* in *ENA1 tos17* insertion lines.

FIGURE S4 | Plant phenotypes of *ena1* knockout mutants (0379 #A and 1060 #A), *GFP-ENA1*- or *ENA1-GFP*-overexpressing rice plants, and WT. Rice plants were grown hydroponically under Fe-sufficient and Fe-deficient conditions. The Fe deficiency treatment lasted for 7 days. **(A)** Shoot length and root length. Error bars represent the standard error (n = 9). **(B)** Relative chlorophyll contents (SPAD values) of the newest yellow leaves and oldest green leaves. **(C,D)** Fe, copper (Cu), Zn, and Mn concentrations in the youngest yellow leaves **(C)** and oldest green leaves **(D)** of *ena1* knockout mutants, *GFP-ENA1*- or *ENA1-GFP*-overexpressing rice plants, and WT after 7 days of Fe-deficient treatment. Values represent means of three replicates. Error bars represent standard deviation. DW, dry weight. **(E)** Root appearance after 7 days of Fe deficiency. Scale bars represent 5 cm.

FIGURE S5 | Gene ontology (GO) terms enriched in the list of genes, whose expression levels were downregulated in the roots of *ena1* knockout mutants compared to WT under Fe-deficient conditions. **(A)** Biological process. **(B)** Molecular function. **(C)** Cellular component.

FIGURE S6 | GO terms enriched in the list of genes, whose expression levels were downregulated in the shoots of *ena1* knockout mutants compared to WT under Fe-deficient conditions. **(A)** Biological process. **(B)** Molecular function. **(C)** Cellular component.

FIGURE S7 | GO terms enriched in the list of genes, whose expression levels were downregulated in the roots of *ena1* knockout mutants compared to WT under Fe-sufficient conditions. **(A)** Cellular component.

FIGURE S8 | GO terms enriched in the list of genes, whose expression was downregulated in the shoots of *ena1* knockout mutants compared to WT under Fe-sufficient conditions. **(A)** Molecular function. **(B)** Cellular component.

TABLE S1 | Primers used in the analysis of *ENA1* tos17 insertion lines.

TABLE S2 | Oligo DNA microarray analysis of ena1 knockout mutant lines.

REFERENCES

Arco, A., and Satrústegui, J. (2005). New mitochondrial carriers: an overview. *Cell. Mol. Life Sci.* 62, 2204–2227. doi: 10.1007/s00018-005-5197-x

Bashir, K., Ishimaru, Y., and Nishizawa, N. K. (2010). Iron uptake and loading into rice grains. *Rice* 3, 122–130. doi: 10.1007/s12284-010-9042-y

Beneš, I., Schreiber, K., Ripperger, H., and Kircheiss, A. (1983). Metal complex formation by nicotianamine, a possible phytosiderophore. *Experientia* 39, 261–262. doi: 10.1007/BF01955293

Buchanan, B. B., Gruissem, W., and Jones, R. L. (2015). *Biochemistry and Molecular Biology of Plants*. Hoboken, NJ: Wiley.

Curie, C., Panaviene, Z., Loulergue, C., Dellaporta, S. L., Briat, J.-F., and Walker, E. L. (2001). Maize yellow stripe1 encodes a membrane protein directly involved in Fe(III) uptake. *Nature* 409, 346–349. doi: 10.1038/35053080

Deinlein, U., Weber, M., Schmidt, H., Rensch, S., Trampczynska, A., Hansen, T. H., et al. (2012). Elevated nicotianamine levels in *Arabidopsis halleri* roots play a key role in zinc hyperaccumulation. *Plant Cell* 24, 708–723. doi: 10.1105/tpc.111.095000

Du, Z., Zhou, X., Ling, Y., Zhang, Z., and Su, Z. (2010). agriGO: a GO analysis toolkit for the agricultural community. *Nucleic Acids Res.* 38, W64–W70. doi: 10.1093/nar/gkq310

Eide, D., Broderius, M., Fett, J., and Guerinot, M. L. (1996). A novel iron-regulated metal transporter from plants identified by functional expression in yeast. *Proc. Natl. Acad. Sci. U.S.A.* 93, 5624–5628. doi: 10.1073/pnas.93.11.5624

Haydon, M. J., and Cobbett, C. S. (2007). A novel major facilitator superfamily protein at the tonoplast influences zinc tolerance and accumulation in *Arabidopsis*. *Plant Physiol.* 143, 1705–1719. doi: 10.1104/pp.106.092015

Haydon, M. J., Kawachi, M., Wirtz, M., Hillmer, S., Hell, R., and Krämer, U. (2012). Vacuolar nicotianamine has critical and distinct roles under iron deficiency and for zinc sequestration in *Arabidopsis*. *Plant Cell* 24, 724–737. doi: 10.1105/tpc.111.095042

Hell, R., and Stephan, U. W. (2003). Iron uptake, trafficking and homeostasis in plants. *Planta* 216, 541–551.

Hiei, Y., Ohta, S., Komari, T., and Kumashiro, T. (1994). Efficient transformation of rice (*Oryza sativa* L.) mediated by Agrobacterium and sequence analysis of the boundaries of the T-DNA. *Plant J.* 6, 271–282. doi: 10.1046/j.1365-313X.1994.6020271.x

Hirochika, H., Sugimoto, K., Otsuki, Y., Tsugawa, H., and Kanda, M. (1996). Retrotransposons of rice involved in mutations induced by tissue culture. *Proc. Natl. Acad. Sci. U.S.A.* 93, 7783–7788. doi: 10.1073/pnas.93.15.7783

Ichikawa, T., Nakazawa, M., Kawashima, M., Iizumi, H., Kuroda, H., Kondou, Y., et al. (2006). The FOX hunting system: an alternative gain-of-function gene hunting technique. *Plant J.* 48, 974–985. doi: 10.1111/j.1365-313X.2006.02924.x

Inoue, H., Higuchi, K., Takahashi, M., Nakanishi, H., Mori, S., and Nishizawa, N. K. (2003). Three rice nicotianamine synthase genes, OsNAS1, OsNAS2, and OsNAS3 are expressed in cells involved in long-distance transport of iron and differentially regulated by iron. *Plant J.* 36, 366–381. doi: 10.1046/j.1365-313X.2003.01878.x

Inoue, H., Kobayashi, T., Nozoye, T., Takahashi, M., Kakei, Y., Suzuki, K., et al. (2009). Rice OsYSL15 is an iron-regulated iron(III)-deoxymugineic acid transporter expressed in the roots and is essential for iron uptake in early growth of the seedlings. *J. Biol. Chem.* 284, 3470–3479. doi: 10.1074/jbc.M806042200

Ishimaru, Y., Suzuki, M., Kobayashi, T., Takahashi, M., Nakanishi, H., Mori, S., et al. (2005). OsZIP4, a novel zinc-regulated zinc transporter in rice. *J. Exp. Bot.* 56, 3207–3214. doi: 10.1093/jxb/eri317

Ishimaru, Y., Suzuki, M., Tsukamoto, T., Suzuki, K., Nakazono, M., Kobayashi, T., et al. (2006). Rice plants take up iron as an Fe3+-phytosiderophore and as Fe2+. *Plant J.* 45, 335–346. doi: 10.1111/j.1365-313X.2005.02624.x

Kakei, Y., Yamaguchi, I., Kobayashi, T., Takahashi, M., Nakanishi, H., Yamakawa, T., et al. (2009). A highly sensitive, quick and simple quantification method for nicotianamine and 2'-deoxymugineic acid from minimum samples

using LC/ESI-TOF-MS achieves functional analysis of these components in plants. *Plant Cell Physiol.* 50, 1988–1993. doi: 10.1093/pcp/pcp141

Karimi, M., Inzé, D., and Depicker, A. (2002). GATEWAY^{TM} vectors for *Agrobacterium*-mediated plant transformation. *Trends Plant Sci.* 7, 193–195. doi: 10.1016/S1360-1385(02)02251-3

Kawai, S., Kamei, S., Matsuda, Y., Ando, R., Kondo, S., Ishizawa, A., et al. (2001). Concentrations of iron and phytosiderophores in xylem sap of iron-deficient barley plants. *Soil Sci. Plant Nutr.* 47, 265–272. doi: 10.1080/00380768.2001.10408390

Kobayashi, T., and Nishizawa, N. K. (2012). Iron uptake, translocation, and regulation in higher plants. *Annu. Rev. Plant Biol.* 63, 131–152. doi: 10.1146/annurev-arplant-042811-105522

Kobayashi, T., Nozoye, T., and Nishizawa, N. K. (2018). Iron transport and its regulation in plants. *Free Radic. Biol. Med.* 133, 11–20. doi: 10.1016/j.freeradbiomed.2018.10.439

Kondou, Y., Higuchi, M., Takahashi, S., Sakurai, T., Ichikawa, T., Kuroda, H., et al. (2009). Systematic approaches to using the FOX hunting system to identify useful rice genes. *Plant J.* 57, 883–894. doi: 10.1111/j.1365-313X.2008.03733.x

Ma, J. F., and Nomoto, K. (1993). Two related biosynthetic pathways of mugineic acids in gramineous plants. *Plant Physiol.* 102, 373–378. doi: 10.1104/pp.102.2.373

Ma, J. F., Taketa, S., Chang, Y.-C., Takeda, K., and Matsumoto, H. (1999). Biosynthesis of phytosiderophores in several Triticeae species with different genomes. *J. Exp. Bot.* 50, 723–726. doi: 10.1093/jxb/50.334.723

Marschner, H. (1995). *Mineral Nutrition of Higher Plants*. London: Academic Press.

Marschner, H., Römheld, V., and Kissel, M. (1986). Different strategies in higher plants in mobilization and uptake of iron. *J. Plant Nutr.* 9, 695–713. doi: 10.1080/01904168609363475

Mihashi, S., and Mori, S. (1989). Characterization of mugineic-acid-Fe transporter in Fe-deficient barley roots using the multi-compartment transport box method. *Biometals* 2, 146–154.

Mori, S. (1999). Iron acquisition by plants. *Curr. Opin. Plant Biol.* 2, 250–253. doi: 10.1016/S1369-5266(99)80043-0

Mori, S., Nishizawa, N., Hayashi, H., Chino, M., Yoshimura, E., and Ishihara, J. (1991). "Why are young rice plants highly susceptible to iron deficiency?," in *Iron Nutrition and Interactions in Plants*, ed. Y. Chen (Berlin: Springer), 175–188.

Mori, S., and Nishizawa, N. K. (1987). Methionine as a dominant precursor of phytosiderophores in graminaceae plants. *Plant Cell Physiol.* 28, 1081–1092.

Negishi, T., Nakanishi, H., Yazaki, J., Kishimoto, N., Fujii, F., Shimbo, K., et al. (2002). cDNA microarray analysis of gene expression during Fe-deficiency stress in barley suggests that polar transport of vesicles is implicated in phytosiderophore secretion in Fe-deficient barley roots. *Plant J.* 30, 83–94. doi: 10.1046/j.1365-313X.2002.01270.x

Nishiyama, R., Kato, M., Nagata, S., Yanagisawa, S., and Yoneyama, T. (2012). Identification of Zn–nicotianamine and Fe–2'-deoxymugineic acid in the phloem sap from rice plants (*Oryza sativa* L.). *Plant Cell Physiol.* 53, 381–390. doi: 10.1093/pcp/pcr188

Nishizawa, N., and Mori, S. (1987). The particular vesicle appearing in barley root cells and its relation to mugineic acid secretion. *J. Plant Nutr.* 10, 1013–1020. doi: 10.1080/01904168709363629

Noma, M., and Noguchi, M. (1976). Occurrence of nicotianamine in higher plants. *Phytochemistry* 15, 1701–1702. doi: 10.1016/S0031-9422(00)97459-4

Nozoye, T., Itai, R. N., Nagasaka, S., Takahashi, M., Nakanishi, H., Mori, S., et al. (2004). Diurnal changes in the expression of genes that participate im phytosiderophore synthesis in rice. *Soil Sci. Plant Nutr.* 50, 1125–1131. doi: 10.1080/00380768.2004.10408585

Nozoye, T., Nagasaka, S., Bashir, K., Takahashi, M., Kobayashi, T., Nakanishi, H., et al. (2014a). Nicotianamine synthase 2 localizes to the vesicles of iron-deficient rice roots, and its mutation in the YXXphi or LL motif causes the disruption of vesicle formation or movement in rice. *Plant J.* 77, 246–260. doi: 10.1111/tpj.12383

Nozoye, T., Tsunoda, K., Nagasaka, S., Bashir, K., Takahashi, M., Kobayashi, T., et al. (2014b). Rice nicotianamine synthase localizes to particular vesicles for proper function. *Plant Signal. Behav.* 9:e28660.

Nozoye, T., Nagasaka, S., Kobayashi, T., Sato, Y., Uozumi, N., Nakanishi, H., et al. (2015). The phytosiderophore efflux transporter TOM2 is involved in metal transport in rice. *J. Biol. Chem.* 290, 27688–27699. doi: 10.1074/jbc.M114.635193

Nozoye, T., Nagasaka, S., Kobayashi, T., Takahashi, M., Sato, Y., Sato, Y., et al. (2011). Phytosiderophore efflux transporters are crucial for iron acquisition in graminaceous plants. *J. Biol. Chem.* 286, 5446–5454. doi: 10.1074/jbc.M110.180026

Nozoye, T., Nakanishi, H., and Nishizawa, N. K. (2013). Characterizing the crucial components of iron homeostasis in the maize mutants ys1 and ys3. *PLoS One* 8:e62567. doi: 10.1371/journal.pone.0062567

Ogo, Y., Itai, R. N., Nakanishi, H., Inoue, H., Kobayashi, T., Suzuki, M., et al. (2006). Isolation and characterization of IRO2, a novel iron-regulated bHLH transcription factor in graminaceous plants. *J. Exp. Bot.* 57, 2867–2878. doi: 10.1093/jxb/erl054

Ogo, Y., Kakei, Y., Itai, R. N., Kobayashi, T., Nakanishi, H., Takahashi, H., et al. (2014). Spatial transcriptomes of iron-deficient and cadmium-stressed rice. *New Phytol.* 201, 781–794. doi: 10.1111/nph.12577

Peret, B., Desnos, T., Jost, R., Kanno, S., Berkowitz, O., and Nussaume, L. (2014). Root architecture responses: in search of phosphate. *Plant Physiol.* 166, 1713–1723. doi: 10.1104/pp.114.244541

Pich, A., Manteuffel, R., Hillmer, S., Scholz, G., and Schmidt, W. (2001). Fe homeostasis in plant cells: does nicotianamine play multiple roles in the regulation of cytoplasmic Fe concentration? *Planta* 213, 967–976.

Rajniak, J., Giehl, R. F. H., Chang, E., Murgia, I., Von Wiren, N., and Sattely, E. S. (2018). Biosynthesis of redox-active metabolites in response to iron deficiency in plants. *Nat. Chem. Biol.* 14, 442–450. doi: 10.1038/s41589-018-0019-2

Robinson, N. J., Procter, C. M., Connolly, E. L., and Guerinot, M. L. (1999). A ferric-chelate reductase for iron uptake from soils. *Nature* 397, 694–697. doi: 10.1038/17800

Rodriguez-Celma, J., Pan, I. C., Li, W., Lan, P., Buckhout, T. J., and Schmidt, W. (2013). The transcriptional response of *Arabidopsis* leaves to Fe deficiency. *Front. Plant Sci.* 4:276. doi: 10.3389/fpls.2013.00276

Römheld, V., and Marschner, H. (1986). Evidence for a specific uptake system for iron phytosiderophores in roots of grasses. *Plant Physiol.* 80, 175–180.

Rudolph, A., Becker, R., Scholz, G., Procházka, Ž, Toman, J., Macek, T., et al. (1985). The occurrence of the amino acid nicotianamine in plants and microorganisms. A reinvestigation. *Biochemie und Physiologie der Pflanzen* 180, 557–563. doi: 10.1016/S0015-3796(85)80036-6

Schaaf, G., Ludewig, U., Erenoglu, B. E., Mori, S., Kitahara, T., and Von Wiren, N. (2004). ZmYS1 functions as a proton-coupled symporter for phytosiderophore- and nicotianamine-chelated metals. *J. Biol. Chem.* 279, 9091–9096. doi: 10.1074/jbc.M311799200

Schmid, N. B., Giehl, R. F., Doll, S., Mock, H. P., Strehmel, N., Scheel, D., et al. (2014). Feruloyl-CoA 6'-Hydroxylase1-dependent coumarins mediate iron acquisition from alkaline substrates in *Arabidopsis*. *Plant Physiol.* 164, 160–172. doi: 10.1104/pp.113.228544

Schuler, M., Rellán-Álvarez, R., Fink-Straube, C., Abadía, J., and Bauer, P. (2012). Nicotianamine functions in the phloem-based transport of iron to sink organs, in pollen development and pollen tube growth in *Arabidopsis*. *Plant Cell* 24, 2380–2400. doi: 10.1105/tpc.112.099077

Shojima, S., Nishizawa, N. K., Fushiya, S., Nozoe, S., Irifune, T., and Mori, S. (1990). Biosynthesis of phytosiderophores : in vitro biosynthesis of 2'-deoxymugineic acid from L-methionine and nicotianamine. *Plant Physiol.* 93, 1497–1503. doi: 10.1104/pp.93.4.1497

Song, A., Li, P., Li, Z., Fan, F., Nikolic, M., and Liang, Y. (2011). The alleviation of zinc toxicity by silicon is related to zinc transport and antioxidative reactions in rice. *Plant Soil* 344, 319–333. doi: 10.1007/s11104-011-0749-3

Suzuki, M., Takahashi, M., Tsukamoto, T., Watanabe, S., Matsuhashi, S., Yazaki, J., et al. (2006). Biosynthesis and secretion of mugineic acid family phytosiderophores in zinc-deficient barley. *Plant J.* 48, 85–97. doi: 10.1111/j.1365-313X.2006.02853.x

Takagi, S., Nomoto, K., and Takemoto, T. (1984). Physiological aspect of mugineic acid, a possible phytosiderophore of graminaceous plants. *J. Plant Nutr.* 7, 469–477. doi: 10.1080/01904168409363213

Takagi, S.-I. (1976). Naturally occurring iron-chelating compounds in oat-and rice-root washings: I. Activity measurement and preliminary characterization.

Soil Sci. Plant Nutr. 22, 423–433. doi: 10.1080/00380768.1976.10433004

Takahashi, M., Terada, Y., Nakai, I., Nakanishi, H., Yoshimura, E., Mori, S., et al. (2003). Role of nicotianamine in the intracellular delivery of metals and plant reproductive development. *Plant Cell* 15, 1263–1280.

Tian, T., Liu, Y., Yan, H., You, Q., Yi, X., Du, Z., et al. (2017). agriGO v2. 0: a GO analysis toolkit for the agricultural community, 2017 update. *Nucleic Acids Res.* 45, W122–W129. doi: 10.1093/nar/gkx382

Tsai, H. H., Rodriguez-Celma, J., Lan, P., Wu, Y. C., Velez-Bermudez, I. C., and Schmidt, W. (2018). Scopoletin 8-hydroxylase-mediated fraxetin production is crucial for iron mobilization. *Plant Physiol.* 177, 194–207. doi: 10.1104/pp.18.00178

Tsukamoto, T., Nakanishi, H., Uchida, H., Watanabe, S., Matsuhashi, S., Mori, S., et al. (2009). (52)Fe translocation in barley as monitored by a positron-emitting tracer imaging system (PETIS): evidence for the direct translocation of Fe from roots to young leaves via phloem. *Plant Cell Physiol.* 50, 48–57. doi: 10.1093/pcp/pcn192

Vert, G., Grotz, N., Dédaldéchamp, F., Gaymard, F., Guerinot, M. L., Briat, J.-F., et al. (2002). IRT1, an *Arabidopsis* transporter essential for iron uptake from the soil and for plant growth. *Plant Cell* 14, 1223–1233. doi: 10.1105/tpc.001388

Von Wirén, N., Klair, S., Bansal, S., Briat, J.-F., Khodr, H., Shioiri, T., et al. (1999). Nicotianamine chelates both FeIII and FeII. Implications for metal transport in plants. *Plant Physiol.* 119, 1107–1114. doi: 10.1104/pp.119.3.1107

Watanabe, E., Shimada, T., Tamura, K., Matsushima, R., Koumoto, Y., Nishimura, M., et al. (2004). An ER-localized form of PV72, a seed-specific vacuolar sorting receptor, interferes the transport of an NPIR-containing proteinase in *Arabidopsis* leaves. *Plant Cell Physiol.* 45, 9–17. doi: 10.1093/pcp/pch012

Conflict of Interest Statement: The authors declare that the research was conducted in the absence of any commercial or financial relationships that could be construed as a potential conflict of interest.

frontiers in Plant Science

ORIGINAL RESEARCH
published: 08 May 2019
doi: 10.3389/fpls.2019.00579

Potassium Ion Channel Gene *OsAKT1* Affects Iron Translocation in Rice Plants Exposed to Iron Toxicity

*Lin-Bo Wu[1], Felix Holtkamp[1], Andriele Wairich[1,2] and Michael Frei[1]**

[1] Department of Plant Nutrition, Institute of Crop Science and Resource Conservation, University of Bonn, Bonn, Germany,
[2] Center for Biotechnology, Federal University of Rio Grande do Sul (UFRGS), Porto Alegre, Brazil

Iron toxicity is one of the most widely spread mineral disorders in anaerobic soils, but the tolerance mechanisms in plants are poorly understood. Here we characterize the involvement of a rice potassium ion channel gene, *OsAKT1*, in Fe toxic conditions. Two knock-down lines of *OsAKT1* together with azygos lines were investigated. Mutant lines did not differ from azygos lines regarding plant growth, gas exchange rate or chlorophyll fluorescence in control conditions. However, loss-of-function of *OsAKT1* increased the sensitivity to excess Fe regarding leaf bronzing symptoms, reactive oxygen species generation, leaf spectral reflectance indices, and chlorophyll fluorescence. Fe toxicity leads to largely reduced uptake of other nutrients into shoots, which illustrates the complexity of Fe stress related to multiple mineral disorders. Less potassium uptake in the mutants compared to azygos lines co-occurred with higher amounts of Fe accumulated in the shoot tissues but not in the roots. These results were consistent with a higher level of Fe loaded into the xylem sap of mutants compared to azygos lines in the early phase of Fe toxicity. In conclusion, *OsAKT1* is crucial for the tolerance of rice against Fe toxicity as K homeostasis affects Fe translocation from root to shoot.

Keywords: abiotic stress, iron toxicity, potassium, potassium ion channel, rice, tolerance

OPEN ACCESS

Edited by:
Sebastien Thomine, Centre National de la Recherche Scientifique (CNRS), France

Reviewed by:
Sergey Shabala, University of Tasmania, Australia
Marta Dell'Orto, University of Milan, Italy

****Correspondence:***
Michael Frei
mfrei@uni-bonn.de

Specialty section:
This article was submitted to Plant Nutrition, a section of the journal Frontiers in Plant Science

Received: *20 January 2019*
Accepted: *18 April 2019*
Published: *08 May 2019*

Citation:
Wu L-B, Holtkamp F, Wairich A and Frei M (2019) Potassium Ion Channel Gene OsAKT1 Affects Iron Translocation in Rice Plants Exposed to Iron Toxicity. Front. Plant Sci. 10:579. doi: 10.3389/fpls.2019.00579

INTRODUCTION

Iron (Fe) is a crucial mineral element for all living organisms due to its property as an electron receptor/donor (Kobayashi et al., 2013). Despite its various roles in photosynthesis, respiration and other physiological processes in plants, Fe is toxic when presenting in excess (Becker and Asch, 2005). In optimal growth conditions, rice plants employ both reduction-based (Strategy I) and chelation-based (Strategy II) strategies to take up Fe from the soil (Römheld and Marschner, 1986; Bughio et al., 2002; Ishimaru et al., 2006). In lowland rice fields that contribute 95% of the world rice production, Fe prevalently occurs in the reduced and soluble ferrous form (Fe^{2+}) due to the low soil redox potential arising from anaerobic conditions, which are formed when soil microorganisms and plant roots deplete oxygen by respiration. Excessive Fe^{2+} are transported via the xylem flow to the shoot leading to Fe toxicity, which is one of the most widely observed nutrient disorders in lowland rice production (Becker and Asch, 2005; Frei et al., 2016). Around 12% of the rice production area in Africa is potentially affected by Fe toxicity (van Oort, 2018). Once excess Fe^{2+} enters the plant cells, they can participate in Fenton reactions, in which Fe^{2+} reacts with hydrogen peroxide (H_2O_2) leading to hydroxyl (OH·) radical production. At the same time, Fe^{2+} is oxidized to Fe^{3+}, which can be reduced back to Fe^{2+} by reducing agents such as ascorbate

(AsA) (Grillet et al., 2014; Wu et al., 2017). Hydroxyl radicals can irreversibly damage various cell components such as DNA, proteins, and lipids (Becana et al., 1998) leading to the formation of visible bronzing spots on leaves (Ponnamperuma et al., 1955). Moreover, Fe toxicity can limit the photosynthesis rate through damaging chlorophyll molecules (Stein et al., 2014). High amounts of free Fe^{2+} in soil solutions can directly damage the root system leading to the reduced uptake of essential nutrients (Wu, 2016). Eventually, rice yield production under Fe toxic conditions is negatively affected. Depending on the timing of occurrence and stress density, the yield loss can range from 15 to 100% (Audebert and Fofana, 2009).

To cope with Fe toxicity, rice plants evolve different tolerance mechanisms, which can be classified into two major categories: exclusion and inclusion. A well-characterized exclusion mechanism is related to the oxidation and precipitation of Fe at the root surface, where root plaque is formed to prevent further excess Fe uptake. This process is mediated by root oxidizing power favored by root architectural traits, which facilitate the transport of oxygen from shoot to root and the diffusion into rhizosphere (Wu et al., 2014). Inclusion mechanisms are associated with the partitioning of excess Fe in the tissues with lower photosynthetic activities such as the leaf sheath (Engel et al., 2012). Vacuole constitutes the main organelle for storing excess free Fe in plants (Thomine and Vert, 2013). Moreover, the ubiquitous Fe-storage protein Ferritin, which can store up to 4000 Fe atoms, was shown to be involved in the tolerance to Fe toxicity in rice (da Silveira et al., 2009; Stein et al., 2009). Additionally, rice plants can achieve tolerance to Fe toxicity through maintaining low redox potential of AsA to avoid the pro-oxidant activity of reduced AsA, because AsA can directly reduce Fe^{3+} to Fe^{2+} thus stimulating the Fenton reaction leading to further oxidative stress (Wu et al., 2017).

Genetic factors of Fe toxicity tolerance in rice have been investigated in many studies using either bi-parental populations or diversity panels (Dufey et al., 2014; Wu et al., 2014; Matthus et al., 2015; Zhang et al., 2017). No major quantitative trait loci (QTL) but rather small to medium effect multi-loci have been mapped so far, pointing to a complex genetic architecture of Fe tolerance in rice. In our previous genome-wide association study (GWAS), we suggested a potassium ion channel gene (*OsAKT1*, LOC_Os01g45990) to be associated with the regulation of shoot Fe concentration (Matthus et al., 2015). *OsAKT1* belongs to the Shaker gene family and encodes an inward potassium ion (K^+) channel that localizes on the plasma membrane (Li et al., 2014). *OsAKT1* acts as one of the essential K^+ channels mediating the K uptake in rice (Fuchs et al., 2005; Obata et al., 2007). K constitutes the most abundant monovalent cation in plant cells and plays crucial roles in various plant physiological processes including photosynthesis, assimilation products transport, and resistance/tolerance to biotic/abiotic stresses (Wang and Wu, 2013). Maintaining adequate K status is essential for plants to confer tolerance to drought (Cakmak, 2005), salinity (Garthwaite et al., 2005), and submergence (Gautam et al., 2016). Under excess Fe conditions, higher sensitivity in *Arabidopsis* plants was associated with impaired K homeostasis due to the NO-mediated K loss possibly via non-selective cation channels (NSCC) (Zhang et al., 2018). In rice, interactions between K status and Fe uptake under excess Fe conditions were observed in several studies (Li et al., 2001; Gao et al., 2014) but the underlying genetic and physiological mechanisms, as well as the role of endogenous K homeostasis in Fe toxicity tolerance, remain elusive.

The aims of this study were (i) to confirm the involvement of the *OsAKT1* gene in Fe toxicity tolerance as proposed in our previous study (Matthus et al., 2015). To achieve this goal, two independent rice mutants of *OsAKT1* were investigated in Fe toxic conditions (1,000 mg L^{-1} = 17.9 mM Fe^{2+} for 5 days) in hydroponics. Plant responses including stress symptoms, reactive oxygen species (ROS) generation, leaf spectral reflectance, gas exchange, and photosynthetic activities were examined in mutants and azygos lines. (ii) Further, we aimed to unravel mechanisms by which K homeostasis affects Fe toxicity tolerance, and the mineral composition of Fe stressed rice plants. To this end, ionomic profiling of different plant tissues along with physiological experiments was conducted with mutant lines for the *OsAKT1* gene.

MATERIALS AND METHODS

Plant Materials

Seeds of two lines NG1928, and NC2778 in Nipponbare (*Oryza sativa* L., ssp. *japonica*) background carrying retrotransposon Tos17 insertions in *OsAKT1* (Potassium ion channel, LOC_Os01g45990) were obtained from the Rice Genome Resource Center of the National Institute of Agrobiological Sciences (NIAS), Tsukuba, Japan (Miyao et al., 2003). According to the Tos17 database[1], gene-specific and Tos17-tail6 primers (**Supplementary Table S1**) were used to genotype the mutant lines. Plants carrying homozygous insertions together with co-segregating wildtypes (azygos) were grown to maturity to obtain seeds for further experiments.

Plant Culture and Screening Experiment

Rice seeds were first soaked in de-mineralized water and germinated for 3 days in the dark at 30°C. Young seedlings were subsequently floated on the solutions containing 0.5 mM $CaCl_2$ and 10 μM $FeCl_3$ in the light for another 7 days in a climate-controlled glasshouse. Natural light was supplemented with artificial lighting to ensure a minimum photosynthetic photon flux density (PPFD) of 600 μmol m^{-2} s^{-1}. The day/night temperature was set to 28/22°C. Homogenous seedlings were selected and transplanted into the 60-L tanks filled with half-strength Yoshida solution with modification (Yoshida et al., 1976; Shrestha et al., 2018). One week later, nutrient solutions were exchanged to full strength solutions with the following composition: 2.86 mM N (as NH_4NO_3), 0.32 mM P (as $NaH_2PO_4{\cdot}2H_2O$), 1.02 mM K (as K_2SO_4), 1 mM Ca (as $CaCl_2$), 1.65 mM Mg (as $MgSO_4{\cdot}7H_2O$), 9.1 μM Mn (as $MnCl_2{\cdot}4H_2O$), 0.52 μM Mo (as $(NH_4)_6{\cdot}Mo_7O_{24}{\cdot}4H_2O$), 18.5 μM B (as H_3BO_3), 0.15 μM Zn (as $ZnSO_4{\cdot}7H_2O$), 0.15 μM Cu (as $CuSO_4{\cdot}5H_2O$), 35.7 μM Fe (as Fe-EDTA).

[1] http://tos.nias.affrc.go.jp

The pH value was adjusted to 5.5 every 2 days, and nutrient solutions were renewed every 10 days. To avoid tangling of roots from different plants affecting root oxidizing power, we used PVC tubes fixed underneath a perforated covering plate to create an independent rhizosphere for every single plant grown in the same tank (Wu et al., 2014). After 4-week-growth, $FeSO_4 \cdot 7H_2O$ was added to the nutrient solutions to start an acute Fe stress of 17.9 mM Fe^{2+}. To prevent the auto-oxidation of Fe^{2+}, nitrogen gas was percolated through the nutrient solutions for 15 min every 2 h to remove the dissolved oxygen partially. After five-day-treatment, leaf bronzing symptoms were scaled from 0 (no symptoms) to 10 (dead leaf) according to Wu et al. (2014). Shoot and root tissues were separately flash frozen with liquid nitrogen and stored at −80°C for further analysis. To investigate the distribution pattern of different elements in various tissues, roots, leaf blades, combined leaf sheaths and culms (termed as SC) were harvested separately for mineral analysis. The experiment was designed as a full factorial design with four replicates and six sub-replicates of each genotype per tank.

Leaf Spectral Reflectance Measurement

Leaf spectral reflectance was monitored on the first and second fully expanded leaves on the main tiller with a PolyPen RP410 device (PSI, Drasov, Czechia) to reveal the stress responses and pigment composition of different lines. Different indices were calculated as follows:

Photochemical reflectance index (PRI) = (R531 – R570)/(R531 + R570) (Gamon et al., 1997); Normalized pigment chlorophyll index (NPCI) = (R680 – R430)/(R680 + R430) (Peñuelas et al., 1994); Greenness index (GI) = R554/R677; Normalized difference vegetation index (NDVI) = (R_{NIR} – R_{RED})/(R_{NIR} + R_{RED}) (Huang et al., 2013). In all equations, R represents the reflectance at a given wavelength.

Gas Exchange and Chlorophyll Fluorescence Measurement

Gas exchange and chlorophyll fluorescence were simultaneously measured with a portable photosynthetic gas exchange system Li-Cor 6400 (LI-COR, Inc., Lincoln, NE, United States). The first and second fully expanded leaves on the main tiller of each plant were measured between 10.00 to 14.00 h on the fifth day after starting the treatment. Reference CO_2 concentration and PPFD were set to 400 ppm and 900 $\mu mol\ m^{-2}\ s^{-1}$, respectively. Chlorophyll fluorescence parameters were taken after saturating flashes with a ratio of 10:90 of blue: red light once the raw fluorescence value was stabilized. The calculations of different parameters follow Höller et al. (2015). Quantum efficiency of photosystem II (PSII) was calculated as ΦPSII = (Fm' - Ft)/Fm' where Fm' is the maximal fluorescence under actinic light and Ft is the steady-state terminal fluorescence. Other parameters including stomatal conductance, transpiration rate, leaf to air vapor pressure deficit, leaf temperature and net photosynthetic rate were also monitored.

DNA, RNA Extraction and Quantitative Reverse Transcription PCR

Genomic DNA was isolated using the PeqGOLD plant DNA mini kit (PeqLab Biotechnologie GmbH, Erlangen, Germany) according to manufacturers' instructions. Total RNA from shoot and root were separately extracted with RNA extraction kits (for shoot samples, peqGOLD RNA kit, Peqlab; for root samples, RNeasy Plant Mini Kit, Qiagen GmbH, Düsseldorf, Germany) following the manufacturers' instructions. During the extraction procedure, genomic DNA was removed with on-column RNAase-free DNAase (shoot, Peqlab; root, Qiagen). Three replicates of root/shoot RNA from each sample were tested for integrity on a bleach agarose gel (Aranda et al., 2012) and for purity using NanoDrop OneC (Thermo Fisher Scientific, Braunschweig, Germany). Afterward, 300 ng of total RNA was reverse transcribed to cDNA with GoScript Reverse Transcription Kit (Promega, Manheim, Germany). Quantitative RT-PCR was conducted using GoTaq qPCR master mix (Promega) with a Bio-rad CFX384 real-time system (Biorad, Munich, Germany). The reaction conditions were set up as follows: an initial denaturation step (5 min, 95°C) followed by 40 cycles of denaturation (15 s, 95°C), annealing/extension (1 min, 60°C). Relative expression of *OsAKT1* was calculated using the comparative ΔΔCT method with the expression level of azygos lines in the control as calibrator and *OsUBQ5* as the endogenous reference (Ashrafuzzaman et al., 2018). The primer sequences used in this study are listed in **Supplementary Table S1**.

H_2O_2 Detection in Leaves

In situ detection of H_2O_2 in leaves was conducted according to Wu et al. (2017). In brief, the first and second youngest fully expanded leaves were detached from the main tiller and washed with 0.05% Triton X-100 followed by rinsing with distilled water three times. Then the leaves were submerged into a solution (pH 3.8) containing 0.5 mg mL^{-1} 3,3′-Diaminobenzidine tetrahydrochloride (Merck KGaA, Darmstadt, Germany) dissolved in Milli-Q water (Merck KGaA) for 12 h in the dark and afterward rinsed again with distilled water. The leaves were subsequently incubated in a bleaching solution containing glycerol, lactic acid, and ethanol at a ratio of 1:1:4 (v/v), at 85°C for 1 h to remove the chlorophyll. H_2O_2 formation was visualized as brown precipitation documented by a camera (550D, Canon Deutschland GmbH, Krefeld, Germany).

Ionomic Profiling in Different Tissues

Rice roots were detached and immersed in the dithionite-citrate-bicarbonate (DCB) solution followed by 4-time rinsing with distilled water to remove the root plaque (Liu et al., 2004). Leaf blades were separated from the shoots leaving the combined leaf sheath and culm. Different tissues including the leaf blade, SC and washed roots were dried at 60°C for 4 days until constant weight. Dry samples were ground to fine powder followed by digestion with 65% HNO_3 in a microwave pressure digestion system (MARS6, CEM GmbH, Kamp-Lintfort, Germany). The digested samples were then diluted to a final volume of 20 mL. Different elements including Fe, Ca, Mg, Cu, Zn, Mn, Ni, and

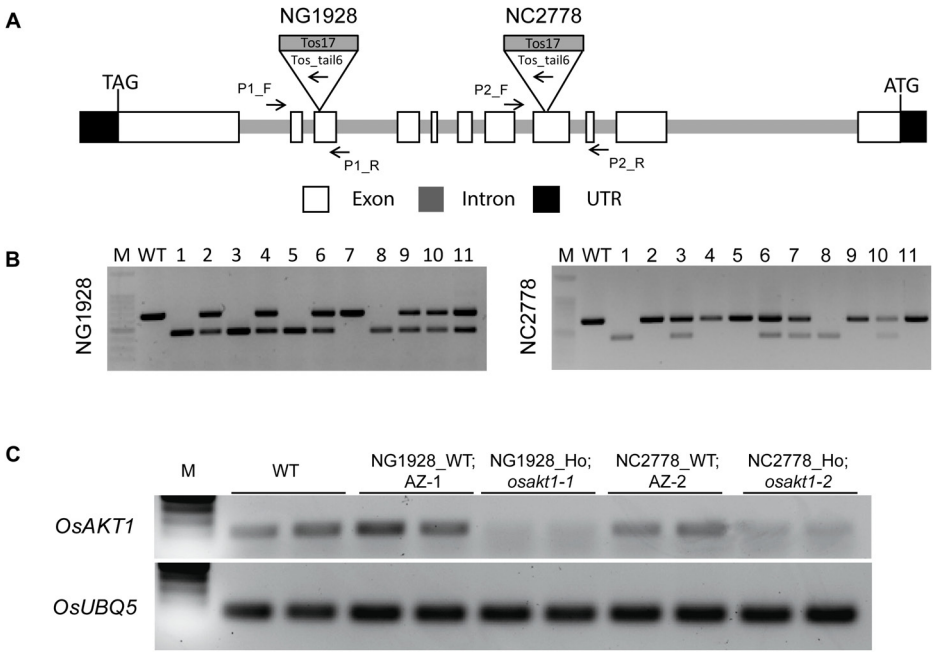

FIGURE 1 | Genotyping and semi-quantitative RT-PCR analysis of the Tos17 insertional lines for potassium ion channel *OsAKT1*. **(A)** Schematic representation of the *OsAKT1* gene structure and Tos17 insertions in two different lines, NG1928 and NC2778. **(B)** Genotyping results of T2 plants of NG1928 and NC2778 line. **(C)** Semi-quantitative RT-PCR of *OsAKT1* in NG1928 and NC2778 segregation lines. Rice ubiquitin gene (*OsUBQ5*) was used as a reference. The sequences of the primers are listed in **Supplementary Table S1**. P1_F, P1_R: gene-specific primers for NG1928; P2_F, P2_R: gene-specific primers for NC2778; Tos_tail6: Tos17 primer; M: DNA marker; WT: Nipponbare; AZ-1: azygos line of NG1928; AZ-2: azygos line of NC2778.

Mo were measured with an Inductively Coupled Plasma Atomic Emission Spectrometry (ICP-OES, Ultima2, Horiba Jobin Yvon GmbH, Bensheim, Germany). K and Na were measured by Atomic Absorption Spectrometry (AAS, Perkin-ELMER 1100B, Überlingen, Germany). Fe concentration in the root plaque extract was also measured with AAS. Root oxidizing power was calculated as the amount of Fe precipitated on the root surface per root dry weight.

Xylem Sap Collection and Fe Determination

Xylem sap was collected from the plants grown in both control and Fe treatment. Two hours after starting the Fe treatments, rice shoots were removed at the position of 1 cm above the basal node. Xylem sap was collected for 3 h and transferred into 1.5 mL centrifuge tubes kept on ice. The xylem sap was then incubated in 10 mM ascorbic acid solution to reduce Fe^{3+} to Fe^{2+}. The total Fe was measured with the colorimetric method using 2-2′ bipyridyl with a microplate reader (Powerwave XSII, BioTek, Bad Reichenhall, Germany) at the wavelength of 522 nm (Hartmann and Asch, 2018).

Statistical Analysis

Two-way analysis of variance (ANOVA) was used to analyze the effects of treatment, genotype, and treatment by genotype interaction on different traits with SPSS software (IBM SPSS Statistics 24, Ehningen, Germany). Within treatments, genotypic differences were analyzed with one-way ANOVA at the significance level of $P < 0.05$. *Post hoc* multiple comparisons for observed values were conducted using the Tukey's test if appropriate. The heatmap for ionomic profiling was generated with Heatmapper[2] (Babicki et al., 2016). Hierarchical clustering for the variation patterns of different elements was conducted using the average linkage with the Pearson's test.

RESULTS

Genotyping and Identification of Rice Mutants of *OsAKT1*

T2 plants of NG1928 and NC2778 were genotyped using triple primer PCR with gene-specific primers and Tos17-tail6 primer (**Figure 1A**). Homozygous plants showed single PCR band differing from wildtype (WT) while heterozygous plants showed two bands (**Figure 1B**). Homozygous lines from NG1928 (plant ID 1, 3, 5 and 8) and NC2778 (Plant ID 1,8) were grown to maturity to obtain T3 seeds together with azygos (AZ) lines (for NG1928, plant ID 7; for NC2778, plant ID 2, 4, 5), in which mutant alleles were segregated out. Semi-quantitative RT-PCR was conducted using homozygous T3 plants (**Figure 1C**) together with their corresponding AZ lines. The homozygous mutant lines of both NG1928 and NC2778 showed reduced expression compared to AZ lines indicating that insertion of

[2]http://www2.heatmapper.ca/

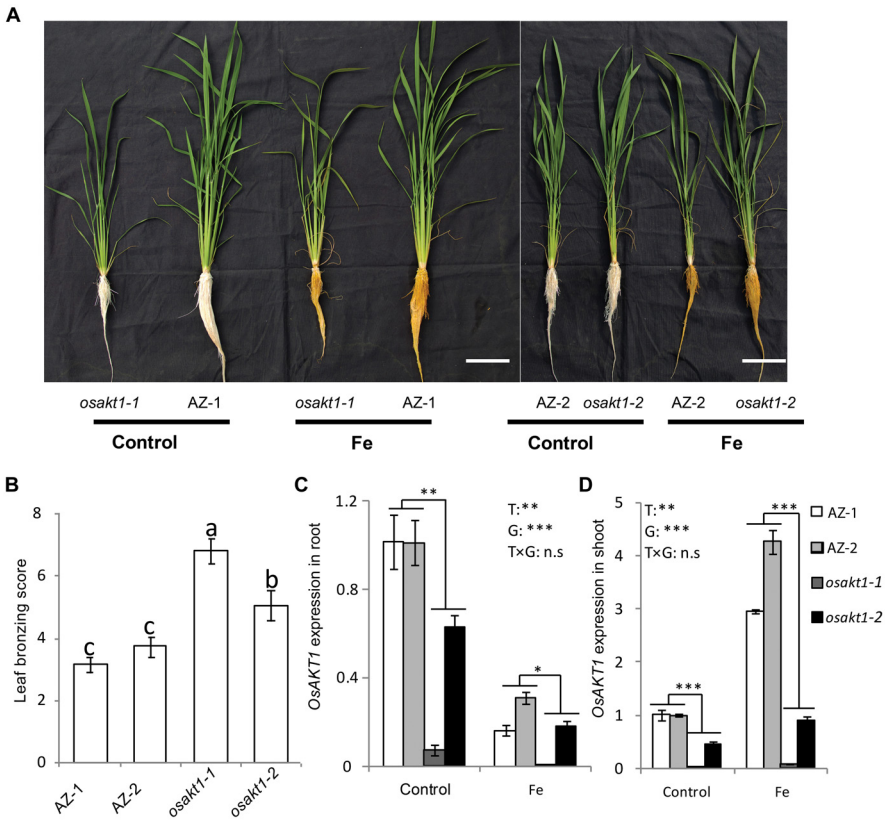

FIGURE 2 | Responses of the *OsAKT1* lines exposed to Fe toxicity (17.9 mM Fe^{2+} for 5 days). **(A)** Photos of *OsAKT1* lines in both control and Fe treatments. **(B)** Leaf bronzing score in Fe treatment. *OsAKT1* expression in the root **(C)** and shoot **(D)**. Vertical bars represent the mean values ± standard errors (*N* = 12 in B, *N* = 3 in C and D). Different letters above the bars indicate the differences were significant at $P < 0.05$ by *post hoc* Tukey's test. T: treatment; G: genotype; T × G: treatment by genotype interaction; * $P < 0.05$; ** $P < 0.01$; *** $P < 0.001$, n.s: not significant. Bar scale = 10 cm.

Tos17 led to the knock-down effect of *OsAKT1* gene. The mutant lines from NG1928 and NC2778 were named as *osakt1-1* and *osakt1-2*, respectively. AZ lines from NG1928 and NC2778 were accordingly named as AZ-1 and AZ-2, respectively.

Responses of *OsAKT1* Mutant Lines to Fe Toxicity

Both AZ and mutant lines showed similar growth after exposure to Fe toxicity (17.9 mM Fe^{2+} for 5 days) without showing reduced shoot or root biomass (**Figure 2A** and **Supplementary Figure S1**). However, Fe treatment led to marked leaf bronzing symptoms in both mutant and AZ lines (**Figure 2B**). Both *osakt1-1* and *osakt1-2* showed higher leaf bronzing score than AZ lines indicating higher sensitivity to Fe toxicity. Relative expression of *OsAKT1* in root and shoot were analyzed with quantitative RT-PCR. Fe treatment significantly suppressed the expression of *OsAKT1* in roots, while the opposite was observed in shoots where *OsAKT1* expression was induced (**Figures 2C,D**). Both *osakt1-1* and *osakt1-2* showed some residual mRNA expression values which were significantly lower than in AZ-1 and AZ-2, consistent with the semi-quantitative RT-PCR (**Figure 1C**). Moreover, the knock-down effect in *osakt1-1* was more pronounced than in *osakt1-2*.

H_2O_2 Detection in Leaves

H_2O_2 generation in leaves was visualized by DAB staining (**Figure 3**). In control conditions, no differences for the H_2O_2 generation between mutant lines and AZ lines were observed. Fe treatment markedly induced the H_2O_2 production in all the lines, but more so in *osakt1-1* and *osakt1-2* than in AZ-1 and AZ-2.

Leaf Spectral Reflectance Indices

Leaf spectral reflectance indices were monitored as stress indicators. Fe treatment significantly reduced the PRI indicating that Fe toxicity can severely limit photochemical reactions thus impairing the photosynthesis process. Moreover, mutant lines showed more pronounced decreases than AZ lines indicating that the loss function of *OsAKT1* leads to higher sensitivity to Fe toxicity (**Figure 4A**). For NPCI, which is inversely related to chlorophyll content, Fe treatment significantly increased the index in both mutant and AZ lines. A significant genotypic difference was only detected in the Fe treatment indicating that mutation of the *OsAKT1* gene led to higher sensitivity to excess Fe (**Figure 4B**). Based on the results, we conclude that *OsAKT1* is crucial for rice plants to maintain the chlorophyll content subjected to Fe stress. Additionally, leaf GI and NDVI were drastically reduced by Fe treatment.

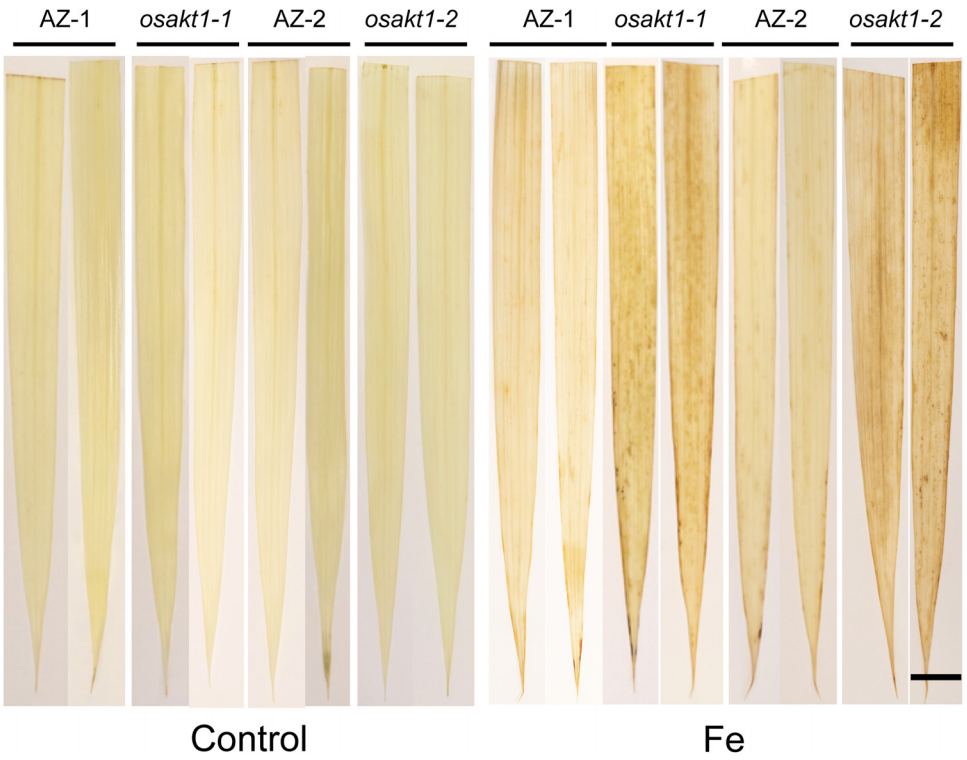

FIGURE 3 | Leaf ROS staining of *OsAKT1* lines in both control and Fe treatment (17.9 mM Fe^{2+} for 5 days). Bar scale = 1 cm. AZ, azygos line.

Both AZ-1 and AZ-2 performed significantly better than the mutant lines in Fe treatment (**Figures 4C,D**). The results indicate the crucial roles of *OsAKT1* in the tolerance to Fe toxicity in rice.

Gas Exchange and Photosynthetic Activity

The impact of Fe toxicity on the photosynthesis was investigated by gas exchange and chlorophyll fluorescence analysis. Stomatal conductance in both AZ and mutants were strongly inhibited by Fe treatment (**Figure 5A**), and mutants showed significantly lower conductance than AZ lines. Furthermore, leaf transpiration rate was significantly decreased in the Fe treatment. A significant difference was observed between mutant and AZ lines (**Figure 5B**) in the Fe treatment. Leaf-to-air water pressure deficit together with leaf temperature was induced by Fe toxicity. For both traits, mutant lines showed a higher degree of responses to Fe toxicity (**Figures 5C,D**).

Regarding net photosynthetic rate (A), photosystem II efficiency (ΦPSII) in both mutant and AZ lines were suppressed by Fe toxicity. In the Fe treatment, *osakt1-1* and *osakt1-2* showed significantly lower net photosynthetic rate than AZ lines (**Figure 5E**). Moreover, the PSII efficiency in mutant lines was significantly reduced by Fe toxicity compared to AZ lines (**Figure 5F**). Therefore, the loss-of-function of *OsAKT1* leads to more sensitivity to Fe stress in terms of photosynthetic activities in rice plants.

Potassium and Fe Measurement in Different Tissues

K and Fe concentrations were analyzed in various tissues including leaf blades, SC, and roots. Fe treatment significantly reduced the K concentrations in shoots (**Figures 6A,C**) but not in the roots (**Figure 6E**). In the control treatment, *osakt1-1* and *osakt1-2* showed decreased K concentration only in the SC compared to AZ lines ($P < 0.01$, **Figure 6C**). However, when exposed to excess Fe, the mutant lines showed consistently lower K concentration in all tissues. Fe treatment markedly increased the Fe concentrations in all tissues ($P < 0.001$, **Figures 6B,D,F**). Moreover, the mutants showed markedly higher Fe concentration in the leaf blade ($P < 0.001$, **Figure 6B**) and SC ($P < 0.05$, **Figure 6D**), but not in the root. Thus the mutation of *OsAKT1* leads to reduced K uptake in the Fe treatment, which in turn enhanced Fe translocation from root to shoot, but did not increase Fe concentrations in the root.

Ionomic Profiling of Rice Plants in Fe Toxicity

The impact of excess Fe on other cations uptake in rice was analyzed by ionomic profiling in different tissues including root, SC and leaf blade (**Figure 7**). In the root, Fe concentration was significantly higher while Mn, Ca and Mo concentrations were lower in the Fe treatment than in control. K concentrations in the mutant lines were significantly lower than in AZ lines ($P < 0.05$), and Fe treatment significantly increased the Fe

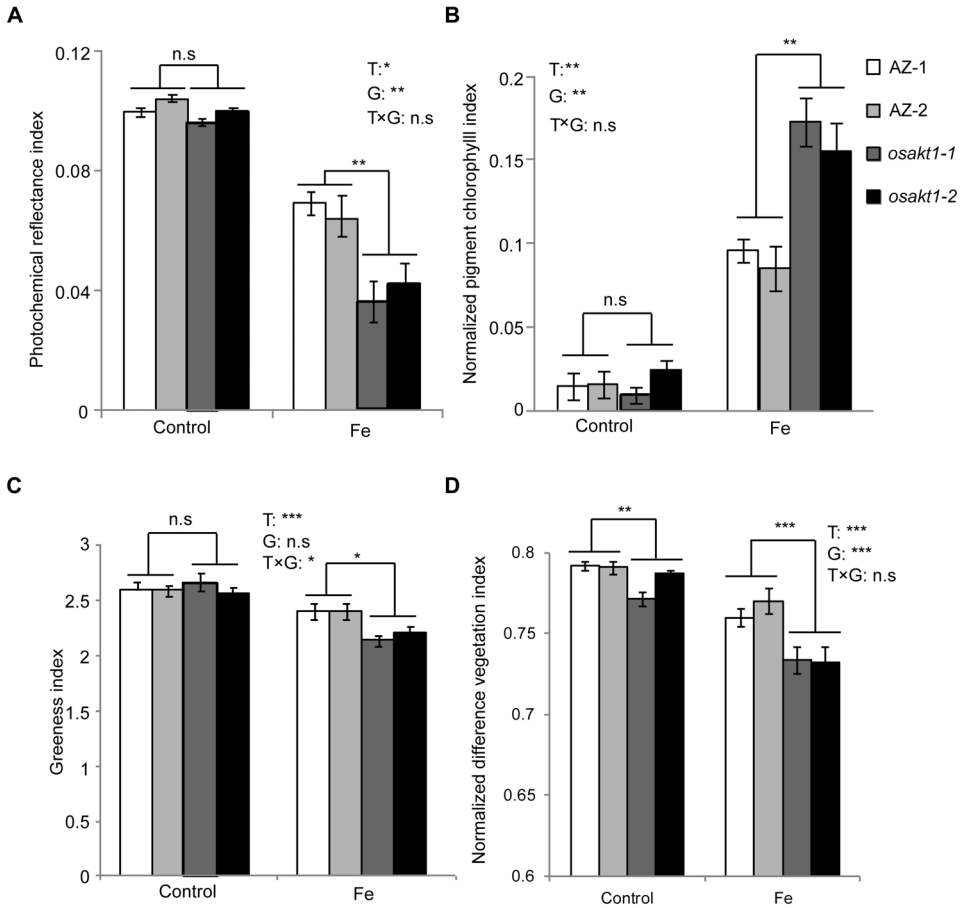

FIGURE 4 | Leaf spectral reflectance indices of *OsAKT1* mutant lines. **(A)** Photochemical reflectance index, **(B)** normalized pigment chlorophyll index, **(C)** greenness index, and **(D)** normalized difference vegetation index. Vertical bars represent mean values ± standard errors ($N = 6$). T: treatment; G: genotype; T × G: treatment by genotype interaction; * $P < 0.05$; ** $P < 0.01$; *** $P < 0.001$; n.s: not significant; AZ: azygos line.

concentration in SC ($P < 0.001$). Moreover, the concentrations of various elements including Mo, Ca, Mg, Mn, Zn, and K were significantly reduced by Fe treatment. Consistent with root tissue, K concentration in SC was also significantly lower in the mutants than in the AZ lines ($P < 0.001$), whereas Fe concentration was significantly higher in the mutants than in the AZ lines. In the leaf blade, the concentrations of multiple elements including Mo, Ca, Mg, Mn, Zn, Cu, and Ni were reduced by Fe treatment. Fe treatment increased Fe concentrations in leaf blades as expected ($P < 0.001$). The mutant lines showed significantly lower K concentrations in leaf blades, which was associated with reduced Cu but increased Fe concentrations than AZ lines ($P < 0.05$). Clustering analysis was conducted to reveal variation patterns of different cations under Fe toxicity. The variation pattern of Fe and K concentrations showed close linkage, indicating physiological interactions between Fe and K in the rice plants subjected to Fe toxicity.

Fe Uptake Gene Expression in Root

Due to the differentially regulated shoot Fe concentrations (leaf blade and SC) between mutants and AZ lines (**Figure 6**), the expression levels of Fe transport genes in root were analyzed to elucidate their possible roles in Fe uptake into the shoot tissues. Four genes including *OsFRDL1, OsIRT1, OsYSL2*, and *OsYSL15* were tested in both control and Fe toxic conditions (**Figure 8**). Fe treatment significantly reduced the expressions of *OsIRT1, OsYSL2*, and *OsYSL15* in the root. However, no genotypic differences were observed in the four genes expressions, indicating the root to shoot Fe transport genes were not affected by the loss-of-function of *OsAKT1*.

Fe Concentration in Root Plaque and Xylem Sap

We further investigated the possible mechanisms involved in Fe translocation from root to shoot under Fe toxicity. That lower Fe concentration in the SC in AZ lines was not due to exclusion at the root surface is confirmed by lack of significant differences in root oxidizing power (**Figure 9A**) between mutants and AZ lines. However, *osakt1-1* and *osakt1-2* showed significantly higher Fe concentration in the xylem sap than AZ lines in the early

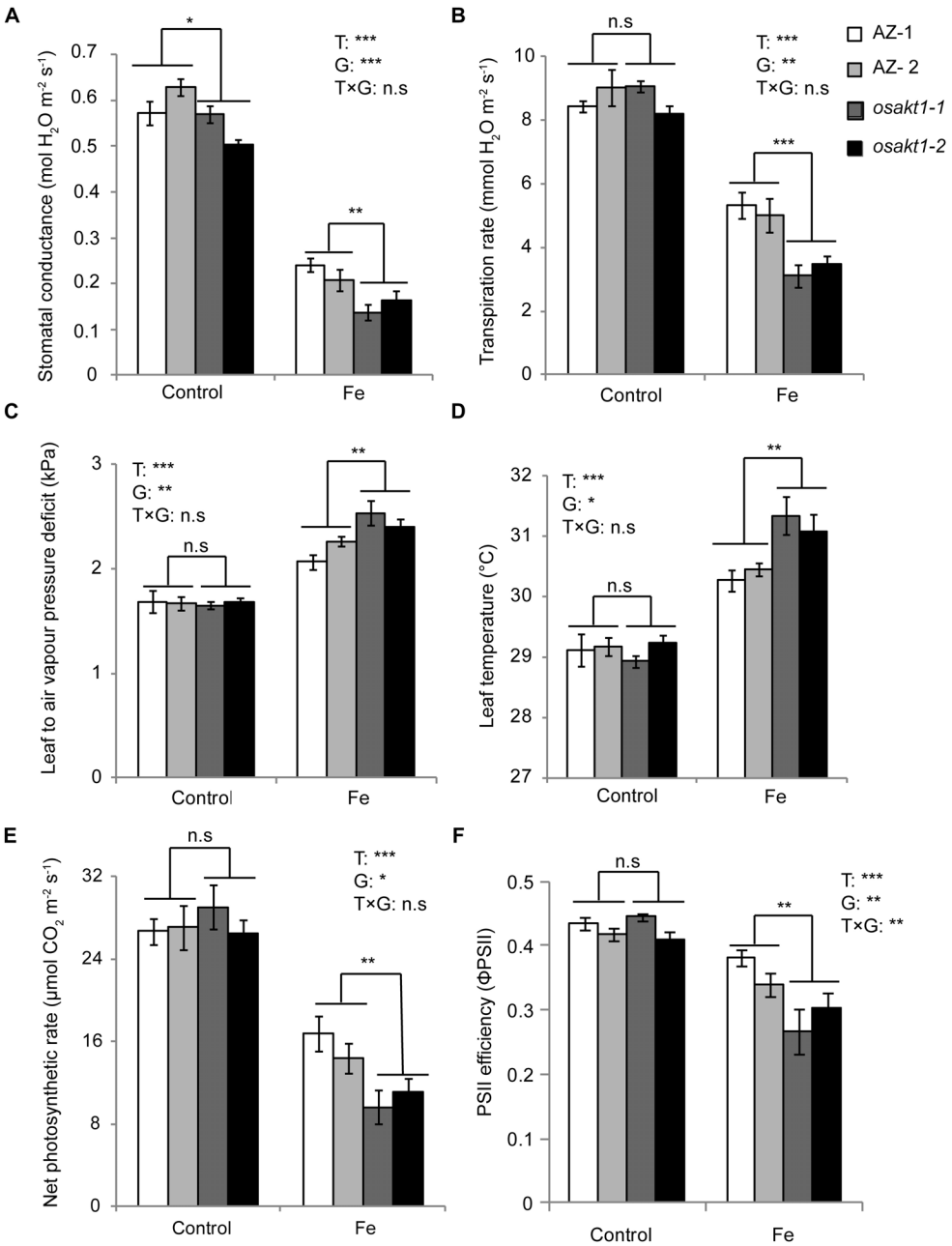

FIGURE 5 | Responses of gas exchange and chlorophyll fluorescence in *OsAKT1* mutant lines exposed to Fe toxicity (17.9 mM Fe^{2+} for 5 days). **(A)** Stomatal conductance, **(B)** transpiration rate, **(C)** leaf to air vapor pressure deficit, **(D)** leaf temperature, **(E)** net photosynthetic rate and **(F)** photosystem II efficiency were measured on the first and second fully expanded leaves of the main tiller. Vertical bars represent mean values ± standard errors ($N = 6$). T: treatment; G: genotype; T × G: treatment by genotype interaction; * $P < 0.05$; ** $P < 0.01$; *** $P < 0.001$; n.s: not significant; AZ: azygos line.

stage (2 h) of Fe stress (**Figure 9B**), indicating that root-to-shoot translocation of Fe was affected due to mutation of *OsAKT1*.

DISCUSSION

In this study, we investigated a potassium ion channel gene *OsAKT1*, which was nominated as a candidate gene underlying an Fe uptake QTL in our previous study (Matthus et al., 2015). In GWAS, *OsAKT1* was identified in a linkage block flanking a highly significant SNP marker on chromosome 1, which was associated with variations of the shoot Fe concentration among 329 Asian rice accessions. By analyzing Tos17 insertional mutants, we confirmed that loss-function of *OsAKT1* in rice led to lower K concentrations in various tissues (**Figures 6A,C,E**), thereby confirming the findings in previous

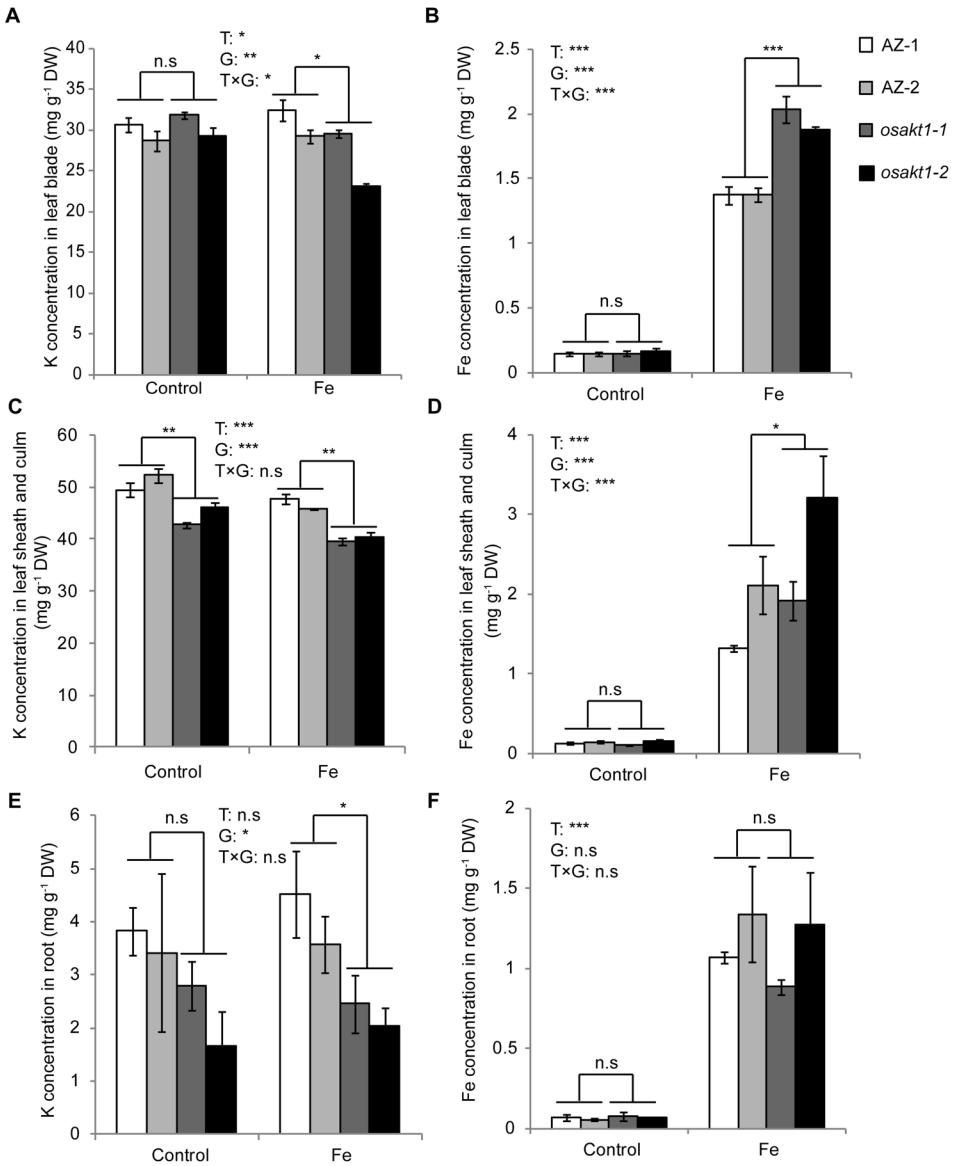

FIGURE 6 | K and Fe concentration in different tissues of *OsAKT1* mutant lines exposed to Fe toxicity (17.9 mM Fe^{2+} for 5 days). **(A)** K concentration in leaf bade, **(B)** Fe concentration in leaf blade, **(C)** K concentration in leaf sheath and culm, **(D)** Fe concentration in leaf sheath and culm, **(E)** K concentration in the root, and **(F)** Fe concentration in the root. Vertical bars represent mean values ± standard errors ($N = 4$). T: treatment, G: genotype, T × G: treatment by genotype interaction. * $P < 0.05$; ** $P < 0.01$; *** $P < 0.001$; n.s: not significant; AZ: azygos line.

reports (Fuchs et al., 2005; Obata et al., 2007). Compared to AZ lines, *OsAKT1* mutants showed similar growth after 5 weeks in control conditions despite lower potassium concentration in the SC (**Figure 6C**). The results were consistent with the findings described by Ahmad et al. (2016), in which, *OsAKT1* mutants showed similar relative growth rate as wildtypes in the absence of stress when rice plants were also grown for 5 weeks. However, Li et al. (2014) observed reduced shoot growth in a T-DNA insertional mutant line for *OsAKT1* compared to the wildtype when both lines were grown only for 1 week. The loss-of-function of *OsAKT1* might be compensated by other K transporters (Ahmad et al., 2016). However, due to the low-capacity transport activities of, e.g., HAK/KUP family transporters (Yang et al., 2014), mutant plants require an extended period to restore growth.

Fe is transported to the shoots via transpiration stream in the xylem (Curie and Briat, 2003). Rice plants responded to excess Fe by decreasing stomatal conductance (**Figure 5A**), thus lowering the transpiration rate (**Figure 5B**), which might be considered as an avoidance mechanism to reduce Fe uptake. However, previous studies reported that sensitive genotypes showed a more pronounced decrease in stomatal conductance and transpiration rate than tolerant genotypes (Dufey et al., 2009; Pereira et al., 2013). It suggests that stomata closure is a stress

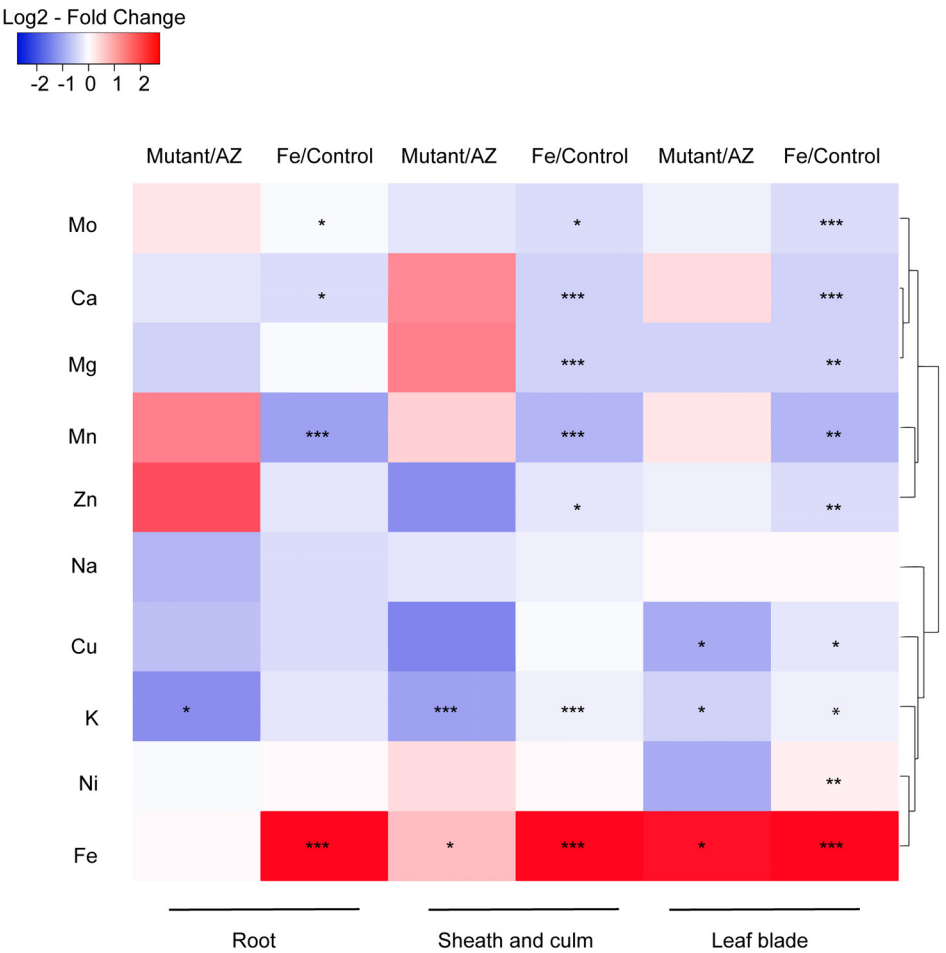

FIGURE 7 | Ionomic profiling of *OsAKT1* lines exposed to Fe toxicity (17.9 mM Fe^{2+} for 5 days). Heatmap was generated using the fold-change value (Log2 transformed) of ions concentrations in various tissues. Blue color indicates the lower element concentration in Fe treatment than control or mutants than azygos lines while red color indicates the opposite results. Only significant differences between treatments or genotypes were shown with asterisks. Hierarchical clustering for the variation patterns of different elements was conducted using the average linkage with the Pearson's test. AZ: azygos lines; * $P < 0.05$; ** $P < 0.01$; *** $P < 0.001$.

symptom rather than a tolerance mechanism of the rice plants subjected to excess Fe. As a consequence of the lower K uptake, mutant lines showed lower stomatal conductance than AZ lines in control conditions (**Figure 5A**). In Fe treatment, mutant lines showed reduced stomatal conductance and transpiration rate than AZ lines indicating more sensitivity (**Figures 5A,B**). Other parameters including ROS generation (**Figure 3**), chlorophyll content (**Figure 4**) and photosynthesis efficiency (**Figure 5E**) also showed the same trend leading to the conclusion that *OsAKT1* is involved in Fe toxicity tolerance in rice.

Apart from inducing oxidative stress in rice plants (Quinet et al., 2012; Höller et al., 2015; Wu et al., 2017), Fe toxicity also affected the uptake of other essential elements into different tissues (**Figure 7**). The reductions in nutrients uptake might be caused by the damage of root systems (Wu, 2016) or by the root plaque formed through the oxidation and precipitation of Fe (Wu et al., 2012, 2014; Zhou et al., 2015). Additionally, excess Fe can reduce the expression of metal (e.g., Zn, Mn) transporter genes in roots as suggested by previous transcriptome analyses (Quinet et al., 2012; Wu et al., 2017). Thus, Fe toxicity leads to multiple nutrient disorders causing negative feedback on growth and physiological traits. In Fe toxic conditions, K homeostasis plays a vital role in regulating excess Fe translocation into shoot tissues.

Interactions between K and excess Fe were previously reported in *Arabidopsis*, in which the tolerance to excess Fe was found to be positively associated with root K status, which was mediated by ethylene and NO (Li et al., 2015; Zhang et al., 2018). Moreover, the application of K can restore primary root growth in *Arabidopsis* plants subjected to excess Fe (Li et al., 2016). However, contradictory results were found in rice studies regarding the interactions between K and Fe stress (Li et al., 2001). K can mitigate Fe stress in rice when it was applied in the form of K_2SO_4 (Yamauchi, 1989; Li et al., 2001), while no protecting effect was observed when K was applied as KCl (Mehraban et al., 2008). In this study, however, we clearly showed that adequate uptake of K could protect rice plants exposed to excess Fe by regulating Fe translocation from root to shoot in Fe toxic conditions (**Figure 7**).

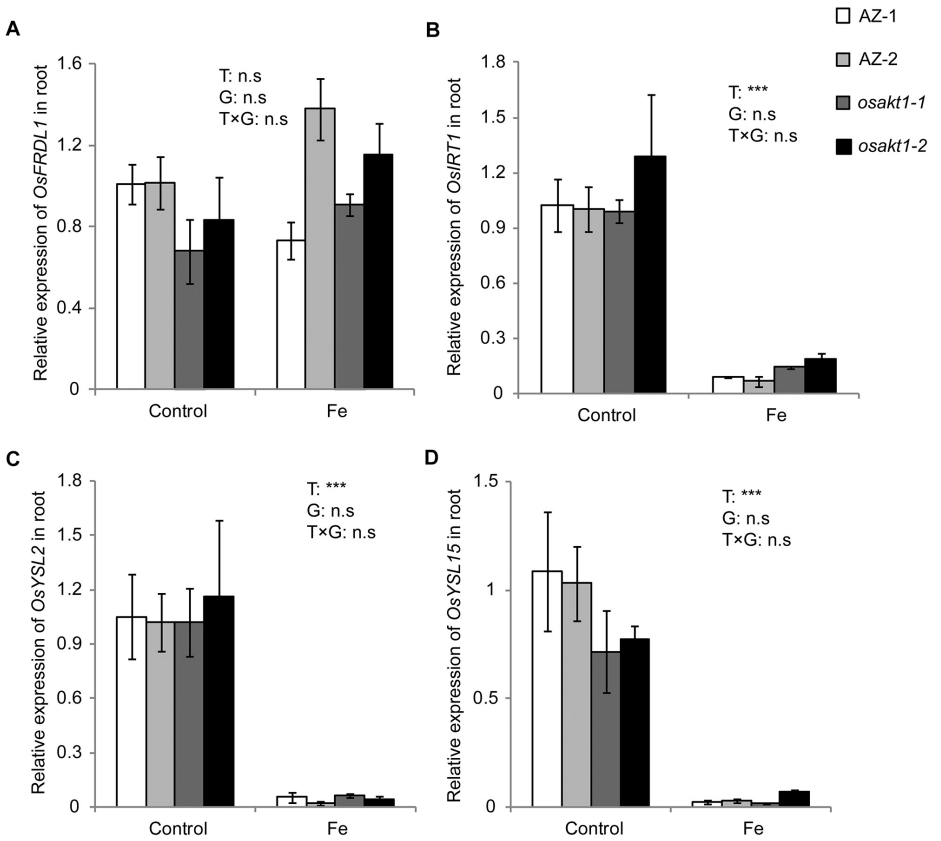

FIGURE 8 | Expression of Fe-transport genes in roots of *OsAKT1* lines exposed to Fe toxicity (17.9 mM Fe^{2+} for 5 days). **(A)** *OsFRDL1*, **(B)** *OsIRT1*, **(C)** *OsYSL2*, and **(D)** *OsYSL15* expression in the root were analyzed with quantitative RT-PCR. Vertical bars represent mean values ± standard errors ($N = 3$). Sequences of the primers used in the test were listed in **Supplementary Table S1**. T: treatment; G: genotype; T × G: treatment by genotype interaction; *** $P < 0.001$, n.s: not significant; AZ: azygos lines.

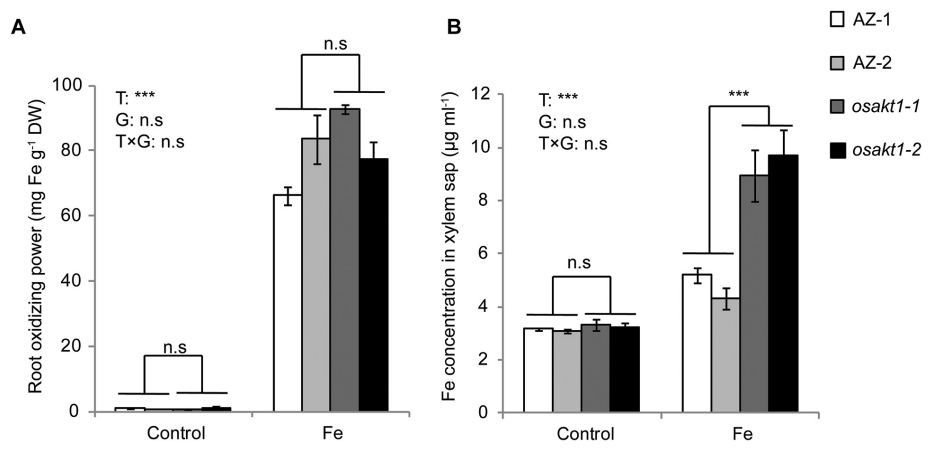

FIGURE 9 | Root oxidizing power and Fe concentration in xylem sap of *OsAKT1* mutant lines exposed to Fe toxicity (17.9 mM Fe^{2+} for 5 days). **(A)** Root oxidizing power. **(B)** Fe concentration in the xylem sap. Vertical bars represent mean values ± standard errors ($N = 3$). T: treatment; G: genotype; T × G: treatment by genotype interaction; *** $P < 0.001$; n.s: not significant; AZ: azygos line.

Long-distance transport of Fe is facilitated by several genes including *OsFRDL1* for Fe translocation to the shoot as a Fe-citrate complex (Yokosho et al., 2009), *OsIRT1* (Ishimaru et al., 2006), *OsYSL2* (Koike et al., 2004), *OsYSL15* (Inoue et al., 2009). The genes responsible for Fe transport were highly induced by Fe deficiency and suppressed by excess Fe (Nozoye et al., 2007;

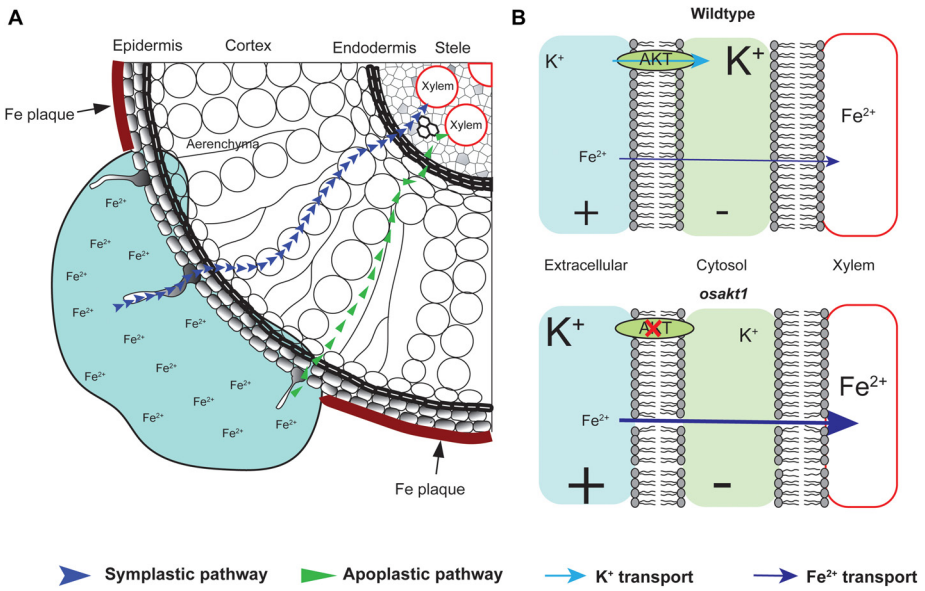

FIGURE 10 | A proposed conceptual model explaining the different xylem Fe concentration observed in *OsAKT1* mutant and wildtype lines. **(A)** In Fe toxic conditions, Fe^{2+} ions enter root cells via both apoplastic and symplastic pathway. Fe plaque formed by root oxidizing power on the root surface did not significantly differ between mutant and wildtype lines. **(B)** Loss-of-function of *OsAKT1* in the mutant lines (lower) leads to lower intracellular K^+ concentration and thus to a higher degree of hyperpolarization of the plasma membrane than wildtypes (Upper). More hyperpolarized membrane will facilitate more Fe^{2+} ions being loaded into the xylem sap and further transported into the shoots. Different font size of K^+ and Fe^{2+} indicates different concentration. +, positively charged; −, negatively charged.

Zheng et al., 2009; Quinet et al., 2012; Wu et al., 2017). In our study, no significant differences were observed for the Fe translocation genes between mutants and AZ lines (**Figure 8**). These observations suggest that the regular Fe transporters play a less critical role in Fe toxic conditions and other physiological processes caused the differences in shoot Fe concentrations between *OsAKT1* mutants and AZ lines.

Fe plaque on root surface is considered as an essential factor affecting shoot Fe concentration in rice plants exposed to Fe toxic conditions, which depends on the root oxidizing power (Engel et al., 2012; Wu et al., 2014). However, no significant differences between mutants and AZ lines were observed for the amount of Fe oxidized and precipitated on the root surface (**Figure 9A**), demonstrating that this mechanism did not explain the differences of shoot Fe concentrations. Therefore we explored the xylem as the primary route of Fe transport from root to shoot via the transpiration stream (Morrissey and Guerinot, 2009). Based on our gas exchange measurements (**Figure 5B**) we can exclude the idea that higher transpiration rate was responsible for Fe accumulation in *OsAKT1* mutants. Instead, higher accumulation of Fe in shoots can be explained with enhanced Fe levels in the xylem sap of *OsAKT1* mutants (**Figure 9B**), which showed significantly lower root K concentrations than AZ lines (**Figure 7**). A conceptual model explaining the different level of Fe in the xylem sap between AZ lines and mutant lines was proposed (**Figure 10**). In Fe toxic conditions, excess Fe^{2+} ions enter the roots via both symplastic and apoplastic pathway (Becker and Asch, 2005). Excess Fe^{2+} ions react with H_2O_2 leading to the generation of hydroxyl radicals, which will directly activate outward-rectifying K^+ channels, e.g., GORK leading to K^+ leak (Demidchik et al., 2010). Moreover, non-selective cation channels (NSCC) can also be activated by excess Fe^{2+} via NO-mediated pathway leading to K^+ loss (Zhang et al., 2018). Massive K^+ leak from the cytosol will hyperpolarize the plasma membrane in root cells (Wang and Wu, 2013). Also due to the loss-of-function of *OsAKT1*, the mutant lines are less capable of restoring cytosolic K^+ content (**Figure 6E**) (Li et al., 2014; Ahmad et al., 2016). The plasma membrane in the mutant lines might show a higher degree of hyperpolarization than the AZ lines, which will facilitate more Fe^{2+} uptake in the roots and further transport to the shoots. These mechanisms were likely involved in a higher level of Fe translocation to the xylem in *OsAKT1* mutant lines.

In conclusion, our study demonstrated the importance of endogenous K homeostasis for the shoot accumulation of Fe in rice plants grown in Fe toxic conditions. Targeting the *OsAKT1* gene as an essential hub of K homeostasis in rice may thus be a promising strategy in the breeding of adapted rice varieties.

AUTHOR CONTRIBUTIONS

L-BW and MF conceived the project, designed the experiments, analyzed the data, and wrote the manuscript. L-BW, FH, and AW conducted the experiments.

FUNDING

This study was financially supported by the Deutsche Forschungsgemeinschaft (DFG, project ID FR2925/2-1).

ACKNOWLEDGMENTS

The authors wish to thank Dr. Jürgen Burkhardt for the support of conducting the gas exchange and chlorophyll fluorescence measurements.

SUPPLEMENTARY MATERIAL

The Supplementary Material for this article can be found online at: https://www.frontiersin.org/articles/10.3389/fpls.2019.00579/full#supplementary-material

REFERENCES

Ahmad, I., Mian, A., and Maathuis, F. J. M. (2016). Overexpression of the rice AKT1 potassium channel affects potassium nutrition and rice drought tolerance. *J. Exp. Bot.* 67, 2689–2698. doi: 10.1093/jxb/erw103

Aranda, P. S., LaJoie, D. M., and Jorcyk, C. L. (2012). Bleach gel: a simple agarose gel for analyzing RNA quality. *Electrophoresis* 33, 366–369. doi: 10.1002/elps.201100335

Ashrafuzzaman, M., Haque, Z., Ali, B., Mathew, B., Yu, P., Hochholdinger, F., et al. (2018). Ethylenediurea (EDU) mitigates the negative effects of ozone in rice: insights into its mode of action. *Plant Cell Environ.* 41, 2882–2898. doi: 10.1111/pce.13423

Audebert, A., and Fofana, M. (2009). Rice yield gap due to iron toxicity in west Africa. *J. Agron. Crop Sci.* 195, 66–76. doi: 10.1111/j.1439-037X.2008.00339.x

Babicki, S., Arndt, D., Marcu, A., Liang, Y., Grant, J. R., Maciejewski, A., et al. (2016). Heatmapper: web-enabled heat mapping for all. *Nucleic Acids Res.* 44, W147–W153. doi: 10.1093/nar/gkw419

Becana, M., Moran, J. F., and Iturbe-Ormaetxe, I. (1998). Iron-dependent oxygen free radical generation in plants subjected to environmental stress: toxicity and antioxidant protection. *Plant Soil* 201, 137–147. doi: 10.1023/a:1004375732137

Becker, M., and Asch, F. (2005). Iron toxicity in rice-conditions and management concepts. *J. Plant Nutr. Soil Sci.* 168, 558–573. doi: 10.1002/jpln.200520504

Bughio, N., Yamaguchi, H., Nishizawa, N. K., Nakanishi, H., and Mori, S. (2002). Cloning an iron-regulated metal transporter from rice. *J. Exp. Bot.* 53, 1677–1682. doi: 10.1093/jxb/erf004

Cakmak, I. (2005). The role of potassium in alleviating detrimental effects of abiotic stresses in plants. *J. Plant Nutr. Soil Sci.* 168, 521–530. doi: 10.1002/jpln.200420485

Curie, C., and Briat, J. F. (2003). Iron transport and signaling in plants. *Annu. Rev. Plant Biol.* 54, 183–206. doi: 10.1146/annurev.arplant.54.031902.135018

da Silveira, V. C., Fadanelli, C., Sperotto, R. A., Stein, R. J., Basso, L. A., Santos, D. S., et al. (2009). Role of ferritin in the rice tolerance to iron overload. *Sci. Agric.* 66, 549–555. doi: 10.1590/s0103-90162009000400019

Demidchik, V., Cuin, T. A., Svistunenko, D., Smith, S. J., Miller, A. J., Shabala, S., et al. (2010). Arabidopsis root K^+-efflux conductance activated by hydroxyl radicals: single-channel properties, genetic basis and involvement in stress-induced cell death. *J. Cell Sci.* 123, 1468–1479. doi: 10.1242/jcs.064352

Dufey, I., Hakizimana, P., Draye, X., Lutts, S., and Bertin, P. (2009). QTL mapping for biomass and physiological parameters linked to resistance mechanisms to ferrous iron toxicity in rice. *Euphytica* 167, 143–160. doi: 10.1007/s10681-008-9870-7

Dufey, I., Mathieu, A.-S., Draye, X., Lutts, S., and Bertin, P. (2014). Construction of an integrated map through comparative studies allows the identification of candidate regions for resistance to ferrous iron toxicity in rice. *Euphytica* 203, 59–69. doi: 10.1007/s10681-014-1255-5

Engel, K., Asch, F., and Becker, M. (2012). Classification of rice genotypes based on their mechanisms of adaptation to iron toxicity. *J. Plant Nutr. Soil Sci.* 175, 871–881. doi: 10.1002/jpln.201100421

Frei, M., Tetteh, R. N., Razafindrazaka, A. L., Fuh, M. A., Wu, L.-B., and Becker, M. (2016). Responses of rice to chronic and acute iron toxicity: genotypic differences and biofortification aspects. *Plant Soil* 408, 149–161. doi: 10.1007/s11104-016-2918-x

Fuchs, I., Stölzle, S., Ivashikina, N., and Hedrich, R. (2005). Rice K^+ uptake channel OsAKT1 is sensitive to salt stress. *Planta* 221, 212–221. doi: 10.1007/s00425-004-1437-9

Gamon, J., Serrano, L., and Surfus, J. (1997). The photochemical reflectance index: an optical indicator of photosynthetic radiation use efficiency across species, functional types, and nutrient levels. *Oecologia* 112, 492–501. doi: 10.1007/s004420050337

Gao, P. P., Zheng, G. H., Wu, Y. H., and Liu, P. (2014). Effect of exogenous potassium on photosynthesis and antioxidant enzymes of rice under iron toxicity. *Russ. J. Plant Physiol.* 61, 47–52. doi: 10.1134/s1021443714010051

Garthwaite, A. J., von Bothmer, R., and Colmer, T. D. (2005). Salt tolerance in wild hordeum species is associated with restricted entry of Na^+ and Cl^- into the shoots. *J. Exp. Bot.* 56, 2365–2378. doi: 10.1093/jxb/eri229

Gautam, P., Lal, B., Tripathi, R., Shahid, M., Baig, M., Maharana, S., et al. (2016). Beneficial effects of potassium application in improving submergence tolerance of rice (*Oryza sativa* L.). *Environ. Exp. Bot.* 128, 18–30. doi: 10.1016/j.envexpbot.2016.04.005

Grillet, L., Ouerdane, L., Flis, P., Hoang, M. T., Isaure, M.-P., Lobinski, R., et al. (2014). Ascorbate efflux as a new strategy for iron reduction and transport in plants. *J. Biol. Chem.* 289, 2515–2525. doi: 10.1074/jbc.M113.514828

Hartmann, J., and Asch, F. (2018). Micro-method to determine iron concentrations in plant tissues using 2, 2′ bipyridine. *J. Plant Nutr. Soil Sci.* 181, 357–363. doi: 10.1002/jpln.201700433

Höller, S., Ueda, Y., Wu, L., Wang, Y., Hajirezaei, M.-R., Ghaffari, M.-R., et al. (2015). Ascorbate biosynthesis and its involvement in stress tolerance and plant development in rice (*Oryza sativa* L.). *Plant Mol. Biol.* 88, 545–560. doi: 10.1007/s11103-015-0341-y

Huang, J., Wang, X., Li, X., Tian, H., and Pan, Z. (2013). Remotely sensed rice yield prediction using multi-temporal NDVI data derived from NOAA's-AVHRR. *PLoS One* 8:e70816. doi: 10.1371/journal.pone.0070816

Inoue, H., Kobayashi, T., Nozoye, T., Takahashi, M., Kakei, Y., Suzuki, K., et al. (2009). Rice OsYSL15 is an iron-regulated iron(III)-deoxymugineic acid transporter expressed in the roots and is essential for iron uptake in early growth of the seedlings. *J. Biol. Chem.* 284, 3470–3479. doi: 10.1074/jbc.M806042200

Ishimaru, Y., Suzuki, M., Tsukamoto, T., Suzuki, K., Nakazono, M., Kobayashi, T., et al. (2006). Rice plants take up iron as an Fe^{3+}-phytosiderophore and as Fe^{2+}. *Plant J.* 45, 335–346. doi: 10.1111/j.1365-313X.2005.02624.x

Kobayashi, T., Nagasaka, S., Senoura, T., Itai, R. N., Nakanishi, H., and Nishizawa, N. K. (2013). Iron-binding haemerythrin RING ubiquitin ligases regulate plant iron responses and accumulation. *Nat. Commun.* 4:2792. doi: 10.1038/ncomms3792

Koike, S., Inoue, H., Mizuno, D., Takahashi, M., Nakanishi, H., Mori, S., et al. (2004). OsYSL2 is a rice metal-Nicotianamine transporter that is regulated by iron and expressed in the phloem. *Plant J.* 39, 415–424. doi: 10.1111/j.1365-313x.2004.02146.x

Li, G., Kronzucker, H. J., and Shi, W. (2016). Root developmental adaptation to Fe toxicity: mechanisms and management. *Plant Signal. Behav.* 11:e1117722. doi: 10.1080/15592324.2015.1117722

Li, G. J., Xu, W. F., Kronzucker, H. J., and Shi, W. M. (2015). Ethylene is critical to the maintenance of primary root growth and Fe homeostasis under Fe stress in Arabidopsis. *J. Exp. Bot.* 66, 2041–2054. doi: 10.1093/jxb/erv005

Li, H., Yang, X., and Luo, A. C. (2001). Ameliorating effect of potassium on iron toxicity in hybrid rice. *J. Plant Nutr.* 24, 1849–1860. doi: 10.1081/pln-100107598

Li, J., Long, Y., Qi, G.-N., Li, J., Xu, Z.-J., Wu, W.-H., et al. (2014). The Os-AKT1 channel is critical for K^+ uptake in rice roots and is modulated by the rice CBL1-CIPK23 complex. *Plant Cell* 26, 3387–3402. doi: 10.1105/tpc.114.123455

Liu, W.-J., Zhu, Y.-G., Smith, F. A., and Smith, S. E. (2004). Do iron plaque and genotypes affect arsenate uptake and translocation by rice seedlings (*Oryza sativa* L.) grown in solution culture? *J. Exp. Bot.* 55, 1707–1713. doi: 10.1093/jxb/erh205

Matthus, E., Wu, L.-B., Ueda, Y., Höller, S., Becker, M., and Frei, M. (2015). Loci, genes, and mechanisms associated with tolerance to ferrous iron toxicity in rice (*Oryza sativa* L.). *Theor. Appl. Genet.* 28, 2085–2098. doi: 10.1007/s00122-015-2569-y

Mehraban, P., Zadeh, A. A., and Sadeghipour, H. R. (2008). Iron toxicity in rice (*Oryza sativa* L.), under different potassium nutrition. *Asian J. Plant Sci.* 7, 251–259. doi: 10.1111/pce.12733

Miyao, A., Tanaka, K., Murata, K., Sawaki, H., Takeda, S., Abe, K., et al. (2003). Target site specificity of the Tos17 retrotransposon shows a preference for insertion within genes and against insertion in retrotransposon-rich regions of the genome. *Plant Cell* 15, 1771–1780. doi: 10.1105/tpc.012559

Morrissey, J., and Guerinot, M. L. (2009). Iron uptake and transport in plants: the good, the bad, and the ionome. *Chem. Rev.* 109, 4553–4567. doi: 10.1021/cr900112r

Nozoye, T., Inoue, H., Takahashi, M., Ishimaru, Y., Nakanishi, H., Mori, S., et al. (2007). The expression of iron homeostasis-related genes during rice germination. *Plant Mol. Biol.* 64, 35–47. doi: 10.1007/s11103-007-9132-4

Obata, T., Kitamoto, H. K., Nakamura, A., Fukuda, A., and Tanaka, Y. (2007). Rice shaker potassium channel oskat1 confers tolerance to salinity stress on yeast and rice cells. *Plant Physiol.* 144, 1978–1985. doi: 10.1104/pp.107.101154

Peñuelas, J., Gamon, J., Fredeen, A., Merino, J., and Field, C. (1994). Reflectance indices associated with physiological changes in nitrogen-and water-limited sunflower leaves. *Remote Sens. Environ.* 48, 135–146. doi: 10.1016/0034-4257(94)90136-8

Pereira, E. G., Oliva, M. A., Rosado-Souza, L., Mendes, G. C., Colares, D. S., Stopato, C. H., et al. (2013). Iron excess affects rice photosynthesis through stomatal and non-stomatal limitations. *Plant Sci.* 201–202, 81–92. doi: 10.1016/j.plantsci.2012.12.003

Ponnamperuma, F. N., Bradfield, R., and Peech, M. (1955). Physiological disease of rice arrtibutable to iron toxicity. *Nature* 175, 265–265. doi: 10.1038/175265a0

Quinet, M., Vromman, D., Clippe, A., Bertin, P., Lequeux, H., Dufey, I., et al. (2012). Combined transcriptomic and physiological approaches reveal strong differences between short- and long-term response of rice (*Oryza sativa*) to iron toxicity. *Plant Cell Environ.* 35, 1837–1859. doi: 10.1111/j.1365-3040.2012.02521.x

Römheld, V., and Marschner, H. (1986). Evidence for a specific uptake system for iron phytosiderophores in roots of grasses. *Plant Physiol.* 80, 175–180. doi: 10.1104/pp.80.1.175

Shrestha, A., Dziwornu, A. K., Ueda, Y., Wu, L.-B., Mathew, B., and Frei, M. (2018). Genome-wide association study to identify candidate loci and genes for Mn toxicity tolerance in rice. *PLoS One* 13:e0192116. doi: 10.1371/journal.pone.0192116

Stein, R. J., Lopes, S. I. G., and Fett, J. P. (2014). Iron toxicity in field-cultivated rice: contrasting tolerance mechanisms in distinct cultivars. *Theor. Exp. Plant Physiol.* 26, 135–146. doi: 10.1007/s40626-014-0013-3

Stein, R. J., Ricachenevsky, F. K., and Fett, J. P. (2009). Differential regulation of the two rice ferritin genes (OsFER1 and OsFER2). *Plant Sci.* 177, 563–569. doi: 10.1016/j.plantsci.2009.08.001

Thomine, S., and Vert, G. (2013). Iron transport in plants: better be safe than sorry. *Curr. Opin. Plant Biol.* 16, 322–327. doi: 10.1016/j.pbi.2013.01.003

van Oort, P. A. J. (2018). Mapping abiotic stresses for rice in Africa: drought, cold, iron toxicity, salinity and sodicity. *Field Crop. Res.* 219, 55–75. doi: 10.1016/j.fcr.2018.01.016

Wang, Y., and Wu, W.-H. (2013). Potassium transport and signaling in higher plants. *Annu. Rev. Plant Biol.* 64, 451–476. doi: 10.1146/annurev-arplant-050312-120153

Wu, C., Ye, Z., Li, H., Wu, S., Deng, D., Zhu, Y., et al. (2012). Do radial oxygen loss and external aeration affect iron plaque formation and arsenic accumulation and speciation in rice? *J. Exp. Bot.* 63, 2961–2970. doi: 10.1093/jxb/ers017

Wu, L.-B. (2016). *Genetic and Physiological Analyses of the Tolerance Mechanisms to Ferrous Iron Toxicity in Rice (Oryza sativa L.)*. Ph.D. thesis, University of Bonn, Bonn, Germany.

Wu, L.-B., Shhadi, M., Gregorio, G., Matthus, E., Becker, M., and Frei, M. (2014). Genetic and physiological analysis of tolerance to acute iron toxicity in rice. *Rice* 7:8. doi: 10.1186/s12284-014-0008-3

Wu, L.-B., Ueda, Y., Lai, S.-K., and Frei, M. (2017). Shoot tolerance mechanisms to iron toxicity in rice (*Oryza sativa* L.). *Plant Cell Environ.* 40, 570–584. doi: 10.1111/pce.12733

Yamauchi, M. (1989). Rice bronzing in Nigeria caused by nutrient imbalances and its control by potassium sulfate application. *Plant Soil* 117, 275–286. doi: 10.1007/bf02220722

Yang, T., Zhang, S., Hu, Y., Wu, F., Hu, Q., Chen, G., et al. (2014). The role of a potassium transporter OsHAK5 in potassium acquisition and transport from roots to shoots in rice at low potassium supply levels. *Plant Physiol.* 166, 945–959. doi: 10.1104/pp.114.246520

Yokosho, K., Yamaji, N., Ueno, D., Mitani, N., and Ma, J. F. (2009). OsFRDL1 is a citrate transporter required for efficient translocation of iron in rice. *Plant Physiol.* 149, 297–305. doi: 10.1104/pp.108.128132

Yoshida, S., Forno, D. A., Cock, J. H., and Gomez, K. A. (1976). *Laboratory Manual for Physiological Studies of Rice*. Manila: International Rice Research Institute.

Zhang, J., Chen, K., Pang, Y., Naveed, S. A., Zhao, X., Wang, X., et al. (2017). QTL mapping and candidate gene analysis of ferrous iron and zinc toxicity tolerance at seedling stage in rice by genome-wide association study. *BMC Genomics* 18:828. doi: 10.1186/s12864-017-4221-5

Zhang, L., Li, G., Wang, M., Di, D., Sun, L., Kronzucker, H. J., et al. (2018). Excess iron stress reduces root tip zone growth through nitric oxide-mediated repression of potassium homeostasis in Arabidopsis. *New Phytol.* 219, 259–274. doi: 10.1111/nph.15157

Zheng, L., Huang, F., Narsai, R., Wu, J., Giraud, E., He, F., et al. (2009). Physiological and transcriptome analysis of iron and phosphorus interaction in rice seedlings. *Plant Physiol.* 151, 262–274. doi: 10.1104/pp.109.141051

Zhou, H., Zeng, M., Zhou, X., Liao, B.-H., Peng, P.-Q., Hu, M., et al. (2015). Heavy metal translocation and accumulation in iron plaques and plant tissues for 32 hybrid rice (*Oryza sativa* L.) cultivars. *Plant Soil* 386, 317–329. doi: 10.1007/s11104-014-2268-5

Conflict of Interest Statement: The authors declare that the research was conducted in the absence of any commercial or financial relationships that could be construed as a potential conflict of interest.

frontiers in Plant Science

MINI REVIEW
published: 14 May 2019
doi: 10.3389/fpls.2019.00605

From Leguminosae/Gramineae Intercropping Systems to See Benefits of Intercropping on Iron Nutrition

*Jing Dai[1,2], Wei Qiu[1], Nanqi Wang[1], Tianqi Wang[1], Hiromi Nakanishi[2] and Yuanmei Zuo[1]**

[1] College of Resources and Environmental Sciences, National Academy of Agriculture Green Development, Key Lab of Plant-Soil Interaction, MOE, China Agricultural University, Beijing, China, [2] Graduate School of Agricultural and Life Sciences, The University of Tokyo, Tokyo, Japan

OPEN ACCESS

Edited by:
Thomas J. Buckhout, Humboldt University of Berlin, Germany

Reviewed by:
Ferenc Fodor, Eötvös Loránd University, Hungary
Tanja Mimmo, Free University of Bozen-Bolzano, Italy

***Correspondence:**
Yuanmei Zuo
zuoym@cau.edu.cn

Specialty section:
This article was submitted to Plant Nutrition, a section of the journal Frontiers in Plant Science

Received: *17 December 2018*
Accepted: *25 April 2019*
Published: *14 May 2019*

Citation:
Dai J, Qiu W, Wang N, Wang T, Nakanishi H and Zuo Y (2019) From Leguminosae/Gramineae Intercropping Systems to See Benefits of Intercropping on Iron Nutrition. Front. Plant Sci. 10:605. doi: 10.3389/fpls.2019.00605

To achieve sustainable development with a growing population while sustaining natural resources, a sustainable intensification of agriculture is necessary. Intercropping is useful for low-input/resource-limited agricultural systems. Iron (Fe) deficiency is a worldwide agricultural problem owing to the low solubility and bioavailability of Fe in alkaline and calcareous soils. Here, we summarize the effects of intercropping systems on Fe nutrition. Several cases showed that intercropping with graminaceous plants could be used to correct Fe nutrition of Leguminosae such as peanut and soybean or fruits such as *Psidium guajava* L., Citrus, grape and pear in calcareous soils. Intercropping systems have strong positive effects on the physicochemical and biochemical characteristics of soil and the microbial community due to interspecific differences and interactions in the rhizosphere. Rhizosphere interactions can increase the bioavailability of Fe with the help of phytosiderophores. Enriched microorganisms may also facilitate the Fe nutrition of crops. A peanut/maize intercropping system could help us understand the dynamics in rhizosphere and molecular mechanism. However, the role of microbiome in regulating Fe acquisition of root and the mechanisms underlying these phenomena in other intercropping system except peanut/maize need further work, which will help better utilize intercropping to increase the efficiency of Fe foraging.

Keywords: iron (Fe), intercropping, rhizosphere, microorganism, exudate

Abbreviations: AMF, arbuscular mycorrhizal fungi; bHLH, basic Helix-Loop-Helix; C/N, Carbon to nitrogen ratio; DIMBOA, 2,4-dihydroxy-7-methoxy-1,4-benzoxazin-3-one; DIMBOA-Glc, 2-(2,4-dihydroxy-7-methoxy-1,4-benzoxazin-3-one)-beta-D-glucopyranose; DMA, 2′ deoxymugineic acid; DMT, divalent metal ion transporter; Fe, iron; FIT, FER-like iron deficiency induced transcription factor; FRO, ferric reductase oxidase; HMT, homocysteine S-methyltransferase; IRT, iron-regulated transporter; JA, jasmonate; Mn, manganese; MTP, metal tolerance protein; NAAT, nicotianamine aminotransferase; NRAMP, natural resistance-associated macrophage protein; P, phosphorus; SAT, serine acetyltransferase; SPAD, soil-plant analysis development; YSL, the yellow stripe-Like family genes; Zn, zinc.

INTERCROPPING WITH GRAMINACEOUS PLANTS FACILITATES THE IRON NUTRITION OF LEGUMINOSAE OR FRUITS IN CALCAREOUS SOILS

Intercropping is an ancient agricultural technology that involves planting two or more crop species together. It contributes to sustainable agriculture, with higher production, higher nutrient availability (Li et al., 2014), effective weed management (Weerarathne et al., 2017), and pest control (Lopes et al., 2016) in resource-limited agricultural systems. Intercropping can improve soil quality and soil phytoavailability due to species complementarity (Li et al., 2014; Cong et al., 2015).

Iron is an essential micronutrient for plant growth. However, the solubilizing ability and bioavailability of Fe is very low in alkaline and calcareous soils, which limits plant growth and development (Guerinot and Yi, 1994). The solubility of Fe in soil is decreased with increasing pH and increasing bicarbonate concentrations, which leads to Fe deficiency in crop production on calcareous soils (Marschner, 2012). Plants have evolved two strategies to take up Fe efficiently in response to Fe deficiency: a reduction-based strategy by non-grasses (Strategy I) and a chelation-based strategy by grasses (Strategy II) (Romheld and Marschner, 1986). Under Fe-limiting conditions, Strategy I plants reinforce the reduction of Fe^{3+} to Fe^{2+}, which is then transported into the root epidermis by Fe-regulated transporters (Robinson et al., 1999; Vert et al., 2002). In this process, Strategy I plants also release protons and phenolic compounds to enhance the bioavailability of Fe (Guerinot and Yi, 1994; Tsai and Schmidt, 2017). Strategy II plants secrete phytosiderophores that can bind Fe^{3+} in the rhizosphere. These complexes are then taken up by yellow stripe-like (YSL) family transporters in the roots (Curie et al., 2001; Inoue et al., 2009).

Several reports have described how intercropping systems can improve the Fe nutrition of crops (**Table 1**), which usually involves intercropping Strategy I plants with graminaceous Strategy II species. With the mutual benefits of intercropping systems, the Fe nutrition of the graminaceous species was also sometimes enhanced.

The peanut/maize intercropping system is often used to investigate interspecies interactions between two species using different Fe uptake strategies. Peanut/maize intercropping can enhance the Fe nutrition of peanuts in calcareous soils (Zuo et al., 2000, 2004; Inal et al., 2007; Dai et al., 2018). Similarly, soybean/maize intercropping with alternating strips and organic fertilizer can increase the Fe concentration in soybean (Dragicevic et al., 2015). Although intercropping with four grass species did not increase the Fe concentration in dry bean tissues, the SPAD value was significantly higher (Omondi and Kniss, 2014). After intercropping with 12 or 24 sorghum seedlings, the Fe concentration in leaves of guava seedlings (*Psidium guajava* L.) increased by 28.2 and 52.2% in Maryut soil, respectively (Kamal et al., 2000). On three different calcareous soils, intercropping with purple false brome (*Brachypodium distachyon*) and barley (*Hordeum vulgare*) enhanced the Fe and chlorophyll concentrations in olive (*Olea europaea*) leaves (Cañasveras et al., 2014). Groundcover with grass is a promising way to enhance the Fe nutrition of fruit trees in orchards. On supplying Fe sulfate to the soil and sowing a mixture of graminaceous species along with pear (*Pyrus communis*) trees in orchards, Fe-deficiency chlorosis symptoms were alleviated (Tagliavini et al., 2000). This was also seen in citrus plants (Cesco et al., 2006) and grape (Bavaresco et al., 2010) in the presence of grass cover species. Green garlic (*Allium sativum* L.) is a non-graminaceous monocot. After intercropping with various amounts of green garlic, the root Fe concentrations of cucumber (*Cucumis sativus* L.) increased, whereas the shoot Fe concentration decreased (Xiao et al., 2013).

All of these effective cases happened in calcareous and/or alkaline soils. The low Fe bioavailability in calcareous soil is induce by pH-related effects. The bicarbonate in calcareous soil can buffer rhizosphere acidification, but also inhibits the expression of ferric reductase, iron transporters and H^+-ATPase genes in Strategy I species such as *Arabidopsis*, pea, tomato and cucumber while has little effect on Strategy II species owing to their chelation-based strategy (Lucena et al., 2007; Marschner, 2012). Compared with graminaceous, non-graminaceous played as gainers in intercropping system on amending Fe nutrition. However, not all the graminaceous could correct the Fe nutrition of partners. The leaves of citrus and peanut did not recover from Fe deficiency chlorosis intercropped with *ys3* maize mutant plants, which is unable to release phytosiderophores (Cesco et al., 2006; Xiong et al., 2013a). It seems that a complementary strategy is necessary to increase the Fe nutrition of Strategy I plants in intercropping systems.

EFFECT OF RHIZOSPHERE CHANGE ON IRON ACQUISITION IN LEGUMINOSAE/GRAMINEAE INTERCROPPING SYSTEMS

The interactions in the rhizosphere affect biogeochemical cycling and nutrient availability, which affect plant growth and tolerance to biotic and abiotic stress (Philippot et al., 2013). The interactions between plant roots and the rhizosphere microbiome are critical for improving plant fitness (Zhalnina et al., 2018). Plant can secret different exudates to rhizosphere affected by environmental factors such as plant growth, nutrient availability and microorganisms (Mimmo et al., 2011), which mediate various aspects of the rhizosphere, including soil nutrient mobilization (Bakker et al., 2018; Canarini et al., 2019). The root exudates including primary metabolites (sugars, amino acids, and organic acids) can shape the rhizosphere microbiome (Badri and Vivanco, 2009). In turn, the associated microorganisms can influence plant health and growth (Huang et al., 2014). The soil microorganisms have a significant effect on nutrient availability for plants in the rhizosphere (Mimmo et al., 2014). The microorganisms can quickly utilize root exudates which affects plant nutrient foraging (Alegria Terrazas et al., 2016). Inoculation with plant growth-promoting rhizobacteria showed

TABLE 1 | The effects of intercropping systems on the iron (Fe) concentration of plant tissues.

Crop	Intercropped	Tissue	Change	Experimental conditions	References
Psidium guajava L.	Maize/Sorghum	Leaf	Increased	Pot	Kamal et al., 2000
Peanut	Maize	Root, shoot, seed	Increased	Field Pot	Zuo et al., 2000, 2004; Inal et al., 2007; Dai et al., 2018
Phaseolus vulgaris L.	Ryegrass/oat/corn/wheat	Leaf	Not Increased[1]	Field	Omondi and Kniss, 2014
Cucumis sativus	*Allium sativum*	Shoot	Decreased	Pot	Xiao et al., 2013
		Root	Increased		
Olive	Purple false brome/barley	Leaf	Increased	Pot	Cañasveras et al., 2014
Soybean	Maize	grain	Increased	Field	Dragicevic et al., 2015
Maize	soybean		increased		
Citrus	Barley/*Poa pratensis*/*Festuca rubra*	Root leaf	Increased	Hydroponics	Cesco et al., 2006
Grape	*Festuca ovina*	Leaf	Increased	Field	Bavaresco et al., 2010
Pear	Graminaceous species*	Leaf	#	Field	Tagliavini et al., 2000

**Mainly Poa spp., Lolium spp., and Festuca spp. [1]After 1 year, the level was lower at the 8 to 16 trifoliate leaf stage, while after 2 years there was no significant difference between intercropping and monocropping. [#]The Fe concentration of leaves was not measured, but the Fe chlorosis was amended and the SPAD value was increased in leaves.*

potential in benefiting the efficiency of nutrient acquisition of root (Pii et al., 2015).

The effects of intercropping systems on soil physicochemical and biochemical characteristics are complicated due to differences among species (Ladygina and Hedlund, 2010). In typical intercropping systems, legumes benefit soil quality by increasing soil carbon and nitrogen sequestration (Cong et al., 2015; Duchene et al., 2017). In a peanut/maize intercropping system, the available soil nitrogen and phosphorus increased in both the peanut and maize rhizosphere compared with monocropping. Furthermore, the soil urease and phosphomonoesterase activities were also improved by intercropping (Li et al., 2016b). Another field experiment showed that the pH and soil available phosphorus (Olsen-P) concentration in the rhizosphere of peanut crops decreased in the intercropping system after the vegetative stage (Guo et al., 2014). However, in seven cucumber intercropping systems, intercropping had no significant effects on physicochemical characteristics such as soil moisture, pH, and the electrical conductivity in two growing seasons (Li and Wu, 2018).

Facing Fe-limited conditions, Strategy I and II plants secrete different compounds into the rhizosphere to facilitate Fe uptake (Chen et al., 2017). The phenolic compounds, such as coumarins and flavins, secreted by Strategy I plants not only mobilize insoluble Fe but also affect the root microorganisms to promote plant health (Siso-Terraza et al., 2016; Tsai and Schmidt, 2017; Verbon et al., 2017; Stringlis et al., 2018). Different species can secrete different coumarins to better adapt to their environments (Rajniak et al., 2018). Secondary metabolites secreted from roots including antibiotics and volatiles play a key role in the performance of bacteria (Schulz-Bohm, 2018). However, the directly effect of secondary metabolites on plant nutrient foraging is barely understood. The roots of cereals such as maize secrete a class of defensive metabolites called benzoxazinoids, such as DIMBOA and DIMBOA-Glc (Hu et al., 2018a,b). They not only alter the root-associated microbiota and suppress herbivore performance but also facilitate the Fe uptake of maize. A recent study in wheat found that heterospecific combinations induced the secretion of DIMBOA (Kong et al., 2018), indicating that intercropping system may promote the secretion of DIMBOA from graminaceous contributing to Fe availability. The phytosiderophores released by graminaceous species are chelators with high affinity for ferric Fe, and can contribute to the diffusion of Fe in soil (Ma, 2005; Kobayashi and Nishizawa, 2012). The intercropped maize secreted more phytosiderophores in a peanut/maize intercropping system (Xiong et al., 2013a; Dai et al., 2018). The available Fe concentration in the rhizosphere of intercropped peanut was significantly higher than that of monocropped peanut (Guo et al., 2014).

In phosphorus-deficient soil, a maize/common bean intercropping system can efficiently increase the rhizosphere microbial biomass by regulating the C/N balance and the P availability (Latati et al., 2016; Latati et al., 2017). In peanut/maize intercropping systems, better Fe status enhances the expression of the Fe^{2+} transporter *AhDMT1* (*Arachis hypogaea* divalent metal ion transporter 1) to improve the formation of nodules and nitrogen fixation in peanut roots (Zuo et al., 2004; Shen et al., 2014). Moreover, maize root exudates can increase nodulation and stimulate nitrogen fixation by fava beans (*Vicia faba)* by promoting flavonoid synthesis in a fava bean/maize intercropping system (Li et al., 2016a). A field experiment showed that peanut/maize intercropping systems increased the abundance of nitrogen-fixing microorganisms, such as *Rhizobium hainanense*, *Rhizobium leguminosarum*, and *Frankia* (Chen et al., 2018). A pot experiment found that peanut/maize intercropping increased not only the abundance of *Rhizobium* but also *Pseudomonas* in the peanut rhizosphere (Li et al., 2018). The siderophore pyoverdine secreted by *Pseudomonas fluorescens* was beneficial to the Fe nutrition and growth of *Arabidopsis* in Fe-limited conditions (Trapet et al., 2016). The maize/legumes intercropping systems enriched the soil biodiversity and spores of AMF in the root-zone soil (Punyalue et al., 2018). Intercropping facilitated nitrogen transfer from soybeans to maize on co-inoculation with AMF, as shown by ^{15}N

labeling (Wang et al., 2016). AMF application in dill/common bean intercropping systems can enhance the Fe, zinc (Zn), and manganese (Mn) contents of dill and its competitive ability against weeds (Weisany et al., 2016a,b).

Bacillus subtilis GB03 and *Azospirillum brasilense* showed a positive effect on Fe nutrition of *Arabidopsis* and cucumber, respectively (Zhang et al., 2009; Pii et al., 2015). But about their abundance change in intercropping was rarely reported. How the plants shape their root microbiome and the effect of the specific root exudates under Fe deficiency need to be investigated. The role of microorganisms in the Fe nutrition of plant is also not fully understood. The microorganisms can increase soluble Fe in soil by decreasing soil pH through nitrification and secreting siderophores, which may be also helpful for the Fe nutrition of plant (Mimmo et al., 2014; Trapet et al., 2016). On another hand, microorganisms are competitive for Fe (Mimmo et al., 2014). In intercropping systems, more attention was paid on the effect of microorganisms on N and P turnover. Understanding the difference of effect between graminaceous and non-graminaceous on rhizosphere microbiome and their corresponding function differences can provide a new perspective for explaining the rhizosphere process in intercropping system. Knowing how the rhizosphere facilitates interactions in intercropping systems could help us to optimize plant performance by engineering the plant rhizosphere.

MOLECULAR MECHANISM UNDERLYING THE BENEFICIAL EFFECTS OF INTERCROPPING ON IRON NUTRITION IN PEANUT/MAIZE INTERCROPPING SYSTEM

Studies of the molecular mechanisms underlying how specific intercropping interactions enhance Fe nutrition only focused on peanut/maize intercropping. In other cases, only the phenomenon was raised. The results of peanut/maize intercropping system can give us a guide to understand the Fe nutrition foraging of Leguminosae/Gramineae intercropping.

Arachis hypogaea iron-regulated transporter 1 (AhIRT1) was the first iron-related transporter to be isolated from the peanut. Ding et al. (2010) found higher *AhIRT1* expression during anthesis in intercropped peanut compared with monocropped peanut. In other studies, the expression of *AhIRT1* was downregulated in intercropped peanut during the reproductive stage (Xiong et al., 2013a,b; Dai et al., 2018). Further work must examine whether the intercropping interactions have a specific effect on the expression of *AhIRT1*. The expression of *AhFRO1* (*Arachis hypogaea* ferric reductase oxidase 1), which encodes a Fe(III)-chelate reductase, was affected by the growth stage in intercropping systems. During the vegetative growth of maize, *AhFRO1* was upregulated in intercropping systems while peanut was already in reproductive stage. During this period, monocropped peanut did not show Fe deficiency chlorosis. Subsequently, *AhFRO1* was downregulated in intercropping systems owing to the better Fe nutrition status. The ferric reductase activity of peanut roots showed a similar tendency, and was higher during the vegetative growth stage and lower during the reproductive growth stage of maize (Guo et al., 2014; Dai et al., 2018). The divalent metal transporter AhNRAMP1 (*Arachis hypogaea* Natural Resistance-Associated Macrophage Protein 1) is also involved in Fe uptake in peanut (Xiong et al., 2012). Both suppression subtractive hybridization and RT-PCR showed that *AhNRAMP1* was upregulated in intercropped peanut during the vegetative stage of maize. In addition, a putative MTP shared similar expression patterns with *AhNRAMP1* in an intercropping system (Dai et al., 2018).

The phytosiderophores secreted by maize chelate and solubilize Fe from the rhizosphere, and this is enhanced by specific intercropping interactions (Xiong et al., 2013a; Dai et al., 2018). The enhanced amino acid metabolism may increase the release of phytosiderophores in maize roots. Homocysteine S-methyltransferase (HMT2) and serine acetyltransferase (SAT1) are directly associated with the methionine metabolism pathway. The phytosiderophore-Fe(III) complex can be absorbed across the plasma membrane of roots by the peanut transporter protein AhYSL1 (*Arachis hypogaea* yellow stripe1-like), a homolog of maize yellow stripe 1 (Xiong et al., 2013a). Several studies have indicated that intercropping also had a positive effect on the expression of *AhYSL1*, especially during the reproductive stage (Xiong et al., 2013a; Guo et al., 2014; Dai et al., 2018). Further work must examine whether the expression of *AhYSL1* is correlated with the phytosiderophores in the rhizosphere. The soil pH and Olsen-P concentration decreased in reproductive stage under the effect of intercropping, while the available Fe concentration was the highest in rhizosphere (Guo et al., 2014). It seems that beneficial effects differ during the vegetative stage owing to dynamic changes in the rhizosphere. However, how the other factors that can influence Fe bioavailability such as rhizospheric organic compounds and the microbiome changes along with growth phase indicates that it is still an open question. Reproductive stage is a critical period of plant development which associates with sink formation (Marschner, 2012). The more nutrient demands in critical period of maize might drive the more release of phytosiderophores, which might induce the expression of *AhYSL1*.

Phytosiderophores are a class of Fe chelators that enhance adaption in the natural environment; these commonly exist in grasses, but not exclusively. 2′-Deoxymugineic acid (DMA) was detected in xylem sap from the olive (*Olea europaea* L.) (Suzuki et al., 2016). As mentioned above, intercropping with purple false brome and barley improved the Fe nutrition of olive trees. However, no study has examined whether the olive can take up DMA-Fe(III) directly, as the peanut can, in an intercropping system (Xiong et al., 2013a). Of course, homologs of the NAAT, aldo-keto reductase (similar to *DMAS*), and *YSL* family genes can be found in dicots by checking GenBank, and this is a stepping-stone for exploring the evolution of the two Fe uptake strategies. In addition, analyzing the function of phytosiderophores can help us to exploit the application of their analogs in agriculture.

The works in peanut/maize intercropping system can provide a case to understand the molecular mechanism how intercropping system benefits the non-graminaceous

Fe nutrition. The further research need be taken in other intercropping systems to see if these cases can be Fe biofortification by intercropping. The driving factors of rhizosphere changes is an important task if one aims at fully understand the biological and ecological mechanism how intercropping system affect Fe turnover.

CONCLUDING REMARKS

The previous works in intercropping system have provided different insights to uncover the effects and mechanisms of intercropping systems on Fe nutrition. Due to the interspecies facilitation of the rhizosphere, especially between Gramineae and Leguminosae, the intercropping systems show more benefits in resource-limited agricultural system including enhancing Fe nutrition. However, we still do not know how plant-microorganisms interactions regulate Fe uptake of root. The microbiome is an essential part to elucidate rhizosphere process in intercropping system. Except peanut/maize intercropping system, whether other Leguminosae/Gramineae intercropping systems can be a promising technology to facilitate Fe nutrition in calcareous/alkaline soils need be addressed further. Based on the links between molecular biology and field practices, it will contribute to a universal guide on correcting Fe deficiency chlorosis in different crops with low-input.

AUTHOR CONTRIBUTIONS

JD summarized and wrote the manuscript. WQ, NW, and TW all made suggestions. HN and YZ revised the manuscript. YZ provided funding for this work as corresponding author.

FUNDING

This study was supported by a grant from National Natural Science Foundation of China (NSFC, Grant No. 31872183), the National Key Research and Development Program of China (2017YFD0202102, 2016YFD0200405, and 2016YFE0101100), and the China Scholarship Council.

REFERENCES

Alegria Terrazas, R., Giles, C., Paterson, E., Robertson-Albertyn, S., Cesco, S., Mimmo, T., et al. (2016). Plant-microbiota interactions as a driver of the mineral turnover in the rhizosphere. *Adv. Appl. Microbiol.* 95, 1–67. doi: 10.1016/bs.aambs.2016.03.001

Badri, D. V., and Vivanco, J. M. (2009). Regulation and function of root exudates. *Plant Cell Environ.* 32, 666–681. doi: 10.1111/j.1365-3040.2008.01926.x

Bakker, P., Pieterse, C. M. J., de Jonge, R., and Berendsen, R. L. (2018). The soil-borne legacy. *Cell* 172, 1178–1180. doi: 10.1016/j.cell.2018.02.024

Bavaresco, L., Goncalves, M. I. V. D. B., Civardi, S., Gatti, M., and Ferrari, F. (2010). Effects of traditional and new methods on overcoming lime-induced chlorosis of grapevine. *Am. J. Enol. Vitic.* 61, 186–190.

Canarini, A., Kaiser, C., Merchant, A., Richter, A., and Wanek, W. (2019). Root exudation of primary metabolites: mechanisms and their roles in plant responses to environmental stimuli. *Front. Plant Sci.* 10:157. doi: 10.3389/fpls.2019.00157

Cañasveras, J. C., del Campillo, M. C., Barron, V., and Torrent, J. (2014). Intercropping with grasses helps to reduce iron chlorosis in olive. *J. Soil Sci. Plant Nut.*14, 554–564.

Cesco, S., Rombola, A. D., Tagliavini, M., Varanini, Z., and Pinton, R. (2006). Phytosiderophores released by graminaceous species promote Fe-59-uptake in citrus. *Plant Soil* 287, 223–233. doi: 10.1007/s11104-006-9069-4

Chen, J., Arafat, Y., Wu, L. K., Xiao, Z. G., Li, Q. S., Khan, M. A., et al. (2018). Shifts in soil microbial community, soil enzymes and crop yield under peanut/maize intercropping with reduced nitrogen levels. *Appl. Soil Ecol.* 124, 327–334. doi: 10.1016/j.apsoil.2017.11.010

Chen, Y. T., Wang, Y., and Yeh, K. C. (2017). Role of root exudates in metal acquisition and tolerance. *Curr. Opin. Plant Biol.* 39, 66–72. doi: 10.1016/j.pbi.2017.06.004

Cong, W. F., Hoffland, E., Li, L., Six, J., Sun, J. H., Bao, X. G., et al. (2015). Intercropping enhances soil carbon and nitrogen. *Glob. Chang Biol.* 21, 1715–1726. doi: 10.1111/gcb.12738

Curie, C., Panaviene, Z., Loulergue, C., Dellaporta, S. L., Briat, J. F., and Walker, E. L. (2001). Maize yellow stripe1 encodes a membrane protein directly involved in Fe(III) uptake. *Nature* 409, 346–349. doi: 10.1038/35053080

Dai, J., Qiu, W., Wang, N., Nakanishi, H., and Zuo, Y. (2018). Comparative transcriptomic analysis of the roots of intercropped peanut and maize reveals novel insights into peanut iron nutrition. *Plant Physiol. Biochem.* 127, 516–524. doi: 10.1016/j.plaphy.2018.04.024

Ding, H., Duan, L., Li, J., Yan, H., Zhao, M., Zhang, F., et al. (2010). Cloning and functional analysis of the peanut iron transporter *AhIRT1* during iron deficiency stress and intercropping with maize. *J. Plant Physiol.* 167, 996–1002. doi: 10.1016/j.jplph.2009.12.019

Dragicevic, V., Oljaca, S., Stojiljkovic, M., Simic, M., Dolijanovic, Z., and Kravic, N. (2015). Effect of the maize-soybean intercropping system on the potential bioavailability of magnesium, iron and zinc. *Crop Pasture Sci.* 66, 1118–1127. doi: 10.1071/Cp14211

Duchene, O., Vian, J. F., and Celette, F. (2017). Intercropping with legume for agroecological cropping systems: complementarity and facilitation processes and the importance of soil microorganisms. A review. *Agric. Ecosyst. Environ.* 240, 148–161. doi: 10.1016/j.agee.2017.02.019

Guerinot, M. L., and Yi, Y. (1994). Iron: nutritious, noxious, and not readily available. *Plant Physiol.* 104, 815–820.

Guo, X., Xiong, H., Shen, H., Qiu, W., Ji, C., Zhang, Z., et al. (2014). Dynamics in the rhizosphere and iron-uptake gene expression in peanut induced by intercropping with maize: role in improving iron nutrition in peanut. *Plant Physiol. Biochem.* 76, 36–43. doi: 10.1016/j.plaphy.2013.12.019

Hu, L., Mateo, P., Ye, M., Zhang, X., Berset, J. D., Handrick, V., et al. (2018a). Plant iron acquisition strategy exploited by an insect herbivore. *Science* 361, 694–697. doi: 10.1126/science.aat4082

Hu, L., Robert, C. A. M., Cadot, S., Zhang, X., Ye, M., Li, B., et al. (2018b). Root exudate metabolites drive plant-soil feedbacks on growth and defense by shaping the rhizosphere microbiota. *Nat. Commun.* 9:2738. doi: 10.1038/s41467-018-05122-7

Huang, X. F., Chaparro, J. M., Reardon, K. F., Zhang, R. F., Shen, Q. R., and Vivanco, J. M. (2014). Rhizosphere interactions: root exudates, microbes, and microbial communities. *Botany* 92, 267–275. doi: 10.1139/cjb-2013-0225

Inal, A., Gunes, A., Zhang, F., and Cakmak, I. (2007). Peanut/maize intercropping induced changes in rhizosphere and nutrient concentrations in shoots. *Plant Physiol. Biochem.* 45, 350–356. doi: 10.1016/j.plaphy.2007.03.016

Inoue, H., Kobayashi, T., Nozoye, T., Takahashi, M., Kakei, Y., Suzuki, K., et al. (2009). Rice OsYSL15 is an iron-regulated iron(III)-deoxymugineic acid transporter expressed in the roots and is essential for iron uptake in early growth of the seedlings. *J. Biol. Chem.* 284, 3470–3479. doi: 10.1074/jbc.M806042200

Kamal, K., Hagagg, L., and Awad, F. (2000). Improved Fe and Zn acquisition by guava seedlings grown in calcareous soils intercropped with graminaceous species. *J. Plant Nutr.* 23, 2071–2080. doi: 10.1080/01904160009382166

Kobayashi, T., and Nishizawa, N. K. (2012). Iron uptake, translocation, and regulation in higher plants. *Annu. Rev. Plant Biol.* 63, 131–152. doi: 10.1146/annurev-arplant-042811-105522

Kong, C. H., Zhang, S. Z., Li, Y. H., Xia, Z. C., Yang, X. F., Meiners, S. J., et al. (2018). Plant neighbor detection and allelochemical response are driven by root-secreted signaling chemicals. *Nat. Commun.* 9:3867. doi: 10.1038/s41467-018-06429-1

Ladygina, N., and Hedlund, K. (2010). Plant species influence microbial diversity and carbon allocation in the rhizosphere. *Soil Biol. Biochem.* 42, 162–168. doi: 10.1016/j.soilbio.2009.10.009

Latati, M., Aouiche, A., Tellah, S., Laribi, A., Benlahrech, S., Kaci, G., et al. (2017). Intercropping maize and common bean enhances microbial carbon and nitrogen availability in low phosphorus soil under mediterranean conditions. *Eur. J. Soil Biol.* 80, 9–18. doi: 10.1016/j.ejsobi.2017.03.003

Latati, M., Bargaz, A., Belarbi, B., Lazali, M., Benlahrech, S., Tellah, S., et al. (2016). The intercropping common bean with maize improves the rhizobial efficiency, resource use and grain yield under low phosphorus availability. *Eur. J. Agron.* 72, 80–90. doi: 10.1016/j.eja.2015.09.015

Li, B., Li, Y. Y., Wu, H. M., Zhang, F. F., Li, C. J., Li, X. X., et al. (2016a). Root exudates drive interspecific facilitation by enhancing nodulation and N2 fixation. *Proc. Natl. Acad. Sci. U.S.A.* 113, 6496–6501. doi: 10.1073/pnas.1523580113

Li, Q. S., Wu, L. K., Chen, J., Khan, M. A., Luo, X. M., and Lin, W. X. (2016b). Biochemical and microbial properties of rhizospheres under maize/peanut intercropping. *J. Int. Agric.* 15, 101–110. doi: 10.1016/S2095-3119(15)61089-9

Li, L., Tilman, D., Lambers, H., and Zhang, F. S. (2014). Plant diversity and overyielding: insights from belowground facilitation of intercropping in agriculture. *New Phytol.* 203, 63–69. doi: 10.1111/nph.12778

Li, Q., Chen, J., Wu, L., Luo, X., Li, N., Arafat, Y., et al. (2018). Belowground interactions impact the soil bacterial community, soil fertility, and crop yield in maize/peanut intercropping systems. *Int. J. Mol. Sci.* 19:622. doi: 10.3390/ijms19020622

Li, S., and Wu, F. (2018). Diversity and co-occurrence patterns of soil bacterial and fungal communities in seven intercropping systems. *Front. Microbiol.* 9:1521. doi: 10.3389/fmicb.2018.01521

Lopes, T., Hatt, S., Xu, Q., Chen, J., Liu, Y., and Francis, F. (2016). Wheat (*Triticum aestivum* L.)-based intercropping systems for biological pest control. *Pest Manag. Sci.* 72, 2193–2202. doi: 10.1002/ps.4332

Lucena, C., Romera, F. J., Rojas, C. L., Garcia, M., Alcantara, E., and Perez-Vicente, R. (2007). Bicarbonate blocks the expression of several genes involved in the physiological responses to Fe deficiency of Strategy I plants. *Funct. Plant Biol.* 34, 1002–1009. doi: 10.1071/Fp07136

Ma, J. F. (2005). Plant root responses to three abundant soil minerals: silicon, aluminum and iron. *Crit. Rev. Plant Sci.* 24, 267–281. doi: 10.1080/07352680500196017

Marschner, P. (2012). *Marschner's Mineral Nutrition of Higher Plants*. Cambridge, MA: Academic press.

Mimmo, T., Del Buono, D., Terzano, R., Tomasi, N., Vigani, G., Crecchio, C., et al. (2014). Rhizospheric organic compounds in the soil-microorganism-plant system: their role in iron availability. *Eur. J. Soil Sci.* 65, 629–642. doi: 10.1111/ejss.12158

Mimmo, T., Hann, S., Jaitz, L., Cesco, S., Gessa, C. E., and Puschenreiter, M. (2011). Time and substrate dependent exudation of carboxylates by *Lupinus albus* L. and *Brassica napus* L. *Plant Physiol. Biochem.* 49, 1272–1278. doi: 10.1016/j.plaphy.2011.08.012

Omondi, E. C., and Kniss, A. R. (2014). Interplanting annual ryegrass, wheat, oat, and corn to mitigate iron deficiency in dry beans. *PLoS One* 9:e115673. doi: 10.1371/journal.pone.0115673

Philippot, L., Raaijmakers, J. M., Lemanceau, P., and van der Putten, W. H. (2013). Going back to the roots: the microbial ecology of the rhizosphere. *Nat. Rev. Microbiol.* 11, 789–799. doi: 10.1038/nrmicro3109

Pii, Y., Mimmo, T., Tomasi, N., Terzano, R., Cesco, S., and Crecchio, C. (2015). Microbial interactions in the rhizosphere: beneficial influences of plant growth-promoting rhizobacteria on nutrient acquisition process. A review. *Biol. Fertil. Soils* 51, 403–415. doi: 10.1007/s00374-015-0996-1

Punyalue, A., Jamjod, S., and Rerkasem, B. (2018). Intercropping maize with legumes for sustainable highland maize production. *Mt. Res. Dev.* 38, 35–44. doi: 10.1659/Mrd-Journal-D-17-00048.1

Rajniak, J., Giehl, R. F. H., Chang, E., Murgia, I., von Wiren, N., and Sattely, E. S. (2018). Biosynthesis of redox-active metabolites in response to iron deficiency in plants. *Nat. Chem. Biol.* 14, 442–450. doi: 10.1038/s41589-018-0019-2

Robinson, N. J., Procter, C. M., Connolly, E. L., and Guerinot, M. L. (1999). A ferric-chelate reductase for iron uptake from soils. *Nature* 397, 694–697. doi: 10.1038/17800

Romheld, V., and Marschner, H. (1986). Evidence for a specific uptake system for iron phytosiderophores in roots of grasses. *Plant Physiol.* 80, 175–180.

Schulz-Bohm, K. (2018). *The Ecological Role of Volatile Mediated Interactions Belowground*. Ph.D. thesis, Wageningen University, Wageningen.

Shen, H., Xiong, H., Guo, X., Wang, P., Duan, P., Zhang, L., et al. (2014). AhDMT1, a Fe(2+) transporter, is involved in improving iron nutrition and N2 fixation in nodules of peanut intercropped with maize in calcareous soils. *Planta* 239, 1065–1077. doi: 10.1007/s00425-014-2033-2

Siso-Terraza, P., Rios, J. J., Abadia, J., Abadia, A., and Alvarez-Fernandez, A. (2016). Flavins secreted by roots of iron-deficient Beta vulgaris enable mining of ferric oxide via reductive mechanisms. *New Phytol.* 209, 733–745. doi: 10.1111/nph.13633

Stringlis, I. A., Yu, K., Feussner, K., de Jonge, R., Van Bentum, S., Van Verk, M. C., et al. (2018). MYB72-dependent coumarin exudation shapes root microbiome assembly to promote plant health. *Proc. Natl. Acad. Sci. U.S.A.* 115, E5213–E5222. doi: 10.1073/pnas.1722335115

Suzuki, M., Nozoye, T., Nagasaka, S., Nakanishi, H., Nishizawa, N. K., and Mori, S. (2016). The detection of endogenous 2'-deoxymugineic acid in olives (*Olea europaea* L.) indicates the biosynthesis of mugineic acid family phytosiderophores in non-graminaceous plants. *Soil Sci. Plant Nutr.* 62, 481–488. doi: 10.1080/00380768.2016.1230724

Tagliavini, M., Abadia, J., Rombola, A. D., Abadia, A., Tsipouridis, C., and Marangoni, B. (2000). Agronomic means for the control of iron deficiency chlorosis in deciduous fruit trees. *J. Plant Nutr.* 23, 2007–2022. doi: 10.1080/01904160009382161

Trapet, P., Avoscan, L., Klinguer, A., Pateyron, S., Citerne, S., Chervin, C., et al. (2016). The *Pseudomonas* fluorescens siderophore pyoverdine weakens arabidopsis thaliana defense in favor of growth in iron-deficient conditions. *Plant Physiol.* 171, 675–693. doi: 10.1104/pp.15.01537

Tsai, H. H., and Schmidt, W. (2017). Mobilization of iron by plant-borne coumarins. *Trends Plant Sci.* 22, 538–548. doi: 10.1016/j.tplants.2017.03.008

Verbon, E. H., Trapet, P. L., Stringlis, I. A., Kruijs, S., Bakker, P., and Pieterse, C. M. J. (2017). Iron and immunity. *Annu. Rev. Phytopathol.* 55, 355–375. doi: 10.1146/annurev-phyto-080516-035537

Vert, G., Grotz, N., Dedaldechamp, F., Gaymard, F., Guerinot, M. L., Briat, J. F., et al. (2002). IRT1, an *Arabidopsis* transporter essential for iron uptake from the soil and for plant growth. *Plant Cell* 14, 1223–1233.

Wang, G., Sheng, L., Zhao, D., Sheng, J., Wang, X., and Liao, H. (2016). Allocation of nitrogen and carbon is regulated by nodulation and mycorrhizal networks in soybean/maize intercropping system. *Front. Plant Sci.* 7:1901. doi: 10.3389/fpls.2016.01901

Weerarathne, L. V. Y., Marambe, B., and Chauhan, B. S. (2017). Does intercropping play a role in alleviating weeds in cassava as a non-chemical tool of weed management? – A review. *Crop Prot.* 95, 81–88. doi: 10.1016/j.cropro.2016.08.028

Weisany, W., Raei, Y., Salmasi, S. Z., Sohrabi, Y., and Ghassemi-Golezani, K. (2016a). Arbuscular mycorrhizal fungi induced changes in rhizosphere, essential oil and mineral nutrients uptake in dill/common bean intercropping system. *Ann. Appl. Biol.* 169, 384–397. doi: 10.1111/aab.12309

Weisany, W., Zehtab-Salmasi, S., Raei, Y., Sohrabi, Y., and Ghassemi-Golezani, K. (2016b). Can arbuscular mycorrhizal fungi improve competitive ability of dill+common bean intercrops against weeds? *Eur. J. Agron.* 75, 60–71. doi: 10.1016/j.eja.2016.01.006

Xiao, X., Cheng, Z., Meng, H., Liu, L., Li, H., and Dong, Y. (2013). Intercropping of green garlic (*Allium sativum* L.) induces nutrient concentration changes in the soil and plants in continuously cropped cucumber (*Cucumis sativus* L.) in a plastic tunnel. *PLoS One* 8:e62173. doi: 10.1371/journal.pone.0062173

Xiong, H., Kakei, Y., Kobayashi, T., Guo, X., Nakazono, M., Takahashi, H., et al. (2013a). Molecular evidence for phytosiderophore-induced improvement of iron nutrition of peanut intercropped with maize in calcareous soil. *Plant Cell Environ.* 36, 1888–1902. doi: 10.1111/pce.12097

Xiong, H., Shen, H., Zhang, L., Zhang, Y., Guo, X., Wang, P., et al. (2013b). Comparative proteomic analysis for assessment of the ecological significance of maize and peanut intercropping. *J. Proteom.* 78, 447–460. doi: 10.1016/j.jprot.2012.10.013

Xiong, H., Kobayashi, T., Kakei, Y., Senoura, T., Nakazono, M., Takahashi, H., et al. (2012). AhNRAMP1 iron transporter is involved in iron acquisition in peanut. *J. Exp. Bot.* 63, 4437–4446. doi: 10.1093/jxb/ers117

Zhalnina, K., Louie, K. B., Hao, Z., Mansoori, N., da Rocha, U. N., Shi, S., et al. (2018). Dynamic root exudate chemistry and microbial substrate preferences drive patterns in rhizosphere microbial community assembly. *Nat. Microbiol.* 3, 470–480. doi: 10.1038/s41564-018-0129-3

Zhang, H., Sun, Y., Xie, X., Kim, M. S., Dowd, S. E., and Paré, P. W. (2009). A soil bacterium regulates plant acquisition of iron via deficiency-inducible mechanisms. *Plant J.* 58, 568–577. doi: 10.1111/j.1365-313X.2009.03803.x

Zuo, Y. M., Liu, Y. X., Zhang, F. S., and Christie, P. (2004). A study on the improvement iron nutrition of peanut intercropping with maize on nitrogen fixation at early stages of growth of peanut on a calcareous soil. *Soil Sci. Plant Nutr.* 50, 1071–1078. doi: 10.1080/00380768.2004.10408576

Zuo, Y. M., Zhang, F. S., Li, X. L., and Cao, Y. P. (2000). Studies on the improvement in iron nutrition of peanut by intercropping with maize on a calcareous soil. *Plant Soil* 220, 13–25. doi: 10.1023/A:1004724219988

Conflict of Interest Statement: The authors declare that the research was conducted in the absence of any commercial or financial relationships that could be construed as a potential conflict of interest.

frontiers in Plant Science

ORIGINAL RESEARCH
published: 16 May 2019
doi: 10.3389/fpls.2019.00627

PRC2-Mediated H3K27me3 Contributes to Transcriptional Regulation of FIT-Dependent Iron Deficiency Response

*Emily Y. Park[1], Kaitlyn M. Tsuyuki[1,2], Fengling Hu[2], Joohyun Lee[1,2] and Jeeyon Jeong[1,2]**

[1] Program in Biochemistry and Biophysics, Amherst College, Amherst, MA, United States, [2] Department of Biology, Amherst College, Amherst, MA, United States

Iron is an essential micronutrient for nearly all organisms, but excessive iron can lead to the formation of cytotoxic reactive oxygen species. Therefore, iron acquisition and homeostasis must be tightly regulated. Plants have evolved complex mechanisms to optimize their use of iron, which is one of the most limiting nutrients in the soil. In particular, transcriptional regulation is vital for regulating iron in plants, and much work has revealed the role of transcription factors on this front. Our study adds novel insights to the transcriptional regulation of iron homeostasis in plants by showing that chromatin remodeling via histone 3 lysine 27 trimethylation (H3K27me3) modulates the expression of FIT-dependent genes under iron deficiency. We provide evidence that FIT-dependent iron acquisition genes, *IRT1* and *FRO2*, as well as *FIT* itself are direct targets of PRC2-mediated H3K27me3. In the *clf* mutant, which lacks the predominant H3K27 tri-methyltransferase, induction of *FIT*, *FRO2*, *IRT1*, and other FIT-regulated genes in roots is significantly higher under iron deficient conditions than in wild type. Furthermore, we observe that *clf* mutants are more tolerant to iron deficiency than wild type, indicating that gene expression levels appear to be limiting the plants ability to access iron. We propose that H3K27me3 attenuates the induction of FIT-target genes under iron deficiency and hypothesize that this may serve as a mechanism to restrict the maximum level of induction of iron acquisition genes to prevent iron overload.

Keywords: iron, FIT, H3K27me3, PRC2, transcription, Arabidopsis

OPEN ACCESS

Edited by:
Wolfgang Schmidt,
Academia Sinica, Taiwan

Reviewed by:
Keqiang Wu,
National Taiwan University, Taiwan
Ping Lan,
Institute of Soil Science (CAS), China

***Correspondence:**
Jeeyon Jeong
jjeong@amherst.edu

Specialty section:
This article was submitted to Plant Nutrition, a section of the journal Frontiers in Plant Science

Received: *19 February 2019*
Accepted: *26 April 2019*
Published: *16 May 2019*

Citation:
Park EY, Tsuyuki KM, Hu F, Lee J and Jeong J (2019) PRC2-Mediated H3K27me3 Contributes to Transcriptional Regulation of FIT-Dependent Iron Deficiency Response. Front. Plant Sci. 10:627. doi: 10.3389/fpls.2019.00627

INTRODUCTION

Much of the micronutrients in the earth's soil is inaccessible to plants, which negatively affects crop yield and quality (Marschner, 2012). In particular, iron is abundant in the earth's crust but is one of the most limiting nutrients for plant growth because it exists as insoluble ferric oxides under aerobic and neutral or alkaline conditions (Colombo et al., 2014). Plants have a unique need for iron as photosynthetic organisms; however, they are exposed to a higher risk of iron-induced toxicity. Hence, plants have evolved a host of delicate mechanisms to tightly control iron acquisition and homeostasis. To improve agriculture and human health, it is crucial to understand the molecular mechanisms behind iron acquisition and regulation in plants.

Dicots, including *Arabidopsis thaliana*, use Strategy I, which implements a reduction-based mechanism for acquiring iron (Jeong et al., 2017). Under iron-deficient conditions, *A. thaliana* extrudes protons through the P-type H^+-ATPases, such as AHA2, and acidifies the rhizosphere to help solubilize Fe^{3+}-chelates (Santi and Schmidt, 2009). PDR9, an ABC transporter, facilitates the export of coumarin-family phenolics into the surrounding rhizosphere and contributes to the formation of an accessible pool of iron in the apoplast (Fourcroy et al., 2014; Clemens and Weber, 2016). FERRIC REDUCTASE OXIDASE 2 (FRO2) reduces ferric iron-chelates to ferrous iron (Robinson et al., 1999), which is then transported into the root epidermal cell by Iron-Regulated Transporter 1 (IRT1) (Connolly et al., 2002; Varotto et al., 2002; Vert et al., 2002).

The iron acquisition process is largely controlled by a sophisticated transcriptional regulatory network. FER-LIKE IRON DEFICIENCY-INDUCED TRANSCRIPTION FACTOR (FIT), the master regulator of the iron deficiency response, is essential for the high-level induction of Strategy I iron acquisition genes and *FIT* loss-of-function mutants are lethal under iron deficient conditions (Colangelo and Guerinot, 2004; Jakoby et al., 2004; Yuan et al., 2005). FIT is a basic-helix-loop-helix (bHLH) transcription factor that dimerizes with bHLH subgroup Ib transcription factors, bHLH38, bHLH39, bHLH100, or bHLH101 to positively regulate its target genes (Yuan et al., 2008; Wang et al., 2013). However, rather than inducing FIT target genes, bHLH100 and bHLH101 may regulate genes involved in distributing iron in tissues and organelles via a FIT-independent pathway (Sivitz et al., 2012). Meanwhile, FIT also interacts with transcription factors of other regulatory networks involving hormones, such as jasmonic acid, ethylene, or gibberellin, as well as bHLH transcription factors of bHLH IIIe and IVa subgroups that control FIT at the transcriptional and posttranslational levels (Lingam et al., 2011; Wild et al., 2016; Naranjo-Arcos et al., 2017; Cui et al., 2018; Tanabe et al., 2018).

Evidence suggests that there are mechanisms upstream of FIT that control iron acquisition. FIT itself is iron-regulated at the transcriptional and post-transcriptional levels. *FIT* is induced by iron deficiency (Colangelo and Guerinot, 2004), but in plants that constitutively express *FIT*, FIT subjected to rapid turnover by proteasomal degradation at the early onset of the iron deficiency response (Sivitz et al., 2011). Recently, an iron-regulated calcium dependent protein kinase, CBL-INTERACTING PROTEIN KINASE (CIPK) 11, was identified as a positive regulator of FIT (Gratz et al., 2019). Meanwhile, IRON MAN (IMA) peptides, also referred as FE-UPTAKE-INDUCING PEPTIDEs (FEPs), were reported as an upstream regulator of the iron uptake pathway (Grillet et al., 2018; Hirayama et al., 2018). Overexpression of the IMA motif was sufficient to trigger the iron deficiency response and lead to accumulation of iron (Grillet et al., 2018), but IMA3/FEP1 was proposed to activate bHLH38/39 via a mechanism independent of FIT, with the expression of FEP1 also being independent of FIT (Hirayama et al., 2018).

In addition to FIT, POPEYE (PYE) is another bHLH transcription factor that plays a major role under iron deficiency (Long et al., 2010). PYE represses genes, such as *NICOTIANMINE SYNTHASE 4* (*NAS4*) and *FERRIC REDUCTASE OXIDASE 3* (*FRO3*), which are involved in root iron mobilization and shoot translocation. NAS4 synthesizes nicotianamine, which chelates iron into a mobile form for vascular translocation (Bauer et al., 2004), and FRO3 is a mitochondrial ferric chelate reductase expressed in the vasculature (Jeong and Connolly, 2009). The expression of *PYE* is tightly correlated with *bHLH39* and *bHLH101* (Long et al., 2010), which are strongly induced by iron deficiency (Yuan et al., 2008). Because bHLH039 is a FIT binding partner, PYE activity mediates widespread transcriptional regulation under iron deficiency through indirect regulation of FIT or with direct interaction with other PYE targets (Long et al., 2010). Although *PYE* is most highly expressed in the root pericycle, PYE protein is found in the nuclei of all root cells under iron deficiency (Long et al., 2010), which implies that PYE might translocate throughout the root and convene with the FIT network. *PYE* is a direct target of bHLH34, and *FIT* and *bHLH38/39/100/101* were also proposed as direct targets of bHLH34 (Li et al., 2016).

Even though the intricate transcriptional network of the iron deficiency response has been extensively studied (Dinneny et al., 2008; Buckhout et al., 2009; Rodríguez-Celma et al., 2013; Mai et al., 2016; Gao et al., 2019), the effect of chromatin structure on iron homeostasis gene expression is not well-understood. In addition to transcription factors, chromatin structure is a major transcriptional regulator in eukaryotes (Li et al., 2007). The covalent chemical modification of the histone tails that modifies the compression and relaxation of the chromatin directly impacts transcription factor and transcriptional machinery access to promoter regions, and thus subsequent gene expression.

Histone 3 lysine 27 trimethylation (H3K27me3) is a well-established repression mark, controlled by the activity of polycomb-group (PcG) protein complexes that play significant roles in regulating gene expression and multicellular development (Köhler and Hennig, 2010; Pu and Sung, 2015). For example, the homeotic MADS box gene *AGAMOUS* (*AG*) is involved in specifying floral organ identity (Bowman et al., 1989; Yanofsky et al., 1990) and has been shown to be regulated by Polycomb Repressive Complex 2 (PRC2)-mediated H3K27me3 activity (Goodrich et al., 1997; Katz et al., 2004). In Arabidopsis, PRC2 specifically catalyzes the trimethylation of H3K27 (Zhang et al., 2007). Silencing occurs when PRC2 trimethylates K27 on histone 3, and the repression mark spreads along the chromatin, ultimately resulting in its compaction (Margueron and Reinberg, 2011). The CURLY LEAF (CLF) and SWINGER (SWN) subunits are responsible for the PRC2 methyltransferase activity in Arabidopsis. While CLF and SWN are partially redundant, CLF is the predominant H3K27 tri-methyltransferase of PRC2 and loss of CLF function results in drastically reduced H3K27me3 deposition (Chanvivattana et al., 2004; Schubert et al., 2006; Zhang et al., 2007; Wang et al., 2016); thus, *clf* mutants are widely used as PCR2 mutants (Lafos et al., 2011; Lu et al., 2011; Zhou et al., 2018). Nearly 20% of Arabidopsis genes were identified as H3K27me3 targets, which predominantly consisted of transcriptionally repressed genes (Turck et al., 2007; Zhang et al., 2007). In plants, H3K27me3 has been understood as a widely used repressive epigenetic mark in response to not only developmental cues, but also abiotic stressors such as

temperature and drought (Probst and Mittelsten Scheid, 2015; Secco et al., 2017).

In this study, we show that post-translational modification of a core histone, histone 3 lysine 27 trimethylation (H3K27me3), modulates the induction of *FIT* and FIT-dependent iron acquisition genes under iron deficiency. Our work reveals that FIT-dependent genes are more pronouncedly induced by iron deficiency in the *clf* mutant, which lacks the major H3K27 trimethyltransferase, than in wild type. Furthermore, we show that *FIT*, *FRO2*, and *IRT1* are direct targets of H3K27me3 and that the *clf* loss-of-function mutant grows better than wild type in conditions with low levels of iron.

MATERIALS AND METHODS

Plant Materials and Growth Conditions

Arabidopsis thaliana ecotype Columbia (Col-0) was used as the wild type. The *clf* mutant line used was *clf-29* (SALK_21003) from the Arabidopsis Biological Resource Center. Arabidopsis seeds were surface-sterilized and plated on B5 media. After stratification, seeds were grown at 22°C under a 16/8 h light/dark cycle in a Conviron A1000 growth chamber. For iron treatments, plants were transferred to iron deficient media (−Fe), Murashige and Skoog (MS) medium with no iron (Caisson MSP33) supplemented with 300 μM ferrozine, or Fe sufficient media (+Fe), MS medium with 100 μM FeNa-EDTA (Caisson MSP34) for 3 days for both gene expression analysis and chromatin immunoprecipitation.

RNA Extraction

Total RNA was extracted from root and shoot tissues using the Plant RNA Isolation Kit (Agilent) per the manufacturer's instructions. The concentration and purity of RNA were measured with NanoDrop One (Thermo Fisher Scientific), and the integrity of RNA was assessed by running a bleach gel (Aranda et al., 2012).

Quantitative RT-PCR

cDNA was synthesized from total RNA using iScript™ Reverse Transcription Supermix (Bio-Rad) following manufacturer's instructions. cDNA samples were then diluted 1:10 with nuclease-free water and used for RT-qPCR analysis with iTaq™ Universal SYBR© Green Supermix (Bio-Rad) following manufacturer's instructions using the CFX Connect™ Real-Time System (Bio-Rad). A melt curve analysis was performed at the end of the qPCR protocol. Relative transcript levels of genes of interest was calculated using the ΔCt method (Schmittgen and Livak, 2008). The expression level of *ACTIN2* (*ACT2*) was used as an internal control. Primers were designed using QuantPrime (Arvidsson et al., 2008). Primer sequences are listed in **Supplementary Table S1**.

RNA-Sequencing and Data Analysis

Three biological replicates of wild type and *clf* roots grown under iron deficient or sufficient conditions were used for RNA-seq analysis. RNA was extracted as described above. cDNA library construction, 150 bp paired-end sequencing on Illumina NovaSeq 6000 platform, and standard RNA-seq analysis were conducted by Novogene. Gene expression was quantified using the union mode of the HTSeq software and reported as FPKM (Fragments Per Kilobase of transcript sequence per Millions base pairs sequenced). All sequencing reads were aligned to the *Arabidopsis thaliana* reference genome, TAIR10[1]. Readcount histograms of the genes of interest was generated using the Integrative Genomics Viewer (IGV), IGV 2.4 (Robinson et al., 2011; Thorvaldsdóttir et al., 2013). Differential gene expression analysis was conducted using DESeq with a threshold set as padj <0.05 using negative binominal distribution for *p*-value estimation and BH for FDR estimation (Anders and Huber, 2010). The Gene Ontology (GO) term annotations were conducted using the enrichment analysis tool (Mi et al., 2017) available via from the Gene Ontology Consortium (Ashburner et al., 2000; The Gene Ontology Consortium, 2017). Statistical analyses of iron regulated genes were performed using R (The R Foundation, Vienna, Austria). The genes used for the analysis shown in **Figure 2** are listed in **Supplementary Table S2**.

Chromatin Immunoprecipitation (ChIP) – qPCR

Wild type and *clf* plants were grown as described above and root tissue was harvested. Native proteins were crosslinked with gDNA using GB buffer (0.4 M sucrose, 10 mM Tris pH 8.0, 1 mM EDTA), 100 mM PMSF, and 37% formaldehyde. Plant tissue was ground in liquid nitrogen by mortar and pestle and sonicated in lysis buffer (500 mM HEPES pH 7.5, 150 mM NaCl, 1 mM EDTA, 1% Triton X-100, 0.1% deoxycholate, 0.1% SDS). Crosslinked DNA was precleared with Protein A Agarose/Salmon Sperm DNA beads (Millipore Sigma, 16-157) for 1 h at 4°C with gentle rotation and then incubated with anti-IgG (Millipore Sigma, 12-370), H3 (AbCam 1791), or H3K27me3 antibodies (Millipore Sigma, 07-449) overnight at 4°C with gentle rotation. Crosslinked DNA was washed in a series with lysis buffer, LNDET buffer (0.25 M LiCl, 1% NP-40, 1% deoxycholate, 1 mM EDTA, 10 mM Tris-HCl pH 8.0), and TE buffer before elution with elution buffer (1% SDS, 0.1 M $NaHCO_3$). Crosslinking was reversed with Proteinase K overnight at 65°C, and DNA was purified using the Zymo-Spin ChIP Kit per manufacturer's instructions. The qPCR was conducted as described above, and gene enrichment was normalized to 10% of input (Haring et al., 2007). Primers were designed using NCBI Primer-BLAST (Ye et al., 2012). Primer sequences are listed in **Supplementary Table S3**.

Low Iron Growth

Wild type and *clf* seeds were surface-sterilized, plated, and grown under light and temperature conditions as described above after stratification. Plants were grown on media with no added iron and 300 μM ferrozine, low iron (10 μM Fe), or sufficient iron (100 μM Fe) for up to 12 days. Low iron media was prepared by adding sterile 10 μM Fe (III)-NaEDTA to MS medium without iron (Caisson MSP33). Root lengths were measured using ImageJ.

[1] www.arabidopsis.org

RESULTS

Iron Acquisition Genes Are More Highly Induced in Roots of *clf* Than in Wild Type

Multiple large-scale epigenomics studies have mapped H3K27me3 target loci in Arabidopsis (Turck et al., 2007; Zhang et al., 2007; Bouyer et al., 2011; Lafos et al., 2011; Lu et al., 2011; Roudier et al., 2011). After a survey of the genome-wide studies, we noted that loci of several iron deficiency response genes, including the major iron acquisition genes, were among those identified to be associated with H3K27me3 (**Table 1**). Such findings suggested that iron homeostasis genes are under the control of H3K27me3 and led us to hypothesize that Arabidopsis might implicate chromatin remodeling to regulate the iron deficiency response. To test this hypothesis and understand the role of H3K27me3 in the iron deficiency response, we examined the expression of iron homeostasis genes that are well-established to be induced under iron deficiency in wild type and *clf* mutant roots. CLF is a core PRC2 component in Arabidopsis, which is largely responsible for the methyltransferase activity of PRC2 (Chanvivattana et al., 2004; Köhler and Hennig, 2010), and *clf* mutants are used as PRC2 mutants (Lafos et al., 2011; Lu et al., 2011; Zhou et al., 2018). Although CLF is partially redundant with SWN, we did not conduct our experiments using the *clf swn* double mutant, which exhibits severe developmental phenotypes and develops into a mass of callus-like tissue that does not differentiate into roots and shoots (Chanvivattana et al., 2004). Because our study focuses on root-specific iron acquisition genes, we conducted experiments using a *clf* single mutant, *clf-29*, which has remarkably reduced levels of H3K27me3 and has been widely used in multiple studies (Bouveret et al., 2006; Schönrock et al., 2006; Xu and Shen, 2008; Zhao et al., 2015; de Lucas et al., 2016; Bellegarde et al., 2018). In addition, we verified expression of iron deficiency response genes and low iron growth phenotypes of a second *clf* mutant, *clf-28*, as shown in **Supplementary Figures S1, S4**.

If iron deficiency response genes are repressed by H3K27me3, their expression will be higher in the *clf* mutant than in wild type. We predicted that these genes might be induced at a higher level in *clf* than in wild type under iron deficient conditions, but still remain at a low basal level under iron sufficient conditions in *clf*. Previous studies have shown that the removal of H3K27me3 is often not sufficient to induce gene expression (Bouyer et al., 2011), and FIT overexpression studies have shown that FIT is inactive under iron sufficiency (Lingam et al., 2011; Meiser et al., 2011). Thus, it is likely that an upstream regulatory mechanism that is activated by the iron deficiency signal will be necessary to trigger the induction of iron acquisition genes.

To test if iron deficiency response genes are differentially regulated in the *clf* mutant, we first quantified the expression of FIT-target genes involved in iron acquisition such as *FIT*, *IRT1*, *FRO2*, and *F6'H1*, in *clf* and wild type roots from iron sufficient and deficient conditions. As expected, in wild type, these genes were highly induced under iron deficiency but barely expressed under iron sufficient conditions (**Figure 1A**). In *clf* roots from iron sufficient conditions, expression of FIT-target genes remained low, consistent with the wild type (**Figure 1A**). However, the induction of *FIT*, *IRT1*, *FRO2*, and *F6'H1* was significantly higher in iron deficient roots of *clf* than in those of wild type (**Figure 1A**). The higher induction of FIT target genes under iron deficient conditions was consistently observed in the second *clf* mutant (**Supplementary Figure S1**). This suggests that H3K27me3 is primarily involved in modulating Strategy I genes under iron deficiency and prevents hyper-induction of these genes.

Next, we examined PYE-dependent genes, *FRO3*, *NAS4*, and *BTS*, which are also known to be induced under iron deficiency (Long et al., 2010). The PYE-dependent genes were highly induced under iron deficient conditions in both wild type and *clf* roots, but their expression levels were comparable between both genotypes (**Figure 1B**). Our qRT-PCR data suggested that H3K27me3 modulates the induction of FIT-dependent genes in response to iron deficiency, whereas PYE-dependent genes are not likely to be under the control of this repression mark under iron deficient conditions. The results also revealed that H3K27me3 is not the primary factor that represses iron deficiency inducible genes under iron sufficient conditions, as neither the FIT- nor PYE-regulated genes tested were expressed in the *clf* mutant in the presence of iron (**Figure 1**).

TABLE 1 | Iron deficiency response genes identified as H3K27me3 targets from existing large scale epigenomic datasets.

Gene ID	Gene name	Annotated function
At1g01580	*Ferric Reductase Oxidase 2* (*FRO2*)	Reduces ferric-chelate iron to ferrous iron
At2g28160	*FER-like iron deficiency transcription factor* (*FIT*)	Regulator of the iron deficiency response
At3g08040	*Ferric Reductase Defective 3* (*FRD3*)	Cation transmembrane transport
At3g13610	*F6'H1*	Iron uptake and production of iron uptake-related fluorescent phenolics
At3g50740	*UDP-Glucosyl Transferase 72E1* (*UGT72E1*)	UDP-glucosyl transferase activity, response to toxic substances
At3g53480	*Pleiotropic Drug Resistance 9* (*PDR9*)/*ATP-binding cassette G37* (*ABCG37*)	Secretion of iron uptake-related fluorescent phenolics
At4g19680	*Iron Regulated Transport 2* (*IRT2*)	Ferrous iron ion transporter
At4g19690	*Iron Regulated Transport 1* (*IRT1*)	Ferrous iron ion transporter

Transcriptomic Analysis of Genes Differentially Regulated by Iron in Wild Type and *clf* Roots

To get a broader sense of the impact of H3K27me3 on the expression of iron homeostasis genes, we conducted RNA-seq analysis with RNA isolated from root tissue of wild type and *clf* mutants treated under iron deficient and sufficient conditions. We identified 310 genes that were differentially up-regulated in iron deficient wild type roots and 581 genes in *clf* roots. As expected, the list of iron-regulated genes included

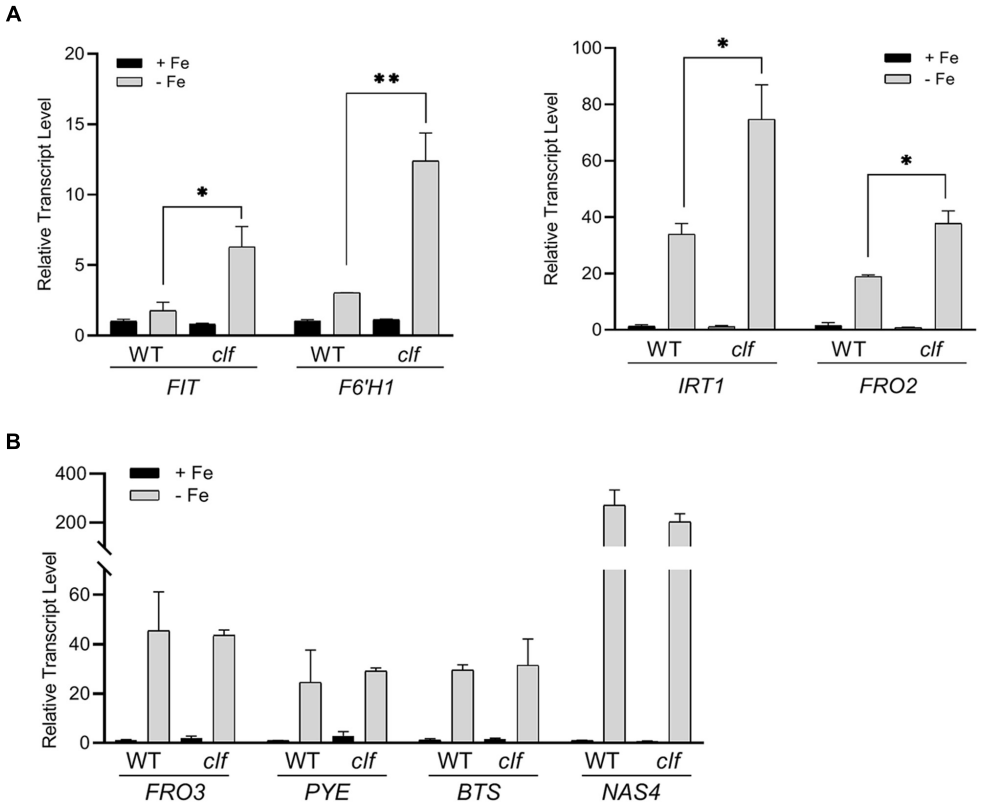

FIGURE 1 | Transcript levels of iron deficiency inducible genes in wild type and *clf* roots. Quantitative RT-PCR was conducted with total RNA extracted from roots of 12-day-old plants grown on B5 without sucrose and then transferred to iron sufficient (+Fe; 100 μM Fe) or iron deficient (–Fe; 300 μM ferrozine) media for 3 days. Transcript levels were normalized to an internal control, *ACT2*, and reported as the expression ratio relative to wild type under iron-sufficient conditions. **(A)** FIT-dependent genes, **(B)** PYE-dependent genes. Mean values of three biological replicates are shown. Error bars represent standard error ($n = 3$). $^{*}p < 0.05$; $^{**}p < 0.01$.

the well-established iron homeostasis genes and other genes previously identified to be regulated by iron (**Figures 2**, **3** and **Supplementary Table S2**). Alignment of the read counts with the FIT-dependent iron deficiency response genes revealed greater induction of these genes in *clf* than in wild type in iron deficient conditions (**Figure 2A**), while PYE-dependent iron deficiency response genes were comparably induced between wild type and *clf* under iron deficiency (**Supplementary Figure S2**). Additionally, it is notable that even under iron sufficient conditions, the read counts for genes in the FIT pathway were consistently higher in *clf* compared to wild type, as opposed to PYE-dependent genes, for which the relative read counts in wild type and *clf* were variable (**Supplementary Figure S3**). This suggests that H3K27me3 takes part in repressing FIT-dependent iron acquisition genes under iron sufficient conditions. The overall read counts of these genes in iron-sufficient *clf* are still low; this signifies that iron-dependent upstream regulators are necessary to fully induce FIT-regulated iron acquisition genes, and explains why the small, yet significant changes were not detectable from our initial qRT-PCR analysis (**Figure 1**).

To visualize the differential expression of multiple FIT- and PYE-dependent iron responsive genes in *clf* compared to wild type, we plotted log2 fold change of *clf* over the log2 fold change of wild type for these genes, along with the line y = x (**Figure 2B**). The fold changes were calculated based on RNA-seq read counts in iron deficient conditions compared to iron sufficient conditions for both wild type and *clf*, and log2-transformation was conducted to obtain approximately normal distributions (**Figure 2C**). We observed a clear trend of FIT-dependent genes more often showing higher fold changes in *clf* than in wild type from the scatter plot and density plot (**Figures 2B,C**). Thus, we performed a randomization test to estimate the null distribution of the proportion of FIT-target genes that were more robustly expressed in *clf* than in wild type. This null distribution was then compared to the observed proportion FIT-dependent genes with a higher fold induction in clf than in wild type under iron deficiency. Based on the randomization test, FIT-target genes were more likely to have higher log fold changes in *clf* compared to PYE-dependent genes ($p < 0.001$; **Figures 2B,C**). Additionally, the induction of FIT-dependent transcripts in *clf* compared to wild type was generally more drastic than that of PYE-dependent transcripts (Mann-Whitney U test, $p < 0.001$). For example, under iron deficiency, expression of FIT-dependent genes such as *FIT*, *FRO2*, and *IRT1* were each approximately 3.9, 13.7, and 11.3-fold induced in wild type, whereas their transcript levels were each approximately 5.0, 40.8, and 22.4-fold induced in *clf*

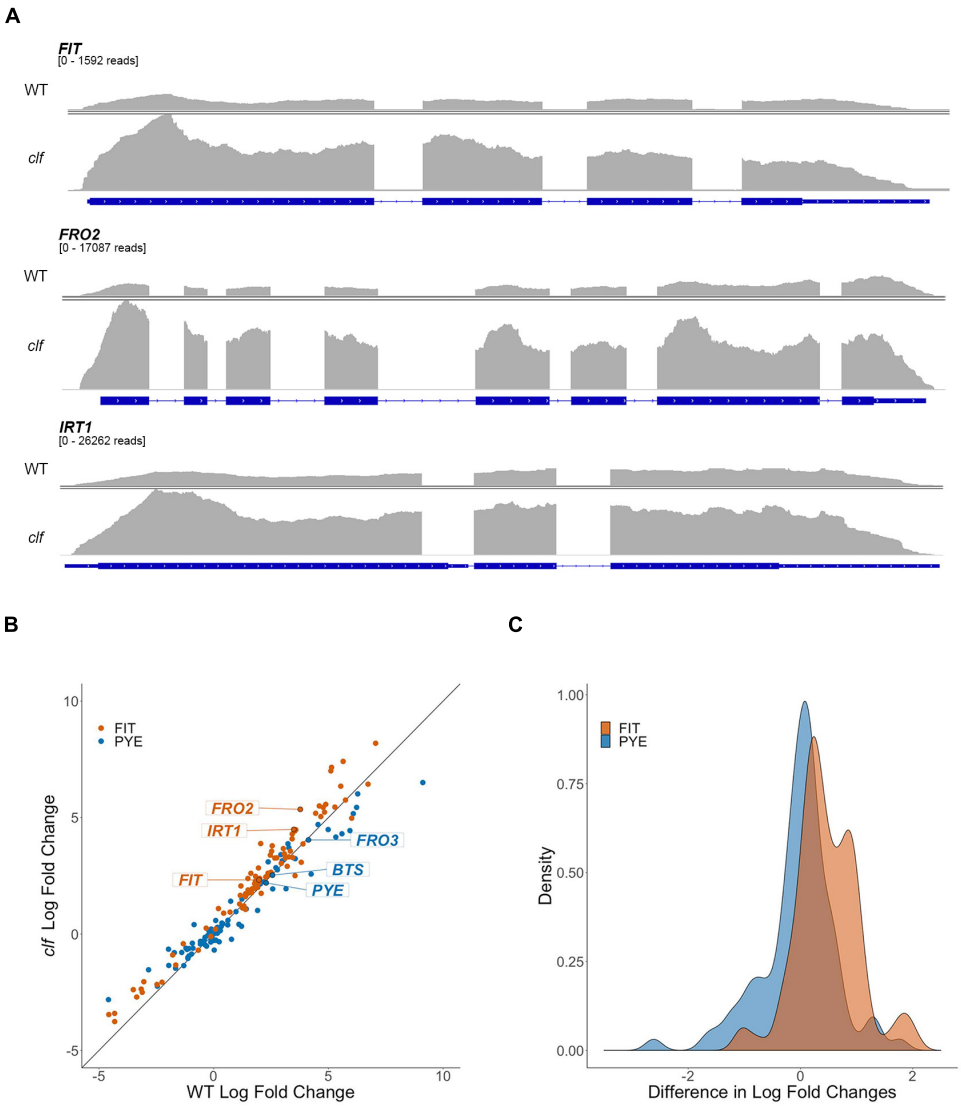

FIGURE 2 | Differential regulation by iron of FIT-dependent iron acquisition genes in *clf* compared to wild type. **(A)** RNA-seq read count histograms of FIT-dependent iron acquisition genes in wild type and *clf* under iron deficiency. Gene diagrams depict introns (line) and exons (boxes) and are aligned with read counts. The read count range, denoted below the gene name, were scaled to the maximum number of reads obtained in *clf*. Read count scale is equivalent for wild type and *clf* within each gene. **(B)** Scatter plot of log2 fold change in *clf* over wild type. y = x line represents non-differential induction of iron acquisition genes between wild type and *clf*. **(C)** Density histogram of differentially induced FIT- and PYE-dependent iron acquisition genes between wild type and *clf*.

roots (**Supplementary Table S2**). On the other hand, fold change inductions of PYE-dependent genes were similar between the two genotypes, with transcript levels of *PYE*, *BTS*, and *FRO3* about 4.9, 5.9, and 17.5 times higher in wild type under iron deficiency and 4.6, 5.7, and 16.4 times higher in *clf* under iron deficiency respectively (**Supplementary Table S2**).

We conducted a hierarchical clustering analysis with 1021 genes that were differentially regulated by iron in wild type or *clf* roots. Genes differentially regulated in response to iron in the roots exhibited generally consistent expression patterns regardless of the genotype (**Figure 3**). From the heat map generated by the cluster analysis, we noted a region of genes that were more robustly repressed under iron sufficient conditions and expressed less under iron deficient conditions in *clf* than in wild type; this group was enriched with genes involved in glutathione metabolism (**Figure 3**, Group 1). Among the genes highly expressed in iron sufficient conditions but downregulated under iron deficiency, genes involved in metabolism, stress responses, and iron homeostasis were over-represented (**Figure 3**, Group 3). Within this group are *FER1* and *FER4*, which encodes ferritins that bind to iron to prevent iron-induced cytotoxicity (Ravet et al., 2009).

In addition, we identified a group of genes up-regulated under iron deficiency but down-regulated under iron sufficient conditions (**Figure 3**, Group 2). This group was enriched with genes iron deficiency response genes, such as those that

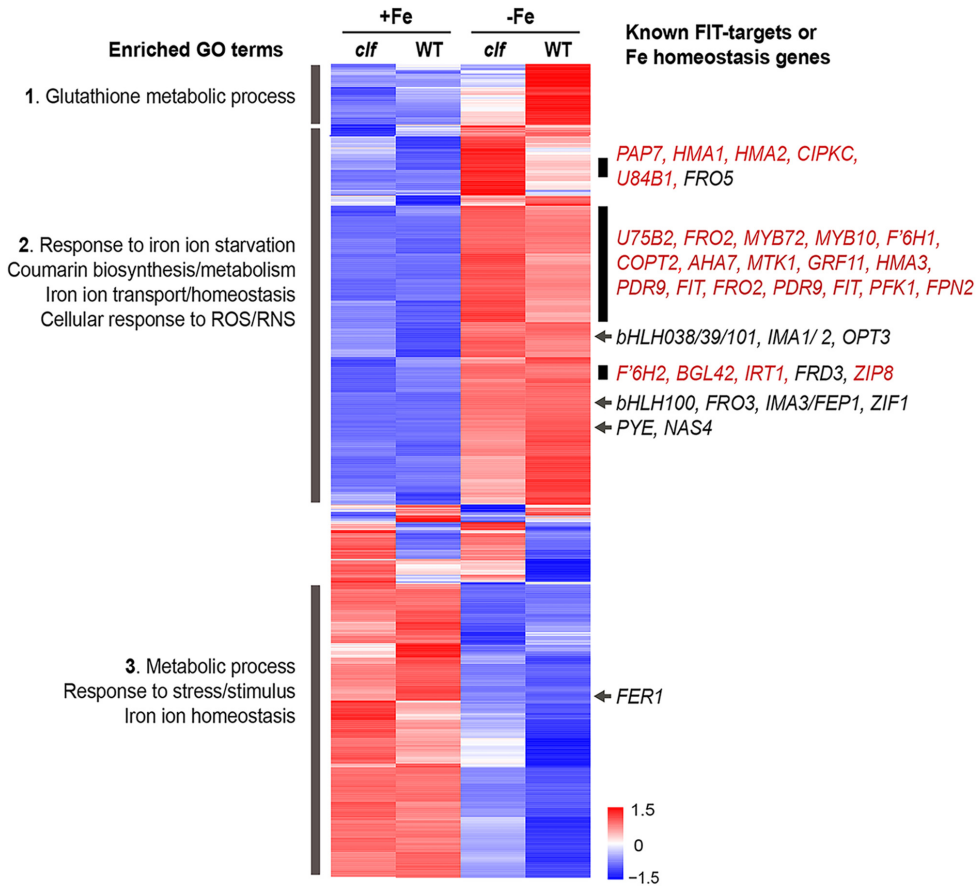

FIGURE 3 | Cluster analysis of genes differentially regulated by iron in wild type and *clf* roots. Heat map of genes differentially regulated by iron in wild type or *clf* root tissue. Enriched GO terms and known iron homeostasis genes or FIT-regulated genes (red) in the subsets highlighted are indicated. Numbers on the scale bar represent standard deviation from the mean.

participate in coumarin synthesis and iron uptake, as well as genes involved in responding to reactive oxygen/nitrogen species (ROS/RNS). Within this group, we noted subsets of genes that had markedly higher levels of transcripts in the *clf* mutant than in wild type (**Figure 3**). These subsets included a high proportion of FIT-dependent genes; about 24% of genes, i.e., 45 out of 191 genes, from this category were previously identified to be regulated by FIT (Colangelo and Guerinot, 2004; Mai et al., 2016). Meanwhile, iron deficiency inducible PYE-dependent genes were distributed throughout the upper half of the heat map. The expression of *bHLH38/39/100/101*, which encode proteins that form heterodimers with FIT, was induced under iron deficiency in both wild type and *clf* (**Figure 3**). However, their induction levels were not significantly different between wild type and *clf* (**Figure 3**). This observation is consistent with our hypothesis that PRC2 affects FIT-regulated genes. In addition, it reveals that *bHLH38/39/100/101* were present and would be able to interact with FIT in both genotypes.

Overall, the RNA-seq results corroborated our findings from the qPCR analysis, confirming that iron acquisition genes were more highly induced by iron deficiency in roots of *clf* loss-of-function mutants compared to wild type. Furthermore, the statistical analyses with fold change induction of iron deficiency response genes (**Figure 2**) and the clustering analysis of genes differentially regulated by iron (**Figure 3**) consistently revealed that FIT-dependent genes are disproportionately more highly induced by iron deficiency in *clf* roots. Such findings from the RNA-seq analysis and our qRT-PCR data (**Figure 1**) strongly suggest that H3K27me3 is attenuating the induction of FIT-regulated genes under iron deficiency.

H3K27me3 Is Deposited on FIT-Dependent Iron Deficiency Response Genes

We conducted chromatin immunoprecipitation followed by qPCR (ChIP-qPCR) using antibodies against H3K27me3 and primers specific to multiple regions of the Strategy I genes, *FIT*, *FRO2*, and *IRT1*, (1) to confirm that these FIT-dependent genes are direct targets of H3K27me3, and (2) to test if H3K27me3 is differentially deposited on these gene loci depending on the iron status of the plant. Primers were designed to target upstream regions of exon 1 in order to perceive maximal H3K27me3 enrichment, which occurs primarily at the promoters

and transcribed genic regions (Zhang et al., 2007). If the FIT-dependent iron deficiency response genes are direct targets of H3K27me3, H3K27me3 should be highly enriched at their loci in wild type. Substantially less H3K27me3 deposition is expected in *clf* regardless of the iron conditions. Additionally, if H3K27me3 is involved in transcriptionally regulating FIT-dependent genes in response to iron, we expected to see differential levels of H3K27me3 enrichment under iron deficient and sufficient conditions.

According to our ChIP-qPCR results, H3K27me3 enrichment at the *FIT*, *FRO2*, and *IRT1* loci was distinctly higher in wild type grown in iron sufficient conditions than in iron deficient wild type or *clf* from either iron condition (**Figure 4**). This provides evidence that the FIT-dependent iron deficiency response genes are direct targets of PRC2-mediated H3K27me3, consistent with the large scale epigenomics studies in which *FIT*, *FRO2*, and *IRT1* were identified as H3K27me3 targets (**Table 1**). Furthermore, our results suggest that H3K27me3 is involved in regulating the iron deficiency response at multiple levels, at the *FIT* locus as well as downstream of FIT at the *FRO2* and *IRT1* loci.

clf Seedlings Are More Resistant to Low Iron Conditions Than Wild Type

Our results showed that FIT-dependent iron acquisition genes are more robustly induced in *clf* roots upon iron deficiency (**Figures 1–3**) and that they are subjected to CLF-mediated H3K27me3 (**Figure 4**). Therefore, we hypothesized that *clf* might be more tolerant to iron deficiency and examined the young seedlings of *clf* and wild type germinated on media that lack iron or are supplemented with a low concentration of iron that is suboptimal for growth. Consistent with our hypothesis, *clf* seedlings grew better than wild type on iron-limiting media, whereas the growth of both wild type and *clf* plants were comparable under iron sufficient conditions (**Figure 5A**). The root length of *clf* mutants was considerably greater than that of wild type when the plants were germinated and grown on low iron media (**Figure 5B** and **Supplementary Figure S4**), which correlated with their high level of iron acquisition gene expression (**Figure 1** and **Supplementary Figure S1**). The overall growth and quantified root length were comparable between wild type and *clf* grown on iron sufficient media (**Figure 5** and **Supplementary Figure S4**), suggesting that the difference in growth observed under low iron conditions was indeed an iron effect rather than a difference due to the genotype. In media without iron, the growth of both wild and *clf* plants was severely impaired (**Supplementary Figure S5**). Consequently, the phenotype of *clf* in low iron suggests that iron acquisition genes are not only robustly induced at the transcriptional level, but also that their enhanced gene expression contributes to better growth under low iron conditions.

DISCUSSION

Precise regulation of gene expression in response to specific cues is fundamental to vital biological processes. At the transcriptional level, transcription factors and chromatin structure controlled by

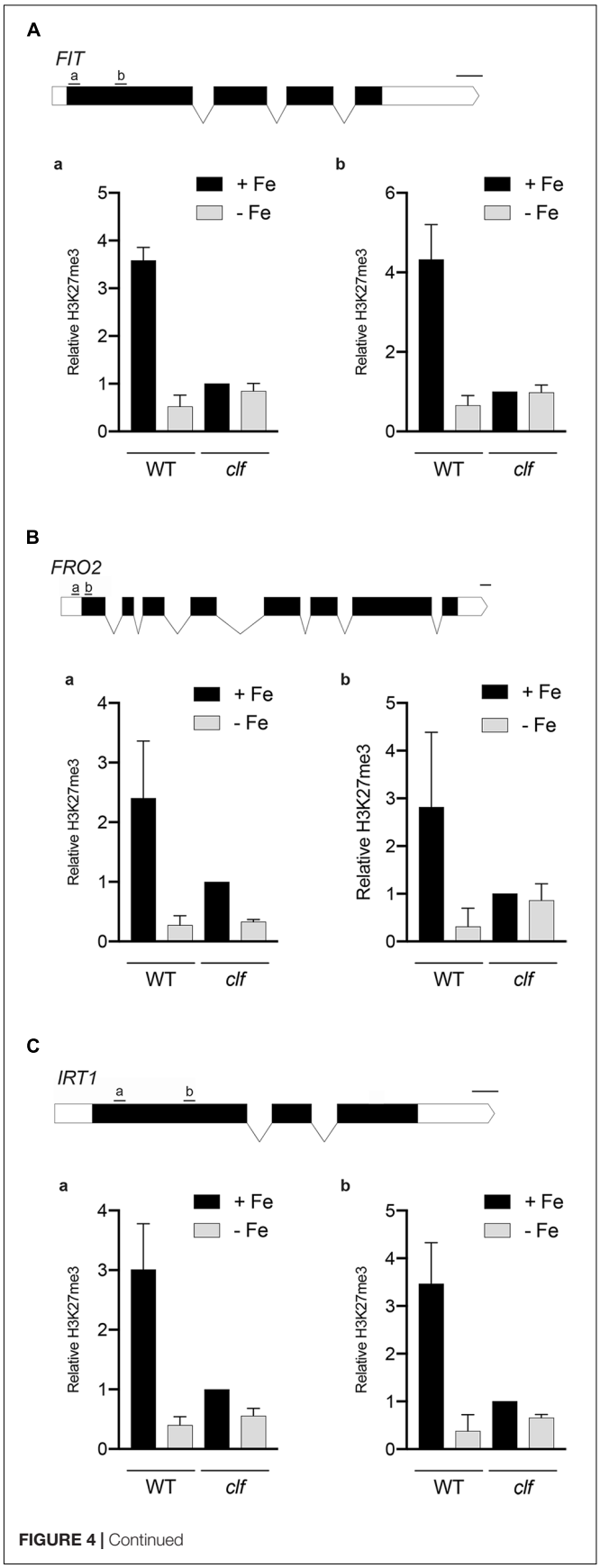

FIGURE 4 | Continued

FIGURE 4 | H3K27me3 enrichment at the loci of iron acquisition genes. H3K27me3 deposition at the indicated regions **(a,b)** of **(A)** *FIT*, **(B)** *FRO2*, and **(C)** *IRT1* gene loci was detected by ChIP-qPCR from wild type and *clf* roots treated under iron deficient (–Fe) or iron sufficient (+Fe) conditions. ChIP-qPCR signal was normalized with input DNA, and H3K27me3 enrichment relative to that in *clf* grown under iron-sufficient conditions was plotted. Error bars represent standard error of the mean of three biological replicates (n = 3). Scale bar above gene diagram represents length for 100 bp.

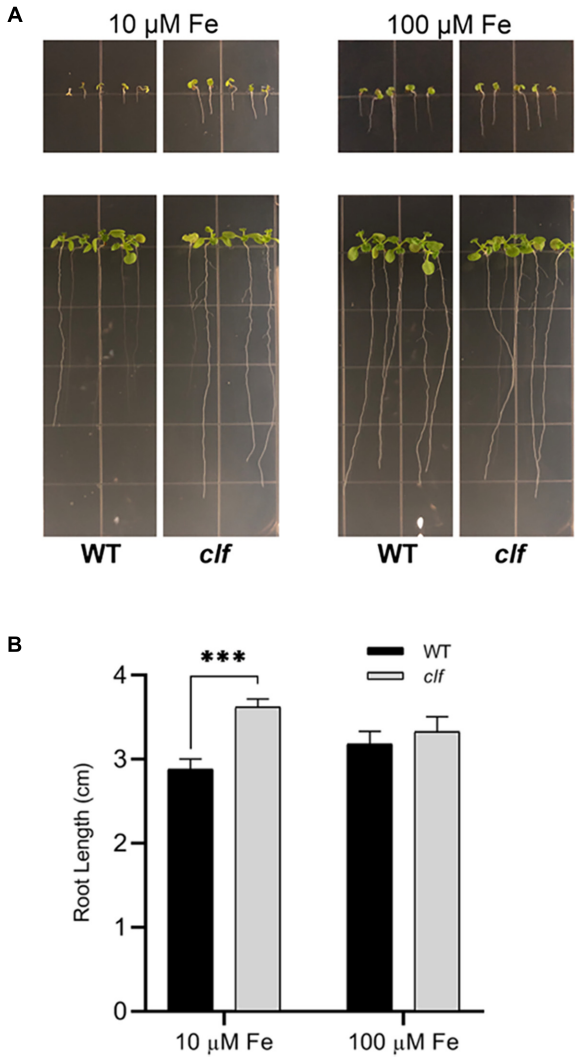

FIGURE 5 | Growth phenotypes of *clf* and wild type under low iron conditions. **(A)** Wild type and *clf* plants were germinated and grown on iron-limiting (10 μM Fe) and iron-sufficient (100 μM Fe) media. Photos in the upper panel were taken 4 days after germination, and Photos in the lower panel were taken 10 days after germination. **(B)** Quantified root length. Mean values of root lengths are shown with standard error (n = 20–24; ***$p < 0.001$).

histone modifications have profound effects on gene expression (Li et al., 2007; Farnham, 2009). The iron deficiency response in plants and subsequent iron acquisition is, to a great extent, regulated at the transcriptional level. Indeed, multiple key transcription factors involved in iron homeostasis have been extensively studied (Gao et al., 2019). However, the impact of chromatin structure on transcriptional regulation of iron homeostasis genes remains to be understood. In this study, we provide evidence that the well-established H3K27me3 repression mark contributes to transcriptional regulation of iron deficiency by fine-tuning the induction of *FIT*-target genes in iron deficient roots.

Based on our findings, we propose a working model for H3K27me3-mediated regulation of the FIT-dependent iron deficiency response (**Figure 6**). Under iron sufficiency, *FIT* is directly targeted by H3K27me3, resulting in repression of its transcription and the subsequent iron deficiency response. The removal of the trimethylation mark is still insufficient for the full induction of *FIT* and its downstream targets, as evidenced by the low expression of these genes in *clf* in the presence of iron (**Figures 1A**, **3**). This implies the involvement of regulatory mechanisms upstream of *FIT* that are responsive to iron. Despite the higher level of *FIT* transcripts detected in iron sufficient *clf* compared to wild type (**Supplementary Figure S2**), without the iron deficiency signal that activates FIT, it is likely that neither *FIT* nor its downstream genes could be fully induced. Upon encountering iron deficiency, H3K27me3 is removed and the iron deficiency signal activates regulators of FIT, which then lead to the pronounced expression of *FIT* and its downstream targets. However, residual H3K27me3 may attenuate the induction of iron acquisition genes in wild type. In *clf*, where there is very little H3K27me3 deposition, *FIT* is more strongly induced than in wild type under iron deficient conditions. Additionally, *FRO2* and *IRT1* are also direct targets of H3K27me3. Therefore, the high-level induction of *FIT* and the lack of H3K27me3 on the *FRO2* and *IRT1* loci are likely to contribute to the augmented induction of these FIT-dependent genes in *clf* roots compared to wild type.

We hypothesize that PRC2-mediated H3K27me3 provides a mechanism to limit the maximum level of induction of iron acquisition. This would be beneficial for plants, as cellular iron levels must be maintained within a very narrow range due to iron's redox properties that can facilitate the production of cytotoxic hydroxyl radicals (Halliwell and Gutteridge, 1992). Multiple studies have shown that the expression of iron acquisition genes is very precisely controlled depending on the iron status of the plant. *FIT*, *FRO2*, and *IRT1* are post-transcriptionally regulated to ensure that their proteins do not accumulate or stay active in the presence of iron (Connolly et al., 2002; Connolly et al., 2003; Colangelo and Guerinot, 2004; Kerkeb et al., 2008; Sivitz et al., 2011; Shin et al., 2013). Additionally, as cytotoxic effects can be caused by the entry of non-iron secondary substrates, IRT1 also undergoes monoubiquitin-dependent endocytosis (Barberon et al., 2011, 2014) and acts as a transceptor that directly senses excess non-iron metals to control self-degradation (Dubeaux et al., 2018). In addition to the regulation at the post-transcriptional and post-translational levels, our findings indicate that a mechanism to avoid overaccumulation of iron is imposed at a much earlier stage prior to transcription. Furthermore, we speculate that H3K27me3 contributes to preventing iron-induced toxicity in wild type roots under iron sufficient conditions, supported by proof of greater

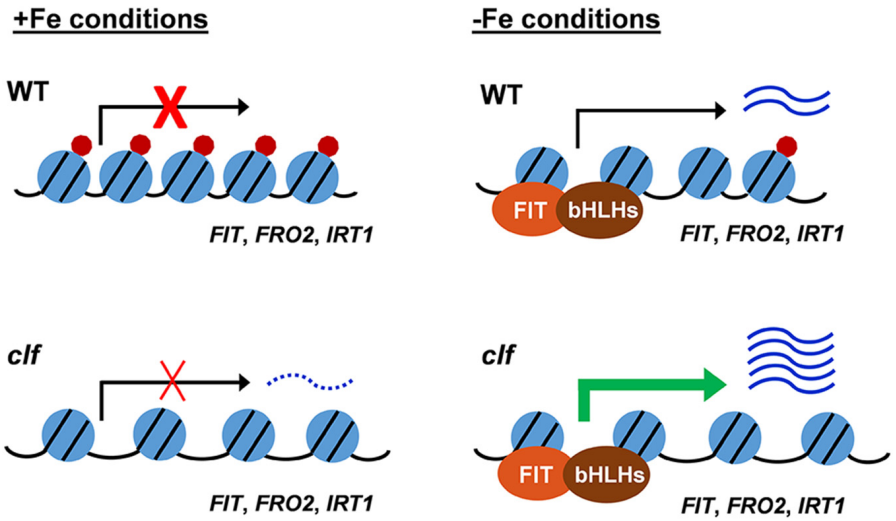

FIGURE 6 | Proposed model for H3K27me3 regulation of the FIT-dependent iron deficiency response. Under iron sufficient conditions, the H3K27me3 deposition on FIT-dependent iron acquisition gene loci prevents the iron deficiency response. In response to iron deficiency, H3K27me3 is partially removed, allowing for the induction of the FIT-dependent acquisition genes. In the *clf* mutant, the H3K27me3 level is significantly reduced. Under iron sufficient conditions, the substantially reduced level of H3K27me3 marks allows for a low-level transcription of FIT-dependent genes and leads to the greater induction of iron acquisition genes under iron deficiency compared to wild type. Under iron sufficient conditions, despite the increased basal level of transcripts in *clf*, the absence of H3K27me3 is not sufficient to induce FIT-dependent iron deficiency response genes as the presence of iron negatively regulates the induction of *FIT*. Blue circles with black lines represent nucleosomes, with core histones and chromatin DNA, red circles represent H3K27me3 deposition, and the distance between blue circles depict euchromatin or heterochromatin structure due to H3K27me3. Arrows indicate active or inactive transcriptional states. Wavy lines represent transcripts of the FIT-dependent iron acquisition, with the dotted wavy line representing basal level of transcription in *clf*.

induction of FIT-dependent genes in *clf* compared to wild type in iron sufficient conditions (**Supplementary Figure S3**). We noted that H3K27me3 deposition at the loci of iron acquisition genes in wild type and *clf* under iron deficiency were comparable based on our ChIP-qPCR results (**Figure 5**). However, this may only appear to be the case due to the limited resolution afforded by probing specific regions by ChIP-qPCR. H3K27me3 deposition may occur at other locations along the gene, and a higher resolution assay such as ChIP-seq may reveal nuances in H3K27me3 enrichment that were not sufficiently detected by the ChIP-qPCR. As a result, it is likely that there is considerably decreased H3K27me3 enrichment on *FIT* and FIT-target genes in *clf* than in wild type under iron deficiency.

Environmentally induced chromatin remodeling has been studied in plants. The best understood example is for vernalization, in which PRC2-mediated chromatin modifications on *FLC* silences its expression in response to prolonged cold (Michaels and Amasino, 1999; Lee et al., 2015). Recently, more research has been conducted to investigate changes in chromatin structure in response to a wide range of abiotic stressors, and changes in histone modification and chromatin remodeling in response to nutrient availability have been observed (Probst and Mittelsten Scheid, 2015; Secco et al., 2017). For example, *NITRATE TRANSPORTER 2.1* (*NRT2.1*), which encodes a high-affinity root nitrate transporter, was found to be subjected to transcriptional repression by PRC2-mediated H3K27me3 (Bellegarde et al., 2018). H3K27me3 down-regulates *NRT2.1* expression under nitrogen limiting conditions, where the gene is most highly expressed.

Transcriptional regulation of a few iron homeostasis genes by histone modifications have been reported. *FERRIC REDUCTASE DEFECTIVE 3* (*FRD3*), which encodes the citrate effluxer that facilitates iron translocation in the xylem (Durrett et al., 2007), was identified as a direct target of GCN5 (Xing et al., 2015). GCN5 mediates acetylation of H3K14 and facilitates the acetylation of H3K9 and H3K27, which is involved in transcriptional activation of a large number of genes (Vlachonasios et al., 2003; Earley et al., 2007; Benhamed et al., 2008). GCN5 was proposed to regulate citrate efflux in root tissues via modulating *FRD3* expression when iron is limited (Xing et al., 2015). However, the induction of iron acquisition genes, such as *IRT1* and *FRO2*, under iron deficiency was not regulated by GCN5 (Xing et al., 2015). Expression of several Ib subgroup bHLH genes involved in the iron uptake process, such as bHLH38, bHLH39, bHLH100, and bHLH101, was reported to be negatively regulated by SKB1-mediated histone H4R3 dimethylation (Fan et al., 2014). It was also observed that *FRO2* and *IRT1* expression was higher in *skb1-1* than in wild type roots under iron deficient and sufficient conditions; nevertheless, *FRO2* and *IRT1* were not direct targets of SKB1 (Fan et al., 2014).

Our study provides a novel understanding of the transcriptional regulation of iron uptake in Arabidopsis by showing that H3K27me3 works upstream of *FIT* to partially repress the FIT-mediated iron deficiency response during iron sufficiency by directly modulating the *FIT*, *FRO2*, and *IRT1* loci. However, we still need to understand the interactions between the H3K27me3 repression mark and the iron-dependent regulatory pathway upstream of FIT. Considering that

H3K27me3-mediated gene repression can be associated with tissue-specific expression of its targets (Lafos et al., 2011), further studies should address if H3K27me3 plays a role in the tissue-specific expression of FIT-dependent iron acquisition genes in the epidermis. Integrative studies to assess the combinatorial view of repression and activation marks will be necessary, and whether iron-induced changes in chromatin are heritable should also be elucidated. A better comprehension of the molecular mechanisms behind chromatin remodeling in response to iron homeostasis will provide critical insights for improving iron nutrition in plants.

DATA AVAILABILITY

The RNA-seq data discussed in this publication have been deposited in NCBI's Gene Expression Omnibus (Edgar et al., 2002) and are accessible through GEO Series accession number GSE126782 (http://www.ncbi.nlm.nih.gov/geo/query/acc.cgi?acc=GSE126782).

AUTHOR CONTRIBUTIONS

JJ and JL conceived the idea. JJ supervised the project. EP and KT conducted the qRT-PCR. EP performed the ChIP-qPCR and prepared the RNA samples for RNA-seq by Novogene. KT performed the low iron growth assays. FH conducted the statistical analyses. EP and JJ primarily wrote the manuscript. All authors reviewed and approved the manuscript.

FUNDING

This work was supported by the Gregory S. Call Undergraduate Research Program (EP, KT, FH, JL, and JJ), Doelling Undergraduate Research Fund (EP and FH), and the National Science Foundation grant to JJ (IOS-1754969).

ACKNOWLEDGMENTS

We thank Amy Wagaman for assistance with statistical analysis, Mary Lou Guerinot for feedback on the manuscript, and Erin Connolly and Elsbeth Walker for helpful discussion. We also thank Angie Kim, Daniel Chung, Leah Kim, Elizabeth Parsons, and Avery Tucker for technical assistance at various stages of this project.

SUPPLEMENTARY MATERIAL

The Supplementary Material for this article can be found online at: https://www.frontiersin.org/articles/10.3389/fpls.2019.00627/full#supplementary-material

REFERENCES

Anders, S., and Huber, W. (2010). Differential expression analysis for sequence count data. *Genome Biol.* 11:R106. doi: 10.1186/gb-2010-11-10-r106

Aranda, P. S., LaJoie, D. M., and Jorcyk, C. L. (2012). Bleach gel: a simple agarose gel for analyzing RNA quality. *Electrophoresis* 33, 366–369. doi: 10.1002/elps.201100335

Arvidsson, S., Kwasniewski, M., Riaño-Pachón, D. M., and Mueller-Roeber, B. (2008). QuantPrime--a flexible tool for reliable high-throughput primer design for quantitative PCR. *BMC Bioinformatics* 9:456. doi: 10.1186/1471-2105-9-465

Ashburner, M., Ball, C. A., Blake, J. A., Botstein, D., Butler, H., Cherry, J. M., et al. (2000). Gene ontology: tool for the unification of biology. The gene ontology consortium. *Nat. Genet.* 25, 25–29. doi: 10.1038/75556

Barberon, M., Dubeaux, G., Kolb, C., Isono, E., Zelazny, E., and Vert, G. (2014). Polarization of IRON-REGULATED TRANSPORTER 1 (IRT1) to the plant-soil interface plays crucial role in metal homeostasis. *Proc. Natl. Acad. Sci. U.S.A.* 111, 8293–8298. doi: 10.1073/pnas.1402262111

Barberon, M., Zelazny, E., Robert, S., Conéjéro, G., Curie, C., Friml, J., et al. (2011). Monoubiquitin-dependent endocytosis of the iron-regulated transporter 1 (IRT1) transporter controls iron uptake in plants. *Proc. Natl. Acad. Sci. U.S.A.* 108, E450–E458. doi: 10.1073/pnas.1100659108

Bauer, P., Thiel, T., Klatte, M., Bereczky, Z., Brumbarova, T., Hell, R., et al. (2004). Analysis of sequence, map position, and gene expression reveals conserved essential genes for iron uptake in *Arabidopsis* and tomato. *Plant Physiol.* 136, 4169–4183. doi: 10.1104/pp.104.047233

Bellegarde, F., Herbert, L., Séré, D., Caillieux, E., Boucherez, J., Fizames, C., et al. (2018). Polycomb repressive complex 2 attenuates the very high expression of the *Arabidopsis* gene NRT2.1. *Sci. Rep.* 8:7905. doi: 10.1038/s41598-018-26349-w

Benhamed, M., Martin-Magniette, M.-L., Taconnat, L., Bitton, F., Servet, C., De Clercq, R., et al. (2008). Genome-scale *Arabidopsis* promoter array identifies targets of the histone acetyltransferase GCN5. *Plant J.* 56, 493–504. doi: 10.1111/j.1365-313X.2008.03606.x

Bouveret, R., Schönrock, N., Gruissem, W., and Hennig, L. (2006). Regulation of flowering time by *Arabidopsis* MSI1. *Development* 133, 1693–1702. doi: 10.1242/dev.02340

Bouyer, D., Roudier, F., Heese, M., Andersen, E. D., Gey, D., Nowack, M. K., et al. (2011). Polycomb repressive complex 2 controls the embryo-to-seedling phase transition. *PLoS Genet.* 7:e1002014. doi: 10.1371/journal.pgen.1002014

Bowman, J. L., Smyth, D. R., and Meyerowitz, E. M. (1989). Genes directing flower development in *Arabidopsis*. *Plant Cell* 1, 37–52. doi: 10.1105/tpc.1.1.37

Buckhout, T. J., Yang, T. J. W., and Schmidt, W. (2009). Early iron-deficiency-induced transcriptional changes in *Arabidopsis* roots as revealed by microarray analyses. *BMC Genomics* 10:147. doi: 10.1186/1471-2164-10-147

Chanvivattana, Y., Bishopp, A., Schubert, D., Stock, C., Moon, Y.-H., Sung, Z. R., et al. (2004). Interaction of Polycomb-group proteins controlling flowering in *Arabidopsis*. *Development* 131, 5263–5276. doi: 10.1242/dev.01400

Clemens, S., and Weber, M. (2016). The essential role of coumarin secretion for Fe acquisition from alkaline soil. *Plant Signal. Behav.* 11:e1114197. doi: 10.1080/15592324.2015.1114197

Colangelo, E. P., and Guerinot, M. L. (2004). The essential basic helix-loop-helix protein FIT1 is required for the iron deficiency response. *Plant Cell* 16, 3400–3412. doi: 10.1105/tpc.104.024315

Colombo, C., Palumbo, G., He, J.-Z., Pinton, R., and Cesco, S. (2014). Review on iron availability in soil: interaction of Fe minerals, plants, and microbes. *J. Soils Sediments* 14, 538–548. doi: 10.1007/s11368-013-0814-z

Connolly, E. L., Campbell, N. H., Grotz, N., Prichard, C. L., and Guerinot, M. L. (2003). Overexpression of the FRO2 ferric chelate reductase confers tolerance to growth on low iron and uncovers posttranscriptional control. *Plant Physiol.* 133, 1102–1110. doi: 10.1104/pp.103.025122

Connolly, E. L., Fett, J. P., and Guerinot, M. L. (2002). Expression of the IRT1 metal transporter is controlled by metals at the levels of transcript and protein accumulation. *Plant Cell* 14, 1347–1357. doi: 10.1105/tpc.001263

Cui, Y., Chen, C.-L., Cui, M., Zhou, W.-J., Wu, H.-L., and Ling, H.-Q. (2018). Four IVa bHLH transcription factors are novel interactors of FIT and mediate

JA inhibition of iron uptake in *Arabidopsis*. *Mol. Plant* 11, 1166–1183. doi: 10.1016/j.molp.2018.06.005

de Lucas, M., Pu, L., Turco, G., Gaudinier, A., Morao, A. K., Harashima, H., et al. (2016). Transcriptional regulation of *Arabidopsis* polycomb repressive complex 2 coordinates cell-type proliferation and differentiation. *Plant Cell* 28, 2616–2631. doi: 10.1105/tpc.15.00744

Dinneny, J. R., Long, T. A., Wang, J. Y., Jung, J. W., Mace, D., Pointer, S., et al. (2008). Cell identity mediates the response of *Arabidopsis* roots to abiotic stress. *Science* 320, 942–945. doi: 10.1126/science.1153795

Dubeaux, G., Neveu, J., Zelazny, E., and Vert, G. (2018). Metal sensing by the IRT1 transporter-receptor orchestrates its own degradation and plant metal nutrition. *Mol. Cell* 69, 953–964.e5. doi: 10.1016/j.molcel.2018.02.009

Durrett, T. P., Gassmann, W., and Rogers, E. E. (2007). The FRD3-mediated efflux of citrate into the root vasculature is necessary for efficient iron translocation. *Plant Physiol.* 144, 197–205. doi: 10.1104/pp.107.097162

Earley, K. W., Shook, M. S., Brower-Toland, B., Hicks, L., and Pikaard, C. S. (2007). In vitro specificities of *Arabidopsis* co-activator histone acetyltransferases: implications for histone hyperacetylation in gene activation. *Plant J.* 52, 615–626. doi: 10.1111/j.1365-313X.2007.03264.x

Edgar, R., Domrachev, M., and Lash, A. E. (2002). Gene Expression omnibus: NCBI gene expression and hybridization array data repository. *Nucleic Acids Res.* 30, 207–210. doi: 10.1093/nar/30.1.207

Fan, H., Zhang, Z., Wang, N., Cui, Y., Sun, H., Liu, Y., et al. (2014). SKB1/PRMT5-mediated histone H4R3 dimethylation of Ib subgroup bHLH genes negatively regulates iron homeostasis in *Arabidopsis thaliana*. *Plant J.* 77, 209–221. doi: 10.1111/tpj.12380

Farnham, P. J. (2009). Insights from genomic profiling of transcription factors. *Nat. Rev. Genet.* 10, 605–616. doi: 10.1038/nrg2636

Fourcroy, P., Sisó-Terraza, P., Sudre, D., Savirón, M., Reyt, G., Gaymard, F., et al. (2014). Involvement of the ABCG37 transporter in secretion of scopoletin and derivatives by *Arabidopsis* roots in response to iron deficiency. *New Phytol.* 201, 155–167. doi: 10.1111/nph.12471

Gao, F., Robe, K., Gaymard, F., Izquierdo, E., and Dubos, C. (2019). The transcriptional control of iron homeostasis in plants: a tale of bHLH transcription factors? *Front. Plant Sci.* 10:6. doi: 10.3389/fpls.2019.00006

Goodrich, J., Puangsomlee, P., Martin, M., Long, D., Meyerowitz, E. M., and Coupland, G. (1997). A polycomb-group gene regulates homeotic gene expression in *Arabidopsis*. *Nature* 386, 44–51. doi: 10.1038/386044a0

Gratz, R., Manishankar, P., Ivanov, R., Köster, P., Mohr, I., Trofimov, K., et al. (2019). CIPK11-dependent phosphorylation modulates FIT activity to promote *Arabidopsis* iron acquisition in response to calcium signaling. *Dev. Cell* 48, 726–740.e10. doi: 10.1016/j.devcel.2019.01.006

Grillet, L., Lan, P., Li, W., Mokkapati, G., and Schmidt, W. (2018). IRON MAN is a ubiquitous family of peptides that control iron transport in plants. *Nat. Plants* 4, 953–963. doi: 10.1038/s41477-018-0266-y

Halliwell, B., and Gutteridge, J. M. (1992). Biologically relevant metal ion-dependent hydroxyl radical generation. An update. *FEBS Lett.* 307, 108–112. doi: 10.1016/0014-5793(92)80911-Y

Haring, M., Offermann, S., Danker, T., Horst, I., Peterhansel, C., and Stam, M. (2007). Chromatin immunoprecipitation: optimization, quantitative analysis and data normalization. *Plant Methods* 3:11. doi: 10.1186/1746-4811-3-11

Hirayama, T., Lei, G. J., Yamaji, N., Nakagawa, N., and Ma, J. F. (2018). The putative peptide gene FEP1 regulates iron deficiency response in *Arabidopsis*. *Plant Cell Physiol.* doi: 10.1093/pcp/pcy145 [Epub ahead of print].

Jakoby, M., Wang, H.-Y., Reidt, W., Weisshaar, B., and Bauer, P. (2004). FRU (BHLH029) is required for induction of iron mobilization genes in *Arabidopsis thaliana*. *FEBS Lett.* 577, 528–534. doi: 10.1016/j.febslet.2004.10.062

Jeong, J., and Connolly, E. L. (2009). Iron uptake mechanisms in plants: functions of the FRO family of ferric reductases. *Plant Sci.* 176, 709–714. doi: 10.1016/j.plantsci.2009.02.011

Jeong, J., Merkovich, A., Clyne, M., and Connolly, E. L. (2017). Directing iron transport in dicots: regulation of iron acquisition and translocation. *Curr. Opin. Plant Biol.* 39, 106–113. doi: 10.1016/j.pbi.2017.06.014

Katz, A., Oliva, M., Mosquna, A., Hakim, O., and Ohad, N. (2004). FIE and CURLY LEAF polycomb proteins interact in the regulation of homeobox gene expression during sporophyte development. *Plant J.* 37, 707–719. doi: 10.1111/j.1365-313X.2003.01996.x

Kerkeb, L., Mukherjee, I., Chatterjee, I., Lahner, B., Salt, D. E., and Connolly, E. L. (2008). Iron-induced turnover of the *Arabidopsis* iron-regulated transporter1 metal transporter requires lysine residues. *Plant Physiol.* 146, 1964–1973. doi: 10.1104/pp.107.113282

Köhler, C., and Hennig, L. (2010). Regulation of cell identity by plant Polycomb and trithorax group proteins. *Curr. Opin. Genet. Dev.* 20, 541–547. doi: 10.1016/j.gde.2010.04.015

Lafos, M., Kroll, P., Hohenstatt, M. L., Thorpe, F. L., Clarenz, O., and Schubert, D. (2011). Dynamic regulation of H3K27 trimethylation during *Arabidopsis* differentiation. *PLoS Genet.* 7:e1002040. doi: 10.1371/journal.pgen.1002040

Lee, J., Yun, J.-Y., Zhao, W., Shen, W.-H., and Amasino, R. M. (2015). A methyltransferase required for proper timing of the vernalization response in *Arabidopsis*. *Proc. Natl. Acad. Sci. U.S.A.* 112, 2269–2274. doi: 10.1073/pnas.1423585112

Li, B., Carey, M., and Workman, J. L. (2007). The role of chromatin during transcription. *Cell* 128, 707–719. doi: 10.1016/j.cell.2007.01.015

Li, X., Zhang, H., Ai, Q., Liang, G., and Yu, D. (2016). Two bHLH transcription factors, bHLH34 and bHLH104, regulate iron homeostasis in *Arabidopsis thaliana*. *Plant Physiol.* 170, 2478–2493. doi: 10.1104/pp.15.01827

Lingam, S., Mohrbacher, J., Brumbarova, T., Potuschak, T., Fink-Straube, C., Blondet, E., et al. (2011). Interaction between the bHLH transcription factor FIT and ethylene insensitive3/ethylene insensitive3-like1 reveals molecular linkage between the regulation of iron acquisition and ethylene signaling in *Arabidopsis*. *Plant Cell* 23, 1815–1829. doi: 10.1105/tpc.111.084715

Long, T. A., Tsukagoshi, H., Busch, W., Lahner, B., Salt, D. E., and Benfey, P. N. (2010). The bHLH transcription factor POPEYE regulates response to iron deficiency in *Arabidopsis* roots. *Plant Cell* 22, 2219–2236. doi: 10.1105/tpc.110.074096

Lu, F., Cui, X., Zhang, S., Jenuwein, T., and Cao, X. (2011). *Arabidopsis* REF6 is a histone H3 lysine 27 demethylase. *Nat. Genet.* 43, 715–719. doi: 10.1038/ng.854

Mai, H.-J., Pateyron, S., and Bauer, P. (2016). Iron homeostasis in *Arabidopsis thaliana*: transcriptomic analyses reveal novel FIT-regulated genes, iron deficiency marker genes and functional gene networks. *BMC Plant Biol.* 16:211. doi: 10.1186/s12870-016-0899-9

Margueron, R., and Reinberg, D. (2011). The Polycomb complex PRC2 and its mark in life. *Nature* 469, 343–349. doi: 10.1038/nature09784

Marschner, P. (2012). *Marschner's Mineral Nutrition of Higher Plants*, 3rd Edn. Cambridge, MA: Academic Press.

Meiser, J., Lingam, S., and Bauer, P. (2011). Posttranslational regulation of the iron deficiency basic helix-loop-helix transcription factor FIT is affected by iron and nitric oxide. *Plant Physiol.* 157, 2154–2166. doi: 10.1104/pp.111.183285

Mi, H., Huang, X., Muruganujan, A., Tang, H., Mills, C., Kang, D., et al. (2017). PANTHER version 11: expanded annotation data from gene ontology and reactome pathways, and data analysis tool enhancements. *Nucleic Acids Res.* 45, D183–D189. doi: 10.1093/nar/gkw1138

Michaels, S. D., and Amasino, R. M. (1999). FLOWERING LOCUS C encodes a novel MADS domain protein that acts as a repressor of flowering. *Plant Cell* 11, 949–956. doi: 10.1105/tpc.11.5.949

Naranjo-Arcos, M. A., Maurer, F., Meiser, J., Pateyron, S., Fink-Straube, C., and Bauer, P. (2017). Dissection of iron signaling and iron accumulation by overexpression of subgroup Ib bHLH039 protein. *Sci. Rep.* 7:10911. doi: 10.1038/s41598-017-11171-7

Probst, A. V., and Mittelsten Scheid, O. (2015). Stress-induced structural changes in plant chromatin. *Curr. Opin. Plant Biol.* 27, 8–16. doi: 10.1016/j.pbi.2015.05.011

Pu, L., and Sung, Z. R. (2015). PcG and trxG in plants - friends or foes. *Trends Genet.* 31, 252–262. doi: 10.1016/j.tig.2015.03.004

Ravet, K., Touraine, B., Boucherez, J., Briat, J.-F., Gaymard, F., and Cellier, F. (2009). Ferritins control interaction between iron homeostasis and oxidative stress in *Arabidopsis*. *Plant J.* 57, 400–412. doi: 10.1111/j.1365-313X.2008.03698.x

Robinson, J. T., Thorvaldsdóttir, H., Winckler, W., Guttman, M., Lander, E. S., Getz, G., et al. (2011). Integrative genomics viewer. *Nat. Biotechnol.* 29, 24–26. doi: 10.1038/nbt.1754

Robinson, N. J., Procter, C. M., Connolly, E. L., and Guerinot, M. L. (1999). A ferric-chelate reductase for iron uptake from soils. *Nature* 397, 694–697. doi: 10.1038/17800

Rodríguez-Celma, J., Pan, I. C., Li, W., Lan, P., Buckhout, T. J., and Schmidt, W. (2013). The transcriptional response of *Arabidopsis* leaves to Fe deficiency. *Front. Plant Sci.* 4:276. doi: 10.3389/fpls.2013.00276

Roudier, F., Ahmed, I., Bérard, C., Sarazin, A., Mary-Huard, T., Cortijo, S., et al. (2011). Integrative epigenomic mapping defines four main chromatin states in *Arabidopsis*. *EMBO J.* 30, 1928–1938. doi: 10.1038/emboj.2011.103

Santi, S., and Schmidt, W. (2009). Dissecting iron deficiency-induced proton extrusion in *Arabidopsis* roots. *New Phytol.* 183, 1072–1084. doi: 10.1111/j.1469-8137.2009.02908.x

Schmittgen, T. D., and Livak, K. J. (2008). Analyzing real-time PCR data by the comparative CT method. *Nat. Protoc.* 3, 1101–1108. doi: 10.1038/nprot.2008.73

Schönrock, N., Bouveret, R., Leroy, O., Borghi, L., Köhler, C., Gruissem, W., et al. (2006). Polycomb-group proteins repress the floral activator AGL19 in the FLC-independent vernalization pathway. *Genes Dev.* 20, 1667–1678. doi: 10.1101/gad.377206

Schubert, D., Primavesi, L., Bishopp, A., Roberts, G., Doonan, J., Jenuwein, T., et al. (2006). Silencing by plant Polycomb-group genes requires dispersed trimethylation of histone H3 at lysine 27. *EMBO J.* 25, 4638–4649. doi: 10.1038/sj.emboj.7601311

Secco, D., Whelan, J., Rouached, H., and Lister, R. (2017). Nutrient stress-induced chromatin changes in plants. *Curr. Opin. Plant Biol.* 39, 1–7. doi: 10.1016/j.pbi.2017.04.001

Shin, L.-J., Lo, J.-C., Chen, G.-H., Callis, J., Fu, H., and Yeh, K.-C. (2013). IRT1 degradation factor1, a ring E3 ubiquitin ligase, regulates the degradation of iron-regulated transporter1 in *Arabidopsis*. *Plant Cell* 25, 3039–3051. doi: 10.1105/tpc.113.115212

Sivitz, A., Grinvalds, C., Barberon, M., Curie, C., and Vert, G. (2011). Proteasome-mediated turnover of the transcriptional activator FIT is required for plant iron-deficiency responses. *Plant J.* 66, 1044–1052. doi: 10.1111/j.1365-313X.2011.04565.x

Sivitz, A. B., Hermand, V., Curie, C., and Vert, G. (2012). *Arabidopsis* bHLH100 and bHLH101 control iron homeostasis via a FIT-independent pathway. *PLoS One* 7:e44843. doi: 10.1371/journal.pone.0044843

Tanabe, N., Noshi, M., Mori, D., Nozawa, K., Tamoi, M., and Shigeoka, S. (2018). The basic helix-loop-helix transcription factor, bHLH11 functions in the iron-uptake system in *Arabidopsis thaliana*. *J. Plant Res.* 132, 93–105. doi: 10.1007/s10265-018-1068-z

The Gene Ontology Consortium (2017). Expansion of the gene ontology knowledgebase and resources. *Nucleic Acids Res.* 45, D331–D338. doi: 10.1093/nar/gkw1108

Thorvaldsdóttir, H., Robinson, J. T., and Mesirov, J. P. (2013). Integrative genomics viewer (IGV): high-performance genomics data visualization and exploration. *Brief Bioinform.* 14, 178–192. doi: 10.1093/bib/bbs017

Turck, F., Roudier, F., Farrona, S., Martin-Magniette, M.-L., Guillaume, E., Buisine, N., et al. (2007). *Arabidopsis* TFL2/LHP1 specifically associates with genes marked by trimethylation of histone H3 lysine 27. *PLoS Genet.* 3:e86. doi: 10.1371/journal.pgen.0030086

Varotto, C., Maiwald, D., Pesaresi, P., Jahns, P., Salamini, F., and Leister, D. (2002). The metal ion transporter IRT1 is necessary for iron homeostasis and efficient photosynthesis in *Arabidopsis thaliana*. *Plant J.* 31, 589–599. doi: 10.1046/j.1365-313X.2002.01381.x

Vert, G., Grotz, N., Dédaldéchamp, F., Gaymard, F., Guerinot, M. L., Briat, J.-F., et al. (2002). IRT1, an *Arabidopsis* transporter essential for iron uptake from the soil and for plant growth. *Plant Cell* 14, 1223–1233. doi: 10.1105/tpc.001388

Vlachonasios, K. E., Thomashow, M. F., and Triezenberg, S. J. (2003). Disruption mutations of ADA2b and GCN5 transcriptional adaptor genes dramatically affect *Arabidopsis* growth, development, and gene expression. *Plant Cell* 15, 626–638. doi: 10.1105/tpc.007922

Wang, H., Liu, C., Cheng, J., Liu, J., Zhang, L., He, C., et al. (2016). *Arabidopsis* flower and embryo developmental genes are repressed in seedlings by different combinations of polycomb group proteins in association with distinct sets of Cis-regulatory elements. *PLoS Genet.* 12:e1005771. doi: 10.1371/journal.pgen.1005771

Wang, N., Cui, Y., Liu, Y., Fan, H., Du, J., Huang, Z., et al. (2013). Requirement and functional redundancy of Ib subgroup bHLH proteins for iron deficiency responses and uptake in *Arabidopsis thaliana*. *Mol. Plant* 6, 503–513. doi: 10.1093/mp/sss089

Wild, M., Davière, J.-M., Regnault, T., Sakvarelidze-Achard, L., Carrera, E., Lopez Diaz, I., et al. (2016). Tissue-specific regulation of gibberellin signaling fine-tunes *Arabidopsis* iron-deficiency responses. *Dev. Cell* 37, 190–200. doi: 10.1016/j.devcel.2016.03.022

Xing, J., Wang, T., Liu, Z., Xu, J., Yao, Y., Hu, Z., et al. (2015). General control nonrepressed protein5-mediated histone acetylation of ferric reductase defective3 contributes to iron homeostasis in *Arabidopsis*. *Plant Physiol.* 168, 1309–1320. doi: 10.1104/pp.15.00397

Xu, L., and Shen, W.-H. (2008). Polycomb silencing of KNOX genes confines shoot stem cell niches in *Arabidopsis*. *Curr. Biol.* 18, 1966–1971. doi: 10.1016/j.cub.2008.11.019

Yanofsky, M. F., Ma, H., Bowman, J. L., Drews, G. N., Feldmann, K. A., and Meyerowitz, E. M. (1990). The protein encoded by the *Arabidopsis* homeotic gene agamous resembles transcription factors. *Nature* 346, 35–39. doi: 10.1038/346035a0

Ye, J., Coulouris, G., Zaretskaya, I., Cutcutache, I., Rozen, S., and Madden, T. L. (2012). Primer-BLAST: a tool to design target-specific primers for polymerase chain reaction. *BMC Bioinform.* 13:134. doi: 10.1186/1471-2105-13-134

Yuan, Y., Wu, H., Wang, N., Li, J., Zhao, W., Du, J., et al. (2008). FIT interacts with AtbHLH38 and AtbHLH39 in regulating iron uptake gene expression for iron homeostasis in *Arabidopsis*. *Cell Res.* 18, 385–397. doi: 10.1038/cr.2008.26

Yuan, Y. X., Zhang, J., Wang, D. W., and Ling, H. Q. (2005). AtbHLH29 of *Arabidopsis thaliana* is a functional ortholog of tomato FER involved in controlling iron acquisition in strategy I plants. *Cell Res.* 15, 613–621. doi: 10.1038/sj.cr.7290331

Zhang, X., Clarenz, O., Cokus, S., Bernatavichute, Y. V., Pellegrini, M., Goodrich, J., et al. (2007). Whole-genome analysis of histone H3 lysine 27 trimethylation in *Arabidopsis*. *PLoS Biol.* 5:e129. doi: 10.1371/journal.pbio.0050129

Zhao, W., Shafiq, S., Berr, A., and Shen, W.-H. (2015). Genome-wide gene expression profiling to investigate molecular phenotypes of *Arabidopsis* mutants deprived in distinct histone methyltransferases and demethylases. *Genomics Data* 4, 143–145. doi: 10.1016/j.gdata.2015.04.006

Zhou, Y., Wang, Y., Krause, K., Yang, T., Dongus, J. A., Zhang, Y., et al. (2018). Telobox motifs recruit CLF/SWN-PRC2 for H3K27me3 deposition via TRB factors in *Arabidopsis*. *Nat. Genet.* 50, 638–644. doi: 10.1038/s41588-018-0109-9

Conflict of Interest Statement: The authors declare that the research was conducted in the absence of any commercial or financial relationships that could be construed as a potential conflict of interest.

frontiers in Plant Science

MINI REVIEW
published: 22 May 2019
doi: 10.3389/fpls.2019.00675

Humic Substances Contribute to Plant Iron Nutrition Acting as Chelators and Biostimulants

*Laura Zanin[1], Nicola Tomasi[1], Stefano Cesco[2], Zeno Varanini[3] and Roberto Pinton[1]**

[1] Dipartimento di Scienze AgroAlimentari, Ambientali e Animali, Università degli Studi di Udine, Udine, Italy, [2] Faculty of Science and Technology, Free University of Bozen-Bolzano, Bolzano, Italy, [3] Dipartimento di Biotecnologie, Università di Verona, Verona, Italy

Improvement of plant iron nutrition as a consequence of metal complexation by humic substances (HS) extracted from different sources has been widely reported. The presence of humified fractions of the organic matter in soil sediments and solutions would contribute, depending on the solubility and the molecular size of HS, to build up a reservoir of Fe available for plants which exude metal ligands and to provide Fe-HS complexes directly usable by plant Fe uptake mechanisms. It has also been shown that HS can promote the physiological mechanisms involved in Fe acquisition acting at the transcriptional and post-transcriptional level. Furthermore, the distribution and allocation of Fe within the plant could be modified when plants were supplied with water soluble Fe-HS complexes as compared with other natural or synthetic chelates. These effects are in line with previous observations showing that treatments with HS were able to induce changes in root morphology and modulate plant membrane activities related to nutrient acquisition, pathways of primary and secondary metabolism, hormonal and reactive oxygen balance. The multifaceted action of HS indicates that soluble Fe-HS complexes, either naturally present in the soil or exogenously supplied to the plants, can promote Fe acquisition in a complex way by providing a readily available iron form in the rhizosphere and by directly affecting plant physiology. Furthermore, the possibility to use Fe-HS of different sources, size and solubility may be considered as an environmental-friendly tool for Fe fertilization of crops.

Keywords: Fe complex, Fe chelates, fulvic acids, root uptake, strategy I, strategy II, water-extractable humic substances (WEHS)

OPEN ACCESS

Edited by:
Thomas J. Buckhout, Humboldt University of Berlin, Germany

Reviewed by:
Marta Fuentes, University of Navarra, Spain
Youry Pii, Free University of Bozen-Bolzano, Italy

****Correspondence:***
Roberto Pinton
roberto.pinton@uniud.it

Specialty section:
This article was submitted to Plant Nutrition, a section of the journal Frontiers in Plant Science

Received: *05 February 2019*
Accepted: *06 May 2019*
Published: *22 May 2019*

Citation:
Zanin L, Tomasi N, Cesco S, Varanini Z and Pinton R (2019) Humic Substances Contribute to Plant Iron Nutrition Acting as Chelators and Biostimulants. Front. Plant Sci. 10:675. doi: 10.3389/fpls.2019.00675

Abbreviations: ABA, abscisic acid; CK, cytokinins; DOM, dissolved organic matter; ET, ethylene; FA, fluvic acids; FRO, ferric chelate reductase; GA, gibberellic acid; HA, humic acids; HS, humic substances; IAA, indole-3-acetic acids; IHS, insoluble HS; IRT, iron transporter; NO, nitric oxide; NRAMP, natural resistance-associated macrophage proteins; PS, phytosiderophores; ROS, reactive oxygen species; TCA, tricarboxylic acid; WEHS, water extractable humic substances.

INTRODUCTION

Soil HS are generally considered as the result of the partial degradation and re-synthesis of organic material, especially of plant residues. They originate from polymerization/polycondensation of phenolic compounds, mainly deriving from microbial lignin degradation. As a consequence, soil HS have a strong aromatic nature; nonetheless, during the condensation process a number of organic molecules including aliphatic chains, peptides, amino acids, fatty acids and sugars can be incorporated, thus forming substances from medium to high molecular weight (Stevenson, 1994). Soil HS could also originate from associations of relatively small humic molecules linked together by hydrophobic interactions and hydrogen bonds (Piccolo, 2002). Humic molecules of different molecular masses can bind together forming a supramolecular humic network; the degree of aggregation may depend on the pH, ionic strength and mineral composition of the solution (Garcia-Mina, 2007; Esfahani et al., 2015).

These processes imply that HS of different molecular size and solubility are present in the soil. Some fractions are present in the soil solution, thus being able to directly interact with plant roots (Chen and Schnitzer, 1978; Gerke, 1997). These latter soluble HS are considered as part of the DOM (Bolan et al., 2011).

Humic substances are routinely extracted from the soil with alkaline solutions and then can be operationally fractionated, based on their different water solubility, into humic (HA) and fluvic (FA) acids (Stevenson, 1994).

Due to their heterogeneity, the molecular structure of soil HS cannot be unequivocally identified. Nevertheless, it has been clearly defined that the presence of some functional groups within their structure are responsible for the observed indirect and direct effects on plant growth and nutrition (Nebbioso and Piccolo, 2011; Muscolo et al., 2013; García et al., 2016a). Indirect effects refer to changes in the chemical and physical properties of soil and rhizosphere, while direct ones indicate actions on plasma membrane (PM)-bound activities and plant metabolic pathways (Varanini and Pinton, 2001; Nardi et al., 2002; Zandonadi et al., 2013; Canellas and Olivares, 2014; Rose et al., 2014; Olaetxea et al., 2018).

The occurrence of HS in soils, as representative of natural organic matter evolution, has been questioned; rather it has been proposed that they are the result of the alkali-based extraction procedure (Lehmann and Kleber, 2015). While this aspect is still under debate (Gerke, 2018; Olk et al., 2019), it is noteworthy that humic-like molecules have been extracted from soils treated with mild extractants (Hayes, 2006), found in aquatic environments (Alberts and Takács, 2004), peat water extracts and soil leachates (Pinton et al., 1997; Vujinovic et al., 2013).

Despite being the chemical nature of HS still controversial, it has been unequivocally demonstrated that organic materials of different origin can provide available Fe to plants as a results of Fe complexation by humic molecules (Chen et al., 2004a; Bocanegra et al., 2006; Kovács et al., 2013; Cieschi et al., 2017). Furthermore, soluble Fe-HS complexes could be formed and directly used by the plants (Pandeya et al., 1998; Pinton et al., 1999). The capacity of HS to complex metals and affect the mechanisms of nutrient acquisition and plant metabolism provide evidence for a multifaceted role of these organic fractions on Fe nutrition.

In the present work, we will summarize recent reports on the role of HS in plant Fe nutrition that can be attributed to their chelating and biostimulant effect, with a special emphasis on effects exerted by the water-soluble fractions.

EFFECTS OF HUMIC SUBSTANCES ON IRON AVAILABILITY

Humic substances are able to form stable complexes with metal micronutrients, due to the presence in their structure of oxygen-, nitrogen- and sulfur-containing functional groups. This, in turn, would help maintaining micronutrients in solution and/or in bioavailable forms at pH values found in most soils (Senesi, 1992; Tipping, 2002). In the case of Fe, highly stable HS complexes mainly involve O-containing groups (carboxylic and phenolic groups) (Senesi, 1992; Tipping, 2002). More recently it was shown that carboxylic acids in aliphatic domains are also involved in Fe(III)-HS complexation (Fuentes et al., 2013).

The stability order of the complexes formed between metals and humic acids has been determined through potentiometric titration and follows the Irving-Williams series. Evaluation of stability constants for metal-HS complexes (Garcia-Mina et al., 2004) showed values somewhat lower than those observed for complexes between Fe and synthetic chelating agents (e.g., EDTA, EDDHA; Lucena, 2003) or organic compounds of biological origin (e.g., organic acids, siderophores, PS, phenols) (von Wirén et al., 2000; Crowley, 2001; Ryan et al., 2001; Mimmo et al., 2014).

Stability and solubility of the complexes are both affected by pH and molar ratio between micronutrients and HS (Chen et al., 2004a; Garcia-Mina, 2006). A high stability would be favored in the 5–9 pH range by a low metal:HS ratio, while a high solubility would be favored by alkaline pH and a low metal:HS ratio. This implies that plants growing in calcareous soils with limited Fe availability could benefit from the formation of stable and soluble Fe-HS complexes (Cieschi and Lucena, 2018), as well as of insoluble complexes with high molecular weight HS (Colombo et al., 2014).

Humic substances can affect Fe availability also through the stabilization of amorphous Fe oxides by high molecular weight humic fractions (Schwertmann, 1991). The poorly crystalline Fe phases, co-precipitated with insoluble HS (IHS) and maintained for a long period in this form, can represent a reservoir of iron suitable, *via* ligand mobilization, for plant Fe nutrition (Colombo et al., 2012, 2014).

The ability of HS to complex Fe can also be important for phosphorous nutrition, since phosphate can be bound to HS by Fe bridges (Gerke, 2010; Urrutia et al., 2013). This process would increase phosphate availability; in fact, complexation of Fe by ligands released by plant roots could promote uptake of both nutrients (Gerke, 1993; Urrutia et al., 2014).

Humic substances are known to be redox reactive and capable of chemically reducing metals including Fe^{3+} (Skogerboe and Wilson, 1981; Struyk and Sposito, 2001). Reduction of Fe^{3+} occurs at significant levels at pH values lower than 4; at higher pH

values reduction is limited by formation of complexes between Fe^{3+} and humic molecules. It has been shown that dissolved and solid-phase HS can accelerate Fe(III)-oxide reduction in sediments (Nevin and Lovley, 2002; Roden et al., 2010) and bioreduction of Fe(III) minerals in soils (Rakshit et al., 2009), by shuttling electrons from bacteria to oxide surfaces.

ROLE OF HUMIC SUBSTANCES AS NATURAL CHELATES

Besides delaying the Fe crystallization processes, HS can contribute to Fe nutrition via formation of water-soluble Fe-HS complexes, which can move in the soil and reach the roots (Pandeya et al., 1998; Garcia-Mina et al., 2004; Chen et al., 2004b). These complexes would act as natural Fe-chelates interacting with plant uptake mechanisms. Using a water-extractable humic fraction (WEHS), purified from a water extract of sphagnum peat, it was demonstrated that a Fe-WEHS complex could be obtained by interaction between the humic fraction and a poorly soluble Fe form (Cesco et al., 2000). Fe-WEHS complex could, in turn, be used by Fe-deficient Strategy-I and Strategy-II plants. Uptake by Strategy-I plants could occur via the Fe(III) reduction-based mechanism (Pinton et al., 1999), while in Strategy-II plants, a ligand exchange between WEHS and PS was conceivably involved (Cesco et al., 2002). Uptake of ^{59}Fe from ^{59}Fe-WEHS complex was measured even at pH values compatible with those found in calcareous soils (Cesco et al., 2002; Tomasi et al., 2013) and the same held true for root Fe(III) reduction in Strategy-I plants (Tomasi et al., 2013; Zamboni et al., 2016). The recovery of Fe-deficient plants following the treatment with Fe-WEHS was paralleled by a stimulation of the acidification capacity of roots, a component of the Fe-deficiency response in Strategy-I plants (Pinton et al., 1999; Tomasi et al., 2013).

Iron from ^{59}Fe-WEHS complex appeared to be accumulated in higher amount within the plant as compared with other natural chelates, such as ^{59}Fe-citrate or ^{59}Fe-PS (Tomasi et al., 2013; Zamboni et al., 2016). Furthermore, a higher translocation of Fe to the leaves was observed in Fe-deficient Strategy-I plants supplied with ^{59}Fe-WEHS (Tomasi et al., 2009; Zanin et al., 2015) as compared with the other two natural Fe-chelates. This behavior was accompanied by an increase of Fe content in the xylem sap (Tomasi et al., 2009). In ^{59}Fe-WEHS-treated cucumber plants Fe was more rapidly allocated into the leaf veins and transferred to interveinal cells (Zanin et al., 2015). Similar effects were reported by Bocanegra et al. (2006) who observed a rapid translocation of Fe from roots to leaves of plants treated with a low molecular weight humic fraction. These results indicate that HS could affect Fe nutrition not only by increasing the metal availability in the soil and in the rhizosphere, but also acting on the mechanisms involved in its uptake and its translocation within the plant.

Supply of HS or Fe-HS complexes has also been shown to affect expression of genes related to Fe-uptake mechanisms. Providing a Fe-WEHS complex to Fe-deficient tomato plants induced an up-regulation of root Fe(III)-chelate reductase (*LeFRO1*) and Fe transporter genes, *LeIRT1* and *LeIRT2* (Tomasi et al., 2013). The increase in transcript abundance was faster and reached a higher level than when Fe-citrate or Fe-PS were used. Aguirre et al. (2009) showed that the treatment of cucumber plants with HS purified from leonardite induced a transient up-regulation of genes involved in the Strategy-I uptake mechanism, that is *CsHA2*, *CsFRO1* and *CsIRT1*, in cucumber roots. These effects were associated with an increase of the root Fe(III) chelate-reductase activity. Billard et al. (2013) showed that a humic fraction isolated from black peat could induce the up-regulation of the *IRT1* gene in both the roots and leaves of rapeseed plants. These results were correlated to a significant increase of the Fe concentration in leaves.

Interestingly, also genes involved in Fe uptake in leaves (*CsFRO1*, *CsIRT1*, *CsNRAMP*) were up-regulated following Fe-WEHS supply to Fe-deficient cucumber plants, as compared with Fe-PS-fed plants (Zanin et al., 2015). The localization of *CsFRO1*, *CsIRT1* transcripts was evident next to the midveins, while *CsNRAMP* expression was detected in the overall mesophyll region, supporting a role of this later gene in the Fe distribution within the whole leaf tissue.

Genome-wide transcriptional analysis revealed that the early response to Fe supply of Fe-deficient tomato plants was strongly influenced by the nature of the chelating agent (Zamboni et al., 2016). In fact, Fe-citrate and Fe-PS modulated, respectively the expression of 728 and 408 genes, showing a fast down-regulation of molecular mechanisms induced by Fe deficiency. On the other hand, Fe-WEHS did not determine relevant changes in the root transcriptome with respect to the Fe-deficient plants, suggesting that roots did not sense the restored cellular Fe accumulation. This behavior would account for the higher Fe accumulation in Fe-WEHS treated plants.

EFFECTS OF HUMIC SUBSTANCES ON ROOT GROWTH AND FUNCTIONS

Treatments of plants with HS have been shown to induce changes in root morphology and modulate plant membrane activities related to nutrient acquisition, pathways of primary and secondary metabolism, hormonal and reactive oxygen balance (Varanini and Pinton, 2001; Nardi et al., 2002; Canellas and Olivares, 2014; Olaetxea et al., 2018; **Figure 1**). These effects, which vary depending on the origin, molecular size and chemical characteristics of HS, suggest an action of these organic fractions on growth promotion and stress resistance in plants.

Many authors observed that plants treated with HS of different origin were able to induce proliferation of lateral roots and root hairs (Canellas et al., 2002; Nardi et al., 2002). This behavior has been related to the activation of signaling pathways involving phytohormones, especially auxin, nitric oxide, Ca^{2+} and ROS (Trevisan et al., 2010; Zandonadi et al., 2010; Mora et al., 2012; Ramos et al., 2015; García et al., 2016b,c). Up-regulation of auxin-regulated genes (Trevisan et al., 2011) and modulation of genes coding for enzymes involved in hormone metabolisms (Zanin et al., 2018) suggest that HS might influence the steady-state equilibrium of different plant hormones. However, stimulation of root growth was observed also independently of hormonal

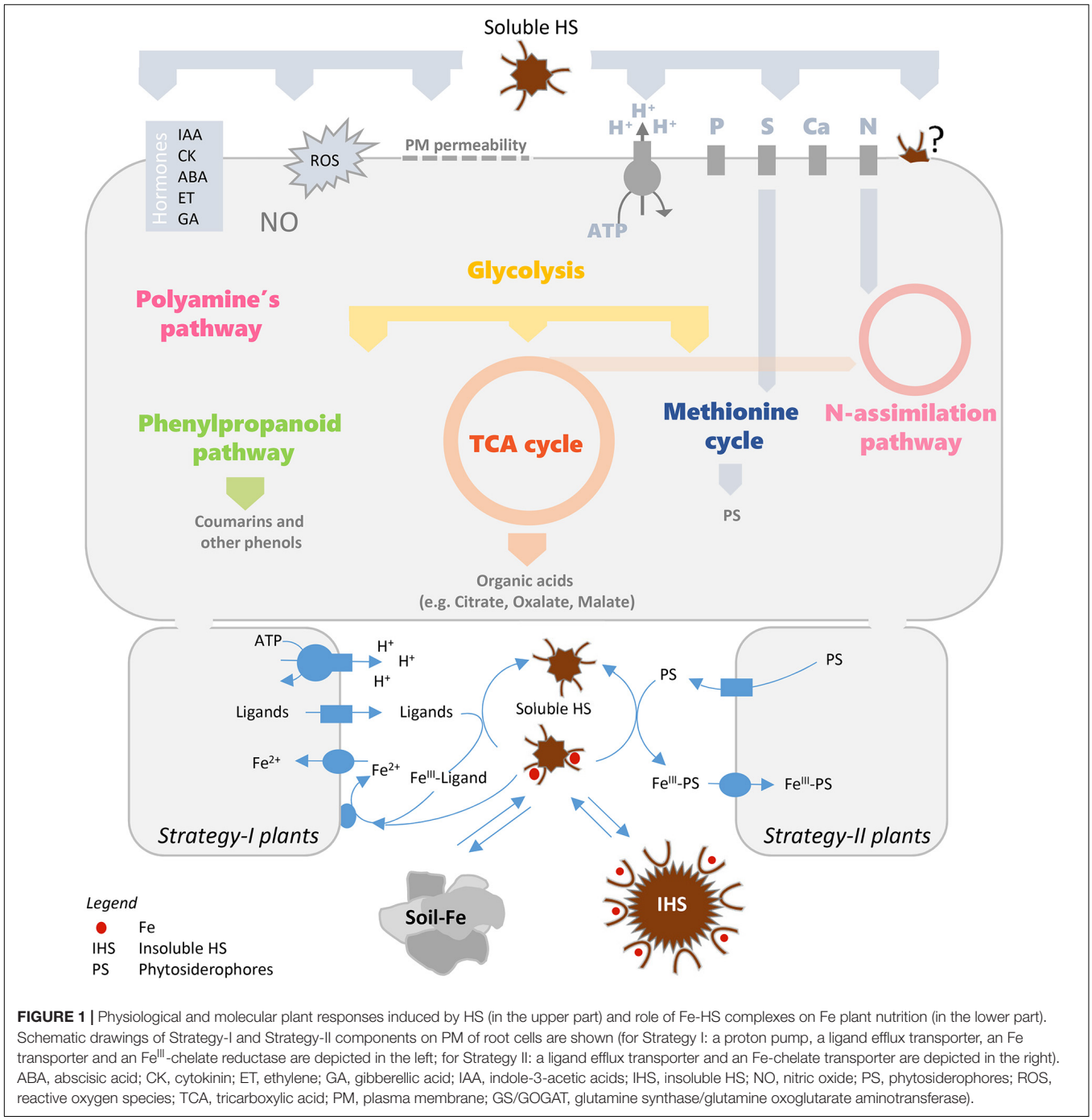

FIGURE 1 | Physiological and molecular plant responses induced by HS (in the upper part) and role of Fe-HS complexes on Fe plant nutrition (in the lower part). Schematic drawings of Strategy-I and Strategy-II components on PM of root cells are shown (for Strategy I: a proton pump, a ligand efflux transporter, an Fe transporter and an Fe^{III}-chelate reductase are depicted in the left; for Strategy II: a ligand efflux transporter and an Fe-chelate transporter are depicted in the right). ABA, abscisic acid; CK, cytokinin; ET, ethylene; GA, gibberellic acid; IAA, indole-3-acetic acids; IHS, insoluble HS; NO, nitric oxide; PS, phytosiderophores; ROS, reactive oxygen species; TCA, tricarboxylic acid; PM, plasma membrane; GS/GOGAT, glutamine synthase/glutamine oxoglutarate aminotransferase).

changes (Schmidt et al., 2007; Mora et al., 2012), suggesting that other signals might be involved in the morphological modifications elicited by HS.

A recognized target of HS action is the root PM H^+-ATPase (Zandonadi et al., 2016). Evidence for activation of the PM proton pump has been observed both at transcriptional and post-transcriptional level and related to proton extrusion (Varanini et al., 1993; Canellas et al., 2002) and uptake of ions, such as nitrate (Pinton et al., 1999; Quaggiotti et al., 2004; Tavares et al., 2017), phosphate (Jindo et al., 2016) and sulfate (Jannin et al., 2012). Besides ion uptake, HS have been shown to promote nitrogen assimilation (Mora et al., 2010; Jannin et al., 2012; Vaccaro et al., 2015; Zanin et al., 2018), carbon metabolism (glycolysis and Krebs cycle; Nardi et al., 2007; Trevisan et al., 2011) and synthesis of secondary metabolites, such as phenylpropanoids (Schiavon et al., 2010; Jannin et al., 2012; García et al., 2016c).

In addition to the stimulation of proton release, HS have been shown to affect rhizodeposition. Humic acids promoted release of anionic species close to region of root acidification [apolar

TABLE 1 | Reports focusing on the role of humic substances in iron plant nutrition.

Humic substances		Crop		HS Treatment	Objectives	Actions	References
Source	**Fraction/ Size**	**Species**	**Organ**				
Humate (from leaf compost)	N/A	*Solanum lycopersicum*	Shoots, Roots	supply of humates (100 mg L^{-1} dm^3)	Influence of sodium humate on the uptake or some ions by tomato seedlings	Facilitated the Fe transport from roots to shoots and stimulated the root uptake of K^+, Rb^+, Mg^{2+} and PO_4^{3-}, while strongly inhibited the Cl^- uptake	Gumiński et al., 1983
FA (from sphagnum peat)	WEHS	*Cucumis sativus, Hordeum vulgaris*	Plants	supply of ^{59}Fe-WEHS (1 μM Fe; 5 mg C_{org} L^{-1} WEHS) up to 3 days	Strategy-I and Strategy-II plant capabilities to use Fe complexed by WEHS	cucumber plants (Strategy I) utilize Fe-WEHS, presumably via reduction of Fe(III)-WEHS by PM Fe reductases, while barley plants (Strategy II) use an indirect mechanism involving ligand exchange between WEHS and PS	Cesco et al., 2002
HA (from mollisol)	N/A	*Helianthus annuus, Hordeum vulgare*	Plants	^{59}Fe-HA complex and EDTA or DTPA (0.1 mM) for 1, 4, or 14 days	Study the release and diffusion of Fe from Fe-HA chelates and its availability to growing plants	EDTA and DTPA attracted and chelated substantial amounts of the ^{59}Fe bonded by the HA, presumably by a ligand exchange process	Bocanegra et al., 2004
HA (from mollisol)	$HA_{100,000}$ (>100 KDa); $HA_{10,000}$ (<10 kDa)	*Helianthus annuus*	Plants	supply of ^{59}Fe-HA (50–100 mg L^{-1}) for 15 days	Plant uptake of iron chelated by humic acids of different size	Rapid translocation of Fe to the leaves; the small size HA10,000 and EDTA were the most efficient in affecting transport of Fe from root to leaf tissue	Bocanegra et al., 2006
HA (from leonardite)		*Cucumis sativus*	Roots	supply of HA (2, 5, 100, and 250 mg C_{org} L^{-1} up to 92 h; 40 μM of Fe were added as Fe-EDTA	Dose effect of HA on Fe-deficient response in cucumber plants	HA treatments transiently up-regulated in roots *CsFRO1*, *CsIRT1* and *CsHA2* expression and increased the Fe(III) chelate-reductase and PM H+-ATPase activity	Aguirre et al., 2009
FA (from sphagnum peat)	WEHS	*Solanum lycopersicum*	Leaves	supply of Fe-WEHS (1 μM Fe; 5 mg C_{org} L^{-1} WEHS) up to 24 h	study on mechanisms induced by Fe-WEHS at the leaf level	efficient use of Fe complexed by WEHS, at least in part, also the activation of Fe-acquisition mechanisms operating at the leaf level (upregulation of *LeFRO1*, *LeIRT1* and *Ferritin2* genes)	Tomasi et al., 2009
Insoluble HS (from Leonardite) and FA (from sphagnum peat)	HMW and WEHS	*Cucumis sativus*	Plants	supply of Fe-HS (0.1–10 μM Fe; 5 mg C_{org} L^{-1} HS) up to 11 days	efficiency of Fe-IHS complexes in alleviating Fe chlorosis	use of Fe insoluble high-molecular weight complexes (Fe-IHS) as an effective product to correct the Fe nutritional disorder	Colombo et al., 2012

(Continued)

TABLE 1 | Continued

Humic substances		Crop		HS Treatment	Objectives	Actions	References
Source	**Fraction/ Size**	**Species**	**Organ**				
high molecular weight HS (HA7 extract from black peat)	0.96–68 kDa	*Brassica napus*	Leaves, Roots	supply of HA7 (100 mg C_{org} L^{-1} HA7) up to 1, 3 or 30 days	Effect of HA treatment on rapeseed nutrition	HA7 incresed the Fe content in shoots and induced the expressionof genes coding for *BnIRT1, BnCOPT2, BnNRAMP3*	Billard et al., 2013
water soluble HS (from Leonardite)	WSHS	*Cucumis sativus*	Plants	supply of Fe-WSHS (20 μM Fe; Fe:LN = 1:1.1) for 1 day	study the use of Fe^{3+}/Fe^{2+} species in Fe-LN for plant nutrition	Fe^{2+}-WSHS use efficiently by plants under hydroponic conditions, while Fe^{3+}-WSHS is used more effectively under calcareous soil conditions	Kovács et al., 2013
FA (from sphagnum peat)	WEHS	*Solanum lycopersicum*	Roots	supply of Fe-WEHS (1 μM Fe; 5 mg C_{org} L^{-1} WEHS) up to 24 h	Physiology and molecular response of Fe-deficient plants	increased the ^{59}Fe hydroxide solubilization, the ^{59}Fe root uptake and gene expression of *LeFRO1* and *LeIRT1* and *LeIRT2*	Tomasi et al., 2013
FA (from sphagnum peat)	WEHS	*Cucumis sativus*	Leaves, Roots	supply of Fe-WEHS (1 μM Fe; 5 mg C_{org} L^{-1} WEHS) up to 5 days	Nutrient allocation in leaves of Fe-deficient lants	Increased root uptake of nitrate, CO_2 assimilation while changed the allocation of several nutrients from the vascular system (K, Cu, and Zn) or trichomes (Ca and Mn) to the entire leaf blade.	Tomasi et al., 2014
FA (from sphagnum peat)	WEHS	*Cucumis sativus*	Leaves	supply of Fe-WEHS (1 μM Fe; 5 mg C_{org} L^{-1} WEHS) up to 5 days	Iron allocation in leaves of Fe-deficient plants	stimulated the Fe accumulation and allocation in leaves, the upregulation of three transcripts: *CsFRO*, *CsIRT* (both localized next to the midveins) and *CsNRAMP* (in the interveinal area)	Zanin et al., 2015
HA (from leonardite)	N/A	*Triticum aestivum*	Shoots, Roots	Fe–HA (Fe 38.2 mg L^{-1}; 98 mg L^{-1} HA)	The effect of Fe-HA on photosynthesis and lipid profile in Fe-deficient plants	Enhanced input of Zn and lipid content in Fe-deficient plants, effect of HAs on the antioxidant status of plants and the plant lipid metabolism	Abros'kin et al., 2016
FA (from sphagnum peat)	WEHS	*Solanum lycopersicum*	Roots	supply of Fe-WEHS (1 μM Fe; 5 mg C_{org} L^{-1} WEHS) for 1 h	Early transcriptomic response in Fe deficient roots	Upregulation of Strategy I components, the feedback regulation of these components does not occured.	Zamboni et al., 2016
humic fraction (from leonardite)	HA, FA	*Glycine max*	Plants	supply of Fe-HS (10–100 μmol Fe pot^{-1}) up to 60 days	Study the Fe-HS use efficiency in soybean roots for Fe nutrition under calcareous conditions	Show the effect of HS accumulation on soybean roots in the iron transport from root to shoot and the Fe-biomineralization to form jarosite on the soybean root surface	Cieschi and Lucena, 2018

sugars from maize roots (Puglisi et al., 2009), impacting soil microbial community in the rhizosphere (Puglisi et al., 2013)]. Increase in root growth was accompanied by a greater release of low molecular weight exudates from maize plants treated with HS (Canellas et al., 2019). On the other hand, it has been reported that organic acids, such as those released by the roots, could disaggregate supramolecular structure of HS releasing low molecular weight humic fractions (Piccolo et al., 2003), which in turn might exert their effects on roots. Regarding this point is noteworthy that accumulation of HS at the root surface and in the apoplast has been observed (García et al., 2012; Kulikova et al., 2014). Furthermore, HS fractions obtained from rhizospheric soil showed different chemical characteristics to those isolated from bulk soil (D'Orazio and Senesi, 2009).

Effects of HS on root growth (signaling pathways), ion uptake (primary and secondary membrane transporters), primary metabolism (nitrogen and carbon), secondary metabolism (phenylpropanoids) and root exudation might be important for Fe acquisition and could improve the response of plants to Fe deprivation (**Figure 1**).

CONCLUSION AND PERSPECTIVE

Plenty of papers in the last decades have proven the capability of HS, isolated from different organic sources, to affect plant growth, nutrition and metabolism.

In natural soils, these substances, due to their heterogeneity and polydispersity, can be present as co-precipitates with mineral parts (e.g., Fe-oxides and clays) or in the solution where they contribute a considerable portion of the DOM.

Low-molecular-weight and water-soluble fractions have been shown to affect functionality of ion transporters operating on the PM of root cells, acting both at transcriptional and post-transcriptional level. This evidence has been achieved mostly using controlled experimental conditions, such as isolated HS and hydroponically grown plants. Conceivably, these HS could directly interact with plant roots, microorganisms and soil particles in the rhizosphere. Thus, study of structural and chemical characteristics of HS present in soil solution and in the rhizosphere are needed to allow the transfer of knowledge obtained in controlled systems to real soil/rhizosphere conditions. This would help to shed light on the direct contribution of HS to plant nutrition and growth and on their usefulness in the field. Evidence of a relationship between chemical structural characteristics of HS obtained from different sources and having variable molecular complexity and the biological effects they exert on plants has been already provided. This kind of studies can now be performed using new analytical techniques thus allowing a full characterization of HS based on their origin, either natural or anthropogenic.

Concerning Fe nutrition, these aspects would be very useful considering the dual role that has been attributed to HS, as chelating compounds and biostimulants (**Table 1**). The capability of HS to form stable complexes with Fe and to directly affect Fe-acquisition mechanisms would account for the relative contribution of Fe-HS complexes to plant Fe nutrition as compared to other Fe-complexes naturally occurring in the rhizosphere.

It is noteworthy that HS induce a "nutrient acquisition response" even when plants are adequately supplied or during the recovery from a deficiency status, affecting functionality and regulation of nutrient uptake mechanisms. The signaling network at the basis of this behavior starts to be elucidated. Furthermore, it has been suggested that the cross-interaction between root exudates and HS might be part of the cross-talk between plant and soil. These features would favor a prompt adaptation of plants to a specific environment.

Another point of interest studying the behavior of HS is their possible use to develop environmentally friendly fertilization tools, being crucial in terms of circular economy. Although their chemical structure is not yet fully understood and the direct transfer of results obtained in controlled conditions to real soil has been questioned, it is quite clear that HS isolated from different organic sources, when added to nutrient solution or to the soil can favor plant nutrition, and especially nitrogen and Fe accumulation. This implies that humic fractions with different chemical and biological properties could be used to tailor HS-based fertilizers with high use efficiency. This tool could be particularly relevant for precision agriculture aimed at limiting external inputs and optimizing the use of natural resources by crops.

AUTHOR CONTRIBUTIONS

LZ, NT, and RP wrote the manuscript and SC and ZV critically revised the manuscript. All authors approved the final version of the manuscript.

FUNDING

This work was supported by Dipartimento di Scienze AgroAlimentari, Ambientali e Animali (Di4A), University of Udine (PRID Startup 2018: DOM-BIO).

REFERENCES

Abros'kin, D. P., Fuentes, M., Garcia-Mina, J. M., Klyain, O. I., Senik, S. V., Volkov, D. S., et al. (2016). The effect of humic acids and their complexes with iron on the functional status of plants grown under iron deficiency. *Euras. Soil Sci.* 49, 1099–1108. doi: 10.1134/s1064229316100021

Aguirre, E., Leménager, D., Bacaicoa, E., Fuentes, M., Baigorri, R., Zamarreño, A. M., et al. (2009). The root application of a purified leonardite humic acid modifies the transcriptional regulation of the main physiological root responses to Fe deficiency in Fe-sufficient cucumber plants. *Plant Physiol. Biochem.* 47, 215–223. doi: 10.1016/j.plaphy.2008.11.013

Alberts, J. J., and Takács, M. (2004). Comparison of the natural fluorescence distribution among size fractions of terrestrial fulvic and humic acids and aquatic natural organic matter. *Org. Geochem.* 35, 1141–1149. doi: 10.1016/j.orggeochem.2004.06.010

Billard, V., Etienne, P., Jannin, L., Garnica, M., Cruz, F., Garcia-Mina, J. M., et al. (2013). Two biostimulants derived from algae or humic acid induce similar responses in the mineral content and gene expression of winter oilseed rape (*Brassica napus* L.). *J. Plant Growth Regul.* 33, 305–316. doi: 10.1007/s00344-013-9372-2

Bocanegra, M. P., Lobartini, J. C., and Orioli, G. A. (2004). Fe-humate as a source of iron for plants. *Commun. Soil Sci. Plant Anal.* 35, 2567–2576. doi: 10.1081/lcss-200030378

Bocanegra, M. P., Lobartini, J. C., and Orioli, G. A. (2006). Plant uptake of iron chelated by humic acids of different molecular weights. *Commun. Soil Sci. Plan.* 37, 239–248. doi: 10.1080/00103620500408779

Bolan, N. S., Adriano, D. C., Kunhikrishnan, A., James, T., McDowell, R., and Senesi, N. (2011). Dissolved organic matter: biogeochemistry, dynamics, and environmental significance in soils. *Adv. Agron.* 110, 1–75.

Canellas, L. P., and Olivares, F. L. (2014). Physiological responses to humic substances as plant growth promoter. *Chem. Biol. Technol. Agric.* 1, 1–11.

Canellas, L. P., Olivares, F. L., Canellas, N. O. A., Mazzei, P., and Piccolo, A. (2019). Humic acids increase the maize seedlings exudation yield. *Chem. Biol. Technol. Agric.* 6:3.

Canellas, L. P., Olivares, F. L., Okorokova-Façanha, A. L., and Façanha, A. R. (2002). Humic acids isolated from earthworm compost enhance root elongation, lateral root emergence, and plasma membrane HC-ATPase activity in maize roots. *Plant Physiol.* 130, 1951–1957. doi: 10.1104/pp.007088

Cesco, S., Nikolic, M., Römheld, V., Varanini, Z., and Pinton, R. (2002). Uptake of 59Fe from soluble 59Fe-humate by cucumber and barley plants. *Plant Soil* 241, 121–128.

Cesco, S., Römheld, V., Varanini, Z., and Pinton, R. (2000). Solubilization of iron by water-extractable humic substances. *J. Plant Nutr. Soil Sci.* 163, 285–290. doi: 10.1002/1522-2624(200006)163:3<285::aid-jpln285>3.0.co;2-z

Chen, Y., Clapp, C. E., and Magen, H. (2004a). Mechanisms of plant growth stimulation by humic substances: the role of organo-iron complexes. *Soil Sci. Plant Nutr.* 50, 1089–1095. doi: 10.1080/00380768.2004.10408579

Chen, Y., De Nobili, M., and Aviad, T. (2004b). "Stimulatory effects of humic substances on plant growth," in *Soil Organic Matter in Sustainable Agriculture*, eds F. Magdoff and R. R. Weil (New York, NY: CRC Press), 103–130.

Chen, Y., and Schnitzer, M. (1978). The surface tension of aqueous solutions of soil humic substances. *Soil Sci.* 125, 7–15. doi: 10.1097/00010694-197801000-00002

Cieschi, M. T., Caballero-Molada, M., Menéndez, N., Naranjo, M. A., and Lucena, J. J. (2017). Long-term effect of a leonardite iron humate improving Fe nutrition as revealed in silico, in vivo, and in field experiments. *J. Agr. Food Chem.* 65, 6554–6563. doi: 10.1021/acs.jafc.7b01804

Cieschi, M. T., and Lucena, J. J. (2018). Iron and humic acid accumulation on soybean roots fertilized with leonardite iron humates under calcareous conditions. *J. Agr. Food Chem.* 66, 13386–13396. doi: 10.1021/acs.jafc.8b04021

Colombo, C., Palumbo, G., He, J. Z., Pinton, R., and Cesco, S. (2014). Review on iron availability in soil: interaction of Fe minerals, plants, and microbes. *J Soils Sed.* 14, 538–548. doi: 10.1007/s11368-013-0814-z

Colombo, C., Palumbo, G., Sellitto, V. M., Rizzardo, C., Tomasi, N., Pinton, R., et al. (2012). Characteristics of insoluble, high molecular weight Fe-humic substances used as plant Fe sources. *Soil Sci. Soc. Am. J.* 76, 1246–1256.

Crowley, D. (2001). "Function of siderophores in the plant rhizosphere," in *The Rhizosphere: Biochemistry and Organic Substances at the Soil-Plant Interface*, eds R. Pinton, Z. Varanini, and P. Nannipieri (New York, NY: Marcel Dekker), 223–261.

D'Orazio, V., and Senesi, N. (2009). Spectroscopic properties of humic acids isolated from the rhizosphere and bulk soil compartments and fractionated by size-exclusion chromatography. *Soil Biol. Biochem.* 41, 1775–1781. doi: 10.1016/j.soilbio.2008.02.001

Esfahani, M. R., Stretz, H. A., and Wells, M. J. M. (2015). Abiotic reversible self-assembly of fulvic and humic acid aggregates in low electrolytic conductivity solutions by dynamic light scattering and zeta potential investigation. *Sci. Total Environ.* 537, 81–92. doi: 10.1016/j.scitotenv.2015.08.001

Fuentes, M., Olaetxea, M., Baigorri, R., Zamarreño, A. M., Etienne, P., Laîné, P., et al. (2013). Main binding sites involved in Fe(III) and Cu(II) complexation in humic-based structures. *J. Geochem. Exp.* 129, 14–17. doi: 10.1016/j.gexplo.2012.12.015

García, A. C., de Souza, L. G. A., Pereira, M. G., Castro, R. N., García-Mina, J. M., Zonta, E., et al. (2016a). Structure-property-function relationship in humic substances to explain the biological activity in plants. *Sci. Rep.* 6:e20798. doi: 10.1038/srep20798

García, A. C., Olaetxea, M., Santos, L. A., Mora, V., Baigorri, R., Fuentes, M., et al. (2016b). Involvement of hormone-and ROS-signaling pathways in the beneficial action of humic substances on plants growing under normal and stressing conditions. *BioMed. Res. Int.* 2016:3747501. doi: 10.1155/2016/3747501

García, A. C., Santos, L. A., de Souza, L. G. A., Tavares, O. C. H., Zonta, E., Gomes, E. T. M., et al. (2016c). Vermicompost humic acids modulate the accumulation and metabolism of ROS in rice plants. *J. Plant Physiol.* 192, 56–63. doi: 10.1016/j.jplph.2016.01.008

García, A. C., Santos, L. A., Izquierdo, F. G., Sperandio, M. V. L., Castro, R. N., and Berbara, R. L. L. (2012). Vermicompost humic acids as an ecological pathway to protect rice plant against oxidative stress. *Ecol. Eng.* 47, 203–208. doi: 10.1016/j.ecoleng.2012.06.011

Garcia-Mina, J. M. (2006). Stability, solubility and maximum metal binding capacity in metal–humic complexes involving humic substances extracted from peat and organic compost. *Org. Geochem.* 37, 1960–1972. doi: 10.1016/j.orggeochem.2006.07.027

Garcia-Mina, J. M. (2007). Advantages and limitations of the use of an extended polyelectrolyte model to describe the proton-Binding process in macromolecular systems. application to a poly(acrylic acid) and a humic acid. *J. Phys. Chem. B* 111, 4488–4494. doi: 10.1021/jp0689518

Garcia-Mina, J. M., Antolín, M. C., and Sanchez-Diaz, M. (2004). Metal-humic complexes and plant micronutrient uptake: a study based on different plant species cultivated in diverse soil types. *Plant Soil* 258, 57–68. doi: 10.1023/b:plso.0000016509.56780.40

Gerke, J. (1993). Solubilization of Fe(III) from humic-Fe complexes, humic/Fe-oxide mixtures and from poorly ordered Fe-oxide by organic acids - consequences for P adsorption. *Z. Pflanzenernähr. Bodenk.* 156, 253–257. doi: 10.1002/jpln.19931560311

Gerke, J. (1997). Aluminum and iron(III) species in the soil solution including organic complexes with citrate and humic substances. *J. Plant Nutr. Soil Sci.* 160, 427–432. doi: 10.1002/jpln.19971600313

Gerke, J. (2010). Humic (organic matter)-Al(Fe)-phosphate complexes: an underestimated phosphate form in soils and source of plant-available phosphate. *Soil Sci.* 175, 417–425. doi: 10.1097/ss.0b013e3181f1b4dd

Gerke, J. (2018). Concepts and misconceptions of humic substances as the stable part of soil organic matter: a review. *Agronomy* 8:76. doi: 10.3390/agronomy8050076

Gumiński, S., Sulej, J., and Glabiszewski, J. (1983). Influence of sodium humate on the uptake of some ions by tomato seedlings. *Acta Soc. Bot. Pol.* 52, 149–164. doi: 10.5586/asbp.1983.017

Hayes, M. H. B. (2006). Solvent systems for the isolation of organic components from soils. *Soil Sci. Soc. Am. J.* 70, 986–994.

Jannin, L., Arkoun, M., Ourry, A., Laîné, P., Goux, D., Garnica, M., et al. (2012). Microarray analysis of humic acid effects on *Brassica napus* growth: involvement of N, C and S metabolisms. *Plant Soil* 359, 297–319. doi: 10.1007/s11104-012-1191-x

Jindo, K., Soares, T. S., Peres, L. E. P., Azevedo, I. G., Aguiar, N. O., Mazzei, P., et al. (2016). Phosphorus speciation and high-affinity transporters are influenced by humic substances. *J. Plant Nutr. Soil Sci.* 179, 206–214. doi: 10.1002/jpln.201500228

Kovács, K., Czech, V., Fodor, F., Solti, A., Lucena, J. J., Santos-Rosell, S., et al. (2013). Characterization of fe–leonardite complexes as novel natural iron fertilizers. *J. Agr. Food Chem.* 61, 12200–12210. doi: 10.1021/jf404455y

Kulikova, N. A., Badun, G. A., Korobkov, V. I., Chernysheva, M. G., Tsvetkova, E. A., Abroskin, D. P., et al. (2014). Accumulation of coal humic acids by wheat seedlings: direct evidence using tritium autoradiography and occurrence in lipid fraction. *J. Plant Nutr. Soil Sci.* 177, 875–883. doi: 10.1002/jpln.201300648

Lehmann, J., and Kleber, M. (2015). The contentious nature of soil organic matter. *Nature* 528, 60–68. doi: 10.1038/nature16069

Lucena, J. J. (2003). Fe chelates for remediation of Fe chlorosis in strategy I plants. *J. Plant Nutr.* 26, 1969–1984. doi: 10.1002/jsfa.5726

Mimmo, T., Del Buono, D., Terzano, R., Tomasi, N., Vigani, G., Crecchio, C., et al. (2014). Rhizospheric organic compounds in the soil–microorganism–plant system: their role in iron availability. *Eur. J. Soil Sci.* 65, 629–642. doi: 10.1111/ejss.12158

Mora, V., Bacaicoa, E., Zamarreño, A. M., Aguirre, E., Garnica, M., Fuentes, M., et al. (2010). Action of humic acid on promotion of cucumber shoot growth involves nitrate-related changes associated with the root-to-shoot distribution of cytokinins, polyamines and mineral nutrients. *J. Plant Physiol.* 167, 633–642. doi: 10.1016/j.jplph.2009.11.018

Mora, V., Baigorri, R., Bacaicoa, E., Zamarreño, A. M., and García-Mina, J. M. (2012). The humic acid-induced changes in the root concentration of nitric oxide, IAA and ethylene do not explain the changes in root architecture caused by humic acid in cucumber. *Environ. Exp. Bot.* 76, 24–32. doi: 10.1016/j.envexpbot.2011.10.001

Muscolo, A., Sidari, M., and Nardi, S. (2013). Humic substance: relationship between structure and activity. deeper information suggests univocal findings. *J. Geochem. Explor.* 129, 57–63. doi: 10.1016/j.gexplo.2012.10.012

Nardi, S., Muscolo, A., Vaccaro, S., Baiano, S., Spaccini, R., and Piccolo, A. (2007). Relationship between molecular characteristics of soil humic fractions and glycolytic pathway and Krebs cycle in maize seedlings. *Soil Biol. Biochem.* 39, 3138–3146. doi: 10.1016/j.soilbio.2007.07.006

Nardi, S., Pizzeghello, D., Muscolo, A., and Vianello, A. (2002). Physiological effects of humic substances on higher plants. *Soil Biol. Biochem.* 34, 1527–1536. doi: 10.1016/s0038-0717(02)00174-8

Nebbioso, A., and Piccolo, P. (2011). Basis of a humeomics science: chemical fractionation and molecular characterization of humic biosuprastructures. *Biomacromolecules* 12, 1187–1199. doi: 10.1021/bm101488e

Nevin, K. P., and Lovley, D. R. (2002). Mechanisms for Fe(III) oxide reduction in sedimentary environments. *Geomicrobiol. J.* 19, 141–159. doi: 10.1080/01490450252864253

Olaetxea, M., De Hita, D., Garcia, C. A., Fuentes, M., Baigorri, R., Mora, V., et al. (2018). Hypothetical framework integrating the main mechanisms involved in the promoting action of rhizospheric humic substances on plant root- and shoot- growth. *Appl. Soil Ecol.* 123, 521–537. doi: 10.1016/j.apsoil.2017.06.007

Olk, D. C., Bloom, P. R., Perdue, E. M., McKnight, D. M., Chen, Y., Farenhorst, A., et al. (2019). Environmental and agricultural relevance of humic fractions extracted by alkali from soils and natural waters. *J. Environ. Qual.* 48, 217–232. doi: 10.2134/jeq2019.02.0041

Pandeya, S. B., Singh, A. K., and Dhar, P. (1998). Influence of fulvic acid on transport of iron in soils and uptake by paddy seedlings. *Plant Soil* 198, 117–125.

Piccolo, A. (2002). The supramolecular structure of humic substances: a novel understanding of humus chemistry and implications in soil science. *Adv. Agron.* 75, 57–134. doi: 10.1016/s0065-2113(02)75003-7

Piccolo, A., Conte, P., Spaccini, R., and Chiarella, M. (2003). Effects of some dicarboxylic acids on the association of dissolved humic substances. *Biol. Fertil. Soils* 37, 255–259.

Pinton, R., Cesco, S., De Nobili, M., Santi, S., and Varanini, Z. (1997). Water and pyrophosphate-extractable humic substances fractions as a source of iron for Fe-deficient cucumber plants. *Biol. Fertil. Soils* 26, 23–27. doi: 10.1007/s003740050337

Pinton, R., Cesco, S., Iacolettig, G., Astolfi, S., and Varanini, Z. (1999). Modulation of NO3- uptake by water-extractable humic substances: involvement of root plasma membrane H+ ATPase. *Plant Soil* 215, 155–161.

Puglisi, E., Fragoulis, G., Ricciuti, P., Cappa, F., Spaccini, R., Piccolo, A., et al. (2009). Effects of a humic acid and its size-fractions on the bacterial community of soil rhizosphere under maize (*Zea mays* L.). *Chemosphere* 77, 829–837. doi: 10.1016/j.chemosphere.2009.07.077

Puglisi, E., Pascazio, S., Suciu, N., Cattani, I., Fait, G., Spaccini, R., et al. (2013). Rhizosphere microbial diversity as influenced by humic substance amendments and chemical composition of rhizodeposits. *J. Geochem. Explor.* 129, 82–94. doi: 10.1016/j.gexplo.2012.10.006

Quaggiotti, S., Ruperti, B., Pizzeghello, D., Francioso, O., Tugnoli, V., and Nardi, S. (2004). Effect of low molecular size humic substances on nitrate uptake and expression of genes involved in nitrate transport in maize (*Zea mays* L.). *J. Exp. Bot.* 55, 803–813. doi: 10.1093/jxb/erh085

Rakshit, S., Uchimiya, M., and Sposito, G. (2009). Iron(III) bioreduction in soil in the presence of added humic substances. *Soil Sci. Soc. Am. J.* 73, 65–71.

Ramos, A. C., Dobbss, L. B., Santos, L. A., Fernandes, M. S., Olivares, F. L., Aguiar, N. O., et al. (2015). Humic matter elicits proton and calcium fluxes and signalling dependent on Ca2+-dependent protein kinase (CDPK) at early stages of lateral plant root development. *Chem. Biol. Tech. Agr.* 2:3. doi: 10.1186/s40538-014-0030-0

Roden, E. E., Kappler, A., Bauer, I., Jiang, J., Paul, A., Stoesser, R., et al. (2010). Extracellular electron transfer through microbial reduction of solid-phase humic substances. *Nat. Geosci.* 3:417. doi: 10.1038/ngeo870

Rose, M. T., Patti, A. F., Little, K. R., Brown, A. L., Jackson, W. R., and Cavagnaro, T. R. (2014). A meta-analysis and review of plant-growth response to humic substances: practical implications for agriculture. *Adv. Agron.* 124, 37–89. doi: 10.1016/b978-0-12-800138-7.00002-4

Ryan, P. R., Delhaize, E., and Jones, D. L. (2001). Function and mechanism of organic anion exudation from plant roots. *Annu. Rev. Plant Phys.* 52, 527–560.

Schiavon, M., Pizzeghello, D., Muscolo, A., Vaccaro, S., Francioso, O., and Nardi, S. (2010). High molecular size humic substances enhance phenylpropanoid metabolism in maize (*Zea mays* L.). *J. Chem. Ecol.* 36, 662–669. doi: 10.1007/s10886-010-9790-6

Schmidt, W., Santi, S., Pinton, R., and Varanini, Z. (2007). Water-extractable humic substances alter root development and epidermal cell pattern in *Arabidopsis*. *Plant Soil* 300, 259–267. doi: 10.1007/s11104-007-9411-5

Schwertmann, U. (1991). Solubility and dissolution of iron oxides. *Plant Soil* 130, 1–25. doi: 10.1007/bf00011851

Senesi, N. (1992). "Metal-Humic substance complexes in the environment. Molecular and mechanistic aspects by multiple spectroscopic approach," in *Biogeochemistry of Trace Metals*, ed. D. M. Adriano (Boca Raton: Lewis Publishers), 429–495.

Skogerboe, R. K., and Wilson, S. A. (1981). Reduction of ionic species by fulvic acid. Wilson A. *Anal. Chem.* 53, 228–232. doi: 10.1021/ac00225a023

Stevenson, F. J. (1994). *Humus Chemistry. Genesis, Composition, Reactions*, 2nd Edn. New York, NY: Wiley.

Struyk, Z., and Sposito, G. (2001). Redox properties of standard humic acids. *Geoderma* 102, 329–346. doi: 10.1016/s0016-7061(01)00040-4

Tavares, O. C. H., Santos, L. A., Ferreira, L. M., Sperandio, M. V. L., da Rocha, J. G., Garcia, A. C., et al. (2017). Humic acid differentially improves nitrate kinetics under low and high-affinity systems and alters the expression of plasma membrane H+-ATPases and nitrate transporters in rice. *Ann. Appl. Biol.* 170, 89–103. doi: 10.1111/aab.12317

Tipping, E. (2002). *Cation Binding by Humic Substances*. Cambridge: Cambridge University Press, 1–434.

Tomasi, N., De Nobili, M., Gottardi, S., Zanin, L., Mimmo, T., Varanini, Z., et al. (2013). Physiological and molecular aspects of Fe acquisition by tomato plants from natural Fe complexes. *Biol. Fertil. Soil* 49, 187–200. doi: 10.1007/s00374-012-0706-1

Tomasi, N., Mimmo, T., Terzano, R., Alfeld, M., Janssens, K., Zanin, L., et al. (2014). Nutrient accumulation in leaves of Fe-deficient cucumber plants treated with natural Fe complexes. *Biol. Fert. Soils* 50, 973–982. doi: 10.1007/s00374-014-0919-6

Tomasi, N., Rizzardo, C., Monte, R., Gottardi, S., Jelali, N., Terzano, R., et al. (2009). Micro-analytical, physiological and molecular aspects of Fe acquisition in leaves of Fe-deficient tomato plants re-supplied with natural Fe-complexes in nutrient solution. *Plant Soil* 325, 25–38. doi: 10.1007/s11104-009-0069-z

Trevisan, S., Botton, A., Vaccaro, S., Vezzaroa, A., Quaggiotti, S., and Nardi, S. (2011). Humic substances affect Arabidopsis physiology by altering the expression of genes involved in primary metabolism, growth and development. *Environ. Exp. Bot.* 74, 45–55. doi: 10.1016/j.envexpbot.2011.04.017

Trevisan, S., Pizzeghello, D., Ruperti, B., Francioso, O., Sassi, A., Palme, K., et al. (2010). Humic substances induce lateral root formation and expression of the early auxin-responsive IAA19 gene and DR5 synthetic element in *Arabidopsis*. *Plant Biol.* 12, 604–614. doi: 10.1111/j.1438-8677.2009.00248.x

Urrutia, O., Erro, J., Guardado, I., Mandado, M., and Garcia-Mina, J. M. (2013). Theoretical chemical characterization of phospho-metal humic complexes and relationships with their effects on both phosphorus soil fixation and phosphorus availability for plants. *J. Sci. Food Agric.* 93, 293–303. doi: 10.1002/jsfa.5756

Urrutia, O., Erro, J., Guardado, I., San Francisco, S., Mandado, M., Baigorri, R., et al. (2014). Physico-chemical characterization of humic-metalphosphate complexes and their potential application to the manufacture of new types of phosphate-based fertilizers. *J. Plant Nutr. Soil Sci.* 177, 128–136. doi: 10.1002/jpln.201200651

Vaccaro, S., Ertani, A., Nebbioso, A., Muscolo, A., Quaggiotti, S., Piccolo, A., et al. (2015). Humic substances stimulate maize nitrogen assimilation and amino acid

metabolism at physiological and molecular level. *Chem. Biol. Technol. Agric.* 2:5. doi: 10.1186/s40538-015-0033-5

Varanini, Z., and Pinton, R. (2001). "Direct versus indirect effects of soil humic substances on plant growth and nutrition," in *The Rizosphere*, eds R. Pinton, Z. Varanini, and P. Nannipieri (Basel: Marcel Dekker), 141–158.

Varanini, Z., Pinton, R., De Biasi, M. G., Astolfi, S., and Maggioni, A. (1993). Low molecular weight humic substances stimulate H+-ATPase activity of plasma membrane vesicles isolated from oat (*Avena sativa* L.) roots. *Plant Soil* 153, 61–69. doi: 10.1007/bf00010544

von Wirén, N., Khodr, H., and Hider, R. C. (2000). Hydroxylated phytosiderophore species possess an enhanced chelate stability and affinity for Iron(III). *Plant Physiol.* 124, 1149–1158. doi: 10.1104/pp.124.3.1149

Vujinovic, T., Contin, M., Cesco, S., Pinton, R., Tomasi, N., Ceccon, P., et al. (2013). "Characterization of humic fractions in leachates from soil under organic and conventional management and their interactions with the root zone," in *Functions of Natural Organic Matter in Changing Environment*, eds J. Xu, J. Wu, and Y. He (Dordrecht: Springer).

Zamboni, A., Zanin, L., Tomasi, N., Avesani, L., Pinton, R., Varanini, Z., et al. (2016). Early transcriptomic response to Fe supply in Fe-deficient tomato plants is strongly influenced by the nature of the chelating agent. *BMC Genomics* 17:35. doi: 10.1186/s12864-015-2331-5

Zandonadi, D. B., Santos, M. P., Busato, J. G., Peres, L. E. P., and Façanha, A. R. (2013). Plant physiology as affected by humified organic matter. *Theor. Exp. Plant Phys.* 25, 12–25.

Zandonadi, D. B., Santos, M. P., Caixeta, L. S., Marinho, E. B., Peres, L. E. P., and Façanha, A. R. (2016). Plant proton pumps as markers of biostimulant action. *Sci. Agric.* 73, 24–28. doi: 10.1590/0103-9016-2015-0076

Zandonadi, D. B., Santos, M. P., Dobbss, L. B., Olivares, F. L., Canellas, L. P., Binzel, M. L., et al. (2010). Nitric oxide mediates humic acids induced root development and plasma membrane H+-ATPase activation. *Planta* 231, 1025–1036. doi: 10.1007/s00425-010-1106-0

Zanin, L., Tomasi, N., Rizzardo, C., Gottardi, S., Terzano, R., Alfeld, M., et al. (2015). Iron allocation in leaves of Fe-deficient cucumber plants fed with natural Fe complexes. *Physiol. Plant.* 154, 82–94. doi: 10.1111/ppl.12296

Zanin, L., Tomasi, N., Zamboni, A., Sega, D., Varanini, Z., and Pinton, R. (2018). Water-extractable humic substances speed up transcriptional response of maize roots to nitrate. *Environ. Exp. Bot.* 147, 167–178. doi: 10.1016/j.envexpbot.2017.12.014

Conflict of Interest Statement: The authors declare that the research was conducted in the absence of any commercial or financial relationships that could be construed as a potential conflict of interest.

The reviewer YP declared a shared affiliation, though no other collaboration, with one of the authors SC to the handling Editor.

frontiers in Plant Science

ORIGINAL RESEARCH
published: 04 June 2019
doi: 10.3389/fpls.2019.00660

Nicotianamine Synthesis by *OsNAS3* Is Important for Mitigating Iron Excess Stress in Rice

*May Sann Aung[1,2], Hiroshi Masuda[1,2], Tomoko Nozoye[3,4], Takanori Kobayashi[1], Jong-Seong Jeon[5], Gynheung An[5] and Naoko K. Nishizawa[1,4]**

[1] Research Institute for Bioresources and Biotechnology, Ishikawa Prefectural University, Ishikawa, Japan, [2] Department of Biological Production, Faculty of Bioresource Sciences, Akita Prefectural University, Akita, Japan, [3] Center for Liberal Arts, Meiji Gakuin University, Kanagawa, Japan, [4] Department of Global Agricultural Sciences, The University of Tokyo, Tokyo, Japan, [5] Crop Biotech Institute and Graduate School of Biotechnology, Kyung Hee University, Yongin, South Korea

Iron (Fe) toxicity in plants causes tissue damage and cellular homeostasis disorders, thereby affecting plant growth and development. Nicotianamine (NA) is a ubiquitous chelator of metal cations and is responsible for metal homeostasis. Rice has three NA synthase (*NAS*) genes, of which the expression of *OsNAS1* and *OsNAS2* but not of *OsNAS3* is strongly induced in response to Fe deficiency. Recently, we found that *OsNAS3* expression is strongly induced with excess Fe in most rice tissues, particularly old leaves, suggesting that it may play a vital role under excess Fe conditions. However, the mechanism by which *OsNAS3* responds to excess Fe in rice remains poorly understood. In this study, we clarified the physiological response of *OsNAS3* expression to excess Fe and the role of NA synthesis in this condition. Promoter *GUS* analyses revealed that *OsNAS3* was widely expressed in roots, especially in vascular bundle, epidermis, exodermis, stem, and old leaf tissues under Fe excess compared to control plants. Nicotianamine and deoxymugineic acid (DMA; a type of phytosiderophore synthesized by Strategy II species) were present in roots and shoots under Fe excess likewise under control conditions. In addition, *OsNAS3* knockout plants were sensitive to excess Fe, exhibiting inferior growth, reduced dry weight, severer leaf bronzing, and greater Fe accumulation in their leaves than non-transformants with excess Fe. We also observed that NA-overproducing rice was tolerant of excess Fe. These results show that NA synthesized by *OsNAS3* under Fe excess condition is to mitigate excess Fe whereas NA synthesized by *OsNAS1* and *OsNAS2* under normal Fe condition is to enhance Fe translocation, suggesting the different roles and functions of the NA existence between these two conditions. Overall, these findings suggest that rice synthesizes NA with *OsNAS3* under Fe excess in roots and shoots, and that NA and DMA within the plant body are important for mitigating excess Fe stress and alleviating other metal deficiencies in rice. This report will be important for the development of tolerant rice adapted to Fe-contaminated soils.

Keywords: iron excess, rice, OsNAS3, nicotianamine, deoxymugineic acid, detoxification

OPEN ACCESS

Edited by:
Wolfgang Schmidt,
Academia Sinica, Taiwan

Reviewed by:
Elsbeth L. Walker,
University of Massachusetts Amherst, United States
Alexander Arthur Theodore Johnson,
The University of Melbourne, Australia

***Correspondence:**
Naoko K. Nishizawa
annaoko@mail.ecc.u-tokyo.ac.jp

Specialty section:
This article was submitted to Plant Nutrition, a section of the journal Frontiers in Plant Science

Received: *31 January 2019*
Accepted: *02 May 2019*
Published: *04 June 2019*

Citation:
Aung MS, Masuda H, Nozoye T, Kobayashi T, Jeon J-S, An G and Nishizawa NK (2019) Nicotianamine Synthesis by OsNAS3 Is Important for Mitigating Iron Excess Stress in Rice. Front. Plant Sci. 10:660. doi: 10.3389/fpls.2019.00660

INTRODUCTION

Iron (Fe) is an essential nutrient for most living organisms and is a key determinant of crop production, yield, and quality; however, it can be toxic when hyperaccumulated within cells. Iron toxicity is one of the most important stressors of rice in many lowland environments worldwide. Iron is reduced from ferric ion [Fe(III)] to more soluble ferrous ion [Fe(II)] when submerged in water. Ferrous ion is more easily dissolved in water ($K_{sp} = 8 \times 10^{-16}$) compared to ferric ion ($K_{sp} = \sim 1 \times 10^{-36}$) at 25°C (Stumm and Lee, 1961). Thus, Fe toxicity occurs more readily in submerged environments with acid soils. Acid soils occupy approximately 30% (or 3950 million hectares) of land worldwide, and approximately 50% of the world's arable land is estimated to be acidic (von Uexküll and Mutert, 1995). Iron toxicity is a serious constraint on rice growth and yield in regions where rice production is high such as China and Southeast Asia, and the regions mainly characterized by acid soils such as ultisols (NRCS, 2005). Iron overload in plants leads to leaf bronzing, tissue damage, and cellular homeostasis disorders. To mitigate this problem and maintain Fe homeostasis within the plant body, plants use strict and sophisticated Fe regulation mechanisms.

Nicotianamine (NA) is a ubiquitous plant-derived chelator of various divalent cations such as Fe^{2+} and Zn^{2+}, and is biosynthesized from S-adenosylmethionine by NA synthase (NAS; Higuchi et al., 1994). All higher plants synthesize NA and utilize it for chelation as well as internal transport of Fe^{2+} and other metal cations to maintain metal homeostasis (Hell and Stephan, 2003; Takahashi et al., 2003). Numerous studies have reported disrupted internal metal transport in NA-defective plants. For example, NA-defective tomato mutant exhibits an iron-deficient phenotype (Pich and Scholz, 1996; Stephan et al., 1996), NA-deficient transgenic tobacco plants have serious chlorosis in young leaves and decreased Fe and zinc (Zn) concentrations in leaves and flowers (Takahashi et al., 2003), and the *Arabidopsis AtNAS* quadruple mutant has a decreased Fe concentration in its seeds (Klatte et al., 2009). Introducing overexpression of a barley *NAS* gene, *HvNAS1*, to tobacco plants leads to increased Fe and Zn concentrations in the leaves, flowers, and seeds (Takahashi et al., 2003). These reports suggest that NA plays an important role in internal Fe transport in higher plants.

In rice, NA is biosynthesized by three NAS enzymes: *OsNAS1*, *OsNAS2*, and *OsNAS3* (Higuchi et al., 2001), all of which exhibit NA synthase activity *in vitro* (Inoue et al., 2003). Among three encoding genes, expression of *OsNAS1* and *OsNAS2* is strongly induced in rice roots and yellow leaves under Fe deficiency, whereas *OsNAS3* expression is mildly induced in roots but is suppressed in leaves under Fe deficiency (Inoue et al., 2003). The sequences of *OsNAS1* and *OsNAS2* are located very close to each other on rice chromosome 3, whereas *OsNAS3* is located on chromosome 7 (Higuchi et al., 2001; Inoue et al., 2003). Many other genes involved in Fe acquisition under Fe deficiency also show Fe deficiency-induced expression changes similar to those of the *OsNAS1* and *OsNAS2* genes, but not that of *OsNAS3* (Kobayashi et al., 2014). Thus, *OsNAS3* has a unique expression pattern compared to *OsNAS1* or *OsNAS2*, and as such, likely plays a different role than *OsNAS1* and *OsNAS2*.

Nicotianamine is not only involved in long-distance Fe transport in rice, but also serves as a substrate for production of deoxymugineic acid (DMA) via a 3″–oxo intermediate by NA aminotransferase (NAAT) and DMA synthase (DMAS) (Mori and Nishizawa, 1987; Shojima et al., 1989). In rice, one *NAAT* gene (*OsNAAT1*) and one *DMAS* gene (*OsDMAS1*) have been isolated (Bashir et al., 2006; Inoue et al., 2008). For DMA, it serves as a type of mugineic acid family phytosiderophore synthesized and secreted from graminaceous plants under Fe-deficient conditions to acquire Fe from the soil (Takagi, 1976; Marschner et al., 1986; Marschner and Romheld, 1994). Iron is thought to chelate with NA and DMA in the rice plant body and is translocated to various tissues including seeds. A correlation has been found between seed NA or DMA concentration and seed Fe concentration in transgenic rice with higher *NAS* expression (Masuda et al., 2009; Johnson et al., 2011).

Nicotianamine also plays a vital role in enhancing the nutritional quality of rice and is a candidate for biofortification of rice. For example, overexpression of the *NAS* gene increases Fe and Zn concentrations in rice seeds (Lee et al., 2009; Masuda et al., 2009; Johnson et al., 2011) and rice *glutelin B1* promoter-driven *OsNAS1* increases Fe concentrations in leaves and polished seeds (Zheng et al., 2010). Nicotianamine works synergistically with other genes to achieve high Fe in rice grains. For example, *HvNAS1*, *GmFER*, and *OsYSL2* (Masuda et al., 2012; Aung et al., 2013), *OsNAS2* and *GmFER* (Trijatmiko et al., 2016), and *AtNAS1*, *AtIRT1*, and *PvFER* (Boonyaves et al., 2017) together contribute to grain Fe accumulation. The increased Fe content in rice grains caused by enhanced *NAS* expression is also bioavailable (Lee et al., 2009). These reports suggest that NA synthesized by NAS enhances Fe translocation within rice plants to the seeds.

Nicotianamine is thought to play vital roles not only in Fe deficiency tolerance and seed Fe accumulation but also in detoxification of excess intracellular Fe (von Wirén et al., 1999). Former studies have shown the importance of NA in heavy metal metabolism in dicot plants (Pich et al., 2001; Takahashi et al., 2003; Douchkov et al., 2005; Kim et al., 2005; Han et al., 2018) and monocot plants (Lee et al., 2009; Aung et al., 2018). For example, among dicot plants, Pich et al. (2001) suggested a possible role of NA in vacuolar sequestration for detoxification of excess Fe in pea and tomato. In other dicots, transgenic *Arabidopsis* and tobacco plants overexpressing *HvNAS1* tolerated excess metal toxicity, particularly Ni (Kim et al., 2005). In addition, overexpression of apple *MxNAS1*, *MxNAS2* and *MxNAS3* genes led to enhanced tolerance to low and high levels of Fe stress in transgenic tomato (Han et al., 2013; Yang et al., 2015) and transgenic *Arabidopsis* by influencing NA synthesis (Han et al., 2018), respectively.

In dicot plants, NA functions exclusively as a metal chelator, as they do not produce MAs. In graminaceous plants, NA plays two roles, functioning not only as a metal chelator for internal transport but also as a precursor of MAs. In the monocot rice, overexpression of *OsNAS3* increased Fe and Zn concentrations and NA levels in grains as well as tolerance to Fe and Zn deficiencies and Zn, copper (Cu), and nickel (Ni) toxicities (Lee et al., 2009). Recently, we reported the transcriptomic analyses of various rice tissues in response to

ferrous Fe toxicity (Aung et al., 2018). The results showed that Fe homeostasis-related genes were suppressed under excess Fe, principally in the roots. In particular, the NA synthase genes *OsNAS1* and *OsNAS2* were clearly suppressed in the roots and junction nodes between the root and shoot (discrimination center, DC). By contrast, *OsNAS3* expression was increased in all tissues in response to excess Fe, by 2- to 10-fold in the roots, 2- to 9-fold in the DC, 2- to 8-fold in stems, 10- to 120-fold in old leaves and 3- to 22-fold in the newest leaves. Under Fe excess, *OsNAS3* expression was as high as that of other important Fe excess-responsive genes, such as those of the Fe storage protein ferritin and vacuolar Fe transporter *OsVIT2* (Aung et al., 2018). These results suggest that NA synthesized by induced *OsNAS3* may play an important role in rice under Fe excess conditions. However, further in-depth analyses of *OsNAS3* are required to elucidate its physiological function in Fe excess and its role in Fe detoxification in rice.

In this study, we clarified the roles of NA and *OsNAS3* in rice under Fe excess conditions. To this end, we analyzed spatial expression patterns in various tissues of *OsNAS3* promoter-*GUS* plants (roots, DC, stems, old leaves, and newest leaves) in response to Fe excess. In addition, the amounts of NA and DMA in roots and shoots were investigated. An *OsNAS3* knockout line was cultivated under control and Fe excess conditions for observation of growth, leaf bronzing, metal concentrations, and Fe histochemical localization. Moreover, tolerance to Fe excess was observed in a NA-overproducing rice line. These results suggest a novel role for NA synthesized by *OsNAS3* in the Fe detoxification process.

MATERIALS AND METHODS

Plant Materials and Growth Conditions in Hydroponic Culture

Plant Cultivation by Hydroponic Culture

Rice seeds were germinated on Murashige and Skoog (MS) medium (Murashige and Skoog, 1962) with and without hygromycin B (50 mg L^{-1}) for transformant and non-transformant (NT) plants, respectively. The seedlings were grown in modified Kasugai's hydroponic culture solution (× 1 Fe; 35.7 μM $FeCl_2$) at pH 5.5 for 1 week, as previously described by Aung et al. (2018), after which the plants were cultivated under conditions of control Fe (× 1 Fe) or ferrous Fe excess (× 70 Fe; 2.50 mM $FeCl_2$) at pH 4.0. The pH of the solution was adjusted to 4.0 every 2 days, and the culture solution was renewed every week. One plant per hill and three or four biological replicates were used for each Fe condition. All experiments were conducted in a greenhouse at 30°C during the 14 h day and 25°C during the 10 h night with natural light.

Growth Analyses of *OsNAS3* Knockout Rice Plants

Rice seeds (*Oryza sativa* L. cv. Hwayoung) of NT and the *OsNAS3* knockout mutant line 2D30228, *osnas3–1* (Lee et al., 2009) were obtained from the Rice T-DNA Insertion Sequence Database (POSTECH; Pohang University of Science and Technology, Pohang, Korea; Jeong et al., 2002). The T-DNA insertion position was described by Lee et al. (2009).

The 18-day-old seedlings (first experiment) or 14-day-old seedlings (second experiment) of knockout and NT plants were cultured hydroponically and exposed to excess Fe in hydroponic culture as described above for 39 days (first experiment) or 23 days (second experiment). Four biological replicates were used for each Fe condition. In both experiments, shoot and root lengths were measured throughout cultivation. The severity of Fe toxicity in leaves was measured after 11 or 17 days of exposure to excess Fe by determining the bronzing score of the fully expanded newest leaf (NL) and older leaves, as previously described by Aung et al. (2018).

Growth Analyses of NAS-Overexpressing Rice Plants

Rice seeds (*O. sativa* L. cv. Tsukinohikari) of NT plants and the T_4 generation of NAS-overexpressing (*Actin* promoter-*HvNAS1*) plants (Masuda et al., 2009) were used for growth analyses. Eighteen-day-old seedlings were cultured hydroponically and exposed to excess Fe in hydroponic culture for 39 days. Plant growth and bronzing scores were measured as described above.

Histochemical Analyses of Promoter-GUS Rice Lines

The seeds of the *OsNAS3* promoter-*GUS* lines (T_3 and T_4 seeds; *O. sativa* L. cv. Tsukinohikari) described by Inoue et al. (2003) were used for histochemical analyses. Fifteen-day-old seedlings were transferred to hydroponic culture and exposed to excess Fe for 14 days. Roots, leaf blades, stems, DCs were cut with a scalpel into approximately 1 cm sections. Then, the sections were embedded into 5% agar and cut into 100 μm transverse, or longitudinal sections by a DTK-1000N MicroSlicer (Dosaka EM Co., Ltd., Kyoto, Japan) as described by Kobayashi et al. (2010). GUS reaction buffer was prepared with 1 mM 5-bromo-4-chloro-3-indolyl-ß-D-glucuronide Cyclohexyl ammonium salt (X-Gluc; Wako, Japan) in staining buffer (100 mM Na_2HPO_4, 1 mM $K_3Fe(CN)_6$, 1 mM $K_4Fe(CN)_6$, and 20% methanol). The samples were subjected to histochemical assays for GUS activity, with vacuum infiltration on ice for 30 min and then incubated at 37°C dark for 7 min for roots, 1 min for DCs, 9 min for stems, 2 h 30 min for old leaves and 1 h for the newest leaves. Once the staining appeared, the reactions of both control and Fe excess sections were stopped at the same time by washing 70% ethanol and then reserved in 70% ethanol. Histochemical localization was observed in both the T_3 and T_4 generations of at least two independent lines under a Zeiss Axion Vision Image 4.2 microscope and a Zeiss Axioskop 2 Plus fluorescence microscope (Carl Zeiss Microscopy, Jena, Germany).

NA and DMA Concentration Analyses

Rice seeds (*O. sativa* L. cv. Tsukinohikari) were used for NA and DMA concentration analyses. Sixteen-day-old rice seedlings were transferred to hydroponic culture, and half were exposed to excess Fe at pH 4.0 for 14 days. Four biological replicates were used in control (× 1 Fe) and Fe excess (× 70 Fe) hydroponic cultures. Leaf and root samples were ground to powder in liquid nitrogen using a mortar and pestle, and then the endogenous

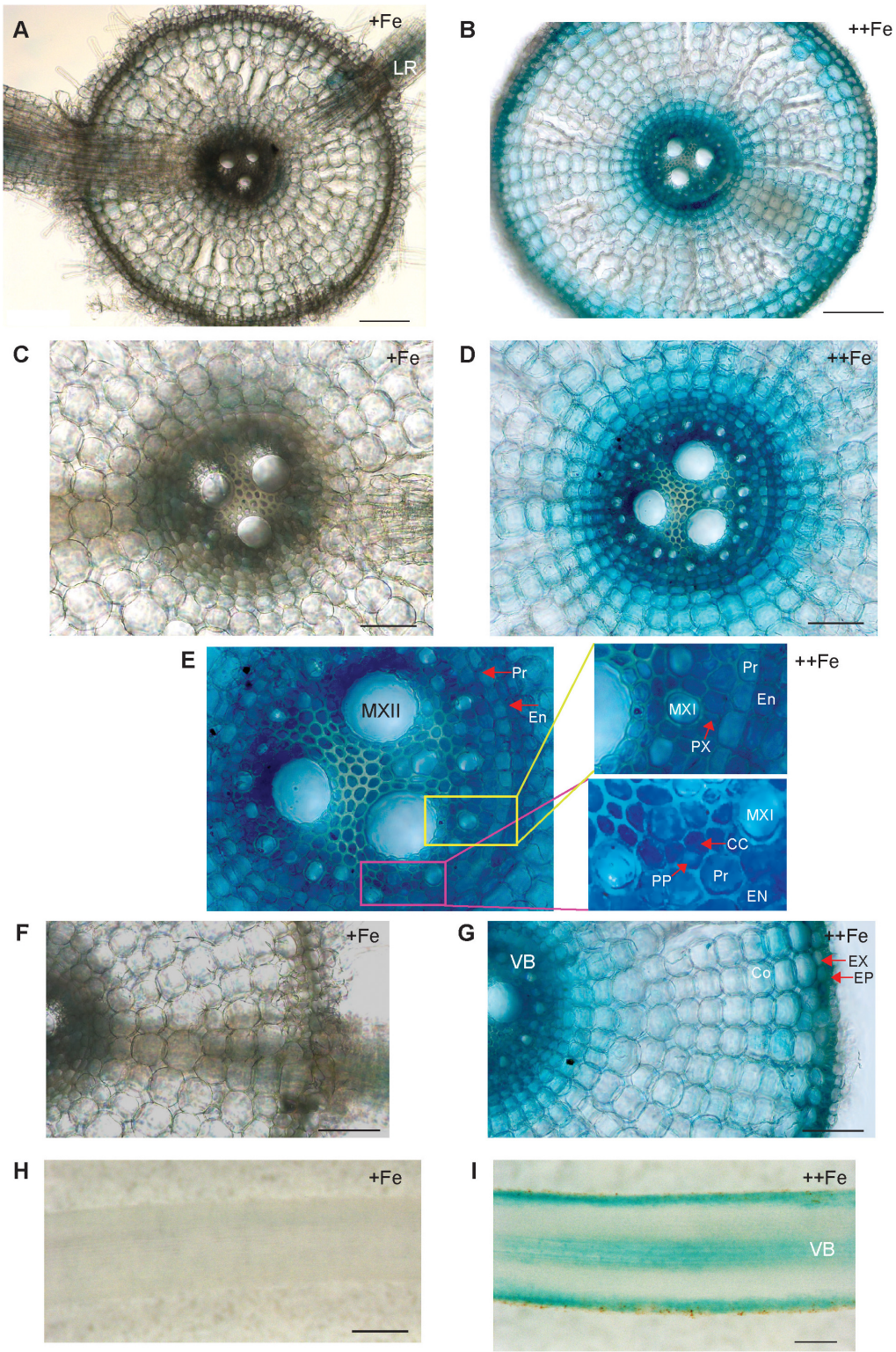

FIGURE 1 | Cellular localization of *OsNAS3* promoter-GUS expression in roots. **(A)** Transverse section of control root. **(B)** Transverse section of Fe-excess root. **(C,D)** Enlarged views of vascular tissues shown in **(A,B)**, respectively. **(E)** An enlarged view of xylem and phloem shown in **(D)**. **(F,G)** Enlarged views of outer root layers shown in **(A,B)**, respectively. **(H)** Longitudinal section of control root. **(I)** Longitudinal section of Fe-excess root. LR, lateral root; MXI, metaxylem I; MXII, metaxylem II; PP, protophloem; CC, companion cells; EN, endodermis; Pr, pericycle; PX, protoxylem; EX, exodermis; EP, epidermis; Co, cortex; VB, vascular bundle. Scale bars: 20 μm for **(A–D,F,G)**; 100 μm for **(H,I)**.

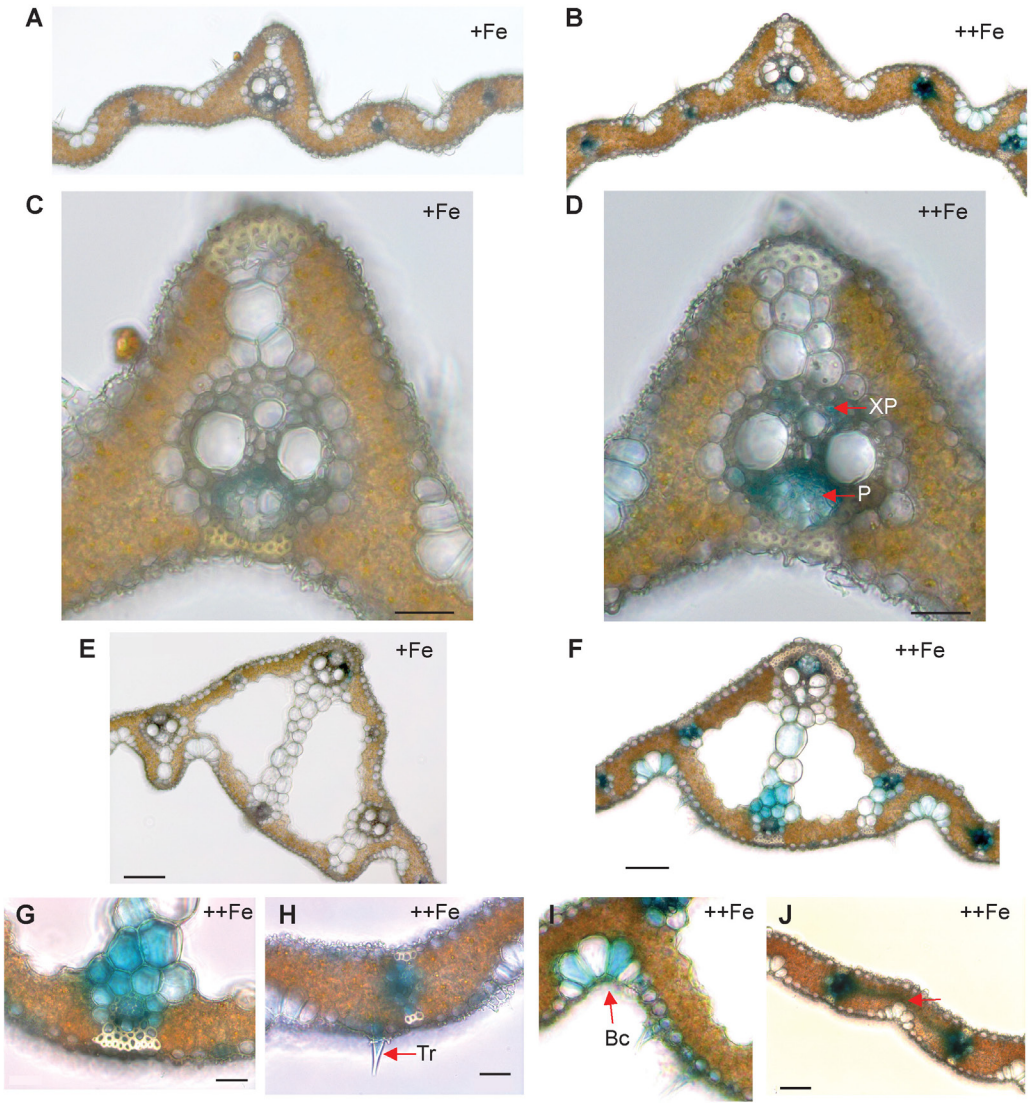

FIGURE 2 | Cellular localization of *OsNAS3* promoter-GUS expression in old leaves. **(A)** Transverse sections of control old leaf. **(B)** Fe-excess old leaf. **(C)** Enlarged view of control leaf. **(D)** Enlarged view of Fe-excess leaf. **(E)** Midrib of control leaf. **(F)** Midrib of Fe-excess leaf. **(G)** An enlarged view of **(F)**. **(H)** Fe excess leaf showing trichome. **(I)** Fe excess leaf showing bulliform cells. **(J)** Vascular vein connecting vascular bundles of Fe-excess leaf shown by arrow. XP, xylem parenchyma; P, phloem; Tr, trichome; Bc, bulliform cells. Scale bars: 20 μm for **(C–J)**.

NA and DMA concentrations of the samples were determined through high-performance liquid chromatography according to the method described by Nozoye et al. (2014).

Metal Concentration Analyses

Samples of roots and shoots (newest leaves and third newest leaves) from control and Fe-treated plants (from the second experiment; 23 days of excess Fe exposure) were collected for metal concentration analyses. The roots were washed with distilled water or Milli-Q water containing 50 mM sodium ethylenediaminetetraacetic acid (Na-EDTA) for control or Fe excess plants, respectively. Root and leaf samples were dried for 3 days at 60°C, and 50–200 mg samples were digested with 2 mL HNO_3 and 2 mL H_2O_2 at 220°C for 20 min using the MARS XPRESS oven (CEM Japan, Tokyo, Japan), and then messed up and filtered as described by Masuda et al. (2009). The concentrations of Fe, Zn, manganese (Mn), and Cu were measured with an inductively coupled plasma atomic emission spectrometer (ICPS-8100; Shimadzu, Kyoto, Japan). Three biological replicates were performed.

Iron Histochemical Localization Analyses

To detect the presence of Fe in the leaf tissues of *OsNAS3* knockout plants, leaf sections from control and Fe excess cultures were obtained (from the second experiment) and placed in ethanol for 24 h to remove the chlorophyll. Then the sections were exposed to a solution containing 2% potassium ferricyanide (Wako Co., Ltd., Tokyo, Japan) and 2% hydrochloric acid

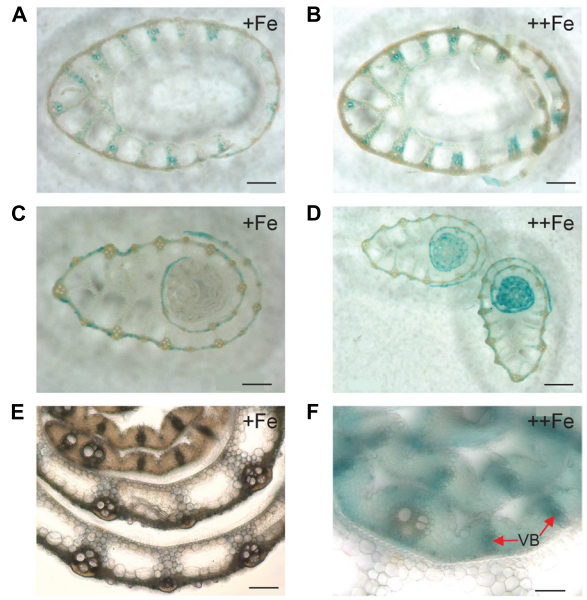

FIGURE 3 | Cellular localization of *OsNAS3* promoter-GUS expression in the stem. **(A)** The outer part of the control stem. **(B)** The outer part of the Fe-excess stem. **(C)** The inner part of the control stem. **(D)** The inner part of the Fe-excess stem. **(E,F)** Enlarged views of **(C,D)**, respectively. VB, vascular bundle. Scale bars: 500 μm for **(A–D)**; 20 μm for **(E–F)**.

(Wako) for 24 h. After rinsing with distilled water, the sections were mounted in distilled water and localization was observed under the Zeiss Axion Vision Image 4.2 microscope (Carl Zeiss Microscopy).

Quantitative Real-Time RT-PCR Analyses

Total RNA from rice prepared for the microarray analyses as described by Aung et al. (2018) was used to confirm the expression patterns of the genes *OsDMAS1* and *OsNAAT1* under Fe excess conditions by quantitative real-time polymerase chain reaction (RT-PCR) analyses. For the expression analyses of *OsNAS3* knockout and NT plants from ×1 Fe and ×70 Fe cultures, rice RNA was extracted from hydroponically grown leaves. For all samples, the first-strand cDNA was synthesized using the ReverTra Ace reverse transcriptase kit (Toyobo, Osaka, Japan) and oligo-d(T)$_{30}$ primers. Then, qPCR was performed in a StepOnePlus^{TM} Real-Time PCR System (Life Technology, Tokyo, Japan) with SYBR Premix Ex Taq II reagent (Takara, Shiga, Japan). The transcript abundance was normalized against the rice *alpha-tubulin* transcript level. The primer sequences used for gene expression analyses were as follows: 5′GCC GGC ATC CCG GCA GCG GAA GAT CA 3′ for *OsDMAS1* FW and 5′ CTC TCT CTC TCG GGC ACG TGC TAG CGT 3′ for *OsDMAS1* RV; 5′-TAAGAGGATAATTGATTTGCTTAC-3′ for *OsNAAT1* FW and 5′-CTGATCATTCCAATCCTAGTACAAT-3′ for *OsNAAT1* RV; 5′ CGA TGA CTG CTT CCA TCG CTT G 3′ for *OsNAS3* FW and 5′ GGC A TG CAT TCA TGC ATG ACT GC 3′ for *OsNAS3* RV; 5′ TCT TCC ACC CTG AGC AGC TC 3′ for *alpha-tubulin* FW and 5′ AAC CTT GGA GAC CAG TGC AG 3′ for *alpha-tubulin* RV.

Statistical Analyses

Statistical analyses were conducted using Microsoft Excel software. Comparisons were made between ×1 Fe and each level of Fe excess in each tissue. For each set of comparisons, a two-sample Student's *t*-test for an equal or unequal variance was performed based on the *F*-test for equal variance.

RESULTS

Expression of *OsNAS3* Was Observed in All Tissues Investigated Under Fe Excess

To uncover the physiological role of *OsNAS3* in Fe excess, the tissue-specific expression of *OsNAS3* was investigated based on histochemical localization in transgenic rice plants with the introduced *OsNAS3* promoter–*GUS* described by Inoue et al. (2003). Expression of *OsNAS3* was observed in every tissue investigated. In the transverse section of roots under control Fe conditions, *OsNAS3* expression was mainly restricted to phloem cells and lateral roots (**Figures 1A,C,F**). Under excess Fe, strong expression was observed throughout the entire root, particularly in the vascular bundles, exodermis, and epidermis of the roots observed in transverse sections (**Figures 1B,D,E,G**). Enlarged transverse sections of the vascular bundle exhibited extremely deep staining in the phloem cells, phloem companion cells, protoxylem, xylem parenchyma cells, and epidermal cells (**Figures 1D,E**). In the longitudinal sections, *OsNAS3* expression in roots was very clear under Fe excess compared to control conditions (**Figures 1H,I**). Expression of *OsNAS3* was observed in lateral roots in rice under both control and Fe excess conditions (**Figure 1A** and **Supplementary Figure S1A**).

In old leaf blades, weak expression of *OsNAS3* under Fe sufficiency was present only in the small vascular bundles and phloem cells of large vascular bundles (**Figures 2A,C**). Under Fe excess, leaves showed stronger expression of *OsNAS3* in the small and large vascular bundles (**Figure 2B**) and xylem parenchyma and phloem cells (**Figure 2D**). In addition, weak expression was observed in extracellular veins and chloroplasts within mesophyll cells in leaves with excess Fe (**Figure 2D** and **Supplementary Figure S1B**). In the midrib of the control Fe leaf, expression was very weak (**Figure 2E**), whereas the Fe excess leaf midrib showed dominant expression of *OsNAS3* in the vascular bundles, bundle sheath cells and adjacent cells, the lower and upper epidermis (**Figures 2F,G**), trichomes (**Figure 2H**), some parts of the bulliform (motor) cells present on the adaxial side of the leaf (**Figure 2I**), and also in the veins connecting small vascular bundles (**Figure 2J**). The outer layer of the stem showed dominant expression under excess Fe than under control (**Figures 3A,B**). In the inner part of the stem, expression of *OsNAS3* in the prospective new leaves that would soon emerge, but were folded inside stem tissue at the time, was more pronounced under excess Fe compared to control Fe condition (**Figures 3C–F**).

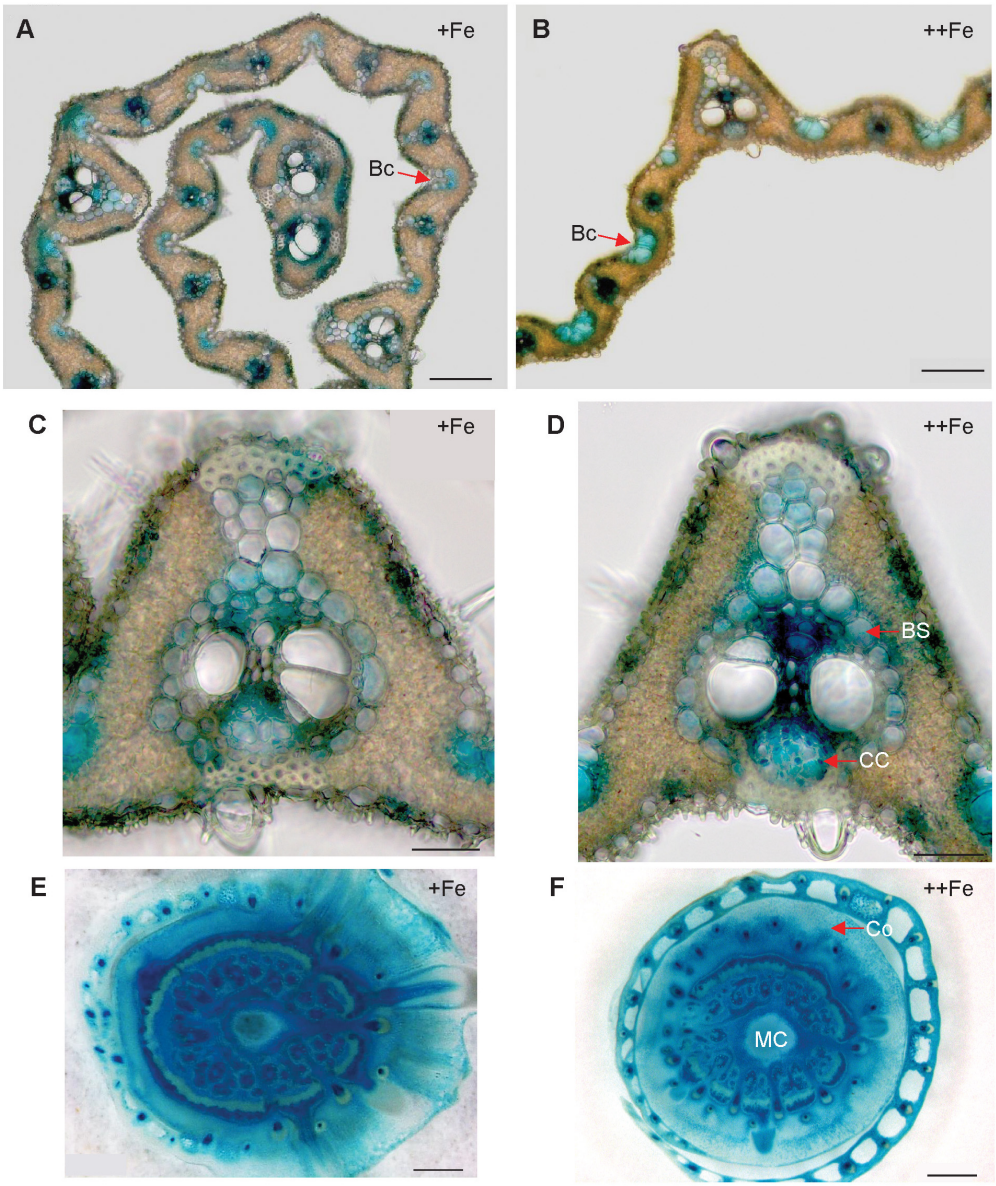

FIGURE 4 | Cellular localization of *OsNAS3* promoter-GUS expression in the newest leaves and DCs. **(A)** Transverse sections of the control newest leaf. **(B)** Fe-excess newest leaf. **(C,D)** Enlarged views of **(A,B)**, respectively. **(E)** Control DC. **(F)** Fe-excess DC. Bc, bulliform cells; BS, bundle sheath cells; CC, companion cells; Co, cortex; MC, medullary cavity. Scale bars: 20 μm for **(A–D)**; 500 μm for **(E,F)**.

In the newest leaves, *OsNAS3* expression patterns were not affected by Fe status (**Figures 4A–D**). Expression was localized to the small and large vascular bundles, bundle sheath cells, some parts of mesophyll cells and collenchyma fibers, and bulliform and epidermis cells of both the abaxial and adaxial surfaces (**Figures 4A–D** and **Supplementary Figures S1C,D**). More dense and dominant GUS activity was observed inside the large vascular bundles of leaves particularly in phloem companion cells under Fe excess than in control leaves. Bulliform cells, which only expressed *OsNAS3* under Fe excess conditions in old leaves, expressed *OsNAS3* in the newest leaves under both control and Fe excess conditions (**Figures 4A,B**). Bundle sheath cells, which did not express *OsNAS3* in old leaves, expressed this gene dominantly in the newest leaves (**Figures 4C,D**). DCs constitutively exhibited strong *OsNAS3* expression, particularly in the thick cortex, medullary cavity, and leaf sheath of the second leaf, whether Fe was sufficient or excessive (**Figures 4E,F** and **Supplementary Figures S1E,F**). Expression patterns were similar for DCs in the control and Fe excess conditions.

Expression of *OsDMAS1* in Various Rice Tissues

To determine whether *OsDMAS1* and *OsNAAT1* are involved in DMA synthesis in rice exposed to excess Fe, we analyzed

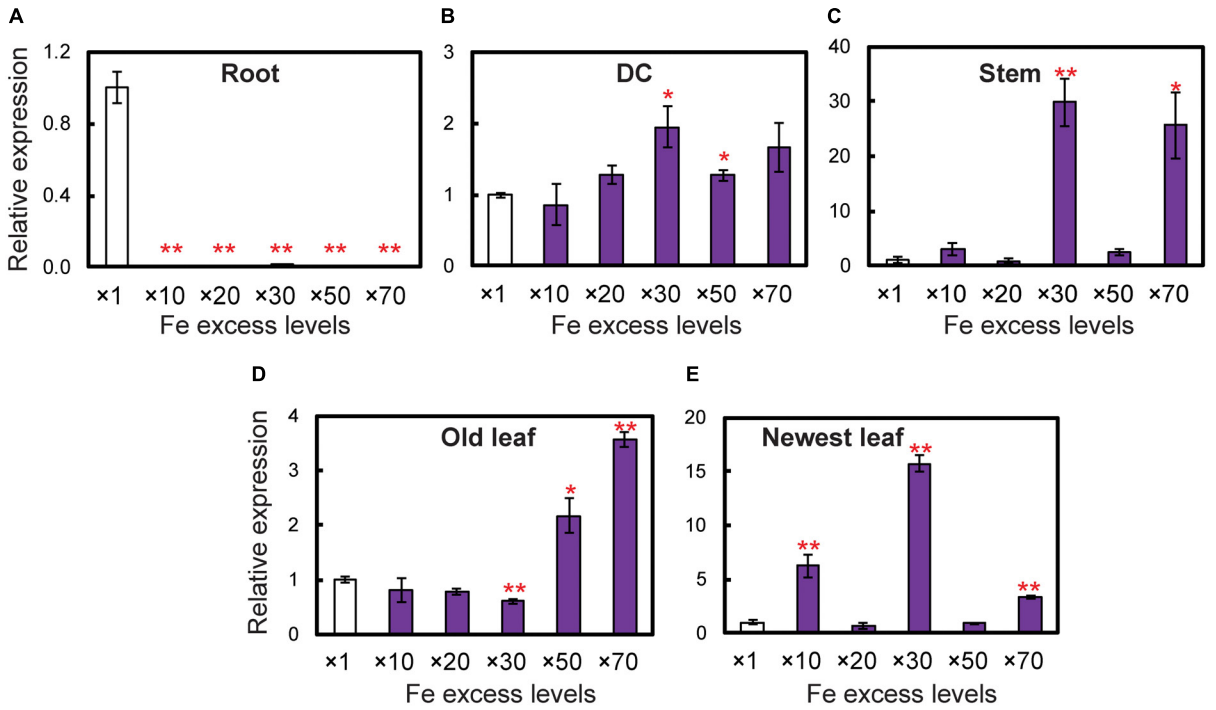

FIGURE 5 | Expression levels of the *OsDMAS1* gene in rice tissues under control and various Fe excess conditions. **(A)** Roots. **(B)** DCs. **(C)** Stems. **(D)** Old leaves. **(E)** Newest leaves. DC, discrimination center. This figure shows confirmation of the microarray results listed in Table 1 of Aung et al. (2018) from qPCR analyses. Error bars represent ± 1 standard error (SE) of the technical variation, $n = 3$. Data were normalized to the observed expression levels of *alpha-tubulin* and presented as relative gene expression in each tissue (×1 Fe = 1). Asterisks above the bars indicate significant differences (*$P < 0.05$; **$P < 0.01$) compared to the control (×1 Fe).

the expression patterns of these genes in various tissues (**Figure 5**). In roots, *OsDMAS1* expression was reduced but not completely suppressed under Fe excess compared to control conditions (**Figure 5A**). In aboveground tissues (i.e., DCs, stems, old leaves and newest leaves), the expression of *OsDMAS1* was similar under both control and Fe excess conditions, or higher under excess Fe conditions (**Figures 5B–E**). We also measured *OsNAAT1* expression, which was reduced in roots, but not completely suppressed. Its levels remained similar or increased with Fe excess in DC, old leaf and newest leaf tissues (**Supplementary Figure S2**).

Endogenous NA and DMA Are Present in Both Roots and Shoots With Excess Fe

Endogenous NA and DMA concentrations were analyzed in roots and shoots of NT rice grown under control and Fe excess conditions, and were present in both roots and shoots under excess Fe and control Fe conditions (**Figure 6**). Shoots had higher concentrations of NA and DMA than roots, and these concentrations did not significantly differ between control and Fe excess plants.

The *OsNAS3* Knockout Plants Are Weaker Under Excess Fe

The *OsNAS3* knockout mutant line described by Lee et al. (2009) was used to investigate the response to Fe excess. The knockout plants and NT were grown in hydroponic cultures with control and excess Fe conditions. We also measured *OsNAS3* expression in knockout plants under control and excess Fe conditions (**Supplementary Figure S3**). Under excess Fe supply, all knockout plants showed growth defects compared to NT plants (**Figures 7A,B** and **Supplementary Figure S4**). The NT plants under Fe-excess set panicles likewise under control Fe conditions but the knockout plants under Fe excess did not (**Figures 7A,B**). Shoot and root growth were significantly suppressed in knockout plants compared to NT under both control and excess Fe conditions (**Figures 7C,D**). Continuous growth was observed in both shoots and roots of all plants under control conditions (**Figures 7C,E**). Inferior shoot growth became pronounced in knockout plants with excess Fe after 7 days, and growth was stunted after 27 days, while root growth retardation occurred earlier, at 5 days after excess Fe exposure (**Figures 7D,F**). In the second experiment, the dry weight of roots and shoots were also measured. The shoot dry weights of the knockout plants were similar with NT under control condition, but reduced 36% in excess Fe compared with NT (**Figure 7G**). The root dry weights of the knockout plants reduced 20% in control condition and 46% in Fe excess condition compared to those of NT (**Figure 7H**). In this experiment, rather than the growth defect, the decrease in dry weight and the leaf bronzing caused by Fe excess damage in knockout plants were more pronounced. Bronzing symptoms on leaves were observed and bronzing scores were recorded for control and

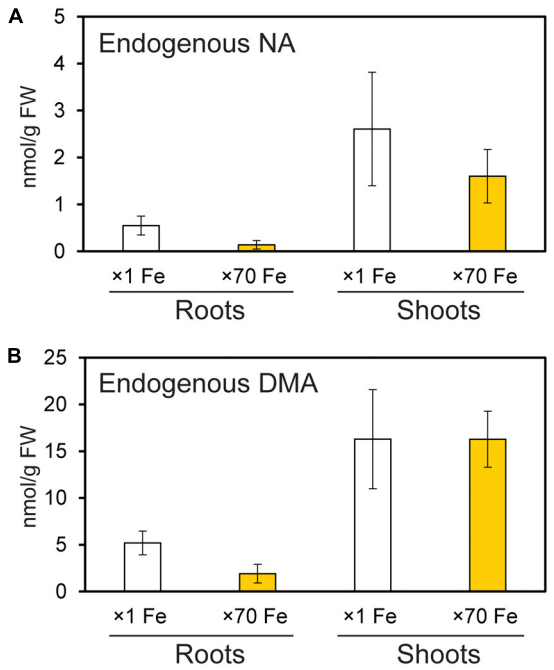

FIGURE 6 | Amounts of endogenous nicotianamine (NA) and deoxymugineic acid (DMA) in the roots and shoots of control and Fe-excess rice. **(A)** The amount of endogenous NA and **(B)** the amount of endogenous DMA in roots and shoots of non-transformant rice under control and Fe excess conditions. Plants were grown hydroponically under control (×1 Fe) and excess ferrous Fe (×70 Fe) conditions at pH 4.0 for 14 days. Error bars represent ± 1 SE of three biological replicates. There were no significant differences between × 1 Fe and × 70 Fe in roots or shoots in **(A,B)**, as determined using a *t*-test (*$P < 0.05$; **$P < 0.01$).

Fe-excess NT and *OsNAS3* knockout plants. All leaves were healthy in both NT and knockout plants under control Fe conditions (**Figure 8A**). By contrast, *OsNAS3* knockout plants showed serious leaf bronzing, particularly in older leaves, with excess Fe compared to NT plants (**Figure 8A**). Higher bronzing scores in all leaves of knockout plants (first to sixth newest leaves) were observed compared to those of NT plants exposed to excess Fe (**Figure 8B**).

We also measured metal concentrations in the newest leaves, third newest leaves (older leaves), and whole roots of *OsNAS3* knockout mutants and NT plants grown for 23 days under either control or Fe excess conditions (**Figure 9**). With excess Fe, both NT and knockout plants showed higher Fe accumulation in the newest leaves, which was even higher in older leaves, compared to the control condition (**Figure 9A**). In particular, *OsNAS3* knockout plants had significantly higher Fe accumulation in both the newest (3 times higher) and older leaves (2 times higher) compared to the NT under excess Fe, while there were no differences from the NT in the control Fe treatment (**Figure 9A**). The Zn and Cu concentration trends did not differ between knockouts and NT under control conditions, but these trends were altered with excess Fe (**Figures 9B,C**). Both NT and knockout plants had higher Zn and lower Cu concentrations in the newest leaves than in older leaves. The concentrations of these metals were similar between the newest and older leaves of knockout plants with excess Fe (**Figures 9B,C**). Under excess Fe, knockout plants tended to have lower Zn in the newest leaves and lower Cu in older leaves compared to NT (**Figures 9B,C**). Mn accumulation was greater in older leaves than the newest leaves in the control condition, and its accumulation decreased with excess Fe in both NT and knockout plants (**Figure 9D**). Under excess Fe conditions, knockout plants tended to have higher Mn accumulation than NT plants, particularly in older leaves. The concentrations of Fe in roots were elevated in both knockouts and NT plants grown under excess Fe compared to control treatments, but there were no significant differences between knockout mutants and NT plants (**Figure 9E**). In roots, plants treated with excess Fe had lower concentrations of Zn, Cu, and Mn (**Figures 9F–H**). These metal accumulations were unaltered between NT and knockout plants, regardless of Fe status (**Figures 9F–H**). To evaluate how Fe is localized in leaf tissues of knockout plants, we observed Fe histochemical localization as deep blue staining using the Prussian blue staining method. Under control Fe conditions, both NT and knockout plants showed low Fe contents in leaves (**Figures 10A,B**). Iron staining was observed with Fe excess in both first and third newest leaves of NT plants (**Figures 10C,E**). Iron staining was more prominent in the newest leaves and in older leaves of Fe-excess knockout plants that exhibited serious leaf bronzing than in NT leaves (**Figures 10D,F**).

Transgenic Line With Elevated NA Production Was More Tolerant to Excess Fe

To further examine the role of NA in the response to excess Fe in rice, a transgenic rice line with 15-fold elevated NA production in shoot tissues via induced expression of barley *HvNAS1* (Masuda et al., 2009) was cultivated under both control and Fe excess conditions, and its growth and morphological characteristics were observed. Under excess Fe, the high-NA line maintained its growth and remained healthy throughout cultivation for 39 days, showing increased tolerance to excess Fe compared to NT plants, and similar growth to NT plants under control conditions (**Supplementary Figure S5**).

DISCUSSION

Expression of *OsNAS3* Is Investigated in Various Tissues Under Fe Excess Conditions

The localization of *OsNAS3* expression was investigated using promoter-*GUS* analyses to determine the physiological role of this gene under Fe excess conditions. The strong expression of *OsNAS3* was observed throughout Fe-excess root cells compared to control roots, suggesting that *OsNAS3* functions deep within roots in the presence of excess Fe. Inoue et al. (2003) showed that *OsNAS3* expression was slightly induced in roots under Fe deficiency. Thus, it is conceivable that *OsNAS3* preferentially works under stress conditions: it may

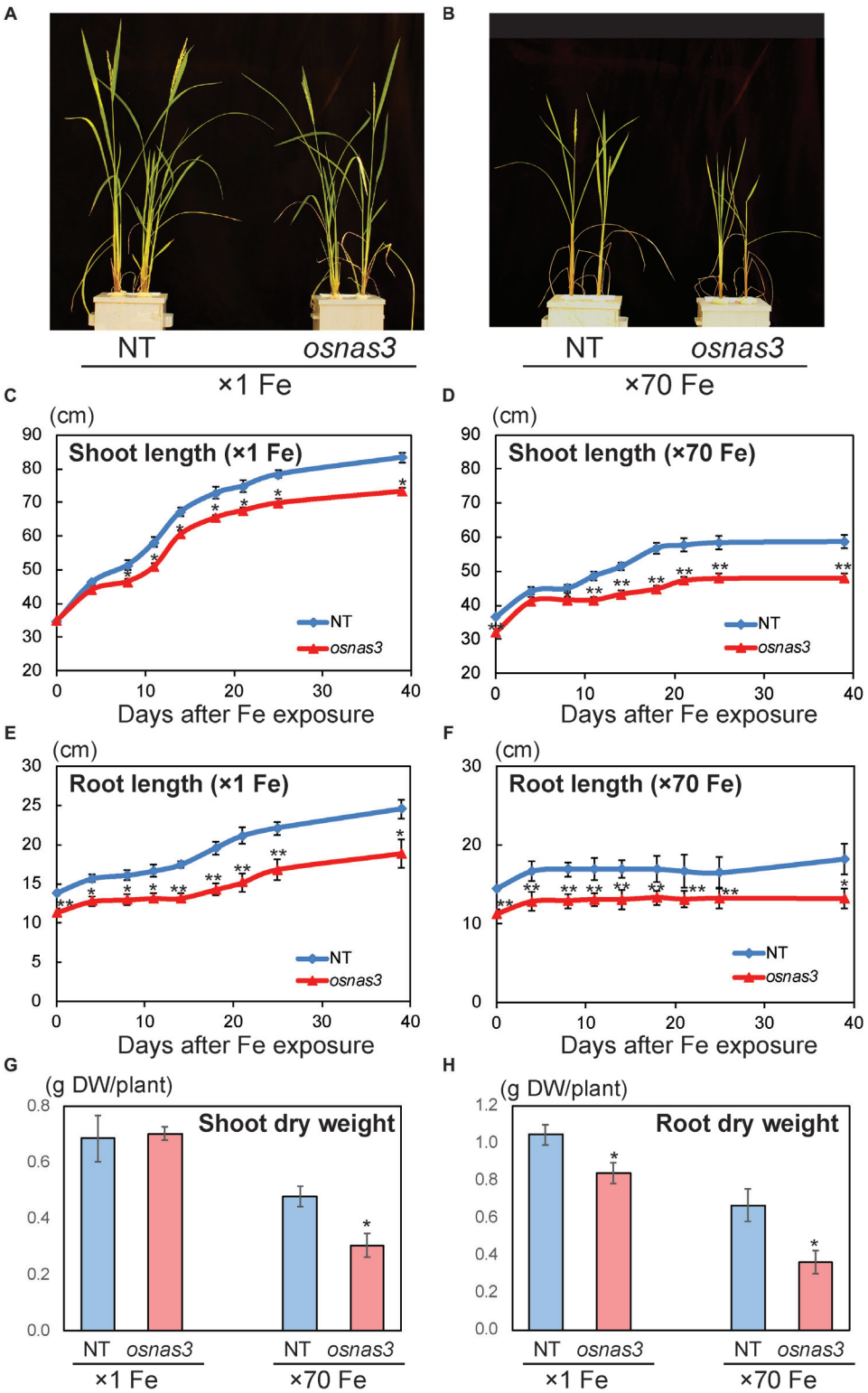

FIGURE 7 | Plant appearance and growth of NT and *OsNAS3* knockout rice. **(A,B)** Appearance of *OsNAS3* knockout plants and non-transformants (NT) under control **(A)** or Fe excess **(B)** conditions after 39-day treatment. **(C,D)** Shoot length under control **(C)** or Fe excess **(D)** conditions. **(E,F)** Root length under control **(E)** or Fe excess **(F)** conditions. **(G,H)** Dry weights of shoots **(G)** and roots **(H)** under control and Fe excess condition at 23 days after transplanting (from 2nd experiment). Error bars represent the standard error (SE) of biological replicates, $n = 4$ for NT and $n = 3$ for knockout plants. Plants were grown hydroponically under control (×1 Fe) or excess ferrous Fe (×70 Fe) conditions at pH 4.0. Asterisks indicate significant differences compared to the NT at each time point or each Fe condition (*$P < 0.05$, **$P < 0.01$).

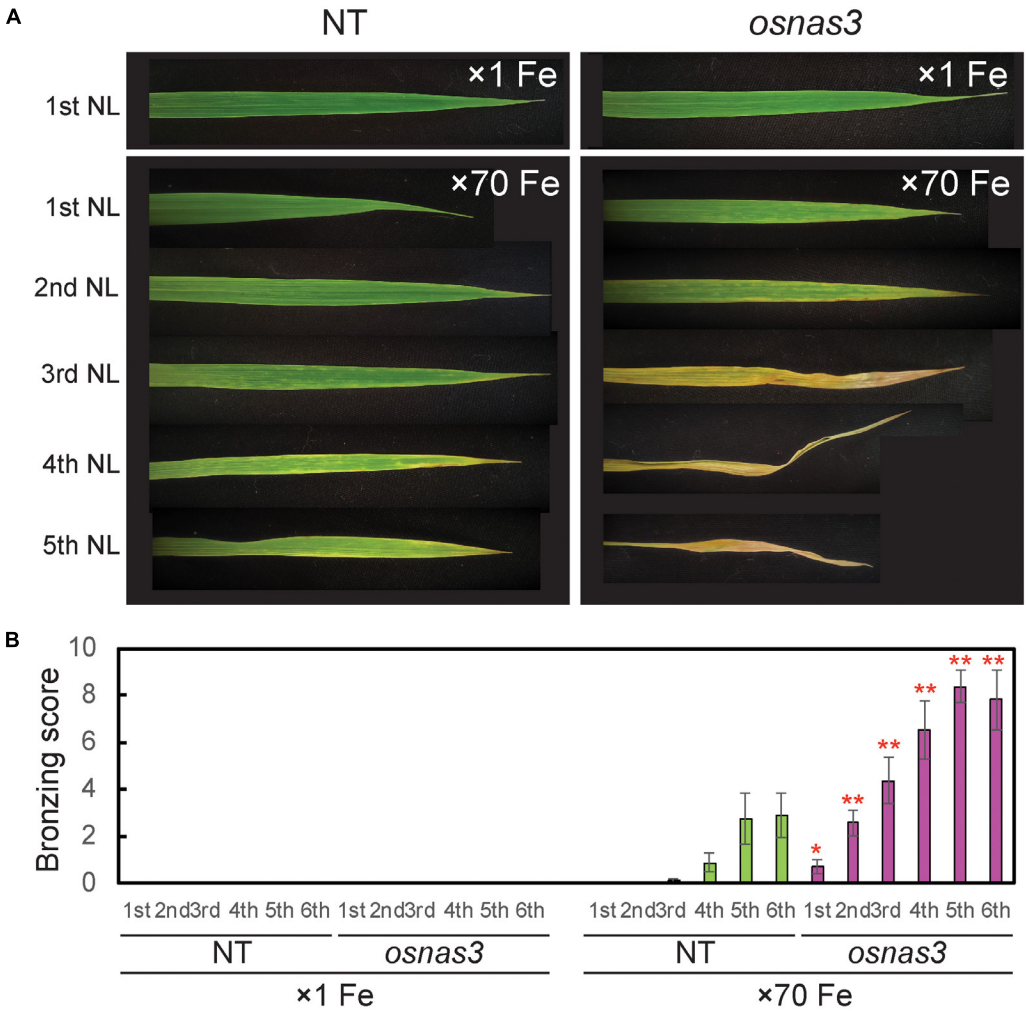

FIGURE 8 | Leaf appearance and leaf bronzing scores of NT and *OsNAS3* knockout rice. **(A)** Bronzing symptoms on representative leaves after 16 days of control or excess Fe stress treatment. The first, second, third, fourth, and fifth newest leaves (NL) are shown. **(B)** Bronzing scores after 17 days of Fe exposure. The first, second, third, fourth, fifth and six newest leaves are indicated on the horizontal axis as 1st, 2nd, 3rd, 4th, 5th, and 6th, respectively. Error bars represent the SE of biological replicates, $n = 8$. Plants were grown hydroponically under control (×1 Fe) and excess ferrous Fe (×70 Fe) conditions at pH 4.0. Asterisks indicate significant differences compared to the NT for each Fe condition and plant part (*$P < 0.05$, **$P < 0.01$).

function in roots weakly under Fe deficiency and strongly under excess Fe conditions.

Under excess Fe, *OsNAS3* expression was particularly dominant in exodermis, epidermis and vascular bundles (**Figure 1**), especially, extremely strong activity was observed in phloem cells, phloem companion cells, protoxylem, xylem parenchyma cells, and epidermal cells (**Figures 1D,E**). These results suggest that NA synthesis due to *OsNAS3* may be involved in the radial movement of Fe to vascular bundle cells, as well as chelating excess Fe in roots and enhancing xylem and phloem loading.

Inoue et al. (2003) reported that under Fe deficiency, *OsNAS3* expression was restricted to the central cylinder cells and did not extend to all root cells, suggesting that unlike *OsNAS1* and *OsNAS2*, *OsNAS3* does not contribute to the enhanced secretion of DMA from Fe-deficient roots. However, DMA accumulation was detected in the xylem sap of Fe-sufficient rice and under control Fe conditions (Kawai et al., 2001; Kakei et al., 2009). Our results also showed DMA accumulation in both control and Fe excess roots (**Figures 5**, **6**). Expression of *OsNAAT1* and *OsDMS1* was observed in both control and excess Fe roots (**Figure 5A** and **Supplementary Figure S2A**), suggesting that NA is further converted into DMA in these cells under control and excess Fe conditions and that not only NA but also DMA may participate in Fe detoxification.

Stronger expression of *OsNAS3* was observed in Fe-excess old leaves compared to control Fe leaves (**Figure 2**). Under control Fe conditions, *OsNAS3* expression was restricted to phloem cells inside the large and small vascular bundles of old leaves (**Figures 2A,C,E**). Strong induction of *OsNAS3* expression in old leaves was also observed through microarray and qPCR analyses (Aung et al., 2018). The GUS analyses

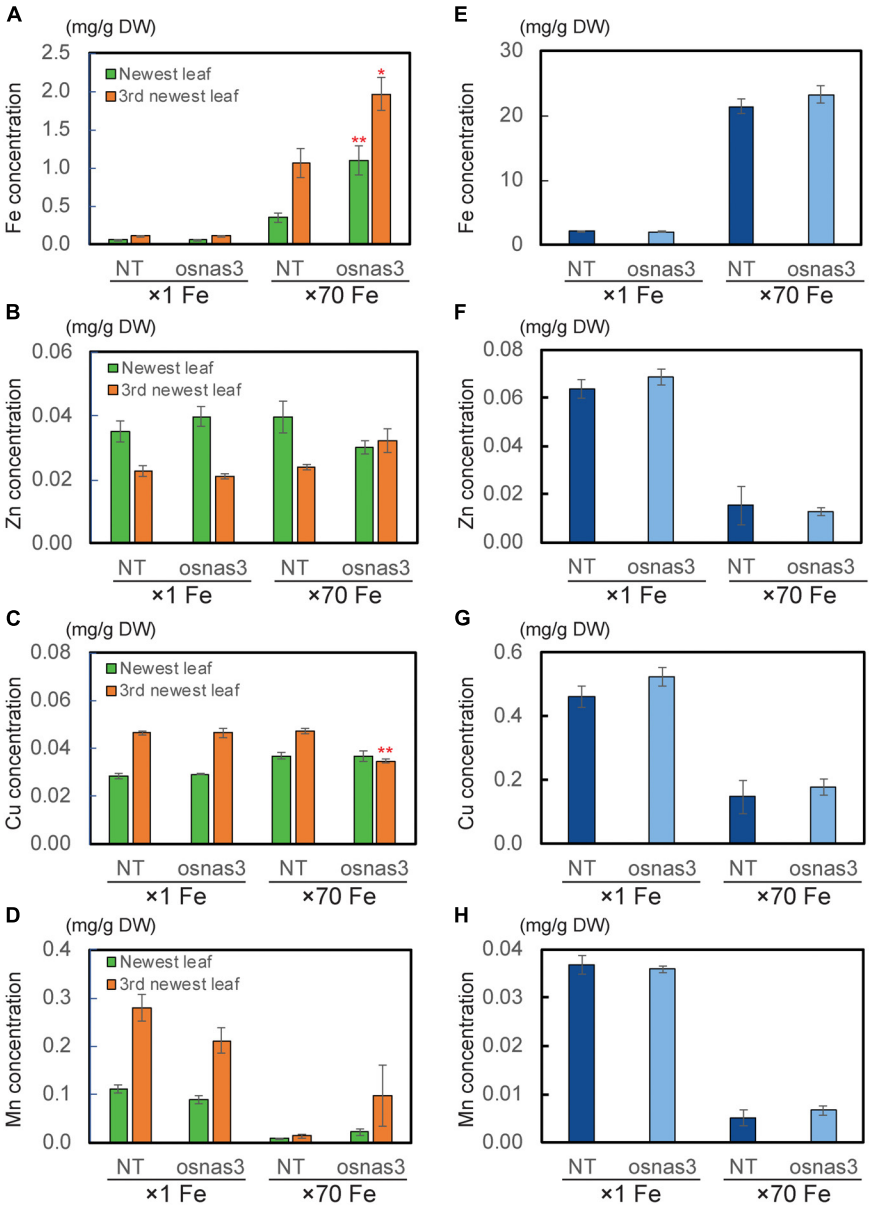

FIGURE 9 | The metal concentrations in NT and *OsNAS3* knockout plants under control and Fe excess conditions. **(A)** Fe, **(B)** Zn, **(C)** Cu and **(D)** Mn concentrations in leaves. **(E)** Fe, **(F)** Zn, **(G)** Cu and **(H)** Mn concentrations in roots. Plants were grown hydroponically under control (×1 Fe) and excess ferrous Fe (×70 Fe) conditions at pH 4.0 for 23 days. Green and orange bars indicate concentrations in the newest and third newest leaves, respectively. Error bars represent ± 1 SE from 3 biological replicates. Asterisks above the bars indicate significant differences compared to NT for each condition and plant part (*$P < 0.05$; **$P < 0.01$).

showed dominant expression in vascular bundles, but only weak expression throughout the leaves, particularly in mesophyll cells. This result might be due to Fe stress causing old leaves to turn bronze in color, associated with cell death due to Fe overload (**Figures 2D,G–J** and **Supplementary Figure S1B**). In this study, we applied strong Fe excess stress to plants (70 times the control level). Thus, an experiment using milder Fe excess stress may be more suitable for identifying differences in old leaves.

Expression of *OsNAS3* was observed in the trichomes of old leaves under excess Fe (**Figure 2H**). The Fe toxicity induces oxidative stress, which in turn causes limitation of photosynthesis. A rice variety that is sensitive to Fe excess showed impairment in light energy partitioning and oxidative damage before the onset of visual symptoms (Pinto et al., 2016). Some plant species accumulate excess metals in trichomes, cuticles or epidermal common cells to avoid greater damage to photosynthetic machinery (Küpper et al., 2000; Robinson et al., 2003; Freeman et al., 2006). Presumably, NA synthesis or allocation in trichomes and epidermal cells may be responsible for protecting leaf photosynthesis during Fe excess stress.

Trichomes and epidermal cells showed high levels of GUS activity in the newest leaves irrespective of Fe status in this study (data not shown). *OsNAS3* expression was also frequently seen in bulliform (motor) cells in old leaves treated with excess Fe (**Figure 2I**). Bulliform cells act as an entrance for light into the mesophyll cells (Clayton and Renvoize, 1986) and participate in the folding of mature leaves to minimize water loss during drought as well as the expansion of young leaves rolled in the apex (Shields, 1951; Jane and Chiang, 1991). Similar *OsNAS3* expression in bulliform cells was observed in Fe-deficient leaves, suggesting a possible role of metals bound to NA in the regulation of water volume in bulliform cells (Inoue et al., 2003). Our result provides further support for *OsNAS3* expression in these cells being for young leaf expansion and protection against water loss induced by excess Fe stress.

Expression of *OsNAS3* was observed in both vascular bundles and mesophyll cells in the newest green leaves of both Fe sufficient and excess conditions (**Figures 4C,D** and **Supplementary Figures S1C,D**). Inoue et al. (2003) showed GUS expression in Fe sufficient green leaf tissue. Nicotianamine produced by *OsNAS3* in the newest leaves may chelate excess Fe to mitigate Fe excess damage to the newest leaves. Iron excess causes a deficiency of other metals, such as Zn (Aung et al., 2018). Thus, NA is thought to support to the transport of other minerals, including Zn, in these leaves. In the inner part of the stem, prospective new leaves folded inside stem tissues showed denser GUS staining under Fe excess conditions compared to the control (**Figures 3C–F**). These very young new leaves inside the inner part of the stem are prone to Fe exposure transported via phloem pathway, but less Fe exposure than the previously extended leaves where Fe is transported via xylem stream from Fe excess roots. Still, protection from Fe excess is thought to be very important for new leaves inside the stem. *OsNAS3* is thought to work in the next set of leaves to emerge when they are folded inside the stem. Discrimination center (DC) is a region that includes the shoot meristem, node, and internode (Mori, 1998; Itoh et al., 2005) and plays an important role in mineral and metabolite transport in graminaceous plants. Iron and other minerals absorbed by the roots first accumulate in the DC and then are distributed to shoots (Tsukamoto et al., 2009). *OsNAS3* is strongly induced in DC under Fe excess (Aung et al., 2018). In this study, the strong expression of *OsNAS3* was localized in DC, regardless of Fe status (**Figures 4E,F** and **Supplementary Figures S1E,F**). Iron chelated with NA controlled by *OsNAS3* in DC might be transported to the shoots through YSL transporters such as *OsYSL17* and *OsYSL18*, which are induced under Fe excess in the roots and DC (Aung et al., 2018).

Endogenous NA and DMA Are Present in Both Roots and Shoots Under Excess Fe

Under both normal and limited Fe conditions, graminaceous plants produce NA, which is further converted into DMA to acquire Fe from the rhizosphere (Takagi, 1976; Marschner et al., 1986). Nicotianamine enhances Fe translocation within plants under both limited and normal Fe conditions (Takahashi et al., 2003). Our results confirmed the presence of NA in control roots

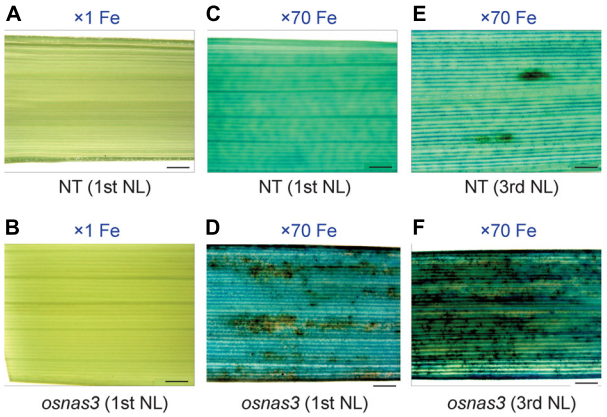

FIGURE 10 | Histochemical Fe localization in leaves of NT and *OsNAS3* knockout rice determined through Prussian blue staining. **(A)** First newest leaf of NT and **(B)** first newest leaf of knockout plant under control Fe conditions. **(C)** First newest leaf of NT, **(D)** first newest leaf of knockout plant, **(E)** third newest leaf of NT and **(F)** third newest leaf of knockout plant under Fe excess conditions. NL, newest leaf. Plants were grown hydroponically under control (×1 Fe) and excess ferrous Fe (× 70 Fe) conditions at pH 4.0 for 23 days. Scale bars: 500 μm.

(**Figure 6**). This NA was produced by *OsNAS1* and *OsNAS2* to enhance Fe translocation under normal condition. On the other hand, under Fe excess condition, plants might not need to produce further NA within the plant to take up more Fe. However, NA and DMA were present in roots and shoots under Fe excess (**Figure 6**). *OsNAS3* was strongly induced in most rice tissues under Fe excess compared to the control (Aung et al., 2018). Thus, this NA might be produced by *OsNAS3*. Under normal Fe condition (x 1 Fe), rice plants should have efforts to take up and translocate Fe within the plant body. Thus, the *OsNAS1* and *OsNAS2* expression was high in roots under x1 Fe condition for the transport of Fe and other metals within the plant body, whereas their expression in roots was extremely low under ×70 Fe condition (Aung et al., 2018). Moreover, the produced NA in roots will be transported to shoot under normal Fe condition together with other metal transportation. Because of this reason, although NA productivity increased by *OsNAS3* under Fe excess, total NA concentrations was the same or slightly reduced under Fe excess condition (**Figure 6**). These results clearly show that the roles and the functions of the NA between these two conditions are different. It is well understood in plant nutrition that NA is used for Fe translocation or a precursor of DMA for Fe uptake. Our finding is that NA and DMA still exist under Fe excess and there is a role of them under Fe excess. The expression of *OsNAAT1* and *OsDMAS1* in roots was reduced but not completely suppressed with excess Fe (**Figure 5A** and **Supplementary Figure S2**). Their expression levels were even higher under Fe excess in the DC, stem, old leaves, and newest leaves (**Figures 5B–E** and **Supplementary Figure S2**; Aung et al., 2018). Thus, DMA may also participate in Fe detoxification processes under Fe excess conditions. Free Fe causes cellular Fe toxicity because it serves as a catalyst in the formation of free radicals from reactive oxygen species via the Fenton reaction. But

Fe chelated with NA does not undergo the Fenton reaction and can be safely sequestered and stored in ferritins or vacuoles within plant tissues. The Fe(II)-NA complexes are poor Fenton reagents, based on their ability to mediate H_2O_2-dependent oxidation of deoxyribose, suggesting that NA has a vital role in scavenging Fe and protecting the cell from Fe-induced oxidative damage (von Wirén et al., 1999). Thus, NA and DMA production by *OsNAS3* under Fe excess conditions is to chelate free excess Fe and thus mitigate Fe excess stress.

Among NAS genes in rice, *OsNAS3* belongs to Clade II, (Mizuno et al., 2003; Bonneau et al., 2016). Bonneau et al. (2016) reported that maize *ZmNAS3*, *ZmNAS4*, *ZmNAS5*, barley *NASHOR2*, wheat *TaNAS9-A*, *TaNAS9-B*, and *TaNAS9-D* are included in Clade II, and among these, wheat *TaNAS9-A* and *TaNAS9-D* have greater relative expression in roots under Fe sufficiency than Fe deficiency. These genes are closely related to *OsNAS3* and they might operate under Fe excess in the same manner as *OsNAS3*. Expression of Clade II *NAS* genes decreased under Fe deficiency and was induced in roots and shoots under normal Fe condition. Thus, Clade II NAS proteins may not contribute to MA biosynthesis under Fe deficiency, but may be involved in NA biosynthesis to support Fe loading of vascular tissues and maintenance of cellular Fe homeostasis (Bonneau et al., 2016).

The *OsNAS3* Knockout Plants Are Sensitive to Fe Excess

The *OsNAS3* knockout plants resulted in impaired shoot and root growth than NT under both control and Fe excess conditions (**Figure 7**). The NT plants under Fe-excess set panicles likewise under control Fe condition but the knockout plants under Fe-excess did not set panicles (**Figures 7A,B**). Dry weights of the knockout plants reduced in both shoots and roots under excess Fe (**Figures 7G,H**). In this study, the leaf bronzing caused by Fe excess damage in knockout plants was more pronounced than the growth defect. Our results consistently indicated that the knockout line was more susceptible to Fe excess than NT plants in terms of leaf bronzing levels and Fe accumulation in the newest leaves and old leaves (third newest leaves) compared to NT plants (**Figures 8**, **9**, **10**). Disruption of *OsNAS3* clearly enhanced Fe accumulation in leaves in response to excess Fe, but only slightly higher Fe accumulation occurred in the roots than in NT roots (**Figures 9A,E**). These results suggest that enhanced Fe toxicity in *OsNAS3* knockout lines might be due to enhanced Fe translocation from roots to shoots. In fact, NA chelates excess Fe and supports its efficient translocation and sequestration, and hence the plant can reduce Fe translocation to shoots. However, high Fe accumulation was observed in Fe-excess shoots, showing that this knockout rice was unable to translocate excess Fe to the suitable tissues in roots. Iron uptake-related transporters such as *OsIRT1*, *OsIRT2*, *OsNRAMP1*, *OsYSL2*, and *OsYSL15* were highly suppressed under Fe excess (Aung et al., 2018). Thus, this high level of Fe accumulation in shoots may be due to Fe uptake by other chelators or other mineral transporters, for example, Zn transporters, which can take up Fe as well as Zn. These results indicate that *OsNAS3* plays an important role in mitigating Fe excess in rice.

In this study, the treatment applied was severe excess ferrous Fe stress (× 70 Fe; 2520 μM Fe^{2+}) compared to the control in the hydroponic culture at low pH (pH 4.0). We also showed that the transgenic line with higher NA production showed tolerance to this severe level of Fe excess stress (**Supplementary Figure S5**). This line accumulated 15 times more NA and 3 times more DMA in its shoots (Masuda et al., 2009). These results suggest that increased NA and DMA biosynthesis might mitigate the damage from excess Fe in the plant.

Role of NA in Fe Excess and Zn Deficiency

Iron excess leads to Zn deficiency. The Zn concentration was decreased under Fe excess in roots of both NT plants and the *OsNAS3* knockout line (**Figure 9F**). The concentrations of Zn decrease proportionally with the increase in Fe excess levels in roots (Aung et al., 2018). Preventing Fe uptake in response to Fe excess may reduce Zn uptake capacity. At the same time, expression of some putative Zn transporter genes such as *OsZIP4*, *OsZIP5*, *OsZIP7*, and *OsZIP9* is strongly induced in Fe excess roots, suggesting that these putative Zn transporters may participate in enhanced Zn transport under Fe excess (Aung et al., 2018). Nicotianamine plays a vital role in intercellular and long-distance transport of Zn to maintain Zn homeostasis in plants (Clemens et al., 2013). The Zn concentration tended to decrease in new leaves and increased in old leaves in knockouts compared to NT plants under Fe excess conditions (**Figure 9B**). The knockout plant was also impaired in Zn translocation and distribution, suggesting that NA produced by *OsNAS3* may be important to maintaining Zn levels in the newest leaves with excess Fe. Interestingly, expression of *OsNAS3* increased in Zn-deficient roots and shoots, but not that of *OsNAS1* or *OsNAS2* (Suzuki et al., 2008). Under Zn deficiency, *OsNAS3* expression is strongly induced in almost all tissues, by about 3 to 8 times (unpublished data). By contrast, under excess Zn, *OsNAS3* was highly repressed in both roots and shoots, while *OsNAS1* and *OsNAS2* were highly induced (Ishimaru et al., 2008). In this study, in addition to NA, DMA was present in roots and shoots under Fe excess (**Figure 6B**). DMA increases Zn translocation in Zn-deficient rice (Suzuki et al., 2008). It indicates another important role of NA synthesized by *OsNAS3* under excess Fe conditions, alleviating Zn deficiency in rice.

CONCLUSION

In this study, we provide evidence that *OsNAS3* is functional and physiologically crucial under excess Fe, acting as an iron-excess induced gene. Our results suggest that NA and DMA synthesized by *OsNAS3* under excess Fe conditions contribute to Fe detoxification in rice. Nicotianamine plays multiple important roles in Fe nutrition in plants, which can be applied to Fe detoxification as well as Fe deficiency tolerance and Fe biofortification.

This finding will contribute to developing Fe toxicity tolerant rice for growth in acidic paddy fields, which has the potential for improving rice yield to feed the increasing global population.

AUTHOR CONTRIBUTIONS

MSA, HM, and NKN designed, led, and coordinated the overall study. MSA performed most of the experiments, analyzed the results, and wrote the manuscript with assistance from HM. TN analyzed the NA and DMA concentrations. GA and J-SJ provided *OsNAS3* knockout seeds. HM, TK, and NKN discussed the results and improved the manuscript.

FUNDING

This research was supported by the Japan Society for the Promotion of Sciences (JSPS) Fellowship Program for Overseas Researchers, MSA (ID No. P04079) and (JSPS KAKENHI Grant No. 14F04079) host researcher NKN, Grant-in-Aid for Young Scientists (JSPS KAKENHI Grant No. 18K14367) to MSA, and the Advanced Low Carbon Technology Research and Development Program (ALCA) of the Japan Science and Technology Agency (Grant No. JPMJAL1107) to NKN.

ACKNOWLEDGMENTS

We thank Dr. Haruhiro Inoue from the National Agriculture and Food Research Organization (NARO) and Dr. Reiko Nakanishi Itai from The University of Tokyo for providing *OsNAS3* promoter-*GUS* seeds. We thank Dr. Sichul Lee for providing seeds of the *OsNAS3* knockout mutant. We also thank the following individuals from Ishikawa Prefectural University: Dr. Tatsuro Hamada for support of research facilities, and Ms. Yukiko Sato, Ms. Reiko Omote, and Ms. Emiko Nakanishi for research assistance.

SUPPLEMENTARY MATERIAL

The Supplementary Material for this article can be found online at: https://www.frontiersin.org/articles/10.3389/fpls.2019.00660/full#supplementary-material

REFERENCES

Aung, M. S., Masuda, H., Kobayashi, T., Nakanishi, H., Yamakawa, T., and Nishizawa, N. K. (2013). Iron biofortification of myanmar rice. *Front. Plant Sci.* 4:158. doi: 10.3389/fpls.2013.00158

Aung, M. S., Masuda, H., Kobayashi, T., and Nishizawa, N. K. (2018). Physiological and transcriptomic analysis of responses to different levels of iron excess stress in various rice tissues. *Soil Sci. Plant Nutr.* 64, 370–385. doi: 10.1080/00380768.2018.1443754

Bashir, K., Inoue, H., Nagasaka, S., Takahashi, M., Nakanishi, H., Mori, S., et al. (2006). Cloning and characterization of deoxymugineic acid synthase genes from graminaceous plants. *J. Biol. Chem.* 281, 32395–32402. doi: 10.1074/jbc.M604133200

Bonneau, J., Baumann, U., Beasley, J., Li, Y., and Johnson, A. A. T. (2016). Identification and molecular characterization of the nicotianamine synthase gene family in bread wheat plant. *Biotech. J.* 14, 2228–2239. doi: 10.1111/pbi.12577

Boonyaves, K., Wu, T.-Y., Gruissem, W., and Bhullar, N. K. (2017). Enhanced grain iron levels in rice expressing an iron-regulated metal transporter, nicotianamine synthase, and ferritin gene cassette. *Front. Plant Sci.* 8:130. doi: 10.3389/fpls.2017.00130

Clayton, W. D., and Renvoize, S. A. (1986). *Genera Graminum – Grasses of the World. Kew Bulletin Additional Series XIII*. London: Her Majestic Stationary Office.

Clemens, S., Deinlein, U., Ahmadi, H., Horeth, S., and Uraguchi, S. (2013). Nicotianamine is a major player in plant Zn homeostasis. *Biometals* 26, 623–632. doi: 10.1007/s10534-013-9643-1

Douchkov, D., Gryczka, C., Stephan, U. W., Hell, R., and Baumlein, H. (2005). Ectopic expression of nicotianamine synthase genes results in improved iron accumulation and increased nickel tolerance in transgenic tobacco. *Plant Cell Environ.* 28, 365–374. doi: 10.1111/j.1365-3040.2005.01273.x

Freeman, J. L., Zhang, L. H., Marcus, M. A., Fakra, S., McGrath, S. P., and Pilon-Smits, E. A. H. (2006). Spatial imaging, speciation, and quantification of selenium in the hyperaccumulator plants *Astragalus bisulcatus* and *Stanleya pinnata*. *Plant Physiol.* 142, 124–134. doi: 10.1104/pp.106.081158

Han, D., Zhang, Z., Ni, B., Ding, H., Liu, W., Li, W., et al. (2018). Isolation and functional analysis of MxNAS3 involved in enhanced iron stress tolerance and abnormal flower in transgenic *Arabidopsis*. *J Plant Int.* 13, 433–441. doi: 10.1080/17429145.2018.1499145

Han, D. G., Yang, G. H., Xu, K. D., Shao, Q., Yu, Z. Y., Wang, B., et al. (2013). Overexpression of a malus xiaojinensis Nas1 gene influences flower development and tolerance to iron stress in transgenic tobacco. *Plant Mol. Biol. Rep.* 31, 802–809. doi: 10.1007/s11105-012-0551-2

Hell, R., and Stephan, U. W. (2003). Iron uptake, trafficking and homeostasis in plants. *Planta* 216, 541–551.

Higuchi, K., Kanazawa, K., Nishizawa, N. K., Chino, M., and Mori, S. (1994). Purification and characterization of nicotianamine synthase from Fe- deficient barley roots. *Plant Soil* 165, 173–179. doi: 10.1007/bf00008059

Higuchi, K., Watanabe, S., Takahashi, M., Kawasaki, S., Nakanishi, H., Nishizawa, N. K., et al. (2001). Nicotianamine synthase gene expression differs in barley and rice under Fe-deficient conditions. *Plant J.* 25, 159–167. doi: 10.1111/j.1365-313x.2001.00951.x

Inoue, H., Higuchi, K., Takahashi, M., Nakanishi, H., Mori, S., and Nishizawa, N. K. (2003). Three rice nicotianamine synthase genes, OsNAS1, OsNAS2, and OsNAS3 are expressed in cells involved in long-distance transport of iron and differentially regulated by iron. *Plant J.* 36, 366–381. doi: 10.1046/j.1365-313X.2003.01878.x

Inoue, H., Takahashi, M., Kobayashi, T., Suzuki, M., Nakanishi, H., Mori, S., et al. (2008). Identification and localization of the rice nicotianamine aminotransferase gene OsNAAT1 expression suggests the site of phytosiderophore synthesis in rice. *Plant Mol. Biol.* 66, 193–203. doi: 10.1007/s11103-007-9262-8

Ishimaru, Y., Suzuki, M., Ogo, Y., Takahashi, M., Nakanishi, H., Mori, S., et al. (2008). Synthesis of nicotianamine and deoxymugineic acid is regulated by OsIRO2 in Zn excess rice plants. *Soil Sci. Plant Nutr.* 54, 417–423. doi: 10.1111/j.1747-0765.2008.00259.x

Itoh, J., Nonomura, K., Ikeda, K., Yamaki, S., Inukai, Y., Yamagishi, H., et al. (2005). Rice plant development: from zygote to spikelet. *Plant Cell Physiol.* 46, 23–47. doi: 10.1093/pcp/pci501

Jane, W. N., and Chiang, S. H. T. (1991). Morphology and development of bulliform cells in arundo formosana hack. *Taiwania* 36, 85–97.

Jeong, D. H., An, S., Kang, H. G., Moon, S., Han, J. J., Park, S., et al. (2002). T-DNA insertional mutagenesis for activation tagging in rice. *Plant Physiol.* 130, 1636–1644. doi: 10.1104/pp.014357

Johnson, A. A. T., Kyriacou, B., Callahan, D. L., Carruthers, L., Stangoulis, J., Lombi, E., et al. (2011). Constitutive overexpression of the OsNAS gene family reveals single gene strategies for effective iron- and zinc-biofortification of rice endosperm. *PLoS One* 6:e24476. doi: 10.1371/journal.pone.0024476

Kakei, Y., Yamaguchi, I., Kobayashi, T., Takahashi, M., Nakanishi, H., Yamakawa, T., et al. (2009). A highly sensitive, quick and simple quantification method for nicotianamine and 2′-deoxymugineic acid from minimum samples using LC/ESI-TOF-MS achieves functional analysis of these components in plants. *Plant Cell Physiol.* 50, 1988–1993. doi: 10.1093/pcp/pcp141

Kawai, S., Kamei, S., Matsuda, Y., Ando, R., Kondo, S., Ishizawa, A., et al. (2001). Concentrations of iron and phytosiderophores in xylem sap of iron-deficient barley plants. *Soil Sci. Plant Nutr.* 47, 265–272. doi: 10.1080/00380768.2001.10408390

Kim, S., Takahashi, M., Higuchi, K., Tsunoda, K., Nakanishi, H., Yoshimura, E., et al. (2005). Increased nicotianamine biosynthesis confers enhanced tolerance of high levels of metals, in particular nickel, to plants. *Plant Cell Physiol.* 46, 1809–1818. doi: 10.1093/pcp/pci196

Klatte, M., Schuler, M., Wirtz, M., Fink-Straube, C., Hell, R., and Bauer, P. (2009). The analysis of arabidopsis nicotianamine synthase mutants reveals functions for nicotianamine in seed iron loading and iron deficiency responses. *Plant Physiol.* 150, 257–271. doi: 10.1104/pp.109.136374

Kobayashi, T., Itai, R. N., and Nishizawa, N. K. (2014). Iron deficiency responses in rice roots. *Rice* 7:27. doi: 10.1186/s12284-014-0027-0

Kobayashi, T., Ogo, Y., Aung, M. S., Nozoye, T., Itai, R. N., Nakanishi, H., et al. (2010). The spatial expression and regulation of transcription factors IDEF1 and IDEF2. *Ann. Bot.* 105, 1109–1117. doi: 10.1093/aob/mcq002

Küpper, H., Lombi, E., Zhao, F. J., and McGrath, S. P. (2000). Cellular compartmentation of cadmium and zinc in relation to other elements in the hyperaccumulator *Arabidopsis halleri*. *Planta* 212, 75–84. doi: 10.1007/s004250000366

Lee, S., Jeon, U. S., Lee, S. J., Kim, Y. K., Persson, D. P., Husted, S., et al. (2009). Iron fortification of rice seeds through activation of the nicotianamine synthase gene. *Proc. Natl. Acad. Sci. U.S.A.* 106, 22014–22019. doi: 10.1073/pnas.0910950106

Marschner, H., and Romheld, V. (1994). Strategies of plants for acquisition of iron. *Plant Soil* 165, 261–274. doi: 10.1007/bf00008069

Marschner, H., Romheld, V., and Kissel, M. (1986). Different strategies in higherplants in mobilization and uptake of iron. *J. Plant Nutr.* 9, 695–713. doi: 10.1080/01904168609363475

Masuda, H., Ishimaru, Y., Aung, M. S., Kobayashi, T., Kakei, Y., Takahashi, M., et al. (2012). Iron biofortification in rice by the introduction of multiple genes involved in iron nutrition. *Sci. Rep.* 2:543. doi: 10.1038/srep00543

Masuda, H., Usuda, K., Kobayashi, T., Ishimaru, Y., Kakei, Y., Takahashi, M., et al. (2009). Overexpression of the barley nicotianamine synthase gene HvNAS1 increase iron and zinc concentrations in rice grains. *Rice* 2, 155–166. doi: 10.1007/s12284-009-9031-1

Mizuno, D., Higuchi, K., Sakamoto, T., Nakanishi, H., Mori, S., and Nishizawa, N. K. (2003). Three nicotianamine synthase genes isolated from maize are differentially regulated by iron nutritional status. *Plant Physiol.* 132, 1989–1997. doi: 10.1104/pp.102.019869

Mori, S. (1998). "Iron transport in graminaceous plants," in *Iron Transport and Storage in Microorganisms, Plants and Animals*. Vol. 35, *Metal Ions in Biological Systems*, eds A. Sigel and H. Sigel (New York, NY: Marcel Dekker), 215–237.

Mori, S., and Nishizawa, N. (1987). Methionine as a dominant precursor of phytosiderophores in graminaceae plants. *Plant Cell Physiol.* 28, 1081–1092.

Murashige, T., and Skoog, F. (1962). A revised medium for rapid growth and bioassay with tobacco tissue cultures. *Physiol Plant.* 15, 473–497. doi: 10.1111/j.1399-3054.1962.tb08052.x

Nozoye, T., Nagasaka, S., Bashir, K., Takahashi, M., Kobayashi, T., Nakanishi, H., et al. (2014). Nicotianamine synthase 2 localizes to the vesicles of iron-deficient rice roots, and its mutation in (the) YXXphi or LL motif causes the disruption of vesicle formation or movement in rice. *Plant J.* 77, 246–260. doi: 10.1111/tpj.12383

NRCS (2005). *Global Soil Regions Map*. Washington, DC: National Resources Conservation Services.

Pich, A., Manteuffel, R., Hillmer, S., Scholz, G., and Schmidt, W. (2001). Fe homeostasis in plant cells: does nicotianamine play multiple roles in the regulation of cytoplasmic Fe concentration? *Planta* 213, 967–976. doi: 10.1007/s004250100573

Pich, A., and Scholz, G. (1996). Translocation of copper and other micronutrients in tomato plants (*Lycopersicon esculentum* Mill.): nicotianamine-stimulated copper transport in the xylem. *J. Exp. Bot.* 47, 41–47. doi: 10.1093/jxb/47.1.41

Pinto, S. D. S., de Souza, A. E., Oliva, M. A., and Pereira, E. G. (2016). Oxidative damage and photosynthetic impairment in tropical rice cultivars upon exposure to excess iron. *Sci. Agricola* 73, 217–226. doi: 10.1590/0103-9016-2015-0288

Robinson, B. H., Lombi, E., Zhao, F. J., and McGrath, S. P. (2003). Uptake and distribution of nickel and other metals in the hyperaccumulator *Berkheya coddii*. *New Phytol.* 158, 279–285. doi: 10.1046/j.1469-8137.2003.00743.x

Shields, L. M. (1951). The involution mechanism in leaves of certain xeric grasses. *Phytomorphology* 1, 225–241.

Shojima, S., Nishizawa, N. K., Fushiya, S., Nozoe, S., Kumashiro, T., Nagata, T., et al. (1989). Biosynthesis of nicotianamine in the suspension-cultured cells of tobacco (*Nicotiana megalosiphon*). *Biol. Metals* 2, 142–145. doi: 10.1007/BF01142552

Stephan, U. W., Schmidke, I., Stephan, V. W., and Scholz, G. (1996). The nicotianamine molecule is made-to-measure for complexation of metal micronutrients in plants. *Biometals* 9, 84–90.

Stumm, W., and Lee, G. F. (1961). Oxygenation of ferrous iron. *Ind. Eng. Chem.* 53, 143–146. doi: 10.1021/ie50614a030

Suzuki, M., Tsukamoto, T., Inoue, H., Watanabe, S., Matsuhashi, S., Takahashi, M., et al. (2008). Deoxymugineic acid increases Zn translocation in Zn-deficient rice plants. *Plant Mol. Biol.* 66, 609. doi: 10.1007/s11103-008-9292-x

Takagi, S. (1976). Naturally occurring iron-chelating compounds in oat- and rice-root washing. I: activity measurement and preliminary characterization. *Soil Sci. Plant Nutr.* 22, 423–433. doi: 10.1080/00380768.1976.10433004

Takahashi, M., Terada, Y., Nakai, I., Nakanishi, H., Yoshimura, E., Mori, S., et al. (2003). The role of nicotianamine in the intracellular delivery of metals and plant reproductive development. *Plant Cell* 15, 1263–1280.

Trijatmiko, K. R., Duenas, C., Tsakirpaloglou, N., Torrizo, L., Arines, F. M., Adeva, C., et al. (2016). Biofortified indica rice attains iron and zinc nutrition dietary targets in the field. *Sci. Rep.* 6:19792. doi: 10.1038/srep19792

Tsukamoto, T., Nakanishi, H., Uchida, H., Watanabe, S., Matsuhashi, S., Mori, S., et al. (2009). 52Fe translocation in barley as monitored by a positron emitting tracer imaging system (PETIS): evidence for the direct translocation of Fe from roots to young leaves via phloem. *Plant Cell Physiol.* 50, 48–57. doi: 10.1093/pcp/pcn192

von Uexküll, H. R., and Mutert, E. (1995). "Global extent, development and economic impact of acid soils," in *Plant–Soil Interactions at Low pH: Principles and Management*, eds R. A. Date, N. J. Grundon, G. E. Raymet, and M. E. Probert (Dordrecht: Kluwer Academic Publishers), 5–19. doi: 10.1007/978-94-011-0221-6_1

von Wirén, N., Klair, S., Bansal, S., Briat, J. F., Khodr, H., Shioiri, T., et al. (1999). Nicotianamine chelates both Fe-III and Fe-II. Implications for metal transport in plants. *Plant Physiol.* 119, 1107–1114. doi: 10.1104/pp.119.3.1107

Yang, G. H., Li, J., Liu, W., Yu, Z. Y., Shi, Y., Lv, B. Y., et al. (2015). Molecular cloning and characterization of MxNAS2, a gene encoding nicotianamine synthase in *Malus xiaojinensis*, with functions in tolerance to iron stress and misshapen flower in transgenic tobacco. *Sci. Hortic.* 183, 77–86. doi: 10.1016/j.scienta.2014.12.014

Zheng, L., Cheng, Z., Ai, C., Jiang, X., Bei, X., Zheng, Y., et al. (2010). Nicotianamine, a novel enhancer of rice iron bioavailability to humans. *PLoS One* 5:e10190. doi: 10.1371/journal.pone.0010190

Conflict of Interest Statement: The authors declare that the research was conducted in the absence of any commercial or financial relationships that could be construed as a potential conflict of interest.

frontiers in Plant Science

ORIGINAL RESEARCH
published: 04 June 2019
doi: 10.3389/fpls.2019.00700

A Vacuolar Membrane Ferric-Chelate Reductase, OsFRO1, Alleviates Fe Toxicity in Rice (*Oryza sativa* L.)

*Lin Li[1], Lingxiao Ye[1,2], Qihui Kong[1] and Huixia Shou[1]**

[1] State Key Laboratory of Plant Physiology and Biochemistry, College of Life Sciences, Zhejiang University, Hangzhou, China,
[2] The Zhejiang University Affiliated 15st Middle School in Hangzhou, Hangzhou, China

Ferric reductase oxidase (*FRO*), the enzyme that reduced ferric iron [Fe (III)] into ferrous iron [Fe (II)], is known to play important roles in Fe absorption and homeostasis in plants that utilize a strategy I mechanism to obtain iron. Rice can use both strategies I and II for Fe uptake depending on the growth conditions. FRO is encoded by two genes in rice genome. Amino acid sequence alignment shows that Os*FRO1* contains all necessary predicted motifs for a functional FRO enzyme, whereas Os*FRO2* lacks a complete transmembrane domain at the N-terminal. Transient expression of OsFRO1: GFP protein fusion revealed that OsFRO1 is localized to the vacuolar membrane in rice protoplast. Os*FRO1* is primarily expressed in leaves and transcript abundance was decreased under excess Fe conditions. Transgenic plants overexpressing Os*FRO1* were more sensitive to Fe toxicity, in contrast RNA interference lines showed more tolerance to Fe excess stress. Furthermore, RNAi lines showed decreased Fe concentrations compared to wild type plants under Fe excess condition. Together these data show that OsFRO1 is involved in reducing ferric Fe into ferrous Fe in the vacuole, and makes the vacuolar stored Fe available to the cytoplasm through Fe (II) or chelated Fe (II) transporters. Under Fe excess condition, the downregulation of *OsFRO1* in the RNAi plants reduced the amount of Fe (II) available for cytoplasm, to alleviate Fe excess toxicity. This indicates that OsFRO1 plays an important role to maintain Fe homeostasis between the cytoplasm and vacuole in rice.

Keywords: rice, ferric reductase oxidase, iron excess, vacuole, iron homeostasis

OPEN ACCESS

Edited by:
Thomas J. Buckhout, Humboldt University of Berlin, Germany

Reviewed by:
Khurram Bashir, RIKEN, Japan
Christian Dubos, Institut National de la Recherche Agronomique (INRA), France

****Correspondence:***
Huixia Shou
huixia@zju.edu.cn

Specialty section:
This article was submitted to Plant Nutrition, a section of the journal Frontiers in Plant Science

Received: *16 February 2019*
Accepted: *13 May 2019*
Published: *04 June 2019*

Citation:
Li L, Ye L, Kong Q and Shou H (2019) A Vacuolar Membrane Ferric-Chelate Reductase, OsFRO1, Alleviates Fe Toxicity in Rice (Oryza sativa L.). Front. Plant Sci. 10:700. doi: 10.3389/fpls.2019.00700

INTRODUCTION

Iron (Fe) is an essential micronutrient for most living organisms. The transition between two oxidation states, the Fe (II) and Fe (III), makes it an indispensable element for multiple biological processes for plant growth (Connorton et al., 2017). Fe participates in various metabolic pathways including photosynthesis, respiration, chlorophyll biosynthesis, and nitrogen fixation (Kobayashi and Nishizawa, 2012; Briat et al., 2015). The redox properties also allow Fe to function as the catalytic component, in the form of heme or Fe–S clusters, in a wide variety of proteins (Guerinot and Yi, 1994).

Although abundant in the Earth's crust Fe bioavailability is strongly restricted by the insolubility of ferric oxide present in well-aerated or alkaline soils, which is not easily accessible for uptake by

plants (Mori, 1999). Fe deficiency retards plant growth and reduces crop yields, but excess Fe also cause toxicity to the plants (Halliwell and Gutteridge, 1992). Plants have two distinct Fe acquisition strategies to obtain Fe from the soil (Römheld and Marschner, 1986; Connorton et al., 2017). Non-grass plants, such as the model plant *Arabidopsis thaliana*, utilize strategy I, which is also known as the reducing strategy. When exposed to Fe-limiting conditions, plants secrete protons and phenolic compounds into the rhizosphere that lower the pH and enhance Fe (III) solubility (Santi and Schmidt, 2009). Fe (III) is reduced to Fe (II) by Ferric Reduction Oxidase 2 (FRO2) localized on the plasma membrane (Robinson et al., 1999). Afterward, Fe (II) is transported across the plasma membrane into the root epidermal cells by the iron-regulated transporter 1 (IRT1) (Eide et al., 1996; Varotto et al., 2002; Vert et al., 2002). Grass plants, such as barley and maize, utilize strategy II which is also called chelating strategy to take up Fe from the soil. In strategy II plants phytosiderophores (PS) are released into the rhizosphere (Kobayashi et al., 2010). After binding Fe (III) in the soil, Fe (III)-PS complexes are taken up by specific transporters belonging to the yellow stripe (YS) or YS like (YSL) family of proteins (Curie et al., 2001; Inoue et al., 2009). Rice has functional IRT1 and IRT2 that allow it to take up Fe (II) directly under submerge conditions (Ishimaru et al., 2006). In addition, rice can secrete phenolic compounds to chelate Fe (III) and solubilize apoplasmic Fe (Bashir et al., 2011; Ishimaru et al., 2011). Thus, rice is considered to use a mixed model for Fe uptake.

Under anaerobic conditions and low pH in flooded soils Fe is present mainly as soluble Fe (II) due to the low redox potential (Becker and Asch, 2005). Fe (II) can be taken up excessively by plant roots, resulting in cellular Fe overloaded, which can be toxic for plants. Fe toxicity has become a widespread nutrient stress affecting the growth of wetland rice, especially in Asia and West Africa (Sahrawat, 2004; Audebert and Fofana, 2009). In plant cells excess amount of Fe (II) contributes to the formation of hydroxyl radicals (·OH) and other reactive oxygen species (ROS) through the Fenton reaction (Fenton, 1984; Becana et al., 1998). These hydroxyl radicals can react with lipids, DNA and proteins, causing irreversible damage and oxidative stress (Briat et al., 1995; Fang et al., 2001). In rice the most obvious symptoms of Fe-overloading stress are leaf bronzing (Asch et al., 2005; Becker and Asch, 2005). Moreover, excess Fe in the soil can damage the root uptake system and adversely affect the acquisition of other nutrients, such as phosphorus, zinc and magnesium, leading to reduced growth and yield loss and even death of plants (Sahrawat, 2004). Thus, the cellular Fe level must be tightly controlled to maintain Fe homeostasis in plants.

The mechanisms for Fe excess tolerance can be divided into three aspects: (1) Avoiding excess Fe accumulation – Fe deposits at the root surface as the Fe plaque and forms a physical barrier to exclude excess Fe uptake (Deng et al., 2010). Reduced Fe translocation from roots to shoots could be important to prevent oxidative stress in leaves. (2) Storing high Fe levels – Fe partitioning into different sub-cellular compartments, mainly apoplast and vacuoles, are crucial to alleviate Fe toxicity (Moore et al., 2014). Ferritins can store up to 4,000 Fe atoms and are considered essential for tolerance to excess Fe (Briat et al., 2010). (3) Scavenging of ROS by antioxidants – Plants may also utilize antioxidants such as ascorbate, glutathione, phenolics or antioxidant enzymes such as superoxide dismutase (SOD), ascorbate peroxidase (APX), and catalase (CAT) to detoxify oxidative molecules (Fang et al., 2001; Wu et al., 2017).

A significantly amount of work has been done on Fe-deficiency in plants. In contrast, the molecular aspects of Fe excess responses remain largely unknown. Several quantitative trait loci (QTL) co-localized on chromosome 1 were reported to be associated with tolerance to Fe excess stress in rice (Wu et al., 2014; Dufey et al., 2015). These results were also confirmed by genome-wide association study (GWAS) (Matthus et al., 2015). A transcriptomic study compared the expression profiling of rice seedlings after short- and long-term exposure to Fe excess (Quinet et al., 2012). It was found that more genes were up- or down-regulated after 3 days than after 3 weeks of Fe excess treatment. Transcriptomic analysis of rice in response to Fe deficiency and excess revealed that there is crosstalk between the two treatments and small open reading frames might play an important role in the response of plants to Fe deficiency and excess (Bashir et al., 2014). OsWRKY80 is the first reported transcription factor induced by Fe excess in plants (Ricachenevsky et al., 2010). However, the biological function of this gene is still under investigation.

Ferric reductase oxidase (FRO), the enzyme to reduce Fe (III) into Fe (II), is known to play important roles in Fe absorption and homeostasis in strategy I plants. There are two *FRO* genes in rice genome, but their function has not yet been characterized. In this study, the predicted amino acid sequence alignment shows that OsFRO1 contains all necessary motifs for a functional FRO enzyme. OsFRO1 is localized in the vacuolar membrane, which is different from other plant FRO proteins previously reported. Under Fe excess conditions, the transcript abundance of Os*FRO1* was decreased in abundance. Knockdown of *OsFRO1* by RNAi alleviated Fe toxicity in transgenic rice. This work indicates that OsFRO1 plays an important role to maintain Fe homeostasis in rice.

MATERIALS AND METHODS

Plant Materials and Growth Conditions

The rice cultivar (*Oryza sativa L.* ssp. *japonica* cv. *Dongjin*) was used for physiological experiments and rice transformations. Seeds were germinated in water for 3 days. After germination uniform seedlings were transferred to nutrient solution containing 1.425 mM NH_4NO_3, 0.323 mM NaH_2PO_4, 0.513 mM K_2SO_4, 0.998 mM $CaCl_2$, 1.643 mM $MgSO_4$, 0.009 mM $MnCl_2$, 0.075 mM $(NH_4)_6Mo_7O_{24}$, 0.019 mM H_3BO_3, 0.155 mM $CuSO_4$, 0.152 mM $ZnSO_4$, 125 μM Fe (II)-EDTA, with pH 5.5 (Yoshida et al., 1976). For gene expression assay, 2-week old seedlings were transferred to normal, Fe deficient or excess nutrient solutions. The solution contains 0, 0.125 mM Fe or 1 mM Fe (II)-EDTA, respectively. Plants were harvested at 7 days after Fe treatment. For phenotypic analysis, 2-week-old

seedlings were grown in nutrient solution with 7 or 0.125 mM Fe (II)-EDTA for 3 days.

All the experiments were carried out in green house with a day/night temperature of 30°C/28°C and a 12 h photoperiod. The nutrient solution was changed every 3 days.

Transient Expression of OsFRO1-GFP and OsFRO2-GFP Fusion Protein

To investigate the subcellular localization of OsFRO1 and OsFRO2, the coding sequences of *OsFRO1* and *OsFRO2* without a stop codon was amplified and cloned into pDEST/CGFP using the gateway system. Rice protoplasts were isolated from 2-week-old seedlings using cellulose R10 and macerozyme R10 as previously described (Ying et al., 2017). Two hundred micro liter of protoplast suspension was transformed with 8∼10 μg plasmid DNA using the PEG (polyethylene glycol)-mediated transformation method (Chen et al., 2011). After incubation at 25°C in the dark for 12 to 14 h, fluorescence images were captured using confocal microscopy.

Vector Construction and Rice Transformation

For over-expression the full-length cDNA of Os*FRO1* was cloned into entry vector pENTR-D-TOPO. After sequencing the LR recombination reaction was performed between an attL-containing entry clone and an attR-containing destination vector pEarlyGate 303 to generate the overexpression (Os*FRO1*-Oe*)* vector. For RNA-interference vector, a 300 bp fragment from the Os*FRO1* coding region was amplified and subcloned into entry vector pDONR201 via BR reaction. Then the fragment was inserted into the destination vector pH7GWIWG2(I) in both a sense and anti-sense orientation to get the interference (Os*FRO1*-Ri) vector (Karimi et al., 2002). For expression pattern analysis, the 1800 bp upstream of the ATG start codon of Os*FRO1* was amplified and cloned into pBI101.3 to generate the P_{OsFRO1}: GUS vector. All the corresponding primers are listed in **Supplementary Table S1**.

The Os*FRO1*-Oe, Os*FRO1*-Ri and P_{OsFRO1}: GUS vectors were transformed into *Agrobacterium* strain EHA101 or EHA105. Transgenic rice plants for the three constructs were regenerated via *Agrobacterium*-mediated transformation as described (Chen et al., 2003).

Histochemical β-Glucuronidase (GUS) Staining

T1 transgenic seeds were germinated and grown in nutrient solution with 125 μM Fe (II)-EDTA. Tissues were immersed immediately in staining solution with 1 mM X-Gluc (5-bromo-4-chloro-3-indolyl-b-D-glucuronidase) overnight at 37°C. Afterward, roots were imbedded in 3% (w/v) agarose (Biowest, Spain). Samples were sectioned to a thickness of 30 μm by vibrating microtome (VT 1000 S, Leica, Bensheim, Germany). The Spur's resin was used to imbed leaves. Sections of 10 μm were cut and the images were observed under a microscope (Eclipse 90i, Nikon, Tokyo, Japan).

Yeast Fe (III) Chelate Reductase Assay

For assaying Fe (III) reduction activity of OsFRO1 and OsFRO2, the full-length cDNA of OsFRO1, OsFRO2 and AtFRO2 were subcloned into pYES2.0 vector to generate pYES2.0-OsFRO1, pYES2.0-OsFRO2 and pYES2.0-AtFRO2, respectively. Constructs were transformed into *S. cerevisiae* wild-type strain BJ2168 using the lithium acetate method according to the manufacturer's manual. Yeast transformants were grown following the protocol described previously (Li et al., 2004). Cells were harvested in the mid-log phase, and Fe (III) chelate reductase activity was quantified based on the absorbance at 562 nm (Yi and Guerinot, 1996).

Total RNA Isolation and Quantitative RT-PCR

Total RNA was extracted from the roots and shoots using TRIzol reagent (Invitrogen, Shanghai, China), according to the manufacturer's instructions. cDNA was synthesized from 2 μg of total RNA using the PrimeScript^{TM} RT reagent Kit (Takara Bio, Inc., Dalian, China). qRT-PCR were conducted using LightCycler 480 SYBR Green I Master Kit (Roche Diagnostics) on a LightCycler480 machine. The relative expression levels were normalized to the housekeeping gene *OsACTIN1* by the formula $2^{-\Delta\Delta Ct}$. The primers for qRT-PCR analysis are given in **Supplementary Table S1**.

Measurement of Element Concentration

To determine the metal concentration in plants, root or shoot samples were dried for 3 days at 80°C. About 0.1 g dry weight was used for digestion. Metal concentration analysis was performed using inductively coupled plasma spectroscopy (ICP-MS, Agilent 7500ce, Santa Clara, CA, United States).

Histochemical Staining for ROS Production

In situ detection of superoxide (O^{2-}) in leaves was conducted using NBT staining as described (Höller et al., 2014). In brief, the expanded leaves were excised and immersed in staining solution containing 0.1% (w/v) NBT, 10 mM sodium azide, 50 mM potassium phosphate (pH 6.4). Vacuum infiltrate the leaves for 30 min until they were completely infiltrated. Afterward, incubate the leaves in 10 mL of staining solution (0.1% NBT) for 15 min. ROS formation was visualized by a scanner (CanoScan 9000F MarkII, Tokyo, Japan).

RESULTS

Identification of OsFRO1 From the Rice Genome

In *Arabidopsis thaliana* there are predicted to be eight *FRO* genes in the genome based on high sequence similarity with *AtFRO2* (Ling et al., 2005). In order to identify *FRO* genes of rice, BLAST searches against the rice genome database using the amino acid sequences of AtFROs were performed. Two putative proteins, named OsFRO1 (LOC_Os04g36720)

and OsFRO2 (LOC_Os04g48930) were found as ortyhologs of AtFROs. Phylogenic analysis of FROs in higher plants showed that OsFRO1 displayed higher similarity to AtFRO7, while OsFRO2 clustered together with three characterized FROs, PsFRO1 (Waters et al., 2002), LeFRO1 (Li et al., 2004), CsFRO1 (Waters et al., 2007) in a small group (**Figure 1A**). OsFRO1 and OsFRO2 have the highest similarity with AtFRO6 (60.9%) and AtFRO2 (58.5%) among the Arabidopsis FROs, respectively (**Figure 1B**).

Plant FROs were identified based on its sequence similarity to human phagocytic NADPH oxidase gp91phox and yeast ferric-chelate reductases such as FREs (Dancis et al., 1990; Babior, 1995). Similar to FREs and gp91phox, AtFRO2 contains the two conserved motifs HPFT and GPYG that are associated with FAD and NADPH binding sites of the cofactor (Robinson et al., 1999). Amino acid sequence alignment of OsFROs with the AtFROs revealed that both OsFRO1 and OsFRO2 contained the two conservative motifs. The FAD binding site of OsFRO1 shared 100% identity with AtFRO6/7 (HPFS), whereas the FAD motif of OsFRO2 is "HPFT," identical to AtFRO2. The NADPH binding site of OsFRO1 is GPYS, identical to the other FROs, whereas that of OsFRO2 is GPYT, different from the functional Arabidopsis FROs analyzed (**Figure 1C**).

The THTMM program was used to predict the membrane topology of two OsFRO proteins, resulting in predictions of 10 transmembrane domains in OsFRO1 and 6 transmembrane domains in OsFRO2 (**Supplementary Figure S1**). OsFRO2 lacks complete transmembrane domains in its N-terminal and might not be functional. Thus, the study is focused on OsFRO1 for further investigation.

OsFRO1 Is Localized on the Tonoplast Membrane

To determine the subcellular localization of OsFRO1 and OsFRO2 GFP was fused to the C terminus of OsFRO1 and OsFRO2 coding regions. The GFP-fusion constructs were transformed into rice protoplasts isolated from stems and leaves of etiolated seedlings. The green fluorescence signal of OsFRO1 was detected in the vacuolar membrane, whereas that of OsFRO2 located mainly in the cytoplasm (**Figure 2**). To further confirm the subcellular localization of OsFRO1, a vacuolar membrane marker, OsSPX-MFS3 (Wang et al., 2015), was co-expressed with OsFRO1 in rice protoplasts. The GFP signal mostly overlapped with the mCherry signal of the vacuolar membrane marker (**Supplementary Figure S2**). Noticeably, the subcellular localization of OsFRO1 was completely different with that of other FROs in plants, since it is the only FRO family member localized to tonoplast to our knowledge. This result indicated that OsFRO1 may play a novel role in Fe homeostasis.

Expression Profile of *OsFRO1*

To investigate the spatial expression of *OsFRO1*, transgenic plants carrying the promoter region of *OsFRO1* fused to the *GUS* gene (P_{OsFRO1}: GUS) were generated. GUS expression was observed in all tissues, including roots, stems, leaves, flowers and seeds (**Figure 3A**). Cross-sections of leaves showed that no staining was observed in bulliform cells and part of epidermal cells (**Figure 3B**). In roots, GUS expression was mainly observed in the mature roots, but not at the young roots. Little staining was detected in root tips (**Figure 3C**). Cross-sections of roots exhibited that GUS expression was observed throughout root except the epidermal cells (**Figure 3D**). In the floral organs, GUS was expressed in stigma and pollen (**Figures 3E–G**). In mature seeds, GUS expression was detected in the glumes (**Figure 3H**). One day after germination, GUS expression was also detected in the endosperm (**Figures 3I,J**).

To gain further insight into the expression pattern of Os*FRO1* the transcript abundance of Os*FRO1* was analyzed in leaves and roots. Results showed that the basal level of Os*FRO1* in leaves was 1000 times as high as that in roots (**Figure 4A**). Similar spatial expression pattern can be found from the microarray data retrieved from GENEVESTIGATOR (**Supplementary Figure S3**). While the mRNA abundance of Os*FRO1* was not affected by Fe deficiency, it is greatly inhibited when plants exposed to solution culture containing excess Fe (**Figure 4B**). In addition, GUS staining of the P_{FRO1}: GUS transgenic plants showed that excess Fe supply significantly suppressed the GUS activity in old leaves, but not in the young leaves (**Figure 4C**).

Knock Down of *OsFRO1* Resulted in More Tolerance to Fe Toxicity in Rice Plants

To determine the biological function of OsFRO1 in Fe homeostasis, *OsFRO1* overexpression (Oe) or the RNA interference (Ri) transgenic lines were generated and the transcript abundance of Os*FRO1* in the Oe and Ri plants was determined by quantitative real-time PCR (qRT-PCR) analyses. The *OsFRO1* transcript abundance were 10–40 times higher in the Oe plants, or 2–5 times lower in the Ri plants, compared to that in the wild type (WT) plants (**Supplementary Figure S4**). Two independent transgenic lines of each construct were selected for further experimental analysis, i.e., Oe-1, Oe-3, Ri-1, and Ri-3.

To evaluate the effect of OsFRO1 on Fe homeostasis, the transgenic plants were grown under Fe deficiency or Fe excess conditions. Under normal or Fe deficient conditions, there was no significant difference in growth performance and Fe concentrations between the transgenic plants and WT control (**Supplementary Figure S5**). When treated with excess Fe for 3 days, all the plants showed bronzing in the leaves, and Fe plaques in roots, which are common symptoms of Fe overaccumulation. The 4^{th} and 5^{th} leaves of the WT and transgenic plants were detached and compared. As shown in **Figure 5A**, *OsFRO1*-Ri lines displayed less bronzing symptom in the leaves compared to WT and Oe plants. No significant differences in plant length or fresh weight were observed between the transgenic plants and WT control (**Figure 5B**).

No significant difference was found in leaf and root Fe concentrations among the WT, Ri, and Oe plants when grown in normal Fe supply condition (**Figure 6A**). Under excess Fe supply condition, the leaf Fe concentrations of the Ri-1 and Ri-3 plants

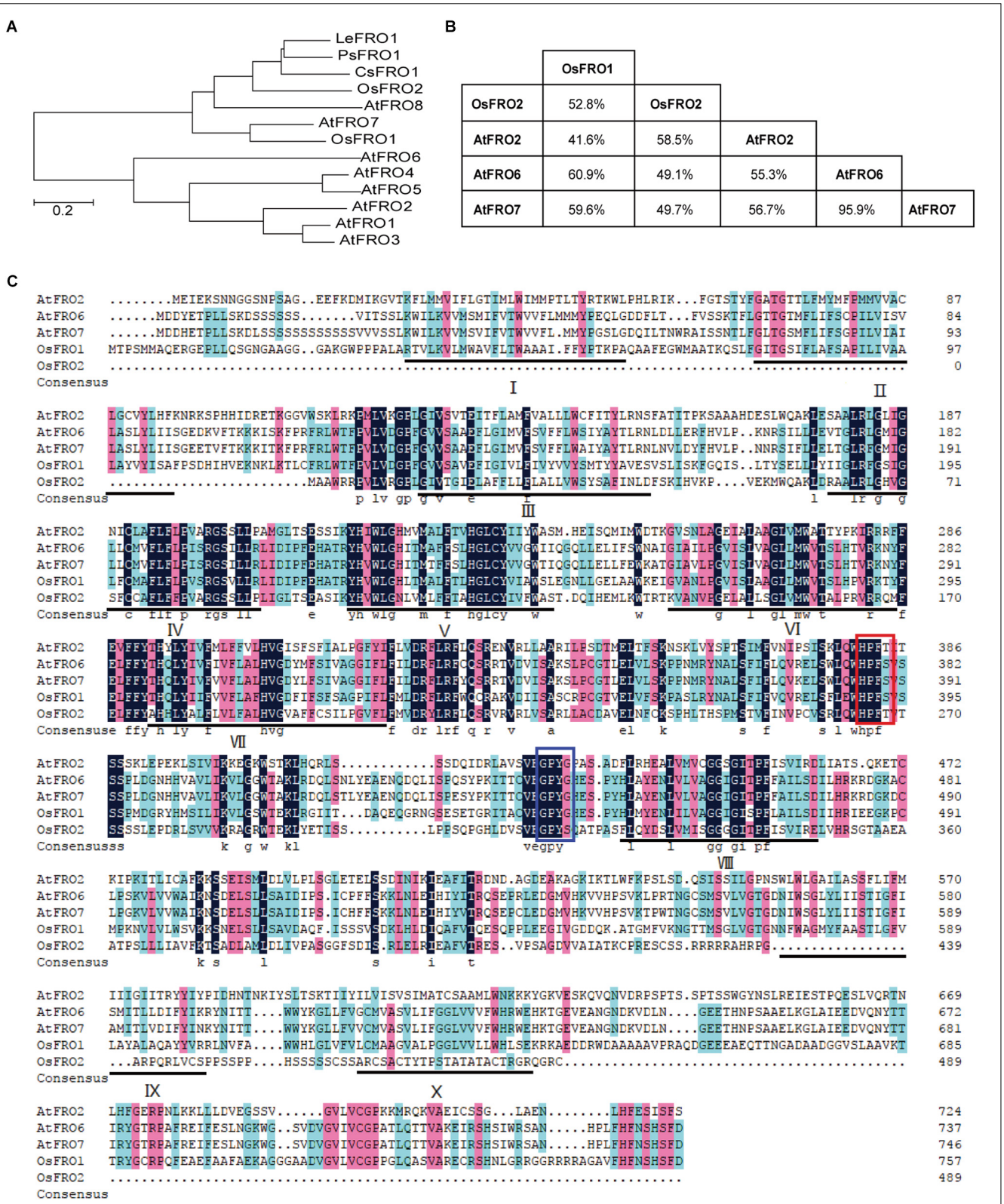

	OsFRO1				
OsFRO2	52.8%	OsFRO2			
AtFRO2	41.6%	58.5%	AtFRO2		
AtFRO6	60.9%	49.1%	55.3%	AtFRO6	
AtFRO7	59.6%	49.7%	56.7%	95.9%	AtFRO7

FIGURE 1 | Phylogenetic analysis and alignments of FROs in plants. **(A)** Phylogenetic analysis of FRO proteins in plants. Amino acid sequences were used and the evolutionary history was conducted in MEGA6 via neighbor-joining method. **(B)** The similarity matrix for FRO proteins from rice and Arabidopsis. **(C)** Amino acids sequences alignment of FRO proteins from rice and Arabidopsis. The FAD and NADPH binding site were highlighted by red and blue boxes, respectively. The locations of the 10 potential transmembrane domains were underlined and numbered I-X.

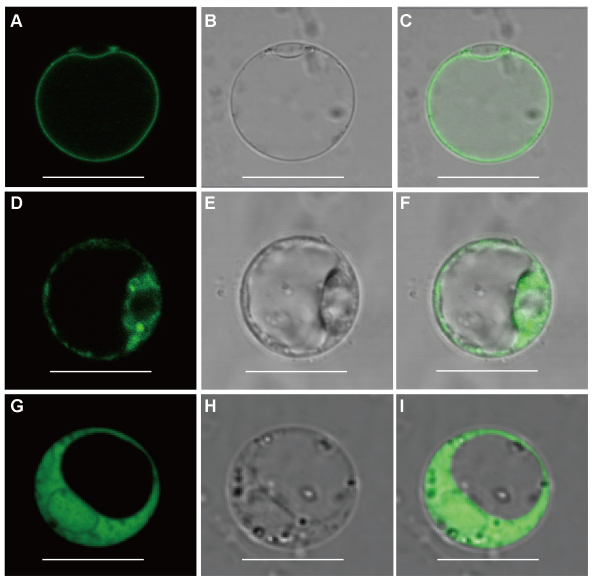

FIGURE 2 | Subcellular localization of OsFRO1 and OsFRO2. **(A)** OsFRO1-GFP expression. **(B)** Bright field image of a protoplast transformed with OsFRO1-GFP. **(C)** Overlay image of **(A,B)**. **(D)** OsFRO2-GFP expression. **(E)** Bright field image of a protoplast transformed with OsFRO2-GFP. **(F)** Overlay image of **(D,E)**. **(G)** 35s-GFP expression. **(H)** Bright field image of a protoplast transformed with 35s-GFP. **(I)** Overlay image of **(G,H)**. Bars = 20 μm.

were significantly ($p < 0.05$) or marginally ($p < 0.1$) lower than WT (**Figure 6A**). In addition, the root Fe concentrations of the Ri-1 and Ri-3 plants were significantly lower than that of WT (**Figure 6B**). There was no significant difference in the Zn, Mn, Cu concentrations among the leaves and roots of *OsFRO1*-Oe and Ri lines compared to WT (**Supplementary Figure S6**).

Knock Down of *OsFRO1* Reduced ROS Accumulation Caused by Excess Fe Stress

Excess Fe resulted an oxidative stress in plants through the formation of ROS by the Fenton reaction (Becana et al., 1998). In order to evaluate the Fe-induced oxidative stress, superoxide ($\cdot O^{2-}$) contents representing the major ROS was estimated using NBT staining. Under Fe excess conditions, all the plants showed typical symptoms of Fe overaccumulation (**Figure 7A**). While the excess Fe supply resulted in significant accumulation of ROS in leaves of WT, Oe and Ri plants, the NBT staining in the *OsFRO1*-Oe leaves was at the highest level (**Figure 7B**). As contrast, the blue staining in Ri leaves were significantly lower than that in WT and Oe leaves. This NBT staining result is in accordance with the bronzing phenotypes described (**Figure 5A**).

DISCUSSION

A rice vacuolar membrane ferric-chelate reductase, OsFRO1, which was down-regulated in shoots under Fe excess conditions was identified in this study. Suppression of the expression of *OsFRO1* by RNAi resulted in tolerant to Fe excess stress in transgenic plants, suggesting that OsFRO1 might be involved in maintaining the Fe balance between the cytoplasm and vacuoles. We propose that OsFRO1 is involved in reducing ferric Fe into ferrous Fe in vacuole, and makes the vacuolar stored Fe available to cytoplasm through Fe (II) or chelated Fe (II) transporters. Under Fe excess condition, the decrease in transcript abundance of Os*FRO1* in the RNAi plants reduced the amount of Fe (II) available for cytoplasm, and therefore alleviates Fe excess toxicity.

Previously, rice FROs were predicted to be non-functional because OsFRO1 and OsFRO2 do not contain perfect conserved HPFT or GPYG motifs compared to Arabidopsis FRO2, which are essential for the binding to the FAD and NADPH in cofactors, respectively (Ishimaru et al., 2006). In the study, we performed a multiple sequence alignment of OsFRO1, OsFRO2, AtFRO2, AtFRO6, and AtFRO7. Results showed that both HPFT and GPYG motifs of OsFRO1 were identical to that of AtFRO6/7 (**Figure 1**), while the GPYG motif of OsFRO2 is not conserved with the four analyzed Arabidopsis FROs. AtFRO6 was demonstrated to be a functional ferric reductase, which could facilitate the reduction of Fe in tobacco leaves (Li et al., 2011). AtFRO7 was reported to be a chloroplast ferric chelate reductase (Jeong et al., 2008). In this regard, OsFRO1 is likely a functional ferric reductase. To test the reductase activity of OsFRO1 and OsFRO2, we performed a Fe (III)-chelate reductase assay in yeast. Unfortunately, we were not able to detect significant Fe (III)-chelate reductase activity in OsFRO1-expressing or OsFRO2-expressing cells, while AtFRO2-expressing cells showed up to fivefold more Fe (III)-chelate reductase activity than cells transformed with an empty vector (**Supplementary Figure S7**). The failure of detection of Fe (III)-chelate reductase activity could be caused by the non-plasma membrane localization of OsFRO1 and OsFRO2 in the yeast (data not shown). Because Fe (III)-chelate reductase activity assay requires the membrane impermeant property of bathophenanthroline disulfonic acid, it is difficult to measure the Fe (III) chelate reductase activity of a non-plasma membrane localized FRO. Similar observation was reported in AtFRO7 (Jeong et al., 2008). AtFRO7 is localized in chloroplasts, whose Fe (III) chelate reductase activity could not be detected in the yeast. Further ferric Fe reductase activity assay in yeast may first fuse the OsFRO1 to a protein targeting signal, for instance, the COOH-terminal domain of Ist2p (Jüschke et al., 2005), to facilitate the trafficking of OsFRO1 protein to the plasma membrane in yeast.

The members of FRO family has been well-documented and characterized in fungi, plants, and mammals. Many of them, such as AtFRO2, AtFRO6 in Arabidopsis and FRE1 in yeast, localize to the plasma membrane (Jeong and Connolly, 2009). There are also a subset of FRO family members localizes to internal membranes, such as Arabidopsis AtFRO7 in chloroplast, AtFRO3 and AtFRO8 in mitochondria, and yeast FRE6 in vacuolar membrane, suggesting functional roles in several subcellular compartments (Singh et al., 2007; Jeong et al., 2008; Jain

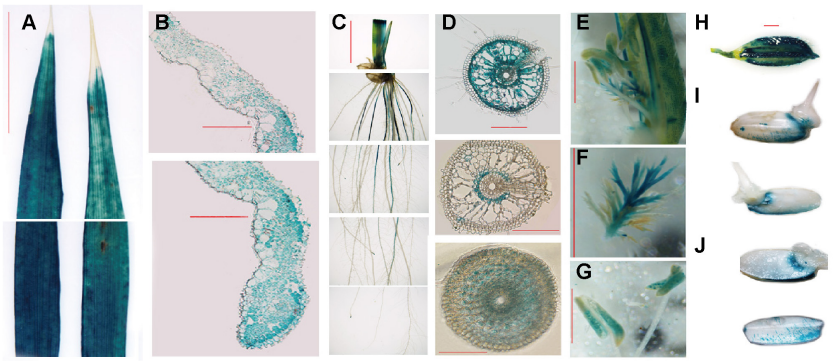

FIGURE 3 | OsFRO1 promoter-driven GUS expression pattern. **(A)** Leaves from 2-week-old seedlings. **(B)** Cross-sections of **(A)**. **(C)** Roots from -week-old seedling. **(D)** Cross-sections of **(C)**. Images of the sections that were close to the root–stem junction (upper panel), 5 cm away from the root tip (middle panel) and 0.5 cm away from the root tip (lower panel). **(E)** GUS staining of the mature flowers. **(F)** Pistil of **(E)**. **(G)** Stamen of **(E)**. **(H)** Seeds before germination. **(I)** Seeds geminated after 1 day. **(J)** Cross-sections of **(I)**. Bar = 1 cm **(A,C)**, Bar = 100 μm **(BD)**, Bar = 1 mm **(E–J)**.

et al., 2014). Vacuoles are considered as the main compartment for excess Fe storage in rice and *Arabidopsis* (Roschzttardtz et al., 2009). Since all known vacuolar transporters, including AtVIT1, AtNRAMP3 and AtNRAMP4, transport Fe across vacuolar membranes in the form of Fe(II) (Lanquar et al., 2005; Kim et al., 2006), it was postulated that Fe reduction might be involved in the vacuolar membrane (Jeong and Connolly, 2009). In yeast, reduction of Fe (III) in vacuoles is carried out by FRE6, which is critical for remobilization of Fe from vacuoles into the cytosol (Raguzzi et al., 1988; Singh et al., 2007). While none of the eight Arabidopsis FROs was reported or predicted to reside on the vacuolar membrane, OsFRO1 was located in the vacuolar membrane in this study. OsFRO1 is likely to reduce Fe (III) into Fe (II) in the vacuolar membrane similar to FRE6 in yeast. The reduced Fe (II) can be transported across the vacuolar membrane into the cytosol by other Fe (II) transporters. Knock down of *OsFRO1* resulted in more tolerance to Fe toxicity in rice plants. The similar phenotype was observed in the rice mutant *MuFRO1* that had a mutation in the *OsFRO1* gene, isolated from a fast neutron mutant library (Ruengphayak et al., 2015). In the Os*FRO1* mutant or knockdown plants, the vacuolar ferric reductase activities are reduced, which might lead to the reduction of the amount of Fe (II) being transported into the cytosol. When exposed to excess Fe, the mutant plants should have less Fe accumulation in the cytosol, and thus showed enhanced tolerance to the excess Fe. The NBT staining showed a significant reduction of ROS accumulation in the *OsFRO1*-Ri leaves, supports this working model for OsFRO1 (**Figure 5A**).

Os*FRO1*-Ri and Os*FRO1* mutant had a similar decrease in root and shoot Fe concentrations (**Figure 6**; Ruengphayak et al., 2015). qRT-PCR was carried out to determine the transcript abundance of genes involving in Fe acquisition and translocation, including *IRT1, FRDL1*, *YSL15*, and no significant difference between WT and Os*FRO1*-Ri plants was detected. This indicates the mechanism by which the Fe concentrations were reduced in the *OsFRO1*-Ri or mutant plants merits more investigation to give insight into Fe sensing and response in rice.

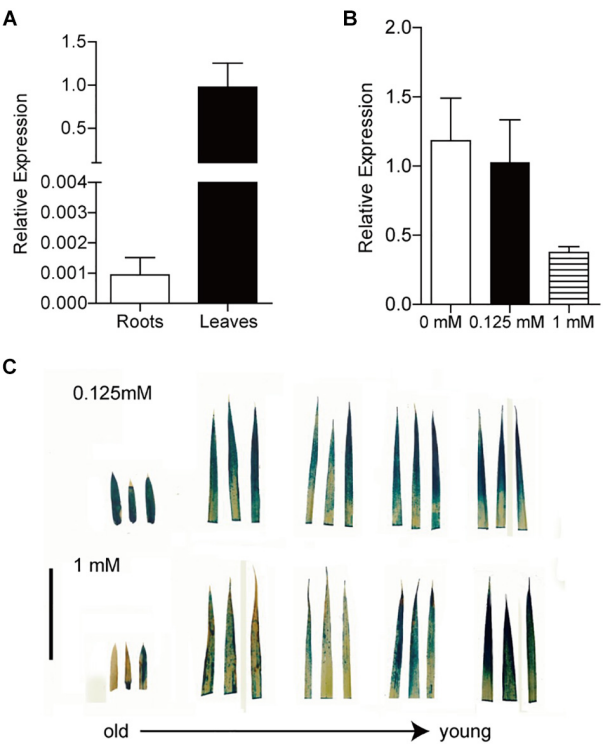

FIGURE 4 | Expression analysis of *OsFRO1* transcript abundance in Rice. **(A)** Transcript abundance of *OsFRO1* in leaves and roots (the expression in leaves was set to 1.0). Seedlings were grown in normal nutrient solution for 3 weeks. Leaves and roots were sampled for RNA extraction. **(B)** Transcript levels of *OsFRO1* under different Fe supply. Two-week-old seedlings cultured in normal nutrient solution (0.125 mM Fe) were transferred to 0 or 1 mM Fe solution for 7 days. Leaves were sampled for RNA extraction. **(C)** GUS staining of P_{OsFRO1}: GUS transgenic seedlings under 1 mM Fe treatment. Bar = 3 cm. Data are shown as the mean ± SD (n = 3).

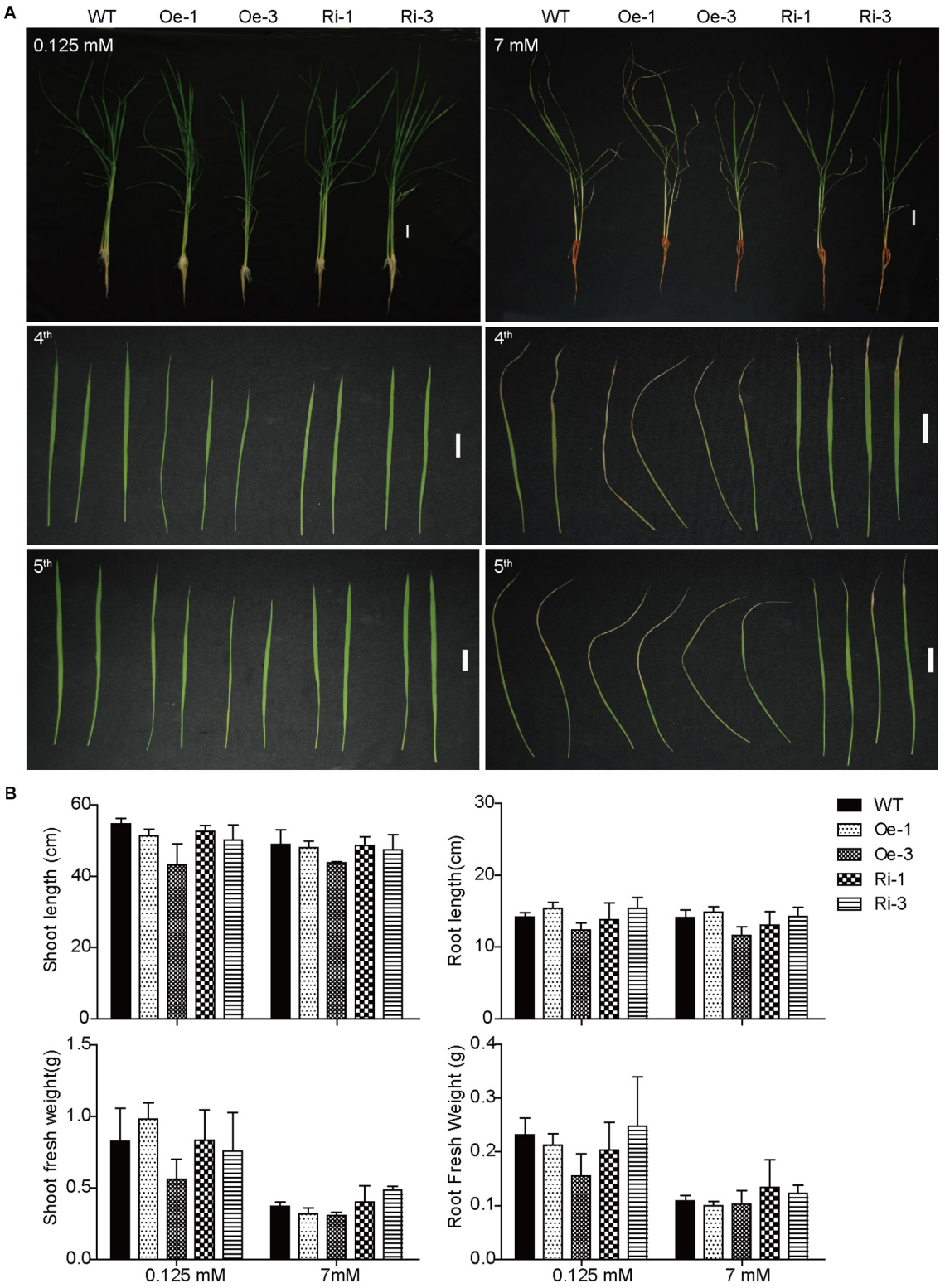

FIGURE 5 | Phenotype analysis of WT and transgenic plants under treatment of excess Fe. **(A)** Growth performance of WT and transgenic plants under normal and Fe excess conditions. Two-week-old plants were grown on nutrient solution supplied with 0.125 or 7 mM Fe (II)-EDTA for 3 days. The fourth and fifth leaves were detached to display their phenotypes. **(B)** Plant length and biomass of WT and transgenic plants under normal and HFe conditions. Bar = 2 cm. Data are shown as the mean and standard deviation (n = 3).

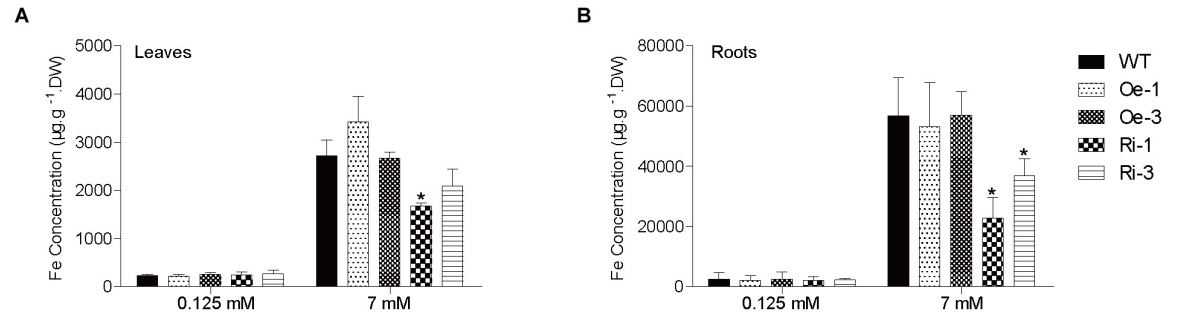

FIGURE 6 | Analysis of Fe concentrations in WT and transgenic plants. Two-week-old plants were grown on nutrient solution supplied with 0.125 or 7 mM Fe (II)-EDTA for 3 days. Fe concentrations in leaves **(A)** and roots **(B)** were measured by ICP-OES. Data are shown as the mean and standard deviation ($n = 3$). Significance of differences compared to WT is indicated by asterisks (Tukey's ANOVA test; $*p < 0.05$).

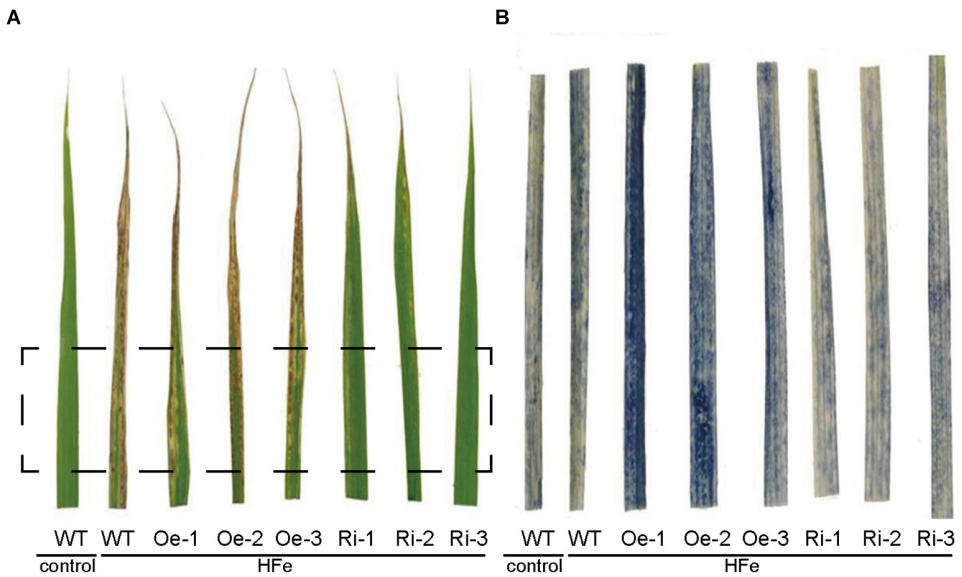

FIGURE 7 | NBT staining of superoxide (O^{2-}) in leaves of WT and transgenic rice plants. Three-week-old seedlings cultured in normal nutrient solution were transferred to nutrient solution containing 1 mM Fe and grown for 7 days. Leaves were detached for visualization. **(A)** The leaf-bronzing symptom of WT and transgenic plants under Fe excess conditions. **(B)** The zoom-in region that correspond to rectangle in **(A)** after NBT staining.

In summary, rice FRO, OsFRO1 was shown to function in the vacuolar membrane to converting Fe (III) into Fe (II). Knockdown of Os*FRO1* could alleviate the Fe excess toxicity.

DATA AVAILABILITY

All datasets generated for this study are included in the manuscript and/or the **Supplementary Files**.

AUTHOR CONTRIBUTIONS

LL carried out most experiments and drafted the manuscript. QK performed the phenotypic analyses and helped in results interpretation. LY helped to conceive the study and its design, and participated in the critical review of the manuscript. HS conceived the study, its design and coordination and helped to draft the manuscript. All authors read and approved the final manuscript.

FUNDING

This work was supported by the 111 project (B14027) and National Natural Science Foundation of China (Grant No. 31401934).

ACKNOWLEDGMENTS

We thank Shelong Zhang for the technical support on confocal microscope manipulation.

SUPPLEMENTARY MATERIAL

The Supplementary Material for this article can be found online at: https://www.frontiersin.org/articles/10.3389/fpls.2019.00700/full#supplementary-material

FIGURE S1 | The predicted membrane topology of FROs in Rice and Arabidopsis.

FIGURE S2 | Subcellular localization of OsFRO1.

FIGURE S3 | Expression levels of OsFRO1 in different tissues **(A)** and different development stages **(B)** based on microarray data retrieved from GENEVESTIGATOR (https://genevestigator.com/gv/).

FIGURE S4 | Identification of *OsFRO1* overexpression and RNAi lines.

FIGURE S5 | Growth performance of WT and transgenic plants.

FIGURE S6 | Analysis of Cu, Zn, Mn concentrations in WT and transgenic plants.

FIGURE S7 | Fe (III) chelate reductase assay in yeast cells.

TABLE S1 | Primers used in this work.

REFERENCES

Asch, F., Becker, M., and Kpongor, D. S. (2005). A quick and efficient screen for resistance to iron toxicity in lowland rice. *J. Plant Nutr. Soil Sci.* 168, 764–773. doi: 10.1002/jpln.200520540

Audebert, A., and Fofana, M. (2009). Rice yield gap due to iron toxicity in West Africa. *J. Agron. Crop Sci.* 195, 66–76. doi: 10.1111/j.1439-037X.2008.00339

Babior, B. M. (1995). The respiratory burst oxidase. *Curr. Opin. Hematol.* 2, 55–60.

Bashir, K., Hanada, K., Shimizu, M., Seki, M., Nakanishi, H., and Nishizawa, N. K. J. R. (2014). Transcriptomic analysis of rice in response to iron deficiency and excess. *Rice* 7:18. doi: 10.1186/s12284-014-0018-1

Bashir, K., Ishimaru, Y., Shimo, H., Kakei, Y., Senoura, T., Takahashi, R., et al. (2011). Rice phenolics efflux transporter 2 (PEZ2) plays an important role in solubilizing apoplasmic iron. *Soil Sci. Plant Nutr.* 57, 803–812. doi: 10.1080/00380768.2011.637305

Becana, M., Moran, J. F., and Iturbe-Ormaetxe, I. (1998). Iron-dependent oxygen free radical generation in plants subjected to environmental stress: toxicity and antioxidant protection. *Plant Soil* 201, 137–147. doi: 10.1023/a:1004375732137

Becker, M., and Asch, F. (2005). Iron toxicity in rice—conditions and management concepts. *J. Plant Nutr. Soil Sci.* 168, 558–573. doi: 10.1002/jpln.200520504

Briat, J.-F., Dubos, C., and Gaymard, F. (2015). Iron nutrition, biomass production, and plant product quality. *Trends Plant Sci.* 20, 33–40. doi: 10.1016/j.tplants.2014.07.005

Briat, J.-F., Duc, C., Ravet, K., and Gaymard, F. (2010). Ferritins and iron storage in plants. *Biochim. Biophys. Acta* 1800, 806–814. doi: 10.1016/j.bbagen.2009.12.003

Briat, J.-F., Fobis-Loisy, I., Grignon, N., Lobréaux, S., Pascal, N., Savino, G., et al. (1995). Cellular and molecular aspects of iron metabolism in plants. *Biol. Cell* 84, 69–81. doi: 10.1016/0248-4900(96)81320-7

Chen, J., Liu, Y., Ni, J., Wang, Y., Bai, Y., Shi, J., et al. (2011). OsPHF1 regulates the plasma membrane localization of low- and high-affinity inorganic phosphate transporters and determines inorganic phosphate uptake and translocation in rice. *Plant Physiol.* 157, 269–278. doi: 10.1104/pp.111.181669

Chen, S. Y., Jin, W. Z., Wang, M. Y., Zhang, F., Zhou, J., Jia, Q. J., et al. (2003). Distribution and characterization of over 1000 T-DNA tags in rice genome. *Plant J.* 36, 105–113. doi: 10.1046/j.1365-313X.2003.01860.x

Connorton, J. M., Balk, J., and Rodríguez-Celma, J. (2017). Iron homeostasis in plants – a brief overview. *Metallomics* 9, 813–823. doi: 10.1039/c7mt00136c

Curie, C., Panaviene, Z., Loulergue, C., Dellaporta, S. L., Briat, J.-F., and Walker, E. L. (2001). Maize yellow stripe1 encodes a membrane protein directly involved in Fe (III) uptake. *Nature* 409, 346–349. doi: 10.1038/35053080

Dancis, A., Klausner, R. D., Hinnebusch, A. G., and Barriocanal, J. G. (1990). Genetic evidence that ferric reductase is required for iron uptake in *Saccharomyces cerevisiae*. *Mol. Cell. Biol.* 10, 2294–2301. doi: 10.1128/mcb.10.5.2294

Deng, D., Wu, S.-C., Wu, F.-Y., Deng, H., and Wong, M.-H. (2010). Effects of root anatomy and Fe plaque on arsenic uptake by rice seedlings grown in solution culture. *Environ. Pollut.* 158, 2589–2595. doi: 10.1016/j.envpol.2010.05.015

Dufey, I., Mathieu, A.-S., Draye, X., Lutts, S., and Bertin, P. (2015). Construction of an integrated map through comparative studies allows the identification of candidate regions for resistance to ferrous iron toxicity in rice. *Euphytica* 203, 59–69. doi: 10.1007/s10681-014-1255-5

Eide, D., Broderius, M., Fett, J., and Guerinot, M. L. (1996). A novel iron-regulated metal transporter from plants identified by functional expression in yeast. *Proc. Natl. Acad. Sci. U.S.A.* 93, 5624–5628. doi: 10.1073/pnas.93.11.5624

Fang, W.-C., Wang, J.-W., Lin, C. C., and Kao, C. H. (2001). Iron induction of lipid peroxidation and effects on antioxidative enzyme activities in rice leaves. *Plant Growth Regul.* 35, 75–80. doi: 10.1023/a:1013879019368

Fenton, M. A. (1984). Oxidation of tartaric acid in presence of iron. *J. Chem. Soc. Trans.* 65, 899–910. doi: 10.1039/ct8946500899

Guerinot, M. L., and Yi, Y. (1994). Iron: nutritious, noxious, and not readily available. *Plant Physiol.* 104, 815–820. doi: 10.1104/pp.104.3.815

Halliwell, B., and Gutteridge, J. M. C. (1992). Biologically relevant metal ion-dependent hydroxyl radical generation an update. *FEBS Lett.* 307, 108–112. doi: 10.1016/0014-5793(92)80911-Y

Höller, S., Meyer, A., and Frei, M. (2014). Zinc deficiency differentially affects redox homeostasis of rice genotypes contrasting in ascorbate level. *J. Plant Physiol.* 171, 1748–1756. doi: 10.1016/j.jplph.2014.08.012

Inoue, H., Kobayashi, T., Nozoye, T., Takahashi, M., Kakei, Y., Suzuki, K., et al. (2009). Rice OsYSL15 is an iron-regulated iron (III)-deoxymugineic acid transporter expressed in the roots and is essential for iron uptake in early growth of the seedlings. *J. Biol. Chem.* 284, 3470–3479. doi: 10.1074/jbc.M806042200

Ishimaru, Y., Kakei, Y., Shimo, H., Bashir, K., Sato, Y., Sato, Y., et al. (2011). A rice phenolic efflux transporter is essential for solubilizing precipitated apoplasmic iron in the plant stele. *J. Biol. Chem.* 286, 24649–24655. doi: 10.1074/jbc.M111.221168

Ishimaru, Y., Suzuki, M., Tsukamoto, T., Suzuki, K., Nakazono, M., Kobayashi, T., et al. (2006). Rice plants take up iron as an Fe^{3+}-phytosiderophore and as Fe^{2+}. *Plant J.* 45, 335–346. doi: 10.1111/j.1365-313X.2005.02624.x

Jain, A., Wilson, G., and Connolly, E. (2014). The diverse roles of FRO family metalloreductases in iron and copper homeostasis. *Front. Plant Sci.* 5:100. doi: 10.3389/fpls.2014.00100

Jeong, J., Cohu, C., Kerkeb, L., Pilon, M., Connolly, E. L., and Guerinot, M. L. (2008). Chloroplast Fe (III) chelate reductase activity is essential for seedling viability under iron limiting conditions. *Proc. Natl. Acad. Sci. U.S.A.* 105, 10619–10624. doi: 10.1073/pnas.0708367105

Jeong, J., and Connolly, E. L. (2009). Iron uptake mechanisms in plants: functions of the FRO family of ferric reductases. *Plant Sci.* 176, 709–714. doi: 10.1016/j.plantsci.2009.02.011

Jüschke, C., Wächter, A., Schwappach, B., and Seedorf, M. (2005). SEC18/NSF-independent, protein-sorting pathway from the yeast cortical ER to the plasma membrane. *J. Cell Biol.* 169, 613–622. doi: 10.1083/jcb.200503033

Karimi, M., Inzé, D., and Depicker, A. (2002). GATEWAY^{TM} vectors for *Agrobacterium*-mediated plant transformation. *Trends Plant Sci.* 7, 193–195. doi: 10.1016/S1360-1385(02)02251-3

Kim, S. A., Punshon, T., Lanzirotti, A., Li, L., Alonso, J. M., Ecker, J. R., et al. (2006). Localization of iron in *Arabidopsis* seed requires the vacuolar membrane transporter VIT1. *Science* 314, 1295–1298. doi: 10.1126/science.1132563

Kobayashi, T., Nakanishi, H., and Nishizawa, N. K. (2010). Recent insights into iron homeostasis and their application in graminaceous crops. *Proc. Jpn. Acad. Ser. B Phys. Biol. Sci.* 86, 900–913. doi: 10.2183/pjab.86.900

Kobayashi, T., and Nishizawa, N. K. (2012). Iron uptake, translocation, and regulation in higher plants. *Annu. Rev. Plant Biol.* 63, 131–152. doi: 10.1146/annurev-arplant-042811-105522

Lanquar, V., Lelièvre, F., Bolte, S., Hamès, C., Alcon, C., Neumann, D., et al. (2005). Mobilization of vacuolar iron by AtNRAMP3 and AtNRAMP4 is essential for seed germination on low iron. *EMBO J.* 24, 4041–4051. doi: 10.1038/sj.emboj.7600864

Li, L., Cheng, X., and Ling, H.-Q. (2004). Isolation and characterization of Fe (III)-chelate reductase gene LeFRO1 in tomato. *Plant Mol. Biol.* 54, 125–136. doi: 10.1023/b:plan.0000028774.82782.16

Li, L.-Y., Cai, Q.-Y., Yu, D.-S., and Guo, C.-H. (2011). Overexpression of AtFRO6 in transgenic tobacco enhances ferric chelate reductase activity in leaves and increases tolerance to iron-deficiency chlorosis. *Mol. Biol. Rep.* 38, 3605–3613. doi: 10.1007/s11033-010-0472-9

Ling, H.-Q., Wu, H., Li, L., Du, J., Cheng, X., and Yuan, Y. (2005). Molecular and biochemical characterization of the Fe (III) chelate reductase gene family in *Arabidopsis thaliana*. *Plant Cell Physiol.* 46, 1505–1514. doi: 10.1093/pcp/pci163

Matthus, E., Wu, L.-B., Ueda, Y., Höller, S., Becker, M., and Frei, M. (2015). Loci, genes, and mechanisms associated with tolerance to ferrous iron toxicity in rice (*Oryza sativa* L.). *Theor. Appl. Genet.* 128, 2085–2098. doi: 10.1007/s00122-015-2569-y

Moore, K. L., Chen, Y., van de Meene, A. M. L., Hughes, L., Liu, W., Geraki, T., et al. (2014). Combined NanoSIMS and synchrotron X-ray fluorescence reveal distinct cellular and subcellular distribution patterns of trace elements in rice tissues. *New Phytol.* 201, 104–115. doi: 10.1111/nph.12497

Mori, S. (1999). Iron acquisition by plants. *Curr. Opin. Plant Biol.* 2, 250–253. doi: 10.1016/S1369-5266(99)80043-0

Quinet, M., Vromman, D., Clippe, A., Bertin, P., Lequeux, H., Dufey, I., et al. (2012). Combined transcriptomic and physiological approaches reveal strong differences between short- and long-term response of rice (*Oryza sativa*) to iron toxicity. *Plant Cell Environ.* 35, 1837–1859. doi: 10.1111/j.1365-3040.2012.02521.x

Raguzzi, F., Lesuisse, E., and Crichton, R. R. (1988). Iron storage in *Saccharomyces cerevisiae*. *FEBS Lett.* 231, 253–258. doi: 10.1016/0014-5793(88)80742-7

Ricachenevsky, F. K., Sperotto, R. A., Menguer, P. K., and Fett, J. P. (2010). Identification of Fe-excess-induced genes in rice shoots reveals a WRKY transcription factor responsive to Fe, drought and senescence. *Mol. Biol. Rep.* 37, 3735–3745. doi: 10.1007/s11033-010-0027-0

Robinson, N. J., Procter, C. M., Connolly, E. L., and Guerinot, M. L. (1999). A ferric-chelate reductase for iron uptake from soils. *Nature* 397, 694–697. doi: 10.1038/17800

Römheld, V., and Marschner, H. (1986). Evidence for a specific uptake system for iron phytosiderophores in roots of grasses. *Plant Physiol.* 80, 175–180. doi: 10.1104/pp.80.1.175

Roschzttardtz, H., Conéjéro, G., Curie, C., and Mari, S. (2009). Identification of the endodermal vacuole as the iron storage compartment in the arabidopsis embryo. *Plant Physiol.* 151, 1329–1338. doi: 10.1104/pp.109.144444

Ruengphayak, S., Ruanjaichon, V., Saensuk, C., Phromphan, S., Tragoonrung, S., Kongkachuichai, R., et al. (2015). Forward screening for seedling tolerance to Fe toxicity reveals a polymorphic mutation in ferric chelate reductase in rice. *Rice* 8:36. doi: 10.1186/s12284-014-0036-z

Sahrawat, K. L. (2004). Iron toxicity in wetland rice and the role of other nutrients. *J. Plant Nutr.* 27, 1471–1504. doi: 10.1081/pln-200025869

Santi, S., and Schmidt, W. (2009). Dissecting iron deficiency-induced proton extrusion in Arabidopsis roots. *New Phytol.* 183, 1072–1084. doi: 10.1111/j.1469-8137.2009.02908.x

Singh, A., Kaur, N., and Kosman, D. J. (2007). The Metalloreductase Fre6p in Fe-efflux from the yeast vacuole. *J. Biol. Chem.* 282, 28619–28626. doi: 10.1074/jbc.M703398200

Varotto, C., Maiwald, D., Pesaresi, P., Jahns, P., Salamini, F., and Leister, D. (2002). The metal ion transporter IRT1 is necessary for iron homeostasis and efficient photosynthesis in *Arabidopsis thaliana*. *Plant J.* 31, 589–599. doi: 10.1046/j.1365-313X.2002.01381

Vert, G., Grotz, N., Dédaldéchamp, F., Gaymard, F., Guerinot, M. L., Briat, J.-F., et al. (2002). IRT1, an arabidopsis transporter essential for iron uptake from the soil and for plant growth. *Plant Cell* 14, 1223–1233. doi: 10.1105/tpc.001388

Wang, C., Yue, W., Ying, Y., Wang, S., Secco, D., Liu, Y., et al. (2015). Rice SPX-major facility superfamily3, a vacuolar phosphate efflux transporter, is involved in maintaining phosphate homeostasis in rice. *J. Plant Physiol.* 169, 2822–2831. doi: 10.1104/pp.15.01005

Waters, B. M., Blevins, D. G., and Eide, D. J. (2002). Characterization of FRO1, a pea ferric-chelate reductase involved in root iron acquisition. *Plant Physiol.* 129, 85–94. doi: 10.1104/pp.010829

Waters, B. M., Lucena, C., Romera, F. J., Jester, G. G., Wynn, A. N., Rojas, C. L., et al. (2007). Ethylene involvement in the regulation of the H+-ATPase CsHA1 gene and of the new isolated ferric reductase CsFRO1 and iron transporter CsIRT1 genes in cucumber plants. *Plant Physiol. Biochem.* 45, 293–301. doi: 10.1016/j.plaphy.2007.03.011

Wu, L. B., Shhadi, M. Y., Gregorio, G., Matthus, E., Becker, M., and Frei, M. (2014). Genetic and physiological analysis of tolerance to acute iron toxicity in rice. *Rice* 7:8. doi: 10.1186/s12284-014-0008-3

Wu, L. B., Ueda, Y., Lai, S.-K., and Frei, M. (2017). Shoot tolerance mechanisms to iron toxicity in rice (*Oryza sativa* L.). *Plant Cell Environ.* 40, 570–584. doi: 10.1111/pce.12733

Yi, Y., and Guerinot, M. L. (1996). Genetic evidence that induction of root Fe (III) chelate reductase activity is necessary for iron uptake under iron deficiency†. *Plant J.* 10, 835–844. doi: 10.1046/j.1365-313x.1996.10050835.x

Ying, Y., Yue, W., Wang, S., Li, S., Wang, M., Zhao, Y., et al. (2017). Two h-Type thioredoxins interact with the E2 ubiquitin conjugase PHO2 to fine-tune phosphate homeostasis in rice. *Plant Physiol.* 173, 812–824. doi: 10.1104/pp.16.01639

Yoshida, S., Forno, D. A., and Cock, J. (1976). *Laboratory Manual for Physiological Studies of Rice*. Los Baños: IRRI.

Conflict of Interest Statement: The authors declare that the research was conducted in the absence of any commercial or financial relationships that could be construed as a potential conflict of interest.

frontiers in Plant Science

PERSPECTIVE
published: 04 June 2019
doi: 10.3389/fpls.2019.00712

Is There a Role for Glutaredoxins and BOLAs in the Perception of the Cellular Iron Status in Plants?

*Pascal Rey[1], Maël Taupin-Broggini[2], Jérémy Couturier[3], Florence Vignols[2] and Nicolas Rouhier[3]**

[1] Plant Protective Proteins Team, CEA, CNRS, BIAM, Aix-Marseille University, Saint-Paul-lez-Durance, France, [2] Biochimie et Physiologie Moléculaire des Plantes, CNRS/INRA/Université de Montpellier/SupAgro, Montpellier, France, [3] Université de Lorraine, INRA, IAM, Nancy, France

OPEN ACCESS

Edited by:
Thomas J. Buckhout, Humboldt University of Berlin, Germany

Reviewed by:
Qingyu Wu, Institute of Agricultural Resources and Regional Planning (CAAS), China
Ping Lan, Institute of Soil Science (CAS), China

***Correspondence:**
Nicolas Rouhier
Nicolas.Rouhier@univ-lorraine.fr

Specialty section:
This article was submitted to Plant Nutrition, a section of the journal Frontiers in Plant Science

Received: *05 March 2019*
Accepted: *14 May 2019*
Published: *04 June 2019*

Citation:
Rey P, Taupin-Broggini M, Couturier J, Vignols F and Rouhier N (2019) Is There a Role for Glutaredoxins and BOLAs in the Perception of the Cellular Iron Status in Plants? Front. Plant Sci. 10:712. doi: 10.3389/fpls.2019.00712

Glutaredoxins (GRXs) have at least three major identified functions. In apoforms, they exhibit oxidoreductase activity controlling notably protein glutathionylation/deglutathionylation. In holoforms, i.e., iron–sulfur (Fe–S) cluster-bridging forms, they act as maturation factors for the biogenesis of Fe–S proteins or as regulators of iron homeostasis contributing directly or indirectly to the sensing of cellular iron status and/or distribution. The latter functions seem intimately connected with the capacity of specific GRXs to form [2Fe–2S] cluster-bridging homodimeric or heterodimeric complexes with BOLA proteins. In yeast species, both proteins modulate the localization and/or activity of transcription factors regulating genes coding for proteins involved in iron uptake and intracellular sequestration in response notably to iron deficiency. Whereas vertebrate GRX and BOLA isoforms may display similar functions, the involved partner proteins are different. We perform here a critical evaluation of the results supporting the implication of both protein families in similar signaling pathways in plants and provide ideas and experimental strategies to delineate further their functions.

Keywords: BOLA, glutaredoxins, iron–sulfur center, maturation factor, iron homeostasis

INTRODUCTION

Many cellular reactions and biological processes require metalloproteins, among which those containing iron (Fe) cofactors such as mononuclear and dinuclear (non-heme) Fe centers, hemes and iron–sulfur (Fe–S) clusters, are particularly crucial. Unlike other metals such as copper or zinc, there is no universal Fe chaperone described and so far, only poly rC-binding proteins (PCBPs) were shown to coordinate Fe entry in the cytosol and serve for the metalation of non-heme Fe enzymes in mammals (Philpott et al., 2017). In contrast, the synthesis/assembly of hemes and Fe–S clusters requires more complex and universally conserved pathways (Couturier et al., 2013; Barupala et al., 2016). The machineries dedicated to the maturation of Fe–S proteins present in mitochondria

and chloroplasts, named ISC (iron–sulfur cluster) and SUF (sulfur mobilization), respectively, are also found in bacteria (Lill, 2009). On the other hand, cytosolic and nuclear Fe–S proteins are maturated via the eukaryote-specific cytosolic iron–sulfur cluster assembly (CIA) machinery, which is, however, dependent on the mitochondrial ISC machinery for sulfur supply (Lill, 2009). Hence, given the high cellular demand for iron, sophisticated systems exist to control Fe uptake and intracellular distribution due to its potential toxicity. Strikingly, the Fe sensing systems and associated transcription factors generally differ in bacteria, yeast/fungi, mammals, and plants, but might include common actors such as glutaredoxins (GRXs) and BOLAs (Couturier et al., 2015).

Two GRX classes, I and II, are present in most organisms whereas additional classes are specific to some species/genus/kingdoms (Alves et al., 2009; Couturier et al., 2009). GRXs of the first class are involved in redox regulation, reducing protein disulfides or glutathione-protein mixed disulfides. GRXs from class II participate in the regulation of Fe homeostasis (Mühlenhoff et al., 2010; Haunhorst et al., 2013) and in the maturation of Fe–S proteins owing to their capacity to ligate and exchange [2Fe–2S] clusters with partner proteins (**Table 1**; Rodríguez-Manzaneque et al., 2002; Bandyopadhyay et al., 2008). They are also referred to as monothiol GRXs or CGFS GRXs owing to their conserved CGFS active site signature.

Regarding the BOLA family, an extensive phylogenetic analysis allowed delineating four groups, namely BOLA1–BOLA4 (Couturier et al., 2014). BOLA1s are present in both bacteria and eukaryotes, BOLA2s and BOLA3s in eukaryotes and BOLA4s in photosynthetic organisms, archaea, and bacteria. Pioneer works revealed functions for *Escherichia coli* BolA in the regulation of cell morphology, possibly as a transcriptional regulator (Aldea et al., 1989), for *Saccharomyces cerevisiae* cytosolic Bol2/Fra2 (Fe repressor of activation 2) in the regulation of iron homeostasis (Lesuisse et al., 2005; Kumánovics et al., 2008), and for mitochondrial BOLAs (human BOLA3 and yeast Bol1, Bol3) in the maturation of Fe–S clusters (**Table 1**; Cameron et al., 2011; Melber et al., 2016; Uzarska et al., 2016).

A very close relationship between class II GRXs and BOLAs was initially evident from genome (gene co-occurrence and clustering, existence of fusion proteins) and large-scale interactomic analyses in various organisms (reviewed in Przybyla-Toscano et al., 2017). Then, the molecular and structural determinants of the complexes were investigated in detail using mutational, spectroscopic and structural analyses on recombinant proteins. This led to demonstrate that class II GRXs and BOLAs form both apo- and holo-heterodimers bridging a [2Fe–2S] cluster, usually more stable than the [2Fe–2S] cluster-bridging GRX homodimers, and to identify the residues serving as ligands (Li and Outten, 2012; Couturier et al., 2015; Przybyla-Toscano et al., 2017). In GRX-BOLA holo-heterodimers, the [2Fe–2S] cluster is ligated using the GRX conserved cysteine, a cysteine from glutathione (as in GRX holo-homodimers), and, on the BOLA side, using a C-terminally located conserved histidine and an histidine or a cysteine in the β1–β2 loop, referred to as [H/C] loop (**Figure 1A**; Li et al., 2011, 2012; Roret et al., 2014; Dlouhy et al., 2016; Nasta et al., 2017).

Hereafter, based on the most recent results and known roles in non-photosynthetic organisms, we discuss the putative or confirmed functions of GRX and BOLA, alone or in complex, in photosynthetic organisms.

THE CLASS II GRX AND BOLA COUPLE PROTEINS PRESENT IN BACTERIA OR IN EUKARYOTE ORGANELLES ARE INVOLVED IN THE SYNTHESIS OF FE–S CLUSTERS

The first evidence about GRX involvement in the biogenesis of Fe–S proteins were obtained from a *S. cerevisiae* mutant for the mitochondrial Grx5 (**Table 1**; Rodríguez-Manzaneque et al., 2002; Mühlenhoff et al., 2003). Orthologs of this single domain-containing GRX are found in bacteria, archaea and plant plastids. The current view is that Grx5 is required for the maturation of all types of Fe–S clusters in mitochondria, receiving a [2Fe–2S] cluster from ISCU-type scaffold proteins and transferring it to ISCA-type transfer proteins for subsequent maturation of [4Fe–4S] proteins (**Figure 1B**). Grx5 is also required for the maturation of nucleo-cytosolic Fe–S proteins and the activation of the Aft1 transcription factor, pointing to its key position in *S. cerevisiae* (see below) (Uzarska et al., 2013). Yeast Bol1 and Bol3, which have the capacity to form heterodimers with Grx5, were later shown to be required for a specific set of mitochondrial [4Fe–4S] proteins, without affecting *de novo* synthesis of [2Fe–2S] proteins (Uzarska et al., 2016). So far, human BOLA3, but not BOLA1, has been demonstrated as required for the maturation of specific Fe–S proteins (**Table 1**; Cameron et al., 2011; Willems et al., 2013). The client proteins are notably the succinate dehydrogenase/complex II and lipoate synthase. Moreover, the fact that *bol1–bol3*Δ mutants are neither affected in the CIA machinery, nor in Aft1 activation, indicates that Grx5 has physiological roles independent of Bol1 and Bol3 (Uzarska et al., 2016). Additional studies suggested that Bol1 indeed acts early in the ISC pathway in concert with Grx5 (possibly only for [4Fe–4S] proteins) whereas Bol3 may preferentially act with NFU1, a late Fe–S cluster transfer protein, to preserve the [4Fe–4S] center found in some specific mitochondrial client proteins, as lipoate synthase, from oxidative damage (**Figure 1B**; Melber et al., 2016).

Concerning bacteria, the sole Grx isoform (Grx4/D) and both BolAs (BolA and IbaG) from *E. coli* were recently shown as implicated in the maturation of the respiratory complexes I and II, but the effects are only visible when multiple genes are mutated (Burschel et al., 2019). This role in maturating Fe–S proteins is consistent with (i) the synthetic lethality of the *Grx4* gene with genes present in the ISC operon (Butland et al., 2008), (ii) the interaction *in vitro* of Grx4 with the MiaB Fe–S protein (Boutigny et al., 2013), and (iii) the capacity of Grx4-BolA and Grx4-IbaG to form the

TABLE 1 | Iron-related phenotypes of *bolA* and *glutaredoxin* mutants from various sources.

	Organism	Protein names	Mutant phenotype(s)	References
Mono-domain (organellar) GRXs	*Saccharomyces cerevisiae*	Grx5	Defaults in Fe–S cluster assembly	Rodríguez-Manzaneque et al., 2002; Mühlenhoff et al., 2003
	Schizosaccharomyces pombe	Grx5	Defaults in Fe–S cluster assembly, decreased amount of mitochondrial DNA, reduced growth, and sensitivity toward oxidants	Chung et al., 2005; Kim et al., 2010
	Danio rerio	GRX5	Embryo lethal	Wingert et al., 2005
	Homo sapiens	GLRX5	Defaults in Fe–S cluster assembly leading to sideroblastic anemia	Camaschella et al., 2007; Ye et al., 2010
	Trypanosoma brucei	1-C-Grx1	Lethal	Comini et al., 2008
	Sinorhizobium meliloti	Grx2	Defaults in Fe–S cluster assembly, deregulation of RirA transcriptional activity, increased intracellular iron content, modified nodule development	Benyamina et al., 2013
	Escherichia coli	Grx4	Sensitivity to iron depletion, defect in respiratory complex I	Yeung et al., 2011; Burschel et al., 2019
	Arabidopsis thaliana	GRXS14	Sensitivity to prolonged darkness	Rey et al., 2017
	Arabidopsis thaliana	GRXS15	Lethal, decreased amounts of lipoate synthase and of lipoic acid dependent H subunits of the glycine cleavage system in RNAi lines	Moseler et al., 2015; Ströher et al., 2016
	Arabidopsis thaliana	GRXS16	None described for co-suppressed and RNAi lines	Rey et al., 2017
Multi-domain (cytosolic) GRXs	*Saccharomyces cerevisiae*	Grx3	Impaired regulation of Aft1/2 and iron homeostasis	Ojeda et al., 2006; Pujol-Carrion et al., 2006
	Saccharomyces cerevisiae	Grx4	Impaired regulation of Aft1/2 and iron homeostasis	Ojeda et al., 2006; Pujol-Carrion et al., 2006
	Saccharomyces cerevisiae	Grx3–Grx4	Lethal in some background. Impaired iron trafficking and assembly of Fe–S proteins, heme, and iron-containing proteins	Pujol-Carrion et al., 2006; Mühlenhoff et al., 2010
	Schizosaccharomyces pombe	Grx4	Lethal	Chung et al., 2005
	Cryptococcus neoformans	Grx4	Slow growth upon iron deprivation	Attarian et al., 2018
	Danio rerio	GRX3	Impaired heme synthesis and Fe–S protein maturation	Haunhorst et al., 2013
	Homo sapiens	GLRX3/PICOT	Decreased activities of cytosolic Fe–S proteins	Haunhorst et al., 2013
	Arabidopsis thaliana	GRXS17	Growth defects (meristem arrest) upon elevated temperature and long photoperiod. No decrease in cytosolic Fe–S protein activity	Cheng et al., 2011; Knuesting et al., 2015; Yu et al., 2017
BOLA	*Saccharomyces cerevisiae*	Bol1	No growth defect and no decrease in Fe–S enzyme activity	Melber et al., 2016; Uzarska et al., 2016
	Saccharomyces cerevisiae	Bol3	Slightly decreased complex II (SDH) activity	Melber et al., 2016; Uzarska et al., 2016
	Saccharomyces cerevisiae	Bol1–Bol3	Decreased activity of lipoic acid-dependent enzymes, aconitase, and respiratory complex II	Melber et al., 2016; Uzarska et al., 2016
	Saccharomyces cerevisiae	Bol2/Fra2	Impaired regulation of Aft1/2 and iron homeostasis	Kumánovics et al., 2008; Uzarska et al., 2016
	Schizosaccharomyces pombe	BolA2/ Fra2	Impaired regulation of the Fep1 transcription factor	Jacques et al., 2014
	Homo sapiens	BOLA1	Oxidation of the mitochondrial GSH pool	Willems et al., 2013
	Homo sapiens	BOLA2	None described for siRNA lines	Frey et al., 2016
	Homo sapiens	BOLA3	Defect in lipoic acid-dependent enzymes and in respiratory complexes I and II	Cameron et al., 2011
	Escherichia coli	BolA	Partial defect in respiratory complex I assembly	Burschel et al., 2019
	Escherichia coli	IbaG	None described	Burschel et al., 2019
	Escherichia coli	BolA – IbaG	Decreased complex II activity	Burschel et al., 2019
	Salmonella typhimurium	BolA	Decreased resistance to acidic and oxidative stresses and decreased virulence	Mil-Homens et al., 2018
	Arabidopsis thaliana	BOLA2	None described under control conditions, increased resistance to oxidative conditions	Qin et al., 2015

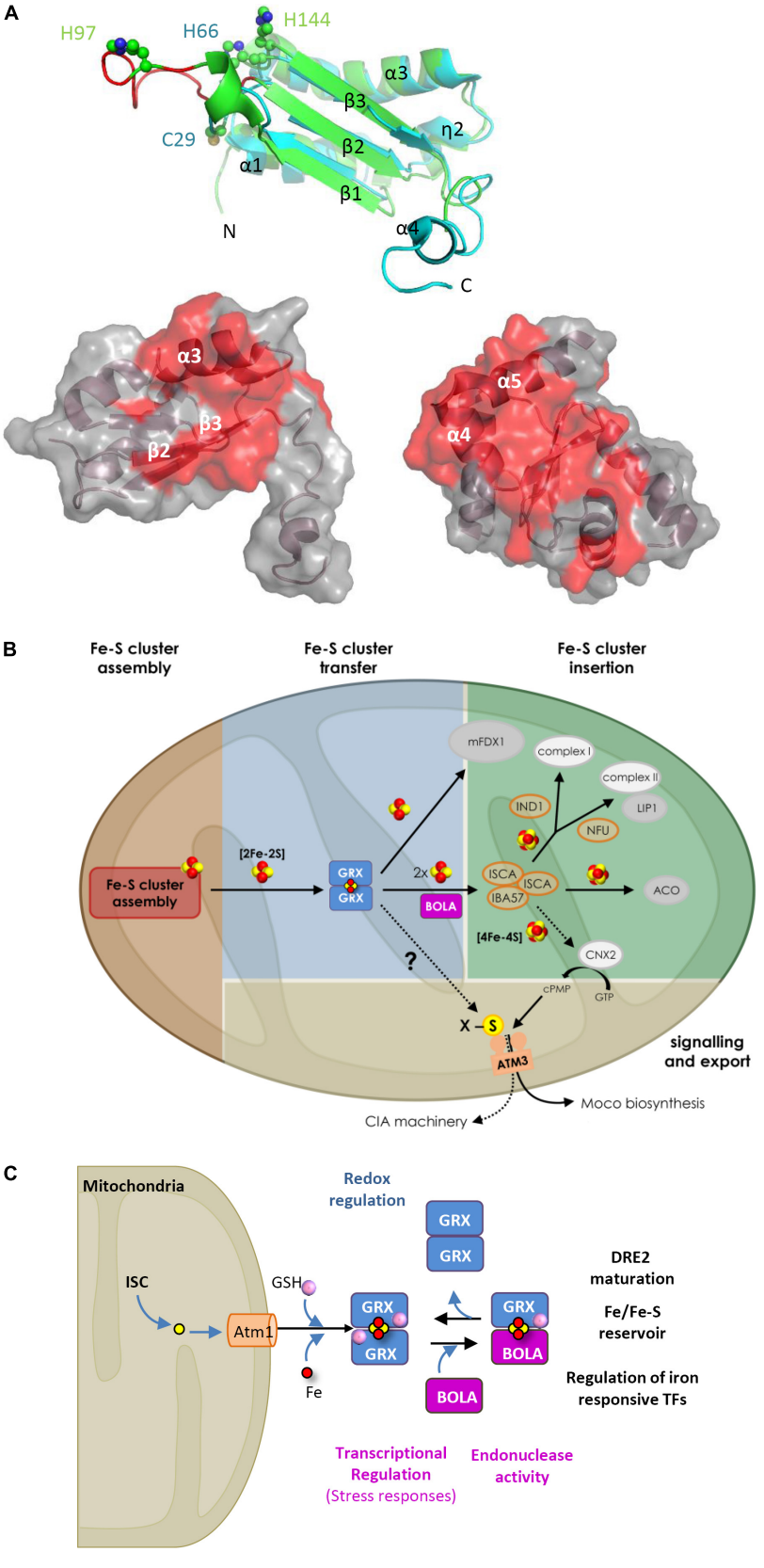

FIGURE 1 | Continued

FIGURE 1 | Properties and hypothetical roles of the class II GRX-BOLA couple in plants. **(A)** Tridimensional structures of plastidial *Arabidopsis thaliana* BOLA1 and GRXS14 proteins highlighting the residues involved in the interactions. On the top, superimposition of AtBOLA1 (green) and AtBOLA2 (blue) structures. Both proteins have a α/β-structure made of four helices and three strands with an α1β1β2η2α3β3α4 (η: 3_{10}-helix) topology (Roret et al., 2014). The β-strands form a central three-stranded β-sheet. In addition to the extended C-terminal part in AtBOLA2, both proteins differ by the length of the β1–β2 loop (in red in BOLA1), referred to as [H/C] loop, and which contains the histidine (His97 in AtBOLA1) or cysteine (Cys29 in AtBOLA2) residues provided by BOLA proteins for Fe–S cluster bridging together with the His66 (AtBOLA2) or His144 (AtBOLA1). The putative DNA binding site in BOLAs is formed by the η2 and α3 helices, the loop containing a specific FXGX signature (type II β-turn), the α3 helix containing a positively charged RHR motif and the β3 strand. Below, from left to right, AtBOLA2 structure showing 18 residues (mainly part of the β2 and β3 strands and α3 helix) identified by NMR titration as involved in the interaction with apo-AtGRXS14; and AtGRXS14 structure showing 32 residues (many present in the C-terminal α3 and α4 helices) identified by NMR titration as involved in the interaction with AtBOLA2 (Roret et al., 2014). These residues, plus some additional ones, are also involved in the formation of the [2Fe–2S] cluster-bridged heterodimer as determined using human proteins (Nasta et al., 2017). **(B)** Hypothetical model for the role of GRXS15 and BOLA4 in plant mitochondria. By analogy with the yeast system, GRXS15 (shortened as GRX) should receive a [2Fe–2S] cluster synthesized *de novo* by a multi-protein assembly complex (details about the proteins involved in the early steps of Fe–S cluster assembly and transfer have been omitted). GRXS15 is supposed to transfer its [2Fe–2S] cluster to client proteins as the mitochondrial ferredoxin 1 (mFDX1) (Moseler et al., 2015) or to ISCA proteins for the reductive conversion of two [2Fe–2S] clusters into a [4Fe–4S] cluster (as shown with human proteins) and its subsequent delivery to client proteins bearing such cluster. In the absence of genetic analysis about *bola4* mutants, the contribution of BOLA4 (shortened as BOLA) for the respective roles of GRXS15 is unclear, but the confirmed interaction between both proteins (Couturier et al., 2014) prompted us to include BOLA at this step as yeast Bol1/3 proteins are only required for the maturation of [4Fe–4S] proteins. The specific defects observed for aconitase (ACO) and lipoic-acid dependent proteins in the *GRXS15* mutant lines indicate a direct or indirect role for GRXS15 in the maturation of both lipoate synthase (LIP1) and aconitase. Finally, whether GRXS15 is required for the maturation and activity of cytosolic and nuclear Fe–S proteins by fueling the CIA machinery as shown for yeast Grx5, or by indirectly contributing to the synthesis of molybdenum cofactor, that is present in several cytosolic Fe–S proteins, is unknown. **(C)** Roles associated with the various oligomeric forms involving nucleo-cytosolic GRXs and BOLAs irrespective of the organisms considered. The color code is as follows: in blue, functions associated with apo-dimeric GRX forms, in purple those associated with apo-BOLA and in black those associated with the GRX homodimeric or GRX-BOLA heterodimeric forms bridging a [2Fe–2S] cluster.

usual [2Fe–2S] cluster-bridging heterodimers (Yeung et al., 2011; Dlouhy et al., 2016). In *Sinorhizobium meliloti*, deletion of the sole class II GRX also leads to impaired maturation of Fe–S proteins and increased intracellular iron content (Benyamina et al., 2013).

In plants, the corresponding mitochondrial GRX is named GRXS15. Knockout Arabidopsis mutants are lethal due to defective embryo development (Moseler et al., 2015). Plants expressing a mutated GRXS15 form modified for its ability to coordinate an Fe–S cluster exhibit severely reduced growth and impaired aconitase activity (Moseler et al., 2015). Additionally, Arabidopsis GRXS15 down-regulated lines display slowed growth and impaired activity of enzymes dependent on lipoic acid, the synthesis of which is ensured by the Fe–S cluster-containing lipoyl synthase (Ströher et al., 2016). Whether GRXS15 fulfills its function in concert with BOLA4, the sole mitochondrial BOLA, remains to be explored, but their interaction was demonstrated in yeast and *in planta* (**Figure 1B**; Couturier et al., 2014). Plants also have class II GRXs (GRXS14 and S16) and mono-domain BOLAs (BOLA1, BOLA4) in plastids (Couturier et al., 2013). So far, *in planta* evidence for their implication in the biogenesis of Fe–S proteins are scarce (**Table 1**). GRXS14-deficient Arabidopsis plants exhibit accelerated chlorophyll loss upon prolonged darkness, a treatment also leading to a decreased abundance of proteins acting in Fe–S cluster metabolism (Rey et al., 2017). Nevertheless, the demonstration that Arabidopsis and/or poplar GRXS14 and GRXS16 interact both with BOLA1 and BOLA4 (Couturier et al., 2014), bind Fe–S clusters alone or in complex (Bandyopadhyay et al., 2008; Dhalleine et al., 2014; Roret et al., 2014) and transfer it to partner proteins (Mapolelo et al., 2013) give strong credence to such a role. Even more importantly, all plant *GRX* and *BOLA* genes complement totally or partially (*GRXS15*) the corresponding yeast *grx5* and *bol1–bol3* mutants, indicating that they possess similar structural and functional determinants (Bandyopadhyay et al., 2008; Moseler et al., 2015; Uzarska et al., 2018).

MULTIPLE FUNCTIONS IN THE REGULATION OF IRON HOMEOSTASIS OF THE CLASS II GRX AND BOLA COUPLE IN THE CYTOSOL/NUCLEUS OF EUKARYOTES

Eukaryote cytosolic class II GRXs are multidomain proteins formed by an N-terminal thioredoxin-like domain fused to one to three GRX domains (Couturier et al., 2009). Most organisms have a single GRX of this type and also a single cytosolic BOLA isoform, referred to as BOLA2/Bol2/Fra2. The pioneering studies showing the involvement of class II GRXs and BOLAs in Fe homeostasis have been conducted in *S. cerevisiae* mutants deregulated in *Grx3*, *Grx4,* and *Bol2/Fra2* genes (**Table 1**; Lesuisse et al., 2005; Ojeda et al., 2006; Pujol-Carrion et al., 2006). In yeast, the regulation of Fe concentration is achieved at the transcriptional level by low- (Aft1 and Aft2) and high-level (Yap5) sensing transcription factors and at the post-transcriptional level by mRNA-binding proteins (Outten and Albetel, 2013). Both types of transcription factors bind [2Fe–2S] clusters allowing them to perceive the cellular Fe or Fe–S cluster status (Poor et al., 2014; Rietzschel et al., 2015). Whereas *Grx4* expression is regulated by Yap5, it is not documented whether Yap5 localization or activity is controlled by a GRX/BOLA complex. Regarding Aft1/Aft2, their subcellular (nuclear vs. cytosolic) localization is controlled by a Fra2-Grx3/4 inhibitory complex (possibly requiring also the aminopeptidase Fra1) (Kumánovics et al., 2008). The current view is that the presence of an Fe–S cluster in the Fra2-Grx3/4 complex is synonymous of iron-replete conditions and of a correct functioning of the ISC machinery (**Figure 1C**;

Kumánovics et al., 2008). By transferring a cluster to Aft1/2, the GRX-BOLA complex should either retain them in the cytosol or promote their dissociation from DNA if in the nucleus (Ueta et al., 2012; Poor et al., 2014).

Some aspects of Fe homeostasis in other yeasts and fungi are also controlled by GRX and/or BOLA. In *Cryptococcus neoformans*, Fe repletion promotes Grx4 relocation from the nucleus to the cytoplasm allowing the regulation of Cir1, a master regulator of Fe-responsive genes (Attarian et al., 2018). In *Schizosaccharomyces pombe*, Fe metabolism is regulated by two transcriptional repressors, the GATA-type iron sensing Fep1 and the CCAAT-binding factor complex subunit Php4 (Brault et al., 2015). Their localization and/or DNA binding activity are regulated by Grx4 and/or Fra2 (reviewed in Outten and Albetel, 2013; Brault et al., 2015). The binding of a [2Fe–2S] cluster between Grx4 and Php4 may promote Php4 release from the CCAAT-binding complex at the DNA targets and suppress its inhibitory effect on the expression of Fe storage genes (Dlouhy et al., 2017). Unlike Php4, the regulation of which does not involve Fra2, the formation of a [2Fe–2S]-Grx4/Fra2 heterodimeric complex is required for regulating Fep1 activation (Jacques et al., 2014; Encinar del Dedo et al., 2015).

In mammals, the regulation of Fe metabolism and homeostasis is ensured by IRP1/2 and RNA-binding proteins (Rouault and Maio, 2017). Under Fe limitation, both IRPs bind to the so-called Iron Responsive Elements (IREs) in untranslated regions of mRNAs coding for proteins implicated in Fe assimilation and homeostasis (Rouault and Maio, 2017). Doing so, they control either mRNA stabilization or translational blocking. Whereas IRP2 release from IREs is mediated by proteasomal degradation (Guo et al., 1995), IRP1 function may depend on GLRX3/PICOT (but also on mitochondrial GLRX5) as it relies on the binding of an Fe–S cluster. Under Fe sufficiency, IRP1 binds a [4Fe–4S] cluster and acts as an aconitase whereas under Fe limitation the protein turns into an apoform binding to IREs. Consequently, IRP1 requires functional mitochondrial and cytosolic Fe–S cluster assembly machineries. Having two GRX domains, human GLRX3 forms homodimers or heterotrimers with two BOLA2 molecules bridging two [2Fe–2S] clusters (Li et al., 2012; Banci et al., 2015b; Frey et al., 2016). It also binds a [4Fe–4S] cluster and transfers it *in vitro* to an apo-IRP1 (Xia et al., 2015). *GLRX3* silencing in human HELA cells decreases the activity of several cytosolic Fe–S proteins, including IRP1 (**Table 1**; Haunhorst et al., 2013). In zebrafish, *GLRX3* deletion impairs heme biosynthesis during embryo development (Haunhorst et al., 2013). All of this indicates important functions of vertebrate GLRX3 in Fe metabolism.

In addition to an Fe sensing function, an Fe or Fe–S cluster trafficking function was proposed for yeast Grx3/4 and the human GLRX3-BOLA2 complex to ensure proper assembly of several types of Fe-containing centers. In fact, most multidomain GRXs are able to rescue the Fe–S cluster maturation defects of the yeast *grx5* mutant (Molina et al., 2004; Bandyopadhyay et al., 2008; Knuesting et al., 2015) suggesting that they have the capacity of exchanging Fe–S clusters. Accordingly, both human GLRX3 homodimers and GLRX3-BOLA2 trimeric complexes bridging two [2Fe–2S] clusters can deliver their clusters to the anamorsin/CIAPIN/DRE2 protein (Banci et al., 2015a,b). From the observation that the maturation of yeast Grx3/4 and human GLRX3-BOLA2 heterodimers requires the mitochondrial ISC machinery but not CIA components (Mühlenhoff et al., 2010; Frey et al., 2016), it is concluded that cytosolic class II GRXs should build their cluster from a sulfur compound exported by the mitochondrial ATM transporter (**Figure 1C**). In yeast *grx3/4*Δ, the Fe or Fe-cofactor insertion in various proteins present in cytosol [catalase, ribonucleotide reductase (RNR)], and mitochondria (complexes II and III, aconitase, Coq7 mono-oxygenase) is altered (Mühlenhoff et al., 2010; Zhang et al., 2011). Moreover, the respective increased and decreased Fe levels in cytosol and mitochondria of Grx3/4 depleted cells pointed to impaired Fe distribution (Mühlenhoff et al., 2010). These additional functions of yeast Grx3/4 are well exemplified in the case of RNR di-iron cofactor biogenesis because Grx4 provides the Fe atoms, but also serves for the maturation of holo-Dre2, that provides the required electrons (Li et al., 2017). A contribution of yeast Bol2 for these functions is unclear even though a general role in cytosolic Fe–S protein maturation is excluded (Uzarska et al., 2016). In human, GLRX3-BOLA2 trimeric complexes bridging two [2Fe–2S] clusters were proposed to constitute a reservoir for delivering Fe or Fe–S cluster to some Fe-containing target proteins based notably on the six–eightfold increased abundance observed in response to elevated iron (Frey et al., 2016).

The function of GRXS17, the sole nucleo-cytosolic class II GRX in plants, has been explored using several approaches. Tandem affinity purification using a tagged GRX form expressed in Arabidopsis cell cultures and seedlings pointed to the association of GRXS17 with CIA components and BOLA2 (Iñigo et al., 2016). The interactions with DRE2 and BOLA2 have been confirmed *in vivo* by binary yeast two-hybrid and BiFC and/or *in vitro* by co-expression in *E. coli* (Couturier et al., 2014; Dhalleine et al., 2014; Iñigo et al., 2016). As GRXs interact with Dre2/Anamorsin in yeast and human cells (Zhang et al., 2011; Banci et al., 2015b), the only direct CIA partner of GRXS17 might be DRE2 and the other proteins part of a complex. Besides, the binding of GRXS17 with putative Fe–S client proteins involved in purine salvage (xanthine dehydrogenase 1) or tRNA modification (thiouridylase subunits 1 and 2) was shown (Iñigo et al., 2016). Thus, one would expect that plants deficient in GRXS17 display a marked phenotype in relation with Fe metabolism, but the analysis of Arabidopsis *grxs17* plants led to relatively complex data. Indeed, their development is only mildly affected under standard growth conditions, but gets severely impaired (elongated leaves, modified shoot apical meristem structure, and altered auxin response) at high temperature or under long photoperiod (Cheng et al., 2011; Knuesting et al., 2015). It is not yet clear whether a redox- and/or an Fe-related function of GRXS17 is responsible for these alterations. In fact, *in vitro* pull-downs performed using the recombinant protein allowed recovering many non-Fe–S proteins including the NF-YC11 transcriptional regulator (Knuesting et al., 2015).

Moreover, there is no variation in the Fe content in mature leaves and only a slight increase in seeds (Yu et al., 2017) of *grxs17* plants that exhibit no or minor decreases in the activity of three Fe–S containing enzymes: aconitase, aldehyde oxidase and xanthine dehydrogenase (Knuesting et al., 2015; Iñigo et al., 2016). On the other hand, GRXS17-deficient lines exhibit a slightly increased sensitivity to genotoxic stress which is reminiscent of mutants compromised in the CIA pathway (Iñigo et al., 2016). Finally, when GRXS17-deficient lines are exposed to Fe deficiency, the primary root growth reduction, that is already visible under standard conditions, is exacerbated and ROS levels are elevated (Iñigo et al., 2016; Yu et al., 2017). Whether plant GRXS17 and BOLA2 act in concert remains unclear. The Arabidopsis *bola2* (incorrectly named *bola3*) mutant displays no phenotype under control conditions and no change in the activity of typical Fe–S enzymes (Qin et al., 2015). Surprisingly, this line is more tolerant to oxidative stress generated by an Fe excess (Qin et al., 2015). In conclusion, *bola2* and *grxs17* plants exhibit relatively mild phenotypes, visible mostly under stress conditions, compared to those described for human and yeast orthologs and to the embryo-lethality of most Arabidopsis mutants defective for early acting CIA components (Bernard et al., 2013). This raises some questions about the exact functions of BOLA2 and GRXS17 in the regulation of Fe homeostasis in plant cells and about the existence of an alternative system, notably for delivering Fe–S clusters to DRE2, whose function is essential.

ROADMAP TOWARD THE UNDERSTANDING OF THE ROLES OF GRX/BOLA COUPLES IN PLANTS

In this section, we propose some ideas and experimental strategies that should warrant deciphering the functions associated to GRX/BOLA couples in plants.

Evidence obtained so far indicate that the class II mono-domain GRXs and BOLAs present in mitochondria of non-plant eukaryotes and in bacteria act as maturation factors for the biogenesis of Fe–S proteins. A similar role seems true for the plant mitochondrial GRXS15, but it is now mandatory to examine whether it also contributes to the maturation of extra-mitochondrial proteins. Another challenge will be to understand why it is essential in plants unlike in yeast. Also, the physiological consequences of *BOLA4* depletion must be investigated to see whether this fits with a function connected to GRXS15. Concerning plastidial proteins (GRXS14, GRXS16, BOLA1, and BOLA4), a role in the maturation of Fe–S proteins still needs to be demonstrated *in planta*, despite they can functionally substitute to their mitochondrial yeast counterparts.

With regard to the cytosolic multi-domain GRXs and BOLAs, a role in Fe metabolism seems evolutionary conserved, but their contribution and partners differ. In yeast, their primary function is to regulate Fe-responsive transcription factors. Additional functions are to ensure a proper Fe distribution toward all types of Fe cofactors (including heme and non-heme Fe centers) and/or to serve for Dre2 maturation, thus contributing to the correct functioning of the CIA machinery. In this case, Grx3/4 have an exclusive or predominant role because the corresponding mutant is lethal or strongly affected, unlike the *bol2/fra2* mutant. Experimental evidence indicate that the involvement of GRX and/or BOLA in DRE2 maturation is likely also true in mammals and plants, but evidence supporting other functions are scarce.

A first prerequisite to future molecular and physiological analyses is to generate the missing single knock-out lines but also multiple knock-out lines for possibly redundant proteins. This would be particularly important to obtain lines combining mutations for GRXS14 and GRXS16, for BOLA1 and BOLA4, but also for GRXS17 and the only other Fe–S ligating GRXs reported so far in the cytosol, namely GRXC1 (Rouhier et al., 2007), or BOLA2. In case the single or multiple mutants are lethal, an option for obtaining viable lines would be to generate RNAi lines as for *GRXS15*, but also dominant negative mutant lines expressing mutated versions of GRX or BOLA unable for instance to ligate the Fe–S cluster, i.e., mutated for the catalytic cysteine of GRXs or the conserved histidine residue of BOLA.

At the physiological level, the growth of these plants should be analyzed under standard conditions, but also under environmental constraints as the shoot phenotypes of *grxs17* mutants are only visible in specific conditions. For the BOLA2-GRXS17 couple, understanding their connection and discriminating between Fe- or redox-related functions will require in particular to assess the phenotypes of the corresponding mutants in the same experimental setup and conditions. Considering the described importance of GSH for ligating Fe–S cluster in GRX homodimer or GRX-BOLA heterodimer and for the maturation of cytosolic Fe–S proteins (Sipos et al., 2002), crossing some of these mutants with mutants having an altered GSH homeostasis would certainly be informative.

In other respects, an obvious strategy is to measure the abundance/activity of representative Fe–S proteins in these lines. However, performing quantitative proteomic and metabolomic approaches may be more informative and help obtaining a broader view of the molecular and cellular mechanisms affected and of the compensations established. It may also rapidly point to metabolic differences existing among mutants.

In all cases, determining the identity of the direct and indirect targets of both GRXs and BOLAs would represent a mandatory information. For instance, the proteins involved in the Fe–S cluster maturation process may act at different steps. Various approaches complementary to quantitative proteomics proved valuable even for detecting supposedly transient interactions among Fe–S cluster donors and acceptors (Touraine et al., 2019). Hence, it is possible to combine it to another non-targeted approach such as co-immunoprecipitation or to binary yeast two-hybrid experiments which has the advantage for instance to allow studying rapidly sequence requirements by mutational analysis.

In summary, the combination of genetic approaches, omics analyses and conventional biochemical tools should

in principle allow better delineating the roles and specificities of GRX/BOLA couples in the maintenance of Fe homeostasis in plants.

DATA AVAILABILITY

All datasets analyzed for this study are included in the manuscript and the Supplementary Files.

AUTHOR CONTRIBUTIONS

All authors wrote the text and approved the final version of the manuscript.

ACKNOWLEDGMENTS

Ms. Anna Moseler is greatly acknowledged for the artwork on **Figure 1**.

FUNDING

The UMR1136 is supported by a grant overseen by the French National Research Agency (ANR) as part of the "Investissements d'Avenir" program (ANR-11-LABX-0002-01, Lab of Excellence ARBRE). The work on plant GRX and BOLA proteins was supported by the Agence Nationale de la Recherche (Grant No. 2010BLAN1616).

REFERENCES

Aldea, M., Garrido, T., Hernández-Chico, C., Vicente, M., and Kushner, S. R. (1989). Induction of a growth-phase-dependent promoter triggers transcription of bolA, an *Escherichia coli* morphogene. *EMBO J.* 8, 3923–3931. doi: 10.1002/j.1460-2075.1989.tb08573.x

Alves, R., Vilaprinyo, E., Sorribas, A., and Herrero, E. (2009). Evolution based on domain combinations: the case of glutaredoxins. *BMC Evol. Biol.* 9:66. doi: 10.1186/1471-2148-9-66

Attarian, R., Hu, G., Sánchez-León, E., Caza, M., Croll, D., Do, E., et al. (2018). The monothiol glutaredoxin grx4 regulates iron homeostasis and virulence in *Cryptococcus neoformans*. *mBio* 9:e02377-18. doi: 10.1128/mBio.02377-18

Banci, L., Camponeschi, F., Ciofi-Baffoni, S., and Muzzioli, R. (2015a). Elucidating the molecular function of human BOLA2 in GRX3-dependent anamorsin maturation pathway. *J. Am. Chem. Soc.* 137, 16133–16143. doi: 10.1021/jacs.5b10592

Banci, L., Ciofi-Baffoni, S., Gajda, K., Muzzioli, R., Peruzzini, R., and Winkelmann, J. (2015b). N-terminal domains mediate [2Fe-2S] cluster transfer from glutaredoxin-3 to anamorsin. *Nat. Chem. Biol.* 11, 772–778. doi: 10.1038/nchembio.1892

Bandyopadhyay, S., Gama, F., Molina-Navarro, M. M., Gualberto, J. M., Claxton, R., Naik, S. G., et al. (2008). Chloroplast monothiol glutaredoxins as scaffold proteins for the assembly and delivery of [2Fe-2S] clusters. *EMBO J.* 27, 1122–1133. doi: 10.1038/emboj.2008.50

Barupala, D. P., Dzul, S. P., Riggs-Gelasco, P. J., and Stemmler, T. L. (2016). Synthesis, delivery and regulation of eukaryotic heme and Fe-S cluster cofactors. *Arch. Biochem. Biophys.* 592, 60–75. doi: 10.1016/j.abb.2016.01.010

Benyamina, S. M., Baldacci-Cresp, F., Couturier, J., Chibani, K., Hopkins, J., Bekki, A., et al. (2013). Two *Sinorhizobium meliloti* glutaredoxins regulate iron metabolism and symbiotic bacteroid differentiation. *Environ. Microbiol.* 15, 795–810. doi: 10.1111/j.1462-2920.2012.02835.x

Bernard, D. G., Netz, D. J. A., Lagny, T. J., Pierik, A. J., and Balk, J. (2013). Requirements of the cytosolic iron-sulfur cluster assembly pathway in *Arabidopsis*. *Philos. Trans. R. Soc. Lond. B. Biol. Sci.* 368:20120259. doi: 10.1098/rstb.2012.0259

Boutigny, S., Saini, A., Baidoo, E. E. K., Yeung, N., Keasling, J. D., and Butland, G. (2013). Physical and functional interactions of a monothiol glutaredoxin and an iron sulfur cluster carrier protein with the sulfur-donating radical S-adenosyl-L-methionine enzyme MiaB. *J. Biol. Chem.* 288, 14200–14211. doi: 10.1074/jbc.M113.460360

Brault, A., Mourer, T., and Labbé, S. (2015). Molecular basis of the regulation of iron homeostasis in fission and filamentous yeasts. *IUBMB Life* 67, 801–815. doi: 10.1002/iub.1441

Burschel, S., Kreuzer Decovic, D., Nuber, F., Stiller, M., Hofmann, M., Zupok, A., et al. (2019). Iron-sulfur cluster carrier proteins involved in the assembly of *Escherichia coli* NADH:ubiquinone oxidoreductase (complex I). *Mol. Microbiol.* 111, 31–45. doi: 10.1111/mmi.14137

Butland, G., Babu, M., Díaz-Mejía, J. J., Bohdana, F., Phanse, S., Gold, B., et al. (2008). eSGA: *E. coli* synthetic genetic array analysis. *Nat. Methods* 5, 789–795. doi: 10.1038/nmeth.1239

Camaschella, C., Campanella, A., De Falco, L., Boschetto, L., Merlini, R., Silvestri, L., et al. (2007). The human counterpart of zebrafish shiraz shows sideroblastic-like microcytic anemia and iron overload. *Blood* 110, 1353–1358. doi: 10.1182/blood-2007-02-072520

Cameron, J. M., Janer, A., Levandovskiy, V., Mackay, N., Rouault, T. A., Tong, W.-H., et al. (2011). Mutations in iron-sulfur cluster scaffold genes NFU1 and BOLA3 cause a fatal deficiency of multiple respiratory chain and 2-oxoacid dehydrogenase enzymes. *Am. J. Hum. Genet.* 89, 486–495. doi: 10.1016/j.ajhg.2011.08.011

Cheng, N.-H., Liu, J.-Z., Liu, X., Wu, Q., Thompson, S. M., Lin, J., et al. (2011). *Arabidopsis* monothiol glutaredoxin, AtGRXS17, is critical for temperature-dependent postembryonic growth and development via modulating auxin response. *J. Biol. Chem.* 286, 20398–20406. doi: 10.1074/jbc.M110.201707

Chung, W.-H., Kim, K.-D., and Roe, J.-H. (2005). Localization and function of three monothiol glutaredoxins in *Schizosaccharomyces pombe*. *Biochem. Biophys. Res. Commun.* 330, 604–610. doi: 10.1016/j.bbrc.2005.02.183

Comini, M. A., Rettig, J., Dirdjaja, N., Hanschmann, E.-M., Berndt, C., and Krauth-Siegel, R. L. (2008). Monothiol glutaredoxin-1 is an essential iron-sulfur protein in the mitochondrion of African trypanosomes. *J. Biol. Chem.* 283, 27785–27798. doi: 10.1074/jbc.M802010200

Couturier, J., Jacquot, J.-P., and Rouhier, N. (2009). Evolution and diversity of glutaredoxins in photosynthetic organisms. *Cell. Mol. Life Sci.* 66, 2539–2557. doi: 10.1007/s00018-009-0054-y

Couturier, J., Przybyla-Toscano, J., Roret, T., Didierjean, C., and Rouhier, N. (2015). The roles of glutaredoxins ligating Fe-S clusters: sensing, transfer or repair functions? *Biochim. Biophys. Acta* 1853, 1513–1527. doi: 10.1016/j.bbamcr.2014.09.018

Couturier, J., Touraine, B., Briat, J.-F., Gaymard, F., and Rouhier, N. (2013). The iron-sulfur cluster assembly machineries in plants: current knowledge and open questions. *Front. Plant Sci.* 4:259. doi: 10.3389/fpls.2013.00259

Couturier, J., Wu, H.-C., Dhalleine, T., Pégeot, H., Sudre, D., Gualberto, J. M., et al. (2014). Monothiol glutaredoxin-BolA interactions: redox control of *Arabidopsis thaliana* BolA2 and SufE1. *Mol. Plant* 7, 187–205. doi: 10.1093/mp/sst156

Dhalleine, T., Rouhier, N., and Couturier, J. (2014). Putative roles of glutaredoxin-BolA holo-heterodimers in plants. *Plant Signal. Behav.* 9:e28564. doi: 10.4161/psb.28564

Dlouhy, A. C., Beaudoin, J., Labbé, S., and Outten, C. E. (2017). *Schizosaccharomyces pombe* Grx4 regulates the transcriptional repressor Php4 via [2Fe-2S] cluster binding. *Met. Integr. Biometal Sci.* 9, 1096–1105. doi: 10.1039/c7mt00144d

Dlouhy, A. C., Li, H., Albetel, A.-N., Zhang, B., Mapolelo, D. T., Randeniya, S., et al. (2016). The *Escherichia coli* BolA protein IbaG forms a histidine-Ligated [2Fe-2S]-bridged complex with Grx4. *Biochemistry* 55, 6869–6879. doi: 10.1021/acs.biochem.6b00812

Encinar del Dedo, J., Gabrielli, N., Carmona, M., Ayté, J., and Hidalgo, E. (2015). A cascade of iron-containing proteins governs the genetic iron starvation response to promote iron uptake and inhibit iron storage in fission yeast. *PLoS Genet.* 11:e1005106. doi: 10.1371/journal.pgen.1005106

Frey, A. G., Palenchar, D. J., Wildemann, J. D., and Philpott, C. C. (2016). A glutaredoxin · bola complex serves as an iron-sulfur cluster chaperone for the cytosolic cluster assembly machinery. *J. Biol. Chem.* 291, 22344–22356. doi: 10.1074/jbc.M116.744946

Guo, B., Phillips, J. D., Yu, Y., and Leibold, E. A. (1995). Iron regulates the intracellular degradation of iron regulatory protein 2 by the proteasome. *J. Biol. Chem.* 270, 21645–21651. doi: 10.1074/jbc.270.37.21645

Haunhorst, P., Hanschmann, E.-M., Bräutigam, L., Stehling, O., Hoffmann, B., Mühlenhoff, U., et al. (2013). Crucial function of vertebrate glutaredoxin 3 (PICOT) in iron homeostasis and hemoglobin maturation. *Mol. Biol. Cell* 24, 1895–1903. doi: 10.1091/mbc.E12-09-0648

Iñigo, S., Durand, A. N., Ritter, A., Le Gall, S., Termathe, M., Klassen, R., et al. (2016). Glutaredoxin GRXS17 associates with the cytosolic iron-sulfur cluster assembly pathway. *Plant Physiol.* 172, 858–873. doi: 10.1104/pp.16.00261

Jacques, J.-F., Mercier, A., Brault, A., Mourer, T., and Labbé, S. (2014). Fra2 is a co-regulator of Fep1 inhibition in response to iron starvation. *PLoS One* 9:e98959. doi: 10.1371/journal.pone.0098959

Kim, K.-D., Chung, W.-H., Kim, H.-J., Lee, K.-C., and Roe, J.-H. (2010). Monothiol glutaredoxin Grx5 interacts with Fe-S scaffold proteins Isa1 and Isa2 and supports Fe-S assembly and DNA integrity in mitochondria of fission yeast. *Biochem. Biophys. Res. Commun.* 392, 467–472. doi: 10.1016/j.bbrc.2010.01.051

Knuesting, J., Riondet, C., Maria, C., Kruse, I., Bécuwe, N., König, N., et al. (2015). Arabidopsis glutaredoxin S17 and its partner, the nuclear factor Y subunit C11/negative cofactor 2α, contribute to maintenance of the shoot apical meristem under long-day photoperiod. *Plant Physiol.* 167, 1643–1658. doi: 10.1104/pp.15.00049

Kumánovics, A., Chen, O. S., Li, L., Bagley, D., Adkins, E. M., Lin, H., et al. (2008). Identification of FRA1 and FRA2 as genes involved in regulating the yeast iron regulon in response to decreased mitochondrial iron-sulfur cluster synthesis. *J. Biol. Chem.* 283, 10276–10286. doi: 10.1074/jbc.M801160200

Lesuisse, E., Knight, S. A. B., Courel, M., Santos, R., Camadro, J.-M., and Dancis, A. (2005). Genome-wide screen for genes with effects on distinct iron uptake activities in *Saccharomyces cerevisiae*. *Genetics* 169, 107–122. doi: 10.1534/genetics.104.035873

Li, H., Mapolelo, D. T., Dingra, N. N., Keller, G., Riggs-Gelasco, P. J., Winge, D. R., et al. (2011). Histidine 103 in Fra2 is an iron-sulfur cluster ligand in the [2Fe-2S] Fra2-Grx3 complex and is required for *in vivo* iron signaling in yeast. *J. Biol. Chem.* 286, 867–876. doi: 10.1074/jbc.M110.184176

Li, H., Mapolelo, D. T., Randeniya, S., Johnson, M. K., and Outten, C. E. (2012). Human glutaredoxin 3 forms [2Fe-2S]-bridged complexes with human BolA2. *Biochemistry* 51, 1687–1696. doi: 10.1021/bi2019089

Li, H., and Outten, C. E. (2012). Monothiol CGFS glutaredoxins and BolA-like proteins: [2Fe-2S] binding partners in iron homeostasis. *Biochemistry* 51, 4377–4389. doi: 10.1021/bi300393z

Li, H., Stümpfig, M., Zhang, C., An, X., Stubbe, J., Lill, R., et al. (2017). The diferric-tyrosyl radical cluster of ribonucleotide reductase and cytosolic iron-sulfur clusters have distinct and similar biogenesis requirements. *J. Biol. Chem.* 292, 11445–11451. doi: 10.1074/jbc.M117.786178

Lill, R. (2009). Function and biogenesis of iron-sulphur proteins. *Nature* 460, 831–838. doi: 10.1038/nature08301

Mapolelo, D. T., Zhang, B., Randeniya, S., Albetel, A.-N., Li, H., Couturier, J., et al. (2013). Monothiol glutaredoxins and A-type proteins: partners in Fe-S cluster trafficking. *Dalton Trans. Camb. Engl.* 2003, 3107–3115. doi: 10.1039/c2dt32263c

Melber, A., Na, U., Vashisht, A., Weiler, B. D., Lill, R., Wohlschlegel, J. A., et al. (2016). Role of Nfu1 and Bol3 in iron-sulfur cluster transfer to mitochondrial clients. *eLife* 5:e15991. doi: 10.7554/eLife.15991

Mil-Homens, D., Barahona, S., Moreira, R. N., Silva, I. J., Pinto, S. N., Fialho, A. M., et al. (2018). Stress response protein bola influences fitness and promotes *Salmonella enterica Serovar Typhimurium* virulence. *Appl. Environ. Microbiol.* 84:e02850-17. doi: 10.1128/AEM.02850-17

Molina, M. M., Bellí, G., de la Torre, M. A., Rodríguez-Manzaneque, M. T., and Herrero, E. (2004). Nuclear monothiol glutaredoxins of *Saccharomyces cerevisiae* can function as mitochondrial glutaredoxins. *J. Biol. Chem.* 279, 51923–51930. doi: 10.1074/jbc.M410219200

Moseler, A., Aller, I., Wagner, S., Nietzel, T., Przybyla-Toscano, J., Mühlenhoff, U., et al. (2015). The mitochondrial monothiol glutaredoxin S15 is essential for iron-sulfur protein maturation in *Arabidopsis thaliana*. *Proc. Natl. Acad. Sci. U.S.A.* 112, 13735–13740. doi: 10.1073/pnas.1510835112

Mühlenhoff, U., Gerber, J., Richhardt, N., and Lill, R. (2003). Components involved in assembly and dislocation of iron-sulfur clusters on the scaffold protein Isu1p. *EMBO J.* 22, 4815–4825. doi: 10.1093/emboj/cdg446

Mühlenhoff, U., Molik, S., Godoy, J. R., Uzarska, M. A., Richter, N., Seubert, A., et al. (2010). Cytosolic monothiol glutaredoxins function in intracellular iron sensing and trafficking via their bound iron-sulfur cluster. *Cell Metab.* 12, 373–385. doi: 10.1016/j.cmet.2010.08.001

Nasta, V., Giachetti, A., Ciofi-Baffoni, S., and Banci, L. (2017). Structural insights into the molecular function of human [2Fe-2S] BOLA1-GRX5 and [2Fe-2S] BOLA3-GRX5 complexes. *Biochim. Biophys. Acta* 1861, 2119–2131. doi: 10.1016/j.bbagen.2017.05.005

Ojeda, L., Keller, G., Muhlenhoff, U., Rutherford, J. C., Lill, R., and Winge, D. R. (2006). Role of glutaredoxin-3 and glutaredoxin-4 in the iron regulation of the Aft1 transcriptional activator in *Saccharomyces cerevisiae*. *J. Biol. Chem.* 281, 17661–17669. doi: 10.1074/jbc.M602165200

Outten, C. E., and Albetel, A.-N. (2013). Iron sensing and regulation in *Saccharomyces cerevisiae*: ironing out the mechanistic details. *Curr. Opin. Microbiol.* 16, 662–668. doi: 10.1016/j.mib.2013.07.020

Philpott, C. C., Ryu, M.-S., Frey, A., and Patel, S. (2017). Cytosolic iron chaperones: proteins delivering iron cofactors in the cytosol of mammalian cells. *J. Biol. Chem.* 292, 12764–12771. doi: 10.1074/jbc.R117.791962

Poor, C. B., Wegner, S. V., Li, H., Dlouhy, A. C., Schuermann, J. P., Sanishvili, R., et al. (2014). Molecular mechanism and structure of the *Saccharomyces cerevisiae* iron regulator Aft2. *Proc. Natl. Acad. Sci. U.S.A.* 111, 4043–4048. doi: 10.1073/pnas.1318869111

Przybyla-Toscano, J., Roret, T., Couturier, J., and Rouhier, N. (2017). "FeS Cluster Assembly: Role of Monothiol Grxs and Nfu Proteins," in *Encyclopedia of Inorganic and Bioinorganic Chemistry*, eds R. A Scott (New York, NY: American Cancer Society), 1–19. doi: 10.1002/9781119951438.eibc2470

Pujol-Carrion, N., Belli, G., Herrero, E., Nogues, A., and de la Torre-Ruiz, M. A. (2006). Glutaredoxins Grx3 and Grx4 regulate nuclear localisation of Aft1 and the oxidative stress response in *Saccharomyces cerevisiae*. *J. Cell Sci.* 119, 4554–4564. doi: 10.1242/jcs.03229

Qin, L., Wang, M., Zuo, J., Feng, X., Liang, X., Wu, Z., et al. (2015). Cytosolic bolA plays a repressive role in the tolerance against excess iron and mv-induced oxidative stress in plants. *PLoS One* 10:e0124887. doi: 10.1371/journal.pone.0124887

Rey, P., Becuwe, N., Tourrette, S., and Rouhier, N. (2017). Involvement of *Arabidopsis* glutaredoxin S14 in the maintenance of chlorophyll content. *Plant Cell Environ.* 40, 2319–2332. doi: 10.1111/pce.13036

Rietzschel, N., Pierik, A. J., Bill, E., Lill, R., and Mühlenhoff, U. (2015). The basic leucine zipper stress response regulator Yap5 senses high-iron conditions by coordination of [2Fe-2S] clusters. *Mol. Cell. Biol.* 35, 370–378. doi: 10.1128/MCB.01033-14

Rodríguez-Manzaneque, M. T., Tamarit, J., Bellí, G., Ros, J., and Herrero, E. (2002). Grx5 is a mitochondrial glutaredoxin required for the activity of iron/sulfur enzymes. *Mol. Biol. Cell* 13, 1109–1121. doi: 10.1091/mbc.01-10-0517

Roret, T., Tsan, P., Couturier, J., Zhang, B., Johnson, M. K., Rouhier, N., et al. (2014). Structural and spectroscopic insights into BolA-glutaredoxin complexes. *J. Biol. Chem.* 289, 24588–24598. doi: 10.1074/jbc.M114.572701

Rouault, T. A., and Maio, N. (2017). Biogenesis and functions of mammalian iron-sulfur proteins in the regulation of iron homeostasis and pivotal metabolic pathways. *J. Biol. Chem.* 292, 12744–12753. doi: 10.1074/jbc.R117.789537

Rouhier, N., Unno, H., Bandyopadhyay, S., Masip, L., Kim, S.-K., Hirasawa, M., et al. (2007). Functional, structural, and spectroscopic characterization of a glutathione-ligated [2Fe-2S] cluster in poplar glutaredoxin C1. *Proc. Natl. Acad. Sci. U.S.A.* 104, 7379–7384. doi: 10.1073/pnas.0702268104

Sipos, K., Lange, H., Fekete, Z., Ullmann, P., Lill, R., and Kispal, G. (2002). Maturation of cytosolic iron-sulfur proteins requires glutathione. *J. Biol. Chem.* 277, 26944–26949. doi: 10.1074/jbc.M200677200

Ströher, E., Grassl, J., Carrie, C., Fenske, R., Whelan, J., and Millar, A. H. (2016). Glutaredoxin S15 is involved in Fe-S cluster transfer in mitochondria

influencing lipoic acid-dependent enzymes, plant growth, and arsenic tolerance in *Arabidopsis*. *Plant Physiol.* 170, 1284–1299. doi: 10.1104/pp.15.01308

Touraine, B., Vignols, F., Przybyla-Toscano, J., Ischebeck, T., Dhalleine, T., Wu, H.-C., et al. (2019). Iron-sulfur protein NFU2 is required for branched-chain amino acid synthesis in Arabidopsis roots. *J. Exp. Bot.* 70, 1875–1889. doi: 10.1093/jxb/erz050

Ueta, R., Fujiwara, N., Iwai, K., and Yamaguchi-Iwai, Y. (2012). Iron-induced dissociation of the Aft1p transcriptional regulator from target gene promoters is an initial event in iron-dependent gene suppression. *Mol. Cell. Biol.* 32, 4998–5008. doi: 10.1128/MCB.00726-12

Uzarska, M. A., Dutkiewicz, R., Freibert, S.-A., Lill, R., and Mühlenhoff, U. (2013). The mitochondrial Hsp70 chaperone Ssq1 facilitates Fe/S cluster transfer from Isu1 to Grx5 by complex formation. *Mol. Biol. Cell* 24, 1830–1841. doi: 10.1091/mbc.E12-09-0644

Uzarska, M. A., Nasta, V., Weiler, B. D., Spantgar, F., Ciofi-Baffoni, S., Saviello, M. R., et al. (2016). Mitochondrial Bol1 and Bol3 function as assembly factors for specific iron-sulfur proteins. *eLife* 5:e16673. doi: 10.7554/eLife.16673

Uzarska, M. A., Przybyla-Toscano, J., Spantgar, F., Zannini, F., Lill, R., Mühlenhoff, U., et al. (2018). Conserved functions of Arabidopsis mitochondrial late-acting maturation factors in the trafficking of iron-sulfur clusters. *Biochim. Biophys. Acta Mol. Cell Res.* 1865, 1250–1259. doi: 10.1016/j.bbamcr.2018.06.003

Willems, P., Wanschers, B. F. J., Esseling, J., Szklarczyk, R., Kudla, U., Duarte, I., et al. (2013). BOLA1 is an aerobic protein that prevents mitochondrial morphology changes induced by glutathione depletion. *Antioxid. Redox Signal.* 18, 129–138. doi: 10.1089/ars.2011.4253

Wingert, R. A., Galloway, J. L., Barut, B., Foott, H., Fraenkel, P., Axe, J. L., et al. (2005). Deficiency of glutaredoxin 5 reveals Fe-S clusters are required for vertebrate haem synthesis. *Nature* 436, 1035–1039. doi: 10.1038/nature03887

Xia, H., Li, B., Zhang, Z., Wang, Q., Qiao, T., and Li, K. (2015). Human glutaredoxin 3 can bind and effectively transfer [4Fe-4S] cluster to apo-iron regulatory protein 1. *Biochem. Biophys. Res. Commun.* 465, 620–624. doi: 10.1016/j.bbrc.2015.08.073

Ye, H., Jeong, S. Y., Ghosh, M. C., Kovtunovych, G., Silvestri, L., Ortillo, D., et al. (2010). Glutaredoxin 5 deficiency causes sideroblastic anemia by specifically impairing heme biosynthesis and depleting cytosolic iron in human erythroblasts. *J. Clin. Invest.* 120, 1749–1761. doi: 10.1172/JCI40372

Yeung, N., Gold, B., Liu, N. L., Prathapam, R., Sterling, H. J., Willams, E. R., et al. (2011). The *E. coli* monothiol glutaredoxin GrxD forms homodimeric and heterodimeric FeS cluster containing complexes. *Biochemistry* 50, 8957–8969. doi: 10.1021/bi2008883

Yu, H., Yang, J., Shi, Y., Donelson, J., Thompson, S. M., Sprague, S., et al. (2017). *Arabidopsis* glutaredoxin S17 contributes to vegetative growth, mineral accumulation, and redox balance during iron deficiency. *Front. Plant Sci.* 8:1045. doi: 10.3389/fpls.2017.01045

Zhang, Y., Liu, L., Wu, X., An, X., Stubbe, J., and Huang, M. (2011). Investigation of in vivo diferric tyrosyl radical formation in *Saccharomyces cerevisiae* Rnr2 protein: requirement of Rnr4 and contribution of Grx3/4 AND Dre2 proteins. *J. Biol. Chem.* 286, 41499–41509. doi: 10.1074/jbc.M111.294074

Conflict of Interest Statement: The authors declare that the research was conducted in the absence of any commercial or financial relationships that could be construed as a potential conflict of interest.

frontiers in Plant Science

ORIGINAL RESEARCH
published: 12 June 2019
doi: 10.3389/fpls.2019.00746

Genotype Variation in Rice (*Oryza sativa* L.) Tolerance to Fe Toxicity Might Be Linked to Root Cell Wall Lignification

*Ricardo José Stein[1], Guilherme Leitão Duarte[2], Lívia Scheunemann[3†], Marta Gomes Spohr[3], Artur Teixeira de Araújo Júnior[2], Felipe Klein Ricachenevsky[4], Luis Mauro Gonçalves Rosa[5], Nilson Ivo Tonin Zanchin[6], Rinaldo Pires dos Santos[3] and Janette Palma Fett[2,3]**

[1] Faculdade Murialdo, Caxias do Sul, Brazil, [2] Centro de Biotecnologia, Universidade Federal do Rio Grande do Sul, Porto Alegre, Brazil, [3] Instituto de Biociências, Universidade Federal do Rio Grande do Sul, Porto Alegre, Brazil, [4] Departamento de Biologia, Universidade Federal de Santa Maria, Santa Maria, Brazil, [5] Departamento de Plantas Forrageiras e Agrometeorologia, Faculdade de Agronomia, Universidade Federal do Rio Grande do Sul, Porto Alegre, Brazil, [6] Instituto Carlos Chagas, Fundação Oswaldo Cruz – FIOCRUZ, Curitiba, Brazil

OPEN ACCESS

Edited by:
Thomas J. Buckhout, Humboldt University of Berlin, Germany

Reviewed by:
Lin-Bo Wu, University of Bonn, Germany
Huixia Shou, Zhejiang University, China

***Correspondence:**
Janette Palma Fett
jpfett@cbiot.ufrgs.br

†Present address:
Lívia Scheunemann, Department of Genetics, Ludwig-Maximilians-Universität, Munich, Germany

Specialty section:
This article was submitted to Plant Nutrition, a section of the journal Frontiers in Plant Science

Received: *29 January 2019*
Accepted: *21 May 2019*
Published: *12 June 2019*

Citation:
Stein RJ, Duarte GL, Scheunemann L, Spohr MG, de Araújo Júnior AT, Ricachenevsky FK, Rosa LMG, Zanchin NIT, Santos RP and Fett JP (2019) Genotype Variation in Rice (Oryza sativa L.) Tolerance to Fe Toxicity Might Be Linked to Root Cell Wall Lignification. Front. Plant Sci. 10:746. doi: 10.3389/fpls.2019.00746

Iron (Fe) is an essential element to plants, but can be harmful if accumulated to toxic concentrations. Fe toxicity can be a major nutritional disorder in rice (*Oryza sativa*) when cultivated under waterlogged conditions, as a result of excessive Fe solubilization of in the soil. However, little is known about the basis of Fe toxicity and tolerance at both physiological and molecular level. To identify mechanisms and potential candidate genes for Fe tolerance in rice, we comparatively analyzed the effects of excess Fe on two cultivars with distinct tolerance to Fe toxicity, EPAGRI 108 (tolerant) and BR-IRGA 409 (susceptible). After excess Fe treatment, BR-IRGA 409 plants showed reduced biomass and photosynthetic parameters, compared to EPAGRI 108. EPAGRI 108 plants accumulated lower amounts of Fe in both shoots and roots compared to BR-IRGA 409. We conducted transcriptomic analyses of roots from susceptible and tolerant plants under control and excess Fe conditions. We found 423 up-regulated and 92 down-regulated genes in the susceptible cultivar, and 42 up-regulated and 305 down-regulated genes in the tolerant one. We observed striking differences in root gene expression profiles following exposure to excess Fe: the two cultivars showed no genes regulated in the same way (up or down in both), and 264 genes were oppositely regulated in both cultivars. Plants from the susceptible cultivar showed down-regulation of known Fe uptake-related genes, indicating that plants are actively decreasing Fe acquisition. On the other hand, plants from the tolerant cultivar showed up-regulation of genes involved in root cell wall biosynthesis and lignification. We confirmed that the tolerant cultivar has increased lignification in the outer layers of the cortex and in the vascular bundle compared to the susceptible cultivar, suggesting that the capacity to avoid excessive Fe uptake could rely in root cell wall remodeling. Moreover, we showed

that increased lignin concentrations in roots might be linked to Fe tolerance in other rice cultivars, suggesting that a similar mechanism might operate in multiple genotypes. Our results indicate that changes in root cell wall and Fe permeability might be related to Fe toxicity tolerance in rice natural variation.

Keywords: iron, rice, lignin, root, exclusion

INTRODUCTION

Iron (Fe) is an essential nutrient for plants. It is involved in oxi-reductive reactions in photosynthesis, respiration and nitrogen assimilation, as well as in other important plant biological processes. Thus, plants have evolved mechanisms to maintain Fe homeostasis when soil concentration is low (Sperotto et al., 2012; Ricachenevsky et al., 2018). However, Fe can also become toxic if accumulated inside the cell, acting as a potent generator of reactive oxygen species (ROS), specially the hydroxyl radical, by the Fenton reaction (Becana et al., 1998). This radical is extremely toxic to cell metabolism, leading to oxidation of biological macromolecules such as lipids, proteins and nucleic acids, causing membrane leakage and even cell death (Blokhina et al., 2003). Thus, plants must maintain Fe concentrations within a narrow range for proper growth and development.

Rice plants are especially prone to Fe toxicity when cultivated under flooded conditions. Well-aerated soils usually have high amounts of ferric Fe (Fe^{3+}), which has low solubility. Waterlogging, however, results in an anoxic and reductive environment that reduces Fe^{3+} to the more soluble Fe^{2+}, which is accumulated in the soil solution (Becker and Asch, 2005). Wetland rice stands for most of the world rice production, and Fe toxicity reduces rice yield by 12 to 100%, depending on the genotype, intensity of Fe toxicity stress and soil fertility status (Sahrawat, 2004). Two distinct types of toxicity have been described in the literature: a true (or real) Fe toxicity – characterized by the accumulation of toxic levels of Fe in the plant body (Sahrawat, 2000; Olaleye et al., 2001; Stein et al., 2009a) and an indirect toxicity, caused by Fe precipitation in the root apoplast – the Fe plaque – resulting in multiple nutritional deficiencies (Sahrawat, 2004).

Different Fe toxicity tolerance mechanisms have been proposed for rice plants: type I consists in Fe exclusion from roots, and uses aerenchyma-derived oxygen or enzymatic activity to oxidize Fe^{2+} into Fe^{3+}, which precipitates as an Fe plaque at the root surface (Wu et al., 2014); type II consists of shoot tolerance to high Fe concentration, likely through compartmentalization via storage within the inner cavity of ferritin proteins (Stein et al., 2009b) or by the action of vacuolar transporters such as VITs (VACUOLAR IRON TRANSPORTER, Zhang et al., 2012); and type III, in the presence of an antioxidant system that detoxifies reactive oxygen species produced via Fenton when Fe is present in excess (Wu et al., 2017). Type I is considered a root-based mechanism, and types II and III are shoot-based mechanisms. Clearly, there is wide variation in tolerance, which depends on the stress duration, strength, and plant developmental stage. Some genotypes may present contrasting phenotypes depending on how the experiments are performed (Wu et al., 2014; Matthus et al., 2015), indicating the need to better understand the underlying physiological and molecular mechanisms of Fe tolerance. Previous work showed that (1) photosynthesis is affected by Fe toxicity (Stein et al., 2009a; Müller et al., 2017); known Fe uptake genes are down-regulated upon high Fe treatment (Finatto et al., 2015); and that early (3 days) and late (3 weeks) Fe toxicity responses are quite different in both roots and shoots (Quinet et al., 2012). However, molecular mechanisms associated with tolerant and sensitive genotypes are underexplored.

Although no causative gene that confers Fe tolerance was cloned, previous studies showed that Fe tolerance in distinct rice genotypes is a quantitative trait, with many QTL already described, all showing small effects (Dufey et al., 2009, 2012, 2015; Wu et al., 2014; Matthus et al., 2015; Zhang et al., 2017). Based on these studies, shoot-based tolerance might be linked to two glutathione S-transferases localized in chromosome 1, which are induced upon Fe stress (Matthus et al., 2015). For root-based mechanisms of Fe exclusion, one QTL co-localizes with OsIRT1, which is a Fe^{2+} transporter involved in the combined strategy for Fe acquisition present in rice (Ishimaru et al., 2006; Sperotto et al., 2012; Ricachenevsky and Sperotto, 2014).

Here, we analyzed the effects of high Fe concentration on two rice cultivars previously characterized as Fe toxicity susceptible and tolerant, BR-IRGA 409 and EPAGRI 108 (Silveira et al., 2007). The two cultivars are commonly used in rice fields in the two southernmost provinces of Brazil, Rio Grande do Sul, and Santa Catarina. Besides physiological characterization, transcriptomic analyses using microarrays were performed, showing markedly different gene expression profiles in the two contrasting cultivars. Our data suggest that tolerance to high Fe in some rice cultivars can be linked to increased lignification, which would in turn result in decreased permeability for Fe radial diffusion in roots and consequently lower root-to-shoot Fe translocation.

RESULTS

BR-IRGA 409 and EPAGRI 108 Susceptibility and Tolerance to Fe Toxicity

BR-IRGA 409 and EPAGRI 108 (hereafter "susceptible" and "tolerant" cultivars) were previously characterized as susceptible and tolerant to Fe toxicity, respectively, based solely on shoot biomass (Silveira et al., 2007). In order to further characterize the physiological responses of these cultivars to high Fe, we exposed plants to 500 ppm (excess Fe) and 6.5 ppm (control) for 9 days.

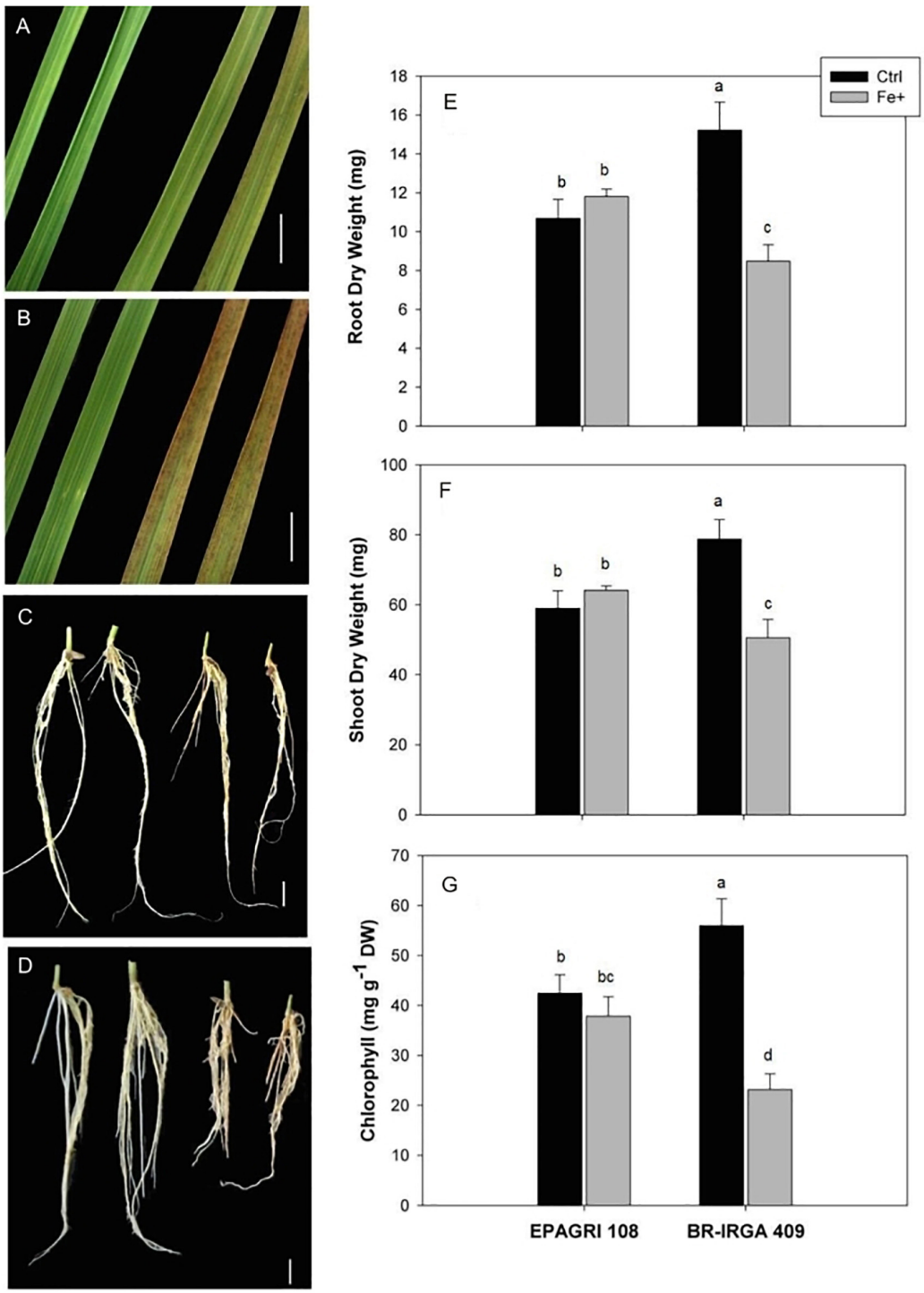

FIGURE 1 | Effects of excess iron in leaves **(A,B)** and roots **(C,D)** from EPAGRI 108 **(A,C)** and BR-IRGA 409 **(B,D)** rice plants exposed for 9 days to control (left) and excess (right) iron treatments. Bars represent 0.5 cm. Root **(E)**, and shoot **(F)** dry weight, and total chlorophyll **(G)** of plants exposed for 9 days to control (Ctrl) or iron excess (Fe+). Each value represents the mean of six replicates ± SE. Distinct letters above the bars indicate significant difference between means (Duncan test, $P \leq 0.05$).

Plants from the susceptible cultivar developed typical symptoms of Fe toxicity, with appearance of bronzing and necrotic lesions on leaves, while roots turned brown/orange (**Figures 1B,D**). The tolerant cultivar showed weaker symptoms of Fe toxicity in both shoots and roots (**Figures 1A,C**). Confirming previous data, shoot and root dry weight of the susceptible cultivar were

TABLE 1 | Iron accumulation and distribution in rice plants from cultivars EPAGRI 108 and BR-IRGA 409 after 9 days of exposure to control (Control) or excess (Fe+) iron treatments.

	EPAGRI 108		BR-IRGA 409	
	Control	Fe+	Control	Fe+
Shoot (mg Fe g^{-1} DW)	0.30 ± 0.02c	1.25 ± 0.11b	0.29 ± 0.03c	2.04 ± 0.21a
Root (mg Fe g^{-1} DW)	0.91 ± 0.16c	1.97 ± 0.23b	0.81 ± 0.15c	2.58 ± 0.2a
Iron plaque (mg Fe g^{-1} DW)	48.07 ± 0.94d	88.81 ± 2.53b	39.04 ± 2.58c	104 ± 2.65a

Each value represents the mean of six replicates. Distinct letters indicate significant difference between means from each parameter ($P \leq 0.05$).

decreased upon excess Fe treatment (**Figures 1E,F**), while no significant differences were observed in shoot and root dry weight in the tolerant cultivar. Exposure to excess Fe also led to a severe reduction of chlorophyll concentration in the susceptible cultivar, but no reduction in the tolerant one (**Figure 1G**). This clearly shows that BR-IRGA 409 and EPAGRI 108 are susceptible and tolerant to excessive Fe in our experimental conditions.

In order to find possible differences in Fe partitioning that could account for differences in tolerance, we quantified Fe concentrations in plants from both cultivars under control and excess Fe conditions (**Table 1**). Interestingly, shoots and roots (after Fe plaque removal – see below) from both cultivars showed comparable concentrations of Fe. Upon excess Fe treatment, shoots, and roots of the susceptible cultivar increased Fe concentration to a largest extent compared to the tolerant one. In shoots the susceptible cultivar had an increase of sevenfold, whereas the tolerant one had a fourfold increase (**Table 1**). In order to account for the larger biomass of the tolerant cultivar (**Figure 1**), we also considered the total Fe content (Fe concentrations in roots and shoots multiplied by the respective dry weights) in both cultivars. The average total Fe contents within plants (roots plus shoots, excluding the "Fe plaque") under the control treatment were 27.8 and 35.3 mg of Fe in EPAGRI 108 and BR-IRGA 409 plants, respectively. Upon excess Fe treatment, those contents reached 100.8 μg Fe in the tolerant cultivar (EPAGRI 108) and 129.4 μg Fe in the susceptible one. Therefore, even with lower biomass, total Fe uptake in plants from the susceptible cultivar was 28% higher than in the tolerant plants. Similarly, the Fe concentration in roots "Fe plaque" was higher in plants submitted to excess Fe treatment than in control plants, again to a larger extent in the susceptible cultivar. Interestingly, root Fe concentration in the "Fe plaque" was lower under excess Fe conditions in the tolerant cultivar than in the susceptible one (**Table 1**). Taken together, these results indicate that EPAGRI 108 is capable of excluding Fe from entering the root symplast, thus decreasing root to shoot Fe translocation.

Gas Exchange Measurements Reflect the Susceptible and Tolerant Phenotypes

Plants of both cultivars were exposed to excess Fe and control conditions for gas exchange measurements. Plants from the susceptible cultivar exposed to excess Fe showed lower rates of light saturated photosynthesis compared to control plants, while plants from the tolerant cultivar showed little difference between treatments (**Figure 2**). Decrease on carbon assimilation in BR-IRGA 409 plants was detected as early as the first day of exposure to excess Fe, with further decrease during the 9 days of treatment. In EPAGRI 108, a similar decrease in carbon assimilation was observed after 1 day of treatment. However, after 6 days of excess Fe treatment, plants from the tolerant cultivar recovered, and the photosynthetic activity reached levels similar to those of the control treatment. Thus, the tolerant cultivar is able to circumvent the effects of Fe toxicity to maintain carbon assimilation.

Different patterns of CO_2 assimilation rates/estimated substomatal CO_2 partial pressure (A/Ci) response curves were observed in tolerant EPAGRI 108 and susceptible BR-IRGA 409 plants (**Figures 3A,B**). Under excess Fe, plants from both cultivars showed a reduction in photosynthetic capacity (the maximum rate of photosynthesis reached under CO_2 saturation as light is already saturating), which was clearer in BR-IRGA 409 plants. Plants from the susceptible cultivar also showed a decrease in the slope of the A/Ci relationship, indicating a reduction in the carboxylation efficiency under excess Fe compared to control conditions (**Figure 3A**). Plants from the tolerant cultivar, however, showed no reduction (**Figure 3B**). Analysis of the response curves by using the model proposed by Farquhar et al. (1980) indicated that excess Fe led to a decrease in maximum carboxylation rate (Vc_{max}, 24.5% reduction) and electron transport rate (J_{max}, 41.7% reduction) after 6 days of exposure only in the susceptible cultivar (BR-IRGA 409), compared to the control treatment. EPAGRI 108 plants showed no statistically significant changes in both parameters (**Table 2**).

The light response curves (**Figures 3C,D**) revealed a clear advantage for the susceptible BR-IRGA 409 plants under non-stressful conditions, while tolerant EPAGRI 108 plants showed no differences when cultivated under control or excess Fe treatments,. Exposure of BR-IRGA 409 plants to excess Fe resulted in a significant reduction (51.9%) on the apparent quantum yield (ϕ_m) as compared to control plants, while a small reduction (6.3%, not significant) was observed in EPAGRI 108 plants (**Table 2**). These data indicate that photosynthesis is only marginally affected by excess Fe in plants from the tolerant cultivar, whereas photosynthetic parameters showed significant decreases in plants from the susceptible one when exposed to excess Fe.

Oxidative Metabolism Is Affected in Leaves of the Susceptible but Not in Tolerant Cultivar Under Excess Fe

Differences in oxidative metabolism were already suggested as possible sources of tolerance to Fe toxicity in rice

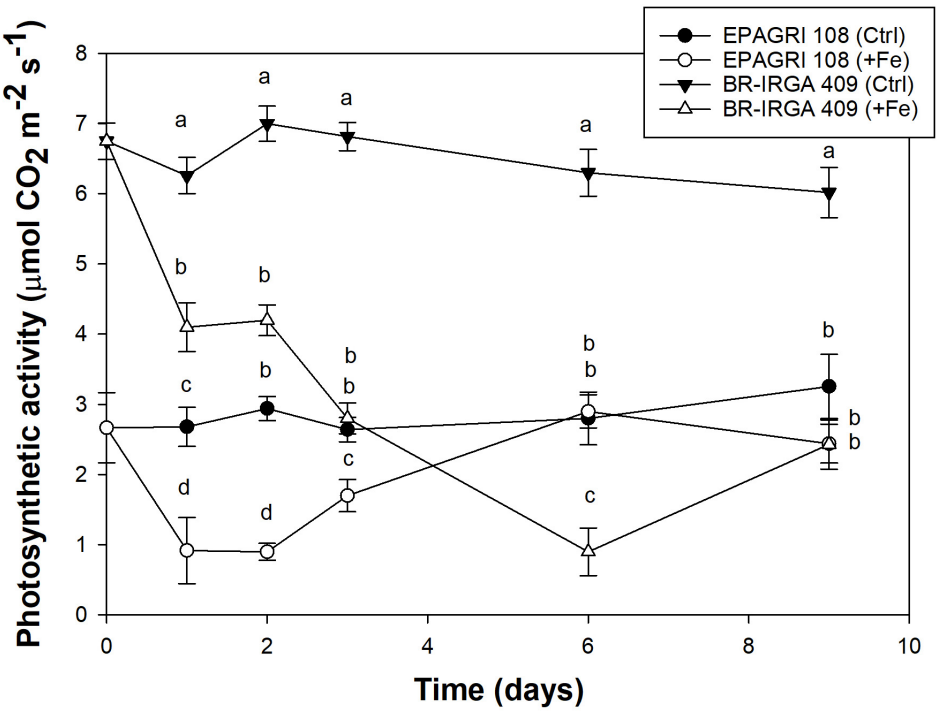

FIGURE 2 | Net CO_2 assimilation rate from cultivars BR-IRGA 409 (circles) and EPAGRI 108 (triangles) rice plants, exposed to control (closed symbols) or excess (open symbols) iron treatments. Gas exchange measurements were performed after 1, 2, 3, 6,and 9 days of exposure to treatments, using the youngest fully expanded leaf from each plant. Each value represents the mean of six replicates ± SE.

(Wu et al., 2017). In the present work, fully expanded leaves from plants of the susceptible cultivar exposed to excess Fe showed higher thiobarbituric acid-reacting substances (TBARS; **Figure 4A**), carbonyl concentration (**Figure 4B**) and H_2O_2 levels (**Figure 4C**) than leaves from plants in control conditions, while no difference could be observed in leaves of the tolerant cultivar (**Figure 4**). These data clearly indicated that excess Fe caused oxidative stress only in the susceptible cultivar (BR-IRGA 409), increasing to oxidation of lipids, proteins and the H_2O_2 accumulation in the leaves, whereas no changes are observed in the tolerant cultivar.

Antioxidative enzyme activities were differentially regulated upon excess Fe in each cultivar. Compared to controls, catalase (CAT) activity was increased by Fe toxicity in both cultivars, whereas ascorbate peroxidase (APX) activity was increased to a higher extent in the susceptible one (**Figures 5A,B**). No difference in superoxide dismutase (SOD) activity was observed in plants from both cultivars submitted to excess Fe compared to controls (**Figure 5C**). Although we cannot rule out a shoot-based mechanism for EPAGRI 108 Fe tolerance (e.g., increased Fe compartmentalization in vacuoles), these data indicate that the tolerant cultivar has few changes in the antioxidant metabolism that could account for the tolerant phenotype. Thus, EPAGRI 108 seems to be at least to some extent tolerant to excessive Fe due to root-based mechanisms.

The Gene Expression Profiles of Plants Exposed to Excess Fe Are Highly Divergent

To evaluate the impact of high levels of Fe on root gene expression profiles of the two rice cultivars, we used the Rice Gene Chip genome array (Affymetrix). Plants from EPAGRI 108 and BR-IRGA 409 cultivars were treated with excess Fe for 3 days. We chose this particular time point based on the photosynthetic activity data, which clearly indicated a slow but consistent increase in the photosynthetic capacity of EPAGRI 108 plants in day three after an initial drop upon exposure to excess Fe on days one and two (**Figure 2**), indicating that this could be the time point when tolerance-related traits started to be expressed. Exposure to excess Fe distinctly affected gene expression in the two cultivars: there were 423 up-regulated and 92 down-regulated genes in the susceptible cultivar BR-IRGA 409, while 43 up-regulated and 310 down-regulated genes were found in the tolerant cultivar EPAGRI 108 (**Figure 6** and **Supplementary Tables S1–S4**). Strikingly, we found that there was no overlap between the responses in the two cultivars: 232 genes up-regulated in the susceptible cultivar were also down regulated in the tolerant one, while 29 down regulated in the susceptible were up regulated in the tolerant one. There were 191 and 15 exclusively up-regulated in the susceptible and tolerant cultivars, respectively; and 64 and 78 down regulated in the

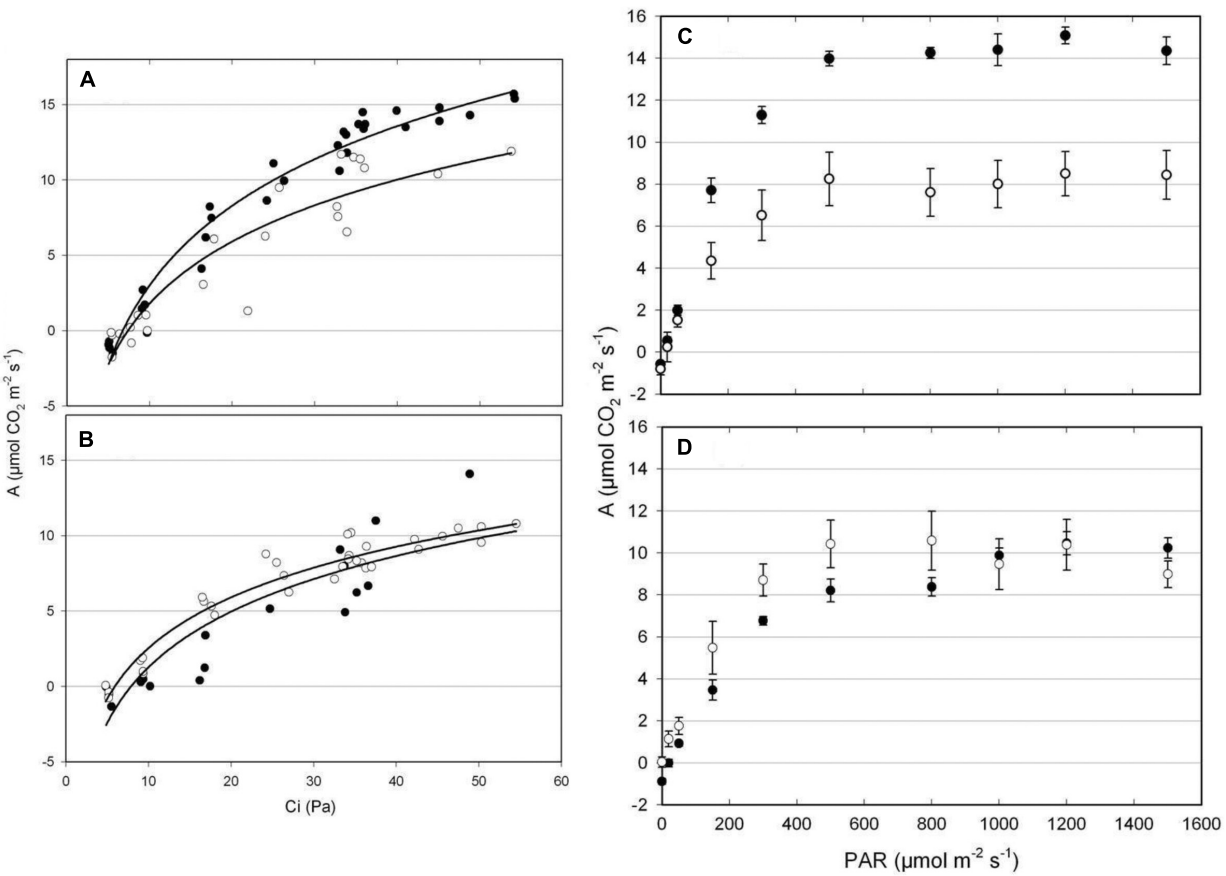

FIGURE 3 | CO_2 response **(A,B)** and light response **(C,D)** curves from BR-IRGA 409 **(A,C)** and EPAGRI 108 **(B,D)** rice plants after 6 days of exposure to control (closed circles) or excess (open circles) iron treatments. Photosynthetic response curves were obtained for the youngest fully expanded leaf from each plant. Each curve represents the measurements obtained from four independent plants. In C and D, means ± SE are shown. A, net CO_2 assimilation rate; Ci, estimated substomatal CO_2 partial pressure; PAR, photosynthetic active radiation.

TABLE 2 | Effects of 6-days exposure to control (Control) or excess (Fe+) iron treatments on photosynthetic parameters of rice plants from cultivars EPAGRI 108 and BR-IRGA 409.

	EPAGRI 108		BR-IRGA 409	
	Control	**Fe+**	**Control**	**Fe+**
Vc_{max} (µmol CO_2 $m^{-2}s^{-1}$)	17.75 ± 2.05c	18.65 ± 1.74c	30.78 ± 0.7a	23.25 ± 2.30b
J_{max} (µmol m^{-2} s^{-1})	58.3 ± 15.27b	65.6 ± 12.52b	111.55 ± 12.59a	65.05 ± 5.73b
ϕ_m (mol CO_2 mol^{-1} photons)	0.0369 ± 0.0059b	0.0394 ± 0.0044b	0.0524 ± 0.0043a	0.0252 ± 0.0056c

Each value represents the mean of four replicates. Distinct letters indicate significant difference between means from each parameter ($P \leq 0.05$). ϕ_m, apparent quantum yield; Vc_{max}, maximum carboxylation rate; J_{max}, electron transport rate.

susceptible and tolerant cultivars, respectively (**Figure 6**). These results were confirmed by RT-qPCR analyses of 13 selected genes (**Figures 7A–M**). The microarray data was confirmed in most cases, with the exception of some genes that are regulated in opposite directions in the two cultivars, which did not show the expected down-regulation. This might be due to the fact that some genes shown as down-regulated in the microarray already have low expression under control conditions. Altogether, these results indicate that these cultivars respond very differently to excess Fe, and confirm the quality of our dataset.

We conducted a Gene Ontology (GO) term enrichment analysis to have an overview of the cultivar-specific response to excess Fe (**Figure 8**). Data clearly showed that the two cultivars have very different enriched categories, and many of them are found in opposite regulation (i.e., up regulated in one cultivar, down regulated in the other). We found that "Ion Transport," "Metal Transport," and "Cation Transport" categories were enriched in the susceptible cultivar up regulated gene set, but not in the tolerant one. We also found many categories related to cell wall enriched in both cultivars. Interestingly, the

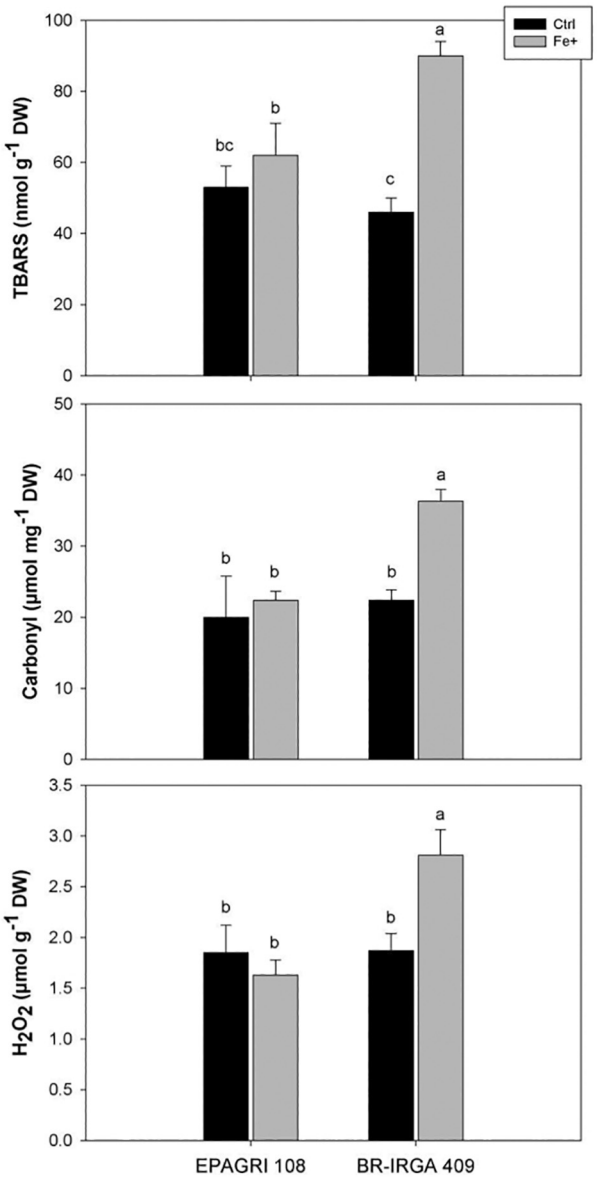

FIGURE 4 | Oxidative damage to lipids and proteins (TBARS and Carbonyl accumulation, respectively) and H_2O_2 accumulation in fully expanded leaves from EPAGRI 108 and BR-IRGA 409 rice plants after 9 days of exposure to control (Ctrl) or excess (Fe+) iron treatments. Each value represents the mean of six replicates ± SE. Distinct letters above the bars indicate significant difference between means (Duncan test, $P \leq 0.05$).

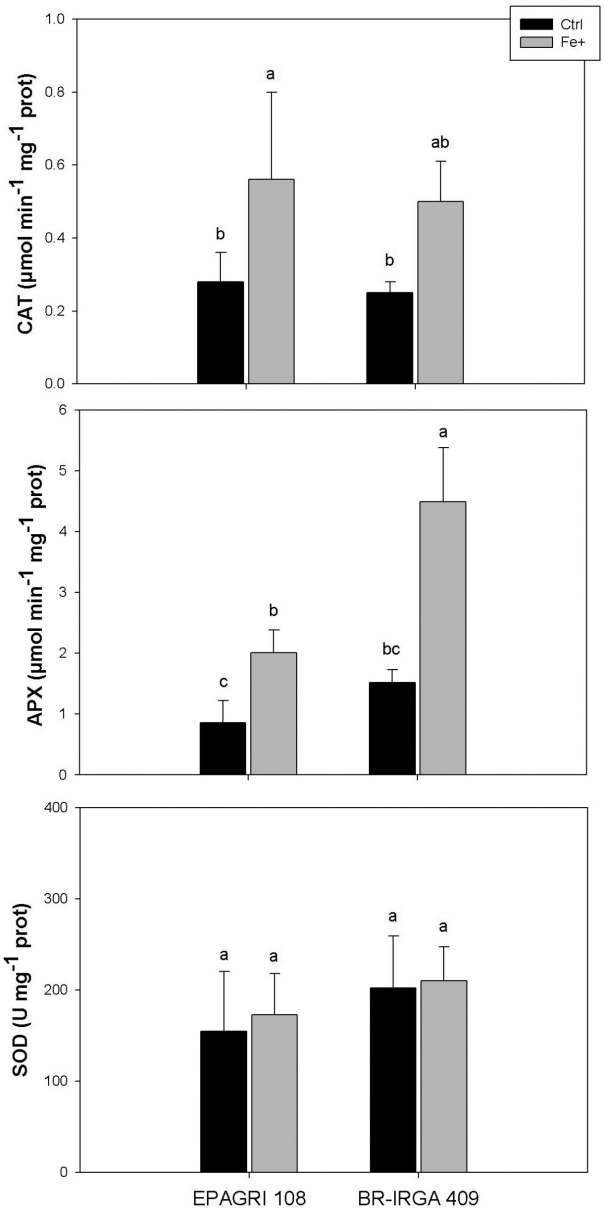

FIGURE 5 | Activity of antioxidant enzymes (CAT, APX, and SOD) in fully expanded leaves from EPAGRI 108 and BR-IRGA 409 rice plants after 9 days exposure to control (Ctrl) or excess (Fe+) iron treatments. Each value represents the mean of six replicates ± SE. Distinct letters above the bars indicate significant difference between means (Duncan test, $P \leq 0.05$).

tolerant cultivar has up regulated categories such as "Cell Wall," "Apoplast," "Extracellular Region," which were all down regulated in the susceptible one. Moreover, the tolerant cultivar did not have categories associated with ion or metal transport up or down regulated (**Figure 8**).

In order to have a more in-depth, gene-by-gene view of the different responses of each cultivar, we analyzed the 15 top regulated genes up- and down-regulated (**Table 3**). We found among the top up-regulated genes in BR-IRGA 409 a vacuolar Fe transporter, OsVIT2, that is responsive to excess Fe (Zhang et al., 2012); an uncharacterized VIT-Like (VTL) transporter (69-fold), similar to the VTL proteins known to mediate Fe transport into vacuoles in Arabidopsis (Gollhofer et al., 2014); OsASR3 (abscisic stress ripening protein; 25-fold), which was already been shown to be responsive to drought stress (Joo et al., 2013), and aluminum toxicity (Arenhart et al., 2013); and one abscisic acid responsive protein (18-fold). Moreover, the well-known Fe-excess responsive Ferritin genes OsFER1

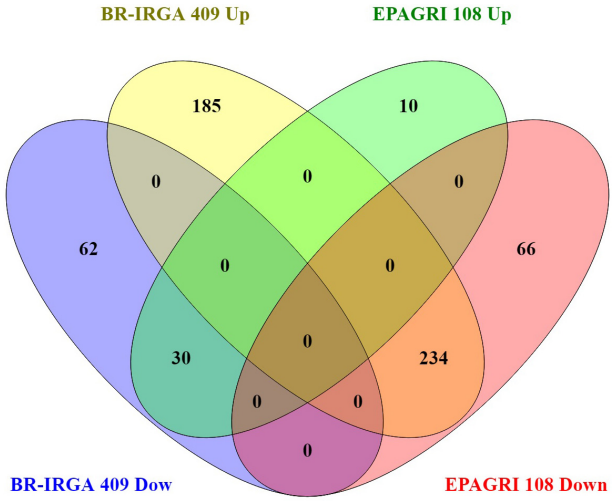

FIGURE 6 | Venn diagram showing overlap between BR-IRGA 409 up-regulated genes, BR-IRGA 409 down-regulated genes, EPAGRI 108 up-regulated genes, and EPAGRI 108 down-regulated genes.

and OsFER2 (Stein et al., 2009b; Ricachenevsky et al., 2010) were also up-regulated in BR-IRGA 409 (3.8- and 4.3 fold, respectively; **Supplementary Table S1**), indicating that these plants are responding as expected to high Fe concentrations.

Conversely, we found several genes related to Fe deficiency responses down-regulated in the susceptible cultivar when exposed to excess Fe (**Table 3** and **Supplementary Table S2**). Among the top 15 down-regulated genes in BR-IRGA 409, eight genes are well-described as being up-regulated under Fe deficiency (Zheng et al., 2009; Grillet et al., 2018), including the Fe(III)-Deoxymugineic acid (DMA) transporter OsYSL15 (-109-fold) and the Fe(II)-Nicotianamine (NA) transporter OsYSL2 (-12-fold); the Fe^{2+} transporters OsIRT1 (-38-fold), and OsNRAMP1 (-13-fold); the DMA biosynthesis-related genes OsNAS1 (-102-fold), OsNAS2 (-63-fold), and OsNAAT1 (-27-fold); and the regulatory peptide OsIMA1 (IRON MAN 1; Grillet et al., 2018). Other genes that are commonly associated with the Fe deficiency regulon were also down regulated, but not among the top 15 genes, such as OsZIFL4/TOM1 (-6.2-fold; Nozoye et al., 2011; Ricachenevsky et al., 2011), OsYSL16 (-3.6-fold; Kakei et al., 2012), and OsMIR (-3.2-fold; Ishimaru et al., 2009). Thus, these results show that BR-IRGA 409 plants are down-regulating Fe acquisition-related genes.

In contrast, the tolerant cultivar EPAGRI 108 showed three dirigent (DIR)-like proteins among the top 15 up-regulated genes (7-, 25-, and 33- fold; **Table 3** and **Supplementary Table S3**), which are related to lignin and lignin biosynthesis (Paniagua et al., 2017); two cell-wall modifying enzymes (Xyloglucan endotransglucosylase/hydrolase protein, 5/2-fold; a beta-glucosidase, 4.7-fold); and three peroxidases (8.4-, 5.7-, and 4.5-fold), which were already linked to metal stress (Kidwai et al., 2019). Interestingly, we found OsIRT1 up-regulated in this cultivar (12-fold), which is the opposite regulation found in the susceptible cultivar BR-IRGA 409. However, the absolute expression levels were extremely low, as shown in RT-qPCR data (**Figure 7**), and might not be physiologically relevant.

Among the top 15 genes down-regulated in EPAGRI 108 cultivar, the three most strongly down-regulated genes are also among the top 15 up-regulated genes in BR-IRGA 409, again demonstrating a clear opposite transcriptional regulation in these two cultivars upon excess Fe. Several Cytochrome P450 genes were also down-regulated (**Table 3**).

Roots of the Tolerant Cultivar Show Increased Lignin Deposition Upon Excess Fe Treatment Compared to the Susceptible One

Based on the microarray data, we hypothesized that the tolerant cultivar might show tolerance to Fe toxicity because of cell wall modifications. Since DIR proteins are involved in lignin biosynthesis, we analyzed lignin deposition in roots of both cultivars under control and excess Fe conditions. We found almost no change in lignin deposition pattern in the susceptible cultivar BR-IRGA 409 when comparing root sections of plants under control (**Figure 9A**) and excess Fe (**Figure 9B**) treatments. However, root sections of plants from the tolerant cultivar EPAGRI 108 cultivated under control (**Figure 9C**) and excess Fe (**Figure 9D**) presented markedly distinct lignin localization.

Lignin deposition in roots of the tolerant cultivar increased both in the outer layers of the cortex (exodermis and sclerenchyma ring, **Figure 9E**), in u-shaped secondary cell wall deposits of the tertiary endodermis around the vascular cylinder, in the primary xylem parenchyma cells (intense red staining), and in the pith parenchyma cells (**Figure 9F**). These results indicate that altered lignin deposition might be involved in the tolerance mechanism found in EPAGRI 108.

Lignin Concentrations in Roots of Susceptible and Tolerant Genotypes

Based on the clear change in lignin deposition, we decided to analyze the lignin concentration in other rice cultivars that might contrast in their Fe tolerance. In order to access Fe tolerance/susceptibility, we used maximum photochemical efficiency (F_V/F_M) values. Our susceptible and tolerant reference cultivars showed markedly different responses to excess Fe: BR-IRGA 409 showed a clear decrease in F_V/F_M value upon excess Fe exposure, whereas EPAGRI 108 showed no difference compared to control plants (**Figure 10A**). Lignin quantification showed that the susceptible cultivar has a decreased in lignin concentration, while the tolerant one showed a slight increase (**Figure 10B**). A set of eight genotypes were also evaluated, and cultivars that showed decreased F_V/F_M values when treated with excessive Fe were considered susceptible, whereas those showing no change (or slight increase in one case) were considered tolerant (**Figure 10A**). Clearly, tolerant cultivars showed increased lignin concentration in roots when plants were treated with

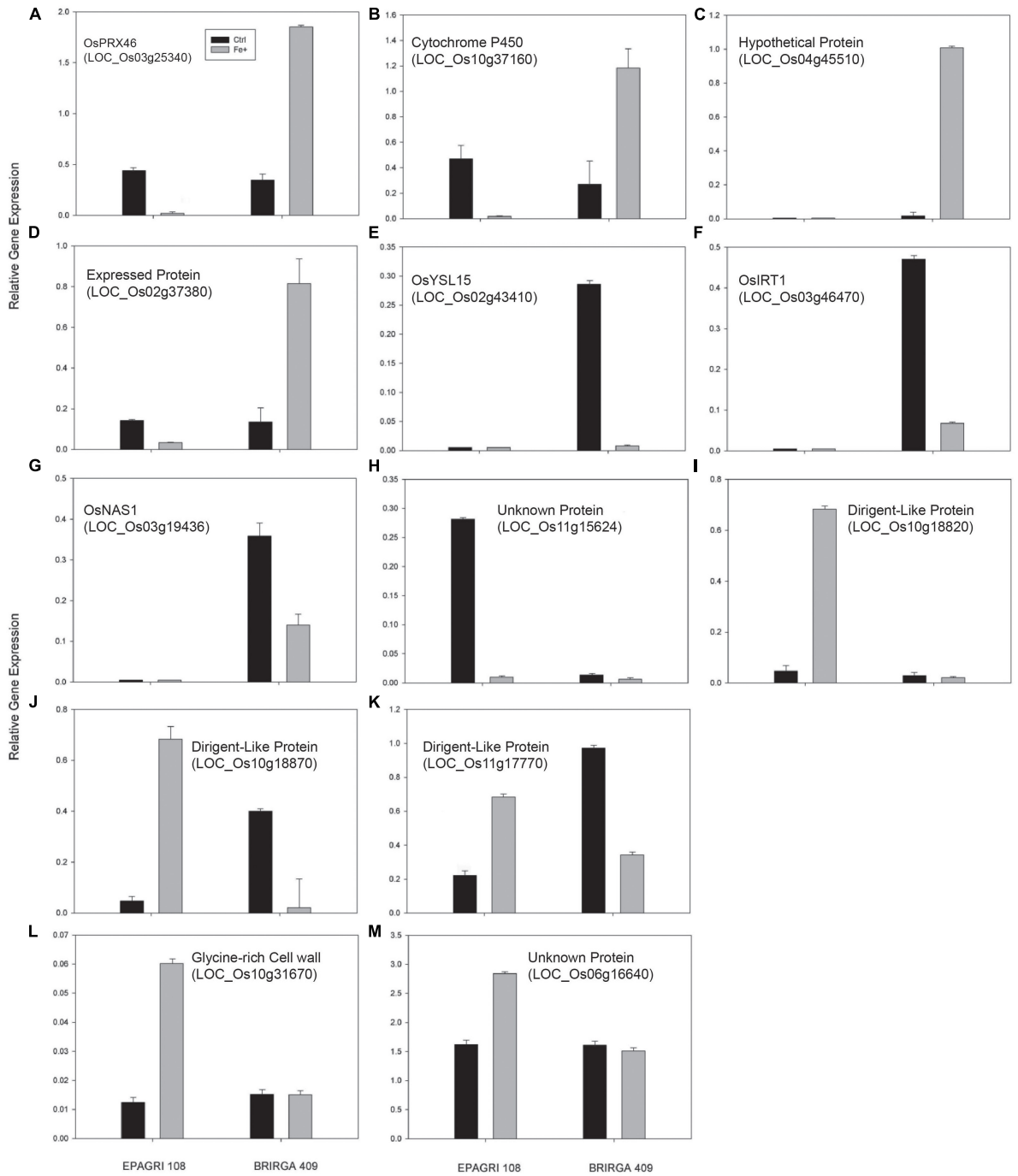

FIGURE 7 | Validation of the microarray analysis by real-time PCR. Relative expression levels by RT-qPCR of selected genes were evaluated in roots of rice plants exposed for 3 days to control or excess iron treatments. **(A)** OsPRX46; **(B)** Cytochrome P450; **(C)** Hypothetical protein; **(D)** Expressed protein; **(E)** OsYSL15; **(F)** OsIRT1; **(G)** OsNAS1; **(H)** Unknown protein; **(I)** Dirigent-Like Protein; **(J)** Dirigent-Like Protein; **(K)** Dirigent-Like Protein; **(L)** GLycine-rich Cell wall protein; **(M)** Unknown protein. All Locus ID numbers are shown.Primers corresponding to all tested genes are listed in **Supplementary Table S5**. Values represent the mean ± SE of three biological replicates (n = 3).

excess Fe (**Figure 10B**). Conversely, susceptible cultivars showed decreased lignin (**Figure 10B**). Data from all ten cultivars were plotted comparing the % of variation in F_V/F_M values and lignin concentration when exposed to excess Fe compared to the same cultivar under control conditions. Tolerant and susceptible genotypes grouped separately (**Figure 10C**), indicating that changes in total lignin concentrations are involved in tolerance to excess Fe.

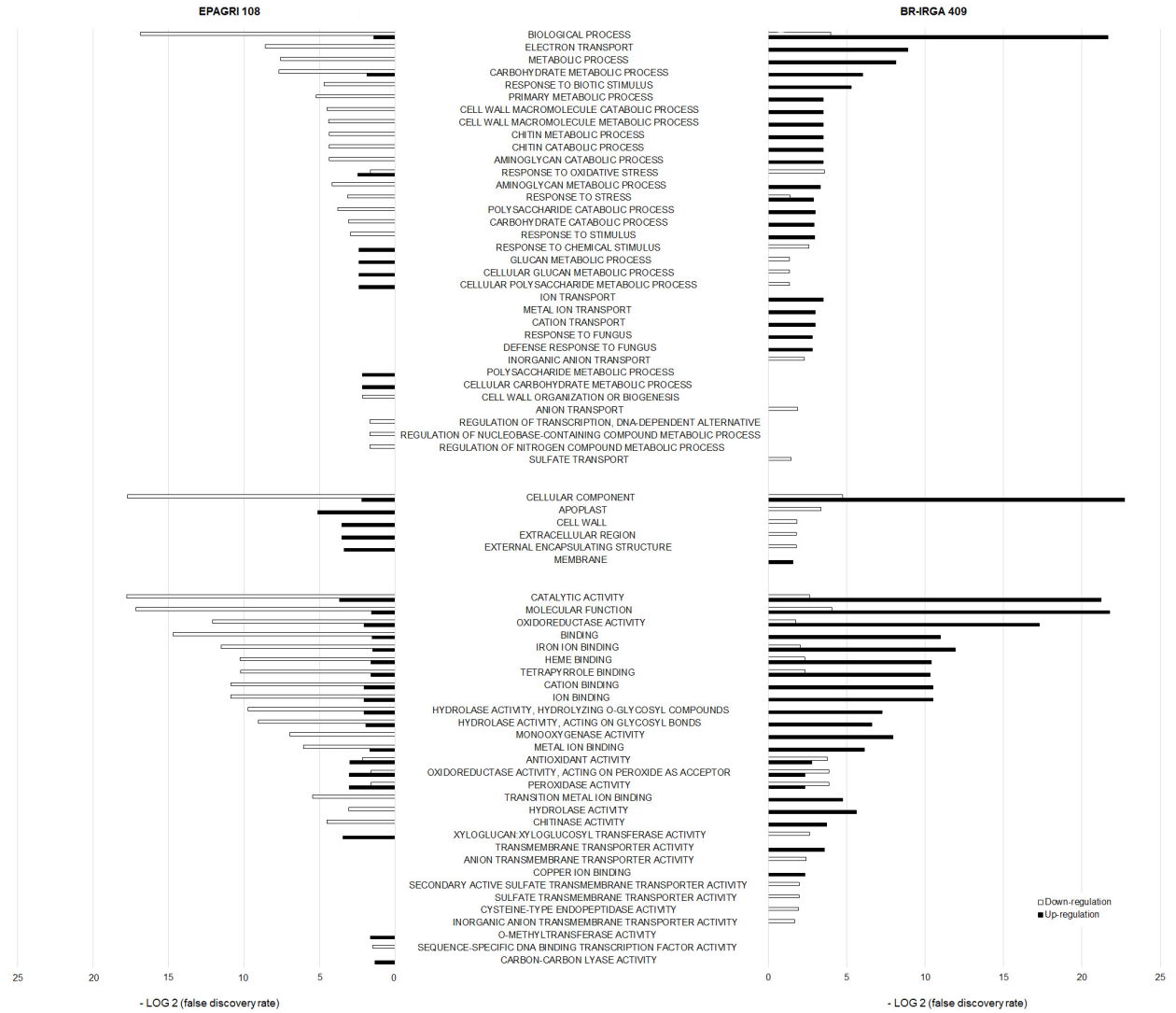

FIGURE 8 | Comparison of Gene Ontology terms enrichment between the two cultivars up- and down regulated genes. Term enrichment is shown as a function of the False Discovery Rate observed. Terms enriched in up- or down-regulated gene sets of either BR-IRGA 409 or EPAGRI 108 are highlighted.

DISCUSSION

Contrasting Physiological Impacts of Excess Fe on the Two Rice Cultivars

Excess Fe led to decreased biomass accumulation (in shoots and roots), loss of chlorophyll and decreased photosynthetic activity in the susceptible BR-IRGA 409 cultivar (**Figures 1–3**). The tolerant cultivar, however, showed no change in biomass or chlorophyll, and slight decrease in photosynthetic parameters, which were mostly recovered during the course of the 9-day excess Fe treatment (**Figures 2**, **3**). Previous work with the same rice cultivars showed that exposure to excess Fe did not indirectly induce deficiency of other nutrients, indicating a direct effect of excess Fe, a result that was later confirmed by field experiments (Silveira et al., 2007; Stein et al., 2009a). The toxic effects were directly related to accumulation of higher levels of Fe in shoots and roots of BR-IRGA 409 plants. Consistently, Olaleye et al. (2001) reported that high concentrations of Fe resulted in decreased plant weight and grain yield, and the growth retardation observed was not attributed to deficiencies of other nutrients, but to physiological problems directly originating from excessive Fe accumulation. Thus, our data confirmed the tolerant and the susceptible traits of these cultivars, validating the experimental approach used in this work.

In this study, photosynthetic activity decreased in plants from both cultivars after the initial period of exposure to excess Fe. However, the tolerant cultivar (EPAGRI 108) was able to fully recover its photosynthetic capacity after 6 days, a reasonable lag period for the induction of its tolerance mechanisms. For this reason, our transcriptomic analyses were performed at 3 days of

TABLE 3 | Top 15 up- and down regulated genes in each cultivar.

Locus TIGR	BR-IRGA 409	EPAGRI 108	Gene description
Up-regulated in BR-IRGA 409			
LOC_Os04g45510	89.22443	−12.244819	hypothetical protein
LOC_Os04g45520	69.78652	−6.165692	VIT-Like Protein
LOC_Os02g37380	54.848434	−37.811863	Expressed protein
LOC_Os10g37160	41.434082	−56.202168	Cytochrome P450 CY89A2
LOC_Os09g23300	37.27906	NDEG	OsVIT2
LOC_Os11g31540	27.535797	−38.461082	BRASSINOSTEROID INSENSITIVE 1-associated receptor kinase 1 precursor, putative, expressed
LOC_Os05g08830	27.033407	−15.521343	Hypothetical protein
LOC_Os03g16030	27.02408	NDEG	17.4 kDa class I heat shock protein 3
LOC_Os01g72900	25.64241	−10.956484	OsASR3 (abscisic stress ripening protein 3)
LOC_Os09g19820	22.898518	−6.1851354	Aminopeptidase-like protein
LOC_Os06g09870	20.326283	−9.836528	Glycine-rich cell wall structural protein 2
LOC_Os01g58960	19.996674	−5.3904	Cytochrome P450 94A1, putative, expressed
LOC_Os07g46920	19.222033	−11.117482	Sex determination protein tasselseed-2, putative, expressed
LOC_Os01g43750	19.13674	−5.59671	Cytochrome P450 72A1, putative, expressed
LOC_Os12g29400	18.903513	NDEG	ABA-responsive protein, putative, expressed
Down-regulated in BR-IRGA 409			
LOC_Os02g43410	−109.300575	NDEG	OsYSL15 (Fe3+-phytosiderophore transporter)
LOC_Os03g19436	−102.14942	NDEG	OsNAS1 (Nicotianamine synthase 1)
LOC_Os03g19420	−63.42101	NDEG	OsNAS2 (Nicotianamine synthase 2)
LOC_Os10g18870	−57.646217	25.752077	Dirigent-like protein
LOC_Os03g46470	−38.56981	12.099378	OsIRT1 (Fe2+ transporter)
LOC_Os01g45914	−30.128687	NDEG	IRON MAN 1
LOC_Os02g20360	−27.718102	NDEG	OsNAAT1 (Nicotianamine aminotransferase)
LOC_Os10g18820	−22.484005	33.883545	Dirigent-like protein
LOC_Os12g36840	−14.281752	NDEG	Pathogenesis-related protein 10
LOC_Os07g15460	−13.20834	NDEG	OsNRAMP1 (putative metal transporter)
LOC_Os11g15624	−12.335097	NDEG	Unknown protein
LOC_Os02g43370	−12.134548	NDEG	OsYSL2 (Fe3+-phytosiderophore transporter)
LOC_Os01g65110	−11.203648	NDEG	Proton-dependent oligopeptide transport (POT) family protein
LOC_Os11g05390	−10.996121	NDEG	Tetracycline transporter protein, putative, expressed
LOC_Os03g22010	−9.311682	5.7919073	OsPrx41 (peroxidase)
Up-regulated in EPAGRI 108			
LOC_Os10g18820	**−22.484005**	**33.883545**	**Dirigent-like protein**
LOC_Os10g18870	**−57.646217**	**25.752077**	**Dirigent-like protein**
LOC_Os06g16640	−3.6726174	13.423064	Carboxyl-terminal peptidase, putative, expressed
LOC_Os04g46810	−7.2157893	12.945946	Cortical cell-delineating protein precursor, putative, expressed
LOC_Os03g46470	**−38.56981**	**12.099378**	**OsIRT1 (Fe2+ transporter)**
LOC_Os10g18760	−8.9875965	11.241121	Jasmonate-induced protein, putative, expressed
LOC_Os02g37260	−3.2897632	10.861882	Expressed protein
LOC_Os01g73170	−6.2279987	8.349177	OsPrx20 (peroxidase)
LOC_Os03g09980	−8.079094	7.5308027	Sulfate transporter 1.2, putative, expressed
LOC_Os11g07770	−8.848223	7.3968105	Dirigent-like protein
LOC_Os05g28770	−7.0391817	6.0021596	Expressed protein
LOC_Os03g22010	**−9.311682**	**5.7919073**	**Peroxidase 2 precursor, putative, expressed**
LOC_Os06g48180	−7.122961	5.211064	Xyloglucan endotransglucosylase/hydrolase protein (OsXTH10, OsXTH11, OsXTH12, or OsXTH18)
LOC_Os09g31430	NDEG	4.727019	Non-cyanogenic beta-glucosidase precursor, putative, expressed
LOC_Os06g20150	−4.356904	4.563937	OsPrx78 (peroxidase)

(Continued)

TABLE 3 | Continued

Locus TIGR	BR-IRGA 409	EPAGRI 108	Gene description
Down-regulated in EPAGRI 108			
LOC_Os10g37160	**41.434082**	**−56.202168**	**Cytochrome P450 CY89A2**
LOC_Os11g31540	**27.535797**	**−38.461082**	**Brassinosteroid insensitive 1-associated receptor kinase 1**
LOC_Os02g37380	**54.848434**	**−37.811863**	**Expressed protein**
LOC_Os11g46000	5.0010676	−30.422861	Von willebrand factor type A domain containing protein
LOC_Os02g36110	12.113743	−21.564749	Cytochrome P450 76C2, putative, expressed
LOC_Os04g10160	8.430319	−18.699465	Cytochrome P450 CYP99A1
LOC_Os04g09920	7.923875	−17.830105	Cytochrome P450 CYP99A1, putative, expressed
LOC_Os01g13610	7.5534124	−17.769463	Isoflavone reductase homolog IRL, putative, expressed
LOC_Os06g35700	6.695192	−17.551943	Reticuline oxidase precursor, putative, expressed
LOC_Os07g44440	13.513653	−16.21314	Peroxiredoxin, putative, expressed
LOC_Os05g08830	**27.033407**	**−15.521343**	**Hypothetical protein**
LOC_Os04g49210	11.567054	−14.981616	Naringenin,2-oxoglutarate 3-dioxygenase, putative, expressed
LOC_Os07g46846	3.5318127	−14.938069	Sex determination protein tasselseed-2, putative, expressed
LOC_Os07g23410	5.9368644	−14.20258	Omega-6 fatty acid desaturase, endoplasmic reticulum isozyme 2, putative, expressed
LOC_Os12g36830	6.6913185	−13.807509	Pathogenesis-related protein 10, putative, expressed

Genes are shown in four blocks (BR-IRGA 409 up-regulated, BR-IRGA 409 down-regulated, EPAGRI 108 up-regulated, EPAGRI 108 down-regulated). Genes that are differentially expressed in both cultivars among the top 15 regulated genes appear in bold. Fold change in both cultivars is also shown (NDEG means Not Differentially Expressed in that cultivar).

exposure to excess Fe. Using A/Ci and light response curves, we could identify the impact of excess Fe on carbon fixation, affecting the maximum carboxylation rate (Vc_{max}), electron transport rate (J_{max}), and maximum apparent quantum yield (ϕ_m) in the susceptible cultivar, but not in the tolerant one (**Table 2**). The reduction in Vc_{max} may result from the reduced rate of electron transport, limiting the amount of available energy for Calvin cycle enzymes. The reduction in chlorophyll concentration associated to lower electron transport rates may indicate a direct effect of excess Fe on the photosynthetic electron transport chain components (either LHCII or $Cytb_6/f$). The toxic effects of Fe in photosynthesis were also observed in *Nicotiana plumbaginifolia* cuttings accompanied by photoinhibition, increased reduction of PSII and higher thylakoid energization (Kampfenkel et al., 1995). Excessive amounts of Fe in thylakoid membranes in the form of cytochrome b_6/f complex showed correlation with photodamage to PSII, derived from excessive production of singlet oxygen in pea plants (Suh et al., 2002).

Data from independent studies showed that BR-IRGA 409 increases photorespiration under excess Fe (Pereira et al., 2013), and together with electron transport rate and carboxylation efficiency were proposed as good parameters to access rice Fe tolerance (Müller et al., 2017). Our tolerant cultivar showed no change in V_{cmax}, J_{max} (**Table 2**), and Fv/Fm (**Figure 9**), in contrast with the susceptible one, which corroborate the use of photosynthetic parameters for easy, non-destructive access to Fe tolerance in rice genotypes (Pereira et al., 2013; Müller et al., 2017).

Mechanisms of Fe Tolerance in the Two Rice Cultivars

Tolerance to Fe toxicity in rice can have three general possible sources of tolerance: Fe exclusion (i.e., avoiding Fe entering plant tissues); Fe uptake and further compartmentalization (i.e., in Fe storage proteins such as Ferritins, or in vacuoles); and Fe uptake associated with increased tolerance to the consequent reactive oxygen species using anti-oxidants (Wu et al., 2014). Of course, one given genotype can combine two or more tolerance mechanisms. Here both cultivars showed comparable concentrations of Fe in shoots and roots under control conditions, whereas exposure to excess Fe induced Fe accumulation in roots and shoots of both cultivars (**Table 1**). The susceptible cultivar, however, showed higher levels of Fe compared to the tolerant one on both organs, suggesting that the tolerant genotype is able to exclude Fe. Exclusion by roots can be achieved by increased oxidation capacity, resulting in higher Fe^{2+} oxidation to Fe^{3+}, Fe precipitation and Fe plaque formation, limiting the absorption of Fe by the root system (Wu et al., 2014). After 9 days of excess Fe treatment, both cultivars showed increased Fe concentrations in the Fe plaque (**Table 1**). However, the susceptible cultivar (BR-IRGA 409) showed significantly higher levels of Fe in the Fe plaque than the tolerant cultivar (**Table 1**). These data suggest that the tolerant cultivar does not have increased oxidation power in roots, which would lead to higher levels of Fe in the apoplast. In fact, EPAGRI 108 decreased levels of Fe in the Fe plaque might be due to increased lignification, which would decrease root oxygen loss and therefore reduce root oxidation power. Thus, these data indicate that EPAGRI 108 tolerance is based at least partially on a distinct mechanism.

The increased Fe concentration in shoots of plants from the tolerant cultivar treated with excess Fe accumulation was significant, but with little effect on the plant phenotype compared to the susceptible one (**Figure 1**). Thus, it is likely that EPAGRI 108 also has Fe shoot – based tolerance as well. This is consistent with the observation that the susceptible cultivar has increased markers for ROS stress, while the tolerant one showed

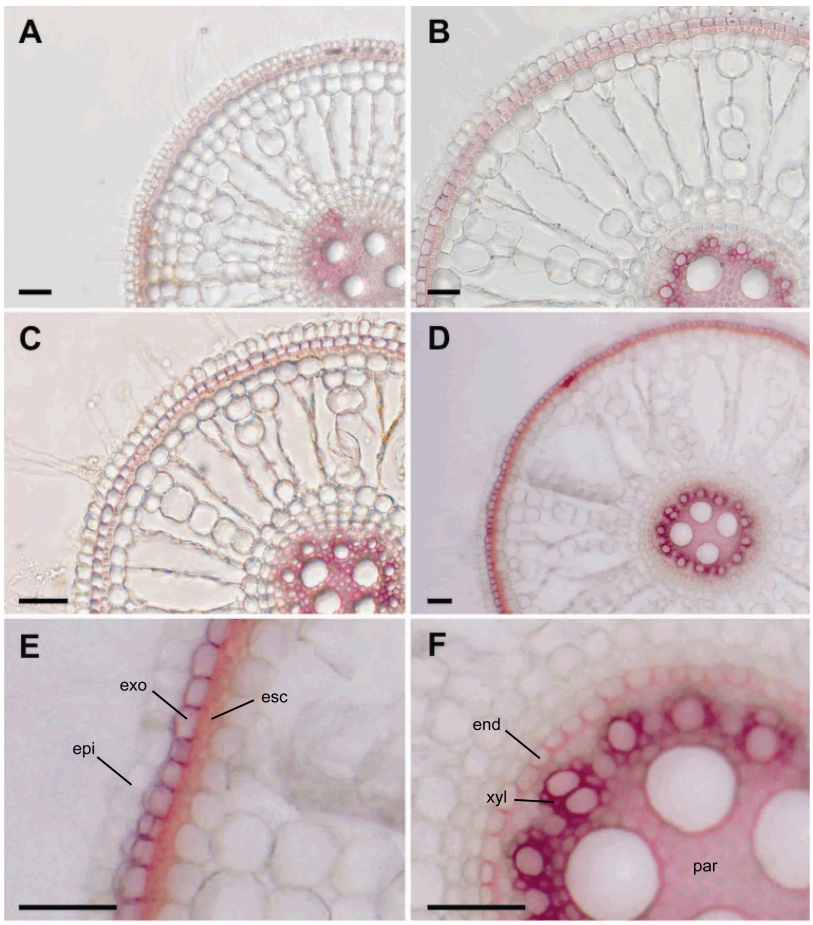

FIGURE 9 | Root lignification under iron excess. Cross-sections of root sectors from BR-IRGA 409 **(A,B)** and EPAGRI 108 **(C,D)** plants maintained for 15 days under control **(A,C)** or iron excess **(B,D)** treatments, showing the extent of lignification (cell walls stained in red) indicated by the Wiesner reaction (acidified phloroglucinol solution). Magnifications from figure **D** show more intense cell wall lignification of exodermis (exo) and esclerenchyma (esc), in the outer layers of the cortex **(E)**, and lignin deposition in endodermis (end), xylem parenchyma (xyl), and pith parenchyma (par) cell walls **(F)**. Scale bars = 100 μm.

no difference compared to controls (**Figure 4**). Enzymatic detoxification of ROS could be involved in Fe toxicity responses (Fang et al., 2001; Majerus et al., 2007). APX activity, which could be part of a ROS tolerance, shoot-based mechanism as previously proposed (Wu et al., 2017), is induced only in the susceptible cultivar (**Figure 5B**), but not in the tolerant. Catalase activity was shown to be slightly higher in the tolerant cultivar (**Figure 5A**). Previous analyses of Fe tolerant and susceptible rice cultivars associated lower dehydroascorbate reductase, higher ascorbate oxidase activity and high rates of ascorbate reduction to tolerance (Wu et al., 2017), which were not tested in our experiments. Thus, EPAGRI 108 should be further investigated to identify the nature of its shoot-based tolerance mechanism.

Fe Homeostasis-Related Genes Are Strongly Regulated in the Susceptible Cultivar

Our data clearly shows that the susceptible BR-IRGA 409 cultivar is responding as expected to Fe toxicity (**Table 3** and **Supplementary Tables S1–S5**). Genes such as OsVIT2, OsFER1, and OsFER2 are up-regulated indicating that plants are compartmentalizing excessive Fe into vacuoles and ferritin holoproteins (Stein et al., 2009b; Zhang et al., 2012). Another interesting finding is that a putative, uncharacterized VTL transporter was one of the highly expressed genes under excess Fe. VTL were shown to transport Fe into the vacuoles in Arabidopsis (Gollhofer et al., 2014), indicating that the rice homolog might be important for Fe detoxification in vacuoles. Moreover, we found two ASR genes, OsASR1 and OsASR3, up-regulated in this cultivar. Both genes are up regulated by aluminum (Al) stress, and OsASR1 is involved in regulating the Al stress response in rice, acting as a transcription factor (Arenhart et al., 2013). Fe and Al stresses are common in acidic soils, and thus ASR proteins might be involved to some extent in Fe toxicity gene regulation as well. Alternatively, Fe and Al stress responses in roots might be convergent, since both result in changes in root length due to decreased elongation. This, however, remains to be tested.

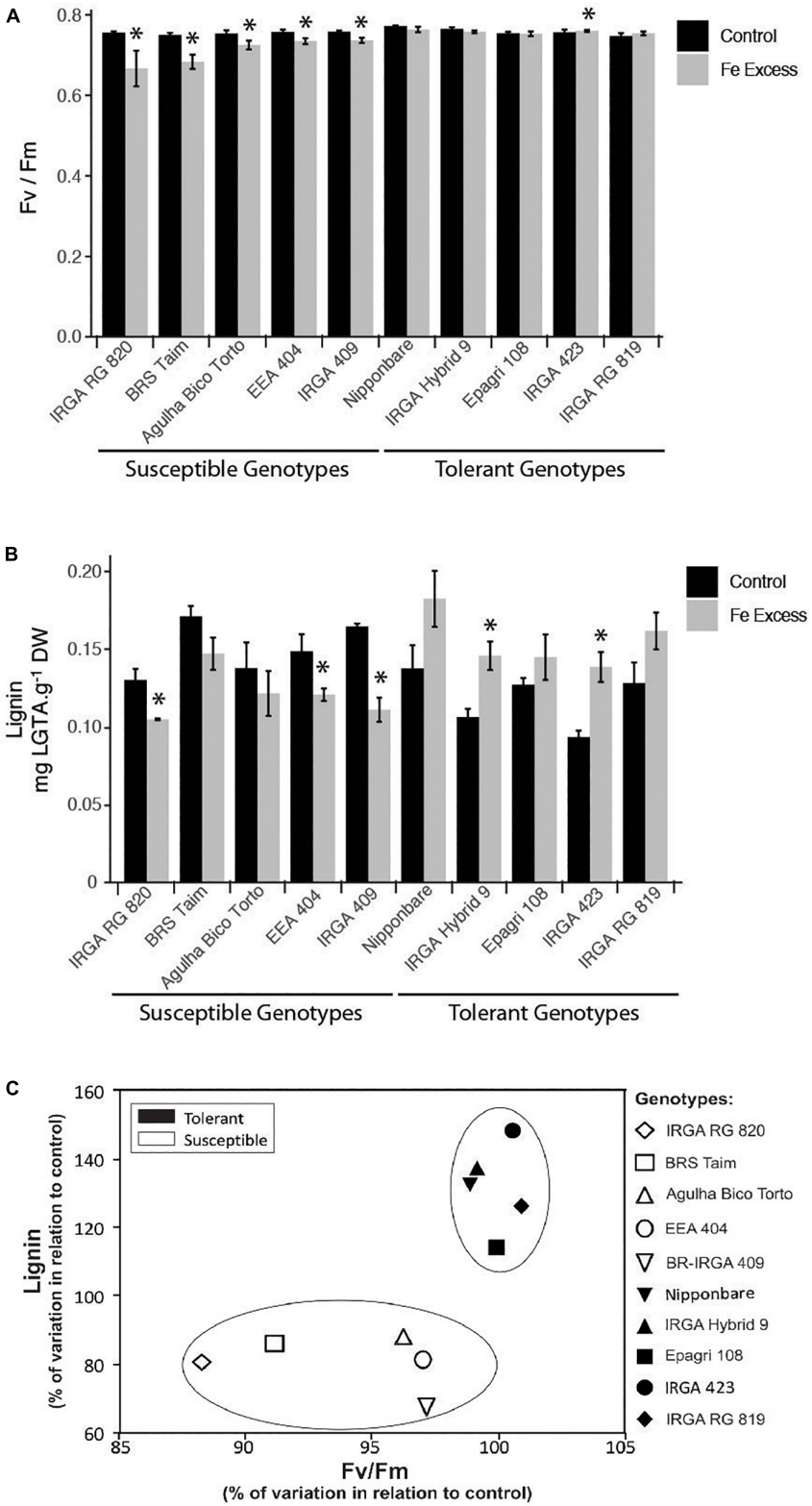

FIGURE 10 | Effects of iron excess in plants from ten rice genotypes exposed to 500 mg L^{-1} $FeSO_4$ (Fe+) or 6.5 mg L^{-1} $FeSO_4$ (Ctrl) for 15 days: maximum photochemical efficiency (F_V/F_M) from leaves **(A)**; lignin concentration from roots **(B)**; and genotype distribution plot **(C)**, based on % variations observed in iron excess treated plants in relation to control plants (% variation in leaf F_V/F_M values against % variation in root lignin concentrations). In **A** and **B**, the asterisks indicate means that are significantly different from control by the Student's *t*-test ($P \leq 0.05$). Experiments were performed using $n = 8$ to 9 plants per genotype.

As already described in other studies, the Fe deficiency responsive genes were down regulated under excess Fe, but exclusively in the susceptible cultivar. Fe uptake transporters OsYSL15, OsIRT1, and OsNRAMP1; nicotianamine and phytosiderophore synthesis enzymes (NAS and NAAT); and phytosiderophore secretion transporter OsZIFL4/TOM1 were among them (**Table 3** and **Supplementary Table S2**). These indicate that plants from the susceptible cultivar are attempting to avoid Fe uptake under excess Fe, and is in agreement with previous observations (Quinet et al., 2012; Bashir et al., 2014). An Fe and Cu transporter, OsYSL16, was also found as down-regulated (**Supplementary Table S2**). OsYSL16 was shown to be important for Fe distribution in rice plants, and its activation-tagging (which results in higher steady-state expression levels) results in increased Fe efficiency (Kakei et al., 2012; Lee et al., 2012). Thus, OsYSL16 decreased expression under excess Fe might be also contributing to avoid Fe accumulation.

Interestingly, we also found the recently described OsIMA1 (LOC_Os01g45914; IRON MAN 1), a small peptide that was clearly involved in regulating the Fe deficiency response in Arabidopsis (Grillet et al., 2018). Microarray data already demonstrated that OsIMA1 was up regulated by Fe deficiency (Zheng et al., 2009) and heterologous expression in Arabidopsis showed it is able to regulate Fe deficiency responses (Grillet et al., 2018). However, OsIMA1 physiological role is not established yet. Our data shows that it may be also important to regulate rice responses to Fe toxicity, likely by down regulating the Fe uptake machinery. In agreement with that, OsMIR, an orphan rice small protein that is also involved in Fe deficiency responses (Ishimaru et al., 2009), was also down regulated in BR-IRGA 409, again indicating the importance of such small regulatory peptides in regulating Fe concentration in plants.

However, it is puzzling that we haven't found any commonly regulated genes in the tolerant cultivar compared to the susceptible one. We considered that 3 days of Fe excess treatment would be a good time point to identify contrasting differences in the two cultivars, based on physiological data. However, we should consider that sampling at later time points, when Fe would build up to higher levels in the tolerant cultivar, could show us similar genes regulated in EPAGRI 108 as observed in the susceptible BR-IRGA 409 after 3 days treatment with Fe excess. A time course transcriptional experiment could reveal the dynamics of this regulation, and how tolerant and susceptible cultivars may differ in the timing at which some genes are up and down regulated. Thus, our non-overlapping expression patterns would likely not be maintained throughout Fe excess responses for more than 3 days.

Root Lignification Might Be Involved in Tolerance to Excess Fe

As inferred from the distinct Fe accumulation and distribution in the plant body between the two studied cultivars, the capacity to accumulate lower levels of Fe greatly contributes to the tolerance character of EPAGRI 108 plants. Based on the gene expression pattern and on the root anatomical analysis described in this work, root cell wall lignification and remodeling could play an important role in providing such a capacity to EPAGRI 108 plants. The tolerant cultivar showed only 42 genes up-regulated by excess Fe after 3 days of exposure. Among these, we found four peroxidases, one laccase and three dirigent proteins, most of them among the top up-regulated genes (**Table 3** and **Supplementary Table S3**) indicating that the dirigent-guided lignin deposition might be up-regulated in the roots of the tolerant cultivar under excess Fe. The synthesis of coniferyl alcohols by peroxidases and laccases is known to lack region and stereoselectivity (Paniagua et al., 2017). Dirigent proteins stipulate, at regional and stereochemical levels, the outcome from the coupling of two molecules of *E*-coniferyl alcohol to produce the lignan (+)-pinoresinol (Davin et al., 1997). One characterized dirigent protein was shown to require the provision of one-electron oxidation through an auxiliary source, such as laccases, peroxidases and monooxygenases for its activity, and to be expressed mainly in lignifying tissues (Burlat et al., 2001). Two enzymes involved in lignin biosynthesis, Caffeoyl-CoA *O*-methyltransferase and *O*-methyltransferase ZRP4 (Raes et al., 2003; Boerjan et al., 2003), were also up-regulated in EPAGRI 108 (**Supplementary Table S3**). These results indicated that lignin deposition might be involved in Fe tolerance observed in EPAGRI 108.

Our data further corroborated this hypothesis showing that other Fe tolerant cultivars induce lignin deposition in roots, whereas Fe susceptible cultivars decrease total lignin (**Figure 10**). A recent work showed that heterologous expression in Arabidopsis of OsPRX38, a rice Class III peroxidase, leads to higher tolerance to arsenic (Kidwai et al., 2019). Interestingly, expression of OsPRX38 caused increased expression lignin biosynthesis genes such as Caffeoyl-CoA *O*-methyltransferase, which results in root lignification, providing an apoplastic barrier for arsenic diffusion and therefore less arsenic uptake by Arabidopsis plants (Kidwai et al., 2019). Similarly, expression of Arabidopsis AtHMA4 (a membrane-localized Zn/Cd efflux transporter) in tobacco resulted in decreased Cd concentration in roots and shoots. Lignin biosynthesis genes were up-regulated when these plants were exposed to Cd, with consequent increased lignification, which blocked apoplastic diffusion of Cd (Siemianowski et al., 2014). Cu excess or Mn excess were also shown to induce lignification in Arabidopsis and rice, respectively (Lequeux et al., 2010; Dziwornu et al., 2018). Our data shows for the first time that lignin biosynthesis is linked to excess Fe responses and to Fe tolerance.

Lignin deposition increased both in the exodermis and in the endodermis, possibly limiting Fe uptake into the root and Fe translocation to the shoot, respectively. The exodermis and the endodermis are the outer- and innermost cortical layers of a root, and serve as filtration sites for the passive movement of ions between the soil solution and the stele (Ma and Peterson, 2003). These are the root tissue layers where rice deposits Casparian strips, which act as apoplastic diffusional barriers (Cai et al., 2011). Interestingly, work in Arabidopsis showed that Casparian strips are entirely made of a lignin polymer without suberin, contrary to what was previously accepted (Naseer et al., 2012). The Casparian strip works as a barrier for nutrient diffusion

both into and out of the stele, which can have consequences for root to shoot translocation of minerals (Doblas et al., 2017; Ricachenevsky et al., 2018). The transcriptional control and further steps for its formation are being dissected in detail. Among these, a dirigent protein named ENHANCED SUBERIN 1 (ESB1)/AtDIR10 was shown as essential for Casparian strip integrity in Arabidopsis (Hosmani et al., 2013). However, rice orthologous proteins to the ones involved in Casparian strip synthesis and maintenance are not among the differentially expressed genes in our datasets. Therefore, lignin deposition in response to excess Fe in the tolerant cultivar is performed by a different set of genes, likely reinforcing the Casparian strip barrier or adding other layers of lignification in similar tissues to avoid Fe diffusion into the roots. Based on our data (**Figure 10**) this new mechanism might be common to other rice cultivars, indicating a new avenue for rice Fe tolerance breeding and engineering.

In EPAGRI 108 roots under iron excess, the additional lignification of cell walls of the xylem parenchyma cells, which surround the tracheal metaxylem elements, may represent an extra barrier against iron translocation. Parenchyma xylem cells are the final water transport route before the tracheal cell entrance, after passage through the epidermis and cortical layers (including exoderm and endoderm). Therefore, an increase in lignification in the parenchyma of the xylem can function as a final "line of defense" against Fe transport (another apoplastic barrier). In the roots of *Brachiaria decumbens*, all xylem cells (i.e., including xylem parenchyma cells) are thickened with an evident deposition of lignin on the wall because of the increased concentration of heavy metals (Gomes et al., 2011).

CONCLUSION

Our results described two rice cultivars, one tolerant and one susceptible, to excess Fe. We provide datasets for gene expression of two contrasting rice cultivars regarding Fe toxicity tolerance under early Fe excess stress. We suggest that tolerance in the EPAGRI 108 cultivar, and likely in other rice germplasm, could be linked to increased cell wall lignification in the root cortex layers (endodermis and exodermis), as well as in the central cylinder (primary xylem and pith parenchyma cell), which would be a new mechanism for rice tolerance to high Fe concentrations. The data provided here could be important for further studying the responses of rice cultivars to Fe excess, and uncovering a possible Fe tolerance mechanism linked to cell wall remodeling.

MATERIALS AND METHODS

Plant Material, Growth, and Treatments

Seeds from rice (*Oryza sativa* L. ssp. *indica*) genotypes used in this work were provided by the Rice Breeding Group from IRGA (Instituto Rio Grandense do Arroz, Brazil). BR-IRGA 409, IRGA RG 820, BRS Taim, Agulha Bico Torto, EEA 404, Nipponbare, IRGA Hybrid 9, EPAGRI 108, IRGA 423, and IRGA RG 819 are part of the germplasm bank of IRGA, and are commonly used for testing different traits in breeding programs of the Institute. The two genotypes used in most experiments are cultivated in southern Brazil and were previously characterized as tolerant (EPAGRI 108) and susceptible (BR-IRGA 409) to Fe toxicity (Silveira et al., 2007). Seeds were surface sterilized in 70% ethanol for 2 min, followed by 1.5% $NaClO_4$ for 1 min, and then washed with abundant distilled water and germinated on moistened filter paper in Petri dishes. The seedlings were kept in the dark during the first 48 h, transferred to 16 h/8 h day/light regime (65 μmol $m^{-2}s^{-1}$ of photosynthetic active radiation) at 28°C for 2 days and then transferred to pots with vermiculite, watered with nutrient solution consisted of 1.42 mM NH_4NO_3; 0.4 mM NaH_2PO_4; 0.5 mM K_2SO_4; 1.7 mM $CaCl_2.2\ H_2O$; 1.7 mM $MgSO_4.7H_2O$; 9.5 μM $MnCl_2.4\ H_2O$; 0.07 μM $(NH_4)_6Mo_7O_{24}.4H_2O$; 20 μM H_3BO_3; 0.16 μM $ZnSO_4.7H_2O$; 0.16 μM $CuSO_4.5H_2O$; 35.6 μM $FeCl_3.6H_2O$, and 0.07 mM citric acid (Yoshida et al., 1976). After 10 days, plants were transferred to hydroponic conditions, using the same nutrient solution, and after 10 more days plants were subjected to excess Fe (500 mg L^{-1} of iron) or control concentration (6.5 mg L^{-1}), both using $FeSO_4$ as the Fe source. To avoid possible effects of sulfur concentrations, Na_2SO_4 was added to the control solution to obtain equimolar sulfur concentration in both treatments. To maintain the concentration and keep Fe soluble, nutrient solutions were replaced every 72 h.

Dry Weight and Chlorophyll Determinations

After 9 days of treatment, plants were separated in shoots and roots, immediately frozen in liquid nitrogen and kept at –20°C until further analysis. Shoots and roots were dried at 60°C to constant weight for the determination of DW. Fully expanded leaves were ground in liquid nitrogen and chlorophyll extracted in acetone 85%. Total chlorophyll (chlorophyll *a*+ chlorophyll *b*) was quantified by measuring absorbance at 663 nm and 645 nm, and the concentrations calculated as in Stein et al. (2009a).

Gas Exchange Measurements

Gas exchange measurements were performed after 1, 2, 3, 6, and 9 days of exposure to the Fe treatments, using a portable photosynthesis system (LI-6400, LiCor Inc., Lincoln, NE, United States). All determinations of photosynthetic rate were performed using a reference CO_2 concentration of 400 μL L^{-1}, 1000 μmol m^{-2} s^{-1} photosynthetic photon flux (PPF) and leaf temperature of 22°C, using only the youngest fully expanded leaf. Light response curves were performed using a reference CO_2 concentration of 400 μL L^{-1}, leaf temperature of 22°C and a PPF range from 1500 to 0 μmol $m^{-2}s^{-1}$. CO_2 response curves were performed using 1000 μmol m^{-2} s^{-1} PPF, leaf temperature of 22°C, with reference CO_2 concentrations ranging from 800 to 50 μL L^{-1}. All photosynthetic response curves were performed using only the youngest fully expanded leaf, after 6 days of exposure of plants to treatments (control and excess Fe), and the photosynthetic parameters were

estimated according to the biochemical model described in Farquhar et al. (1980).

Fe Concentration in Shoots, Roots, and Fe Plaque

To determine the Fe concentration in the Fe plaque, root systems were washed in abundant distilled water and immediately incubated for 3 h in cold dithionite-citrate-bicarbonate solution (Taylor and Crowder, 1983) and the Fe concentration determined by atomic absorption spectrometry (Varian-Model Spectra 10/20, Victoria, VIC, Australia). After extraction of Fe plaque, root systems were washed in distilled water and dried at 60°C. Dry samples (shoots and roots) were ashed at 500°C for 3 h. Ashes were digested with concentrated HCl and Fe was quantified by atomic absorption spectrometry.

Oxidative Damage to Lipids, Proteins, and H_2O_2 Determination

Lipid peroxides were extracted in 80% ethanol from fully expanded leaves and lipid peroxidation determined by measuring the concentration of TBARS as described by Hodges et al. (1999). Oxidative damage to proteins was determined by the quantification of carbonyl groups, by derivatization with 2,4-dinitrophenyl-hydrazine. Fully expanded leaves were ground in cold extraction buffer [50 mM Tris (pH 8.0), 2 mM EDTA, 1 mM phenylmethylsulfonyl fluoride and 1 mM benzamidine], centrifuged at 12,000 × *g* for 15 min at 4°C, and the supernatants immediately used for carbonyl determination according to Levine et al. (1990) and normalized with the protein concentration determined using the dye-binding method (Bradford, 1976). H_2O_2 was quantified spectrophotometrically (Cintra 5, GBC Scientific Equipment, Victoria, VIC, Australia) after extraction with 0.1% trichloroacetic acid and reaction with KI in the dark (Alexieva et al., 2001). The amount of H_2O_2 was calculated using a standard curve prepared with known concentrations.

Antioxidant Enzymes Activity

For all enzymatic activity determinations, fully expanded leaves were ground in cold extraction buffer containing 50 mM of sodium phosphate buffer (pH 7.4), 1% (w/v) polyvinylpyrrolidone, 1 mM EDTA, 1 mM phenylmethylsulfonyl fluoride, and 1 mM benzamidine. The homogenate was centrifuged at 12,000 × *g* for 15 min at 4°C and the supernatant immediately used for enzymatic assays.

Ascorbate peroxidase activity was determined according to Klapheck et al. (1990), from the decrease in absorbance at 290 nm; CAT activity was determined following the decrease of absorbance at 240 nm due to H_2O_2 consumption (Cakmak and Marschner, 1992); and SOD activity was quantified as described by Beyer and Fridovich (1987), using 15 min of illumination and recording the absorbance at 560 nm. All enzymatic assays were performed at 25°C as initial activities, with no lag period, and total protein concentration determined by the dye-binding method (Bradford, 1976).

Global Gene Expression Analysis and Real-Time PCR

For global gene expression analysis, highly purified total RNA was obtained using NucleoSpin RNA II (Macherey-Nagel) from roots of EPAGRI 108 and BR-IRGA 409 plants exposed for 3 days to control or excess Fe conditions. RNA purity and quality was assessed by absorbance measurement (260 and 280 nm ratio) and by analysis on a Bioanalyzer (Agilent Technologies). Global gene expressions analyses were performed using the GeneChip Rice Genome Array (Affymetrix), which contains probes to query 51,279 transcripts representing two rice subspecies, with approximately 48,564 transcripts from *japonica* and 1,260 transcripts from the *indica* subspecies, respectively. 5 μg of total RNA were used as starting material for each sample, which were labeled using the one-cycle target labeling and control reagents (Affymetrix). Target preparation, micro-chip hybridization, washing, staining, and scanning were carried out according to manufacturer's instructions (Affymetrix). The Affymetrix GeneChip Operating Software 1.2.1 was used for washing and scanning in the Fluidics Station 450 (Affymetrix) and the Scanner 3300 (Affymetrix), respectively. Sample quality was assessed by examining the 3′ to 5′ intensity ratios of the Poly-A and hybridization controls, and the housekeeping genes. For further data analysis, the probe intensity files (.cel) were imported into the ArrayAssist software (Stratagene) and normalization and probe summarization were performed using the Robust Multichip Analysis algorithm (Irizarry et al., 2003), followed by variance stabilization. Variance stabilization was performed to suppress noise by addition of a fixed quantity to all linear scale signal values.

To identify differentially expressed genes, a Student's *t*-test (using $P \leq 0.05$) was performed and the genes that showed significant differences and were up- or down-regulated by threefold or more were considered to be differentially expressed. Averages from three biological replicates for each sample were used for analysis.

The results from the microarray analysis were validated by real-time PCR. Total RNA was isolated from roots of rice plants exposed for 3 days to control or excess Fe treatments, and one microgram was treated with DNAse and reverse transcribed. Polymerase chain reactions were performed in a StepOne real time PCR System (Applied Biosystems), using SYBR® Green (Invitrogen) to monitor dsDNA synthesis. The following standard thermal profile was used for all PCRs: 95°C for 5 min; 40 cycles of 95°C for 15 s, 60°C for 10 s, 72°C for 15 s, and 60°C for 35 s. Relative expression was determined based on Schmittgen and Livak (2008) method with slight modifications, as described previously (Dametto et al., 2015). Primer sequences corresponding to all tested genes are listed in **Supplementary Table S5**. The microarray data obtained is publicly available at Gene Expression Omnibus[1] under the accession number GSE131287.

[1] https://www.ncbi.nlm.nih.gov/geo/

Gene Ontology Analyses and Venn Diagram

Gene Ontology analyses were performed using PlantGSEA[2]. The 20 most highly enriched categories were selected, and showed with false discovery rate transformed to Log_{10} base. Categories were separated in "Biological Process," "Cellular Component," and "Molecular Function." The Venn diagram was generated using Venny[3].

Histochemical Staining

Plants were harvested after 15 days of treatment. The five millimeters most distal from the root tip were harvested from each root and fixed in 1.5 mL of 2.5% (w/v) glutaraldehyde and 3% (w/v) formaldehyde in phosphate buffer (pH 7.2). Hand-cut transverse sections were taken from fixed roots, after phosphate buffer (pH 7.2) washing followed by rinse in distilled water. The presence of lignin was determined by the Wiesner reaction (Wiesner, 1878), which gives a characteristic red coloration due to cinnamic aldehydes contained in lignified cell walls (Pomar et al., 2002), when viewed under bright field light microscopy. Sections of the roots were soaked in 1:1 aqueous solution of 2% (w/v) phloroglucinol and 70% (v/v) HCl, transferred to a glass-slide, topped with one drop of glycerin and covered with a cover slip. Observations and images were made using a Leica DM light microscope equipped with a Leica DFC500 Digital Camera system.

Chlorophyll *a* Fluorescence

Chlorophyll fluorescence was evaluated using a portable Chlorophyll Fluorometer (OS-30p Opti-Sciences Inc., Hudson, NH, United States). The fast kinetics rising transient (OJIP) measurements were made on attached youngest fully expanded leaves, which were dark-adapted for 12 h. For these measurements, eight plants from each genotype and treatment were used. The F_V/F_M ratio or trapping probability, TR0/ABS, which is the probability that an absorbed photon will be trapped by the Photosystem II reaction center with the resultant reduction of Q_A (primary electron acceptor of Photosystem II) was estimated from the JIP test parameters (Strasser and Strasser, 1995; Krüger et al., 1997). Experiments were performed using $n = 8$ to 9 plants per genotype.

Lignin Quantification

After 15 days of treatment, roots of nine plants from each genotype were harvested and dried in an oven (60°C, 9 days). The eight millimeters most distal from the root tip were harvested from each root for lignin analysis. Root lignin concentration was determined from the protein-free cell wall fraction by the formation and quantification of lignin-thioglycolic acid (LTGA) (Santos et al., 2004, modified proportionally to use 0.05 g of dry roots per sample). The LTGA pellets were dried at 60°C, dissolved in 0.5 M NaOH and diluted to yield an appropriate absorbance for spectrophotometric determination at 280 nm. For lignin's standard curve preparation, different concentrations from 0.005 to 0.5 mg ml^{-1} of lignin (Aldrich 37,096-7 Lignin, alkali, 2-hydroxy-propyl ether) were prepared in the same way (reaction with thioglycolic acid and HCl) and the absorbance at 280 nm was determined. Lignin concentration was expressed as milligram LTGA per gram of dry weight. Experiments were performed using $n = 8$ to 9 plants per genotype.

Statistical Analysis

Means from most physiological and biochemical analyses were compared by ANOVA, followed by Duncan test, according to Quinn and Keough (2002). F_V/F_M and lignin concentration means were compared to the respective controls by the Student's *t*-test ($P \leq 0.05$) using the SPSS Base 12.0 for Windows (SPSS Inc., Chicago, IL, United States). Differences were considered significant when $P \leq 0.05$.

DATA AVAILABILITY

All datasets for this study are included in the manuscript and the **Supplementary Files**. The microarray data obtained in this work is available at Gene Expression Omnibus[4] under the accession number GSE131287.

AUTHOR CONTRIBUTIONS

RJS and JPF conceived the study. RJS, GLD, LS, and MGS conducted the experiments. RJS, AdAJ, FKR, LMGR, NITZ, RS, and JPF analyzed the data. JPF, LMGR, NITZ, and RJS provided the experimental tools. RJS, FKR, and JPF wrote the manuscript. All authors approved the current version of the manuscript.

FUNDING

This work was supported by CNPq (Conselho Nacional de Desenvolvimento Científico e Tecnológico – Brazil), CAPES (Coordenação de Aperfeiçoamento de Pessoal de Nível Superior – Brazil), FAPERGS (Fundação de Apoio à Pesquisa do Estado do Rio Grande do Sul), FAPESP (Fundação de Apoio à Pesquisa do Estado de São Paulo), and CIAT (Centro Internacional de Agricultura Tropical).

ACKNOWLEDGMENTS

The authors thank IRGA (Instituto Rio Grandense do Arroz) for kindly providing rice seeds and access to atomic absorption spectrometry equipment.

SUPPLEMENTARY MATERIAL

The Supplementary Material for this article can be found online at: https://www.frontiersin.org/articles/10.3389/fpls.2019.00746/full#supplementary-material

[2]http://structuralbiology.cau.edu.cn/PlantGSEA/analysis.php

[3]http://bioinfogp.cnb.csic.es/tools/venny/

[4]https://www.ncbi.nlm.nih.gov/geo/

REFERENCES

Alexieva, V., Sergiev, S., Mapelli, S., and Karanov, E. (2001). The effect of drought and ultraviolet radiation on growth and stress markers in pea and wheat. *Plant Cell Environ.* 24, 1337–1344.

Arenhart, R. A., Lima, J. C., Pedron, M., Carvalho, F. E., Silveira, J. A., Rosa, S. B., et al. (2013). Involvement of ASR genes in aluminium tolerance mechanisms in rice. *Plant Cell Environ.* 36, 52–67. doi: 10.1111/j.1365-3040.2012.02553.x

Bashir, K., Hanada, K., Shimizu, M., Seki, M., Nakanishi, H., and Nishizawa, N. K. (2014). Transcriptomic analysis of rice in response to iron deficiency and excess. *Rice* 7, :18. doi: 10.1186/s12284-014-0018-1

Becana, M., Moran, J. F., and Iturbe-Ormaetxe, I. (1998). Iron-dependent oxygen free radical generation in plants subjected to environmental stress: toxicity and antioxidant protection. *Plant Soil* 201, 137–147.

Becker, M., and Asch, F. (2005). Iron toxicity in rice—conditions and management concepts. *J. Plant Nutr. Soil Sci.* 168, 558–573.

Beyer, W. F., and Fridovich, I. (1987). Assaying of superoxide dismutase activity: some large consequences of minor changes in conditions. *Anal. Biochem.* 161, 559–566.

Blokhina, O., Virolainen, E., and Fagerstedt, K. V. (2003). Antioxidants, oxidative damage and oxygen deprivation stress: a review. *Ann. Bot.* 91, 179–194.

Boerjan, W., Ralph, J., and Baucher, M. (2003). Lignin biosynthesis. *Ann. Rev. Plant Biol.* 54, 519–546.

Bradford, M. M. (1976). A rapid and sensitive method for the quantitation of microgram quantities of protein utilizing the principle of protein-dye binding. *Anal. Biochem.* 72, 248–254.

Burlat, V., Kwon, M., Davin, L. B., and Lewis, N. G. (2001). Dirigent proteins and dirigent sites in lignifying tissues. *Phytochemistry* 57, 883–897.

Cai, X., Chen, T., Zhou, Q., Xu, L., Qu, L., Hua, X., et al. (2011). Development of casparian strip in rice cultivars. *Plant Signal. Behav.* 6, 59–65.

Cakmak, I., and Marschner, H. (1992). Magnesium deficiency and high light intensity enhance activities of superoxide dismutase, ascorbate peroxidase and glutathione reductase in bean leaves. *Plant Physiol.* 98, 1222–1227.

Dametto, A., Sperotto, R. A., Adamski, J. M., Blasi, É. A., Cargnelutti, D., de Oliveira, L. F., et al. (2015). Cold tolerance in rice germinating seeds revealed by deep RNAseq analysis of contrasting indica genotypes. *Plant Sci.* 238, 1–12. doi: 10.1016/j.plantsci.2015.05.009

Davin, L. B., Wang, H. B., Crowell, A. L., Bedgar, D. L., Martin, D. M., Sarkanen, S., et al. (1997). Stereoselective bimolecular phenoxy radical coupling by an auxiliary (dirigent) protein without an active center. *Science* 275, 362–366.

Doblas, V. G., Geldner, N., and Barberon, M. (2017). The endodermis, a tightly controlled barrier for nutrients. *Curr. Opin. Plant Biol.* 39, 136–143. doi: 10.1016/j.pbi.2017.06.010

Dufey, I., Hakizimana, P., Draye, X., Lutts, S., and Bertin, P. (2009). QTL mapping for biomass and physiological parameters linked to resistance mechanisms to ferrous iron toxicity in rice. *Euphytica* 167, 143–160.

Dufey, I., Hiel, M. P., Hakizimana, P., Draye, X., Lutts, S., Koné, B., et al. (2012). Multienvironment quantitative trait loci mapping and consistency across environments of resistance mechanisms to ferrous iron toxicity in rice. *Crop Sci.* 52, 539–550.

Dufey, I., Mathieu, A.-S., Draye, X., Lutts, S., and Bertin, P. (2015). Construc- tion of an integrated map through comparative studies allows the identification of candidate regions for resistance to ferrous iron toxicity in rice. *Euphytica* 203, 59–69.

Dziwornu, A. K., Shrestha, A., Matthus, E., Ali, B., Wu, L. B., and Frei, M. (2018). Responses of contrasting rice genotypes to excess manganese and their implications for lignin synthesis. *Plant Physiol. Biochem.* 123, 252–259. doi: 10.1016/j.plaphy.2017.12.018

Fang, W. C., Wang, J. W., Lin, C. C., and Kao, C. H. (2001). Iron induction of lipid peroxidation and effects on antioxidative enzymes activities in rice leaves. *Plant Growth Regul.* 35, 75–80.

Farquhar, G. D., Von Caemmerer, S., and Berry, J. A. (1980). A biochemical model of photosynthetic CO2 assimilation in leaves of C3 species. *Planta* 149, 78–90. doi: 10.1007/BF00386231

Finatto, T., de Oliveira, A. C., Chaparro, C., da Maia, L. C., Farias, D. R., Woyann, L. G., et al. (2015). Abiotic stress and genome dynamics: specific genes and transposable elements response to iron excess in rice. *Rice* 8, :13. doi: 10.1186/s12284-015-0045-6

Gollhofer, J., Timofeev, R., Lan, P., Schmidt, W., and Buckhout, T. J. (2014). Vacuolar-iron-transporter1-like proteins mediate iron homeostasis in *Arabidopsis*. *PLoS One* 9:e110468. doi: 10.1371/journal.pone.0110468

Gomes, M. P., Marques, T. C. L. S. M., Nogueira, M. O. G., Castro, E. M., and Soares, A. M. (2011). Ecophysiological and anatomical changes due to uptake and accumulation of heavy metal in *Brachiaria decumbens*. *Sci. Agric.* 68, 566–573. doi: 10.1590/S0103-90162011000500009

Grillet, L., Lan, P., Li, W., Mokkapati, G., and Schmidt, W. (2018). IRON MAN is a ubiquitous family of peptides that control iron transport in plants. *Nat. Plants* 4, 953–963. doi: 10.1038/s41477-018-0266-y

Hodges, D. M., DeLong, J. M., Forney, C. F., and Prange, R. K. (1999). Improving the thiobarbituric acid-reactive-substances assay for estimating lipid peroxidation in plant tissues containing anthocyanin and other interfering compounds. *Planta* 207, 604–611.

Hosmani, P. S., Kamiya, T., Danku, J., Naseer, S., Geldner, N., Guerinot, M. L., et al. (2013). Dirigent domain-containing protein is part of the machinery required for formation of the lignin-based casparian strip in the root. *Proc.eedings of the Natl.ional Acad.emy of Sci.ences, U.S.A.* 110, 14498–14503. doi: 10.1073/pnas.1308412110

Irizarry, R. A., Bolstad, B. M., Collin, F., Cope, L. M., Bridget, H., and Terence, P. (2003). Summaries of affymetrix genechip probe level data. *Nucleic Acids Res.* 31, e15.

Ishimaru, Y., Bashir, K., Fujimoto, M., An, G., Itai, R. N., Tsutsumi, N., et al. (2009). Rice-specific mitochondrial iron-regulated gene (MIR) plays an important role in iron homeostasis. *Mol. Plant* 2, 1059–1066. doi: 10.1093/mp/ssp051

Ishimaru, Y., Suzuki, M., Tsukamoto, T., Suzuki, K., Nakazono, M., Kobayashi, T., et al. (2006). Rice plants take up iron as an Fe3+-phytosiderophore and as Fe2+. *Plant J.ournal* 45, 335–346. doi: 10.1111/j.1365-313X.2005.02624.x

Joo, J., Lee, Y. H., Kim, Y. K., Nahm, B. H., and Song, S. I. (2013). Abiotic stress responsive rice ASR1 and ASR3 exhibit different tissue-dependent sugar and hormone-sensitivities. *Mol. Cells* 35, 421–435. doi: 10.1007/s10059-013-0036-7

Kakei, Y., Ishimaru, Y., Kobayashi, T., Yamakawa, T., Nakanishi, H., and Nishizawa, N. K. (2012). OsYSL16 plays a role in the allocation of iron. *Plant Mol. Biol.* 79, 583–594. doi: 10.1007/s11103-012-9930-1

Kampfenkel, K., van Montagu, M., and Inzé, D. (1995). Effects of iron excess on *Nicotiana plumbaginifolia*. Implications to oxidative stress. *Plant Physiol.* 107, 725–735.

Kidwai, M., Dhar, Y. V., Gautam, N., Tiwari, M., Ahmad, I. Z., Asif, M. H., et al. (2019). *Oryza sativa* class III peroxidase (OsPRX38) overexpression in *Arabidopsis thaliana* reduces arsenic accumulation due to apoplastic lignification. *J. Hazard. Mater.* 362, 383–393. doi: 10.1016/j.jhazmat.2018.09.029

Klapheck, S., Zimmer, I., and Cosse, H. (1990). Scavenging of hydrogen peroxide in the endosperm of *Ricinus communis* by ascorbate peroxidase. *Plant Cell Physiol.* 31:, 1005–1013.

Krüger, G. H. J., Tsimilli-Michael, M., and Strasser, R. J. (1997). Light stress provokes plastic and elastic modifications in structure and function of photosystem II in camellia leaves. *Physiol. Plant.* 101, 265–277.

Lee, S., Ryoo, N., Jeon, J. S., Guerinot, M. L., and An, G. (2012). Activation of rice yellow stripe1-like 16 (OsYSL16) enhances iron efficiency. *Mol. Cells* 33, 117–126. doi: 10.1007/s10059-012-2165-9

Lequeux, H., Hermans, C., Lutts, S., and Verbruggen, N. (2010). Response to copper excess in *Arabidopsis thaliana*: impact on the root system architecture, hormone distribution, lignin accumulation and mineral profile. *Plant Physiol. Biochem.* 48, 673–682. doi: 10.1016/j.plaphy.2010.05.005

Levine, R. L., Garland, D., Oliver, C. N., Amici, A., Climent, I., Lenz, A., et al. (1990). Determination of carbonyl content in oxidatively modified proteins. *Methods Enzymol.* 186, 464–478.

Ma, F., and Peterson, C. A. (2003). Current insides into the development, structure, and chemistry of the endodermis and exodermis of roots. *Can. J. Bot.* 81, 405–421.

Majerus, V., Bertin, P., Swenden, V., Fortemps, A., Lobreaux, S., and Lutts, S. (2007). Organ-dependent responses of the african rice to short-term iron toxicity: fer- ritin regulation and antioxidative responses. *Biol.ogia Plant.arum* 51, 303–312.

Matthus, E., Wu, L. B., Ueda, Y., Höller, S., Becker, M., and Frei, M. (2015). Loci, genes, and mechanisms associated with tolerance to ferrous iron toxicity in rice (*Oryza sativa* L.). *Theor. Appl. Genet.* 128, 2085–2098. doi: 10.1007/s00122-015-2569-y

Müller, C., Silveira, S. F. D. S., Daloso, D. M., Mendes, G. C., Merchant, A., Kuki, K. N., et al. (2017). Ecophysiological responses to excess iron in lowland and upland rice cultivars. *Chemosphere* 189, 123–133. doi: 10.1016/j.chemosphere.2017.09.033

Naseer, S., Lee, Y., Lapierre, C., Franke, R., Nawrath, C., and Geldner, N. (2012). Casparian strip diffusion barrier in *Arabidopsis* is made of a lignin polymer without suberin. *Proc. Natl. Acad. Sci. U.S.A.* 109, 10101–10106. doi: 10.1073/pnas.1205726109

Nozoye, T., Nagasaka, S., Kobayashi, T., Takahashi, M., Sato, Y., Sato, Y., et al. (2011). Phytosiderophore efflux transporters are crucial for iron acquisition in graminaceous plants. *J. Biol. Chem.* 286, 5446–5454. doi: 10.1074/jbc.M110.180026

Olaleye, A. O., Tabi, F. O., Ogunkule, A. O., Singh, B. N., and Sahrawat, K. L. (2001). Effect of toxic iron concentration on the growth of lowland rice. *J. Plant Nutr.* 24, 441–457.

Paniagua, C., Bilkova, A., Jackson, P., Dabravolski, S., Riber, W., Didi, V., et al. (2017). Dirigent proteins in plants: modulating cell wall metabolism during abiotic and biotic stress exposure. *J. Exp. Bot.* 68, 3287–3301. doi: 10.1093/jxb/erx141

Pereira, E. G., Oliva, M. A., Rosado-Souza, L., Mendes, G. C., Colares, D. S., Stopato, C. H., et al. (2013). Iron excess affects rice photosynthesis through stomatal and non-stomatal limitations. *Plant Sci.* 20, 81–92. doi: 10.1016/j.plantsci.2012.12.003

Pomar, F., Merino, F., and Barcelo, A. R. (2002). O-4- linked coniferyl and sinapyl aldehydes in lignifying cell walls are the main targets of the wiesner (phloroglucinol-HCl) reaction. *Protoplasma* 220, 17–28. doi: 10.1007/s00709-002-0030-y

Quinn, G. P., and Keough, M. J. (2002). *Experimental Design and Data Analysis for Biologists*. Cambridge: Cambridge University Press, 738.

Quinet, M., Vromman, D., Clippe, A., Bertin, P., Lequeux, H., Dufey, I., et al. (2012). Combined transcriptomic and physiological approaches reveal strong differences between short- and long-term response of rice (*Oryza sativa*) to iron toxicity. *Plant Cell Environ.* 35, 1837–1859. doi: 10.1111/j.1365-3040.2012.02521.x

Raes, J., Rohde, A., Christensen, J. H., Van de Peer, Y., and Boerjan, W. (2003). Genome-wide characterization of the lignification toolbox in *Arabidopsis*. *Plant Physiol.* 1, 1051–1071.

Ricachenevsky, F. K., de Araújo Junior, A. T., Fett, J. P., and Sperotto, R. A. (2018). You shall not pass: root vacuoles as a symplastic checkpoint for metal translocation to shoots and possible application to grain nutritional quality. *Front. Plant Sci.* 9:412. doi: 10.3389/fpls.2018.00412

Ricachenevsky, F. K., and Sperotto, R. A. (2014). There and back again, or always there? The evolution of rice combined strategy for Fe uptake. *Front. Plant Sci.* 5:89. doi: 10.3389/fpls.2014.00189

Ricachenevsky, F. K., Sperotto, R. A., Menguer, P. K., and Fett, J. P. (2010). Identification of Fe-excess-induced genes in rice shoots reveals a WRKY transcription factor responsive to Fe, drought and senescence. *Mol. Biol. Rep.* 37, 3735–3745. doi: 10.1007/s11033-010-0027-0

Ricachenevsky, F. K., Sperotto, R. A., Menguer, P. K., Sperb, E. R., Lopes, K. L., and Fett, J. P. (2011). ZINC-induced facilitator-like family in plants: lineage-specific expansion in monocotyledons and conserved genomic and expression features among rice (*Oryza sativa*) paralogs. *BMC Plant Biol.* 11:20. doi: 10.1186/1471-2229-11-20

Sahrawat, K. L. (2000). Elemental composition of rice plants as affected by iron toxicity under field conditions. *Commun. Soil Sci. Plant Anal.* 31, 2819–2827.

Sahrawat, K. L. (2004). Iron toxicity in wetland rice and the role of other nutrients. *J. Plant Nutr.* 27, 1471–1504.

Santos, W. D., Ferrarese, M. L. L., Finger, A., Teixeira, A. C. N., and Ferrarese-Filho, O. (2004). Lignification and related enzymes in soybean root growth-inhibition by ferulic acid. *J. Chem. Ecol.* 30, 1203–1212.

Schmittgen, T. D., and Livak, K. J. (2008). Analyzing real-time PCR data by the comparative CT method. *Nat.ure Protoc.* 3, 1101–1108.

Siemianowski, O., Barabasz, A., Kendziorek, M., Ruszczynska, A., Bulska, E., Williams, L. E., et al. (2014). HMA4 expression in tobacco reduces Cd accumulation due to the induction of the apoplastic barrier. *J. Exp. Bot.* 65, 1125–1139. doi: 10.1093/jxb/ert471

Silveira, V. C., Oliveira, A. P., Sperotto, R. A., Espindola, L., Amaral, L., Dias, J. F., et al. (2007). Influence of iron on mineral status of two rice (*Oryza sativa* L.) cultivars. *Braz. J. Plant Physiol.* 19, 127–139.

Sperotto, R. A., Ricachenevsky, F. K., Waldow Vde, A., and Fett, J. P. (2012). Iron biofortification in rice: it"s a long way to the top. *Plant Sci.* 190, 24–39. doi: 10.1016/j.plantsci.2012.03.004

Strasser, B. J., and Strasser, R. J. (1995). "Measuring fast fluorescence transients to address environmental questions: the JIP test," in: *Mathis P (ed) Photosynthesis: From Light to Biosphere* (Dordrecht: Kluwer Acadamic Publishers), 977–980.

Stein, R. J., Duarte, G. L., Spohr, M. G., Lopes, S. I. G., and Fett, J. P. (2009a). Distinct physiological responses of two rice cultivars subjected to iron toxicity under field conditions. *Ann. Appl. Biol.* 154, 269–277.

Stein, R. J., Ricachenevsky, F. K., and Fett, J. P. (2009b). Differential regulation of the two rice ferritin genes (OsFER1 and OsFER2). *Plant Sci.* 177, 563–569.

Suh, H., Kim, C. S., Lee, J., and Jung, J. (2002). Photodynamic effect of iron excess on photosystem II function in pea plants. *Photochem. Photobiol.* 75, 513–518.

Taylor, G., and Crowder, A. A. (1983). Use of the DCB technique for extraction of hydrous iron oxides from roots of wetland plants. *Am. J. Bot.* 70, 1254–1257.

Wiesner, J. (1878). Note űber das verhalten des phloroglucins und einiger verwandter körper zur verholzten zellmembrane. *Sitzungsber Akad Wiss Math-naturw Kl* 77, 60–66.

Wu, L.-B., Shhadi, M., Gregorio, G., Matthus, E., Becker, M., and Frei, M. (2014). Genetic and physiological analysis of tolerance to acute iron tox- icity in rice. *Rice* 7, :8. doi: 10.1186/s12284-014-0008-3

Wu, L. B., Ueda, Y., Lai, S. K., and Frei, M. (2017). Shoot tolerance mechanisms to iron toxicity in rice (*Oryza sativa* L.). *Plant Cell Environ.* 40, 570–584. doi: 10.1111/pce.12733

Yoshida, S., Forno, D. A., Cock, J. H., and Gomez, K. A. (1976). *Laboratory Manual for Physiological Studies of Rice*, 3rd Edn. Manila: International Rice Research Institutes, 61.

Zhang, J., Chen, K., Pang, Y., Naveed, S. A., Zhao, X., Wang, X., et al. (2017). QTL mapping and candidate gene analysis of ferrous iron and zinc toxicity tolerance at seedling stage in rice by genome-wide association study. *BMC Genomics* 18:828. doi: 10.1186/s12864-017-4221-5

Zhang, Y., Xu, Y. H., Yi, H. Y., and Gong, J. M. (2012). Vacuolar membrane transporters OsVIT1 and OsVIT2 modulate iron translocation between flag leaves and seeds in rice. *Plant J.* 72, 400–410. doi: 10.1111/j.1365-313X.2012.05088.x

Zheng, L., Huang, F., Narsai, R., Wu, J., Giraud, E., He, F., et al. (2009). Physiological and transcriptome analysis of iron and phosphorus interaction in rice seedlings. *Plant Physiol.* 151, 262–274. doi: 10.1104/pp.109.141051

Conflict of Interest Statement: The authors declare that the research was conducted in the absence of any commercial or financial relationships that could be construed as a potential conflict of interest.

frontiers in Plant Science

REVIEW
published: 26 June 2019
doi: 10.3389/fpls.2019.00844

FIT-Binding Proteins and Their Functions in the Regulation of Fe Homeostasis

Huilan Wu[1] *and Hong-Qing Ling*[1,2]*

[1] *The State Key Laboratory of Plant Cell and Chromosome Engineering, Institute of Genetics and Developmental Biology, Chinese Academy of Sciences, Beijing, China,* [2] *College of Life Sciences, University of Chinese Academy of Sciences, Beijing, China*

Iron, as an essential micronutrient, is required by all living organisms. In plants, the deficiency and excess of iron will impair their growth and development. For maintaining a proper intracellular iron concentration, plants evolved different regulation mechanisms to tightly control iron uptake, translocation and storage. FIT, a bHLH transcription factor, is the master regulator of the iron deficiency responses and homeostasis in Arabidopsis. It interacts with different proteins, functioning in controlling the expression of various genes involved in iron uptake and homeostasis. In this review, we summarize the recent progress in the studies of FIT and FIT-binding proteins, and give an overview of FIT-regulated network in iron deficiency response and homeostasis.

Keywords: Arabidopsis, plant nutrition, iron, FIT, FIT-binding protein, transcriptional regulation

OPEN ACCESS

Edited by:
Sebastien Thomine, Centre National de la Recherche Scientifique (CNRS), France

Reviewed by:
Gang Liang, Xishuangbanna Tropical Botanical Garden (CAS), China
Petra Bauer, Saarland University, Germany
Christian Dubos, Institut National de la Recherche Agronomique (INRA), France

***Correspondence:**
Hong-Qing Ling
hqling@genetics.ac.cn

Specialty section:
This article was submitted to Plant Nutrition, a section of the journal Frontiers in Plant Science

Received: *31 January 2019*
Accepted: *12 June 2019*
Published: *26 June 2019*

Citation:
Wu H and Ling H-Q (2019) FIT-Binding Proteins and Their Functions in the Regulation of Fe Homeostasis. Front. Plant Sci. 10:844. doi: 10.3389/fpls.2019.00844

INTRODUCTION

Iron plays an essential role in a variety of biologic processes in plants, such as photosynthesis, respiration, nitrogen fixation and vitamin synthesis (Schmidt, 2003; Hansch and Mendel, 2009; Jeong and Guerinot, 2009; Zhao et al., 2011). Although iron is the fourth most abundant element in the earth's crust, the deficiency of iron is one of the factors mostly limiting plant growth because it is mainly present as insoluble form Fe^{3+} and not available for plants in soil, especially in the neutral and basic soil. In order to overcome iron deficiency, plant developed the reduction-based (strategy I) and chelation-based (strategy II) mechanisms to mobilize and enhance iron uptake from soil (Marschner et al., 1986; Römheld and Marschner, 1986). All dicots and non-graminaceous plants use the strategy I mechanism whereas grasses apply the strategy II. Under iron limitation condition, the strategy I plants secrete proton and phenolic compounds from roots to rhizosphere for increasing the solubility of ferric iron (Santi and Schmidt, 2009; Fourcroy et al., 2014); the mobilized ferric iron will then be reduced to ferrous iron on root surface by the ferric chelate reductase, such as Ferric Reduction Oxidase2 (FRO2) (Robinson et al., 1999); finally, the reduced ferrous iron will be transported into root epidermal cells by the metal transporter Iron-Regulated Transporter1 (IRT1) (Vert et al., 2002). The strategy II plants (grasses) secrete phytosiderophores (PS) from roots into soil to chelate Fe(III), and the PS-Fe(III) complex will be transported into root cells by YS1 under the stress of iron deficiency (Takagi et al., 1984; Mori and Nishizawa, 1987; Curie et al., 2001). On the other hand, excessive iron can generate oxidative stress in cells and become toxic for plants. Therefore, the uptake, translocation and storage of iron in plants should be carefully regulated.

In strategy I plants, the expression of many genes is induced or upregulated at transcriptional level under iron limitation. In the processes, transcription factors are required and play important

roles. *FER*, the first isolated regulatory gene of iron homeostasis from tomato, encodes a typical basic helix-loop-helix protein (Ling et al., 2002). The *FER*-null mutant *T3238fer*, which was caused by the insertion of a Ty1-copia-like element in the first exon of *FER* (Cheng et al., 2009), lost the whole iron deficiency responses. The expression of ferric-chelate reductase *LeFRO1* and ferrous transporter *LeIRT1* was not able to be upregulated in the mutant at the stress of iron deficiency (Ling et al., 2002; Li et al., 2004). The mutant showed severe chlorosis and died at young seedling stage under normal culture condition. FIT (AtbHLH29/FRU), a FER ortholog in Arabidopsis, was confirmed to enable complementation of the defective function in *T3238fer* (Yuan et al., 2005). The *FIT*-null mutant *fit-1* and *fit-3* generated by T-DNA insertion showed similar phenotypes as tomato *T3238fer*. The transcription of *FRO2* and *IRT1* in *fit-1* and *fit-3* was severely impaired (Colangelo and Guerinot, 2004; Jakoby et al., 2004). Microarray analysis showed that 72 genes upregulated under iron deficiency in wild type were completely or partially deregulated in the mutant *fit-1* (such as *AHA2*, *IRT1*, *IRT2, NRAMP1*, and *NAS1*), some of which were proposed to be its direct targets (Colangelo and Guerinot, 2004; Jakoby et al., 2004; Yuan et al., 2008; Ivanov et al., 2011; Sivitz et al., 2012; Wang et al., 2013). Recently, the list of FIT-regulated genes was expanded (Mai et al., 2016). As a key factor in the transcriptional regulation of Fe uptake and homeostasis, the expression of *FIT* is tightly regulated at transcriptional and posttranscriptional levels.

In this review, we summarize the recent progress in the studies of FIT and several of its interaction partners in *Arabidopsis thaliana* (a model plant of strategy I plants), and give an overview of FIT-related regulation pathway in iron deficiency responses and homeostasis of strategy I plants.

REGULATORS INTERACTED WITH FIT IN INITIATING IRON DEFICIENCY RESPONSES

Ib Subgroup of bHLH Transcription Factors

As shown in introduction, FIT, an ortholog of tomato FER, is a key transcription factor in the control of iron deficiency responses and homeostasis in *Arabidopsis thaliana* (Colangelo and Guerinot, 2004; Jakoby et al., 2004; Yuan et al., 2005). However, overexpression of *FIT* didn't result in obvious phenotypical and physiological alterations, compared to wild type (Colangelo and Guerinot, 2004; Jakoby et al., 2004; Yuan et al., 2005; Meiser et al., 2011; Sivitz et al., 2011; Gratz et al., 2019). Based on these, it was suggested that FIT is essential, but it alone is not sufficient for the activation of iron deficiency responses and the effective iron uptake system in Arabidopsis. Indeed, Yuan et al. (2008) and Wang et al. (2013) revealed that the Ib subgroup of bHLH transcription factors bHLH038, bHLH039, bHLH100, and bHLH101 were able to interact with FIT to form the heterodimer of FIT/bHLH38, FIT/bHLH39, FIT/bHLH100, and FIT/bHLH101 in plant cells. Further, they did the transcriptional activation assay, and showed that the co-expression of *FIT* with one of the Ib subgroup of bHLH transcription factors enabled to activate *GUS* expression driven by either the *FRO2* or the *IRT1* promoter in yeast cells, suggesting that the formed heterodimer complex could bind to the promoter of iron uptake genes *FRO2* and *IRT1*, and directly activated their expression (Yuan et al., 2008; Wang et al., 2013). The expression of the four Ib bHLH genes was dependent on iron status, and strongly upregulated in root and leaf under iron starvation (Vorwieger et al., 2007; Wang et al., 2007). The plants double overexpressing *FIT* with *bHLH38*, *bHLH39*, *bHLH100,* or *bHLH101* changed the expression patterns of *FRO2* and *IRT1* from induced to a constitutive expression regardless iron status (Yuan et al., 2008; Wang et al., 2013). Phenotypically, the transgenic plants revealed a higher ferric-chelate reductase activity in root and accumulated more iron in shoot than wild type and the plants overexpressing of *bHLH38*, *bHLH39*, *bHLH100,* or *bHLH101* alone. The four Ib bHLH genes have a high sequence identity, and function redundantly in the regulation of iron uptake and homeostasis. Therefore, the single and double mutants of the four genes did not show obviously phenotypical and physiological alterations, whereas their triple mutant bHLH38/100/101 and bHLH39/100/101 exhibited sensitivity to iron limitation and chlorotic phenotype, compared to wild type (Wang et al., 2013). Additionally, they found that the four bHLH proteins possessed different significance in regulation of iron-deficiency responses and uptake (bHLH 39 > bHLH101 > bHLH38 > bHLH100). The similar results were also reported by Sivitz et al. (2012) and Maurer et al. (2014). They did not observed an obvious effect on the expression of iron acquisition genes in double knocking out-mutant *bhlh100bhlh101* and triple knocking-out mutant *bhlh39bhlh100bhlh101* (*3xbhlh*).

In addition to the activation function, Cui et al. (2018) recently reported that Ib bHLH proteins have a stabilization function for FIT in plant cells. They detected abundant FIT protein accumulation in roots of plants overexpressing *FIT* and *bHLH38*, but not in the roots of plants overexpressing *FIT* alone under iron-sufficient conditions. Further, they also observed that the roots of *bHLH38*-overexpressing plants accumulated much more FIT under iron sufficiency and protected JA-induced FIT degradation under JA treatment, compared to wild type. Based on the data, they speculated that the Ib subgroup of bHLH transcription factors might play a role in the protection of FIT from degradation. Alternatively, the phenomenon may be caused by higher expression of *FIT* in bHLH38-overexpressing plants and *FIT* and *bHLH38* double overexpressing plants. However, as reported by Yuan et al. (2008), over expression of *bHLH038* did not change the expressional level of *FIT*, compared with wild type. Anyway, more experiments are needed to confirm it.

The expression of the Ib bHLH genes was controlled genetically and epigenetically at transcription level. Shk1 binding protein 1 (SKB1/AtPRMT5), which catalyzes the symmetric dimethylation of histone H4R3 (H4R3sme2), was identified to be involved in iron homeostasis in Arabidopsis, while the SKB1 lesion mutant exhibited higher iron content in shoots and more tolerance to iron deficiency, compared to wild type (Fan et al., 2013). The expression of *SKB1* was not dependent on iron, but the level of H4R3sme2 mediated by SKB1 was clearly

related to iron status in plants. Chromatin immunoprecipitation (ChIP) and genome-wide ChIP-seq results showed that SKB1 associated with the chromatin in the promoter region of *bHLH38*, *bHLH39*, *bHLH100* and *bHLH101*, and symmetrically dimethylated histone H4R3 (Fan et al., 2013). Iron deficiency may cause an increase in the disassociation of SKB1 from chromatin of the four Ib bHLH genes and resulted in a decrease of H4R3sme2 level, thereby elevating their transcription and enhancing iron uptake.

At genetic control, a recent report showed that the expression of *bHLH38*, *bHLH39*, *bHLH100,* and *bHLH101* was positively regulated by bHLH034, bHLH104, bHLH105, and bHLH115, which are classified as the IVc subgroup of bHLH transcription factors. The mutants of IVc bHLH transcription factors displayed sensitivity to iron deficiency, including reduced root length, chlorotic leaves, and decreased ferric chelate reductase activity (Zhang et al., 2015; Li et al., 2016; Liang et al., 2017). Under both Fe-sufficient and Fe-deficient conditions, the transcript levels of *bHLH38*, *bHLH39*, *bHLH100,* and *bHLH101* were always lower in the mutants of IVc bHLH transcription factors than in wild-type plants. Transient expression assays and ChIP experiments confirmed that IVc bHLH transcription factors were able to directly activate the promoters of *bHLH38*, *bHLH39*, *bHLH100,* and *bHLH101* (Zhang et al., 2015; Li et al., 2016; Liang et al., 2017).

EIN3 and EIL1

As known for a long time, ethylene as a phytohormone plays important roles in iron deficiency responses. Its molecular mechanism has been elucidated recently. Lingam et al. (2011) reported that EIN3 (Ethylene Insensitive 3) and EIL1 (EIN3-Like 1), two transcription factors involved in the ethylene signaling pathway, can interact with FIT, and showed that the interaction of FIT with EIN3 and EIL1 was required for FIT accumulation, and contributes to the expression of FIT-downstream genes. Loss function of *EIN3* and *EIL1* led to the significant reduction of FIT accumulation even under iron deficiency condition.

MED16 and MED25

During the transcription process, Mediator, a large protein complex comprising more than 20 subunits, is required and functions as a bridge connecting the RNA polymerase II (Pol II) complex and specific transcriptional activators (Asturias et al., 1999). Through interaction with specific transcription activators, Mediator coordinates and transfers the developmental and environmental signals to the transcriptional machinery to regulate the expression of corresponding genes (Bäckström et al., 2007; Mathur et al., 2011; Zhang et al., 2012). MED16 (Mediator subunit 16) and MED25 (Mediator subunit 25), organized in the tail module of the Mediator, have been recently identified to be involved in the regulation of Fe-dependent gene expression (Yang et al., 2014; Zhang et al., 2014). Loss of MED16 or MED25 led to a declined expression of some iron deficiency response genes, such as *FRO2*, *IRT1* and *AHA2*, under iron deficiency condition. The mutant *med16* and *med25* showed hypersensitivity to the stress of iron limitation. Zhang et al. (2014) demonstrated that MED16 functioned in the interaction with FIT to enhance the expression of FIT-dependent genes by recruiting FIT-bHLH complex to their promoters. Additionally, Yang et al. (2014) found that MED25 was able to interact with MED16, EIN3 and EIL1, which may play some roles in FIT stabilization.

CIPK11

Cytosolic Ca^{2+} as the second messenger is an important signaling molecule to transduce developmental and environmental cues to activate physiological processes in plants. Recently, Tian et al. (2016) and Gratz et al. (2019) used the method of fluorescence resonance energy transfer (FRET), and observed an increased cytoplasm Ca^{2+} concentration in primary roots under iron deficiency. Further, they physiologically characterized the loss-of-function mutants of *CIPK11*, *CIPK23,* and *CBL1*/*CBL9* on iron deficiency medium, and demonstrated that calcium-dependent CBL-CIPK pathway was involved in response to iron deficiency in Arabidopsis. With yeast-two-hybrid and BiFC assay, Gratz et al. (2019) confirmed that CIPK11 was positively involved in iron deficiency response through directly interaction with FIT. *CIPK11* transcript abundance was significantly elevated under iron deficiency, and its expression pattern was similarly to the *FIT* in the early differentiation root zone, in which iron uptake occurs predominantly (Gratz et al., 2019). Loss of CIPK11 function resulted in the partial inactivation of the iron deficiency responses and reduced the iron content in seed. *In vitro* assay displayed that CIPK11 as a kinase enabled phosphorylation of FIT at Ser271 amino acid (Gratz et al., 2019). Further, using a series of molecular methods including *fit-3* mutant complementation assay, protein homo- and hetero-dimerization assay in yeast and planta, transcription self-activation capacity assay and fluorescence recovery after photobleaching analysis (Gratz et al., 2019), they revealed that phosphorylation of Ser272 amino acid modulated FIT nuclear accumulation, homo-dimerization, interaction with bHLH039 and transcriptional activity, and proposed that FIT phosphorylation status determines its activity.

REGULATORS INTERACTED WITH FIT IN REPRESSING IRON DEFICIENCY RESPONSES

ZAT12

As known, H_2O_2 as a signal is involved in many abiotic stresses (Mittler and Blumwald, 2015). Increase in H_2O_2 accumulation was observed in plant roots under the deficiency of potassium, nitrogen, phosphorus and iron (Ranieri et al., 2001; Shin et al., 2005; Sun et al., 2007). Recently, Le et al. (2016) reported that zinc finger of *Arabidopsis thaliana* 12 (ZAT12) functioned in the negative regulation of plant responses to prolonged iron deficiency stress. ZAT12 is a marker of abiotic stress and its expression is induced by oxidative stress. Thus, a molecular connection between Fe deficiency and the oxidative stress response was illustrated. *ZAT12* was expressed mainly in the root early differentiation and elongation zone, and responded to iron deficiency in the late stage, compared with Fe sufficiency. Using yeast-two-hybrid approach and BiFC assay in plant, they

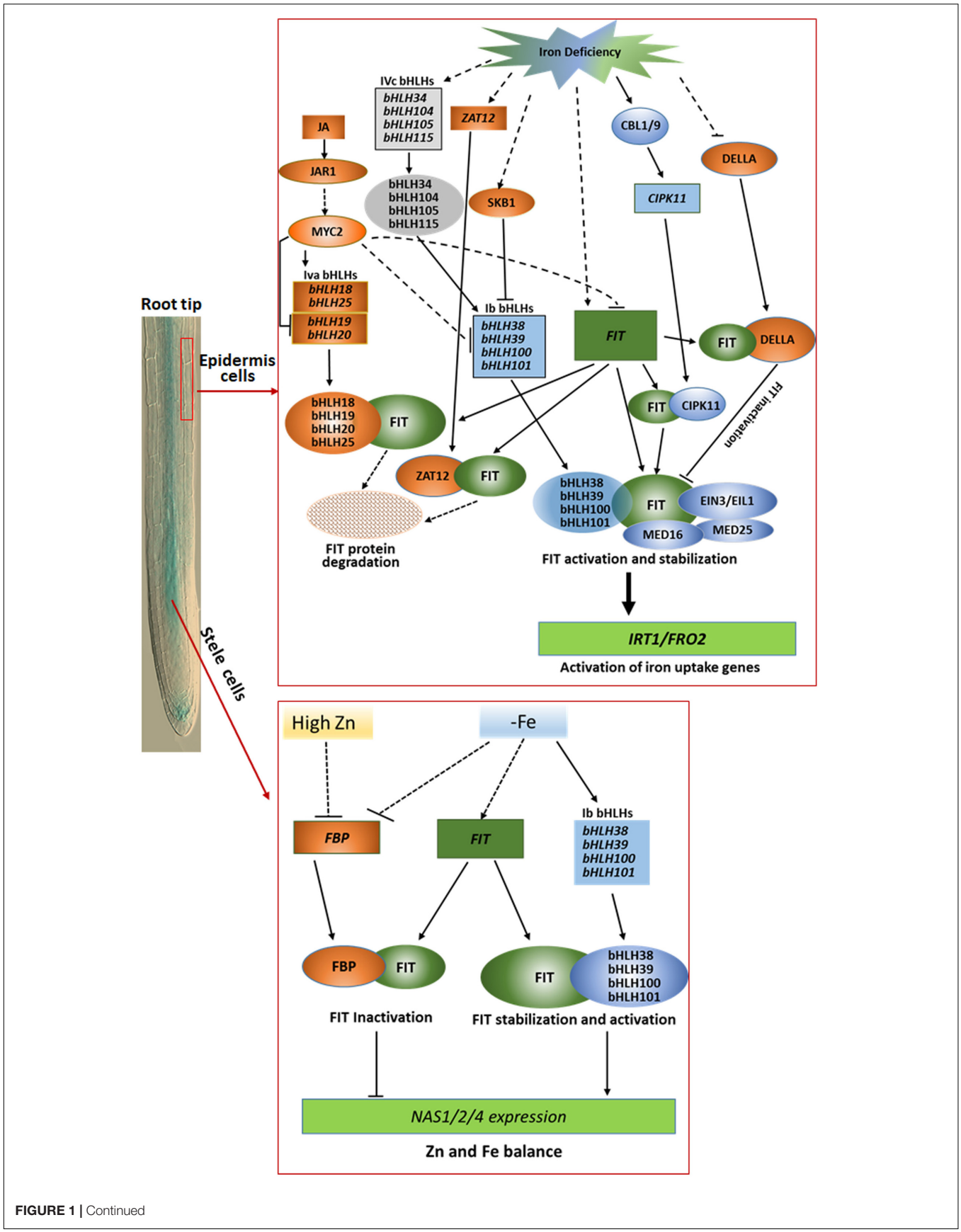

FIGURE 1 | Continued

FIGURE 1 | Outline of the regulation networks and functions of FIT-binding proteins in iron deficiency responses and homeostasis in root epidermis cells (upper part) and stele cells (lower part). In root epidermal cells, Ib bHLHs, MED16, MED25, EIN3/EIL1, and CIPK11 as positive modulators interacts with the key regulator FIT, functioning in activation of the expression of iron acquisition genes such as *FRO2* and *IRT1* under iron limitation condition, whereas DELLA, ZAT12, and IVa bHLHs as negative modulators compete with Ib bHLHs to bind FIT for negative regulation of FIT activity for avoidance of excessive iron uptake. In stele cells, FBP as a negative regulator sequestered FIT to obstruct the heterodimer formation of FIT with Ib bHLH protein to downregulate the expression of *NAS1*, *NAS2,* and *NAS4* for balancing Fe and Zn homeostasis in Arabidopsis under low iron or high Zn stress condition. The rectangles represent transcripts of the corresponding genes, and the ovals mean proteins indicated. The blue and orange color depicted positive and negative regulators, respectively. The solid and dotted lines separately indicate the known and unknown regulation processes.

demonstrated that the EAR motif of ZAT12 interacted with FIT-C terminus. Based on the result that *FIT* expression was down-regulated and *ZAT12* expression was up-regulated under iron deficiency with H_2O_2 stress, ZAT12 should be a repressor of FIT. The formation of FIT-ZAT12 complexes in root cells would inactivate the FIT under prolonged Fe deficiency condition.

DELLA

Iron deficiency will trigger obvious changes in root architecture, such as reduced primary root length and increased frequency of root hairs, as well as high affinity iron uptake mechanism. Exogenous gibberellin (GA) treatment has been shown to promote the expression of *IRT1*, *FRO2*, *bHLH38,* and *bHLH39* in the GA-deficient mutant *ga3ox1ga3ox2* (the double-knockout mutant of GA biosynthetic gene *GA3OX1* and *GA3OX2* which are involved in later steps of the gibberellic acid biosynthesis), although the expression of *FIT* was not induced by the application of GA (Matsuoka et al., 2014). Recently, Wild et al. (2016) demonstrated that GA signaling was involved in the iron deficiency response by interaction of DELLA with protein FIT, bHLH38, and bHLH39. DELLA-FIT interaction did not interfere with the formation of FIT-Ib bHLH heterodimer, but impaired the binding capacity of the FIT-Ib bHLH complex to corresponding promoters. DELLA protein exists in all tissues of root under normal condition. Under iron deficiency, DELLA protein will accumulate in the root meristem to repress the root growth, and degrade in the epidermis cells of the differentiation zone, relieving FIT from the DELLA-FIT complex for activating the expression of iron uptake genes (Wild et al., 2016).

FBP

Under iron deficiency, plants will upregulate the expression of Fe transporter *IRT1* in strategy I plants. Due to the low substrate specificity of IRT1 protein, other divalent transition metals, such as Zn, will be transported into root cells. Thus, the excessive Zn will be acquired into root cells from the environment, and result in toxicity to the plant under the condition of iron limitation. To keep the Zn balance and detoxify in cells, plant will up-regulate the expression of some genes related to sequestration and chelation of Zn. Chen et al. (2018) used yeast-two-hybrid approach and identified a novel FIT-binding protein (FBP), which is involved in the distribution and balance of Fe and Zn homeostasis. They confirmed that FBP sequestered FIT to obstruct the heterodimer formation of FIT with Ib bHLH protein in the root stele and negatively regulated the expression of *NAS1, NAS2,* and *NAS4* genes to balance the Fe and Zn homeostasis in Arabidopsis. FBP transcript abundance significantly reduced along with increased Zn concentration. The plants with loss function of *FBP* displayed the elevated expression of *NAS* genes, and tolerance to excessive Zn stress (Chen et al., 2018). Further, they did DNA-protein binding and transcriptional activation analysis, and confirmed that FBP inhibited the binding of FIT-Ib bHLH heterodimer to the promoters of *NAS* genes. The negative regulation caused by sequestration of FIT is restricted in the root stele, but not in epidemic cells, because *FBP* only expressed in the root stele. Considering that FIT protein accumulation was comparable in roots of *FBP*-null mutant *fbp* with wild type under high Zn condition (Chen et al., 2018), the main function of FBP looks like to inactivate FIT by blocking heterodimer formation with Ib bHLH proteins, but not for its degradation.

IVa bHLH Transcription Factors

Jasmonic acid (JA) as a negative factor represses the upregulated expression of *FIT*, *IRT1* and *FRO2* under iron deficiency (Maurer et al., 2011). The depressed regulation mechanism has been elucidated recently. Cui et al. (2018) identified the IVa subgroup of bHLH transcription factors (bHLH18, bHLH19, bHLH20, and bHLH25), which are involved in the repressed regulation of iron deficiency responses under JA present. The four IVa bHLH genes expressed mainly in roots and responded to JA. Characterization of the single, double, triple and quadruple mutants of the four IVa bHLH genes revealed that the four bHLH transcription factors functioned redundantly in the JA-mediated inhibition of iron acquisition in Arabidopsis. Immunoblot analysis showed that bHLH18, bHLH19, bHLH20, and bHLH25 interacted with FIT and promoted its degradation mediated by JA under iron deficiency. Based on that the plants overexpressing Ib bHLH genes can alleviate JA-mediated FIT protein degradation, and exhibit more tolerance to iron deficiency under JA present, Cui et al. (2018) speculated that the main function of the four IVa bHLH proteins might be to compete with Ib bHLH proteins to bind FIT and stimulates its degradation. Further, they demonstrated that JA-promoted degradation of the FIT protein is through the 26S proteasome pathway. Additionally, they showed that MYC2 and JAR1, critical components of the JA signaling pathway, differentially regulated the expression of *bHLH18*, *bHLH19*, *bHLH20,* and bHLH25 to modulate FIT protein accumulation, and MYC2 depressed the expression of *FIT* and the four Ib bHLH genes at transcription level. Taken together, upregulated expression of IVa bHLH genes and downregulated expression of *FIT* and Ib bHLH genes under JA present result in lower accumulation of activators FIT and Ib bHLH proteins, consequently downregulating the expression of the iron-uptake genes *IRT1* and *FRO2*. Considering that JA is an important

integrator that balances plant growth and defense responses, the JA-mediated suppression of iron acquisition in plants should play some important roles in defense responses against biotic and abiotic stresses to promote plant survival.

CONCLUSION

As described above, the proteins encoded by 15 different genes have been confirmed to bind FIT during last several years in Arabidopsis. Their functions can be generally summarized into three categories, and outlined in **Figure 1**. The first group contains the four Ib bHLH proteins, CIPK11, MED16, EIN3, and EIL1. The eight proteins as positive regulators bind to FIT, and function as stabilizer and activator of FIT in iron deficiency responses and homeostasis. The second one is the four IVa bHLH proteins mediated by JA signal pathway and ZAT12. They play as negative regulators to enhance the degradation of FIT protein via interaction with FIT. The last group includes DELLA and FBP, which compete with Ib bHLH proteins to bind FIT, and inactivate its functions. These findings obviously reveal a new insight for understanding the regulation mechanisms of iron uptake and homeostasis in strategy I plants. Although a great progress has been made in studying the molecular regulation mechanisms of iron deficiency responses and homeostasis in strategy I plants in the past two decades, there are still many questions that are not answered. For example, iron uptake and homeostasis are tightly regulated dependent on iron status in plants, how does plant sense the iron status in cells and in environment, and how is the iron signal transduced in plants? As shown in **Figure 1**, some proteins, such as DELLA and FBP, involved in iron deficiency responses and homeostasis function only in a specific region or cell type of root, we still do not know what is the molecular mechanism(s) accurately controlling their spatial expression and functional patterns. As a key regulator, expression of *FIT* is controlled at transcriptional and posttranscriptional level. However, we do still not well know the regulation mechanisms.

AUTHOR CONTRIBUTIONS

Both authors listed have made a substantial, direct and intellectual contribution to the work, and approved it for publication.

FUNDING

This work was supported by the National Natural Science Foundation of China (Grant No. 31870225).

REFERENCES

Asturias, F. J., Jiang, Y. W., Myers, L. C., Gustafsson, C. M., and Kornberg, R. D. (1999). Conserved structures of mediator and RNA polymerase II holoenzyme. *Science* 283, 985–987. doi: 10.1126/science.283.5404.985

Bäckström, S., Elfving, N., Nilsson, R., Wingsle, G., and Bjorklund, S. (2007). Purification of a plant mediator from *Arabidopsis thaliana* identifies PFT1 as the Med25 subunit. *Mol. Cell.* 26, 717–729. doi: 10.1016/j.molcel.2007.05.007

Chen, C. L., Cui, Y., Cui, M., Zhou, W. J., Wu, H. L., and Ling, H. Q. (2018). A FIT-binding protein is involved in modulating iron and zinc homeostasis in Arabidopsis. *Plant Cell Environ.* 41, 1698–1714. doi: 10.1111/pce.13321

Cheng, X., Zhang, D., Cheng, Z., Keller, B., and Ling, H. Q. (2009). A new family of Ty1-copia-like retrotransposons originated in the tomato genome by a recent horizontal transfer event. *Genetics* 181, 1183–1193. doi: 10.1534/genetics.108.099150

Colangelo, E. P., and Guerinot, M. L. (2004). The essential basic helix-loop-helix protein FIT1 is required for the iron deficiency response. *Plant Cell* 16, 3400–3412. doi: 10.1105/tpc.104.024315

Cui, Y., Chen, C. L., Cui, M., Zhou, W. J., Wu, H. L., and Ling, H. Q. (2018). Four IVa bHLH transcription factors are novel interactors of FIT and mediate JA inhibition of iron uptake in Arabidopsis. *Mol. Plant* 11, 1166–1183. doi: 10.1016/j.molp.2018.06.005

Curie, C., Panaviene, Z., Loulergue, C., Dellaporta, S. L., Briat, J.-F., and Walker, E. L. (2001). Maize yellow stripe1 encodes a membrane protein directly involved in Fe (III) uptake. *Nature* 409, 346–349. doi: 10.1038/35053080

Fan, H., Zhang, Z., Wang, N., Cui, Y., Sun, H., Liu, Y., et al. (2013). SKB1/PRMT5 mediated histone H4R3 dimethylation of Ib subgroup bHLH genes negatively regulates iron homeostasis in *Arabidopsis thaliana*. *Plant J.* 77, 209–221. doi: 10.1111/tpj.12380

Fourcroy, P., Siso-Terraza, P., Sudre, D., Saviron, M., Reyt, G., Gaymard, F., et al. (2014). Involvement of the ABCG37 transporter in secretion of scopoletin and derivatives by Arabidopsis roots in response to iron deficiency. *New Phytol.* 201, 155–167. doi: 10.1111/nph.12471

Gratz, R., Manishankar, P., Ivanov, R., Koster, P., Mohr, I., Trofimov, K., et al. (2019). CIPK11-dependent phosphorylation modulates FIT activity to promote Arabidopsis iron acquisition in response to calcium signaling. *Dev. Cell* 48, 726–740. doi: 10.1016/j.devcel.2019.01.006

Hansch, R., and Mendel, R. R. (2009). Physiological functions of mineral micronutrients (Cu, Zn, Mn, Fe, Ni, Mo, B, Cl). *Curr. Opin. Plant Biol.* 12, 259–266. doi: 10.1016/j.pbi.2009.05.006

Ivanov, R., Brumbarova, T., and Bauer, P. (2011). Fitting into the harsh reality: regulation of iron deficiency responses in dicotyledonous plants. *Mol. Plant* 5, 27–42. doi: 10.1093/mp/ssr065

Jakoby, M., Wang, H. Y., Reidt, W., Weisshaar, B., and Bauer, P. (2004). FRU (BHLH029) is required for induction of iron mobilization genes in *Arabidopsis thaliana*. *FEBS Lett.* 577, 528–534. doi: 10.1016/j.febslet.2004.10.062

Jeong, J., and Guerinot, M. L. (2009). Homing in on iron homeostasis in plants. *Trends Plant Sci.* 14, 280–285. doi: 10.1016/j.tplants.2009.02.006

Le, C. T., Brumbarova, T., Ivanov, R., Stoof, C., Weber, E., Mohrbacher, J., et al. (2016). Zinc finger of *Arabidopsis thaliana*12 (ZAT12) interacts with fer-LIKE iron deficiency-induced transcription factor (FIT) linking iron deficiency and oxidative stress responses. *Plant Physiol.* 170, 540–557. doi: 10.1104/pp.15.01589

Li, L., Cheng, X., and Ling, H. Q. (2004). Isolation and characterization of Fe(III)-chelate reductase gene LeFRO1 in tomato. *Plant Mol. Biol.* 54, 125–136. doi: 10.1023/b:plan.0000028774.82782.16

Li, X., Zhang, H., Ai, Q., Liang, G., and Yu, D. (2016). Two bHLH transcription factors, bHLH34 and bHLH104, regulate iron homeostasis in *Arabidopsis thaliana*. *Plant Physiol.* 170, 2478–2493. doi: 10.1104/pp.15.01827

Liang, G., Zhang, H., Li, X., Ai, Q., and Yu, D. (2017). bHLH transcription factor bHLH115 regulates iron homeostasis in *Arabidopsis thaliana*. *J. Exp. Bot.* 68, 1743–1755. doi: 10.1093/jxb/erx043

Ling, H. Q., Bauer, P., Bereczky, Z., Keller, B., and Ganal, M. (2002). The tomato fer gene encoding a bHLH protein controls iron-uptake responses in roots. *Proc. Natl. Acad. Sci. U.S.A.* 99, 13938–13943. doi: 10.1073/pnas.212448699

Lingam, S., Mohrbacher, J., Brumbarova, T., Potuschak, T., Fink-Straube, C., Blondet, E., et al. (2011). Interaction between the bHLH transcription factor FIT and ethylene insensitive3/ethylene insensitive3-like1 reveals molecular linkage between the regulation of iron acquisition and ethylene signaling in Arabidopsis. *Plant Cell* 23, 1815–1829. doi: 10.1105/tpc.111.084715

Mai, H. J., Pateyron, S., and Bauer, P. (2016). Iron homeostasis in *Arabidopsis thaliana*: transcriptomic analyses reveal novel FIT-regulated genes, iron deficiency marker genes and functional gene networks. *BMC Plant Biol.* 16:211. doi: 0.1186/s12870-016-0899-9

Marschner, H., Römheld, V., and Kissel, M. (1986). Different strategies in higher plants in mobilization and uptake of iron. *J. Plant Nutr.* 9, 695–713. doi: 10.1080/01904168609363475

Mathur, S., Vyas, S., Kapoor, S., and Tyagi, A. K. (2011). The mediator complex in plants: structure, phylogeny and expression profiling of representative genes in a dicot (*Arabidopsis thaliana*) and a monocot (*Oryza sativa*) during reproduction and abiotic stress. *Plant Physiol.* 157, 1609–1627. doi: 10.1104/pp.111.188300

Matsuoka, K., Furukawa, J., Bidadi, H., Asahina, M., Yamaguchi, S., and Satoh, S. (2014). Gibberellin-induced expression of Fe uptake-related genes in Arabidopsis. *Plant Cell Physiol.* 55, 87–98. doi: 10.1093/pcp/pct160

Maurer, F., Muller, S., and Bauer, P. (2011). Suppression of fe deficiency gene expression by jasmonate. *Plant Physiol. Biochem.* 49, 530–536. doi: 10.1016/j.plaphy.2011.01.025

Maurer, F., Naranjo Arcos, M. A., and Bauer, P. (2014). Responses of a triple mutant defective in three iron deficiency-induced basic helix-loop-helix genes of the subgroup Ib (2) to iron deficiency and salicylic acid. *PLoS One* 9:e99234. doi: 10.1371/journal.pone.0099234

Meiser, J., Lingam, S., and Bauer, P. (2011). Posttranslational regulation of the iron deficiency basic helix-loop-helix transcription factor FIT is affected by iron and nitric oxide. *Plant Physiol.* 157, 2154–2166. doi: 10.1104/pp.111.183285

Mittler, R., and Blumwald, E. (2015). The roles of ROS and ABA in systemic acquired acclimation. *Plant Cell* 27, 64–70. doi: 10.1105/tpc.114.133090

Mori, S., and Nishizawa, N. (1987). Methionine as a dominant precursor of phytosiderophores in graminaceae plants. *Plant Cell Physiol.* 28, 1081–1092.

Ranieri, A., Castagna, A., Baldan, B., and Soldatini, G. F. (2001). Iron deficiency differently affects peroxidase isoforms in sunflower. *J. Exp. Bot.* 52, 25–35. doi: 10.1093/jxb/52.354.25

Robinson, N. J., Procter, C. M., Connolly, E. L., and Guerinot, M. L. (1999). A ferric-chelate reductase for iron uptake from soils. *Nature* 397, 694–697. doi: 10.1038/17800

Römheld, V., and Marschner, H. (1986). Evidence for a specific uptake system for iron phytosiderophores in roots of grasses. *Plant Physiol.* 80, 175–180. doi: 10.1104/pp.80.1.175

Santi, S., and Schmidt, W. (2009). Dissecting iron deficiency-induced proton extrusion in Arabidopsis roots. *New Phytol.* 183, 1072–1084. doi: 10.1111/j.1469-8137.2009.02908.x

Schmidt, W. (2003). Iron solutions: acquisition strategies and signaling pathways in plants. *Trends Plant Sci.* 8, 188–193. doi: 10.1016/s1360-1385(03)00048-7

Shin, R., Berg, R. H., and Schachtman, D. P. (2005). Reactive oxygen species and root hairs in Arabidopsis root response to nitrogen, phosphorus and potassium deficiency. *Plant Cell Physiol.* 46, 1350–1357. doi: 10.1093/pcp/pci145

Sivitz, A., Grinvalds, C., Barberon, M., Curie, C., and Vert, G. (2011). Proteasome mediated turnover of the transcriptional activator FIT is required for plant iron-deficiency responses. *Plant J.* 66, 1044–1052. doi: 10.1111/j.1365-313X.2011.04565.x

Sivitz, A. B., Hermand, V., Curie, C. V., and Vert, G. (2012). Arabidopsis bHLH100 and bHLH101 control iron homeostasis via a FIT-independent pathway. *PLoS One* 7:e44843. doi: 10.1371/journal.pone.0044843

Sun, B., Jing, Y., Chen, K., Song, L., Chen, F., and Zhang, L. (2007). Protective effect of nitric oxide on iron deficiency-induced oxidative stress in maize (Zea mays). *J. Plant Physiol.* 164, 536–543. doi: 10.1016/j.jplph.2006.02.011

Takagi, S., Nomoto, K., and Takemoto, T. (1984). Physiological aspect of mugineic acid, a possible phytosiderophore of graminaceous plants. *J. Plant Nutr.* 7, 469–477. doi: 10.1080/01904168409363213

Tian, Q., Zhang, X., Yang, A., Wang, T., and Zhang, W. H. (2016). CIPK23 is involved in iron acquisition of Arabidopsis by affecting ferric chelate reductase activity. *Plant Sci.* 246, 70–79. doi: 10.1016/j.plantsci.2016.01.010

Vert, G., Grotz, N., Dedaldechamp, F., Gaymard, F., Guerinot, M. L., Briat, J. F., et al. (2002). IRT1, an Arabidopsis transporter essential for iron uptake from the soil and for plant growth. *Plant Cell* 14, 1223–1233. doi: 10.1105/tpc.001388

Vorwieger, A., Gryczka, C., Czihal, A., Douchkov, D., Tiedemann, J., Mock, H. P., et al. (2007). Iron assimilation and transcription factor controlled synthesis of riboflavin in plants. *Planta* 226, 147–158. doi: 10.1007/s00425-006-0476-9

Wang, H. Y., Klatte, M., Jakoby, M., Baumlein, H., Weisshaar, B., and Bauer, P. (2007). Iron deficiency-mediated stress regulation of four subgroup Ib BHLH genes in *Arabidopsis thaliana*. *Planta* 226, 897–908. doi: 10.1007/s00425-007-0535-x

Wang, N., Cui, Y., Liu, Y., Fan, H., Du, J., Huang, Z., et al. (2013). Requirement and functional redundancy of Ib subgroup bHLH proteins for iron deficiency responses and uptake in *Arabidopsis thaliana*. *Mol. Plant* 6, 503–513. doi: 10.1093/mp/sss089

Wild, M., Davie're, J.-M., Regnault, T., Sakvarelidze-Achard, L., Carrera, E., Lopez Diaz, I., et al. (2016). Tissue-specific regulation of gibberellin signaling fine-tunes Arabidopsis iron-deficiency responses. *Dev. Cell* 37, 190–200. doi: 10.1016/j.devcel.2016.03.022

Yang, Y., Ou, B., Zhang, J. Z., Si, W., Gu, H. Y., Qin, G. J., et al. (2014). The Arabidopsis mediator subunit MED16 regulates iron homeostasis by associating with EIN3/EIL1 through subunit MED25. *Plant J.* 77, 838–851. doi: 10.1111/tpj.12440

Yuan, Y., Wu, H., Wang, N., Li, J., Zhao, W., Du, J., et al. (2008). FIT interacts with AtbHLH38 and AtbHLH39 in regulating iron uptake gene expression for iron homeostasis in Arabidopsis. *Cell Res.* 18, 385–397. doi: 10.1038/cr.2008.26

Yuan, Y. X., Zhang, J., Wang, D. W., and Ling, H. Q. (2005). AtbHLH29 of *Arabidopsis thaliana* is a functional ortholog of tomato FER involved in controlling iron acquisition in strategy I plants. *Cell Res.* 15, 613–621. doi: 10.1038/sj.cr.7290331

Zhang, J., Liu, B., Li, M., Feng, D., Jin, H., Wang, P., et al. (2015). The bHLH transcription factor bHLH104 interacts with IAA-LEUCINE RESISTANT3 and modulates iron homeostasis in Arabidopsis. *Plant Cell* 27, 787–805. doi: 10.1105/tpc.114.132704

Zhang, X., Wang, C., Zhang, Y., Sun, Y., and Mou, Z. (2012). The Arabidopsis mediator complex subunit16 positively regulates salicylate-mediated systemic acquired resistance and jasmonate/ethylene-induced defense pathways. *Plant Cell* 24, 4294–4309. doi: 10.1105/tpc.112.103317

Zhang, Y., Wu, H. L., Wang, N., Fan, H. J., Chen, C. L., Cui, Y., et al. (2014). Mediator subunit 16 functions in the regulation of iron uptake gene expression in Arabidopsis. *New Phytol.* 203, 770–783. doi: 10.1111/nph.12860

Zhao, W., Cheng, X., Huang, Z., Fan, H., Wu, H., and Ling, H. Q. (2011). Tomato LeTHIC is an Fe-requiring HMP-P synthase involved in thiamine synthesis and regulated by multiple factors. *Plant Cell Physiol.* 52, 967–982. doi: 10.1093/pcp/pcr048

Conflict of Interest Statement: The authors declare that the research was conducted in the absence of any commercial or financial relationships that could be construed as a potential conflict of interest.

frontiers in Plant Science

ORIGINAL RESEARCH
published: 12 July 2019
doi: 10.3389/fpls.2019.00907

The Conservation of VIT1-Dependent Iron Distribution in Seeds

Seckin Eroglu[1], Nur Karaca[2], Katarina Vogel-Mikus[3,4], Anja Kavčič[3], Ertugrul Filiz[5] and Bahattin Tanyolac[2]*

[1] Department of Genetics and Bioengineering, Izmir University of Economics, Izmir, Turkey, [2] Department of Bioengineering, Ege University, Izmir, Turkey, [3] Department of Biology, University of Ljubljana, Ljubljana, Slovenia, [4] Jozef Stefan Institute, Ljubljana, Slovenia, [5] Department of Crop and Animal Production, Cilimli Vocational School, Duzce University, Duzce, Turkey

One third of people suffer from anemia, with iron (Fe) deficiency being the most common reason. The human diet includes seeds of staple crops, which contain Fe that is poorly bioavailable. One reason for low bioavailability is that these seeds store Fe in cellular compartments that also contain antinutrients, such as phytate. Thus, several studies have focused on decreasing phytate concentrations. In theory, as an alternative approach, Fe reserves might be directed to cellular compartments that are free of phytate, such as plastids. However, it is not known if seed plastid can represent a major Fe storage compartment in nature. To discover distinct types of Fe storage in nature, we investigated metal localizations in the seeds of more than twenty species using histochemical or X-ray based techniques. Results showed that in Rosids, the largest clade of eudicots, Fe reserves were primarily confined to the embryo of the seeds. Furthermore, inside the embryos, Fe accumulated specifically in the endodermal cell layer, a well-known feature that is mediated by VACUOLAR IRON TRANSPORTER1 (VIT1) in model plant *Arabidopsis thaliana*. In rice, Fe enrichment is lost around the provasculature in the mutants of VIT1 orthologs. Finally, in *Carica papaya*, Fe accumulated in numerous organelles resembling plastids; however, these organelles accumulated reserve proteins but not ferritin, failing to prove to be plastids. By investigating Fe distribution in distinct plant lineages, this study failed to discover distinct Fe storage patterns that can be useful for biofortification. However, it revealed Fe enrichment is widely conserved in the endodermal cell layer in a VIT1-dependent manner in the plant kingdom.

Keywords: biofortification, seed, iron, metal, vit1, plastid, synchrotron, homeostasis

OPEN ACCESS

Edited by:
Thomas J. Buckhout, Humboldt University of Berlin, Germany

Reviewed by:
Louis Grillet, Academia Sinica, Taiwan
James Connorton, John Innes Centre (JIC), United Kingdom

****Correspondence:***
Seckin Eroglu
erogluseckin@gmail.com

Specialty section:
This article was submitted to Plant Nutrition, a section of the journal Frontiers in Plant Science

Received: *19 December 2018*
Accepted: *26 June 2019*
Published: *12 July 2019*

Citation:
Eroglu S, Karaca N, Vogel-Mikus K, Kavčič A, Filiz E and Tanyolac B (2019) The Conservation of VIT1-Dependent Iron Distribution in Seeds. Front. Plant Sci. 10:907. doi: 10.3389/fpls.2019.00907

INTRODUCTION

One third of people suffer from anemia, with iron (Fe) deficiency being the most common reason (Kassebaum et al., 2014). Human diets are largely based on plants, which are often a poor source of Fe (Gibson et al., 2010). This is because corn, wheat, and rice kernels contain low concentrations of total Fe, and a large part of it cannot be absorbed by the human digestive system (Borg et al., 2009). To combat Fe deficiency, increasing bioavailable Fe (biofortification) of seeds has been suggested as the most sustainable approach (Shahzad et al., 2014).

Classical breeding, genetic engineering and other methods have been applied to increase Fe concentration in seeds (Murgia et al., 2012). Classical breeding has resulted in limited success, especially when natural cultivars show low variability in seed Fe levels. Genetic engineering

methods have been shown to successfully increase Fe levels in major crops such as rice and wheat (Lee et al., 2009; Connorton et al., 2017). This increase has been mainly achieved by overexpressing proteins that boost the Fe storage capacity of the cells, eventually forcing the mother plant to divert more Fe into the seeds. Most of the biofortification approaches have targeted increasing concentration of Fe, but its low bioavailability is another major concern.

Bioavailability determines the portion of Fe that can be absorbed by the human digestive system. Fe absorption is affected by the form of Fe, which may lead to less than ten percent of the total Fe intake (Hurrell and Egli, 2010). Staple crop species accumulate Fe in cells that contain metal binding molecules, with phytate being the most important. Fe releases from phytate due to the presence of phytases to support germination (Hegeman and Grabau, 2001). However, humans do not possess phytase, therefore phytates act as antinutrients to humans. To increase Fe bioavailability, several studies have aimed at decreasing phytate concentrations (Shi et al., 2007; Reddy et al., 2017). Such a decrease has been achieved but at the expense of growth (Warkentin et al., 2012). An alternative approach could be to redirect Fe from phytate-containing compartments to phytate-free compartments. In nature, at a subcellular level, Fe accumulates in vacuoles, plastids, cytosol or elsewhere (Otegui et al., 2002; Cvitanich et al., 2010). In vacuoles, Fe accumulates in globules where it binds to phytate (Davila-Hicks et al., 2004; Lanquar et al., 2005). In plastids, Fe binds to ferritin protein (Waldo et al., 1995; Briat et al., 2010). In contrast to phytate-bound Fe, ferritin-bound Fe is bioavailable (Davila-Hicks et al., 2004). Thus, optimizing seed Fe for human nutrition requires not only increasing Fe concentration but also its bioavailability, which is strictly dependent on its subcellular level distribution.

The advances in Fe imaging techniques have allowed detailed investigations of Fe localization in the small seeds of *Arabidopsis thaliana* (Eroglu, 2018). The X-ray synchrotron fluorescence imaging technique identified nonhomogenous distribution of Fe throughout the embryo and revealed an Fe-enriched hotspot around the provascular strands (Kim et al., 2006). However, the emerging technique failed to pinpoint the specific cells that are overaccumulating Fe. Such a resolution has been achieved with the use of an enhanced version of classical Perls staining, namely, Perls/DAB (Roschzttardtz et al., 2009). Perls/DAB revealed that the Fe enrichment around provascular strands is confined to endodermal cells (Roschzttardtz et al., 2009; Ramos et al., 2013).

The genetic basis of endodermal Fe accumulation has been tackled by the comparison of T-DNA insertion mutants of *A. thaliana*. Two individual lines lost the endodermal Fe enrichment when mutated in the *VACUOLAR IRON TRANSPORTER1 (VIT1)* gene (Kim et al., 2006; Eroglu et al., 2017). *VIT1* localized to the tonoplast, expressed in the stele, and complemented the Fe hypersensitivity of yeast when expressed heterologously; suggesting it imports Fe into the vacuoles of endodermal cells (Kim et al., 2006). Disruption of VIT1 relocalized Fe from the endodermal to the subepidermal cell layer in *vit1* mutants. *vit1* mutants further lost the subepidermal Fe enrichment when mutated in *METAL TOLERANCE PROTEIN8 (MTP8)* (Eroglu et al., 2016, 2017; Eroglu, 2018). Similar to *VIT1*, *MTP8* localized to the tonoplast and complemented the Fe hypersensitivity of yeast (Eroglu et al., 2017). The disruption of *VIT1* and *MTP8* together relocalized Fe throughout the embryo homogeneously. In conclusion, analysis of loss-of-function mutants of *A. thaliana* shows that metal transporters determine where metals will be stored in the mature seed. This indicates that if a suitable Fe transporter protein is used, it might be possible to direct Fe to certain organelles that are free of antinutrients.

Our research aim was to identify a seed Fe transporter that can be useful to direct Fe to the plastids. *A. thaliana* accumulates Fe almost exclusively inside the vacuoles, therefore failing to be a suitable model for such an approach. Fe distribution in the seeds of other plants is poorly known. To find plastid targeting Fe transporters, we screened Fe distributions in seeds belonging to distinct plant lineages. Based on what is known from the model plant, we hypothesized that Fe concentrated regions will indicate the presence of a transporter. To this end, we examined the seeds of more than 20 different species belonging to several different plant orders by using Perls/DAB histochemical staining or synchrotron X-ray fluorescence spectroscopy.

MATERIALS AND METHODS

Collection of Seeds

Seeds were obtained from gene banks, local suppliers, or personally collected (**Table 1**). Rice T−DNA insertion mutants *vit1-1* (*Os04g0463400* Zhonghua11 background) and *vit2-1* (Knock out line of Os09g0396900, Dongjin genetic background) and wild type (Dongjin) were courtesy of Dr. Ji-Ming Gong (Zhang et al., 2012).

Perls Staining and DAB/H_2O_2 Intensification (Perls/DAB)

Wherever possible (embryos were large, could easily be isolated, seed coat was sufficiently soft to be cut, and high magnification was not needed), samples were directly (i.e., without fixation) stained by Perls (**Figures 4A,B**) or Perls/DAB (**Figures 2C**, **3D**) (Roschzttardtz et al., 2009). In other cases, *in situ* protocol was used. For direct Perls staining, samples were vacuum infiltrated in 4% (v/v) HCl and 4% (w/v) K-ferrocyanide (Perls stain solution) for 15 min and incubated for 30 min at room temperature (Stacey et al., 2008). If the Fe signal was weak, it was intensified using DAB (Roschzttardtz et al., 2009). Perls-stained samples were incubated in a methanol solution containing 0.01 M NaN_3 and 0.3% (v/v) H_2O_2 for 1 h, and then washed with 0.1 M phosphate buffer (pH 7.4). For the intensification reaction, samples were incubated between 10 and 30 min in a 0.1 M phosphate buffer (pH 7.4) solution containing 0.025% (w/v) DAB, 0.005% (v/v) H_2O_2, and 0.005% (w/v) $CoCl_2$. The reaction was stopped by rinsing with distilled water.

For *in situ* Perls staining, seeds were first fixed in 10% formalin and then dehydrated in an ethanol series (30%, 40%,. . ., 100%). Seeds were cleared with xylene. Seeds that were still

TABLE 1 | Seeds used in the study.

Species	Source
Linum usitatiss	National Genebank, Menemen, Turkey
Medicago truncatula	National Genebank, Menemen, Turkey
Cucumis sativus	National Genebank, Menemen, Turkey
Citrullus lanatus	National Genebank, Menemen, Turkey
Cannabis sativa	National Genebank, Menemen, Turkey
Euonymus europaeus	National Genebank, Menemen, Turkey
Alyssum sibiricum	National Genebank, Menemen, Turkey
Brassica oleracea	National Genebank, Menemen, Turkey
Gossypium arboreum	National Genebank, Menemen, Turkey
Batis maritima	Kew Gardens, London, England
Moringa peregrina	Kew Gardens, London, England
Eucalyptus elata	Kew Gardens, London, England
Geranium carolinianum	Kew Gardens, London, England
Brassica napus	Genebank, Gatersleben, Germany
Limnanthes douglasii	Botanischer Garten, Marburg, Germany
Arabidopsis thaliana	Arabidopsis Biological Resource Center, Ohio, United States
Reseda lutea	Personally collected*
Noccaea praecox	Personally collected**
Carica papaya	Commercial
Arachis hypogaea	Commercial
Solanum lycopersicum	Commercial
Capparis spinosa	Commercial

**Çilden et al., 2018* ***Collected from Pb, Zn polluted site, Mežica, Slovenia (Vogel-Mikus et al., 2005).*

too hard to cut were further incubated in 20% formic acid for 45 min. Seeds were then embedded in wax and 10–30 μm sections were cut. Sections were deparaffinized by incubation at 65°C for 15 min following a xylene treatment for 15 min, and were stained with Perls/DAB according to Roschzttardtz et al. (2009). Sections were treated with 4% (v/v) HCl and 4% (w/v) K-ferrocyanide (Perls stain solution) for 15 min and incubated for 30 min at room temperature (Stacey et al., 2008). DAB intensification was applied as described in Meguro et al. (2007). For the intensification reaction, the sections were incubated between 10 and 30 min in a 0.1 M phosphate buffer (pH 7.4) solution containing 0.025% (w/v) DAB (Sigma), 0.005% (v/v) H_2O_2, and 0.005% (w/v) $CoCl_2$ (intensification solution). The reaction was stopped by rinsing samples with distilled water. Samples were imaged with a light microscope (Axioskop; Carl Zeiss, Jena, Germany).

For iodine staining, sections were stained with Gram's iodine solution (6.7 g potassium iodide and 3.3 g iodine dissolved in 1L H2O; Ward's science) for at least 5 s.

For Naphthol Blue–Black staining of proteins, slides were placed in 0.1% (w/v) Naphthol Blue–Black, 10% (v/v) acetic acid for 5 min. For immunohistochemistry, after deparaffinization, tissues were rehydrated by ethanol series and hybridization was conducted according to Paciorek et al. (2006). Anti-rabbit secondary antibody was conjugated with Alexa-488 and was used with 1:800 dilution (Jackson ImmunoResearch, West Grow, PA, United States).

X-Ray Fluorescence

X-ray fluorescence imaging of *Brassica napus*, *Moringa peregrine*, and *Euonymus europaeus* was performed at XRF beamline of Synchrotron Elettra (Karydas et al., 2018) on 60 μm seed cross-sections. The seeds were imbibed overnight at 4°C, flash frozen in propane cooled with liquid nitrogen, embedded in tissue freezing medium (Leica, Germany), and cut using CM3060 Leica Cryostat (Vogel-Mikuš et al., 2014). The sections were sandwiched between two 2.5 μm Mylar foil and scanned by 75 × 75 μm beam at an excitation energy of 10 KeV. Obtained XRF spectra were fitted by PyMCA software (Solé et al., 2007) and quantified (Kump and Vogel-Mikuš, 2018). Imaging of element distribution in *Noccaea praecox* was performed by micro-PIXE as described (Vogel-Mikus et al., 2007; Vogel-Mikuš et al., 2008).

Bioinformatics Analyses

VIT1 protein sequences were derived from the Phytozome database 12.1.6 version[1] (Goodstein et al., 2011) for bioinformatics analyses. The following plants were included: *A. thaliana* (AT2G01770), *Carica papaya* (evm.model.supercontig_2.168), *Cucumis sativus* (Cucsa.174130.1, Cucsa.012090, and Cucsa.012100), *Linum usitatiss* (Lus10021809), *Medicago truncatula* (Medtr8g105790 and Medtr8g105810), *Eucalyptus grandis* (Eucgr.B02690, Eucgr.B02691, and Eucgr.G02084), *B. napus* (A0A078JDR3), *Gossypium arboreum* (A0A0B0MD68), *Arachis duranensis* (XP_020996537.1), *Arachis ipaensis* (XP_020977382.1), *Brachypodium distachyon* (Bradi4g29720 and Bradi5g12570), *Brassica rapa* (Brara.B03068 and Brara.F03456), *Chlamydomonas reinhardtii* (Cre02.g099500 and Cre02.g107550), *Glycine max* (Glyma.05G24060 and Glyma.08G047500), *Gossypium raimondii* (Gorai.013G029700), *Zea mays* (GRMZM2G074672 and GRMZM2G107306), *Vitis vinifera* (GSVIVG01011628001 and GSVIVG01011629001), *Oryza sativa* (LOC_Os04g38940 and LOC_Os09g23300), *Phaseolus vulgaris* (Phvul.002G322800 and Phvul.002G322900), *Populus trichocarpa* (Potri.010G104100 and Potri.010G104200), *Physcomitrella patens* (Pp3c2_34540), *Prunus persica* (Prupe.1G335200 and Prupe.1G335300), *Sorghum bicolor* (Sobic.002G194600 and Sobic.006G109000), and *Solanum lycopersicum* (Solyc04g008060). Protein domains were detected using Pfam 31.0[2] (Finn et al., 2015). Sequence length, molecular weight, and isoelectric point (*pI*) were determined by using the ExPASy ProtParam tool[3] (Gasteiger et al., 2005). The transmembrane helices were predicted by using The HMMTOP transmembrane topology prediction server version 2.0[4] (Tusnady and Simon, 2001). The phylogenetic tree of VIT1s was constructed with MEGA 7.0.2 software (Kumar et al., 2016) using maximum likelihood (ML) method with 1000 bootstraps. The evolutionary distances were computed using the Poisson correction method (Zuckerkandl and Pauling, 1965).

[1]https://phytozome.jgi.doe.gov/pz/portal.html#
[2]https://pfam.xfam.org/
[3]https://web.expasy.org/protparam/
[4]http://www.enzim.hu/hmmtop/

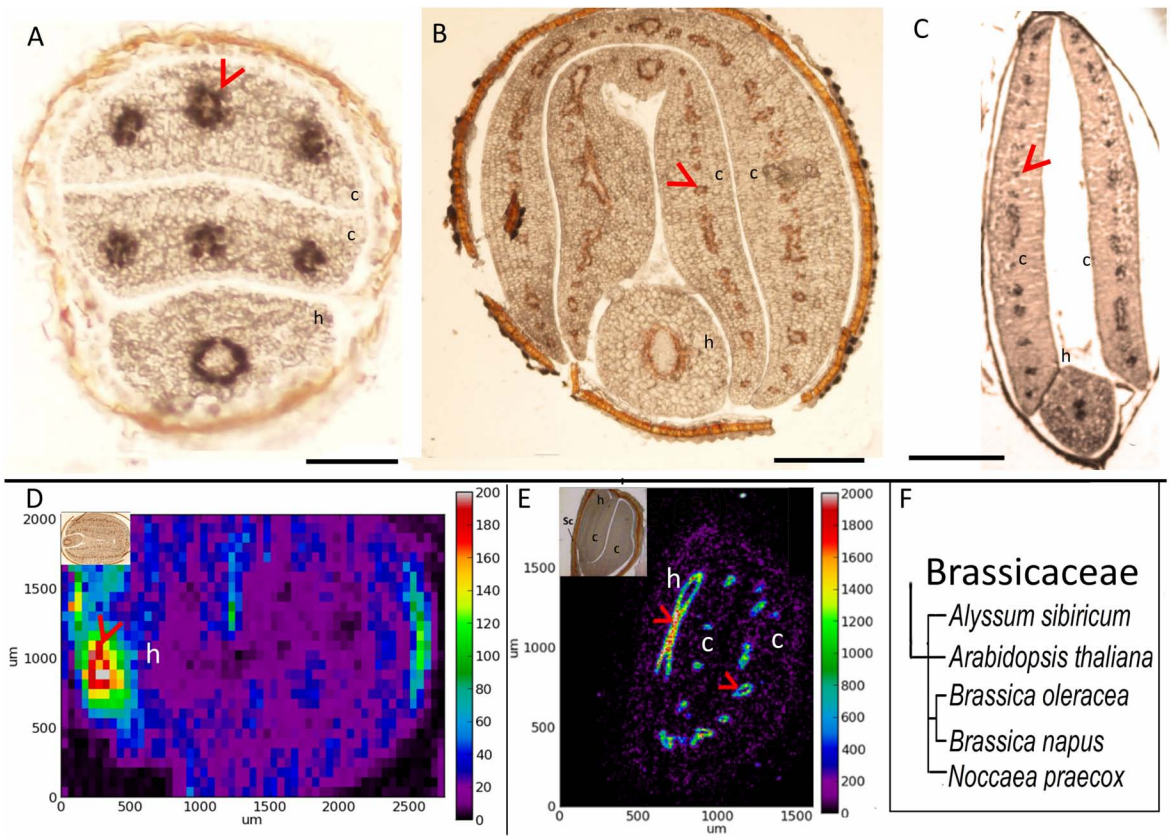

FIGURE 1 | Fe accumulates in the endodermis of Brassicaceae family. **(A–C)** Perls/DAB-stained seed cross sections. Cross sections were stained with Perls/DAB and observed under light microscope. From left to right: *Arabidopsis thaliana*, *Brassica oleracea*, and *Alyssum sibiricum*. Brown regions surrounding the embryos are seed coats. These were already brown before the staining; thus, the color does not reflect the stained Fe. Fe appeared as black stains in panels **(A)** and **(C)**, and brown in panel **(B)**. Circular-shaped staining in *Arabidopsis thaliana* corresponds to the endodermal cells surrounding the provascular strands. **(D,E)** Synchrotron X-Ray fluorescence images of relative Fe distribution in the seeds. **(D)** *Brassica napus* and **(E)** *Noccaea praecox*. **(F)** Branch of the taxonomic tree, for the whole tree refer to **Figure 8**. This branch shows species that were examined for Fe reserves in Brassicaceae family and used as a visual aid. Note that *Arabidopsis thaliana*, *Alyssum sibiricum*, and *Noccaea praecox*, consist of a single pair of cotyledons, but both *Brassica napus* and *Brassica oleracea* consist of a pair of inner and an outer cotyledons. Bar represents 0.1 mm in panel **(A)**, 0.5 mm in panels **(B,C)**. c, cotyledon; h, hypocotyl. Red arrow heads point to examples of specific Fe accumulation pattern, closed rings around provasculature of cotyledons **(A–C,E),** and hypocotyl **(D)**.

Identity values (%) of VIT1s were analyzed using the NCBI blastp tool.[5]

In silico expression data of soybean *VIT1* were obtained using the Seed Gene Network Database (www.seedgenenetwork.com). Arabidopsis *VIT1* gene number AT2G01770 was submitted. That submission returned soybean (*G. max*) GeneChip Expression Profile for Probe Set – Gma.6465.1.S1_a_at corresponding to *Glyma01g40600*. The signal data of individual experiments were obtained from the original file (Geo number: GSE46906).

RESULTS

Fe Accumulates in Endodermis in Brassicaceae Family

To investigate how Fe distribution differs between *A. thaliana* and other members of Brassicaceae, by using Perls/DAB method and X-ray synchrotron analysis, we compared Fe distribution in several different Brassicaceae species. *A. thaliana* showed circular Fe-enriched regions in cotyledons and hypocotyl (**Figure 1A**), confirming previous reports (Kim et al., 2006; Eroglu, 2018). This region corresponds to the endodermis (Roschzttardtz et al., 2009). Similar to *A. thaliana* (**Figure 1A**), all other members of Brassicaceae showed circular Fe-enriched regions, both in cotyledons and the hypocotyl (**Figures 1B–E**). Fe rings seemingly overlap the region surrounding provascular bundles, most probably endodermis, based on extrapolation from *A. thaliana*. *B. napus*, and *Brassica oleracea* contained conduplicate cotyledons (i.e., inner and outer), both of which exhibited the same Fe distribution pattern (**Figures 1B,D**). Despite the similarities in these patterns, variations were also observed between species. In contrast to *A. thaliana* (**Figure 1A**), the Fe-enriched region of *B. napus* was not confined to a single cell layer in the hypocotyl (**Figure 1C**). Furthermore, *Alyssum sibiricum* showed two adjacent Fe-enriched circles instead of one in its hypocotyl (**Figure 1D**). Taken together, results showed that

[5]https://blast.ncbi.nlm.nih.gov/Blast.cgi?PAGE=Proteins

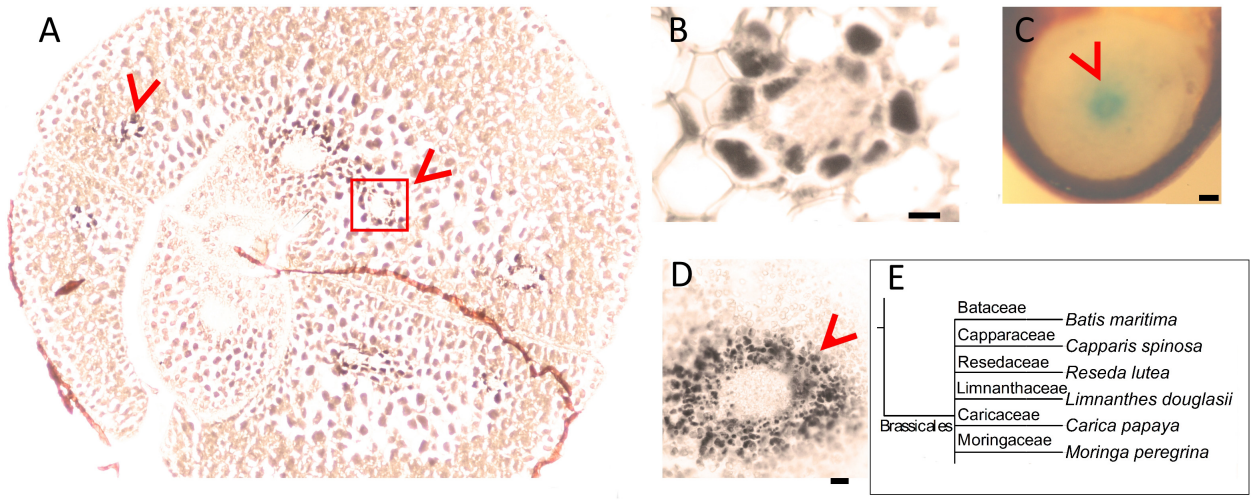

FIGURE 2 | Fe-enriched endodermis is conserved in Brassicales order. Seed cross sections were stained either with Perls or with Perls/DAB and observed under light microscope. **(A)** *Limnanthes douglasii*. **(B)** Higher magnification of the red square in panel **(A)**. **(C)** Hypocotyl of *Capparis spinosa*. **(D)** Hypocotyl of *Batis maritima*. **(B–D)** Focusses on vascular tissues. Fe staining appeared black in panels **(A,B,D)** and blue in panel **(C)**. Brown colored structure partially surrounding the embryo in panel **(A)** is the seed coat. This was already brown before the staining; thus, the color does not reflect the stained Fe. This branch shows species that were examined for Fe reserves in Brassicaceae family and used as a visual aid. Bar is 0.1 mm for panel **(A,C)**; 0.01 mm for panel **(B,D)**. **(E)** Branch of the taxonomic tree, for the whole tree refer to **Figure 8**. This branch shows species that were examined for Fe reserves in the same order but different families and used as a visual aid. Red arrow heads point to examples of specific Fe accumulation pattern, closed rings around provasculature of cotyledons **(A,B)** and hypocotyl **(C,D)**.

not only *A. thaliana,* but also other Brassicaceae species store main Fe reserves in the endodermis.

Conservation of Fe-Enriched Endodermis in the Order Brassicales

Next, we assessed whether the conserved Fe pattern in *A. thaliana* seed extends beyond the family level to the order level. We searched for ring-like Fe distribution patterns around the provasculature of either the cotyledon or the hypocotyl, which was typical of Brassicaceae. We stained distinct species belonging to Brassicales by either Perls alone (for Fe-rich samples) or with DAB intensification (for Fe-poor samples) to reach a balance in staining intensity. In *Limnanthes douglasii* embryos, all cells showed the staining. At first glance, stained cells did not exclusively correspond to the endodermis (**Figure 2A**). However, closer examination revealed that cells around the provascular bundles of cotyledons were slightly enriched with Fe (**Figure 2B**). In *Capparis spinosa*, Perls staining without DAB amplification revealed that Fe accumulated close to the central cylinder of the hypocotyl (**Figure 2C**). In *Batis maritima*, Fe accumulated in several cell layers surrounding the provasculature, including the endodermis (**Figure 2E**). Taken together, an Fe-enriched endodermis is conserved in plants at least in order level.

Fe Accumulation in the Endodermis Beyond the Order Brassicales

Brassicales with 16 other orders together constitute a large clade of flowering plants, namely, Rosids (Chase et al., 2016). We next pursued the Fe distribution in species that belong to Rosids (**Table 1**). *G. arboreum* showed ring-like Fe distribution around provasculature (**Figure 3A**), similar to typical Fe-stained endodermal cells. Furthermore, the rest of the cells were devoid of staining, indicating endodermis represented the main Fe reserves in the embryo. Likewise, *Eucalyptus elata* also showed Fe enrichment in the endodermis of the cotyledon. However, that of hypocotyl did not show the same enrichment (**Figure 3B**). We examined two species that belong to the Fagales order, namely, *M. truncatula* and *Arachis hypogaea* (**Figures 3C,D**). *M. truncatula* showed circular Fe-stained regions in the cotyledons, which represented the largest Fe pool in the embryo (**Figure 3C**). In contrast to *M. truncatula*, Fe seemingly accumulated homogeneously in *A. hypogaea* However, closer examination of *A. hypogaea* revealed provascular strands were enriched in Fe (**Figure 3D**).

Conservation of VIT1 Sequence in Species That Do Not Show an Fe-Enriched Endodermis

In *A. thaliana* seed, Fe enrichment in the endodermis is dependent on a functional VIT1 protein (Kim et al., 2006). We failed to observe an Fe-enriched endodermis in some species. To evaluate how conserved VIT1 is in these species, VIT1 protein sequences in distinct plants were compared (**Figure 4**). First, to get a general picture, 34 sequences were determined and compared from 18 plant species (**Figure 4A**). In contrast to *A. thaliana*, which had only one VIT1, most plants showed two copies. Interestingly, in *V. vinifera*, one of the two copies of VIT1 clustered with monocot VITs in the phylogenetic tree. *E. grandis* contained three homologs of VIT1, one of which was distinctly

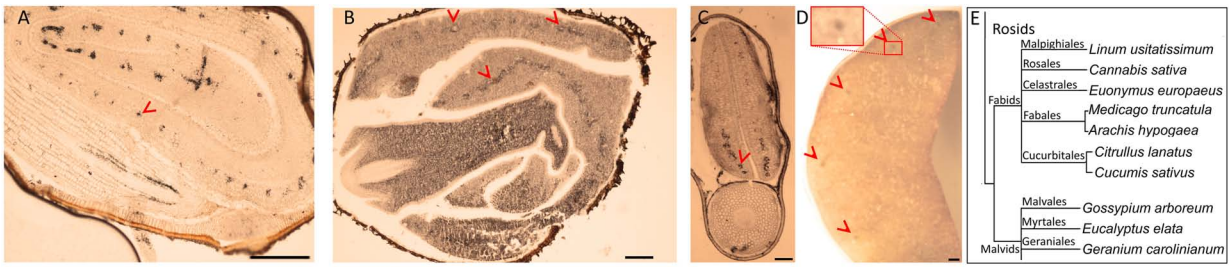

FIGURE 3 | Fe-enriched endodermis is conserved in distinct plant orders. Seed cross sections belonging to members of various orders were stained with Perls/DAB and observed under light microscope. From panels **(A–C)**, *Gossypium arboreum*. *Eucalyptus elata* and *M. truncatula*, respectively. **(D)** Single cotyledon of *Arachis hypogaea*. Fe staining appeared black in panels **(A–C)** and brown in panel **(D)**. Outer brown–black cover in panels **(A–C)** are seed coats. These were already brown before the staining, thus the color do not reflect the stained Fe. In panel **(A)**, longitudinal section of hypocotyl and cross section of folded cotyledons can be differentiated. Red arrow heads show Fe enrichment surrounding the provascular strands of cotyledons. **(E)** Branch of the taxonomic tree, for the whole tree refer to **Figure 8**. This branch shows species that were examined for Fe reserves in distinct orders and used as a visual aid. Note that only selected examples from panel **(E)** is shown through **(A–D)**. Bar is 1 mm for panel **(A)** and 0.1 mm for panels **(B–D)**. Red arrow heads point to examples of specific Fe accumulation pattern, closed rings around provasculature of cotyledons.

diverged. These data suggest that VIT1 is well-conserved in distinct plant lineages (**Supplementary Figures 1**, **2**).

We next assessed the conservation of VIT1 protein sequence in species that were used in Fe staining. The whole genome sequence was available only for *A. thaliana*, *C. papaya*, *Cucumis sativus*, *L. usitatiss*, *M. truncatula*, *E. grandis*, *B. napus*, *G. arboreum*, and *Arachis sp.* (**Supplementary Figure 3**). VIT1 sequences of all ten species consisted of 245–265 amino acids with five transmembrane helices and clustered in three subgroups (**Supplementary Table 1**). All contained the VIT1 domain structure (PF01988) (**Supplementary Figure 2**). Protein BLAST analyses showed that identity values (%) of *Arabidopsis* and the other nine VIT1s ranged from 29 to 92% (**Supplementary Figure 3**). We found the highest identity value between *Arabidopsis* and *B. napus* (92%), followed by *M. truncatula* and *Linum usitasiss* (83%), while the lowest was found between *A. thaliana* and *Arachis* spp. (29%), indicating variations of *VIT1* genes in plants. All three VIT1 subgroups included members that stored Fe around the provasculature. Therefore, although some species did not exhibit a VIT1-dependent Fe enrichment in the endodermis (**Supplementary Figure 4**), their VIT1 sequences did not diverge from others.

In *A. thaliana*, analysis of *ProVIT1::GUS* lines showed *VIT1* is preferentially expressed in the provasculature (Kim et al., 2006; Eroglu et al., 2017). To investigate whether spatial VIT1 expression is conserved in VIT1 orthologs, we compared expression of *VIT1* orthologs using publicly available microarray databases. We found that *VIT1* signal was highest in the provasculature in soybean embryo (**Figure 4B**). This data indicated spatial expression pattern is conserved in VIT1 orthologs.

Furthermore, to investigate whether VIT1's function is also conserved, we compared Fe distributions in mutants of VIT1 orthologs. VIT1 orthologs have been reported to involve in Fe distribution in rice embryo (Zhang et al., 2012; Bashir et al., 2013); however, precise description of the effect was lacking due to the low resolution, where Perls staining was applied without DAB amplification. Perls/DAB staining revealed that Fe specifically concentrated around the provasculature in wild type rice and not in single *vit1* nor *vit2* mutants (**Figure 4C**). Fe accumulated less heterogeneously among embryonic tissues in those compared to the wild type. This data suggested Fe enrichment around provasculature is conserved and mediated by VIT1 homologs in rice.

Organ, Tissue, and Subcellular Level Variations in Seed Fe Storage

Perls staining revealed Fe storing protein bodies show great variation in the structure. *C. papaya* seed showed intense staining in the center corresponding to the embryo – even though the DAB intensification step was skipped –; while the peripheries were devoid of staining, corresponding to the endosperm (**Figures 5A,B**). At the tissue and subcellular level, staining was confined to organelles similar to leucoplasts regarding the shape, size, and number (**Figure 5C**). Distribution of this organelle did not differ between the endodermis and other cell layers. Since a specific group of seed leucoplasts store starch (i.e., amyloplast), we next investigated whether Fe-accumulating organelles belong to that group. Iodine and periodic acid could only weakly stained those (data not shown), failing to show these organelles accumulate starch. Next, since Fe in plastids is associated with ferritin, using immunohistochemistry, we investigated if Fe accumulating organelle contains ferritin. Ferritin fluorescence were observed in the embryo cells but outside of those organelles (**Figure 5D**). Instead, unlike plastids, these organelles accumulated proteins, as shown by Naphthol Blue–Black staining (**Figure 5E**). Taken together, these data suggested accumulating organelles in *C. papaya* were indeed protein storage vacuoles or globules similar to many other plant seeds, despite their distinct relative size and appearance.

Nutrients accumulate usually in embryo part of the seeds. We found that in addition to the embryo, the endosperm and even the seed coat can significantly store Fe in a few Rosid species. For example, *E. europaeus* contained a large endosperm, which was intensely stained by Perls/DAB (**Figures 6A,B**).

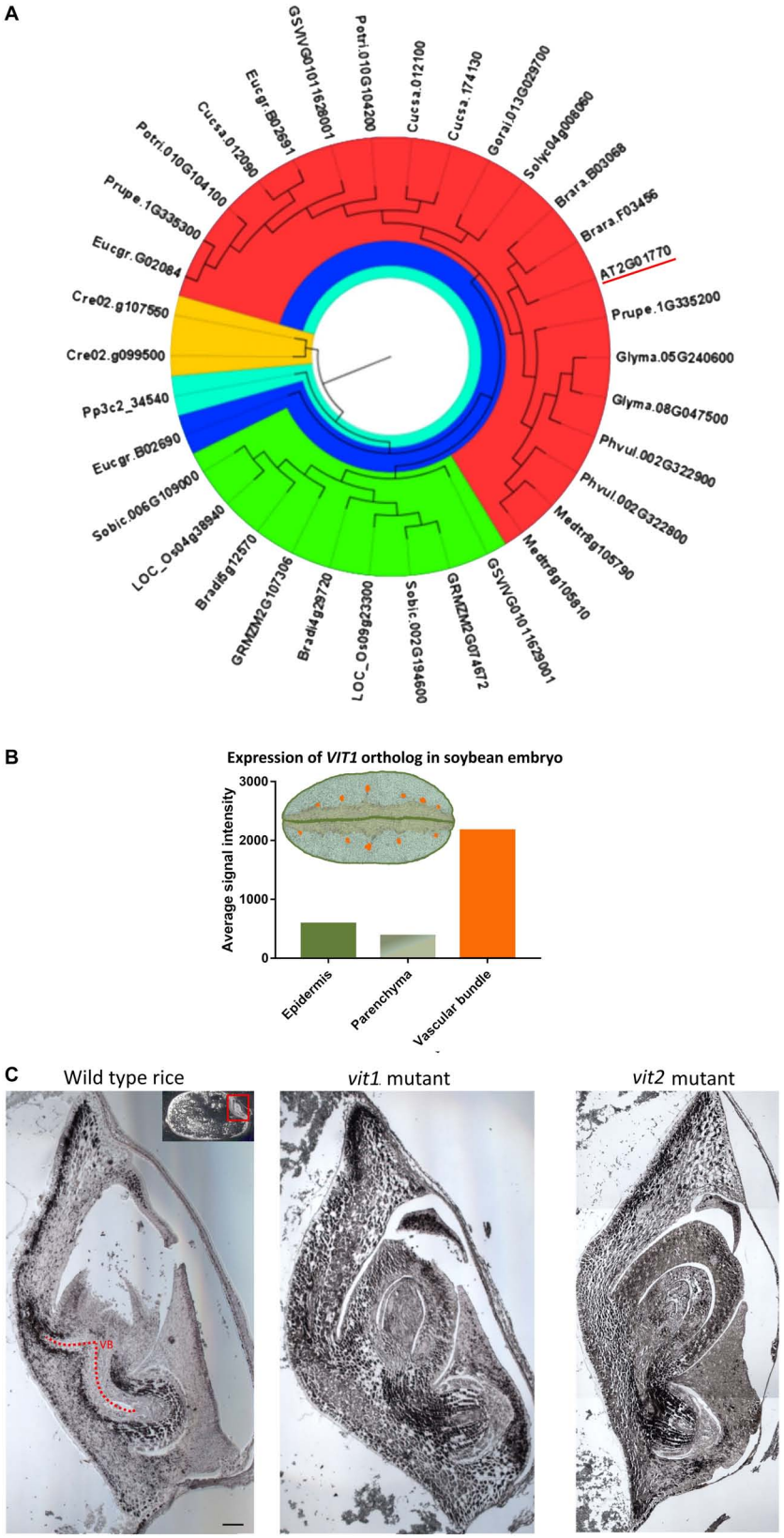

FIGURE 4 | Continued

FIGURE 4 | Conservation of VIT1 sequence, expression and function. **(A)** Phylogenetic distribution of VIT1 orthologs in 18 different plant species from monocots, dicots and lower plants. Phylogeny was constructed by MEGA 7 with ML method for 1000 bootstraps using putative 34 VIT1 protein sequences. The red segment includes only dicots. Green segment includes only monocots except for one member of *Vitis vinifera*. The blue segment shows a diverged dicot member of *E. grandis*. Orange and cyan colors show algal and moss species, respectively. VIT1 from *Arabidopsis thaliana* is underlined. For details on analyzed sequences, refer to materials and method section. **(B)** Expression of *VIT1* ortholog (*Glyma01g40600*) in embryo tissues of soybean (Microarray data retrieved from www.seedgenenetwork.net). The picture illustrates the soybean (*Glycine max*) tissues: green, epidermis; orange vascular bundles; rest, parenchyma. **(C)** Impact of *VIT1* orthologs in Fe distribution of rice (*Oryza sativa*) embryo. Unlike dicots, monocots such as rice do not have well defined organs. Longitudinal sections of whole rice embryos were obtained from either wild type or mutant rice (*VIT1* or *VIT2* genes were either substantially knocked down or knocked out), stained by Perls/DAB (black color) and Fe distribution in the embryos were compared. Region with red line corresponds to provascular bundles (VB) in rice embryo. Red arrow heads point specific Fe accumulation pattern around provasculature. Bar is 0.1 mm.

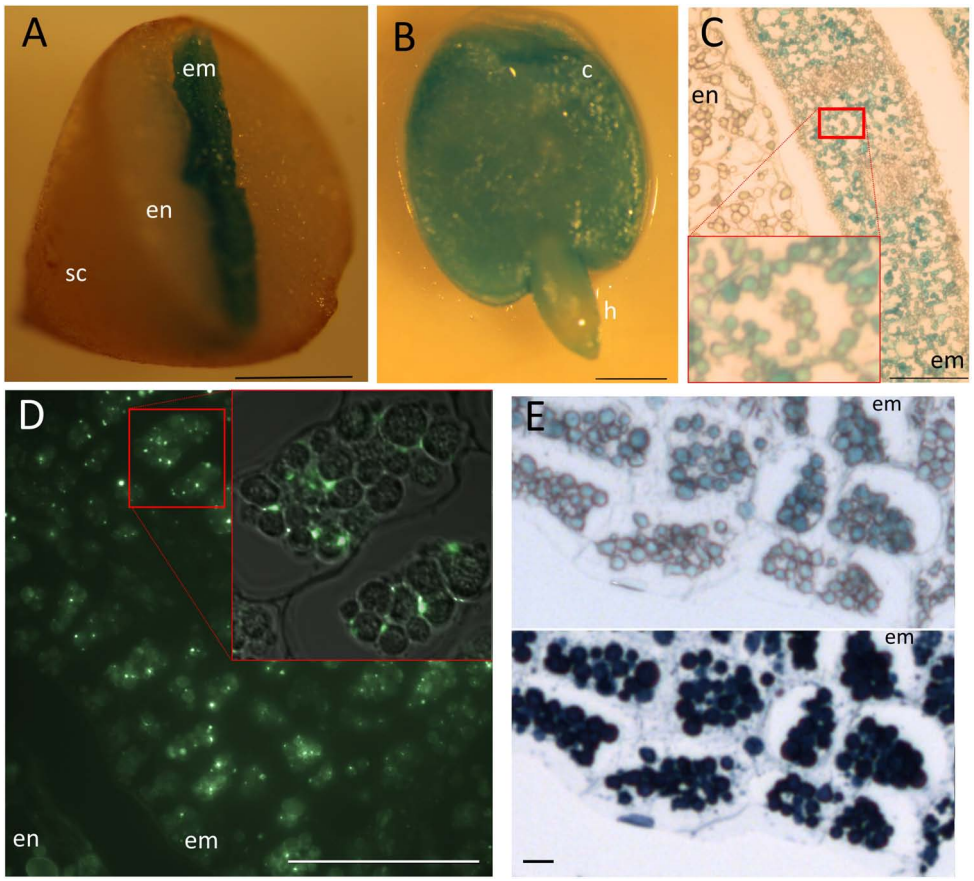

FIGURE 5 | Fe storage in *Carica papaya*. Distribution of Fe as subcellular hotspots in *Carica papaya* seeds. *Carica papaya* seeds were cleaned from the pericarp. **(A)** Seeds were cut into half by hand and were stained by Perls. **(B)** Whole embryo was isolated from the seed and was stained by perls. **(C)** Perls-stained thin cross section of a cotyledon. Red squares indicate close up. **(D)** Immunohistochemistry using ferritin antibodies. Bright green spots indicate ferritin presence. Red square indicates closeup, fluorescence image overlayed on top of the light microscopy image to indicate localization of fluorescent spots with regards to the Fe storing organelles. **(E)** Juxtaposition of Fe-stained and protein-stained regions of the embryo cross sections. The same cross section was first stained by Perls, pictured (top panel) and then stained by Naphthol Blue–Black, pictured again (bottom panel). Blue color in panel **(A–C)** and in the top panel of **(E)** indicate stained Fe. Note, the cellular position and number of the organelles slightly differ in panel **(C)**, compared with **(D)** and **(E)**. The difference might be due to a fixation artifact or cross sectioning from distinct regions of the embryos. Dark blue color in the bottom panel of **(E)** indicates presence of proteins. sc, seed coat; en, endosperm; c, cotyledon; h, hypocotyl; em, embryo. Bar is 1 mm for panels **(A,B)**; 0.05 mm for panel **(D)**; 0.1 mm for panel **(C)**; 0.01 mm for panel **(E)**.

As another example, the seed coat of *Moringa peregrina* was stained by Perls/DAB (**Figures 6C,D**). Interestingly, the staining intensity was higher in its seed coat compared with its embryo (**Figure 6C**), indicating that the seed coat is a major Fe accumulation site in *M. peregrina*.

Finally, the distinct distribution of Fe in *E. europaeus* and *M. peregrina* seeds was further investigated by synchrotron X-ray fluorescence spectrometry. Synchrotron X-ray fluorescence confirmed the Fe accumulation in the endosperm of *E. europaeus* and in the inner seed coat of *M. peregrina* (**Figure 7**). In addition to Fe, synchrotron analysis further revealed the distribution of other metals. In *E. europaeus*, phosphorus (P) and Mn localized homogeneously through the embryo and endosperm, while zinc (Zn) localized exclusively in the embryo. In *M. peregrina*, Fe

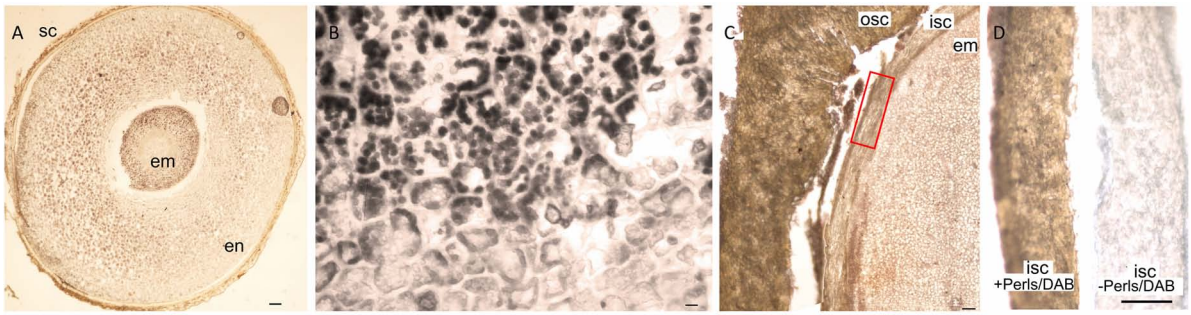

FIGURE 6 | Unusual Fe storage in the endosperm and in the seed coat. Fe staining in *Euonymus europaeus* and *Moringa peregrina.* Cross sections were stained with Perls/DAB and observed under light microscope. **(A)** *Euonymus europaeus*. **(B)** A close-up to endosperm tissue of *Euonymus europaeus*. **(C)** *Moringa peregrina*, focused on a small part of the seed. Embryo, inner and outer sections of the seed coats are visible. *Moringa peregrina* does not possess an endosperm and has a thick two-layered seed coat. **(D)** Dissected inner seed coats of *Moringa peregrina.* Left, Perls/DAB stained, right unstained control. Fe staining appeared brown in panels **(A,C,D)** and black in panel **(B)**. Seed coat in panel **(A)** and outer seed coat in panel **(C)** were already brown before the staining, thus the color does not reflect the stained Fe. In contrast, inner seed coat of *Moringa peregrina* is white, and brown color in panel **(C)** shows the stained Fe. sc, seed coat; en, endosperm; osc, outer seed coat; isc, inner seed coat; em, embryo. Bar is 0.1 mm for panel **(A)**, 0.01 mm for panel **(B)**, 1mm for panels **(C,D)**.

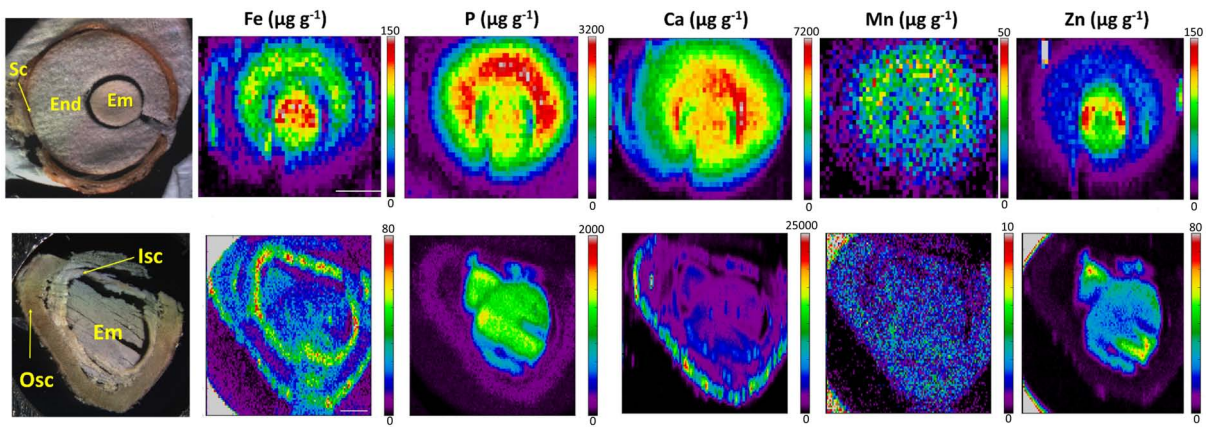

FIGURE 7 | X-ray fluorescence spectroscopy confirms endosperm and seed coat accumulate Fe. Spatial distribution of metals in *Euonymus europaeus* (**top panel**) and *Moringa peregrina* (**bottom panel**). The first column of images shows light microscopy images. Other columns show distribution of elements; Fe, P, Ca, Mn, and Zn, respectively. Colorbar indicates concentration. sc, seed coat; en, endosperm; isc, inner seed coat; osc, outer seed coat; em, embryo. Bar is 1 mm.

concentration was high not only in the inner seed coat as previously revealed by Perls/DAB (**Figure 6**) but also in the outer seed coat (**Figure 7**). Fe localized specifically to the outer side of the outer seed coat and throughout the inner seed coat. The outer seed coat of *M. peregrina* accumulated calcium (Ca), spatially overlapping Fe, but not other metals. Zn accumulated exclusively in the embryo.

DISCUSSION

We screened seeds that belong to distinct plant lineages using Perls/DAB staining and X-ray-based methods to find Fe-accumulating plastids. Although we failed to identify such seeds, our approach revealed seed Fe storage patterns in distinct plant lineages. Among those, Fe enrichment around provasculature is well conserved in Rosids which is dependent on orthologs of VIT1.

Fe accumulates almost exclusively in the embryos in Rosids (**Figures 1–3**, **5** and in all other plants that were examined in **Figure 8**). In contrast, monocots store large quantities of Fe also in the endosperm, specifically in the aleurone layer (Lu et al., 2013; Singh et al., 2013, 2014; Vatansever et al., 2017). This organ level difference in Fe partition may be explained by the decrease in endosperm size during evolution (Forbis et al., 2002; Finch-Savage and Leubner-Metzger, 2006). Branches that appear early, such as monocots, almost never possess an embryo occupying more than half of the total seed volume. In contrast, branches that appeared later (e.g., Rosids) can possess embryo that may fill almost the entire seed. In the latter, the endosperm shrinks as the seed develops and the embryo eventually occupies most of the seed volume. Since the endosperm is a nutritive tissue, as it degrades, nutrient storage function must be taken over by the embryo itself. Therefore, we suggest that the metal accumulation in the endosperm, at least for Fe, is taken over by the embryo as an evolutionary trend.

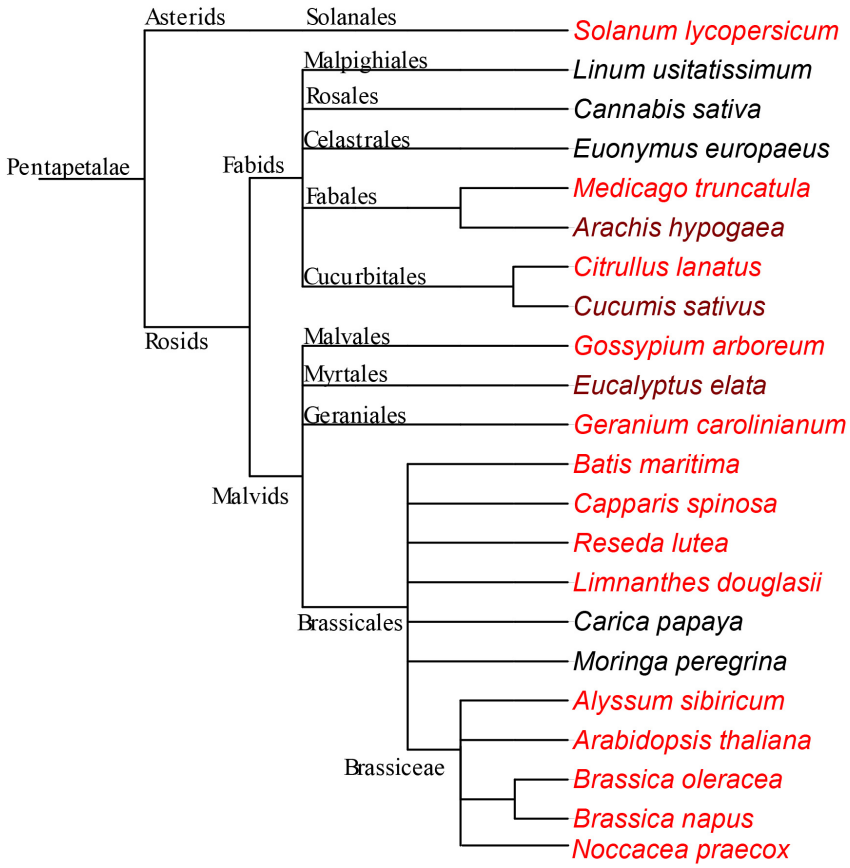

FIGURE 8 | Fe-enriched endodermis is a conserved feature in Rosids. Schema representing species that are used in this study. The phylogenetic tree was generated using NCBI taxonomy database and exported with the version 3 of the Interactive Tree of Life (iTOL) (Letunic and Bork, 2016). Both dark and light red colored species were enriched with Fe around provascular strands. In the darker-red-colored species, endodermis Fe does not represent the highest concentration of Fe, in contrast to the lighter-red-colored species. The species which are not red, do not specifically accumulate large Fe reserves in their endodermis. See discussion for the interpretation of the negative data.

Besides the general trends, Fe may accumulate in distinct organs and cellular compartments. The destination of nutrients must be the embryo, as the mature seed coat is dead while the endosperm is sterile. However, Fe accumulates in the seed coat higher than the embryo in rare cases (**Figures 6**, **7**; Cvitanich et al., 2010; Moraghan et al., 2002). This can be related to the presence of chelators in the seed coat, such as tannins, which immobilize metal nutrients (Lombardi-Boccia et al., 1995). The function of trapped Fe reserves in the seed coat should be addressed in the future. In this regard, since most seed coats are naturally colored; Perls staining may fail to detect Fe; however, this problem can be circumvented by using fluorescent dyes (Park et al., 2014). In contrast to Fe, Zn is not trapped in the seed coat (**Figure 7**). This might be due to its lower affinity to tannins and other polyphenols (Santos-Buelga and Scalbert, 2000). In Rosids, the endosperm rarely stores a significant amount of Fe (only in a few species, see **Figures 6A,B**, **7** and **Supplementary Figure 4**). Interestingly, X-ray fluorescence showed Fe in the endosperm colocalizes with phosphorus (P) (**Figure 7A**). Localization of P usually mirrors phytate distribution in seeds, indicating Fe might be trapped by phytate in the endosperm before it can reach the embryo (Iwai et al., 2012). In summary, the principal storage organ for Fe in Rosid seeds is the embryo; however, Fe reserves can be restrained on the way to the embryo, most likely due to the immobilization by chelation in the endosperm or in the seed coat.

Carica papaya showed the most concentrated Fe hotspots among all the analyzed seeds. Despite the presence of a large endosperm, the Fe signal from Perls staining appeared exclusively in the embryo (**Figure 5A**), specifically localized in homogeneously distributed organelles similar to plastids (**Figure 5B**). To the best of our knowledge, plastids have never been reported as representing the main Fe reserves in any seeds. For example, Cvitanich et al. (2010) determined a large number of amyloplasts in beans, which even contain Fe-binding ferritin proteins; but these plastids were devoid of Perls stain. In papaya, we found that Fe accumulating organelles are related to protein storage vacuoles based on the absence of ferritin (**Figure 5D**) and presence of proteins (**Figure 5E**). Protein storage vacuole is the only vacuole plant seeds has and contain phytate enriched globules, where Fe reserves reside (Lanquar et al., 2005; Regvar et al., 2011). These globules are separated from each

other, but often detected as a single aggregate under microscope (Roschzttardtz et al., 2009; Eroglu et al., 2017) which might be an artifact due to fixation (Herman and Larkins, 1999). Interestingly, in papaya, proteins aggregated in separated compartments (**Figure 5**). These compartments seemed to localize in the cytosol instead of being enclosed by a protein storage vacuole.

Endodermis represents the major conserved Fe hotspot in distinct plant lineages (**Figure 8**). In few species, Fe-enriched cells go beyond the single endodermal cell layer to nearby cortex cells [compare **Figure 2B** with 2D, also see Ibeas et al. (2017)]. Therefore, the question arises whether VIT1 can also localize to cortex cells in addition to the endodermis. VIT1 is able to localize to the inner-most cortex cells in the absence of the endodermis (Roschzttardtz et al., 2009), which may indicate – regardless of whether it is restricted to a single cell layer or not – that the typical ring-shaped Fe localization close proximity to provascular strands is due to VIT1. VIT1 plasticity may not be limited to the different number of cell layers and may extent to different subcellular localization. In beans, instead of the vacuole, Fe accumulated in the cytosol of endodermal cells (Cvitanich et al., 2010), indicating VIT1 orthologs can localize to the plasma membrane (as opposed to tonoplast in Arabidopsis). Taken together, these variations indicate the core signature of VIT1-mediated Fe accumulation in plants is the enrichment around the provasculature, not the confinement in the single cell layer nor the compartmentalization into the vacuole.

Although VIT1-mediated Fe enrichment was conserved, few species lacked this phenotype (**Figures 5**–**8**). This may raise the question of whether VIT1 has been lost in these species during the course of evolution. However, this is unlikely due to conservation of a VIT1 domain in species which lack a Fe-enriched endodermis (PF01988) (**Figure 4A** and **Supplementary Figures 2**, **3**). Alternatively, we hypothesize that other transporters might have taken over VIT1's function in these species. Studies with loss of function mutants indicate that Fe patterns are eventually determined by a single dominant transporter (Kim et al., 2006; Eroglu et al., 2017). For example, in *A. thaliana*, VIT1's presence prevents another protein, MTP8, from storing Fe. Likewise, when a more preferential Fe transporter is present, VIT1 may still mediate Fe accumulation (i.e., Fe-enriched endodermis) but to a much lesser extent. Furthermore, the nature of techniques used in the study is biased in revealing a less pronounced Fe store in the presence of a highly pronounced one, making it likely to miss VIT1's impact in the presence of a stronger metal transporter. For instance, X-ray analysis (Kim et al., 2006) or Perls/DAB staining (**Figure 1A**) fail to detect any Fe in cortex or epidermal cells in the presence of the large endodermal Fe pool, although they constitute half of the total seed Fe (Ramos et al., 2013). Taken together, VIT1 and its associated phenotype is well-conserved despite some seeds showing alternative Fe hotspots.

Rosids is a huge lineage including 80,000 species belonging to 147 families, comprising more than a third of all angiosperms (Soltis, 2005; Hedges and Kumar, 2009). The current study shows Rosid seeds store Fe in the embryo. This Fe is not equally distributed but most often concentrated in the innermost cell layers, the endodermis and sometimes the cortex, in a VIT1-dependent manner. This phenotype goes beyond dicots and may extend to monocots as shown in rice. Future studies should examine other clades beyond Rosids to pinpoint at which stage of plant evolution the Fe-enriched endodermis appeared as a new feature.

AUTHOR CONTRIBUTIONS

SE and NK collected the seeds and performed the histochemistry. KV-M and AK carried out the X-ray analyses. EF performed the bioinformatics. SE and BT conceived and planned the project. SE wrote the manuscript with the contributions of all the authors.

FUNDING

This study was partially supported by the ARRS (Slovenian Research Agency) (P1-0212, J7-9418, and J7-9398) and internal fundings. The research leading to this result has been supported by the project CALIPSOplus under Grant Agreement 730872 from the EU Framework Programme for Research and Innovation HORIZON 2020.

ACKNOWLEDGMENTS

Thanks to Asci Murat Mihladiz (Capparis Research & Development Center, Burdur, Turkey) and Dr. Emre Cilden (Hacettepe University, Ankara, Turkey) for sharing seed stocks with us. We gratefully acknowledge Dr. Ali Veral and his team, especially Ebru Çanlı (Ege University Hospital, Izmir, Turkey) for excellent technical help in preparing the histological sections. Thanks to Recep Vatansever and Ferhat Celep for fruitful discussions. We also acknowledge Primoz Pelicon and Primoz Vavpetič (JSI) for their help with PIXE analysis and Iva Bozicevic Mihalic (Elettra Sincrotrone Trieste) for her help with the synchrotron measurements. Elettra was acknowledged for the provision of the beamtime (Project 20175078).

SUPPLEMENTARY MATERIAL

The Supplementary Material for this article can be found online at: https://www.frontiersin.org/articles/10.3389/fpls.2019.00907/full#supplementary-material

REFERENCES

Bashir, K., Takahashi, R., Akhtar, S., Ishimaru, Y., Nakanishi, H., and Nishizawa, N. K. (2013). The knockdown of OsVIT2 and MIT affects iron localization in rice seed. *Rice* 6:31. doi: 10.1186/1939-8433-6-31

Borg, S., Brinch-Pedersen, H., Tauris, B., and Holm, P. B. (2009). Iron transport, deposition and bioavailability in the wheat and barley grain. *Plant Soil* 325, 15–24. doi: 10.1007/s11104-009-0046-6

Briat, J.-F., Duc, C., Ravet, K., and Gaymard, F. (2010). Ferritins and iron storage in plants. *Biochim. Biophys. Acta*

BBA Gen. Subj. 1800, 806–814. doi: 10.1016/j.bbagen.2009.12.003

Chase, M. W., Christenhusz, M. J. M., Fay, M. F., Byng, J. W., Judd, W. S., Soltis, D. E., et al. (2016). An update of the angiosperm phylogeny group classification for the orders and families of flowering plants: APG IV. *Bot. J. Linn. Soc.* 181, 1–20. doi: 10.1111/boj.12385

Çilden, E., Yildirimli, Ş, Zare, G., and Martín-Bravo, S. (2018). Rediscovery of the restricted endemic *Reseda balansae* (Resedaceae) in Turkey. *Phytotaxa* 362, 87–96.

Connorton, J. M., Jones, E. R., Rodríguez-Ramiro, I., Fairweather-Tait, S., Uauy, C., and Balk, J. (2017). Wheat vacuolar iron transporter TaVIT2 Transports Fe and Mn and Is effective for biofortification. *Plant Physiol.* 174, 2434–2444. doi: 10.1104/pp.17.00672

Cvitanich, C., Przybyłowicz, W. J., Urbanski, D. F., Jurkiewicz, A. M., Mesjasz-Przybyłowicz, J., Blair, M. W., et al. (2010). Iron and ferritin accumulate in separate cellular locations in Phaseolus seeds. *BMC Plant Biol.* 10:26. doi: 10.1186/1471-2229-10-26

Davila-Hicks, P., Theil, E. C., and Lönnerdal, B. (2004). Iron in ferritin or in salts (ferrous sulfate) is equally bioavailable in nonanemic women. *Am. J. Clin. Nutr.* 80, 936–940. doi: 10.1093/ajcn/80.4.936

Eroglu, S. (2018). "Chapter Four - Metal transport in the developing plant seed," in *Advances in Botanical Research*, ed. C. Maurel (Cambridge, MA: Academic Press), 91–113. doi: 10.1016/bs.abr.2018.09.010

Eroglu, S., Giehl, R. F. H., Meier, B., Takahashi, M., Terada, Y., Ignatyev, K., et al. (2017). Metal tolerance protein 8 mediates manganese homeostasis and iron reallocation during seed development and germination. *Plant Physiol.* 174, 1633–1647. doi: 10.1104/pp.16.01646

Eroglu, S., Meier, B., von Wirén, N., and Peiter, E. (2016). The vacuolar manganese transporter MTP8 determines tolerance to iron deficiency-induced chlorosis in *Arabidopsis*. *Plant Physiol.* 170, 1030–1045. doi: 10.1104/pp.15.01194

Finch-Savage, W. E., and Leubner-Metzger, G. (2006). Seed dormancy and the control of germination. *New Phytol.* 171, 501–523.

Finn, R. D., Coggill, P., Eberhardt, R. Y., Eddy, S. R., Mistry, J., Mitchell, A. L., et al. (2015). The Pfam protein families database: towards a more sustainable future. *Nucleic Acids Res.* 44, 279–285. doi: 10.1093/nar/gkv1344

Forbis, T. A., Floyd, S. K., and de Queiroz, A. (2002). The evolution of embryo size in angiosperms and other seed plants: implications for the evolution of seed dormancy. *Evolution* 56, 2112–2125. doi: 10.1111/j.0014-3820.2002.tb00137.x

Gasteiger, E., Hoogland, C., Gattiker, A., Wilkins, M. R., Appel, R. D., and Bairoch, A. (2005). "Protein identification and analysis tools on the ExPASy server," in *The Proteomics Protocols Handbook*, ed. J. M. Walker (Berlin: Springer), 571–607. doi: 10.1385/1-59259-890-0:571

Gibson, R. S., Bailey, K. B., Gibbs, M., and Ferguson, E. L. (2010). A review of phytate, iron, zinc, and calcium concentrations in plant-based complementary foods used in low-income countries and implications for bioavailability. *Food Nutr. Bull.* 31, 134–146.

Goodstein, D. M., Shu, S., Howson, R., Neupane, R., Hayes, R. D., Fazo, J., et al. (2011). Phytozome: a comparative platform for green plant genomics. *Nucleic Acids Res.* 40, 1178–1186. doi: 10.1093/nar/gkr944

Hedges, S. B., and Kumar, S. (2009). *The Timetree of Life*. Oxford: OUP Oxford.

Hegeman, C. E., and Grabau, E. A. (2001). A novel phytase with sequence similarity to purple acid phosphatases is expressed in cotyledons of germinating soybean seedlings. *Plant Physiol.* 126, 1598–1608. doi: 10.1104/pp.126.4.1598

Herman, E. M., and Larkins, B. A. (1999). Protein storage bodies and vacuoles. *Plant Cell* 11, 601–613. doi: 10.1105/tpc.11.4.601

Hurrell, R., and Egli, I. (2010). Iron bioavailability and dietary reference values. *Am. J. Clin. Nutr.* 91, 1461–1467.

Ibeas, M. A., Grant-Grant, S., Navarro, N., Perez, M. F., and Roschzttardtz, H. (2017). Dynamic subcellular localization of iron during embryo development in Brassicaceae seeds. *Front. Plant Sci.* 8:2186. doi: 10.3389/fpls.2017.02186

Iwai, T., Takahashi, M., Oda, K., Terada, Y., and Yoshida, K. T. (2012). Dynamic changes in the distribution of minerals in relation to phytic-acid accumulation during rice seed development. *Plant Physiol.* 160, 2007–2014. doi: 10.1104/pp.112.206573

Karydas, A. G., Czyzycki, M., Leani, J. J., Migliori, A., Osan, J., Bogovac, M., et al. (2018). An IAEA multi-technique X-ray spectrometry endstation at Elettra Sincrotrone Trieste: benchmarking results and interdisciplinary applications. *J. Synchrotron Radiat.* 25, 189–203. doi: 10.1107/S1600577517016332

Kassebaum, N. J., Jasrasaria, R., Naghavi, M., Wulf, S. K., Johns, N., Lozano, R., et al. (2014). A systematic analysis of global anemia burden from 1990 to 2010. *Blood* 123, 615–624. doi: 10.1182/blood-2013-06-508325

Kim, S. A., Punshon, T., Lanzirotti, A., Li, L., Alonso, J. M., Ecker, J. R., et al. (2006). Localization of iron in *Arabidopsis* seed requires the vacuolar membrane transporter VIT1. *Science* 314, 1295–1298. doi: 10.1126/science.1132563

Kumar, S., Stecher, G., and Tamura, K. (2016). MEGA7: molecular evolutionary genetics analysis version 7.0 for bigger datasets. *Mol. Biol. Evol.* 33, 1870–1874. doi: 10.1093/molbev/msw054

Kump, P., and Vogel-Mikuš, K. (2018). Quantification of 2D elemental distribution maps of intermediate-thick biological sections by low energy synchrotron $\upmu$-X-ray fluorescence spectrometry. *J. Instrum.* 13:C05014.

Lanquar, V., Lelièvre, F., Bolte, S., Hamès, C., Alcon, C., Neumann, D., et al. (2005). Mobilization of vacuolar iron by AtNRAMP3 and AtNRAMP4 is essential for seed germination on low iron. *EMBO J.* 24, 4041–4051. doi: 10.1038/sj.emboj.7600864

Lee, S., Jeon, U. S., Lee, S. J., Kim, Y.-K., Persson, D. P., Husted, S., et al. (2009). Iron fortification of rice seeds through activation of the nicotianamine synthase gene. *Proc. Natl. Acad. Sci. U.S.A.* 106, 22014–22019. doi: 10.1073/pnas.0910950106

Letunic, I., and Bork, P. (2016). Interactive tree of life (iTOL) v3: an online tool for the display and annotation of phylogenetic and other trees. *Nucleic Acids Res.* 44, 242–245. doi: 10.1093/nar/gkw290

Lombardi-Boccia, G., De Santis, N., Di Lullo, G., and Carnovale, E. (1995). Impact of processing on Fe dialysability from bean (*Phaseolus vulgaris* L.). *Food Chem.* 2, 191–195. doi: 10.1016/0308-8146(95)90787-8

Lu, L., Tian, S., Liao, H., Zhang, J., Yang, X., Labavitch, J. M., et al. (2013). Analysis of metal element distributions in rice (*Oryza sativa* L.) seeds and relocation during germination based on X-Ray fluorescence imaging of Zn, Fe, K, Ca, and Mn. *PLoS One* 8:e57360. doi: 10.1371/journal.pone.0057360

Meguro, R., Asano, Y., Odagiri, S., Li, C., Iwatsuki, H., and Shoumura, K. (2007). Nonheme-iron histochemistry for light and electron microscopy: a historical, theoretical and technical review. *Arch. Histol. Cytol.* 70, 1–19. doi: 10.1679/aohc.70.1

Moraghan, J., Padilla, J., Etchevers, J., Grafton, K., and Acosta-Gallegos, J. (2002). Iron accumulation in seed of common bean. *Plant Soil* 246, 175–183.

Murgia, I., Arosio, P., Tarantino, D., and Soave, C. (2012). Biofortification for combating 'hidden hunger' for iron. *Trends Plant Sci.* 17, 47–55. doi: 10.1016/j.tplants.2011.10.003

Otegui, M. S., Capp, R., and Staehelin, L. A. (2002). Developing seeds of *Arabidopsis* store different minerals in two types of vacuoles and in the endoplasmic reticulum. *Plant Cell* 14, 1311–1327. doi: 10.1105/tpc.010486

Paciorek, T., Sauer, M., Balla, J., Wiśniewska, J., and Friml, J. (2006). Immunocytochemical technique for protein localization in sections of plant tissues. *Nat. Protoc.* 1, 104–107. doi: 10.1038/nprot.2006.16

Park, M.-J., Jung, H.-S., Kim, Y.-J., Kwon, Y.-J., Lee, J.-K., and Park, C.-M. (2014). High-sensitivity fluorescence imaging of iron in plant tissues. *Chem. Commun.* 50, 8547–8549. doi: 10.1039/c4cc02132k

Ramos, M. S., Khodja, H., Mary, V., and Thomine, S. (2013). Using μPIXE for quantitative mapping of metal concentration in *Arabidopsis thaliana* seeds. *Front. Plant Sci.* 4:168. doi: 10.3389/fpls.2013.00168

Reddy, C. S., Kim, S.-C., and Kaul, T. (2017). Genetically modified phytase crops role in sustainable plant and animal nutrition and ecological development: a review. *3 Biotech* 7:195. doi: 10.1007/s13205-017-0797-3

Regvar, M., Eichert, D., Kaulich, B., Gianoncelli, A., Pongrac, P., Vogel-Mikuš, K., et al. (2011). New insights into globoids of protein storage vacuoles in wheat aleurone using synchrotron soft X-ray microscopy. *J. Exp. Bot.* 62, 3929–3939. doi: 10.1093/jxb/err090

Roschzttardtz, H., Conejero, G., Curie, C., and Mari, S. (2009). Identification of the endodermal vacuole as the iron storage compartment in the *Arabidopsis* embryo. *Plant Physiol.* 151, 1329–1338. doi: 10.1104/pp.109.144444

Santos-Buelga, C., and Scalbert, A. (2000). Proanthocyanidins and tannin-like compounds – nature, occurrence, dietary intake and effects on nutrition and health. *J. Sci. Food Agric.* 80, 1094–1117. doi: 10.1002/(sici)1097-0010(20000515)80:7<1094::aid-jsfa569>3.0.co;2-1

Shahzad, Z., Rouached, H., and Rakha, A. (2014). Combating mineral malnutrition through iron and zinc biofortification of cereals: Fe and Zn biofortification of cereals. . .. *Compr. Rev. Food Sci. Food Saf.* 13, 329–346. doi: 10.1111/1541-4337.12063

Shi, J., Wang, H., Schellin, K., Li, B., Faller, M., Stoop, J. M., et al. (2007). Embryo-specific silencing of a transporter reduces phytic acid content of maize and soybean seeds. *Nat. Biotechnol.* 25, 930–937. doi: 10.1038/nbt1322

Singh, S. P., Vogel-Mikuš, K., Arèon, I., Vavpetiè, P., Jeromel, L., Pelicon, P., et al. (2013). Pattern of iron distribution in maternal and filial tissues in wheat grains with contrasting levels of iron. *J. Exp. Bot.* 64, 3249–3260. doi: 10.1093/jxb/ert160

Singh, S. P., Vogel-Mikuš, K., Vavpetiè, P., Jeromel, L., Pelicon, P., Kumar, J., et al. (2014). Spatial X-ray fluorescence micro-imaging of minerals in grain tissues of wheat and related genotypes. *Planta* 240, 277–289. doi: 10.1007/s00425-014-2084-4

Solé, V. A. A., Papillon, E., Cotte, M., Walter, P. H., and Susini, J. (2007). A multiplatform code for the analysis of energy-dispersive X-ray fluorescence spectra. *Spectrochim. Acta Part B At. Spectrosc.* 62, 63–68. doi: 10.1016/j.sab.2006.12.002

Soltis, P. S. (2005). Ancient and recent polyploidy in angiosperms. *New Phytol.* 166, 5–8. doi: 10.1111/j.1469-8137.2005.01379.x

Stacey, M. G., Patel, A., McClain, W. E., Mathieu, M., Remley, M., Rogers, E. E., et al. (2008). The Arabidopsis AtOPT3 protein functions in metal homeostasis and movement of iron to developing seeds. *Plant Physiol.* 146, 589–601. doi: 10.1104/pp.107.108183

Tusnady, G. E., and Simon, I. (2001). The HMMTOP transmembrane topology prediction server. *Bioinformatics* 17, 849–850. doi: 10.1093/bioinformatics/17.9.849

Vatansever, R., Filiz, E., and Eroglu, S. (2017). Genome-wide exploration of metal tolerance protein (MTP) genes in common wheat (*Triticum aestivum*): insights into metal homeostasis and biofortification. *Biometals* 30, 217–235. doi: 10.1007/s10534-017-9997-x

Vogel-Mikus, K., Drobne, D., and Regvar, M. (2005). Zn, Cd and Pb accumulation and arbuscular mycorrhizal colonisation of pennycress *Thlaspi praecox* Wulf. (*Brassicaceae*) from the vicinity of a lead mine and smelter in Slovenia. *Environ. Pollut. Barking Essex* 1987, 233–242. doi: 10.1016/j.envpol.2004.06.021

Vogel-Mikus, K., Pongrac, P., Kump, P., Necemer, M., Simcic, J., Pelicon, P., et al. (2007). Localisation and quantification of elements within seeds of Cd/Zn hyperaccumulator *Thlaspi praecox* by micro-PIXE. *Environ. Pollut. Barking Essex* 1987, 50–59. doi: 10.1016/j.envpol.2006.08.026

Vogel-Mikuš, K., Pongrac, P., and Pelicon, P. (2014). Micro-PIXE elemental mapping for ionome studies of crop plants. *Int. J. PIXE* 24, 217–233. doi: 10.1142/s0129083514400142

Vogel-Mikuš, K., Simčič, J., Pelicon, P., Budnar, M., Kump, P., Neèemer, M., et al. (2008). Comparison of essential and non-essential element distribution in leaves of the Cd/Zn hyperaccumulator *Thlaspi praecox* as revealed by micro-PIXE. *Plant Cell Environ.* 31, 1484–1496. doi: 10.1111/j.1365-3040.2008.01858.x

Waldo, G. S., Wright, E., Whang, Z. H., Briat, J. F., Theil, E. C., and Sayers, D. E. (1995). Formation of the ferritin iron mineral occurs in plastids (An X-Ray Absorption Spectroscopy Study. *Plant Physiol.* 109, 797–802. doi: 10.1104/pp.109.3.797

Warkentin, T. D., Delgerjav, O., Arganosa, G., Rehman, A. U., Bett, K. E., Anbessa, Y., et al. (2012). Development and characterization of low-phytate pea. *Crop Sci.* 52, 74–78.

Zhang, Y., Xu, Y.-H., Yi, H.-Y., and Gong, J.-M. (2012). Vacuolar membrane transporters OsVIT1 and OsVIT2 modulate iron translocation between flag leaves and seeds in rice. *Plant J.* 72, 400–410. doi: 10.1111/j.1365-313X.2012.05088.x

Zuckerkandl, E., and Pauling, L. (1965). "Evolutionary divergence and convergence in proteins," in *Evolving Genes and Proteins*, eds V. Bryson and H. J. Vogel (New York, NY: Academic Press), 97–166. doi: 10.1016/b978-1-4832-2734-4.50017-6

Conflict of Interest Statement: The authors declare that the research was conducted in the absence of any commercial or financial relationships that could be construed as a potential conflict of interest.

frontiers in Plant Science

MINI REVIEW
published: 16 July 2019
doi: 10.3389/fpls.2019.00833

Genetic Biofortification to Enrich Rice and Wheat Grain Iron: From Genes to Product

*Yvonne Ludwig and Inez H. Slamet-Loedin**

Trait and Genome Engineering Cluster, Strategic Innovation Platform, International Rice Research Institute, Los Baños, Philippines

The micronutrient iron (Fe) is not only essential for plant survival and proliferation but also crucial for healthy human growth and development. Rice and wheat are the two leading staples globally; unfortunately, popular rice and wheat cultivars only have a minuscule amount of Fe content and mainly present in the outer bran layers. Unavailability of considerable Fe-rich rice and wheat germplasms limits the potential of conventional breeding to develop this micronutrient trait in both staples. Agronomic biofortification, defined as soil and foliar fertilizer application, has potential but remains quite challenging to improve grain Fe to the significant level. In contrast, recent accomplishments in genetic biofortification can help to develop Fe-enriched cereal grains to sustainably address the problem of "hidden hunger" when the roadmap from proof of concept to product and adoption can be achieved. Here, we highlight the different genetic biofortification strategies for rice and wheat and path to develop a product.

Keywords: biofortification, iron, rice, wheat, genes

OPEN ACCESS

Edited by:
Thomas J. Buckhout, Humboldt University of Berlin, Germany

Reviewed by:
Khurram Bashir, RIKEN, Japan
Soumitra Paul, University of Calcutta, India

***Correspondence:**
Inez H. Slamet-Loedin
I.Slamet-Loedin@irri.org

Specialty section:
This article was submitted to Plant Nutrition, a section of the journal Frontiers in Plant Science

Received: *28 January 2019*
Accepted: *11 June 2019*
Published: *16 July 2019*

Citation:
Ludwig Y and Slamet-Loedin IH (2019) Genetic Biofortification to Enrich Rice and Wheat Grain Iron: From Genes to Product. Front. Plant Sci. 10:833. doi: 10.3389/fpls.2019.00833

INTRODUCTION

"Hidden hunger," the cause of inadequate intake of key micronutrients, is a major problem globally affecting around 2 billion people worldwide, and 30–40% (GBD 2015 Disease and Injury Incidence and Prevalence Collaborators, 2016) of it is caused by iron (Fe) deficiency anemia (IDA). The people most vulnerable to IDA are women and children. IDA can hamper cognitive and physical development, reduce immunity, and enhance the risk of maternal and perinatal mortality. The breeding target to fulfill the 30% estimated average requirement (EAR) of woman and children recommended by the HarvestPlus program for Fe is 13 μg/g in polished rice or around five to sixfold increase of grain Fe in popular rice. While in wheat, it is 59 μg/g (dry weight) of Fe or around twofold (Bouis et al., 2011).

In developing and less developed countries, it is challenging to provide access to a more diverse diet that can ameliorate the micronutrient deficiency. Biofortification, the enhancement of bioavailable micronutrient in the edible parts of staple food by either conventional plant breeding, biotechnology techniques, or agronomic approaches can help to alleviate malnutrition in the regions where the main source of calories and micronutrients come from staples (Bouis and Saltzman, 2017).

PLANT FE UPTAKE AND TRANSLOCATION

Iron is an essential micronutrient in plants and is required frequently in various processes such as photosynthesis, respiration, or chlorophyll biosynthesis. Different strategies are known for the uptake of low soluble Fe(III) oxyhydrate from the rhizosphere in higher plants: (a) Strategy I (non-Graminaceae) implicating reduction of ferric Fe(III) chelate reduction at the root surface to allow absorption of ferrous Fe(II) at plasma membrane, (b) Strategy II (Graminaceae) is the chelation strategy involving mugineic acid (MA) biosynthesis and secretion, and (c) a combination of both (Connorton et al., 2017a).

Major key genes of uptake in Strategy I for dicots and non-grass species were identified from Arabidopsis, namely ferric-chelate reductase oxidase 2 (FRO2) (Robinson et al., 1999), Fe-regulated transporter 1 (IRT1) (Eide et al., 1996), and a large number of H^+-ATPase (HA) genes that are responsible for proton and phenolic compound excretion into the rhizosphere to enhance the solubility of ferric ions (Kobayashi and Nishizawa, 2012).

Strategy II plants such as rice, wheat, barley, and maize secrete the high Fe affinity organic molecule phytosiderophore (PS), a MA family into the rhizosphere (Kobayashi et al., 2005; Suzuki et al., 2006; Borrill et al., 2014; Bashir et al., 2017). The basic scheme for genes involved in Fe homeostasis in rice as the model system is presented in **Figure 1**. The uptake and translocation process in wheat is similar to rice and has been comprehensively reviewed (Borrill et al., 2014; Connorton et al., 2017a).

The synthesis of MA is a conserved pathway starting from *S*-adenosyl-L-methionine and covers consecutive enzymatic reactions of nicotianamine synthase (NAS), nicotianamine aminotransferase (NAAT), and deoxymugineic acid synthase (DMAS) genes, producing the precursor of nine known types of MAs: 2′-deoxymugineic acid (DMA) (Higuchi et al., 1999; Takahashi et al., 1999; Bashir et al., 2006; Kobayashi and Nishizawa, 2012). In rice, the expression of these genes is highly affected by the level of Fe availability in the soil; most genes were identified in response to Fe deficiency. NAS is localized on the membrane of vesicles in root cells, while NAAT is within these vesicles, proposing the location of the MA biosynthesis. Interestingly, a diurnal pattern is known for the secretion of MA, with its peak in the morning hours (Takagi et al., 1984; Suzuki et al., 2006). The secretion of MA into the rhizosphere is facilitated by the expression of TOM1 (transporter of MA family PSs). TOM1 was first identified in rice and barley and belongs to the major facilitator superfamily (MFS), which is one of the largest group of membrane transport proteins that promote the transit of substrates across cell membranes in response to chemiosmotic ion gradient (Nozoye et al., 2011). Fe–MA complexes are then built and taken up by YELLOW STRIPE 1 (YS1) and YELLOW STRIPE 1-like (YSL1) transporter into root cells (Curie et al., 2001; Inoue et al., 2009). The Fe(III)–DMA complex absorbed in root cell cytosols is likely reduced by ascorbate and altered to be Fe(II)–NA. The cytosolic Fe(II)–NA then excreted to the xylem and created complexes predominantly with citrate or with DMA (Fe–DMA) and transport further (Yoneyama et al., 2015).

In addition to the strategy II Fe(III)–DMA complex and OsYSL15 transporter, rice carries a ferrous transporter (OsIRT1) in its genome, which allows the direct uptake of Fe(II). On the root surface, rice shows a low ferric-chelate reductase activity, indicating an adaptation to submerge and anaerobic conditions (Ishimaru et al., 2006). Other metal transporters were identified for both strategies like ZIP (zinc-regulated transporter, IRT-like protein) family or natural resistance-associated macrophage protein (NRAMP) (Guerinot, 2000; Lanquar et al., 2005; Calliatte et al., 2010).

A complex cascade involves in the Fe translocation in higher plants, including xylem and phloem loading/unloading, transport, and retranslocation within the plant from source to sink organ (Kim and Guerinot, 2007). To facilitate this translocation, different chelators such as citrate, MAs, and nicotianamine (NA) play a crucial role in symplast heavy metal homeostasis (Garcia-Oliveira et al., 2018). The cytosolic Fe(II)–NA then excreted to the xylem and created complexes predominantly with citrate or with DMA (Fe–DMA) and transport further in rice phloem while remaining to bind to DMA, citrate, and proteins (Yoneyama et al., 2015). FERRIC REDUCTASE DEFECTIVE LIKE 1 (OsFRDL1) in rice (**Figure 1**) encodes a citrate efflux transporter required for Fe translocation. This gene is primarily expressed in root pericycle cells. Knockout plants of OsFRDL1 display a mild defect in Fe homeostasis, which suggests alternative chelators for Fe xylem transport (Inoue et al., 2004; Yokosho et al., 2009).

The YSL family members (influx transporter) are involved in metal–NA chelate translocation (Curie et al., 2009). The rice YSL family consists of 18 members. The OsYSL2 transporter is responsible for the long-distance transfer into sink tissues like leaves and grains (Koike et al., 2004). It is a carrier of Fe(II)–NA, but not Fe(III)–MAs. The transport of Fe(III)–DMA is performed by OsYSL15, which is responsible for Fe root absorption and internal translocation for long distance as well as seedling growth. The Fe transporter OsYSL18 is specifically expressed in reproductive organ, such as the pollen and pollen tube, which suggests a specific role in fertilization. It also can be found in the phloem of laminar joints, indicating a part in phloem Fe transport (Kobayashi and Nishizawa, 2012). The ferrous transporter OsIRT1 and DMA effluxer TOM1 seem not only to be involved in Fe uptake but also in Fe translocation within the plant, due to its expression in vascular tissue in rice (Ishimaru et al., 2006; Nozoye et al., 2011). While the two efflux transporter of NA 1 (ENA1) and ENA2 were involved in NA transport (Nozoye et al., 2011).

BIOFORTIFICATION: AGRONOMIC VS./AND GENETIC IN RICE AND WHEAT

Agronomic Biofortification

Cereal grain micronutrient content can be enriched through agronomic biofortification, which is a fertilizer-based application

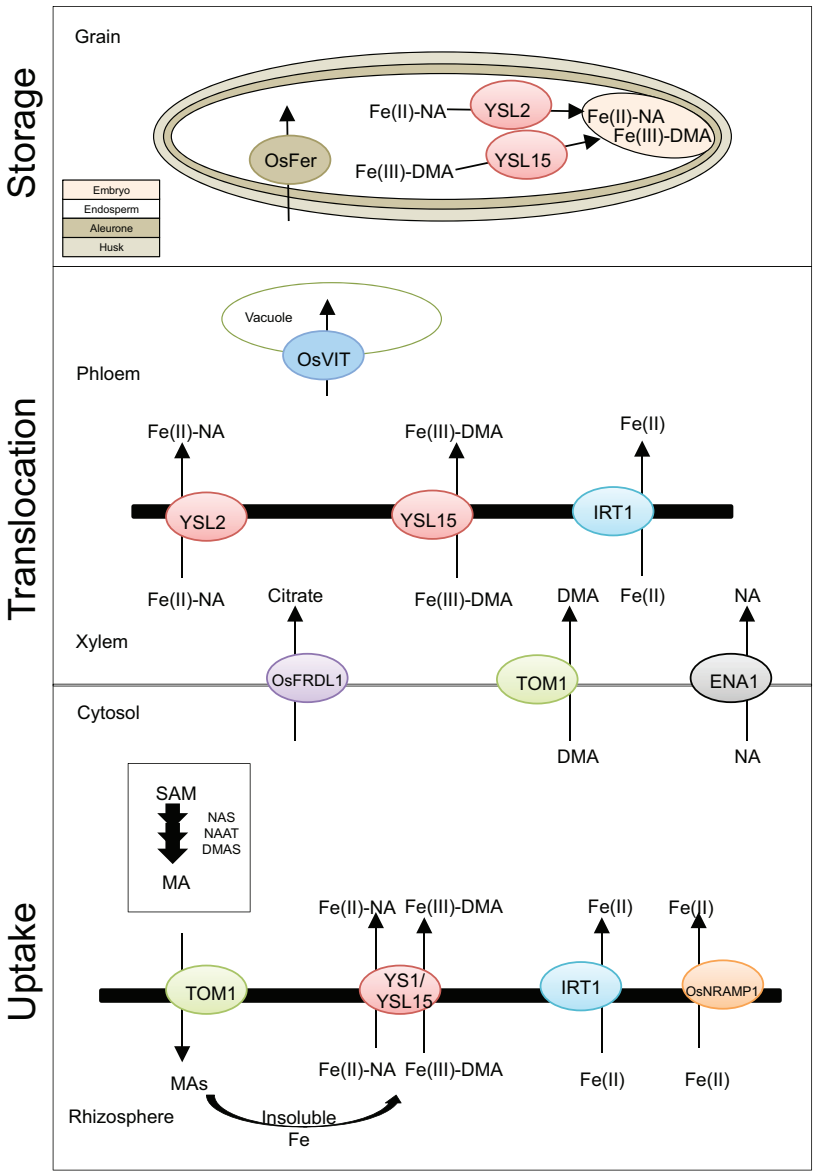

FIGURE 1 | Basic scheme of iron uptake, translocation, and storage in rice. Presented are known genes involved in iron uptake and transport within the rice plant. TOM1, transporter of mugineic acid family phytosiderophores 1; YS1, yellow strip1; YSL15, yellow stripe 1-like; IRT1, iron-regulated transporter; OsNRAMP1, natural resistance-associated macrophage protein 1; OsFRDL1, ferric reductase defective like1; ENA, efflux transporter of nicotianamine; OsVIT, vacuolar iron transporter; OsFER, ferritin; MA, mugineic acid; DMA, 2′-deoxymugineic acid; NA, nicotianamine; SAM, *S*-adenosyl-L-methionine; NAS, nicotianamine synthase; NAAT, nicotianamine aminotransferase; DMAS, deoxymugineic acid synthase.

method to soil or to plant foliar (Cakmak and Kutman, 2017). Soil agronomic biofortification is easy and can be quite cost-effective (Garg et al., 2018). It is a short time solution, important to complement the genetic biofortification, particularly when the soil in the target region is limited to a readily available pool of micronutrient (Cakmak and Kutman, 2017). For rice, the main challenge is the translocation of the mineral from the vegetative part to the grain (Mabesa et al., 2013; Slamet-Loedin et al., 2015), since it is mostly grown in lowland irrigated areas where Fe is highly available.

Foliar feeding is established via plant tissue test or visual foliar. It is affected by endogenous (leaf anatomy), exogenous (pH, soil), as well as environmental factors. After foliar Fe application, it takes the plants 10–20 days to absorb 50% of the micronutrient (Alshall and El-Ramady, 2017). In contrast with the promising results of foliar fertilizer application to improve grain Zn in rice (Cakmak, 2008; Cakmak and Kutman, 2017), the increase of grain Fe using foliar fortification was modest. A similar phenomenon was observed in wheat, neither soil nor foliar applications in inorganic form (e.g., $FeSO_4$) or chelated form (e.g., Fe–EDTA, Fe–EDDHA, or Fe–citrate) were

reported to be effective for increasing grain Fe concentrations (Cakmak, 2008). A minor increase in grain Fe was observed with Fe-EDTA application and also nitrogen application in wheat (Cakmak and Kutman, 2017). Another study showed a foliar application of Fe–amino acid (Fe AA) modestly increased grain Fe concentration by 14.5% on average in rice and by 32.5% when 1% (w/v) NA was added (Yuan et al., 2012). A foliar application to reach a significant increase in grain Fe for biofortification remains challenging.

Genetic Biofortification

Efforts to enrich Fe in the rice grain by conventional breeding are constrained by the limited natural variation of polished grain Fe in rice germplasm. Over 20,000 different accessions of rice germplasm were tested and displayed a maximum of only 5–8 mg kg^{-1} in polished rice grains (Gregorio et al., 2000; Graham, 2003). To date none of the conventional breeding and molecular marker approaches reached grain Fe breeding target in rice and wheat to fulfill 30% EAR in women and children; therefore, this review focuses on the genetic biofortification through transgenic approaches.

To facilitate an efficient and targeted genetic biofortification in rice five key steps can be addressed: (a) enhanced uptake, (b) increase translocation to grain, (c) specialization of Fe storage toward endosperm, (d) decrease of anti-nutritions, and (e) increase of bioavailability (Mulualem, 2015). Both single approach or combination of multiple approaches have been applied in genetic biofortification. The first attempt to obtain an Fe-enriched rice was reported by Goto et al. (1999, **Table 1**), focusing on improving the Fe storage protein. An increase of grain Fe concentration was attained in brown rice (up to 38 μg/g) compared to the wildtype Japonica cv. Kitaake (∼14.3 μg/g) through ectopic overexpression (OE) of SoyFerH1 in the endosperm. Several studies followed using a similar approach of OE lines of SoyferH1, differing in the genetic background (Swarna, IR68144, BR29, IR64, M12) and usage of promoters (OsGluB1, OsGtbl, CluB1, GluB4, OsG1b) (Slamet-Loedin et al., 2015). In two attempts, an elevated Fe level in the polished rice (up to ∼9.2 or ∼7.6 μg/g) was obtained and stable over several generations (Khalekuzzaman et al., 2006; Oliva et al., 2014); however, in particular case, there was no significant increase observed (Drakakaki et al., 2000). Not only was the soybean storage gene utilized to improve the Fe levels within the grain, but also the effect of overexpressing the rice ferritin gene (OsFer2) was analyzed. Higher Fe concentrations were found in T3 rice seeds (up to ∼15.9 μg/g) compared to the control Indica cv. Pusa-Sugandh II with ∼7 μg/g (Paul et al., 2012). Other studies focus on the genes for Fe uptake and translocation in the plant such as the development of OE lines of OsYSL15 (Lee et al., 2009a), responsible for the uptake of Fe(III)–DMA, and OsYSL2 (Ishimaru et al., 2010) for the uptake of Fe(II)–NA from the rhizosphere. The OsYSL2 OE study indicated a higher Fe content of ∼7.5 μg/g in polished rice compared to its counterpart (∼1.8 μg/g) in the T1 generation (**Table 1**). Only minimal elevated Fe concentrations were detected for OsYSL15 OE lines in T1 brown rice (Lee et al., 2009a), similar to the OE of OsYSL9 (Senoura et al., 2017). The alternative approach is to increase the expression of the NAS genes in rice, either by adding a 35S promoter enhancer in OsNAS3 and OsNAS2 gene through T-DNA activation tagging (Lee et al., 2009b, 2012), or by an endosperm OE of OsNAS1 (Zheng et al., 2010), or constitutive OE of OsNAS2 gene (Johnson et al., 2011). The endosperm OE of OsNAS1 resulted in 19 μg/g Fe level in brown rice compared to its wildtype (12 μ/g) and reduced to 5 mg/g after polishing (Zheng et al., 2010). Better results were achieved in the OE OsNAS2 plants with a Fe level-up to 19 μg/g in polished rice (Johnson et al., 2011) in comparison with the Nipponbare wildtype (4.5 μg/g), or in the OsNAS3 and OsNAS2 activation tag plants with 12 and 10 μg/g Fe in milled rice respectively compared to the wildtype (4 μg/g) (Lee et al., 2009b, 2012). A high Fe increase up to 55 μg/g was reported in the endosperm of japonica rice by OE of OsNAS1 and HvNAAT genes (Diaz-Benito et al., 2018). The Fe level is exceptionally high for the starchy endosperm suggesting either Fe contamination or the presence aleurone layer. The Fe level in the earlier generation was 18 μg/g (Banakar et al., 2017b) that already fulfill the nutritive target.

A few studies use the silencing approach to reduce the Fe content in rice grain. Zhang et al. (2012) developed vascular Fe transport (OsVIT) silencing lines, aiming to interrupt the transport of Fe into the flag leaves. A comparable approach was used by Bashir et al. (2013), achieving a Fe level of ∼8 μg/g in polished rice. Only one gene involved in the Fe deficiency response was used to increase the Fe concentration till now. The constitutive expression of OsIRO2 resulted in ∼15.5 μg/g Fe in T1 brown rice seeds in comparison with the wildtype (∼6 μg/g) (Ogo et al., 2011).

The most promising results for Fe-enriched rice grains in tropical Indica rice were developed by Trijatmiko et al. (2016) and Wu et al. (2019) by multigene OE. By expressing the endosperm storage gene PvFER, the chelator AtNAS1 gene and an intracellular iron stores AtNRAMP3 in one cassette, the level of 13.65 μg/g iron was reached in the greenhouse condition (Wu et al., 2019). A slightly higher level of Fe of 15 μg/g concentration in polished grain Fe coupled with high Zn was shown in the results of Trijatmiko et al. (2016) in two field trials (**Table 1**; Trijatmiko et al., 2016). Generally, the field condition resulted in a lower grain Fe compared to the glasshouse setting (Masuda et al., 2012). These reported studies serve as a proof of concept for the potential product of Fe-biofortified rice.

In wheat, using the marker-assisted breeding a modest increase in Fe by 18% was observed in near-isogenic lines of NAM-B1 (Distelfeld et al., 2007). The first transgenic approach in wheat reported a significant increase in grain Fe achieved by the OE of the wheat FERRITIN gene (Borg et al., 2012; **Table 1**). This OE of TaFer1-A gene increased to 50–85% higher Fe content in wheat grains; however, the TaFer1-A genes presence was not stable over the generations (Borg, personal communication). The recent report (Singh et al., 2017b) showed significant progress that OE of OsNAS2 produced up to 93.1 μg/g of Fe in the wheat grain in the greenhouse, it surpasses the recommended nutritive breeding target. While using VACUOLAR IRON TRANSPORTER (TaVIT), a double of Fe concentration was obtained in flour but not in whole grain (Connorton et al., 2017b). Another recent study OE of OsNAS2 in wheat (Beasley et al.,

TABLE 1 | Review on transgenic approaches to develop iron-rich rice and wheat grains.

	Iron ([c] in μg/g)		Generation	Seed status	Growth condition	Cultivar	References
	TG	WT					
RICE			**Genes involved in iron uptake and translocation**				
Rice gene overexpression							
OsIRT1	~12	~10	T3	Brown	Paddy field	Japonica cv. Dongjin	Lee and An, 2009
TOM1	~18	~15	T1	Brown	Hydroponic	Japonica cv. Tsukinohikari	Nozoye et al., 2011
OsYSL15	~14	~12	T1	Brown	Paddy field	Japonica cv. Dongjin	Lee et al., 2009a
OsNAS1	up to ~19	~12		Brown	Field	Japonica cv. Xiushui 110	Zheng et al., 2010
OsNAS2	~10	~4		Milled	Greenhouse	Japonica cv. Dongjin	Lee et al., 2012
OsNAS3	~12	~4	T1	Milled	Greenhouse	*Oryza sativa* L. (cv EYI 105)	Lee et al., 2009b
OsYSL2	~7.5	~1.8	T1	Polished	Glasshouse	Japonica cv. Tsukinohikari	Ishimaru et al., 2010
OsNAS1, OsNAS2, OSNAS3	up to ~19	~4.5	T1	Polished	Glasshouse	Japonica cv. Nipponbare	Johnson et al., 2011
OsNAS1	up to ~40	~20	T4	Endosperm	Greenhouse	*Oryza sativa* L. (cv EYI 105)	Diaz-Benito et al., 2018
OsYSL13	~15	~11		Brown	Greenhouse	Japonica cv. Zhonghua 11	Zhang et al., 2018
Overexpression of gene of different species							
HvNAS1	~8.5	~4	T2	Polished	Greenhouse	Japonica cv. Tsukinohikari	Masuda et al., 2009
HvYS1	up to ~9	~4	T2	Polished		*Oryza sativa* L. (cv EYI 105)	Banakar et al., 2017a
AtIRT1	up to ~4.86	~2.28	T3	Polished	Greenhouse	Japonica cv. Taipei 309	Boonyaves et al., 2016
			Genes involved in storage				
Rice gene overexpression							
OsFer2	up to ~15.9	~7	T3	Milled	Greenhouse	Indica cv. Pusa-Sugandh II	Paul et al., 2012
Soybean gene overexpression							
SoyferH1	up to ~38	~14.3	T1	Brown	Greenhouse	Japonica cv. Kitaake	Goto et al., 1999
SoyferH1	up to ~25	~17	T3–T6	Brown	Greenhouse	Japonica cv. Kitaake	Qu et al., 2005
SoyferH1	~18	~18	T2	Brown	Greenhouse	Indica cv. M12	Drakakaki et al., 2000
SoyferH1	up to ~37	~10	T2	Milled	Screenhouse	Indica cv. IR68144	Vasconcelos et al., 2003
SoyferH1	up to ~16	~6.75	BC2F5	Milled	Greenhouse	Indica cv. Swarna	Paul et al., 2014
SoyferH1	up to ~9.2	~3.8	T3	Polished	Greenhouse	Indica cv. BR29	Khalekuzzaman et al., 2006
SoyferH1	up to ~7.6	~3.3	T4	Polished	Greenhouse	Indica cv. IR64	Oliva et al., 2014
			Genes involved in iron deficiency response				
Rice gene overexpression							
OsIRO2	up to ~15.5	~6	T1	Brown	Greenhouse	Japonica cv. Tsukinohikari	Ogo et al., 2011
			Genes involved in inter-cellular/intra-cellular transport and storage				
Rice gene silencing/knock-down mutant							
OsVIT1	~26	~20		Brown	Paddy field	Japonica cv. Zhonghua 11	Zhang et al., 2012
OsVIT2	~28	~20		Brown	Paddy field	Japonica cv. Dongjin	Zhang et al., 2012
OsVIT2	~8	~5		Polished		Japonica cv. Dongjin	Bashir et al., 2013
OsYSL9	up to ~2.5	1		Polished		Japonica cv. Tsukinohikari	Senoura et al., 2017
OsDMAS1	~5	~5		Polished		Japonica cv. Dongjin	Bashir et al., 2017
			Combined strategies				
Multigene overexpression							
PyFerritin+rgMT+phyA	~22	~10	T1	Brown	Greenhouse	Japonica cv. Taipei 309	Lucca et al., 2002
OsYSL2+, SoyFerH2+, HvNAS1	up to ~4	~1	T3	Polished	Paddy field	Japonica cv. Tsukinohikari	Masuda et al., 2012
HvNAS1, HvNAS1+, HvNAAT, IDS3	up to ~7.3	~5.8	T1	Polished	Paddy field	Japonica cv. Tsukinohikari	Suzuki et al., 2008
HvNAS1+, OsYSL2, SoyFerH2+	~6.3 (~5.02)	~3.2 (~1.46)	T1(T2)	Polished	Greenhouse	Tropical Japonica cv. Paw San Yin	Aung et al., 2013
AtNAS1+, Pvferritin+, Afphytase	up to ~7	~1	T1	Polished	Hydroponic	Japonica cv. Taipei 309	Wirth et al., 2009

(Continued)

TABLE 1 | Continued

AtIRT1, PvFERRITIN, AtNAS1	up to ∼10.46	∼2.7	T2	Polished	Greenhouse	Japonica cv. Nipponbare	Boonyaves et al., 2017
GmFERRITIN, OsNAS2	∼15	∼2.5	T3	Polished	Field	Indica cv. IR64	Trijatmiko et al., 2016
AtNAS1, AtFRD3, PvFer	up to ∼11.08	∼2.05	T3	Polished	Greenhouse	Japonica cv. Nipponbare	Wu et al., 2018
AtNAS1, PvFer, AtNRAMP3	up to ∼13.65	∼2.72	T2	Polished	Greenhouse	Indica cv. IR64	Wu et al., 2019
AtNAS1, PvFER, ZmPSY, PaCRT1	up to ∼6.02	∼1.82	T3	Polished	Greenhouse	Japonica cv. Nipponbare	Singh et al., 2017a
OsNAS1, HvNAATb	up to ∼55	∼20	T4	Endosperm	Greenhouse	*Oryza sativa* L. (cv EYI 105)	Diaz-Benito et al., 2018
OsNAS1, HvHAATb	∼up to 18	∼4	T3	Endosperm	Hydroponic	*Oryza sativa* L. (cv EYI 105)	Banakar et al., 2017b
WHEAT							
Genes involved in iron uptake and translocation							
Single gene over expression							
OsNAS2	up to ∼80	40		Whole grain	Field	*Triticum aestivum* (cv Bob White)	Beasley et al., 2019
OsNAS2	up to ∼22	14		Flour	Field	*Triticum aestivum* (cv Bob White)	Beasley et al., 2019
Genes involved in storage							
Ta FERRITIN	Up to ∼130	72	T2	Whole grain	Greenhouse	*Triticum aestivum* (cv Bob White)	Borg et al., 2012
Ta FERRITIN	Average 88.5	70	T2	Flour	*Greenhouse*	*Triticum aestivum* (cv Bob White)	Borg et al., 2012
Genes involved in inter-cellular/intra-cellular transport and storage							
Ta VIT	Up to 20	10	T1	Flour			Connorton et al., 2017b
Combined strategy							
Multigene overexpression							
OsNAS2 +/or PvFERRITIN	up to ∼93.1	42.7	T4	Whole grain	Greenhouse	*Triticum aestivum* (cv Bob White)	Singh et al., 2017b
OsNAS2, +/or PvFERRITIN	53.3	21.4		Flour	Greenhouse	*Triticum aestivum* (cv Bob White)	Singh et al., 2017b

2019) reported up to 80 μg/g of Fe concentration in wheat grain under field condition.

Potential of Genome Editing Approaches

A recent development in the genome editing tool, Clustered Regulatory Interspaced Palindromic Repeats (CRISPR) for precise modification within the genome, gives researchers a possibility for accurate targeting of genes or genomic regions. This technology has been used in rice to improve yield and stress resistance (Jaganathan et al., 2018; Mishra et al., 2018). The potential example to use CRISPR-based approach is to knockdown OsVIT2 to achieve the increase of grain Fe, similar to the published T-DNA insertion silencing of this gene (Bashir et al., 2013) in different rice cultivars. The development of Fe-enriched rice and wheat grains can also benefit from this method by tweaking the expression of genes involved in Fe homeostasis by editing the regulatory element of Fe homeostasis genes.

TRAIT SELECTION AND POST-HARVEST EFFECT ON IRON AND BIOAVAILABILITY

The accuracy of grain Fe measurement requires consistent preparation, contamination free, and a standardized processing method to reach a consistent milling degree to select the product. The most accurate technique for Fe measurement is ICP-OES (Elzain et al., 2016).

Unpolished brown rice and wheat have a higher concentration and variation of Fe in the aleurone layers, wherein most of the Fe in rice and wheat is stored. Fe in cereal is stored in vacuoles in complex with phytate (Borg et al., 2012), and localized in the aleurone layer and embryo parts. Minimal phytate amount has been detected in the endosperm (Saenchai et al., 2016). Depending on the genotype, the rice bran can have one to five aleurone layers (Del Rosario et al., 1968). Unfortunately, dietary factors that inhibit cereal Fe absorption in human include phytic acid (myoinositol hexaphosphate) together with polyphenols (Gibson et al., 2010; Moretti et al., 2014), tannins, fiber, or hemagglutinins (Welch and Graham, 2004; Holme et al., 2012). Fe in cereal bran is chelated by phytic acid and forms an insoluble complex in the gastrointestinal tract (Iqbal et al., 1994). Rice is predominantly consumed in polished form, while wheat consumption is mixed between brown and white flour. To effectively reduce the "hidden hunger," it is crucial that the added biofortified grain Fe is bioavailable.

Iron bound to ferritin is most likely to be highly available (Lönnerdal et al., 2006). NA has also been suggested as a Fe bioavailability enhancer in rice (Zheng et al., 2010). The correlation of the bioavailability of grain Fe with the presence of NA and ferritin was shown in rice (Trijatmiko et al., 2016).

Recently in wheat, the OE lines of OsNAS2 show that the endosperm Fe is not co-localized with phosphorous but likely with NA (Beasley et al., 2019).

PATHWAY OF A GENETIC BIOFORTIFICATION: PROOF OF CONCEPT TO A PRODUCT

The path from proof of concept to the product started from the development of commercial event amenable for deregulation, the trait and agronomic testing phase in multiple confined fields, the regulatory science phase, and varietal registration phase (McDougall, 2011). To pass the regulatory requirement, GM rice needs to be screened for single locus insertion containing one or more copies and characterized at the molecular level of the actual insert, the absence of vector backbone or other unintended change, and heritability and followed by comprehensive food and environmental safety studies to prove product safety (Heck et al., 2005). In the biofortification study by Trijatmiko et al. (2016), the highest concentrations were obtained in the lines having two copies of transgenes in one insertion locus. Insertion of more than one copy of a transgene does not impede event deregulation as has been shown in some commercially released crops events (Canola-23-18-17, Soya-GU262) with multiple copies (Health Canada, 1999; ISAAA, 2019).

Collection of a comprehensive safety data of food and feed use of Fe-biofortified rice to develop a robust safety regulatory dossier is crucial. In most countries, the assessment follows the Codex Alimentarius guideline, which requires the description of the donor organism; genetic modification and its characterization; and assessment of the possible toxicity, allergenicity, and compositional analysis (FAO, 2003). For the environmental evaluation of nutrition trait, the necessary assessment could be to monitor the relevant insect pest population and change in seed vigor to assess the weediness potential.

Development and submission of a robust biosafety dossier, an excellent agronomic performance, enhancement of Fe bioavailability, and bioefficacy (Bouis and Saltzman, 2017) within the local context of the staple food processing, cooking, and eating habit, and a strong support of the seed sector and health sector in target countries will lay a path for deployment and adoption of Fe-enriched rice. Significant progress in genetic biofortification in recent years can provide a sustainable food-based solution to complement other interventions to reduce iron deficiency anemia in the target communities.

AUTHOR CONTRIBUTIONS

Both authors listed have made a substantial, direct and intellectual contribution to the work, and approved it for publication.

FUNDING

This work was supported by the HarvestPlus – title: Developing high-iron and high-zinc transgenic rice to alleviate iron deficiency in Bangladesh and Southeast Asia Agreement No. 2015H5315 and the BMGF Healthier Rice Project.

ACKNOWLEDGMENTS

We are grateful to Russell Reinke, the IRRI healthier rice project leader, Joe Tohme, The HarvestPlus biotech project coordinator, and Lawrence Kent, the BMGF program officer for Healthier rice for their support.

REFERENCES

Alshall, T., and El-Ramady, H. (2017). Foliar application: from plant nutrition to biofortification. *Environ. Biodiver. Soil Secur.* 1, 71–83. doi: 10.21608/jenvbs.2017.1089.1006

Aung, M. S., Masuda, H., Kobayashi, T., Nakanishi, H., Yamakawa, T., and Nishizawa, N. K. (2013). Iron biofortification of myanmar rice. *Front. Plant Sci.* 4:158. doi: 10.3389/fpls.2013.00158

Banakar, R., Alvarez-Fernandez, A., Abadia, J., Capell, T., and Christou, P. (2017a). The expression of heterologous Fe (III) phytosiderophore transporter HvYS1 in rice increases Fe uptake, translocation and seed loading and excludes heavy metals by selective Fe transport. *Plant Biotechnol. J.* 15, 423–432. doi: 10.1111/pbi.12637

Banakar, R., Alvarez-Fernandez, A., Diaz-Benito, P., Abadia, J., Capell, T., and Christou, P. (2017b). Phytosiderophores determine thresholds for iron and zinc accumulation in biofortified rice endosperm while inhibiting the accumulation of cadmium. *J. Exp. Bot.* 68, 4983–4995. doi: 10.1093/jxb/erx304

Bashir, K., Inoue, H., Nagasaka, S., Takahashi, M., Nakanishi, H., Mori, S., et al. (2006). Cloning and characterization of deoxymugineic acid synthase genes from graminaceous plants. *J. Biol. Chem.* 281, 32395–32402. doi: 10.1074/jbc.m604133200

Bashir, K., Nozoye, T., Nagasaka, S., Rasheed, S., Miyauchi, N., Seki, M., et al. (2017). Paralogs and mutants show that one DMA synthase functions in iron homeostasis in rice. *J. Exp. Bot.* 68, 1785–1795. doi: 10.1093/jxb/erx065

Bashir, K., Takahashi, R., Akhtar, S., Ishimaru, Y., Nakanishi, H., and Nishizawa, N. K. (2013). The knockdown of OsVIT2 and MIT affects iron localization in rice seed. *Rice* 6:31. doi: 10.1186/1939-8433-6-31

Beasley, J. T., Bonneau, J. P., Sanchez-Palacios, J. T., Moreno-Moyano, L. T., Callahan, D. L., Tako, E., et al. (2019). Metabolic engineering of bread wheat improves grain iron concentration and bioavailability. *Plant Biotechnol. J.* doi: 10.1111/pbi.13074 [Epub ahead of print].

Boonyaves, K., Gruissem, W., and Bhullar, N. K. (2016). NOD promoter-controlled AtIRT1 expression functions synergistically with NAS and FERRITIN genes to increase iron in rice grains. *Plant Mol. Biol.* 90, 207–215. doi: 10.1007/s11103-015-0404-0

Boonyaves, K., Wu, T.-Y., Gruissem, W., and Bhullar, N. K. (2017). Enhanced Grain iron levels in rice expressing an iron-regulated metal transporter, nicotianamine synthase, and ferritin gene cassette. *Front. Plant Sci.* 8:130. doi: 10.3389/fpls.2017.00130

Borg, S., Brinch-Pedersen, H., Tauris, B., Madsen, L. H., Darbani, B., Noeparvar, S., et al. (2012). Wheat ferritins: improving the iron content of the wheat grain. *J. Cereal Sci.* 56, 204–213. doi: 10.1016/J.Jcs.2012.03.005

Borrill, P., Connorton, J. M., Balk, J., Miller, A. J., Sanders, D., and Uauy, C. (2014). Biofortification of wheat grain with iron and zinc: integrating novel genomic resources and knowledge from model crops. *Front. Plant Sci.* 5:53. doi: 10.3389/fpls.2014.00053

Bouis, H. E., Hotz, C., McClafferty, B., Meenakshi, J. V., and Pfeiffer, W. H. (2011). Biofortification: a new tool to reduce micronutrient malnutrient. *Food Nutr. Bull.* 32, S31–S40. doi: 10.1021/es010549d

Bouis, H. E., and Saltzman, A. (2017). Improving nutrition through biofortification: a review of evidence from HarvestPlus, 2003 through 2016. *Glob. Food Secur.* 12, 49–58. doi: 10.1016/j.gfs.2017.01.009

Cakmak, I. (2008). Enrichment of cereal grains with zinc: Agronomic or genetic biofortification? *Plant Soil* 302, 1–17. doi: 10.1007/s11104-007-9466-3

Cakmak, I., and Kutman, U. B. (2017). Agronomic biofortification of cereals with zinc: a review. *Eur. J. Soil Sci.* 69, 172–180. doi: 10.1111/ejss.12437

Calliatte, R., Schikora, A., Briat, J. F., Mari, S., and Curie, C. (2010). High-affinity manganese uptake by the metal transporter NRAMP1 is essential for *Arabidopsis* growth in low manganese conditions. *Plant Cell* 22, 904–917. doi: 10.1105/tpc.109.073023

Connorton, J. M., Balk, J., and Rodriguez-Celma, J. (2017a). Iron homeostasis in plants – a brief overview. *Metallomics* 9, 813–823. doi: 10.1039/c7mt00136c

Connorton, J. M., Jones, E. R., Rodríguez-Ramiro, I., Fairweather-Tait, S., Uauy, C., and Balk, J. (2017b). Wheat vacuolar iron transporter TaVIT2 transports Fe and Mn and is effective for biofortification. *Plant Physiol.* 174, 2434–2444. doi: 10.1104/pp.17.00672

Curie, C., Cassin, G., Couch, D., Divol, F., Higuchi, K., Le, Jean M, et al. (2009). Metal movement within the plant: contribution of nicotianamine and yellow stripe 1-like transporter. *Ann. Bot.* 103, 1–11. doi: 10.1093/aob/mcn207

Curie, C., Panaviene, Z., Loulergue, C., Dellaporta, S. L., Briat, J. F., and Walker, E. L. (2001). Maize yellow stripe 1 encodes a membrane protein directly involved in Fe(III) uptake. *Nature* 409, 346–349. doi: 10.1038/35053080

Del Rosario, A. R., Briones, V. P., Vidal, A. J., and Juliano, B. O. (1968). Composition and endosperm structure of developing and mature rice kernel. *Cereal Chem.* 45, 225–235.

Diaz-Benito, P., Banakar, R., Rodriguez-Menendez, S., Capell, T., Pereiro, R., Christou, P., et al. (2018). Iron and zinc in the embryo and endosperm of rice (*Oryza sativa* L.) seeds in contrasting 2'-deoxymugineic acid/ nicotianamine scenarios. *Front. Plant Sci.* 9:1190. doi: 10.3389/fpls.2018.01190

Distelfeld, A., Cakmak, I., Peleg, Z., Ozturk, L., Yazici, A. M., Budak, H., et al. (2007). Multiple QTL-effects of wheat Gpc-B1 locus on grain protein and micronutrient concentrations. *Physiol. Plant* 129, 635–643. doi: 10.1111/j.1399-3054.2006.00841.x

Drakakaki, G., Christou, P., and Stöger, E. (2000). Constitutive expression of soybean ferritin cDNA in transgenic wheat and rice results in increased iron levels in vegetative tissues but not in seeds. *Transgenic Res.* 9, 445–452. doi: 10.1023/A:1026534009483

Eide, D., Broderius, M., Fett, J., and Guerinot, M. L. (1996). A novel iron-regulated metal transporter from plants identified by functional expression in yeast. *Proc. Natl. Acad. Sci. U.S.A.* 93, 5624–5628. doi: 10.1073/pnas.93.11.5624

Elzain, A. H., Ebrahim, A. M., and Ali Eltoum, M. S. (2016). Comparison between XRF, PIXE and ICP-OES Techniques Applied For Analysis of Some Medicinal Plants. *IOSR-JAC* 9, 6–12. doi: 10.9790/5736-090401 0612

FAO (2003). *Guideline for the Conduct of Food Safety Assessment of Foods Derived From Recombinant-DNA Plants*. Available at: http://www.fao.org/fileadmin/user_upload/gmfp/docs/CAC.GL_45_2003.pdf (accessed June 12, 2019).

Garcia-Oliveira, A. L., Chander, S., Ortiz, R., Menkir, A., and Gedil, M. (2018). Genetic basis and breeding perspectives of grain iron and zinc enrichment in cereals. *Front. Plant Sci.* 9:937. doi: 10.3389/fpls.2018.00937

Garg, M., Sharma, N., Sharma, S., Kapoor, P., Kumar, A., Chunduri, V., et al. (2018). Biofortified crops generated by breeding, agronomy, and transgenic approaches are improving lives of millions of people around the world. *Front. Nutr.* 5:12. doi: 10.3389/fnut.2018.00012

GBD 2015 Disease and Injury Incidence and Prevalence Collaborators (2016). Global, regional, and national incidence, prevalence, and years lived with disability for 310 diseases and injuries, 1990–2015: a systematic analysis for the Global Burden of Disease Study 2015. *Lancet* 388, 1545–1602. doi: 10.1016/S0140-6736(16)31678-6

Gibson, R. S., Bailey, K. B., Gibbs, M., and Ferguson, E. L. (2010). A review of phytate, iron, zinc, and calcium concentrations in plant-based complementary foods used in low-income countries and implications for bioavailability. *Food Nutr. Bull.* 31(2 Suppl.), S134–S146. doi: 10.1177/15648265100312 S206

Goto, F., Yoshihara, T., Shigemoto, N., Toki, S., and Takaiwa, F. (1999). Iron fortification of rice seed by the soybean ferritin gene. *Nat. Biotechnol.* 17, 282–286. doi: 10.1038/7029

Graham, R. D. (2003). Biofortification: a global challenge. *Int. Rice Res. Notes* 28, 4–8.

Gregorio, G. B., Senadhira, D., Htut, H., and Graham, R. D. (2000). Breeding for trace mineral density in rice. *Food Nutr. Bull.* 21, 382–386. doi: 10.1177/156482650002100407

Guerinot, M. L. (2000). The ZIP family of metal transporters. *Biochim. Biophys. Acta* 1465, 190–198. doi: 10.1016/s0005-2736(00)00138-3

Health Canada (1999). *ARCHIVED - High Lauric Acid Canola Lines 23-198, 23-18-17*. Available at: https://www.canada.ca/en/health-canada/services/food-nutrition/genetically-modified-foods-other-novel-foods/approved-products/high-lauric-acid-canola-lines-23-198-23-18-17.html (accessed October, 1999).

Heck, G. R., Armstrong, C. L., Astwood, J. D., Behr, C. F., Bookout, J. T., Brown, S. M., et al. (2005). Development and characterization of a CP4 EPSPS-based, glyphosate-tolerant corn event. *Crop Sci.* 44, 329–339. doi: 10.2135/cropsci2005.0329

Higuchi, K., Suzuki, K., Nakanishi, H., Yamaguchi, H., Nishizawa, N. K., and Mori, S. (1999). Cloning of nicotianamine synthase genes, novel genes involved in the biosynthesis of phytosiderophores. *Plant Physiol.* 119, 471–479.

Holme, I. B., Dioisio, G., Brinch-Pedersen, H., Wendt, T., Madsen, C. K., Vincze, E., et al. (2012). Cisgenic barley with improved phytase activity. *Plant Biotechnol. J.* 10, 237–247. doi: 10.1111/j.1467-7652.2011.00660.x

Inoue, H., Kobayashi, T., Nozoye, T., Takahashi, M., Kakei, Y., Suzuki, K., et al. (2009). Rice OsYSL15 is an iron-regulated iron(III)-deoxymugineic acid transporter expressed in the roots and is essential for iron uptake in early growth of the seedlings. *J. Biol. Chem.* 284, 3470–3479. doi: 10.1074/jbc.M806042200

Inoue, H., Suzuji, M., Takahashi, M., Nakanishi, H., Mori, S., and Nishizawa, N. K. (2004). A rice FRD3-like (OsFRDL1) gene is expressed in the cells involved in long-distance transport. *Soil Sci. Plant Nutr.* 50, 1133–1140. doi: 10.1080/00380768.2004.10408586

Iqbal, T. H., Lewis, K. O., and Copper, B. T. (1994). Phytase activity in the human and rat small intestine. *Gut* 35, 1233–1236. doi: 10.1136/gut.35.9.1233

ISAAA (2019). *International Service for the Acquisition of Agri-Biotech Applications*. http://www.isaaa.org/gmapprovaldatabase/event/default.asp?EventID=164

Ishimaru, Y., Masuda, H., Bashir, K., Inoue, H., Tsukamoto, T., Takahashi, M., et al. (2010). Rice metal-nicotianamine transporter, OsYSL2, is required for the long-distance transport of iron and manganese. *Plant J.* 62, 379–390. doi: 10.1111/j.1365-313X.2010.04158.x

Ishimaru, Y., Suzuki, M., Tsukamoto, T., Suzuki, K., Nakazono, M., Kobayashi, T., et al. (2006). Rice plants take up iron as an Fe3+-phytosiderophore and as Fe2+. *Plant J.* 45, 335–346. doi: 10.1111/j.1365-313x.2005.02624.x

Jaganathan, D., Ramasamy, K., Sellamuthu, G., Jayabalan, S., and Venkataraman, G. (2018). CRISPR for crop improvement: an update review. *Front. Plant Sci.* 9:985. doi: 10.3389/fpls.2018.00985

Johnson, A. A. T., Kyriacou, B., Callahan, D. L., Carruthers, L., Stangoulis, J., Lombi, E., et al. (2011). Constitutive overexpression of OsNAS gene family reveals single-gene strategies for effective iron- and zinc- biofortification of rice endosperm. *PLoS One* 6:e24476. doi: 10.1371/journal.pone.0024476

Khalekuzzaman, M., Datta, K., Oliva, N., Alam, M. F., Joarder, I., and Datta, S. K. (2006). Stable integration, expression and inheritance of the ferritin gene in transgenic elite indica rice cultivar BR29 with enhanced iron level in the endosperm. *Indian J.* 5, 26–31.

Kim, S. A., and Guerinot, M. L. (2007). Mining iron: iron uptake and transport in plants. *FEBS Lett.* 581, 2273–2280. doi: 10.1016/j.febslet.2007.04.043

Kobayashi, T., and Nishizawa, N. K. (2012). Iron uptake, translocation, and regulation in higher plants. *Annu. Rev. Plant Biol.* 63, 131–152. doi: 10.1146/annurev-arplant-042811-105522

Kobayashi, T., Suzuki, M., Inoue, H., Itai, R. N., Takahashi, M., Nakanishi, H., et al. (2005). Expression of iron-acquisition-related genes in iron-deficient rice is co-ordinately induced by partially conserved iron-deficiency-responsive elements. *J. Exp. Bot.* 56, 1305–1316. doi: 10.1093/jxb/eri131

Koike, S., Inoue, H., Mizuno, D., Takahashi, M., Nakanishi, H., Mori, S., et al. (2004). OsYSL2 is a rice metal-nicotianamine transporter that is regulated by

iron and expressed in phloem. *Plant J.* 39, 415–424. doi: 10.1111/j.1365-313x.2004.02146.x

Lanquar, V., Lelièvre, F., Bolte, S., Hamès, C., Alcon, C., Neumann, D., et al. (2005). Mobilization of vacuolar iron by AtNRAMP3 and At NRAMP4 is essential for seed germination on low iron. *EMBO J.* 24, 4041–4051. doi: 10.1038/sj.emboj.7600864

Lee, S., and An, G. (2009). Over-expression of OsIRT leads to increased iron and zinc accumulations in rice. *Plant. Cell Environ.* 32, 408–416. doi: 10.1111/j.1365-3040.2009.01935.x

Lee, S., Chiecko, J. C., Kim, S. A., Walker, E. L., Lee, Y., Guerinot, M. L., et al. (2009a). Disruption of OsYSL15 leads to iron inefficiency in rice plants. *Plant Physiol.* 150, 786–800. doi: 10.1104/pp.109.135418

Lee, S., Jeon, U. S., Lee, S. J., Kim, Y.-K., Persson, D. P., Husted, S., et al. (2009b). Iron fortification of rice seeds through activation of the nicotianamine synthase gene. *Proc. Natl. Acad. Sci. U.S.A.* 106, 22014–22019. doi: 10.1073/pnas.0910950106

Lee, S., Kim, Y.-S., Jeon, U.-S., Kim, Y.-K., Schjoerring, J. K., and An, G. (2012). Activation of rice nicotianamine synthase 2 (OsNAS2) enhances iron availability for biofortification. *Mol. Cells* 33, 269–275. doi: 10.1007/s10059-012-2231-3

Lönnerdal, B., Bryant, A., Liu, X., and Theil, E. C. (2006). Iron absorption from soybean ferritin in nonanemic women. *Am. J. Clin. Nutr.* 83, 103–107. doi: 10.1093/ajcn/83.1.103

Lucca, P., Hurrell, R., and Potrykus, I. (2002). Fighting iron deficiency anemia with iron-rich rice. *J. Am. Coll. Nutr.* 21, 184–190. doi: 10.1080/07315724.2002.10719264

Mabesa, R. L., Impa, S. M., Grewal, D., and Johnson-Beebout, S. E. (2013). Contrasting grain-Zn response of biofortification rice (*Oryza sativa* L.) breeding lines to foliar Zn application. *Field Crops Res.* 149, 223–233. doi: 10.1016/j.fcr.2013.05.012

Masuda, H., Ishimaru, Y., Aung, M. S., Kobayashi, T., Kakei, Y., Takahashi, M., et al. (2012). Iron biofortification in rice by the introduction of multiple genes involved in iron nutrition. *Sci. Rep.* 2, 1–7. doi: 10.1038/srep00543

Masuda, H., Usuda, K., Kobayashi, T., Ishimaru, Y., Kakei, Y., Takahashi, M., et al. (2009). Overexpression of the barley nicotianamine synthase gene HvNAS1 increases iron and zinc concentrations in rice grains. *Rice* 2, 155–166. doi: 10.1007/s12284-009-9031-9031

McDougall, A. (2011). *The Cost and Time Involved in the Discovery, Development and Authorisation of a New Plant Biotechnology Derived Trait, a Consultancy Study for Crop Life International*. Available at: https://croplife.org/wp-content/uploads/2014/04/Getting-a-Biotech-Crop-to-Market-Phillips-McDougall-Study.pdf (accessed April 14, 2015).

Mishra, R., Joshi, R. K., and Zhao, K. (2018). Genome editing in rice: recent advances, challenges, and future implications. *Front. Plant Sci.* 9:1361. doi: 10.33389/fpls.2018.01361

Moretti, D., Biebinger, R., Bruins, M. J., Hoeft, B., and Kraemer, K. (2014). Bioavailability of iron, zinc, folic acid, and vitamin A from fortified maize. *Ann. N. Y. Acad. Sci.* 1312, 54–65. doi: 10.1111/nyas.12297

Mulualem, T. (2015). Application of bio-fortification through plant breeding to improve the value of staple crops. *Biomed. Biotechnol.* 3, 11–19. doi: 10.12691/bb-3-1-3

Nozoye, T., Nagaska, S., Kobayashi, T., Takahashi, M., Sato, Y., Sato, Y., et al. (2011). Phytosiderophore efflux transporters are crucial for iron acquisition in graminaceous plants. *J. Biol. Chem.* 286, 5446–5454. doi: 10.1074/jbc.M110.180026

Ogo, Y., Itai, R. N., Kobayashi, T., Aung, M. S., Nakanishi, H., and Nishizawa, N. K. (2011). OsIRO2 is responsible for iron utilization in rice and improves growth and yield in calcareous soil. *Plant Mol. Biol.* 75, 593–605. doi: 10.1007/s11103-011-9752-6

Oliva, N., Chadha-Mohanty, P., Poletti, S., Abrigo, E., Atienza, G., Torrizo, L., et al. (2014). Large-scale production and evaluation of marker-free indica rice IR64 expressing phytoferritin genes. *Mol. Breed.* 33, 23–37. doi: 10.1007/s11032-013-9931-z

Paul, S., Ali, N., Datta, S. K., and Datta, K. (2014). Development of an iron-enriched high-yieldings indica rice cultivar by introgression of a high-iron trait from transgenic iron-biofortified rice. *Plant Foods Hum. Nutr.* 69, 203–208. doi: 10.1007/s11130-014-0431-z

Paul, S., Ali, N., Gayen, D., Datta, S. K., and Datta, K. (2012). Molecular breeding of Osfer2 gene to increase iron nutrition in rice grain. *GM Crops Food* 3, 310–316. doi: 10.4161/gmcr.22104

Qu, L. Q., Yoshihara, T., Ooyama, A., Goto, F., and Takaiwa, F. (2005). Iron accumulation does not parallel the high expression level of ferritin in transgenic rice seeds. *Planta* 222, 225–233. doi: 10.1007/s00425-005-1530-8

Robinson, N. J., Procter, C. M., Connolly, E. L., and Guerinot, M. L. (1999). A ferric-chelate reductase for iron uptake from soils. *Nature* 397, 694–697. doi: 10.1038/17800

Saenchai, C., Prom-u-thai, C., Lordkaew, S., Rouached, H., and Rerkasem, B. (2016). Distribution of iron and Zn in plant and grain of different rice genotypes grown under aerobic and wetland conditions. *J. Cereal Sci.* 71, 108–115. doi: 10.1016/j.jcs.2016.08.007

Senoura, T., Sakashita, E., Kobayashi, T., Takahashi, M., Aung, M. S., Masuda, H., et al. (2017). The iron-chelate transporter OsYSL9 plays a role in iron distribution in developing rice grains. *Plant Mol. Biol.* 95, 375–387. doi: 10.1007/s11103-017-0656-y

Singh, S. P., Gruissem, W., and Bhullar, N. K. (2017a). Single genetic locus improvement if iron, zinc and β-carotene content in rice grains. *Sci. Rep.* 7: 6883. doi: 10.1038/s41598-017-07198-5

Singh, S. P., Keller, B., Gruissem, W., and Bhullar, N. K. (2017b). Rice nicotianamine synthase 2 expression improves dietary iron and zinc levels in wheat. *Theor. Appl. Genet* 130, 283–292. doi: 10.1007/s00122-016-2808-x

Slamet-Loedin, I. H., Johnson-Beebout, S. E., Impa, S., and Tsakirpaloglou, N. (2015). Enriching rice with Zn and Fe while minimizing Cd risk. *Front. Plant Sci.* 6:121. doi: 10.3389/fpls.2015.00121

Suzuki, M., Morikawa, K. C., Nakanishi, H., Takahashi, M., Saigusa, M., Mori, S., et al. (2008). Transgenic rice lines that include barley genes have increased tolerance to low iron availability in a calcareous paddy soil. *Soil Sci. Plant Nutr.* 54, 77–85. doi: 10.1111/j.1747-0765.2007.00205.x

Suzuki, M., Takahashi, M., Tsukamoto, T., Watanabe, S., Matsuhashi, S., Yazaki, J., et al. (2006). Biosynthesis and secretion of mugineic acid family phytosiderophores in zinc-deficient barely. *Plant J.* 48, 85–97. doi: 10.1111/j.1365-313x.2006.02853.x

Takagi, S., Nomoto, K., and Takemoto, S. (1984). Physiological aspect of mugineic acid, a possible phytosiderophore of graminaceous plants. *J. Plant Nutr.* 7, 469–477. doi: 10.1080/01904168409363213

Takahashi, M., Yamaguchi, H., Nakanishi, H., Shioiri, T., Nishizawa, N. K., and Mori, S. (1999). Cloning two genes for nicotianamine aminotransferase, a critical enzyme in iron acquisition (StrategyII) in graminaceous plants. *Plant Physiol.* 121, 947–956. doi: 10.1104/pp.121.3.947

Trijatmiko, K. R., Dueñas, C., Tsakirpaloglou, N., Torrizo, L., Arines, F. M., Adeva, C., et al. (2016). Biofortified indica rice attains iron and zinc nutrition dietary targets in the field. *Sci. Rep.* 6:19792. doi: 10.1038/srep19792

Vasconcelos, M., Datta, K., Oliva, N., Khalekuzzaman, M., Torrizo, L., Krishnan, S., et al. (2003). Enhanced iron and zinc accumulation in transgenic rice with the ferritin gene. *Plant Sci.* 164, 371–378. doi: 10.1016/S0168-9452(02)00421-1

Welch, R. M., and Graham, R. D. (2004). Breeding for micronutrients in staple food crops from human nutrition perspective. *J. Exp. Bot.* 55, 353–365. doi: 10.1093/jxb/erh064

Wirth, J., Poletti, S., Aeschlimann, B., Yakandawala, N., Drosse, B., Osorio, S., et al. (2009). Rice endosperm iron biofortification by targeted and synergistic action of nicotianamine synthase and ferritin. *Plant Biotechnol. J.* 7, 631–644. doi: 10.111/j.1467-7652.2009.00430.x

Wu, T.-Y., Gruissem, W., and Bhullar, N. K. (2018). Facilitated citrate-dependent iron translocation increases rice endosperm iron and zinc concentrations. *Plant Sci.* 270, 13–22. doi: 10.1016/.plantsci.2018.02.002

Wu, T.-Y., Gruissem, W., and Bhullar, N. K. (2019). Targeting intracellular transport combined with efficient uptake and storage significantly increases grain iron and zinc levels in rice. *Plant Biotechnol. J.* 17, 9–20. doi: 10.111/pbi.12943

Yokosho, K., Yamaji, N., Ueno, D., Mitani, N., and Ma, J. F. (2009). OsFRDL1 is a citrate transporter required for efficient translocation of iron in rice. *Plant Physiol.* 149, 297–305. doi: 10.1104/pp.108.128132

Yoneyama, T., Ishikawa, S., and Fujimaki, S. (2015). Route and regulation of zinc, cadmium, and iron transport in rice plants (*Oryza sativa* L.) during

vegetative growth and grain filling: Metal transporters, metal speciation, grain Cd reduction and Zn and Fe biofortification. *Int. J. Mol. Sci.* 16, 19111–19129. doi: 10.3390/ijms160819111

Yuan, L., Wu, L., Yang, C., and Lv, Q. (2012). Effects of iron and zinc foliar applications on rice plants and their grain accumulation and grain nutritional quality. *J. Sci. Food Agric.* 93, 254–261. doi: 10.1002/jsfa.5749

Zhang, C., Shinwari, K. I., Luo, L., and Zheng, L. (2018). OsYSL13 is involved in iron distribution in rice. *Int. J. Mol. Sci.* 19:3537. doi: 10.3390/ijms19113537

Zhang, Y., Xu, Y.-H., Yi, H.-Y., and Gong, J.-M. (2012). Vacuolar membrane transporters OsVIT1 and OsVIT2 modulate iron translocation between flag leaves and seeds in rice. *Plant J.* 72, 400–410. doi: 10.1111/j.1365-313X.2012.05088.x

Zheng, L., Cheng, Z., Ai, C., Jiang, X., Bei, X., Zheng, Y., et al. (2010). Nicotianamine, a novel enhancer of rice iron bioavailability to humans. *PLoS One* 5:e10190. doi: 10.1371/journal.pone.0010190

Conflict of Interest Statement: The authors declare that the research was conducted in the absence of any commercial or financial relationships that could be construed as a potential conflict of interest.

frontiers in Plant Science

ORIGINAL RESEARCH
published: 10 October 2019
doi: 10.3389/fpls.2019.01237

Ethylene and Phloem Signals Are Involved in the Regulation of Responses to Fe and P Deficiencies in Roots of Strategy I Plants

Carlos Lucena[1], Rafael Porras[2], María J. García[1], Esteban Alcántara[3], Rafael Pérez-Vicente[1], Ángel M. Zamarreño[4], Eva Bacaicoa[4], José M. García-Mina[4], Aaron P. Smith[5] and Francisco J. Romera[3]*

[1] Department of Botany, Ecology and Plant Physiology, Campus de Excelencia Internacional Agroalimentario CeiA3, Universidad de Córdoba, Córdoba, Spain, [2] IFAPA, Centro Alameda del Obispo, Córdoba, Spain, [3] Department of Agronomy, Campus de Excelencia Internacional Agroalimentario CeiA3, Universidad de Córdoba, Córdoba, Spain, [4] Department of Environmental Biology, Faculty of Sciences, Universidad de Navarra, Pamplona (Navarra), Spain, [5] Department of Biological Sciences, Louisiana State University, Baton Rouge, LA, United States

OPEN ACCESS

Edited by:
Wolfgang Schmidt, Academia Sinica, Taiwan

Reviewed by:
Maribela Pestana, University of Algarve, Portugal
Jitender Giri, National Institute of Plant Genome Research (NIPGR), India

***Correspondence:**
Carlos Lucena
b42lulec@uco.es

Specialty section:
This article was submitted to Plant Nutrition, a section of the journal Frontiers in Plant Science

Received: 31 January 2019
Accepted: 05 September 2019
Published: 10 October 2019

Citation:
Lucena C, Porras R, García MJ, Alcántara E, Pérez-Vicente R, Zamarreño ÁM, Bacaicoa E, García-Mina JM, Smith AP and Romera FJ (2019) Ethylene and Phloem Signals Are Involved in the Regulation of Responses to Fe and P Deficiencies in Roots of Strategy I Plants. Front. Plant Sci. 10:1237. doi: 10.3389/fpls.2019.01237

Iron (Fe) and phosphorus (P) are two essential mineral nutrients whose acquisition by plants presents important environmental and economic implications. Both elements are abundant in most soils but scarcely available to plants. To prevent Fe or P deficiency dicot plants initiate morphological and physiological responses in their roots aimed to specifically acquire these elements. The existence of common signals in Fe and P deficiency pathways suggests the signaling factors must act in conjunction with distinct nutrient-specific signals in order to confer tolerance to each deficiency. Previous works have shown the existence of cross talk between responses to Fe and P deficiency, but details of the associated signaling pathways remain unclear. Herein, the impact of foliar application of either P or Fe on P and Fe responses was studied in P- or Fe-deficient plants of *Arabidopsis thaliana*, including mutants exhibiting altered Fe or P homeostasis. Ferric reductase and acid phosphatase activities in roots were determined as well as the expression of genes related to P and Fe acquisition. The results obtained showed that Fe deficiency induces the expression of P acquisition genes and phosphatase activity, whereas P deficiency induces the expression of Fe acquisition genes and ferric reductase activity, although only transitorily. Importantly, these responses were reversed upon foliar application of either Fe or P on nutrient-starved plants. Taken together, the results reveal interactions between P- and Fe-related phloem signals originating in the shoots that likely interact with hormones in the roots to initiate adaptive mechanisms to tolerate deficiency of each nutrient.

Keywords: ethylene, iron, phloem, phosphorus, signals

INTRODUCTION

Iron (Fe) and phosphorus (P) are two essential elements for plant growth (Marschner, 1995). Both elements are abundant in most soils but are present in chemical forms generally not available to plants. As a result, plants enhance acquisition of Fe and P through morphological and physiological responses in their roots. Deficiency of either nutrient initiates similar root responses, such as development of subapical root hairs or cluster roots and the acidification of the rhizosphere or the production of organic acids (Lucena et al., 2015; Song and Liu, 2015; Neumann, 2016; Stetter et al., 2017; Bhosale et al., 2018; Lucena et al., 2018). A defining feature of Strategy I plants is the need to reduce Fe(III), the most abundant form of Fe in soils, to Fe(II), prior to acquisition. In *Arabidopsis*, this Fe(III) reduction is catalyzed by a ferric reductase (EC 1.16.1.17) encoded by the *FRO2* gene, whereas Fe(II) uptake is mediated by a transporter encoded by the *IRT1* gene (Walker and Connolly, 2008; Ivanov et al., 2012). Both genes are up-regulated under Fe deficiency and are activated by specific bHLH transcription factors, which are also up regulated by Fe deficiency. These bHLH transcription factors include FIT, bHLH38, bHLH39, and others in *Arabidopsis* (Yuan et al., 2008; Ivanov et al., 2012; Brumbarova et al., 2015). Some of the physiological responses to phosphate (Pi) starvation include the up-regulation of Pi transporters (e.g. AtPht1;4, also named AtPT2) and of phosphatase activities (e.g. AtPAP17, also named AtACP5) (Zhang et al., 2014). del Pozo et al. (1999) purified and sequenced the N-terminal region of a Pi starvation induced acid phosphatase (encoded by the *AtPAP17* gene) from *Arabidopsis thaliana*. PAP17 shares the characteristics of type 5 acid phosphatases, a class of purple acid phosphatases (PAP) stimulated under low P availability. Recent studies have demonstrated that secretion of PAPs can facilitate utilization of organic P in the rhizosphere (Wang et al., 2009; Robinson et al., 2012; Mehra et al., 2017).

Studies in recent years have demonstrated an important role of MYB type transcription factors on the expression of genes that initiate responses to Fe or P deficiency. *AtMYB72* increases its transcription under Fe deficiency and is involved in some Fe deficiency responses (García et al., 2010). Most transcription factors that induce P deficiency responses belong to the MYB family (Müller et al., 2007). Of particular note, the *Arabidopsis* MYB transcription factors AtPHR1 and AtPHR2 ("Phosphate Starvation Response" 1 and 2 respectively), are crucial for P deficiency signaling (Rubio et al., 2001; Franco-Zorrilla et al., 2004; Todd et al., 2004; Bari et al., 2006; Mehra et al., 2017).

In previous works, it has been found that P deficiency induces the expression of Fe-related genes; that Fe deficiency induces the expression of P-related genes and that both deficiencies induce the expression of ethylene-related genes (reviewed in García et al., 2015; Lucena et al., 2015; Lucena et al., 2018). Taken together, these results suggest the existence of cross talk between Fe and P deficiency. The upregulation of Fe acquisition genes under P deficiency is generally associated to the increased accumulation of Fe in leaves (Wang Y. H. et al., 2002; Misson et al., 2005; Hirsch et al., 2006; Ward et al., 2008; Zheng et al., 2009; Abel, 2011; Perea-García et al., 2013; Wang et al., 2014, Lucena et al., 2018). On the other hand, P fertilization excess causes Fe chlorosis in calcareous soils (Romera et al., 1992; Sánchez-Rodriguez et al., 2013; Henry et al., 2017) and Fe deficiency affects P content in leaves (de Kock, 1955).

Either work in the nineties revealed links between ethylene and responses to deficiencies of Fe (Romera and Alcántara, 1994) and P (Borch et al., 1999). Although the regulation of the genes related to these responses is not totally understood, ethylene has since been implicated in the activation of both Fe-related genes (*AtFIT*, *AtFRO2*, and *AtIRT1*; Lucena et al., 2006; Lucena et al., 2015; Lucena et al., 2018; García et al., 2011; García et al., 2015) and P-related genes (*AtPht1;4* and *AtPAP17*; Lei et al., 2011; Roldán et al., 2013). In all cases, the activating effect of ethylene was dependent on the Fe or P status of the plants (García et al., 2011; Lei et al., 2011; Neumann, 2016; Liu et al., 2017), which suggests the involvement of signals other than ethylene in gene activation (García et al., 2013). García et al. (2013) showed that the foliar application of Fe blocked the expression of Fe-acquisition genes in the *Arabidopsis* wild-type cultivar Col-0 but not in the *Arabidopsis opt3-2* mutant, which suggests the existence of a Fe-related repressive signal moving in the phloem. This mutant harbors a T-DNA insertion in the *AtOPT3* promoter resulting in reduced *AtOPT3* expression (Stacey et al., 2008). Recently, *AtOPT3* has been implicated in the transport of Fe ions into the phloem (Zhai et al., 2014). In relation to ethylene, the *opt3* mutant produces more ACC in Fe-sufficient roots than the wild-type cultivar Col-0 (García et al., 2018). In agreement with this, it also presents constitutive activation of several ethylene-related genes in Fe-sufficient roots (García et al., 2018). These results suggest that a Fe-related repressive signal entering the phloem through OPT3 blocks ethylene synthesis in roots (**Figure 9**; García et al., 2018).

The *Arabidopsis pho2* mutant is impaired in the sensing of P-related phloem signals coming from leaves to roots and overaccumulates Pi in leaves under Pi-replete conditions (Bari et al., 2006; Chiou and Lin, 2011). Micrografting experiments revealed that a *pho2* root genotype is sufficient to yield leaf Pi over-accumulation (Bari et al., 2006). *PHO2* encodes an ubiquitin-conjugating E2 enzyme, that targets proteins involved in P acquisition, like Pht1;4, and P loading into the xylem, like PHO1, for degradation (**Figure 9**; Chiou and Lin, 2011; Liu et al., 2012; Ham et al., 2018; Wang et al., 2018). Probably, PHO2 is also implicated in the regulation of PPAs protein stability (Wang and Liu, 2018). Under P deficiency, increased miRNA399, that participates in the cleavage of *PHO2* mRNA, enhances plant P acquisition and translocation by reducing the level of PHO2 protein (**Figure 9**; Chiou and Lin, 2011; Liu et al., 2012; Ham et al., 2018; Wang et al., 2018). miRNA399 is upregulated earlier in shoots than in roots and it has been proposed that its movement through the phloem acts as a systemic signal. In this sense, PHO2 is recognized as a systemic root sensor of shoot-derived P-related signals (Chiou and Lin, 2011).

The role of signals besides ethylene in the regulation of Fe and P acquisition genes is also supported by the fact that the *Arabidopsis* constitutive ethylene mutant *ctr1* does not present constitutive expression of either Fe-related genes (García et al., 2014) or P-related genes (Lei et al., 2011) when grown in complete

nutrient solution. Among the non-ethylene signals involved in the regulation of Fe- or P-related genes have been proposed a Fe-peptide (García et al., 2013) and the miRNA399 described above (Pant et al., 2009; Kumar et al., 2017), both moving through the phloem. These signals could interact with ethylene and confer specificity to the responses to Fe or P deficiency, avoiding the induction of the specific responses when ethylene increases due to other nutrient deficiencies or stresses. Besides the specificity conferred by these non-ethylene signals, ethylene itself could confer specificity to the responses to Fe or P deficiency by acting through different signaling pathways in each case. For example, P deficiency did not induce the expression of P-related genes in the *Arabidopsis* ethylene insensitive mutants *ein2* and *etr1* (Lei et al., 2011), whereas Fe deficiency induced the expression of Fe-related genes in both mutants (Lucena et al., 2006; García et al., 2013). Taken together, the above results indicate that ethylene could regulate different nutrient responses by acting in conjunction with other signals and also by acting through different signaling pathways. More knowledge of the specific aspects of the regulation by ethylene of the responses to these deficiencies is necessary to understand the interactions between Fe and P. In this work we have further studied the existence of cross talks between the responses to Fe and P deficiency, taking into account the time course of both deficiencies and the existence of cross talks between Fe and P phloem signals. For this, we have studied Fe and P deficiency responses in *A. thaliana* Col-0, *opt3-2*, and *pho2* mutants, impaired in the transport of Fe through the phloem (*opt3-2*) or P homeostasis (*pho2*). The results obtained show that Fe deficiency induces the expression of P acquisition genes and phosphatase activity while P deficiency transitorily induces the expression of Fe acquisition genes and ferric reductase activity. Moreover, the foliar application of either Fe or P diminished the phosphatase activity and the expression of P-related genes in P deficient plants and the ferric reductase activity in Fe deficient plants. Taken together, the results show additional interactions between P and Fe signals originating in the shoots, and suggest that Fe- or P-related phloem signals can interact with ethylene for the regulation of the responses to their deficiencies.

MATERIALS AND METHODS

Plant Material, Growth Conditions and Treatments

To analyze the effect of Fe or P deficiency and its interactions with Fe or P phloem signals on the induction of Fe or P deficiency responses and the expression of Fe or P acquisition genes, we used wild-type *Arabidopsis* [*A. thaliana* (L.) Heynh ecotype Columbia Col-0] and two *Arabidopsis* mutants [*opt3-2* (characterized by Stacey et al., 2008) and *pho2* (characterized by Delhaize and Randall, 1995)], which are affected in the transport of Fe (*opt3-2*) or sensing of P-related signals (*pho2*) in the phloem. Seeds of the *A. thaliana* mutants used in this study were obtained from Dr. Stacey (*opt3-2*) and Dr. Smith (coauthor of this research work; *pho2*). *Arabidopsis* plants were grown under controlled conditions as previously described (Lucena et al., 2006; Lucena et al., 2007). Briefly, seeds were germinated and, when appropriate, seedlings were transferred to individual containers of 70 ml volume with complete nutrient solution continuously aerated. The nutrient solution had the following composition: 2 mM $Ca(NO_3)_2$, 0.75 mM K_2SO_4, 0.5 mM KH_2PO_4, 0.65 mM $MgSO_4$, 50 μM KCl, 10 μM H_3BO_3, 1 μM $MnSO_4$, 0.5 μM $CuSO_4$, 0.5 μM $ZnSO_4$, 0.05 μM $(NH_4)_6Mo_7O_{24}$, and 20 μM Fe-EDDHA. When plants were 45-days-old, they were transferred from this complete nutrient solution to the different treatments. Nutrient solutions were renewed every week previously to the treatments but not during the treatments.

The treatments imposed were: Control: complete nutrient solution with 40 μM FeEDDHA and P; –Fe: nutrient solution without Fe for 2 days; –P: nutrient solution without P (0.5 mM KH_2PO_4 was not added to the nutrient solution, instead 0.5 mM KCl was added) for 7 days; –Fe–P: nutrient solution without Fe (the last 2 days) and without P for 7 days. The duration of the treatments was of 2 days for Fe deficiency and of 7 days for P deficiency because this is the time (in our experimental conditions of hydroponic culture system) for plants to exhibit maximal induction of their Fe or P acquisition genes. After these periods of time (2 days without Fe and 7 days without P) plants were remove for different assessments. Six replicates were used per each control or deficiency treatment.

In some treatments, the shoots were sprayed with 0.05% $FeSO_4$ or 0.35% KH_2PO_4, both dissolved in deionized water, just 24 h before the end of the assay. A hand pressure sprayer was used for the foliar treatments.

Acid Phosphatase Activity Determination

It was determined as previously described (Zakhleniuk et al., 2001). Briefly, roots of intact plants were placed in Petri dishes containing a solution with 5-bromo-4-chloro-3′-indolyphosphate p-toluidine salt (BCIP) 0.01% (w/v) for 4 h. Blue color of roots is higher with increased acid phosphatase activity. After 4 h, photographs of roots were taken with a stereoscopic microscope.

Root Ferric Reductase Activity Determination

It was determined as previously described (Lucena et al., 2006; Lucena et al., 2007). Briefly, intact plants were placed in a Fe(III) reduction assay solution containing Fe(III)-EDTA and Ferrozine for 60 min. The ferric reductase activity was determined spectrophotometrically by measuring the absorbance (562 nm) of the Fe(II)-Ferrozine complex and using an extinction coefficient of 29,800 $M^{-1}cm^{-1}$. After the reduction assay, roots were excised and weighed, and the results were expressed on a root fresh weight basis. Finally, the roots were collected and kept at −80°C for subsequent analysis of mRNA levels. Each experiment was repeated at least twice and representative results are presented. Data are given as means ± SE (n = 6).

Analysis of Root ACC Content

The extraction, purification, and quantification of ACC (1-aminocyclopropane-1-carboxylic acid) was carried out using the method described by Mora et al. (2012). Briefly,

ACC of roots was extracted with 20 µl of d_4ACC [3 µg/ml in acetonitrile/acetic acid 0.2% (90/10)] and 3 ml of MeOH/H_2O/HCOOH (15/4/1, v/v/v) at −20°C. Purification was carried out using a Strata C18-E cartridge (Ref 8B-S001-FBJ, Phenomenex, Torrance, CA, USA) preconditioned with 4 ml of methanol and 2 ml of MeOH/H_2O/HCOOH (15/4/1, v/v/v). Finally the eluted fraction was centrifuged (10,000 rpm, 8 min) and injected in the LC/MS/MS systems, so ACC was quantified by HPLC linked to a 3200 QTRAP LC/MS/MS system (Applied Biosystems/MDS Sciex, Ontario, Canada), equipped with a turbo ion spray interface.

qRT-PCR Analysis

Roots were ground to a fine powder with a mortar and pestle in liquid nitrogen. Total RNA was extracted using the Tri Reagent solution (Molecular Research Center, Inc., Cincinnati, OH) according to the manufacturer's instructions. M-MLV reverse transcriptase (Promega, Madison, WI) was used to generate cDNA with 3 µg of total RNA from roots as template and random hexamers or oligo dT(20) as primers. Prior to cDNA synthesis, RNA was treated with DNAse to eliminate possible contamination by genomic DNA, being DNase inactivated later, adding 50 mM EDTA. Negative controls included all reaction components except M-MLV enzyme. One tenth of each RT reaction was used as PCR template.

The study of gene expression by qRT-PCR was performed using a qRT-PCR Bio-Rad (CFX connect), and the SYBR Green Bio-RAD PCR Master Mix, following the manufacturer's instructions. *SAND1* and *YLS8* genes were used as reference genes to normalize the results of qRT-PCR. The Pfaffl method was used to calculate the relative expression levels. Primer pairs for *Arabidopsis* genes were designed as follows: (5′-3′) AtFRO2F (TGG TTG CCA CAT CTG CGT AT); AtFRO2R (TCG ATA TGG TGT GGC GAC TT); AtIRT1F (TGT CTC TTT TGC AAT CTG TCC A); AtIRT1R (AGG AGC TCC AAC ACC AAT CA); AtPAP17F (CCT CCA AGT ACG TTT CAT CGA TCC); AtPAP17R (CCG TGG CGG ACA TTA ACG AT).AtPht1;4F (CTT TTT CGG GTG GCT TGG TG); AtPht1;4R (AGC TTT TGG CTC ATG TCC GA).

Statistical Analysis

All experiments were repeated at least twice and representative results are presented. A nonlinear regression test was applied to verify the relationship between number of hours under P deficiency conditions, genes expression and ferric reductase activity. The best regression model was chosen from many combinations of terms based, Akaike information criterion modified for small data sets, the model standard deviation and the coefficient of determination (R^2). The analysis was performer by using analytical software 10.

The values of qRT-PCR represent the mean ± SE of three independent biological replicates. The values of other determinations (ferric reductase activity or ACC concentration) represent the mean ± SE of six replicates. Within each gene or genotype, different letters indicate significant differences ($P < 0.05$) among treatments using one-way analysis of variance (ANOVA) followed by a Duncan's multiple range test. Dunnett's test was also used when one or several mutants were compared with the WT for the +Fe treatment and when different treatments were compared with a control. In this latter case, ** indicate significant differences ($P < 0.05$).

RESULTS

P Deficiency Induces the Enhancement of Ferric Reductase Activity and the Expression of Fe Acquisition Genes

The early effect of P deficiency on ferric reductase activity and on *AtFRO2* and *AtIRT1* expression (both are Fe acquisition genes) in *Arabidopsis* wild-type Columbia (Col-0) plants is shown in **Figure 1**. Just 3–6 h after transferring the plants to P deficiency conditions, both the ferric reductase activity and the Fe acquisition genes *AtFRO2* and *AtIRT1* were induced (**Figures 1A–D**). The induction observed progressively decreased after 6 h of deficiency.

Fe Deficiency Induces Acid Phosphatase Activity and the Expression of P Acquisition Genes

In relation to the P acquisition genes, both *AtPht1;4* and *AtPAP17* transcripts were detected in roots of Fe deficient plants compared to the control plants after 2 days of deficiency (**Figure 2**). Fe deficiency also induced phosphatase activity after 2 days (see **Figure 5A**).

ACC Concentration is Higher in Both *opt3-2* and *pho2* Roots Than in Col-0 Roots

To look further into the relationship of ethylene with both deficiencies (see Introduction section; Nagarajan and Smith, 2012; Lucena et al., 2015), the effect of Fe, P, or Fe and P deficiency on ACC (an ethylene precursor) production was determined. As shown in **Figure 3**, both *opt3-2* and *pho2* mutant roots exhibited higher ACC concentrations than Col-0 roots in all treatments.

Fe or P Foliar Applications Has a Differential Inhibitory Effect on Ferric Reductase Activity in Col-0 Plants or in *opt3-2* and *pho2* Mutant Plants

To study the cross talk between shoot Fe and P derived signals, we studied the effect of foliar applications of Fe or P on both Fe- and P-physiological responses. At first, the effects of the foliar applications of Fe or P on the ferric reductase activity was studied in Fe-, P-, and Fe–P-deficient plants of Col-0 and of the *opt3-2* and *pho2* mutants (**Figure 4**). These mutants are affected in the transport of Fe (*opt3-2*) or sensing of P-related signals (*pho2*) in the phloem. The induction of ferric reductase activity caused by -Fe (2 days) or –Fe–P (the last 2 days and 7 days, respectively) deficient treatments was drastically inhibited by the foliar application of Fe and, to a lesser extent, by the foliar application of P (**Figure 4A**).

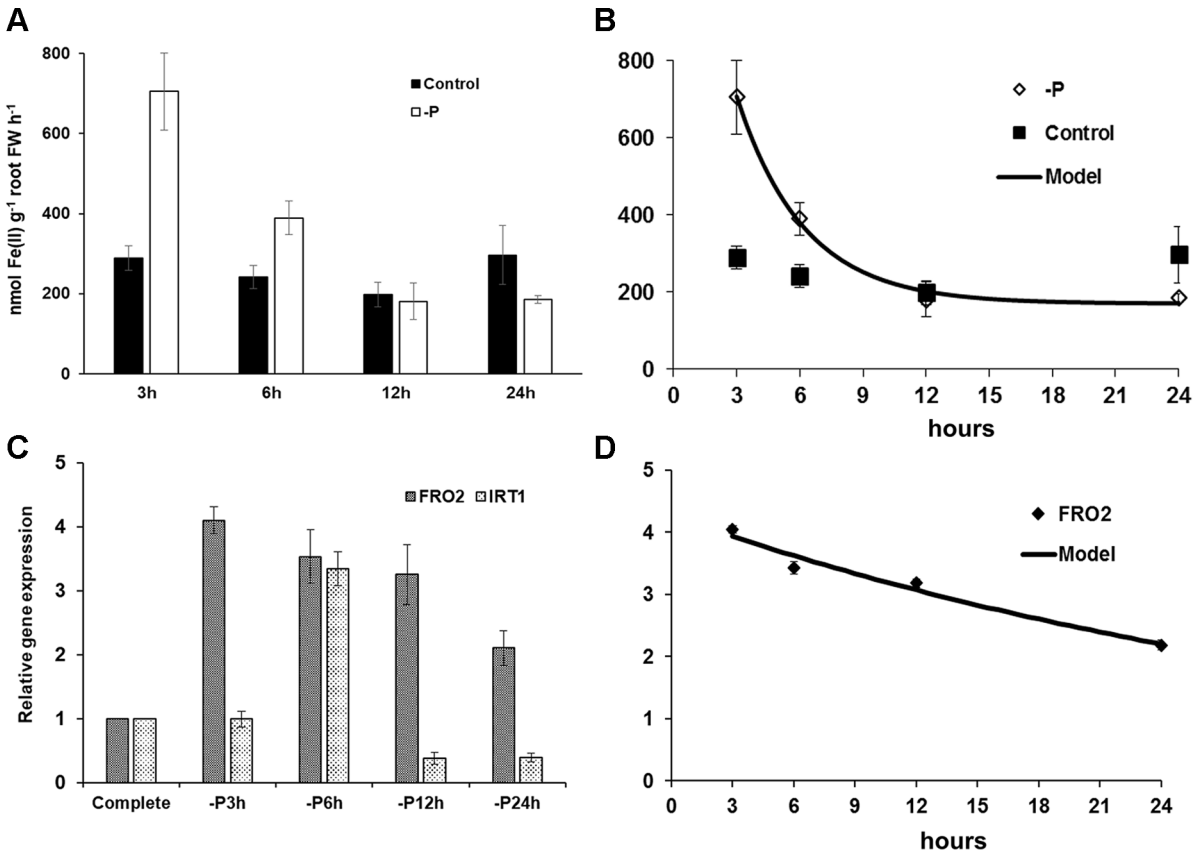

FIGURE 1 | Effect of P deficiency on ferric reductase activity **(A)** and on *AtFRO2* and *AtIRT1* expression (both are Fe acquisition genes) **(C)** in *Arabidopsis* wild-type Columbia plants (Col-0). Plants were grown in a complete nutrient solution and some of them transferred to nutrient solution without P for 3, 6, 12, or 24 h. For ferric reductase activity **(A)**, data are given as means ± SE (n = 6). **(C)** qRT-PCR was performed using total RNA from roots as template and gene-specific primers to amplify partial cDNAs of *AtFRO2* and *AtIRT1*. *SAND1* and *YLS8* were used as reference genes to normalize the results obtained by qRT-PCR. Data represent the mean ± SE of three independent biological replicates and two technical replicates. A nonlinear regression test was applied over ferric reductase activity **(B)** $R^2 = 0.995$; standard deviation = 27.33 and over *AtFRO2* expression **(D)** $R^2 = 0.966$; standard deviation = 0.246.

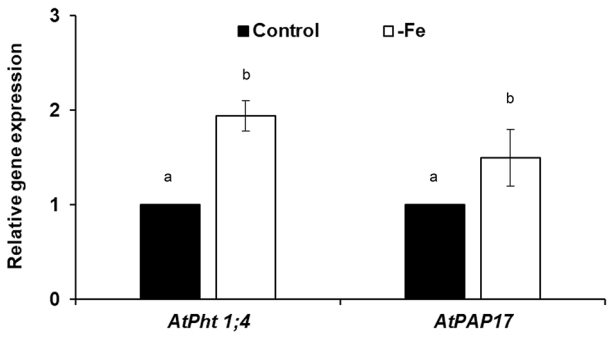

FIGURE 2 | Effect of Fe deficiency on *AtPht1;4* and *AtPAP17* expression (both are P acquisition genes), in *Arabidopsis* wild-type Columbia plants (Col-0). Plants were grown in a complete nutrient solution and some of them transferred to nutrient solution without Fe for 2 days. Quantitative RT-PCR was performed using total RNA from roots as template and gene-specific primers to amplify partial cDNAs of *AtPht1;4* and *AtPAP17*. *SAND1* and *YLS8* were used as reference genes to normalize the results obtained by qRT-PCR. Relative expression was calculated in relation to Control. Data represent the mean ± SE of three independent biological replicates and two technical replicates. Within each gene, bars with different letters indicate significant differences ($P < 0.05$).

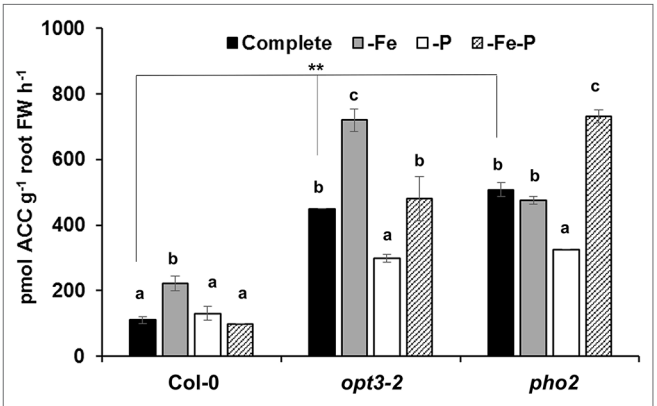

FIGURE 3 | Effect of Fe-, P- or Fe- and P- deficiency on ACC production in *Arabidopsis* wild-type Col-0, *opt3-2* and *pho2* plants. Plants were grown in a complete nutrient solution and some of them transferred to nutrient solution without Fe, P, or Fe and P for 2 days. ACC production of roots was determined as previously described Mora et al. (2012). Data represent the mean ± SE (n = 6). Within each genotype, bars with different letters indicate significant differences ($P < 0.05$). Significant difference between the +Fe from Col-0, *opt3-2* and *pho2* is also indicated: **$P < 0.05$.

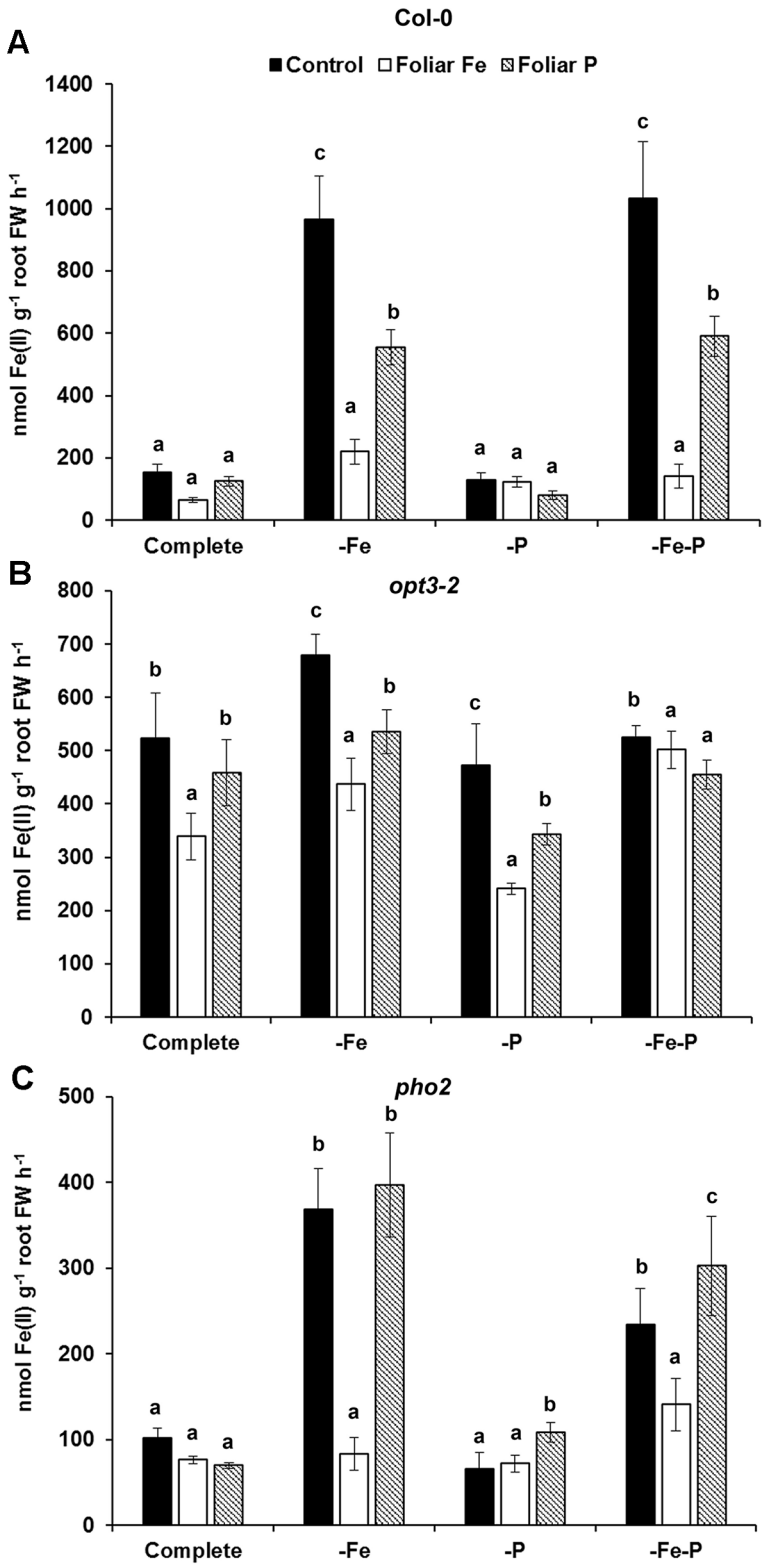

FIGURE 4 | Effect of the foliar application of Fe or P on the ferric reductase activity of Fe-, P- or Fe- and P-deficient *Arabidopsis* wild-type Col-0 **(A)**, *opt3-2* **(B)** and *pho2* **(C)** plants. *opt3-2* and *pho2* are mutants affected in the transport of Fe (*opt3-2*) or sensing of P-related signals (*pho2*) in the phloem, respectively. Deficient treatment were: without Fe (–Fe) for 2 days; without P (–P), for 7 days; and without Fe and P (–Fe–P) (–Fe the last 2 days and –P for 7 days). Some of the plants were sprayed with 0.05% $FeSO_4$ or 0.35% KH_2PO_4 just 24 h before the end of the assay. One day later, the ferric reductase activity was determined. Data are given as means ± SE (n = 6). Within each deficiency treatment, bars with different letters indicate significant differences ($P < 0.05$).

The inhibition caused by the foliar application of either Fe or P was less in the *opt3-2* mutant, which exhibits constitutive induction of Fe responses (**Figure 4B**). In the *pho2* mutant, the foliar application of Fe inhibited the induction of the ferric reductase activity caused by the –Fe or –Fe–P treatments while the foliar application of P did not (**Figure 4C**).

Fe or P Foliar Applications Has a Differential Inhibitory Effect on Acid Phosphatase Activity and on the Expression of *AtPAP17* in Col-0 Plants or in *opt3-2* and *pho2* Mutant Plants

The effects of the foliar application of Fe or P on the acid phosphatase activity and on the expression of *AtPAP17* was studied in Fe, P, and Fe–P deficient plants of Col-0 (**Figure 5**) and of the *opt3-2* (**Figure 6**) and *pho2* mutants (**Figure 7**). All deficiency treatments applied caused induction of the phosphatase activity (**Figure 5A**) and *AtPAP17* expression (**Figure 5B**) in Col-0 plants. Just 2 and 7 days under Fe or P deficiency, respectively, were enough to induce both the phosphatase activity and *AtPAP17* expression (**Figures 5A**, **B**). These inductions were strongly inhibited by the foliar application of either Fe or P (**Figures 5A**, **B**). The induction of both phosphatase activity and *AtPAP17* expression in *opt3-2* and *pho2* was detected in –P and –Fe–P treatments, but not –Fe treatment (**Figures 6** and **7**). In contrast to Col-0, the inhibitory effect of the foliar application of Fe or P on the induction of both phosphatase activity and *AtPAP17* expression did not occur in either mutant (**Figures 6A**, **B** and **7A**, **B**). It could appreciate a slightly inhibitory effect of the foliar application of both Fe and P, only in –Fe–P treatment of *opt3-2* mutant plants (**Figure 6B**).

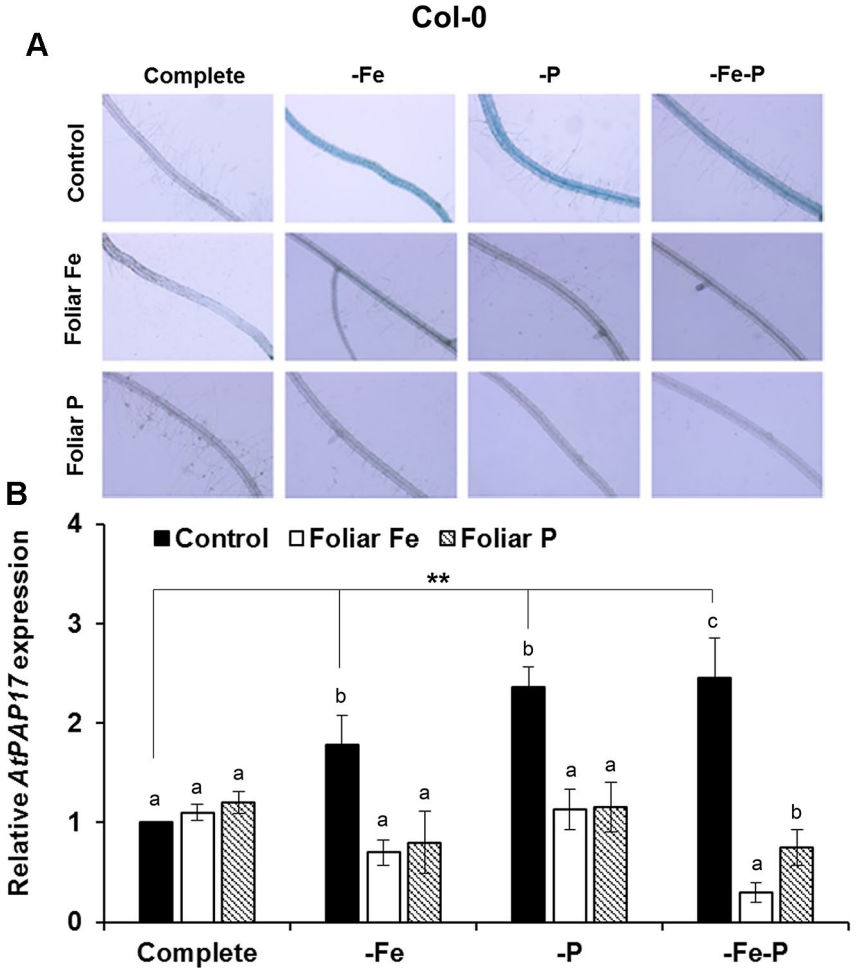

FIGURE 5 | Effect of the foliar application of Fe or P on acid phosphatase activity **(A)** and on the expression of its encoding gene, *AtPAP17* **(B)**, in Fe-, P- or Fe- and P-deficient *Arabidopsis* wild-type Col-0 plants. For acid phosphatase activity determination, roots of intact plants were incubated in a solution containing a phosphated organic substrate (BCIP), for 4 h. Quantitative RT-PCR was performed using total RNA from roots as template and gene-specific primer to amplify partial cDNAs of *AtPAP17*. *SAND1* and *YLS8* were used as reference genes to normalize the results obtained by qRT-PCR. Data represent the mean ± SE of three independent biological replicates and two technical replicates. Within each deficiency treatment, bars with different letters indicate significant differences ($P < 0.05$). Significant difference between the control treatments is also indicated: $^{**}P < 0.05$.

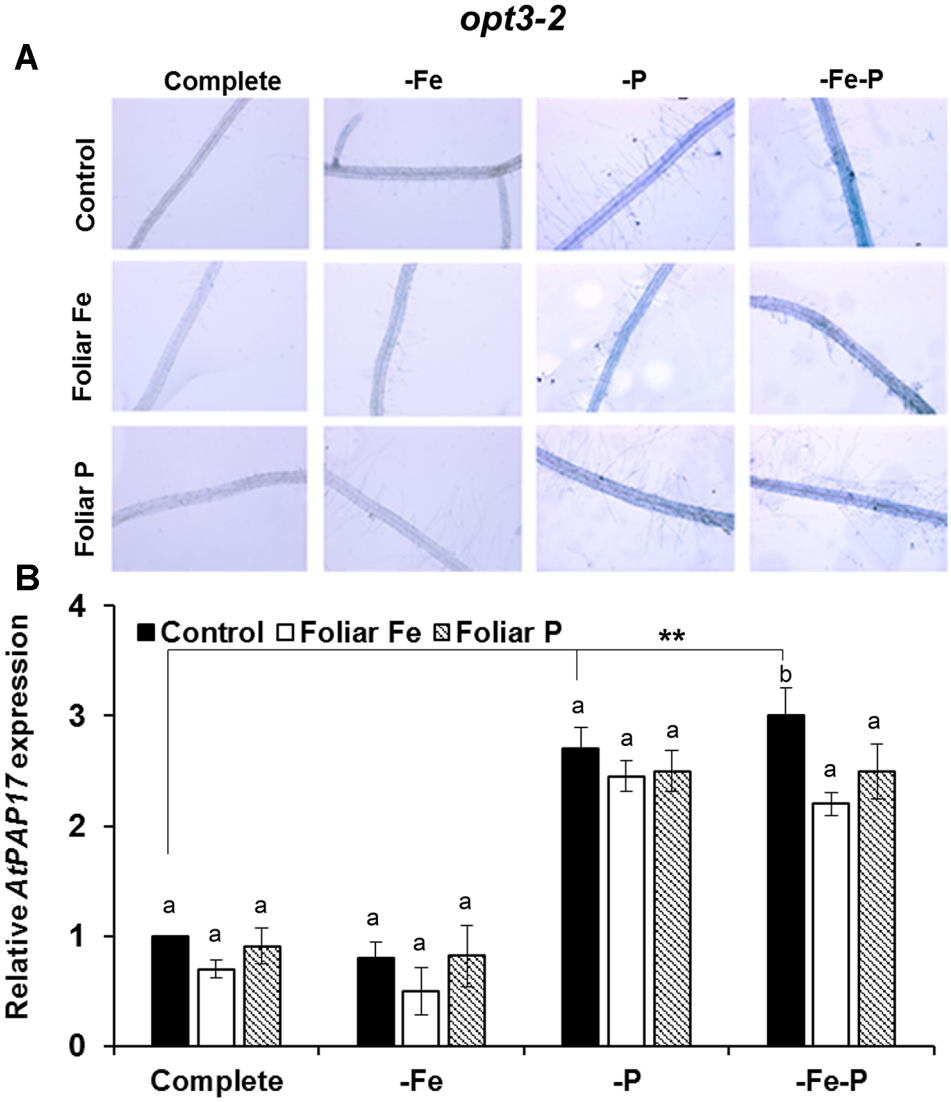

FIGURE 6 | Effect of the foliar application of Fe or P on acid phosphatase activity **(A)** and on the expression of its encoding gene, *AtPAP17* **(B)**, in Fe-, P- or Fe and P-deficient *Arabidopsis opt3-2* mutant plants. This mutant is impaired in the phloematic transport of Fe. For acid phosphatase activity determination, roots of intact plants were incubated in a solution containing a phosphated organic substrate (BCIP), for 4 h. Quantitative RT-PCR was performed using total RNA from roots as template and gene-specific primer to amplify partial cDNAs of *AtPAP17*. *SAND1* and *YLS8* were used as reference genes to normalize the results obtained by qRT-PCR. Data represent the mean ± SE of three independent biological replicates and two technical replicates. Within each deficiency treatment, bars with different letters indicate significant differences ($P < 0.05$). Significant difference between the control treatments is also indicated: **$P < 0.05$.

In general, phosphatase activity and *AtPAP17* expression levels were strongly correlated (**Figures 5A**, **B**, **6A**, **B**, and **7A**, **B**).

opt3-2 Roots Present Constitutive Activation of Fe Acquisition Genes Under Complete Nutrient Solution but Not of P Acquisition Genes

The results presented above suggest the existence of cross talk between Fe and P deficiency responses. However, this does not exclude the existence of specific signals that confer specificity to each deficiency. To analyze this possibility, we determined the expression of both Fe and P acquisition genes in the *opt3-2* mutant, which presents constitutive expression of Fe acquisition genes, even when grown under Fe sufficient conditions (Stacey et al., 2008; García et al., 2013). As shown in **Figures 8A**, **B**, this mutant exhibits almost constitutive activation of Fe acquisition genes in the different treatments. However, the P acquisition genes are not constitutively activated. They are only induced under P or Fe and P deficiency conditions (**Figures 8C**, **D**).

DISCUSSION

Previous works have shown the existence of cross talk between the responses to Fe and P deficiency in such a way that P deficiency induces the expression of Fe responses and Fe

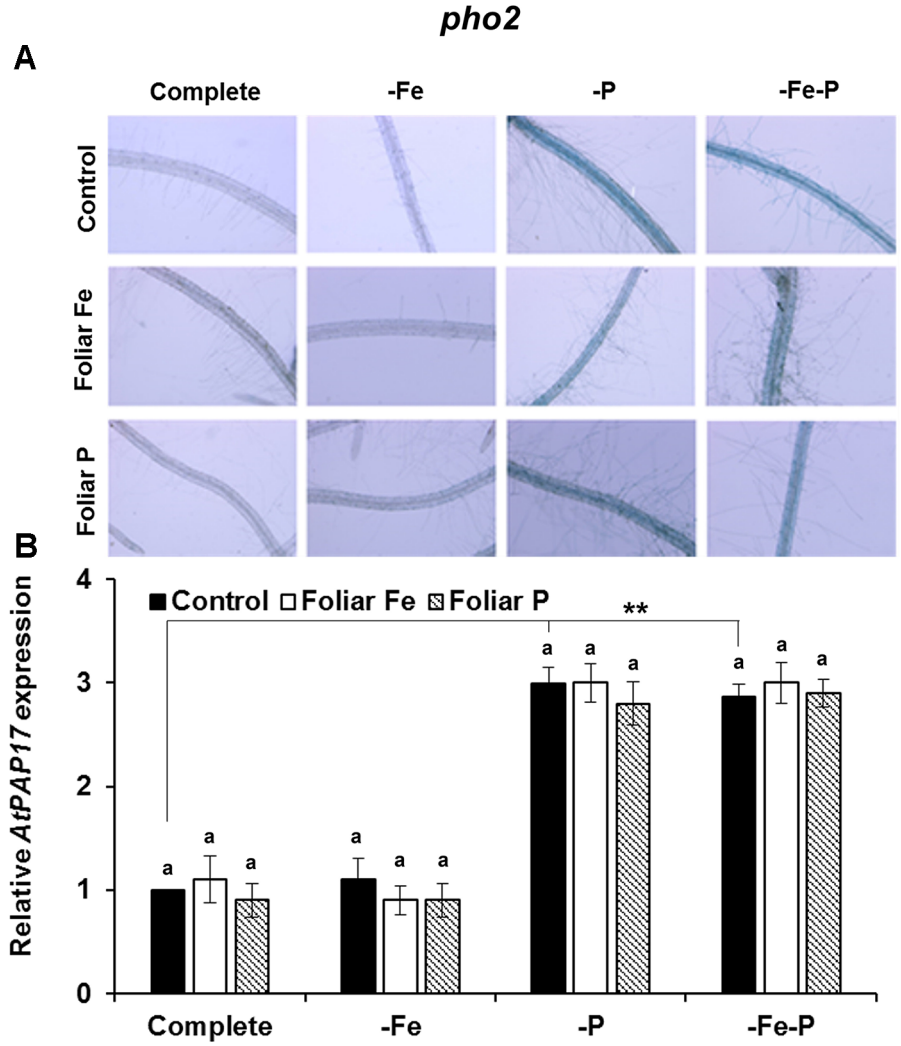

FIGURE 7 | Effect of the foliar application of Fe or P on acid phosphatase activity **(A)** and on the expression of its encoding gene, *AtPAP17* **(B)**, in Fe-, P- or Fe- and P-deficient *Arabidopsis pho2* mutant plants. This mutant is affected on sensing of P-related signals (*pho2*) in the phloem. For acid phosphatase activity determination, roots of intact plants were incubated in a solution containing a phosphated organic substrate (BCIP), for 4 h. Quantitative RT-PCR was performed using total RNA from roots as template and gene-specific primer to amplify partial cDNAs of *AtPAP17*. *SAND1* and *YLS8* were used as reference genes to normalize the results obtained by qRT-PCR. Data represent the mean ± SE of three independent biological replicates and two technical replicates. Within each deficiency treatment, bars with different letters indicate significant differences ($P < 0.05$). Significant difference between the control treatments is also indicated: **$P < 0.05$.

deficiency induces the expression of P responses. Those works have preferentially analyzed the expression of Fe- and P-related genes and Fe and P content in leaves (de Kock, 1955; Wang et al., 2002; Misson et al., 2005; Hirsch et al., 2006; Ward et al., 2008; Zheng et al., 2009; Abel, 2011; Perea-García et al., 2013; Wang et al., 2014). However, no studies have investigated the effect of each deficiency on some activities related to the other deficiency, such as ferric reductase activity (encoded by the *AtFRO2* gene in *Arabidopsis*) or phosphatase activity (encoded by the *AtPAP17* gene and other related genes in *Arabidopsis*). We think that, besides gene expression, it is important to determine these activities to better understand the cross talk between Fe and P deficiency because of the possible effects of post-transcriptional regulation. Additionally, we consider it important to study the time course of each deficiency on the induction of genes related to the other deficiency and the possible cross talk between shoot derived signals associated with each deficiency.

In this work, similar to previous works (see above), the results obtained show that P deficiency can induce the expression of some Fe acquisition genes, like *AtFRO2* and *AtIRT1* (**Figures 1C**, **D**; Wang et al., 2002; Misson et al., 2005; Wang et al., 2014), while Fe deficiency can induce the expression of some P acquisition genes, like *AtPht1;4* and *AtPAP17* (**Figure 2**). These results match with others obtained by microarray analysis showing an early transcriptional response of both *AtPht1;4* and

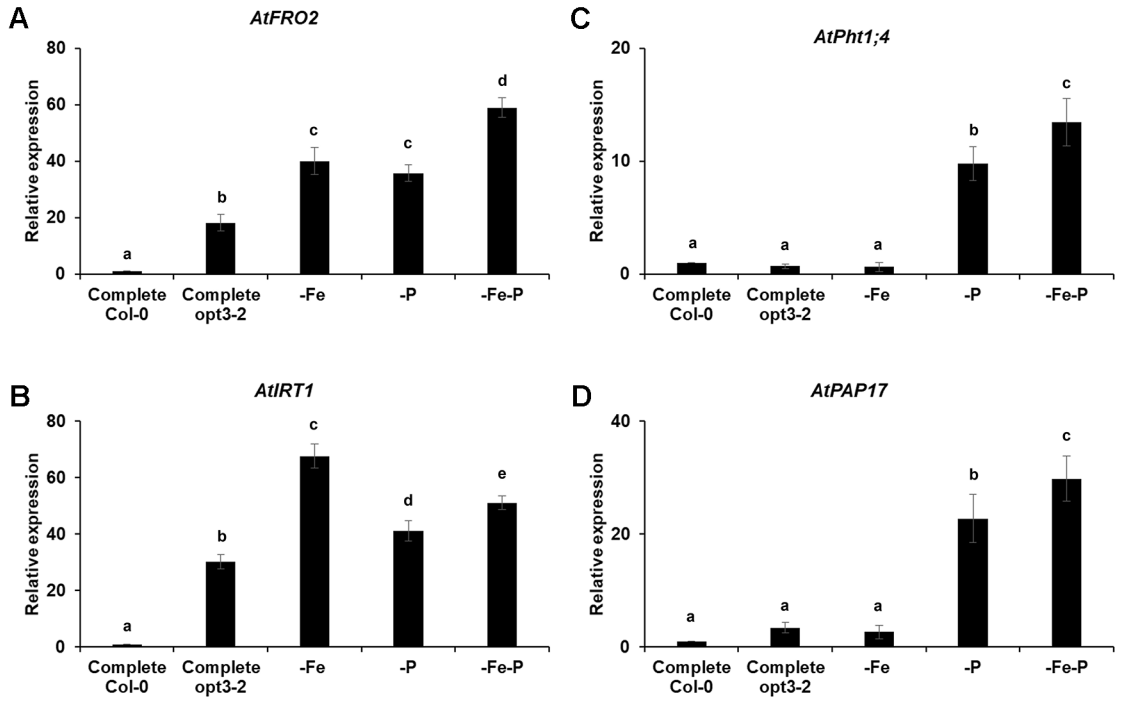

FIGURE 8 | Effect of Fe-, P- or Fe- and P- deficiency on P acquisition gene expression **(C** and **D)** and Fe acquisition gene expression **(A** and **B)** in *Arabidopsis opt3-2* mutant plants. Plants were grown in a complete nutrient solution and some of them transferred to nutrient solution without Fe, P, or Fe and P for 2 days. Quantitative RT-PCR was performed using total RNA from roots as template and gene-specific primers to amplify partial cDNAs of *AtPht1;4, AtPAP17, AtFRO2* and *AtIRT1*. *SAND1* and *YLS8* were used as reference genes to normalize the results obtained by qRT-PCR. Data represent the mean ± SE of three independent biological replicates and two technical replicates. Within each gene, bars with different letters indicate significant differences ($P < 0.05$).

AtPAP17 to Fe deficiency (1–3 days growing without Fe) in roots of *Arabidopsis* plants (Thimm et al., 2001). The induction of the Fe acquisition genes by P deficiency occurred early, after 3 h (*AtFRO2*) and 6 h (*AtIRT1*) of the deficiency treatment, and then the induction tended to disappear (**Figures 1C**, **D**), which suggests the presence of specific Fe inhibitory signals. Moreover, the ferric reductase activity was induced only transitorily (**Figures 1A**, **B**) and decreased faster than the expression of the *AtFRO2* gene (**Figures 1C**, **D**), suggesting the possible existence of a post-transcriptional regulation by Fe (Connolly et al., 2003). In relation to Fe deficiency, it induced the expression of P acquisition genes and phosphatase activity after 2 days of deficiency (**Figures 2** and **5**), even before the induction caused by P deficiency itself (**Figure 5**). The induction of the phosphatase activity by Fe deficiency (**Figure 5A**) was not as transitory as the induction of ferric reductase by P deficiency (**Figure 1A**). This result is somewhat surprising since the induction of phosphatase activity is a response traditionally associated with P deficiency (Bari et al., 2006; Lei et al., 2011). The possible role of phosphatase activity on Fe nutrition is not known and warrants further investigation.

The existence of cross talk between the responses to Fe and P deficiency could be associated with common signals in the activation of both nutrient deficiency responses, such as ethylene (Nagarajan and Smith, 2012; García et al., 2015; Lucena et al., 2015; Song and Liu, 2015; Neumann, 2016; Lucena et al., 2018), nitric oxide (NO; Graziano and Lamattina, 2007; Meng et al., 2012) and auxin (Chen et al., 2010; Miura et al., 2011; Bhosale et al., 2018). In relation to ethylene, the results presented in **Figure 3** show that *opt3-2* and *pho2*, which exhibit constitutive Fe or P responses, respectively, have greater ACC content in roots than Col-0. Since both mutants are affected in the transport of Fe (*opt3-2*) or in the sensing of P-related signals (*pho2*) in the phloem (Bari et al., 2006; García et al., 2013), their higher ACC accumulation suggests that phloem-Fe signals and phloem-P signals can inhibit directly, or indirectly, ACC synthesis and, presumably, ethylene synthesis. These phloem signals should come from the shoots, as previously suggested (Buhtz et al., 2010; García et al., 2013).

To study the possible cross talk of Fe and P shoot-derived signals with the responses to both deficiencies, we sprayed leaves of Col-0, *opt3-2* and *pho2* plants with Fe or P, and analyzed their effects in roots. The foliar application of Fe inhibited the ferric reductase activity in Col-0 (**Figure 4A**) and in the *pho2* mutant (**Figure 4C**) while it had less effect in the *opt3-2* mutant (**Figure 4B**). This latter effect agrees with previous results (García et al., 2013). Curiously, the foliar application of P also inhibited the ferric reductase activity in Col-0 plants, less than the Fe application (**Figure 4A**), but had no effect on *pho2* (**Figure 4C**) and hardly in *opt3-2* (**Figure 4B**). These results suggest that there are Fe and P shoot-derived signals

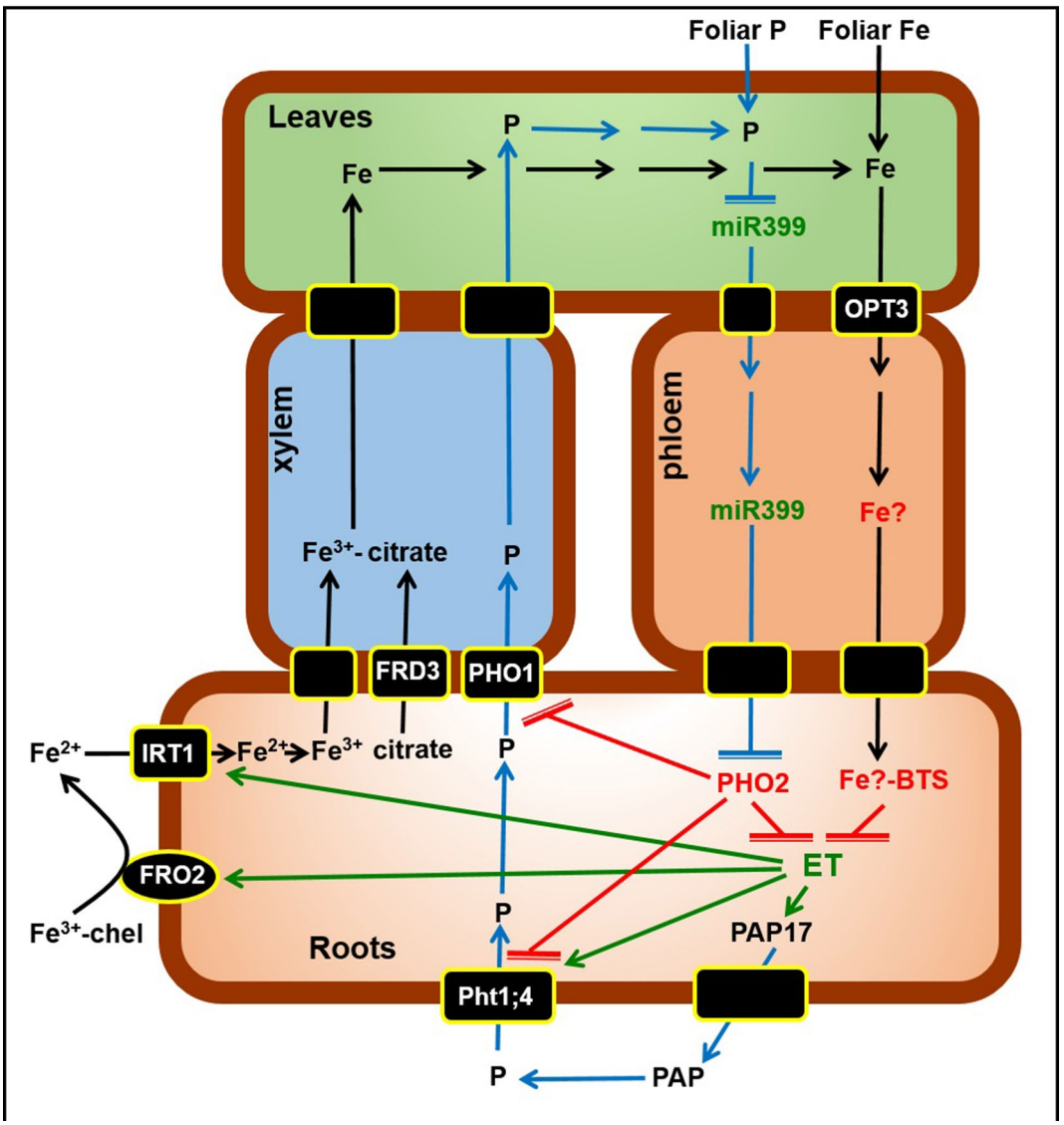

FIGURE 9 | Working Model to explain the role of ethylene and P-related and Fe-related phloem signals on the regulation of Fe and P acquisition genes. Once inside roots, Fe (black arrows) is translocated to leaves through the xylem, bound to citrate (provided by the FRD3 transporter). In shoots, some Fe can enter the phloem through the OPT3 transporter, and moves back to roots probably bound to a chelating agent (Fe)?. In roots, this Fe? can be sensed by the Brutus protein (BTS) that blocks the expression of the Fe acquisition genes *FRO2* and *IRT1*, probably because inhibits the synthesis of ethylene (ET), which has been involved in their upregulation. P (blue arrows) is absorbed through P transporters, like Pht1;4, and then loaded into the xylem through transporters like PHO1. Under P deficiency, miR399 in shoots increases and moves through the phloem to roots where suppresses PHO2. PHO2 participates in the degradation of Pht1;4 and PHO1, and probably inhibits ethylene synthesis. Consequently, under P deficiency, the suppression of PHO2 by miR399 can permit the stabilization of Pht1;4 and PHO1, and the synthesis of ethylene, which has been involved in the upregulation of *Pht1;4* and *PAP17*, encoding a phosphatase (PAP). In green are components whose expression, activity and/or content is known to increase under Fe or P deficiency while in red are components whose expression, activity and/or content is known to increase under Fe or P sufficiency. For more details, see text. (→: promotion; ⊤: inhibition). Working model based on Chiou and Lin (2011) and García et al. (2018).

moving through the phloem that are inhibitory and that both Fe and P signals are interrelated. This interrelation is further supported when analysing phosphatase activity and the expression of one of its encoding genes, *AtPAP17*. As shown in **Figure 5**, the foliar application of either Fe or P drastically inhibited the phosphatase activity and *AtPAP17* expression in Col-0. However, neither Fe nor P application appreciably inhibited these P responses in either mutant (**Figures 6** and **7**).

Despite the existence of common signals involved in the activation of responses to both nutrient deficiencies, like ethylene (**Figure 3**), and the cross talk between shoot-derived signals (see previous paragraph), some results presented in this work suggest the existence of specific signals that block the activation of the responses to one deficiency when the deficiency is caused by the other element. For example, the expression of Fe acquisition genes is almost constitutively activated in the *opt3-2* mutant (**Figures 8A**,

B) while the expression of P acquisition genes is not (**Figures 8C**, **D**). This suggests that the absence of the phloem-Fe signal related to OPT3 depresses the expression of Fe acquisition genes (García et al., 2013) but not that of P acquisition genes, probably because there are specific P signals that block it.

According to the results obtained in this study we propose a Working Model to explain the role of ethylene and P-related and Fe-related phloem signals on the regulation of Fe and P acquisition genes (**Figure 9**). Once inside roots, Fe (black arrows) is translocated to leaves through the xylem, bound to citrate (provided by the FRD3 transporter). In shoots, some Fe can enter the phloem through the OPT3 transporter, and moves back to roots probably bound to a chelating agent (Fe)?. In roots, this Fe? can be sensed by the Brutus protein (BTS) that blocks the expression of the Fe acquisition genes *FRO2* and *IRT1*, probably because it inhibits the synthesis of ethylene (ET), which has been involved in their upregulation. P (blue arrows) is absorbed through P transporters, like Pht1;4, and then loaded into the xylem through transporters like PHO1. Under P deficiency, miR399 in shoots increases and moves through the phloem to roots where it suppresses PHO2. PHO2 participates in the degradation of Pht1;4 and PHO1, and probably inhibits ethylene synthesis. Consequently, under P deficiency, the suppression of PHO2 by miR399 can permit the stabilization of Pht1;4 and PHO1, and the synthesis of ethylene, which has been involved in the upregulation of *Pht1;4* and *PAP17*, encoding a phosphatase (PAP).

In conclusion, the results obtained in this work further support the cross talk between Fe and P deficiency responses since Fe deficiency induces the expression of P acquisition genes and the phosphatase activity, and P deficiency induces the expression of Fe acquisition genes and the ferric reductase activity. In most cases, like the induction of Fe acquisition genes and ferric reductase activity by P deficiency, this occurs very transitorily, probably due to the existence of Fe-related inhibitory signals and because of the post-transcriptional regulation of FRO2 by Fe. The cross talk between both deficiencies could be related to the existence of common signals, like ethylene, implicated in the activation of their responses. Besides ethylene, the results obtained with the foliar application of Fe or P show additional interactions between P and Fe inhibitory signals coming from the shoots, and suggest that Fe- or P-related phloem signals could interact with ethylene in the regulation of the responses to their deficiencies.

AUTHOR CONTRIBUTIONS

CL and FR designed the experiments after discussions with JG-M and MG; RP and MG conducted the laboratory work; ÁZ and EB determined ACC; AS, EA, RP-V, and CL wrote the manuscript.

FUNDING

This work was supported by the European Regional Development Fund from the European Union, the "Ministerio de Economía y Competitividad" (Projects AGL2013- 40822-R and AGL2015-65104-P); the "Junta de Andalucía" (Research Groups AGR115 and BIO159) and the economic contribution of the Company TimacAgro Spain (Roullier Group).

ACKNOWLEDGMENTS

We thank Dr. Joaquin Romero, of the University of Córdoba (Spain), for his support and valuable contribution in the statistical analysis of results.

REFERENCES

Abel, S. (2011). Phosphate sensing in root development. *Curr. Opin. Plant Biol.* 14, 303–309. doi: 10.1016/j.pbi.2011.04.007

Bari, R., Pant, B. D., Stitt, M., and Scheible, W. R. (2006). PHO2, microRNA399, and PHR1 define a phosphate- pathway in plants. *Plant Physiol.* 141, 988–999. doi: 10.1104/pp.106.079707

Borch, K., Bouma, T. J., Lynch, J. P., and Brown, K. M. (1999). Ethylene: a regulator of root architectural responses to soil phosphorus availability. *Plant Cell Environ.* 22, 425–431. doi: 10.1046/j.1365-3040.1999.00405.x

Bhosale, R., Giri, J., Pandey, B. K., Giehl, R. F., Hartmann, A., Traini, R., et al. (2018). A mechanistic framework for auxin dependent *Arabidopsis* root hair elongation to low external phosphate. *Nat. Commun.* 9 (1), 1409–1417. doi: 10.1038/s41467-018-03851-3

Brumbarova, T., Bauer, P., and Ivanov, R. (2015). Molecular mechanisms governing *Arabidopsis* iron uptake. *Trends Plant Sci.* 20, 124–133. doi: 10.1016/j.tplants.2014.11.004

Buhtz, A., Pieritz, J., Springer, F., and Kehr, J. (2010). Phloem small RNAs, nutrient stress responses, and systemic mobility. *BMC Plant Biol.* 10, 64. doi: 10.1186/1471-2229-10-64

Connolly, E. L., Campbell, N. H., Grotz, N., Prichard, C. L., and Guerinot, M. L. (2003). Overexpression of the FRO2 ferric chelate reductase confers tolerance to growth on low iron and uncovers posttranscriptional control. *Plant Physiol.* 133, 1102–1110. doi: 10.1104/pp.103.025122

Chen, W. W., Yang, J. L., Qin, C., Jin, C. W., Mo, J. H., Ye, T., et al. (2010). Nitric oxide acts downstream of auxin to trigger root ferric-chelate reductase activity in response to iron deficiency in *Arabidopsis thaliana*. *Plant Physiol.* 154, 810–819. doi: 10.1104/pp.110.161109

Chiou, T. J., and Lin, S. I. (2011). Network in sensing phosphate availability in plants. *Annu Rev Plant Biol.* 62, 185–206. doi: 10.1146/annurev-arplant-042110-103849

de Kock, P. C. (1955). Iron nutrition of plants at high pH. *Soil Sci.* 79, 167–175. doi: 10.1097/00010694-195503000-00001

Delhaize, E., and Randall, P. J. (1995). Characterization of a phosphate accumulator mutant of *Arabidopsis thaliana*. *Plant Physiol.* 107, 207–213. doi: 10.1104/pp.107.1.207

del Pozo, J. C., Allona, I., Rubio, V., Leyva, A., de la Peña, A., Aragoncillo, C., et al. (1999). A type 5 acid phosphatase gene from *Arabidopsis thaliana* is induced by phosphate starvation and by som other types of phosphate mobilising/oxidative stress conditions. *Plant J.* 19, 579–589. doi: 10.1046/j.1365-313X.1999.00562.x

Franco-Zorrilla, J. M., González, E., Bustos, R., Linhares, F., Leyva, A., and Paz-Ares, J. (2004). The transcriptional control of plant responses to phosphate limitation. *J. Exp. Bot.* 55, 285–293. doi: 10.1093/jxb/erh009

García, M. J., Lucena, C., Romera, F. J., Alcántara, E., and Pérez-Vicente, R. (2010). Ethylene and nitric oxide involvement in the up-regulation of key genes related to iron acquisition and homeostasis in *Arabidopsis*. *J. Exp. Bot.* 61, 3885–3899. doi: 10.1093/jxb/erq203

García, M. J., Suárez, V., Romera, F. J., Alcántara, E., and Pérez-Vicente, R. (2011). A new model involving ethylene, nitric oxide and Fe to explain the regulation of Fe-acquisition genes in Strategy I plants. *Plant Physiol. Biochem.* 49, 537–544. doi: 10.1016/j.plaphy.2011.01.019

García, M. J., Romera, F. J., Stacey, M. G., Stacey, G., Villar, E., Alcántara, E., et al. (2013). Shoot to root communication is necessary to control the expression of iron-acquisition genes in Strategy I plants. *Planta* 237, 65–75. doi: 10.1007/s00425-012-1757-0

García, M.J., García-Mateo, M.J., Lucena, C., Romera, F.J.,Rojas, C.L., Alcántara, E., et al. (2014). Hypoxia and bicarbonate could block the expression of iron acquisition genes in Strategy I plants by affecting ethylene synthesis and signaling in different ways. *Physiol. Plant*. 150, 95–106. doi: 10.1111/ppl. 12076

García, M. J., Romera, F. J., Lucena, C., Alcántara, E., and Pérez-Vicente, R. (2015). Ethylene and the regulation of physiological and morphological responses to nutrient deficiencies. *Plant Physiol.* 169, 51–60. doi: 10.1104/pp.15.00708

García, M. J., Corpas, F. J., Lucena, C., Alcántara, E., Pérez-Vicente, R., Zamarreño, Á.M., et al. (2018). A shoot Fe pathway requiring the OPT3 transporter controls GSNO reductase and ethylene in *Arabidopsis thaliana* roots. *Front. Plant Sci.* 9, 1325–1341. doi: 10.3389/fpls.2018.01325

Graziano, M., and Lamattina, L. (2007). Nitric oxide accumulation is required for molecular and physiological responses to iron deficiency in tomato roots. *Plant J.* 52, 949–960. doi: 10.1111/j.1365-313X.2007.03283.x

Ham, B. K., Chen, J., Yan, Y., and Lucas, W. J. (2018). Insights into plant phosphate sensing and signaling. *Curr. Opi. Biotech* 49, 1–9. doi: 10.1016/j.copbio.2017.07.005

Henry, J. B., McCall, I., Jackson, B., and Whipker, B. E. (2017). Growth response of herbaceous ornamental to phosphorus fertilization. *Hortscience* 52, 1362–1367. doi: 10.21273/HORTSCI12256-17

Hirsch, J., Marin, E., Floriani, M., Chiarenza, S., Richaud, P., Nussaume, L., et al. (2006). Phosphate deficiency promotes modification of iron distribution in *Arabidopsis* plants. *Biochimie*. 88, 1767–1771. doi: 10.1016/j.biochi.2006.05.007

Ivanov, R., Brumbarova, T., and Bauer, P. (2012). Fitting into the harsh reality: regulation of iron-deficiency responses in dicotyledonous plants. *Mol. Plant* 5, 27–42. doi: 10.1093/mp/ssr065

Kumar, S., Verma, S., and Trivedi, P. K. (2017). Involvement of Small RNAs in phosphorus and sulfur sensing, and stress: current update. *Front. Plant. Sci.* 8, 285. doi: 10.3389/fpls.2017.00285

Lei, M., Zhu, C., Liu, Y., Karthikeyan, A. S., Bressan, R. A., Raghothama, K. G., et al. (2011). Ethylene is involved in regulation of phosphate starvation-induced gene expression and production of acid phosphatases and anthocyanin in *Arabidopsis*. *New Phytol.* 189, 1084–1095. doi: 10.1111/j.1469-8137.2010.03555.x

Liu, T. Y., Huang, T. K., Tseng, C. Y., Lai, Y. S., Lin, S. I., Lin, W. Y., et al. (2012). PHO2-dependent degradation of PHO1 modulates phosphate homeostasis in *Arabidopsis*. *Plant Cell* 24 (5), 2168–2183. doi: 10.1105/tpc.112.096636

Liu, W., Li, Q., Wang, Y., Wu, T., Yang, Y., Zhang, X., et al. (2017). Ethylene response factor AtERF72 negatively regulates *Arabidopsis thaliana* response to iron deficiency. *Biochem. Biophys. Res. Commun.* 491, 862–868. doi: 10.1016/j.bbrc.2017.04.014

Lucena, C., Waters, B. M., Romera, F. J., García, M. J., Morales, M., Alcántara, E., et al. (2006). Ethylene could influence ferric reductase, iron transporter and H^+-ATPase gene expression by affecting FER (or FER-like) gene activity. *J. Exp. Bot.* 57, 4145–4154. doi: 10.1093/jxb/erl189

Lucena, C., Romera, F. J., Rojas, C. L., García, M. J., Alcántara, E., and Pérez-Vicente, R. (2007). Bicarbonate blocks the expression of several genes involved in the physiological responses to Fe deficiency of Strategy I plants. *Funct. Plant Biol.* 34, 1002–1009. doi: 10.1071/FP07136

Lucena, C., Romera, F. J., García, M. J., Alcántara, A., and Pérez-Vicente, R. (2015). Ethylene participates in the regulation of Fe deficiency responses in Strategy I plants and in rice. *Front. Plant Sci.* 6, 1056. doi: 10.3389/fpls.2015.01056

Lucena, C., Porras, R., Romena, F. J., Alcántara, E., and Pérez-Vicente, R. (2018). Similarities and differences in the acquisition of Fe and P by dicot plants. *Agronomy* 8, 148–163. doi: 10.3390/agronomy8080148

Marschner, H. (1995). *Mineral nutrition of higher plants*. 2nd ed edition. London: Academic Press.

Meng, Z. B., Chen, L. Q., Suo, D., Li, G. X., Tang, C. X., and Zheng, S. J. (2012). Nitric oxide is the shared signalling molecule in phosphorus- and iron deficiency- induced formation of cluster roots in white lupin (*Lupinus albus*). *Ann. Bot.* 109, 1055–1064. doi: 10.1093/aob/mcs024

Mehra, P., Pandey, B. K., and Giri, J. (2017). Improvement in phosphate acquisition and utilization by a secretory purple acid phosphatase (OsPAP21b) in rice. *Plant Biotech. J.* 15 (8), 1054–1067. doi: 10.1111/pbi.12699

Misson, J., Raghothama, K. G., Jain, A., Jouhet, J., Block, M. A., Bligny, R., et al. (2005). A genome-wide transcriptional analysis using Arabidopsis thaliana Affymetrix gene chips determined plant responses to phosphate deprivation. *Proc. Natl. Acad. Sci. Biol.* 102, 11934–11939. doi: 10.1073/pnas.0505266102

Miura, K., Lee, J., Gong, Q., Ma, S., Jin, J. B., Yoo, C. Y., et al. (2011). SIZ1 regulation of phosphate starvation induced root architecture remodeling involves the control of auxin accumulation. *Plant Physiol.* 155, 1000–1012. doi: 10.1104/pp.110.165191

Mora, V., Baigorri, R., Bacaicoa, E., Zamarreño, A. M., and García-Mina, J. M. (2012). The humic acid-induced changes in the root concentration of nitric oxide, IAA and ethylene do not explain the changes in root architecture caused by humic acid in cucumber. *Environ. Exp. Bot.* 76, 24–32. doi: 10.1016/j.envexpbot.2011.10.001

Müller, R., Morant, M., Jarmer, H., Nilsson, L., and Nielsen, T. H. (2007). Genome wide analysis of the *Arabidopsis* leaf transcriptome reveals interaction of phosphate and sugar metabolism. *Plant Physiol.* 143, 156–171. doi: 10.1104/pp.106.090167

Nagarajan, V. K., and Smith, A. P. (2012). Ethylene´s role in phosphate starvation: more than just a root growth regulator. *Plant Cell Physiol.* 53 (2), 277–286. doi: 10.1093/pcp/pcr186

Neumann, G. (2016). The role of ethylene in plant adaptations for phosphate acquisition in soils—A review. *Front. Plant Sci.* 6, 1224. doi: 10.3389/fpls.2015.01224

Pant, B. D., Musialak-Lange, M., Nuc, P., May, P., Buhtz, A., Kehr, J. et al. (2009). Identification of nutrient-responsive *Arabidopsis* and rapeseed microARNs by comprehensive real-time polymerase chain reaction profiling and small RNA sequencing. *Plant Physiol.* 150, 1541–1555. doi: 10.1104/pp.109.139139

Perea-García, A., García-Molina, A., Andres-Colas, N., Vera-Sirera, F., Perez-Amador, M. A., Puig, S., et al. (2013). *Arabidopsis* copper transport protein COPT2 participates in the cross talk between iron deficiency responses and low-phosphate. *Plant Physiol.* 162, 180–194. doi: 10.1104/pp.112.212407

Robinson, W. D., Park, J., Tran, H. T., Del Vecchio, H. A., Ying, S., Zins, J. L., et al. (2012). The secreted purple acid phosphatase isozymes AtPAP12 and AtPAP26 play a pivotal role in extracellular phosphate-scavenging by *Arabidopsis thaliana*. *J. Exp. Bot.* 63 (18), 6531–6542. doi: 10.1093/jxb/ers309

Romera, F. J., Alcantara, E., and de la Guardia, M. D. (1992). Effects of bicarbonate, phosphate and high pH on the reducing capacity of Fe-deficient sunflower and cucumber plants. *J. Plant Nutr.* 15, 1519–1530. doi: 10.1080/01904169209364418

Romera, F. J., and Alcántara, E. (1994). Iron-deficiency stress responses in cucumber (*Cucumis sativus* L.) roots. A possible role for ethylene? *Plant Physiol.* 105, 1133–1138. doi: 10.1104/pp.105.4.1133

Roldán, M., Dinh, P., Leung, S., and McManus, M. T. (2013). Ethylene and the responses of plants to phosphate deficiency. *AoB PLANTS* 5, plt013. doi: 10.1093/aobpla/plt013

Rubio, V., Linhares, F., Solano, R., Martín, A. C., Iglesias, J., Leyva, A. et al. (2001). A conversed MYB transcription factor involved in phosphate starvation both in vascular plants and in unicellular algae. *Genes Dev.* 15, 2122–2133. doi: 10.1101/gad.204401

Sánchez-Rodriguez, A. R., del Campillo, M. C., and Torrent, J. (2013). Phosphate aggravates iron chlorosis in carbonate–iron oxide systems. *Plant Soil* 373, 31–42. doi: 10.1007/s11104-013-1785-y

Stacey, M. G., Patel, A., McClain, W. E., Mathieu, M., Remley, M., Rogers, E. E., et al. (2008). The *Arabidopsis* AtOPT3 protein functions in metal homeostasis and movement of iron to developing seeds. *Plant Physiol.* 146, 589–601. doi: 10.1104/pp.107.108183

Stetter, M. G., Benz, M., and Ludewig, U. (2017). Increased root hair density by loss of WRKY6 in *Arabidopsis thaliana*. *Peer J.* 5, e2891. doi: 10.7717/peerj.2891

Song, L., and Liu, D. (2015). Ethylene and plant responses to phosphate deficiency. *Front. Plant Sci.* 6, 796. doi: 10.3389/fpls.2015.00796

Thimm, O., Essigmann, B., Kloska, S., Altmann, T., and Buckhout, T. J. (2001). Response of *Arabidopsis* to iron deficiency stress as revealed by microarray analysis. *Plant Physiol.* 127 (3), 1030–1043. doi: 10.1104/pp.010191

Todd, C. D., Zeng, P., Rodríguez, A. M., Hoyos., M. E., and Polacco, J. C. (2004). Transcripts of MYB-like genes respond to phosphorus and nitrogen deprivation in *Arabidopsis*. *Planta* 219, 1003–1009. doi: 10.1007/s00425-004-1305-7

Walker, E. L., and Connolly, E. L. (2008). Time to pump iron: iron-deficiency mechanisms of higher plants. *Curr. Opin. Plant Biol.* 11, 530–535. doi: 10.1016/j.pbi.2008.06.013

Wang, Y. H., Garvin, D. F., and Kochian, L. V. (2002). Rapid introduction of regulatory and transporter genes in response to phosphorus, potassium, and

iron deficiencies in tomato roots. Evidence for cross talk and root/rhizosphere-mediated signals. *Plant Physiol.* 130, 1370. doi: 10.1104/pp.008854

Wang, K. L. C., Li, H., and Ecker, J. R. (2002). Ethylene biosynthesis and networks. *Plant Cell* 2002, S131–S151. doi: 10.1105/tpc.001768

Wang, X., Wang, Y., Tian, J., Lim, B. L., Yan, X., and Liao, H. (2009). Overexpressing AtPAP15 enhances phosphorus efficiency in soybean. *Plant Physiol.* 151, 233–240. doi: 10.1104/pp.109.138891

Wang, Z., Straub, D., Yang, H., Kania, A., Shen, J., Ludewig, U., et al. (2014). The regulatory network of cluster-root function and development in phosphate deficient white lupin (*Lupinus albus*) identified by transcriptome sequencing. *Physiol. Plant* 151, 323–338. doi: 10.1111/ppl.12187

Wang, F., Deng, M., Xu, J., Zhu, X., and Mao, C. (2018). Molecular mechanisms of phosphate transport and in higher plants. *Semin. Cell Develop. Biol.* 74, 114–122. doi: 10.1016/j.semcdb.2017.06.013

Wang, L., and Liu, D. (2018). Functions and regulation of phosphate starvation-induced secreted acid phosphatases in higher plants. *Plant Sci.* 271, 108–116. doi: 10.1016/j.plantsci.2018.03.013

Ward, J. T., Lahner, B., Yakubova, E., Salt, D. E., and Raghothama, K. G. (2008). The effect of iron on the primary root elongation of *Arabidopsis* during phosphate deficiency. *Plant Physiol.* 147, 1181–1191. doi: 10.1104/pp.108.118562

Yuan, Y., Wu, H., Wang, N., Li, J., Zhao, W., Du, J., et al. (2008). FIT interacts with AtbHLH38 and AtbHLH39 in regulating iron uptake gene expression for iron homeostasis in *Arabidopsis*. *Cell Res.* 18, 385–397. doi: 10.1038/cr.2008.26

Zakhleniuk, O. V., Raines, C. A., and Lloyd, J. C. (2001). Pho3: a phosphorus-deficient mutant of *Arabidopsis thaliana* (L.) Heynh. *Planta* 212, 529–534. doi: 10.1007/s004250000450

Zhai, Z., Gayomba, S. R., Jung, H., Vimalakumari, N. K., Piñeros, M., Craft, E., et al. (2014). OPT3 is a Phloem-specific iron transporter that is essential for systemic iron and redistriburtion of iron and cadmium in *Arabidopsis. Plant Cell* 26, 2249–2264. doi: 10.1105/tpc.114.123737

Zhang, Z., Hong, L., and William, J. L. (2014). Molecular mechanisms underlying phosphate sensing, and adaptation in plants. *J. Integrative Plant Biol.* 56, 192–220. doi: 10.1111/jipb.12163

Zheng, L., Huang, F., Narsai, R., Wu, J., Giraud, E., He, F., et al. (2009). Physiological and transcriptome analysis of iron and phosphorus interaction in rice seedlings. *Plant Physiol.* 151, 262–274. doi: 10.1104/pp.109.141051

Conflict of Interest: The authors declare that the research was conducted in the absence of any commercial or financial relationships that could be construed as a potential conflict of interest.

frontiers in Plant Science

ORIGINAL RESEARCH
published: 18 October 2019
doi: 10.3389/fpls.2019.01179

Enhancement of Iron Acquisition in Rice by the Mugineic Acid Synthase Gene With Ferric Iron Reductase Gene and *OsIRO2* Confers Tolerance in Submerged and Nonsubmerged Calcareous Soils

Hiroshi Masuda[1,2], *May Sann Aung*[1,2], *Takanori Kobayashi*[1], *Tatsuro Hamada*[1] *and Naoko K. Nishizawa*[1]*

[1] *Research Institute for Bioresources and Biotechnology, Ishikawa Prefectural University, Ishikawa, Japan,* [2] *Department of Biological Production, Faculty of Bioresource Sciences, Akita Prefectural University, Akita, Japan*

OPEN ACCESS

Edited by:
Wolfgang Schmidt, Academia Sinica, Taiwan

Reviewed by:
An Yang, Chinese Academy of Sciences, China
Rumen Ivanov, Heinrich Heine University of Düsseldorf, Germany
Erin L. Connolly, Pennsylvania State University, United States

***Correspondence:**
Naoko K. Nishizawa
annaoko@mail.ecc.u-tokyo.ac.jp

Specialty section:
This article was submitted to Plant Nutrition, a section of the journal Frontiers in Plant Science

Received: *30 January 2019*
Accepted: *29 August 2019*
Published: *18 October 2019*

Citation:
Masuda H, Aung MS, Kobayashi T, Hamada T and Nishizawa NK (2019) Enhancement of Iron Acquisition in Rice by the Mugineic Acid Synthase Gene With Ferric Iron Reductase Gene and OsIRO2 Confers Tolerance in Submerged and Nonsubmerged Calcareous Soils. Front. Plant Sci. 10:1179. doi: 10.3389/fpls.2019.01179

Iron (Fe) is an essential micronutrient for plants. Plants encounter Fe deficiency when grown in calcareous soil with low Fe availability, leading to reduced crop yield and agricultural problem. Rice acquires Fe from the soil *via* Strategy I–related system (ferrous ion uptake by OsIRT1) and Strategy II system (ferric ion uptake by chelation). However, rice plants have a weak ability in Fe(III) reduction and phytosiderophore secretion. We previously produced an Fe deficiency–tolerant rice harboring *OsIRT1* promoter-*refre1/372* (for higher Fe(III) reductase ability) and a *35S* promoter-*OsIRO2* (for higher phytosiderophore secretion). In this study, we produced a new Fe deficiency–tolerant rice by the additional introduction of a barley *IDS3* genome fragment with *refre1/372* and *OsIRO2* (named as IRI lines) for further enhancement in Strategy II phytosiderophore productivity and better growth performance in various environments. Our results show that an enhanced tolerance was observed in *OsIRO2* introduced line at the early growth stage, *refre1/372* introduced line in the late stage, and RI line in all stages among five types of cultivation method. Moreover, we demonstrated that new IRI rice lines exhibited enhanced tolerance to Fe deficiency compared to nontransgenic (NT) rice and rice lines harboring the overexpressing *OsIRO2* or the *IDS3* fragment under submerged calcareous soil. The yields of IRI lines were ninefold higher than the NT line. Furthermore, under Fe-limited nonsubmerged calcareous soil condition (a new cultivation condition), IRI lines also conferred enhanced tolerance than NT, lines introducing only the *OsIRT1* promoter-*refre1/372* or overexpressing *OsIRO2*, and lines harboring both. Our results demonstrate that further enhancement of the Strategy II Fe uptake system by the mugineic acid synthase gene in addition to Fe uptake by enhanced ferric Fe reduction and phytosiderophore production in rice contributes Fe deficiency tolerance and broaden its utility in calcareous soil cultivation under paddy or nonpaddy field conditions.

Keywords: iron deficiency, transgenic rice, phytosiderophore, biomass, calcareous soil, *OsIRO2*, *IDS3*

INTRODUCTION

Iron (Fe) is an essential micronutrient for the survival of most living organisms including plants. Approximately 30% of the Earth's surface is covered by calcareous soil. There is an abundant amount of Fe in the soil. However, Fe is sparingly soluble under aerobic conditions, particularly in calcareous soil at high pH because Fe in soil mainly exists in its oxidized form (Fe^{3+}) (Marschner, 1995). Plants often suffer from Fe deficiency when cultivated in calcareous soil and exhibit chlorosis symptoms primarily on young leaves, consequently affecting plant growth, crop yield, and quality. Therefore, producing Fe deficiency–tolerant crops will contribute to increasing crop production in widespread calcareous soils to fulfill the food demand for increasing world population.

Iron acquisition in higher plants is mediated by two major strategies: Strategy I and Strategy II (Römheld and Marschner, 1986). Under conditions of low Fe availability in soil, nongraminaceous species employ the Fe reduction system (Strategy I), in which Fe(III) in soil is first reduced to Fe^{2+} by Fe(III)-chelate reductase FRO2 in roots (Robinson et al., 1999), which is assumed to be the rate-limiting step of Fe uptake from soil (Connolly et al., 2003). Then, the resulting Fe^{2+} is transported across the plasma membrane of the roots by the Fe-regulated transporter, IRT1 (Eide et al., 1996). Rice (*Oryza sativa* L.) is a gramineous plant, but it also uses a part of the Strategy I system, which is a direct Fe^{2+} uptake system facilitated by the ferrous transporter OsIRT1 (Bughio et al., 2002; Ishimaru et al., 2006). Rice is typically cultivated in anaerobic paddy fields where abundant Fe^{2+} is readily available to plants because of the low redox potential. This is probably a reason why rice plants possess Fe^{2+} uptake system, although it is a gramineous plant (Bughio et al., 2002; Ishimaru et al., 2006). However, rice has limited Fe uptake efficiency due to its low Fe(III)-chelate reductase activity (Ishimaru et al., 2006) and also a lack of a complete Strategy I system.

All graminaceous species including rice employ Fe chelation system (Strategy II), in which plants synthesize and secrete mugineic acid family phytosiderophores (MAs) into the soil to acquire Fe. The biosynthetic pathway of MAs from methionine has been elucidated (Mori and Nishizawa, 1987; Shojima et al., 1990). In this pathway, nicotianamine (NA) is biosynthesized from three *S*-adenosyl-L-methionine by NA synthase (NAS) (Higuchi et al., 1999). Nicotianamine is synthesized into 2′-deoxymugineic acid (DMA) by NA aminotransferase (NAAT) (Takahashi et al., 1999; Inoue et al., 2008) and DMA synthase (DMAS) (Bashir et al., 2006). Rice plants synthesize DMA in root and secrete them to rhizospheres to chelate Fe(III), and the resulting Fe(III)–DMA complexes are transported into the plant roots *via* the Fe(III)-DMA transporter, OsYSL15 (Inoue et al., 2009; Lee et al., 2009). In many graminaceous species, DMA is further converted into various MAs by deoxygenases, such as IDS3 and IDS2 in barley (Nakanishi et al., 2000; Kobayashi et al., 2001). However, rice secretes only lower levels of MAs compared to other graminaceous species (Takagi, 1976; Marschner et al., 1986). This is a reason why rice is more susceptible to Fe deficiency than the other graminaceous plants.

Iron acquisition of the rice plant can be increased by transgenic approaches. In order to enhance MAs biosynthesis in the plant *via* Strategy II–based approach, first, Takahashi et al. (2001) introduced a barley genome fragment that contained the *HvNAAT-A* and *HvNAAT-B* genes into the rice, and the transgenic rice secreted higher amount of phytosiderophore than nontransgenic (NT) and exhibited tolerance to Fe deficiency in calcareous soil. In addition, Suzuki et al. (2008) developed transgenic rice lines carrying the barley genomic fragments containing genes (*HvNAS1*, or *HvNAS1* plus *HvNAAT-A* and *-B*, or *IDS3*), and all lines demonstrated tolerance to Fe deficiency when they were grown in a field with calcareous soil. Moreover, Masuda et al. (2013) also showed that combined introduction of the barley genomic fragments of MA synthesis genes (*HvNAS1*, *HvNAAT-A* and *–B,* and *IDS3*) into rice led to enhanced Fe deficiency tolerance and increased Fe concentration in grains. All these results suggested that improvement of phytosiderophore productivity in rice can obviously enhance Fe uptake and Fe deficiency tolerance in rice. The other Strategy II–based approach is the enhancement of Fe acquisition by overexpressing the transcription factor in rice. Ogo et al. (2006, 2007) identified an Fe deficiency–inducible basic helix-loop-helix transcription factor (OsIRO2), which mainly controls Strategy II–related Fe uptake key genes such as *OsNAS1*, *OsNAS2*, *OsNAAT1*, *OsDMAS1*, *TOM1*, and *OsYSL15*. When *OsIRO2* was introduced under the control of the constitutive cauliflower mosaic virus *35S* promoter into rice, the transformants had a larger amount of DMA secretion than NT plants and showed enhanced tolerance to Fe limitation in calcareous soil (Ogo et al., 2007; Ogo et al., 2011).

The Strategy I–based approach is the enhancement of Fe(III)-chelate reductase activity in the plant. Oki et al. (2004) artificially reconstructed and mutagenized to generate *refre1/372* from yeast Fe(III)-chelate reductase gene, *FRE1*. Refre1/372 shows increased enzymatic activity at alkaline pH, and it renders the transgenic tobacco plants resistant to Fe deficiency in calcareous soil (Oki et al., 2004). Ishimaru et al. (2007) introduced *refre1/372* into rice under the control of the *OsIRT1* promoter. The transgenic rice plants had enhanced Fe(III)-chelate reductase activity and conferred enhanced tolerance to Fe deficiency in calcareous soil (Ishimaru et al., 2007). Furthermore, these lines had a higher rate of Fe uptake and were 7.9-fold higher in grain yield than NT plants.

We recently developed an Fe deficiency–tolerant rice lines harboring *OsIRT1* promoter-*refre1/372* and overexpression of *OsIRO2* (Masuda et al., 2017). The introduction of a combination of two genes (*refre1/372* and *OsIRO2*; called "RI line") was more effective to provide Fe deficiency tolerance in rice than the single introduction of either gene in early growth stage under water-submerged conditions (Masuda et al., 2017). However, in this cultivation condition alone, the advantage of the combination of *refre1/372* and *OsIRO2* was not clear at a late period of growth and yields compared to *refre1/372* alone. Moreover, the contribution of OsIRO2 alone may not be enough for the elevation of Fe deficiency tolerance at the late growth period. *IDS3* is a MAs biosynthesis gene, which is responsible for enhancing Fe uptake and translocation. Thus, further enhancement of Strategy II

Fe uptake system by *IDS3* in rice together with *refre1/372* and *OsIRO2* is expected to be effective in enhancing Fe deficiency tolerance in calcareous soils.

In the present study, first, we observed the response of Refre1 line, OsIRO2 line, and RI lines to various cultivation conditions in calcareous soil and investigated the contribution of Fe deficiency tolerance by introducing *refre1/372*, *OsIRO2,* or combination of both genes. Then, we engineered a new construct and produced a rice line harboring an *IDS3* genome fragment, *OsIRT1* promoter-*refre1/372*, and *35S* promoter-*OsIRO2*. These transgenic lines possess *IDS3-refre1/372-OsIRO2* and are referred to as "IRI lines." The growth and yield of rice are also highly influenced by other cultivation conditions such as water level and the type of fertilizers. Thus, we also observed the Fe deficiency tolerance and response of IRI lines compared to NT plants, the *OsIRO2* line, *Refre1* line, and RI line in calcareous soil under submerged and nonsubmerged conditions.

MATERIALS AND METHODS

Production of *IDS3-Refre1/372-OsIRO2* (IRI) Rice Lines

The plasmid pIG121Hm containing a *35S* promoter-*OsIRO2*, *OsIRT1* promoter-*refre1/372*, and *IDS3* genome fragment was prepared as follows: the vector of RI line containing the *OsIRT1* promoter-refre1/372 and *35S* promoter-*OsIRO2* (Masuda et al., 2017) has a *Pme*I restriction enzyme site between RB and *35S-NPTII-tNOS* of the pIG121Hm vector (**Figure S1**). The *IDS3* genome fragment (Nakanishi et al., 2000) was digested by *Kpn*I and *Bam*HI, blunted by T4 DNA polymerase, and ligated to the RI vector, which was digested with *Pme*I. Then, the *IDS3-OsIRT1* promoter-*refre1/372-35S-OsIRO2*-pIG121Hm vector was obtained and named as IRI vector (**Figure S1**). Insertion of the *IDS3* genome fragment in the IRI vector was confirmed by polymerase chain reaction (PCR) with *IDS3* forward and reverse primers (5′-AAG CTT ACT GGT TGG ACG GTA TTT CA-3′ and 5′-GGA TCC ACG GGC CAC ATG ATC CA-3′, respectively), as well as by sequencing. *Agrobacterium tumefaciens* (strain C58) was used to introduce the IRI construct into the rice (*O. sativa* L. cv. Tsukinohikari) according to the modified method outlined in Hiei et al. (1994). Seventy-three regenerated plants were obtained. Gene insertion in regenerated plants was confirmed by genomic PCR. Then, IRI transformants were cultivated in a greenhouse at 28°C under natural light, and mature T_1 seeds and also T_2 seeds of the next generation were obtained for further analyses.

RNA Extraction and Quantitative Real-Time Reverse Transcription–PCR Analyses

The rice seeds of NT and IRI transgenic rice (T_2 seeds) were germinated for 17 days on Murashige and Skoog (1962) (MS) medium with and without hygromycin B (50 mg/L) for transformants and NT, respectively, at 28°C under 24-h light conditions. During the acclimation period of plantlets for 5 days, a leaf was sampled from each plantlet for the analyses of *OsIRO2* expression as described below. Then, IRI lines with higher expression of *OsIRO2* and NT plantlets were cultivated in an Fe-deficient hydroponic culture solution containing 122 mg/L K_2SO_4, 7.5 mg/L KCl, 14 mg/L KH_2PO_4, 472 mg/L $Ca(NO_3)_2 \cdot 4H_2O$, 123 mg/L $MgSO_4 \cdot 7H_2O$, 0.62 mg/L H_3BO_3, 0.12 mg/L $MnSO_4 \cdot 5H_2O$, 0.14 mg/L $ZnSO_4 \cdot 7H_2O$, 0.05 mg/L $CuSO_4 \cdot 5H_2O$, and 0.012 mg/L $(NH_4)_6Mo_7O_{24}$ as described in Masuda et al. (2017). The pH of the culture solution was adjusted to 5.5 every 2 days. After 6 days, roots were sampled for the analyses of *OsIRO2*, *refre1/372*, and *IDS3* gene expression. Total RNA was extracted from leaves or roots using an RNeasy Plant Mini Kit (Qiagen, Hilden, Germany). From extracted total RNA, the first-strand cDNA was synthesized using a ReverTra Ace qPCR reverse transcriptase (RT) Kit with gDNA remover (Toyobo, Osaka, Japan). Quantitative real-time RT-PCR was carried out using a StepOnePlus™ Real-Time PCR system (Applied Biosystems, Foster City, CA, USA) and SYBR Green (Takara, Shiga, Japan). The primers used for gene expression analyses were as follows: 5′-GGC ATG GCT CCC ATC GT-3′ and 5′-AAC AAG CTG ACC TGA ACC ATG A-3′ for *OsIRO2*, 5′-GGA AAG CTT CGT CTT CGC TTC-3′ and 5′-GAC CTC ATC ACG ACC AC TG-3′ for *IDS3*, and 5′-CCG AGA AGG TCT TCA GGA AC-3′ and 5′-CAT CCA TCC TAG TGT GTG GC-3′ for *refre1/372*. The plasmids that contain *HvNAS1*, *OsIRO2*, *IDS3*, or rice α-*tubulin* were diluted certain number of target gene copies (such as 10^3, 10^4, 10^5, or 10^6 copy/μl) and used as standard template. We performed real-time RT-PCR together with unknown cDNA template and standard templates, and then the copy number in unknown cDNA template was calculated based on standard line method. Transcript levels were normalized to the observed expression levels of α-*tubulin* by the primers 5′-TCT TCC ACC CTG AGC AGC TC-3′ and 5′-AAC CTT GGA GAC CAG TGC AG-3′, and the data is shown as "copy number of target gene/copy number of α-*tubulin*". By agarose gel electrophoresis method, the sizes of the amplified fragments were confirmed.

Growth Analyses of RI Lines on Calcareous Soil Under Different Water and Fertilizer Conditions

For the growth analyses in calcareous soil, T_3 seeds of RI line No. 22 (Masuda et al., 2017), T_3 seeds of Refre1 line No. 7 (Ishimaru et al., 2007), T_2 seeds of IRO2 line No. 2 (Ogo et al., 2007, OX2), and NT seeds were used. Seeds were surface sterilized and germinated on MS medium with or without hygromycin B, at 28°C for 20 days. Then, after acclimation of germinated plantlets for 3 days, five plants of each line were transplanted to a pot containing 700 ml calcareous soil. This calcareous soil contains soluble CaO: 39.6% and Fe_2O_3: 1.7% with pH 8.9, and the source of the soil is Takaoka City, Toyama, Japan (Nihonkai Kougyou, Japan). To prevent pest contamination, the soil was autoclaved and used just before transplanting. Then, the plantlets were cultivated in the following five patterns: 1) Plants were supplied with the slow-release fertilizer Eco-long total 70 (ELT70; the fertilizer releases NPK and micronutrients within 70 days) containing nitrogen (N):phosphorus (P):potassium (K) (13%, 11%, 13%)

with the micronutrients 0.20% Fe as EDTA-Na-Fe(III), 0.050% Cu, 0.015% Zn, and 0.020% Mo (JCAM AGRI, Co., Ltd., Tokyo, Japan) at a rate of 3 g/pot, and the water level of the container was maintained at lower than half of the pot height. 2) Plants were supplied with the slow-release fertilizer Eco-long 70 (EL70) containing N:P:K (14%, 12%, 14%) without micronutrients (JCAM AGRI, Co., Ltd.) at a rate of 3 g/pot, and the water level was maintained at lower than half of the pot height. 3) Hydroponic culture solution (50 ml) with Fe (components described above) was applied as fertilizer to each plant every 2 days, and the water level was maintained at lower than half of the pot height. 4) Hydroponic culture solution without Fe (components described above) was applied as a fertilizer into the whole cultivation box, and submerged conditions (water levels continuously higher than 2 cm of the pot height) were used. 5) ELT70 fertilizer was added at a rate of 3 g/pot, and the water level was maintained at higher than 3 cm above the pot height. A netting sheet was spread on the basal holes of the pot in order to avoid the roots from growing outside the pots. After setting up all conditions, the plants were cultivated in a greenhouse at 28°C under natural light. The SPAD value of the newest leaf and the shoot height were measured every 3 days by a SPAD-502 chlorophyll meter (Konica Minolta, Japan). Plants were harvested after seed maturation at 109 days after transplanting, and weights of panicles and straw were measured.

Selection of IRI Lines on Calcareous Soil

Plantlets of IRI T_2 lines with higher expression of *OsIRO2*, *Refre1/372*, and *IDS3*, as well as NT plantlets, were prepared as described above. Then, two plants of each line were transferred to a pot containing 700 ml calcareous soil as described above. A netting sheet was covered on the basal holes of the pot. Then, ELT40 (3.5 g/pot) and ELT70 (3.5g/pot) or hydroponic culture solution with or without Fe (50 ml/pot *per* week) was added as fertilizer. Submerged conditions (level of water continuously higher than 3 cm above the pot height) were used. The plants were cultivated in a greenhouse at 28°C under natural light. The shoot length and the SPAD value of the newest leaf were measured every 3 days throughout the cultivation. Then the lines with higher shoot length and higher SPAD value were selected for further analysis.

Growth Analyses of IRI Lines on Calcareous Soils Under Submerged and Nonsubmerged Conditions

For the growth analyses of IRI lines on calcareous soil, T_3 plantlets of IRI lines 1, 4, and 65; T_3 plantlets of the RI line (Masuda et al., 2017; line No. 22); Refre1 line (Ishimaru et al., 2007; line No. 7); and IRO2 line (Ogo et al., 2007; OX2 line); T_5 plantlets of the *IDS3* genome line (generated by Kobayashi et al., 2001 and tested the Fe deficiency tolerance in the field by Suzuki et al., 2008); and NT plantlets were prepared and cultivated in the following two patterns: 1) For the first experiment, individual plantlet was grown in each pot containing 1 kg of calcareous soil (as described above) with 3.5 g of ELT70 and 3.5 g of ELT140 fertilizers. A netting sheet was placed on the base of each pot. The growing method was the same as described in Masuda et al. (2017). The level of water was maintained at higher than 3 cm of the pot height. 2) For the second experiment, the same lines (T_3 plants of IRI lines) were cultivated in a pot containing 1 kg calcareous soil, and 50 ml hydroponic culture solution without Fe was added as fertilizer to each pot every 3 days. Water was maintained at higher than 3 cm above the bottom of the cultivation box (one-fourth of the pot height). Shoot height and the SPAD value of the newest leaf were measured every 3 days. Weights of the plants were measured at 115 days after transplanting.

Statistical Analyses

We used four biological replications (n = 4) for each variety for calcareous cultivation. Analysis of variance *via* Student's *t*-test was used to examine the experimental data from calcareous soil cultivation, such as plant height, SPAD value, and dry weights of panicles. Statistical analysis was performed using JMP14 software (SAS Institute, Cary, NC, USA); $p < 0.05$ was considered statistically significant.

RESULTS

Production of Triple-Inserted IRI Lines and Selection of Lines With Higher Gene Expression Under Fe-Deficiency Conditions

For the enhancement of Fe acquisition in rice, the IRI vector harboring the *IDS3-OsIRT1* promoter-*Refre1/372-35S-OsIRO2* was produced and introduced into rice plants by *Agrobacterium*-mediated transformation (**Figure 1A**, **Figure S1**). We obtained 73 regenerated lines, from which we selected the lines with higher expression levels of *OsIRO2* from the shoot of the T_2 plants (**Figure 1B**). Next, the lines with higher expression of all three introduced genes (*OsIRO2*, *refre1/372*, and *IDS3*) were achieved by the real-time quantitative RT-PCR analysis of the roots of selected IRI lines grown in Fe-deficient hydroponic solution (**Figures 1C**–**E**). The expression levels of *OsIRO2* in the IRI lines were higher than those in the NT line (**Figure 1C**). The expression levels of *refre1/372* and *IDS3* were detected in IRI lines but not in the NT line (**Figures 1D**, **E**). Therefore, the nine T_2 IRI lines with higher gene expression (lines 1-3, 3-1, 4-2, 6, 8, 11-1, 12, 65-2, and 73-1) were used for growth analyses and further investigation.

Water Levels and Types of Fertilizers Influence Plant Growth of RI Lines

In order to determine the growth conditions that reflect the clear roles of individual gene and combined genes, first, Refre1 line, OsIRO2 line and RI line were grown on calcareous soil under five different cultivation conditions with varied fertilizer and water supply as follows.

Cultivation condition (1): When plants were grown with NPK fertilizer with micronutrients (ELT70) and under nonsubmerged conditions (**Figure S2A**), the growth of OsIRO2 line, Refre1

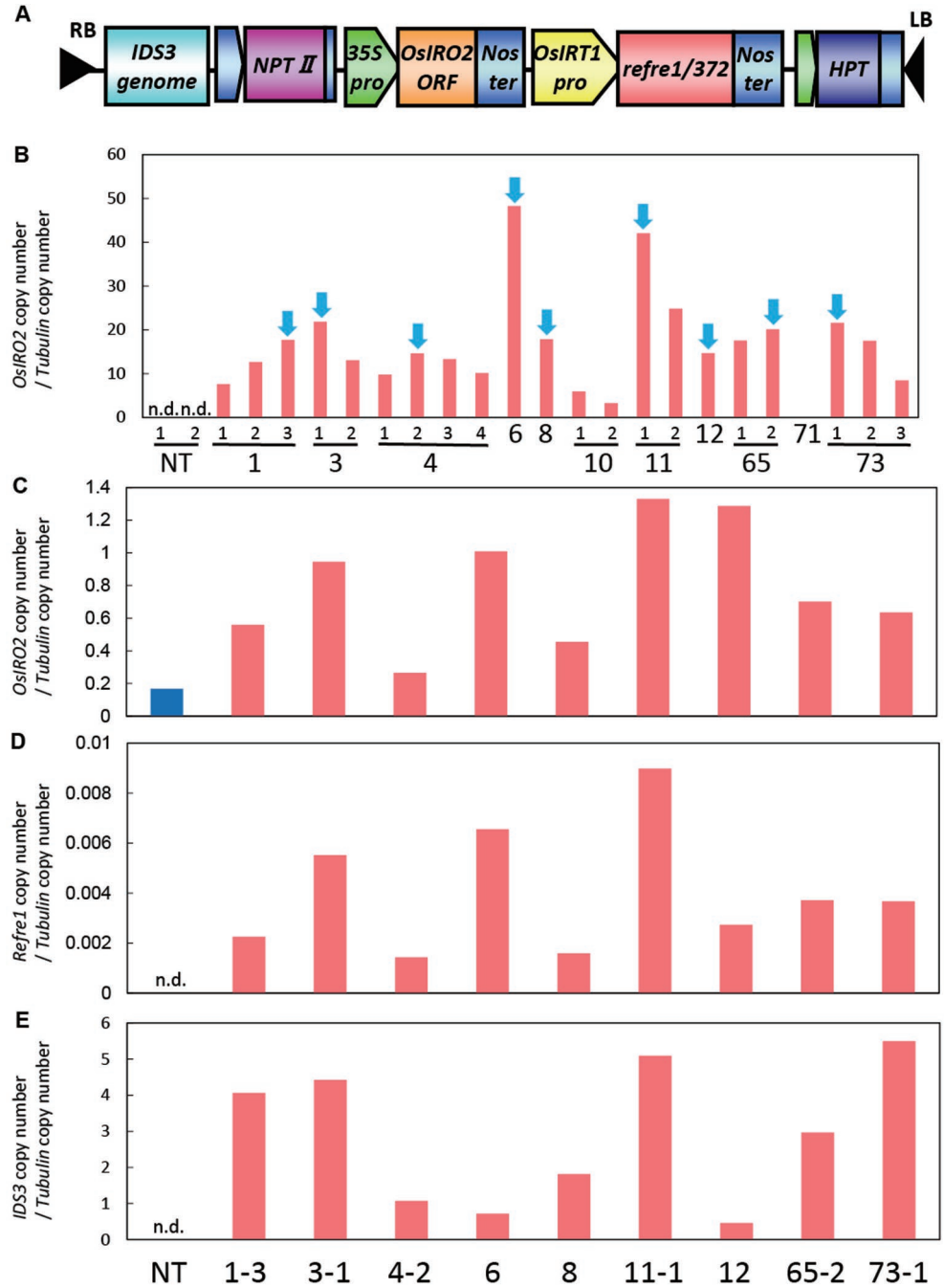

FIGURE 1 | Vector construction and gene expression analyses of IRI rice lines. **(A)** Vector construction of IRI. This vector was introduced into rice cultivar Tsukinohikari by *Agrobacterium*-mediated rice transformation to produce IRI lines. **(B)** Gene expression analyses of *OsIRO2* by real-time RT-PCR for line selection. Leaves were sampled from T_2 IRI lines and nontransgenic (NT) plants germinated on MS medium. The IRI lines with higher gene expression shown by blue arrows were selected for further analyses. **(C–E)** Expression of the three inserted genes, *OsIRO2*, *refre1/372*, and *IDS3*, respectively, in Fe deficiency roots by real-time RT-PCR. Roots were sampled from T_2 IRI lines and NT plants cultivated in Fe-deficient hydroponic culture for 1 week. The expression levels were normalized with *rice* α-*tubulin*, and data shown represent target gene copy number/α-*tubulin* copy number (n = 1). n.d., not determined.

line, and RI line 22 was better than NT during vegetative stage (**Figure S2B**). However, all plants set panicles similarly during the maturation stage (**Figure S2D**), and there were no significant differences in the yields of all lines compared to NT lines (**Figure S2E**). The SPAD value was higher in RI line 22 compared to the OsIRO2, Refre1, and NT lines (**Figure S2C**).

Cultivation condition (2): When plants were grown with NPK fertilizer without micronutrients (EL70) and under

nonsubmerged conditions (**Figure S3**), some NT plants died, but the transgenic lines survived (**Figure S3C**). The growth of the transgenic lines was better than the NT lines (**Figure S3A**). The SPAD values of the OsIRO2 and RI 22 lines were higher than NT and Refre1 lines in this condition (**Figure S3B**).

Cultivation condition (3): When plants were grown with an application of Fe-sufficient hydroponic solution under nonsubmerged conditions (**Figure S4A**), the growth, the SPAD values, and the yields of all transgenic lines were better than NT lines (**Figure S4**).

Cultivation condition (4): When plants were grown with application of hydroponic solution without Fe under submerged conditions (**Figure S5A**), the growth, SPAD values, and the yields of RI line 22 were better compared to the IRO2 and Refre1 lines, which were better than those of the NT lines (**Figures S5B–E**). In the early growth stage, the SPAD value of the OsIRO2 line was better than the Refre1 line (**Figures S5B, D**), and it exhibited the same trend as described in Masuda et al. (2017).

Cultivation condition (5): When plants were grown with NPK fertilizer with micronutrients (ELT70) and under submerged conditions (**Figure S6**), the RI line 22 and Refre1 grew better than the NT and OsIRO2 lines (**Figures S6A–D**).

We used nonsubmerged conditions for cultivation condition (1), (2), and (3) and submerged conditions for cultivation conditions (4) and (5). In this study, our results show that between the single introduction lines, Refre1 line was more tolerant than the IRO2 line under most cultivation conditions especially in the middle and late growth stages under cultivation conditions (1) and (5) (**Figures S2C**, **S6C**). On the other hand, the OsIRO2 line showed a better SPAD value especially in early growth stages, and the value decreased to the NT level in the middle and late growth stages under cultivation conditions (1) and (4) (**Figures S2C**, **S5D**).

Fe Deficiency Tolerance of IRI Lines Under Various Cultivation Conditions

To further enhance Strategy II Fe uptake in rice, we focused on the introduction of the *IDS3*, a mugineic acid synthase gene of barley. We generated a new rice IRI line harboring the *IDS3* genome fragment, *OsIRT1* promoter-*refre1/372*, and *35S* promoter-*OsIRO2* (**Figure 1A**, **Figure S1A**). When nine T_2 IRI lines with higher gene expression (lines 1-3, 3-1, 4-2, 6, 8, 11-1, 12, 65-2, and 73-1) were cultivated on calcareous soil with ELT70 fertilizer (NPK with micronutrients) under water-submerged conditions, the IRI rice plants exhibited superior Fe deficiency tolerance, while NT plants died (**Figure 2A**). The growth of IRI lines was better than that of NT lines (**Figure 2B**). In particular, the plant heights of lines 1-3, 3-1, 4-2, and 65-2 were better than the other lines. The SPAD values of lines 1-3 and 65-2 were higher than other lines, including NT lines (**Figure 2C**). The weights of panicles in lines 1-3 and 65-2 were also higher than other lines, including NT lines (**Figure 2D**). Thus, lines 1-3 and 65-2 were selected from this cultivation for further analyses.

Next, we grew the same lines in a calcareous soil under another cultivation condition, i.e., with Fe or without Fe hydroponic solution fertilizer under nonsubmerged conditions (**Figure 3**). With Fe-sufficient hydroponic solution fertilizer, although transgenic lines exhibited higher plant growth and SPAD values, a clear difference between each line and the NT lines was not apparent (**Figures 3A–C**). With the addition of Fe-deficient hydroponic solution, transgenic lines showed better growth and SPAD values compared to NT lines (**Figures 3D–F**). In particular, IRI line 4-2 showed better growth performance than other lines (**Figures 3E**, **F**). Thus, we also selected IRI line 4-2 for further analyses of calcareous soil cultivation.

Growth of IRI Lines Under Fe-Sufficient Water-Submerged Conditions

To compare the contributions of individual genes introduced into IRI lines, we grew the previously produced IRO2 line (Ogo et al., 2007), Refre1 line (Ishimaru et al., 2007), IDS3 line (Masuda et al., 2008), and RI line No. 22 (Masuda et al., 2017) together with IRI and NT lines. When the plants were cultivated with ELT fertilizer (NPK plus micronutrients) under water-submerged condition (**Figure S7A**), IRI lines and all other transformants exhibited better growth than NT (**Figure 4A**). Especially, the IRI and Refre1 lines showed superior growth performance and Fe deficiency tolerance than the NT lines (**Figures 4B**, **C**). IRI lines 1-3, 4-2, and 65-2 and the Refre1 line showed better growth and SPAD values compared to the IDS3, IRO2, and NT lines (**Figures 4D**, **E**). The yields (panicle weight) and biomass (straw weight) of transgenic lines were higher than those of NT lines (**Table 1**, **Figure S8A**). The dry weights of straw were measured from the plants harvested at 150 days after transplanting for submerged condition (**Figure S8A**). After that long period, the other tested transgenic lines were also recovered likewise IRI and Refre1 lines especially under submerged condition (**Figure S8A**). However, there were remarkable differences in growth and SPAD among the lines (**Figures 4D**, **E**). Our results showed the Refre1 line was tolerant to Fe deficiency likewise IRI lines in this cultivation condition.

Growth of IRI Lines Under Fe-Limited Nonsubmerged Conditions

Transgenic and NT lines were cultivated on calcareous soil with Fe-deficient hydroponic solution fertilizer under nonsubmerged conditions (**Figure S7B**). In this cultivation condition, IDS3 and all IRI lines (line 1-3, 4-2, and 65-2) showed greenish leaves compared to NT, Refre1, IRO2, and RI22 lines, which showed clear Fe-deficiency chlorosis symptoms on leaves (**Figure 5A**). There was less difference in plant growth (**Figure 5B**). However, the SPAD values of IRI lines 1-3, 4-2, and 65-2 and IDS3 lines were higher than those of Refre1, IRO2, and RI line 22 (**Figure 5C**). The dry weights of straw were also measured from the plants harvested at 105 days after transplanting for nonsubmerged condition (**Figure S8B**). In this cultivation condition, the biomasses of the IRI lines, IDS line, and IRO2 line were better than those of Refre1 line, RI line 22, and NT (**Table 1**, **Figure S8B**).

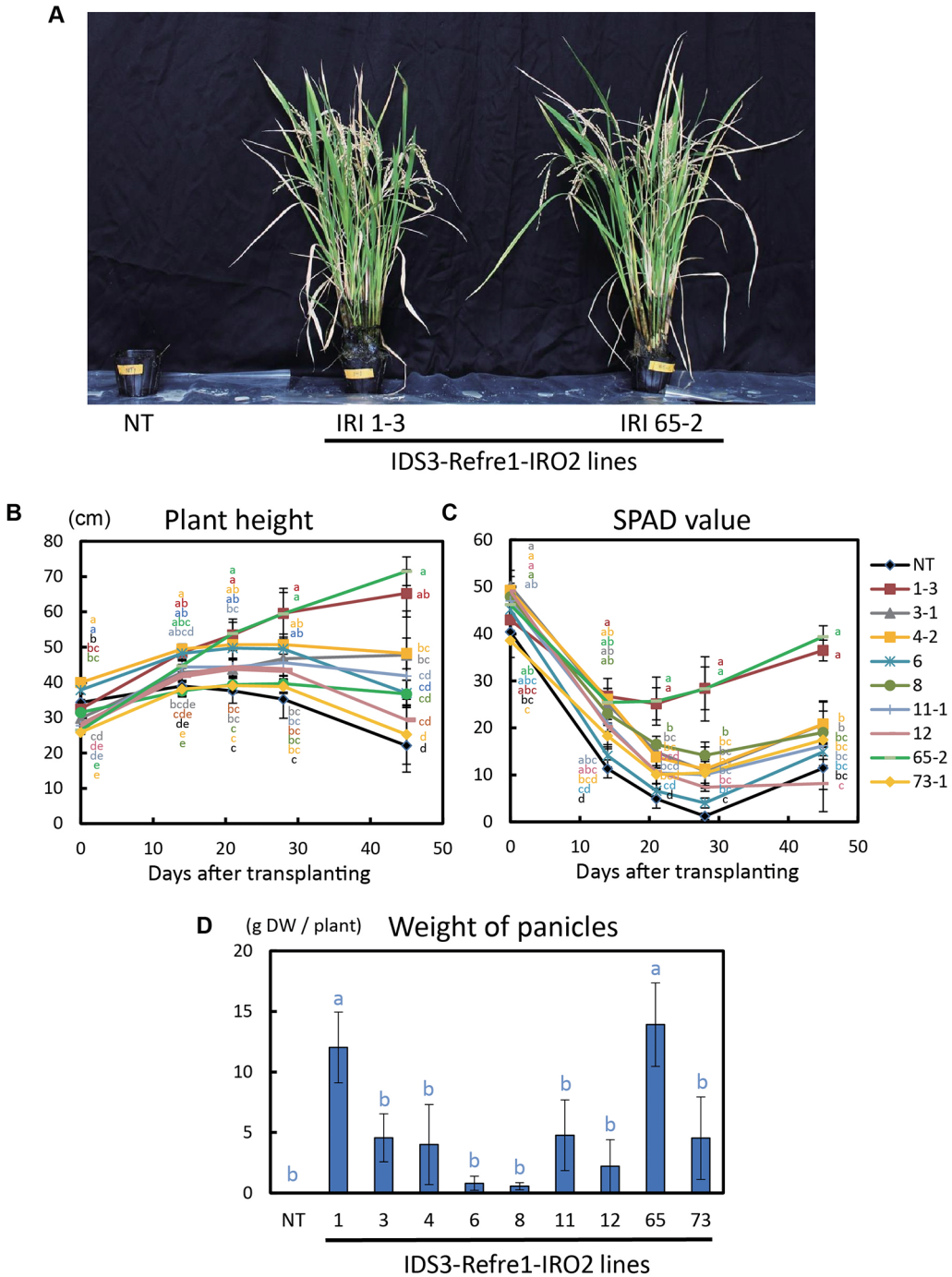

FIGURE 2 | Growth test of IRI rice lines compared to NT on calcareous soil under water submerged condition. **(A)** Plant appearance at 117 days after transplanting. **(B)** Plant height. **(C)** SPAD value of the newest leaves. **(D)** Weight of panicles. NT, nontransgenic rice; Numbers, T_2 plants of IRI lines. Error bars represent ± 1 standard error (SE) of biological replicates (n = 4). Values with different letters were significantly different by Student's *t*-test ($p < 0.05$).

DISCUSSION

Water Levels and Fertilizer Types Influence Plant Growth of RI Lines

In our previous study (Masuda et al., 2017), the growth at late periods and yields between Refre1 and RI lines were similar, and the contribution of OsIRO2 to Fe deficiency tolerance was not clear. The plant growth is highly influenced by cultivation practices such as water levels and types of fertilizers, and thus the important roles of individual gene and combined genes on the stages of plant life would be interesting. In fact, the water level is not consistently maintained in real paddy field

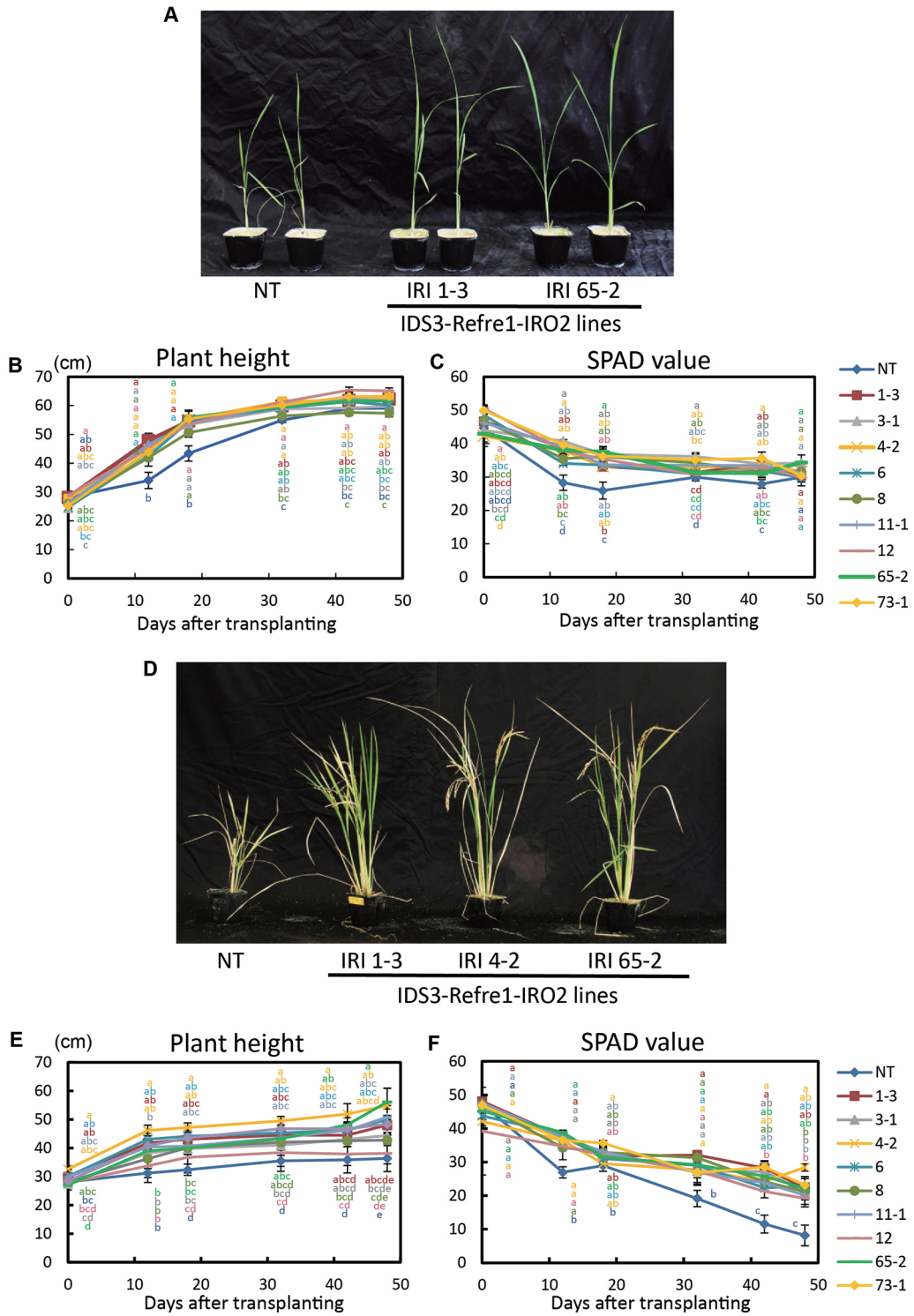

FIGURE 3 | Growth test of IRI rice lines compared to NT on calcareous soil under non–water-submerged condition. **(A)** Plant appearance at 17 days after transplanting, **(B)** Plant height and **(C)** SPAD value of the newest leaves of the plants supplied by 50 ml Fe-sufficient hydroponic solution fertilizer to each pot every 3 days. **(D)** Plant appearance at 176 days after transplanting, **(E)** plant height, and **(F)** SPAD value of the newest leaves of the plants supplied by 50 ml Fe-deficient hydroponic solution fertilizer to each pot every 3 days. NT, nontransgenic rice; Numbers, T_2 plants of IRI lines. Error bars represent ± 1 SE of biological replicates (n = 4). Values with different letters were significantly different by Student *t* test ($p < 0.05$).

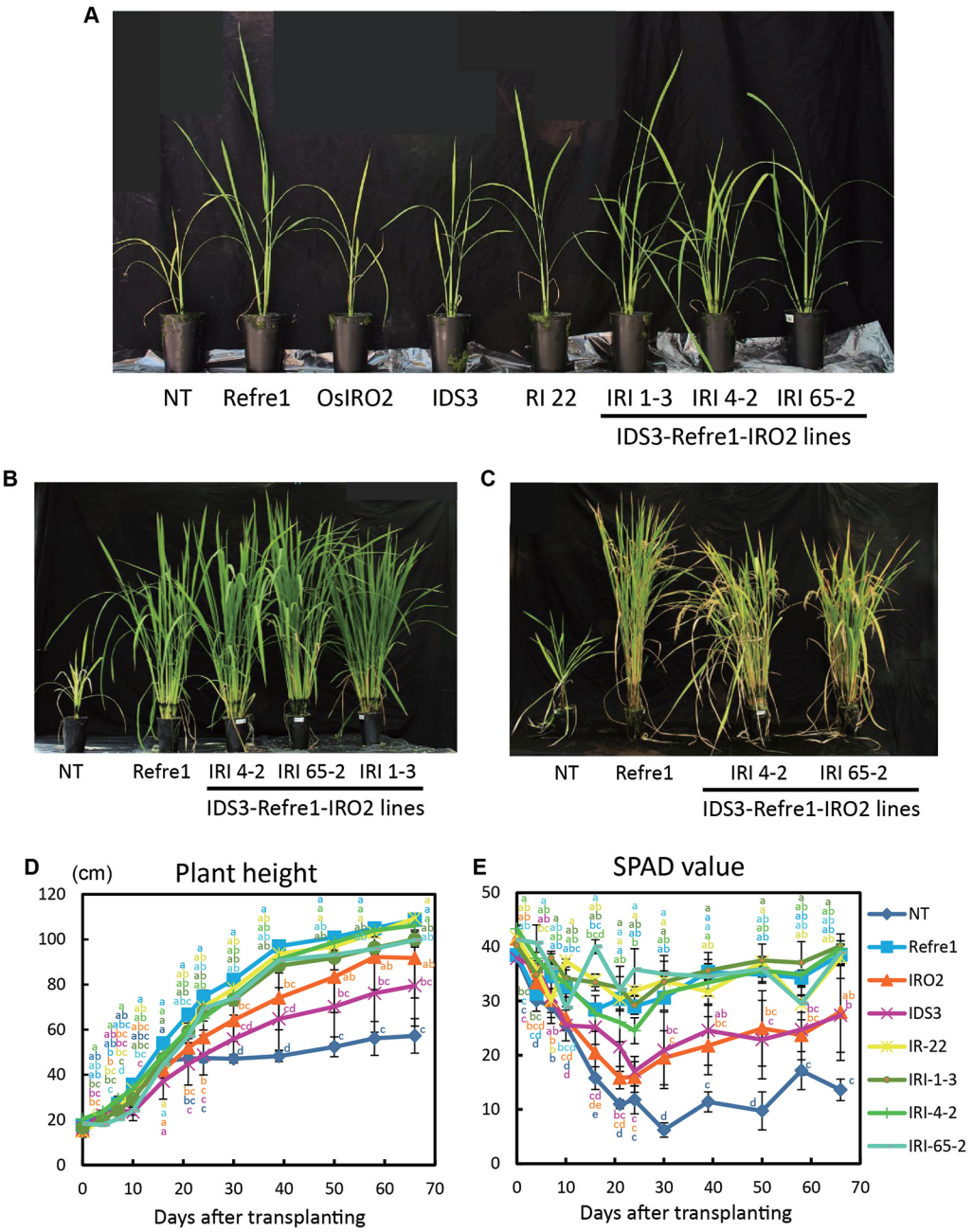

FIGURE 4 | Growth test of IRI lines compared to NT and other lines on calcareous soil treated with Fe-sufficient fertilizer under water-submerged condition. **(A)** Plant appearances of all lines at 25 days after transplanting (DAT). **(B)** Plant appearances of IRI lines compared to NT and Refre1 lines during the vegetative stage at 73 DAT. **(C)** Plant appearances of IRI lines compared to NT and Refre1 lines during the maturation stage at 137 DAT. **(D)** Plant height. **(E)** SPAD value of the newest leaves. ELT fertilizer (NPK plus micronutrients) was applied to the soil. NT, nontransgenic rice; Refre1, line with *OsIRT1* promoter-*refre1*; IRO2, line with *35S* promoter-*OsIRO2*; IDS3, line with *IDS3* genome fragment; RI-22, line with *35S* promoter-*OsIRO2* and *OsIRT1* promoter-*refre1* No. 22; IRI, lines with *IDS3* genome fragment, *OsIRT1* promoter-*refre1*, and *35S* promoter-*OsIRO2*. Error bars represent ± 1 SE of biological replicates (n = 4). Values with different letters were significantly different by Student *t* test ($p < 0.05$).

cultivation of rice. The Fe status in soil changes depending on the water level: Fe is mostly in precipitate form as ferric oxide under nonsubmerged condition, but it exists as a ferrous ion under submerged condition. Thus, the water level is an important factor in the cultivation of rice to resist Fe deficiency stress. Morikawa et al. (2004) used three types of fertilizer for rice cultivation (c.v. Tsukinohikari) in calcareous paddy fields: EL70, which includes only NPK (defined as CRF NPK in the study); ELT70, which includes NPK plus micronutrients (CRF M1 in the study); and ELT140, which also includes NPK plus

TABLE 1 | Plant tolerance under calcareous soil cultivation with different water conditions.

Lines	Submerged condition - Calcareous soil		Nonsubmerged condition - Calcareous soil	
	Growth (Height, SPAD)	Biomass / Yield (g/plant)	Growth (Height, SPAD)	Biomass (g/plant)
NT	✕ (57.3 ±7.7 cm, 13.6 ±2.0)	✕ (15.5±3.6 /4.9±3.2)	✕ (71.1 ±0.7 cm, 13.75 ±1.6)	✕ (3.1±0.2)
Refre1	◎ (108.8 ±2.9 cm, 38.5 ±1.8)	◎ (90.7±14.2 / 9.6±6.9)	△ (76.5 ±1.5 cm, 20.2 ±4.9)	△ (3.9±0.3)
IRO2	○ (91.8 ±17.7 cm, 28.0 ±8.9)	○ (54.5±21.3 /23.0± 9.7)	○ (79 ±2.0 cm, 22.9 ±1.8)	○ (5.0±0.4)
Refre1-IRO2 (RI line)	◎ (109.4±1.1 cm, 38.0 ±1.5)	◎ (53.9±5.0/26.0± 4.9)	○ (75.8 ±1.8 cm, 25.0 ±6.8)	△ (4.1±0.6)
IDS3	△ (79.5 ±17.9 cm, 27.4 ±6.8)	○ (36.9±17.2/14.0± 7.6)	◎ (79.6 ±3.3 cm, 36.1 ±2.1)	○ (5.3±0.2)
IDS3-Refre1-IRO2 (IRI line)	◎ (106.1 ±1.9 cm, 39.7 ±1.4)	◎ (50.0±10.3/21.4± 6.7)	◎ (81.8 ±1.6 cm, 36.9 ±2.4)	○ (5.2±0.4)

✕, *very poor or weak;* △, *slightly good tolerance;* ○, *good tolerance;* ◎, *excellent tolerance.* ± *showed the standard error n = 4. The height of submerged condition, the SPAD of submerged condition, the height of nonsubmerged condition, and the SPAD of nonsubmerged conditions shown in the parentheses are referenced on 66 days after transplanting (DAT), 66 DAT, 33 DAT, 63 DAT, respectively. NT, nontransgenic rice. RI line represents RI line 22. IRI line represents IRI line 4-2.*

micronutrients (CRF M2 in the study). All plants died when treated with EL fertilizer alone. The plants could not survive without micronutrient supplementation in the calcareous paddy field (Morikawa et al., 2004). It suggests that the type of fertilizer is another important factor for rice cultivation in calcareous soil.

Thus, we assumed that the determination of cultivation condition is important for Fe deficiency tolerance of plants grown on calcareous soil. In order to determine the growth conditions that reflect clear roles of individual gene and combined genes, we grew Refre1 line, OsIRO2 line, and RI line in five different cultivation conditions with varied fertilizers and water supplies with five different cultivation conditions (**Figures S2–S6**). In all five cultivation conditions, the RI line showed the best growth. Our results suggested that, as concluded in Masuda et al. (2017), the combined introduction of *35S-IRO2* and *OsIRT1* promoter-*refre1* enhanced Fe deficiency tolerance in rice in calcareous soil than the single gene introduction.

In this study, our results show that among the single gene introduced lines, Refre1 line was more tolerant than the IRO2 line under most cultivation conditions except the early growth stage in cultivation condition (4) (**Figures S5B–D**). Under cultivation conditions (1) and (4), although the OsIRO2 line showed a better SPAD value in early growth stages, the value decreased to the NT level in the middle and late growth stages (**Figures S2C**, **S5D**). OsIRO2 plants may have grown well in the early growth stages because of increased expression of *OsIRO2*. However, in the middle and late growth stages, when plants grew larger and consequently the Fe demand of the plants increased further, the Fe uptake ability was not well enhanced by the introduction of *35S-OsIRO2* alone. We considered the further enhancement of the Strategy II Fe uptake system in rice would be required to produce higher Fe deficiency tolerance for calcareous soil cultivation.

IRI Lines Exhibit Strong Fe Deficiency Tolerance Under Various Cultivation Conditions Compared to NT

We additionally introduced a barley mugineic acid synthase gene, *IDS3*, for the further enhancement of Strategy II Fe uptake in rice. Most of the rice variety including Tsukinohikari, the variety tested, can produce until only DMA, but it cannot produce mugineic acid (Kobayashi et al., 2001). When rice expresses *IDS3* by the introduction of the barley *IDS3* genome fragment, it can produce mugineic acid together with DMA, and the total amount of MAs secretion also increases (Kobayashi et al., 2001). Introduction of the *IDS3* genome fragment in rice enhances Fe translocation and increases seed Fe concentration (Masuda et al., 2008) and also enhances Fe deficiency tolerance in field cultivation on calcareous soil (Suzuki et al., 2008). We successfully generated IRI plants harboring the *IDS3* genome fragment, *OsIRT1* promoter-*refre1/372*, and *35S* promoter-*OsIRO2* (**Figure 1**, **Figure S1A**). IRI lines demonstrated excellent growth and superior Fe deficiency tolerance, while NT plants died when cultivated on calcareous soils with ELT fertilizer under submerged condition (**Figure 2**). Additional cultivation conditions with different fertilizer types were also used to determine the growth response on calcareous soils under nonsubmerged conditions (**Figure 3**). IRI lines exhibited higher growth and SPAD values in both fertilizer types (**Figure 3**), but there was no clear difference between each line and the NT lines with Fe-sufficient hydroponic fertilizer (**Figures 3A–C**), while a clear difference can be observed with Fe-deficient hydroponic fertilizer (**Figures 3D–F**). In this study, the two introduced genes, *OsIRT1* promoter-*refre1/372* and the *IDS3* genome fragment, were under the control of Fe deficiency–inducible promoters. Because of this fact, it may be indistinguishable that higher gene expression was as a result of the trait of particular lines or Fe deficiency. In our results, the gene expression of IRI lines 1-3, 4-2, and 65-2 was not the highest among the lines tested, but

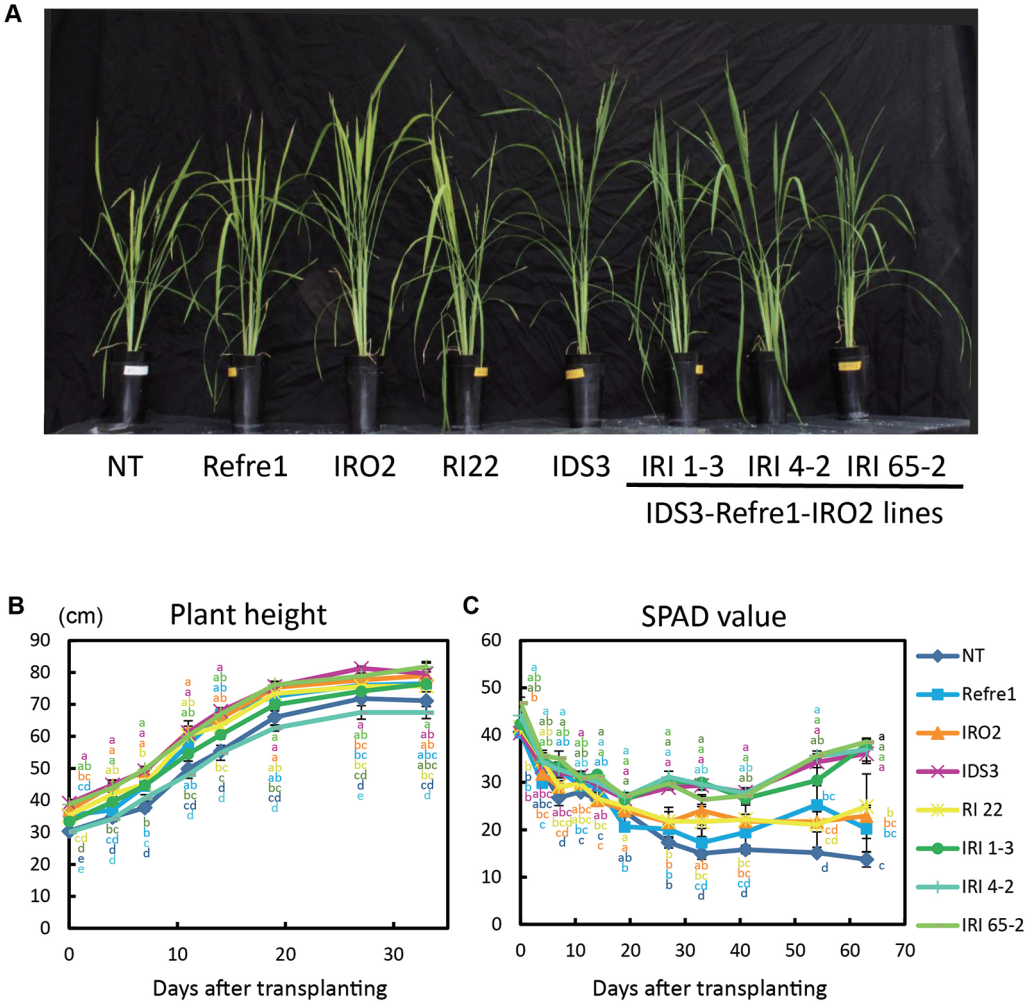

FIGURE 5 | Growth test of IRI lines compared to NT and other lines on calcareous soil treated with Fe-deficient fertilizer under non–water-submerged condition. **(A)** Plant growth and appearances at 66 days after transplanting. **(B)** Plant height. **(C)** SPAD value of the newest leaves. Iron-deficient hydroponic solution fertilizer was applied to the soil. NT, nontransgenic rice; Refre1, line with *OsIRT1* promoter-*Refre1*; IRO2, line with *35S* promoter-*OsIRO2*; IDS3, line with *IDS3* genome fragment; RI-22, line with *35S* promoter-*OsIRO2* and *OsIRT1* promoter-*refre1* No. 22; IRI, lines with *IDS3* genome fragment, *OsIRT1* promoter-*refre1*, and *35S* promoter-*OsIRO2*. Error bars represent ± 1 SE of biological replicates (n = 4). Values with different letters were significantly different by Student *t* test ($p < 0.05$).

these lines showed remarkable Fe deficiency tolerance (**Figures 1B–E**), suggesting the need for line selection based on not only gene expression but also Fe deficiency tolerance.

IRI Lines Showed Better Growth Under Fe-Sufficient Water-Submerged Conditions

To investigate the roles and contributions of individual genes introduced into IRI lines, all transformants were cultivated on calcareous soils with ELT fertilizer under water-submerged condition (**Figure S7A**). As a result, all transformants showed better growth than NT (**Figure 4A**). Especially, all IRI lines 1-3, 4-2, and 65-2 and the Refre1 line exhibited superior growth performance and Fe deficiency tolerance with high SPAD values compared to the IDS3, IRO2, and NT lines (**Figures 4B–E**). Our results showed the Refre1 line was tolerant to Fe deficiency likewise IRI lines (**Figure 4**). In fact, under anaerobic water-submerged condition, normal paddy soil has a large number of ferrous ions, especially in low pH soil. However, calcareous soil does not contain abundant soluble ferrous ions because of its high pH, and NT plants cannot take up Fe easily. Thus, under this water-submerged condition on high pH calcareous soil, *OsIRT1* promoter-*refre1/372* reduces ferric ions to ferrous form at the root surface, and ferrous form of Fe reduced by refre1/372 is easier to maintain in the reduction state of water-submerged cultivation and easier to take up directly by the OsIRT1 ferrous ion transporter in rice roots. This might be the main reason for the strong tolerance of the Refre1 line in this cultivation. *OsIRT1* promoter-refre1/372 showed high Fe(III)-chelate reductase activity and Fe deficiency–tolerant in calcareous soil (Ishimaru et al., 2007).

Another reason is partly that Refre1 line used MAs, which might be produced and released by the OsIRO2, IDS3, RI, and IRI lines under this cultivation condition. *OsIRO2*-overexpressing rice secreted DMA about 1.7 times (Ogo et al., 2007), and IDS3 rice secreted MAs about two times (Kobayashi et al., 2001) more than did NT plants. Because of the above reason, Refre1 was already stronger than NT under submerged condition. Therefore, these DMA and MAs produced by single, double, and triple introduced lines might be efficiently used by Refre1 line. In fact, the effect of MAs is lower, and MAs strategy is less effective under submerged condition. Thus, OsIRO2 and IDS3 lines were weak in this condition, and there was less difference between Refre1 and double introduced line. On the other hand, Refre1 rice had advantages in this condition.

As reported in Masuda et al. (2017), we confirmed *OsIRO2* overexpression improved Fe deficiency tolerance at the early growth stage of the plants under submerged conditions (**Figures S2C**, **S3B**) and nonsubmerged condition (**Figure S5D**). OsIRO2 is an important transcription factor that regulates the genes involved in Strategy II–related Fe uptake and translocation (Ogo et al., 2007; Ogo et al., 2011). Moreover, OsIRO2 positively regulates the expression of NA and DMA biosynthesis genes, and DMA and Fe(III)-DMA transporters under both Fe-deficient and -sufficient conditions, and *OsIRO2* overexpression confers increased DMA secretion under Fe-deficiency condition (Ogo et al., 2007; Ogo et al., 2011). Thus, it is thought that the IRO2 line is constantly ready for Strategy II–based tolerance to Fe deficiency before Fe deficiency arises, resulting in early growth tolerance in calcareous soil cultivation (Masuda et al., 2017). However, *refre1/372* was expressed under the control of the *OsIRT1* promoter, which induces gene expression mainly under Fe-deficient conditions in roots of the Refre1 line. Thus, the Refre1 line is prone to meet Fe deficiency before inducing tolerance (Masuda et al., 2017). As a result, there was a comparatively low SPAD value and weak tolerance of the Refre1 line to Fe-deficient conditions during the first week of growth in calcareous soils (**Figures 4E**, **5C**, **Figures S3B**, **S5D**).

During the middle and late stages of cultivation, IRI lines, RI lines, and the Refre1 line exhibited superior tolerance compared to the NT, IRO2, and IDS3 lines (**Figure 4**). The trends were the same as reported in Masuda et al. (2017). The Fe(III)-chelate reductase activity of Refre1 line was two times higher than that of NT line under Fe-deficient conditions (Masuda et al., 2017). This advantage might confer Refre1 line, and the lines possess *refre1/372* to be more resilient than the NT line during the middle and late growth stages of growth in calcareous soils. On the other hand, the IRO2 line and IDS3 line exhibited weak tolerance during these growth stages (**Figure 4**). MAs productivity was enhanced by the introduction of *OsIRO2* or *IDS3*. However, under water-sufficient condition, diffusion of MA phytosiderophores produced and released from roots might be increased under such condition, and the concentration of MAs in rhizosphere decreased. The dose-dependent DMA application to hydroponic culture solution affects the improvement of Fe nutrition (Araki et al., 2015). Therefore, improvement of the reduction strategy mediated by *refre1/372* would be highly effective in supporting Fe acquisition when Strategy II–based uptake is insufficient during the middle and late growth stages under water-submerged condition.

IRI Lines With the Additional Introduction of an *IDS3* Genome Fragment Are Effective Under Fe-Limited Nonsubmerged Conditions

When transgenic and NT lines were cultivated on calcareous soil with Fe-deficient hydroponic fertilizer under nonsubmerged conditions, NT, Refre1, IRO2, and RI22 lines showed clear Fe-deficiency chlorosis symptoms on leaves, whereas IDS3 and all IRI lines exhibited greenish healthy leaves, and their SPAD values were higher than those of Refre1, IRO2, and RI line 22 (**Figures 5A**, **C**). Our results indicate that the Refre1 line did not tolerate under nonsubmerged condition (**Figure 5**). The reason for this could be that ferric ions which were reduced by *refre1/372* on root surface might be oxidized easily in the oxidation state under nonsubmerged conditions and difficult to take up by *OsIRT1* in rice roots.

OsIRO2 and RI lines also did not tolerate in this condition compared to NT. It might be because of two reasons. 1) The productivity of MA which normal rice cannot produce and secrete is important. NT, Refre1, OsIRO2, and RI plants can produce only until DMA. On the other hand, IDS3 line and IRI lines can produce both DMA and MA. MA is more efficient than DMA. 2) *OsIRO2* expression of the NT plant is very low under Fe-sufficient conditions compared to that of *35S*-promoter *OsIRO2* plant (Ogo et al., 2006), whereas it is dramatically high under Fe-deficiency conditions (Masuda et al., 2017). Thus, in middle and late growth stages of Fe-deficiency conditions in calcareous soils, this Fe deficiency–induced function of endogenous *OsIRO2* might outcome smaller contribution of *OsIRO2* overexpression in the IRO2 line than NT line and thus, the advantageous of *35S*-promoter *OsIRO2* gene is reduced compared to NT (Masuda et al., 2017, **Figures 4** and **5**). In this study, the contribution degree of the *35S-OsIRO2* cassette when introduced together with *IDS3* genome and *refre1/372* is still unclear because the Fe deficiency tolerance of the line harboring refre1 and the *IDS3* genomic fragment has not been examined yet for comparison. Thus, in further study, the line harboring *Refre1-IDS3* cassette may be valuable as control compared with IRI lines to observe whether the *35S-OsIRO2* cassette is essential or not together with *IDS3* genome and *refre1/372* to achieve Fe deficiency tolerance.

Our results confirm that the contribution of OsIRO2 alone was insufficient for the elevation of Fe deficiency tolerance at the late growth period. On the other hand, MAs biosynthesis gene IDS3 complements this necessity. Under nonsubmerged conditions, phytosiderophore produced and secreted to root rhizosphere might not diffuse and effectively contributed to uptake Fe in IDS3 line and IRI lines. IDS3 line and IRI line maintained high SPAD value and showed remarkable tolerance under nonsubmerged condition (**Figures 5A**, **C**). We show that IRI rice with further improvement of Strategy II Fe uptake system mediated by *IDS3* obviously can enhance Fe deficiency tolerance in the rice.

IRI Lines Confers Further Enhancement of Fe Acquisition and Tolerance in Rice in Both Submerged and Nonsubmerged Calcareous Soils

In the present study, we showed that IRI lines exhibit better growth performance and Fe deficiency tolerance than NT and other lines under various cultivation conditions. Table 1 illustrates the toleration levels of these lines to Fe deficiency, and their biomass and yields. In this study, "single inserted line (Refre1)" shows tolerance under submerged condition (**Figure 4**) but less tolerance under nonsubmerged condition (**Figure 5**). "Single inserted line (OsIRO2)" shows tolerance under nonsubmerged condition (for the early stage) (**Figure 5**) but less tolerance under submerged condition (**Figure 4**). "Single inserted line (IDS3 genome)" shows tolerance under nonsubmerged condition (for the late stage) (**Figure 5**) but less tolerance under submerged condition (**Figure 4**). "Double inserted line (Refre1+OsIRO2)" shows tolerance under submerged condition (**Figure 4**) but less tolerance under nonsubmerged condition compared to a single inserted IDS3 line (**Figure 5**). "Triple inserted line (Refre1+OsIRO2+IDS3)" shows tolerance under both submerged condition (likewise Refre1) and nonsubmerged condition (likewise OsIRO2 and IDS3). In practical field cultivation, the water level is difficult to manage by farmers especially in developing countries with weak irrigation and drainage system. For example, Refre1 line may produce a high yield in the year of enough rainfall, however, it will be under risk of dying when less rainfall or drought period continues. IRO2 or IDS3 line is expected to survive under less rainfall period, however, it cannot produce enough yield in abundant rainfall season. On the other hand, new rice, IRI line, may grow healthy under less rainfall or drought condition and may also produce high yield under abundant rainfall condition. This is the superiority of the IRI rice, and it will be important for breeding and practical application. Our results confirm that IRI rice with the additional insertion of the *IDS3* genome fragment also contributes to improved Fe deficiency tolerance in rice under water-limited conditions. MAs, which are produced by IDS3, might further contribute to the uptake of precipitated ferric iron in a calcareous soil under water-limited cultivation.

CONCLUSIONS

This study confirms that IRI rice lines with the *IDS3* genome fragment, *OsIRT1*promoter-*refre1/372*, and *35S-OsIRO2* exhibit increased Fe deficiency tolerance under various cultivation conditions on calcareous soil. The effects of these three genes in increasing Fe deficiency tolerance were additive, not synergistic. However, under real field cultivation, water supply and nutrient conditions will vary dramatically and are difficult to control by rice farmers in many cases. It is important to produce crops with Fe deficiency tolerance in both submerged and nonsubmerged conditions, and IRI rice has a superior performance of consistent Fe deficiency tolerance in various cultivation conditions; the presence of all three genes in rice improves Fe deficiency tolerance to a greater extent than the single or double introduction. Our results will help improve growth performance and grain yields of diverse rice cultivars grown in calcareous soil to meet the food demand by the increasing world population.

AUTHOR CONTRIBUTIONS

HM, MSA, and NN designed and coordinated the overall study. HM conducted all experiments, analyzed the data and wrote the manuscript, with assistance from MSA. TH provides some research facilities and technical suggestions. TK discussed the results and made suggestions. NN improved the manuscript.

FUNDING

This research was supported by the Advanced Low Carbon Technology Research and Development Program from the Japan Science and Technology Agency (JST; Grant Number JPMJAL1107 to NN) and JST research fund from the Japan Ministry of Science and Culture (to NN).

ACKNOWLEDGMENTS

We thank Nihonkai Kougyo (Toyama, Japan) for kindly providing calcareous soil. We are grateful to Dr. Yuko Ogo, Dr. Yasuhiro Ishimaru, and Dr. Hiromi Nakanishi for providing OsIRO2, Refre1, and IDS3 lines. We thank Dr. Takeshi Senoura for discussion and advice. We also thank Ms. Konishi Akane, Ms. May Linn Aung, and Ms. Mariko Sakashita from Ishikawa Prefectural University (Nonoichi, Ishikawa, Japan) for the assistance with experiments.

SUPPLEMENTARY MATERIAL

The Supplementary Material for this article can be found online at: https://www.frontiersin.org/articles/10.3389/fpls.2019.01179/full#supplementary-material

REFERENCES

Araki, R., Kousaka, K., Namba, K., Murata, Y., and Murata, J. (2015). 2′-Deoxymugineic acid promoters growth of rice (*Oryza sativa* L.) by orchestrating iron and nitrate uptake processes under high pH conditions. *Plant J.* 81, 233–246. doi: 10.1111/tpj.12722

Bashir, K., Inoue, H., Nagasaka, S., Takahashi, M., Nakanishi, H., Mori, S., et al. (2006). Cloning and characterization of deoxymugineic acid synthase genes from graminaceous plants. *J. Biol. Chem.* 281, 32395–32402. doi: 10.1074/jbc.M604133200

Bughio, N., Yamaguchi, H., Nishizawa, N. K., Nakanishi, H., and Mori, S. (2002). Cloning an iron-regulated metal transporter from rice. *J. Exp. Bot.* 53, 1677–1682. doi: 10.1093/jxb/erf004

Connolly, E. L., Campbell, N. H., Grotz, N., Prichard, C. L., and Guerinot, M. L. (2003). Overexpression of the FRO2 ferric chelate reductase confers tolerance to growth on low iron and uncovers posttranscriptional control. *Plant Physiol.* 113, 1102–1110. doi: 10.1104/pp.103.025122

Eide, D., Brodrius, M., Fett, J., and Guerinot, M. L. (1996). A novel iron-regulated metal transporter from plants identified by functional expression in yeast. *Proc. Natl. Aca. Sci. U.S.A.* 93, 5624–5628. doi: 10.1073/pnas.93.11.5624

Hiei, Y., Ohta, S., Komari, T., and Kumashiro, T. (1994). Efficient transformation of rice (*Oryza sativa* L.) mediated by Agrobacterium and sequence analysis of the bounderies of the T-DNA. *Plant J.* 6, 271–282. doi: 10.1046/j.1365-313X.1994.6020271.x

Higuchi, K., Suzuki, K., Nakanishi, H., Yamaguchi, H., Nishizawa, N. K., and Mori, S. (1999). Cloning of nicotianamine synthase genes, novel genes involved in the biosynthesis of phytosiderophores. *Plant Physiol.* 119, 471–479. doi: 10.1104/pp.119.2.471

Inoue, H., Kobayashi, T., Nozoye, T., Takahashi, M., Kakei, Y., Suzuki, K., et al. (2009). Rice OsYSL15 is an iron-regulated iron(III)-deoxymugineic acid transporter expressed in the roots and is essential for iron uptake in early growth of the seedlings. *J. Biol. Chem.* 284, 3470–3479. doi: 10.1074/jbc.M806042200

Inoue, H., Takahashi, M., Kobayashi, T., Suzuki, M., Nakanishi, H., Mori, S., et al. (2008). Identification and localisation of the rice nicotianamine aminotransferase gene *OsNAAT1* expression suggests the site of phytosiderophore synthesis in rice. *Plant Mol. Biol.* 66, 193–203. doi: 10.1007/s11103-007-9262-8

Ishimaru, Y., Kim, S., Tsukamoto, T., Oki, H., Kobayashi, T., Watanabe, S., et al. (2007). Mutational reconstructed ferric chelate reductase confers enhanced tolerance in rice to iron deficiency in calcareous soil. *Proc. Natl. Aca. Sci. U.S.A.* 104, 7373–7378. doi: 10.1073/pnas.0610555104

Ishimaru, Y., Suzuki, M., Tsukamoto, T., Suzuki, K., Nakazono, M., Kobayashi, T., et al. (2006). Rice plants take up iron as an Fe^{3+}-phytosiderophore and as Fe^{2+}. *Plant J.* 45, 335–346. doi: 10.1111/j.1365-313X.2005.02624.x

Kobayashi, T., Nakanishi, H., Takahashi, M., Kawasaki, S., Nishizawa, N. K., and Mori, S. (2001). *In vivo* evidence that *Ids3* from *Hordeum vulgare* encodes a dioxygenase that converts 2′-deoxymugineic acid to mugineic acid in transgenic rice. *Planta.* 212, 864–871. doi: 10.1007/s004250000453

Lee, S., Chiecko, J. C., Kim, S. A., Walker, E. L., Lee, Y., Guerinot, M. L., et al. (2009). Disruption of *OsYSL15* leads to iron inefficiency in rice plants. *Plant Physiol.* 150, 786–800. doi: 10.1104/pp.109.135418

Marschner, H. (1995). *Mineral nutrition of higher plants. 2nd edition*. (London: Academic Press).

Marschner, H., Römheld, V., and Kissel, M. (1986). Different strategies in higher plants in mobilization and uptake of iron. *J. Plant Nut.* 9, 695–713. doi: 10.1080/01904168609363475

Masuda, H., Kobayashi, T., Ishimaru, Y., Takahashi, M., Aung, M. S., Nakanishi, H., et al. (2013). Iron-biofortification in rice by the introduction of three barley genes participated in mugineic acid biosynthesis with soybean ferritin gene. *Front. Plant Sci.* 4, 132. doi: 10.3389/fpls.2013.00132

Masuda, H., Shimoshi, E., Hamada, T., Senoura, T., Kobayashi, T., Aung, M. S., et al. (2017). A new transgenic rice line exhibiting enhanced ferric iron reduction and phytosiderophore production confers tolerance to low iron availability in calcareous soil. *PLoS ONE* 12 (3), e0173441. doi: 10.1371/journal.pone.0173441

Masuda, H., Suzuki, M., Morikawa, K. C., Kobayashi, T., Nakanishi, H., Takahashi, M., et al. (2008). Increase in iron and zinc concentrations in rice grains *via the* introduction of barley genes involved in phytosiderophore synthesis. *Rice* 1, 100–108. doi: 10.1007/s12284-008-9007-6

Mori, S., and Nishizawa, N. K. (1987). Methionine as a dominant precursor of phytosiderophore in graminaceae plant. *Plant Cell Physiol.* 28, 1081–1092. doi: 10.1093/oxfordjournals.pcp.a077388

Morikawa, C. K., Saigusa, M., Nakanishi, H., Nishizawa, N. K., Hasegawa, K., and Mori, S. (2004). Co-situs application of controlled-release fertilizers to alleviate iron chlorosis of paddy rice grown in calcareous soil. *Soil Sci. Plant Nutr.* 50, 1013–1021. doi: 10.1080/00380768.2004.10408568

Murashige, T., and Skoog, F. (1962). A revised medium for rapid growth and bioassay with tobacco tissue cultures. *Physiol. Plant.* 15, 473–497. doi: 10.1111/j.1399-3054.1962.tb08052.x

Nakanishi, H., Yamaguchi, H., Sasakuma, T., Nishizawa, N. K., and Mori, S. (2000). Two dioxygenase genes, *Ids3* and *Ids2*, from *Hordeum vulgare* are involved in the biosynthesis of mugineic acid family phytosiderophores. *Plant Mol. Biol.* 44, 199–207. doi: 10.1023/A:1006491521586

Ogo, Y., Itai, R. N., Nakanishi, H., Inoue, H., Kobayashi, T., Suzuki, M., et al. (2006). Isolation and characterization of IRO2, a novel iron-regulated bHLH transcription factor in graminaceous plants. *J. Exp. Bot.* 57, 2867–2878. doi: 10.1093/jxb/erl054

Ogo, Y., Itai, R. N., Nakanishi, H., Kobayashi, T., Takahashi, M., Mori, S., et al. (2007). The rice bHLH protein OsIRO2 is an essential regulator of the genes involved in Fe uptake under Fe deficient conditions. *Plant J.* 51, 366–377. doi: 10.1111/j.1365-313X.2007.03149.x

Ogo, Y., Itai, R. N., Kobayashi, T., Aung, M. S., Nakanishi, H., and Nishizawa, N. K. (2011). OsIRO2 is responsible for iron utilization in rice and improves growth and yield in calcareous soil. *Plant Mol. Biol.* 75, 593–605. doi: 10.1007/s11103-011-9752-6

Oki, H., Kim, S., Nakanishi, H., Takahashi, M., Yamaguchi, H., Mori, S., et al. (2004). Directed evolution of yeast ferric reductase to produce plants with tolerance to iron deficiency in alkaline soils. *Soil Sci. Plant Nutr.* 50, 1159–1165. doi: 10.1080/00380768.2004.10408589

Robinson, N. J., Procter, C. M., Connolly, E. L., and Guerinot, M. L. (1999). A ferric-chelate reductase for iron uptake from soils. *Nature.* 397, 694–697. doi: 10.1038/17800

Römheld, V., and Marschner, M. (1986). Evidence for a specific uptake system for iron phytosiderophores in roots of grasses. *Plant Physiol.* 80, 175–180. doi: 10.1104/pp.80.1.175

Shojima, S., Nishizawa, N. K., Fushiya, S., Nozoe, S., Irifune, T., and Mori, S. (1990). Biosynthesis of phytosiderophores—*in vitro* biosynthesis of 2′-deoxymugineic acid from l-methionine and nicotianamine. *Plant Physiol.* 93, 1497–1503. doi: 10.1104/pp.93.4.1497

Suzuki, M., Morikawa, C., Nakanishi, H., Takahashi, M., Saigusa, M., Mori, S., et al. (2008). Transgenic rice lines that include barley genes have increased tolerance to low iron availability in a calcareous paddy soil. *Soil Sci. Plant Nutr.* 54, 77–85. doi: 10.1111/j.1747-0765.2007.00205.x

Takagi, S. (1976). Naturally occurring iron-chelating compounds in oat- and rice-root washings. I. Activity measurement and preliminary characterization. *Soil Sci. Plant Nutr.* 22, 423–433. doi: 10.1080/00380768.1976.10433004

Takahashi, M., Nakanishi, H., Kawasaki, S., Nishizawa, N. K., and Mori, S. (2001). Enhanced tolerance of rice to low iron availability in alkaline soils using barley nicotianamine aminotransferase genes. *Nat. Biotech.* 19, 466–469. doi: 10.1038/88143

Takahashi, M., Yamaguchi, H., Nakanishi, H., Shioiri, T., Nishizawa, N. K., and Mori, S. (1999). Cloning two genes for nicotianamine aminotransferase, a critical enzyme in iron acquisition (Strategy II) in graminaceous plants. *Plant Physiol.* 121, 947–956 doi: 10.1104/pp.121.3.947.

Conflict of Interest: The authors declare that the research was conducted in the absence of any commercial or financial relationships that could be construed as a potential conflict of interest.

frontiers in Plant Science

ORIGINAL RESEARCH
published: 29 October 2019
doi: 10.3389/fpls.2019.01264

OPEN ACCESS

Edited by:
Thomas J. Buckhout, Humboldt University of Berlin, Germany

Reviewed by:
Thomas Eitinger, Humboldt University of Berlin, Germany
Wayne Versaw, Texas A&M University, United States

***Correspondence:**
Katrin Philippar
katrin.philippar@uni-saarland.de

†These authors have contributed equally to this work

‡Present Address:
Lena Voith von Voithenberg
IBM Research Zürich, Rüschlikon, Switzerland
Jiyoung Park
Division of Biological Sciences, University of California San Diego, La Jolla CA, United States
Roland Stübe
Haupt Pharma Wolfratshausen GmbH, Aenova Holding GmbH, Wolfratshausen, Germany

Specialty section:
This article was submitted to Plant Nutrition, a section of the journal Frontiers in Plant Science

Received: *13 February 2019*
Accepted: *11 September 2019*
Published: *29 October 2019*

Citation:
Voith von Voithenberg L, Park J, Stübe R, Lux C, Lee Y and Philippar K (2019) A Novel Prokaryote-Type ECF/ABC Transporter Module in Chloroplast Metal Homeostasis. Front. Plant Sci. 10:1264. doi: 10.3389/fpls.2019.01264

A Novel Prokaryote-Type ECF/ABC Transporter Module in Chloroplast Metal Homeostasis

Lena Voith von Voithenberg[1†‡], Jiyoung Park[2†‡], Roland Stübe[1‡], Christopher Lux[3], Youngsook Lee[2] and Katrin Philippar[3]*

[1] Plant Biochemistry and Physiology, Department of Biology I, LMU München, Planegg-Martinsried, Germany, [2] Department of Life Science, Pohang University of Science and Technology, Pohang, South Korea, [3] Plant Biology, Center for Human and Molecular Biology (ZHMB), Saarland University, Saarbrücken, Germany

During evolution, chloroplasts, which originated by endosymbiosis of a prokaryotic ancestor of today's cyanobacteria with a eukaryotic host cell, were established as the site for photosynthesis. Therefore, chloroplast organelles are loaded with transition metals including iron, copper, and manganese, which are essential for photosynthetic electron transport due to their redox capacity. Although transport, storage, and cofactor-assembly of metal ions in chloroplasts are tightly controlled and crucial throughout plant growth and development, knowledge on the molecular nature of chloroplast metal-transport proteins is still fragmentary. Here, we characterized the soluble, ATP-binding ABC-transporter subunits ABCI10 and ABCI11 in *Arabidopsis thaliana*, which show similarities to components of prokaryotic, multisubunit ABC transporters. Both ABCI10 and ABCI11 proteins appear to be strongly attached to chloroplast-intrinsic membranes, most likely inner envelopes for ABCI10 and possibly plastoglobuli for ABCI11. Loss of ABCI10 and ABCI11 gene products in *Arabidopsis* leads to extremely dwarfed, albino plants showing impaired chloroplast biogenesis and deregulated metal homeostasis. Further, we identified the membrane-intrinsic protein ABCI12 as potential interaction partner for ABCI10 in the inner envelope. Our results suggest that ABCI12 inserts into the chloroplast inner envelope membrane most likely with five predicted α-helical transmembrane domains and represents the membrane-intrinsic subunit of a prokaryotic-type, energy-coupling factor (ECF) ABC-transporter complex. In bacteria, these multisubunit ECF importers are widely distributed for the uptake of nickel and cobalt metal ions as well as for import of vitamins and several other metabolites. Therefore, we propose that ABCI10 (as the ATPase A-subunit) and ABCI12 (as the membrane-intrinsic, energy-coupling T-subunit) are part of a novel, chloroplast envelope-localized, AAT energy-coupling module of a prokaryotic-type ECF transporter, most likely involved in metal ion uptake.

Keywords: ABC transporter, chloroplast, energy-coupling factor transporter, inner envelope membrane, iron transport, metal homeostasis

INTRODUCTION

Chloroplasts originated about 3 billion years ago by endosymbiosis of an ancestor of today's cyanobacteria with a mitochondria-containing host cell (Gould et al., 2008; Zimorski et al., 2014). During evolution, chloroplasts were established as the site for photosynthesis and thus became the basis for all life dependent on oxygen and carbohydrate supply. To fulfill this task, chloroplast organelles are loaded with the transition metals iron (Fe), copper (Cu), and manganese (Mn), which are essential for photosynthetic electron transport due to their redox capacity (Yruela, 2013). In consequence, chloroplasts represent the Fe-richest system in plant cells (Raven et al., 1999). However, evolutionary improvement of oxygenic photosynthesis in turn required tight control of metal transport and distribution since metal-catalyzed generation of reactive oxygen species (ROS) causes oxidative damage. This is most acute in chloroplasts, where oxygen radicals and transition metals are side by side and ROS-production is a usual feature of photosynthetic electron transport (Asada, 1999; Mubarakshina et al., 2010). Thus, on the one hand, when chelated or bound by proteins, chloroplast-intrinsic metals are a prerequisite for photoautotrophic life, but on the other hand become toxic when present in their highly reactive, radical generating, free ionic forms (Briat et al., 2010; Halliwell and Gutteridge, 1992). In consequence, transport, storage and cofactor-assembly of metal ions in chloroplasts have to be tightly controlled and are crucial throughout plant growth and development [for overview see (Thomine and Vert, 2013; Bashir et al., 2016; Lopez-Millan et al., 2016; Vigani et al., 2019)].

Due to their endosymbiotic origin, chloroplasts are surrounded by two membranes similar to their Gram-negative prokaryotic ancestors. Whereas the inner envelope (IE) membrane of chloroplasts presumably was derived mainly from the bacterial plasma membrane, the chloroplast outer envelope (OE), however, largely originated from the outer membrane of the Gram-negative cyanobacterial-like endosymbiont (Block et al., 2007). In the IE, numerous transporter proteins for metabolites and ions have been characterized (Weber and Linka, 2011; Finazzi et al., 2015; Marchand et al., 2018). These channels and transporters are facilitating the exchange of ions and metabolic products between plastids and the cytoplasm. Transmembrane-spanning domains of these proteins are built by hydrophobic α-helices. In contrast, characteristic channels of the outer membrane in Gram-negative bacteria and the chloroplast OE span the membrane in the form of β-strands that are organized to form a barrel-like pore structure (Duy et al., 2007a; Zeth and Thein, 2010). In chloroplasts, these solute pores like the OE proteins OEP21, OEP24, OEP37 and OEP40 (Pohlmeyer et al., 1998; Bölter et al., 1999; Goetze et al., 2006; Harsman et al., 2016) are essential parts of the outer membrane permeom for metabolites and ions (Breuers et al., 2011).

The metal transport mechanisms of chloroplasts (Lopez-Millan et al., 2016; Nouet et al., 2011; Vigani et al., 2019) are not as well-known as strategies occurring in root plasma membranes for iron acquisition, i.e., reduction-based Fe^{2+}-transport (strategy I) and transport of chelated Fe^{III} [strategy II; see (Morrissey and Guerinot, 2009; Kobayashi and Nishizawa, 2012; Brumbarova et al., 2015)]. However, research on the molecular identity of chloroplast iron transport systems suggests that several protein families may play a role in Fe-uptake and export [for overview see (Nouet et al., 2011; Finazzi et al., 2015; Lopez-Millan et al., 2016)]. Chloroplasts inherited a series of solute transporters from their prokaryotic ancestors (Tyra et al., 2007), including components of metal transport systems like the ancient, Fe-uptake permease PIC1 of cyanobacterial origin (Duy et al., 2007b) or the prokaryotic-type ATP-binding cassette (ABC) transporter subunit ABCI11/NAP14 (Shimoni-Shor et al., 2010). The permease PIC1 previously also has been described as Tic21, a putative IE translocon component, which could participate in import of nuclear-encoded plastid proteins from the cytosol (Teng et al., 2006). However, a direct functional analysis of Tic21/PIC1 for protein transport is lacking. In 2009, a protein complex of about 1 MDa was identified at the chloroplast IE membrane containing the putative translocon channel Tic20, a large fraction (about 900 kDa) of yet unidentified membrane proteins, and also small amounts of Tic21/PIC1 (Kikuchi et al., 2009). More recent publications, however, which lead to the identification of the other proteins in this potential protein translocation core, demonstrated that Tic21/PIC1 does not co-purify with this 1 MDa complex (Kikuchi et al., 2013; Nakai, 2015). Therefore, the previously described function of PIC1 in protein import seems to be obsolete [for discussion see (Duy et al., 2007b; Duy et al., 2011; Lopez-Millan et al., 2016)]. Further, transporters of prokaryotic origin are involved in the shuttling of Mn across the IE and thylakoid membranes in chloroplasts (Eisenhut et al., 2018; Krieger-Liszkay and Thomine, 2018; Zhang et al., 2018) as well as membranes of the cyanobacterium *Synecocystis PCC6803* (Brandenburg et al., 2017; Gandini et al., 2017). Therefore, metal transport mechanisms of prokaryotes, in particular those of Gram-negative bacteria and cyanobacteria (Braun and Hantke, 2011; Lau et al., 2016), today can serve as blueprint for chloroplasts of land plants. Proteins that transport metals across the OE have not been identified yet nevertheless they might be represented by ß-barrel channel pores like OEPs or the protein translocon channel Toc75. In Gram-negative *E. coli* and also in cyanobacteria, Fe uptake across the OM occurs *via* receptor-gated ß-barrel channels also called TonB-dependent transporters (TBDTs), which transport Fe^{III}-chelates and are energized by the TonB system at the plasma membrane (Kranzler et al., 2013; Braun, 2014; Rudolf et al., 2015). Whereas physiological data point to a reduction based transport of divalent Fe^{2+} or Mn^{2+} for metal uptake across the IE membrane (Shingles et al., 2001; Shingles et al., 2002; Solti et al., 2012; Solti et al., 2014), chelated iron most likely in the form of Fe^{III}-citrate complexes is shuttled over the OE membrane (Bughio et al., 1997; Solti et al., 2012; Solti et al., 2016; Müller et al., 2018). For a recent update on intracellular iron transport in plants, we refer to Vigani et al. (2019).

In plants, an exceptionally high number of ABC transporters exists, which are involved in the transport and distribution of numerous metabolites and ions, including metals, hormones, and lipid compounds. In consequence, functional ABC-transporter systems are crucial for plant growth and development (Do et al., 2018; Hwang et al., 2016). The classical, eukaryotic ABC transporters are composed of two nucleotide

binding (NBD) and two transmembrane (TMD) permease subunits. Depending if these four subunits are encoded by one or two genes, the proteins are categorized as full- or half-size ABC transporters, respectively (Verrier et al., 2008; Theodoulou and Kerr, 2015). For functional half-size transporters, a homo- or heterodimer of NBD-TMD or TMD-NBD proteins can be assembled. In addition to these eukaryotic ABC-transporters sorted into subfamilies A-D and G, plants possess a collection of ABC proteins bearing similarities to components of prokaryotic, multisubunit ABC transporters (Verrier et al., 2008; Theodoulou and Kerr, 2015). In general, canonical, prokaryotic ABC transporters as well assemble as dimers of two NBD and two TMD proteins, however, for importers, an additional substrate binding protein (SBP) exists (Eitinger et al., 2011; Theodoulou and Kerr, 2015). In contrast to the operon arrangement of prokaryotes, however, in plants, separate intron-containing genes, which are scattered throughout the genome, encode for the subunits of these transporters. Thereby, the correct identification of the single subunits that form one functional ABC complex is hindered. In the first inventory of plant ABC transporters, several of the prokaryotic-type, soluble NBD-subunits were designated as non-intrinsic ABC proteins (NAPs) (Sanchez-Fernandez et al., 2001). However, later on, most of the NAPs were grouped into ABC protein subfamily I (Verrier et al., 2008). Well in line with their prokaryotic features, most of these *Arabidopsis* ABCI proteins characterized so far are localized in the endosymbiotically derived organelles chloroplasts and mitochondria. These include ABCI1/NAP10 (NBD), ABCI2 (TMD) for the cytochrome *c* maturation complex in mitochondria (Rayapuram et al., 2007), and ABCI6/NAP7 (NBD), ABCI7, and ABCI8 for the iron-sulfur cluster biogenesis complex in chloroplasts (Xu and Möller, 2004). The well characterized TGD1/ABCI4 (TMD), TGD2/ABCI5 (SBP), and TGD3/ABCI13 (NBD) ABC transporter complex in the chloroplast IE is responsible for the import of eukaryotic acyl lipids, synthesized in the ER (Xu et al., 2003; Lu et al., 2007; Xu et al., 2010; Roston et al., 2012). Further, the NBD protein ABCI17/NAP3 was described to bind to ABCI16/ALS3 (TMD) in the tonoplast and to be implicated in root metal homeostasis (Fe, Al) and signaling under phosphate deficiency (Huang et al., 2010; Belal et al., 2015; Dong et al., 2017; Wang et al., 2019). Only for the TGD complex, a distinct membrane transport function, i.e., lipid import into chloroplasts, is described. With its NBD-TMD-SBP subunit arrangement, TGD1-3 corresponds to the full canonical ABC importer assembly in prokaryotes. ABCI1-ABCI2 (cytC maturation in mitochondria) and ABCI17-ABCI16 (root metal homeostasis, signaling at phosphate deficiency) are supposed to assemble as NBD-TMD dimers. The NBD ATPase ABCI6 for FeS cluster biogenesis in chloroplasts, however, interacts with ABCI7 and ABCI8, which are soluble proteins that do not belong to an ABC transporter assembly. The chloroplast intrinsic NBD-subunit ABCI11/NAP14 in *Arabidopsis* and rice (here designated as Os-ABCI8) was described to play a pivotal role in metal homeostasis, although a direct involvement in transport or interaction with membrane-intrinsic ABC transporter subunits so far has not been demonstrated (Shimoni-Shor et al., 2010; Zeng et al., 2017).

In addition to the canonical NBD-TMD-SBP ABC-complexes for metabolite and ion uptake, prokaryotes contain a differently organized class of importing ABC proteins, also known as energy-coupling factor (ECF) transporters (Rodionov et al., 2009; Eitinger et al., 2011; Theodoulou and Kerr, 2015; Rempel et al., 2019). Central to these ECF protein complexes is the energy-coupling module AAT, which consists of two NBD ATPase-subunits (A) and one energy-transducing, transmembrane subunit T. The A subunits contain the classical ATPase and ABC transporter signature motifs within the RecA and helical subdomains (Davidson et al., 2008; Wilkens, 2015). Both A proteins bind to a single T protein either as homodimer (A1, A1), heterodimer (A1, A2), or a pair of ATPase domains fused in a single polypeptide (A1-A2) (Rodionov et al., 2009; Eitinger et al., 2011). In contrast to the canonical prokaryotic ABC importers (see above), the substrate-binding subunit of ECF transporters (S) is a membrane-intrinsic protein. ECF-type ABC importers are divided into two subgroups, depending if they contain a dedicated energy-coupling module for each S subunit (group I) or a shared AAT module that can be combined with various substrate-binding S components (group II) (Rodionov et al., 2009; Eitinger et al., 2011; Rempel et al., 2019). Besides several other metabolites, group I ECF transporters in bacteria are described to transport biotin (BioMNY complex; Hebbeln et al., 2007) and are widely distributed for the uptake of cobalt and nickel metal ions *via* CbiMNQO and NikMNQO complexes, respectively (Rodionov et al., 2006). Because of the high substrate variability of the different S components, which form complexes with an invariant EcfAAT module, group II ECF transporters have a broad range of substrate metabolites, including folate (FolT transporter; Neubauer et al., 2009; Rodionov et al., 2009) as well as other vitamins, metabolites, cofactors, and precursors thereof (Eitinger et al., 2011).

Currently, five crystal structures of full group II complexes and one structure of a group I ECF transporter are resolved (Rempel et al., 2019). Among them, the CbiMQO core complex (group I, EcfAATS) from *Rhodobacter capsulatus* (Bao et al., 2017) and the structure of FolT2 (group II, EcfA1A2TS) from *Lactobacillus delbrueckii* (Swier et al., 2016) allow insight into the molecular mechanism for divalent metal and folate transport, respectively (Rempel et al., 2019). The ATPase subunits (A components) contain all domains (RecA, helical subdomains) and motifs described for ABC transporter NBD subunits (Davidson et al., 2008; Wilkens, 2015). In addition, ECF transporter ATPases are characterized by a special arrangement of the negatively charged groove that exists on the surface of the AA dimer. This groove, which is formed by the so-called Q-helix and the first helix of the helical subdomain of each A subunit, is responsible for contact with the T subunit (Karpowich and Wang, 2013; Rempel et al., 2019). The Q-helix is specific for polypeptide chains of ECF transporter ATPases and forms a highly conserved, short helical turn with a conserved amino acid motif. This six-residue helix, named after the invariant glutamine (Q), allows correct positioning of a conserved acidic amino acid from the helical subdomain within the groove of the AA dimer. Thereby, this acidic and negatively charged residue of each A subunit is enabled to bind to the strictly conserved and positively charged

arginine (X-R-X motif) in one of the two coupling helices of the membrane-intrinsic T subunit (Swier et al., 2016; Bao et al., 2017; Rempel et al., 2019). Furthermore, a conserved negatively charged amino acid (aspartate or glutamate) of the Q-helix itself forms an intramolecular interaction with a specific arginine of the "LSGGQ" motif in the helical subdomain of each A component (Karpowich and Wang, 2013). Thereby, the Q-helix is essential for transport activity of ECF transporters and significantly contributes to the strong interactions described between ATPase and T subunits of prokaryotic ECF importers (Bao et al., 2017; Rempel et al., 2019). ATPase proteins of group II ECF transporters further are characterized by short, C-terminal helices, which contribute to dimerization and are absent in many ATPases of group I ECF transporters (Rodionov et al., 2009; Karpowich and Wang, 2013). T subunits of different ECF transporters contain a varying amount of α-helical transmembrane domains (between 4 and 8) and the coupling domain for contact with both A proteins. This coupling domain comprises two long α-helices that are arranged in an X shape at the cytosolic face of the membrane (Bao et al., 2017; Rempel et al., 2019). At the C-terminal end of each of these coupling helices, a conserved arginine motif (X-R-X, mostly Ala-Arg-Gly) (Eitinger et al., 2011) mediates interaction with the groove of the AA dimer (see above) and is essential for ECF complex assembly as well as ATPase activity (Neubauer et al., 2009). Transport by ECF importers is energized by ATP hydrolysis *via* the AA dimer, which in turn most likely induces a swing like movement of the transmembrane helices of subunit T [for details on mechanisms see (Bao et al., 2017; Rempel et al., 2019)]. Substrate specificity of each transporter complex is defined by the S components, which have a core of six α-helical membrane domains arranged in a cylindrical bundle. The variable substrate binding side is located in a pocket at the extracellular side of the membrane (Rempel et al., 2019). Group I S components for Ni and Co metal ECF transporters—i.e., NikM and CbiM—contain an additional, N-terminal α-helix that is involved in substrate binding with its first two amino acids. In addition, these metal ion ECF transporter complexes assemble with a third, short membrane-spanning domain (two α-helices)—i.e., subunit N in NikMNQO and CbiMNQO (Eitinger et al., 2011).

In eukaryotes, assembly of ECF transporter subunits, however, has never been described before. A plant-specific T subunit, predicted to be targeted to chloroplasts and corresponding to cyanobacterial T proteins, was identified by *in silico* analyses (Rodionov et al., 2009; Eitinger et al., 2011). However, the corresponding ATPase and substrate binding subunits remain elusive. Only in the chloroplast genome of the freshwater green algae *Mesostigma viride*, a single BioY ortholog (S-component) was discovered (Hebbeln et al., 2007). Due to their endosymbiotic origin and high metal content, chloroplasts represent the most probable site for metal-transporting ECF proteins. Furthermore, chloroplast import of metabolites is essential for cellular metabolism, e.g., biotin uptake for plastid-intrinsic *de novo* fatty acid biosynthesis. Our results on the chloroplast-localized ABCI proteins ABCI10 and ABCI12 here for the first time point to such an ECF ABC-transporter core complex in the IE membrane of chloroplasts. Therefore, we propose that ABCI10 (as the ATPase A subunit) and ABCI12 (as the membrane-intrinsic, energy coupling T subunit) in the chloroplast IE represent the energy-coupling module of a novel, prokaryotic type ECF-transporter complex.

MATERIALS AND METHODS

Plant Material and Growth Conditions

All experiments were performed on *Arabidopsis thaliana* ecotype Col-0 (Lehle Seeds, Round Rock, USA). The T-DNA insertion lines SALK_027278 (*abci10-1*), GABI_946_B10 (*abci10-2*), GABI_969_D10 (*abci10-3*), CS16225/EMB2751 (*abci10-4*), and SALK_116866 (*abci11-1*) were purchased from NASC (University of Nottingham), GABI-Kat (Max Planck Institute for Plant Breeding Research), and ABRC (Ohio State University). Please note that *abci11-1* under the name *nap14-1* has been characterized previously by Shimoni-Shor et al. (2010). Before sowing, seeds were surface-sterilized and vernalized at 4°C to synchronize germination.

Plants were grown in ½ Murashige and Skoog (MS) plates containing 0.8% agar and 1-1.5% sucrose in a controlled environment with a 16 h light (100 μmol/m^2·s)/8 h dark cycle at 22°C/18°C. Due to the sterility of the homozygous knockout lines *abci10-1*, *abci10-3*, *abci10-4*, and *abci11-1*, seeds of heterozygous mutant plants were sown to obtain homozygous mutant progeny. In case grown for more than 3 weeks, only homozygous *abci10* and *abci11* plantlets were transferred to new ½ MS plates. To observe developing seeds, siliques were gently opened by fine forceps at 9–10 days after flowering. To examine growth under excess manganese, homozygous *abci10-1*, *abci10-4*, and *abci11-1* as well as wild-type plants were germinated for 1–2 weeks on control ½ MS plates and subsequently transferred to ½ MS plates supplemented with 0, 0.5, 0.75, or 1.0 mM $MnSO_4$. Growth phenotypes were documented 2 weeks after transfer to Mn-supplemented media. Dry weight of *abci10-1*, *abci10-3*, and *abci11-1* homozygous knockout mutants, the corresponding segregated wild-type lines, and Col-0 was determined from 3-week-old seedlings grown on ½ MS media, supplemented with 0, 5, 20, 100, 300, and 1000 μM Fe. Prior to freeze-drying for 4–8 h, 2–15 individual plantlets were sampled per data point. Dry weight was determined by a special accuracy weighing machine.

GFP, RFP, and YFP Fusion Proteins

To yield the ABCI10-GFP and ABCI11-GFP constructs (lab of JP/YL), the coding sequences of At-ABCI10 and At-ABCI11 without stop codons were ligated into the 326sGFP vector (Clonetech) using the XbaI site. For ABCI11-mRFP and ABCI12-mRFP constructs, the coding sequences of At-ABCI11 and At-ABCI12 without stop codons were ligated into the 326mRFP (Clonetech) vector using the XbaI site. For PIC1-mRFP, the coding sequence of At-PIC1 without stop codon was ligated into the 326mRFP vector (Clonetech) with the BamHI site. The PGL35-YFP construct was a kind gift from Felix Kessler (Vidi et al., 2006).

In a second approach by the group of KP, C-terminal fusions of GFP and YFP to the preproteins of ABCI10, ABCI11, and ABCI12 were constructed by subcloning PCR-amplified cDNA into the pENTR/D/TOPO and further into the p2GWF7(GFP)

and pB7YWG2(YFP) plasmid vectors (Karimi et al., 2002) using the Gateway cloning system (Invitrogen). PIC1/pK7FWG2 (Duy et al., 2007b) and FSD1/pPOL (Chang et al., 2014) were used as controls.

Protoplast Isolation and Transient Expression

Wild-type *Arabidopsis* plants were grown on soil pots and mesophyll protoplasts were isolated as described (Duy et al., 2007b) from rosette leaves by enzymatic digestion using an enzyme solution [400 mM mannitol, 20 mM KCl, 20 mM MES-KOH pH 5.7, 10 mM $CaCl_2$, 0.25% w/v Macerozyme R-10 (Yakult), 1% w/v Cellulase R-10 (Yakult), 0.1% w/v bovine serum albumin]. Healthy mesophyll protoplasts were transformed by the polyethylene glycol method (Abel and Theologis, 1998; Duy et al., 2007b), and fluorescent signals were observed using the respective microscopes. To isolate protoplasts from *abci10-1* and *abci11-1* homozygous mutants, plants were grown on ½ MS plates for 3–4 weeks, and whole plants were used for enzymatic digestion using the enzyme solution. Overnight incubation of the mutant plants in the enzyme solution improved protoplast isolation.

Microscopy

Confocal images in the lab of JP/YL were observed using an Olympus FV1000 confocal laser scanning microscope (Olympus) with spectral settings of excitation at 488 nm and emission at 500–530 nm for GFP, ex 543 nm/em 575–630 nm for RFP, and ex 515 nm/em 520–560 nm for YFP. Fluorescent images were observed using a Zeiss Axioskop2 microscope (Zeiss) with spectral settings of excitation at 455–495 nm and emission at 505–555 nm for GFP, ex 540–552 nm/em 575–640 nm for RFP, and ex 546/12 nm/em 575–640 nm for chlorophyll autofluorescence.

Images in the group of KP were recorded with a confocal laser scanning microscope (Leica, TCS SP5). Here, protoplasts were examined using the 63x1.3 glycerine-immersion objective with excitation using the argon laser (ex 488 nm for GFP, ex 524 nm for YFP). The emitted light of GFP and YFP was detected at 509 nm and 527 nm, respectively. Chlorophyll auto-fluorescence was monitored at 497–524 nm. When appropriate, the bright field images of samples were imaged with the transmitted light photomultiplier. All images of LVvV, RS were processed with Leica LA SAF Lite (Leica).

Ultrastructural analysis by transmission electron microscopy was conducted as described (Duy et al., 2007b).

Measurement of Ion and Chlorophyll Contents

Homozygous *abci10* and *abci11* mutant plants were grown in ½ MS plates for 34 days, and shoots or whole tissues were collected separately for ICP-MS measurements. Wild-type plants were grown for 15 or 16 days. Plant tissues were rinsed twice with 2 mM K^+- phosphate buffer (pH 5.7) and once with ice-cold water. Samples were digested with 11 N HNO_3 at 100°C for 6 h to 1 day. After samples were completely digested, they were diluted with distilled water, and ion contents were analyzed using an ICP-MS spectrometer (ELAN DRC-e; Perkin-Elmer). Ni and Mo contents as well as chlorophyll were determined in 20-day-old seedlings as described (Duy et al., 2007b; Duy et al., 2011).

Transcript Level Profiling

Quantitative real-time RT-PCR was performed as described previously (Duy et al., 2007b) using a LightCycler (Roche). All signals were normalized to the signal of actin cDNA fragments from *Actin* 2 and 8 (At3g18780 and At1g49240).

Antiserum Production

To raise antisera against At-ABCI10 and At-ABCI11, cDNA was PCR-amplified on the respective SALK pUNI clones U62184 and U51365 (Yamada et al., 2003). The resulting mature versions of At-ABCI10 and At-ABCI11 were subcloned into the pET21d (Novagen) plasmid vector and used for overexpression after transforming *E. coli* BL21(DE3) cells (Novagen). Rapidly growing cells with an OD_{600} of 0.6 were induced with 0.6 mM isopropyl1-thio-b-D-galactopyranoside (IPTG) for 3 h at 37°C. Afterwards, pelleted cells (4°C, 6,000g, 15 min) were resuspended in cell lysis solution (50 mM Tris-HCl, pH 8.0, 25% [w/v] sucrose, 1 mM EDTA, 100 mg/ml DNase) and sonicated three times for 30 s. Inclusion bodies were collected by centrifugation at 4°C and 20,000g for 30 min. The resulting pellet was resuspended in buffer A (50 mM NaPP, pH 8.0, 100 mM NaCl, 2 mM β-mercaptoethanol, and 8 M urea), and remaining insoluble material was separated by centrifugation. The major fraction of overexpressed recombinant At-ABCI10 and At-ABCI11 protein was present in the urea-soluble supernatant. Both proteins were purified *via* their C-terminal polyhistidine tags using Ni-NTA-Sepharose as described (Harsman et al., 2016) and eluted in buffer A including increasing imidazole concentrations (100–500 mM). After addition of 1% [w/v] SDS, the purified recombinant mature At-ABCI10 and At-ABCI11 proteins were used as antigenes to raise antibodies in rabbit (Pineda Antibody Service). Antisera for marker proteins were produced as described previously (Küchler et al., 2002; Duy et al., 2007b; Philippar et al., 2007).

Immunoblot Analysis

For immunoblot analysis, pea and *Arabidopsis* chloroplasts were isolated and subfractionated as described (Duy et al., 2007b; Li et al., 2015). Total proteins from seedling tissue grinded in liquid nitrogen were extracted for 30 min on ice in buffer (50 mM Tris-HCl, pH 8.0; 50 mM EDTA; 2% LDS; 10 mM DTT; 100 mM PMSF). Cell debris was pelleted for 15 min at 14,000g, 4°C.

For protein extraction and solubilization, pea IE membrane vesicles were pelleted by centrifugation at 256,000g, 4°C for 10 min and resuspended in either 1 M NaCl, 0.1 M Na_2CO_3 (pH 11.3), 6 M urea, or 1% Triton X-100, followed by incubation for 20 min on ice or for urea extraction at RT. Afterwards, IE membranes corresponding to 20 µg protein for each assay were separated into membranes and solubilized proteins by centrifugation at 100,000g, 4°C for 10 min.

All protein fractions were separated by SDS-PAGE and transferred to Immobilon-P PVDF membrane (Millipore) for immunoblot analysis. Polyclonal antisera against recombinant At-ABCI10 and At-ABCI11 proteins were used in 1:500 and 1:2,000 dilution (0.1 M Tris-HCl pH 7.5, 0.15 M NaCl, 0.2% Tween 20). The antisera against At-PIC1, Tic62, LHC, and pSSU were diluted 1:1,000–1:5,000, and serum against OEP16.1 was used in 1:500 dilution. Secondary, alkaline phosphatase coupled antibodies (Sigma-Aldrich) were diluted 1:5,000. Nonspecific signals were blocked by 1% or 3% skim milk powder and 0.03% or 0.1% BSA. Blots were stained using the alkaline phosphatase reaction in the presence of nitroblue tetrazolium and bromochloroindolyl phosphate as substrate.

Co-Immunoprecipitation

Coupling of protein-A-sepharose to the antibodies against At-ABCI10 and At-ABCI11 or the respective pre-immune sera was done in advance. Therefore, for each assay, 40 µl of protein-A-sepharose was incubated with 10 µl of the antiserum in 0.2 M triethanolamine (pH 8.2) at room temperature for 1 h. Following a washing step with triethanolamine, coupling was achieved using 20 mM dimethyl pimelimidate and incubation at RT for 1 h. Unspecific binding was reduced by incubation of the sepharose-antibody suspension with triethanolamine for 1 h. Following three washing steps with IP buffer (50 mM Tris/HCl, pH 7.5, 150 mM NaCl), the antibody-coupled sepharose was kept at 4°C for 20 h.

Isolated and purified pea IE membranes (corresponding to 70 µg protein) were solubilized with 0.5% dodecylmaltoside in IP buffer on ice for 1 h by repeated pipetting (every 10 min). After centrifugation at 100,000g for 10 min, 4°C, the protein-containing supernatant was diluted 1:10 in IP buffer. Subsequently, the solubilized and diluted IE proteins were added to the antibody-coupled protein-A-sepharose and incubated at room-temperature for 2 h. Sepharose beads were washed three times in IP buffer with 0.05% dodecylmaltoside and once with IP buffer without detergent. Elution was performed using SDS PAGE loading buffer without ß-mercaptoethanol, and separation from the sepharose beads was achieved using a Micro Bio-Spin Chromatography Column (BioRad). Load, flow-through, washes, and elution fractions were analyzed by SDS-PAGE and immunoblotting.

RESULTS

Our database and literature search for prokaryotic-like ABC-transporter subunits, which might contribute to chloroplast metal transport in *Arabidopis* identified At-ABCI10 (At4g33460), At-ABCI11 (At5g14100), and At-ABCI12 (At3g21580) as promising candidates. All three proteins are predicted to be targeted to chloroplasts and were grouped into the prokaryotic-type CBY/Y179 subfamily of *Arabidopsis* and rice ABC transport systems (Garcia et al., 2004; Verrier et al., 2008), annotated with a potential function in metal transport. ABCI10 and ABCI11—also known as NAP13 and NAP14 for non-intrinsic ABC protein 13 and 14, respectively—are soluble NBD ATPase-subunits. Since the two proteins are encoded by separate genes and do not include a TMD-permease subunit, which is common for eukaryotic full- or half-size ABC transporters, ABCI10 and ABCI11 belong to group I of prokaryotic-type, multisubunit ABC-transporters in plants (Verrier et al., 2008). At-ABCI11/NAP14 has previously been reported to localize to the chloroplast stroma and has already been implicated with a function in chloroplast Fe-homeostasis (Shimoni-Shor et al., 2010). Similar results were obtained for the orthologous protein Os-ABCI7 in rice (*Oryza sativa*; Zeng et al., 2017). Please note that Zeng and co-authors (2017) unfortunately named this protein Os-ABCI8, whereas the consortium-annotated name in Verrier et al. (2008) is Os-ABCI7 for the NBD-subunit orthologous to At-ABCI11/NAP14 (compare **Figure 1A**). Os-ABCI8 instead is the consortium and database name for the rice transmembrane-protein relative to At-ABCI12. ABCI12 in *Arabidopsis* also is encoded by a separate gene, is predicted to contain five transmembrane α-helices, and most likely represents the membrane-intrinsic T subunit of a non-classical, prokaryotic-type ECF ABC-transporter complex that was identified by *in silico* analyses and named "plant T protein" (Eitinger et al., 2011). In general, plant ABCI10, 11, and 12 polypeptides are nucleus encoded and contain predicted N-terminal chloroplast targeting peptides (Aramemnon database; Schwacke et al., 2003). In the AT_CHLORO proteome database, all three proteins are assigned to the chloroplast envelope (Ferro et al., 2010). However, only for ABCI10, peptides have been experimentally detected in purified "mixed" envelopes from *Arabidopsis* (Froehlich et al., 2003), envelope preparations from maize (*Zea mays;* Bräutigam et al., 2008), and IE membranes from pea (*Pisum sativum;* Gutierrez-Carbonell et al., 2014).

ABCI10 and ABCI11 Are Prokaryotic-Type NBD-Domain ATPase Subunits

In *Arabidopsis*, the mature proteins ABCI10 and ABCI11 are predicted to be 223aa and 229aa long with a molecular mass of 24.4 kDa and 25.3 kDa, respectively. Both contain the classical ATPase motifs Walker A, Walker B, Q-, D-, and H-loop, which form the nucleotide-binding site (Gaudet and Wiley 2001) as well as the ABC transporter signature motif LSGGQ in the helical subdomain specific for NBD subunits of ABC transporters (Davidson et al., 2008; Wilkens, 2015) (**Figure 1A**). Furthermore, an "ABC_cobalt_CbiO_domain 1" [conserved protein domain family (CDD) cd03225] is annotated to span the entire sequence of the mature At-ABCI10 and At-ABCI11 proteins (GenPept entries NP_195072, NP_196914). CbiO in bacteria has been shown to be the ATPase subunit A in group I ECF-transporters named CbiMNQO for import of cobalt ions (Rodionov et al., 2006; Rodionov et al., 2009), which has recently been crystallized from *R. capsulatus* as CbiMQO core (Bao et al., 2017). Since At-ABCI10 and At-ABCI11 represent separately encoded NBD subunits of ABC transporter complexes, their prokaryotic origin seems obvious (Verrier et al., 2008; Theodoulou and Kerr, 2015). Both proteins are conserved in the "green lineage" with relatives in dicots, monocots, mosses, green microalgae, and cyanobacteria (**Supplementary Figures 1**, **2**).

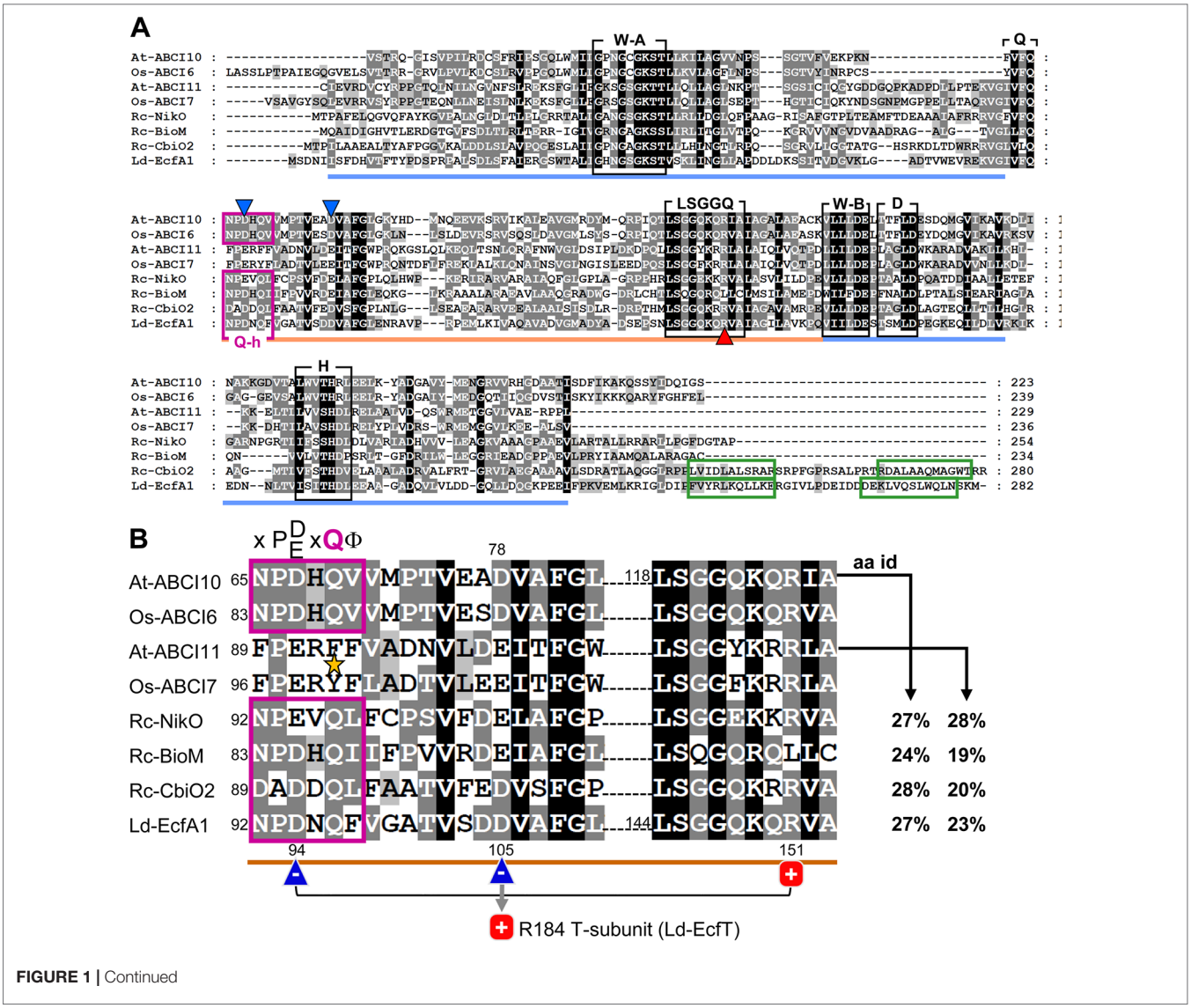

FIGURE 1 | Continued

Although ABCI10 and ABCI11 include all domains of ABC transporter ATPases, their amino acid sequences and predicted secondary structures show some differences. While At-ABCI10 and the identified relatives from plants and cyanobacteria contain the so-called Q-helix motif, described to be specific for ATPase A components of bacterial ECF transporters (Karpowich and Wang, 2013; Rempel et al., 2019), this X-P-D/E-X-Q-Φ consensus sequence is not conserved in ABCI11 proteins (**Figure 1**, **Supplementary Figures 1, 2**). In comparison to Q-helix motifs of ECF A subunits from *R. capsulatus* (NikO, BioM, CbiO2) and from *L. delbrueckii* (EcfA1), ABCI10 from *Arabidopsis* and ABCI6 from rice have the amino acid stretch N-P-D-H-Q-V, including the conserved proline (P), acidic aspartate (D), and glutamine (Q) residues (**Figure 1A,B**). Thus, a short α-helical turn is predicted for the Q-helix of ABCI10, very similar to that of the crystallized CbiO2 and EcfA1 proteins (**Figure 1C**). In general, the Q-helix motif directly follows the Q-loop region and thereby is placed at the beginning of the helical subdomain of ECF transporter ATPases. The detailed structures of CbiO2 and EcfA1/A2 in the complexes CbiMQO (Co-uptake) and ECF-FolT (folate transport) (Swier et al., 2016; Bao et al., 2017) reveal that the Q-helix is essential for interaction of a conserved aspartate residue in the helical subdomain of A subunits (D_{102} of CbiO2, D_{105} of EcfA1) with a conserved arginine motif in the coupling helices of subunit T (**Figure 1B**). Furthermore, another invariant acidic residue in the Q-helix itself can form an intramolecular interaction with a conserved arginine in the LSGGQ motif of each A subunit. In contrast to ABCI10-family proteins, the full Q-helix motif is not present in At-ABCI11 and its plant or cyanobacterial relatives (**Figure 1, Supplementary Figure 2**). In At-ABCI11 and Os-ABCI7, the invariant polar glutamine (Q) residue is replaced by hydrophobic phenylalanine and tyrosine residues, respectively (**Figure 1B**). In consequence, the predicted α-helix in the amino acid stretch corresponding to the Q-helix is longer and less confident for At-ABCI11

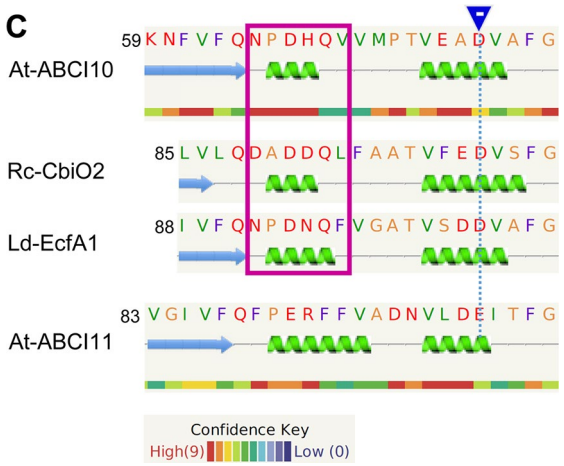

FIGURE 1 | ABCI10 and ABCI11 proteins. **(A)** Amino acid sequences of mature *Arabidopsis* At-ABCI10 (Q8H1R4), At-ABCI11 (Q8LEF6), rice Os-ABCI6 (Q5ZD09), Os-ABCI7 (Q2R434), and the bacterial ECF transporter A subunits NikO (D5AQY6), BioM (D5ARH0), CbiO2 (O68106) from *Rhodobacter capsulatus* and EcfA1 (Q1GBJ0) from *Lactobacillus delbrueckii*. UniProtKB accession numbers are given in brackets (UniProt Consortium, 2018), and chloroplast targeting peptides were predicted by ChloroP (Emanuelsson et al., 1999). Please note that in rice, the protein Os-ABCI7 (Q2R434) was named Os-ABCI8 by Zeng et al. (2017). The conserved motifs Walker A, Walker B, Q-loop, D-loop, and H-loop (black boxes) form the nucleotide binding sites in the RecA domain (blue line). The ABC-transporter ATPase specific helical subdomain (orange line) contains the signature motif LSGGQ. The Q-helix (purple box) and the two α-helices in the C-terminal domain of CbiO2 and EcfA1 (green boxes) are indicated. Conserved negative acidic residues are highlighted by blue, and the conserved positively charged arginines are highlighted by red triangles. All motifs and domains are depicted according to the crystal structures of Rc-CbiO2 and Ld-EcfA1 in the CbiMQO and FolT2 complexes (pdb entries 5X3X and 5D7T). **(B)** Highlighted Q-helix (purple box) and helical subdomain region from alignment in **(A)**. In ECF transporter A subunits, the Q-helix with the specific motif X-P-D/E-X-Q-Φ (X is any, Φ a hydrophobic amino acid) directly follows the Q-loop that connects the RecA and helical subdomain [see **(A)**]. The invariant glutamine (Q) residue of the Q-helix is absent in ABCI11 proteins (asterisk). According to the crystal structure of FolT2 (Swier et al., 2016; Rempel et al., 2019), the conserved acidic and negatively charged residue (blue triangle) in the Q-helix of EcfA1 (D_{94}) forms an intramolecular interaction with the conserved positive arginine (R_{151}) in the LSGGQ motif (red square). Further, the invariant acidic residue in the first helix of the helical subdomain (D_{105} of LcfA1) is positioned at the surface of the negatively charged groove of the EcfA1A2 dimer and binds to the conserved arginine (R_{184}) in the coupling helix 2 of the membrane-intrinsic EcfT subunit (compare **Supplementary Figure 10**). The amino acid identities (aa id) of the full mature At-ABCI10 and At-ABCI11 proteins to Rc-NikO, Rc-BioM, Rc-CbiO2, and Ld-EcfA1 are indicated. **(C)** Secondary structure and disorder prediction by Phyre2 (Kelley et al., 2015) reveals that the Q-helix predicted for At-ABCI10 most likely forms a short helical turn specific for ECF transporter ATPase subunits like CbiO2 and EcfA1. In contrast, substitution of the conserved polar glutamine (Q) by a hydrophobic phenylalanine (F) in At-ABCI11 leads to a less confident prediction of a longer helix. In consequence, the acidic glutamate in the first α-helix of the helical subdomain of At-ABCI11 (dotted blue line) might not be positioned for proper interaction with residues of a membrane-intrinsic T-subunit.

(**Figure 1C**). Thus, the correct and ECF-specific formation of the groove in ABCI11 ATPase subunits for specific interaction with membrane-intrinsic T-components of an ECF transporter might not be possible.

Therefore, we propose that At-ABCI10 most likely represents an ATPase A subunit of a prokaryotic-type ECF transporter. ATPases of all prokaryotic group II ECF transporters (like EcfA1 from FolT) and of some group I proteins (like CbiO2 from CbiMNQO, compare **Figure 1A**) are characterized by an additional C-terminal helical extension that is proposed to act in dimer formation in the absence of ATP and to have a regulatory function (Rodionov et al., 2009; Rempel et al., 2019). Since this C-terminus is absent in ABCI10, the protein most likely groups to type-I ECF transporters like NikO from NikMNQO or BioM from BioMNY (**Figure 1A**). In contrast to ABCI10, At-ABCI11/NAP14 might correspond to an ATPase NBD-domain subunit of a canonical prokaryotic-type ABC transporter similar to TGD3/ABCI13 in the TGD complex for lipid import into chloroplasts (Lu et al., 2007) or to other organelle intrinsic NAP proteins. This hypothesis is further supported by the finding that *in silico* structural modeling (Phyre2; Kelley et al., 2015) for At-ABCI10 gives the most likely hit to the ECF transporter A subunit CbiO2 from *R. capsulatus* (PDB database entry 5X3X; 100% confidence, 37% aa identity). At-ABCI11 instead shows the most similar structure (100% confidence, 33% identity) to the NBD subunit of a hypothetical prokaryotic maltose/maltodextrin ABC transporter (PDB database entry 2IT1). When comparing all single ATPase NBD-subunits from the ABCI family of *Arabiodpsis* ABC transporters (Verrier et al., 2008), only At-ABCI10 has the full characteristic Q-helix consensus motif, indicating that this protein might be the only prokaryotic-type ECF ATPase in the dicot model plant (**Supplementary Figure 3**).

ABCI10 and ABCI11 Attach to Chloroplast-Intrinsic Membranes

To verify the subcellular localization of At-ABCI10 and At-ABCI11, we performed *in vivo* GFP-targeting assays by transiently transforming *Arabidopsis* leaf mesophyll protoplasts with the ABCI proteins tagged with fluorescent proteins at the C-terminal end (**Figure 2**). Protoplasts transformed with ABCI10-GFP or ABCI11-GFP both exhibited fluorescence signals only in chloroplasts as suggested by sequence prediction (**Figures 2A, B**). However, signal patterns of GFP tagged to ABCI10 and ABCI11

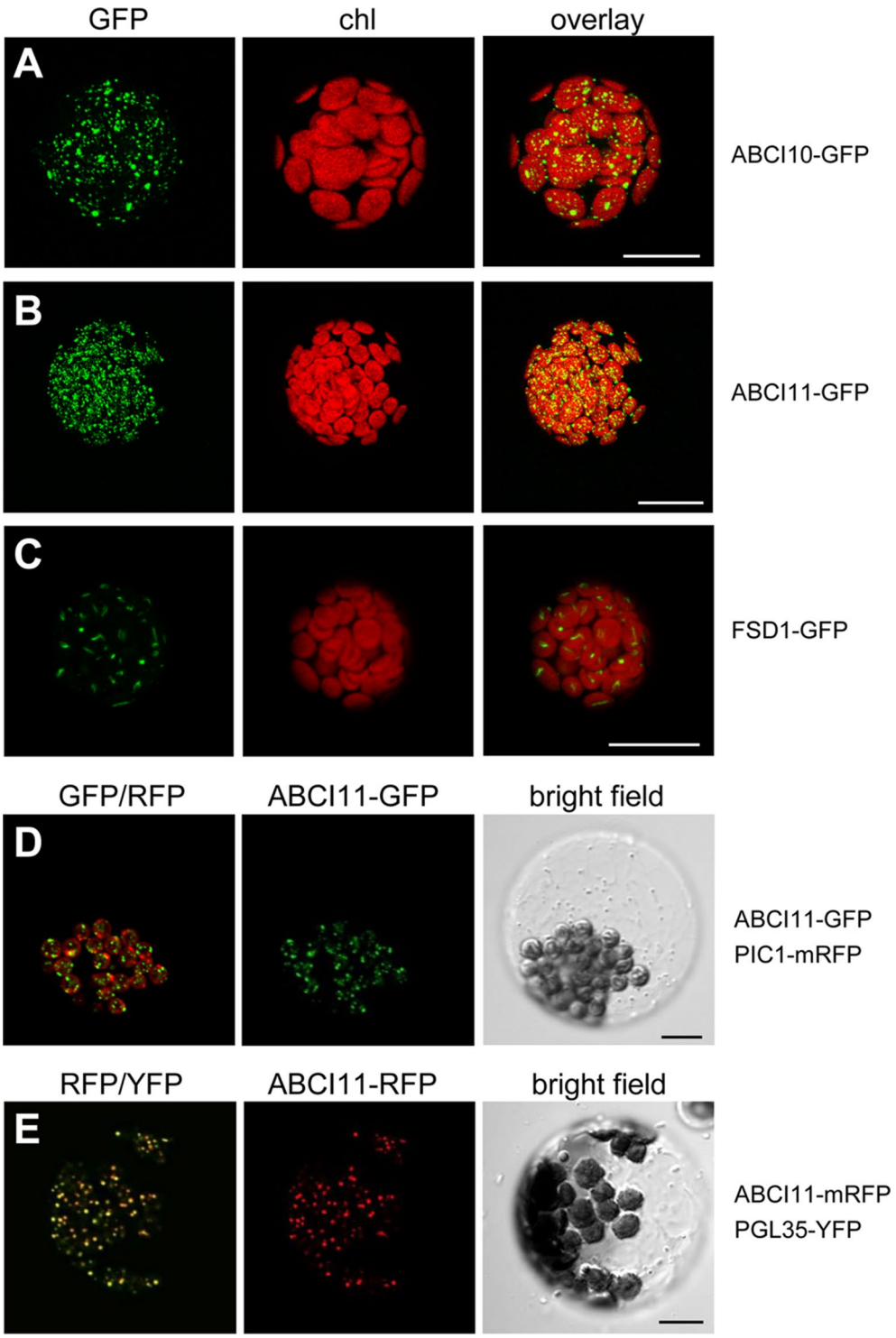

FIGURE 2 | At-ABCI10 and At-ABCI11 are targeted to chloroplasts. *In vivo* GFP-targeting of At-ABCI10 and At-ABCI11. *Arabidopsis* leaf protoplasts were transiently transformed with constructs for At-ABCI10-GFP **(A)**, At-ABCI11-GFP **(B)**, FSD1-GFP [chloroplast stroma marker; (Chang et al., 2014)] **(C)**, as well as At-ABCI11-GFP co-expressed with PIC1-mRFP **(D)** and At-ABCI11-mRFP co-expressed with PGL35-YFP **(E)**. Images in **(A–C)** show GFP-signals (left), chlorophyll fluorescence (middle), as well as an overlay of both (right). Images in **(D,E)** display an overlay of the respective GFP/RFP and RFP/YFP fluorescence (left), signals of At-ABCI11 constructs (middle) as well as a bright field image of the protoplast. Scale bars = 10 μm.

were slightly dissimilar and clearly different from the stroma-targeted protein control FSD1 (Fe-superoxide dismutase 1; Chang et al., 2014; Kliebenstein et al., 1998). In each chloroplast, FSD1-GFP proteins represented a single signal inside the stroma that was surrounded by the bowl-shaped thylakoid membrane systems (**Figure 2C**). In contrast, the multiple punctuate stains of ABCI10-GFP seemed to be more around the chloroplasts periphery, suggesting its localization at the envelope region (**Figure 2A**). Distribution of ABCI11-GFP fluorescence was more uniform as shown by numerous dots all-over each chloroplast (**Figure 2B**). For fluorescence signals by non-chloroplast targeted cytosolic GFP, please see Chang et al. (2014). To examine these unexpected GFP-signals of ABCI11 in more detail, we co-expressed ABCI11 tagged proteins with chloroplast-intrinsic marker proteins PIC1-RFP (**Figure 2D**) or PGL35-YFP (Vidi et al., 2006; **Figure 2E**). The Fe-permease PIC1 is localized in the IE of chloroplasts (Duy et al., 2007b), while the plastoglobulin PGL35 is mostly targeted to plastoglobuli, which are plastid-intrinsic lipoprotein particles surrounded by monolayer lipid membranes (Shanmugabalaji et al., 2013). While signals for ABCI11-GFP did not show any overlap with those for PIC1-RFP at the envelopes surrounding the chloroplasts (**Figure 2D**), the superimposition of ABCI11-RFP and PGL35-YFP fluorescence was almost complete (**Figure 2E**), suggesting attachment to ABCI11 to plastoglobuli (van Wijk and Kessler, 2017).

To confirm the results of *in vivo* GFP-targeting assays, which sometimes could be misleading due to artificial overexpression, we further tested for subcellular localization of ABCI10 and ABCI11 proteins by immunoblot analysis using isolated and sub-fractionated chloroplasts (**Figure 3**). Therefore, we generated antisera against the purified recombinant mature proteins At-ABCI10 and At-ABCI11 (**Supplementary Figure 4**). Immunoblot analysis using chloroplast membranes from pea (*Pisum sativum*; **Figure 3A**) showed that ABCI11 runs at a molecular weight of about 28–29 kDa, well in line with the size of the purified, recombinant mature At-ABCI11 protein (**Supplementary Figure 4**). In the pea IE fraction, the antiserum directed against *Arabidopsis* ABCI11 stains a double band that might be due to unspecific interaction, possibly with another chloroplast NBD-protein from pea or to alternative processing of the mature polypeptide. Instead, α-At-ABCI10 in pea IE stains a single band at 27 kDa (**Figure 3A**), nicely reflecting the size of the recombinant protein (**Supplementary Figure 4**) and the fact that the mature ABCI10 is about 1 kDa smaller than ABCI11. In addition, we tested both antisera on *Arabidopsis* chloroplast and tissue preparations from wild type and *abci10*, *abci11* knockout mutants, where we could assign signals to endogenous At-ABCI10 and At-ABCI11 proteins (**Supplementary Figure 5**). Surprisingly, the immunoblot analyses showed ABCI10 and ABCI11 only in chloroplast IE membrane fractions and not in the stroma, as would be expected for soluble ATPase proteins without any transmembrane domains (**Figure 3**). The purity of the pea IE membranes was confirmed with controls against the stroma marker protein LSU, the thylakoid marker protein LHC, the OE protein OEP16.1, and the IE-intrinsic PIC1 (**Figure 3A**).

To follow the observed unusual attachment of soluble ABCI10 and ABCI11 proteins to the IE membrane of chloroplasts in more detail, we treated purified pea IE vesicles with high ionic strength and high pH buffers as well as denaturing and detergent agents (**Figure 3B**). Subsequent separation of membranes by centrifugation, followed by immunoblot analysis can reveal if proteins are still attached to/intrinsic to membranes or upon treatment are dissolved into the soluble fraction. In our assays, neither high salt nor high pH could detach both ABCI10 and ABCI11 from the membrane pellet (**Figure 3B**, left panel). Since ABCI10 and ABCI11 do not contain any membrane-spanning, hydrophobic domains, this indicates that most likely both proteins attach to the IE membrane *via* strong interactions with a membrane-embedded anchor protein. For ABCI11, this interaction might be slightly weaker and/or different, because some protein traces were washed from the membrane to the supernatant by salt and high pH treatment (**Figure 3B**, triangle). Denaturation of proteins and membranes by urea as well as membrane solubilization by the detergent Triton X-100 successfully moved ABCI10 and ABCI11 proteins to the soluble supernatant (**Figure 3B**, right panel). Thus, upon urea treatment, the potential anchor proteins and interaction sites for ABCI proteins would be denatured and therefore release ABCI10 and ABCI11 from the membranes. Some residual amounts of proteins in the membrane fraction after detergent usage most likely are due to incomplete solubilization of membranes and anchor proteins. As control we used the antiserum for PIC1, which contains four predicted hydrophobic, membrane-spanning α-helical domains (Duy et al., 2007b; Duy et al., 2011). PIC1—as expected for an IE transmembrane protein—was detected in the soluble fraction only after membrane disruption by Triton X-100. Instead, Tic62, which attaches more loosely to the inner leaflet of the IE membrane (Küchler et al., 2002; Stengel et al., 2008), was already partly solubilized by high salt, high pH and urea (**Figure 3B**).

In summary, our results on the subcellular and suborganellar localization of ABCI10 and ABCI11 point to their strong attachment to chloroplast membranes possibly *via* interaction with potential membrane-intrinsic subunits of prokaryotic-type ABC transporter complexes. ABCI10 is most likely anchored to the IE membrane, while ABCI11 might be attached to the lipid monolayer of plastoglobuli that might co-purify with IE membranes upon isolation.

The Loss of ABCI10 as well as of ABCI11 Impairs Plant Growth and Chloroplast Biogenesis

To follow the role of ABCI10 and ABCI11 *in planta*, we characterized the mutant lines *abci10-1*, *abci10-2*, *abci10-3*, *abci10-4*, and *abci11-1* in *Arabidopsis* (**Supplementary Figures 5, 6, 7**). Please note that under the name *nap14-1*, the line *abci11-1* was already described in detail by Shimoni-Shor et al. (2010). The generation of specific antisera, however, now enabled us to probe for protein levels (**Supplementary Figure 5D**). Both, the loss of either At-ABCI10 or At-ABCI11 proteins led to impaired segregation of homozygous mutant alleles, most likely due to partial embryo and/or seed lethality (**Supplementary Figure 5E, F**). For *abci10*, the observed embryo lethality is well

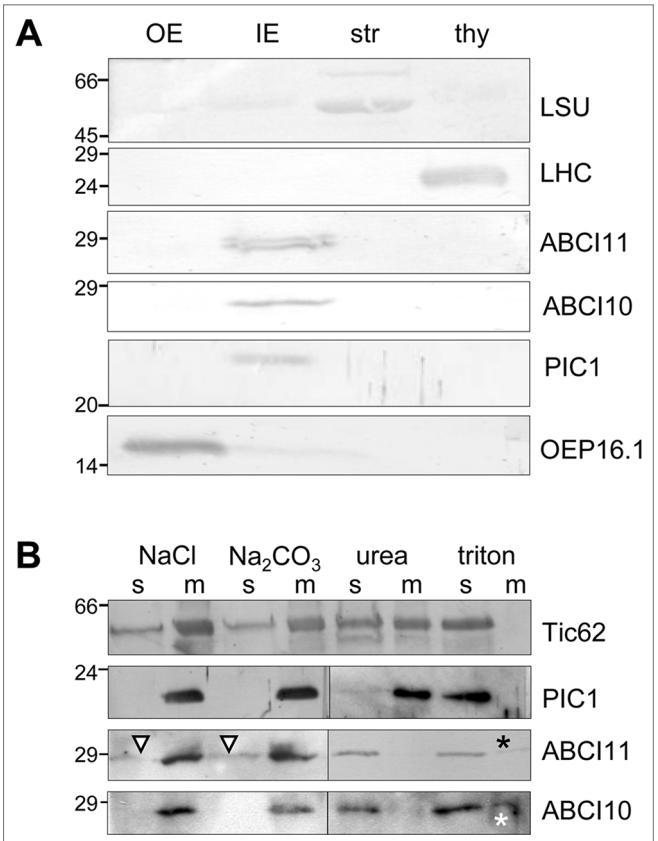

FIGURE 3 | ABCI10 and ABCI11 attach to chloroplast IE membranes. Immunoblot analysis of ABCI10 and ABCI11 localization in chloroplast subfractions. Numbers indicate molecular mass of proteins in kDa. **(A)** Intact isolated chloroplasts from pea (*Pisum sativum*) were fractionated into outer (OE) and inner (IE) envelope membranes, stroma (str) and thylakoids (thy). Equal protein amounts (10 µg) were separated by SDS-PAGE and were subjected to immunoblot analysis using antisera against the mature proteins At-ABCI10 and At-ABCI11, respectively. Antisera against the marker proteins LSU (large subunit rubisco, stroma), LHC (light harvesting complex, thylakoids), OEP16.1 (outer envelope protein of 16 kDa, OE), and PIC1 (Fe-uptake, IE) were used as controls. **(B)** After treatment with either high ionic strength (1M NaCl, pH 8), high pH buffer (Na_2CO_3, pH 11.3), denaturing agent (6 M urea) or detergent (1% Triton X-100), pea IE membranes (20 µg protein for each assay) were fractionated into insoluble, membrane-intrinsic (m) and soluble proteins (s) by ultracentrifugation. Subsequently, proteins were separated by SDS-PAGE and subjected to immunoblot analysis using antisera against At-ABCI10 and At-ABCI11. Antisera against the marker proteins Tic62 (loosely attached to IE membranes) and PIC1 (IE membrane-intrinsic, hydrophobic permease) were used as controls. Triangles and asterisks indicate trace amounts of ABCI11 in soluble fractions after high salt, high pH treatment and residual signals of ABCI10, ABCI11 in membrane fractions after detergent solubilization, respectively.

in line with the annotation of the protein as "embryo defective 2751" (Universal Protein resource UniProtKB - Q8H1R4; UniProt Consortium, 2018). Homozygous plantlets of knockout lines, namely, *abci10-1*, *abci10-3*, *abci10-4*, and *abci11-1*, did not survive on soil, but had to be grown on sucrose-supplemented media and mutant lines had to be propagated in the heterozygous state. Knockout mutant plantlets for *At-ABCI10* or *At-ABCI11* were characterized by an extremely dwarf and chlorophyll-less phenotype (**Figure 4A** and **Supplementary Figures 6D, 7A, B**). The line *abci10-2* with a T-DNA insertion in the 3' untranslated region of *At-ABCI10* (**Supplementary Figure 5A**) and therefore not representing a loss-of-function mutant, however, did not show a chlorotic appearance in the homozygous state (**Supplementary Figure 7A**). Leaf structures of *abci10*, *abci11* knockouts were deformed, and mesophyll cells of seedlings were smaller than wild type and did not contain fully developed chloroplasts with chlorophyll (**Figure 4B**). For *ABCI11*, this phenotype has been described previously for *abci11-1/nap14-1* (Shimoni-Shor et al., 2010) and mutation of the corresponding rice ortholog (Zeng et al., 2017). In our phenotype analysis, *abci11-1* showed some trace amounts of green color in seedling leaves as well as in plastid structures of isolated protoplasts (**Figure 4**). By chlorophyll analysis, we here could show that *abci11-1* seedlings still contain residual Chl *a* and Chl *b* (about 18-fold less than Col-0 wild type), whereas the green pigments were below the detection limit in *abci10-1* (**Figure 4A**). Seedling size as well as fresh and dry weight (**Supplementary Figure 7B**) however, did not differ significantly between *abci10* and *abci11* knockout plants. Thus, we can conclude that the albino phenotype of *abci10* knockout lines is more severe than that of *abci11*.

Ultrastructural analysis of plastids by transmission electron microscopy confirmed the strongly impaired chloroplast biogenesis in *abci10-1* as well as in *abci11-1* mutants (**Figure 5**). Whereas thylakoid membrane systems were completely absent in *abci10-1*, some prothylakoid like structures were detected in *abci11-1* plastids, again pointing to a more severe effect of the loss of At-ABCI10 function. Common to both mutant lines, however, was some electron-dense material that accumulated in the plastid stroma (**Figure 5**).

In summary, the loss of At-ABCI10 as well as of At-ABCI11 function causes a strong dwarf and albino phenotype, and severely affects chloroplast and in particular thylakoid biogenesis, a phenotype that is reminiscent of de-regulated metal homeostasis (Varotto et al., 2002; Ravet et al., 2009; Briat et al., 2010; Shimoni-Shor et al., 2010; Duy et al., 2011). In particular, the completely albino appearance of the three independent *abci10* knockout mutant lines (*abci10-1*, *abci10-3*, *abci10-4*) is very similar to that of loss-of-function mutants of the chloroplast Fe-uptake permease PIC1 (Duy et al., 2007b). Since the chlorotic phenotype is quite pleiotropic, we can, however, not exclude involvement of secondary effects or other metabolic pathways. The difference in the strength of chlorosis of *abci10* and *abci11* confirms the observed potential diverse suborganellar localization and suggests slightly different contribution of ABCI10 and ABCI11 to cellular metabolism.

ABCI10 and ABCI11 Are Crucial for Metal Homeostasis

To follow a potential function of At-ABCI10 and At-ABCI11 in metal homeostasis, we determined metal contents in seedling and shoot tissues of wild type and *abci10-1*, *abci10-4, abci11-1* mutant lines (**Figure 6** and **Supplementary Figure 6E**). Whereas magnesium and potassium content did not change to a considerable extend in mutants when compared to

wild type, the levels of transition metals exhibited pronounced alterations that were very similar in *abci10* and *abci11* lines. Prominent and most significant changes were observed for iron (Fe) and manganese (Mn), which play a central role in photosynthetic electron transport. All mutant lines *abci10-1*, *abci10-4*, and *abci11-1* displayed a two- to threefold increase in Fe-levels in shoots and entire seedlings when compared to wild type (**Figure 6A** and **Supplementary Figure 6E**). In contrast, Mn levels in mutant shoot tissue did not vary substantially, but in entire mutant plantlets were reduced to about half of the wild-type levels, indicating a more important role of Mn for root tissue (**Figure 6C**). The latter is supported by the finding that reduced root growth of *abci10-1*, *abci10-4*, and *abci11-1* can be partially rescued by additional Mn supply (**Supplementary Figures 6F, 7C**). Fe addition to the medium, however, failed to prevent dwarfism of *abci10*, *abci11* knockout lines (**Supplementary Figure 7B**), well in line with the general Fe-overload measured. For zinc (Zn) and copper (Cu) as well as for nickel (Ni) and molybdenum (Mo), we observed increased levels in shoot tissue of *abci10*, *abci11* mutants, but a decrease of Zn and no change for Cu in entire seedlings (**Figures 6B, D, E** and **Supplementary Figure 6E**). Again, these findings indicate a severely impaired transition metal homeostasis in chloroplast-dominated shoot tissue that might lead to reduced uptake of Zn and also of Mn (see above) by mutant roots. The changes of metal content for *abci11-1* plantlets determined in this study—except for the decrease of Mn in complete seedlings—are well in line with the data previously published by Shimoni-Shor et al. (2010), who used separated shoot and root tissue. The observed iron overload in all mutant plants and the increase in shoot transition metals might explain the chlorotic and necrotic phenotypes, which are likely to be due to ROS stress generated by too many free metal ions.

To further link the function of ABCI10 and ABCI11 with iron in chloroplasts, we examined the gene expression levels of proteins related to Fe-homeostasis and transport in chloroplasts in *abci10-1* and *abci11-1* lines (**Figure 7**). First, we could demonstrate that expression of *At-ABCI11* is slightly down-regulated in *abci10-1* and *vice versa At-ABCI10* transcripts are decreased in *abci11-1* (**Figure 7A**). This behavior might indicate that ABCI10 and ABCI11 are functioning in separate pathways and cannot complement the function of each other. Moreover, transcripts of the Fe-uptake permease *PIC1* and the chloroplast ferric chelate reductase *FRO7* (**Figure 7B**) are significantly reduced in both mutant lines, pointing to a down-regulation of the potential reductive Fe-uptake pathway in plastids of *abci10-1* and *abci11-1* (compare Vigani et al., 2019). Transcripts of the major ferritin Fe-storage proteins *FER1* and *FER4* in the chloroplast stroma, however, remained at wild-type levels in both mutant lines (**Figure 7C**).

In conclusion, loss-of-function mutants of At-ABCI10 and At-ABCI11 are characterized by a de-regulated transition metal homeostasis, which is most pronounced for increased Fe- and decreased Mn-levels, both metals essential for photosynthesis. Although similar in their dwarf and for *abci10* also in albino appearance, *abci10-1* and *abci11-1* here behave opposite to knockout mutants of the chloroplast Fe-uptake permease PIC1, which shows no change in Fe-levels but a pronounced up-regulation of ferritin transcripts and proteins (Duy et al., 2007b).

ABCI10 Appears to Interact With ABCI12 at the Chloroplast IE

In order to identify potential IE membrane-intrinsic interaction partners for ABCI10 and ABCI11, we performed co-immunoprecipitation assays with the respective antisera on solubilized IE membrane vesicles from pea chloroplasts. Interestingly, the antiserum for At-ABCI10 precipitated a protein band around 50 kDa, which was identified to contain peptides of the pea ortholog to At-ABCI12 (**Supplementary Figure 8**). In contrast, this protein was not precipitated by α-ABCI11 or the respective pre-immune sera, indicating that the potential interaction with ABCI12 seems to be specific for ABCI10. For *Arabidopsis* At-ABCI12 (At3g21580), a chloroplast targeting peptide of 63 aa (ChloroP; Emanuelsson et al., 1999) and five α-helical transmembrane domains are predicted (Aramemnon database; Schwacke et al., 2003). To confirm the potential insertion of At-ABCI12 into the chloroplast envelope, we performed *in vivo* GFP targeting assays by transiently transforming isolated *Arabidopsis* protoplasts with At-ABCI12-GFP constructs (**Figure 8A**). Very similar to the chloroplast IE-intrinsic control At-PIC1-GFP (**Figure 8B**), At-ABCI12 targeted GFP fluorescence appeared around the chloroplast periphery, indicating insertion into the chloroplast envelope, most likely IE membranes. For a verification of the interaction of ABCI10 and ABCI12, we further co-transformed At-ABCI10-YFP and an over-expression construct for At-ABCI12. As observed previously (compare **Figure 2A**), At-ABCI10-YFP signals when transformed alone were punctuate at the periphery of chloroplasts (**Figure 8C**). In combination with overexpression of At-ABCI12 in the same protoplasts (co-transformation of both constructs), however, the YFP fluorescence of At-ABCI10 moved to a clear ring-like pattern around the chloroplast envelopes (**Figure 8D**). The same behavior was observed for co-expression of At-ABCI10-GFP and At-ABCI12-RFP, but not for At-ABCI11-GFP and At-ABCI12-RFP (**Supplementary Figure 9**).

Thus, fluorescence patterns of single and co-transformed At-ABCI10, At-ABCI11, and At-ABCI12 constructs confirm co-immunoprecipitation assays and indicate that indeed ABCI12 seems to interact with ABCI10 but not with ABCI11. Thereby, ABCI12 appears to anchor the potential ECF ATPase-subunit ABCI10 to the IE membrane of chloroplasts.

ABCI12: Subunit T of a Potential Chloroplast ECF ABC Transporter

The mature At-ABCI12 protein is expected to be 328 aa long with a size of about 36 kDa. In UniProt/InterPro databases (accession Q944H2), At-ABCI12 is annotated to be an ABC/ECF transporter transmembrane component (IPR003339 family). Further, the protein was already mentioned as "plant T protein," belonging to a plant-specific ECF transporter T

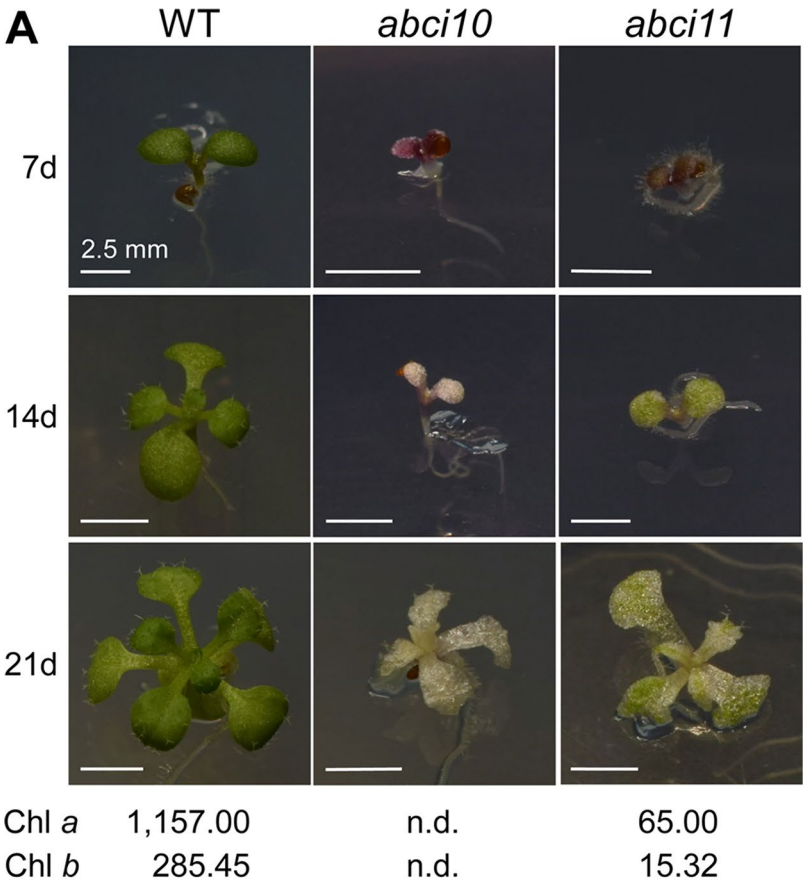

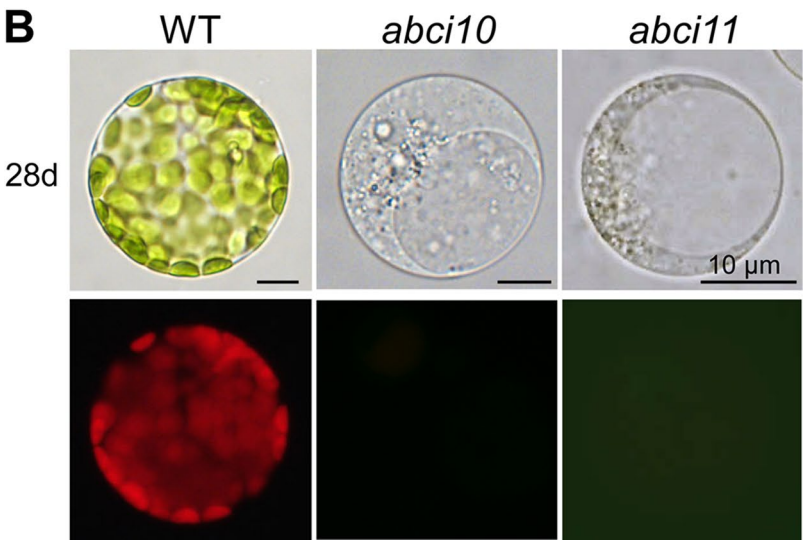

FIGURE 4 | ABCI10 and ABCI11 loss-of-function mutants are dwarfed albino plants. **(A)** Seedlings of Col-0 wild type, *abci10-1*, and *abci11-1* knockout mutants grown for 7, 14, and 21 days on agar medium supplemented with sucrose. Scale bars = 2.5 mm. Chlorophyll *a* and chlorophyll *b* content was measured in 21-day-old plantlets. Mean values (ng chlorophyll/mg freshweight) from two independent extractions on each time 9 (Col-0), 16 (*abci10*), and 26 (*acbi11*) pooled individuals are shown. n.d., not detectable. **(B)** Protoplasts isolated from 28-day-old seedlings depicted in **(A)**. The upper panel shows bright field images, which document absence of mature chloroplasts in *abci10-1* and *abci11-1* mutants. The lower panel depicts chlorophyll autofluorescence of the same protoplasts. Please note that plastid structures in protoplasts of *abci11-1* appear to be slightly greenish. Scale bars = 10 µm.

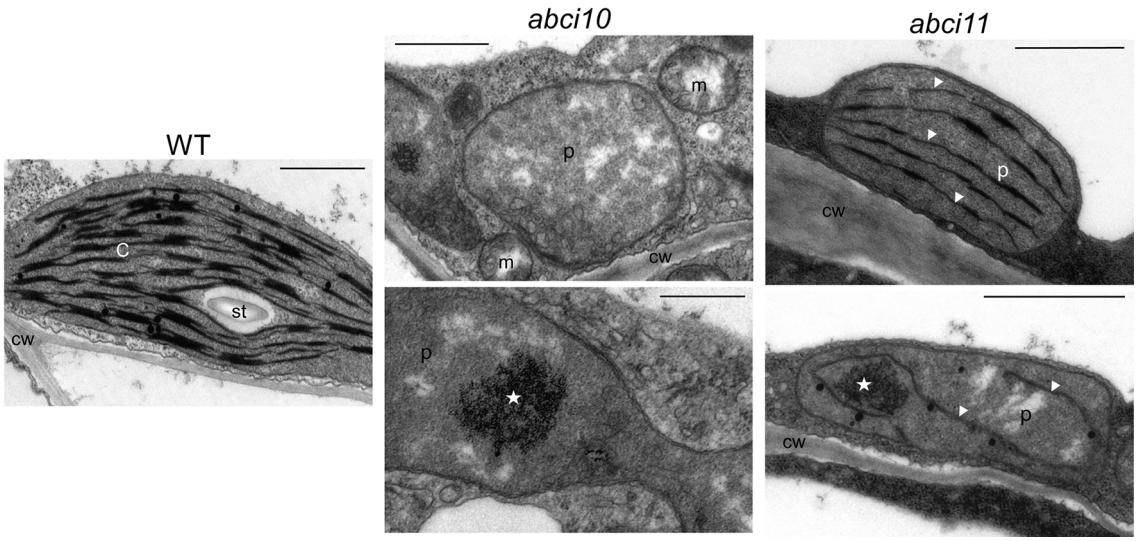

FIGURE 5 | Chloroplast biogenesis is impaired in *abci10-1* and *abci11-1* knockouts.Transmission electron microscopic pictures of plastids from 21-day-old *abci10-1* and *abci11-1* mutant and Col-0 wild-type seedlings. Asterisks indicate electron dense clusters visible in plastids of *abci10-1* and *abci11-1* mutants. Arrowheads highlight prothylakoid-like membranes in *abci11-1*. Scale bars = 1 µm. c, chloroplast; cw, cell wall; m, mitochondrium; p, plastid; st, starch grain.

subunit with similarity to cyanobacterial proteins (Eitinger et al., 2011). The crystal structures of CbiQ2 and EcfT in the complexes CbiMQO (group I, Co-uptake; Bao et al., 2017) and ECF-FolT (group II, folate transport; Swier et al., 2016) reveal details in structure function relations of T subunits and therefore were selected for comparison with At-ABCI12. In addition, we choose NikQ (group I, Ni-transport) and BioN (group I, biotin transport), the latter only with four α-helical membrane domains (**Supplementary Figure 10**). Here, At-ABCI12 and its ortholog Os-ABCi8 from rice show structural similarity to T subunits with 5 α-helical transmembrane domains, namely, NikQ, CbiQ2, and EcfT from ECF complexes for Ni, Co, and folate transport (NikMNQO, CbiMNQO, and FolT, respectively; Rodionov et al., 2006; Neubauer et al., 2009; Rodionov et al., 2009). Like for ABCI10 and ABCI11, orthologs of ABCI12 are found in the green lineage in dicots, monocots, mosses, green algae, and cyanobacteria (**Supplementary Figure 11**). However, ABCI12 relatives appear to be absent in *Gloeobacter*, i.e., cyanobacteria without thylakoid membrane systems. In comparison to non-photosynthetic prokaryotes, it becomes evident that plant and cyanobacterial T proteins contain an additional stretch—about 35 amino acids for At-ABCI12—between transmembrane helix 3 and 4 (**Figure 9A**, **Supplementary Figures 10, 11**; compare Eitinger et al., 2011).

Structural modeling of the mature At-ABCI12 (Phyre2; Kelley et al., 2015) gives a structure prediction also with five transmembrane helices known for most EcfT proteins (group II) and many T subunits of group I transporters (Eitinger et al., 2011) with considerable confidence (**Figure 9A**). Common and conserved for all T proteins of ECF transporters are the two coupling helices with the highly conserved X-R-X motifs, crucial for interaction with the negatively charged residues in the groove of the ATPase AA dimer (compare **Figure 1**) at the cytosolic face of the membrane (Neubauer et al., 2009; Rempel et al., 2019). In At-ABCI12, these conserved arginines can be found at the C-terminal end of each of the coupling helices ch2 (R_{242}) and ch3 (R_{283}) (**Figure 9**). Since ABCI12 most likely inserts into the IE membrane of chloroplasts, we propose that these two coupling helices are facing to the stroma and thereby can mediate interaction with the groove of a potential ABCI10 AA dimer (**Figure 9B**).

DISCUSSION

In our study on potential metal transporters of prokaryotic origin in *Arabidopsis* chloroplasts, we identified the soluble NBD ABC-transporter subunits At-ABCI10 and At-ABCI11. By *in vivo* GFP-targeting and immunoblot analysis, we could unequivocally show that both proteins are chloroplast intrinsic. Thereby, we confirmed previous results on ABCI11/NAP14 in *Arabidopsis* and rice (Shimoni-Shor et al., 2010; Zeng et al., 2017). Our *in vivo* GFP-targeting assays in the homologous *Arabidopsis* protoplast system appeared to allow to distinguish signal distribution within different regions of the chloroplast stroma—i.e., soluble for the control FSD1 or membrane attached for ABCI11 (plastoglobuli) and ABCI10 (envelope). However, interpretation of data and biological relevance of these observations requires a second, independent approach such as immunoblot analysis. The latter revealed to our surprise that both ABCI10 and ABCI11 appeared to be strongly attached to chloroplast IE membranes. For At-ABCI11 *in vivo* GFP-targeting assays in addition point to a possible attachment to plastoglobuli (PG), which still has to be verified. On the one hand, transient overexpression of fluorescent-tagged proteins could result in ectopic, non-endogenous localization of the

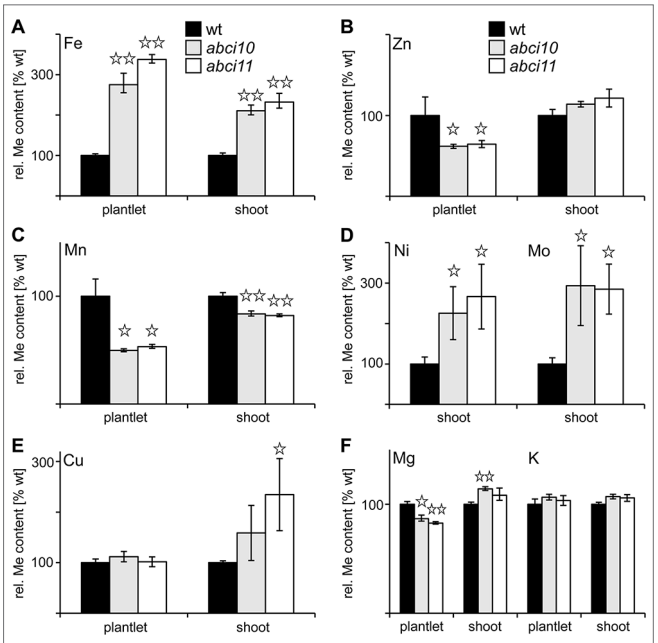

FIGURE 6 | Knockouts of *At-ABCI10* and *At-ABCI11* have a de-regulated metal content. Metal contents for iron **(A)**, zinc **(B)**, manganese **(C)**, nickel, molybdenum **(D)**, copper **(E)** and magnesium, potassium **(F)** were determined in entire plantlets and separated shoot tissue of 15-day-old wild type (wt, black bars) as well as 34-day-old *abci10-1* (grey bars) and *abci11-1* (white bars) mutant lines. Please note that for Ni and Mo in (D) shoot tissue of 20-day old seedlings was used. The respective metal content (n = 3 ± SD) is given relative to the level in wt, which was set to 100%. Data points with significant difference to wt according to Student's t-test are indicated by *($p < 0.05$) and ** ($p < 0.01$).

proteins. On the other hand, PG membranes might co-purify with the IE membrane vesicles during purification steps. Further, it should also be noted that a number of studies on plastoglobule proteomics did not find ABCI11 (Ytterberg et al., 2006; Lundquist et al., 2012; van Wijk and Kessler, 2017). In proteomics of chloroplast envelopes, ABCI11 was also not experimentally detected, but only annotated to the IE (Ferro et al., 2010). Thus, if the sub-organellar distribution of the ABCI11 protein is only at plastoglobuli or maybe at both IE and PG lipid layers, still has to be clarified in the future. Here, detailed suborganellar immuno-localization by electron microscopy techniques and the identification of ABCI11-interacting proteins would help to unveil the precise localization and function of ABCI11 proteins in chloroplasts. Depending on the interaction partner, At-ABCI11/NAP14 might either represent an ATPase NBD-domain subunit of a canonical prokaryotic-type ABC transporter or function as non-ABC transporter, organelle-intrinsic NAP protein. Within the plant ABC-transporter inventory in subfamily I (Verrier et al., 2008), the TGD1-3 complex—NBD-TMD-SBP subunit arrangement—as well as the NBD-TMD dimers ABCI1-ABCI2 and ABCI17-ABCI16 are examples for a canonical prokaryotic-type ABC importer assembly (for details on functions see Xu et al., 2003; Lu et al., 2007; Rayapuram et al., 2007; Huang et al., 2010; Xu et al., 2010; Roston et al., 2012; Belal et al., 2015; Dong et al., 2017; Wang et al., 2019). The NBD ATPase ABCI6 for FeS cluster biogenesis in chloroplasts, however, interacts with ABCI7, ABCI8, which are soluble proteins that do not belong to an ABC transporter assembly (Xu and Möller, 2004). To our knowledge, no more single transmembrane subunits of either canonical TMD- or ECF T-type with still unknown partners are annotated in the plant ABC transporter superfamily (Verrier et al., 2008). Therefore, an interaction of ABCI11 with protein partners similar to ABCI7, ABCI8 for FeS cluster biogenesis seems to be most likely. Thus, ABCI11/NAP14 appears to group into the "non-intrinsic ABC protein" NAP family and bind to a still unknown partner protein at plastoglobuli and/or IE membranes. We can, however, not include that some still anonymous membrane-intrinsic proteins for interaction with ABCI11 are present in the chloroplast proteome.

For At-ABCI10 instead, interpretation of the data is more straightforward and points to a strong attachment to the IE membrane from the stroma side. i) At-ABCI10 was the only protein of the three examined in this study, for which peptides have been experimentally detected in purified envelopes from *Arabidopsis* (Froehlich et al., 2003), envelope preparations from maize (Bräutigam et al., 2008), and IE membranes from pea (Gutierrez-Carbonell et al., 2014). ii) No signals of fluorescence-tagged At-ABCI10 have been associated with plastoglobuli. iii) Attachment of ABCI10 to IE membranes seems to be a bit stronger than for ABCI11. iv) The presence of the conserved Q-helix motif in ABCI10, which indicates that in the *Arabidopsis* ABCI family only ABCI10 represents a potential ATPase A subunit of an ECF AAT module. v) Identification of ABCI12 as potential ECF T-subunit interaction partner and IE membrane-anchor for ABCI10.

The loss-of-function of ABCI10 as well as of ACBI11 in *Arabidopsis*, however, severely impacts plant growth and development as documented by the dwarf, albino appearance of seedlings as well as partial embryo lethality and the fact that homozygous lines are unable to reproduce. Furthermore, chloroplast and in particular thylakoid biogenesis are defect. Since on the chloroplast ultrastructural level and in their completely albino appearance, phenotypes of *abci10* knockouts appear to be more severe than those of *abci11*, a function of both proteins in different pathways is plausible. This hypothesis is further supported by the finding that gene expression in seedlings of both *At-ABCI10* and *At-ABCI11* is not up-regulated for complementation in the respective knockout mutants. However, although somewhat different in their suborganellar distribution, both At-ABCI10 and At-ABCI11 are clearly associated with a function in cellular metal homeostasis. The latter also has been documented previously for mutants of rice and *Arabidopsis* ABCI11 (Shimoni-Shor et al., 2010; Zeng et al., 2017). In the stroma of *abci10* and *abci11* mutant plastids, we detected accumulations of electron-dense material, which resemble that of ferritin protein clusters found in *pic1* knockout plastids (compare Duy et al., 2007b). Thus, in addition to deregulated metal content and reduced transcripts of *PIC1* and *FRO7* genes for chloroplast Fe-uptake in *abci10*, *abci11* mutant seedlings, these ferritin-like clusters in *abci10* and *abci11* plastids point to unbalanced chloroplast metal homeostasis. Different to the strong increase of ferritin transcript and protein in *pic1*, gene expression of ferritin, however, appeared not to

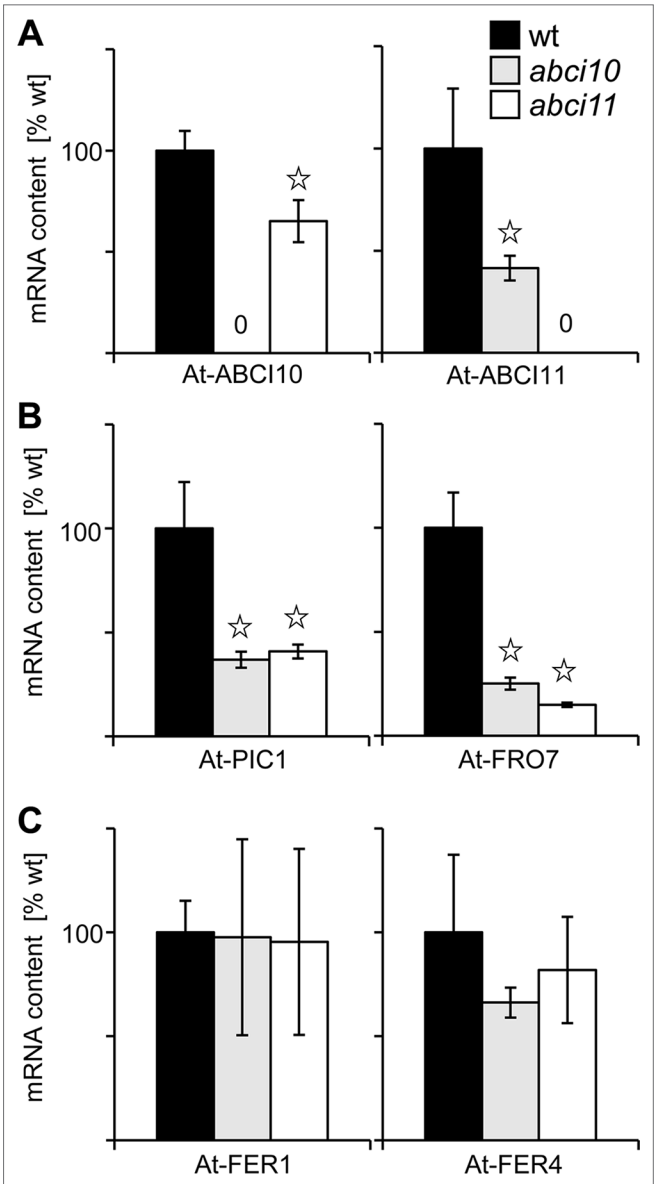

FIGURE 7 | Knockouts of *At-ABCI10* and *At-ABCI11* show differential expression of chloroplast Fe-homeostasis and transport genes. Transcript levels were determined by qRT PCR on RNA isolated from 20-day-old seedlings of wild type (wt, black bars) as well as *abci10-1* (grey bars) and *abci11-1* (white bars) mutant lines. The mRNA content (n = 3 ± SD) of At-ABCI10, At-ABCI11 **(A)**, At-PIC1, At-FRO7 **(B)**, and At-FER1, At-FER4 **(C)** was normalized to 10.000 actin transcripts and calculated relative to the corresponding wild type, which was set to 100%. Data points with significant difference to wt according to Student's t-test are indicated by * ($p < 0.05$).

be regulated in *abci10* and *abci11*. Furthermore, also increased Fe-levels in *abci10* and *abci11*, which are absent in *pic1* (Duy et al., 2007b), point to different cellular regulation in response to the loss of PIC1 and ABCI10, ABCI11. Interestingly, *At-ABCI10*, *At-ABCI11*, and *At-ABCI12* genes show a very similar expression pattern when compared to *At-PIC1*. For all four genes, transcripts peak in green shoot tissues and are almost absent in roots (see developmental map at *Arabidopsis* eFP browser; https://bar.utoronto.ca/efp_arabidopsis/cgi-bin/efpWeb.cgi). The absolute transcript levels for *At-ABCI10*, *At-ABCI11,* and *At-ABCI12*, however, are about 10-fold less than for *At-PIC1*. The partial rescue of dwarf root growth in *abci10* and *abci11* mutants by Mn supplementation also indicates a role for both proteins in metal homeostasis. A pronounced decrease of Mn as well as of Zn was observed only in entire *abci10* and *abci11* seedlings but not in separated shoot tissue. Thus, our findings indicate a severely impaired transition metal homeostasis in chloroplast-dominated shoot tissue. This implies that in response to transition metal overload in shoots, and in particular to the prominent overall increase of Fe, *abci10* and *abci11* mutants might down-regulate root metal acquisition systems. Thus, it is likely that the root growth rescue by Mn is due to secondary effects and not directly linked to a function of ABCI10 and ABCi11 in root plastids. Most likely, ABCI10 (IE attached) and ABCI11 (PG associated) due to their distinct distribution in the chloroplast stroma and their potential assembly with separate protein complexes fulfill different tasks. However, both are crucial for transition metal homeostasis in chloroplasts and thereby closely linked to photosynthetic performance. For the latter, impact of ABCI10 seems to be larger than that of ABCI11, since the albino phenotype of *abci10* knockouts is more severe.

The observed interaction of ABCI10 with ABCI12 at the chloroplast IE membrane suggests that both proteins are part of a prokaryotic-type ECF ABC-transporter. Here, ABCI10 would represent the ATP-binding subunit A, and ABCI12 the membrane-intrinsic, energy-transducing subunit T (**Figure 9B**). According to the working models developed for the prokaryotic CbiMNQO (group I ECF for Co-uptake; Bao et al., 2017) and FolT2 (group II, folate import; Swier et al., 2016), the coupling helices ch2 and ch3 of plant ABCI12 could anchor an ABCI10 dimer at the inner leaflet of the IE membrane (**Figure 9B**). In general, hydrophobic and hydrophilic interactions between the coupling helices of ECF T-subunits and the groove of AA dimers are described (Swier et al., 2016; Bao et al., 2017). In particular, ionic interactions *via* the two conserved positively charged arginine motifs at the end of ch2 and ch3 from the T component and the negatively charged aspartate residues in the helical subdomain of each A protein contribute to the AAT module assembly (Rempel et al., 2019). For the mature ABCI12 protein, these residues are represented by arginine 242 (ch2) and 283 (ch3), the conserved aspartate in the mature ABCI10 sequence is at position 78 (**Figure 9B**). Thereby, the observed unusually strong attachment of ABCI10 to IE membranes could be explained. If ABCI10 functions as homodimer or maybe in combination with another ATPase A subunit still has to be clarified. However, since ABCI10 represents the only ABC ATPase with the ECF transporter specific Q-helix motif in *Arabidopsis*, a function as homomeric AA component is most likely. Furthermore, ABCI10 proteins do not contain the C-terminal α-helical stretch (compare **Figure 1**), which is mandatory for ECF group II but only optional for group I transporters (Eitinger et al., 2011; Rempel et al., 2019). Thus, the potential ABCI10/ABCI10-ABCI12 AAT module in the IE membrane of chloroplasts, most likely belongs to group I ECF importers.

In bacteria, these group I ECF transporters are described to import divalent Co or Ni metal ions (CbiMNQO, NikMNQO) as

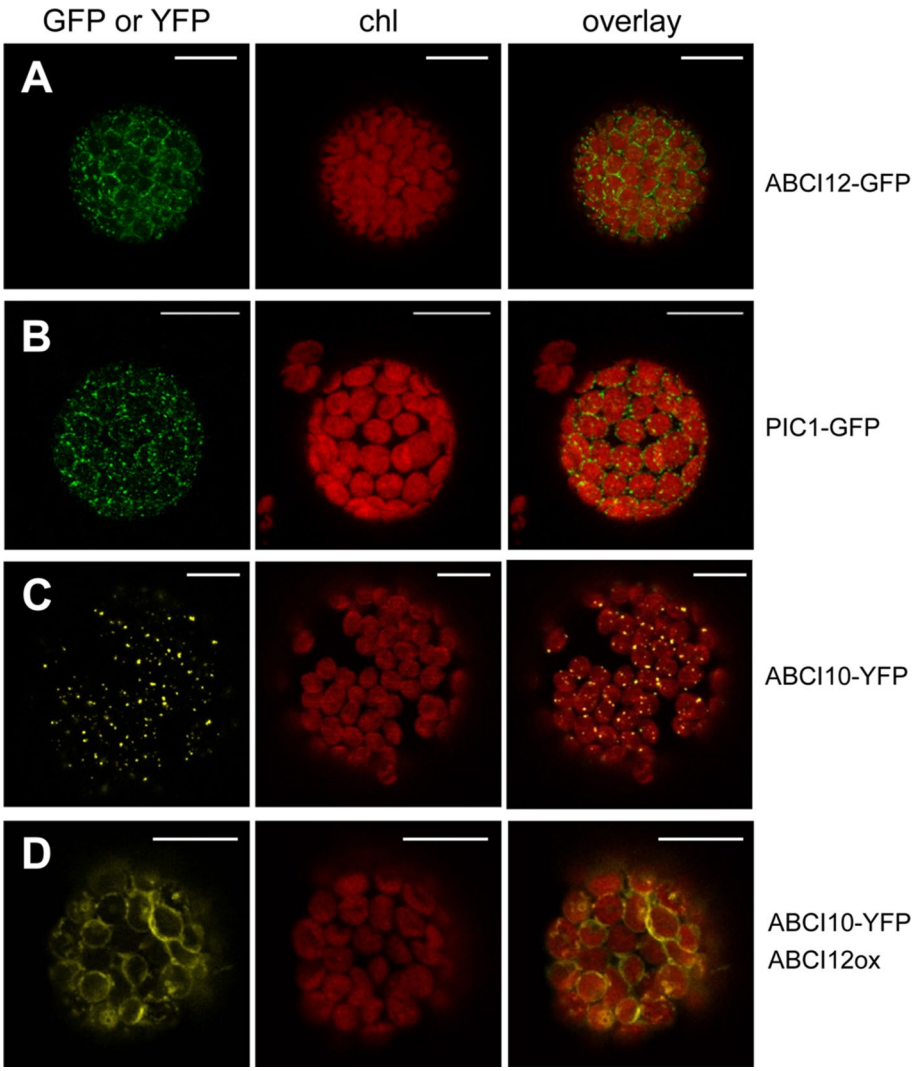

FIGURE 8 | At-ABCI12 in the chloroplast envelope targets At-ABCI10 to the IE membrane. *Arabidopsis* leaf protoplasts were transiently transformed with constructs for At-ABCI12-GFP **(A)**, At-PIC1-GFP [chloroplast IE marker; (Duy et al. 2007b)] **(B)**, At-ABCI10-YFP **(C)**, as well as At-ABCI10-YFP when co-expressed with an At-ABCI12 construct **(D)**. Images show GFP- **(A,B)** and YFP-signals **(C,D)** (left), chlorophyll fluorescence (middle), as well as an overlay of both (right). Scale bar = 10 µm.

well as metabolites like biotin (BioMNY), methyl-thioadenosine or precursors for queuosine, methionine, thiamine, or cobalamin (Rodionov et al., 2009; Eitinger et al., 2011). Transport specificity is defined by the corresponding substrate-binding protein S, whose origin and features are still enigmatic for the potential chloroplast ABCI10/ABCI10-ABCI12 module. In general, a chloroplast ECF-complex mediated uptake of divalent metal ions for photosynthetic electron transport or import of biotin, which is synthesized in mitochondria but central for *de novo* fatty acid biosynthesis in chloroplasts, is probable. Since *abci10* knockout lines show a strong albino phenotype, similar to that of loss-of-function lines for the chloroplast Fe-uptake permease PIC1 (Duy et al., 2007b; Duy et al., 2011; Gong et al., 2015), it is however tempting to speculate that ABCI10 in chloroplasts is involved in transition metal uptake as well. Thereby, the potential ABCI10/ABCI10-ABCI12 module would provide a bypass for PIC1 in IE membranes, which, however, has a distinct impact on cellular metal homeostasis. Furthermore, PIC1 (Duy et al., 2007b) and ABCI12 orthologous proteins seem to be absent in the thylakoid-less green algae *Gloeobacter* pointing to a transport function closely linked to thylakoid membrane processes such as photosynthetic electron transport that requires a high amount of transition metals (Fe, Mn, Cu). In addition, the plant and cyanobacterial specific amino acid stretch between tm3 and tm4 of T subunits (compare **Figure 9B**; Eitinger et al., 2011) indicates a specification linked to performance of oxygenic photosynthesis. Since tm3 is described to contribute to conformational flexibility between membrane-intrinsic and coupling domains of ECF T-subunits and together with the other hydrophobic tms is involved in interaction with the membrane-intrinsic S component (Rempel et al., 2019), this "photosynthesis"-specific stretch in ABCI12

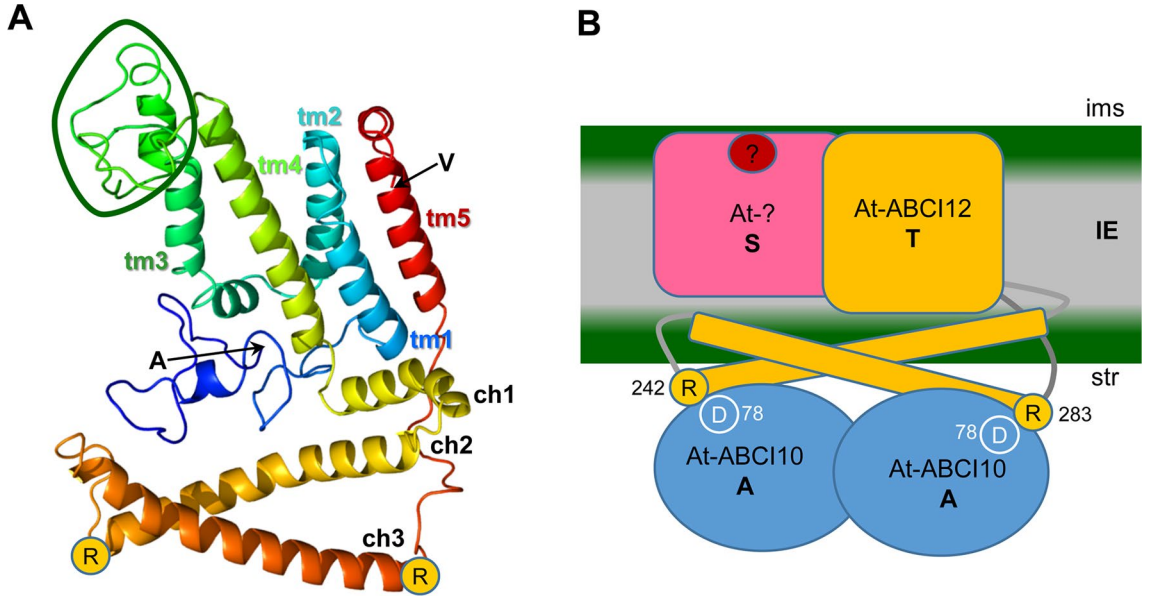

FIGURE 9 | ABCI12 as T subunit of a chloroplast ECF ABC transporter. **(A)** The secondary structure of mature At-ABCI12 (79% modelled at >90% confidence) was predicted by Phyre[2] (Kelley et al. 2015) in comparison to the structure of four bacterial ECF transporter complexes (templates 5js7, c4huqT [FolT folate transport], c4rfsT [panthothenate transport], c5x3xq [CbiMQO Co-transport]. N- and C-terminal amino acids of the mature ABCI12 (alanine and valine, respectively) as well as the conserved arginine residues (R) at the end of ch2 and ch3 are indicated. Please note that the structures of the N-terminus (blue ribbon) and of the loop between tm3 and tm4, which is specific for plant and cyanobacterial ABCI12 relatives (green circle), are predicted with low confidence, whereas helices are strongly supported by the model. ch1-3, coupling α-helices; tm1-5, transmembrane α-helices 1-5. **(B)** According to the working hypothesis, At-ABCI12 (orange) in the IE membrane would represent the energy transducing subunit T of a chloroplast ECF transporter AAT module. ch2 and ch3 of ABCI12 could bind with R_{242} and R_{283} to conserved aspartate residues (D_{78}) in the groove of an At-ABCI10 ATPase homodimer (AA subunit, blue) at the inner leaflet of the IE. The membrane-intrinsic substrate-binding subunit S (pink) as well as the substrate (red dot), however, are still unknown. ims, intermembrane space; str, stroma.

proteins might define the still unknown substrate-specificity of the potential chloroplast AAT module. Because specificity of transport proteins for divalent metal ions in general is low (Kobayashi and Nishizawa, 2012), we propose that ABCI10/ABCI10-ABCI12 might be involved in chloroplast uptake of Fe and Mn ions.

Involvement of ABCI10 and ABCI12 in chloroplast biotin uptake seems rather unlikely, because the five transmembrane structure predicted for ABCI12 is not common for BioN T subunits in ECF biotin transporters. Further, since the chloroplast stroma is the only site for *de novo* fatty acid synthesis in plant cells, disruption of biotin import essential for the first step of this pathway would most likely lead to complete embryo lethality rather than to the chlorotic and dwarf appearance and only partial embryo lethality observed in *abci10* knockouts. Indeed, strict embryo abortion is observed in knockout mutants of the biotin-carboxyl carrier protein BCCP2 (Li et al., 2011), which delivers biotin for carboxylation in the heteromeric acetyl-CoA carboxylase complex in the chloroplast stroma (Li-Beisson et al., 2013).

In summary, it is tempting to speculate that ABCI10 as homodimer and ABCI12 in the IE membrane can form an AAT energy-coupling module of a novel, chloroplast ECF ABC importer that most likely has a prokaryotic origin and is involved in transition metal uptake. A conclusion on assembly and transport specificity of a potential group I ECF transport, mediated by an ABCI10/ABCI10-ABCI12 module however, is only possible with the still lacking identification of the substrate-binding component(s) and direct functional as well as interaction assays for such a complex.

DATA AVAILABILITY STATEMENT

All datasets generated for this study are included in the manuscript/**Supplementary Files**.

AUTHOR CONTRIBUTIONS

JP, YL, and KP conceived and designed experiments. LV and JP characterized mutant plants and phenotypes, performed GFP-targeting assays, and analyzed metal contents. LV conducted co-immunoprecipitation assays and qRT-PCR analysis. RS purified recombinant proteins and contributed to immunoblot analysis and co-transformation of protoplasts. CL contributed to phenotyping of mutant lines. KP performed structural and sequence analysis of ABCI proteins and wrote the manuscript together with JP.

FUNDING

This work was funded by the DFG (Deutsche Forschungsgemeinschaft) grants PH73/3-2, -3 to KP, a Human

Frontier Science Program long-term postdoctoral fellowship to JP, and in part was supported by the National Research Foundation of Korea (NRF) grant (2018R1A2A1A05018173) funded by the Korean government (Ministry of Science and ICT) to YL.

ACKNOWLEDGMENTS

We would like to acknowledge excellent technical assistance by Karl Mayer, and we thank Daniela Duy for in-depth discussions and help. We are grateful to Jürgen Soll for his constant support of our research and to Gerhard Wanner/Daniela Duy for electron microscopic pictures.

SUPPLEMENTARY MATERIAL

The Supplementary Material for this article can be found online at: https://www.frontiersin.org/articles/10.3389/fpls.2019.01264/full#supplementary-material

REFERENCES

Abel, S., and Theologis, A. (1998). Transient gene expression in protoplasts of *Arabidopsis thaliana*. *Methods Mol. Biol.* 82, 209–217. doi: 10.1385/0-89603-391-0:209

Asada, K. (1999). The water-water cycle in chloroplasts: scavenging of active oxygen and dissipation of excess photons. *Annu. Rev. Plant Physiol. Plant Mol. Biol.* 50, 601–639. doi: 10.1146/annurev.arplant.50.1.601

Bao, Z., Qi, X., Hong, S., Xu, K., He, F., Zhang, M., et al. (2017). Structure and mechanism of a group-I cobalt energy coupling factor transporter. *Cell Res.* 27, 675–687. doi: 10.1038/cr.2017.38

Bashir, K., Rasheed, S., Kobayashi, T., Seki, M., and Nishizawa, N. K. (2016). Regulating subcellular metal homeostasis: the key to crop improvement. *Front. Plant Sci.* 7, 1192. doi: 10.3389/fpls.2016.01192

Belal, R., Tang, R., Li, Y., Mabrouk, Y., Badr, E., and Luan, S. (2015). An ABC transporter complex encoded by Aluminum Sensitive 3 and NAP3 is required for phosphate deficiency responses in *Arabidopsis*. *Biochem. Biophys. Res. Commun.* 463, 18–23. doi: 10.1016/j.bbrc.2015.05.009

Block, M. A., Douce, R., Joyard, J., and Rolland, N. (2007). Chloroplast envelope membranes: a dynamic interface between plastids and the cytosol. *Photosynth. Res.* 92, 225–244. doi: 10.1007/s11120-007-9195-8

Bölter, B., Soll, J., Hill, K., Hemmler, R., and Wagner, R. (1999). A rectifying ATP-regulated solute channel in the chloroplastic outer envelope from pea. *EMBO J.* 18, 5505–5516. doi: 10.1093/emboj/18.20.5505

Brandenburg, F., Schoffman, H., Kurz, S., Kramer, U., Keren, N., Weber, A. P., et al. (2017). The synechocystis manganese exporter Mnx is essential for manganese homeostasis in cyanobacteria. *Plant Physiol.* 173, 1798–1810. doi: 10.1104/pp.16.01895

Braun, V. (2014). "Energy-coupled transport across the outer membrane of Gram-negative bacteria," in *Bacterial membranes: structural and molecular biology*. Ed. H. F. R. Remaut (U.K: Caister Academic Press).

Braun, V., and Hantke, K. (2011). Recent insights into iron import by bacteria. *Curr. Opin. Chem. Biol.* 15, 328–334. doi: 10.1016/j.cbpa.2011.01.005

Bräutigam, A., Hoffmann-Benning, S., and Weber, A. P. (2008). Comparative proteomics of chloroplast envelopes from C3 and C4 plants reveals specific adaptations of the plastid envelope to C4 photosynthesis and candidate proteins required for maintaining C4 metabolite fluxes. *Plant Physiol.* 148, 568–579. doi: 10.1104/pp.108.121012

Breuers, F. K., Brautigam, A., and Weber, A. P. (2011). The plastid outer envelope—a highly dynamic interface between plastid and cytoplasm. *Front. Plant Sci.* 2, 97. doi: 10.3389/fpls.2011.00097

Briat, J. F., Ravet, K., Arnaud, N., Duc, C., Boucherez, J., Touraine, B., et al. (2010). New insights into ferritin synthesis and function highlight a link between iron homeostasis and oxidative stress in plants. *Ann. Bot.* 105, 811–822. doi: 10.1093/aob/mcp128

Brumbarova, T., Bauer, P., and Ivanov, R. (2015). Molecular mechanisms governing *Arabidopsis* iron uptake. *Trends Plant Sci.* 20, 124–133. doi: 10.1016/j.tplants.2014.11.004

Bughio, N., Takahashi, M., Yoshimura, E., Nishizawa, N. K., and Mori, S. (1997). Light-dependent iron transport into isolated barley chloroplasts. *Plant Cell Phys.* 38, 101–105. doi: 10.1093/oxfordjournals.pcp.a029079

Chang, W., Soll, J., and Bolter, B. (2014). A new member of the psToc159 family contributes to distinct protein targeting pathways in pea chloroplasts. *Front. Plant Sci.* 5, 239. doi: 10.3389/fpls.2014.00239

Davidson, A. L., Dassa, E., Orelle, C., and Chen, J. (2008). Structure, function, and evolution of bacterial ATP-binding cassette systems. *Microbiol. Mol. Biol. Rev.* 72, 317–364. doi: 10.1128/MMBR.00031-07

Do, T. H. T., Martinoia, E., and Lee, Y. (2018). Functions of ABC transporters in plant growth and development. *Curr. Opin. Plant Biol.* 41, 32–38. doi: 10.1016/j.pbi.2017.08.003

Dong, J., Pineros, M. A., Li, X., Yang, H., Liu, Y., Murphy, A. S., et al. (2017). An *Arabidopsis* ABC transporter mediates phosphate deficiency-induced remodeling of root architecture by modulating iron homeostasis in roots. *Mol. Plant* 10, 244–259. doi: 10.1016/j.molp.2016.11.001

Duy, D., Soll, J., and Philippar, K. (2007a). Solute channels of the outer membrane: from bacteria to chloroplasts. *Biol. Chem.* 388, 879–889. doi: 10.1515/BC.2007.120

Duy, D., Wanner, G., Meda, A. R., von Wiren, N., Soll, J., and Philippar, K. (2007b). PIC1, an ancient permease in *Arabidopsis* chloroplasts, mediates iron transport. *Plant Cell* 19, 986–1006. doi: 10.1105/tpc.106.047407

Duy, D., Stübe, R., Wanner, G., and Philippar, K. (2011). The chloroplast permease PIC1 regulates plant growth and development by directing homeostasis and transport of iron. *Plant Physiol.* 155, 1709–1722. doi: 10.1104/pp.110.170233

Eisenhut, M., Hoecker, N., Schmidt, S. B., Basgaran, R. M., Flachbart, S., Jahns, P., et al. (2018). The plastid envelope CHLOROPLAST MANGANESE TRANSPORTER1 is essential for manganese homeostasis in *Arabidopsis*. *Mol. Plant* 11, 955–969. doi: 10.1016/j.molp.2018.04.008

Eitinger, T., Rodionov, D. A., Grote, M., and Schneider, E. (2011). Canonical and ECF-type ATP-binding cassette importers in prokaryotes: diversity in modular organization and cellular functions. *FEMS Microbiol. Rev.* 35, 3–67. doi: 10.1111/j.1574-6976.2010.00230.x

Emanuelsson, O., Nielsen, H., and Von Heijne, G. (1999). ChloroP, a neural network-based method for predicting chloroplast transit peptides and their cleavage sites. *Protein Sci.* 8, 978–984. doi: 10.1110/ps.8.5.978

Ferro, M., Brugiere, S., Salvi, D., Seigneurin-Berny, D., Court, M., Moyet, L., et al. (2010). AT_CHLORO, a comprehensive chloroplast proteome database with subplastidial localization and curated information on envelope proteins. *Mol. Cell Proteomics* 9, 1063–1084. doi: 10.1074/mcp.M900325-MCP200

Finazzi, G., Petroutsos, D., Tomizioli, M., Flori, S., Sautron, E., Villanova, V., et al. (2015). Ions channels/transporters and chloroplast regulation. *Cell Calcium* 58, 86–97. doi: 10.1016/j.ceca.2014.10.002

Froehlich, J. E., Wilkerson, C. G., Ray, W. K., McAndrew, R. S., Osteryoung, K. W., Gage, D. A., et al. (2003). Proteomic study of the *Arabidopsis* thaliana chloroplastic envelope membrane utilizing alternatives to traditional two-dimensional electrophoresis. *J. Proteome Res.* 2, 413–425. doi: 10.1021/pr034025j

Gandini, C., Schmidt, S. B., Husted, S., Schneider, A., and Leister, D. (2017). The transporter SynPAM71 is located in the plasma membrane and thylakoids, and mediates manganese tolerance in Synechocystis PCC6803. *New Phytol.* 215, 256–268. doi: 10.1111/nph.14526

Garcia, O., Bouige, P., Forestier, C., and Dassa, E. (2004). Inventory and comparative analysis of rice and *Arabidopsis* ATP-binding cassette (ABC) systems. *J. Mol. Biol.* 343, 249–265. doi: 10.1016/j.jmb.2004.07.093

Gaudet, R., and Wiley, D. C. (2001). Structure of the ABC ATPase domain of human TAP1, the transporter associated with antigen processing. *EMBO J.* 20, 4964–4972. doi: 10.1093/emboj/20.17.4964

Goetze, T. A., Philippar, K., Ilkavets, I., Soll, J., and Wagner, R. (2006). OEP37 is a new member of the chloroplast outer membrane ion channels. *J. Biol. Chem.* 281, 17989–17998. doi: 10.1074/jbc.M600700200

Gong, X., Guo, C., Terachi, T., Cai, H., and Yu, D. (2015). Tobacco PIC1 mediates iron transport and regulates chloroplast development. *Plant Mol. Biol. Rep.* 33, 401–413. doi: 10.1007/s11105-014-0758-5

Gould, S. B., Waller, R. F., and McFadden, G. I. (2008). Plastid Evolution. *Annu. Rev.Plant Biol.* 59, 491–517. doi: 10.1146/annurev.arplant.59.032607.092915

Gutierrez-Carbonell, E., Takahashi, D., Lattanzio, G., Rodriguez-Celma, J., Kehr, J., Soll, J., et al. (2014). The distinct functional roles of the inner and outer chloroplast envelope of Pea (Pisum sativum) as revealed by proteomic approaches. *J. Proteome Res.* 13, 2941–2953. doi: 10.1021/pr500106s

Halliwell, B., and Gutteridge, J. M. C. (1992). Biologically relevant metal ion-dependent hydroxyl radical generation - an update. *FEBS Lett.* 307, 108–112. doi: 10.1016/0014-5793(92)80911-Y

Harsman, A., Schock, A., Hemmis, B., Wahl, V., Jeshen, I., Bartsch, P., et al. (2016). OEP40, a regulated glucose-permeable beta-barrel solute channel in the chloroplast outer envelope membrane. *J. Biol. Chem.* 291, 17848–17860. doi: 10.1074/jbc.M115.712398

Hebbeln, P., Rodionov, D. A., Alfandega, A., and Eitinger, T. (2007). Biotin uptake in prokaryotes by solute transporters with an optional ATP-binding cassette-containing module. *Proc. Natl. Acad. Sci. U. S. A.* 104, 2909–2914. doi: 10.1073/pnas.0609905104

Huang, C. F., Yamaji, N., and Ma, J. F. (2010). Knockout of a bacterial-type ATP-binding cassette transporter gene, AtSTAR1, results in increased aluminum sensitivity in *Arabidopsis*. *Plant Physiol.* 153, 1669–1677. doi: 10.1104/pp.110.155028

Hwang, J. U., Song, W. Y., Hong, D., Ko, D., Yamaoka, Y., Jang, S., et al. (2016). Plant ABC transporters enable many unique aspects of a terrestrial plant's lifestyle. *Mol. Plant* 9, 338–355. doi: 10.1016/j.molp.2016.02.003

Karimi, M., Inze, D., and Depicker, A. (2002). GATEWAY vectors for Agrobacterium-mediated plant transformation. *Trends Plant Sci.* 7, 193–195. doi: 10.1016/S1360-1385(02)02251-3

Karpowich, N. K., and Wang, D. N. (2013). Assembly and mechanism of a group II ECF transporter. *Proc. Natl. Acad. Sci. U. S. A.* 110, 2534–2539. doi: 10.1073/pnas.1217361110

Kelley, L. A., Mezulis, S., Yates, C. M., Wass, M. N., and Sternberg, M. J. (2015). The Phyre2 web portal for protein modeling, prediction and analysis. *Nat. Protoc.* 10, 845–858. doi: 10.1038/nprot.2015.053

Kikuchi, S., Oishi, M., Hirabayashi, Y., Lee, D. W., Hwang, I., and Nakai, M. (2009). A 1-megadalton translocation complex containing Tic20 and Tic21 mediates chloroplast protein import at the inner envelope membrane. *Plant Cell* 21, 1781–1797. doi: 10.1105/tpc.108.063552

Kikuchi, S., Bedard, J., Hirano, M., Hirabayashi, Y., Oishi, M., Imai, M., et al. (2013). Uncovering the protein translocon at the chloroplast inner envelope membrane. *Science* 339, 571–574. doi: 10.1126/science.1229262

Kliebenstein, D. J., Monde, R. A., and Last, R. L. (1998). Superoxide dismutase in *Arabidopsis:* an eclectic enzyme family with disparate regulation and protein localization. *Plant Physiol.* 118, 637–650. doi: 10.1104/pp.118.2.637

Kobayashi, T., and Nishizawa, N. K. (2012). Iron uptake, translocation, and regulation in higher plants. *Annu. Rev. Plant Biol.* 63, 131–152. doi: 10.1146/annurev-arplant-042811-105522

Kranzler, C., Rudolf, M., Keren, N., and Schleiff, E. (2013). Iron in cyanobacteria. *Advan. Bot. Res.* 65, 57–105. doi: 10.1016/B978-0-12-394313-2.00003-2

Krieger-Liszkay, A., and Thomine, S. (2018). Importing manganese into the chloroplast: many membranes to cross. *Mol. Plant* 11, 1109–1111. doi: 10.1016/j.molp.2018.07.006

Küchler, M., Decker, S., Hörmann, F., Soll, J., and Heins, L. (2002). Protein import into chloroplasts involves redox-regulated proteins. *EMBO J.* 21, 6136–6145. doi: 10.1093/emboj/cdf621

Lau, C. K., Krewulak, K. D., and Vogel, H. J. (2016). Bacterial ferrous iron transport: the Feo system. *FEMS Microbiol. Rev.* 40, 273–298. doi: 10.1093/femsre/fuv049

Li-Beisson, Y., Shorrosh, B., Beisson, F., Andersson, M. X., Arondel, V., Bates, P. D., et al. (2013). Acyl-lipid metabolism. *Arabidopsis Book* 11, e0161. doi: 10.1199/tab.0161

Li, N., Gügel, I. L., Giavalisco, P., Zeisler, V., Schreiber, L., Soll, J., et al. (2015). FAX1, a novel membrane protein mediating plastid fatty acid export. *PLoS Biology* 13, e1002053. doi: 10.1371/journal.pbio.1002053

Li, X., Ilarslan, H., Brachova, L., Qian, H. R., Li, L., Che, P., et al. (2011). Reverse-genetic analysis of the two biotin-containing subunit genes of the heteromeric acetyl-coenzyme A carboxylase in *Arabidopsis* indicates a unidirectional functional redundancy. *Plant Physiol.* 155, 293–314. doi: 10.1104/pp.110.165910

Lopez-Millan, A. F., Duy, D., and Philippar, K. (2016). Chloroplast iron transport proteins—function and impact on plant physiology. *Front. Plant Sci.* 7, 178. doi: 10.3389/fpls.2016.00178

Lu, B. B., Xu, C. C., Awai, K., Jones, A. D., and Benning, C. (2007). A small ATPase protein of *Arabidopsis,* TGD3, involved in chloroplast lipid import. *J. Biol. Chem.* 282, 35945–35953. doi: 10.1074/jbc.M704063200

Lundquist, P. K., Poliakov, A., Bhuiyan, N. H., Zybailov, B., Sun, Q., and van Wijk, K. J. (2012). The functional network of the *Arabidopsis* plastoglobule proteome based on quantitative proteomics and genome-wide coexpression analysis. *Plant Physiol.* 158, 1172–1192. doi: 10.1104/pp.111.193144

Marchand, J., Heydarizadeh, P., Schoefs, B., and Spetea, C. (2018). Ion and metabolite transport in the chloroplast of algae: lessons from land plants. *Cell. Mol. Life Sci.* 75, 2153–2176. doi: 10.1007/s00018-018-2793-0

Morrissey, J., and Guerinot, M. L. (2009). Iron uptake and transport in plants: the good, the bad, and the ionome. *Chem. Rev.* 109, 4553–4567. doi: 10.1021/cr900112r

Mubarakshina, M. M., Ivanov, B. N., Naydov, I. A., Hillier, W., Badger, M. R., and Krieger-Liszkay, A. (2010). Production and diffusion of chloroplastic H2O2 and its implication to signalling. *J. Ex. Bot.* 61, 3577–3587. doi: 10.1093/jxb/erq171

Müller, B., Pham, H. D., Kovács, K., Kavak, Y., Gyuris, B., Sági-Kazár, M., et al. (2018). "Iron uptake machinery of chloroplasts tends to utilise stoichiometric ferric-citrate complexes in Brassica napus," in *19th International Symposium on Iron Nutrition and Interactions in Plants*. Ed. W. Schmidt (Taipei, Taiwan: Academia Sinica), 40.

Nakai, M. (2015). The TIC complex uncovered: the alternative view on the molecular mechanism of protein translocation across the inner envelope membrane of chloroplasts. *Biochim. Biophys. Acta* 1847, 957–967. doi: 10.1016/j.bbabio.2015.02.011

Neubauer, O., Alfandega, A., Schoknecht, J., Sternberg, U., Pohlmann, A., and Eitinger, T. (2009). Two essential arginine residues in the T components of energy-coupling factor transporters. *J. Bacteriol.* 191, 6482–6488. doi: 10.1128/JB.00965-09

Nouet, C., Motte, P., and Hanikenne, M. (2011). Chloroplastic and mitochondrial metal homeostasis. *Trends Plant Sci* 16, 395–404. doi: 10.1016/j.tplants.2011.03.005

Philippar, K., Geis, T., Ilkavets, I., Oster, U., Schwenkert, S., Meurer, J., et al. (2007). Chloroplast biogenesis: the use of mutants to study the etioplast-chloroplast transition. *Proc. Natl. Acad. Sci. U. S. A.* 104, 678–683. doi: 10.1073/pnas.0610062104

Pohlmeyer, K., Soll, J., Grimm, R., Hill, K., and Wagner, R. (1998). A high-conductance solute channel in the chloroplastic outer envelope from Pea. *Plant Cell* 10, 1207–1216. doi: 10.1105/tpc.10.7.1207

Raven, J. A., Evans, M. C. E., and Korb, R. E. (1999). The role of trace metals in photosynthetic electron transport in O 2 evolving organisms. *Photosynth. Res.* 60, 111–149. doi: 10.1023/A:1006282714942

Ravet, K., Touraine, B., Boucherez, J., Briat, J. F., Gaymard, F., and Cellier, F. (2009). Ferritins control interaction between iron homeostasis and oxidative stress in *Arabidopsis*. *Plant J.* 57, 400–412. doi: 10.1111/j.1365-313X.2008.03698.x

Rayapuram, N., Hagenmuller, J., Grienenberger, J. M., Giege, P., and Bonnard, G. (2007). AtCCMA interacts with AtCcmB to form a novel mitochondrial ABC transporter involved in cytochrome c maturation in *Arabidopsis*. *J. Biol. Chem.* 282, 21015–21023. doi: 10.1074/jbc.M704091200

Rempel, S., Stanek, W. K., and Slotboom, D. J. (2019). Energy-coupling factor-type ATP-binding cassette transporters. *Annu. Rev. Biochem.* 88, 551–576. doi: 10.1146/annurev-biochem-013118-111705

Rodionov, D. A., Hebbeln, P., Gelfand, M. S., and Eitinger, T. (2006). Comparative and functional genomic analysis of prokaryotic nickel and cobalt uptake transporters: evidence for a novel group of ATP-binding cassette transporters. *J. Bacteriol.* 188, 317–327. doi: 10.1128/JB.188.1.317-327.2006

Rodionov, D. A., Hebbeln, P., Eudes, A., ter Beek, J., Rodionova, I. A., Erkens, G. B., et al. (2009). A novel class of modular transporters for vitamins in prokaryotes. *J. Bacteriol.* 191, 42–51. doi: 10.1128/JB.01208-08

Roston, R. L., Gao, J., Murcha, M. W., Whelan, J., and Benning, C. (2012). TGD1, -2, and -3 proteins involved in lipid trafficking form ATP-binding cassette

(ABC) transporter with multiple substrate-binding proteins. *J. Biol. Chem.* 287, 21406–21415. doi: 10.1074/jbc.M112.370213

Rudolf, M., Kranzler, C., Lis, H., Margulis, K., Stevanovic, M., Keren, N., et al. (2015). Multiple modes of iron uptake by the filamentous, siderophore-producing cyanobacterium, Anabaena sp. PCC 7120. *Mol. Microbiol.* 97, 577–588. doi: 10.1111/mmi.13049

Sanchez-Fernandez, R., Davies, T. G., Coleman, J. O., and Rea, P. A. (2001). The *Arabidopsis* thaliana ABC protein superfamily, a complete inventory. *J. Biol. Chem.* 276, 30231–30244. doi: 10.1074/jbc.M103104200

Schwacke, R., Schneider, A., van der Graaff, E., Fischer, K., Catoni, E., Desimone, M., et al. (2003). ARAMEMNON, a novel database for *Arabidopsis* integral membrane proteins. *Plant Physiol.* 131, 16–26. doi: 10.1104/pp.011577

Shanmugabalaji, V., Besagni, C., Piller, L. E., Douet, V., Ruf, S., Bock, R., et al. (2013). Dual targeting of a mature plastoglobulin/fibrillin fusion protein to chloroplast plastoglobules and thylakoids in transplastomic tobacco plants. *Plant Mol. Biol.* 81, 13–25. doi: 10.1007/s11103-012-9977-z

Shimoni-Shor, E., Hassidim, M., Yuval-Naeh, N., and Keren, N. (2010). Disruption of Nap14, a plastid-localized non-intrinsic ABC protein in *Arabidopsis thaliana* results in the over-accumulation of transition metals and in aberrant chloroplast structures. *Plant Cell Environ.* 33, 1029–1038. doi: 10.1111/j.1365-3040.2010.02124.x

Shingles, R., North, M., and McCarty, R. E. (2001). Direct measurement of ferrous ion transport across membranes using a sensitive fluorometric assay. *Anal. Biochem.* 296, 106–113. doi: 10.1006/abio.2001.5209

Shingles, R., North, M., and McCarty, R. E. (2002). Ferrous ion transport across chloroplast inner envelope membranes. *Plant Physiol.* 128, 1022–1030. doi: 10.1104/pp.010858

Solti, A., Kovacs, K., Basa, B., Vertes, A., Sarvari, E., and Fodor, F. (2012). Uptake and incorporation of iron in sugar beet chloroplasts. *Plant Physiol. Biochem.* 52, 91–97. doi: 10.1016/j.plaphy.2011.11.010

Solti, A., Muller, B., Czech, V., Sarvari, E., and Fodor, F. (2014). Functional characterization of the chloroplast ferric chelate oxidoreductase enzyme. *New Phytol.* 202, 920–928. doi: 10.1111/nph.12715

Solti, A., Kovacs, K., Muller, B., Vazquez, S., Hamar, E., Pham, H. D., et al. (2016). Does a voltage-sensitive outer envelope transport mechanism contributes to the chloroplast iron uptake? *Planta* 244, 1303–1313. doi: 10.1007/s00425-016-2586-3

Stengel, A., Benz, P., Balsera, M., Soll, J., and Bolter, B. (2008). TIC62 redox-regulated translocon composition and dynamics. *J. Biol. Chem.* 283, 6656–6667. doi: 10.1074/jbc.M706719200

Swier, L. J., Guskov, A., and Slotboom, D. J. (2016). Structural insight in the toppling mechanism of an energy-coupling factor transporter. *Nat. Commun.* 7, 11072. doi: 10.1038/ncomms11072

Teng, Y. S., Su, Y. S., Chen, L. J., Lee, Y. J., Hwang, I., and Li, H. M. (2006). Tic21 is an essential translocon component for protein translocation across the chloroplast inner envelope membrane. *Plant Cell* 18, 2247–2257. doi: 10.1105/tpc.106.044305

Theodoulou, F. L., and Kerr, I. D. (2015). ABC transporter research: going strong 40 years on. *Biochem. Soc. Trans.* 43, 1033–1040. doi: 10.1042/BST20150139

Thomine, S., and Vert, G. (2013). Iron transport in plants: better be safe than sorry. *Curr. Opin. Plant Biol.* 16, 322–327. doi: 10.1016/j.pbi.2013.01.003

Tyra, H. M., Linka, M., Weber, A. P., and Bhattacharya, D. (2007). Host origin of plastid solute transporters in the first photosynthetic eukaryotes. *Genome Biol.* 8, R212. doi: 10.1186/gb-2007-8-10-r212

UniProt Consortium, T. (2018). UniProt: the universal protein knowledgebase. *Nuc. Acids Res.* 46, 2699. doi: 10.1093/nar/gky092

van Wijk, K. J., and Kessler, F. (2017). Plastoglobuli: plastid microcompartments with integrated functions in metabolism, plastid developmental transitions, and environmental adaptation. *Annu. Rev. Plant Biol.* 68, 253–289. doi: 10.1146/annurev-arplant-043015-111737

Varotto, C., Maiwald, D., Pesaresi, P., Jahns, P., Salamini, F., and Leister, D. (2002). The metal ion transporter IRT1 is necessary for iron homeostasis and efficient photosynthesis in *Arabidopsis thaliana*. *Plant J.* 31, 589–599. doi: 10.1046/j.1365-313X.2002.01381.x

Verrier, P. J., Bird, D., Buria, B., Dassa, E., Forestier, C., Geisler, M., et al. (2008). Plant ABC proteins - a unified nomenclature and updated inventory. *Trends Plant Sci.* 13, 151–159. doi: 10.1016/j.tplants.2008.02.001

Vidi, P. A., Kanwischer, M., Baginsky, S., Austin, J. R., Csucs, G., Dormann, P., et al. (2006). Tocopherol cyclase (VTE1) localization and vitamin E accumulation in chloroplast plastoglobule lipoprotein particles. *J. Biol. Chem.* 281, 11225–11234. doi: 10.1074/jbc.M511939200

Vigani, G., Solti, A., Thomine, S., and Philippar, K. (2019). Essential and detrimental - an update on intracellular iron trafficking and homeostasis. *Plant Cell Physiol.* 60, 1420–1439. doi: 10.1093/pcp/pcz091

Wang, X., Wang, Z., Zheng, Z., Dong, J., Song, L., Sui, L., et al. (2019). Genetic dissection of Fe-dependent signaling in root developmental responses to phosphate deficiency. *Plant Physiol.* 179, 300–316. doi: 10.1104/pp.18.00907

Weber, A. P., and Linka, N. (2011). Connecting the plastid: transporters of the plastid envelope and their role in linking plastidial with cytosolic metabolism. *Annu. Rev. Plant Biol.* 62, 53–77. doi: 10.1146/annurev-arplant-042110-103903

Wilkens, S. (2015). Structure and mechanism of ABC transporters. *F1000Prime Rep.* 7, 14. doi: 10.12703/P7-14

Xu, C., Moellering, E. R., Muthan, B., Fan, J., and Benning, C. (2010). Lipid transport mediated by *Arabidopsis* TGD proteins is unidirectional from the endoplasmic reticulum to the plastid. *Plant Cell Physiol.* 51, 1019–1028. doi: 10.1093/pcp/pcq053

Xu, C. C., Fan, J. L., Riekhof, W., Froehlich, J. E., and Benning, C. (2003). A permease-like protein involved in ER to thylakoid lipid transfer in *Arabidopsis*. *EMBO J.* 22, 2370–2379. doi: 10.1093/emboj/cdg234

Xu, X. M., and Möller, S. G. (2004). AtNAP7 is a plastidic SufC-like ATP-binding cassette/ATPase essential for *Arabidopsis* embryogenesis. *Proc. Natl. Acad. Sci. U. S. A.* 101, 9143–9148. doi: 10.1073/pnas.0400799101

Yamada, K., Lim, J., Dale, J. M., Chen, H., Shinn, P., Palm, C. J., et al. (2003). Empirical analysis of transcriptional activity in the *Arabidopsis* genome. *Science* 302, 842–846. doi: 10.1126/science.1088305

Yruela, I. (2013). Transition metals in plant photosynthesis. *Metallomics* 5, 1090–1109. doi: 10.1039/c3mt00086a

Ytterberg, A. J., Peltier, J. B., and van Wijk, K. J. (2006). Protein profiling of plastoglobules in chloroplasts and chromoplasts. A surprising site for differential accumulation of metabolic enzymes. *Plant Physiol.* 140, 984–997. doi: 10.1104/pp.105.076083

Zeng, X., Tang, R., Guo, H., Ke, S., Teng, B., Hung, Y. H., et al. (2017). A naturally occurring conditional albino mutant in rice caused by defects in the plastid-localized OsABCI8 transporter. *Plant Mol. Biol.* 94, 137–148. doi: 10.1007/s11103-017-0598-4

Zeth, K., and Thein, M. (2010). Porins in prokaryotes and eukaryotes: common themes and variations. *Biochem. J.* 431, 13–22. doi: 10.1042/BJ20100371

Zhang, B., Zhang, C., Liu, C., Jing, Y., Wang, Y., Jin, L., et al. (2018). Inner envelope CHLOROPLAST MANGANESE TRANSPORTER 1 supports manganese homeostasis and phototrophic growth in *Arabidopsis*. *Mol. Plant* 11, 943–954. doi: 10.1016/j.molp.2018.04.007

Zimorski, V., Ku, C., Martin, W. F., and Gould, S. B. (2014). Endosymbiotic theory for organelle origins. *Curr. Oppin Microbiol.* 22, 38–48. doi: 10.1016/j.mib.2014.09.008

Conflict of Interest: The authors declare that the research was conducted in the absence of any commercial or financial relationships that could be construed as a potential conflict of interest.

frontiers in Plant Science

ORIGINAL RESEARCH
published: 19 November 2019
doi: 10.3389/fpls.2019.01487

Automated Imaging, Tracking, and Analytics Pipeline for Differentiating Environmental Effects on Root Meristematic Cell Division

Eli Buckner[1†], Imani Madison[2†], Hsuan Chou[2], Anna Matthiadis[2], Charles E. Melvin[2], Rosangela Sozzani[2], Cranos Williams[1] and Terri A. Long[2*]*

[1] Electrical and Computer Engineering Department, North Carolina State University, Raleigh, NC, United States, [2] Plant and Microbial Biology Department, North Carolina State University, Raleigh, NC, United States

OPEN ACCESS

Edited by:
Thomas J. Buckhout, Humboldt University of Berlin, Germany

Reviewed by:
Dierk Wanke, University of Tübingen, Germany
Marta Wilton Vasconcelos, Catholic University of Portugal, Portugal

***Correspondence:**
Cranos Williams
cmwilli5@ncsu.edu
Terri A. Long
terri_long@ncsu.edu

†These authors have contributed equally to this work

Specialty section:
This article was submitted to Plant Nutrition, a section of the journal Frontiers in Plant Science

Received: 27 February 2019
Accepted: 28 October 2019
Published: 19 November 2019

Citation:
Buckner E, Madison I, Chou H, Matthadis A, Melvin CE, Sozzani R, Williams C and Long TA (2019) Automated Imaging, Tracking, and Analytics Pipeline for Differentiating Environmental Effects on Root Meristematic Cell Division. Front. Plant Sci. 10:1487. doi: 10.3389/fpls.2019.01487

Exposure of plants to abiotic stresses, whether individually or in combination, triggers dynamic changes to gene regulation. These responses induce distinct changes in phenotypic characteristics, enabling the plant to adapt to changing environments. For example, iron deficiency and heat stress have been shown to alter root development by reducing primary root growth and reducing cell proliferation, respectively. Currently, identifying the dynamic temporal coordination of genetic responses to combined abiotic stresses remains a bottleneck. This is, in part, due to an inability to isolate specific intervals in developmental time where differential activity in plant stress responses plays a critical role. Here, we observed that iron deficiency, in combination with temporary heat stress, suppresses the expression of iron deficiency-responsive pPYE::LUC (POPEYE::luciferase) and pBTS::LUC (BRUTUS::luciferase) reporter genes. Moreover, root growth was suppressed less under combined iron deficiency and heat stress than under either single stress condition. To further explore the interaction between pathways, we also created a computer vision pipeline to extract, analyze, and compare high-dimensional dynamic spatial and temporal cellular data in response to heat and iron deficiency stress conditions at high temporal resolution. Specifically, we used fluorescence light sheet microscopy to image *Arabidopsis thaliana* roots expressing CYCB1;1:GFP, a marker for cell entry into mitosis, every 20 min for 24 h exposed to either iron sufficiency, iron deficiency, heat stress, or combined iron deficiency and heat stress. Our pipeline extracted spatiotemporal metrics from these time-course data. These metrics showed that the persistency and timing of CYCB1;1:GFP signal were uniquely different under combined iron deficiency and heat stress conditions versus the single stress conditions. These metrics also indicated that the spatiotemporal characteristics of the CYCB1;1:GFP signal under combined stress were more dissimilar to the control response than the response seen under iron deficiency for the majority of the 24-h experiment. Moreover, the combined stress response was less dissimilar to the control than the response seen under heat stress. This indicated that pathways activated when the plant is exposed to both iron deficiency and heat stress affected CYCB1;1:GFP spatiotemporal function antagonistically.

Keywords: light sheet imaging, image analysis, cell cycle progression, heat stress and iron deficiency stresses, combined stresses

INTRODUCTION

Abiotic stresses, such as low iron bioavailability (iron deficiency, −Fe) or high ambient temperatures (heat stress, Heat), negatively impact key important plant processes, including growth, development, and reproduction. The effects of iron deficiency stress range from impaired chlorophyll biosynthesis and chloroplast maintenance in shoots to reduced cellular respiration and mitochondrial development in roots (Thimm et al., 2001; López-Bucio et al., 2003; Rout and Sahoo, 2015). Additionally, iron deficiency generally results in reduced primary root growth in favor of increased lateral root growth due to modulations in cell division within the primary and lateral root meristems (López-Bucio et al., 2003; Gharagozloo et al., 2008; Gruber et al., 2013; Hilo et al., 2017). Similarly, heat stress impairs photosynthesis, resulting in reduced biomass, reduced primary root growth, and arrested cell division within the root meristem (Larkindale et al., 2005; Wahid et al., 2007; Zhao et al., 2014). Overall, heat stress impairs many cellular processes via a cytotoxic accumulation of Reactive Oxygen Species (ROS), while also hindering enzyme and membrane function (Larkindale et al., 2005; Mangelsen et al., 2011; Tsukagoshi, 2012). Heat stress also increases the rate of cells transitioning into the elongation zone within the root meristem (Feraru et al., 2019). At its most severe, heat stress causes apoptosis (Larkindale et al., 2005). Moreover, heat stress has been implicated in several unrelated stress pathways, such as heavy metal and oxidative stresses (Larkindale et al., 2005; Kilian et al., 2007; Swindell et al., 2007; Hahn et al., 2013). While these stress response studies have shed light on many physiological and molecular effects, iron deficiency stress and heat stress responses have been traditionally studied in isolation. Given that, in field conditions, it is common for plants to experience stresses in combination rather than as isolated stress events (Thimm et al., 2001; Suzuki et al., 2014; Corrales et al., 2017; Carvalho et al., 2018), it is necessary to understand the existence of any interplay between stress response pathways when plants are exposed to multiple stresses. Experimental and computational tools that extract spatial and temporal similarities/differences in the molecular response of plants under both combinatorial and individual stresses would provide insight into the existence of interplay between two stress response pathways. This type of analysis requires quantifying how these stresses, both individually and combinatorially, contribute to the magnitude of each respective stress response with respect to a control condition. This analysis requires identifying the existence of an interaction between stress pathways. If there is interaction, it is also necessary to understand how the interaction influences function (antagonistically or agonistically).

While recent studies have indicated that there does not exist a universal stress regulator in plants, there is evidence for commonality in transcriptional regulation within groups of stress types, particularly in heat stress responses (Kilian et al., 2007; Swindell et al., 2007; Iyer-Pascuzzi et al., 2011; Kilian et al., 2012; Hahn et al., 2013; Zandalinas et al., 2018). A commonly observed phenomenon for the response of plants under stress is a change in cell cycle progression in actively proliferating regions such as the root meristem (Skirycz et al., 2011). Obtaining data that quantifies the time, location, and duration in which cell cycle progression is altered under single and combinatorial stress conditions could provide substantial insight into the interplay between iron deficiency and heat stress response pathways that are activated under combinatorial stress conditions. These data may also provide quantitative insight into how plants regulate overall cell proliferation; a key aspect of organ growth (Sakamoto et al., 2016).

In this work, we theorize that the comparison of spatiotemporal cell cycle patterns extracted from single and combinatorial stress data may allow us to 1) infer the temporal characteristics of stress specific pathways under combinatorial stress conditions, and 2) decipher whether stress specific pathways interact with one another and if that interaction functions antagonistically. We first quantified the dynamics of transcriptional luciferase fusions for two known −Fe response genes, POPEYE (PYE) and BRUTUS (BTS) in response to iron deficiency stress (−Fe), heat stress (Heat), and a combination of both stresses (−Fe+Heat). Since plants can be exposed to high temperature fluctuations over a 24-h period in field conditions, heat stress experimental regimes typically involve a short application of heat (60–90 mins) (Yeh et al., 2012; Silva-Correia et al., 2014). For this reason, we chose to implement heat stress by applying 38°C for 80 min. However, we applied iron deficiency stress for the full 24 h because this is a nutritional stress that plants are more commonly exposed to for days or longer. We observed that under the combinatorial −Fe+Heat stress condition, transcriptional activation of these genes is suppressed by Heat within the 24-h time frame, revealing antagonism between the output of these stress pathways with respect to these −Fe response genes. To gain further insight into how these combinatorial stress conditions affect molecular mechanisms associated with root development, we developed a computational approach to extract non-iron deficiency specific high-dimensional data from microscopy images obtained after exposing *Arabidopsis thaliana* seedlings expressing CYCB1;1:GFP (a proxy for cell entry into division) (Menges et al., 2005; de Luis Balaguer et al., 2016; Schnittger and De Veylder, 2018) to these conditions. We used Light Sheet Fluorescence Microscopy (LSFM), which offers low phototoxicity in fluorescent molecules, to acquire high temporal imaging data over 24-h time-course experiments (Reynaud et al., 2015; Ovečka et al., 2018). We developed the BioVision Tracker (BVT) image analysis pipeline to analyze root growth dynamics and track CYCB1;1:GFP expression within the meristematic region of the root over time. We used these tracking data to extract spatiotemporal metrics, which captured similarities and differences in spatiotemporal CYCB1;1:GFP expression patterns over fine intervals of time in response to −Fe, Heat, and −Fe+Heat. We show that our computational pipeline was capable of extracting useful spatiotemporal metrics from high throughput microscopy images, which revealed that Heat and −Fe responses interact with one another in an antagonistic manner. This technology facilitates the design of further studies with unprecedented specificity into how simultaneous plant stress responses function on a given output, which will potentially inform agricultural efforts in maintaining consistent crop growth despite impending climate and environmental changes.

RESULTS

Iron Deficiency Responsive Genes Are Suppressed When Introduced to Both Iron Deficiency and Heat Shock

To gain insight into if and how Heat stress affects the –Fe response under combinatorial stress, we examined the dynamics of transcriptional luciferase fusions for two known –Fe response genes, *POPEYE* and *BRUTUS* in *A. thaliana* seedlings. PYE acts as a regulator to many iron deficiency-specific genes while BTS is tightly coregulated with PYE such that both genes are transcriptionally induced in response to –Fe (Long et al., 2010). Two independent transgenic lines expressing pPOPEYE::luciferase (pPYE::LUC4-2 and pPYE::LUC5-5) or BRUTUS::luciferase (pBTS::LUC5-1 and pBTS::LUC2-3) were exposed to either 1) control media (Control); 2), –Fe media (–Fe), 3) control media and subjected to 80 min of heat stress (Heat); or 4) –Fe media and subjected to 80 min of heat stress (–Fe+Heat) (**Figures 1A**, **B**; see *Materials and Methods*). We performed a bioluminescence assay for our treatments to measure p*BTS::LUC* and p*PYE::LUC* expression levels in response to our variety of stress conditions. We observed that the expression levels of p*PYE::LUC* and p*BTS::LUC* were significantly higher for –Fe compared to the Control and Heat conditions within 12 h of the experiment ($p < 0.05$) (**Figures 1C, D** and **Supplementary Figure 2**). This was expected since *POPEYE* and *BRUTUS* are upregulated within 12 h of –Fe induction based on previous studies (Long et al., 2010). However, the expression levels were significantly higher under the –Fe than under the –Fe+Heat condition within 16 h for p*BTS::LUC* and within 18 h for p*PYE::LUC* ($p < 0.05$). This result was unexpected since BRUTUS and POPEYE are not known to be heat stress-responsive and it was not anticipated that exposure to –Fe+Heat would significantly disrupt the expression of either *BRUTUS* or *POPEYE*. These statistically different expression profiles suggest that there was interaction between the two pathways under a combination of stress. Furthermore, p*BTS::LUC* and p*PYE::LUC* expression levels appear to be suppressed when Heat is added in combination to –Fe which suggests the pathways are functioning antagonistically with one another. Therefore, we investigated further into the interplay of these two stress pathways by looking at root growth and molecular markers correlated with root growth and cell division that are not specific to either stress to determine if there exist similar antagonistic characteristics on the root itself.

Imaging Pipeline and Root Growth Assay Shows Root Growth Rate is Higher in –Fe+Heat Than in –Fe or Heat Alone

To gain insight into these stress responses at the molecular and physiological level, we grew *A. thaliana* CYCB1;1:GFP seedlings in a MAGIC growth and imaging chamber (de Luis Balaguer et al., 2016) for 4 days and subsequently imaged them by a light sheet microscope every 20 min for 24 h under the same conditions as was used in the luciferase assay (**Figures 2A**, **B**). Since cell division is a contributor to root growth, second to root cell elongation, we chose CYCB1;1:GFP as a proxy for cell division because of its significant involvement in signaling mitosis (López-Bucio et al., 2003; Tsukagoshi, 2012). We chose to observe CYCB1;1:GFP every 20 min because CYCB1;1 expression, on average, has a duration of 3 h, which gave us about nine samples per occurrence (Yin et al., 2014). Using the digital images from both the fluorescent and brightfield channels of the light sheet microscope, we segmented, processed, and tracked CYCB1;1:GFP Regions of Interest (ROI) within the root

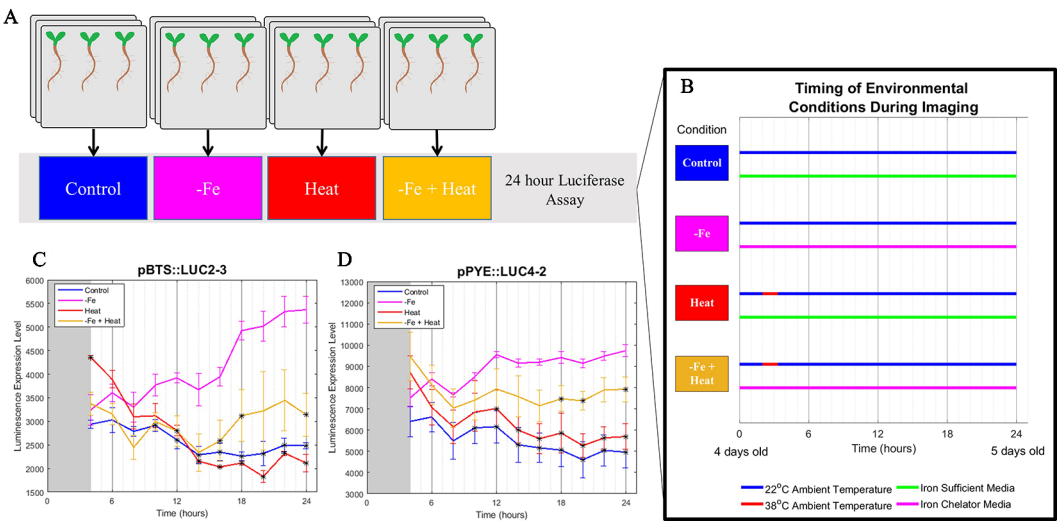

FIGURE 1 | Bioluminescence assay on POPEYE and BRUTUS. **(A**, **B)** A 24-h bioluminescence assay was performed to measure the expression levels of two major iron deficiency response genes POPEYE (PYE) and BRUTUS (BTS). Two lines each of pPYE::LUC (pPYE::LUC5-5 and pPYE::LUC4-2) and pBTS::LUC (pBTS::LUC5-1 and pBTS::LUC2-3) seedlings were grown on plates for 4 days and then exposed to Control, –Fe, Heat, or –Fe+Heat conditions (three biological replicates containing three seedlings for each condition). **(C**, **D)** Imaging began at 4 h and was conducted every 2 h following. These luminescence expression signals show that the expression of BRUTUS and POPEYE were suppressed over time when the seedlings were introduced to –Fe+Heat in comparison to –Fe (*$p < 0.05$ in comparison to the –Fe condition using a two-sample t-test). Here, lines pBTS::LUC2-3 and pPYE::LUC4-2 are shown, whereas supplementary material shows all four lines. Error bars show the standard error across biological replicates.

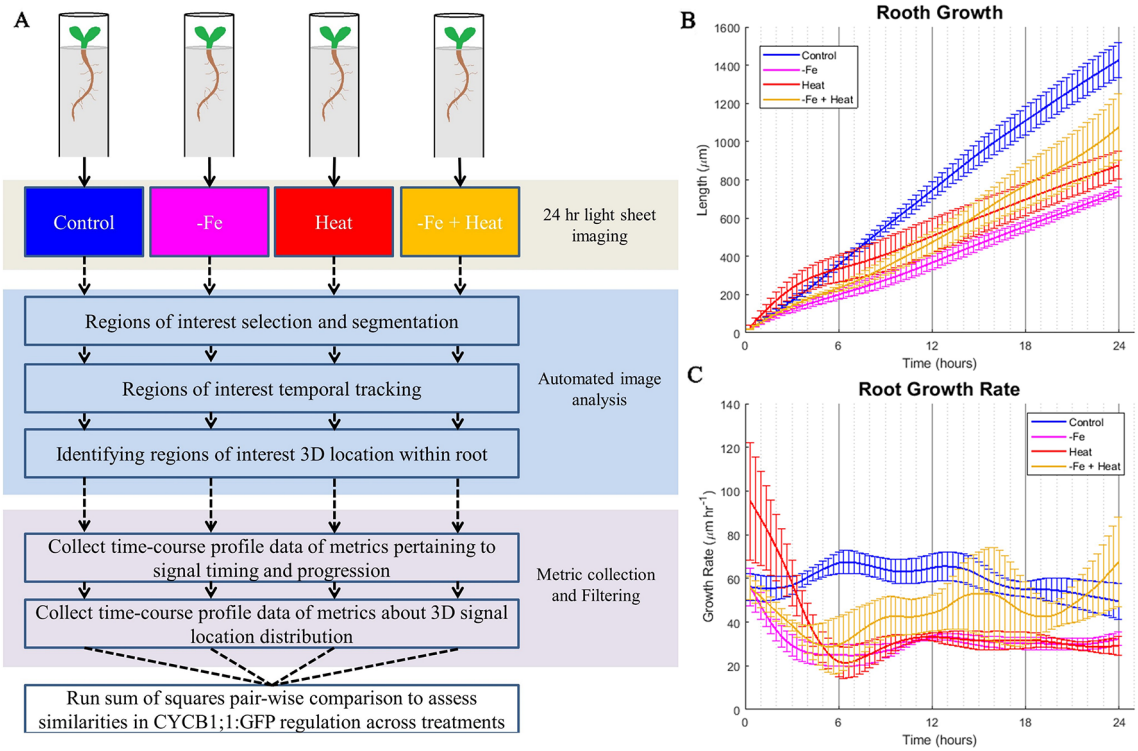

FIGURE 2 | Overall computational pipeline and root growth assays. **(A)** The overall flow of our experimental setup and computational approach. *A. thaliana* plants were grown in FEP tubes for 4 days and then treated to 1 of 4 of the same environmental conditions as the luciferase assay for 24 h while being imaged within the ZEISS Lightsheet Z.1 every 20 min. CYCB1;1:GFP, a proxy for entry into cell division, was visualized through a fluorescent channel. The images were then processed to segment, track, and locate CYCB1;1:GFP fluorescent regions of interest within the 3D locations of the root. Then, metrics were derived from the automated image analysis data to give temporal profiles of spatiotemporal CYCB1;1 data from fluorescent signals. These profiles were used to quantify similarities of cell division regulation across stress conditions. The total root growth during the course of the experiment **(B)** and the root growth rate **(C)** was recorded every 20 min over the 24 experiment for n = 3 to 4 biological replicates.

with our custom automated image analysis software as described below in Development of an Automated Image Analysis Software to Extract Quantitative Spatiotemporal Metrics of CYCB1;1:GFP (adapted from Buckner et al., 2018). We utilized the tracking portion of our pipeline to assess root growth by quantifying the global movement of the root between sequential images. These data were collected every 20 min, aggregated into a time signal, and filtered using a low-pass filter to reduce noise and jitter (see *Materials and Methods*). As expected, the –Fe, Heat, and –Fe+Heat conditions resulted in stunted overall root growth within the scope of the 24-h experiment (**Figure 2B**). However, for the –Fe+Heat condition, the total root growth over the 24 h was more than the total root growth under either of the individual stress conditions (**Figure 2B**). By observing the root growth rate over time (**Figure 2C**) we were able to conclude that after 5 h of the experiment, the rate in which roots undergoing –Fe+Heat conditions were growing was faster than the roots undergoing –Fe or Heat conditions individually. This suggests that due to the response to both of these stresses, an interaction between pathways may have occurred to result in increased root growth rate. Although our assay does not indicate the specific molecular mechanism by which this interaction occurred, the interaction appear antagonistic since the suppression of root growth was decreased under the combinatorial condition.

To further assess the characteristics that this combination of stresses induced at the molecular level, we modified our existing computational pipeline (Buckner et al., 2018) to provide an automated process for collecting temporal characteristics of cells newly expressing CYCB1;1:GFP as well as the perdurance of CYCB1;1:GFP signal. It also collected spatial information of where in the root the CYCB1;1:GFP signal was detected. These CYCB1;1:GFP ROI tracking data were used to generate profiles of 10 spatiotemporal metrics (Material and Methods) over the 24-h experimental period. The temporal profiles of these 10 metrics were analyzed and compared numerically using a sum of squares approach to quantify similarities and differences between single and combinatorial stress responses (**Figure 2A**).

Development of an Automated Image Analysis Software to Extract Quantitative Spatiotemporal Metrics of CYCB1;1:GFP

We developed the BioVision Tracker (BVT) image analysis software to track ROIs in the time course microscopy images using a method that we adapted from our previously developed algorithm (Buckner et al., 2018). BVT first processes 3D fluorescence microscopy images (**Figure 3A**) by selecting ROIs

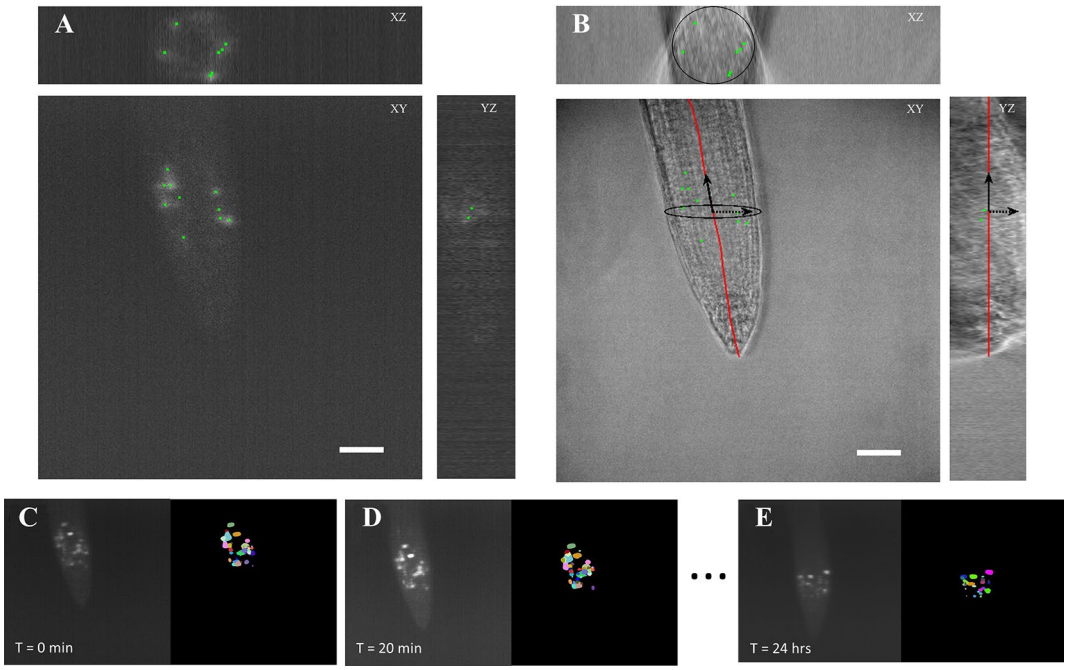

FIGURE 3 | Automated image analysis on 3D light sheet microscopy images. **(A)** A 3D fluorescent image was taken every 20 min capturing ROIs of the CYCB1;1:GFP signal. The image analysis software distinguished the different ROIs as individual instances. **(B)** A corresponding 3D brightfield image was taken every 20 min in the light sheet growth chamber to capture the overall structure of the *A. thaliana* root. The ROI locations were on to the processed coordinate system of the root. Scale bars = 50 μm. **(C–E)** Segmentation and tracking of the 3D images max projected onto 2D images. Segmented ROIs of the same color indicates the same region in different time stamps.

using an image intensity threshold and segmenting each ROI using a watershed algorithm for each image in the time-course (**Figures 3C–E**). BVT then uses image registration techniques to track the movement of the ROIs within the scope of the microscope's field of view over time (**Figures 3C–E**). Additionally, BVT is able to define a root-specific coordinate system that localizes the ROIs within specific portions of the root by processing the 3D images from the Brightfield channel (**Figure 3B**). This is done by using an unsupervised clustering algorithm on the Brightfield image's gradient data to estimate which voxels in the image contain root tissue and which do not (Buckner et al., 2018).

We processed the images taken by the light sheet using the BVT software to provide tracking information about ROIs that fluoresce the CYCB1;1:GFP signal in the meristematic region of the roots. We extracted two major categories of data from this software: 1) the location of each ROI with respect to the distance from the tip of the root and the longitudinal axis and 2) the tracking information about which ROIs continued to produce signal in sequentially sampled images and for how long (**Figure 3**). These data were aggregated for each environmental condition (Control, −Fe, Heat, and −Fe+Heat) and used to produce 10 spatiotemporal metrics that capture the characteristics of the CYCB1;1:GFP signal under single and combinatorial stress.

The 10 spatiotemporal metrics, derived from the BVT tracking data characterized the spatiotemporal CYCB1;1:GFP ROI dynamics for each condition in 20-min increments over the 24-h experimental period. **Table 1** gives the definition of 6 of the 10 metrics, along with the biological implications as it relates to CYCB1;1:GFP. The remaining four metrics are described in the *Materials and Methods*. **Figure 4** shows 6 of the 10 spatiotemporal metrics that were collected to measure the temporal dynamics of the CYCB1;1:GFP expression. The additional four metrics were collected to measure overall spatial distributions of CYCB1;1:GFP signal over time with respect to the distance from the tip and the longitudinal axis of the root and are shown in **Supplementary Figure 1**.

The data from each of the 10 metrics were transformed into 10 time signals using a low pass digital filter across all conditions. The value of the time signal at a given time stamp was computed by averaging the data for the corresponding metric around that specific time (see *Materials and Methods*). This approach provided a way of reducing noise and jitter in the spatiotemporal metrics as sliding windows can behave much like a low pass filter. We first observed that the metrics describing spatial measurements did not show obvious distinctive differences between the temporal profiles of the different environmental conditions (**Supplementary Figure 1**). However, we found that CYCB1;1:GFP timing and progression were both greatly affected and highly dynamic under iron deficiency stress, heat stress, and a combination of both stresses when compared to the control over 24 h (**Figure 3**, **Table 1**).

To assess how single and combinatorial stresses altered CYCB1;1:GFP expression duration with respect to the control, we further examined the metrics associated with persistency (PERSISTENCY AVERAGE, PERSISTENCY SPREAD, and PERSISTENT ADDITIVE) and timing (AVERAGE NUMBER, NEW APPEARANCES, and TRACK END) in greater detail. We first examined metrics associated with persistency, or the amount

TABLE 1 | Temporal metric descriptions.

Metric	Technical description	Biological description (CYCB1;1)
PERSISTENCY AVERAGE	Each ROI tracked from the software has a persistency value which is the amount of time (in hours) that ROI has been and will be tracked from the images. This metric is the average persistency measure of ROIs at a time point.	An increase in this metric suggests a longer sustained CYCB1;1 signal
PERSISTENCY SPREAD	The standard deviation of persistency measures of the ROIs at a time point.	An increase in this metric suggests that the duration of time of sustained CYCB1;1 signal in cells is highly variable.
PERSISTENT ADDITIVE	The cumulative sum of all ROI persistency measures at a time point.	An increase in this metric suggests higher overall CYCB1;1 production in the meristematic region
AVERAGE NUMBER	The number of ROIs detected by the software at a time point.	An increase in this metric suggests more individual cells are producing CYCB1;1
NEW APPEARANCES	The number of ROIs that first appear at a time point.	An increase in this metric suggests more cells are beginning to produce CYCB1;1
TRACK END	The number of ROIs that cease to be tracked at a time point	An increase in this metric suggests more cells are ceasing to produce CYCB1;1

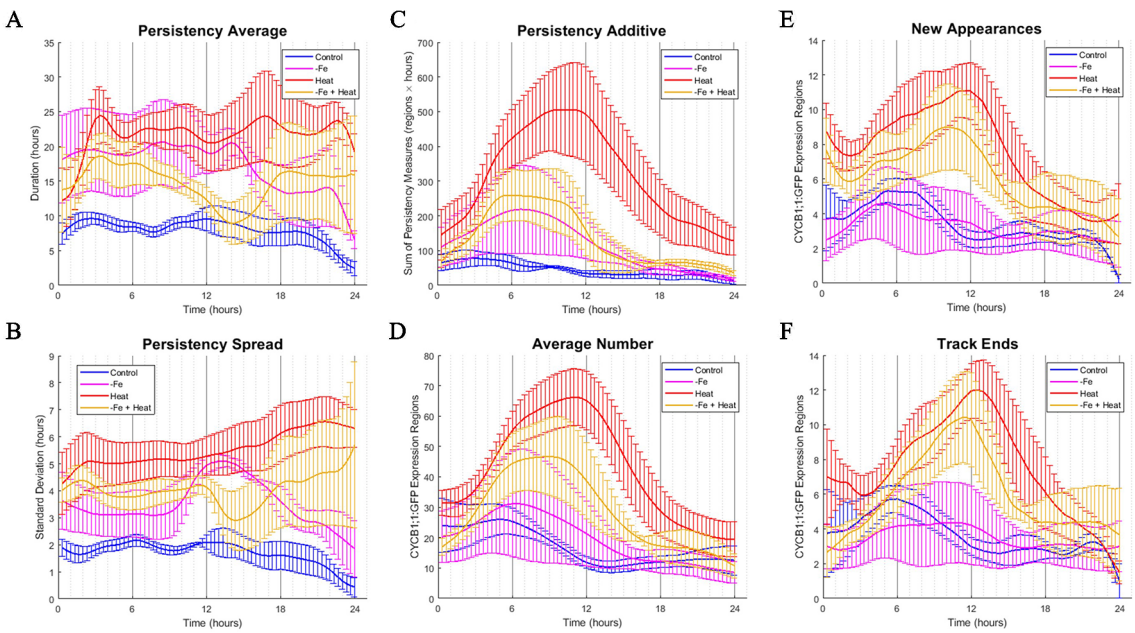

FIGURE 4 | Time-course profiles of individual metrics obtained from the image analysis software. **(A–F)** Metrics obtained from image analysis of all conditions over a 24-h time period. Error bars indicate standard error from the biological replicates (n = 3 to 4). **(A)** PERSISTENCY AVERAGE metric showing the average time (in hours) that ROIs were tracked. This corresponds to how long cells were expressing CYCB1;1:GFP. **(B)** PERSISTENCY SPREAD metric showing the standard deviation of ROI persistency measures. This corresponds to the variety of lengths of time that cells expressed CYCB1;1:GFP. **(C)** PERSISTENT ADDITIVE metric showing the cumulative sum of persistency measures from detected ROIs at any one time. **(D)** AVERAGE NUMBER metric showing the average number of ROIs detected by the software at any one time. An increase in AVERAGE NUMBER corresponds to an increased number of cells producing CYCB1;1:GFP **(E)** NEW APPEARANCES metric showing the average number of newly appearing ROIs at any one time. This corresponds to the average number of new cells expressing CYCB1;1:GFP **(F)** TRACK END metric showing the average number of ROIs ceasing to be tracked by the software at any one time.

of time (in hours) a uniquely identified ROI is tracked, as it relates to the average persistency across all detected ROIs at a given time stamp (PERSISTENCY AVERAGE), the variation around this average, (PERSISTENCY SPREAD), and additive sum of persistency of all detected ROIs (PERSISTENT ADDITIVE). These signals are shown in **Figures 4A–C**, respectively. We note that overall, under control conditions, these metrics remain constant with little variation. This suggests that the progression of cell cycle remains relatively constant for the portion of the cycle in which CYCB1;1:GFP is active over a 24-h period when no stress is applied. We also look at metrics associated with the timing of CYCB1;1:GFP characteristics, such as the average number of ROIs detected at a given time stamp (AVERAGE NUMBER), the number of new ROIs that appear at that time stamp (NEW APPEARANCES), and the number of ROIs that are no longer detectable at that time point (TRACK END). These signals are shown in **Figures 4D–F**, respectively. For the control, **Figures 4D–F** showed a maximum value around 6 h for these timing metrics, indicating that under control conditions regions currently expressing, starting to express, and ceasing to express CYCB1;1:GFP had peaked around this time. We compared the characteristics of these timing and persistency metrics under

control conditions to the metrics obtained under −Fe, Heat, and −Fe+Heat conditions to assessing differences in magnitude and temporal characteristics.

We observed that the PERSISTENCY AVERAGE and PERSISTENCY SPREAD signals were consistently higher for all three stress conditions than for the control while also maintaining larger variation throughout most of the 24-h window (**Figures 4A**, **B**). These results suggest that there is an increase in the length of time uniquely identified ROIs are tracked under these stresses which could potentially imply a stall in cell cycle, specifically during the stage of mitosis. While the data suggests increased persistence for all three stress conditions, the profiles of these two metrics for the −Fe+Heat condition does not appear to strictly follow that of either single stress. Furthermore, it appears that the PERSISTENCY AVERAGE of the −Fe+Heat condition was lower than either single stress which may be associated with higher growth rates for this condition especially between 12 and 18 h in which −Fe+Heat and Control values of PERSISTENCY AVERAGE overlapped closely. During the same 12–18-h period, root growth rate (**Figure 2C**) under −Fe+Heat conditions accelerated to similar growth rates under Control conditions, which never occurred in either single stresses. Overall, this suggests a unique response in CYCB1;1:GFP persistency that correlates with altered root growth rate induced by combining −Fe and Heat.

The PERSISTENT ADDITIVE and AVERAGE NUMBER signals (**Figures 4C**, **D**) show similar increases in all three stress conditions in that all three contained a peak between 3 and 12 h. Thus, the data that our software collected was able to capture specific time points in which events associated with cell division spike. This spike could be explained by 1) the duration of time that cell division was being prolonged was increased for all stress conditions, 2) the rate in number of cells initiating division was larger than the rate of cells actually dividing, and/or 3) there was an increase of stress-induced DNA damage in cells since CYCB1;1 has also been shown to be produced in earlier stages of the cell cycle after DNA damage occurs is present in the cell (Schnittger and De Veylder, 2018). However, further experiments examining these time points would be needed to further conclude specifics about the effects of iron and heat stress on the cell cycle.

Finally, we examine the characteristics of the NEW APPEARANCES and TRACK END signals under stress conditions and compare them to the characteristics seen under the control. For the NEW APPEARANCES signal, we observed that for Heat, the increase of newly appearing ROIs was sustained and peaked around 12 h in contrast to both the control and −Fe conditions, which were sustained but peaked at less than 6 h. Finally, for the TRACK END signal, we observed delayed peaks for each stress condition compared to the control, where the peaks for each stress condition were located around 12 h.

Our computational approach allowed us to collect information that captured the dynamics of many spatiotemporal cell cycle characteristics in response to stress at an unprecedented resolution. Our method allowed us to extract many observations by expanding the data collected from image analysis into quantitative metrics. We observed that CYCB1;1:GFP was perdured in response to all three types of stress introduced here. We also found that many of the profiles for the −Fe+Heat condition had peaks and valleys at different times than either the −Fe or Heat conditions alone and, in most cases, the magnitude of response was different in −Fe+Heat than the profiles of either −Fe or Heat. This suggests that the time and the degree to which plants respond to −Fe+Heat with respect to CYCB1;1:GFP is distinct from that which occurs in response to −Fe or Heat individually. Therefore, we further investigated by aggregating all metrics collectively in a high-dimensional space to assess when, and to what degree, plants initiate specific stress responses, and how combining these stresses might affect these responses.

Image Analysis Reveal That Characteristics of CYCB1;1:GFP in Combined Stress Are Different Than Single Stresses

To identify similarities in spatiotemporal CYCB1;1:GFP behaviors between experimental conditions, we computed the sum of squared difference (SS) across all 10 metrics for all pairwise combination of stress vs. the control at each 20-min time point. Each metric was normalized between 0 and 1 so that no single metric would bear more weight than another. **Figure 5A** shows the SS values for each stress condition in comparison to the control. Note that a larger SS value corresponds to increased dissimilarity between the compared conditions.

We found that the spatiotemporal CYCB1;1:GFP data of the Heat and −Fe+Heat stress conditions diverged in behavior from the control early in the time course, which is indicated by increasing SS values for these curves within the first 3 h (**Figure 5A**), whereas the −Fe condition diverges very slightly from the control throughout the entire 24-h span. The SS values comparing the similarity between the Heat and Control conditions show distinctively different characteristics compared to the −Fe vs. Control profile in magnitude and timing, showing intervals of both increasing dissimilarity (0–12 h and 20–24 h, **Figure 5A**) and decreasing dissimilarity (12–20 h, **Figure 5A**). SS values for the −Fe+Heat vs. Control are different in magnitude from the aforementioned SS values, where the characteristics are more similar to the control than the Heat condition but less similar to the control than the −Fe experiment for most of the time course. This was further affirmed by looking at the integration of these SS signals over the entire 24-h experiment to assess overall dissimilarity (**Figure 5B**). This suggests that, according to our pipeline analysis, an interaction between stress pathways exists, but the overall effect on CYCB1;1:GFP expression is antagonistic.

DISCUSSION AND CONCLUSION

Abiotic stresses affect development, in part, by altering the size, shape and number of cells, which is controlled by progression through the cell cycle. Our computational approach of using image analysis to quantify root growth showed that growth was inhibited more in −Fe and Heat conditions than in −Fe+Heat conditions. Furthermore, our approach was used to extract spatiotemporal gene expression data. This allowed us to observe many aspects of how and when CYCB1;1:GFP patterns are altered due to iron deficiency stress, heat stress, and a combination of both conditions, which have certain implications on cell division. We found that

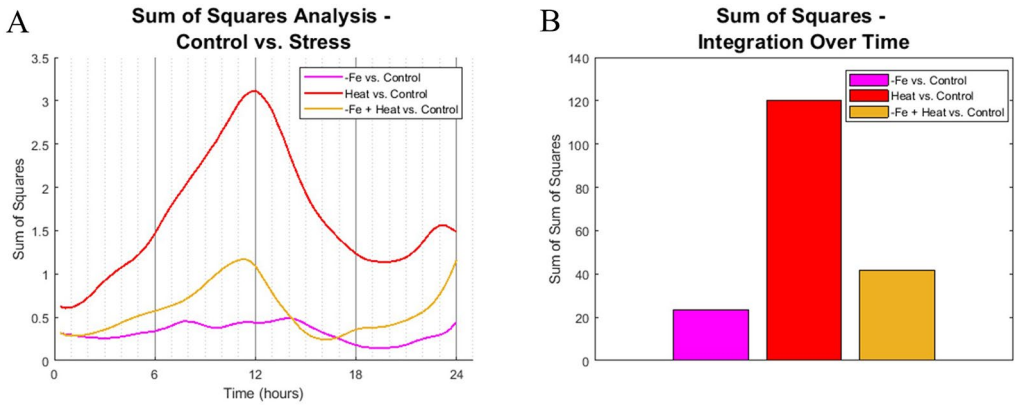

FIGURE 5 | Sum of squares comparison of conditions. **(A)** Sum of squares analysis was performed every 20 min interval by comparing the high dimensional CYCB1;1:GFP data of stress-inducing experiments to the control. **(B)** The profiles from **(A)** were integrated across time to get overall dynamic similarities between treatments.

overall, CYCB1;1 spatiotemporal patterns were affected by both of these stresses individually and combinationatorially in as early as 3 h. However, the timing and magnitude to which they were affected appeared to differ under combined stress condition compared to single stress conditions alone. Our observation of CYCB1;1:GFP tracking revealed there to be an apparent temporal relationship between the temporal prolonging of CYCB1;1:GFP expression and root growth inhibition which could explain the increased root growth in the −Fe+Heat condition since the combined stress condition had overall lower PERSISTENCY AVERAGE; however, root growth is a physiological outcome that is controlled by a network of genes, and by assessing the characteristics of CYCB1;1:GFP, one may not be able to conclude causation of root growth, particularly because root cell elongation had likely been affected by either stress, which would also contribute to root elongation. Thus, we show how our approach has the potential to reveal underlying mechanisms by observing molecular and organ level characteristics at high temporal resolution. We conclude from these observations that these two stress pathways could interact which may cause the plant to regulate genes in a completely unique way apart from iron deficiency or heat stresses alone resulting in an antagonistic outcome on the biological reporters we have selected.

Our results are consistent with previous studies that have concluded not only that plant gene regulation cannot be predicted in many combinatorial stresses just by observing the regulation of each stress response individually, but also that combinatorial stresses trigger unique stress responses relative to that of single stress responses (Kilian et al., 2012; Rivero et al., 2014). Moreover, with respect to iron-centric studies, increased iron availability is implicated in promoting both root meristematic cell division and *CYCB1* expression in petunia and has established roles in regulating primary root elongation (Landsberg, 1996; López-Bucio et al., 2003; Gharagozloo et al., 2008; Gruber et al., 2013; Hilo et al., 2017). Furthermore, heat stress is also known to reduce primary root growth and promote G2/M phase arrest in root meristematic cells (Zhao et al., 2014). Established relationships with either iron or heat stress within roots are consistent with our findings of apparent cell cycle arrest, based on dynamics changes in CYCB1;1:GFP, in all stress conditions. Little is known about the combinatorial interactions of heat and iron stress in plants, particularly in root cells. However, it has been shown that moderate heat stress causes ferroptosis-like cell death in root hair cells. Ferroptosis, identified first in animal cells, is a type of cell death that occurs in response to moderate heat stress and is dependent on cellular iron availability and mediated by ROS accumulation (Mushegian, 2017). In recent studies, ferroptosis-like cell death has been identified in root hair cells in which moderate heat stress induces cell death that is mediated by ROS accumulation, as in animal cells (Distéfano et al., 2017). However, in combination with iron chelators, heat stress is unable to induce cell death; thus, iron deficiency via chelation has been shown to attenuate a moderate heat stress response (Distéfano et al., 2017). Similarly, our results suggest that heat stress and iron deficiency, which was induced by iron chelation, interact in an opposing manner to regulate the cellular life cycle. Moreover, heat stress triggers ROS production, resulting in either root acclimation to stress or cell death; however, heat stress in combination with other abiotic stresses, such as drought or salinity, results in unique patterns of ROS production relative to those produced by heat single stress (Kilian et al., 2012; Choudhury et al., 2017). It is likely that heat stress responses, in concert with iron deficiency stress responses function antagonistically to each other so that cellular ROS production is inhibited and, thus, ROS-induced or iron-dependent (ferroptosis) cell death was mitigated. Moreover, it is also possible that the stress responses induced by iron deficiency primed, or acclimated, the root to the subsequent heat stress condition, especially since priming, or desensitization of a plant from one stress by another previous stress has been observed (Kilian et al., 2012).

Since iron deficiency causes the malnutrition of billions of individuals worldwide and there is currently a rise in global temperatures, it is very likely that these two stresses commonly appear in combination to many crops all over the world (Stein, 2010). While our laboratory growth conditions may not fully reflect field conditions in which crops are grown, we attempted to emulate aspects of field-like characteristics such as a short (80 min) heat stress application and constant 24-h iron deficiency

application, which is commonly used to reflect fluctuating heat over a 24-h period and prolong nutrient deficiencies, respectively. Our findings and methods shed new light on how plant responses to combinatorial stress conditions may be non-intuitive. Moreover, we provide a computational approach that can be adapted to study a broad application of spatiotemporal dynamics of gene regulation under diverse developmental and environmental conditions. We have designed our approach such that it can be customizable to many different applications for gaining insight on the effects that environment has on plant growth. Specifically, our approach can be used to transform high volumes of fluorescence microscopy image data, containing specimens with fluorescent-tagged genetic markers, into quantitative spatiotemporal metrics. These metrics can then, as shown here, give biological insight into the timing and characteristics of plant responses under single and multiple stresses.

MATERIALS AND METHODS

Plant Growth and Seed Preparation

The *Arabidopsis thaliana* pCYCLINB1;1:CYCLINB1;1::GFP in a Columbia (Col-0) background was used for all experiments. Seeds were sterilized in 70% ethanol for 5 min followed by incubation in 30% bleach and 0.02% Triton X-100 for 15 min. Then, seeds were rinsed 3 times in sterile water and stratified at 4°C for at least 2 days. Seeds were germinated and grown in a MAGIC 3D printed growth chamber as described in (de Luis Balaguer et al., 2016). Each seed was germinated in 13-mm-long FEP tube, containing iron-sufficient (+Fe) MS low gelling media, consisting of standard Murashige and Skoog medium with 0.05% MES (w/v), 1% (w/v) sucrose, 0.4% (w/v) low gelling agar, and 0.1-mM FeEDTA substituted for iron sulfate. Each tube was oriented vertically, held upright by standard +Fe MS solid media in plates which were kept at 22°C under a 16-h-light and an 8-h-dark period in environmentally-controlled plant growth chambers (Percival Scientific).

On the 4th day after planting, seedlings were prepared for imaging. To induce iron deficiency, +Fe low gelling medium was replaced with −Fe low gelling medium, which had the same composition of +MS low gelling media, except that 300 μM ferrozine was added as an iron chelator. For the biological replicates that were induced with heat stress, the imaging chamber was programmed to incubate the specimens at 38°C for 80 min starting at the 2-h mark from the beginning of the imaging experiment. For all other times outside of the heat stress window and for specimens not induced with heat stress, the chamber was programmed to incubate at 22°C. Each experiment, iron sufficient (+Fe), iron deficient (−Fe), heat stress (Heat), and iron deficient with heat stress (−Fe+Heat), used 3–4 seedlings as individual replicates.

Light Sheet Microscopy and Imaging Chamber

The ZEISS Lightsheet Z.1 microscope (Carl Zeiss, Germany) was used for all imaging experiments. All settings related to imaging configuration and imaging chamber environment of the microscope were adjusted using the ZEN software from ZEISS.

The MAGIC chamber was lowered into the light sheet where the meristematic region of each root was imaged using a W Plan-Apochromat 20x/1.0 NA objective (Carl Zeiss, Germany). Two image channels were taken simultaneously of each plant, a 3D fluorescent channel and a 3D brightfield channel. In the fluorescent channel, the laser was set to single-side excitation with settings of 488 nm, 50 mW, laser intensity set to 60%, and the exposure time was set to 29.97 ms. The SBS LP 560 beam splitter and BP505-545 emission filter were used to detect GFP emissions. Both the fluorescent images and the brightfield images were taken at a pixel resolution of 0.23 μm × 0.23 μm and a z-slice interval of 3.33 μm. The microscope was programmed to image each root every 20 min for 24 h. Every 20 min from the beginning to the end of any experiment is considered a timestamp. This time interval was chosen because it was determined to be a good sampling frequency for observing cell cycle changes in *A. thaliana*.

Dynamic Cell Cycle Metrics Descriptions and Low Pass Filtering

The images taken from the light sheet were processed to track fluorescent CYCB1;1:GFP ROI over space and time using the BioVision Tracker software (Buckner et al., 2018). We further processed the data about the ROIs that were collected from the software into metrics that help characterize average spatiotemporal CYCB1;1:GFP signal patterns at any one time stamp. The following metrics were collected for each image that was taken.

1. PERSISTENCY AVERAGE (X_1)—The average persistency measure of all ROIs detected.
2. PERSISTENCY SPREAD (X_2)—This is the standard deviation of collected persistency measures from all ROIs in a single time point.
3. PERSISTENCY ADDITIVE (X_3)—Each ROI has a persistency measure which is the length of time that each ROI has been and will be tracked (in hours). Persistency additive is the sum of all visible ROI's persistency measures in a single time point.
4. AVERAGE NUMBER (X_4)—This is the average number of ROIs detected at any one time stamp.
5. NEW APPEARANCE (X_5)—This is the number of ROIs that first appear and begin to be tracked in the evaluated time stamp.
6. TRACK END (X_6)—This is the number of ROIs that stopped being visible during that time stamp and thus stopped being tracked at that time.
7. TIP DISTANCE AVERAGE (X_7)—This is the average distance away from the tip (in microns) ROIs appeared within the root at that time stamp.
8. TIP DISTANCE SPREAD (X_8)—This is the standard deviation of ROI distances away from the tip of the root at that time stamp.
9. CENTER DISTANCE AVERAGE (X_9)—This is the average distance away from the longitudinal axis (in microns) ROIs appeared within the root at that time stamp.
10. CENTER DISTANCE SPREAD (X_{10})—This is the standard deviation of ROI distances away from the longitudinal axis of the root at that time stamp.

These 10 metrics were collected for each 20-min imaging timestamp across all replicates in each environmental condition. Let $X^r_{i,k}(n)$,represent the discrete time signal for metric k, condition i, replicate r, and time stamp t, and let $h(n)$ represent the following digital filter.

$$h(n) = \sum_{k=-4}^{S} \frac{1}{10}\delta(n-k),$$

where δ is the Dirac delta function.

All time signals were filtered by convolving them with $h(n)$.

$$F^r_{i,k}(n) = X^r_{i,k}(n) * h(n)$$

The overall metric profiles were calculated using the average filtered signal across all replicates in each environmental condition. Here, R_i is the number of biological replicates used for each condition i.

$$p_{i,k}(n) = \frac{1}{R_i}\sum_{r=1}^{R_i} F^r_{i,k}(n)$$

Sum of Squares Pairwise Comparisons

Each metric profile was aggregated together to create a 10-dimensional profile. Here, T stands for the transpose operation of a matrix.

$$P_i(n) = [p_{i,1}(n)^T, p_{i,2}(\mathrm{n})^T, \ldots, p_{i,10}(n)^T]^T$$

To compare any two profiles ($P_i(n)$ vs. $P_j(n)$), first each metric was normalized between 0 and 1.

$$P'_i(n) = M^{-1} \times P_i(n),$$

where M is a 10 × 10-diagonal matrix that contains the highest observed value across all experiments for each of the 10 metrics.

A sum of squares (SS) operation was then completed across all metrics.

$$\underline{SS_{i,j}}(n) = \underline{1_{1\times 10}} \times ((P'_1(n) - P'_j(n)) \circ (\mathrm{P}'_i(n) - P'_j(n)))$$

To evaluate the overall SS value across all time (SST), the SS values for each time stamp were summed together. Here, N is the number of total time stamps found in the imaging experiment, which is 72 for this study.

$$SST_{i,j} = \underline{SS_{i,j}}(n) \times \underline{1_{N\times 1}}$$

MAGIC Root Growth Assay

Using the 24-h time-course image data from the environmental experiments, a growth vector was calculated to represent the growth of the root between any two consecutive time stamps using image registration in the BioVision Tracker Software. The magnitude of each growth vector $g^r_i(n)$ was determined using a euclidean distance calculation for each replicate r, condition i, and time stamp n. This magnitude was translated into distances in microns from distances in voxels using the voxel resolution value (α) obtained from the light sheet metadata. For each root, the total growth at time stamp n was calculated using the following equation.

$$G^r_i(n) = \sum_{\mu=1}^{n} \alpha g^r_i(\mu)$$

Bioluminescence Assay

The promoter sequences of BTS: (3,000 bp) using 5'-caccATGAGATGAAATGTCTTATCTTTAT-3' and 5'-TTCC CCCAAAGCTTATCTCCGTTTT -3', and PYE: (1,120 bp) 5'-ca ccACCGCAAAACTATATATAGTATTT-3' and 5'-CTTTGCTTT TATTACAGAACAAGA-3', were amplified from genomic DNA from Columbia (Col-0) as the template. Each promoter region was cloned into pENTR/D-TOPO then transferred to the pFLASH vector, containing the firefly luciferase gene, containing a spectinomycin resistance gene. Transformation and selection proceeded as described in Long et al., 2010. The resultant reporter lines *pBTS::LUC5-1*, *pBTS::LUC2-3*, *pPYE::LUC4-2,* and *pPYE::LUC5-5* were germinated on iron sufficient MS media for 4 days. On the 4th day, seedlings were transferred to new (iron sufficient or iron deficient) media plates. Seedlings were sprayed with 5-mM D-luciferin (Goldbio) in 0.1% Triton X-100 8 h prior to transferring. After transfer, plates were acclimated in the percival for 2 h then half of the plates were put in a 38°C water bath for 80 min (as described above). Bioluminescence imaging was performed and the first image was taken 4 h after transfer. Images were acquired every 2 h with exposure times of 20 min across 2 consecutive days. Images were processed using software ImageJ (Schneider et al., 2012). All experimental treatments contain three biological replicates (n = 3) with three seedlings for each replicate. A two-sample t-test was run for all pairwise comparisons using the MATLAB function ttest2.m.

DATA AVAILABILITY STATEMENT

The datasets generated for this study are available on request to the corresponding author.

AUTHOR CONTRIBUTIONS

EB and IM collected data, analyzed the data, and wrote the manuscript. HC, AM, and CM collected data. RS, CW, and TL provided expert guidance and helped in writing the manuscript.

FUNDING

EB was supported by the GAANN Fellowship in Molecular Biotechnology (grant #P200A160061). IM was supported by

a fellowship from the Southern Regional Education Board (SREB) Doctoral Scholars Program. AM was supported by the National Science Foundation (grant 1120937, grant 1252376, and grant 1247427). Support to RS was provided by the National Science Foundation (NSF) (CAREER MCB 1453130). RS and TL were funded bilaterally by the NSF and the Biotechnology and Biological Sciences Research Council (BBSRC) (NSF MCB-1517058). TL, CW, and HC were supported by NSF MCB-1247427. TL is also funded by the USDA National Institute of Food and Agriculture, Hatch Project (Accession Number 101090). HC is also supported by a North Carolina Agriculture and Life Sciences Research Foundation's Innovation Award.

SUPPLEMENTARY MATERIAL

The Supplementary Material for this article can be found online at: https://www.frontiersin.org/articles/10.3389/fpls.2019.01487/full#supplementary-material

REFERENCES

Buckner, E., Ottley, C., Williams, C., de Luis Balaguer, A., Melvin, C. E., and Rosangela Sozzani, R. (2018). "Tracking gene expression via light sheet microscopy and computer vision in living organisms". *2018 40th Annual International Conference of the IEEE Engineering in Medicine and Biology Society (EMBC)*. (IEEE), Honolulu, HI. 818–821. doi: 10.1109/EMBC.2018.8512416

Carvalho, A., Leal, F., Matos, M., and Jse Lima-Brito, J. (2018). "Effects of heat stress in the leaf mitotic cell cycle and chromosomes of four wine-producing grapevine varieties". *Protoplasma* 255 (6), 1725–1740. doi: 10.1007/s00709-018-1267-4

Choudhury, F. K., Rivero, R. M., Blumwald, E., and Mittler, R. (2017). Reactive oxygen species, abiotic stress and stress combination. *Plant J.* 90 (5), 856–867. doi: 10.1111/tpj.13299

Corrales, A. R., Carrillo, L., Lasierra, P., Nebauer, S. G., Dominguez-Figueroa, J., and Renau-Morata, B. (2017). "Multifaceted role of cycling DOF factor 3 (CDF3) in the regulation of flowering time and abiotic stress responses in *Arabidopsis*". *Plant Cell Environ.* 40 (5), 748–764. doi: 10.1111/pce.12894

de Luis Balaguer, M. A., Ramos-Pezzotti, M., Rahhal, M. B., Melvin, C. E., Johannes, E., and Horn, T. J. (2016). "Multi-sample arabidopsis growth and imaging chamber (MAGIC) for long term imaging in the ZEISS lightsheet Z.1". *Dev. Biol.* 419 (1), 19–25. doi: 10.1016/j.ydbio.2016.05.029

Distéfano, A., Martin, M., Córdoba, J., Bellido, A., D'Ippólito, S., Colman, S., et al. (2017). "Heat stress induces ferroptosis-like cell death in plants". *J. Cell Biol.* 216 (2), 463–476. doi: 10.1083/jcb.201605110

Feraru, E., Feraru, M. I., Barbez, E., Waidmann, S., Sun, L., Gaidora, A., and Kleine-Vehn, J. (2019). "PILS6 is a temperature-sensitive regulator of nuclear auxin input and organ growth in *Arabidopsis thaliana*". *Proc. Natl. Acad. Sci.* 116(9), pp.3893-3898. doi: 10.1073/pnas.1814015116

Gharagozloo, M., Khoshdel, Z., Amirghofran, Z., Zahra Khoshdel, and Zahra Amirghofran. (2008). "The effect of an iron (III) chelator, silybin, on the proliferation and cell cycle of jurkat cells: A comparison with desferrioxamine." *Eur. J. Pharmacol.* 589(1–3): 1–7. doi: 10.1016/j.ejphar.2008.03.059

Gruber, B. D., Giehl, R. F. H., Friedel, S., and von Wirén, N. (2013). "Plasticity of the Arabidopsis root system under nutrient deficiencies". *Plant Physiol.* 163 (1), 161–179. doi: 10.1104/pp.113.218453

Hahn, A., Kilian, J., Mohrholz, A., Ladwig, F., Peschke, F., Dautel, R., et al. (2013). Plant core environmental stress response genes are systemically coordinated during abiotic stresses. *Int. J. Mol. Sci.* 14 (4), 7617–7641. doi: 10.3390/ijms14047617

Hilo, A., Shahinnia, F., Druege, U., Franken, P., Melzer, M., and Rutten, T. (2017). "A specific role of iron in promoting meristematic cell division during adventitious root formation". *J. Exp. Bot.* 68 (15), 4233–4247. doi: 10.1093/jxb/erx248

Iyer-Pascuzzi, A. S., Jackson, T., Cui, H., Petricka, J. J., Busch, W., and Tsukagoshi, H. (2011). "Cell identity regulators link development and stress responses in the *Arabidopsis* root". *Dev. Cell* 21 (4), 770–782. doi: 10.1016/j.devcel.2011.09.009

Kilian, J., Whitehead, D., Horak, J., Wanke, D., Weinl, S., Batistic, O., et al. (2007). "The AtGenExpress global stress expression data set: protocols, evaluation and model data analysis of UV-B light, drought and cold stress responses". *Plant J.* 50 (2), 347–363. doi: 10.1111/j.1365-313X.2007.03052.x

Kilian, J., Peschke, F., Berendzen, K. W., Harter, K., and Wanke, D. (2012). Prerequisites, performance and profits of transcriptional profiling the abiotic stress response. *BBA - Gene Regul. Mech.* 1819 (2), 166–175. doi: 10.1016/j.bbagrm.2011.09.005

López-Bucio, J., Cruz-Ramírez, A., and Herrera-Estrella, L. (2003). "The role of nutrient availability in regulating root architecture". *Curr. Opin. In Plant Biol.* 6 (3), 280–287. doi: 10.1016/S1369-5266(03)00035-9

Landsberg, E. (1996). Hormonal regulation of iron-stress response in sunflower roots: A morphological and cytological investigation. *Protoplasma* 194 (1–2), 69–80. doi: 10.1007/BF01273169

Larkindale, J., Hall, J. D., Knight, M. R., and Vierling, E. (2005). "Heat stress phenotypes of *Arabidopsis* mutants implicate multiple signaling pathways in the acquisition of thermotolerance". *Plant Physiol.* 138 (2), 882–897. doi: 10.1104/pp.105.062257

Long, T. A., Tsukagoshi, H., Busch, W., Lahner, B., Salt, D. E., and Benfey, P. N. (2010). "The bHLH transcription factor POPEYE regulates response to iron deficiency in Arabidopsis roots." *The Plant Cell*, 22 (7), 2219–2236. doi: 10.1105/tpc.110.074096

Mangelsen, E., Kilian, J., Harter, K., Jansson, C., Wanke, D., and Sundberg, E. (2011). Transcriptome analysis of high-temperature stress in developing barley caryopses: early stress responses and effects on storage compound biosynthesis. *Mol. Plant* 4 (1), 97–115. doi: 10.1093/mp/ssq058

Menges, M., De Jager, S. M., Gruissem, W., and Murray, J. A. H. (2005). "Global analysis of the core cell cycle regulators of *Arabidopsis* identifies novel genes, reveals multiple and highly specific profiles of expression and provides a coherent model for plant cell cycle control". *Plant J.* 41 (4), 546–566. doi: 10.1111/j.1365-313X.2004.02319

Mushegian, A. A. (2017). Ferroptosis-like cell death in plants. *Sci. Signaling* 10 (468). doi: 10.1126/scisignal.aan0450. doi: 10.1126/scisignal.aan0450

Ovečka, M., von Wangenheim, D., Tomančák, P., Šamajová, O., Komis, G., and Šamaj, J. (2018). "Multiscale imaging of plant development by light-sheet fluorescence microscopy". *Nat. Plants* 4 (9), 639–650. doi: 10.1038/s41477-018-0238-2

Reynaud, E. G., Peychl, J., Huisken, J., and Tomancak, P. (2015). "Guide to light-sheet microscopy for adventurous biologists". *Nat. Methods* 12 (1), 30–34. doi: 10.1038/nmeth.3222

Rivero, R. M., Mestre, T. C., Mittler, R. O. N., Rubio, F., Gargia-Sanchez, F., and Martinez, V. (2014). "The combined effect of salinity and heat reveals a specific physiological, biochemical and molecular response in tomato plants". *Plant Cell Environ.* 37 (5), 1059–1073. doi: 10.1111/pce.12199

Rout, G. R., and Sahoo, S. (2015). "Role of iron in plant growth and metabolism". *Rev. In Agric. Sci.* 3, 1–24. doi: 10.7831/ras.3.1

Sakamoto, T., Sakamoto, Y., & Matsunaga, S. (2016). Cell Division and Cell Growth. In Molecular Cell Biology of the Growth and Differentiation of Plant Cells (pp. 86–98). Boca Raton, FL: CRC Press, Taylor & Francis Group. doi: 10.1201/b2031

Schneider, C. A., Rasband, W. S., and Eliceiri, K. W. (2012). "NIH image to ImageJ: 25 years of image analysis". *Nat. Methods* 9 (7), 671–675. doi: 10.1038/nmeth.2089

Schnittger, A., and De Veylder, L. (2018). "The dual face of cyclin B1". *Trends In Plant Sci.* 23 (6), 475–478. doi: 10.1016/j.tplants.2018.03.015

Silva-Correia, J., Freitas, S., Tavares, R. M., Lino-Neto, T., and Azevedo, H. (2014). Phenotypic analysis of the Arabidopsis heat stress response during germination and early seedling development. *Plant Methods* 10, 7 (2014) doi: 10.1186/1746-4811-10-7

Skirycz, A., Claeys, H., De Bodt, S., Oikawa, A., Shinoda, S., and Andriankaja, M. (2011). "Pause-and-stop: the effects of osmotic stress on cell proliferation

during early leaf development in *Arabidopsis* and a Role for ethylene signaling in cell cycle arrest". *Plant Cell* 23 (5), 1876–1888. doi: 10.1105/tpc.111.084160

Stein, A. J. (2010). "Global impacts of human mineral malnutrition". *Plant Soil* 335 (1–2), 133–154. doi: 10.1007/s11104-009-0228-2

Suzuki, N., Rivero, R. M., Shulaev, V., Blumwald, E., and Mittler, R. (2014). "Abiotic and biotic stress combinations". *New Phytol.* 203 (1), 32–43. doi: 10.1111/nph.12797

Swindell, W. R., Huebner, M., and Weber, A. P. (2007). "Transcriptional profiling of *Arabidopsis* heat shock proteins and transcription factors reveals extensive overlap between heat and non-heat stress response pathways". *BMC Genomics* 8 (1), 125. doi: 10.1186/1471-2164-8-125

Thimm, O., Essigmann, B., Kloska, S., Altmann, T., and Buckhout, T. J. (2001). "Response of *Arabidopsis* to iron deficiency stress as revealed by microarray analysis". *Plant Physiol.* 127 (3), 1030–1043. doi: 10.1104/pp.010191

Tsukagoshi, H. (2012). "Defective root growth triggered by oxidative stress is controlled through the expression of cell cycle-related genes". *Plant Sci.* 197, 30–39. doi: 10.1016/j.plantsci.2012.08.011

Wahid, A., Gelani, S., Ashraf, M., and Foolad, M. R. (2007). "Heat tolerance in plants: An overview." *Environ. Exp. Bot.* 61 (3), 199–223. doi: 10.1016/j.envexpbot.2007.05.011

Yeh, C. H., Kaplinsky, N. J., Hu, C., and Charng, Y. Y. (2012). Some like it hot, some like it warm: phenotyping to explore thermotolerance diversity. *Plant Sci.* 195, 10–23. doi: 10.1016/j.plantsci.2012.06.004

Yin, K., Ueda, M., Takagi, H., Kajihara, T., Sugamata Aki, S., Nobusawa, T., et al. (2014). "A dual-color marker system for in vivo visualization of cell cycle progression in *Arabidopsis*". *Plant J.* 80 (3), 541–552. doi: 10.1111/tpj.12652

Zandalinas, S. I., Mittler, R., Balfagón, D., Arbona, V., and Gómez-Cadenas, A. (2018). "Plant adaptations to the combination of drought and high temperatures". *Physiol. Plant.* 162 (1), 2–12. doi: 10.1111/ppl.12540

Zhao, L., Wang, P., Hou, H., Zhang, H., Wang, Y., and Yan, S. (2014). "Transcriptional regulation of cell cycle genes in response to abiotic stresses correlates with dynamic changes in histone modifications in maize". *PloS One* 9 (8), e106070. doi: 10.1371/journal.pone.0106070

Conflict of Interest: The authors declare that the research was conducted in the absence of any commercial or financial relationships that could be construed as a potential conflict of interest.

frontiers in Plant Science

ORIGINAL RESEARCH
published: 25 November 2019
doi: 10.3389/fpls.2019.01449

Mitochondrial Iron Transporters (MIT1 and MIT2) Are Essential for Iron Homeostasis and Embryogenesis in *Arabidopsis thaliana*

Anshika Jain[1†], *Zachary S. Dashner*[2] *and Erin L. Connolly*[1,2*]

[1] Department of Biological Sciences, University of South Carolina, Columbia, SC, United States, [2] Department of Plant Science, The Pennsylvania State University, University Park, PA, United States

OPEN ACCESS

Edited by:
Thomas J. Buckhout,
Humboldt University of Berlin,
Germany

Reviewed by:
Katrin Philippar,
Universität des Saarlandes,
Germany
Kuo-Chen Yen,
Academia Sinica, Taiwan

***Correspondence:**
Erin L. Connolly
elc18@psu.edu

†Present address:
Anshika Jain,
Eunice Kennedy Shriver National Institute of Child Health and Human Development, National Institutes of Health (NIH), Bethesda, MD, United States

Specialty section:
This article was submitted to Plant Nutrition, a section of the journal Frontiers in Plant Science

Received: 19 April 2019
Accepted: 17 October 2019
Published: 25 November 2019

Citation:
Jain A, Dashner ZS and Connolly EL (2019) Mitochondrial Iron Transporters (MIT1 and MIT2) Are Essential for Iron Homeostasis and Embryogenesis in Arabidopsis thaliana. Front. Plant Sci. 10:1449. doi: 10.3389/fpls.2019.01449

Iron (Fe) is an essential nutrient for virtually all organisms, where it functions in critical electron transfer processes, like those involved in respiration. Photosynthetic organisms have special requirements for Fe due to its importance in photosynthesis. While the importance of Fe for mitochondria- and chloroplast-localized processes is clear, our understanding of the molecular mechanisms that underlie the trafficking of Fe to these compartments is not complete. Here, we describe the Arabidopsis mitochondrial iron transporters, MIT1 and MIT2, that belong to the mitochondrial carrier family (MCF) of transport proteins. MIT1 and MIT2 display considerable homology with known mitochondrial Fe transporters of other organisms. Expression of MIT1 or MIT2 rescues the phenotype of the yeast *mrs3mrs4* mutant, which is defective in mitochondrial iron transport. Although the Arabidopsis *mit1* and *mit2* single mutants do not show any significant visible phenotypes, the double mutant *mit1mit2* displays embryo lethality. Analysis of a *mit1*$^{-/-}$/*mit2*$^{+/-}$ line revealed that MIT1 and MIT2 are essential for iron acquisition by mitochondria and proper mitochondrial function. In addition, loss of *MIT* function results in mislocalization of Fe, which in turn causes upregulation of the root high affinity Fe uptake pathway. Thus, MIT1 and MIT2 are required for the maintenance of both mitochondrial and whole plant Fe homeostasis, which, in turn, is important for the proper growth and development of the plant.

Keywords: mitochondria, iron, mitochondrial iron transport, arabidopsis, iron homeostasis

INTRODUCTION

Iron (Fe) is an essential element that is required for numerous biochemical processes in cells. It readily accepts and donates electrons, and functions as a part of redox centers where it serves as a cofactor for various enzymes and proteins. The molecular details of Fe uptake in plants are reasonably well described (Kobayashi and Nishizawa 2012; Jeong et al., 2017). Grasses like rice, barley, and maize utilize a chelation-based strategy in which Fe uptake from the rhizosphere is mediated by phytosiderophores such as deoxymugineic acid. Studies in rice and barley have shown that in response to iron limitation, phytosiderophores (PSs) are exported by transporter of mugineic acid (TOM1) and Fe-PS complexes are subsequently imported by YS1, a member of the oligopeptide transporter family (Curie et al., 2001; Inoue et al., 2009; Nozoye et al., 2011; Connorton et al., 2017). Dicots such as Arabidopsis, on the other

hand, use a reduction-based strategy in which insoluble ferric chelates in the rhizosphere are solubilized *via* proton extrusion mediated by the H^+ ATPase AHA2 and coumarin secretion (Santi and Schmidt, 2009; Jeong et al., 2017). Upon solubilization, the rhizospheric ferric chelates are reduced to ferrous ions by a root surface-localized ferric chelate reductase, FRO2 (Robinson et al., 1999; Connolly et al., 2003) and subsequently imported into the root epidermal cells by a high affinity iron transporter, IRT1 (Eide et al., 1996; Vert et al., 2002; Jeong and Connolly, 2009). In addition to its role in iron uptake from the soil, IRT1 also functions in the import of other divalent cations such as Mn^{2+}, Zn^{2+}, Co^{2+} and Cd^{2+} (Eide et al., 1996; Korshunova et al., 1999; Vert et al., 2002; Grossoehme et al., 2006).

Cells prioritize delivery of Fe to mitochondria to maintain the proper functioning of iron-requiring biochemical processes such as Fe-S cluster biosynthesis, apoptosis, and respiration. Numerous respiratory complex subunits utilize iron (Fe-S clusters, heme, and/or non-heme iron) as their cofactors (Philpott and Ryu, 2014). Mitochondria also function as manufacturing sites for synthesis of Fe-S clusters in all organisms and heme groups in non-photosynthetic organisms (Yoon and Cowan, 2004; Balk and Pilon, 2011; Rouault, 2014; Rouault, 2015). Despite its importance, the mechanisms that control mitochondrial Fe metabolism are not fully understood in plants. While Fe export out of the mitochondria is an open question in all living systems, several reports have shed light on iron import to mitochondria (Froschauer et al., 2013; Jain and Connolly, 2013; Vigani et al., 2019).

The yeast mitoferrin proteins MRS3 and MRS4 (Mitochondrial RNA Splicing proteins) were the first proteins shown to function in mitochondrial iron uptake (Foury and Roganti, 2002). These high affinity iron transporters move iron across the mitochondrial inner membrane in a pH- and concentration-dependent manner (Froschauer et al., 2009). The accumulation of Fe, heme, and Fe-S clusters in yeast mitochondria was shown to be directly proportional to the expression levels of MRS3 and MRS4 in yeast overexpression lines (Foury and Roganti, 2002; Muhlenhoff et al., 2003). MRS3 and MRS4 deletion mutants display a growth phenotype only under Fe-limiting conditions (Muhlenhoff et al., 2003), suggesting the presence of a low affinity Fe transporter that functions under Fe-sufficient conditions. Rim2, a pyrimidine nucleotide exchanger, has been shown to function as an alternative route for mitochondrial Fe transport in yeast (Yoon et al., 2011). Additionally, a recent study utilized *mrs3mrs4* mutant cells to identify a low molecular mass pool of Fe that serves as the feedstock for Fe-S cluster assembly and heme synthesis in yeast (Moore et al., 2018). This study also showed that Fe homeostasis is disrupted in *mrs3mrs4* mutants (Moore et al., 2018).

Homologs of yeast mitoferrins have been described in zebrafish (Shaw et al., 2006; Paradkar et al., 2009), Drosophila (Metzendorf et al., 2009) and rice (Bashir et al., 2011). Drosophila mitoferrin (Dmfrn) is essential for spermatogenesis and loss of Dmfrn leads to male sterility (Metzendorf et al., 2009). The zebrafish *frascatii* (*mfrn1*) mutant displays impaired heme synthesis which leads to severe defects in erythropoiesis and subsequent death of the embryo (Shaw et al., 2006). A related protein, Mfrn2, fails to rescue the defective erythropoetic phenotype of the *mfrn1* mutant. While the role of Mfrn2 is not clear at the organismal level, both Mfrn1 and Mfrn2 were shown to be responsible for Fe transport in the mitochondria of nonerythroid cells (Paradkar et al., 2009). A recent *in vitro* study revealed that Mfrn1 transports free iron (rather than chelated iron complexes) in addition to Co, Cu, Zn, and Mn (Christenson et al., 2018).

The mitoferrin ortholog identified in rice (mitochondrial iron transporter [MIT]) was shown to be responsible for mitochondrial iron acquisition (Bashir et al., 2011). While *mit* knockout mutants are embryo lethal, *mit* knock-down lines exhibit a poor growth phenotype, reduced mitochondrial iron, and increased total Fe in the shoots, suggesting that Fe is mislocalized in *mit* cells. The expression level of the gene coding for the Vacuolar Iron Transporter1 (*VIT1*) is upregulated in the absence of *MIT* in rice (Bashir et al., 2011). Overall, the loss of mitoferrin function in different species results in severely retarded growth and embryo lethal phenotypes (Muhlenhoff et al., 2003; Shaw et al., 2006; Paradkar et al., 2009; Bashir et al., 2011).

In this study, we report the characterization of previously unidentified mitochondrial iron transporters in dicots for the first time. We cloned and characterized two mitochondrial iron transporters (MIT1 and MIT2) from Arabidopsis and demonstrate their importance for mitochondrial iron acquisition as well as for the maintenance of Fe homeostasis in plants. We observed that the loss of MIT1 and MIT2 together results in reduced levels of mitochondrial iron, as well as impaired mitochondrial biochemical function as evidenced by changes in the relative abundance of various respiratory subunits and aconitase levels. Our results also show that MIT1 and MIT2 function redundantly and are essential for embryogenesis. Although rice and Arabidopsis MITs show functional similarities, here we describe key differences between mitochondrial iron transport in dicots and monocots.

MATERIALS AND METHODS

Plant Lines and Plant Growth Conditions

T-DNA insertion mutants [SALK_013388 for *MIT1*(At2g30160) and SALK_096697 for *MIT2* (At1g07030)] were obtained from the Arabidopsis Biological Research Center (ABRC). The *mit1mit2* double mutant was generated using artificial microRNA technology as described below (Schwab et al., 2006). Wild type Arabidopsis (Col-*0* or Col *gl-1*) was used as a control in all the experiments. Seeds were surface sterilized with 25% bleach and 0.02% SDS. After thorough washing with dH2O, seeds were imbibed in the dark for 2 days at 4°C. Seedlings were grown on Gamborg's B5 media (Phytotechnology Laboratories) supplemented with 2% sucrose, 1mM MES, and 0.6% agar, pH 5.8 for 2 weeks under constant light (80 mmol/m^{-2}/s^{-2}) at 22°C. To induce iron deficiency, plants were transferred after 2 weeks from B5 media to 300 μM ferrozine [3-(2-pyridyl)-5,6-diphenyl-1,2,4 triazine sulfonate] containing media (Fe-deficient media) for an additional 3 days as described previously (Connolly et al., 2002). Plants were also grown with and without added Fe (but without an Fe chelator) as follows: 1/2X MS media, 0.6% agar, pH 5.8 supplemented with either 50 μM Fe(III)-EDTA (Fe-sufficient media) or no additional Fe (Fe drop-out media) for 2.5 weeks.

Plants were grown in Metro-Mix360/perlite/vermiculite (5:1:1) under 16 hr light; 8hr dark or were grown hydroponically under constant light. The composition of the hydroponics nutrient solution was as follows: 0.75 mM K_2SO_4, 0.1 mM KH_2PO_4, 2.0 mM $Ca(NO_3)_2$, 0.65 mM $MgSO_4$, 0.05 mM KCl, 10 μM H_3BO_3, 1 μM $MnSO_4$, 0.05 μM $ZnSO_4$, 0.05 μM $CuSO_4$, 0.005 μM $(NH_4)_6Mo_7O_{24}$, with no added Fe (Fe drop-out media) (Kerkeb et al., 2008); media was replaced weekly.

Cloning

For the generation of *35S-MIT1-YFP* and *35S-MIT2-YFP* constructs, the full length cDNAs for *MIT1* and *MIT2*, already cloned in an entry vector (D-TOPO, Life Technologies) were ordered from The Arabidopsis Information Resource (TAIR). In order to obtain *MIT-YFP* fusion constructs, full length CDS lacking the stop codons of *MIT1* and *MIT2* were amplified using gene specific primers (*MIT1* FP: 5′ CACCATGGCAACAGAAGCAACAACC-3′, *MIT1* RP: 5′AGCTGCGTTTGCTTCACCATTGAG-3′, *MIT2* FP: 5′-CACCATGGCTACGGAGGCTACAAC-3′, *MIT2* RP: 5′-GGCAGAGTTTGAATCGACATTGAAG-3′). These DNA fragments were then subcloned into pENTER/D-TOPO and recombined into pEARLY Gateway101 (Life Technologies); these constructs were then transformed into *Agrobacterium tumefaciencs GV3101* using standard cloning and transformation techniques (Koncz and Schell, 1986).

To generate the *pMIT1-GUS* and *pMIT2-GUS* constructs, primers were designed to amplify a 1.5-kb region upstream of *MIT1* and a 0.75-kb region (limited by the presence of another gene upstream on the chromosome) upstream of *MIT2* from the genomic DNA (*pMIT1* FP: 5′ GGTACCCTTTAGTTTAACCGCCGCAT-3′, *pMIT1* RP: 5′GAATTCTTTCTCTATCAATGCAAACCAGAA-3′, *pMIT2* FP: 5′GGTACCTTGTGGAAGAAAGATCAAATCTTG-3′, *pMIT2* RP: 5′GAATTCATCATCAACACAAACCTGGAAA-3′). *pMIT1* was cloned into HindIII/EcoRI sites and similarly *pMIT2* was cloned into HindIII/BamH1 sites of pCAMBIA1381Xa. These clones were transformed into Agrobacterium *GV3101*. Arabidopsis (Col *gl-1*) was then transformed using the floral dip protocol (Clough and Bent, 1998).

Artificial microRNA lines designed to knockdown expression of both *MIT1* and *MIT2* (*amiRmit1mit2*) were developed using the Web MicroRNA Designer (Schwab et al., 2006) as previously reported (Bernal et al., 2012). The targeting microRNA (TATATAGTAGCGAAAACGCCG) was designed to target both *MIT1* and *MIT2* using the following primers: *mit1mit2miR*-sense: 5′GATATATAGTAGCGAAAACGCCGTCTCTCTTTTGTATTCC3′, *mit1mit2miR*-antisense: 5′GACGGCGTTTTCGCTACTATATATCAAAGAGAATCAATGA3′ and *mit1mit2miR**sense: 5′GACGACGTTTTCGCTTCTATATTTCACAGGTCGTGATATG3′, and *mit1mit2miR**antisense: 5′GAAATATAGAAGCGAAAACGTCGTCTACATATATATTCCT3′. The fragment was amplified by overlapping PCR using a template plasmid (pRS300), a kind gift from Dr. Detlef Weigel [http://www.weigelworld.org; (Schwab et al., 2006)]. The amplicon was further cloned into the Not1 and Xho1 sites of 35S-pBARN (LeClere and Bartel, 2001).

For the yeast complementation assay, the *MIT1* and *MIT2* cDNAs were amplified from Col-*0* cDNA and cloned into the BamHI and XhoI sites of pRS426 (a kind gift from Dr. Jerry Kaplan) using the following sets of primers. *MIT1* FP: 5′-CGCGGATCCATGGTAGAAAACTCGTCGAGTAATAATTCAACAAGGCCAATTCCAGCAATACCTATGGATCTACCCTTTCATCCAGCAATCATCGTT-3′, *MIT1* RP: 5′-CCGCTCGAGTTATCACTTGTCATCGTCATCCTTGTAATCACCACCAGCTGCGTTTGCTTCACCATT-3′, *MIT2* FP: 5′-CGCGGATCCATGGTAGAAAACTCGTCGAGTAATAATTCAACAAGGCCAATTCCAGCAATACCTATGGATCTACCCCCGGATTTCAAACCGGAAATC-3′, *MIT2* RP: 5′-CCGCTCGAGTTATCACTTGTCATCGTCATCCTTGTAATCACCACCGGCAGTGTTTGAATCGACATT-3′.

Subcellular Localization

Onion peel epidermis cells were transiently transformed with the *35S-MIT1-YFP* and *35S-MIT2-YFP* constructs as described (Sun et al., 2007). The transformed onion peels were rinsed with water and stained with 150 nM MitoTracker Orange (CMTMRos; Life Technologies). Fluorescence images were generated using a Zeiss LSM 700 meta confocal system. An argon laser at 488 nm and at 535 nm provided the excitation for YFP and MitoTracker Orange (CMTMRos), respectively. Emission of YFP was collected between 505 and 530 nm, and emission of MitoTracker was collected between 585 and 615 nm. Zen lite 2011 software was used to analyze the fluorescence images.

GUS Histochemical Staining

Two-week-old seedlings of the homozygous T4 generation were used for GUS histochemical staining using X-Gluc (5-bromo-4-chloro-3-indonyl β-D glucoronide; Thermo Scientific) as a substrate as described in (Jefferson et al., 1987; Divol et al., 2013). The staining was performed on five independent, single-insertion, homozygous lines grown on B5 media, and representative lines are shown.

RNA Isolation and Transcript Analysis

Total RNA was extracted from 100 mg frozen tissue of 2-week-old seedlings grown on standard Gamborg's B5 media using TRIzol reagent (Sigma). DNase1 treatment (New England Biolabs) was conducted on 3.5 μg of the total RNA for 15 min. Superscript First strand Synthesis system (Life Technologies) was used to prepare the cDNA from total RNA according to the manufacturer's instructions (Mukherjee et al., 2006). Quantitative real-time PCR (qRT-PCR) was performed as described (Fraga et al., 2008). The following primers were used for q-RT PCR of *MIT1* and *MIT2* on the T-DNA mutants and the *amiRmit1mit2* mutant *MIT1* FP: CATGCTGTTGGAGCAGAGGA, *MIT1* RP: CACAACCACACACACCCTGA; *MIT2* FP: AGTTGCAATGTCAGGGTGTGT, *MIT2* RP: CGGGAGCCATCCCCTTAGAA. Primers to study the levels of *MIT1* and *MIT2* in the roots and shoots of WT plants are as follows: *MIT1* FP:

5′-AGACGCAGTTGCAATGTCAG-3′, *MIT1* RP: 5′-AGCC ATCCTCTAGCAAGTCCT-3′, *MIT2* FP: 5′-CGCTTGATG TTGTCAAGACG-3′, *MIT2* RP: 5′-AGGAGCATGGAAGA GCATTCT-3′, *Actin* FP: 5′-CCTTTGTTGCTGTTGACTA CGA-3′, *Actin* RP: 5′-GAACAAGACTTCTGGGCATCT-3′. Semi-qRT-PCR was performed using the following primers (Marone et al., 2001). *MIT1*: 5′-CACCATGG CAACAGAAGCAACAACC-3′, *MIT1* RP: 5′-AGCTGCGTT TGCTTCACCATTGAG-3′, *MIT2* FP: 5′- ATGGCTACGG AGGCTACAAC-3′, *MIT2* RP: 5′-GGCAGAGTTTGAATC GACATTGAAG-3′.

Yeast Complementation Assay

The following primers were designed to tag the protein with FLAG and substitute the 1st- 22 amino acids of MIT1 and MIT2 with the yeast MRS3 leader peptide to ensure proper targeting of the Arabidopsis proteins to the mitochondria of yeast cells (Shaw et al., 2006). *MIT1* FP: 5′ CGCGGATCCATGGTAGAAAACTCGTCGAGTAAT AATTC A A C A A G G C C A A T T C C A G C A A T A C C T A T G G A T CTACCCTTTCATCCAGCAATCATCGTT 3′, *MIT1* RP: 5′CCGCTCGAGTTATCACTTGTCATCGTCATCCTTGTAA TCACCACCAGC TGCGTTTGCTTCACCATT 3′; 5′ *MIT2* FP: CGCGGATCCATGGTAGAAAACTCGTCGAGT AATAATT C A A C A A G G C C A A T T C C A G C A A T A C C T A T G G A TCTACCCCCGGATTTCAAACCGGAAATC 3′, *MIT2* RP: 5′ CCGCTCGAGTTATCACTTGTCATCGTCATCCTTG TAATCACCACCGGCAGTGTTTGAATCGACATT 3′. The *mrs3mrs4* yeast strain was transformed with the empty vector (pRS426-ADH), the vector containing the *MRS3* ORF (positive control) or the vector containing *MIT1-FLAG* or *MIT2-FLAG* (Pan et al., 2004). Yeast strains were grown in liquid SD-URA medium, and serial dilutions were prepared (OD_{600} 1, 0.1 and 0.01). 10µl of the dilutions were plated as spots on the SD-URA plates containing either 0.1mM $FeSO_4$ or 0.1mM bathophenanthroline disulfonate (BPS) as described (Li and Kaplan, 2004). The plates were incubated at 30°C for 4 days.

Ferric Reductase Assay

For the ferric reductase activity assay, plants were grown on Gamborg's B5 media for 2 weeks and then transferred to Fe-sufficient (50 µM Fe-EDTA) or Fe-deficient media (300 µM ferrozine) for 3 days (Connolly et al., 2003). For the measurement of reductase activity, the roots of the intact seedlings were submerged in 300µl assay solution comprised of 50 µM Fe(III) EDTA and 300µM ferrozine and placed in the dark for 20 min. The absorbance of the assay solution was then measured at 562 nm, and the activity was normalized to the fresh weight of the roots (Robinson et al., 1999; Connolly et al., 2003). Reported data are based on 10 biological replicates. A Student's *t*-test was used to perform the statistical analysis.

Mitochondrial Fractionation and Purification

Mitochondria were prepared from seedlings grown in B5 or 1/2X MS media (with or without Fe) for 2.5 weeks. A total of 40 to 50 g of tissue was ground in 100 ml of ice-cold extraction buffer containing 0.3 M sucrose, 25 mM MOPS pH 7.5, 0.2% (w/v) BSA, 0.6% (w/v) polyvinyl-pyrrolidone 40, 2 mM EGTA, and 4 mM cysteine. All procedures were carried out at 4°C. The extract was filtered through two layers of Miracloth and centrifuged at 6,500*g* for 5 min. The supernatant was then further centrifuged at 18,000*g* for 15 min. The pellet, thus obtained was gently resuspended in extraction buffer, and the aforementioned centrifugation steps were repeated again. The resulting crude organelle pellet was resuspended in the extraction buffer and layered on a 32% (v/v) continuous Percoll gradient solution (0.25M sucrose, 10 mM MOPS, 1 mM EDTA, 0.5% PVP-40, 0.1% BSA, 1 mM glycine). The gradient was centrifuged at 40,000*g* for 2 h 30 min and the mitochondria, visible as a whitish/light-brown ring, were collected. The purified mitochondria were washed twice by resuspending in wash buffer containing 0.3 M sucrose, 5 mM MOPS followed by centrifugation at 18,000*g* for 15 min. The final mitochondrial pellet was resuspended in wash buffer containing 100 mM PMSF (Branco-Price et al., 2005). Mitochondrial protein concentrations were determined using the BCA assay (Pierce).

Elemental Analysis

For elemental analysis of mitochondria, samples were digested overnight in 250 µl concentrated HNO_3 and 50 µl concentrated HCl at 60°C. The digested samples were centrifuged at 14,000*g* for 1 min, and the supernatant was diluted to obtain a final concentration of 2.5% HNO_3. Samples were analyzed on a Thermo Elemental PQ ExCell ICP-MS using a glass conical nebulizer drawing 1 ml per min. The activity of three biological replicates was averaged for each genotype. The elemental analysis on the 44-day-old aerial tissues of soil-grown plants was conducted using ICP-MS at the University of Aberdeen as described (Lahner et al., 2003). A Student's *t*-test was used to perform the statistical analysis.

Western Blot Analysis

Protein lysates (25 µg) were separated by SDS-PAGE and transferred to PVDF (Fisher Scientific) membrane by electroblotting. Membranes were probed with IRT1 (Connolly et al., 2002), ferritin, actin, PSB-a, IDH, COX2, Histone3 (Agrisera), or aconitase antibodies and chemiluminescence detection was carried out as described (Connolly et al., 2002). Two micrograms of mitochondrial proteins were separated for aconitase antibody detection. Aconitase antibody was a kind gift from Dr. Janneke Balk (Luo et al., 2012).

Blue Native Polyacrylamide Gel Electrophoresis (BN-PAGE) and In-Gel Assay

20 µg of the resuspended mitochondrial fraction enriched in respiratory complexes was subjected to BN-PAGE according to (Schagger and von Jagow, 1991) and the in-gel assay for complex I was carried out according to (Sabar et al., 2005). Gels were incubated with 0.2 mM NADH (Sigma) and 0.1% (w/v) nitroblue tetrazolium (Sigma) in 0.1 M Tris-HCl 7.4 for complex I/NADH dehydrogenase activities. The relative intensities of the complex I bands were calculated using ImageJ software (Schneider et al., 2012).

RESULTS

MIT1 and MIT2 Functionally Complement a Yeast Mitoferrin Mutant

A sequence homology-based search for yeast mitoferrin (MRS3 and MRS4) orthologs in the *Arabidopsis* genome yielded two proteins—MIT1 (At2g30160) and MIT2 (At1g07030). MIT1 and MIT2 are 81% identical to each other at the amino acid level and share 38% sequence identity to yeast and 32% identity with zebrafish mitoferrins. These proteins belong to the mitochondrial substrate carrier family (MCF) of protein transporters and exhibit their characteristic Mitochondrial Energy Transfer Signature (METS-P-x-[DE]-x-[LIVAT]-[RK]-x-[LRH]-[LIVMFY]-[QGAIVM]) on the matrix side of the protein (**Figure 1**) (Nelson et al., 1998; Millar and Heazlewood, 2003). Additionally, MIT1 and MIT2 also exhibit the highly conserved putative signature Fe binding motifs (GXXXAHXXY, MN, and A) on transmembrane helices II, IV, and VI, respectively (Walker, 1992; Kunji and Robinson, 2006). Two mutagenesis-based studies have identified the residues important for Fe transport in yeast MRS3 and

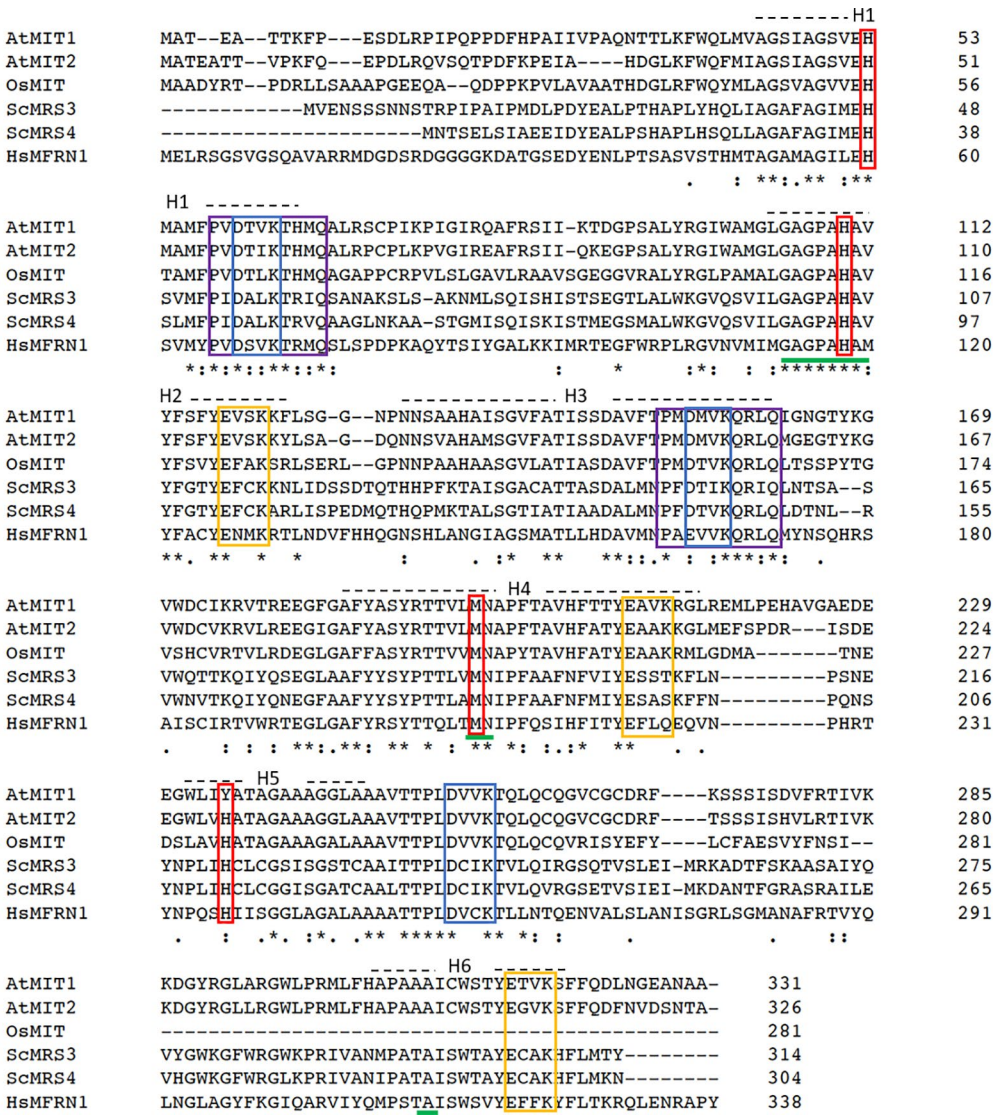

FIGURE 1 | Mitochondrial iron transporters in Arabidopsis exhibit sequence conservation for the residues significant for mitochondrial Fe transport. Sequence alignment *of* Arabidopsis AtMIT1 and AtMIT2 with mitoferrins from rice (OsMIT), yeast (ScMRS3, ScMRS4) and human (HsMfrn1) generated using CLUSTAL O. Sequences of the six predicted transmembrane helices on these proteins are depicted by H1-H6. The Mitochondrial Energy Transfer Signature (METS-P-x-[DE]-x-[LIVAT]-[RK]-x-[LRH]-[LIVMFY]-[QGAIVM]) identified in AtMIT1 and AtMIT2 is indicated by the purple boxes. The putative Fe-binding motifs are underlined in green, and the residues implicated in Fe transport are indicated in red boxes (MIT1 Fe binding motifs: H53, H110, M196, Y235). Conserved [DE]-xx-[RK] motifs putatively forming the salt bridges on the cytosolic and the matrix side of the membrane are indicated in yellow and blue boxes, respectively. An * (asterisk) indicates positions which have a single, fully conserved residue. A : (colon) indicates conservation between groups of strongly similar properties (roughly equivalent to scoring > 0.5 in the Gonnet PAM 250 matrix). A . (period) indicates conservation between groups of weakly similar properties (roughly equivalent to scoring =< 0.5 and > 0 in the Gonnet PAM 250 matrix).

O. niloticus Mfrn1. The results from these studies report the importance of three conserved histidines (H48, H105, and to a lesser extent, H222 in MRS3) and a methionine (M207 in Mfrn1) in the transport of Fe (Brazzolotto et al., 2014; Christenson et al., 2018). The H222 in MRS3 is conserved in MIT2, however, is replaced by another potential Fe-ligand, a tyrosine, in MIT1. Furthermore, two motifs ([DE]-xx-[RK]) that likely form salt-bridge networks on each side of the membrane have been previously hypothesized to facilitate solute transport by MCF proteins. Mutagenesis of the residues building the putative salt-bridge networks were shown to either affect the integrity of the protein or result in loss of transport activity (Christenson et al., 2018). Interestingly, these residues were also identified in MIT1 and MIT2 (**Figure 1**). Thus, despite the relatively low sequence identity between the orthologs, the residues important for Fe transport appear to be conserved across species.

The yeast genes, *MRS3* and *MRS4* encode functional mitochondrial iron transporters that mediate the uptake of Fe^{2+} to the mitochondria. The double mutant, *mrs3mrs4* exhibits a growth sensitive phenotype under low Fe conditions (Muhlenhoff et al., 2003). To test if Arabidopsis MIT1 and MIT2 are functional orthologs of MRS3 and MRS4, we cloned *MIT1* and *MIT2* separately into a yeast expression vector (pRS426-ADH) and transformed them into the *mrs3mrs4* yeast background to assess their ability to complement the poor growth phenotype of the mutant strain. To ensure proper targeting of the Arabidopsis proteins to the yeast mitochondria, the endogenous targeting sequences (1st-22 amino acids) of MIT1 and MIT2 were substituted with the mitochondrial leader sequence (1st-22 amino acids) of MRS3 (as employed in Shaw et al., 2006). The yeast *MRS3* clone and the empty vector were used as positive and negative controls, respectively. The *mrs3mrs4* strain transformed with *MIT1*, *MIT2*, *MRS3*, or the empty vector. The resulting strains were spotted side-by-side on Fe-sufficient and Fe-deficient media. No phenotypic differences were observed between the different strains under Fe sufficiency. Interestingly, similar to yeast MRS3, both MIT1 and MIT2 were able to partially rescue the slow growth phenotype of *mrs3mrs4* under Fe deficiency (**Figure 2**). In contrast, the empty vector strain was unable to grow well on Fe-deficient media. These results show that Arabidopsis MIT1 and MIT2 can rescue the loss of function phenotype of mitochondrial iron transporters in yeast. Differences in the efficiency of complementation by MIT1 and MIT2 could be due to expression and/or targeting of the Arabidopsis proteins in yeast.

MIT1 and MIT2 Localize to Mitochondria in Plants

MIT1 and MIT2 have been previously predicted to localize to the mitochondria due to their possession of the METS (Millar and Heazlewood, 2003). To investigate their subcellular localization *in planta,* the *MIT1* and *MIT2* clones, driven by the *35S* promoter were fused in frame with a YFP tag (*35S-MIT1-YFP* and *35S-MIT2-YFP*) and these constructs were transiently transformed into onion peel epidermis *via* particle bombardment. The transformed epidermis peels were co-stained with a mitochondrial marker (MitoTracker Orange) and were further analyzed for fluorescence using confocal microscopy. Both MIT1 and MIT2 colocalized with the mitochondrial marker thus confirming their localization to mitochondria (**Figures 3A, B**). To further confirm the localization, *35S-MIT1-YFP* and *35S-MIT2-YFP* stable transgenic Arabidopsis lines along with the empty vector line

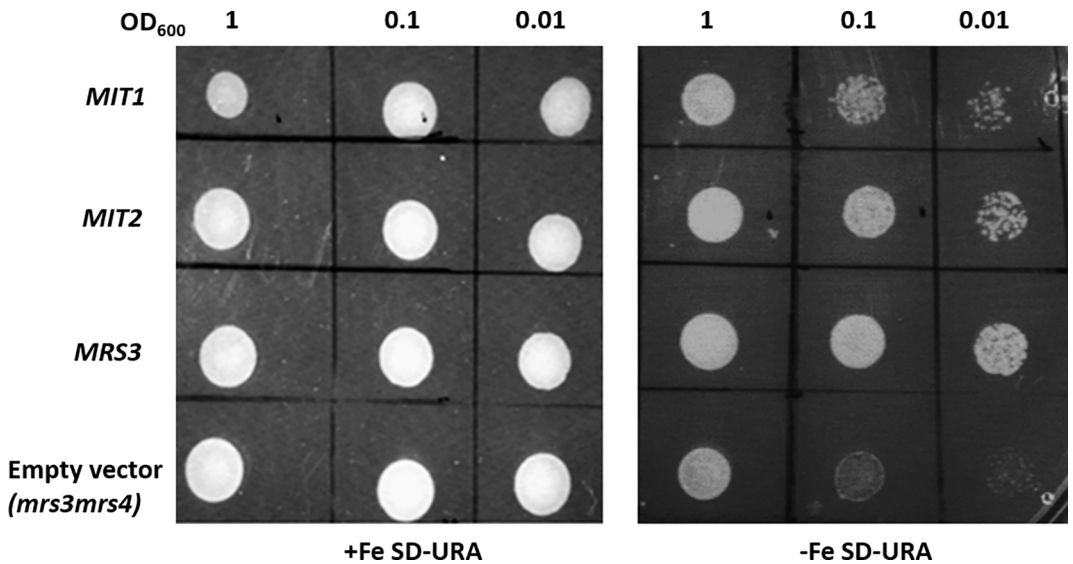

FIGURE 2 | Arabidopsis MIT1 and MIT2 complement the defective growth phenotype of *mrs3mrs4* on Fe-deficient media. *mrs3mrs4* was transformed with *MIT1, MIT2, MRS3* (positive control) and the empty vector (pRS426-ADH; negative control). Three serial dilutions corresponding to OD_{600} of 1, 0.1 and 0.01 of the transformed yeast were assayed for growth complementation on SD-uracil plates under Fe-sufficient (0.1mM $FeSO_4$) or Fe-deficient (0.1mM BPS) conditions.

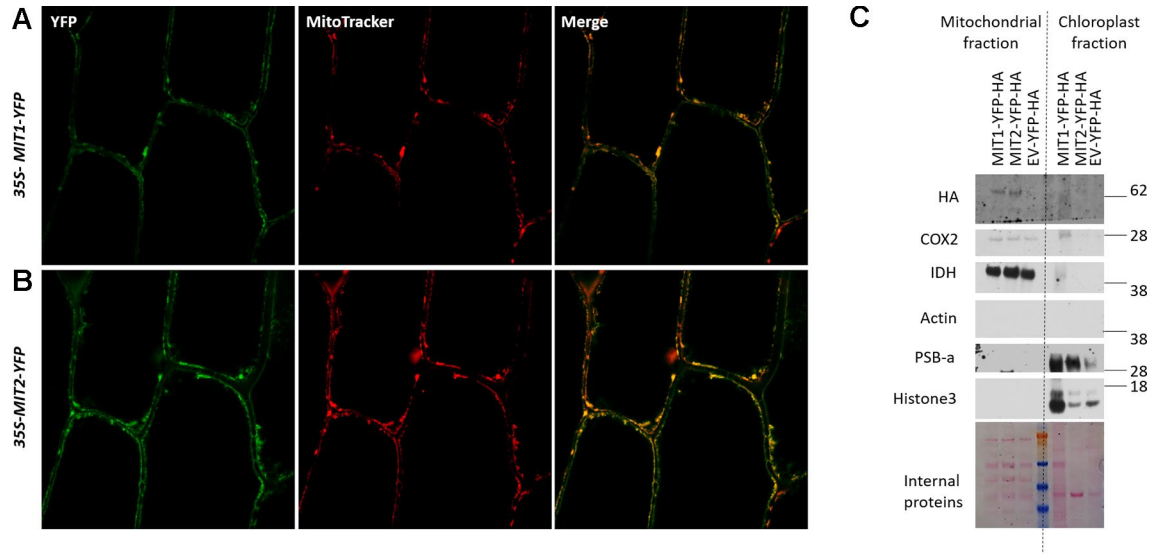

FIGURE 3 | Mitochondrial localization of MIT proteins. Confocal images of onion peel epidermis transiently transformed with **(A)** *35S-MIT1-YFP* and **(B)** *35S-MIT2-YFP* constructs. The cells were co-stained with the mitochondria specific marker, MitoTracker Orange. **(C)** Mitochondria were purified from 2-week-old Arabidopsis *MIT1-YFP-HA*, *MIT2-YFP-HA* and the empty vector (*EV-YFP-HA*) transgenic lines grown on B5 media. 25 µg of the purified protein was separated by the SDS-PAGE. The localization of MIT1 and MIT2 was tested by immunoblotting with an anti-HA antibody. The chloroplast fraction (comprised of broken thylakoids/chloroplasts) separated from the mitochondrial fraction during ultracentrifugation were used as a control. The purity of the mitochondria was tested by immunoblotting the purified mitochondria against different cellular markers including COX2 and IDH (mitochondrial proteins), Actin (cytosolic protein), PSB-a (chloroplast protein) and Histone3 (nuclear protein). Ponceau S-stained proteins were used as a loading control. Note: the chloroplast MIT1-YFP-HA lane is overloaded relative to the MIT2-YFP-HA and EV-YFP-HA lanes.

were also generated. We purified the mitochondria from these lines and assessed the localization of MIT1 and MIT2 *via* western blot. The purity of the mitochondria was analyzed by probing against various known markers of other subcellular compartments. These studies confirmed the localization of both proteins to the mitochondria (**Figure 3C**). In addition, it is important to note that C-terminally tagged MIT1 and MIT2 were able to rescue the yeast *mrs3mrs4* mutant, so presumably, these tags do not disrupt transporter function.

Expression Pattern Analysis of *MIT1* and *MIT2*

Publicly-available gene expression data shows that *MIT1* and *MIT2* are expressed throughout development. However, the expression of both genes is the highest in the seed and young developing seedlings (http://bar.utoronto.ca/efp/cgi-bin/efpWeb.cgi). To study the spatial expression patterns of *MIT1* and *MIT2,* we generated stable transgenic lines transformed with β-glucuronidase (GUS) reporter constructs driven by either the *MIT1* or *MIT2* endogenous promoters. GUS histochemical staining was performed on 2-week-old seedlings, and the staining was observed in both shoots and roots of the young seedlings of *pMIT1-GUS*, as well as *pMIT2-GUS* (**Figures 4A–G**). These results confirm that *MIT1* and *MIT2* are ubiquitously expressed. In addition, the promoter activity for both genes is notably pronounced in the vascular cylinder of the plant as previously observed (Dinneny et al., 2008). In fact, *MIT1* and *MIT2* were identified as genes whose expression is particularly high in the pericycle (Long et al., 2010).

Next, we looked at the expression levels of *MIT1* and *MIT2* in the roots and shoots of Col-*0* (WT) seedlings under Fe-deficient and Fe-sufficient conditions by quantitative RT-PCR (**Figure 5**). Both the genes are expressed in shoots as well as roots. Both *MIT1* and *MIT2* show a modest decrease in mRNA levels upon Fe limitation in shoots but no response to Fe limitation in the roots of 2-week-old seedlings. Thus, our data indicate that unlike rice *MIT*, the expression of *MIT1* and *MIT2* in Arabidopsis is not strongly regulated by Fe availability. Similar results were observed previously in microarray analysis performed on Arabidopsis seedlings grown under +/-Fe conditions (Long et al., 2010). This data is supported by RNA sequencing of the *nramp3nramp4* line (which is defective in Fe remobilization from vacuoles) (Bastow et al., 2018). While the other markers of Fe-deficiency such as putative mitochondrial Fe reductase *FRO3*, the root epidermis Fe reductase *FRO2* and the root epidermis Fe transporter *IRT1* were upregulated in *nramp3nramp4,* expression of *MIT1* and *MIT2* is unaffected in the same background (Bastow et al., 2018). Thus, it appears that MIT expression is not strongly regulated by Fe status in Arabidopsis.

MIT1 and MIT2 Are Essential for Embryogenesis

To investigate the role of *MIT1* and *MIT2 in planta*, T-DNA insertion mutants (SALK_013388 for *MIT1* and SALK_096697

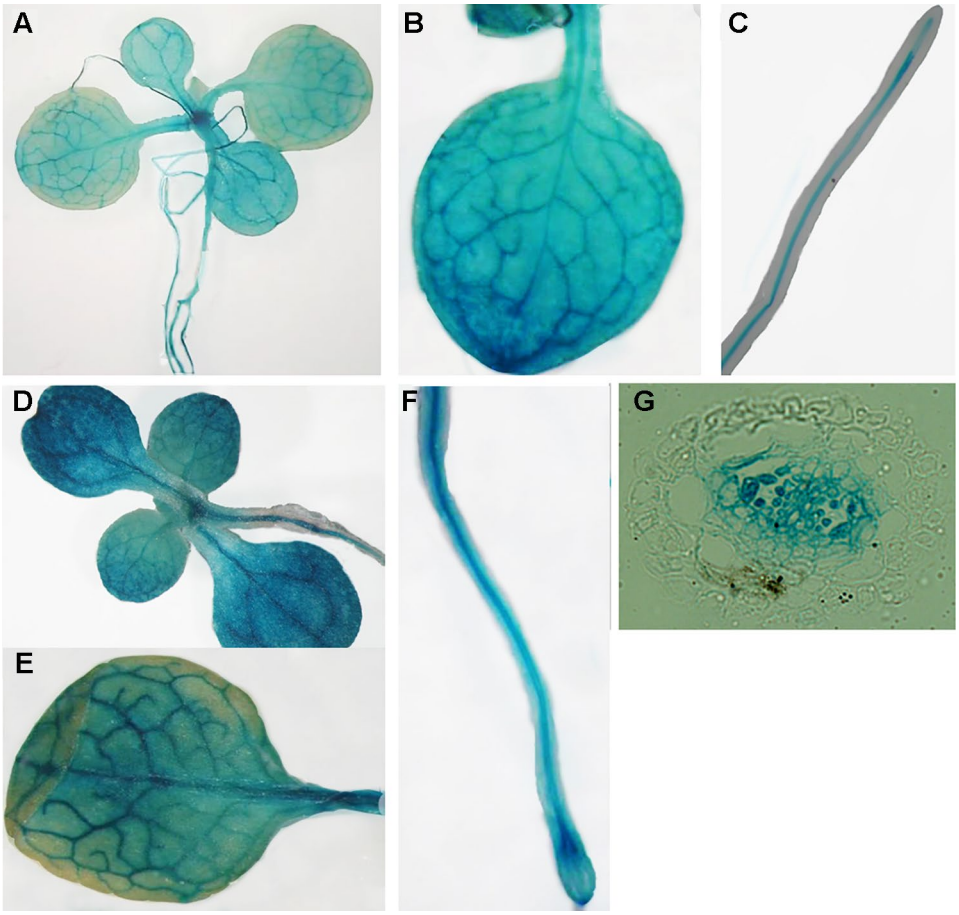

FIGURE 4 | Expression analysis of *MIT1* and *MIT2*. GUS histochemical staining of 2-week-old seedlings grown in B5 media. **(A-C)** *pMIT1-GUS* and **(D-F)** *pMIT2-GUS*. **(G)** Root cross-section of *pMIT2-GUS*.

for *MIT2*) were obtained from the ABRC. *MIT1* (At2g30160) is 1862 bp long with two exons. *MIT2* (At1g07030) is a 2405 bp long gene with two exons and a single intron each. While the *mit1* mutant (SALK_013388) has an insertion in its first exon, 246 bases after the translation start site, the *mit2* (SALK_096697) mutant has a single T-DNA insertion in the intron, 1592 bases after the translation start site (**Figure 6A**). Single-insertion homozygous mutants, (*mit1* and *mit2*) were confirmed by back-crossing the mutants with the WT and PCR genotyping. The heterozygous F1 generation obtained after backcrossing was allowed to self-cross which resulted in a progeny population of 1:2:1 (WT: heterozygous: homozygous) in the following generation (F2). These lines were grown and genotyped for three more generations to ensure a single insertion. The true breeding lines thus obtained were propagated as homozygous single insertion. Transcript levels in the mutants were measured by quantitative and semi-quantitative RT-PCR (**Figures 6B** and **S1A**). The *mit1* insertion resulted in an almost complete knockout with 98% reduction in the *MIT1* transcript abundance while the insertion in the *mit2* line resulted in 85% knockdown of *MIT2* transcript abundance (**Figure 6B**).

The visible phenotypes of the single mutants were indistinguishable from the wild type (data not shown). We therefore hypothesized that MIT1 and MIT2 function redundantly, and so the individual *mit1* and *mit2* T-DNA insertion lines were crossed together to obtain a double knockout line *mit1mit2*. However, we failed to obtain a line homozygous for both *mit1* and *mit2*. Dissection of the siliques of self-crossed $mit1^{--}/mit2^{+-}$ revealed an embryo lethal phenotype presumably due to the loss of both *MIT1* and *MIT2* (**Figures 7A–F**). Similar results were observed by self-crossing the $mit1^{+-}/mit^{--}$ line (image not shown). 6.6% of embryos were aborted in the heterozygous $mit1^{--}/mit2^{+-}$, while 20.4% and 20.8% of embryos were aborted in the self-crossed lines $mit1^{--}/mit2^{+-}$ and $mit1^{+-}/mit2^{--}$ respectively (**Figure 7G**). The statistical significance of these ratios was confirmed by chi-square test (chi-square value <3.84). The fact that the *mit2* mutation does not result in a full knockout may account for the fact that we observed less than the predicted 25% embryo lethality. These results demonstrate that the two genes are functionally redundant and MIT function is essential for embryogenesis. All further experiments for the functional analysis of MIT function were performed using the

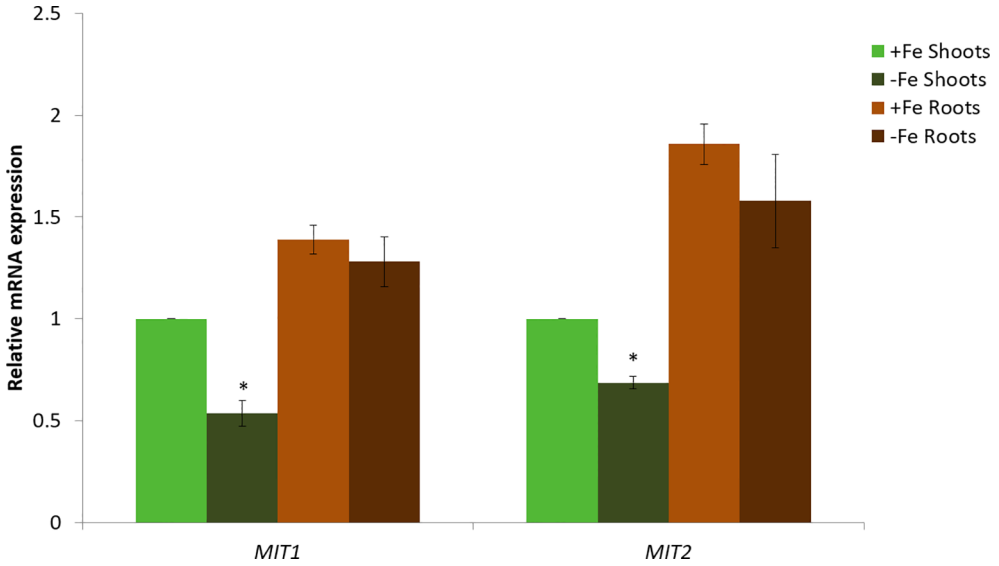

FIGURE 5 | Quantitative RT-PCR expression analysis of *MIT1* and *MIT2* in shoots and roots of WT seedlings grown in standard B5 media for 2 weeks and then transferred to Fe-sufficient or Fe-deficient media for 3 days. The mRNA levels for both *MIT1* and *MIT2* from +Fe shoot was set at 1 and the relative abundance of the two transcripts were determined in the other tissues. Actin was used as a reference gene to normalize mRNA values. Values represent the mean of 3 biological replicates, and error bars indicate standard deviation. Significance ($p < 0.05$) was assessed using the Student's *t*-test; significant differences in the transcript abundance between +Fe and –Fe shoots is represented by an asterisk.

mit1^{--}*/mit2*$^{+-}$ line due to a stronger transcript suppression in this line as compared to *mit1*$^{+-}$*/mit2*$^{--}$ (**Figure S1B**).

Artificial microRNA lines targeting both *MIT1* and *MIT2* (*amiRmit1mit2)* were constructed to confirm the double mutant phenotypes. Five independent lines were tested, and the one (A17) with the lowest transcript abundance (with a 30% reduction in *MIT1* and 88% reduction in *MIT2* levels) of *MIT1* and *MIT2* was chosen for all further experiments (**Figure 6C**). Due to only a partial reduction of transcript abundance, the *amiRmit1mit2* mutant did not exhibit an embryo lethal phenotype but it was subject to further phenotypic profiling (along with *mit1*$^{--}$*/mit2*$^{+-}$*)* as described below.

MIT1 and MIT2 Mediate Mitochondrial Iron Uptake in Arabidopsis

Yeast mitoferrins are believed to function predominantly under low Fe conditions (Froschauer et al., 2009). To study the role of MIT1 and MIT2 in mitochondrial Fe homeostasis, we purified mitochondria from the WT and the *mit1*$^{--}$*/mit2*$^{+-}$ mutant grown in Fe-sufficient and Fe drop-out media. It is important to note that the mitochondria prepared from *mit1*$^{--}$*/mit2*$^{+-}$ were obtained from a population that was homozygous for the *mit1* mutation but was segregating for *mit2*. Since several respiratory subunits require Fe-S clusters and/or heme as their cofactor, Fe-limitation is consequently expected to affect the integrity and the function of the electron transport chain in mitochondria. Therefore, we first investigated the effect of loss of MIT1 and MIT2 on the respiratory complexes by separating solubilized mitochondrial proteins on a blue native gel. While no significant difference was observed between the WT and *mit1*$^{--}$*/mit2*$^{+-}$ mutant mitochondria obtained from Fe-sufficient conditions, significant changes in the relative abundance of the complexes and supercomplexes close to 1 megadalton (typically complex I and its supercomplexes) were observed in the *mit1*$^{--}$*/mit2*$^{+-}$ mutant mitochondria isolated from plants grown in Fe drop-out media (**Figure 8A**). To confirm, we performed in-gel staining for complex I and found a 40% reduction in complex I levels in the mutant mitochondria (**Figure 8B**). A 30.2% reduction in complex I was also observed in the *amiRmit1mit2* mutant mitochondria isolated from seedlings grown in Fe drop-out conditions (**Figure S2A**). We also examined the protein levels of aconitase, a [4Fe-4S] cluster protein, involved in the TCA cycle in mitochondria. Previous studies have shown that Fe deficiency results in reduced aconitase abundance (Ross and Eisenstein, 2002). As expected, reduced aconitase protein levels were observed in the mitochondrial as well as total cellular extracts of *mit* mutants grown in the Fe drop-out conditions (**Figure 8C**). Since the loss of MIT1 and MIT2 had a more pronounced effect in Fe-limited conditions, we measured the elemental profile of mitochondria prepared from 2.5-week-old WT and *mit1*$^{--}$*/mit2*$^{+-}$ seedlings grown on Fe drop-out media. The Fe levels in mitochondrial preparations of the *mit1*$^{--}$*/mit2*$^{+-}$ mutant were significantly reduced (by 43%) as compared with WT (**Figure 8D**). The *amiRmit1mit2* lines also show a reduction in mitochondrial Fe content (**Figure S2B**). Interestingly, these mutants also show an increased accumulation of Zn in their mitochondria (**Figures 8E** and **S2B**), suggesting cross-talk between Fe and Zn homeostasis. The Mn content of the mitochondria was unchanged (**Figures 8F** and **S2C**), and the levels of Cu and Co were below the detection limit. These results indicate that in the absence of MIT1 and MIT2, mitochondrial iron import is severely compromised resulting in

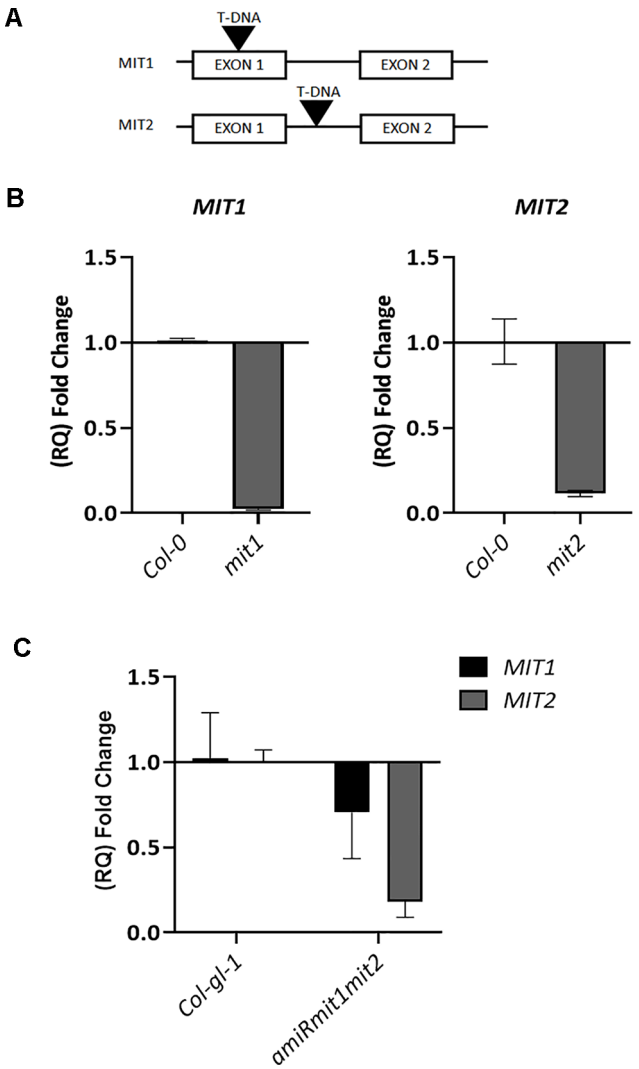

FIGURE 6 | Genetic analysis of *mit1* and *mit2* mutants. **(A)** Gene structure of the *mit1* and *mit2* T-DNA insertion mutants. The insertion in *mit1* was identified in its first exon, 246 bases after the translation start site, the insertion in *mit2* is located in the intron, 1592 bases after the translation start site. **(B)** Relative quantification (RQ) of *MIT1 and MIT2* transcript levels by quantitative RT-PCR in *mit1* and *mit2*, respectively. **(C)** Relative quantification (RQ) of *MIT1* and *MIT2* in Col-*gl-1* and *amiRmit1mit2* lines. Actin was used a control. The values represent the mean of two to three biological replicates, and error bars indicate standard deviation. The RNA was harvested from 2.5-week-old seedlings grown in Fe-sufficient media.

significant loss of Fe-requiring proteins and their biochemical activities. Moreover, the loss of MIT1 and MIT2 appears to be significant for mitochondrial function primarily under Fe drop-out conditions, suggesting the possible existence of an alternate Fe uptake pathway in mitochondria.

mit Mutants Display Altered Whole-Plant Iron Homeostasis

To gain insight into the effect of loss of MIT function on iron homeostasis at the whole plant level, we measured the elemental profile of the shoots of 44-day-old mature, soil grown plants (WT, *mit1, mit2, mit1*$^{--}$*/mit2*$^{+-}$, *mit1*$^{+-}$*/mit2*$^{--}$, and *amiRmit1mit2*) by ICP-MS. Shoot Fe levels showed slight to no change in the mutant lines as compared to the WT (**Figures 9A** and **S2D**). However, all the mutants exhibited the well-described Fe deficiency signature phenotype (Baxter et al., 2008) as shown by elevated levels of Mn, Zn, and Co observed in the shoots of the *mit1, mit2* and the double mutants (**Figures 9B–D**). Additionally, these mutants also accumulated significant amounts of Cu (**Figure 9E**). The elemental profile observed in *mit* lines suggests that these lines perceive Fe deficiency, which in turn results in increased uptake of Zn and other divalent metals potentially *via* IRT1, although Fe levels remain relatively stable, likely due to tight control on Fe homeostasis to prevent its overaccumulation.

To test the hypothesis that loss of MIT function results in upregulation of Fe deficiency responses, we measured the levels of two root Fe deficiency markers. First, we measured root surface ferric reductase activity and showed that while ferric reductase activity is not altered in the single *mit1* and *mit2*

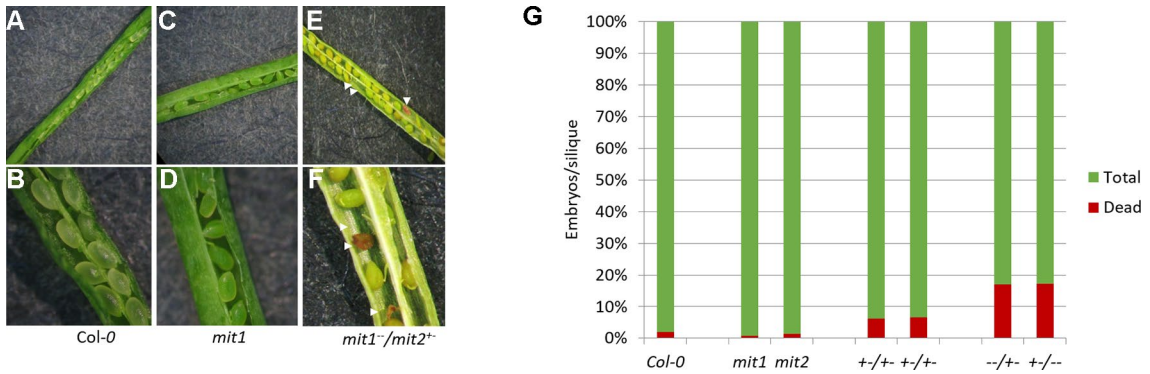

FIGURE 7 | *mit1mit2* mutation is embryonically lethal. Dissected siliques of **(A**, **B)** WT, **(C**, **D)** *mit1*, **(E**, **F)** *mit1*$^{--}$*/mit2*$^{+-}$. The aborted embryos (red embryos and empty spaces in the silique; indicated by white arrows) show the embryonic lethality of *mit1mit2* homozygous mutants. **(G)** Quantification of aborted embryos in different *mit* mutant backgrounds. *mit1*$^{--}$*/mit2*$^{+-}$ is represented as $^{--}$/$^{+-}$ and *mit1*$^{+-}$*/mit2*$^{--}$ is represented as +−/−−. Approximately 500 seeds were counted from 10 to 12 individual siliques per genotype.

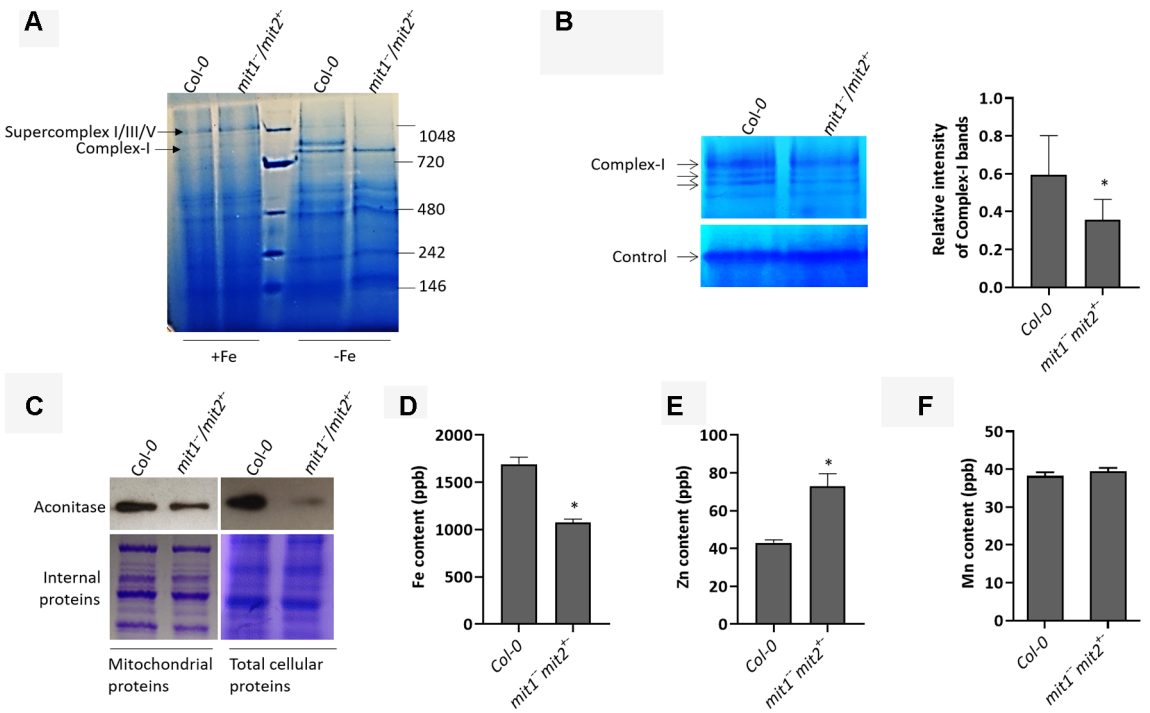

FIGURE 8 | MITs are important for mitochondrial iron acquisition/import. **(A)** Separation of 20 µg solubilized mitochondrial fraction of Col-*0* and the *mit1*$^{--}$*/mit2*$^{+-}$ mutant grown in Fe-sufficient (+Fe) or Fe drop-out media (-Fe) by blue-native gel electrophoresis (BN-PAGE). **(B)** In-gel enzyme activity assay for complex I on mitochondrial extract separated by BN-PAGE. The arrows indicate complex I and its supercomplexes. Non-specific staining at the bottom of the gel was used as the loading control. The staining in the WT and the mutant was quantified using ImageJ software. **(C)** Immunoblots showing aconitase protein levels in mitochondrial and total protein extracts. Coomassie stained internal proteins were used as a loading control. Total mitochondrial **(D)** Fe content, **(E)** Zn content, and **(F)** Mn content as measured by ICP-MS (shown is the mean of three technical replicates; error bars represent standard deviation). Significance was assessed using the student's *t*-test. An asterisk represents a p value < 0.05. The mitochondria for all the experiments **(B**-**F)** were isolated from 2.5-week-old seedlings grown on Fe drop-out media.

mutants, the *mit1*$^{--}$*/mit2*$^{+-}$ and *amiRmit1mit2* lines display significant increases in induction of ferric reductase activity under Fe deficiency as compared to WT (**Figures 10A** and **S2E**). Similarly, IRT1 protein levels are also significantly higher in the mutant lines (**Figures 10B** and **S2F**). Furthermore, we also observed a significant elevation in ferritin levels in *mit* mutant shoots (**Figure 10C**) in Arabidopsis supporting the hypothesis that Fe homeostasis is disrupted in *mit* plants.

In addition to these molecular phenotypes, we also observed the general growth and development of *mit* loss of function lines. While the soil grown mutants did not show any visible phenotypic differences from the WT, *mit* mutants lines appeared to be chlorotic and displayed a compromised growth phenotype when grown hydroponically in Fe drop-out media (**Figures 11A** and **S3**). This phenotype could be rescued *via* exogenous supply of 5 μM Fe(III)-EDDHA, suggesting that MIT loss-of-function phenotypes are due to altered Fe metabolism (**Figure 11B**).

DISCUSSION

Mitochondrial Fe is generally known to be required for two major biochemical pathways: Fe-S cluster biogenesis and heme synthesis. Despite its importance, Fe transport across the mitochondrial membrane is still not fully understood. Our studies in Arabidopsis have identified two putative mitochondrial metalloreductases (FRO3 and FRO8), of which FRO3 is hypothesized to play a role in mitochondrial iron transport based on the fact that it can reduce Fe in a

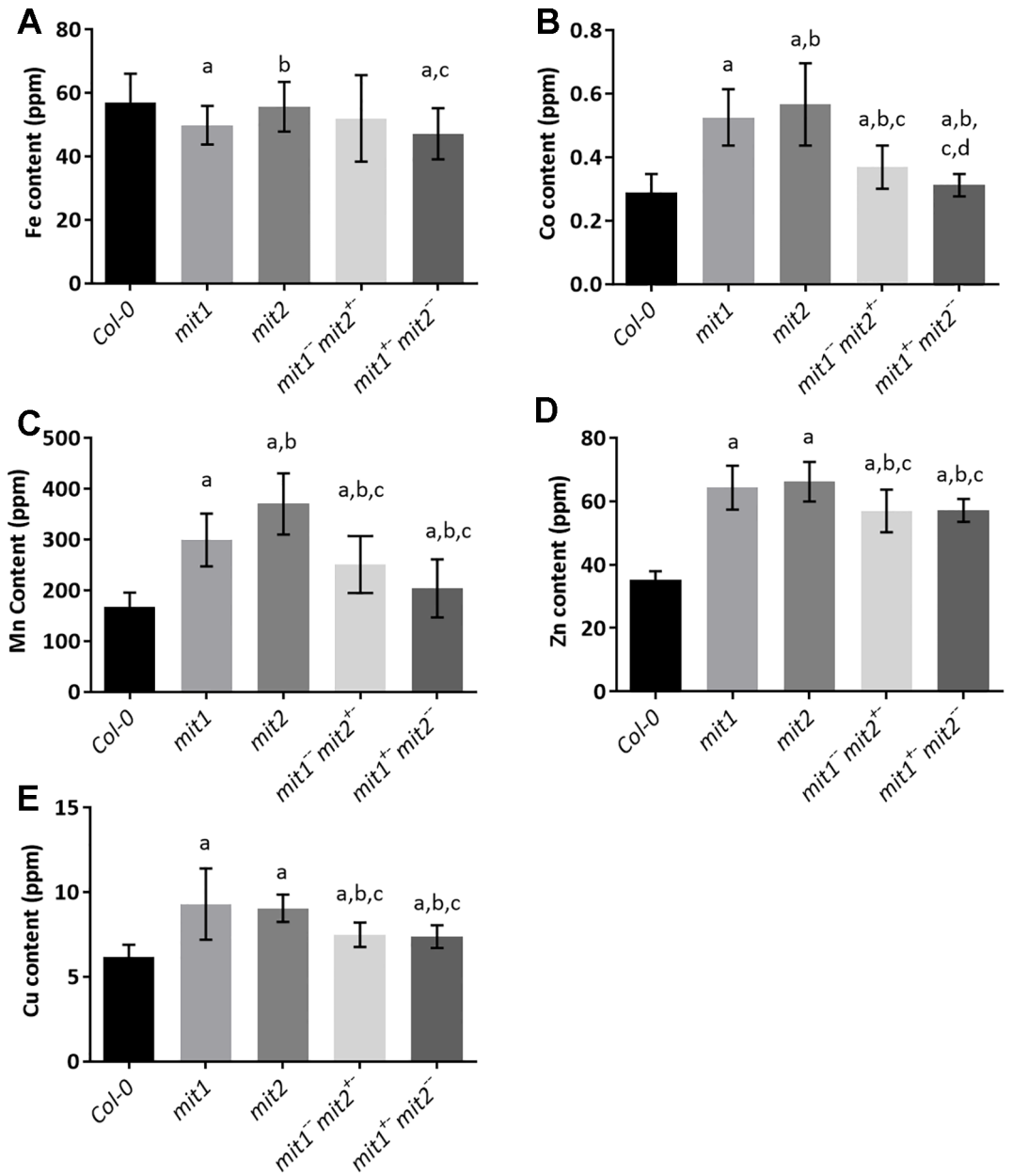

FIGURE 9 | *mit* mutants exhibit iron deficiency. Levels of **(A)** Fe, **(B)** Co, **(C)** Mn, **(D)** Zn, **(E)** Cu in the shoots of plants grown in soil in short day conditions for 44 days. Values shown are an average of 13 biological replicates and error bars represent standard deviation. Significance was assessed using the Student's *t*-test. A p value < 0.05 compared to Col-*0*, *mit1*, *mit2*, *mit1*$^{-}$/*mit2*$^{+-}$ is represented by a, b, c, d respectively.

heterologous system (Wu et al., 2005), is broadly expressed and is upregulated by Fe limitation (Mukherjee et al., 2006; Jain et al., 2014). Although proteins involved in Fe export from plant mitochondria remain unidentified, a recent study has shown that ATM3 (a member of the ATP Binding Cassette (ABC) family) exports glutathione polysulphide for the assembly of cytosolic Fe-S clusters in Arabidopsis (Schaedler et al., 2014). In this paper, we provide evidence that yeast MRS3 and MRS4 orthologs, MIT1 and MIT2 function redundantly as mitochondrial iron transporters in Arabidopsis.

Mitochondrial carrier family (MCF) proteins are small 30kDa proteins that localize to the inner mitochondrial membrane (IMM) and are involved in the transport of a wide variety of solutes from the inner membrane space (IMS) into the mitochondrial matrix (Walker, 1992; Palmieri, 2013). The outer mitochondrial membrane (OMM) possesses porin proteins which allow the free movement of various small molecules across the membrane. The IMM, on the other hand, is selectively permeable, and therefore requires transporters to shuttle polar solutes across the membrane. MCF proteins have a tripartite structure, with six transmembrane domains forming a barrel for substrate transport, which is closed at the matrix side by a salt-bridge network that is located at the bottom of the cavity (Pebay-Peyroula et al., 2003; Kunji and Robinson, 2006). Arabidopsis MIT1 and MIT2 belong to the MCF protein

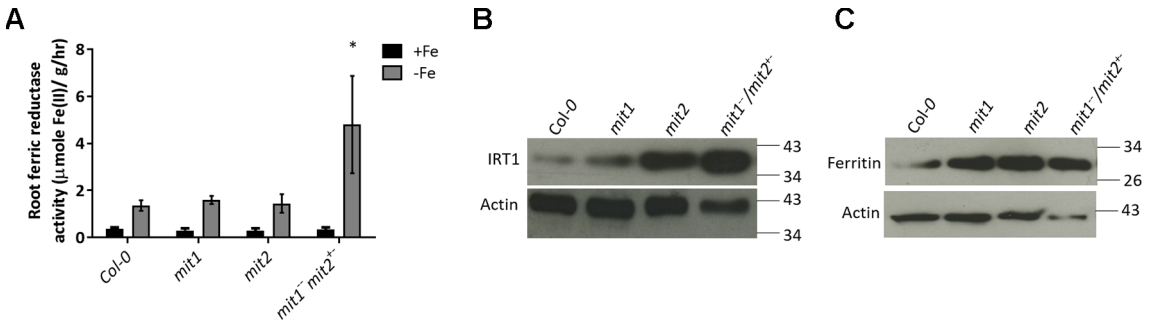

FIGURE 10 | *mit* mutants exhibit altered Fe homeostasis under Fe deficiency. **(A)** Root ferric reductase activity assay on seedlings grown in Fe-sufficient or Fe-deficient media. The activity was normalized to root fresh weight. Values shown are an average of 10 biological replicates. Error bars in all the graphs indicate standard deviation. Significance was assessed using the student's *t*-test. The asterisk represents a p < value 0.05 as compared to Col-*0*. Seedlings were grown on standard B5 media for 2 weeks and then transferred to Fe-sufficient (50 µM Fe(III)-EDTA) or Fe-deficient (300 µM ferrozine media) for 3 days. **(B)** Immunoblot of IRT1 protein levels in the roots of *mit* mutants grown on standard B5 media for 2 weeks and then transferred to Fe-deficient conditions for 3 days. **(C)** Immunoblot of ferritin levels in shoots of 2.5-week-old *mit* seedlings grown in Fe-sufficient media. 25 µg of protein lysate was loaded per lane for the immunoblots.

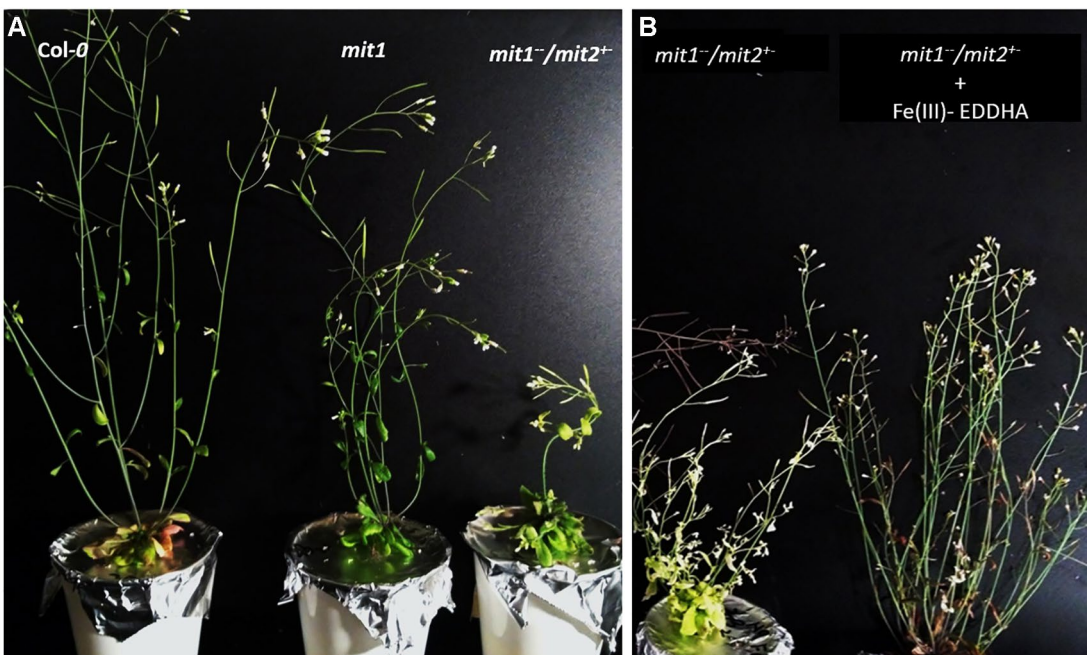

FIGURE 11 | Growth phenotype of mit loss-of-function lines in Fe-deficient conditions. **(A)** Compromised growth phenotype of five-week old *mit1⁻⁻/mit2⁺⁻* grown hydroponically in Fe drop-out media. **(B)** Six-week old plants grown hydroponically in Fe drop-out media supplemented with 5 µM Fe (III)-EDDHA after 3 weeks.

family and therefore likely reside at the IMM of mitochondria (Picault et al., 2004). A recent report described amino acid residues of Mfrn1 and MRS3 that are important for Fe transport across the membrane (Brazzolotto et al., 2014; Christenson et al., 2018). The presence of these residues in the Arabidopsis MIT1 and MIT2 amino acid sequences (**Figure 1**) support their roles as mitochondrial Fe transporters (Kunji and Robinson, 2006; Brazzolotto et al., 2014; Connorton et al., 2017; Christenson et al., 2018). Expression of *35S-MIT-YFP* constructs in onion peel epidermal cells allowed us to show that MIT1 and MIT2 are indeed localized to mitochondria (**Figure 3**). The functional role of MIT1 and MIT2 as mitochondrial Fe transporters was confirmed by complementation of the yeast mitoferrin mutant (*mrs3mrs4*) (**Figure 2**).

To better understand the molecular function of *MIT1* and *MIT2 in planta*, we identified T-DNA insertion mutants of *MIT1* and *MIT2* (**Figure 6**). The redundancy in the roles of mitoferrins has been previously observed in mammalian non-erythroid cells, as well as yeast in terms of biochemical properties and kinetic profiles for Fe^{2+} uptake (Paradkar et al., 2009; Brazzolotto et al., 2014). While the double mutant was embryo lethal, no obvious growth defects were noted when the single mutants were grown in soil or on MS agar plates (data not shown). Similar to the *mit1mit2* double mutant, the frataxin mutant (*atfh*) also exhibits an embryo lethal phenotype (Vazzola et al., 2007). Despite the accumulation of excess mitochondrial Fe, *atfh* mutants are unable to direct their Fe reserves for proper utilization, resulting in compromised Fe-requiring biochemical reactions in the cell (Maliandi et al., 2011; Jain and Connolly, 2013). Interestingly, it has been suggested that frataxin functions in donating Fe for heme synthesis in plant mitochondria. (Armas et al., 2019). Thus, adequate supply of Fe and its proper utilization appears to be obligatory for embryogenesis and survival.

To validate their role in mitochondrial Fe transport *in planta*, we studied the effect of loss of MITs on mitochondrial Fe homeostasis. Loss of MIT1 and MIT2 results in reduced mitochondrial Fe but elevated mitochondrial Zn (**Figures 8** and **S2**). A few regulators have been reported in the literature which function to sense Fe availability based on the ratio of Fe to other metals such as Zn in the cell (Kobayashi et al., 2013). The Fe and Zn binding sites on these regulators sense the imbalance between the two elements to trigger the Fe deficiency response (Kobayashi et al., 2013). Although mitochondrial Fe sensors in plants are still unknown, the aforementioned mechanism may explain the up-regulation of the Fe deficiency pathway in response to the altered elemental profile of $mit1^{--}/mit2^{+-}$ mitochondria (**Figure 8**). Reduced complex I activity and depleted aconitase levels in the mutants further substantiate the significance of MITs in mitochondrial iron trafficking and homeostasis (**Figures 8** and **S2**). These data corroborate the results of a recent study that used transcriptomic and metabolomic profiling to shed light upon the effects of *mit* knockdown on primary metabolism in rice (Vigani et al., 2016).

Mitochondrial iron transporters have been characterized in several species. While mitoferrins/MITs seem to be the major iron importers, they are not the sole transporters of Fe into the mitochondrial matrix. Mitoferrins/MITs appear to be particularly important during the early stages of development (**Figure 7**) (Muhlenhoff et al., 2003; Shaw et al., 2006; Bashir et al., 2011). In addition, the presence of other low affinity mitochondrial Fe transporters or non-specific divalent metal transporters have been reported in the literature (Yoon et al., 2011; Małas et al., 2018; Migocka et al., 2019); such transporters may be responsible for Fe import under normal to high cytosolic Fe conditions (Jain and Connolly 2013). Whether MIT1 and MIT2 can shuttle other ions other than Fe is not clear at this point but a role of their orthologs, Mfrn1, MRS3 and MRS4 in transporting other cations has been reported in the past (Muhlenhoff et al., 2003; Froschauer et al., 2009; Froschauer et al., 2009). In general, mitoferrins play a crucial role in heme and Fe-S cluster biosynthesis in yeast, zebrafish, and mammals; however, their role in plants may be limited to Fe-S cluster synthesis since definitive proof of mitochondrial heme synthesis in plants is lacking (Muhlenhoff et al., 2003; Shaw et al., 2006; Paradkar et al., 2009; Bashir et al., 2011; Jain and Connolly, 2013; Rouault, 2016). In fact, we measured total catalase activity (heme containing enzyme) and observed no difference in the activities in lysates prepared from WT and *mit* mutant backgrounds (data not shown). Nevertheless, MITs seem to be the major mitochondrial Fe transporters, and their significance in mitochondrial and cellular Fe homeostasis is clear.

Given that *mit* mutants displayed reduced Fe content and altered Fe metabolism in the mitochondria, we sought to examine Fe metabolism in whole tissues. The Arabidopsis *mit* mutants show an onset of the Fe deficiency response in roots (**Figure 10**), although shoot Fe content is not dramatically altered in *mit* lines, all the mutants show elevated accumulation of other divalent metal ions, such as Zn, Mn, and Co (**Figure 9**). This phenotype has been previously described as the Fe deficiency signature phenotype (Baxter et al., 2008; Walker and Connolly, 2008). In Arabidopsis, *IRT1* expression responds to Fe deficiency; however, IRT1 non-specifically transports various other metals, such as Mn, Co, Zn, and Cd, along with Fe (Connolly et al., 2002; Eide et al., 1996; Korshunova et al., 1999; Rogers et al., 2000; Vert et al., 2002). These results suggest that cells monitor mitochondrial Fe levels and upregulate the root Fe uptake machinery when mitochondrial Fe levels fall too low. In addition to this, *mit* mutants in Arabidopsis also exhibit significantly elevated shoot Cu levels. This is presumably because Fe deficiency is known to up-regulate a high affinity Copper Transporter (COPT2), which in turn leads to accumulation of Cu in the shoots (Perea-Garcia et al., 2013). This elevated Cu uptake is thought to aid in maintaining metal homeostasis as it allows the plant to switch from Fe-utilization to Cu-utilization pathways, which in turn, helps in the prioritization of Fe and eventual recovery from Fe deficiency (Yamasaki et al., 2009; Garcia et al., 2019).

The *MIT1* and *MIT2* promoters are active throughout the plant with the highest activity in the vasculature (**Figure 4**). The expression of both MIT1 and MIT2 has been observed as early as the stage of seed hydration, at a time when mitochondria become bioenergetically active (Paszkiewicz et al., 2017). However, the two genes are expressed at different levels at different stages of plant growth (www.travadb.org, Arabidopsis efpbrowser) which suggests that they may have different roles in iron metabolism. In recent years, significant progress has been made in elucidation of transcriptional

networks that respond to Fe deficiency. One such network is the PYE network that functions in the pericycle (Long et al., 2010). According to this study, although MITs are expressed in the pericycle and the stele, their expression is not regulated by PYE or Fe availability (Dinneny et al., 2008; Long et al., 2010). Interestingly, while *MIT1* and *MIT2* are not highly regulated by Fe or Cu availability, *MIT1* is regulated by FIT (Mai et al., 2016) and *MIT1* and *MIT2* are regulated by SPL7 (the master regulator of copper-deficient responses) in roots and shoots, respectively (Bernal et al., 2012). This suggests that (similar to human mitoferrins) (Paradkar et al., 2009), while MIT1 and MIT2 are functionally redundant, they may have somewhat specialized functions that remain to be elucidated.

In summary, our results show that *Arabidopsis* MIT1 and MIT2 function in mitochondrial Fe import and together play an essential role in maintenance of cellular and mitochondrial Fe homeostasis. These proteins also are essential for embryogenesis and metabolism under iron-limiting conditions. It is interesting that Arabidopsis, a dicot, has two genes that encode mitochondrial Fe importers, while the monocot rice has just one. Furthermore, it is important to note that loss of MIT function in *Arabidopsis* as compared to rice affects Fe deficiency responses and elemental profiles differently; the consequences of these differences will be the basis for future studies. This work contributes to a comprehensive understanding of Fe homeostasis in plants which may, in turn, help in formulation of strategies to develop Fe-fortified food crops and/or crops that show enhanced performance on marginal soils.

DATA AVAILABILITY STATEMENT

All datasets generated for this study are included in the article/ **Supplementary Material**.

AUTHOR CONTRIBUTIONS

AJ designed and performed the experiments, analyzed the data and wrote the manuscript. ZD performed qRT-PCR experiments on the mutant lines. EC designed and supervised the study, analyzed the data and wrote the manuscript.

ACKNOWLEDGMENTS

We are grateful for funding from NSF IOS (award 1456881) and NSF PGRP (award 144435). We would like to thank Dr. David Salt and John Danku for ICP-MS analysis of Arabidopsis plants, Dr. Jerry Kaplan for the pRS426-ADH vector and the *mrs3mrs4* yeast strain and Dr. Janneke Balk for the aconitase antibody and for her help with BN-PAGE experiments.

SUPPLEMENTARY MATERIAL

The Supplementary Material for this article can be found online at: https://www.frontiersin.org/articles/10.3389/fpls.2019.01449/full#supplementary-material

REFERENCES

Armas, A. M., Balparda, M., Terenzi, A., Busi, M. V., Pagani, M. A., and Gomez-Casati, D. F. (2019). Ferrochelatase activity of plant frataxin. *Biochimie* 156, 118–122. doi: 10.1016/j.biochi.2018.10.009

Balk, J., and Pilon, M. (2011). Ancient and essential: the assembly of iron-sulfur clusters in plants. *Trends Plant Sci.* 16 (4), 218–226. doi: 10.1016/j.tplants.2010.12.006

Bashir, K., Ishimaru, Y., Shimo, H., Nagasaka, S., Fujimoto, M., Takanashi, H., et al. (2011). The rice mitochondrial iron transporter is essential for plant growth. *Nat. Commun.* 2 (1), 322. doi: 10.1038/ncomms1326

Bastow, E. L., Garcia de la Torre, V. S., Maclean, A. E., Green, R. T., Merlot, S., Thomine, S., et al. (2018). Vacuolar iron stores gated by NRAMP3 and NRAMP4 are the primary source of iron in germinating seeds. *Plant Physiol.* 177 (3), 1267–1276. doi: 10.1104/pp.18.00478

Baxter, I. R., Vitek, O., Lahner, B., Muthukumar, B., Borghi, M., Morrissey, J., et al. (2008). The leaf ionome as a multivariable system to detect a plant's physiological status. *Proc. Natl. Acad. Sci.* 105 (33), 12081. doi: 10.1073/pnas.0804175105

Bernal, M., Casero, D., Singh, V., Wilson, G. T., Grande, A., Yang, H., et al. (2012). Transcriptome sequencing identifies SPL7-regulated copper acquisition genes FRO4/FRO5 and the copper dependence of iron homeostasis in Arabidopsis. *Plant Cell* 24 (2), 738–761. doi: 10.1105/tpc.111.090431

Branco-Price, C., Kawaguchi, R., Ferreira, R. B., and Bailey-Serres, J. (2005). Genome-wide analysis of transcript abundance and translation in Arabidopsis seedlings subjected to oxygen deprivation. *Ann. Bot.* 96 (4), 647–660. doi: 10.1093/aob/mci217

Brazzolotto, X., Pierrel, F., and Pelosi, L. (2014). Three conserved histidine residues contribute to mitochondrial iron transport through mitoferrins. *Biochem. J.* 460 (1), 79–89. doi: 10.1042/BJ20140107

Christenson, E. T., Gallegos, A. S., and Banerjee, A. (2018). *In vitro* reconstitution, functional dissection, and mutational analysis of metal ion transport by Mitoferrin-1. *J. Biol. Chem.* 293 (10), 3819–3828. doi: 10.1074/jbc.M117.817478

Clough, S. J., and Bent, A. F. (1998). Floral dip: a simplified method forAgrobacterium-mediated transformation ofArabidopsis thaliana. *Plant J.* 16 (6), 735–743. doi: 10.1046/j.1365-313x.1998.00343.x

Connolly, E. L., Campbell, N. H., Grotz, N., Prichard, C. L., and Guerinot, M. L. (2003). Overexpression of the FRO2 ferric chelate reductase confers tolerance to growth on low iron and uncovers posttranscriptional control. *Plant Physiol.* 133 (3), 1102–1110. doi: 10.1104/pp.103.025122

Connolly, E. L., Fett, J. P., and Guerinot, M. L. (2002). Expression of the IRT1 metal transporter is controlled by metals at the levels of transcript and protein Accumulation. *Plant Cell* 14 (6), 1347. doi: 10.1105/tpc.001263

Connorton, J. M., Balk, J., and Rodriguez-Celma, J. (2017). Iron homeostasis in plants - a brief overview. *Metallomics* 9 (7), 813–823. doi: 10.1039/C7MT00136C

Curie, C., Panaviene, Z., Loulergue, C., Dellaporta, S. L., Briat, J. F., and Walker, E. L. (2001). Maize yellow stripe1 encodes a membrane protein directly involved in Fe(III) uptake. *Nature* 409 (6818), 346–349. doi: 10.1038/35053080

Dinneny, J., Long, T., Wang, J., Jung, J., Mace, D., Pointer, S., et al. (2008). Cell identity mediates the response of Arabidopsis roots to abiotic stress. *Science* 320, 942– 945. doi: 10.1126/science.1153795

Divol, F., Couch, D., Conejero, G., Roschzttardt, H., Mari, S., and Curie, C. (2013). The Arabidopsis YELLOW STRIPE LIKE4 and 6 transporters control iron release from the chloroplast. *Plant Cell* 19, 19. doi: 10.1105/tpc.112.107672

Eide, D., Broderius, M., Fett, J., and Guerinot, M. L. (1996). A novel iron-regulated metal transporter from plants identified by functional expression in yeast. *Proc. Natl. Acad. Sci. U.S.A.* 93 (11), 5624–5628. doi: 10.1073/pnas.93.11.5624

Foury, F., and Roganti, T. (2002). Deletion of the mitochondrial carrier genes MRS3 and MRS4 suppresses mitochondrial iron accumulation in a yeast frataxin-deficient strain. *J. Biol. Chem.* 277 (27), 24475–24483. doi: 10.1074/jbc.M111789200

Fraga, D., Meulia, T., and Fenster, S. (2008). Real-Time PCR. *Curr. Protoc. Essent. Lab. Tech.* (1), 10.13.11–10.13.34. doi: 10.1002/9780470089941.et1003s00

Froschauer, E. M., Rietzschel, N., Hassler, M. R., Binder, M., Schweyen, R. J., Lill, R., et al. (2013). The mitochondrial carrier Rim2 co-imports pyrimidine nucleotides and iron. *Biochem. J.* 455 (1), 57. doi: 10.1042/BJ20130144

Froschauer, E. M., Schweyen, R. J., and Wiesenberger, G. (2009). The yeast mitochondrial carrier proteins Mrs3p/Mrs4p mediate iron transport across the inner mitochondrial membrane. *Biochim. Biophys. Acta* 1788 (5), 1044–1050. doi: 10.1016/j.bbamem.2009.03.004

Garcia, L., Mansilla, N., Ocampos, N., Pagani, M. A., Welchen, E., and Gonzalez, D. H. (2019). The mitochondrial copper chaperone COX19 influences copper and iron homeostasis in arabidopsis. *Plant Mol. Biol.* 99 (6), 621–638. doi: 10.1007/s11103-019-00840-y

Grossoehme, N. E., Akilesh, S., Guerinot, M. L., and Wilcox, D. E. (2006). Metal-binding thermodynamics of the histidine-rich sequence from the metal-transport protein IRT1 of Arabidopsis thaliana. *Inorg. Chem.* 45 (21), 8500–8508. doi: 10.1021/ic0606431

Inoue, H., Kobayashi, T., Nozoye, T., Takahashi, M., Kakei, Y., Suzuki, K., et al. (2009). Rice OsYSL15 Is an iron-regulated Iron(III)-Deoxymugineic acid transporter expressed in the roots and Is essential for iron uptake in early growth of the seedlings. *J. Biol. Chem.* 284 (6), 3470–3479. doi: 10.1074/jbc.M806042200

Jain, A., and Connolly, E. L. (2013). Mitochondrial iron transport and homeostasis in plants. *Front. Plant Sci.* 4 (348), doi: 10.3389/fpls.2013.00348

Jain, A., Wilson, G., and Connolly, E. (2014). The diverse roles of FRO family metalloreductases in iron and copper homeostasis. *Front. Plant Sci.* 5, 100. doi: 10.3389/fpls.2014.00100

Jefferson, R. A., Kavanagh, T. A., and Bevan, M. W. (1987). GUS fusions: beta-glucuronidase as a sensitive and versatile gene fusion marker in higher plants. *EMBO J.* 6 (13), 3901–3907. doi: 10.1002/j.1460-2075.1987.tb02730.x

Jeong, J., and Connolly, E. L. (2009). Iron uptake mechanisms in plants: functions of the FRO family of ferric reductases. *Plant Sci.* 176 (6), 709–714. doi: 10.1016/j.plantsci.2009.02.011

Jeong, J., Merkovich, A., Clyne, M., and Connolly, E. L. (2017). Directing iron transport in dicots: regulation of iron acquisition and translocation. *Curr. Opin. Plant Biol.* 39, 106–113. doi: 10.1016/j.pbi.2017.06.014

Kerkeb, L., Mukherjee, I., Chatterjee, I., Lahner, B., Salt, D. E., and Connolly, E. L. (2008). Iron-induced turnover of the Arabidopsis IRON-REGULATED TRANSPORTER1 metal transporter requires lysine residues. *Plant Physiol.* 146 (4), 1964–1973. doi: 10.1104/pp.107.113282

Kobayashi, T., Nagasaka, S., Senoura, T., Itai, R. N., Nakanishi, H., and Nishizawa, N. K. (2013). Iron-binding Haemerythrin RING ubiquitin ligases regulate plant iron responses and accumulation. *Nat. Commun.* 4, 2792. doi: 10.1038/ncomms3792

Kobayashi, T., and Nishizawa, N. K. (2012). Iron uptake, translocation, and regulation in higher plants. *Annu. Rev. Plant Biol.* 63 (1), 131–152. doi: 10.1146/annurev-arplant-042811-105522

Koncz, C., and Schell, J. (1986). The promoter of TL-DNA gene 5 controls the tissue-specific expression of chimaeric genes carried by a novel type of Agrobacterium binary vector. *Mol. Gen. Genet.* 204 (3), 383–396. doi: 10.1007/BF00331014

Korshunova, Y. O., Eide, D., Clark, W. G., Guerinot, M. L., and Pakrasi, H. B. (1999). The IRT1 protein from Arabidopsis thaliana is a metal transporter with a broad substrate range. *Plant Mol. Biol.* 40 (1), 37–44. doi: 10.1023/A:1026438615520

Kunji, E. R., and Robinson, A. J. (2006). The conserved substrate binding site of mitochondrial carriers. *Biochim. Biophys. Acta* 1757 (9-10), 1237–1248. doi: 10.1016/j.bbabio.2006.03.021

Lahner, B., Gong, J., Mahmoudian, M., Smith, E. L., Abid, K. B., Rogers, E. E., et al. (2003). Genomic scale profiling of nutrient and trace elements in Arabidopsis thaliana. *Nat. Biotechnol.* 21 (10), 1215–1221. doi: 10.1038/nbt865

LeClere, S., and Bartel, B. (2001). A library of Arabidopsis 35S-cDNA lines for identifying novel mutants. *Plant Mol. Biol.* 46 (6), 695–703. doi: 10.1023/A:1011699722052

Li, L., and Kaplan, J. (2004). A mitochondrial-vacuolar signaling pathway in yeast that affects iron and copper metabolism. *J. Biol. Chem.* 279 (32), 33653–33661. doi: 10.1074/jbc.M403146200

Long, T. A., Tsukagoshi, H., Busch, W., Lahner, B., Salt, D. E., and Benfey, P. N. (2010). The bHLH transcription factor POPEYE regulates response to iron deficiency in Arabidopsis roots. *Plant Cell* 22 (7), 2219–2236. doi: 10.1105/tpc.110.074096

Luo, D., Bernard, D. G., Balk, J., Hai, H., and Cui, X. (2012). The DUF59 family gene AE7 acts in the cytosolic iron-sulfur cluster assembly pathway to maintain nuclear genome integrity in Arabidopsis. *Plant Cell* 24 (10), 4135–4148. doi: 10.1105/tpc.112.102608

Mai, H.-J., Pateyron, S., and Bauer, P. (2016). Iron homeostasis in Arabidopsis thaliana: transcriptomic analyses reveal novel FIT-regulated genes, iron deficiency marker genes and functional gene networks. *BMC Plant Biol.* 16 (1), 211. doi: 10.1186/s12870-016-0899-9

Małas, K., Migocka, M., Maciaszczyk-Dziubinska, E., Garbiec, A., and Posyniak, E. (2018). Metal tolerance protein MTP6 affects mitochondrial iron and manganese homeostasis in cucumber. *J. Exp. Bot.* 70 (1), 285–300. doi: 10.1093/jxb/ery342

Maliandi, M. V., Busi, M. V., Turowski, V. R., Leaden, L., Araya, A., and Gomez-Casati, D. F. (2011). The mitochondrial protein frataxin is essential for heme biosynthesis in plants. *FEBS J.* 278 (3), 470–481. doi: 10.1111/j.1742-4658.2010.07968.x

Marone, M., Mozzetti, S., De Ritis, D., Pierelli, L., and Scambia, G. (2001). Semiquantitative RT-PCR analysis to assess the expression levels of multiple transcripts from the same sample. *Biol. Procedures Online* 3, 19–25. doi: 10.1251/bpo20

Metzendorf, C., Wu, W., and Lind, M. I. (2009). Overexpression of Drosophila mitoferrin in l(2)mbn cells results in dysregulation of Fer1HCH expression. *Biochem. J.* 421 (3), 463–471. doi: 10.1042/BJ20082231

Migocka, M., Maciaszczyk-Dziubinska, E., Malas, K., Posyniak, E., and Garbiec, A. (2019). Metal tolerance protein MTP6 affects mitochondrial iron and manganese homeostasis in cucumber. *J. Exp. Bot.* 70 (1), 285–300. doi: 10.1093/jxb/ery342

Millar, A. H., and Heazlewood, J. L. (2003). Genomic and proteomic analysis of mitochondrial carrier proteins in Arabidopsis. *Plant Physiol.* 131 (2), 443. doi: 10.1104/pp.009985

Moore, M. J., Wofford, J. D., Dancis, A., and Lindahl, P. A. (2018). Recovery of mrs3Δmrs4Δ Saccharomyces cerevisiae Cells under iron-sufficient conditions and the role of Fe580. *Biochemistry* 57 (5), 672–683. doi: 10.1021/acs.biochem.7b01034

Muhlenhoff, U., Stadler, J. A., Richhardt, N., Seubert, A., Eickhorst, T., Schweyen, R. J., et al. (2003). A specific role of the yeast mitochondrial carriers MRS3/4p in mitochondrial iron acquisition under iron-limiting conditions. *J. Biol. Chem.* 278 (42), 40612–40620. doi: 10.1074/jbc.M307847200

Mukherjee, I., Campbell, N. H., Ash, J. S., and Connolly, E. L. (2006). Expression profiling of the Arabidopsis ferric chelate reductase (FRO) gene family reveals differential regulation by iron and copper. *Planta* 223 (6), 1178–1190. doi: 10.1007/s00425-005-0165-0

Nelson, D. R., Felix, C. M., and Swanson, J. M. (1998). Highly conserved charge-pair networks in the mitochondrial carrier family. *J. Mol. Biol.* 277 (2), 285–308. doi: 10.1006/jmbi.1997.1594

Nozoye, T., Nagasaka, S., Kobayashi, T., Takahashi, M., Sato, Y., Sato, Y., et al. (2011). Phytosiderophore efflux transporters are crucial for iron acquisition in Graminaceous Plants. *J. Biol. Chem.* 286 (7), 5446–5454. doi: 10.1074/jbc.M110.180026

Palmieri, F. (2013). The mitochondrial transporter family SLC25: identification, properties and physiopathology. *Mol. Aspects Med.* 34 (2-3), 465–484. doi: 10.1016/j.mam.2012.05.005

Pan, X., Yuan, D. S., Xiang, D., Wang, X., Sookhai-Mahadeo, S., Bader, J. S., et al. (2004). A robust toolkit for functional profiling of the yeast genome. *Mol. Cell* 16 (3), 487–496. doi: 10.1016/j.molcel.2004.09.035

Paradkar, P. N., Zumbrennen, K. B., Paw, B. H., Ward, D. M., and Kaplan, J. (2009). Regulation of mitochondrial iron import through differential turnover of mitoferrin 1 and mitoferrin 2. *Mol. Cell. Biol.* 29 (4), 1007–1016. doi: 10.1128/MCB.01685-08

Paszkiewicz, G., Gualberto, J. M., Benamar, A., Macherel, D., and Logan, D. C. (2017). Arabidopsis seed mitochondria are bioenergetically active immediately upon imbibition and specialize via biogenesis in preparation for autotrophic growth. *Plant Cell* 29 (1), 109–128. doi: 10.1105/tpc.16.00700

Pebay-Peyroula, E., Dahout-Gonzalez, C., Kahn, R., Trézéguet, V., Lauquin, G. J. M., and Brandolin, G. (2003). Structure of mitochondrial ADP/ATP carrier in complex with carboxyatractyloside. *Nature* 426, 39. doi: 10.1038/nature02056

Perea-Garcia, A., Garcia-Molina, A., Andres-Colas, N., Vera-Sirera, F., Perez-Amador, M. A., Puig, S., et al. (2013). Arabidopsis copper transport protein COPT2 participates in the cross talk between iron deficiency responses and low-phosphate signaling. *Plant Physiol.* 162 (1), 180–194. doi: 10.1104/pp.112.212407

Philpott, C. C., and Ryu, M.-S. (2014). Special delivery: distributing iron in the cytosol of mammalian cells. *Front. Pharmacol.* 5, 173. doi: 10.3389/fphar.2014.00173

Picault, N., Hodges, M., Palmieri, L., and Palmieri, F. (2004). The growing family of mitochondrial carriers in Arabidopsis. *Trends Plant Sci.* 9 (3), 138–146. doi: 10.1016/j.tplants.2004.01.007

Robinson, N. J., Procter, C. M., Connolly, E. L., and Guerinot, M. L. (1999). A ferric-chelate reductase for iron uptake from soils. *Nature* 397 (6721), 694–697. doi: 10.1038/17800

Rogers, E. E., Eide, D. J., and Guerinot, M. L. (2000). Altered selectivity in an Arabidopsis metal transporter. *Proc. Natl. Acad. Sci. U.S.A.* 97 (22), 12356–12360. doi: 10.1073/pnas.210214197

Ross, K. L., and Eisenstein, R. S. (2002). Iron deficiency decreases mitochondrial aconitase abundance and citrate concentration without affecting tricarboxylic acid cycle capacity in rat liver. *J. Nutr.* 132 (4), 643–651. doi: 10.1093/jn/132.4.643

Rouault, T. A. (2014). Mammalian iron-sulphur proteins: novel insights into biogenesis and function. *Nat. Rev. Mol. Cell Biol.* 16 (1), 45–55. doi: 10.1038/nrm3909

Rouault, T. A. (2015). Iron-sulfur proteins hiding in plain sight. *Nat. Chem. Biol.* 11 (7), 442–445. doi: 10.1038/nchembio.1843

Rouault, T. A. (2016). Mitochondrial iron overload: causes and consequences. *Curr. Opin. Genet. Dev.* 38, 31–37. doi: 10.1016/j.gde.2016.02.004

Sabar, M., Balk, J., and Leaver, C. J. (2005). Histochemical staining and quantification of plant mitochondrial respiratory chain complexes using blue-native polyacrylamide gel electrophoresis. *Plant J.* 44 (5), 893–901. doi: 10.1111/j.1365-313X.2005.02577.x

Santi, S., and Schmidt, W. (2009). Dissecting iron deficiency-induced proton extrusion in Arabidopsis roots. *New Phytol.* 183 (4), 1072–1084. doi: 10.1111/j.1469-8137.2009.02908.x

Schaedler, T. A., Thornton, J. D., Kruse, I., Schwarzlander, M., Meyer, A. J., van Veen, H. W., et al. (2014). A conserved mitochondrial ATP-binding cassette transporter exports glutathione polysulfide for cytosolic metal cofactor assembly. *J. Biol. Chem.* doi: 10.1074/jbc.M114.553438

Schagger, H., and von Jagow, G. (1991). Blue native electrophoresis for isolation of membrane protein complexes in enzymatically active form. *Anal. Biochem.* 199 (2), 223–231. doi: 10.1016/0003-2697(91)90094-A

Schneider, C. A., Rasband, W. S., and Eliceiri, K. W. (2012). NIH Image to ImageJ: 25 years of image analysis. *Nat. Methods* 9 (7), 671–675. doi: 10.1038/nmeth.2089

Schwab, R., Ossowski, S., Riester, M., Warthmann, N., and Weigel, D. (2006). Highly specific gene silencing by artificial microRNAs in Arabidopsis. *Plant Cell Online* 18 (5), 1121–1133. doi: 10.1105/tpc.105.039834

Shaw, G. C., Cope, J. J., Li, L., Corson, K., Hersey, C., Ackermann, G. E., et al. (2006). Mitoferrin is essential for erythroid iron assimilation. *Nature* 440 (7080), 96–100. doi: 10.1038/nature04512

Sun, W., Cao, Z., Li, Y., Zhao, Y., and Zhang, H. (2007). A simple and effective method for protein subcellular localization using Agrobacterium-mediated transformation of onion epidermal cells. *Biologia* 62 (5), 529–532. doi: 10.2478/s11756-007-0104-6

Vazzola, V., Losa, A., Soave, C., and Murgia, I. (2007). Knockout of frataxin gene causes embryo lethality in Arabidopsis. *FEBS Lett.* 581 (4), 667–672. doi: 10.1016/j.febslet.2007.01.030

Vert, G., Grotz, N., Dedaldechamp, F., Gaymard, F., Guerinot, M. L., Briat, J. F., et al. (2002). IRT1, an Arabidopsis transporter essential for iron uptake from the soil and for plant growth. *Plant Cell* 14 (6), 1223–1233. doi: 10.1105/tpc.001388

Vigani, G., Bashir, K., Ishimaru, Y., Lehmann, M., Casiraghi, F. M., Nakanishi, H., et al. (2016). Knocking down mitochondrial iron transporter (MIT) reprograms primary and secondary metabolism in rice plants. *J. Exp. Bot.* 67 (5), 1357–1368. doi: 10.1093/jxb/erv531

Vigani, G., Solti, Á, Thomine, S., and Philippar, K. (2019). Essential and detrimental — an update on intracellular iron trafficking and homeostasis. *Plant Cell Physiol.* 60 (7), 1420–1439. doi: 10.1093/pcp/pcz091

Walker, E. L., and Connolly, E. L. (2008). Time to pump iron: iron-deficiency-signaling mechanisms of higher plants. *Curr. Opin. Plant Biol.* 11 (5), 530–535. doi: 10.1016/j.pbi.2008.06.013

Walker, J. E. (1992). The mitochondrial transporter family. *Curr. Opin. Struct. Biol.* 2 (4), 519–526. doi: 10.1016/0959-440X(92)90081-H

Wu, H., Li, L., Du, J., Yuan, Y., Cheng, X., and Ling, H. Q. (2005). Molecular and biochemical characterization of the Fe(III) chelate reductase gene family in Arabidopsis thaliana. *Plant Cell Physiol.* 46 (9), 1505–1514. doi: 10.1093/pcp/pci163

Yamasaki, H., Hayashi, M., Fukazawa, M., Kobayashi, Y., and Shikanai, T. (2009). SQUAMOSA promoter binding protein-like7 is a central regulator for Copper homeostasis in Arabidopsis. *Plant Cell* 21 (1), 347–361. doi: 10.1105/tpc.108.060137

Yoon, H., Zhang, Y., Pain, J., Lyver, E. R., Lesuisse, E., Pain, D., et al. (2011). Rim2, a pyrimidine nucleotide exchanger, is needed for iron utilization in mitochondria. *Biochem. J.* 440 (1), 137–146. doi: 10.1042/BJ20111036

Yoon, T., and Cowan, J. A. (2004). Frataxin-mediated iron delivery to ferrochelatase in the final step of heme biosynthesis. *J. Biol. Chem.* 279 (25), 25943–25946. doi: 10.1074/jbc.C400107200

Conflict of Interest: The authors declare that the research was conducted in the absence of any commercial or financial relationships that could be construed as a potential conflict of interest.

Advantages of publishing in Frontiers

OPEN ACCESS
Articles are free to read for greatest visibility and readership

FAST PUBLICATION
Around 90 days from submission to decision

HIGH QUALITY PEER-REVIEW
Rigorous, collaborative, and constructive peer-review

TRANSPARENT PEER-REVIEW
Editors and reviewers acknowledged by name on published articles

Frontiers
Avenue du Tribunal-Fédéral 34
1005 Lausanne | Switzerland

Visit us: www.frontiersin.org
Contact us: info@frontiersin.org | +41 21 510 17 00

REPRODUCIBILITY OF RESEARCH
Support open data and methods to enhance research reproducibility

DIGITAL PUBLISHING
Articles designed for optimal readership across devices

FOLLOW US
@frontiersin

IMPACT METRICS
Advanced article metrics track visibility across digital media

EXTENSIVE PROMOTION
Marketing and promotion of impactful research

LOOP RESEARCH NETWORK
Our network increases your article's readership